COMATCOMP 09

AEMAC

ASOCIACIÓN ESPAÑOLA DE MATERIALES COMPUESTOS

ACTAS DEL VIII CONGRESO NACIONAL DE MATERIALES COMPUESTOS

PROCEEDINGS OF V INTERNATIONAL CONFERENCE ON SCIENCE AND TECHNOLOGY OF COMPOSITE MATERIALS

Donostia - San Sebastián, 7, 8 y 9 de octubre de 2009

Editores:

Alfredo Güemes (UPM)
Jose Kenny (UNIPG-CSIC)
Alejandro Ureña (URJC)
Analía Vázquez (UBA)
Iñaki Mondragon (UPV/EHU)

COMATCOMP 09

Depósito legal: SS-1067-2009
I.S.B.N.: En trámite
Imprime: Gráficas San Martín

COMATCOMP 09

PRESENTACIÓN

Los congresos nacionales de materiales compuestos (MATCOMP), organizados con periodicidad bienal por la Asociación Española de Materiales Compuestos (AEMAC) desde 1995, constituyen el encuentro más importante de la comunidad académica, científica y empresarial del campo de los materiales compuestos en España. Lo mismo ocurre a nivel iberoamericano con las conferencias internacionales de materiales composites (COMAT), organizadas en diversos países desde 2001.

El objetivo principal de dichos eventos ha sido servir de foro de comunicación entre la comunidad empresarial, técnica y científica para promover la investigación, el desarrollo, la innovación, el uso y la difusión de los materiales compuestos. Así mismo, los congresos MATCOMP y COMAT son sensibles con los aspectos relacionados con la formación profesional (técnica y científica) de las futuras generaciones de profesionales de la Comunidad iberoamericana.

Por los motivos aludidos, AEMAC considera los congresos MATCOMP como su principal activo y contribución dentro de la labor de promoción de los Materiales Compuestos que desarrolla desde su fundación.

Para su VIII Congreso Nacional, celebrada del 7 al 9 de octubre de 2009, la Junta Directiva de AEMAC escogió el Palacio Miramar de la ciudad de Donostia - San Sebastián, situado a las orillas del mar, y consideró adecuado desarrollarlo conjuntamente con la V Conferencia Internacional COMAT, y de ahí la denominación COMATCOMP.

El Comité local ha estado formado por Faustino Mujika, Jalel Labidi, Loli Martin, Koro de la Caba, Arantxa Eceiza, Mª Angeles Corcuera, Ainhoa Arrese, Itziar Adarraga, Cristina Marieta, Rodrigo Llano-Ponte, Jose Angel Ramos, Cristina Peña, Galder Kortaberria, Nagore Gabilondo, Aitor Arbelaiz e Iñaki Mondragon, todos ellos miembros del Grupo 'Materiales + Tecnologías' sito en la Escuela Politécnica de Donostia - San Sebastián de la Universidad del País Vasco/Euskal Herriko Unibertsitatea.

Se han presentado del orden de 300 ponencias, aumentando la cifra de años anteriores, lo que demuestra el incremento de actividad dentro de esta área, así como su diversificación temática. A todos los autores queremos expresar nuestro agradecimiento por el esfuerzo en la preparación de su ponencia.

Donostia - San Sebastián, 21 de septiembre de 2009

INVITED LECTURES - CONFERENCIAS PLENARIAS

T1. POLYMER-MATRIX COMPOSITES MATERIALES COMPUESTOS DE MATRIZ POLIMÉRICA

T2. ADVANCED COMPOSITES IN INDUSTRIAL APPLICATIONS MATERIALES COMPUESTOS AVANZADOS EN APLICACIONES INDUSTRIALES

T3. METAL-MATRIX COMPOSITES MATERIALES COMPUESTOS DE MATRIZ METÁLICA

T4. OTHER MATRIX COMPOSITES
MATERIALES COMPUESTOS DE OTRAS MATRICES

T5. BIOCOMPOSITES FOR SPECIFIC APPLICATIONS BIOCOMPOSITES PARA APLICACIONES ESPECÍFICAS

T6. NANOCOMPOSITES

T7. MANUFACTURING
PROCESADO

T8. MODELLING
MODELIZACIÓN

T9. MECHANICAL AND PHYSICAL BEHAVIOUR COMPORTAMIENTO FÍSICO Y MECÁNICO

INVITED LECTURES
CONFERENCIAS PLENARIAS

Composite materials. Future developments in aeronautical applications

Jose Sanchez
AIRBUS, Pº. John Lennon s/n 28906 Getafe, Madrid

During last decades a huge increase in the use of organic matrix composite materials has been noted in the aerospace industry. This fact is related with the benefits that these materials offer in the structural performance of the manufactured components as well as in service improvements to the system operators. At the same time the metallic industry has been losing market share for aerospace structural application, which could be related with lack of innovation effort and also with the strong conviction that aerospace business of this companies and related manufacturing companies was so strong that never an emerging industry will take part of his business. The same situation could appear in the comings years but in this case the industry that will suffer the threat will be the composites one. This fact is coming due to lack of innovation in the manufacturing technologies field, as well as in the new materials covering both fibers and resin. A disruptive technology has to be developed in the coming years in order to increase or at least to maintain the today market share in the aerospace market. A special effort has to be performed in the manufacturing area, where new processes and automatization technologies in the dry fiber field are required. The future will be related with the composites plant layout that will allow the OOA technologies, in any of the technological fields of today development. In the materials area a new concept of multifunctionallity is emerging. New resins an fibers has to be developed with a special emphasis to solve the today drawbacks but considering ecoephiciency and final cost as the key drivers for future developments.

Nanostructured cellulose composites

Lars A. Berglund
Dept of Fiber and Polymer Technology and Wallenberg Wood Science Center, Royal Inst of Technology, SE-10044 Stockholm, Sweden

SUMMARY

Cellulose has interesting physical properties. In the form of nanoparticles, it can strongly reinforce elastomers. Recently, it has become economically feasible to make microfibrillated cellulose from wood. Thermoset composites show high modulus and strength, but are brittle. With proper strategy, it is possible to make nanopaper of high toughness. This can be used with plasticized starch to make ductile nanocomposites of high strength and reduced moisture sorption. The cell walls of starch biofoams can also be reinforced by nanocellulose to give strongly enhanced properties . Cellulose surfaces can be grafted by polymer brushes and also modified by adsorption. Cellulose nanofibers thus provides new opportunities to molecular scale tailored interfaces, and high cellulose content so that tough nanocomposites can be prepared with much improved performance as compared with cellulose microcomposites based on plant fibers.

1. INTRODUCTION

Cellulosic biocomposites in current use are based on plant fibers in polymer matrices. The fibers are typically on the order of 30 micrometers in diameter and several millimetres or centimetres in length. Such biocomposites are used in automotive and furniture applications, as well as building applications including decking boards based on polyolefins and wood saw dust. These biocomposites suffer from brittleness due to the early debonding between hydrophilic particulate fillers and hydrophobic matrices. In addition, smell due to degradation of amorpous polysaccharides and lignin can be a problem in melt-processed biocomposites, as well as discolouring. Moisture adsorption in the lignocellulosic fibers can also cause significant problems in terms of lowered strength and hygroscopic swelling or warpage. It is therefore of interest to investigate if it possible to improve the performance of biocomposites by the use of cellulose nanofibers as reinforcement. The following is a brief review of such work carried out in the Biocomposites group at KTH (Royal Inst of Technology in Stockholm) during the past couple of years.

2. NANOFIBER PROPERTIES AND POTENTIAL FOR FIBER/MATRIX INTERACTION – MOLECULAR DYNAMICS INSIGHTS

As we go down in scale for the reinforcement fiber in composites, molecular aspects of both the fiber and fiber/matrix interface become more important. In this context, molecular dynamics simulation becomes of interest. The work by Bergenstråhle et al (2007) analyzes the cellulose crystal in terms of its thermal expansion coefficient and its elastic properties. The cellulose crystal consists of extended cellulose chains in the longitudinal direction of the crystal. Although intermolecular hydrogen bonds are present, the intramolecular hydrogen bonds are the most critical with respect to the high elastic modulus and low thermal expansion. The calculated longitudinal modulus of the crystal is 156 GPa. Compared with the modulus of steel (200 GPa), this is a respectable number, and it is clear that cellulose nanofibers have potential as a biocomposite reinforcement phase.

On the surface of the cellulose crystal, hydroxyl groups are present. They are potential "handles" for further chemical modification of the reinforcement, and can also interact spontaneously with appropriate polymer matrices surrounding the nanofibers. For instance, amorphous polysaccharides from plants such as starch and xyloglucan are of interest as environmentally friendly matrices. Since they are chemically somewhat related to cellulose (polysaccharides based on sugar ring repeat units), there is potential for favourable nanofiber-matrix interaction by physical mechanisms only. In an effort to start understanding the mechanisms for physical adsorption of polysaccharides to cellulose crystal surfaces, Bergenstråhle et al (2009) studied model polysaccharides adsorbing to cellulose surfaces. The nature of the molecular interaction was studied in great detail, as well as the effect of water and initial conformation as the molecule was pulled off the cellulose surface. Bergenstråhle et al (2008) also analyzed the effect of caprolactone grafting on the interaction between modified cellulose surfaces and caprolactone model molecules. The favourable effect of polycaprolactone grafting to cellulose on cellulose-polycaprolactone interaction was later confirmed experimentally (Lönnberg et al, 2008).

2. ELASTOMER REINFORCEMENT

Elastomers can also be reinforced by cellulose nanoparticles. This was demonstrated by Wu et al (2007). An amorphous thermoplastic polyurethane was polymerized in the presence of cellulose nanoparticles based on microcrystalline cellulose. Such nanoparticles have fairly short aspect ratio, but are highly functional with respect to polyurethanes. Covalent as well as hydrogen bonding interaction between the cellulose and the polyurethane will take place. These nanocomposites showed very high strength. The reason is that the elastomer network is improved by interaction with the nanoscale filler. The filler is integrated with the molecular network, so that the effective cross-link density increases. Since the nanaoparticles are very small and show strong filler-matrix adhesion, the strain-to-failure is not reduced as compared with the non-filled elastomer reference. In fact, it is somewhat increased. Since the nanocellulose particles also have a fibrous geometry and high stiffness, this also contributes to the observed reinforcement effect.

3. NANOFIBER PREPARATION

Cellulose nanofibers can be prepared by cellulose-producing bacteria, by acid hydrolysis of plant fibers, and by other related routes. In the present study, focus is on microfibrillated cellulose from wood pulp of high cellulose content. It was found that the energy required for mechanical disintegration of such pulp fibers into cellulose nanofibers, could be reduced significantly. One such method is to use enzymatic pre-treatment of the pulp with endoglucanase, in combination with beating of the fibers (Henriksson et al 2007). It seems this is causing the plant fibers to swell and this facilitates the mechanical disintegration step, so that it becomes economically feasible to make cellulose nanofibers in large quantities. An image of the resulting nanofibers is presented in Figure 1.

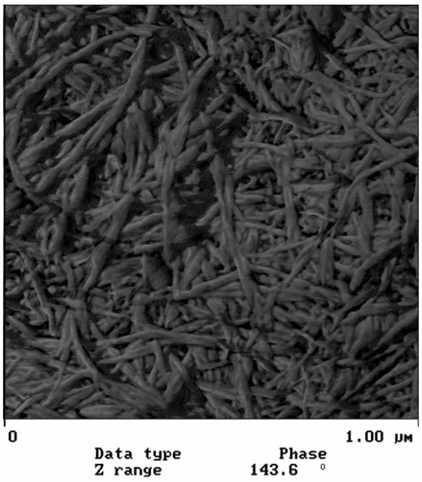

Fig. 1. AFM image of the surface of nanopaper based on cellulose nanofibers from wood pulp. (Image by Prof I Mondragon and colleagues at Univ of the Basque Country).

4. NANOPAPER AND NANOCOMPOSITE PERFORMANCE

Cellulose nanofibers are present as a suspension in water of about 1% concentration by weight. These suspensions can be cast to form films, which actually have a nanopaper structure. Compared with conventional paper, the structure has lower porosity, and the scale of the fibrous phase is three orders of magnitude smaller.

If such nanopaper structures are impregnated by monomers and polymerized to form a glassy thermoset, the resulting material can be strong but is also brittle with a strain-to-failure of only a few percent (Henriksson, Berglund (2007)). If the matrix is highly plasticized, the resulting biocomposite obtains an interesting combination of strength, modulus and high toughness (Svagan et al, 2007). Possibly, the reason is less localized failure initiation processes. These starch-based materials also showed strongly reduced moisture diffusion rates due to the presence of the nanocellulose (Svagan et al 2009). By selection of high molar mass cellulose, careful preparation, charged nanofibers and suitable porosity, it was then possible to prepare cellulose nanopaper of remarkable mechanical properties in uniaxial tension (random-in-the-plane nanofiber orientation), see Figure 2. Recently, even stronger nanopaper composites have been prepared, exceeding 300 MPa in strength (Zhou et al, 2009). In the newest nanocomposites, each individual nanofiber is surrounded by a matrix of hydrated amorphous polysaccharide, a truly nanostructured composite.

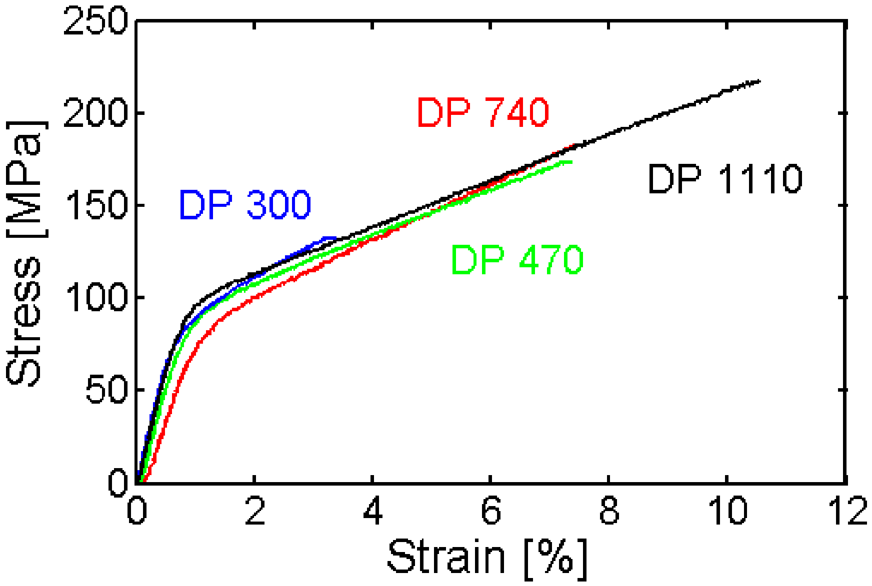

Fig. 2. Stress-strain curve in uniaxial tension of cellulose nanopaper with random-in-the-plane nanofiber orientation distribution. The porosity is in the range 15-20%, and the modulus is 15 GPa. DP numbers correspond to estimated degree of polymerization of the cellulose in the cellulose nanofibers (Figure based on data in Henriksson et al, 2008).

5. FOAMS AND AEROGELS

Polymer foams based on starch are of interest as replacement of petroleum-based expanded polystyrene (EPS) packaging materials. However, the properties of starch foams are much inferior to EPS due to the moisture sensitivity of starch. For this reason, polymer foams were prepared with cellulose nanofiber reinforcement of the foam cell walls, see Figure 3. As a consequence, very strong reinforcement effects were observed (Svagan et al, 2008). The newest materials based on cellulose nanofibers and amylopectin starch show better mechanical properties than EPS in uniaxial compression, also in the presence of humid atmosphere (50% RH and room temperature). Also aerogels with only a few percent by volume of solid material with exceptional mechanical performance and robustness have been prepared (Pääkkö et al, 2008).

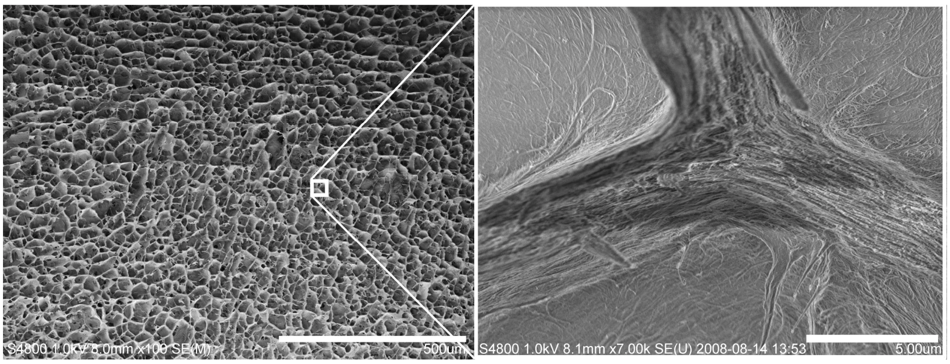

Fig. 3. Structure of nanocomposite foam based on starch and cellulose nanofibers from wood pulp. Left image is cell structure (scale bar 50 micrometers) and right image reveals signs of cellulose nanofibers present in the cell wall. (FE-SEM images by A Svagan)

6. CONCLUSIONS

Cellulose nanofibers can be disintegrated from wood pulp in economically favourable ways. These low-cost nanofibers can be used in nanopaper films, and nanostructured biocomposites showing exceptional mechanical performance. The reason is nanoscale interaction between nanofibers which can be tuned so that nanofibers slip with respect to each other during deformation. Failure is non-localized, and this makes it possible to combine high modulus with high strength and toughness, thereby increasing the designed property space of biocomposites. A key issue is controlled porosity, since these materials can be designed so that mechanical properties are not strongly reduced by porosity.

ACKNOWLEDGMENT

Financial support is gratefully acknowledged, and contributors include SSF (Biomime), Vinnova (BiMac Innovation), EU (Sustaincomp) and the Wallenberg foundation (WWSC).

REFERENCES

BERGENSTRÅHLE, M, BERGLUND, LA, MAZEAU, K, Thermal response in crystalline I beta cellulose: A molecular dynamics study, J PHYS CHEM B, 2007, 111, 9138

BERGENSTRÅHLE M, K MAZEAU, LA BERGLUND, *European Polymer Journal, 44, 2008*, *3662*

BERGENSTRÅHLE M, E. THORMANN, N. NORDGREN AND L.A. BERGLUND, Langmuir, 2009, accepted.

HENRIKSSON, M, HENRIKSSON, G, BERGLUND, LA, LINDSTROM, T, enzyme-assisted preparation of microfibrillated cellulose (MFC) …, EUR POLYMER J, 2007, 43, 3434

HENRIKSSON, M, BERGLUND, LA, Structure and properties of cellulose nanocomposite films containing melamine formaldehyde, J APPL POL SCI, 2007, 106, 2817

HENRIKSSON, M, BERGLUND, LA, ISAKSSON, P, LINDSTROM, T, NISHINO, T, Cellulose nanopaper structures of high toughness, BIOMACROMOL, 2008, 9, 1579

LÖNNBERG H, L FOGELSTRÖM, MASA SAMIR, L BERGLUND, E MALMSTRÖM, A HULT, Surface grafting of microfibrillated cellulose with poly(□-caprolactone) – Synthesis and characterization, *European Polymer Journal*, *44, 2008*, *2991*

PÄÄKKÖ M, J VAPAAVUORI, R SILVENNOINEN, H KOSONEN, M ANKERFORS, T LINDSTRÖM, L A BERGLUND AND O IKKALA, *Soft Matter*, 2008, 4, 2492

SVAGAN, AJ, SAMIR, MASA, BERGLUND, LA, Biomimetic polysaccharide nanocomposites of high cellulose content and high toughness, BIOMACROMOL, 2007, 8, 2556

SVAGAN A, HEDENQVIST M, BERGLUND LA, Reduced water vapour sorption in cellulose nanocomposite with starch matrix, Composites Science and Technology, 2009, in press

SVAGAN, AJ, SAMIR, MASA, BERGLUND, LA, Biomimetic foams of high mechanical performance based on nanostructured cell walls, ADV MAT, 2008, 20, 1263

WU, QJ, HENRIKSSON, M, LIU, X, BERGLUND, LA, A high strength nanocomposite based on microcrystalline cellulose and polyurethane, BIOMACROMOL, 2007, 8, 3687

ZHOU Q, E MALM, H NILSSON, P T LARSSON, T IVERSEN, L A. BERGLUND, V BULONE, High-Strength Nanopaper from Biomimetic Compartmentalized Cellulosic Nanofibers**,** *Soft Matter, 2009,* accepted.

The use of composite materials in Formula 1 motor racing

Gary Savage
Brawn GP Formula 1 Team
Brackley, Northamptonshire. NN13 7BD. United Kingdom

SUMMARY

The introduction of fibre reinforced composite chassis was one of the most significant developments in the history of Grand Prix motor racing. Technology advances gained from these advanced materials have produced cars that are lighter, faster and safer than ever before. The manufacture of Formula 1 cars is now dominated by composites. Much of the development within Formula 1 has shadowed that taking place within the aerospace industry. This is not surprising when one considers the similarity of their objectives. Formula 1 cars develop revolutionarily every year and evolutionarily for every race due to the intense level of competition between the teams. The exploitation of composites within the F1 business is, as a consequence, far more advanced than in any other business.

1. INTRODUCTION

The general arrangement of single seat racing cars has remained the same since the early 1960s. The central component, which accommodates the driver, fuel cell and front suspension assembly, is the chassis. This is a semi-monocoque shell structure which is more like the cockpit of a jet fighter aircraft than anything one would expect to find on the road. The engine, in addition to providing propulsion, is a structural member joining the front and rear of the chassis. It is attached directly to the rear of this unit by high strength metal studs. The assembly is completed by the addition of the gearbox and rear suspension assembly. The gearbox, in addition to carrying the transmission is the rear section of the chassis. The car's primary structure of chassis, engine and gearbox (Figure 1) may be considered as a "torsion-beam" arrangement carrying the inertial loads to their reaction points at the four corners.

Figure 1: The “primary structure” of a formula 1 car consists of chassis, engine and gearbox.

The secondary structures (bodywork, floor, wing configurations and cooler ducting etc.) are arranged around and attached to the primary structure at various points (Figure 2).

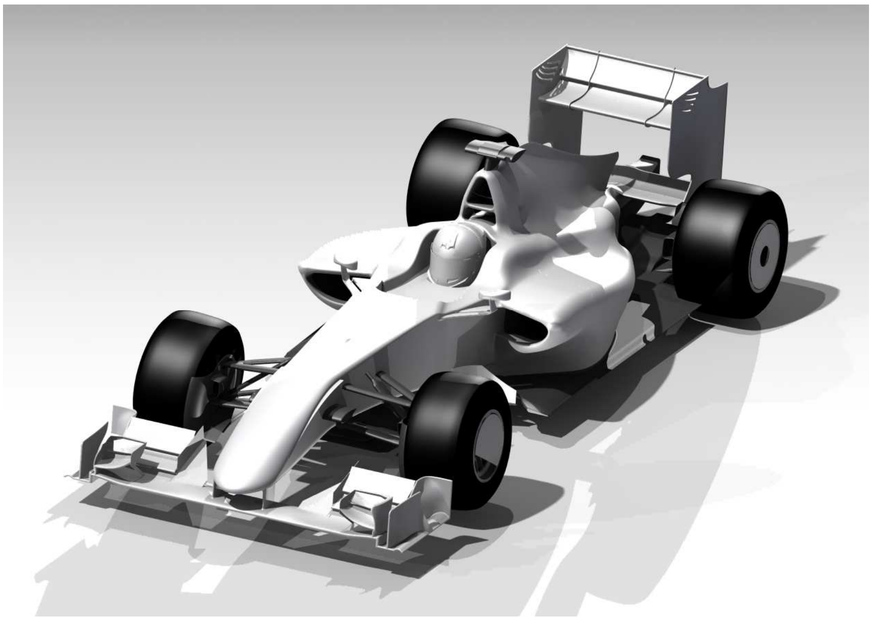

Figure 2: Complete car with secondary structures added.

A Formula 1 car is driven “on the limit”, that is to say one aims to operate the car as close to the point where its longitudinal g is just about to be overcome due to the lateral g from cornering. The car must be “set-up” for each individual circuit in order to optimise performance. Changes are made to the aerodynamic devices and the suspension elements (springs, dampers, anti-roll bars and so on) in an attempt to improve its lap time. Changes in the performance levels of the various sub-components must be manifest in the balance of the car. Clearly this will not occur if the structure transmitting the loads is not of adequate stiffness. In common with many other engineering disciplines, the designers of Formula 1 racing cars are required to comply with a stringent set of regulations. The rules are imposed by the FIA, the Sport’s governing body. Constraints are laid down on geometry, strength and weight. Strict limitations are placed on the overall dimensions of the cars and the sizing of the driver envelope within the cockpit. A series of statutory regulations have been introduced over the years which are continually updated to improve safety. Consequently, the chassis has developed a secondary function of a “survival cell” to protect the pilot in the event of a crash. A number of tests must be performed in the presence of an official prior to the car being certified for Grand Prix usage. The regulation limiting the minimum weight of the car plus driver to 605kg is of great significance. Building a car to the weight limit is a vital task if it is to be competitive.

It has been estimated that a mass of 20kg above the weight limit equates to a loss of 0.4 seconds around a typical Grand Prix circuit. Less than half a second does not sound very much, but during a full race distance this amounts to half a lap or several grid positions during a qualifying session. With modern materials it is relatively easy to build a car which satisfies all of the statutory requirements whilst still being well under the minimum weight limit. Consequently the majority of the cars are required to carry ballast (generally in the form of a heavy metal such as tungsten) in order to make up the deficit. At first glance therefore it may seem fruitless to continually aim to reduce the mass of components only to increase the amount of ballast carried. Lowering the weight of the chassis is still of benefit however. An F1 car is always accelerating, either positively under the influence of the engine or negatively under braking. Lower mass enables the engineers to alter the car’s mass balance and thus greatly influence its handling characteristics. The pursuits of lower weight and improved performance have both stimulated the introduction of new technology in both design and construction. The structural components of the car must be stiff, strong enough to satisfy the loading requirements, tolerant of and resistant to, impact damage and be of minimum weight. The solution to this problem is achieved by optimising the geometry, the quality of construction and by using the most appropriate materials. The quest for maximum structural efficiency has resulted in a progression of different technologies throughout the history of Grand Prix racing which has now converged upon composite materials.

2. DEVELOPMENT OF COMPOSITE STRUCTURES IN FORMULA 1 RACING

The first documented uses of composite construction in racing cars date back to the late 1920’s and early 1930’s in the form of wood and steel chassis. These early vehicles tended to be home built and raced so there is very little documented data concerning their performance. It is most likely however that the use of wood as a chassis material was due in the main to cheapness and convenience rather than to enhance performance. Up until the early 1950’s the predominant method of formula 1 chassis construction consisted of a tubular aluminium space frame surrounded by hand worked aluminium body panels. At that time random orientation glass mat and polyester resins (Glass Reinforced Plastic) developed in wartime research became widely available. This material allowed the relatively cheap production of complex compound curvature bodywork which replaced aluminium. The use of GRP panelling continued right through to the late 1980's.

The first truly composite chassis was built in the early 1960's by Cooper cars. The structure consisted of a hand worked aluminium outer skin, an aluminium honeycomb core and a GRP inner skin. A single piece outer skin was produced from a number of panels to form the final aerodynamic surface of the car. The aluminium honeycomb core was then bonded to the inside of the outer skin using a phenolic resin film adhesive. The inner skin of GRP was similarly bonded to the structure in a separate operation. Although the car never actually reached the track, it was to become the basis of Formula 1 chassis design for the next two decades. In the mid-to-late 1970's the preferred method of composite chassis construction used aluminium skinned, aluminium honeycomb material fabricated using the "cut and fold" method. The tubs were formed from pre-bonded sheeting which was routed, folded and riveted into the appropriate shape (Figure 3). The various teams involved later pre-formed the skins prior to bonding to the core using an epoxy film adhesive.

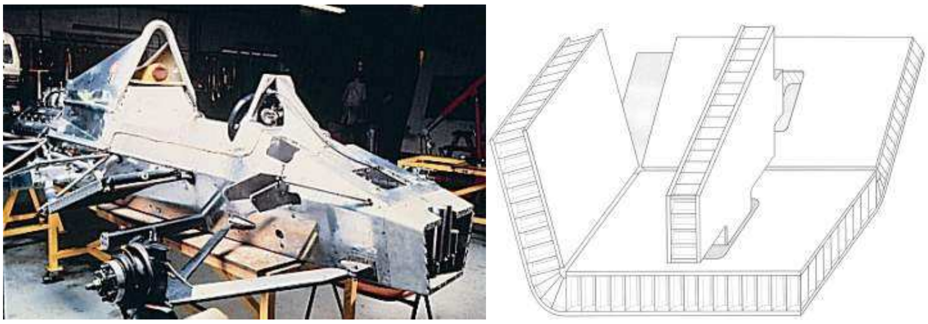

Figure 3: "Cut and fold" aluminium honeycomb chassis (late 1970's).

Carbon fibre composite chassis were first introduced by the McLaren team in 1980 (1). They consisted of pseudo-monolithic arrangement laid up over a "male" mould or mandrel using unidirectional (UD) carbon fibre prepreg tape (Figure 4). The mandrel, made of cast and machined aluminium alloy, was dismantled for removal through the cockpit opening following an autoclave cure of the composite. A three stage cure was required: one for the inner composite skin, a second to cure the epoxy film adhesive which attached the honeycomb core and a third for a further adhesive layer and the structure's outer skin. The basic design and manufacturing process remained essentially unchanged for a number of years and was still the basis of chassis construction at McLaren up until the 1992 season. In 1980 the reputation of composites with respect to impact loading was very poor as a result of problems experienced in aero-engine components in the early 1970's and some dramatic in-service failures of early race car components. Indeed many designers of repute expressed grave doubts as to the suitability of such brittle materials in what is a highly stressed application. Despite the reservations of many of their competitors, the McLaren MP4/1, the first carbon fibre monocoque racing car (Figure 5) proved so successful that it was soon copied, in one form or another, by every other team.

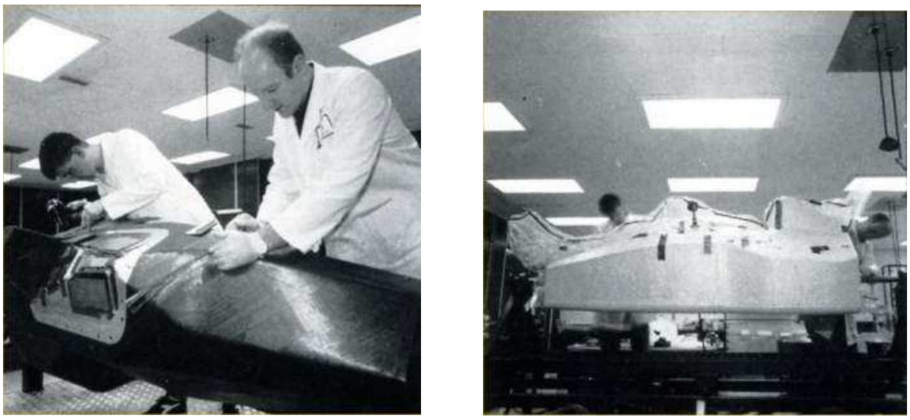

Figure 4: "Male moulded" chassis manufacture

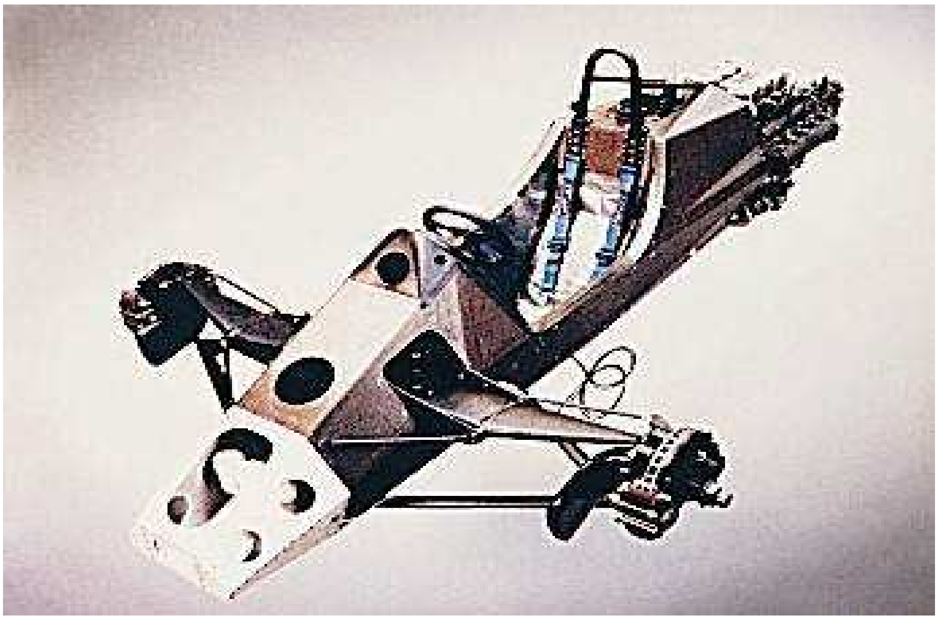

Figure 5: The first carbon monocoque McLaren MP4/1 (1980).

The 1981 season became something of a "war of attrition" for McLaren with a number of cars being accidentally crashed several times during both testing and racing. It became clear that in addition to improved mechanical properties and lower weight of the composite chassis, the damage caused by accidents was constrained in the locality of the impact. Repairs could be executed quickly and effectively with little or no loss in performance. The ability to sustain and undergo repair to minor damage is all very well, but what concerned the designers most was the ability to withstand a major collision. At the 1981 Italian Grand Prix, John Watson lost control of his McLaren and smashed violently into the barriers. He was able to walk away from the debris unscathed (Figure 6). This incident went a long way to removing the doubts in the minds of those unconvinced of the safety of carbon fibre composites under high strain rate loading. The energy absorbing properties of composites have subsequently made a great contribution to the safety record of the sport.

Figure 6: MP4/1 chassis following large impact.

The next major advance in chassis construction occurred in 1983 at one of the smaller teams. The German ATS team developed a tub fabricated inside female composite tooling. The two halves of the structure were made from woven fabric reinforced prepreg and joined at the centre line (Figure 7). Female moulding makes far more efficient use of the available aerodynamic envelope since only a minimum of secondary bodywork is needed to cover it. It also provides an opportunity to optimise the geometry and thus improve its structural efficiency. The BMW powered ATS was never a leading contender but generally considered to be one of the strongest and stiffest chassis on the circuit. Developments in aerodynamic shaping, structural analysis and laminating techniques have ensured continuous development of the chassis and other composite pieces.

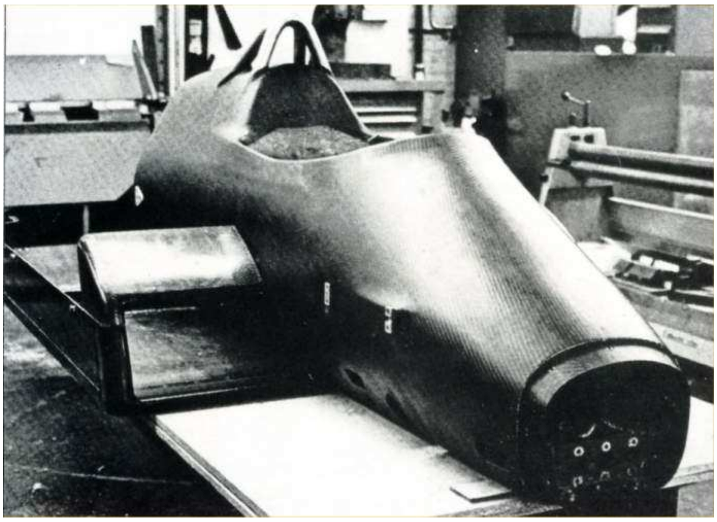

Figure 7: Female moulded ATS D6 (1983).

During the design of the MP4/1, McLaren used carbon composites wherever they offered advantages in mechanical properties or a reduction in complexity of design. Since that time there has been a continual process of metals replacement within the sport. In the early 1990's, Savage and Leaper from McLaren developed composite suspension members (2). Composite suspension components are now used by the all of teams (Figure 8).

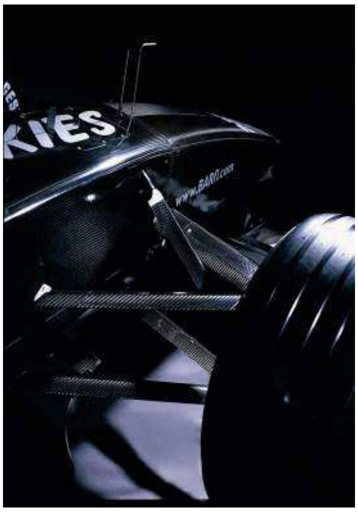

Figure 8: Composite suspension.

In addition to the obvious weight savings, composite push rods and wishbones etc. have almost infinite fatigue durability and so can be made far more cost effective than the steel parts which they replaced. The latest innovation was the introduction of a composite gearbox by the Arrows and Stewart teams in 1998 although the true potential of these structures was only fully realised from 2004 by the BAR-Honda team (3). Composite gearboxes (Figure 9) are significantly lighter than traditional alloy boxes, up to 25% stiffer, can be operated at higher temperatures and are easy to modify and repair. The design and logistics etc are not insignificant such that to this day they are not universally used on the F1 grid.

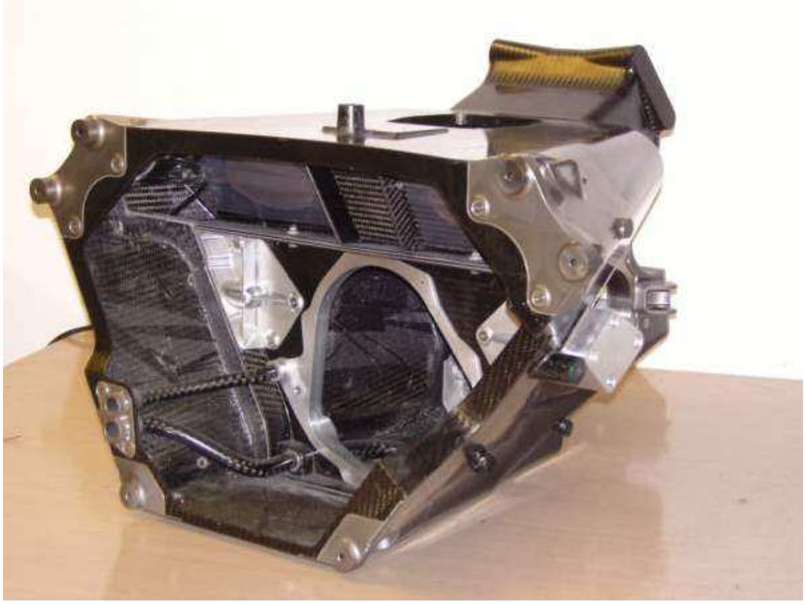

Figure 9: Composite gearbox.

Carbon fibre composites now make up almost 85% of the volume of a contemporary Formula 1 car whilst accounting for less than 30% of its mass. In addition to the chassis there is composite bodywork, cooling ducts for the radiators and brakes, front, rear and side crash structures, suspension, gearbox and the steering wheel and column. In addition to the structural materials a number of “speciality” composites are also used. These include carbon-carbon brakes and clutches, and ablatives in and around the exhaust ports (4).

3. MATERIALS SELECTION

In the production of the race cars the aim is to keep the number of composite materials to a minimum. This enables a tighter control on logistics and quality control, and allows for a more complete understanding of their properties. Materials selection is defined by a “rolling specification”. The incumbent in each materials class is used to define the property requirements. Should a new material prove superior, following extensive testing and trials, it will simply replace the old one. The aim is for the highest possible stiffness and strength whilst maintaining an acceptable minimum value of impact related properties (strain to failure, damage tolerance, matrix toughness etc.) as defined by testing and experience. Anisotropy of fibre composites means that a complete structural characterisation of a composite material requires far more property definition and data collection (Table 1) than is necessary for metals and alloys. The properties of fibre reinforced composites are also statistically complex such that one measures a distribution of properties rather than a discrete value. Unlike metals, composite production requires the carrying out of a complex chemical reaction, the cure. The successful execution of the cure is vital in determining the properties of the composite. Finally the properties of the composite are particularly sensitive to fibre alignment.

E_{11T} E_{11C}	Tensile, Compressive Modulus, Fibre Direction
E_{22T} E_{22C}	Tensile, Compressive Modulus, Transverse Direction
G_{12} G_{23} G_{31}	Shear Modulus
ν_{12}	Poisson's Ratio, In-Plane
σ_{11T} σ_{11C}	Tensile, Compressive Strength, Fibre Direction
σ_{22T} σ_{22C}	Tensile, Compressive Strength, Transverse Direction
τ_{12}	In-Plane Shear Strength
ILSS	Interlaminar Shear Strength
σ_b	Bearing Strength
ρ	Density
t	Ply Thickness
T_g	Glass Transition Temperature
G_{1C}	Strain Energy Release Rate
SEA	Specific Energy Absorption

Table 1 - Mechanical properties required to fully characterise a fibre reinforced composite material.

4. DESIGN PROCESS

The media will often refer to the "designer" of the car as though it were the product of a single individual. In reality it is more likely the result of the combined efforts of 30 or more people, each having responsibility for a particular specialisation. Aerodynamicists are sometimes singled out because the external shape of the car is its most obvious feature. The design of a new car begins with concept studies. Nowadays this is an ongoing iterative process involving constant wind tunnel testing and Computational Fluid Dynamics (CFD). The project definition phase usually occurs during the late summer and involves finalising the general configuration of the major car components. Computer Aided Design (CAD) facilities are used to generate the "electronic master" of the external geometry, optimise the suspension dynamics and organise the internal packaging of the layout. Computer Aided Manufacturing (CAM) software uses this geometry database to produce cutter path information for the machining of metal components and production of the master patterns for composite parts. When they are complete, moulds are taken from the patterns ready for the start of component production. While these activities are in progress, detail design of the structures and bodywork will continue.

The design of the monocoque is extremely complex as a consequence of the multitude of forces acting upon it. As the central element of the car all of the other load bearing structures are directly attached to it. Forces are fed in through the front suspension as the car responds to circuit perturbations and driving manoeuvres; loads are similarly fed in through the engine and gearbox/rear suspension assemblies. Aerodynamic loads are fed in via the wings and floor and there are even forces from within due to the g-forces from the driver on his seat and safety harness mountings. The car must resist the various forces effectively if it is to contribute to the overall performance of the car. It is necessary therefore to design sufficient stiffness into the chassis to minimise deflection under load. The prerequisite is for torsional rigidity to resist twisting loads (5). At the same time there is a requirement for beam stiffness to resist lateral or longitudinal bending loads, and local reinforcement at the points where loading feeds in directly (suspension pick-ups etc.). A further design obligation is impact resistance. The chassis needs to be strong enough to protect the driver in the event of an accident, and must be proved so by passing the FIA's statutory safety tests (6).

The complexity of its geometry and the materials used result in the chassis structure being difficult to analyse. The present designs are semi-quantitative combination of experience and evolution with Finite Element Analysis (FEA). Breaking down the structure into a finite number of elements on a computer enables analysis of its behaviour under the influence of a wide variety of loading regimes. Once an analysis has been completed the results are displayed in graphical form, with values colour co-ordinated to aid interpretation (Figure 10). The deformations of a component under load can be represented in such a way that extremely small movements are artificially exaggerated, making it easier to identify the areas where reinforcement is required. However sophisticated the computer analysis however, the software makes a number of assumptions and estimations on the true behaviour of the structure and materials behaviour. It is paramount therefore that the FEA is carried out in parallel with mechanical testing of representative coupons and components to verify the results before committing to final lay up (7).

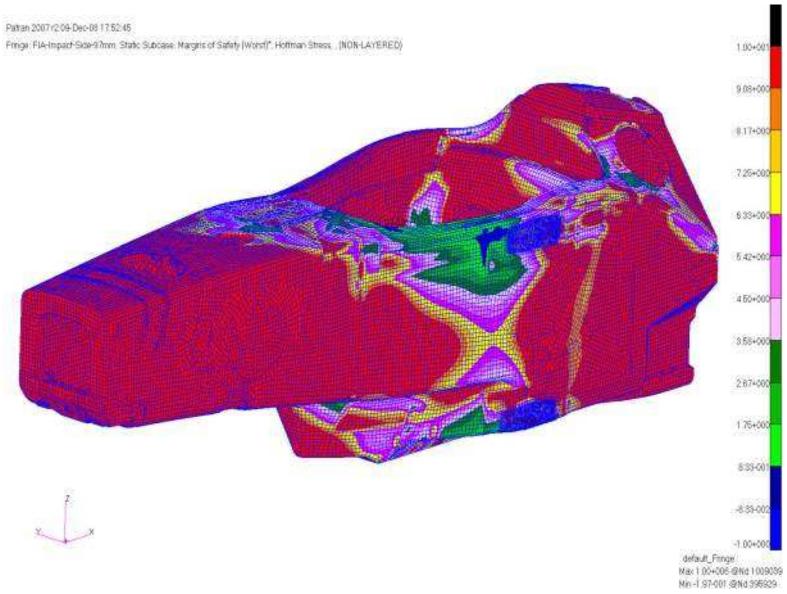

Figure 10: Chassis finite element analysis.

The loading on a Formula 1 car is now better understood than ever before. On-board data logging equipment linked to transducers provides a sound basis for the data to be used in the design of the structure. These, together with the FIA test loads define the basic requirements for strength and stiffness. Beyond this it is always necessary to design for the highest strength situation. One certainty in motor racing is that cars will at some time crash. The use of FEA enables a reduction in weight of the various components by lowering the margin for error needed in the design procedure. Furthermore stress concentrations likely to result in structural failure can be identified and eliminated. It cannot be emphasised too strongly however that whilst the computer stress analysis is a very useful tool, its results must be backed up with a reliable test programme to overcome any of the technique's shortcomings (Figure 11). Failures are generally down to small aspects of detail design and materials selection rather than inadequacies in the overall concept.

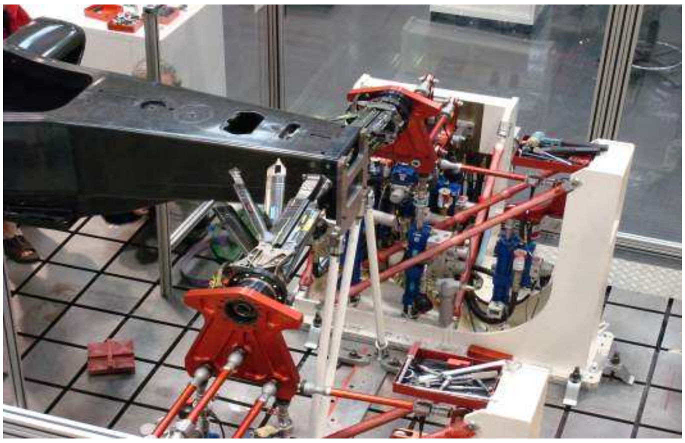

Figure 11: Strength, stiffness and durability testing on a chassis and front suspension assembly.

There is a potential conflict between the need for stiffness and the requirement for impact resistance since the higher the stiffness of the fibres used the less resilience they have. This conflict is resolved by using a combination of fibre types and, where possible, defining a smoothly flowing shape avoiding sharp corners and joggles which act as stress concentrations. A further potential contradiction arises because aerodynamic considerations play a key role in defining the shape of many of the cars' components, so a design compromise must be reached. The chassis' inner and outer skins typically consist of a number of "general plies" oriented at ±45° to provide torsional stiffness. In regions where greater strength or rigidity are required there may be significantly more material with fibres oriented so as to most efficiently react the loads. The lay up of the area directly surrounding the driver is required to afford protection from "sharp-force penetration". As such it must correspond to the lay up of a control panel which has passed an official test (8).

The structural arrangement of the chassis is such that the outer shell is reduced to the minimum number of parts. Generally this consists of two: a top and bottom section. Bulkheads are positioned so as to feed suspension point-loads into the structure and enclose the cockpit bay. Engine mounting studs fit into solid inserts bonded within the honeycomb shell. The gearbox may be considered as the "rear chassis" such that the same design considerations as for the monocoque apply (except for the anti-penetration requirement). Composite gearboxes are generally thin monolithic shells with metallic or composite transverse bulkheads which impart stiffness and carry the "working parts". Bodywork components, the engine cover and side-pods, and the cooling ducts, require good, accurate aerodynamic surfaces, moderate stiffness and minimum mass. Sandwich construction and low density materials such as carbon composites provide an ideal solution for these parts. The floor presents a greater design challenge in that it is required to fulfil a range of different tasks. It forms the mandatory bottom of the car between the wheels whilst performing as an aerodynamic device generating sizeable quantities of down-force. Impact is also an obvious criterion as is vibration tolerance. In common with the chassis, wing structures need to exploit the specific stiffness and strength characteristics of carbon/epoxy laminates, minimum deflection under load being required and tolerance of a high degree of vibration. The accuracy of a wing's profile is crucial to its performance. Prepreg moulding techniques accomplish this very well. Suspension components undergo loading in predetermined directions and so are ideal for exploiting the anisotropy of composites.

5. LINKING DESIGN TO PRODUCTION

When designing a component from composites it is never sufficient to consider the finished item alone. It is always necessary to think about how it will be manufactured in terms of the lay-up through the mould design stage and back as far as the configuration of the master pattern. It is very often necessary to seek a compromise between the simplest way to produce a part and the most elegant design configuration. Components are formed by stacking layers of oriented prepreg into a mould prior to curing under heat and pressure in an autoclave (Figure 12). Composites are particularly demanding with respect to optimisation and process control since there are so many potential variables. Parameters such as ply thickness, fibre type, ply orientation, matrix materials and the number of plies present F1 teams with an almost infinite variety of possible combinations for achieving a wide range of mechanical performance.

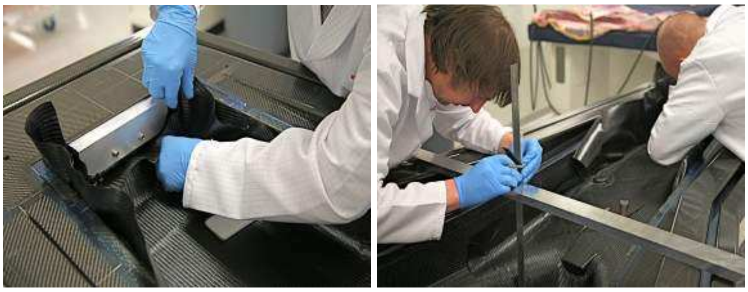

Figure 12: Hand laminating with pre-preg.

One of the most difficult tasks facing the composites design engineer is creating accurate design documentation to enable the conversion of flat-sheet raw material into a complex double curvature component. This becomes even more challenging as changes are made to the design. A recent trend has been the use of optimisation software tools which augment the CAD software to provide a seamless link from the 3D CAD model to the manufacturing floor. Composites application software is able to automatically generate material tables, sequence charts, ply lay-up protocols and lay-up diagrams. As changes are made to the design, the documentation can be automatically updated to accommodate those changes, shortening lead times and preventing mistakes. The overall aim is to simplify the production of components essentially providing a simple set of instructions akin to those used to assemble a hobby model kit in order to guarantee continuity and reproducibility of manufacture. The software allows for the direct translation of compound curves into flat patterns and is able to drive CNC cutting machines which produce a kit of parts ready for assembly.

One particularly beneficial aid to manufacture is the use of what are known as "ply books". Complex constructions are broken down into simple ply by ply steps presented, as the name suggests, in a book format. Each page of the book represents a single ply in the lay up and contains all the information required (material, shape details, start and finish points etc.) to enable an efficient sequential assembly. An example page from a ply book for the manufacture of a composite engine air box is shown in Figure 13. Originally these books were produced by a separate operation once the design was complete. Nowadays they tend to be produced (and updated automatically when necessary) by the optimisation software package.

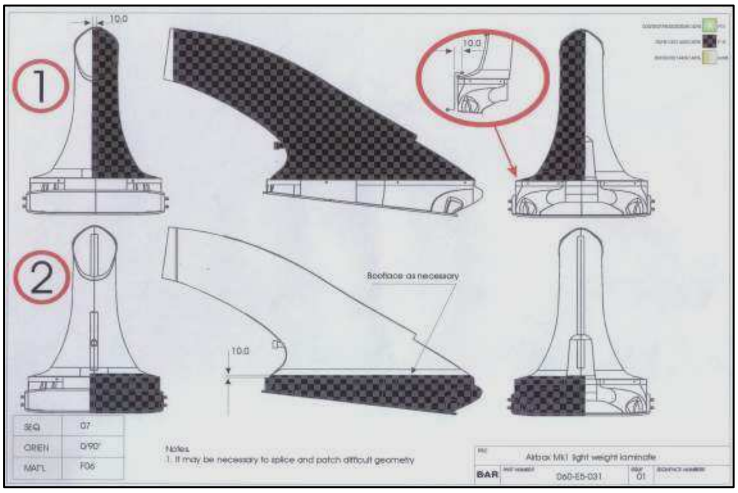

Figure 13: Example page from a ply book

6. COMPONENT MANUFACTURE

Before the components can be produced, a full sized pattern must be produced for each part. The patterns are used to make moulds into which the composite plies are laid up. The most common method for the production of the patterns begins with the appropriate data from the CAD system being fed into a 5-axis CNC milling machine. The milling machine cuts the patterns from a tooling block material (generally a solid epoxy resin containing glass micro-spheres) (Figure 14).

Figure 14: Cutting a pattern.

As supplied the slabs of tooling material are only 50mm deep so the larger patterns must be made by stacking and gluing several slabs together. When the cutting process is complete the patterns are rubbed down by hand using “wet or dry” silicon carbide abrasive paper. This operation, known as *shaping*, ensures that the interfaces between adjoining patterns are blended together and removes any machining marks left by the mill. A coat of epoxy paint is then applied to the moulding surfaces to seal and protect them (Figure 15). Finally the patterns are checked for accuracy using a 3-axis digitising machine.

Figure 15: Finished pattern prepared for moulding.

The moulds from which the composite components are made are produced by laying up a carbon epoxy “tooling prepreg” on the patterns to form a reflected image of the final part (Figure 16). The laminating process followed for the moulds is identical to that employed when making components except that they are always single skins unlike many of the parts made from them which are often honeycomb structures. The tooling prepregs contain a specially formulated epoxy resin which cures at a relatively low temperature of 60°C or less. This is done in order improve the accuracy of reproduction by avoiding heat expansion and distortion in the patterns. Following the cure, the moulds are post cured in a programmable oven to increase the glass transition temperature of the resin. It is important to note that one of the most significant advantages of composite fabrication is the tooling is extremely quick to produce (3 days or less if time scales are tight) and, more often than not, is less expensive than a single unit of the parts made from it. This is particularly advantageous when the production run is small. In certain applications CNC machined aluminium moulds are used for expediency or a one-off component may be taken directly from tooling block, but composite moulds are generally preferred because their resistance to distortion and expansion during the curing cycle produces a more accurate component.

Figure 16: Composite engine cover mould.

Prepreg lay-up of F1 composite parts is accomplished almost entirely by hand and follows accepted practices and procedures. Plies are laminated to the orientations specified in an appropriately configured mould, a vacuum bag is applied and curing takes place in an autoclave to the recommended cycle. The laminating operation is carried out in a controlled environment under *clean room* conditions. The laying up of the prepregs within the moulds is a meticulous process, in which highly skilled and experienced operators must closely follow the documentation provided by the design engineer. The labour intensive nature of the laminating process is one of the main drawbacks of composite materials. When all of the plies have been laid up and the final pressure de-bulk completed, the assembly is enveloped in a new vacuum bag and returned to the autoclave for curing.

Hollow sectioned components such as wings and suspension pieces are consolidated using the *internal pressure bag* technique. Pressure bags also involve the use of vacuum but are more complex, applying additional pressure to the assembly through an elastomeric bag. The bag is open to the autoclave gas ensuring isostatic pressure on the mould tool. A variation on this theme involves the use of a solid metallic or elastomeric mandrel. Consolidation pressure is generated by the thermal expansion of the mandrel against the mould and laminate. Great care must be taken with this method since the pressure generated is not the same as the autoclave gas. It is very easy to make the mandrel too small and have poor consolidation, or too large creating a huge pressure which can damage the mould. Single skin components are cured at 7 bar pressure at the recommended temperature for 1 to 2 hours. Sandwich constructions are cured in two or three stages, the first skin being cured at full (7 bar) autoclave pressure and the subsequent film adhesives, honeycomb core, inserts and inner skin cured at a pressure safe for the core (typically 3.5 bar) (Figure 17).

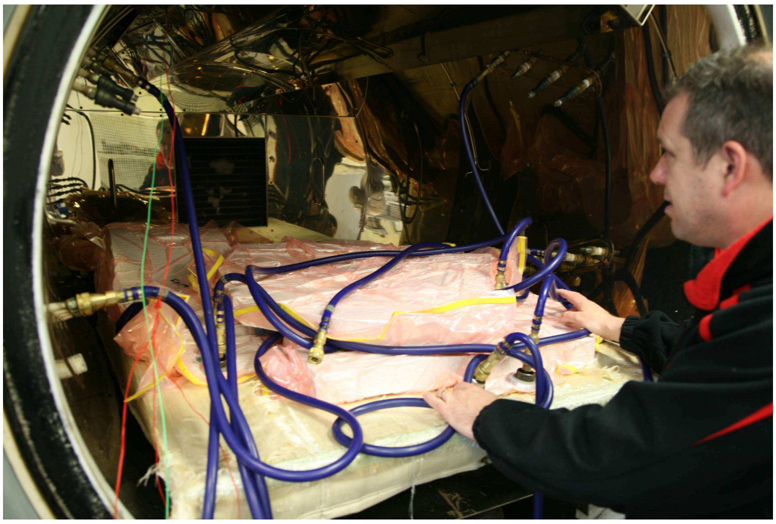

Figure 17: Autoclave cure.

Points where bolts and other fasteners pass through the honeycomb core are locally reinforced using *inserts*. Inserts are solid composite or metallic pieces which are supplied to the laminators pre-cut and are positioned in predetermined cut outs in the honeycomb core. The inserts serve to spread point loading over a larger surface of the composite and thus reduce stress concentrations. They also prevent the bolts etc. from moving under load which crush the honeycomb core and ultimately fracture the composite skin. The layer of aluminium or aramid (“Nomex”) honeycomb material sandwiched between the two skins varies in thickness depending on the structural design. A film adhesive is applied between the skins and the core creating a strong bond when cured.

The majority of structures are assembled by adhesively bonding a number of parts together. Adhesive bonding is a particularly effective method of assembling complex structures, especially those made from different materials (Figure 18). Provided the joint is well designed, the adhesive bond ought to be one of the strongest aspects of the structure and most certainly should not be the life limiting factor. This of course pre-supposes that the joint has been correctly executed. The major factors determining the integrity of an adhesive bond are selection of the most appropriate adhesive, joint design, preparation of the bonding surfaces and strict quality control in production and condition monitoring in service. Finishing of the structures generally involves drilling and tapping etc. the various holes used for attachments. The holes are drilled on a 5-axis CNC milling machine using data supplied by the CAD model and are used, in the case of the monocoque for example, for the fitting of suspension pick-ups and bodywork etc.

Figure 18: Adhesively bonding a gearbox assembly

7. SAFETY AND SURVIVABILITY

The area of crash safety allows us to explode another of the myths surrounding composite materials, that they have poor impact performance. The mechanisms which would occur during the destruction of a metallic race car chassis may be illustrated by considering the axial collapse of a thin walled metal tube under impact. Following an initial peak load, which initiates the process, energy will be absorbed as a result of the work done in the formation of plastic hinges which develop progressively along the tube (Figure 19). This may be demonstrated quite simply by stamping on top of a soft drinks can and then trying to imagine what it would be like to be in it at the time!

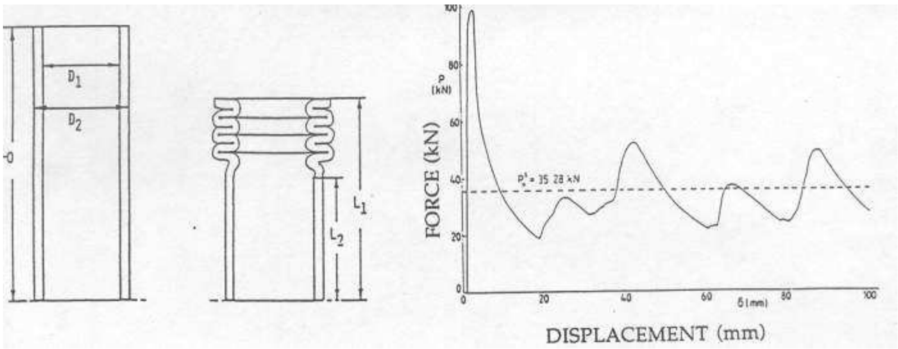

Figure 19: Energy absorption by metallic structures.

In contrast the failure of a composite chassis does not involve plastic deformation. The immense stiffness of a carbon fibre monocoque is such that its elastic limit will not be exceeded. This high stiffness serves to transmit the load from point of impact further into the structure with the result that higher loads can be absorbed without permanent damage Once the load in the locality of the impact has exceeded the absolute strength of the laminate, failure in that area is total as the composite progressively tears itself to pieces (Figure 20).

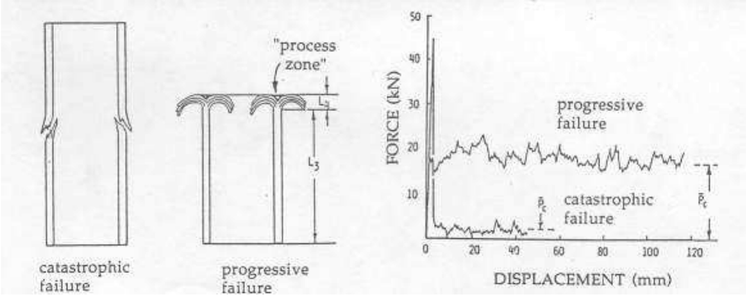

Figure 20: Energy absorption by composite structures.

The energy absorbing properties of composite materials may be described in terms of “work of fracture” which arises from the mechanisms occurring during failure. The inherent brittleness of composites ensures that they do not undergo the yield process characteristic of ductile metals, but, on the application of load, deform elastically up to the point of fracture. A number of modes of deformation are available to complex multiphase composite materials. The primary energy absorbing mechanisms in fibre reinforced plastics are:

1. Cracking and fracture of the fibres
2. Matrix fracture
3. Debonding (pull out) of fibres from the matrix, and
4. Delamination of the layers making up the structure.

A composite body thus disintegrates both structurally and microscopically during an impact event. The core material in aluminium honeycomb cored sandwich structures also adds to the energy absorbing mechanism. Referring to our original analogy, metal honeycombs may be considered as a large array of small soft drinks cans which squash and absorb energy on impact. Once the mechanisms by which composites dissipate energy have been discerned, steps may be taken to engineer the structure to improve driver survivability. The energy absorption properties of composite cars have dramatically improved the safety record of Formula One. It is now fairly commonplace to see drivers survive crashes that previously would almost certainly have claimed their lives. The fatal accidents of the 1994 season showed however that the sport can never be made 100% safe. In order to minimise the risk to drivers and spectators, the FIA require that each car built by the teams must pass a stringent set of safety tests. The tests are upgraded every year as the knowledge of structural design improves and following survivability research carried out by the governing body's medical team. The tests consist of a number of static loads applied to the survival cell to verify its integrity, and impact tests on mandatory front (nose box) rear and side impact structures (Figure 21). The tests must be carried out in the presence of an FIA official. There must be no damage to the survival cell and, in the case of the impact tests, the magnitude of deceleration must be within the limits set by the medical experts as being survivable. Driver survivability relies upon the chassis behaving as a survival cell (essentially a suit of armour) protecting the driver from the impact whilst the energy absorbing structures dissipate the kinetic energy and limit the load transmitted into the monocoque and driver (6).

Figure 21: FIA nose crash test.

8. CONCLUSION

From the outset, motor racing teams have striven to exploit leading edge technology in their quest for victory. Formula 1 stands at the very pinnacle of the sport in terms of popularity, funding and technology. Over the last three decades the sport has developed into a multi-billion dollar business commanding immense global coverage. The major teams now operate on budgets of the order of several tens of millions of dollars as they prepare to "do battle", via the global media, witnessed by a significant proportion of the world's population. An increasing percentage of the teams' budgets are invested in new technology. The extent of this investment has been so great that cynical observers have dubbed the sport "the search for the unfair advantage". Joking aside, the aura of state-of–the-art science and engineering adds much to the allure and increasing appeal of the races. The introduction of fibre reinforced composite chassis was one of the most significant developments in the history of Grand Prix motor racing. Technological advances gained from these advanced materials have produced cars that are lighter, faster and safer than ever before. Composite materials can only be exploited to their full potential if one understands the complete process from raw materials until components are withdrawn from service. The key to success is the ability to obtain the optimum solution to the package of pilot, engine, tyres, aerodynamics, technical innovation and reliability. Composites materials science and engineering has had a significant, often pivotal, roll in the development of Formula 1.

REFERENCES

1. Savage, GM. Metals and materials 7, 10, 617 (1991).
2. Savage, GM. Race Tech. 1, 1(1995).
3. Savage, GM., Proc "Carbon fiber 2007", Washington DC, USA. (Dec 2007).
4. Savage, GM., "Carbon-carbon composites", Chapman and Hall (1993).
5. Savage, GM. J. STA, 140, 18 (2000).
6. Savage, GM., Proc. Anales De Mecanica de la Fractura, 18, 274, Baiona (Vigo), Spain, (Mar. 2001).
7. Savage, GM. Proc. "Transfac 06" San-Sebastian, Spain (Oct 2006).
8. Savage, GM "Development of Penetration Resistance in the Survival Cell of a Formula 1 Racing Car" to be published in Engineering Failure Analysis (Elsevier).

Potentialities of 'New' lignocellulosic fibers

J. R.M. d'Almeida
Materials Engineering Department,
Pontifícia Universidade Católica do Rio de Janeiro, Rio de Janeiro, Brazil

SUMMARY

The use of lignocellulosic fibers and other lignocellulosic materials is increasing due to the many advantages they present over synthetic fibers specially regarding energy consumption, and neutrality in respect to CO_2 emission. Several lignocellulosic fibers, such as sisal, coir, jute and flax are well described, but many other fibers such as piassava (*Attalea funifera*) and caroa (*Neoglaziovia variegata*), as well as the fibers obtained from the dried fruit of the sponge gourd (*Luffa cylindrica*) and from the fibrous protective envelop of ubuçu (*Manicaria saccifera*), or those obtained from processing the stem of the pupunha (*Bactris gasipaes*) palm, present mechanical properties and/or structural characteristics that are suitable to their use in composites. In this work, several characteristics of these 'new' fibers are presented and are compared to those from lignocellulosic fibers already used to reinforce polymer-matrix composites. Questions regarding the availability, and present day usages of these fibers are also presented. Several possibilities of products fabricated from composites manufactured from these fibers, such as vertical blinds, are proposed and their vantages and disadvantages in respect to traditional products are discussed.

1. INTRODUCTION

Lignocellulosic fibers are an ecologically friendly, biodegradable, and renewable resource, that can be used to advantage in many applications. For example, nowadays, lignocellulosic fiber-reinforced composites are being used by the automotive industry, where interior door panels and cushion seats are manufactured using coir, flax or sisal fibers (Marsh 2003). To many countries, like Brazil, the increasing value of these fibers can strongly contribute to set rural works on plantations at the countryside, avoiding an undesirable migration to towns, and the consequent accompanying problems due to the impoverishment of a large percentage of the population. Another very important aspect to be highlighted when dealing with lignocellulosic fibers is that they are neutral in respect to CO_2 emission (Mohanty *et al* 2002), being therefore in context with the Kyoto protocol.

Besides several well established and studied fibers, like jute, sisal and curaua, other fibers and also 'timber like' materials can be considered as potential elements to reinforce composites or to be used in structural elements. Among these 'new' lignocellulosic fibers one can cite, for example, banana fibers (Satyanarayana *et al* 2007) that are extracted from many species of banana trees (*Musa sp.*), are disseminated worldwide and are a low price material obtained from the cut and disregarded banana tree. Although largely available, and studied for many decades now, these fibers have not yet gained a place at the composite market. Other less common fibers such as piassava (*Attalea funifera*) and caroa (*Neoglaziovia variegata*), as well as the fibers obtained from the dried fruit of the sponge gourd (*Luffa cylindrica*) and from the fibrous protective envelop of ubuçu (*Manicaria saccifera*) or those obtained from processing the stem of the pupunha (*Bactris gasipaes*) palm, or from the pseudo stem of this palm itself, present mechanical properties and/or structural characteristics that are suitable to their use in composites.

In this work, several characteristics of these ‘new’ fibers are presented and are compared to those from lignocellulosic fibers already used to reinforce polymer-matrix composites. Questions regarding the availability, and present day marked of these fibers are also presented. Several possibilities of products fabricated from composites manufactured from these fibers are also presented and their vantages and disadvantages in respect to traditional products are discussed.

2. CHARACTERISTICS OF THE “NEW” LIGNOCELLULOSIC FIBERS

2.1 Piassava (*Attalea funifera*) and Caroa (*Neoglaziovia variegata*)

Piassava are stiff and waterproof fibers extracted from a palm tree of natural occurrence at the Brazilian Atlantic rain forest. Its natural incidence range is close to the coastal zone (up to 60 km inland) and it is mainly concentrated between 13^{o}S and 17^{o}S latitudes. The fibers are up to 4 m long with an average width of 1.1 mm.

The production of piassava fibers is steadily increasing over the past years and, nowadays, it amounts to about 100.000 metric tons per year (d’Almeida *et al* 2006b). The main use of these fibers is for industrial and domestic brooms, industrial brushes, ropes and baskets, carpets and roofs. The market of piassava fibers amounts to around US $20 million yearly, and it is estimated that 20% of the fiber production is disregarded as by the transformation industries. Figure 1 shows an overall view of the leftover piassava fibers. Most of these fibers have lengths varying between 5 and 25 cm (Aquino *et al* 2001), and the critical length for stress transfer using a polyester resin as the composite matrix, is about 15 mm (Aquino *et al* 2003). Therefore, these leftover fibers, that do not meet the requisites for the traditional uses cited above, are long enough to be used as reinforcement in fiber composites.

Fig. 1. Leftover piassava fibers.

Caroa was traditionally used for the fabrication of ropes and hessian cloths a century ago, but its use declined, and now it has no economic importance. Caroa is a native bush that spontaneously grows in the semi-arid north-eastern region of Brazil. It belongs to the *Bromeliacea* family and yields soft, white, flexible fibres that are extracted from its leaves and are processed like sisal fibres. The fibre length can vary from 80 cm to 1.6 m, and are being used almost exclusively for cordage and very coarse fabrics and ropes for local consume. Baskets and other artisan-made pieces are also being manufactured from caroa fibres.

Table 1 lists some properties of piassava (*Attalea funifera*) and caroa (*Neoglaziovia variegata*) fibers (d'Almeida *et al* 2006b; d'Almeida *et al* 2008). The properties for jute, coir and sisal are also included for comparison (Bledzki and Gassan 1999).

Table 1. Mechanical properties of some lignocellulosic fibers.

Fiber	Tensile strength (MPa)	Young's modulus (GPa)
Piassava	133 ± 13.5	6.2
Caroa	81-315	5-8
Jute	393-773	26.5
Sisal	511-635	9.4-22
Coir	106-270	4-6

From the data in Table 1, one can see that that both caroa and piassava are low-modulus, low-strength fibers, but with mechanical properties comparable with those from coir. It is important to highlight here, however, that coir fibres are being used by car manufacturers to reinforce several non-structural parts (Marsh 2003).

Piassava has another interesting aspect related to the presence of Si rich arrays of protrusions at their surfaces, Fig.2. These surface features are believed to serve as anchoring points for the resin matrix. Therefore, piassava reinforced polyester matrix composites have good mechanical properties, even using untreated piassava fibers (Aquino *et al* 2001). If the fibers are surface treated, however, the array of protrusions is fully uncovered, as the one presented at Fig.2 (d'Almeida *et al* 2006b). Coir fibers also present similar topographic features (Prasad *et al* 1983; Calado *et al* 2000).

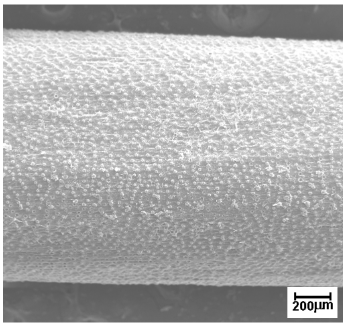

Fig. 2. Surface of mercerized piassava fibers revealing the Si arrays of protrusions covering the entire fiber length.

Both fibers have a great potential to be used in composites. The already existent piassava leftover has an estimated potential of US$ 4,000,000.00/year, without interfering with the traditional use of this fiber. Caroa can have an outstanding effect upon the economy of a very poor region of the Brazilian semi-arid region, if their use in composites increases. The past economical importance of this fiber can be best understood if we realize that even a city was once named by this fiber, namely Caraolina, at the state of Pernanbuco.

2.2 Sponge gourd (*Luffa cylindrica*) and Ubuçu (*Manicaria saccifera*)

Sponge gourd is a subtropical plant abundant in China, Japan, and other countries in Asia as well as in Central and South America. Its fruit has a fibrous vascular system that forms a natural honeycomb structure when dried, Fig.3. The density of the dried vascular system varies from the surface to the core, where a more open structure is present (Boynard and d'Almeida 2000). The overall area weight of this structure is very low (0.078 g/cm^2) and the fibers' diameters typically vary from 270 to 400 μm.

Fig. 3. Aspect of the dried vascular system of the fruit of sponge gourd. Gourds can differ both in size and format depending on their particular sub-species.

Nowadays, sponges are being used mainly as bath scrubbers. However, sponges can also be used in high technological applications such as absorbent materials to reduce pollutants from liquid effluents (Hassan 2006) and substrates to porous ceramics (Colombo and Stankiewicz 2006). The use of untreated sponge gourds to not improve the mechanical properties of polymer matrix composites, however, the composite toughness is greatly improved, because cracks are deflected by the 3-dimensional network of the fibers (Boynard and d'Almeida 2000).

Derivatization treatments produce strong surface modifications on sponge gourd and can increase the fiber/matrix adhesion (d'Almeida *et al* 2006a) increasing the possibility of using sponge gourd in composites, not only as a filler to deflect cracks but also as reinforcement material.

Ubuçu is a natural palm found in the Brazilian Amazon estuary. This palm has its fruits protected by a fibrous sac, called tururi, from where fibers can be extracted, Fig.4. Nowadays, these fibers are almost exclusively used in artisan crafts. In the state of Amapá it is also used to cover houses because the fibers are waterproof. Some designers are now introducing these fibers at fashion sectors producing clothes and other accessories.

Fig. 4. General aspect of the ubuçu fiber.

Although used for long time by natives, the properties of ubuçu are not yet determined, but the fibrous sac forms a natural weave, as observed at Fig.5. Its use in chairs and other furniture with thermoplastic polymers are under development and are promising.

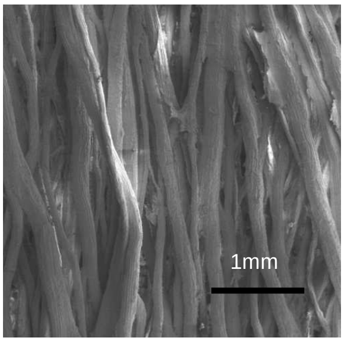

Fig. 5. Aspect of the fibrous envelope of the ubuçu fruits.

2.3 Pupunha (*Bactris gasipaes*)

Pupunha, named in English as Pejibaye or Palm Beach (Mora-Urpí *et al* 1997), is a native palm, occurring at tropical forests of South and Central America. This palm is, nowadays, harvested in large plantations, and it is used for the sustainable production of heart of palm, avoiding the predatory exploration of other native palms, such as açaí (*Euterpe oleraceae*) and jussara (*Euterpe edulis*), that have longer growing cycles and that were being predatorily exploited almost to exhaustion.

Harvesting of pupunha palm has a great economic potential, yielding approximately 1 metric ton of heart of palm per hectare, and its production can begin after 18 to 24 months after seeding, instead of almost 7 years when other palms, like jussara, are considered.

The pseudo-stem of the palm has a “timber like” appearance, and can be collected at plantations after cutting the palm, Fig.6. The outer region of the stem looks like a hardwood, and, therefore, can be an alternative route for obtaining wood-like materials, with several advantages, such as: availability, environmental preservation, and a relatively low cost.

Fig. 6. The stem of the pupunha palm after being cut. The inset highlights the outer region from where a "timber like" material can be obtained. Short fibers can be obtained from inner region.

Table 2 shows the flexural mechanical properties of pupunha planks (Bacellar and d'Almeida 2009), and lists for comparison the properties of some hardwoods largely used to make furnitures, namely: jatobá (*Hymenaea courbaril*) and maçaramduba (*Manilkara amazonica*) (Dias and Lahr 2004). The properties of two hardwood - black oak and white ash - and two softwood - yellow cedar and balsam fir - species from the northern hemisphere are also listed for comparison (Green *et al* 1999). Table 2 also presents the properties of a common glass-fiber composite with a volume fraction of fibers of 30 %. Two points are to be highlighted, namely: i) the high values of the flexural mechanical properties of pupunha, that are, in fact, higher than those of the hardwoods, and ii) the very low standard deviations measured for all flexural properties. This is a very interesting aspect from a practical point of view, and is not commonplace when lignocellulosic materials are under analysis.

Table 2. Flexural mechanical properties of pupunha and some other structural woods and composites.

Material	Flexural strength (MPa)	Flexural modulus (GPa)
Pupunha	214.3 ± 12.3	20.3 ± 1.1
Jatobá	159	22.9
Maçaranduba	136	21.9
Black Oak	57-96	8-11
White Ash	66-103	9.9-12
Yellow Cedar	44-77	7.9-9.8
Balsam Fir	63-38	8.6-10
GF composite	358 ± 56	20 ± 2,17

Finally, and no more important when flooring or furniture are under consideration the visual aspect of this timber like material is both unique and beautiful, and also mimics wooden surfaces, as shown in Fig. 7.

Fig. 7. Visual aspect of the timber like pupunha plank machined along the pupunha trunk length. (www.lets-evo.net/skateboard/2007/01/23/compensado-de-pupunha).

3. CONCLUSIONS

The five lignocellulosic materials here presented are on a very embryonic stage regarding their use in composites or as a structural lignocellulosic material. However, they all present properties or have a structural architecture suitable to be more largely used in composites.

Obviously, it has to be pointed out that many other "new" fibers are available to be studied. Several lignocellulosic materials such as the fibers from the fruit of the açaí (*Euterpe oleraceae*) palm or the fibers from the African oil palm (*Elaeis guineensis*), to cite just a few, have both large quantities and/or present environmental challenges that also qualify their analysis to be used in composites.

The availability of large amounts of a certain type of lignocellulosic fiber can be a positive aspect when an uncommon fiber is under analysis, but we can not forget that sustainability passes also by the use of local resources, promoting the development of the local population.

ACKNOWLEDGMENT

The author acknowledge the Brazilian funding agency CNPQ for financial support and to COMATCOMP 09 organization for the support and invitation.

REFERENCES

AQUINO, R.C.M.P., D'ALMEIDA, J.R.M., MONTEIRO, S.N. (2001). Flexural Mechanical properties of piassava fibers (*Attalea funifera*)- resin matrix composites. *J.Mater.Sci.Letters*. 20(11), 1017-1019.

AQUINO, R.C.M.P., MONTEIRO, S.N., D'ALMEIDA, J.R.M. (2003). Evaluation of the critical fiber length of piassava (*Attalea funifera*) fibers using the pullout test. *J.Mater.Sci.Letters*. 22(21), 1495-1497.

BACELLAR, R.S., D'ALMEIDA, J.R.M. (2009). Mechanical Properties of Pupunha (*Bactris gasipaes*) Palm. Proceedings of the 9th International Conference on Chemical and Process Engineering, 10-13 May, Rome, Italy. CD-Rom, Paper A120.

BLEDZKI, A.K., GASSAN, J. (1999). Composites reinforced with cellulose based fibres. *Prog. Polym. Sci*. 24(2), 221-274.

BOYNARD, C.A., D'ALMEIDA, J.R.M. (2000). Morphological characterization and mechanical behavior of sponge gourd (*Luffa cylindrica*)-polyester composite materials. Polym.-Plast.Technol.Eng. 39(3), 489-499.

CALADO, V., BARRETO, D.W., D'ALMEIDA, J.R.M. (2000). The effect of a chemical treatment on the structure and morphology of coir fibers. *J.Mater.Sci.Letters*. 19(23), 2151–2153.

COLOMBO, P., STANKIEWICZ, E.P. (2006). Other Developments and Special Applications. In: Cellular Ceramics. Scheffler, M. and Colombo, P. (Eds). New York: John Wiley and Sons. pp. 596-620.

D'ALMEIDA, A.L.F.S, BARRETO, D.W., CALADO, V., D'ALMEIDA, J.R.M. (2006a). Effects of Derivatization on Sponge Gourd (*Luffa cylindrica*) Fibres. *Polym.Polym.Comp.* 14(1), 73-80.

D'ALMEIDA, J.R.M., AQUINO, R.C.M.P., MONTEIRO, S.N. (2006b). Tensile mechanical properties, morphological aspects and chemical characterization of piassava (Attalea funifera) fibers. *Comp. Part A*. 37(9), 1473-1479.

D'ALMEIDA, J.R.M., D'ALMEIDA, A.L.F.S., DE CARVALHO, L.H. (2008). Mechanical, morphological, and structural characteristics of caroa (*Neoglaziovia variegata*) fibres. *Polym.Polym.Comp.* 16(9), 589-595.

DIAS, F.M., LAHR, F.A.R. (2004). Strength and stiffness properties of wood estimated through the specific gravity. *Sci.Forestalis*. 65(1), 102-113. (*in Portuguese*)

GREEN, D.W., WINANDY, J.E., KRETSCHMANN, D.E. (1999). Mechanical properties of wood. In: Wood Handbook. Madison, WI: Forest Product Society. Ch.4.

HASSAN, M.L. (2006). Quaternization and anion exchange capacity of Sponge Gourd (*Luffa cylindrica*). *J.Appl.Polym.Sci.* 101(4), 2495-2503.

MARSH, G. (2003). Next step for automotive materials. *Mater. Today*. 6(4), 36-64.

MOHANTY, A.K., MISRA, M., DRZAL, L.T. (2002). Sustainable Bio-Composites from Renewable Resources: Opportunities and Challenges in the Green Materials World. *J.Polym.Environ*. 10(1/2), 19-26.

MORA-URPÍ, J., WEBER, J.C., CLEMENT, C.R. (1997). Peach palm. *Bactris gasipaes* Kunth. Rome: Gatersleben/International Plant Genetic Resources Institute.

PRASAD, S.V., PAVITHRAM, C., ROHATGI. P.K. (1983). Alkali treatment of coir fibres for coir–polyester composites. *J.Mater.Sci.* 18(5),1443–1454.

SATYANARAYANA K.G., GUIMARÃES, J.L., WYPYCH, F. (2007). Studies on lignocellulosic fibers of Brazil. Part I: Source, production, morphology, properties and applications. *Comp. Part A*. 38(7), 1694–1709.

Recent contributions to the realm of composites from renewable resources

Alessandro Gandini
CICECO and Chemistry Department, University of Aveiro, 3810-198 Aveiro, Portugal

SUMMARY

The purpose of this lecture is to provide an update on our recent work on composite materials in which the matrix and/or the reinforcing or blending elements of polymers derived from renewable resources, as opposed to petroleum-based counterparts. Within the context of macromolecular matrices, attention will be focussed on chitosan, starch and both lignin and cellulose derivatives, whereas appropriately modified cellulose fibres, natural rubber beads and starch granules will be discussed in terms of dispersed charges. A particularly noble approach will also be described which calls upon the partial oxypropylation of cellulose fibres and starch granules in order to generate single-component composite materials in which the outer portion of these substrates is converted into a thermo-plastic sleeve, while their inner regions remain pristine.

1. INTRODUCTION

The use of renewable resources as an alternative to dwindling fossil counterparts to provide new sources of energy, chemical commodities and macromolecular materials has become one of the most active research and development topics in the last decade. Both public and private interests have been steadily growing in terms of sponsoring research covering fundamental and applied aspects. The concept of the ***biorefinery*** (Kamm *et al.,* 2006) has become an accepted paradigm which has sprung into numerous pilot plant approaches and recently some actual industrial-scale prototypes. The aim of this burgeoning activity is to achieve an intelligent and rational exploitation of all the components of a given biomass substrate, albeit through different strategies.

Within this vast enterprise we have been focussing on the specific issue of developing novel macromolecular materials based on renewable resources in order to demonstrate the feasibility of producing polymers with properties and applications as viable as those of the currently used petroleum-based plastics (Gandini, 2008, Belgacem and Gandini, 2008a). The present lecture will limit its contents to the specific issue of composite materials where either the matrix or the reinforcing element, *or both*, are derived from the exploitation of the biomass.

2. CELLULOSE FIBRES

The use of lingo-cellulosic fibres as reinforcing elements in composite materials incorporating macromolecular matrices has been a highly popular research topic for several decades and continues to motivate a high number of laboratories throughout the world. This is not surprising considering the obvious advantages associated with these natural filaments, their ubiquity, albeit in different morphologies and chemical compositions, when compared with their glass counterparts. Recent reviews provide a rather thorough account of the state of the art (Belgacem and Gandini, 2008b, Belgacem and Gandini, 2005) and therefore, after a brief general introduction, only the most relevant results obtained in our laboratory will be highlighted here. These include (i) the surface chemical modification of cellulose fibres with fatty acid moieties (i.e. another renewable resource) in order to attain a high degree of compatibility with polyolefin matrices through both chemical affinity and chain entanglements (Freire *et al.* 2006); (ii) the in-depth chemical modification of these fibres by the same fatty acids (Freire *et al.*, 2006) or by partial oxypropylation (Gandini *et al.*, 2005) in order to generate a sleeve of thermoplastic material around the fibres while maintaining their pristine semi-crystalline inner morphology, thus giving rise to a two-phase material which can be readily turned into a composite by hot pressing; (iii) the synthesis of hybrid compositions associating inorganic nanoparticles to the fibres, and their inclusion into different matrices.

3. STARCH

The interest in this renewable resource as a precursor to novel polymers is at present as hot an issue as that of the exploitation of cellulose fibres. Thermoplastic starch (TPS) represents a very promising set of materials given the global availability of its natural substrate at a low price and its efficient biodegradability (Carvalho, 2008). The major obstacles confronted by the application of TPS are their modest mechanical properties and, even worse, their excessive sensitivity to moisture. Several studies will be discussed in this context, namely (i) the preparation of starch cellulose composites; (ii) the incorporation of natural rubber into TPS (Carvalho *et a*l. 2003); (iii) the surface treatment of TPS objects with hydrophobic reagents (Carvalho *et a*l. 2005); (iv) the search for more suitable natural plasticizers; and (v) the partial oxypropylation of starch granules to prepare single-component composite materials (Gandini *et al.,* 2007) following the same strategy as that mentioned above for cellulose fibres.

4. CHITOSAN

Although chitosan is not, as such, a natural polymer, it is very readily prepared by the hydrolysis of the amide moieties of its natural precursor chitin and it is therefore customary to consider chitosan as a renewable resource. Whereas cellulose, starch and many other renewable resources used for the preparation of novel polymers are derived from the vegetable biomass, chitosan is the leading exception as a polymer predominantly obtained from the animal realm, e.g. crustaceans. The properties of this polysaccharide, including its exceptional film-forming aptitude and biocide efficiency, have spurred a vast amount of research devoted to its possible applications, as such, or after appropriate modifications (Peniche *et al*, 2008)). We have been interested in the elaboration of composites associating a chitosan matrix with bacterial cellulose and this ongoing investigation will be discussed here together with the preparation of other composites with paper-based substrates.

REFERENCES

BELGACEM, M.N., GANDINI, A. (2005), *Compos. Interface*, 12, 41.
BELGACEM, M.N., GANDINI, A., Eds. (2008a), *Monomers, Polymers and Composites from Renewable Resources,* Elsevier, Amsterdam.
BELGACEM, M.N., GANDINI, A. (2008b), *Surface Modification of Cellulose Fibres*, in *Monomers, Polymers and Composites from Renewable Resources*, Elsevier, Amsterdam, Chapter 18.
CARVALHO, A.J.F., GANDINI, A., JOB, A.E., ALVES, N., CURRVELO, A.A.S. (2003), *Carbonydr. Polym.*, 53, 95.
CARVALHO, A.J.F., GANDINI, CURRVELO, A.A.S. (2005), *Ind. Crops Prods.,* 21, 331.
CARVALHO, A.J.F. (2008), *Starch: Major Sources, Properties and Applications in Thermoplastic Materials,* in *Monomers, Polymers and Composites from Renewable Resources*, Elsevier, Amsterdam, Chapter 15.
FREIRE, C.S.R., GANDINI, A. PASCAL NETO, C., SILVESTRE, A.J.D., BELGACEM, M.N. (2006), *J. Appl. Polym. Sci*., 100, 1093.
GANDINI, A, CURVELO A.A.S., PASQUINI; D., DE MENEZES, A.J. (2005), *Polymer*, 46, 10611.
GANDINI, A, CURVELO A.A.S., PASQUINI; D., DE MENEZES, A.J. (2007), *Biomacromlecules*, 8, 2047.
GANDINI, A. (2008), *Macromolecules*, 41, 9491.
KAMM, B., GRUBER, P.R., KAMM, M. (2006), *Biorefineries – Industrial Processes and Products*, Wiley-VCH, Weinheim, Vols. 1 and 2.
PENICHE, C. ARGUELLES-MONAL, W., GOYCOOLEA, F.M. (2008), *Chitin and Chitosan: Major Sources, Properties and Applications*, in *Monomers, Polymers and Composites from Renewable Resources*, Elsevier, Amsterdam, Chapter 25.

T1. POLYMER-MATRIX COMPOSITES
MATERIALES COMPUESTOS DE MATRIZ POLIMÉRICA

Polypropylene impregnation improvement into glass fiber woven roving by in-situ polymerization

M. Etcheverry, M.L. Ferreira, N. Capiati, S. Barbosa
Planta Piloto de Ingeniería Química (UNS - CONICET) - Bahía Blanca, Argentina

ABSTRACT

The adhesion between matrix and fibers is an essential factor in the final performance of thermoplastic-based polymer composite materials. The interfacial adhesion of the polypropylene (PP) and glass fibers (GF) can be highly improved by chemical anchoring between PP and GF. The use of thermoplastics in high performance composites, is not large because polymer high viscosity that impedes the impregnation in mats or woven fibers. In this sense, direct polymerization also enhances the infiltration because the polymer is formed in-situ from a gas.
In this work, a methodology for direct polymerization of PP onto GF is proposed. The reaction route includes an initial contact with methylaluminoxane (MAO) and hydroxy-α-olefin to generate the anchorage points on the fiber surface, followed by a propylene polymerization catalyzed by $EtInd_2ZrCl_2$ (metallocene)/MAO. As a result of this reaction, PP chains grow by copolymerization of propylene with the olefin anchored to the GF surface. This procedure was carried out either on continuous strand or on woven roving. The PP/GF adhesion, as well as, the PP impregnation was characterized by Scanning Electron Microscopy (SEM) with X-ray Disperse Energy Microanalysis on line (SEM/EDX) on cryogenic fracture surfaces. All properties were so improved, fiber surface change their character from hydrophilic to hydrophobic, then surface adhesion was duplicated, and resin infiltration is so enhanced.

1. INTRODUCTION

The strengthening of matrix-reinforcement interphases has been the goal of a great amount of research in thermoplastic composite materials. Different kinds of treatments, like fiber surface modification, are necessary to improve the compatibility and the interfacial adhesion [Gatenholm et al., 1993]. Untreated inorganic fibers, embedded in a thermoplastic matrix lead to unstable interfaces, and the stress applied to the composite is not efficiently transferred from the matrix to the fiber. Poor matrix–fiber adhesion generally comes from incomplete wetting of fibers by the liquid polymer, promoting the void formation at the interface. So, an adequate surface modification becomes necessary to improve the fiber wetting. Also, the use of thermoplastics in high performance composites, is not large because polymer high viscosity that impedes the impregnation in fiber woven roving or mats.

In previous work, a new approach to increase polypropylene-fiber adhesion based on “in situ¨ propylene polymerization onto fibers was proposed [Etcheverry et al., 2008]. In this sense, chemical anchoring of the matrix on glass fibers was performed by direct metallocenic propylene polymerization then, the improvement of the polymer impregnation into woven roving is expected because the polymer is formed in-situ from a gas, allowing the PP/GF well impregnated laminates The experimental in-situ polymerization route involves an initial contact with methilaluminoxane (MAO) and hydroxy-α-olefin (comonomer) to generate the anchorage points on fiber surface following of propylene polymerization catalyzed by $EtInd_2ZrCl_2$ (metallocene)/MAO. As a result of this reaction, PP chains grow by copolymerization of propylene with the olefin anchored through MAO to the glass fiber surface. The surface morphology and the amount of grafting PP is a function of the amount of the comonomer used [Barbosa et al., 2001]. The optimal comonomer concentration in terms of adhesion improvements was 1% [Etcheverry et al., 2008]. In the present work, the reaction was performed onto glass fibers woven rovings with different weft path. PP infiltration into the woven roving was analyzed for different reaction conditions and types of woven roving.

2. EXPERIMENTAL

Microcomposites preparation: The polymerization reaction was performed directly on two types of woven rovings with different weft path (namely short and large), kindly supplied by Vetrotex Argentina. A commercial PP film with nominal thickness of 78 μm, was supplied by MG Lavorazioni Materie Plastiche (Vicenza, Italy). The microcomposites are typical PP/GF/PP "sandwich" samples prepared by compression molding at 160 °C with 15 Kg/cm^2 during 1 min.

Morphological Characterization: To establish the penetrability within the polymeric matrix, microcomposites samples were cryogenically fractured surfaces were observed by scanning electron microscope (SEM). This analysis was carried out with a Jeol- 35 CF with Microanalysis Energy Dispersive system (EDX) EDAX DX-4, and the scanning electron micrographs were taken on Au-coated fractured surfaces.

3. RESULTS AND DISCUSION

Figure 1 shows SEM micrographs of short weft path woven roving as provided, in situ polymerized with 1% of comonomer (best condition from adhesion analysis) and sandwich samples using this two woven rovings. The PP grafted onto fibers in polymerized samples (Fig 1b) is evident by comparison with untreated ones (Fig. 1a). To corroborate it, EDX analysis was performed and it shows a large carbon peak in the polymerized sample and no one in pure fibers. The PP improvement in woven infiltration using polymerized samples is evident by the comparison of figs 1c and 1d. Untreated samples shows neat PP films in the borders and only near the edge of the woven PP is observed. In the case of treated samples, the PP penetration into the woven was completed and PP is observed in the center of the woven. It is possible to conclude that, although the woven weft is so closed, the PP infiltration is successfully and it seems a promised route to perform well impregnated PP/GF woven laminates.

In figure 2, SEM micrographs of large woven roving as provided and in situ polymerized with 1% of comonomer are shown. The polymerization reaction was also successful. As expected it is not a function of the woven weft. In this figure sandwich samples are presented, using woven untreated, polymerized with 1% of comonomer and with 1% of comonomer. In a previous work [Barbosa et al., 2001], it was demonstrated that the grafted PP, obtained with 4% of comonomer, covers the entire fiber surface but it length is small than grafted chains obtained with 1%. However, the adhesion is not the best.

The infiltration seems not to be affected by the graft PP morphology, in both conditions the infiltration was successful by comparison with sample sandwich obtained with not treated woven (Fig. 2c). In it, the film remains in the woven surface, demonstrating that infiltration not change with the weft of the woven. The reasons of the resin infiltration enhancement is that the woven rovings are preimpregnated with the polymer first to lamination; as usually is done in thermoset based composite laminated. The methodology proposed is a way to obtain prepregs of glass fiber woven rovings for thermoplastic resins, especially for polypropylene.

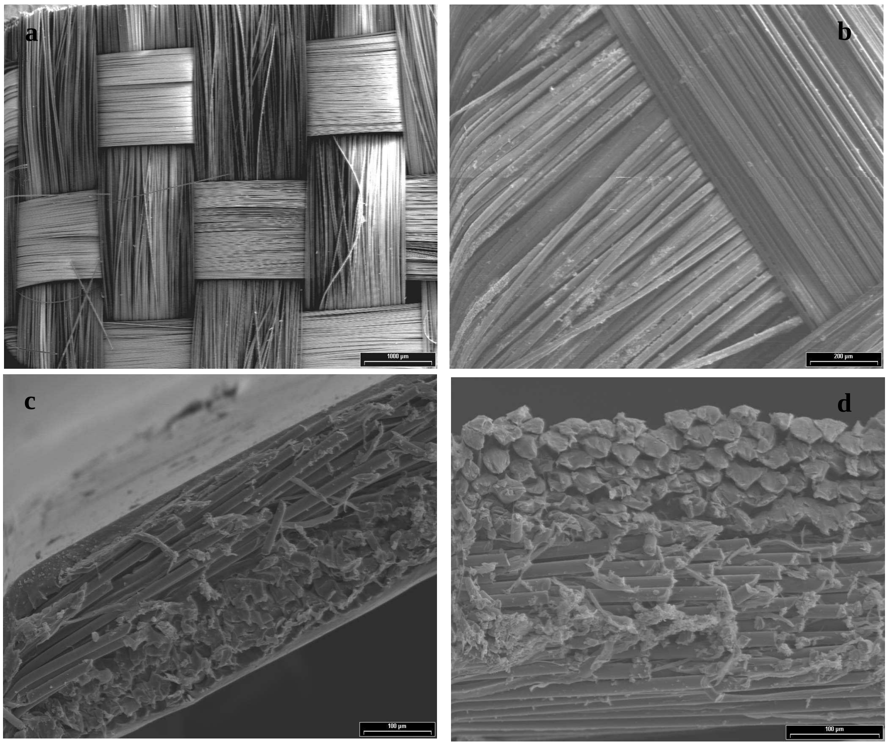

Figure 1. SEM micrographs of woven roving with short weft path, a) As provided (20x), b) In situ polymerized with 1% of comonomer (100x), c) Sandwich PP/woven roving (without treatment)/PP (150x), d) Sandwich PP/woven roving (polymerized -1 %)/PP (200x).

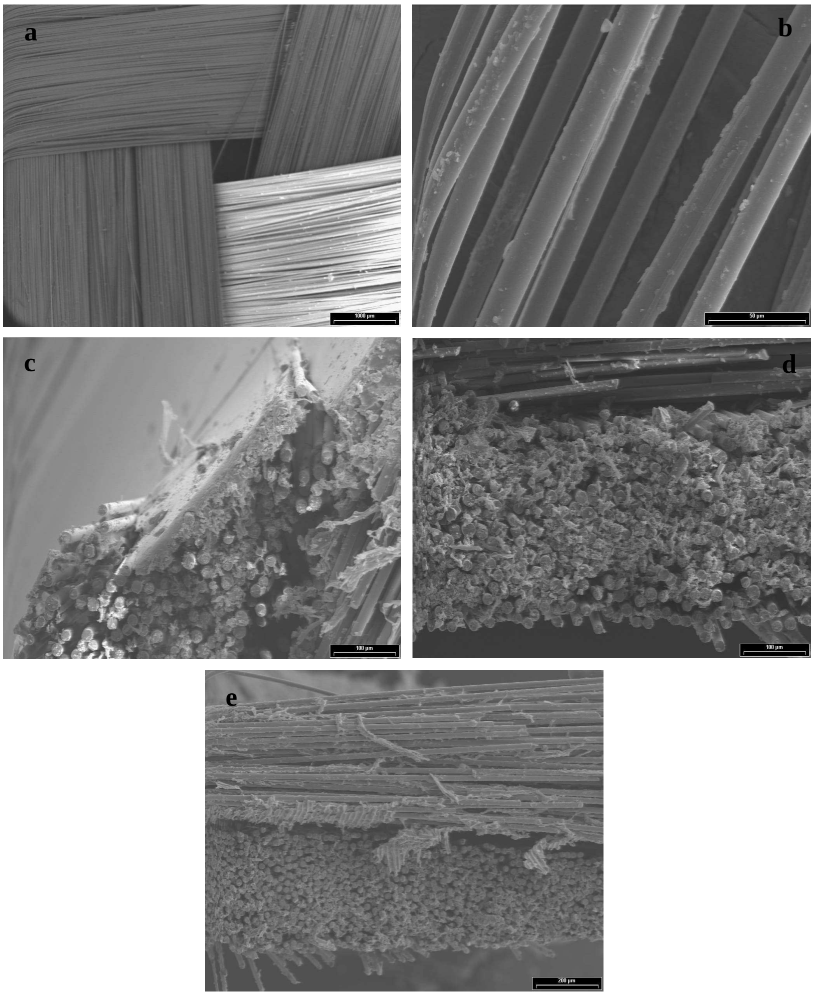

Figure 2. SEM micrographs of woven roving with large weft path, a) As provided (20x), b) In situ polymerized with 1% of comonomer (150x), c) Sandwich PP/woven roving (without treatment)/PP (500x), d) Sandwich PP/woven roving (polymerized-1%)/PP (500x), e) Sandwich PP/woven roving (polymerized-4 %)/PP (200x).

REFERENCES

BARBOSA, S. E.; FERREIRA, M.L.; DAMIANI D.E.; CAPIATI N.J. (2001) Copolymerization of polypropylene and functionalized linear α-olefin onto glass fibers
J Appl Polym Sci, 81, 1266–1276.

ETCHEVERRY, M.; FERREIRA, M.L.; CAPIATI, N.J.; PEGORETTI, A.; BARBOSA, S.E.. (2008) Strengthening of polypropylene–glass fiber interface by direct metallocenic polymerization of propylene onto the fibers *Composites: Part A*, 39, 1915–1923

GATENHOLM, P., FELIX, J. KLASON, AND J. KUBÁT. (1993) Methods for Improvement of Properties of Cellulose-Polymer Composites in *Wood fiber/polymer composites: fundamental concepts, process, and material options*; (M. P. Wolcott, ed.), 20-24 Madison: Forest Product Society; Proc. of the 1st Wood Fiber-Plastic Composite Conference in Madison, WI.

Raman spectroscopic study of the effect of plasma treatment on the interfacial properties of single fibre/epoxy composites

K. Tamargo-Martínez[1], A. Martínez-Alonso[1], M. Gracia[2], J.I. Paredes[1], J.M.D. Tascón[1], M.A. Montes-Morán[1]
1. Instituto Nacional del Carbón, CSIC, Apartado 73, 33080 Oviedo
2. Instituto de Química Fisica "Rocasolano", CSIC, Serrano 119, 28006 Madrid

SUMMARY

The interfacial micromechanics of single poly(*p*-phenylene terephthalamide (PPTA) and poly(*p*-phenylene benzobisoxazole (PBO) fibres embedded in an epoxy resin has been investigated by determining the distribution of interfacial shear stress along the fibres. The effects of an oxygen plasma treatment on the interfacial shear stress of the fibres are discussed. In order to determine the changes in the surface chemistry and morphology, XPS, SEM and AFM studies were performed as well. Raman Spectroscopy has been used to map the strain along the fibre when the composite is subjected to tensile loads. The quality of the interface was improved after the surface treatment, supporting the ability of cold plasma oxidation to enhance the adhesion of high-performance fibres to epoxy resins. It was concluded that the increase in surface nanoroughness and the chemical modifications at the fibre surface contribute in a cooperative way to the improvement of the fibre/matrix adhesion.

1. INTRODUCTION

The quality of interfaces in single fibre-reinforced composite systems is usually characterized by means of fibre pull-out, fibre push-in or fragmentation (Jang-Kyo and Yiu-Wing, 1998) micromechanical tests. For some particular fibre/matrix systems, Raman spectroscopy has been implemented in these tests to obtain strain/stress maps along the fibre during the matrix loading. The use of this technique in composite-related studies relies on the phenomenon that when high-performance fibres are deformed, some of the bands in their Raman spectra shift in a well-defined way. This has been already reported for both PBO and PPTA fibres, for which both a shift towards lower wavenumbers and a widening of the Raman band associated with the symmetric vibration mode of the *para*- phenylene rings (1613 cm^{-1} for PPTA, and 1620 cm^{-1} for PBO) occur when the fibres are deformed in tension (Kitagawa et al. 2001, So et al. 2003, Young 1995, Young and Eichhorn 2006). The band shift is directly proportional to the applied strain (or stress). In this work, this approach has been used to analyse the interfacial behaviour of monofilamentar composites made from epoxy resin and the two above types of fibres exposed or not to an oxygen plasma, a treatment intended to improve the strength of the fibre-matrix interaction.

2. EXPERIMENTAL

PPTA (Kevlar-29® from DuPont, referred to as sample K) and PBO (Zylon® HM from Toyobo, sample Z) fibres with a diameter of 12.1 μm and 11.2 μm, respectively, were exposed to an oxygen plasma generated in a Technics Plasma 200-G apparatus by means of 2.45 GHz microwaves using 70 W power, 1 mbar O_2 pressure and a treatment time of 4 min (KO 4 and ZO 4 samples). Single-fibre model composites (Fig. 1c) were prepared from either pristine or plasma-treated fibres. The matrix used for composite preparation was an epoxy resin (Araldite LY/CH 5052 from Huntsman), obtained by mixing 100 parts by weight (ppw) of LY5052 Araldite resin and 38 ppw of CH5052. Raman spectra were carried out using an HR 800 Jobin Yvon Horiba spectrometer equipped with a CCD detector. An incident beam with a wavelength in the near infrared (λ = 785 nm) was used. The beam, 2 µm in diameter, was focused on the sample surface using an optical microscope (BXFM, from Olympus) coupled to the spectrometer. The dependence of the peak position of the selected Raman bands on axial stress was performed on a lab-made stress rig, used to break single filament tabs (Fig. 1b). The model composites were deformed in a Minimat straining rig. The strain on the composites was monitored using strain gauges connected to a digital multimeter. Raman measurements on these model composites were carried out following the experimental set-up depicted on Fig. 1a.

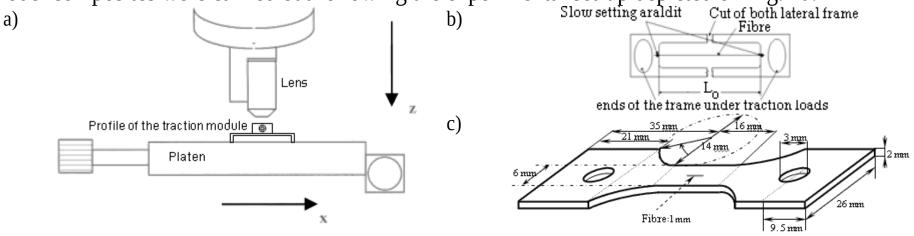

Figure 1. Setup for *in-situ* monitoring of the traction tests using Raman spectroscopy (a), and specimens for tensile tests of single filaments (b) and single-fibre epoxy systems (c). For the single filaments tensile tests, gauge lengths (L_0) of 20, 50 and 60 mm were used.

3. RESULTS AND DISCUSSION

In order to obtain the stress (or strain) distribution along a fibre embedded in a matrix (σ_f, eq. (1)), it is first required to know the variation of a Raman band position (*k*) with stress (or deformation) for the single filament. The values obtained for *k* in the single filament tensile tests are shown in Table 1. The standard deviations obtained indicate that no substantial differences exist between the untreated and plasma-treated fibres.

Length (mm)	$(d\Delta\overline{\vartheta}/d\sigma)\ (cm^{-1}.GPa^{-1})$			
	K	KO 4	Z	ZO 4
20	-3.6	-3.4	-3.2	-3.4
50	-3.6	-3.5	-3.0	-3.1
60	-3.6	-2.9	-4.0	-3.1
Average	**-3.6 ± 0.0**	**-3.3 ± 0.3**	**-3.4 ± 0.5**	**-3.2 ± 0.2**

Table 1. Values of the Raman band shift due to stress for the PPTA (K and KO 4) and PBO fibres (Z and ZO 4).

The corresponding axial stress distributions along the fibre embedded in the epoxy resin (σ_f) were thus calculated (open symbols on Fig. 2, a.1 and b.1) at 8 µm intervals according to eq. (1). Cubic spline fits (solid lines) were applied to the experimental data.

$$\sigma_f = \frac{\Delta\overline{\vartheta_{f,m}}}{k}\begin{Bmatrix} \Delta\overline{\vartheta_{f,m}} : \mathit{Shift\ of\ the\ Raman\ band\ with\ the\ applied\ strain} \\ k : \mathit{Stress\ sensitivity\ facotr\ or\ stress\ calibration\ parameter} \end{Bmatrix} \quad (1)$$

Finally, interfacial shear stress distributions are obtained by differentiating the cubic spline fits of the fibre stress distribution, at each particular matrix level of deformation (ε_m):

$$\tau_i = \frac{r}{2}\cdot\frac{d\sigma_f}{dx} \quad (2)$$

The distributions for σ_f and τ_i fitted approximately the predictions for several proposed micromechanical models (full, partial or total debonding) for short fibre-reinforced systems

(Tamargo-Martínez, 2007). For the PPTA-based systems, it can be said that the obtained experimental results fit the full adhesion model up to 2.0% deformation. As predicted, the absolute maxima of the interfacial shear stress correspond to the ends of the fibre (see Fig. 2-a.2). However, for the PBO composites, the fibre starts to undergo debonding just above 1.0% of matrix deformation. Therefore, only 30% of the PBO fibre that remains fully bound to the epoxy resin at a matrix deformation of 2.0%. Above 3.00% deformation, σ_f for the epoxy-PPTA system exhibits a slight depression in the central area of the fibre (Fig. 2-a.1). The presence of two consecutive max/min pairs in the interfacial shear stress (Fig. 2-a.2) indicates the beginning of the fibre fragmentation. For the epoxy-Z system, σ_f exhibits an "inverted V" shape, i.e., the fibre has been almost totally debonded.

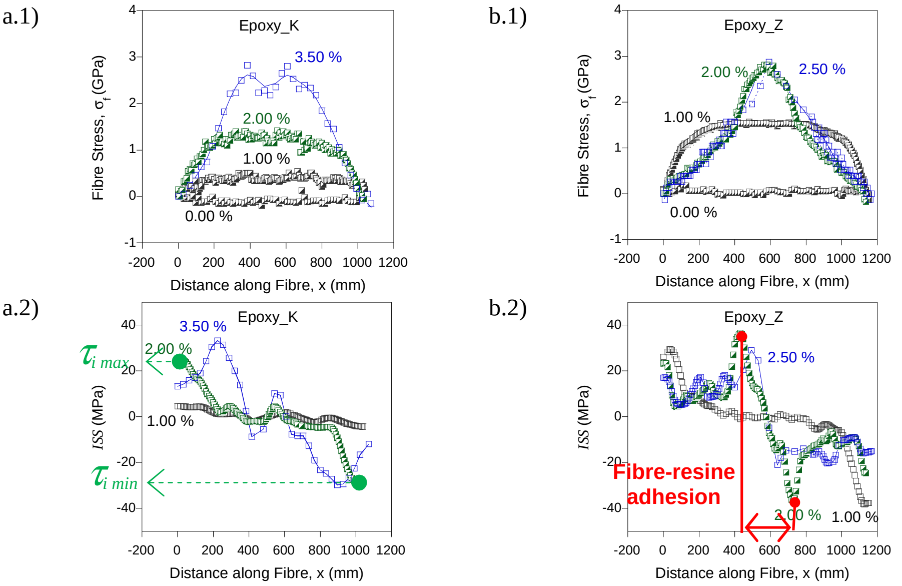

Figure 2. Variation of fibre stress with distance along a PPTA fibre (a.1) or PBO fibre (b.1) at various levels of matrix strain, and interfacial shear stress distributions of the corresponding epoxy systems (a.2 and b.2).

The absolute maxima of the interfacial shear stress (τ_m) increases with increasing matrix deformation until a limit value is attained, above which τ_m remains approximately constant (Fig. 3).

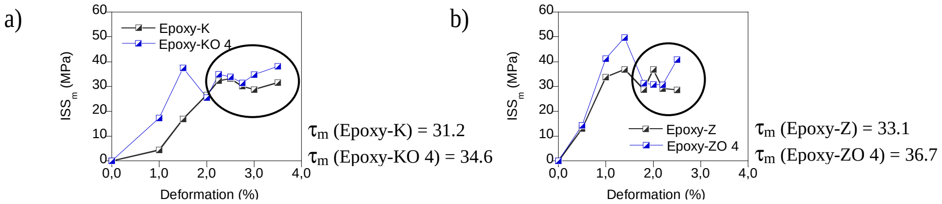

Figure 3. Dependence of the average interfacial shear strength ($ISS_m = 0.5\,[\tau_{imax} + \tau_{imin}]$) upon matrix strain for the epoxy-PPTA (a) and epoxy-PBO (b) systems.

These absolute maxima were used to calculate the average interfacial shear strength (ISS_m) in the fibre-resin adhesion zone. As Table 2 shows, this magnitude is larger (by ~10.0%) for the systems reinforced with the two oxygen plasma-treated fibre samples. The friction shear stress (τ_{ISSf}) provides an estimate of the physicochemical activity in the real contact area in the non-adhesion zone. This magnitude was calculated by averaging the ISS_f data obtained in the range of applied stress in which the fibre begins to be debonded from the resin. These values were approximately constant (within the range tested in this work) for the PPTA-based systems, but decreased by more than 50% for the PBO-based ones (data not shown). This indicates that in the case of PBO the interface is destroyed. The friction shear stress increases following oxygen plasma exposure of the two types of reinforcing fibre (data not shown). τ_{ISSf} follows the same trend as described before for ISS_m, i.e., it is larger for the systems reinforced with KO 4 (~15.0%) and ZO 4 (~35.0%). The interface quality is closely related, besides the friction shear stress, with the interfacial shear stress distributions generated during the deformation process. From this perspective, one can conclude that the oxygen plasma treatment increases the adhesion of PPTA and PBO to the epoxy resin. Atomic force microscopy (AFM) (images not shown) has revealed that the oxygen plasma treatment brings about an increase in the degree of surface roughness of the two types of fibre. It has also been shown that the surfaces of both PPTA and PBO undergo a certain swelling following plasma treatment. For the former, this behaviour has been attributed to incorporation of polar oxygenated groups (Paredes et al. 2006). In the case of PBO, changes observed in the high-resolution XPS spectra of the C(1s), O(1s) and N(1s) core levels (not shown) have been associated to functional groups like amide, carbonyl, imide, and nitrile (Tamargo-Martínez, 2007), which would be responsible for the observed ZO 4 surface swelling.

4. CONCLUSION

The excellent mechanical properties of the PBO and PPTA fibres remain unchanged following the oxygen plasma treatments carried out in this work. The adhesion of the modified fibres (KO 4 and ZO 4) to an epoxy resin was stronger than that of the corresponding pristine fibres. The interfacial shear strength was higher for the PBO-based systems than for the PPTA-based ones. The tensile behaviour of the fibre-reinforced systems when submitted to external efforts was different for the two studied types of fibre. Oxygen plasma treatment brought about an improvement in both mechanical and chemical interactions of the two types of polymeric fibres with the epoxy resin.

ACKNOWLEDGMENT

Financial support from the Spanish MEC (project CTQ2005-01905-C04-02-PPQ).

REFERENCES

JANG-KYO, K., YIU-WING M. (1998). Measurements of interface /interlaminar properties, *in Engineered Interfaces in Fiber reinforced composites* (Eds. Jang-Kyo, K., Yiu-Wing M.), Elsevier Science Ldt., Kindlington, Oxford OX5 (UK).

KITAGAWA, T., YABUKI, K., YOUNG, R.J. (2001). An investigation into the relationship between processing, structure and properties for high-modulus PBO fibres. Part 1. Raman bands shifts and broadening in tension and compression. *Polymer*, 42, 2101-2112.

PAREDES, J.I., VILLAR-RODIL, S., TAMARGO-MARTÍNEZ, K., MARTÍNEZ-ALONSO, A., TASCÓN, J.M.D. (2006). Real-time monitoring of polymer swelling on the nanometer scale by atomic force microscopy. *Langmuir*, 22, 4728-4733.

SO, C.L., BENNETT, J.A., SIRICHAISIT, J., YOUNG, R.J. (2003). Compressive behavior of rigid rod polymer fibres and their adhesion to composites matrixes. *Plastics, Rubber and Composites*, 32, 199-205.

SO, C.L., YOUNG, R.J. (2001). Interfacial failure in poly(*p*-phenylene benzobisoxazole) (PBO)/epoxy single fibibre pull-out specimens. Composites A, 32, 445-455.

TAMARGO-MARTÍNEZ, K. “Fibras poliméricas avanzadas: modificación superficial e interfacial”. Doctoral Thesis, Oviedo University, Oviedo, Spain, 2007.

YOUNG, R.J. (1995). Monitoring deformation processes in high-performance fibres using Raman spectroscopy. *J. Text. Inst.*, 86, 360-381.

YOUNG, R.J., EICHHORN, S.J. (2006). Deformation mechanisms in polymer fibres and nanocomposites. *Polymer*, 48, 2-18.

Thermoplastic reinforcement for thermoset composites: solubility measurements in epoxy resins

D. Dumont, D. Daoust, M. Sclavons, J. Devaux
Unité de Chimie et de Physique des Hauts Polymères, Université catholique de Louvain,
1 Croix du Sud, 1348, Louvain-la-Neuve, Belgium, e-mail: david.dumont@uclouvain.be
D. Seveno, J. de Coninck
Physics of Surfaces and Interfaces Laboratory,
Université de Mons, Parc Initialis, Bât. Materia Nova, 7000, Mons, Belgium

SUMMARY

The stitching of soluble thermoplastic (TP) yarns into the carbon fibre preform is a possible approach for toughening of composites with epoxy matrix processed by Resin Transfer Moulding (RTM). Polyethersulfone (PES) and phenoxy are evaluated in terms of solubility using Differential Scanning Calorimetry (DSC) and dissolution of a yarn into epoxy resins. A higher solubility of phenoxy in epoxy resins is observed compared to PES. Moreover, the dissolution and the diffusion of the TP can be improved by adapting the resin composition and the temperature to influence the local composition and therefrom, the blend microstructure after the reaction induced phase separation.

1. INTRODUCTION

High functionality epoxy resins used as polymer matrices for continuous fibres composites produced using the RTM process are suitable for aeronautic applications due to the high performances of the thermoset (TS) network. The introduction of soluble TP yarns in the dry preform (Beier et al., 2008) improve its ease-of-handling and potentially the matrix properties (Martinez et al., 2000) thanks to the microstructure resulting from the phase separation induced by the crosslinking reaction in the TS/TP blend. Moreover, TP can act as carrier to deliver (nano)particles in epoxy resins to enhance locally electrical, thermal or mechanical properties like toughness. The local microstructure and the filler distribution depend among other things on the dissolution and the diffusion of the TP in the epoxy resin which requires to be controlled (Naffakh et al., 2006). Therefore, the aim of this study is to assess the solubility of amorphous TPs in epoxy resins to allow their exploitation as nanofiller carrier to reinforce the thermoset network.

2. EXPERIMENTAL

A high and a low T_g amorphous TP, respectively polyethersulfone (PES, Radel A-200 from Solvay Advanced Polymers, T_g=220°C) and, poly(hydroxyether of bisphenol A) (phenoxy, PKHP200 from InChem, T_g=92°C) were compared in terms of solubility in resin components and dissolution kinetics of a TP yarn in reactive epoxy resins. The HexFlow RTM6 resin developed to fulfil the requirements of the aerospace industries in RTM and chosen as reference contains tetraglycidyl-4,4'-methylene dianiline (TGMDA, Araldite MY 721 from Huntsman), 4,4'-methylenebis-(2,6-diethyl)-aniline (MDEA, Lonzacure M-DEA kr) and 4,4'-methylenebis-(2-isopropyl-6-methyl)-aniline (MMIPA from Acros organics). Other resin compositions were tested by using triglycidyl para-aminophenol (TGAP, Araldite MY 0510 from Huntsman) and/or diethyltoluenediamine

(DETDA, Lonzacure DETDA 80, 77–81% 3,5-diethyltoluene-2,4-diamine and 18–22% 3,5-diethyltoluene-2,6-diamine). Epoxy resins TGAP-DETDA and TGMDA-DETDA are compound of stoechiometric amounts of epoxide and aromatic diamine. The molecular structures of the resin monomers and the TPs are summarized in table 1.

Diamines	Epoxides
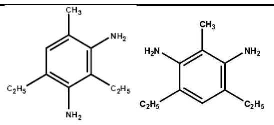 Diethyltoluenediamine (DETDA) 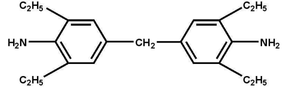 4,4’-methylenebis-(2,6-diethyl)-aniline (MDEA)	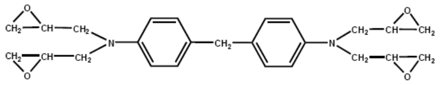 Tetraglycidyl -4,4’-methylene dianiline (TGMDA) 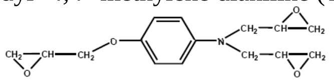 Triglycidyl para-aminophenol (TGAP)
	Thermoplastics
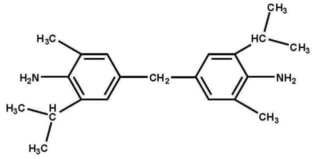 4,4’-methylenebis-(2-isopropyl-6-methyl)-aniline (MMIPA)	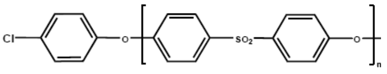 Polyethersulfone (PES) 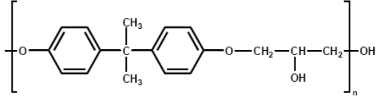 Poly(hydroxyether of bisphenol A) (phenoxy)

Table 1. Molecular structures of epoxides, diamines and thermoplastics

Dissolution temperature measurements of 10wt% TP in the form of powder in the epoxides and the diamines were performed on a Mettler Toledo DSC 822^{e} in 40 µl aluminum pans with sample weights between 15 and 20mg. Indium and copper were used for temperature and enthalpy calibration. The samples were heated from 25 to 200°C at various heating speeds (1, 5 and 10°C/minute).

To follow the thermal dissolution of TP yarns in epoxy resins, a 100µm diameter fibre (95<d<105µm) was placed in 50mg resin between two microscope glass slides and fitted into a Mettler FP82HT hot stage monitored by a Mettler FP90 central processor. The yarn diameter evolution was continuously observed with an Olympus BX51 optical microscope connected to a ColorviewI camera. The TP yarns were made by drawing the soft polymer extruded in a corotating twin-screw batch-type mini-extruder (DSM $15cm^3$) during 5 minutes at 150 rpm at 220°C for the phenoxy and at 340°C for the PES. Phenoxy nanocomposites yarns containing 1wt% unfunctionalized multiwall carbon nanotubes (MWNTs) Nanocyl7000 were produced using the same conditions.

To determine TP diffusion profiles, Raman spectra acquisitions were made on the phase separated samples after dissolution and diffusion at 10µm intervals, perpendicularly to the initial yarn direction using a DXR Raman microscope from Thermo Scientific with an incident laser excitation wavelength of 780nm.

3. THERMOPLASTIC SOLUBILITY IN RESIN COMPONENTS

The DSC solubility measurements are characterized by a low exothermic heat flow signal for PES (endothermic for phenoxy). The heating rate effect on the solubilization heat flow is evidenced on figure 1.a. It must be as low as possible to ensure an equilibrium measurement but high enough for exact solubility determination. The lower solubilization temperatures of the PES in the TGAP and the DETDA compared respectively to the TGMDA and the RTM6 diamines are shown on figure 1.b. Moreover, the phenoxy solubility in TGMDA is higher than for PES.

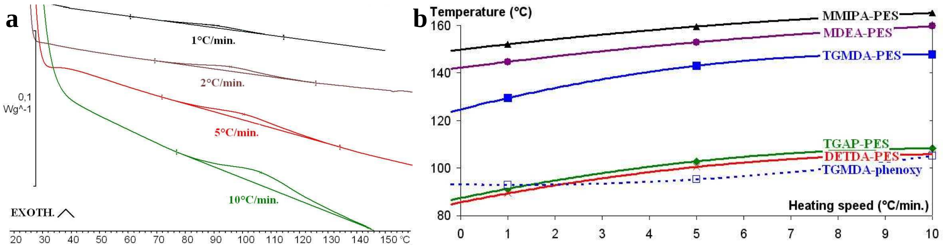

Fig. 1. a) Influence of the heating rate on the solubilization heat flow of PES in TGMDA b) Temperature of the signal maximum vs. heating rate

4. DISSOLUTION OF THERMOPLASTIC YARNS IN EPOXY RESINS

The TP yarn dissolution must be completed before too high viscosity increase of the resin resulting from the crosslinking reaction. Figure 2.a illustrates the improvement of the dissolution kinetics in the TGMDA-DETDA and particularly in the TGAP-DETDA resin compared to the RTM6 resin. Moreover, figure 2.b confirms the higher solubility of phenoxy than PES in epoxy resins.

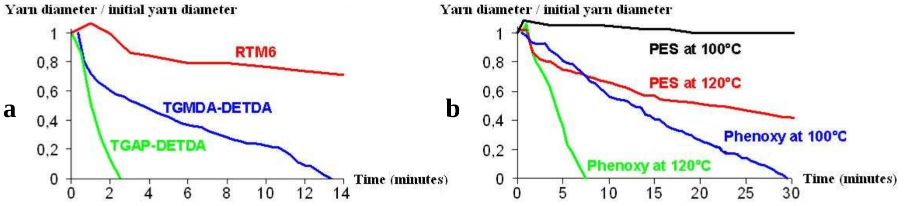

Fig. 2. Yarn diameter evolution in epoxy resins: a) Influence of the resin (PES yarn at 140°C) b) Influence of temperature and TP (TGMDA-DETDA resin)

5. DIFFUSION PROFILES IN EPOXY RESINS

By computing the intensity ratio between a TP (1111cm^{-1} for phenoxy and 1148cm^{-1} for PES) or MWNTs (1311cm^{-1}) and an epoxide characteristic band (795cm^{-1} or 1190cm^{-1} for TGMDA and 825cm^{-1} for TGAP), Raman imaging allows the determination of diffusion profiles. Fig 3.a shows the TP concentration gradient remaining at phase separation. Due to the higher solubility of phenoxy, its diffusion is favored compared to PES. At 120°C, the diffusion of PES is better in the TGAP-DETDA resin than in TGMDA-DETDA or in RTM6 although its higher reactivity induces a shorter diffusion period before gelation. Figure 3.b suggests that for a phenoxy yarn filled with 1wt% MWNTs, the nanotubes have no significant influence on the phenoxy diffusion and that the normalized nanotube and phenoxy profiles are similar in this case.

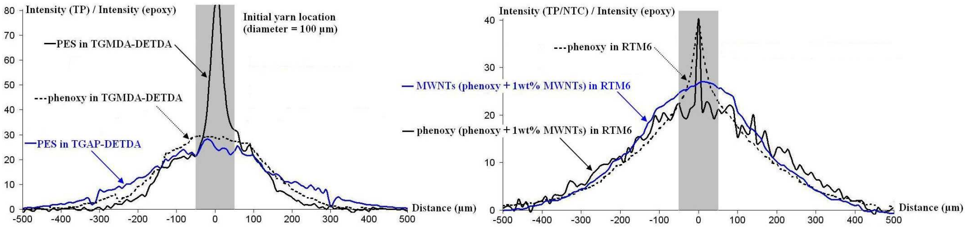

Fig. 3. Diffusion profiles at 120 °C after phase separation (Raman spectroscopy)

6. COMPARISON WITH NUMERICAL SIMULATIONS

A new insight of the solubilization and diffusion processes of phenoxy and PES in the epoxy resins was given by molecular mechanics and dynamics techniques using a COMPASS force field of the MaterialsStudio 4.1 software. It was found that the TGMDA molecule has a greater affinity for phenoxy than for PES and that DETDA and TGAP molecules are more favourable to PES than respectively MDEA (or MMIPA) and TGMDA because of a better diffusion process.

7. CONCLUSIONS

The phenoxy and PES solubilites in epoxy resins allow the yarn dissolution and diffusion of such TP and their exploitation as MWNTs carrier to reinforce thermoset composite matrices. Phenoxy can be dissolved in the RTM6 resin while for PES new epoxy resin compositions are proposed to improve the solubility. The DSC measurements coupled with the numerical simulations give information to predict and to understand the yarn dissolution in the reactive resins.

ACKNOWLEDGMENT

The authors want to be grateful to FRIA and “Région Wallonne” for the financial support and to InChem and Lonza for the phenoxy and Lonzacure DETDA80 supply.

REFERENCES

-BEIER, U., WOLFF-FABRIS, F., FISCHER, F., SANDLER, J.K.W., ALTSTADT, V., HULDER, G., SCHMACHTENBERG, E., SPANNER, H., WEIMER, C., ROSER, T., BUCHS, W. (2008) Mechanical performance of carbon fibre-reinforced composites based on preforms stitched with innovative low-melting temperature and matrix soluble TP yarns, *Composites Part A: Applied Sc. and Manufact.*, 39 (9), 1572-1581.

-MARTINEZ, I., MARTINA, M.D., ECEIZAA, A., OYANGURENB, P., MONDRAGON, I. (2000) Phase separation in polysulfone-modified epoxy mixtures. Relationships between curing conditions, morphology and ultimate behavior, *Polymer*, 41 (3), 1027-1035.

-NAFFAKH, M., DUMON, M., GERARD, J. F. (2006) Study of a Reactive Epoxy-Amine Resin Enabling In Situ Dissolution of TP Films during RTM for Toughening Composites, *Composites Science and Technology*, 66 (10), 1376-1384.

Solubility and diffusion of thermoplastic reinforcement in epoxy resins: a molecular dynamics study

D. Seveno, J. de Coninck
Physics of surfaces and interfaces Laboratory,
Université de Mons, Parc Initialis, Bât. MateriaNova. 7000 Mons, Belgium
D. Dumont, D. Daoust, M. Sclavons, J. Devaux
Unité de Chimie et de Physique des Hauts Polymères (POLY), Université catholique de Louvain, 1 Croix du Sud, 1348, Louvain-la-Neuve, Belgium

SUMMARY

Molecular simulations are used to study, at the molecular level, the mechanisms which control the solubility and diffusion of thermoplastic polymers (TP) into epoxy resins (TS). First, the solubilities of Polythersulfone (PES) and phenoxy are estimated via the calculation of the free energy of mixing based on molecular mechanics calculations. Then, the diffusion of the TP in the components of the TS is simulated via molecular dynamics. Thanks to these simulations, it is found that phenoxy shows a greater affinity to the epoxy resins than PES and that alternative resin formulations can improve the diffusion process of the TP.

1. INTRODUCTION

The addition of thermoplastic reinforcement to a high functionality epoxy resin is a way to increase its toughness and make it suitable for aeronautic applications where the Resin Transfer Moulding (RTM) process is widely used. Because of its high viscosity, the thermoplastic is preferably introduced in the form of yarn in the dry fibre perform. In such cases, the epoxy resin must act as an efficient solvent, to solubilize the yarn and ensure the diffusion of the thermoplastic molecules before the resin reticulates. The microstructure resulting from the phase separation induced by the crosslinking reaction of the epoxy resins potentially improves the matrix properties. The thermoplastics considered are the polyethersulfone (PES) and poly(hydroxyether bisphenol A) (phenoxy). The epoxy systems are Hexflow RTM6 (TGMDA, MDEA, MMIPA) resin and alternative resins composed of an epoxide, triglycidyl p-aminophenol (TGAP) and a liquid aromatic diamine, diethyltoluenediamine (DETDA). Results obtained by Differential Scanning Calorimetry and the observations of the dissolution of thermoplastic yarn using optical microscopy have shown that the use of the phenoxy thermoplastic is appropriate for the RTM6 resin whereas the level of solubilization and diffusion of the PES thermoplastic in the RTM6 resin is increased when the TGAP-DETDA resin is used. From a theoretical point of view, the calculation of the solubility parameters via the group contribution method is not able to explain the experimental results. Numerical simulations (molecular mechanics and dynamics) are then considered to give new insight into the solubilization and diffusion mechanisms at molecular level.

1. THEORETICAL PREDICTION: SOLUBILITY PARAMETER

A quick method to estimate the solubility of a polymer in a solvent is to calculate the solubility parameter, δ, from the group contribution method (the Hoftyser and Van

Krevelen method is here used). δ is given by $\delta^2 = \delta_d{}^2 + \delta_p{}^2 + \delta_h{}^2$ where δ_d, δ_p, and δ_h are respectively the dispersive, the polar, and the hydrogen components of δ. The affinity between the molecules can be estimated by calculating

$$\Delta\delta_{ij} = \sqrt{4\left(\delta_d^i - \delta_d^j\right)^2 + \left(\delta_p^i - \delta_p^j\right)^2 + \left(\delta_h^i - \delta_h^j\right)^2} \qquad (1)$$

which represents the distance in term of solubility between the molecules *i* and *j*. In Table 1, it can be seen that the TGMDA molecule is the most favorable one for both TP. The TGAP and DETDA molecules are disfavorables as the distances between these molecules and the TP are larger than the ones between respectively the TGMDA and either the MDEA or MMIPA molecules.

	RTM6				
	TGMDA	MDEA	MMIPA	TGAP	DETDA
PES	3.29	5.19	3.39	6.17	9.32
phenoxy	2.45	6.92	4.93	4.02	9.68

Table 1. $\Delta\delta$ in $\mathrm{MPa}^{1/2}$ between the TP and the components of the resins.

It is therefore not possible to explain why phenoxy is more soluble in the RTM6 than PES and why the TGAP and DETDA molecules are better solvent than respectively the TGMDA and MDEA (or MMIPA) ones. It is then necessary to go a step further in the modelling of the interactions between the molecules by considering molecular simulations. The molecular mechanics technique is first used to estimate the free energy of mixing between the TP and the epoxide and diamino molecules.

2. FREE ENERGY OF MIXING/ MOLECULAR MECHANICS

In the frame of the Flory-Huggins model, the free energy of mixing is modelled by:

$$\Delta G_M = RT \frac{\phi_A}{n_A} \ln \phi_A + \frac{\phi_B}{n_B} \ln \phi_B + \chi_{AB}\phi_A\phi_B \qquad (2)$$

with ΔG_M the free energy of mixing, *T* the temperature, *R* the Boltzmann constant, n_A and n_B the degree of polymerization of the components A and B, ϕ_A and ϕ_B the volume fraction of component A and B, and χ_{AB} the Flory-Huggins interaction parameter. If ΔG_M is negative, the two substances are mutually soluble. The interaction parameter is defined as:

$$\chi_{AB} = \frac{E_{AB}^{mix}}{RT} \qquad (3)$$

where E_{AB}^{mix} is the mixing energy, i.e. the difference in free energy due to interaction between the mixed and pure state. The mixing energy (extended Flory-Huggins model) is given by :

$$E_{AB}^{mix} = \frac{1}{2}\left(Z_{AB}E_{AB} + Z_{BA}E_{BA} - Z_{AA}E_{AA} - Z_{BB}E_{BB}\right) \tag{4}$$

where E_{ij} is the energy of interaction between the components *i* and *j*, and Z_{ij} is the number of molecules of component *j* that can be packed around a single molecule of component *i*. E_{ij} and Z_{ij} were calculated using the Blends module and the COMPASS forcefield of the MaterialsStudio 4.1 software. The results, partially illustrated by Fig. 1, showed that the phenoxy-TGMDA interaction is clearly favorable whereras the others ΔG_M are weaker but still negative except for the DETDA which is slightly positive.

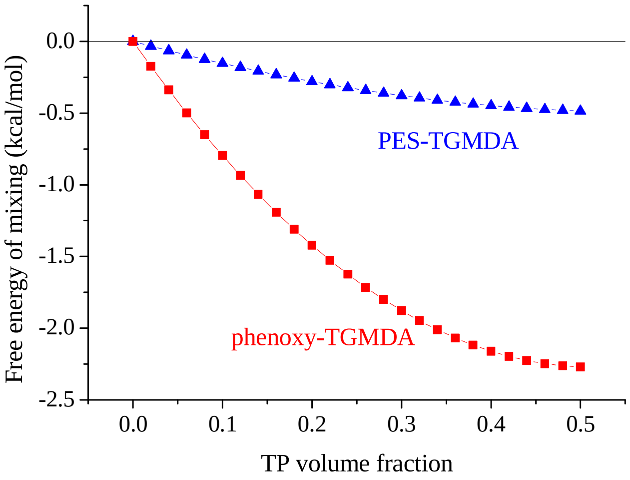

Fig. 1. Free energy of mixing of the TP in the TGMDA molecules at T=100 °C.

3. DIFFUSION COEFFICIENT: MOLECULAR DYNAMICS

Molecular dynamics consist in generating successive configurations of a molecular system by applying Newton's second law of motion $\vec{F} = m\vec{a}$ where *F* is the force on atoms, *m* is the mass of the atom and *a* its acceleration. The force derives from a potential given by a forcefield (COMPASS). Contrary to the molecular mechanics method, the temperature is here a key parameter of the simulation which controls the kinetic energy of the molecules. The method considered here consists in constructing a 3D cell (with periodic boundary conditions) made of TP (25% in weight) and either epoxide or diamino molecules. For a given temperature, an NPT (isothermal-isobaric ensemble) simulation was first run to reach the equilibrium density. A NVT (canonical ensemble) simulation was then performed to study the motion of the TP molecules. Each simulation lasts 100 ps. The diffusion coefficient is obtained by measuring the mean square displacement of molecules over long times. For example, Fig. 2 shows that the coefficient diffusion versus the temperature of phenoxy in the DETDA is higher than in the MDEA-MMIPA molecules.

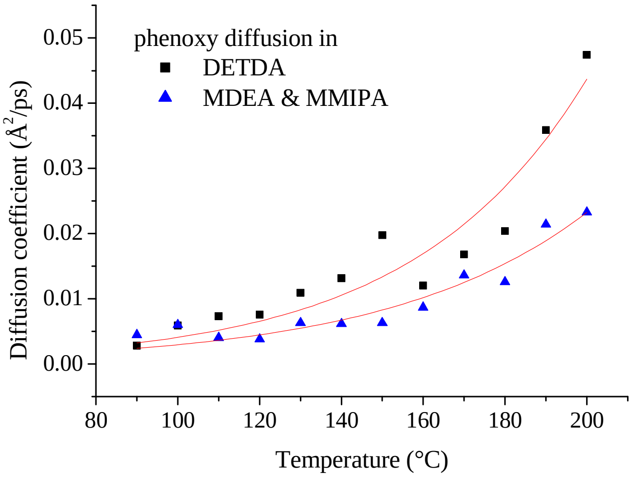

Fig. 2. Coefficient diffusions of phenoxy in the diamino molecules versus the temperature. The full lines are a guide to the eye.

For PES, it is found that the DETDA and the TGAP molecules are more favorable than respectively MDEA (or MMIPA) and TGMDA because of a better diffusion process.

3. CONCLUSIONS

Molecular mechanics and dynamics are used to give a new insight of the solubilisation and diffusion processes of phenoxy and PES in the Hexflow RTM6 resin and alternative resins. It is found that the TGMDA molecule has a greater affinity to phenoxy than to PES and that DETDA and TGAP molecules are more favorables to PES than respectively MDEA (or MMIPA) and TGMDA because of a better diffusion process.

ACKNOWLEDGMENT

The authors acknowledge the Région Wallonne and the FNRS for their financial support.

Effect of chemical modification on the mechanical properties of coconut/ HIPS composites

K.C.C. Carvalho, H.J.C. Voorwald, M.O.H. Cioffi
Fatigue and Aeronautic Materials Research Group, Materials and Technologies Depart.
São Paulo State University. Guaratinguetá Campus, Engineering College

SUMMARY

In the present work, the effect of chemical modification on the mechanical properties of coconut fibers/HIPS composites was studied. Cellulose fibers from coconut were obtained by pre-treatment with 10% sodium hydroxide solution. These fibers were mixed with the polymeric matrix (HIPS) in a thermokinetic mixer, in which fibers were responsible for 10 to 30 wt% in the composition. After the mixture, composites were dried, ground in mill and placed in an injector camera according to ASTM D-638 specification. In order to determine the influence of chemical treatment on the mechanical properties of coconut fibers/HIPS composites specimens were tested in tensile mode and fractures surface composites were analysed by scanning electron microscopy. Results of tensile tests showed a small variation of the average values of tension strength. On the other hand, it was observed an increase of 31% on the values of tensile modulus of composites compared to the pure HIPS.

1. INTRODUCTION

New environmental legislation as well as consumer pressure has forced manufacturing industries to search for new materials that can substitute for conventional non-renewable reinforcing materials such as carbon or glass fibers. Because of this, in the recent years the use of natural fibers like banana, sisal, hemp and flax, jute, coconut, and oil palm have attracted scientists and technologists for applications in consumer goods, low-cost housing and other civil structures (Jústiz-Smith et to. 2008; Spinacé et to. 2009; El-Taybe et to. 2009). Plant fibers are very attractive for composites materials because to the low cost, low density, non-toxicity, no abrasion during processing and recyclability (Spinacé et to. 2009). However, the use of natural fibers in composites materials has some drawbacks such as poor hydrophobic polymer matrix compatibility, tendency to form aggregates during processing and low resistance to moisture and variability of composition (Bessadok et to. 2009). On the other hand, various treatments are being used to improve fibers/matrix compatibility. This process is considered critical as development phase of these materials due to strong interfiber hydrogen bonding, which holds the fibers together. Methods for surface modification can be physical or chemical according to superficial modification approach of the fiber (Bessadok et to. 2009).

In the present work coconut fibers treated with alkaline solution, in order to improve the fiber/matrix compatibility, were mixture with HIPS and the mechanical properties of the coconut fibers/HIPS composites was available.

2. EXPERIMENTAL

2.1 Preparation of treated cellulose fibers

Cellulose fibers from coconut were obtained by pre-treated with alkaline solution of NaOH 10 wt%, following by filtration and dried at 50 ° C for 24 hours.

2.2 Composites preparation

Treated coconut fibers were mixed with the polymeric matrix (HIPS) in a thermokinetic mixer, model MH-50H, with speed rate maintained at 5250 rpm, in which fibers were responsible for 10 and 30 wt% in the composition. After the mixture, composites were dried and ground in mill, model RONE. Then coconut fibers/HIPS composites, were placed in an injector camera at 200°C and 2 ºC min-1 heating rate. The melted material was injected in a required dimensions pre-warm mold (210°C) to obtain tensile specimen.

2.3 Tensile Tests

Composites and pure HIPS were analysed in a Shimatzu testing machine (model AG-X 50kN). Tests were carried out according to ASTM standards D638 with 5 mm.min^{-1} crosshead speed.

2.2 Scanning electron microscopy

Specimens submitted to tensile tests were cut and the composite intact fracture surface was analyzed in a LEO 1450V scanning electron microscopy with tungsten filament operating at 20 kV, utilizing low vacuum technique and work distance of 12 mm. Also were analysed treated and untreated coconut fibers.

3. RESULTS AND DISCUSSIONS

3.1 Scanning electron microscopy

The effect of chemical treatment on surface fibers could be available by scanning electron microscopy technique. Fig. 1 presents the micrographs of untreated and treated coconut fibers. One may see that the surface of coconut fiber is covered with a layer of substances, due to the presence of extractives, part of the constitution of natural fibers.

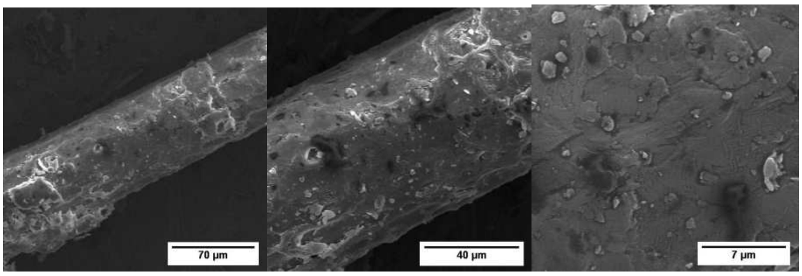

(a) (b) (c)

Fig. 1. SEM of untreated coconut fiber: (a) 500x; (b) 1000x and (c) 5000x.

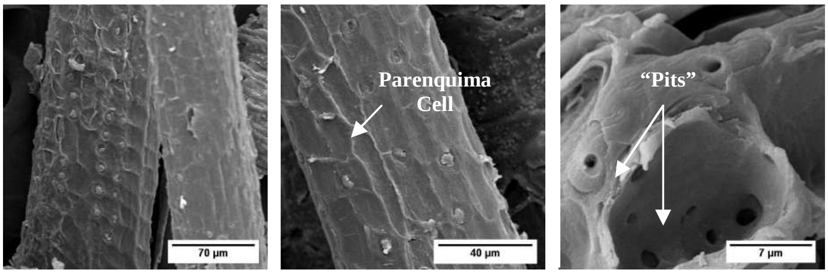

(a) (b) (c)

Fig. 2. SEM of treated coconut fibers: (a) 500x; (b) 1000x and (c) 5000x.

After the chemical treatment, Fig. 2, it was observed a roughness surface with the presence of parenquima cell and pits that are also observed by Huang Gu (2009). The chemical treatment with NaOH removes extractives, as waxes and oil, from the surface of the fibers and thus increases the overall rugosity of the surface, and consequently improves the mechanical bonding between polimeric matrix and coconut fibers in the composite preparation.

3.1 Scanning electron microscopy

Table 1 indicates mechanical properties of treated coconut fibers/HIPS composites and pure HIPS, in special the effect of chemical modification on coconut fibers. The volume fraction of the coconut fibers in the composites was 10 and 30 wt %.

Table 1. Mechanical properties of the materials.

Samples	**Properties**		
	Elongation at break (tensile) (%)	**Tensile strength (MPa)**	**Tensile modulus (MPa)**
HIPS	0.81 ±0.02	20.70 ±0.62	3045.68 ±81.42
Coconut fibers (10%)/HIPS composites	0.78 ±0.04	20.83 ±0.12	3146.90 ±242.01
Coconut fibers (30%)/HIPS composites	0.62 ±0.03	23.00 ±0.62	3977.34 ±133.80

(Reinforcement in wt%)

Treated coconut fibers/HIPS composites show decrease in elongation at break compared to the pure HIPS, which confirms the reinforcement in the matrix. However the reinforcement was not effective to increase resistance coconut fibers (10%)/composite. On the other hand, the addition fibers can contribute to the strength and modulus increase, which exhibited an increase of 31%, compared to the pure HIPS. Therefore amount reinforcement influenced in the mechanical properties and these results may be explained by the poor interaction observed between fibers and matrix during the mixture process, confirming that the chemical treatment it was not good to improves the fiber and matrix adhesion. This can be observed by the fracture surface on the Fig 3.

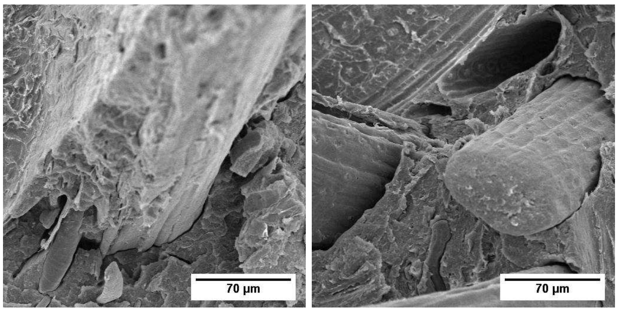

(a) (b)

Fig. 3. SEM of treated coconut fibers/HIPS composites (500x)
(a) 10 wt%; (b) 30 wt%.

4. CONCLUSIONS

The chemical treatment on the surface of coconut fibers it was responsible to remove the extractive and increasing the roughness of the surface, but in the other hand it was not totally effective to improve the adhesion between the fiber and matrix. The lack of adhesion can be also observed in the results of tensile tests that showed small variation of the average values of tensile strenght.

ACKNOWLEDGMENT

The authors want to be grateful FAPESP and Capes for fellowships and financial support.

REFERENCES

BESSADOK,A.;ROUDESLI,S.;MARAIS,S.;FOLLAIN,N.;LEBRUN,L.(2009). Alfa fibres for unsaturated polyester composites reinforcement: Effects of chemical treatments on mechanical and permeation properties. *Composites: Part A., 40,184-195.*

EL-TAYBE, N.S.M. (2009). Development and characterisation of low-cost polymeric composite materials. *Materials and Design., 30,1151-1160.*

GU, H. (2009). Tensile behaviours of the coir fibre and related composites after NaOH treatment. *Materials & Design*, 30, 3931-3934.

JÚSTIZ-SMITH,N.G.;VIRGO,G.J.; BUCHANAN,V.E. (2008). Potential of Jamaican banana, coconut coir and bagasse fibres as composite materials. *Materials Characterization.,59, 1275-1278.*

SPINACÉ, M.A.A.; LAMBERT, C.S.; FERMOSELLI,K.K.G.;DE PAOLI, M.A. (2009). Characterisation of lignocellulosic curaua fibres. *Carbohydrate and Polymers., 40,1151-1160.*

Development and mechanical characterisation of polypropylene composites with different micro- and nano-sized fillers

L. Famá, E. Pérez, C. Bernal
Advanced Materials Group, INTECIN (UBA-CONICET), Department of Mechanical Engineering– Engineering Faculty, University of Buenos Aires
Av. Paseo Colón 850 – C1063ACV – Buenos Aires, ARGENTINA
V. Alvarez, C.J. Pérez
Polymer Division. Materials Science and Technology Research Institute (INTEMA)
National University of Mar del Plata - National Research Council (CONICET),
Av. Juan B. Justo 4302 - B7608FDQ - Mar del Plata, ARGENTINA

ABSTRACT

In this work, polypropylene (PP) and different fillers (organo-modified clay, SiO_2 nanoparticles, Al_2O_3 nanoparticles or $CaCO_3$ particles) were mixed in an intensive mixer. Uniaxial tensile tests and falling weight impact tests were performed for the matrix and the different composites. All composites obtained were stiffer than neat matrix in agreement with expectations. The composite with $CaCO_3$ also exhibited improved ductility and tensile toughness in comparison to other materials without any loss in tensile strength. However, biaxial impact response of all composites was worse than that of the matrix. SEM observations showed that all fillers were mostly present as big aggregates which could in part responsible for the mechanical behaviour observed.

1. INTRODUCTION

The incorporation of inorganic fillers into polymers is a widely used practice in industry to obtain materials with improved physical and mechanical properties such as stiffness, strength, fracture resistance, impact toughness, wear resistance, hardness, among others (Fu et al. 2008), (Kiss et al. 2007). Good processability at low cost is also required.

The composite mechanical properties are strongly related to the matrix (nature, crystallization, morphology) (Mukhopadhyay et al. 2003), filler (size, surface area, aspect ratio, surface treatment, volume fraction, dispersion of the fillers and its adhesion to the matrix) (Fu et al. 2008, Thio et al. 2004, Wu et al. 2002) and processing conditions (rheological conditions, moulding temperature, cooling rate) (Díez-Gutiérrez et al. 1999, Mukhopadhyay et al. 2003). Advantages from the incorporation of fillers can only be obtained if they do not form aggregates (Kiss et al. 2007).

In this work, polypropylene (PP) based composites with 5 wt. % of different fillers (organo-modified clay, SiO_2 nanoparticles, Al_2O_3 nanoparticles or $CaCO_3$ particles) were prepared. The aim of this work was to study the effect of the incorporation of these fillers in the materials mechanical behaviour.

2. EXPERIMENTAL

A commercial grade PP homopolymer (PP 1100N) delivered by Petroquímica Cuyo, (Mendoza, Argentina), with a melt flow index of 11g/10 min and a density of 0.9 g/ml was used as the matrix of the composites. PP and 5 wt. % of different fillers: organo-modified clay, SiO_2 nanoparticles, Al2O$_3$ nanoparticles or $CaCO_3$ particles were mixed in an intensive mixer at 190 ºC and 100 r.p.m. Then, composites films were compression moulded in a hydraulic press by 50 bar at 190 °C for 10 min. The morphology of the composites was determined from SEM micrographs of cryogenic fracture surfaces.

Uniaxial tensile tests were performed on dog-bone specimens in an Instron dynamometer 4467 at 5 mm/min in accordance with ASTM D-638-02 standard recommendations. Stress–strain curves were obtained from these tests. Young's modulus, tensile strength, ultimate strain and tensile toughness were determined from these curves. A minimum of 4 specimens were tested for each system, the average values of the mechanical parameters and their standard deviations were calculated.

Biaxial impact tests were also carried out in a falling weight Fractovis (Ceast, Italy) at 1 m/s on discs. Fracture energy was determined from these tests.

3. RESULTS AND DISCUSSION

Figure 1 shows typical nominal tensile stress-strain curves for the PP matrix and the different composites investigated. Neat matrix and the composites with Al_2O_3 or $CaCO_3$ displayed some degree of strain softening, being the latter the composite with the highest ductility and toughness among all materials as it will be shown later. The composites with SiO_2 nanoparticles or clay, on the contrary, completely failed at maximum stress without any signs of strain softening. As a result, they exhibited lower ductility and toughness in comparison to other materials. In spite of the significant differences in the tensile behaviour observed among the different composites investigated, fractured samples were macroscopically similar with no necking before fracture.

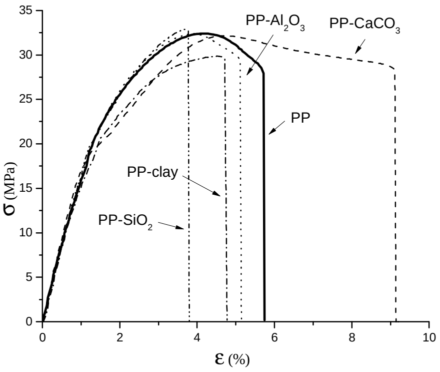

Figure 1. Nominal stress-strain curves for the PP matrix and the composites.

As it can be observed in Table 1, the incorporation of the fillers into PP led to slightly stiffer materials than neat matrix as expected from the incorporation of rigid fillers into a polymer, whereas tensile strength was not significantly changed. It should also be noted that strain at break and tensile toughness was also considerably improved by adding $CaCO_3$ to PP.

Material	Young´s modulus, E (MPa)	Ultimate strength, σ_u (MPa)	Strain at break, ε_b (%)	Tensile toughness (J)	Fracture energy (J/m)	Volume fraction (%)
PP	1.55±0.03	32.79±1.12	5.7±0.1	1.44±0.01	754±96	-------
PP-Al_2O_3	1.57±0.05	32.83±0.64	5.45±0.5	1.36±0.15	432±59	1.2
PP-$CaCO_3$	1.75±0.02	33.00±1.22	9.55±0.07	2.45±0.07	363±20	1.6
PP-Clay	1.73±0.07	29.83±0.01	4.3±0.5	0.96±0.11	322±87	2.8
PP-SiO_2	1.69±0.04	32.48±0.55	3.65±0.07	0.80±0.05	302±19	2

Table 1. Mechanical properties of the PP matrix and the different composites.

Fully brittle force-displacement traces were obtained in biaxial impact tests for all materials (Figure 2). The composites (Table 1) displayed significantly worse mechanical performance under out-of-plane impact loading than the PP matrix, probably as a result of the restriction to matrix plastic deformation imposed by the rigid fillers at the high strain rates of impact (Antich et al., 2006) and/or a poor dispersion of the fillers in the matrix.

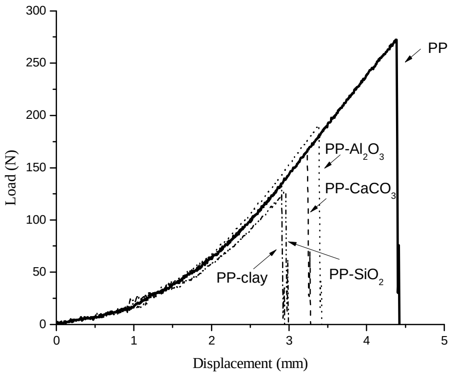

Figure 2. Force-time records obtained under out-of-plane impact loading.

The morphology of the composites was studied by SEM (Figure 3). It was observed that all fillers were mostly present as big aggregates which could be partially the reason for the mechanical performance obtained in our composites as stated before.

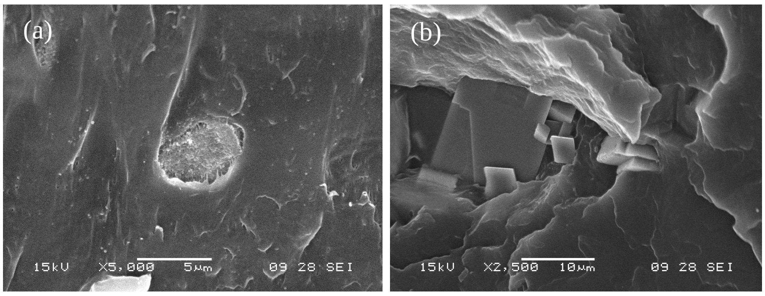

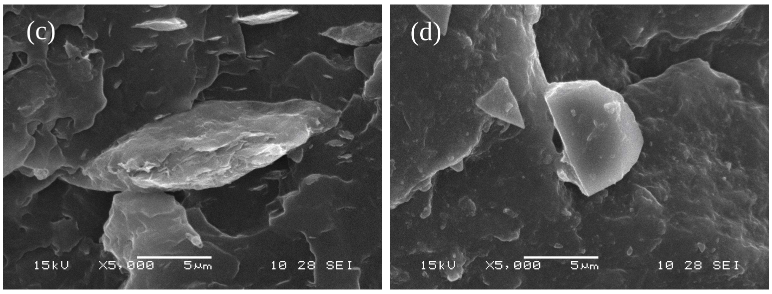

Figure 3. SEM micrographs of the fracture surfaces of the different composites. (a) PP-Al_2O_3, (b) PP-$CaCO_3$, (c) PP-Clay, (d) PP-SiO_2.

4. CONCLUSIONS

In this work, different micro- and nano-sized composites were developed and mechanically characterised.

All composites exhibited higher stiffness values than neat matrix as expected from the addition of less compliant fillers to the polymer matrix whereas tensile strength values were not significantly different from that of PP.

The composite with $CaCO_3$ also exhibited improved ductility and tensile toughness respect to the other materials.

However, in biaxial impact tests, all composites displayed lower fracture energy values than the PP matrix. This could be explained in terms of the restriction to matrix plastic deformation imposed by the rigid fillers especially at the high strain rates of impact and/or the poor dispersion of fillers in the matrix confirmed by SEM.

Further work is in progress to develop PP composites with higher amount of fillers and with MAPP as a coupling agent in order to improve the dispersion of the filler and the adhesion between components and therefore, to change the composites properties.

REFERENCES

ANTICH, P., VÁZQUEZ, A., MONDRAGON, I, BERNAL, C. (2006). Mechanical Behavior of High Impact Polystyrene Reinforced with Short Sisal Fibers. *Composites, Part A*, 37, 139-150.

DÍEZ-GUTIÉRREZ, S., RODRÍGUEZ-PÉREZ, M. A., DE SAJA, J. A., VELASCO, J. I. (1999). Dynamic mechanical analysis of injection-moulded discs of polypropylene and untreated and silane-treated talc-filled polypropylene. *Polymer*., 40, 5345-5353.

FU, Y. S.-Y., FENG, X.-Q., LAUKE, B., MAI, Y.-W. (2008). Effects of particle size, particle/matrix interface adhesion and particle loading on mechanical properties of particulate-polymer composites. *Composites Part B: engineering*, 39, 933-961.

KISS, A., FEKETE, E., PUKÁNSZKY, B. (2007). Aggregation of $CaCO_3$ particles in PP composites: Effect of surface coating. *Composites science and technology*, 67, 1574-1583.

MUKHOPADHYAY, S., DEOPURA, B. L., ALAGIRUSWAMY, R. (2003). Interface behavior in polypropylene composites. *Journal of Thermoplastic Composite Materials*, 16, 479-494.

THIO, Y. S., ARGON, A. S., COHEN, R. E. (2004). Role of interfacial adhesion strength on toughening polypropylene with rigid particles. Polymer, 45,3139-3147.

WU, C. L., ZHANG, M. Q., RONG, M. Z., Klaus, F. (2002). Tensile performance improvement of low nanoparticles filled-polypropylene composites. *Composites science and technology*, 62, 1327-1340.

Local effects on the fibre-matrix interfacial adhesion testing in fibre reinforced composites by the pushin/push-out test

J.M. Molina-Aldareguia[1], M. Rodriguez[1], C. González[1,2], J. Llorca[1,2]
[1]IMDEA-Materials, c/ Profesor Aranguren s/n, 28040 Madrid (Spain)
[2]Dept of Materials Science, Escuela de Ingenieros de Caminos, Polytechnic University of Madrid, c/ Profesor Aranguren s/n, 28040 Madrid (Spain)
*jon.molina@imdea.org

ABSTRACT

The strength and toughness of composites depend on the properties of the fiber/matrix interface. Thus, a method for quantifying the interfacial properties must be established to support the design and computational micro-mechanical modeling of fiber-reinforced composites. Nevertheless, the evaluation of interfacial properties remains a controversial issue among researchers of composite materials due to experimental and interpretation difficulties.

Several methods exist to test interfacial adhesion in composite materials such as pull-out, microbond and push-in/push-out tests. Some of them can only be applied to single fibre matrix composites, like the microbond test, and others are difficult to perform on brittle fibres due to premature fracture of the fibre. Push-in/push-out tests, consisting on pushing the fibre with a microindenter on a bulk specimen (push-in) or a thin membrane (pushout), constitute a powerful technique that can be applied directly on a composite laminate. However, the interfacial adhesion values obtained from different tests (microbond, push-in) often differ and even the results from one type of test are subjected to a large scatter. This is partly due to the fact that the existing analytical solutions that are typically used to interpret the experimental data do not take into account the constrain effect of the surrounding fibres and/or the partial decohesion of the matrix/fibre interface.

To overcome this limitation, we have carried out a careful micromechanical modeling of the push-out/push-in test, coupled with experimental adhesion testing in a glass fibre reinforced epoxy matrix composite. The models address the interfacial fracture process, utilizing interface cohesive elements at the fiber–matrix interface. The results focus on constrain effects due to the local configuration of the surrounding fibers and help determine the required distance from the tested fiber to its surrounding neighbors to minimize the constraint effect on the measured interfacial properties.

Utilización simultánea de técnicas de MDSC y fotocalorimetría en el estudio de la vitrificación y el curado de fotopolímeros

C.A. Gracia-Fernández, C. Del Rio, D. Dávila, P. Davies
TA Instruments división de Waters Cromatografía, Avda. Europa, 21 Parque
Empresarial La Moraleja 28108- Alcobendas Madrid
cgracia@tainstruments.com

RESUMEN

Con el desarrollo de polímeros cuya reacción de curado es iniciada o catalizada por luz UV/visible, la fotocalorimetría se convierte en una técnica básica para el estudio de dichos materiales. En este trabajo se presentan datos en los que se combina la técnica de MDSC (Modulated DSC) con la fotocalorimetería por lo que es posible obtener tiempos de vitrificación en curados isotermos a través del seguimiento de la Capacidad Calorífica. Se ha estudiado el comportamiento de dichos tiempos de vitrificación en función de la intensidad de luz y de la temperatura de curado isotermo. Se ha visto que el tiempo de vitrificación es muy dependiente de la intensidad de luz y muy poco dependiente de la temperatura de curado en un rango de temperaturas entre 25 y 45º C.

1. INTRODUCCIÓN

Es sabido que los polímeros termoendurecibles son en la actualidad uno de los tipos de polímeros con más proyección tanto a nivel científico como industrial. Con el objetivo de monitorizar el curado de este tipo de materiales se utiliza de forma extensa la calorimetría diferencial de barrido así como la calorimetría diferencial de barrido modulada. Dicho proceso de curado puede realizarse utilizando calor o una fuente de luz ultravioleta. (Bruce Prime, 1997) por lo que la fotocalorimetría se convierte en una herramienta fundamental en el estudio de este tipo de materiales. La fotopolimerización se basa fundamentalmente en dos mecanismos 1) la propagación por radicales libres con acrilatos o metacrilatos (Joshi et. Al. 1963) (como en este caso) o 2) la apertura del anillo epoxídico y la adicción de enlace doble con esteres vinílicos. La información que proporciona la técnica de MDSC es extremadamente valiosa. La MDSC ha sido utilizada con éxito por ejemplo, en la obtención de tiempos de vitrificación en curados isotermos, Hasta el momento, la técnica de MDSC no así sido utilizada en combinación con el proceso de curado mediante luz UV. En este trabajo se propone un nuevo tipo de ensayos en los que se combina la calorimetría diferencial de barrido modulada con el curado a través de luz ultravioleta.

2. EXPERIMENTAL

Los ensayos calorimétricos se realizaron en modo isotermo a 3 temperaturas diferentes y 3 intensidades de luz diferentes para observar la influencia de dichos parámetros en el proceso de curado y en el tiempo de vitrificación.

2.1 Materiales Utilizados

La muestra utilizada ha sido un producto commercial denominado Reactmer Paste (Shofu Inc.). El material se comercializado en único contenedor por lo que no es necesario que el usuario realice la mezcla. Este material es utilizado en aplicaciones dentales como por ejemplo empastes. Parte de la composición de este producto es: Fluoroaluminosilicato en estado vítreo y ácido 4-acriloxietiltrimetilitico y resina de dimetacrilato.

2.2 Técnicas Utilizadas

Las medidas de MDSC fueron realizadas con un Q2000 (TA Instruments). Las calibraciones de temperatura, flujo de calor, y capacidad calorífica, fueron realizados mediante estándares de indio y zafiro. Las condiciones de modulación utilizadas en los ensayos de curado isotermo fueron: amplitud de 0.5 K y periodo de 40 s. La masa de las muestras fue aproximadamente de 10-14 mg. El flujo de gas e purga de nitrógeno fue de 50 ml min^{-1}. Las Temperaturas de ensayos han sido 25, 35 y 45º C. En la calorimetría diferencial de barrido modulada se superpone una modulación sinusoidal (oscilación) a la rampa de enfriamiento o calentamiento lineal convencional para proporcionar un perfil, en el cual, la temperatura media de la muestra cambia de forma continua con el tiempo pero no de manera lineal. Se define entonces el módulo de la capacidad calorífica reversing como:

$$C_{prev} = K_{c_p} \frac{A_{HF}}{A_T w} \qquad (1)$$

Donde T_0 es la temperatura inicial del experimento, β es la velocidad de calentamiento, A_T es la amplitud de la onda sinusoidal de temperatura, w es la frecuencia de la oscilación. A_{HF} la amplitud del flujo de calor modulado y K_{Cp} es una constante de calibración. El estudio de la reacción de curado se basa en las medidas de flujo de calor total lo cual nos permite calcular el grado de conversión α de la misma forma que en DSC convencional. El estudio del fenómeno de la vitrificación se basa en la evolución de la Cp_{rev} (Swier S. et. al. 1999).

La fotocalorimetría involucra la introducción de una luz UV/Visible a una muestra a la vez que se realiza el ensayo calorimétrico. Estos experimentos miden el calor emitido por la muestra durante la reacción iniciada por los fotones de longitud de onda determinada. Generalmente la intensidad de dicha luz es medida por un radiómetro externo. Un nuevo accesorio de fotocalorimetría ha sido desarrollado a la par de la de la tecnología Tzero. Por lo tanto, es posible medir simultáneamente la energía incidente en el termopar de referencia y en el termopar de muestra, realizar ensayos en dos muestras simultáneamente y lo que nos ocupa en este trabajo, la posibilidad de realizar ensayos de MDSC® en modo quasi-isotermo ala vez que el propio experimento de fotocalorimetría. El fotocalorímetro utilizado utiliza el diseño de fotometría de filtros con una lámpara de mercurio de ata presión que proporciona una rango de luz con un rango espectral de 250 a 650nm. Dicho rango se puede acotar a 320 hasta 500 nm con los filtros adecuados. La intensidad de luz es ajustable entre 1 y 2000 mW/cm^2 (0.01 a 20 kW/m^2).

3. RESULTADOS EXPERIMENTALES

En la Figura 1 se muestra un resultado típico de un curado por luz UV/Visible. Después de permanecer en régimen isotermo 10.5 min. el programa de control dispara la luz UV/Visible que incide simultáneamente sobre la cápsula abierta de muestra y sobre la cápsula de referencia . Dicha luz fotoinicia la reacción de curado que es medida por el DSC. En el análisis de dicho flujo de calor puede utilizarse el método de las derivadas parciales con lo que tendríamos la conversión en función del tiempo para esa temperatura. Si se quisiera tener en cuenta que la energía de curado durante dicho pulso puede no ser la del curado total podríamos obtener la curva de la conversión referenciada a la conversión obtenida en ese isotermo durante ese tiempo de exposición a la luz.

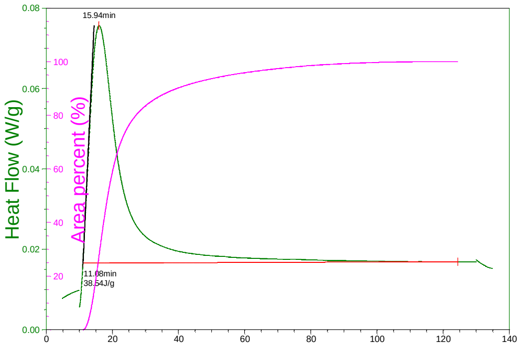

Fig. 1. Flujo de Calor y conversión en función del tiempo para un fotocurado.

Tal y como se ha comentado, mediante MDSC, es posible obtener la evolución de la capacidad calorífica en función del tiempo lo que proporciona información acerca del tiempo de vitrificación de manera directa como punto de inflexión de la disminución de la Cp en dicha vitrificación. Este parámetro es importante ya que marca el paso de control químico de la reacción a control difusivo.

En la Figura 2 se muestra la evolución de dicha capacidad calorífica en función del tiempo. Se ha tomado como tiempo de vitrificación al mínimo en la derivada del Cprev que matemáticamente es el punto de inflexión de la Cprev.

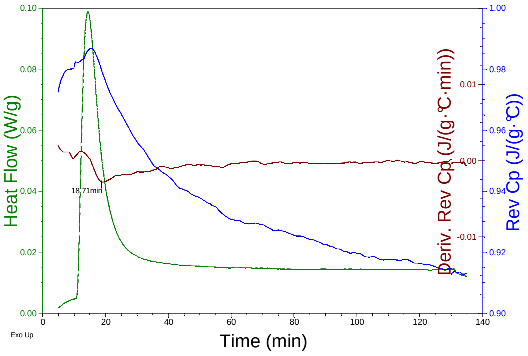

Fig. 2. Flujo de Calor, Cprev y derivada de la Cprev en función del tiempo.

Dichos valores de tiempos de vitrificación se han obtenido para varias intensidades de luz a la temperatura de 25 ºC (Tabla 1) así como para varias temperaturas a las intensidad de 2.3 mW/cm^2 (Tabla 2).

Intensity (mW/cm2)	Vitri Cp rev
6.8	3.2
2.3	10.4
1.5	46

Tabla 1. Tiempos de vitrificación en función de la intensidad de luz a la T de 25 ºC.

Intensity (mW/cm2)	Vitri Cp rev
25	10.4
35	8.4
45	8.3

Tabla 2. Tiempos de vitrificación en función de la temperatura a una intensidad de 2.3 mW/cm^2.

De ambas tablas se deduce que el tiempo de vitrificación y por lo tanto de curado depende enormemente de la intensidad de luz, disminuyendo la aumentar dicha intensidad, así como es prácticamente independiente de la temperatura, al menos en el rango de temperaturas estudiado.

4. CONCLUSIONES

Se deduce de los ensayos del presente estudio que es posible obtener, mediante el uso del MDSC, tiempos de vitrificación a diferentes intensidades de luz o temperaturas en curados fotoiniciados gracias al seguimiento de la capacidad calorífica del material lo que permite a su vez un estudio más profundo de dicho proceso. Los resultados muestran la dependencia del tiempo de vitrificación con la intensidad de luz y la indepencia con la temperatura en el rango de temperaturas estudiado.

REFERENCIAS

PRIME R. B.,(1997) *"Thermosets"*, Thermal Characterization of Polymeric Materials, E. A. Turi (Ed.), Academic Press, Vol. 2, 1997, pp. 1420-1427.
SWIER S.,VAN MELE B.;(1999) *Termoquímica Acta* 330, 175-180. (1999)
JOSHI R. M. MCCURDY K. G., LAIDER K. J., (1963) J. Polymer Sci., 56, 313

Acción de la humedad en el curado de un mortero de polímero a base de resina poliéster

P. Raimonda, C. Mantero, D. Mosca
Instituto de Ensayo de Materiales, Facultad de Ingeniería – UDELAR,
Montevideo, Uruguay

RESUMEN

Los morteros a base de polímeros termo rígidos, con su composición totalmente homogénea gracias a su estudiada y selecta combinación de áridos y resinas, logran mantener unas características físicas y mecánicas excelentes a lo largo del tiempo.

Este material, también llamado hormigón o concreto de polímero, ofrece cualidades muy superiores frente a los materiales tradicionales y ha supuesto un avance decisivo dentro del sector. Su mayor desventaja radica cuando los áridos empleados contienen humedad, ésta interfiere actuando como un agente disociante impidiendo la cohesión entre la matriz de resina y el agregado, resultando un material de menor resistencia.

En este trabajo se estudia la forma de eliminar este problema mediante el uso de agentes desecantes. Para ello se estudian las propiedades mecánicas de los morteros obtenidos corrigiendo el problema de la humedad y se comparan frente a las de un mortero obtenido con arena seca.

Los resultados muestran que el agregado de dichos agentes mejora las propiedades mecánicas del mortero frente a los hechos con arena húmeda pero están por debajo de los valores obtenidos utilizando arena seca. También se observa una acción bastante diferente entre los distintos agentes desecantes y una limitación en la cantidad de humedad que puede contener la arena para ser tratada con los mismos.

1. INTRODUCCIÓN

Los polímeros de concreto (PC) constituyen un material relativamente nuevo, compuesto por un sistema en el cual una resina orgánica actúa como aglomerante de un sistema inorgánico compuesto por grava o arena. Se produce mediante la mezcla de una resina termo rígida en estado líquido y el agregado inorgánico. Para lograr el posterior curado se adicionan iniciadores y/o aceleradores como agentes promotores de la reticulación. Por lo tanto, los polímeros de concreto (PC), consisten en una mezcla de agregados inorgánicos de granulometría predefinida, para lograr mejores propiedades, unidos por una resina en lugar de cemento y agua habituales del concreto tradicional.

Las resinas poliéster, epoxi y metilmetacrilato son las más usadas (Marohn, 1977). Las características más destacadas que hacen de este PC un material de alta calidad frente a uno tradicional son: reducido porcentaje de absorción de agua (Mebarkia et all, 1995), muy buena durabilidad e inalterabilidad frente a las distintas condiciones climáticas, alta resistencia química, muy buena resistencia al choque y a la flexión, rápido tiempo de curado, y un mínimo desgaste por abrasión, etc. (Krauss, et all, 1989; Vipulanandan et all, 1990; Ohama et all, 1979 y Feldman, 1989).

La desventaja principal para su empleo es la existencia de humedad en los áridos, la que actúa como agente disociante, impidiendo la cohesión entre la resina y el árido. La resina al no mojar la superficie del árido impide la correcta adhesión entre ambos ya que las moléculas de agua forman una película envolvente sobre la partícula del agregado evitando su unión directa con la matriz polimérica inhibiendo los enlaces químicos secundarios durante el curado, resultando en propiedades mecánicas inferiores.

El objetivo de este trabajo es estudiar la acción que tiene la incorporación de distintos agentes desecantes para controlar la humedad, comparando las resistencias mecánicas de compresión y de flexión del mortero obtenido. Como referencia se utiliza la misma composición de mezcla con la arena previamente secada. La resina poliéster empleada es del tipo 10203 preacelerada. Como agente de curado se empleó peróxido de metil etil cetona, empleándose como acelerante una solución de octoato de cobalto. El árido utilizado es una arena extraída del río Santa Lucía, Uruguay (tamiz malla 355 milímetros).

2. PARTE EXPERIMENTAL

Para la reticulación de la resina se usó una relación en peso del acelerante del 3.0 % y de catalizador del 0.3 % con respecto a la cantidad de resina utilizada. La composición del mortero: 15 % de resina y un 85 % de árido (Proszek, et all, 2000).

La arena se acondicionó para eliminar la humedad mediante secado durante 24 horas a 110º C. La mezcla de áridos con las distintas proporciones de humedad a ensayar fue preparada a partir de arena seca, mediante el agregado de agua destilada. (Kreis, 1977; Toensmeier, 1989). Para la eliminación del problema de la humedad de los áridos fueron escogidos como agentes desecantes el óxido de calcio (CaO), el sulfato de cobre ($CuSO_4$) y el cloruro de calcio ($CaCl_2$). Para aprovechar su máxima capacidad de absorción, previo a su utilización fueron desecados en estufa durante 24 horas a las temperaturas indicadas en la bibliografía (Hodgman et all, 1957).

Todos los ensayos mecánicos se realizaron según norma EN 196-01:1994.

Las primeras pruebas fueron realizadas sobre morteros de resina con arena seca, obteniéndose así los valores de referencia de las propiedades mecánicas.

Luego se procedió a ensayar formulaciones para observar el efecto del agua en las propiedades del mortero con distintas proporciones de humedad: 1%, 3 %, 5 % y 10%, sin el agregado en este caso de los agentes desecantes.

La siguiente etapa fue repetir la operativa de trabajo con la corrección del problema del agua al agregar el agente desecante. La proporción de este fue función de la capacidad de absorción de cada uno, dejándolo actuar durante 24 horas, pasando luego a la confección de las probetas de ensayo. Los resultados se resumen en las tablas 1 y 2.

Desecante	**Compresión kg/cm^2**	**Flexión kg/cm^2**
Sin	445	91
CaO		
$CuSO_4$	618	142
$CaCl_2$	30	0

Tabla 1. Resultados experimentales obtenidos en morteros con 1 % de humedad

Desecante	**Compresión (kg/cm^2)**	**Flexión (kg/cm^2)**
Sin	-	-
CaO	381	103
$CuSO_4$	455	99
$CaCl_2$	42	10

Tabla 2. Resultados experimentales obtenidos en morteros con 3 % de humedad

3. DISCUSIÓN DE LOS RESULTADOS

De la parte experimental se observó que:

Para las probetas de referencia, obtenidas con arena seca, era posible desmoldarlas a los 30 minutos de elaboradas. El tiempo disponible de manipulación era de 15 minutos aproximadamente, después del cual el material se hacía muy difícil de procesar. Para el caso de las probetas con humedad este tiempo podía llegar hasta los 45 minutos.

Las probetas con 1% de agua y sin agente desecante, endurecieron al cabo de 2 horas.

Las probetas con una humedad del 3% y sin agente desecante, no endurecieron al cabo de las 2 horas, estando endurecidas y prontas para desmoldar a las 24 horas.

Para las probetas con 5% de agua, sin agregado de agentes desecantes, si bien fue posible desmoldarlas no tenían la consistencia adecuada a las 2 horas, la que lograban después de 72 horas, por lo cual fueron descartadas, lo que descartó la realización de los ensayos de probetas obtenidas con agentes desecantes y con esa proporción de humedad.

Las probetas con una humedad del 10% y sin agregado de desecante no curaron.

Las probetas con una humedad del 1% y con cualquiera de los agentes desecantes, endurecieron al cabo de 2 horas y era posible desmoldarlas.

Las probetas con una humedad del 3% y con agregado de desecante, sólo las que contenían $CuSO_4$ endurecieron al cabo de 2 horas, pudiendo ser desmoldadas a las 24 horas.

De los resultados se observa que:

Sólo en el caso del $CuSO_4$ como agente desecante se obtuvieron prácticamente los mismos valores de resistencia a la compresión que los obtenidos con arena seca.

Los valores de resistencia a la flexión en todos los casos fueron inferiores al valor de referencia, siendo el más próximo el material que utilizó $CuSO_4$. Con la utilización del CaO se logran mejorar los valores con respecto al material húmedo pero no se alcanza a corregir completamente el problema de la humedad.

Las probetas que utilizaron $CaCl_2$ no reflejaron en sus valores la mayor capacidad de secado de este agente debido a su reacción extremadamente rápida con la humedad ambiente a pesar de las precauciones tenidas en el proceso.

4. CONCLUSIÓN

Si bien la formulación utilizada para el mortero de polímero no fue optimizada para obtener los mejores valores de las propiedades evaluadas, si sirve para estudiar el efecto de la humedad en el valor de las mismas y como se puede solucionarse mediante el agregado de agentes desecantes.

Solo con un tipo de agente desecante, el sulfato de cobre, se logra corregir el problema del agua y se obtienen valores similares a los obtenidos con arena seca.

Con los otros agentes se observa que los valores de las propiedades mecánicas mejoran con respecto a los obtenidos con arena húmeda pero no llegan a los valores que se obtienen con arena seca.

Con contenidos de humedad en el árido superiores al 5 % el efecto del agente desecante no es adecuado ya que comienza a incidir en las propiedades la presencia del mismo utilizado al afectar la relación arena resina del mortero.

BIBLIOGRAFIA

FELDMAN D. Polymmeric Building Materials, USA, Elsevier Applied Science, 1989.

HODGMAN, C., WEAST, R., SELBY, S. Handbook of Chemistry and Physics, USA, Chemical Rubber Publishing Co., 1957.

KRAUSS, PAUL D. El hormigón de polímero ayuda a mantener el movimiento del tráfico con mantenimiento mínimo. Revista de plásticos modernos, v40, N 396 p. 909-910, 1989.

KREIS, REINER, Posibilidades de aplicación del hormigón de resina sintética, Revista de plásticos modernos, XXVIII, N249, p.379-382, 1977

KREIS, REINER. Máquinas y equipos para fabricar, transformar y trabajar hormigón a base de resinas sintéticas, Revista de plásticos modernos,XXVIII, N252, p. 843-846, 1977.

MAROHN, KLAUS. Elementos de hormigón a base de resinas sintéticas para construcciones subterráneas, Revista de plásticos modernos, v XXVIII, N251, p. 691-695, 1977.

MEBARKIA S., VIPULANANDAN C., Mechanical properties and water difusión in poliéster polymer concrete, Journal of Engineering Mechanics, v121, N 12, p. 1359-1365, 1995

OHAMA, Y., DEMURA, K., KOMIYAMA M., Length Change of Polyester Resin Concrete, Plastic Mortars, Selants and Caulaking Compounds, v79, N 47 p. 67-78, 1979.

PROSZEK, J., DAL MOLIN, D.C., DE SOUZA, C., PAULETTI, C., Concreto polimero, In. XXIX Jornadas Sudamericanas de Ingeniería Estructural, -Jubileo Prof. Ricaldoni, 2000, Punta del Este, Uruguay.

SEYMOUR, RAYMOND B. Avances en hormigón plástico, Revista de plásticos modernos, XXXIV, N327, p. 309-310,1983.

TOENSMEIER, PATRICK A., ¿Cuál es el futuro del moldeo de hormigón de polímero?, Revista de plásticos modernos, v40, N395, p. 750-752, 1989.

Effect of chemical modification on mechanical properties of textile fibers/HDPE composites

C.A.A. Lima
'Universidade Federal de Alfenas, Campus Poços de Caldas, Brazil
D.R. Mulinari, H.J.C. Voorwald, M.O.H. Cioffi, P.H. Ozaki
Grupo de Fadiga e Materiais Aeronáuticos (DMT/FEG). Universidade Estadual Paulista, Brazil

ABSTRACT

In the work, mechanical properties of textile fibers/HDPE composites were studied. Residues textile fibers were treated with 10% sulfuric acid solution, followed by centrifugation, to remove impurities such as waxes, pectins and hemicellulosics fibers and analyzed by FTIR. These fibers were mixed with the polymeric matrix (HDPE) in a thermokinetic mixer, model MH-50H, with speed rate maintained at 5250 rpm, in which fibers were responsible for 5 to 15 wt% in the composition. After the mixture, composites were dried, ground in mill and placed in an injector camera according to ASTM D-638 specification. Results showed the addition of fibers in matrix increased the tensile strength and modulus compared to the matrix polymeric.

1. INTRODUCTION

The utilization of lignocellulosic materials in the production of polymeric composites is attractive particularly because of low cost and high volume applications, as well as advantages other, low density, availability of renewable natural resources, biodegradability and the concern with environment (Satyanarayana *et al*., 2008; Farag, 2008).

Many studies have been developed on composites containing natural lignocellulosic fibers from agroindustrial or agricultural residues (Zah *et al*., 2008; Lei *et al*., 2007). Depending on their origin, natural fibers can be grouped into bast (jute, flax, hemp, kenaf), leaf (pineapple, sisal, henequen), and seed or fruit fibers (coir, cotton, oil palm). Cellulose is the main component of natural fibers, and the elementary unit of a cellulose macromolecule is anhydro-Dglucose, which contains three hydroxyl (OH) groups. However, the hydrophilic nature of these natural fibers is a major disadvantage for their application as reinforcement for polymeric composites.

There are several strategies of surface modifications to improve the compatibility between cellulose fibers and polymer matrices. The methods for surface modification can be physical or chemical according to the way they modify the fibre surface. Other frequently used treatments are bleaching, esterification, silane treatment, use of compatibilizer, plasma treatment, acetylation, alkali treatment and treatment with other chemicals (Mulinari *et al*., 2009; GU, 2009).

Many researches have been conducted to study the mechanical properties, especially interfacial performances of the composites based on natural fibers due to the poor interfacial bonding between the hydrophilic natural fibers and the hydrophobic polymer matrices (Li *et al*., 2008; Luz *et al*., 2008).

The objective of this work was to study the effect of chemical modification on mechanical properties of residue textile fibers/HDPE composites.

2. EXPERIMENTAL

2.1 Chemical modification residue textile fibers

To remove the soluble extractives and to facilitate adhesion between fibers and matrix, the residue textile fibers were modified by pre-treatment with 10% sulfuric acid solution, followed by centrifugation.

2.2 FTIR characterization

The chemical structure of textile fibers modified and non-modified was evaluated by FTIR. FTIR spectra were obtained on a FTIR spectrophotometer (Perkin Elmer). Samples were prepared by mixing the materials and KBr in a proportion 1.5:300 (w/w). For all spectra, 16 scans were accumulated with a 4 cm^{-1} resolution.

2.3 Composites preparation

Residue textile fibers modified were mixed with the HDPE in a thermokinetic mixer, model MH-50H, with speed rate maintained at 5250 rpm, in which fibers were responsible for 5 to 15 wt% in the composition. After the mixture, composites were dried and ground in mill, model RONE. Composites and pure HDPE were placed in an injector camera at 165 ^{o}C and 2 °C min^{-1} heating rate in a required dimensions pre-warm mold to obtain tensile specimen.

2.4 Mechanical properties

The mechanical strength of residue textile fibers reinforced HDPE composites was determined using an INSTRON universal-testing machine (model 8801). Tests were carried out according to ASTM standards D638 with 10 $mm.min^{-1}$ crosshead speed. Tensile strength and modulus values are average results of five tested specimens.

3. RESULTS AND DISCUSSION

3.1 FTIR characterization

Infrared spectra of residue textile non-modified and modified are displayed in Fig. 1.

The most visible differences between the spectra of residue textile fibers modified and modified are the modifications of the signal at 2885 cm^{-1} and 1732 cm^{-1}, characteristics of the stretching of symmetrical CH groups and stretching of unconjugated CO groups present in polysaccharides and xylans. Considering the first region, the ratio between intensity of the C-H stretching band (~2900 cm^{-1}) is lower in the spectrum of the residue textile fibers modified material than that observed for the residue textile fibers non-modified. On the other hand, at the second region it may be observed modifications, especially in the ratio between the intensities of the C=O stretching band (~1730 cm^{-1}).

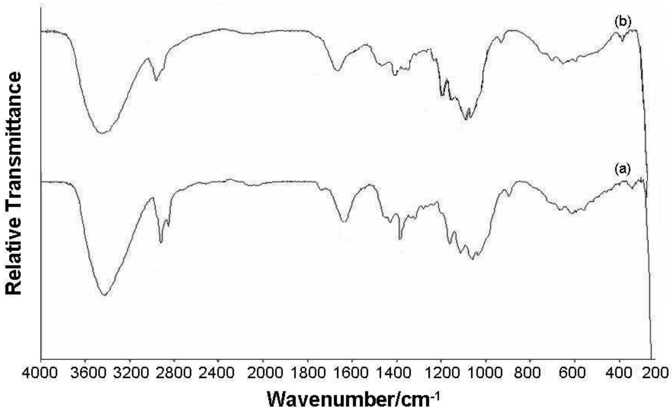

Figure 1. FTIR spectra: (a) residue textile non-modified (b) residue textile modified.

3.2 Mechanical Properties

Table 1 indicates the mechanical properties of residue textile fibers/HDPE composites and pure HDPE, in special the effect of chemical modification on residue textile fibers. Residue textile fibers/ HDPE composites show decrease in elongation at break in comparison to high-density polyethylene. With respect to tensile strength, it was obtained higher average value compared to the pure HDPE, but composites presented results similar. Therefore an amount reinforcement influenced in the tensile modulus.

Table 1. Mechanical properties of the composite.

Samples	*Properties*		
	Elongation at break (%)	*Tensile strength (MPa)*	*Tensile modulus (MPa)*
HDPE	8.9 ± 0.8	15.7 ± 1.1	732.45 ± 90.6
Residue textile fibers modified/HDPE 5%	7.2 ± 0.05	24.1 ± 0.3	1364.1 ± 42.3
Residue textile fibers modified/HDPE 15%	6.2 ± 0.01	23.9 ± 0.15	1557.3 ± 14.25

Reinforcement in wt%.

These results may be explained by the good interaction observed between fibers and matrix during the mixture process, confirming that fibers modification improves the fiber and matrix adhesion. This can be observed by the fracture surface. SEM micrograph of the fractured surface for the composite is shown in Fig. 2. It corresponds to surface of fractured residue textile fibers/HDPE composite 15 wt%.

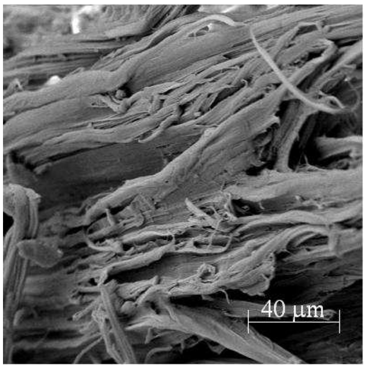

Figure 2. SEM of residue textile fibers modified (15 wt%)/HDPE composite 1000X.

4. CONCLUSIONS

The use of residue textile fibers as an alternative reinforcement in thermoplastics was verified. Modified fibers were studied to demonstrate the effect on mechanical properties and the practicability of processing these fibers with thermoplastics. Results were successfully accomplished and it was verified an improvement in the tensile strength and modulus compared to the high-density polyethylene.

ACKNOWLEDGEMENTS

The authors are grateful for the research support by CAPES.

REFERENCES

FARAG, M.M. (2008). Quantitative methods of materials substitution: Application to automotive components. *Materials & Design*, 29, 374-380.

GU, H. (2009). Tensile behaviours of the coir fibre and related composites after NaOH treatment. *Materials & Design*, 30, 3931-3934.

LEI Y, WU Q, YAO F, XU Y. (2007). Preparation and properties of recycled HDPE/natural fiber composites. Compos Part A, 38, 1664–1674.

LI, Y., HU, C., YU, Y. (2008). Interfacial studies of sisal fiber reinforced high density polyethylene (HDPE) composites. *Compos. Part A*, 39, p.570-579.

LUZ, S. M., DEL TIO, J., ROCHA, G. J. R., GONÇALVES, A. R., DEL'ARCO, A. P. (2008). Cellulose and cellulignin from sugarcane bagasse reinforced polypropylene composites: Effect of acetylation on mechanical and thermal properties. *Compos. Part A*, 39, p1362–1369.

MULINARI, D.R., VOORWALD, H.J.C., CIOFFI, M.O.H., DA SILVA, M.L.C.P., DA CRUZ, T.G., SARON, C. (2009). Sugarcane bagasse cellulose/HDPE composites obtained by extrusion. *Compos. Sci. Technol.*, 69, 214-219.

SATYANARAYANA, K.G., GUIMARÃES, J.L., WYPYCH, F. (2008). Studies on lignocellulosic fibers of Brazil. Part I: Source, production, morphology, properties and applications. *Compos Part A,*, 38, 1694–1709.

ZAH R, HISCHIER R, LEÃO AL, BRAUN I. (2007). Curauá fibers in the automobile industry - a sustainability assessment. J Cleaner Prod, 15, 1032-40.

Fly ash composites as insulation in circular pipes

A.L. Pande
CIET, Raipur (C.G.), India
G.P. Naik
Dy. Director DTE Govt. of C.G.
Raipur, India
Correspondence Address: alpande@gmail.com

Abstract

Fly ash, the waste product of thermal power plants, may become threat to environment if proper disposal/use of it is not found out. Fly ash only about 15% is used for different purpose like making bricks, concrete, cement and roads etc. out of approximately 100 million ton the rest is used for landfills or simply lying on the site of disposal. There is a need to find out the other area for use. In this backdrop an effort is made to find out whether fly ash with some other material like plaster of paris or cement as composites could be used as insulation.

The main processes adopted are as follows:

Different samples of different composition of ash, cement, lime and plaster of paris is made and its physical properties like density, strength water absorption, thermal conductivity are observed. Finally only two composites are selected for experimental work as lagging, one is 70% ash, 10% cement, 10% lime and 10% plaster of paris named composite-A and the other 50% ash and 50% plaster of paris named composite-B.

The molding process with the help of a concentric PVC pipe was tedious process. It takes a lot of time to finally shape up a consistent and durable lagging over a C.I. pipe. After drying of lagging the temperature drop is recorded for different fixed length of pipe in case of bare (unlagged) pipe and lagged pipes with the two composites at different flow rate 95, 85, 75, 65, 55, kg/hr and inlet temperature 50^0, 60^0 & 70^0 C as variables. Atmospheric temperature is also noted. Based on these data the % heat loss and over all heat transfer coefficient are calculated. A graph for temperature drop, a chart for percent heat loss and a graph for over all heat transfer is plotted with distance, flow rate and inlet temp. From the results it can be concluded that both the composites behave like insulation where lagging-A gives 7% less heat loss in comparison to bare; it is 10% in case of lagging-B. Future scope in this area is required with a broad range of composition and thickness of composites, flow rate and inlet temperature as variables. So that final claim can be made about its feasibility, durability, viability as insulation.

Polymer composites as advanced materials for aerospace aplications

[1]I. Dinca, [2]A. Bara, [2]C. Banciu, [1]A. Stefan, [1]A. Stan , [1]S. Gaman,
[1]V. Manoliu, [2]D. Patroi, [2]V. Marinescu
[1] National Institute for Aerospace Research "Elie Carafoli", Iuliu Maniu 220 Bd.,
Bucharest, Romania
[2] National Institute for Research and Development in Electrical Engineering ICPE-CA
Bucharest, 313 Splaiul Unirii, Bucharest 3, 030138

ABSTRACT

Nanocomposites are a new class of advanced, nanometer-scale multiphase polymer composites that often display enhanced physical properties.

Nanocomposites are synthesized by dispersing inorganic exfoliated nanostructurated materials (nanocarbons, nanoclays) into polymer matrix.

Because of the stiffness of carbon nanotubes, they are ideal candidates for structural application, for example high strength, low weight and high performance composites.

A study regarding mechanical properties of some polymer-anorganic nanostructurated materials is presented. The work also concentrates on the nanofiller's influence concerning rheological and tribological properties of nanocomposites.

As polymers, epoxy and polyamide-6 resins and as fillers single and multi-wall carbon nanotubes, carbon nanofibers, laser synthesized amorphous nanocarbon and montmorillonite, (1%, 2%, 5% by weight) were used.

Ultrasonic methods were used to disperse nanofillers. The work presents thermo-mechanical properties and TEM analysis of the above mentioned polymer-based composites. The relative good dispersion and increase of the mechanical strength were revealed.

Biodegradable composites based on polycaprolactone and natural reinforcements with optimized properties

A. Vazquez
Laboratory of Polymer and Composites (INTECIN). Engineering Faculty, University of Buenos Aires, Argentina
L. Ludueña, M. Casco, R. Ollier, V. Alvarez
Research Institute of Material Science and Technology (INTEMA), Engineering Faculty, National University of Mar del Plata - Mar del Plata - Argentina

ABSTRACT

The main objective of this work was to obtain biodegradable composites from polycaprolactone and natural reinforcement with optimized mechanical properties by the chemical modification of bentonite or surface treatments on cellulose fibers. Ammonium and phosphonium salts were used as clay modifiers at different concentrations and times of reactions whereas alkaline-treatments (5, 10, 15 and 20 wt.% of NaOH and 10 wt.% of KOH); acetylation (with glacial acetic acid 1 or 2 hours followed by catalyzed acetic anhydride) and esterification (treatments with stearic and lauric acids) were applied to cellulose fibers. Modified bentonites and cellulose fibers (TGA; DSC; FTIR; WAXS, water absorption; contact angle; SEM) were characterized and most compatible were used to prepare composites (15 wt.%) and nanocomposites (5 wt.%). Mechanical properties were correlated with chemical modifications.

INTRODUCTION

Due to environmental problems, the development biodegradable polymeric products to be used as packaging, are receiving growing attention (Lepoittevin et.al. 2002). Polycaprolactone (PCL) which is biodegradable and biocompatible polyester with a number of potential applications from agricultural usage to biomedical devices (Dubois et.al. 1991) belongs to this class of synthetic biodegradable polymers. Its performance can be greatly enhanced by incorporation of fillers. One possibility is to add natural fibers giving to the final material the additional benefit of complete biodegradability (Mohanty et al 2000). The use of natural fibers (Roohani et. al. 2008) is based on their low-cost, renewability, low densities and low abrasively. Nevertheless, this kind of reinforcements displayed opposite polar behavior with respect to hydrophobic matrices. So, it is necessary to modify the fibers (Plackett and Vázquez 2004) but especially at the surface in order to prevent the destruction of the integrity and thus, their mechanical properties. Another possibility is to incorporate nano-fillers. The nanoparticles mostly used to reinforce polymeric materials are layered silicates. Among them, the use of bentonite is interesting due to environmental and economic factors, their natural abundance, and their mechanical and chemical resistance. In order to achieve better properties it is necessary to obtain a totally exfoliated structure (where silicate layers are completely and uniformly dispersed in a continuous polymeric matrix) but the tendency of the particles to agglomerate has been difficult to overcome in addition to its hydrophilic character, so it is necessary to make a previous treatment. The most popular one consists on converting these hydrophilic silicates to organophilic ones. The hydrated cations that are in the interlayer can be easily replaced by other positively charged surfactants such as alkyl ammonium or phosphonium cations. The modified clay has less surface energy and is more compatible with hydrophobic polymers whose are able to introduce inside the galleries under defined processing conditions.

The aim of this work was to perform different chemical treatments (alkaline, acetylation and esterification) to cellulose fibers and chemical modification to the bentonite (with ammonium and phosphonium salts) in order to improve the reinforcement/polymer compatibility and to obtain biodegradable composites and nanocomposites with optimized final properties. These final products can be used in food package industry

MATERIALS AND METHODS

Polycaprolactone M_n = 80.000 gr/mol (Sigma Aldrich) was used as a matrix. Bentonite was supplied by Minarmco S.A. (Neuquén, Argentine). Cellulose was obtained from cotton by following a previously reported procedure: (Moran et al.).

Modification of bentonites

a) Tributilhexadecylphosphonium bromide (Hedley et al 2007). 2.5 gr of clay were dispersed in 100 ml of deionised water. Then, the aqueous solution of TBHP of the corresponding concentration was added. The mixture was stirred for 4 h at 70 ºC.

b) Octadecylammonium chloride (Bala et al., 2000). Adequate quantities of octadecyl amine, HCl and distilled water were weighted. The mixture was heated at 80 ºC for few minutes in order to protonate the amine. After that, 2.5 gr of clay were dispersed in 100 ml of deionized water at 80 ºC and the ammonium solution was added. The mixture was stirred vigorous keeping the temperature constant.

Modification of cellulose

a) Alkaline treatments: cellulose fibers (2.5 g) were treated with (100 ml) of 5, 10, 15 and 20 wt% of NaOH and 10 wt% of KOH 1 h at 30 ºC under continuous stirring.

b) Acetylation: cellulose fibers (2.5 g) were treated with glacial acetic acid (125 ml) at room temperature by using a shaker for 1 or 2 h. After this process, acetic anhydride (50 ml) with 2 drops of H_2SO_4 was added for 5 min.

c) Esterification: The reactions were carried out under reflux for 4 hr using 2 g of cellulose, 100 ml of toluene and 0.44 ml of dodecanoyl chloride and 0.5 ml of pyridine or 0.57 g of octadecanoyl chloride and 0.6 ml of pyridine. Then was filtered and the modified cellulose was submitted to a soxhlet extraction with acetone for two days.

Characterization of original and modified reinforcements

X-Ray patterns: PW1710 diffractometer with a CuKα generator at room temperature.

Thermogravimetric Analysis (TGA): Shimadzu TGA-50 (25 to 1000 ºC) at 10 ºC/min

FTIR measurements: FTIR Genesis II (4000 - 600 cm-^{1}) at room temperature.

Water absorption tests: 90 % RH. Before tests, samples were dried under vacuum.

Contact angle measurements: Compacts powders were prepared in a press. Sessile drops of ethylene glycol and diiodomethane were formed on the surface of the solids.

Scanning Electron Microscopy (SEM) JEOL JSM-6460 LV. Diameter of at least 100 fibers of each treatment was measured in order to make a statistical distribution.

Characterization of composites (PCL+ 15wt% cellulose or PCL + 5 wt% bentonite)

Differential Scanning Calorimetry (DSC): Shimadzu DSC-50 from 25 to 400 ºC at 10 ºC/min under nitrogen. The degree of crystallinity was calculated from these curves.

Mechanical properties: Tensile tests in a Instron 4467 at 50 mm/min. Before tests, all specimens were preconditioned at 65 % RH (relative humidity).

RESULTS AND DISCUSSION

Modified bentonites. In the case of phosphonium salt, there was a little increase in the interlayer spacing as *f* increased were pristine bentonite was used Comparing the same surfactant amount, by changing the pristine clay for saturated one ; the difference between is negligible (the same as the saturated respect to pristine one). Regarding the octadecylamomniumm modifications, all of them produced and increase on the interlaminar spacing. By using 1.5 CEC it is clear that the stirring time had not an important effect on d001 (average 1.74 nm). On the other hand increasing f (from 1.5 to 3.0), only a marginal augment on this parameter was observed. It is interesting to note that for the lower f (1.5 CEC), there were no important effect of saturation but for higher f (3.0 CEC) the differences are quite notable being d_{001} superior for Na+ saturated bentonite.. One interesting result from TGA experiments is that the water content (obtained from residual mass curve until 130 ºC); it is understandable that all modifications produced an undoubtly decrease on the absorbed water which in turns indicates enhance on the hydrophobicity. By comparing TBDP clays it is possible to observe that the increment on the modifier concentration has a direct effect on the organic content, as it was expected. On the other hand, it is also clear that the effectively of the modifier is improved for saturated bentonite. In the case of ODAC, no important changes were observed as a function neither of time; nor in the TGA curves neither in the organic content (around 2.8 ± 0.7 % in these three cases). This is also coherent with the behavior observed for d001. On the other hand, by increasing the modifier concentration for a fixed time, an important increase on the organic content was detected. (from 3 to 12 %) whereas the changes in the interlayer spacing was not so high, so that, it is quite possible that some part of the organic modifier did not enter in the clay galleries. For the same time and modifier concentration, the organic content was higher in the case of saturated clay in this case also the interlayer space was higher, specially in the case of the higher modifier concentration giving the idea that the introduction of the modifier inside the clay was effective. The thermal stability of phosphonium modified clays is higher than that of the ammonium modified ones. It is interesting to note that the temperature for maximum rate of mass loss decreased for saturated clay and also for higher quantities of surfactant. Polarity was really low in all cases but especially when high surfactant amounts were employed. This result is also interesting because the water absorption (which was also reduced) gives idea about the complete clay and this latter about the external hidrophobicity which became important to interact with the hydrophobic thermoplastic polymers.

Modified cellulose fibers. Alkaline treatment produced a decrease on the crystallinity index (FTIR and DRX) accompanied by the change of cellulose arrangement (from I to II); an increase on the water uptake (water absorption test) due to a higher polarity (contact angle test) and the exposition of free hydroxyl groups on the surface. On the other hand, acetylation generated fibers with higher crystallinity, without changing the cellulose (I), and lower polarity degree and water absorption (according to the surface groups). In the case of esterification, the crystallinity did not show important variations (being always cellulose I) but the water absorption and the polarity decreased until zero; and a strong reduction on the fibers aspect ratio with respect to untreated cellulose was observed. The esterification indexes confirmed that these treatments took place only at the surface.

Composites: 15 wt% of celluloses (untreated; Cel10KOH; Cel20KOH; CelAc2h; CelEsterC12 and CelEsterC18) were added to PCL producing composites. Alkaline treatments did not improve the compatibility with the matrix but it slightly increased the cellulose aspect ratio (*l/d*) (better matrix/fiber load transference efficiency). The esterification treatment produced the opposite result where the best compatibility with the matrix but strong reduction on the fibers *l/d* was achieved. Best composites properties were found with the 2 hours acetylated fibers with good matrix/fiber compatibility and slight decrease on the cellulose *l/d*. Mathematical models were used to correlate experimental mechanical behavior. Best agreement was obtained by the Hull´s model which takes into account the matrix-fiber adhesion and the *l/d*.

Nanocomposites: 5 wt% of bentonites (1; 2; 3; 9 and 11) were added to PCL producing nanoomposites. DRX pattern indicates probably intercalation or some degree of exfoliation of the clay platelets between polymeric chains. All clays act as nucleation agent because X_{cr} increased when bentonites were incorporated. Whereas the stiffness increased in all cases, the tensile strength decreased for PCL/clay 3. The elongation at break decreased in all cases because the intercalation of the clay reduces the plasticity of the polymer. The water vapor rate, whose are very important for packaging, decreased in all cases.

CONCLUSIONS

The results obtained in the present study indicates that increasing the matrix/filler compatibility is one way to improve the mechanical properties of PCL/filler composites but other variables should always be taken into account. Future works will be conducted on changing the processing parameters as another strategy to improve the final behavior of such materials.

ACKNONWLEDGEMENTS

Authors acknowledge to (PICT1560) and CONICET (PIP 6254) for the financial support.

REFERENCES

BALA P, SAMANTARAY BK, SRIVASTAVA SK (2000) Synthesis and characterization of Na-montmorillonite-alkylammonium intercalation compounds *Mat Resear Bull* 35, 1717-1724

DUBOIS P, JACOBS C, JEROME R, TEYSSIE P (1991). Macromolecular engineering of polylactones and polylactides. 4. Mechanism and kinetics of lactide homopolymerization by aluminum isopropoxide. *Macromolecules,* 24(9), 2266-2270.

HEDLEY CB, YUAN G, THENG BKG (2007) Thermal analysis of montmorillonites modified with quaternary phosphonium and ammonium surfactants *Applied Clay Science* 35, 180-188

LEPOITTEVIN B, DEVALCKENAERE M, PANTOUSTIER N, ALEXANDRE M, KUBIES D, CALBERG C, JÉROME R, DUBOIS P. (2002).Poly (ε-caprolactone)/clay nanocomposites prepared by melt intercalation:. *Polymer,* 43(14):4017-4023.

MOHANTY AK, MISRA M, HINRICHSEN G. BIOFIBERS (2000). Biodegradable Polymers and Biocomposites: An Overview. *Macromol Mater Eng,* 277(1), 1-24.

MORÁN J, ALVAREZ V, CYRAS VP, VÁZQUEZ A (2008) Extraction of Cellulose and Preparation of Nano-Cellulose from Sisal Fibers. . *Cellulose,* 15, 149-159.

PLACKETT D, VÁZQUEZ A. (2004) Polymer composites and the environmental. In: Caroline Baillie, Editor, Cambridge: Woodhead Publishers, p. 123-153.

ROOHANI M, HABIBI Y, BELGACEM NM, EBRAHIM G, KARIMI AN, DUFRESNE A. (2008) Cellulose whiskers reinforced polyvinyl alcohol copolymers nanocomposites. *European Polymer Journal,* 44(8), 2489-2498.

Characterisation of the swelling properties of new PVA membranes for DMFC

A. Martínez Felipe, L. Santonja Blasco, E. Ballester Sarrias, A. Ribes Greus
Institute of Materials Technology, Escuela Técnica Superior de Ingeniería del Diseño,
Camino de Vera s/n 46022, Universidad Politécnica de Valencia, Valencia, España

ABSTRACT

Poly(vynil alcohol) (PVA) membranes for DMFC were prepared by using sulfo succinic acid (SSA) as crosslinking agent. Different series of PVA-SSA membranes were prepared by varying the hydrolysis degree of the PVA substrate and the concentration of SSA. Additionally, the membranes were submitted to swelling tests in water at 35ºC. The influence of the PVA substrate and SSA concentration on the preparation procedure of the membranes, the posterior thermal treatment and the solvent absorption were studied by Fourier Transform Infrared Spectroscopy (FTIR) and Thermogravimetric Analysis (TGA). The results indicated changes in the molecular environment of the groups corresponding to PVA, SSA and water through all the preparation process and the swelling tests. Such changes especially concerned the polar groups and the new ester groups. There was also evidence of the existence of free and bounded water in the crosslinked PVA-SSA membranes. The results suggest that there were noticeable changes in the nature of the solvent absorbed in the polymers once the network is formed. The discrimination of the type of water absorbed is paramount to predict the behaviour of the membranes in DMFC, since the proton conductivity and also the *crossover* phenomenon are extremely depending on the water contents.

1. INTRODUCTION

Fuel cells (FC) have emerged as a promising alternative to the use of conventional fossil fuels (Blomen 1993). FC provide electrical energy through the electrochemical reactions of a fuel and an oxidizing agent. In particular, fuel cells working at low temperature have a great potential in portable applications because of their flexibility and low weight. The electrolyte in low temperature fuel cells is a polymeric membrane (Polymer Electrolyte Membrane, PEM) which separates the electrodes and also transports the protons from the anode to the cathode. Fuel cells operating with hydrogen have high yields and a very low environmental impact, with and only generate water and heat as subproducts. However, the use of hydrogen presents several limitations due to the problems related to its production, storage and delivery. As an alternative, Direct Methanol Fuel Cells (DMFC) use methanol in the anode for their oxidation, avoiding the problems related to the storage and delivery of hydrogen. However DMFC still present some limitations based on poor anodic oxidation and other mass transfer effects. Among the different problems related to DMFC, the so-called "*crossover*" phenomenon is one of the most important and causes efficiency losses of up to 30% (Hoogers 2003). Crossover consists on the flow of unreacted methanol molecules from the anode to the cathode. The methanol reacts with the oxygen and no electrical power is produced.

The occurrence of crossover in PEM is attributed to the linkage between the transport mechanisms of water, methanol and protons through the membrane. In general terms, a reduction in the methanol permeability usually leads to a reduction in the water contents in the polymer, and a decrease in the proton conductivity. As a result, attempts to reduce crossover usually decrease the cell performance (Kreuer. 2001). The new PEM materials for DMFC usually consist on polymers with a biphasic structure containing a hydrophobic matrix with proton conducting groups. This leads to a phase separated system with non-polar backbone and polar domains through where water and protons are usually transferred. Since water is an active agent in the proton and methanol transport, it is important to know its chemical and physical state inside the polymer in different conditions, with the aim to design materials which can reduce *crossover* in DMFC (Deluca, 2006).

2. EXPERIMENTAL PROCEDURE

Poly(vynil alcohol) (PVA) with different hydrolysis degrees were used as substrates for the preparation of crosslinked membranes. PVA has been extensively tested as a new material for DMFC electrolytes due to its high affinity towards water in alcohol aqueous solutions (Pivovar et al 1999). The use of different hydrolysis was important to analyse the effect of the OH concentration on the interactions with the solvent and also in the membranes preparation.

In order to enhance the stability and the proton conductivity of the membranes, PVA was crosslinked with sulfo succinic acid (SSA) by esterification. The preparation of the membranes followed a typical procedure. First the PVA was dissolved into water (10%, wt. percentage) during 6 hours at 90ºC. After cooling down, the corresponding SSA amounts were added and the mixture was stirred at 25ºC during 24 hours. The resulting solution was then cast on a Teflon sheet and allowed to dry at room temperature, until no weigh loss was observed (5 – 7 days). The PVA-SSA membranes were then submitted to a thermal treatment at 110ºC during 2 hours to activate the crosslinking reaction.

Different PVA-SSA membranes were prepared, using hydrolysis degrees of 89%, 96% and 99% and SSA concentrations (C_{SSA}) between 0% (substrate) and 30% in weight percentage of SSA. Some of the membranes were also submitted to swelling tests at 35ºC during 1 week in water and methanol binary mixtures with different compositions.

The interactions of the groups of the PVA-SSA membranes and the solvents were analysed by using Attenuated Total Reflectance-Fourier Transform Infrared Spectroscopy (ATR - FTIR). Thermogravimetric analysis (TGA) was used to study the thermal stability of the materials as well as the state of the solvent.

3. RESULTS AND DISCUSSION

3.1. PVA-SSA membranes before the heat treatment

The experimental results corresponding to the PVA-SSA membranes evidenced changes in the initial components even before the heat treatment was carried out (Figure 1). There were noticeable variations in the absorption bands of the most representative groups of PVA once the membranes were obtained. A reduction in the absorbance related to the OH band (ν ~ 3600 – 3000 cm^{-1}) and an increase in the bands related to the ester bond (ν ~ 1720 cm^{-1} for C=O stretching and ν ~ 1250 cm^{-1} for COC stretching) were observed, suggesting that some chemical reaction is occurring even without the thermal treatment. These changes respect to the substrates were also visible in the TGA results through the study of the Derivative thermogravimetric (DTG) curves. A new process of weigh loss which is related to the presence of tightly bound water appears in the 100ºC – 175ºC region in the PVA-SSA membranes. The curves also show an increase in the weight loss related to the degradation of the polymer backbone and the residual weight at 700ºC. The increase in the thermal stability of the polymer suggests the formation of a crosslinked structure.

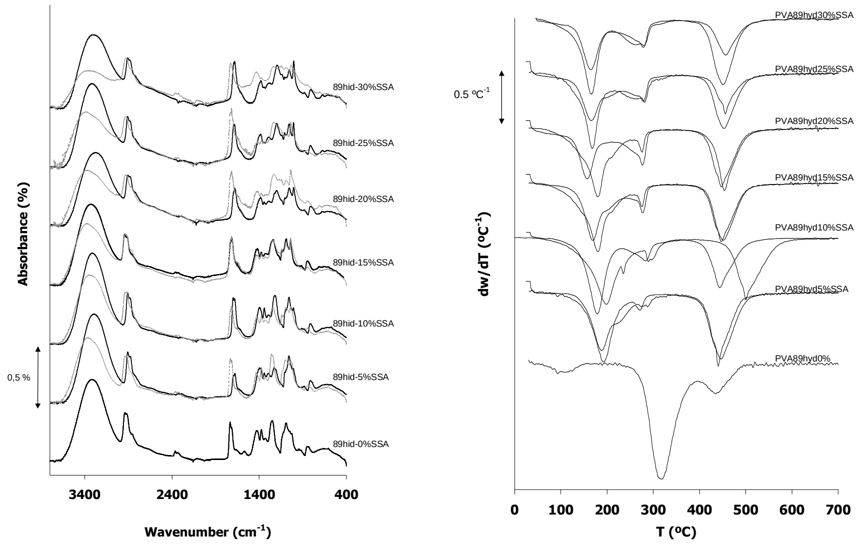

a) ATR - FTIR curves **b) DTG curves**

Figure 1. Experimental results of PVA/SSA membranes before (solid lines) and after (dashed lines) heat treatment

3.2. PVA-SSA membranes after the heat treatment

The FTIR spectra of the PVA-SSA membranes show some deviations after being submitted to the thermal treatment. There is a progressive decrease of the bands related to the OH groups of PVA and an increase in those related to the ester bond. This fact indicates the extension of esterification by the thermal treatment. The results also show that the effect of C_{SSA} in the membranes was different depending on the PVA substrate being more accused for higher hydrolysed PVA. The TGA results also displayed the extension of esterification, for higher residual values were obtained. It was remarkable that the amount of tightly bounded water was not very affected after the thermal treatment. In general terms, it was seen that the thermal treatment was more effective in PVA substrates with higher hydrolysis degrees.

3.3 Effect of solvent absorption in the PVA-SSA membranes.

The presence of solvent in the PVA-SSA membranes was clearly detected by TGA, but also in the FTIR OH stretching and bending vibration regions (ν~3000 cm^{-1} and ν~1650 cm^{-1} respectively). The presence of tightly bounded water was assigned to a tail band in the ν > 1720 cm^{-1} region, indicating the presence of protonated solvent clusters, and also to a new weigh loss peak in the DTG curves around 150ºC. These changes were accompanied with a red-shift in the frequencies of the IR bands of the polar groups (C=O and SO_3), but with a blue-shift in those corresponding to the OH groups. This suggests that the tightly bounded water is related to polar regions rather than to the remaining OH groups in the polymer backbone. Similar behaviour is observed for commercial membranes used in fuel cells and indicates the existence of a cluster-like structure.

On the other hand, the results corresponding to the membranes submerged in water and methanol suggest that the solvent absorbed is mainly contributing to the so-called free water. This indicates that the diffusion of solvent through the polymer can be hindered after the polymer net-work is formed, but the tightly-water is still present in the polymer. Such discrimination of the water typologies can be crucial to discriminate the processes of proton conductivity through vehicular (free water) and hopping (OH bonding with PVA and bounded water).

CONCLUSIONS

The hydrolysis degree of the PVA substrate is an important parameter in the preparation and properties of crosslinked PVA-SSA membranes for DMFC. The changes in the chemical interactions and thermal stability of the components of the membranes were studied by FTIR and TGA. The results revealed that the yield of the esterification depended on the concentration of crosslinking agent but also on the hydrolysis degree. There were also changes on the effect of the thermal treatment on the different PVA substrates. It was observed that the water absorbed after the crosslinked structure was formed was different to that initially present in the substrates and in the PVA-SSA membranes. All these fact can be important to discriminate the mechanisms of proton diffusivity through the electrolytes and therefore to enhance their behaviour against *crossover* in DMFC.

ACKNOWLEDGEMENTS

The authors would like to acknowledge the Spanish Ministry of Education and Science for its financial support through the research project ENE2007-67584-C03-01 and through the awarding of a pre-doctoral grant in the Program for the Formation of University Academic Staff - 2004.

REFERENCES

Blomen, L., (1993), *Fuel Cell Systems*, Ed. Plenum Press, New York
Deluca N.W., Elabd, Journal of Polymer Science 44, 2006, 2201
Hoogers, G., (2003) *Fuel Cell Technology Handbook*, CRC Press, Nueva York,
Kreuer, K.D. Journal of Membrane Science 185, 2001, 29
Pivovar B. S., Wang Y., Cussler E.L., Journal of Membrane Science 154 (1999) 155-162

Stimuli responsive ferrogels based on functionalized magnetic nanoparticles for different biomedical application

I. Craciunescu, A. Nan, R. Turcu, I. Kacso, I. Bratu, C. Leostean
National Institute for Research and Development of Isotopic and
Molecular Technologies, Cluj-Napoca, Romania
L. Vekas
Romanian Academy, Timisoara Branch, Magnetic Fluids Laboratory, Timisoara,
Romania

SUMMARY

Temperature – sensitive poly (N-isopropyl acrylamide) pNIPA gels were synthesized with nano size iron oxide ferrofluids (Fe_3O_4) using N, N'-methylene bis-acrylamide (BIS) as the crosslinking agent, obtaining a new type of material, named ferrogel. The swelling characteristics of these ferrogels at distinct compositions, as a function of temperature were investigated. It was found that the pNIPA ferrogels demonstrated the temperature – responsive nature, and it also showed good reversibility.

The FTIR spectra of pNIPA ferrogel samples, showed the absorption region of the specific chemical groups associated with pNIPA and the Fe_3O_4 magnetic nanoparticles.

The drug release experiments were performed using atenolol (AT) in simulated gastric and intestinal media. The amount of released drug was determined by UV spectroscopy at characteristic wavelength of the drug, using a calibration curve obtained from a series of drug solution with standard concentration

1. INTRODUCTION

Hydrogels are one of the most promising types of polymers being used for new material development and are polymeric material that do not dissolve in water at a physiological temperature and pH, but swell considerably in an aqueous medium. Hydrogels show reversible volume phase transition depending on external stimuli such as temperature, solvent, ionic strength, pH, electrical or magnetic field and this properties made them promising materials in biotechnology, pharmaceutical and industrial application (Tanaka et to 2005).

Hydrogels have been used extensively in the development of the smart delivery system, because the hydrogels can protect the drug from hostile environments like the presence of enzyme and low pH in the stomach. Hydrogels can also control drug release by changing the gel structure in response to environmental stimuli (Qin et to 2001). Among theme, temperature and pH responsive hydrogels have been the most widely studied, because these two factors have a physiological significance.

Temperature responsive hydrogels exhibit a volume phase transition at a certain temperature; wich causes a sudden change in the solution state. These polymers become insoluble upon heating and have a so-called lower critical solution temperature (LCST). Poly (N-isopropyl acrylamide) (PNIPA) is probably the most extensively used because of its lower LCST in the range of 25 - 32° C, close to the body temperature (Ebara et to 2000).

By combination of this temperature sensitive polymers with nano solid or fluid magnetic materials displays novel and often enhanced properties compared to the traditional materials. Due to their sensitivities to both magnetic fields and temperature, this magnetic – field sensitive hydrogels, named ferrogels, offer a high potential application in the design of a targeting drug delivery system which is considered a safe and effective way for tissue specific release of drug.

In the present study we prepared PNIPA ferrogels to develop a dual sensitive system against both temperature and magnetic field. This study deals with the synthesis, characterization and the temperature dependence of the swelling behavior for PNIPA ferrogels. Atenolol was encapsulated into magnetic hydrogel and the drug release behaviour of the magnetic sensitive hydrogel for drug eluting stents application was investigated in this paper.

2. Experimental

2.1. Preparation of the pNIPA ferrogels

Different ratios of monomer N-isopropyl acrylamide (NIPA) and N, N'-methylene bis-acrylamide (BIS), like catalyst were dissolved in 3 ml of deionized water. After N_2 gas bubbling for 10 min to deoxygenate the solution, different concentrations of ferrofluid were added and sonicated for 30 minutes. 1 wt % ammonium persulphate (APS) as redox accelerator was added to the solution. The mixture was kept to react for 2 h at 60°C and after that, 24 h at room temperature.

2.2. *Swelling experiments of the hydrogels*

The swelling ratio was measured gravimetrically in two different phosphate buffer solutions, a neutral solution with pH = 7 and an acid solution with pH = 2. The dry ferrogel samples were immersed in solution with pH 7 and 2 at different temperatures, until they swelled to equilibrium. After excessive surface water removed with filter paper, the swollen samples were weighed time to time. The swelling ratio can be calculated as a function of time (Garcia et to 2004).

$$Swelling\ ratio\left(\%\right)=\frac{W_s-W_d}{W_d}\cdot 100 \tag{1}$$

where W_s represents the weight of theswollen state of the sample at a given time and W_d is the weight of the sample in the dry state.

2.3. Characterization

Fourier transform infrared spectroscopy (FTIR) was used to confirm the structure of PVA and PNIPA hydrogels and ferrogels. Infrared absorption spectra were recorded with a FTIR JASCO – 6100 spectrometer on pressed pellet prepared from dry hydrogels and ferrogels, embedded in KBr, in the 500 – 4000 cm^{-1} spectral range. The amount of released AT was determined at 225 nm with a UV Jasco V-550 spectrometer.

2.4. *Drug release experiment*

The release rate experiments were performed at 25°C under unstirred condition in pH 7.0 phosphate buffer solution. The ferrogels containing a known amount of drug (AT) were added to the release medium (50 ml) at a given time interval, the samples were withdrawn and assayed for the amount of released AT as a function of time. The amount of released AT was determined by UV-VIS spectroscopy at 225 nm using a calibration curve constructed from a series of AT solutions with standard concentrations. The results are expressed as cumulative release ratios.

3. Results and discussion

3.1. *FTIR spectrum of the PNIPA ferrogel*

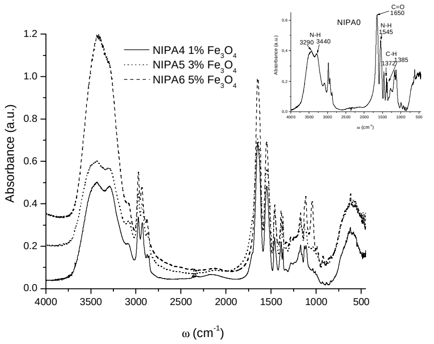

Figure 1. FTIR spectra of NIPA ferrogels
Inset: FTIR spectrum of NIPA hydrogel

FTIR spectra of NIPA ferrogels are presented in Figure 1, and the FTIR spectrum of NIPA hydrogel in the inset.

From the FTIR spectrum of hydrogel (inset Fig.1) there is a carbonyl stretching vibration (amide I) at 1650 cm^{-1}, N-H bending vibration (amide at 1545 cm^{-1}) and two typical peaks of C-H vibration of –CH(CH$_3$)$_2$ at 1372 cm^{-1} and 1385 cm^{-1} are confirmed. A broad peak between 3440 cm^{-1} and 3290 cm^{-1} is also observed due to N-H stretching of NIPA repeating units. Also the presence of the characteristic bands of magnetite (Fe$_3$O$_4$) located around 600 cm^{-1} is observed.

3.2. Swelling studies

In the previous stage of the polymer dissolution the solvent molecules go into the polymeric mass, swell it until chain separation and is incorporated into the solution, in opposition to the intermolecular forces (e.g. van der Waals, electrostatic, etc.) that exist between them. However, if the polymer is not soluble, a solvent diffusion to the polymeric mass and from the polymeric mass to the medium will only exist. Then, the polymer swelling will occur. The equilibrium swelling will be reached when both solvent diffusion are equal.

The water content at different times can be calculated from Eq. (1). Temperature responsive hydrogels exhibit a volume phase transition at a lower critical solution temperature (LCST), which causes a change in the solvation state. The change in the hydratation state, which causes the volume phase transition, reflects competing hydrogen bonding properties, where intra- and inter- molecular hydrogen bonding of the polymer molecules are favorised compared to a solubilisation by water. The time dependent swelling behavior of the pNIPA ferrogels at pH = 7 buffer solution and three different temperature are shown in Figure 2. It can be observed that the swelling ratio of the ferrogels decrease with the increasing of temperature. This behavior is attributed to the collapse of the pNIPA chain around of 37°C, leading the hydrogel to assume a more hydrophobic state

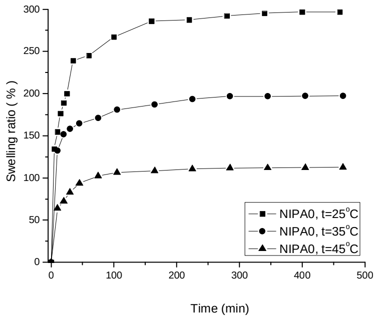

Figure 2. Swelling ratios for pNIPA ferrogels as a function of time for different temperatures.

3.3. *Drug release studies*

All the hydrogels and ferrogels containing a known amount of atenolol were added to the release medium (50 mL of phosphate buffer solution pH = 7). The total concentration of atenolol in this medium is calculated at 0.02 mM.

The amount of drug at any selected time was calculated from the atenolol (AT) calibration curve. Figure 3 shows the calibration curve for AT at 225 nm determined by UV-VIS spectroscopy. Figure 4 shows the release profile (delivered atenolol concentration) of the prepared samples of pNIPA in physiological fluid (buffer solution of pH = 7) By studying the release profile of atenolol (Figure 4) one can observe that in pNIPA ferrogels a higher release rate (max. 50 %) is obtained at 25°C and pH = 7. The reason of this release behavior seems to be the nature of the ferrogels. The drug in the ferrogels could be released as a result of the ferrogels volume change and the interaction between the polymer network and atenolol. Because the experiments are made at pH = 7, there is electrostatic repulsion between -OH of atenolol and –COO$^-$ of pNIPA ferrogels that accelerates the atenolol release (Guo et to 2007). Also, it can be observed that the fractional released is directly proportional to the concentration of magnetic nanoparticles. This result indicates that the higher concentration of magnetic nanoparticles in the ferrogels creates larger surface areas to diffuse the drug.

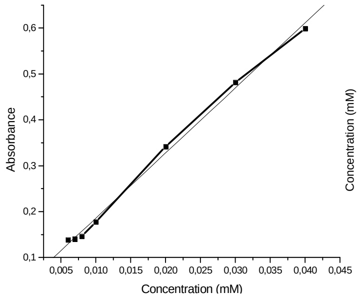

Figure 3. Calibration curve for atenolol (AT).

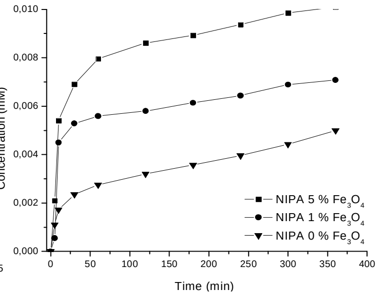

Figure 4. The release profile of atenolol of pNIPA

4. Conclusions

pNIPA hydrogels and ferrogels (based on ferrofluid, a stable dispersion of magnetite nanoparticles in water) were synthesized. The polymerization of pNIPA containing the surface modified magnetic nanoparticles was confirmed by Fourier transform spectroscopy (FTIR). Its swelling behavior showed better temperature sensitivity in buffer solution at different temperature. The Atenolol release from the hydrogels and ferrogels was affected by the nature of the polymeric matrix and is directly proportional to the concentration of magnetic nanoparticles. All these results indicate that the pNIPA ferrogels can be used as a temperature responsive orally administered drug delivery system.

5. References

Ebara M, Aoyagi T, Sakai K and Okama T (2000) *Macromolecules* **33** 8312
Garcia D M, Escobar J L, Noa Y, Bade N, Hernaez E and Katime I (2004) *European Polymer Jornal* **40** 1683
Guo B L and Gao Q Y (2007) *Carbohydrate Research* **342** 2416
Qin J and Park K (2001) *Advanced Drug Delivery Reviews* **53** 321
Tanaka Y, Gong J P and Osada Y (2005) *Prog. Polym. Sci.* **30** 1

Geopolymers based on metakaolin and fly ash alkali activated

I. Petre*, F. Amzica*, S. Stoleriu**
* Research Division, S.C. CEPROCIM SA, Bucharest, Romania
** University POLITEHNICA Bucharest, Romania

ABSTRACT

The properties of the geopolymers based on alkali activated of metakaolin (MK) and fly ash are influenced impacted by the type, concentration and amount of alkali activator used, as well as by the hydrothermal conditions.

Metakaolin and fly ash - based geopolymer has been synthesized from metakaolin and fly ash under activation of NaOH solution (8, 10, 12 mol/L) and sodium silicate solution. The pastes were mechanically mixed for 5 minutes to complete homogenization, cast into cylindrical mold, and vibrated for 60 seconds. The samples were cured at temperatures between 20° and 60°C in oven for 24 hours. The compressive strength, apparent density and open porosity of the geopolymers were measured. The effect of concentration of NaOH solution and temperature on the mechanical properties of the geopolymer was investigated by means of scanning electron microscopy (SEM), infrared spectrometry (IR), and thermal analysis (DTA/TG) IR analyses emphasized amorphous character of the geopolymer. Content of the amorphous phase in increased along with the increase of alkali concentration. SEM results show the synthesized geopolymer maintained layer structure of metakaolinite. The DTA/TG data allow quantifying of the reaction products in the alkaline activated geopolymers.

In general, the results followed expected trends and there were clear correlations between activator composition, microstructure and strength.

Studying the effect of acid treatment of carbon fibers on the flexural properties of unsaturated polyester resin composites

B. Fathi[1]**, M. Esfandeh**[2]**, A. Khalifeh Soltani**[1]
[1]Composites Research Centre, Materials & Manufacturing Processes Department,
Malek Ashtar University of Technology, Tehran, Iran
[2]Iran Polymer & Petrochemical Institute, Composites & Adhesives Department, P. O. Box 14965/115, Tehran, Iran

ABSTRACT

In fiber reinforced composites, the interface of fiber/matrix plays an important role in the mechanical performance of the composite. Carbon fibers are mainly applied in the reinforcement of polymeric matrices. However, when applied without previous surface treatment, these fibers produce composites with low interlaminar shear strength (ILSS).

In this study, the surface modification of PAN based carbon fiber by various concentrations of Sulfuric Acid is investigated. To this end, Atomic Force Microscopy was employed to capture the corresponding changes in the surface roughness of the carbon fiber and the results were compared with that of the non-treated fibers. Moreover, using treated and non-treated fibers, several Carbon fiber/Unsaturated Polyester composite rods were prepared by Pultrusion and their Flexural properties were determined by three point bending and dynamic mechanical-thermal analysis. Finally, the corresponding results were compared together.

The results indicated that the carbon fiber surface roughness increases over the whole investigated concentration range but the fiber diameter decreases at high concentrations. Furthermore, composite rods that were made from treated fibers exhibited improved machanical properties. It is also found that treating the fiber decreases the magnitude of $\tan\delta$. Besides, the flexural strength of the specimen treated by 10% wt Acid concentration increased. Since all other parameters were kept constant over the tests, the differences observed in the composite behavior can only be attributed to the interfacial phenomena.

Effect of interface modification with styrene-co-maleic anhydride oligomers on the mechanical properties of recycled polystyrene-lignocellulosic fiber composites

M. Poletto, J. Dettenborn, M. Zeni, A.J. Zattera
Caxias do Sul University (UCS), Chemical Engineering Department, 95070-560
Caxias do Sul /RS, Brazil

ABSTRACT

This work has the aim to study techniques of green composites manufacturing. Industrial region of Caxias do Sul-Brazil, generates a big amount of industrial and urban wastes. The furniture industry generates wastes of sawdust of *Pinus elliotti* and nowadays there is a large amount of EPS (expanded polystyrene) being deposited in the city landfill. The first phase of the work was the manufacturing of the composites sawdust /EPS in a twin-screw extruder with temperature below 200°C using 20 wt% of sawdust. The effect of the addition of three styrene-co-maleic anhydride oligomers with different content of maleic anhydride, 30%, 25% and 20% (w/w), as commercial interfacial modification agent on sawdust / EPS composite properties was studied. Were incorporated 1, 2 and 4% in weight of coupling agents (SMA 2000, SMA 3000 and SMA EF40) in the composites. Mechanical properties, such as tensile strength, flexural strength, impact strength, tensile and flexural modulus were analyzed. This interface modification improves the compatibility of hydrophilic sawdust with hydrophobic EPS residues. It has been observed that the addition of oligomers improves the mechanical properties of the composites with the incorporation of 2% in weight of coupling agents. The mechanical properties showed to be dependent on content of maleic anhydride in the coupling agent. Scanning electron microscopy (SEM) was used to investigate the fiber surfaces of lignocellulosic material and the fiber-matrix interfaces.

Solubility of the HPMC/PVA blends for control of the release of drugs

V. dos Santos, V.W. Angeli, K.C.B. de Souza, G.A. Carvalho, J.S. Fávero, D.S. Miron, R.N. Brandalise
University of Caxias do Sul – RS, Brazil

ABSTRACT

Many systems used to coat tablets for controlled release of drugs use polymers. This work proposes to evaluate the solubility of the blend of Hydroxypropylmethyl cellulose (HPMC) and Poly (vinyl alcohol) (PVA) compared to the isolated polymers and in solutions with pH of biological fluids, 6.0 and 1.2. The HPMC/PVA compositions tested were 100/0, 75/25, 50/50, 25/75 and 0/100. The blends were performed in a reactor, 80°C, 20min, at a concentration of 5%, in aqueous solution. The characterization of polymers and blends could show the immiscibility of the compositions by SEM, a displacement of the beginning of the fusion process to higher temperatures with increased PVA content in the DSC blends. Using FTIR the models presented coinciding absorption bands between coinciding absorption bands between 3400–3000cm^{-1}, 2835cm^{-1}, 2840cm^{-1} and 1120–1020cm^{-1}. The solubility results showed that the HPMC becomes completely soluble in the test pH and that the PVA allows the control of blend solubility. Theophyline granules containing HPMC/PVA 25/75 in the matrix were coated with hydro alcoholic solution prepared with the same blends of polymers. The resulting granules were used in the preparation of capsules containing 200mg of theophylline. Capsule dissolution profile was monitored by UV absorbance at maximum of theophylline at 269 nm. There was immediate release of theophylline, 78.4% after 30 minutes and 97.4% after 120 minutes.

Influence of liquid rubber/clay combination on mechanical behaviour of epoxies

J. Rotrekl, I. Kelnar, L. Kaprálková
Institute of Macromolecular Chemistry, Academy of Sciences of the Czech Republic,
Heyrovsky Sq. 2, 162 06 Prague, Czech Republic

SUMMARY

The potential of simultaneous application of hyperbranched polyesters or functionalized nitrile rubbers and organophilized montmorillonite to upgrade properties of epoxy resins is shown. The effects of various morphologies of dispersed phases on mechanical behaviour and basic aspects influencing formation of the structure such as blending protocol, application of components with various functionality and polyfunctional precursors are demonstrated.

1. INTRODUCTION

Epoxy resins are one of the most important classes of thermosetting polymers. They are widely used in various fields of coating, high-performance adhesives and in other applications. Cured epoxy resins are characterized by high chemical and corrosion resistance as well as good mechanical and thermal properties. However, they are not suited for some applications because they are brittle and show poor resistance to crack propagation, low impact strength and low toughness.

The aim of our efforts was to increase toughness of epoxy resins without significantly deteriorating other important properties. One of the most successful methods involves the addition of suitable rubber such as amine-terminated (ATBN) and carboxyl-terminated (CTBN) butadiene-acrylonitrile copolymers. A recent method of choice is the use of hyperbranched polyesters (HBP). Its main disadvantage is a decrease in modulus and strength. In the present study application of liquid rubber together with organophilized montmorillonite was investigated in order to obtain tough epoxy resins with better balanced mechanical properties.

2. MATERIALS

The materials used are: DGEBA epoxy resin PRX 217 (5M, Czech Republic), curing agent Laromin C260, hyperbranched polyester Boltorn H2003 with 12 terminal OH groups, MW 2300 (Perstorp Sweden), nitrile-terminated acrylonitrile-butadiene rubber Hycar ATBN 1300 x 16 and carboxyl-terminated acrylonitrile-butadiene Hycar CTBN 1300x8 (Nano Resins), and organophilized montmorillonites Cloisite 30B (C30) and Cloisite 15A (C15) (Southern Clay Products, USA).

3. RESULTS AND DISCUSSION

As shown in Table 1, the highest impact strength was obtained by addition of 10 % of HBP. Surprisingly, addition of HBP also increases the modulus. The temperature dependence of the storage modulus (Fig. 1) shows that addition of HBP increases the modulus only up to 80 °C with a subsequent decrease, whereas a simultaneous addition of C30 extends this interval.

For the systems with C30 preblended with HBP, a significant increase in strength was observed.

Composition	σ_b (MPa)	ε_b (%)	*E* (MPa)	*a* (kJ.m^{-2}) notched
PRX 217	65	5.6	1925	4.6
PRX 217/H2003 95/5	63	4.0	2483	3.0
PRX 217/H2003 90/10	63	5.5	2160	6.0
PRX 217/C30 95/5	60	3.7	2278	1.9
PRX 217/ (preblend H2003/C30 90/10) 90/10	88	6.0	2175	2.6

Table 1. Mechanical properties of epoxy/HBP/organophilized montmorillonite composites

An analogous dependence of the loss modulus (Fig. 2) shows that the HBP-epoxy systems are partly miscible. This fact is proved also by SEM of acetone-etched samples where no rubber domain was observed.

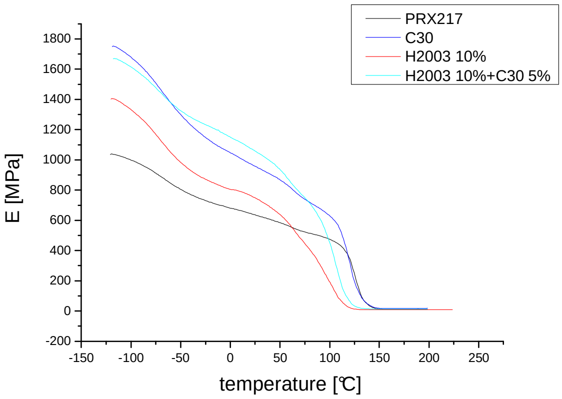

Fig.1. Dynamical mechanical analysis - temperature dependence of storage modulus of epoxy/HBP/organophilized montmorillonite composites

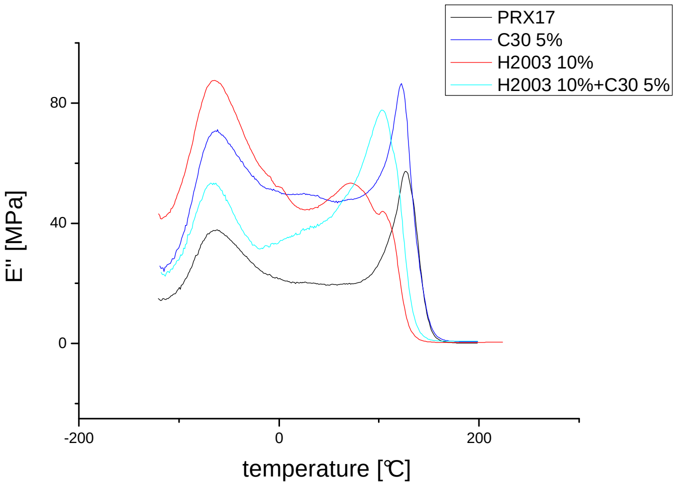

Fig.2. DMA - temperature dependence of loss modulus of epoxy/HBP/organophilized montmorillonite composites

The samples with clay and ATBN/CTBN were prepared by preblending clay with nitrile rubber only and adding the mixture to epoxy resin.

The results in Table 2 show that addition of ATBN increases the impact strength while decreasing the modulus of the composites. Addition of clay to an analogous system leads to an increase in the modulus without decreasing the impact strength. The systems with CTBN exhibit higher moduli, but their impact strength is not as favorable as in the case of ATBN. The particle sizes in both systems are similar (ca. 300 nm); they were not influenced by addition of clay. Different mechanical properties are probably due to different morphology of particles. The structure of inclusions is shown in Fig. 3. The system with ATBN forms mixed inclusions with clay, while CTBN forms an agglomerated structure.

Table 2. Mechanical properties of epoxy/ATBN(CTBN)/organophilized montmorillonite composites[a]

Composition	σ_b (MPa)	ε_b (%)	*E* (MPa)	*a* (kJ.m^{-2}) unnotched
PRX217	65	5.5	1925	28
PRX217/ATBN 90/10	51	4.2	1683	48.5
PRX217/(ATBN/C15 75/25) 90/10	48	3.6	1792	48.5
PRX217/(CTBN/C30 95/5) 90/10	49	4.1	2015	21

[a] Preblend of C30 (C15) in ATBN or CTBN was used.

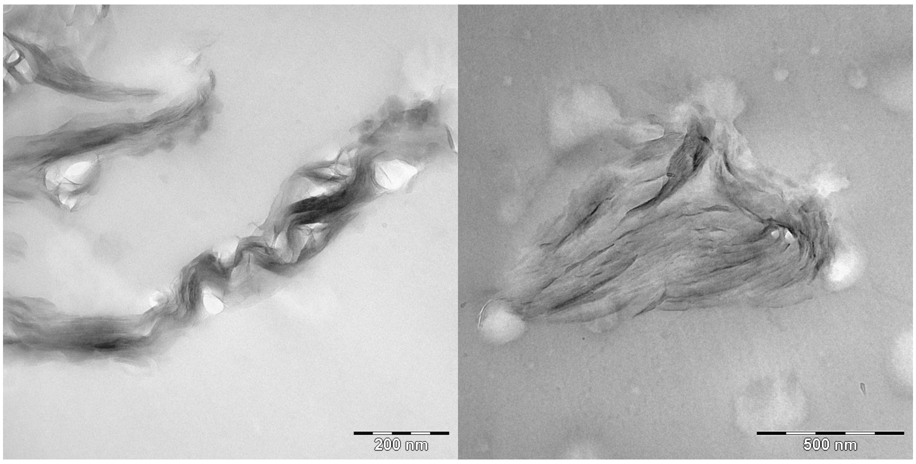

Fig.3. TEM of PRX217/ATBN/C30 (left), PRX217/CTBN/C30 (right)

4. CONCLUSION

The study shows that addition of a combination of organophilized clay with hyperbranched polyesters can lead to a significantly enhanced strength composites. An analogous addition of the clay to liquid nitrile rubber/epoxy blends can balance some of the drawbacks of liquid rubber while maintaining its desirable properties

ACKNOWLEDGMENT

This work was supported by the Grant Agency of the Academy of Sciences of the Czech Republic (grant No IAA200500904)

Análisis cinético y de curado mediante DSC de una resina epoxi reforzada con SiC nanométrico y micrométrico

J. Abenojar, M.A. Martínez
Grupo de Comportamiento en Servicio de Materiales. Universidad Carlos III de Madrid.
Av. Universidad, 30. 28911 Leganés, España
J.C. del Real
Departamento de Ingeniería Mecánica. Universidad Pontificia Comillas de Madrid
(ICAI), Alberto Aguilera, 23, 28015 Madrid, España

RESUMEN

En este trabajo se estudia el curado de una resina epoxi cargada con SiC, mediante calorimetría diferencial de barrido (DSC). Se sigue el método isotérmico, fijando la temperatura a 25 ºC, siguiendo la evolución con el tiempo durante 3 horas y realizando un dinámico subiendo la temperatura hasta 150 ºC a razón de 10 ºC/min. De esta forma se obtiene el calor necesario para curar la resina totalmente. La combinación de los dos métodos permite calcular el grado de conversión del PMC.

Se utiliza SiC en dos proporciones (6 y 12%) y en dos granulometrías (10 μm y nanométrico). El epoxi utilizado es una resina comercial que cura a temperatura ambiente durante 24 h.

El objetivo del trabajo es determinar las cinéticas de curados de los PMC's estudiados, comparándolos con el epoxi para ver la influencia de la carga en estos materiales.

1. INTRODUCCIÓN

El proceso de curado de las resinas termoestables es complejo e incluye varios procesos reactivos. Como resultado de todos estos procesos, el sistema libera calor durante el curado. Esta liberación de calor se puede seguir mediante un DSC.

El avance de la reacción es directamente proporcional a la cantidad de calor generado y el máximo grado de conversión se alcanza cuando hayan reaccionado todos los enlaces susceptibles de hacerlo. Así, el grado de conversión alcanzado en un tiempo t será:

$$\alpha = \Delta H_t/\Delta H_R \qquad (1)$$

Idealmente, ΔH_R es el calor total liberado cuando un material no curado cura completamente y su valor debe ser constante para una resina, independientemente del método de determinación.

La velocidad de reacción $d\alpha/dt$, a presión y temperatura constante, está relacionada con una función que refleja las concentraciones de especies reactivas $f(\alpha)$, a través de la constante de velocidad k.

Para el estudio de reacciones de curado en termoestables, Hoire et al. (1970), Sourour et al. (1976), Pusatcioglu et al. (1979) y Abadie et al. (1992), suelen utilizar el mecanismo llamado de orden n o el autocatalítico. Estos dos modelos corresponden a casos particulares de la ecuación (2), donde n, m y p son constantes y su valor depende del modelo de reacción escogido.

$$f(\alpha) = (1-\alpha)^n \alpha^m (-\ln(1-\alpha))^p \qquad (2)$$

Según Doulah (1980) y Gorbachez (1980) no se puede hablar de ordenes de reacción en reacciones heterogéneas, por eso cuando se utilizan los modelos de orden n y autocatalítico, al no saber que otros procesos reactivos pueden estar implicados, los parámetros calculados tienen un significado formal.

2. PROCEDIMIENTO EXPERIMENTAL

2.1 Materiales

La resina epoxi utilizada fue un DGEBA standard, Epofer EX 401, y el endurecedor fue el Epofer 432, suministrados por Feroca Composites (Madrid, España). Esta resina bicomponente cura a temperatura ambiente, aproximadamente en 24 horas.
El SiC se usa en proporciones del 6 y 12% y procede de diferentes casas comerciales dependiendo de su granulometría. El carburo de silicio nanométrico es suministrado por la empresa Bioker Research, S.L. (Oviedo, España). Las partículas micrométricas de 10 μm fueron suministradas por Carburos Navarro, S.A. (Cuenca, España).

2.2. Técnicas empleadas

El DSC utilizado es de la marca Mettler Toledo (Barcelona, España). El programa que se ha seguido es una isoterma a 25 ºC durante 180 minutos y después un dinámico hasta 150 ºC, a 10 ºC/min, determinándose tanto el calor isotérmico como el residual (que nos da el tramo dinámico), siendo la suma de ambos el ΔH_R de la ecuación (1).
Se utilizan las ecuaciones cinéticas llamadas autocatalíticas o de orden n. Para el cálculo de los parámetros cinéticos se sigue el método de Kamal et al. (1973), que utiliza la ecuación (3), aunque hay otros autores como Macan et al. (2005) para resinas epoxis utilizan el método de Kenny, que es una modificación de Kamal.

$$d\alpha/dt = k_1(1-\alpha)^n + k_2(1-\alpha)^n \alpha^m \qquad (3)$$

3. RESULTADOS

En general la adición de SiC aumenta el grado de curado a las 3 horas, aunque este incremento no esta relacionado con el porcentaje añadido, ya que dependiendo de la granulometría del SiC la variación es diferente (Figura 1). El mayor incremento corresponde al material con un 6% de SiC nano, mientras que para el 12% el grado de curado es igual que el del epoxi. Cuando se adiciona SiC micro la variación se invierte. El mayor grado de conversión corresponde a las adiciones del 12% mientras que las del 6% solo están ligeramente por encima al epoxi.
A las 3 horas a 25 ºC el material base alcanza un 56% de conversión, el epofer + 6%SiC nano alcanza el 71%, mientras que el epofer + 12%SiC nano, se queda en 56%. Esto significa que la adición del 6% de SiC nano hace más rápida la reacción de curado, mientras que cantidades superiores no le afectan. Con el SiC micro el efecto es el inverso. La reacción de curado es más rápida con mayores cantidades de partículas.

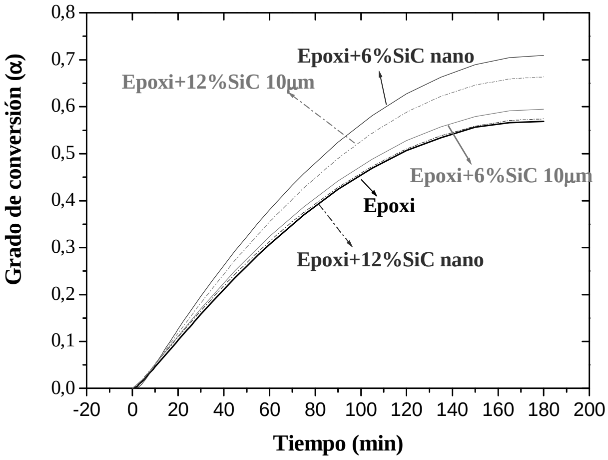

Figura 1. Variación del grado de conversión en relación al porcentaje y la granulometría del SiC adicionado

Datos cinéticos	Epoxi	Epoxi +6%SiC nano	Epoxi +12%SiC nano	Epoxi + 6%SiC 10µm	Epoxi +12%SiC 10µm
k_1	0.00211	0.00059	0.00263	0.00447	0.00428
k_2	0.01163	0.01403	0.00651	0.04516	0.03207
n	2.48951	1.78253	1.56400	3.58967	2.74574
m	0.33487	0.20657	0.19093	1.03798	0.87495
n+m	2.82438	1.98910	1.75493	4.62765	3.62069
R^2	0.94792	0.89209	0.94394	0.94558	0.94377

Tabla 1. Datos del ajuste de la ecuación de Kamal al curado de los PMC's

Al aplicar la ecuación de Kamal (3) al curado de estos materiales (Tabla 1), hay un aumento en el orden de reacción total (n+m) con la adición de SiC micro y un descenso, aunque no tan importante con el nano. El ajuste en general es similar en todas las curvas. Además la k_2 es mayor que la k_1 por lo que la reacción autocatalítica es más rápida que la de orden n.

Si se aplica solo la parte autocatalítica de la ecuación a los materiales compuestos, las diferencias en el orden total de reacción (n+m) es menor (Tabla 2), estando entre 2 y 2,7. Por ello, es de esperar un aporte importante a la ecuación de velocidad de la parte de orden n de la reacción, sobre todo en los materiales cargados con partículas micrométricas. También se puede observar que el ajuste a la parte autocatalítica de la reacción es bastante peor. Sin embargo, para los materiales cargados con nanopartículas la contribución de la parte de orden n a la velocidad de reacción es menos importante, ya que los ordenes de reacción totales son ligeramente superiores a los encontrados teniendo en cuenta los dos aportes. Los valores de k son similares en todos ellos y solo para el epoxi y el epoxi cargado con 6% de nano, este valor es similar al k_2 (Tabla 1).

Datos cinéticos	**Epoxi**	**Epoxi +6%SiC nano**	**Epoxi +12%SiC nano**	**Epoxi +6%SiC 10μm**	**Epoxi +12%SiC 10μm**
k	0.01185	0.01495	0.01028	0.01536	0.01611
n	2.3339	1.80706	2.02015	2.42576	2.00104
m	0.20742	0.2145	0.15026	0.28166	0.28705
n+m	2.54132	2.02156	2.17041	2.70742	2.28809
R^2	0.90488	0.8852	0.87199	0.4574	0.56022

Tabla 2. Datos del ajuste de la ecuación autocatalítica al curado de los PMC's

4. CONCLUSIONES

En general tanto el grado de conversión como el calor utilizado en el curado dependen del tamaño de las partículas de SiC utilizadas. Para las partículas micrométricas y para el 6% de nano, el calor empleado en la reacción es mayor al igual que el grado de conversión que el del material base, aumentando con el porcentaje. Sin embargo para las adiciones del 12% no hay apenas variación.

Para las variables cinéticas se produce un aumento en el orden de reacción total con la adición de partículas micrométricas y un descenso, aunque no tan importante con las partículas nanométricas. La k_2 es mayor que la k_1 por lo que la reacción autocatalítica es más rápida que la de orden n.

Se produce un aporte bastante importante a la ecuación de velocidad de la parte de orden n de la reacción, sobre todo en los materiales con partículas micrométricas.

REFERENCIAS

ABADIE, M. J. M., SAKKAS, D. (1992) Etude cinetique de la reticulation du polyester isophtalique insature par DSC—I. Etude isotherme. *Europ. Polym. J.*, 28, 873-879

DOULAH, M. S. (1980) Determination of kinetic parameters by thermoanalytical techniques. *Thermochim. Acta*, 35, 263-265

GORBACHEZ, V. M. (1980) Some aspects of Sestak's generalized kinetic equation in thermal analysis., *J. Thermal Anal. Calorim.*, 18, 193-197.

HORIE, K., MITA, I., KAMBE, H. (1970). Calorimetric investigation of polymerization reactions. IV. Curing reaction of polyester fumarate with styrene, *J. Polym. Sci. A-1: Polym. Chem.*, 8, 2839-2852

KAMAL, M. R., SOUROUR, S. (1973) Kinetics and thermal characterization of thermoset cure. *Polym. Eng. Sci.*, 13, 59-64

MACAN, J., BRNARDIC, I., IVANKOVIC, M., MENCER. H. J. (2005) DSC study of cure kinetics of DGBA-based epoxy resin with poly(oxypropylene) diamine. *J. Termal Anal. Calorim.*, 81, 369–373

PUSATCIOGLU, S. Y., FRICKE, A. L., HASSLER, J. C. (1979) Heats of reaction and kinetics of a thermoset polyester**.** *J. App. Polym. Sci.*, 24, 937-946

SOUROUR, S., KAMAL, M. R. (1976) Differential scanning calorimetry of epoxy cure: isothermal cure kinetics. *Thermochim. Acta*, 14, 41-59

Prediction of mechanical properties of composites of HDPE/HA/EAA

C. Albano
Laboratorio de Polímeros, Centro de Química, IVIC, Caracas, Venezuela. UCV,
Facultad de Ingeniería, Escuela de Ingeniería Química, Caracas, Venezuela.
R. Perera
Departamento de Mecánica, USB, Caracas, Venezuela
L. Cataño, A. Karam
Laboratorio de Polímeros, Centro de Química, IVIC, Caracas, Venezuela
G. González
Departamento de Ingeniería, IVIC, Caracas, Venezuela.

SUMMARY

The mechanical properties of composites of high-density polyethylene with hydroxyapatite (HDPE/HA) using an ethylene-acrylic acid copolymer (EAA) are analyzed using different mathematical models. A comparison with the experimental results established that the Guth and Kerner theoretical models can be used to predict the Young’s modulus. On the contrary, the values obtained by the Verbeek model did not show a good agreement with the experimental data, because different factors, such as the reinforcement’s aspect ratio, the interfacial adhesion, porosity and binder contents, that influence the mechanical properties.

1. INTRODUCTION

There have been several theoretical models developed to predict the Young’s modulus of reinforced polymers obtained by injection moulding, compression moulding, etc. In this investigation, the models by Verbeek (2003), Guth (1945) and Kerner (1956) were used for predicting Young’s modulus values of composites of high-density polyethylene with hydroxyapatite (HDPE/HA) using an ethylene-acrylic acid copolymer (EAA). Additionally, the Nicolais-Narkis (1971) and Kunori-Geil (1980) models for predicting the polymer-filler interaction were employed.

2. EXPERIMENTAL

A commercial high-density polyethylene (MFR = 5 dg/min) was used as the polymeric matrix. Two ethylene-acrylic acid random block copolymers (EAA) containing 5 and 20 wt% of acrylic acid were used in two different concentrations: 2 and 10 wt%.

HA granules were prepared through a precipitation reaction between calcium hydroxide and ammonium phosphate solutions. Composites were prepared in an internal mixer at 160 °C and at a screw rate of 50 rpm.

Mechanical properties were measured using an Instron Universal Testing Machine (model 4204) at 50 mm/min. The samples were cut out from compression molded sheets to a size recommended by ASTM-638 standard procedure.

The morphology of the composites was evaluated by transmission electron microscopy (TEM). Thermal decomposition analyses were performed in order to elucidate the thermal stability of the evaluated samples. Differential scanning calorimetry analyses were carried out and the crystallinity degrees, melting and crystallization peak temperatures were also determined.

3. RESULTS AND DISCUSSION

Figure 1 shows that the experimental values of the Young’s modulus of HDPE/HA composites are close to those obtained using the Guth and Kerner models. This is attributed to the fact that some of the assumptions made by those models, such as no polymer-filler interactions and increased viscosity due to the filler addition, are indeed the case. Both the experimental and the theoretical values indicate that the incorporation of HA slightly increases the rigidity of HDPE through the restriction in the mobility of the polymer molecules.

Verbeek’s model does not show a good agreement with experimental data, due to the fact that the more important assumptions of the model, such as the particle size and packing efficiency of the reinforcement, as well as its aspect ratio and a perfect polymer-filler interaction, are not followed by the composite. Additionally, this model indicates that a reinforcement effect of the added particles (filler) can only be attained when their aspect ratio is larger than a critical value of around 4. In this study, this factor (aspect ratio) is affected by the filler dispersion and the presence of agglomerates. Furthermore, the porosity of the final product, which increases with the HA content, originates that the experimental results be lower than the values of theYoung’s modulus obtained through the model.

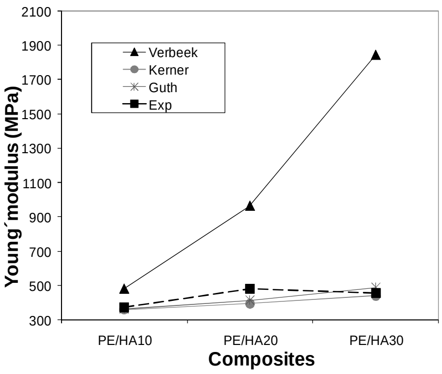

Figure 1: Prediction of the Young’s modulus values of composites.

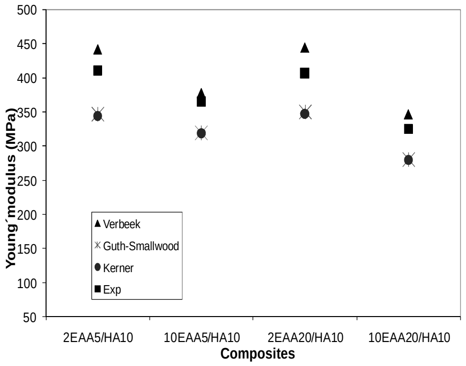

Figure 2: Prediction of the Young’s modulus values of composites with 10 wt.% and copolymers.

When the copolymers were incorporated into the HDPE/HA composites (Figures 2-4), the behavior of the Young’s modulus obtained through the use of the already mentioned models differs from the experimental values depending on the HA content, the AA content of the copolymers and the copolymers concentration. The Guth and Kerner models do not take into consideration factors such as the change of volume on stretching, the shape of rod-like filler particles embedded in a continuous matrix, which makes that the experimental values of the Young’s modulus be slightly higher than those predicted by the models. This behavior was observed in all samples, independently of the HA and copolymer contents. Hence, no improvement in the polymer-filler adhesion due to the presence of the compatibilizers (copolymers) can be inferred.

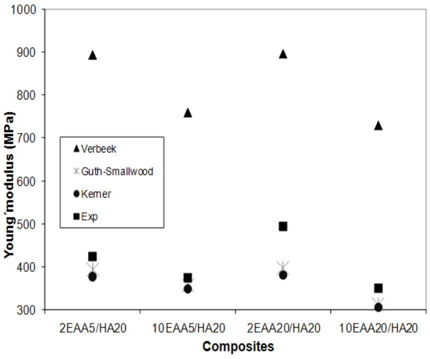

Figure 3: Prediction of the Young’s modulus values of composites with 20 wt.% and copolymers.

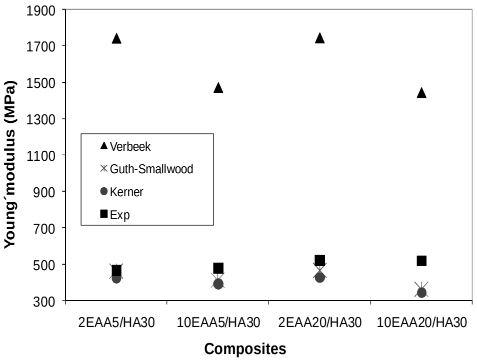

Figure 4: Prediction of the Young’s modulus values of composites with 30 wt.% and copolymers.

At low filler contents (10wt.% of HA), it is possible to enhance the filler dispersion through the addition of the copolymers, but not a true polymer-filler interaction is achieved, which could explain the slight deviations between the experimental and theoretical values predicted by Verbeek’s model. On the contrary, with increased contents of HA (20 and 30wt.%), even with the addition of the copolymers, the Verbeek’s model become unsuitable for determining the composite’s Young modulus. This fact is attributed to the already mentioned factors, as well as to a poor wetting (poor polymer-filler adhesion) on the pores of the composites. Good wetting would result in less porosity, which would increase the Young’s modulus of the material.

The equations of Nicolais-Narkis and Kunori-Geil theoretical models relate the tensile strength with a proportionality parameters “P” and “a” which are stress concentration parameters. A higher value of these parameters corresponds to a stronger stress concentration. The values of “P” and “a” are shown in table 1. As it can be seen, these values decrease with the increase in the HA content. This effect depends on the acrylic acid present in the copolymers and on the copolymer contents. For composites with 10 wt.% of HA, part of the copolymer could be located in the matrix, originating defects which produce stress concentration. On the contrary, at higher HA contents, there is a higher amount of OH groups, and a slight increase in the interactions (though weak) with the carboxylic groups of AA is produced. This implies lower amounts of the copolymer in the polymeric matrix, increased tensile strength values and decreased “P” and “a” values in the composites.

Other factors affecting the experimental Young’s modulus values are the decrease in the crystallinity degree of the matrix, due to the addition of the copolymers, as well as in its thermal stability, determined through the activation energy values.

Parameters	Copolymers	10 wt.% HA	20 wt.% HA	30 wt.% HA
P	0	5.59092984	-0.02289678	-0.39369345
	2(5)	4.87352894	0.44485178	1.21902669
	2(20)	5.31018405	-0.55933569	-0.79213019
	10(5)	5.60074231	0.93222616	0.07826436
	10(20)	7.50436234	2.73812813	-0.49804593
a	0	25.9442758	-0.05518706	-0.77407897
	2(5)	21.089557	1.11749138	2.95711435
	2(20)	23.9508278	-1.28987626	-1.49306655
	10(5)	26.0163782	2.45304864	0.16244827
	10(20)	44.809537	8.92839102	-0.96820611

Table 1: Adhesion parameters of the composites

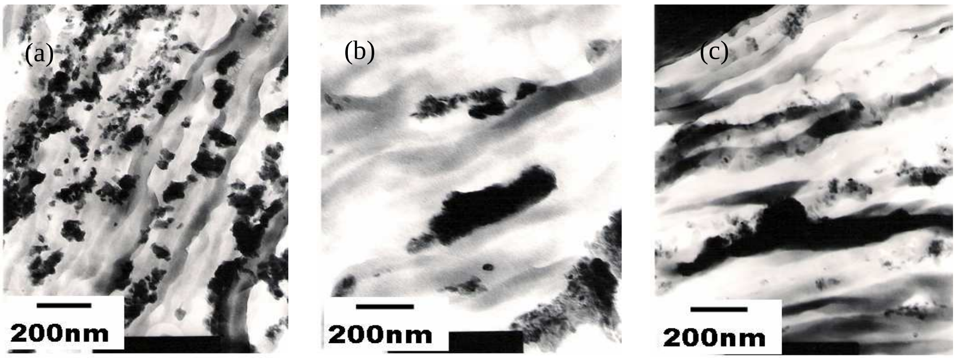

Figure 5: Micrographs of composites with 30wt.% of HA: a) HDPE/HA; b) HDPE/HA/2EAA5; c) HDPE/HA/2EAA20.

Additionally, the morphology of the composites (Figure 5) indicates that there is not a significant increase in the polymer-filler interaction, although better filler dispersion is attained.

REFERENCES

GUTH E. (1945). *J. Appl. Phys.*, 16, 20-25.
KERNER E. H. (1956). *Proc. Phys. Soc.*, 69 (B), 808-813.
KUNORI T., GEIL. P. H. (1980). *J. Macromol. Sci. Phys.*, B18, 135-175.
NICOLAIS L., NARKIS M. (1971). *Polym. Eng. Sci.*, 11, 194-199.
VERBEEKC. J. R. (2003). *Materials Letters*, 57, 1919-1924.

Evaluation of the HPMC/PVA blend in the production of granules for controlled release of theophyline

R. Brandalise
Centro de Ciências Exatas e Tecnologia
Grupo de Tecnologia de Polímeros
Universidade de Caxias do Sul / Caxias do Sul / Brazil
V. Santos, G.A. Carvalho
Centro de Ciências Exatas e Tecnologia
Grupo de Tecnologia de Polímeros
Universidade de Caxias do Sul / Caxias do Sul / Brazil
J. Favero, H.B. da Rosa, D.S. Miron, V.W. Angeli, K.B.C. Souza
Laboratório de Tecnologia Farmacêutica e Controle de Qualidade, Centro de Ciências da Saúde (CECS), Universidade de Caxias do Sul, Caxias do Sul, RS

ABSTRACT

The search for therapies aimed at reducing the adverse effects of some drugs is one of the goals to be achieved in the development of new pharmaceutical forms. The main components for formulations of film coating are polymeric. The drug used in the study was theophyline. This work is proposed to evaluate the morphology and the characteristic solubility of the polymer hydroxypropylmethyl cellulose (HPMC), poly (vinyl alcohol) (PVA) and blend HPMC/PVA-25/75 in medium that simulate the pH of intestinal fluid and stomach. Granules were developed with theophyline and HPMC/PVA-25/75 with further development of capsules. Synergism was observed between the components of the blend in the composition of HPMC/PVA-25/75. The use of PVA in a larger quantity in the blend allows the control of the solubilization in the HCl 0.1 M medium, besides being a water-soluble polymer which makes the process of coating a clean technology when compared to conventional coatings.

1. INTRODUCTION

Polymers are widely explored in pharmaceutics and the mechanism and kinetics of drug release is based on the pharmaceutical forms, depend on the solubility, swelling and polymer erosion properties. For water-soluble drugs, release occurs mainly by diffusion with a limited contribution of matrix erosion and anomalous diffusion resulting from the relaxation of the polymeric chains (Hardy et al. 2007). Different pharmaceutical forms are prepared in order to release the drug immediately into the gastrointestinal system or to modify the release profile using polymer blends with different solubilities in biological fluids.

HPMC is widely used, because of its safety, variety of viscosities and types of substitutions (McPhillips et al. 1999). PVA has been studied in drug release, and when it is at a high percentage, it speeds up drug release (Strübing et al. 2006). Theophyline, used in the experiment, is employed to treat bronchial asthma, and presents a low therapeutic index. It requires constant monitoring of its plasma concentrations to avoid adverse effects. The present study aims to prepare and characterize blends with HPMC/PVA in order to modify the physicochemical properties of the pure polymers and their applicability in drug release.

2. EXPERIMENTAL

2.1 Preparation and characterization of the HPMC/PVA blend

Films of pure polymers and the HPMC/PVA blend at a proportion of 25/75 (w/w) were prepared in an aqueous solution at a concentration of 5% (w/v), in reactors at 80 °C. The solutions were then distributed onto Petri plates and dried in an oven with circulating air (Tecnal, model TE-394/2) at 40 ºC, for 10 hours, or until the water had evaporated completely. The polymers and the blend, in the form of films, were weighed at a proportion of 1:30, in triplicate, and to these a phosphate buffer solution was added, with a pH 6.0, or HCl with a pH 1.2. The mixtures were stirring for 40 minutes. After this period the solubility of polymers was observed in the medium used (USP 2008).

2.2 Production of theophyline granules with HPMC/PVA - 25/75

Theophyline granules were prepared using the HPMC/PVA 25/75 blend as a matrix and as coating (Table 1). The granule matrix was obtained from the HPMC/PVA 25/75 films ground in an IKA-Werke, model A11 basic cryogenic mill. Ethanol (70%) was used as granulator liquid.

Component	Function	Concentration (%)
Teophylline	Active principle	51.3
HPMC/PVA	Matrix	43.6
HPMC/PVA	Agglutinant/Coating	5.1

Table 1. Composition of the theophyline granule with HPMC/PVA 25/75.

The wet mass was dried in an oven at 55 ºC for 20 min, and then calibrated with sieves (with a mesh 24 (1.18 mm) and 14 (0.72mm). The granules collected in the mesh 14 sieve were coated by adding agglutinant solution and later dried at 55 ºC for 20 min. The process was repeated four times to obtain the theophyline-coated granules.

2.3 Evaluation of the dissolution of capsules containing theophyline granules

The theophyline granules were encapsulated so as to obtain a 200 mg dose, and microcrystalline cellulose was used as excipient. The capsules were assayed in a Nova Etica dissolutor, using 900 mL of HCl 0.1 M medium, basket apparatus, 75 rpm, and detection at 269 nm. When necessary, the samples from the dissolutor were diluted to adjust the concentration to the standard curve (4.0 – 6.0 μg/mL of theophylline).

3. RESULTS

Figure 1 illustrates the SEM micrographs of the cryogenic fracture surface of the test specimens of polymers HPMC and PVA, and of HPMC/PVA 25/75 blend.

In the HPMC/PVA 25/75 composition, whose matrix is PVA, a synergism could be seen between the blend components. SEM allowed looking at obtaining theophyline granules with a homogeneous shape and size, based on a HPMC/PVA blend (Figure 2.a). After the granulation process, regions could be seen on the granule surface, characteristic of HPMC/PVA (25/75) film. However, these regions are intercalated by distinct domains of the polymers that make up the blend (Figure 2.b). The dimensions of the granule projection in Figure 2.a were: 1.09 mm and 1.01 mm.

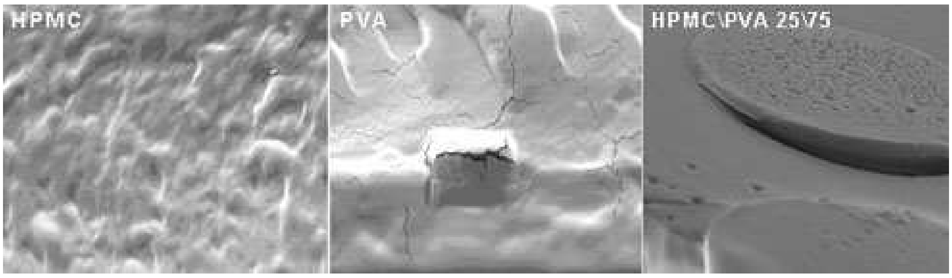

Figure 1. SEM micrographs of polymers HPMC, PVA and HPMC/PVA 25/75 blend (1000x).

Figure 2. SEM micrograph of the theophyline granules using blend HPMC/PVA 25/75 - a(35x) and b (1000x);

3.1 Solubility of the polymers and of HPMC/PVA – 25/75 blend in different media

Table 2 shows the results of solubility of the polymers and HPMC/PVA 25/75 blend in the phosphate buffer solutions (pH 6.0) and hydrochloric acid solution (pH 1.2).

Samples	Phosphate buffer (pH 6.0)	HCl solution (pH 1.2)
HPMC	Solubilized	Solubilized
PVA	Solubilized	Partially solubilized
HPMC/PVA-25/75	Partially solubilized	Partially solubilized

Table 2. Solubility of polymers HPMC, PVA and HPMC/PVA 25/75 blends in the phosphate buffer solutions (pH=6) and HCl solution (pH=1.2) during 40 minute.

According to the solubility results presented, it could be observed that the HPMC presents a good solubility in the buffers used, while PVA does not have the same profile, and it is soluble in pH 6.0 which simulates the pH of the bowel, and less soluble in the HCl solution which simulates the stomach fluid. In the results obtained at a proportion of 25/75 the polymers used were not fully soluble. In the phosphate buffer, and in the HCl solution it is perceived that with any amount of PVA there is less solubility, and this polymer may be the controller of drug solubility.

The capsules dissolution test showed that 78.4% of the drug was released after 30 min and 97.4% after 120 minutes, indicating that the drug is released immediately from the granules. Increasing the number of times (four times) that the granules were coated (adding polymer/drying/adding polymer) improved the results of the dissolution, which were: 52.2% in 30 min and 65.9% in 120 min.

4. CONCLUSIONS

The morphological evaluation of the granules developed with theophylline and the HPMC/PVA-25/75 blend led to the conclusion that granulates could be obtained, but the coating of the granules was not homogeneous. HPMC is completely solubilized in the media that simulate the pH of the stomach and intestine, and PVA is the polymer that allows controlling the solubility of the blend in the media, with different pH. In this way, PVA can potentially control drug solubilization, contributing to obtaining modified release systems.

ACKNOWLEDGMENTS

Universidade de Caxias do Sul, BIC/UCS; Empresa VITAMED.

REFERENCES

HARDY, I.J., WINDBERG-BAARUP, A., A.; NERI, C., BYWAY, P.V., BOOTH, S.W., FITZPATRICK, S. (2007) Modulation of drug release kinetics from hydroxypropyl methyl cellulose matrix tablets using polyvinyl pyrrolidone. *Int. J. Pharmaceut.*, 337, 246-253.

STRÜBING, S., METZ, H., MÄDER, K. (2006) Mechanistic analysis of drug release from tablets with membrane controlled drug delivery. *European Journal of Pharmaceutics and Biopharmaceutics*, 66, 113-119.

MCPHILLIPS, H., CRAIG, D. Q. M., ROYALL, P. G., HILL, V. L. (1999) Characterisation of the glass transition of HPMC using modulated temperature differential scanning calorimetry. *International Journal of* Pharmaceutics, 180, 83-90.

USP 27 United States Pharmacopeial Convention. Usp Nf 2003: the official compendia of standards. Rockville, MD, USA: United States Pharmacopeial Convention, 2003.

A possibility for utilization of phosphogypsum like a mineral filler for polyolefin composites

Y. Denev, B. Bogdanov, G. Denev, A. Popov
Organic Chemical Technologies Department**.** Faculty of Technical Sciences**,** Prof. Assen Zlatarov University, 8010 Burgas, BULGARIA

SUMMARY

The possibility for utilization of phosphogypsum (solid waste by-product from phosphoric acid industry) like mineral filler for composites based on polyolefines (polyethylene and polypropylene) was investigated. The reinforcing of composites with phosphogypsum is intended to enhance the properties and reduce the costs of the materials. The polyolefines were filled with micron-sized phosphogypsum (waste calcium sulfate) particles through melt compounding. The phosphogypsum particles were mixed with polymers at the various weight percentages of 10% to 100% phosphogypsum. The results from the tensile tests of polyethylene/phosphogypsum reinforced composites are that the 60 wt % filler content showed the highest value for maximum tensile properties. The same conclusions were made discussing polypropylene/phosphogypsum composites but at different filler content (10 wt %). The Young modulus increases with reinforcing that proves existence of good adhesion between mineral filler and the polymer matrix. The polyolefin/phosphogypsum composites also show completely different rheological behavior from the neat polymers, such as loss of Newtonian region. There is an attempt to predict mechanical properties of filled composites using theoretical models. The results above indicate that the phosphogypsum particles have a good bonding between its surface and matrix and they are effective mineral filler for polyolefin composites.

1. INTRODUCTION

The filling of polymers is one of the most widely used methods for modification of the polymers. The main task of filling with mineral fillers is to improve some of the basic characteristics of the polymers. The second task is to reduce cost of the polymer products. The first goal is achieved more hard, because the two-phased system characteristics are determined by various factors such filler chemistry nature, disperse composition, package density etc (Rothon et. to 2002). Polyethene is probably the most commonly used polymer in everyday life. It is the polymer that is used to make grocery bags, shampoo bottles, children's toys, and even bullet-proof vests (Vasile et. to 2005). Polypropylene (PP) underwent phenomenal growth in production and use throughout the world during the latter half of the 20th century. From the early 1960s until the oil crisis of the early 1970s, the growth rate was nearly 25% annually (Karian et. to 2003). The phosphogypsum ($CaSO_4.2H_2O$) is a waste by-product from phosphoric acid production. His amount is nearly 4 tones with respect to the 1 tone acid. That creates serious predicaments at its conservation and consists in serious ecological problem (Ahmedov et. to 1980; Evengika et. to 1990). This by-product is deposited on thousands of hectares of landfills and dumping grounds. The world’s total amount of accumulated phosphogypsum is billions of tons. Its use as the mineral filler on polymeric materials is one of the directions for its more skilled use (Kowalska et. to 2002). The phosphogypsum characteristics are suitable for using like mineral filler. Its merits with respect to the wide used mineral fillers that have gone as the crayon, the terra alba, the talc etc. are their low hardness by Mohs (2-3), acid resistance, his crystalline structure and the great variety of the crystalline alterations (Valancius et. to 2005; Nielsen et. to 1974)

2. MATERIALS

Materials. Polyethylene (PE), polypropylene (PP) and $CaSO_4.2H_2O$ filler.

3. RESULTS AND DISCUSSION

Depending on the nature and amount of other modifiers and fillers, calcium sulphate as additive gives rise to enhanced mechanical properties, improved hardness, attrition resistance, chemical resistance, fire resistance and to reduced shrinkage as also to damping of vibrations in thermoplastic materials. Mineral filler composites have emerged as realistic alternative to active filler-reinforced composites in many applications. The SEM micrographs of an untreated phosphogypsum ($CaSO_4$ hemi-hydrate) are shown on figure 1.

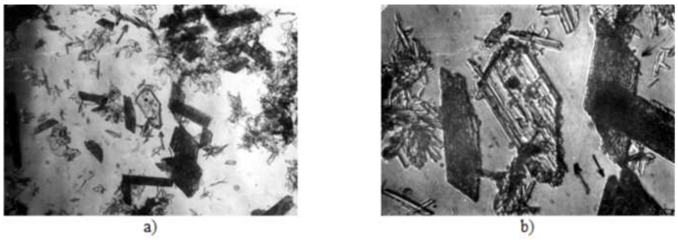

Fig.1. SEM micrographs of neat phosphogypsum ($CaSO_4.1/2H_2O$)
a) x133; b) x373.

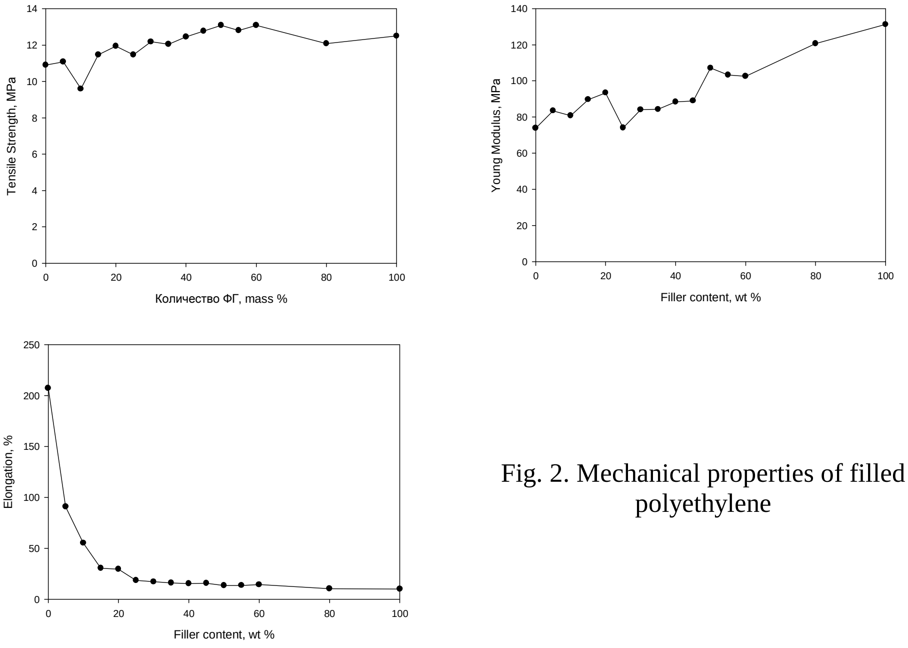

Fig. 2. Mechanical properties of filled polyethylene

The particle size distribution of phosphogypsum is shot as average particle diameter is between 20 and 30 μm. This size is above the particle size of common used mineral fillers but with suitable modification this factor can be overcome.

In the beginning of polyethylene filling (at 10 wt%) was occurred strong decreasing in deformation (fig. 2). At 30 wt% filling this tendency keeps his growth but slowly. At the same time relative elongation of samples decreases probably for the increasing in defects number (fig. 2). At this filling degree the tensile strength and Young modulus change slightly. By increasing of filler content the tendency of decreasing in relative elongation keeps.

The Young modulus significant increases but the tensile strength keeps stable even though weak decrease tendency (fig. 2). The filling of polyethylene with 60 wt% is optimal concentration for this system. (fig. 2). This significant improvement in mechanical behavior of polyethene composites proves the effectiveness of phosphogypsum like mineral filler for polyolefins.

The mechanical behavior of reinforced PP composites demonstrates changes similar to these in most used poyolefin-polyethylene. The main difference between PE and PP occurred in tensile strength change of composite with 10 wt % PG – the tensile strength increases significantly. This phenomena can be explained with some structural effects of phosphogypsum on polypropylene composites. The Young modulus increases to filler content of 10 wt % and after this slightly decreases in whole interval of phosphogypsum content. The reinfocement of PP with 60 wt % filler is optimal phosphogypsum concentration because the mechanical properties have good values and after this concentration the matrix and filler mixing is very difficult.

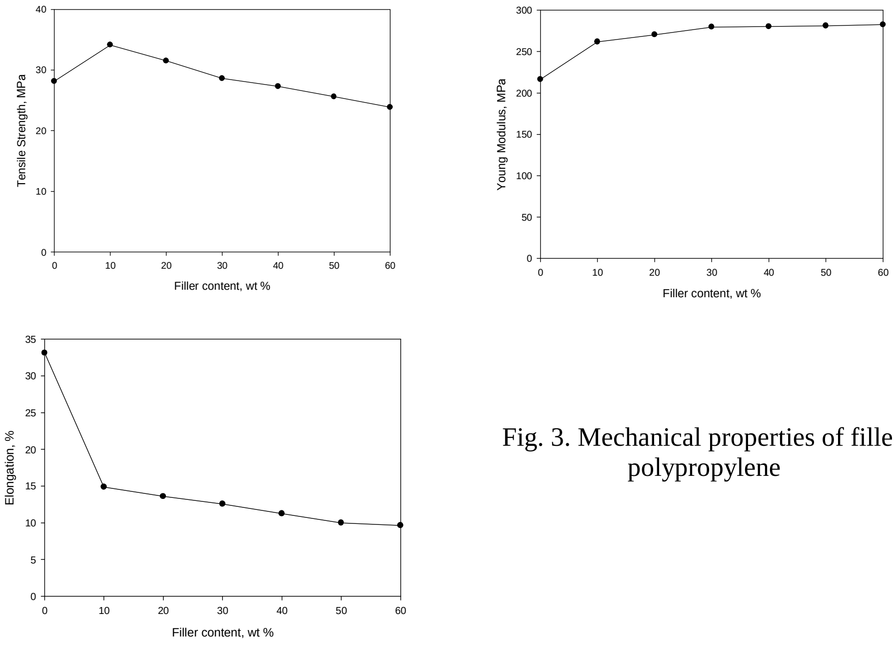

Fig. 3. Mechanical properties of filled polypropylene

4. CONCLUSION

The possibility for a utilization of the waste phosphogypsum like effective light mineral filler for polyolefin composites was investigated. The carried out experiments show positive changes in mechanical behavior of obtained composites.

There is attempt to predict mechanical properties of filled polyolefin composites using theoretical models. The modulus of filled polymers can be predicted more easily than other mechanical properties of filled polymer systems. The degree of polymer-filler interactions plays an important roll in determining the tensile strength of filled polymers. The results above indicate that the phosphogypsum particle has a good bonding between its surface and matrix.

This confirms the possibility for using of phosphogypsum like effective mineral filler for polyolefin composites which obtain characteristics like low hardness, acid and hydroxides resistance etc. compared to widely used chalk.

REFERENCES

1.AHMEDOV MA, TA Atakuzin, (1980) Fosfogips (Phosphogypsum), Fan, Tashkent
2.EVENGIKA SD, AA Novikova, (1990) Fosfogips i ego ispolzovanie (Phosphogypsum and its Use). Moscow
3.KARIAN H., Handbook of Polypropylene and Polyproplene Composites, II ed. Marcel Dekker, 2003
4.KOWALSKA E, WIELGOZE Z (2002), *J Reinf Plast Compos*, 21, 1043-1052
5.KOWLASKA E, WIELGOZE Z (2002), *J Reinf Plast Compos*, 21, 1013-1026
6.NIELSEN L. E., Mechanical Properties of Polymer and Composites, 2, Marcel Dekker, N.Y., 1974
7.ROTHON R.N., Particulate Fillers for Polymers, First Edition, 2002
8.SINGH NB, MIDDENDORF B, (2007) *Prog Cryst Growth Charact Mater*, 53, 57-77
9.VALANCIUS Z, NIZEVICIENE D, LESKEVCIENE V, KYBARTIENE N, *Ceram Silik*, 49(2), 2005, 20-125
10.VASILE C. and PASCU M., Practical Guide to Polyethene, Rapra Technology, 2005

The curing reaction kinetics of epoxy/anhydride/silica systems

E. Díaz
Departamento Ingeniería Ingeniería M.M. y CC. de Materiales, E.T.S. de Náutica y Máquinas Navales. Universidad del País Vasco/EHU
I. Irastorza, R. García, I. Ibañez
Departamento de CC. y TT. de la navegación Maq. Y CC. Navales, E.T.S. de Náutica y Máquinas Navales. Universidad del País Vasco/EHU
R. Valenciano, S. Anasagasti
Departamento de Química-Física. Facultad de Ciencias. Universidad del País Vasco/EHU

SUMMARY

Advances in the electricity industry have led to increasing demands for epoxy/anhydride/silica insulation systems. In this present study, the curing reaction kinetics of two epoxy systems are investigated using non-isothermal differential scanning calorimetry (DSC). Their mixtures were isothermally cured under vacuum at 130 ºC for differing lengths of time, and their glass transition temperatures, T_g, activation energies, E_A, and other parameters were determined by DSC. Interest in such systems centres on their industrial applications, for which reason it was decided to study high silica loadings, cured at 130º C; a curing temperature that was shown to be the most appropriate for these systems in all cases, as it prevented cracks and structural defects in the moulding production processes.

1. INTRODUCTION

The Araldite B_{41} epoxy resin used in this study is a diglycidyl ether of bisphenol-A epoxy resin (DGEBA). It was cured with a mixture of tetrahydrophthalic acid anhydride (THPA) and phthalic acid anhydride (PPA) that acted as hardeners in the presence of a SiO_2 mineral filler in the first system (ETFS). The weight ratios of the epoxy/THPA/FPA/SiO_2 epoxy mixture were 100/30/20/250. In the second system (ETFSA), the accelerator DY 068 (tertiary amine) was also used, the weight ratios of which were 100/30/20/350/5. In the present study, the cure kinetics of two encapsulated epoxy systems were studied using non-isothermal DSC. Two systems with high silica loadings were cured at 130 ºC, which is considered the optimal temperature to ensure a quick cure and to prevent cracks and structural defects in the moulding production processes. The research seeks to provide information on optimising the curing conditions of highly silica-loaded epoxy/anhydride systems.

2. RESULTS AND DISCUSSION

Initially, the total reaction heats, ΔH_T, were determined as $\Delta H_T = 65.55$ J/g for the ETFS system and as $\Delta H_T = 12.63$ J/g for the ETFSA system. These values are considerably smaller than those obtained by Ho Park et al. (1996), Yang et al. (1999) for epoxy/anhydrides systems without silica, whereas our silica-loaded systems hinder the global curing process. The exothermic peak presented by the dynamic thermogram indicates that a polymerisation reaction has taken place. A first analysis of the sharp exothermic curing peak allows us to determine the temperature of maximum effectiveness (maximum of the peak) and the polymerisation heat, as well as the glass transition temperature.

Tables I and II respectively show the results of the dynamic scans for the ETFS and ETFSA samples, providing detailed data on: Curing time t (minutes), Residual reaction heat ΔH_{res} (Joule/gram), Peak temperature T_{peak} (ºC), Degree of conversion α, Rate constant of reaction k (miliseconds), Reaction order.

t (min)	**ΔH_{res} (J/g)**	**T_{peak} (ºC)**	**T_g (ºC)**	**α**	**ln k**	**$k*10^3$ (s^{-1})**	**Reaction Order**
0	65.55	248.0	-13.9	0	-5.1	6.3	1.1
30	63.39	238.3	0.9	0.033	-5.4	4.5	1.1
60	55.77	247.7	8.3	0.149	-5.1	6.0	1.1
90	45.81	259.7	14.2	0.301	-5.0	7.0	1.2
120	18.99	274.0	20.6	0.710	-4.5	11.0	0.9
180	13.44	275.8	37.8	0.795	-4.4	11.7	1.0
240	10.64	245.1	44.1	0.838	-5.1	5.8	1.2
300	10.02	235.2	45.9	0.847	-5.6	3.7	1.2
360	8.85	242.0	52.7	0.865	-5.3	4.8	1.1
420	8.20	236.7	62.6	0,875	-5.4	4.4	1.3
480	6.95	234.5	68.1	0.894	-5.7	3.2	1.1
600	2.35	235.3	81.9	0.954	-5.6	3.7	1.1
720	1.90	242.9	96.7	0.961	-5.2	5.3	0.9
13140	0.37	233.5	97.9	0.974	-5.8	3.0	1.1

Table I. Kinetic parameters for the ETFS system.

It may be observed that both the temperature of maximum effectiveness, and the glass transition temperature of the two systems increase with the curing time, because the material increases its reticulation level. The heat removed in the reaction decreases for the same reason, while both the reaction order to monomer and the rate constant remain constant. However, these parameters cannot predict whether or not there will be changes in the reaction mechanism. As the resin system underwent a series of complex reactions, the variations noted in the values of the reaction order to monomer within the temperature range might be due to variations in the mechanism prompted by the reaction temperatures.

In the first (ETFS) system, conversion rates of 100 % were not reached within the time span under study, which is related to the high silica content. It does not reach a curing degree of 100 % within a reasonable period of time because the load content hinders the curing process.

In the ETFSA system, the curing temperature is higher or similar to the glass transition temperature reached by the material. As reticulation progresses, the T_g increases and there arrives an instant where it coincides with the curing temperature (130 ºC), which triggers the phenomenon of vitrification of the material as studied by Kenny et al. (1996), Riera (1991) and Monserrat et al. (1992). After this point, the T_g increases more slowly, and the polymer is abnormally found in a vitreous state. It has been demonstrated by the same authors that, prior to vitrification, the reaction is kinetically controlled at first and is subsequently controlled by diffusion, when a decrease in the reaction speed takes place.

t (min)	**ΔH_{res} (J/g)**	**T_{peak}(ºC)**	**T_g (ºC)**	**α**	**ln k**	**$k_* 10^3$ (s^{-1})**	**Reaction order**
0	12.63	191.9	-12.7	0	-4.9	7.3	1.0
30	10.27	194.1	12.6	0.187	-4.8	8.2	1.3
60	3.69	191.4	42.9	0.708	-5.0	6.4	1.0
90	3.49	208.8	56.6	0.724	-4.7	9.3	0.9
120	0.73	203.6	74.5	0.942	-4.7	8.9	1.2
180	0.50	243.0	93.3	0.960	-2.9	54.4	0.9
240	0.34	223.5	101.5	0.973	-4.6	10.0	1.0
300	0.27	232.7	110.9	0.978	-3.4	34.4	1.0
360	0.07	228.7	137.6	0.994	-4.1	16.1	0.9
420	0.07	236.4	138.7	0.995	-3.4	34.8	0.9
480	0.03	228.0	140.9	0.997	-4.5	11.2	1.3
540	0.01	257.0	137.1	0.999	-2.8	57.9	1.1
600	0.01	239.8	139.1	0.999	-3.2	40.3	1.1
9060	0.01	229.4	137.1	0.999	-3.9	19.9	0.7

Table II. Kinetic parameters for the ETFSA system.

The T_g associated with the resin softening point is a good indicator of the grade of curing of the material. The importance of curing the resin above the T_g is that it produces a material with good mechanical properties as Ivankovic et al. (2003) have pointed out. The T_g of the uncured samples was –13.9 and –12.7 ºC for the ETFS and ETFSA systems, respectively. The glass transition temperature increased to over 97.9 ºC, for the ETFS sample cured for 13140 minutes, and to 137.1 ºC for the ETFSA sample for 9060 minutes (see tables I and II). The increase in the glass transition temperature disappears over long periods of curing, indicating the end of the cure reaction. The fact that the Tg does not increase linearly with the conversion degree may be explained by the epoxy/hardener relationship that lies outside the stechiometric mixing ratio (excess of hardener), which causes it to modify the magnitude and the characteristics of the formed network. An excessive amount of hardener is not incorporated into the network, acting instead as a plastifier in the curing process and later being incorporated into the main polymer as a flexifier, which can be beneficial in terms of processing the material and reducing its fragility.

Finally, the activation energy of the curing processes has been calculated in terms of its kinetics. The equations of the straight lines are compared with the Arrhenius law in their logarithmic form (Eq.1) and we thereby obtain the value of the activation energy, E_A, and the pre-exponential factor, ln Z, as presented by Yang et al. (1999) and by Lee et al. (1997)

$$\mathrm{Ln}\ k(T) = \ln Z - E_A/RT \qquad (1)$$

The value obtained for the system ETFS is E_A= 65.6 kJ/mol and for the ETFSA E_A= 69.2 kJ/mol. The pre-exponential factor A was 21216.7 for ETFS and 355755.9 for ETFSA.

3. CONCLUSIONS

The experiments show a vitrification effect when the curing temperature is lower than the T_g of the resin.

The ETFSA system cures more quickly and a greater T_g is reached in the presence of the accelerator. The conversion degree is almost 100 % in the ETFSA system.

The activation energies obtained in this experiment were 65.6 and 69.2 kJ/mol for the ETFS and ETFSA systems, respectively.

4. REFERENCES

1. Ho Park W, Keun Lee J, Jeong Kwon K (1996) Polymer Journal, 28:407-411.
2. Ivankovic M, Incarnato L, Kenny JM, Nicolais L (2003) Journal of Applied Polymer Science, 90:3012-3019.
3. Kenny JM, Opaclicki M (1996) Composites, 27:229.
4. Lee SY, Shim MJ, Kim SW (1997) Mater. Chem. Phy., 48:36-40.
5. Monserrat S (1992) J. Apply. Polym. Sci., 44:545.
6. Riera J, Teixidó (1991) Pinturas y Acabados, 187:87.
7. Yang LF, Yao KA, Koh W (1999) Journal of Applied Polymer Science, 73:1501-1508.

ACKNOWLEDGMENTS

Financial support was provided by the University of the Basque Country and by the Basque Government. The authors are grateful to Arteche Electrotécnica Hnos. for supplying the materials.

Modificación superficial de materiales poliméricos mediante plasma atmosférico

N. Encinas, B. Díaz-Benito, J. Abenojar, M.A. Martínez
Dpto de Ciencia e Ingeniería de los Materiales e Ingeniería Química, IAAB
Grupo de Comportamiento en Servicio de Materiales. Universidad Carlos III de Madrid. Av.Universidad, 30. 28911-Leganés-España

RESUMEN

La nula reactividad química (baja energía superficial) de la mayoría de superficies plásticas hace que puedan ser mojados por muy pocos líquidos y no permite lograr, por ejemplo, una unión adhesiva adecuada. Los métodos habituales para aumentar la energía superficial de materiales poliméricos son la abrasión mecánica, el uso de disolventes químicos o el tratamiento con plasma en corona o en llama.El tratamiento superficial mediante la tecnología de plasma es un método rápido, limpio (no se genera ningún tipo de residuo ambiental) y efectivo para la mejora de las propiedades de adhesión de vía aumento de su energía superficial debido a la creación de grupos polares en la superficie.

En el presente estudio se tratan probetas de cuatro materiales poliméricos (polietileno de alta y baja densidad, polipropileno y silicona) con un aparato de plasma atmosférico de Plasmatreat a tiempos 0, 3 minutos, 24, 200, 500 y 750 horas .

Se observa una relación clara entre las variaciones de la energía superficial y sus componentes dispersiva y polar con el tiempo de aplicación del plasma.

Resulta interesante la recuperación con el tiempo que sufren las superficies poliméricas, especialmente en el caso de la silicona.

1. INTRODUCCIÓN

Termodinámicamente la tensión superficial viene definida como la tendencia de un líquido a disminuir su área superficial hasta que la energía de superficie potencial sea mínima, condición necesaria para que el equilibrio sea estable (I. Levine et al). Numéricamente igual a la proporción de aumento de la energía superficial con el área. Viene dada por la ecuación de Young (ec.1):

$$\gamma_s = \gamma_{sl} + \gamma_l . \cos\theta \qquad (1)$$

El ángulo de contacto Θ es aquel que forma la superficie de un líquido al entrar en contacto con un sólido, da una definición de la noción de mojabilidad, e indica los parámetros que se requieren medir para el cálculo de la misma. Así, para $\Theta = 90º$ se dará un mojado total de la superficie, mientras que para $\Theta > 90º$ (implica $\gamma_s<\gamma_l$) el líquido formará gotas sobre la superficie sin mojarla.

Existen varios métodos para la medida de la energía superficial de un sólido, entre los que se encuentran los basados en medidas de ángulo de contacto que, conociendo la tensión superficial de un líquido de referencia permiten calcular la energía superficial a través de distintos cálculos (Owens, Kaelble, Wu et al).

1.1 Superficies poliméricas. Tratamientos Superficiales

El aumento de la energía superficial de los materiales poliméricos por encima de la tensión superficial de los líquidos o adhesivos favorece los mecanismos de adhesión o pintura, así como su durabilidad, al permitir que mojen la totalidad del área del polímero a tratar. Debido a las excelentes propiedades intrínsecas, bajo coste y facilidad de procesado de estos materiales, los tratamientos superficiales que transforman los polímeros en productos de alto valor añadido han adquirido importancia en la industria de los plásticos .Estos tratamientos tienen como objetivo desarrollar fuerza y durabilidad en las uniones adhesivas al lograr un contacto intermolecular adecuado. Ello se consigue eliminando las capas superficiales que recubren el sólido, la creación de grupos específicos, la introducción de entrecruzamiento superficial, el aumento de la energía superficial, la modificación de la morfología superficial por variación de la cristalinidad o rugosidad, mejora de la lubricación, protección de los adherentes antes de la unión adhesiva y lograr un contacto íntimo adhesivo-adherente.

1.2 Tratamiento con plasma atmosférico

El tratamiento superficial mediante plasma es un método rápido, limpio (no se genera ningún tipo de residuo ambiental) y efectivo para la mejora de las propiedades de adhesión. El plasma es generado mediante la aplicación de energía (H. Conrads et el) a un gas a fin de reorganizar la estructura electrónica de las especies y generar iones y otras especies excitadas. La energía transferida a la superficie sobre la que se aplica el plasma produce, entre otros efectos, la ionización de O_2, N_2 y especies neutras superficiales, generación de especies reactivas con grupos que contienen –OH y –NH, nanorugosidad superficial, limpieza de superficies por volatilización de impurezas, aumento de la energía superficial, deposición química de nuevas especies, etc. El flujo de plasma provoca la sustitución de átomos de baja energía de la superficie polimérica por otras funcionalidades más reactivas, como podrían ser hidroxilos (-OH), aminas (-NH), carbonilos (-CO), al bombardear el material con electrones de energía mayor que la de ruptura de los enlaces moleculares superficiales. Este proceso de creación de grupos polares en la superficie polimérica lleva a un aumento de la energía superficial y mojabilidad de la misma

2. PROCEDIMIENTO EXPERIMENTAL

2.1 Materiales utilizados

Los ensayos se llevan a cabo sobre piezas de cuatro plásticos comerciales: polietileno de alta densidad (HDPE, $\rho_{20ºC}$=910-990 kg/m^3 ISO 118), polietileno de baja densidad (LDPE), polipropileno (PP) y silicona. Las características de estos materiales son suministradas por las casas comerciales. La limpieza de las superficies se realiza con el disolvente metil-etil-cetona (MEK).

2.2 Ángulo de contacto

Se evalúa la humectación de los materiales plásticos tanto recibidos como tras el tratamiento de plasma calculando la variación en su energía libre superficial a través de medidas de ángulo de contacto utilizando un equipo OCA 15 plus de DataPhysics (Neurtek Instruments, Eibar, Guipúzcoa, España). Se sigue la metodología propuesta en la prenorma prEN 828:2009 Las muestras son limpiadas con metil-etil-cetona (MEK) y colocadas dentro de una cámara termostatizada a (24 ± 2)ºC, que previamente se ha saturado con vapor del correspondiente líquido de medida durante al menos 5 min. Se hacen medidas con gotas de agua desionizada, glicerol, nitrometano, etilenglicol, diiodometano y 1,5-pentanodiol, con 4 µL de volumen. El método de cálculo elegido es el Owens-Wendt-Rabel-Kaelble (OWRK).

2.3 Plasma Atmosférico

Se utiliza un equipo de Plasma Treat GmbH (Steinhagen, Alemania) que opera a una frecuencia de 17 kHz y a tensión de descarga de 20 kV. Está provisto de una boquilla rotatoria a 1900 rpm que expele el flujo de plasma a una presión de trabajo de 2 bar. Se tratan los plásticos (previamente limpiados con metil-etil-cetona) a tiempos 0 min, 3 min, 24 h, 200 h, 500 h y 750 h y controlando la velocidad de trabajo (1 y 10 mm/min). La boquilla se sitúa a 6 mm de la muestra. Las muestras son almacenadas durante los tiempos de estudio a temperatura ambiente en condiciones libres de contaminación. Se realiza un estudio de la variación de energía superficial de las probetas a lo largo del tiempo, a través de las medidas de ángulo de contacto anteriormente descritas.

2.4 Microscopía Electrónica de Barrido (SEM)

Las variaciones en morfología superficial de los materiales ensayados (previamente metalizadas con oro mediante un equipo de sputtering), son evaluadas por medio de un Microscopio Electrónico de Barrido (Philips XL-30, FEI EUROPE, Eindhoven, Holanda). La energía de los electrones es de 15 kV, y la microsonda EDAX generará el microanálisis de la superficie.

3. RESULTADOS

El aumento de energía superficial se da en los momentos iniciales posteriores a la aplicación del plasma (fig.1). En todos los plásticos, exceptuando la silicona la mejora en la mojabilidad se mantiene constante en el tiempo durante 750 h. El caso de la silicona resulta especialmente interesante, pues se observa un gran incremento en todas las componentes de la energía superficial al inicio del tratamiento, pero al cabo de tan sólo 24 horas, los valores iniciales se recuperan totalmente.

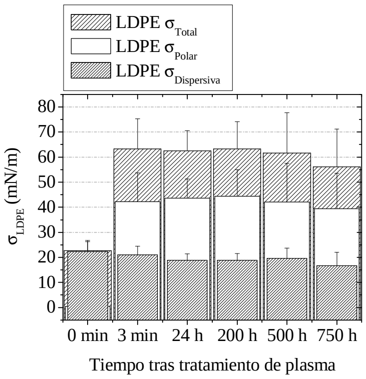

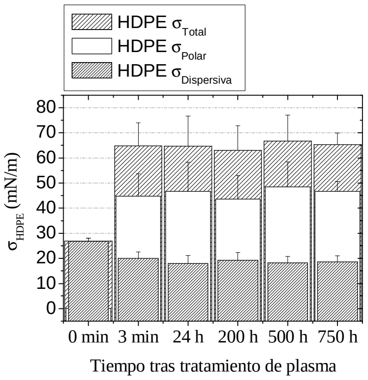

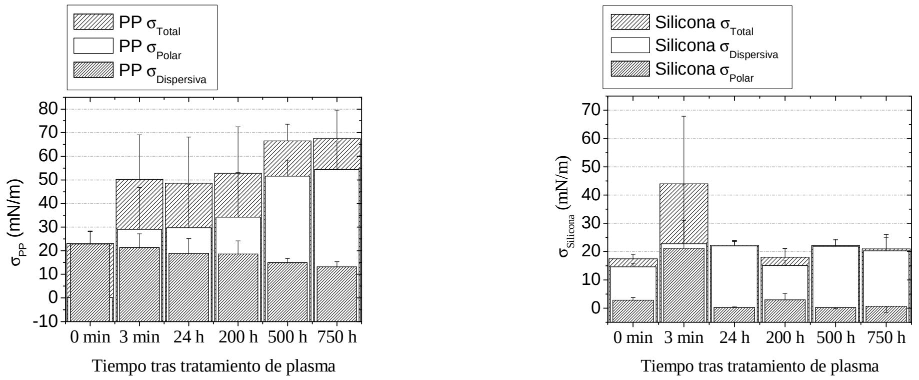

Fig. 1. Componentes de la energía superficial de los cuatro materiales plásticos.

Tras estudiar dos condiciones de aplicación de plasma, a 1 y 10 mm/min, se determina que la óptima será aquella que permita mayor tiempo de aplicación del tratamiento superficial sin dañar la superficie, es decir, 1 mm/min.

4. CONCLUSIONES

El tratamiento mediante plasma genera un aumento notable en la componente total de la energía superficial, y, especialmente, en su fracción polar, manteniéndose la dispersiva aproximadamente constante durante todos los tiempos estudiados (de 0 a 750 horas) en todos los materiales excepto la silicona. Por tanto, la tecnologia de plasma atmosfèrico se considera una tècnica adecuada para la mejora en la resistencia de uniones adhesivas en materiales polimèricos.

5. REFERENCIAS

J. ABENOJAR, R. Torregrosa-Coque, M. A. Martínez, J. M. Martín-Martínez, Surface modifications of polycarbonate (PC) and acrylonitrile butadiene styrene (ABS) copolymer by treatment with atmospheric plasma, Surface and Coatings Technology, **203** (2009) 2173-2180

H. CONRADS, M. Schmidt, Plasma generation and plasma sources, *Plasma Sources Sci. Technol.* **9** (2000) 441-454

D. H. KAELBLE, J. Adhesion, **2**, 66 (1970)

I. LEVINE, Físico Química 4ªEd., McGraw-Hill, 380-382 (1996)

Norma ISO 1183: Methods for determining the density of non-cellular plastics

Norma prEN 828:2009-06-02: Adhesives. Wettability. Determination by measurement of contact angle and surface free energy of solid surface.

D. K. OWENS, R. C. Wendt, J. Appl. Polym. Sci., **13**, 1741 (1969)

P. FAUCHAIS, A. Vardelle, B. Dussoubs, Quo vadis thermal spraying?, *J. Therm. Spray Technol.* **10** (1) (2004) 44-66

S. WU, J. Polym. Sci, **C34**, 19 (1971)

Elastomeric sheets produced with silicone and polyaniline for use as microwave absorbing material

L.C. Folgueras
Comando-Geral de Tecnologia Aeroespacial, Instituto de Aeronáutica e Espaço, Divisão de Materiais, São José dos Campos-SP, Brazil.
M.C. Rezende
Comando-Geral de Tecnologia Aeroespacial, Instituto de Aeronáutica e Espaço, Divisão de Materiais, São José dos Campos-SP, Brazil.

ABSTRACT

The purpose of this work is to processing sheets of radiation absorbing materials flexible from silicon substrate with the polyaniline conductor polymer and deposited in metal. Processed materials were evaluated this electromagnetic properties considering the incident radiation attenuation in the frequency range of 8 to 12 GHz (X-band). The electric permittivity and permeability of the sheets was obtained from the measured scattering parameters by using the waveguide technique and reflectivity was NRL technique. The obtained sheets attenuated the electromagnetic radiation in approximately 90%, this result allows its use as microwave absorbers.

1. INTRODUCTION

The radiation absorbing materials (RAMs), when used in the military area, are an important tool used by the electronic war, due to the possibility of obtaining camouflage of targets by radar. The absorbing structures are the various processed materials whose function is to attenuate the electromagnetic radiation, thus allowing the production of paints, composites, thin films etc. These structures are obtained by the addition of the absorber center into matrices and then deposited in supports. The knowledge of the materials processing technology by means of the combination of components, additives and polymeric matrices with appropriate values of dielectric constant and loss tangent is decisive in the final application of the product and makes its function vary from transmitters to radar absorbers. There are several materials that can be used as polymeric matrix; the silicone, polyurethane and epoxy resins are a lot used in the aeronautics industry for having appropriate properties to this sector, such as a greater resistance to erosion and also physical-chemical and mechanical; and they also have high service temperatures (Hull, 1981).

In order to choose the matrix that will be used to process the electromagnetic radiation material, it is essential to observe the dielectric constant values which, in this case, should not be higher than the unit. This way, the RAM will not have an impedance that differs from the environment (air), allowing the electromagnetic wave to penetrate in the material; and by complex phenomena, active in the material medium, accomplish the absorption of the incident wave. The additives to be used could be some kinds of absorbing centers, such as: carbon black, conducting polymer, inorganic materials, ferrites and carbonyl iron (Lee, 1991; Fauveaux et al., 2003; Folgueras et al., 2008). Depending on the type of interaction with the electromagnetic wave, they can be classified in two types: dielectric loss materials and magnetic loss materials, which are those that interact with the wave electrical and magnetic field, respectively (Lee, 1991).

In this context, aiming at aeronautical application, the absorbing composites were obtained from silicone rubber and the conducting polymer polyaniline, due to its electrical conductivity modulation, which allows their utilization as a microwave electromagnetic radiation absorbing center.

2. EXPERIMENTAL

2.1 Production of the sheets

For the processing of the radiation absorbing composites it was used the silicone rubber RTV 630, a bicomponent system from GE Brazil, which meets the requisites for the aeronautical utilization and also for the RAM processing, since it is transparent to radar. As a radiation absorbing center, it was used the conducting polymer polyaniline, which was synthesized in lab scale (Folgueras et al., 2008). From the aniline oxidation by the oxidizing agent ammonium peroxydisulfate, in acid medium (dodecylbenzenesulponic acid), and used in its electricity conducting state. The mixture of the absorbing center in the matrix was produced by mechanical mixing for its complete homogeneity and then poured into steel molds (dimensions of 30 cm x 30 cm), in order to obtain sheets and the repeatability of the process. After the cure, which was achieved at temperature of 60°C, the sheet was adhered to an aluminum plate of aeronautical use.

2.2 Electromagnetic measurements

The electromagnetic characterization of the processed materials was performed by measurements of the reflectivity/absorption of the incident radiation in the material, applying the Naval Research Laboratory (NRL) arc method (Lee, 1991). Such device consists of a wooden arc-shaped structure which enables the positioning of the horn antennas that emit and receive radio frequency according to the X-band range of the electromagnetic spectrum (from 8 to 12 GHz). The samples were positioned in the center of the arc curvature, on a pedestal and the antennas are placed in the center at the highest position of the arc, pointing to the center of the analyzed sample. This device is coupled to a spectrum analyzer Anritsu (model MS 2668C) and to a frequency generator Agilent Technologies (model 83752A). The reference material used to evaluate the efficiency of the processed RAM's was an aluminum plate 100% reflector or 0% absorber.

For the evaluation of the electrical permittivity and magnetic permeability of the processed materials, it was used the waveguide technique at the X-band frequency. For this, the rectangular waveguide (closed system) was coupled to a vector spectrum analyzer Agilent Technologies (model 8510C) connected to S-parameter Test Hewlett Packard 8510A and also to a synthesized frequency generator. The complex parameters were obtained by using the Agilent Technologies software, in communication with the vector system and based on the measurements of the S-parameters (reflection and transmission coefficients, S_{11} e S_{21}, respectively).

3. RESULTS AND DISCUSSION

The processing of the sheets enabled the production of RAM composites with low specific mass and thickness, showing values of approximately 4 kg/ m^2 and 3.2 mm, respectively. Figure 1 shows the results of the composite materials regarding the absorption of electromagnetic radiation which were obtained through the NRL "arc" technique. The black horizontal line corresponds to the evaluation of the reference material, which is the metal plate without the application of RAM used in the reflectivity/absorption measurements, being it 100% reflector, that is to say 0% of absorption. We notice that at the frequency of 8 GHz it presents -10dB of absorption of the incident radiation in the material, which corresponds to 90% of attenuation, and at the frequency of 12 GHz, it presents -5 dB (60%) of absorption. This characterizes that this material is resonant (or narrowband) absorber with a maximum of approximately 9,5 GHz, absorbing -10dB, which corresponds to the attenuation of 90%

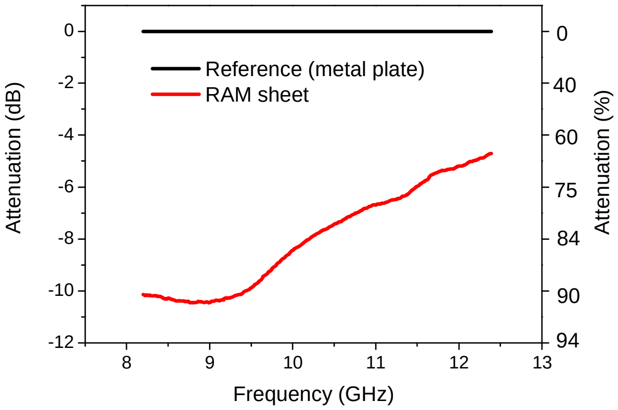

Fig. 1. Attenuation of the incident radiation

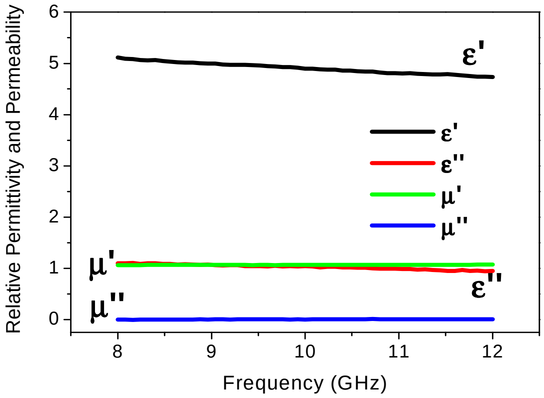

Fig. 2. Relative electric permittivity (ε) and magnetic permeability (μ).

Figure 2 shows the dielectric losses of the elastomeric sheets processed with polyaniline and silicon. It can be observed that the profile of the complex values related to the relative permittivity frequency are: 5.3 and 1.0 for real and imaginary parts, respectively. As the processed material is a dielectric RAM, the values of magnetic losses are low that they can be disregarded (μ'=1, μ"=0). The real relative permittivity values (ε = ε' + ε"j) are always higher than the unit. A material which presents value zero of dielectric loss it will have the values of the permittivity complex parameters ε'=1 e ε"=0,. So, it does not store energy (ε'=1) and, consequently, it does not present losses (ε"=0). Thus, the higher the imaginary component is, the higher the capacity of material loss will be. A material with low dielectric loss can store energy, but it will not dissipate a lot of the energy stored. When, a material with high value of dielectric loss, does not actually store energy, but a certain amount will be converted into thermal energy inside the material, that is, the material absorbs the electromagnetic energy instead of storing it.

3. CONCLUSION

Based on the results obtained in this work, we can conclude that the dielectric composites materials developed has the potential to be used as radiation absorbing materials. And it presents good radiation absorption results, with maximum attenuation of 90%. The polyaniline involved by the silicon matrix provide the formation of conduction paths, allowing the loss of incident radiation by electrical conduction.
The materials processed had low specific mass, less than 4 kg/m^2, which is smaller than magnetic RAMs based on, for example, carbonyl iron materials which have specific masses of 12 k/gm^2. The lower density of PAni-based RAMs increases the number of potential uses for this material.

ACKNOWLEDGEMENT

The authors wish to thank the Comando-Geral de Tecnologia Aeroespacial (CTA) for the technical support and the Brazilian government funding agency CNPq (Project numbers: 301583/2006-4 and 559246/2008-0) for financial support.

REFERENCES

FAUVEAUX, S., WOJKIEWICZ, J.L.; MIANE, J.L. (2003) Broadband electromagnetic shields using polyaniline composites. *Electromagnetics*, 23, 8, 617-627.

FOLGUERAS, L.C., REZENDE, M.C.(2008) Multilayer radar absorbing material processing by using polymeric nonwoven and conducting polymer. *Mat. Res.*, 11, 3, 245-249.

HULL, D. (1981) *An introduction to composite materials*. Cambridge University Press.

LEE, S.M. (1991). *International Encyclopedia of Composites.* New York: VCH Publishers.

Evaluación de aleaciones de residuos plásticos de RSU y de invernadero como matrices para materiales compuestos

J. Acosta[1], C. Fonseca[1], T. Aguinaco [1], M.U. de la Orden[2],
J. Martínez Urreaga[3], C. González Sánchez[4]
[1] Departamento de Química Industrial y Polímeros, Universidad Politécnica de Madrid,
Ronda de Valencia 3, 28012 Madrid. e-mail carmen.fonseca@upm.es
[2] Departamento de Química Orgánica I, EU de Óptica, Universidad
Complutense de Madrid. C/ Arcos de Jalón, s/n, 28037- Madrid
[3]Departamento de Ingeniería Química Industrial y del Medio Ambiente, ETSI
Industriales, Universidad Politécnica de Madrid. C/ José Gutiérrez Abascal, 2, 28006-
Madrid
[4] Departamento de Ingeniera Química y Tecnología del Medio Ambiente.
Universidad de Oviedo. C/ Julian Clavería s/n.33071-Oviedo

RESUMEN

Se han estudiado diversas mezclas de residuos plásticos agrarios y residuos plásticos de post-consumo, con objeto de ser evaluadas como matrices para materiales compuestos. Las mezclas se caracterizaron mediante ensayos espectroscópicos, mecánicos y térmicos. Los resultados indican que pueden obtenerse buenas propiedades mezclando ambas materias primas en las proporciones adecuadas y que las aleaciones obtenidas tienen interés como matrices para materiales compuestos con refuerzos lignocelulósicos.

1. INTRODUCCIÓN

La utilización de materiales plásticos en el sector agrícola ha experimentado en las últimas décadas un incremento permanente (1). Sin embargo, este desarrollo trae como consecuencia la generación de residuos plásticos que deben tratarse convenientemente para minimizar el impacto ambiental y ahorrar recursos naturales.

El objetivo del presente trabajo es la utilización de estos residuos en la fabricación de materiales compuestos, reforzados con materiales lignocelulósicos. Se han preparado mezclas de residuos plásticos agrarios (AF) y residuos plásticos de post-consumo (RU) en diferentes proporciones. Para cada una de esas proporciones, se realizaron ensayos mecánicos, térmicos y espectroscópicos para seleccionar las mezclas con mejores propiedades globales, es decir, las más adecuadas para ser usadas como matrices.

2. MATERIALES DE PARTIDA

Se ha trabajado, además de con plásticos de RU, con tres tipos de granzas recicladas procedentes de dos empresas recicladoras de residuos plásticos de origen agrícola, BEFESA PLÁSTICOS S.L. e IBACPLAST. Se ha utilizado como material virgen de referencia un compuesto para uso agrario de REPSOL (CA-2131A).

El análisis FTIR de las granzas recicladas indica que se trata de polietileno con pequeñas cantidades de EVA (entre 2,5 y 4,5%), tal como cabía esperar de residuos de origen agrario. Por otra parte, al análisis UV-Visible, de Fluorescencia y FTIR indica que contienen cantidades apreciables, aunque inferiores a los plásticos vírgenes, de los aditivos estabilizantes originales. En la Fig. 1, la banda centrada a 225 nm se ha asignado, en función de la bibliografía (2) a aditivos fotoestabilizantes que se han perdido, en distinta proporción, durante el uso. La figura 1 muestra también que los residuos muestran absorción a λ > 250 nm, que parece corresponder a productos de la degradación de los plásticos durante el uso. Estos aditivos pueden ser un valor añadido de cara al uso de residuos de origen agrario en la fabricación de materiales compuestos.

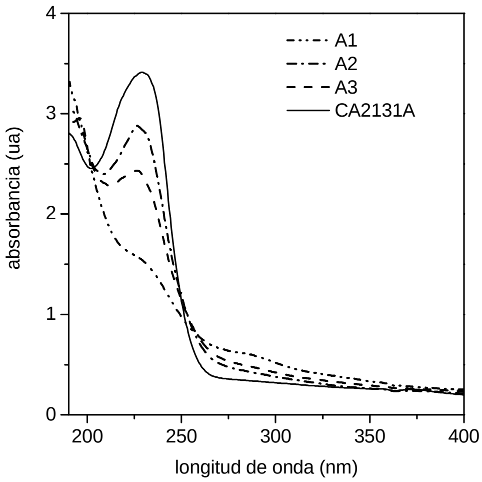

Fig. 1. Absorbancia frente a longitud de onda granzas recicladas en comparación con la original

Los resultados del análisis térmico indican que las temperaturas de fusión de las granzas recicladas de origen agrario son similares a las del material virgen, aunque los picos son más anchos como corresponde a materiales menos homogéneos. Las cristalinidades, entre 32,3 y 33,7, son inferiores a la del plástico virgen de referencia, 40,7. Los tiempos de inducción a la oxidación (TIO) son extremadamente bajos en las recicladas, inferiores a los dos minutos, lo que se considera insuficiente para plásticos que han de someterse a un nuevo procesado por extrusión e inyección, en la fabricación de los nuevos materiales compuestos. En cuanto a las propiedades mecánicas, las granzas recicladas presentan menores valores de tensión y deformación a rotura, como resultado de la degradación experimentada.

Como resultado de todas estas medidas, se seleccionó una de las granzas recicladas de origen agrario, la que presentaba mejores propiedades en conjunto, como material de partida. En todo caso, como las propiedades de estas granzas eran limitadas, debido a la severa degradación de los plásticos agrarios, se consideró la conveniencia de mezclar con plásticos de RSU, para mejorar algunas propiedades.

3. MEZCLAS DE RECICLADOS AGRARIOS Y DE RESIDUOS URBANOS

Se obtuvieron pequeñas cantidades de mezclas de reciclado agrario (A) y residuos plásticos de post-consumo urbano (RU) empleando una mezcladora de rodillos (160ºC, 5 min.). Las proporciones de A variaron entre 20 y 80% (códigos AFRU28 y AFRU82).

3.1. Análisis espectroscópico

Las mezclas de reciclados agrarios y urbanos, AFRU, muestran la presencia de aditivos procedentes de ambos residuos, así como de productos formados como resultado de la degradación, en el análisis espectroscópico. Este análisis muestra también la presencia de dobles enlaces residuales, procedentes en su mayoría del residuo urbano RU. La Figura 2, que recoge los espectros FTIR de mezclas con diferentes proporciones, muestra cómo la banda centrada a 908, que puede asignarse a esos dobles enlaces residuales, crece con el contenido en RU.

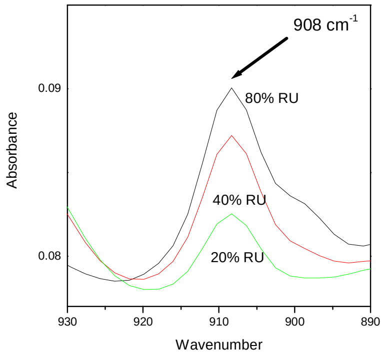

Fig. 2. Absorbancia frente a longitud de onda de mezclas en distintas proporciones de residuos agrarios y urbanos.

La presencia de estos dobles enlaces residuales se considera interesante, puesto que abre la posibilidad de buscar entrecruzamientos entre los distintos plásticos presentes en las mezclas, para mejorar la homogeneidad de las mezclas y, por tanto, algunas de sus propiedades.

3.2. Análisis Térmico: Calorimetría Diferencial de Barrido

Tabla 1. Temperaturas de fusión y tiempos de inducción para la oxidación de mezclas de reciclados agrarios y urbanos.

MATERIAL	Tm (ºC)	TIO (minutos)
A	111,69	0,81
RU	134,01	3,12
AFRU82	130,16 110,16	0,90
AFRU64	132,63 108,77	1,02
AFRU46	133,86	1,35
AFRU28	133,36	2,28

Los valores medidos de la temperatura de fusión indican que los reciclados de origen urbano son principalmente polietileno de alta densidad, mientras que los agrarios son en su mayoría polietileno de baja, como se ha mencionado antes. Los valores de Tm de la Tabla 1 muestran también problemas de compatibilidad y falta de homogeneidad en algunas de las mezclas obtenidas. Concretamente, las mezclas con proporciones más altas de reciclado agrario, como AFRU82, muestran claramente dos picos de fusión, uno correspondiente al reciclado agrario y otro al RU. En cuanto a los porcentajes de cristalinidad, los resultados del análisis térmico muestran un aumento en las mezclas en la medida que aumenta el contenido de RU.

Los valores de TIO van aumentando también a medida que aumenta la proporción de RU en la mezcla, debido a que éste material se encuentra menos degradado que los plásticos procedentes de los residuos agrarios. Este es un caso en el que la adición de RU a los reciclados de origen agrario supone una mejora en una propiedad. En cualquier caso, los valores de las mezclas siguen siendo bajos, insuficientes para su procesado, por lo que se necesita la readitivación con antioxidantes.

3.3. Caracterización mecánica

En las condiciones de los ensayos de impacto realizados (Izod con entalla) las mezclas de ambos plásticos reciclados rompen todas, debido a la presencia de RU y a problemas de falta de homogeneidad, salvo la mezcla AFRU82 que es la que presenta menos contenido en RU. En cualquier caso, la presencia de reciclado agrario causa un incremento significativo en la resistencia al impacto.

Los ensayos de tracción se realizaron a una velocidad de 5mm/min, de acuerdo a la norma UNE-EN-ISO 527-1. Se obtuvieron resultados que presentaban una gran variabilidad. La deformación en el punto de fluencia aumenta con la proporción de reciclado agrario. En cambio, la tensión de fluencia aumenta con la proporción de RU. El módulo de Young, determinado a una velocidad de 1 mm/min según norma UNE-EN-ISO 527-2, aumenta a medida que aumenta la proporción de RU, el plástico más cristalino de la mezcla.

Estos resultados de la caracterización mecánica se analizaron en conjunto con los obtenidos en el análisis térmico y el espectroscópico de las mismas mezclas. En función de este análisis conjunto, se decidió que la mezcla AFRU64 era la más apropiada para actuar como matriz en los materiales compuestos reforzados con fibras lignocelulósicas.

4. CONCLUSIONES

- Los resultados obtenidos en la caracterización de mezclas de reciclados agrarios y urbanos han aportado información necesaria para seleccionar el material a emplear como matriz para la fabricación de materiales compuestos. La mezcla con mejores propiedades en conjunto es la que contiene 60% de residuo agrario y 40% de residuo de post-consumo (AFRU64).
- Las aleaciones de plásticos reciclados de origen agrario y post-consumo urbano muestran una baja resistencia a la oxidación, que los hace poco adecuados para ser procesados por extrusión-inyección, que es el método habitual de fabricación de materiales compuestos, por lo que se necesitaría readitivar con antioxidante.
- Algunas de las aleaciones estudiadas muestran una gran variabilidad en las propiedades mecánicas, debido a problemas de falta de homogeneidad en la mezcla. La mejora de la homogeneidad y, por ende, de las propiedades térmicas y mecánicas de las mezclas, es muy importante para aumentar la aplicabilidad de los residuos plásticos de uso agrario en la fabricación de materiales compuestos.

REFERENCIAS

1. N. Tzankova Dintcheva, F.P. La Mantia, D. Acierno, L. Di Maio, G. Camino, F. Trotta, M.P. Luda, M. Paci. Polym. Degrad. Stab. 72 (2001) 141-146.
2. M. Scoponi, S. Cimmino, M. Kaci. Polymer 41(2000) 7969-7980.

5-fenil-3-hidroxi-4-pentenonitrilo y 5-fenil-3-oxo-4-pentenonitrilo. Tautomerismo y polimerización

J.M. Giussi, M.S. Cortizo, P.E. Allegretti
Laboratorio LADECOR, División Química Orgánica
Instituto de Investigaciones Fisicoquímicas Teóricas y Aplicadas
Departamento de Química, Facultad de Ciencias Exactas, Universidad Nacional de La Plata, Argentina

RESUMEN

Se han sintetizado 5-fenil-3-hidroxi-4-pentenonitrilo y 5-fenil-3-oxo-4-pentenonitrilo. La polimerizabilidad de ambos monómeros se encuentra afectada por la presencia de los diferentes tautómeros existentes en las condiciones empleadas. En fase gaseosa se estudió el equilibrio tautomérico de los correspondientes monómeros mediante cromatografía gaseosa con detección por espectrometría de masa (GC-MS) y en solución mediante espectrometría de Resonancia Magnética Nuclear (NMR). Se seleccionaron solventes en los que se favorezca la presencia de alguno de los tautómeros y se llevó a condiciones de polimerización radical térmica, evaluando el efecto de la variación del tiempo de reacción sobre el rendimiento de polimerización y propiedades de polímeros finales, los cuales se caracterizaron mediante RMN y cromatografía de exclusión molecular.

1. INTRODUCCIÓN

En compuestos carbonílicos con capacidad de tautomerizar el equilibrio favorece ampliamente la forma ceto, por lo que la forma enólica suele ser muy minoritaria (Allegretti 2000, 2003, 2004 y 2005). Algunos compuestos vinílicos con sustituyentes tautoméricos han sido investigados como monómeros en reacciones de polimerización radical con el objetivo de analizar el efecto de la relación entre la estructura tautomérica y la polimerizabilidad (Masuda 1996). Así también, se ha estudiado la cinética de polimerización radical de β-dicetonas y β-cetoésteres en solventes de variada polaridad (Masuda 1987, 1989). Hasta el presente no se han estudiado monómeros que exhiban estructuras tautoméricas derivadas de β-hidroxinitrilos y β-cetonitrilos. Para el siguiente trabajo se seleccionó el 4-metil-3-oxo-4-pentenonitrilo y su análogo hidroxilado, 3-hidroxi-4-metil-4-pentenonitrilo para evaluar la influencia del equilibrio tautomérico presente en dichos compuestos sobre su polimerizabilidad radical térmica.

1.1 PROCEDIMIENTO EXPERIMENTAL.

Los monómeros se han sintetizado a través de la adaptación de métodos encontrado en la literatura para compuestos similares (Zibuck 1993); (Collins 1972). Los polímeros se sintetizaron en tubos sellados con 2,2´-azoisobutironitrilo (AIBN) como iniciador en los solventes seleccionados. Los polímeros obtenidos se aislaron por precipitación con metanol. Por último, para su purificación, se disolvieron en tolueno y se reprecipitaron con metanol.

Determinaciones Estructurales

a. Cromatografía Gaseosa-Espectrometría de Masa. Estas determinaciones se llevaron a cabo inyectando soluciones metanólicas (1 µl) en un cromatógrafo HP 5890 acoplado a un detector selectivo de masas HP 5972.

b- Resonancia Magnética Nuclear. Los espectros ^{1}H-N.M.R y ^{13}C-N.M.R, han sido realizados en un espectrómetro Varian Mercury Plus, 200 MHz. Para la caracterización de los polímeros obtenidos las soluciones se prepararon en cloroformo-d$_1$ y los espectros ^{1}H-N.M.R y ^{13}C-N.M.R y bidimensional se registraron a 35ºC.

c- Cálculos Computacionales. Los cálculos teóricos semi-empíricos AM1 se realizaron utilizando el programa HyperChem$^{®12}$ para estimar la energía relativa de cada tautómero aislado y compararlo con los resultados obtenidos por CG-MS.

d- Determinación de los pesos moleculares promedio y distribución mediante cromatografía de exclusión molecular (SEC). El solvente de elusión seleccionado fue tetrahidrofurano (THF). Las concentraciones fueron de 6 mg/ml. La calibración se hizo empleando estándar de poliestireno.

1.2 RESULTADOS Y DISCUSIÓN. *Monómeros*

Cromatografía Gaseosa-Espectrometría de Masa**:** El esquema 1 muestra las posibles estructuras tautoméricas para el 5-fenil-3-hidroxi-4-pentenonitrilo.

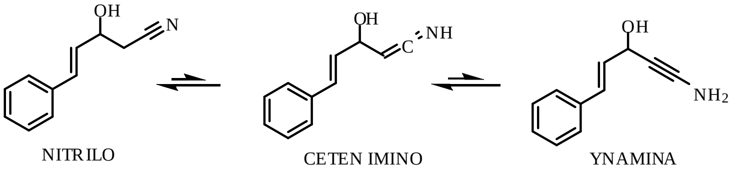

Esquema 1. Posibles estructuras tautoméricas para el 5-fenil-3-hidroxi-4-pentenonitrilo

Con el fin de evaluar la presencia de los diferentes tautómeros, se han asignado picos provenientes de fragmentaciones específicas para cada uno. Del análisis del espectro de masa, se concluyó que estaban presentes el tautómero nitrilo y cetenimina. No se pudo asignar un pico que provenga exclusivamente de la forma ynamina, esto quedó justificado con los cálculos semi-empíricos AM$_1$. El esquema 2 muestra las posibles estructuras tautoméricas para el 5-fenil-3-oxo-4-pentenonitrilo.

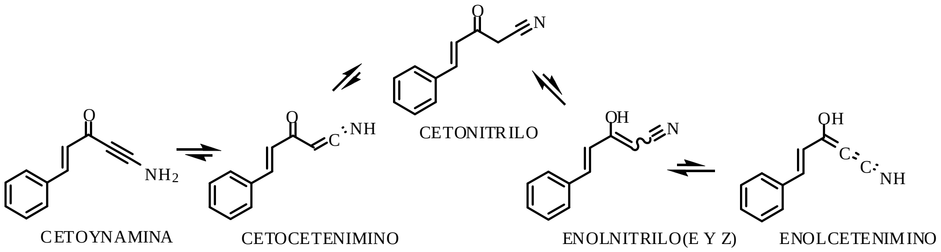

Esquema 2. Posibles estructuras tautoméricas para el 5-fenil-3-oxo-4-pentenonitrilo.

Del análisis del espectro de masa, se concluyó que estaban presentes el tautómero cetonitrilo, enolnitrilo y cetocetenimina. No se pudieron asignar picos que provengan exclusivamente de la forma enolcetenimino y cetoynamina, esta observación también quedó perfectamente justificado con los calculos semi-empíricos AM$_1$, que indicaron una gran energía relativa para estos tautómeros. No se observó separación cromatográfica de los tautómeros considerados (probablemente debido a la rápida velocidad de interconversión), de manera que sus espectros son la superposición de los espectros de los diferentes tautómeros.

Resonancia Magnética Nuclear: El espectro ^{1}H-NMR del 5-fenil-3-oxo-4-pentenonitrilo muestra una evidencia experimental adicional de la coexistencia de los tautómeros cetonitrilo y enolnitrilo. El equilibrio nitrilo-cetenimino para ambos compuestos, no puede observarse por esta técnica. Las constantes de equilibrio operacionales en solución se calcularon como relación de las áreas integradas de los picos a $\delta = 3.81$ y $\delta = 4.37$. En la tabla 1 se arrojar estos resultados para los solventes seleccionados.

Tabla 1. Fracción cetónica y constante de equilibrio tautomérica operacional para 5-fenil-3-oxo-4-pentenonitrilo en los solventes seleccionados

Solvente	Fracción Ceto	K_T^*
benceno	0,990	0.010
cloroformo	0,974	0,027
acetona	0.694	0.440
acetonitrilo	0,352	1.841
DMSO	0.125	7.000
$^*K_T$=[tautómero enol-nitrilo]/[tautómero ceto-nitrilo]		

Polímeros. Para este trabajo solo se incluye la polimerización de 5-fenil-3-oxo-4-pentenonitrilo debido a que es el monómero que en solución contiene presente formas tautoméricas apreciables. La polimerización de este compuesto fue cinéticamente investigada a 60ºC en benceno y en acetonitrilo, usando AIBN como iniciador. Como puede verse en la figura 1 hay una pequeña diferencia en la velocidad de polimerización (Rp), siendo un poco mayor en acetonitrilo que en benceno.

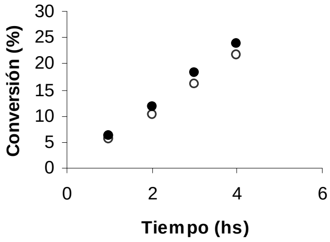

Figura 1. Curvas de tiempo-conversión en acetonitrilo (•) y benceno (○)

Las investigaciones cinéticas arrojaron ecuaciones de velocidad 1 y 2

Resonancia Magnética Nuclear: El análisis de los espectros ^{1}H-NMR y ^{13}C-NMR y bidimensional de los polímeros obtenidos muestra la presencia de los tautómeros estudiados en el polímero final, se ven señales asignables a hidrógenos cetónicos y enólicos.

Cromatografía de exclusión molecular: Del análisis de los elugramas obtenidos para los distintos tiempos de reacción se puede observar una respuesta positiva del peso molecular promedio en peso (M_w) con el tiempo de reacción. En el caso en el que la polimerización fue en benceno, luego de la cuarta hora el M_w bajo y la polidispersidad aumentó y en el caso en que la polimerización fue en acetonitrilo, luego de la tercer hora se vió este fenómeno. Esto puede estar asociado, más allá del efecto del solvente sobre la polimerización, a la naturaleza del monómero. Se sabe que los grupos hidroxilos son capturadores de radicales, por lo que pueden ser los responsables de este comportamiento.

2. ECUACIONES Y FÓRMULAS

(1) $Rp = k\,[\text{Monómero}]^{1.32}\,[\text{AIBN}]^{0.43}$ en acetonitrilo

(2) $Rp = k\,[\text{Monómero}]^{1.25}\,[\text{AIBN}]^{0.45}$ en benceno

3. CONCLUSIONES

La polimerizabilidad para 5-fenil-3-oxo-4-pentenonitrilo se encuentra afectada por la presencia de los diferentes tautómeros, mostrando una cinética mayor para el caso de que la concentración del tautómero enolnitrilo sea la predominante. El análisis de los polímeros finales muestra la coexistencia de ambas formas tautoméricas sobre los polímeros resultantes. La polidispersidad del polímero es mayor cuando el monómero mayoritario es el enolnitrilo.

REFERENCIAS

ALLEGRETTI, P., CÁNEPA, A., BRAVO, R., CASTRO, E., FURLONG, J. (2000). Mass spectrometric analysis and theoretical calculations for the occurrence of tautomeric structures of selected (2H)isoquinolinones. Asian Journal of Spectroscopy, Vol. 4, p. 133-137.

ALLEGRETTI, P., CORTIZO, S., GUZMÁN, C., CASTRO, E., FURLONG, P. (2003). Tautomerism of lactones and related compounds. Mass spectrometric data and theoretical calculations. Arkivoc. Vol X, p. 24-31.

ALLEGRETTI, P., SCHIAVONI, M., CORTIZO, S., CASTRO, E., FURLONG, J. (2004). “Enol and enethioenol occurrence for some ketones and thioketones. Mass Spectrometry and Theoretical Calculations. International Journal of Molecular Sciences. Vol 5, p. 294-300.

ALLEGRETTI, P., MILAZZO, C., FURLONG, J. (2005). Mass Spectrometry as a Tool for the Determination of Heats of Tautomerization of Thioamides in Gas Phase. European Journal of Mass Spectrometry, Vol. 11, p. 53-64.

COLLINS, J., HESS, W. (1972). Aldehydes from primary alcohols by oxidation with chromium trioxide: heptanal; Organic Syntheses, Vol. 52, p.5-9.

MASUDA, S., MINAGAWA, K. (1996). Tautomers as monomers and initiators. Progress in Polymer Science, Vol 21, p. 557-591.

MASUDA, S., TANAKA, M., OTA, T. (1987). Polymerizable tautomers. V. Solvent effects on radical polymerization and copolymerization of 5-hexene-2,4-dione. Polymer, Vol 28, p. 1945-1949.

MASUDA, S., TANAKA, M., OTA, T. (1989). Polymerizable tautomers. VI. Solvent effects on polymerization and copolymerization of ethyl 4-methyl-3-oxo-4-pentenoate; Journal of Polymer Science Part A: Polymer Chemistry. Ed, 27, p.855-863.

ZIBUCK, R., STREIBER, J. (1993). Ethyl 3-oxo-4-pentenoate (Nazarov´s Reagent); Organic Syntheses, Vol. 71, p.236-239.

Síntesis y caracterización de materiales compósitos PVC/ABS/TULE modificando sus propiedades con material compatibilizante

I.L. González-Antonio
Estudiante de Maestría en Tecnología Avanzada del Centro de Investigación en Ciencia Aplicada y Tecnología Avanzada del Instituto Politécnico Nacional Unidad Altamira
CICATA-IPN UA. Km 14.5 Carretera Tampico-Puerto Industrial Altamira C. P. 89600, Altamira, Tamaulipas, igonzaleza0801@ipn.mx
A. López-Marure, M.J. Ulloa, A. Flores-Vela
Instituto Politécnico Nacional, Grupo de Ingeniería en Procesamiento de Materiales
CICATA-IPN UA. Km 14.5 Carretera Tampico-Puerto Industrial Altamira C. P. 89600, Altamira, Tamaulipas, arlopez@ipn.mx, afloresv@ipn.mx

RESUMEN

En esta investigación se pretende elaborar un material compósito PVC/ABS/Tule que presente aumento de propiedades con respecto a las de cada constituyente por separado. Se resalta el uso de la fibra vegetal Tule como refuezo mecánico, la cual se considera una especie invasora en la laguna El Chairel (ubicada en la Ciudad de Tampico, Tamaulipas, México). Es importante mencionar que las ventajas de las fibras naturales sobre los materiales de refuerzo tradicionales son su bajo costo, baja densidad, elevada rigidez, buenas propiedades térmicas, biodegradabilidad y en términos generales excelentes propiedades mecánicas. Además, se encuentran disponibles en grandes cantidades y representan una fuente renovable continua. Asimismo, resulta interesante agregar un compatibilizante para lograr una buena interacción química y así mejorar las propiedades fisicoquímicas y mecánicas del material compósito.

Se trabajó con una relación de PVC/ABS 70:30, en base a estudios anteriores, con diferentes porcentajes de Tule (1% y 5%). Los resultados de la caracterización del material compósito PVC/ABS/Tule mediante la técnica de Analisis Dinamico Mecánico (ADM), mostraron un aumento en la temperatura de transición vítrea (Tg) con respecto a la mezcla PVC/ABS (87°C a 110°C), por lo que es posible concluir que el compósito presenta mayor resistencia térmica. Además, con un 5% de Tule, existe un aumento considerable en el Modulo de Pérdida (325 MPa a 525 MPa), indicando una mayor homogeneidad entre la matriz polimérica y el refuerzo. Sin embargo, mediante las pruebas de resistencia a la tensión, se obtuvo un decremento considerable en el modulo de elasticidad, lo que es posible remediar adicionando Acido Poliláctico (PLA) como agente de acoplamiento.

1. INTRODUCCIÓN

Actualmente existe una gran tendencia por lo natural y la protección del ambiente y en ese sentido, se estimulan los estudios e investigaciones sobre la utilización de fibras de origen vegetal como refuerzo de materiales compósitos. El refuerzo utilizado en la presente investigación es el Tule (*Typha domingensis).* Se trata de una fibra vegetal que se encuentra en grandes cantidades en los vasos lacustres de la zona que comprenden las ciudades Tampico, Madero y Altamira, en el estado de Tamaulipas, México. Sin embargo, en esta ocasión se extrae específicamente de la laguna El Chairel, ubicada en la ciudad de Tampico (22°10´12” Latitud Norte y 97°51´14” Longitud Oeste, al nivel de mar). El exceso de Tule en esta laguna provoca una disminución en la concentración de oxígeno disuelto y consecuentemente un problema ambiental en el agua, además, su crecimiento desmedido evita el aprovechamiento de las lagunas con fines recreativos. Basados en lo anterior, es posible aprovechar esta fibra vegetal con fines industriales como refuerzo mecánico en la síntesis de materiales compósitos PVC/ABS/Tule.

Cuando la adhesión entre la fibra vegetal y la matriz no es eficaz, las fibras no funcionan como un material de refuerzo efectivo. Las fibras celulósicas tienden a formar agregados y por lo tanto no pueden mezclarse bien con la matriz no polar, lo cual evita alcanzar una distribución uniforme en la matriz. Las características superficiales de la fibra de refuerzo son un factor que influye en la distribución de esfuerzos desde la matriz a la fibra. Por esta razón se suele recurrir a tratamientos para la modificación de superficie mediante la incorporación de compatibilizantes para lograr una buena dispersión y una mejora significativa en las propiedades mecánicas de los materiales compuestos.

El agente compatibilizante permite que el tiempo de mezclado se reduzca, disminuyendo costos, mejorando la apariencia de las muestras y evitando los problemas de delaminación, que podrían presentarse en el material sin compatibilizar por el método de compresión. Es bien conocido también que un compatibilizador polimérico puede servir a la vez como modificador de impacto mediante la incorporación de la cantidad adecuada, en un sistema apropiado, utilizando una técnica de procesamiento viable.

2. METODOLOGÍA

El método utilizado fue el siguiente:

a) Recolección del Tule a bordo de una embarcación en diferentes puntos de la laguna El Chairel.
b) Caracterización química (EITF), térmica (DSC y DMA) y estructuralmente (DRX y SEM) de las resinas de ABS y PVC vírgenes, así como el Tule antes de ser tratado.
c) Limpieza del Tule con agua para retirar los residuos no deseados, corte del mismo en trozos con una longitud aproximada de 1 cm, y después secarlos a temperatura ambiente, concluyendo con el secado en la estufa a 80° C por 24 horas. Para eliminar las fibras de mayor tamaño se trituró la fibra y enseguida se cribó. Es importante trabajar con tamaño de partícula de 100µm. El tratamiento químico de las fibras se realizó con una mezcla de CH_3COOH/H_2O_2 50-50 durante 4 horas para la extracción de celulosa. Para finalizar el tratamiento de la fibra, se lavó con agua destilada y se secó nuevamente a 60°C por 24 horas.
d) Síntesis del material compósito, primeramente sin compatibilizante por el método de compresión y en forma de placas. Posteriormente, elaborar el material compósito PVC/ABS/Tule con diferentes porcentajes de Tule (1% y 5%).
e) Medición de las propiedades químicas del material compósito, utilizando las técnicas de EITF, DSC, DRX SEM y DMA, así como las propiedades mecánicas realizando pruebas de tensión y de impacto Izod.

f) Análisis del efecto compatibilizante del PLA sobre la matriz polimérica, realizando el material compósito con compatibilizante. Para ello, se agregan diferentes porcentajes del compatibilizante (1%, 2%, 5% y 10%).
g) Medición de las propiedades químicas del material compósito con el agente compatibilizante, utilizando las técnicas de EITF, DSC, DRX, SEM y DMA, así como las propiedades mecánicas realizando pruebas de tensión y de impacto Izod.

3. RESULTADOS PRELIMINARES

Se elaboro el material compósito PVC/ABS/Tule a base de una mezcla de PVC/ABS (70:30) con diferentes porcentajes de Tule (1% y 5%). Mediante la caracterización por la técnica de Análisis Dinámico Mecánico se pudo apreciar que con un 5% de Tule existe un aumento gradual en la Tg, con respecto a la mezcla PVC/ABS, indicando una mayor homogeneidad entre la matriz polimérica y el refuerzo. Además, el compósito es térmicamente más resistente que la mezcla (Figura 1).

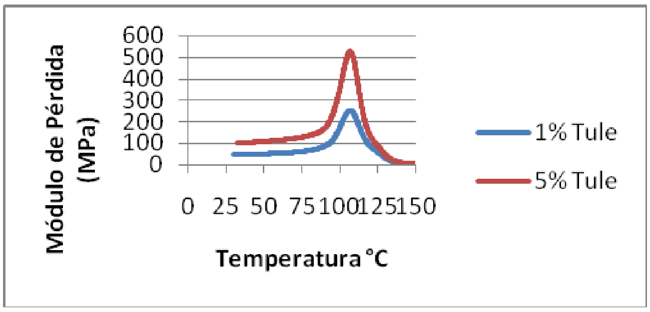

Figura 1. Detección de la Tg mediante el Módulo de Perdida (E”) del material compósito PVC/ABS/Tule a diferentes composiciones.

Los resultados de resistencia a la tensión nos indican un decremento considerable en el modulo de elasticidad con respecto a la mezcla PVC/ABS (70:30). Para solucionar lo anterior se usara Acido Poliláctico (APL) como agente compatibilizante con lo que se espera mejorar la adhesión matriz polimérica/refuerzo así como el incremento de las propiedades mecánicas, ya que en estudios anteriores con PVC/ABS este polímero ha presentado óptimos beneficios, principalmente en el aumento de la resistencia al impacto (López Ramos, 2008).

4. CONCLUSIONES

El presente proyecto tiene un gran impacto social, científico, económico y ambiental, ya que se espera obtener un compósito con buenas propiedades químicas, estructurales y mecánicas, entre ellas alta resistencia al impacto, propiedad que en la actualidad es considerada la más importante en la industria puesto que con base a esta, se establecen los campos de aplicación.

Además, parte muy importante del proyecto, es el uso del APL como agente compatibilizante, el cual permite una mejor adhesión entre la matriz polimérica y el refuerzo, ya que es posible que se adhiera químicamente a la superficie de la fibra, además, es compatible con la matriz.

REFERENCIAS

[1] Aroon V. Shenoy. Rheology of Filled Polymer System. Kluber Academic Publisher. Pagina 16-17.

[2] Arellano Ortega S. Contribución al estudio limnológico de la laguna El Ch Tampico, Tamaulipas, México. Escuela de Ciencias Biológicas Universida Noreste. Tesis de licenciatura. México 1987.

[3] Comisión Nacional para el Conocimiento y uso de la Biodiversidad. Sistema Integrado de Información Taxonómica Malezas de México: Typha domingensis México 2006.

[4] Vallejos M. A. Aprovechamiento integral del Cannabis sativa como material de refuerzo/carga del polipropileno, Tesis de Doctorado. Universidad de Girona. España 2006.

[5] Yu-Tao Zheng, De-Rong Cao, Dong-Shan Wang, Jiu-Ji Chen. Study on the interface modification of bagasse fibre and the mechanical properties of its composite with PVC. China 2006.

[6] Krause E. Materiales compuestos basados en polipropileno y fibras naturales modificadas químicamente por procesamiento reactivo. Centro de Investigación y Desarrollo Tecnológico para la Industria Plástica- INTI. Tesis de doctorado. Argentina 2002.

[7] Mascareñas Espino S. K. Estudio del Efecto Compatibilizante del Copolímero SAN en Mezclas PVC/ABS, Tesis de Maestría. Centro de Investigación en Ciencia Aplicada y Tecnología Avanzada del IPN Unidad Altamira 2008.

[8] López Ramos A P. Elaboración de Materiales Compósitos PVC/ABS Y Bagazo de Caña. Tesis de Maestría. Centro de Investigación en Ciencia Aplicada y Tecnología Avanzada del IPN Unidad Altamira 2008.

Photooxidative behavior of polyethylene films by DSC and FTIR

A.M.C. Grisa, M. Zeni, C. Longo, T. Simioni, R.N. Brandalise
Centro de Ciências Exatas e Tecnologia, Universidade de Caxias do Sul-RS- Brazil

SUMMARY

Most of the synthetic polymers are susceptible to degradation initiated by UV and visible light. The photooxidative behaviors of polyethylene (PE) films have been investigated by FTIR spectroscopy by carbonyl index (IC). Relative intensities of the ester carbonyl band at 1740 cm^{-1}; keto carbonyl band at 1715 cm^{-1} and the double bond band at 1640 cm^{-1} (vinyl index) to that of the methylene band at 1465 cm^{-1} for the PE show the interest for studies of degradation of polyethylene. In this work we have studied crystallinity index (Xc) of the neat PE and PE with blue colorant by Differential Scanning Calorimetry (DSC) and FTIR spectroscopy after 240 hours of irradiation for UV. The crystallinity index (Xc) have been investigated for method suggested by Kaisersberger et al. and Zerbi et al. for DSC. For the neat PE and PE with blue colorant, was evidenced the formation of carbonyl groups after photooxidation. In the IC, it was observed for the crystallinity of the PE is increase after irradiation UV, for the method by Kaisersberger. The values of Xc calculated by the method of Kaisersberger proved to be superior to those obtained by Zerbi et al. By the method of Zerbi et al. did not show significant difference in the crystallinity index after irradiation of polymers.

1. INTRODUCTION

Polyethylenes (HDPE & LDPE) are the most commonly used synthetic polymers and is important to know the extent of degradation of these polymers under UV light. The degradation rate depends on the environment and the type of polymer. Aldehyde and ketone carbonyl groups are common products during processing and the effect of processing on the subsequent degradation behavior is significant (White and Turnbull, 1994).

The photo-oxidation of LDPE proceeds by a free radical mechanism through the formation of hydroperoxides that decompose to new free radicals and the process is autocatalytic. Photodegradation of HDPE occurs in the first stage on the amorphous phase of the material (Valdez-Gonzalez et al. 1999). During photooxidation of PE the amount of hydroperoxides is small and carbonyl compounds are the main products. For PEs, both cross-linking and chain scission may take place concurrently as a result of weathering exposure.

Recent Fourier transformation infrared spectroscopy (FTIR), Differential Scaning Calorimetry (DSC) studies on various polyolefins show the following order light stability LDPE>HDPE> metalocene. Hydroperoxide levels also appear to be important and correlate with the carbonyl index oxidation rates. For HDPE the degradation decreases with the increase of polymer crystallinity (Allen et al., 2000).

In this work we have studied crystallinity index (Xc) and carbonyl index (IC) of the neat PE and PE with blue colorant by DSC and FTIR spectroscopy respectively after 240 hours of irradiation for UV.

2. EXPERIMENTAL

The neat PE and the blue PE films (mixture of LDPE and HDPE) were used in the current study. The photoirradiation of the films was carried out in a accelerated weathering chamber, Conexum Matérias Primas IND LTDA, at temperature 60ºC for 240 hours under atmosphere of condensation at 40ºC. The materials were submitted to the action of weathering in agreement with adapted norm ASTM G154-00.

Chemical structures of the of the neat PE and PE with blue colorant films before and after photoirradiation were monitored using Fourier transform infrared analyzer (FTIR) model Impact 400 Nicolet. The keto carbonyl, ester carbonyl, vinyl indices were measured from the FTIR spectrum sing the following formulae. Relative intensities of the ester carbonyl band at 1740 cm^{-1}; keto carbonyl band at 1715 cm^{-1} and the double bond band at 1640 cm^{-1} (vinyl index) to that of the methylene band at 1465 cm^{-1} were evaluated (Albertsson et al., 1987):

Keto carbonyl bond index = I_{1715}/I_{1465};
Ester carbonyl bond index = I_{1740}/I_{1465};
Vinyl bond index = I_{1640}/I_{1465}.

The differential scanning calorimeter (DSC) measurements were carried out in a Shimadzu DSC-50 Instruments. The samples were heated from room temperature to 180ºC at a constant heating rate of 10˚C/min and held isothermally at that temperature for 1 min. The second run from-100 to 180ºC was carried out at the same heating rate. The measurements were carried out under nitrogen flow of 50mL/min.

The crystallinity index of the polymers was calculated through the expression (Equation 1) suggested by Kaisersberger et al., (1994).

$$X_c = (\Delta H_f\,\text{polymer} / \Delta H_{f\ 100\%}) \times 100 \qquad (1)$$

Where X_c is the crystallinity index (%), $\Delta H_{f\ polymer}$ is the fusion enthalpy of the polymer normalized to its content in the blend, and $\Delta H_{f\ 100\%}$ is the fusion enthalpy of the hypothetically 100% crystalline polymer, 293 $J.g^{-1}$ (Fu et al., 2005) for the HDPE and 140 $J.g^{-1}$ for the LDPE (Abd El-Rehim,2204).

Crystallinity of PE was determined using the method described by Zerbi et al.,(1989). The percentage of the crystalline content, X, can be calculated using Equation. (2):

$$X = 100 - \frac{(1 - Ia/l\ Ib/1{,}233}{1 + (Ia/Ib)} \times (100) \qquad (2)$$

Where *Ia and Ib* are absorbance values from the bands at 1474 and 1464 cm^{-1} or at 730 and 720 cm^{-1}, respectively.

3. RESULTS AND DISCUSSION

The structural analyses for FTIR, the neat PE and PE with blue colorant compared after and before photoirradiation, showed formation of new absorbances (Figure 1a-1b). The most significant changes in the FTIR spectra were in the carbonyl (1785-1700 cm^{-1}). The doublet peaks observed in PEs at 1474–1464 cm^{-1} and 730–720 cm^{-1} correspond to polyethylene crystalline content (1474 and 730 cm^{-1}) and amorphous content (1464 and

720 cm^{-1}). The PE blue after exposition UV showed evolution of the hydroperoxide band (3700-3100 cm^{-1}).

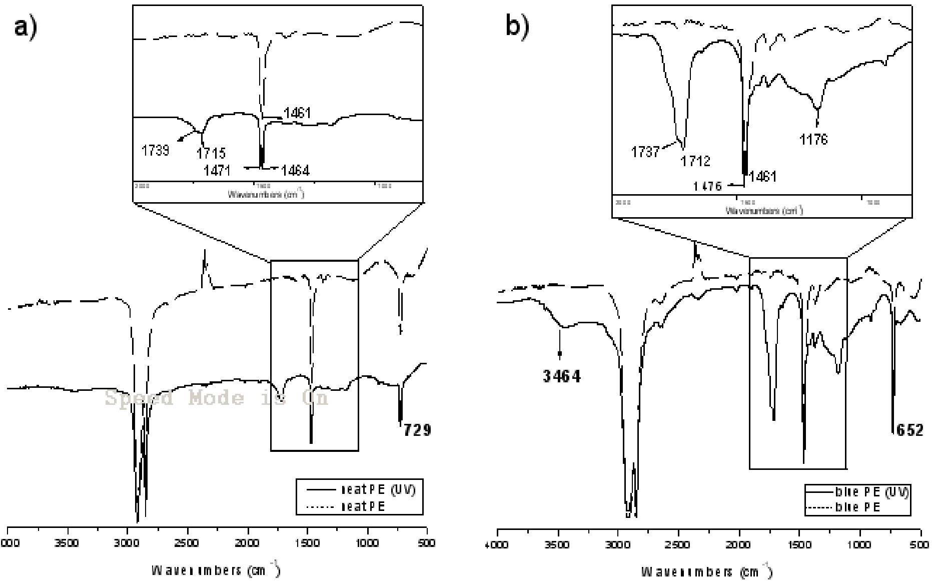

Fig.1. FTIR spectra (a) neat PE and (b) blue PE after and before photoirradiation

The carbonyl index, keto, ester and vinyl bond index before and after 240 hours of irradiation for UV and crystallinity index investigated for method suggested by Kaisersberger et al. and Zerbi et al are summarized in Table1.

Tabela 1. Carbonyl index, keto, ester, vinyl bond and crystallinity index after 240 hours of irradiation for UV

Samples	Neat PE (0h UV)	Neat PE (240h UV)	PE blue (0h UV)	PE blue (240h UV)
Keto carbonyl bond index (I_{1715}/I_{1465})	NI	0.11	0,18	0,27
Ester carbonyl bond index (I_{1740}/I_{1465})	0,01	0,10	NI	0,27
Vinyl bond index (I_{1640}/I_{1465})	NI	NI	NI	0,03
Xc Kaisersberger	74,4	76,7	51,83	81,62
Xc Zerbi	62	62	61	63

NI- unidentified

For neat PE and PE with blue colorant, was evidence the formation of carbonyl groups after photooxidation. The presence of carbonyl groups in degraded polymers indicates that oxidation has taken place and also means that the material is vulnerable to further degradation for UV.

The blue PE films (mixture of LDPE and HDPE) showed higher values of IC because crystallinity, morphology and different polymer matrix embedded additives (chromophoric groups) are all factors affecting the fate and rate of PE degradation and may accelerate the process.

In the crystallinity index, it was observed for the crystallinity of the PE is increase after irradiation UV, for the method by Kaisersberger. The processes of reticulation of the HDPE can favor the formation of crystals in the PE blue. For the neat PE to increase the crystallinity index was not as clear, justified by the presence of ramifications of LDPE.

4. CONCLUSIONS

The results of spectroscopy for FTIR analyses of the samples indicated possible changes in the chemical structure during photooxidation.

The values of Xc calculated by the method of Kaisersberger proved to be superior to those obtained by Zerbi et al. By the method of Zerbi et al did not show significant difference in the crystallinity index after irradiation of polymers.

ACKNOWLEDGMENT

The authors thank to UCS, CNPq for the support.

REFERENCES

ABD EL-REHIM, H.A., HEGAZY, E. A., ALI, A. M., RABIE, A.M. (2004). Synergistic effect of combining UV-sunlight–soil burial treatment on the biodegradation rate of LDPE/starch blends *J. of Photochemistry and Photobiology A*: Chemistry , 163, 547-556.

ALBERTSSON, A.C, ANDERSSON, S.O, KARLSSON, S. (1987). The mechanisms of biodegradation of polyethylene. *Polym Degrad Stab*., 18, 73-87.

ALLEN, N. S., EDGE, M, HOLDSWORTH, D., RAHMAN, A., CATALINA, F., FONTAN, E., ESACALONA, A. M., SIBON, F. F. (2000). Ageing and spectroscopic properties of polyethylenes comparasion with metalocens polymer. *J. Poly. Degrad. Stab.*, 20, 57-67

AMERICAN SOCIETY FOR TESTING MATERIALS, ASTM G154-00a – Standard practice for operating fluorescent light apparatus for UV exposure of nonmetallic materials.

VALDEZ-GONZALEZ A., CERVANTES-UC, J.M., VELEVA, L.(1999). Mineral filler influence on the photo-oxidation of high density polyethylene. *Polymer Degrad. Stab*,.63, 253-260

KAISERSBERGER, E.; KNAPPE, S.; MÖHLER, H.; RAHNER, S. (1994). Thermal analysis for polymer engineering. *NETZSCH Annual for Science and Industry*, 3, 3-81.

WHITE, J. R. and TURNBULL, A. (1994). Weathering of polymers:mechanisms of degradation and stabilization, testing strategies and modelling. *J. Matter Science*, 29, 584-613

Error estimation in the fiber orientation determination of injected LFRT

J. López, R. Navarro, F. Parres, S. Ferrándiz
Dept. of Mechanical and Materials Engineering. Higher Polytechnic School of Alcoy.
Polytechnic University of Valencia. Pl. Ferrándiz Carbonell, s/n, 03801 Alcoy, Spain
jlopezm@mcm.upv.es

ABSTRACT

There are various techniques that can allow us to measure the fiber orientation. Some of it could not be described as an automatic, because it would force us to make such an individual measurement which would transform it into a rather tedious task. Other techniques (Thomason, 2001) can help us do this like automatic way and therefore enable to obtain the resulting of fibers distribution function.

Wetherhold, Scout (1990) explains different methods that can allow the fiber orientation function distribution and it can be checked manually, but hardly automatable and exportable to the field work in a company. The quantitative description of the fiber orientation it's explained by Advani (1987), Tucker (1987) and Thomason (2001), Nath, Phelps, JH (2009). An example of fiber orientation identification is the work of Yasuda (2004).

In summary, although the proposed methods for measuring the orientation, new applications continue to appear to improve the measurements. In our case, designing an operating procedure (Ferrándiz, 2007) capable of performing many of analysis applicable to the study of thermoplastics reinforced with long glass fibers.

1. INTRODUCTION

The increased use of composite materials in the manufacture of structural elements has been remarkable over the last decade. Thus, traditional materials such as aluminum, steel or wood applications are giving way to advanced composite materials. The polymer matrix composite materials have excellent relations of stiffness versus weight or resistance versus weight.

For these reasons can be found different composites ranges based on the type of fiber mixed with the polypropylene.

We need an analysis tool that enables an effective and fast part examination in different process conditions, injection techniques that are varied (pressure, temperature, materials, molds, injection speeds, etc.).

Wetherhold and Scout (1990) set out two different methods to measure manually the fiber orientation function.

One method that can be used is that of diffraction by applying the Fraunhofer diffractometer (McGee on alli, 1984) or performing a simulation of the diffractometer using the Fourier transform. The fiber orientation can be obtained by intensity analysis along the central circular border at the Fourier image. The distribution function for particular angle is proportional to the intensity in the Fourier plane at the same angle rotated pi/2. This system is applied to the compression molding samples (Vahlund, 2001).

Another way is to use the Hough Transform (Russ, 2002). This is a technique to discover how an image is. It‘s based on image transforming points in a parameters space. The idea is to find parameterization curves as straight lines, circles and polynomial functions. The most commonly used to perform edge detection is the Canny filter (Kumar, Murthy, 2001).

In our case has been designed an operational procedure capable of performing a large number of analysis and applied to the study of long glass fiber reinforced thermoplastics.

To this end our work is structured in the following stages:

-Data retrieval.

-Design of an algorithm that allow the processing of the images in an automated manner, with minimal user intervention and which do not lead to a miscalculation high.

Study and determination of the error obtained in the process of entering and identifying the frequency and the fiber orientation function.

2. EXPERIMENTAL

Samples were injected through an injection Mateu & Sole Meteor 270/75 model. The optical material has been used has been a magnifying glass Olympus SZ-CTV model in which the lenses have been used for 4 and 5x magnification. This system incorporates a magnifying lens adapter camera.

The camera used to catch the images of the samples is a Cammedia Olympus C-3030 zoom. The material was used to perform the surgical procedure of checks has been reinforced with a PP 50% Long Glass Fiber, brand Celstran ™ PP-GF50-04 0403P10/10, home © Ticona. The pellets are cylindrical and 10 mm length medium sized

3. RESULTS AND DISCUSION

As has been previously listed steps to be followed to complete the work through the data. This has been carried out several tests two-dimensional image capture. The two-dimensional image capture offers the possibility to determine the fiber orientation in the work layer and suppose an easier way to make the catch of the same images with same results.

In the second way is a procedure designed algorithms that allow the processing of the images like automated way, with minimal user intervention and which do not lead to a miscalculation high. Finally the error determination obtained in the capturing process and identifying the frequency and fiber orientation function.

Higher differences, Table 1 left, the values are 3, 6, 7 and 11 that when there are interferences between the fibers. The values adopted a mean deviation of 1.91%, which indicates an acceptable deviation. If we make an analysis of the values of the matrix vector orientation, and 11, we also observe interesting results, table 1 right.

Sample	Label	measured angle	teorical angle	dif %
1	img14513	134,8	135	0,123
2	img14513	45,221	45	-0,491
3	img14513	96,945	90	-7,717
4	img14513	45,194	45	-0,431
5	img14513	130,892	135	3,191
6	img14513	49,542	45	-10,093
7	img14513	100,574	90	-11,749
8	img14513	132,901	135	1,555
9	img14513	134,439	135	0,416
10	img14513	46,211	45	-2,691
11	img14513	126,745	135	6,115
12	img14513	45,494	45	-1,098
			average	-1,906

sample	measured angle	theoretical angle	a11	diff %
1	134,834	135	0,497	0,579
2	45,221	45	0,496	0,771
3	96,945	90	0,015	0
4	45,194	45	0,497	0,677
5	130,692	135	0,425	14,981
6	49,542	45	0,421	15,788
7	100,574	90	0,034	0
8	132,901	135	0,463	7,32
9	134,439	135	0,49	1,958
10	46,211	45	0,479	4,226
11	126,745	135	0,358	28,41
12	45,494	45	0,491	1,724
		average		7,644

Table 1. Values with interference

The average observed value a11 measured the gap are 0.389 including all values. When compared with the theoretical values, we see that the value goes up to 0.417. This represents an average relative deviation of 7.64%. If we compare with respect to the theoretical values made real, we see that we reached an error of 22%. If, by contrast, is a distorting filter elements we see that errors are kept at values of 5.33%, which can be a pretty good result. As a final test trials on which an image may appear multiple fibers of different lengths and which may appear in different orientations. As with previous examples have been applied to the calculations of the values of a11 of the matrix element of the vector orientation and the final has been obtained averaging all the values a11. The result shows an image measured with a highly oriented fibers, values of 0.8 (the range 0.5-1). This value is the value compared with the fiber theoretical calculation. It can be seen that the average value of the element a11 of the matrix is 0.875 compared to 0.801 of the measured value. This gives us a difference of 8.4% which we regard as deviation or error of measurement, which can be considered acceptable. The values of the testing procedure, we note that there is a small increase in error, Figure 2, as we have increased the complexity of the images of the fibers, and especially the interaction and intersection between them.

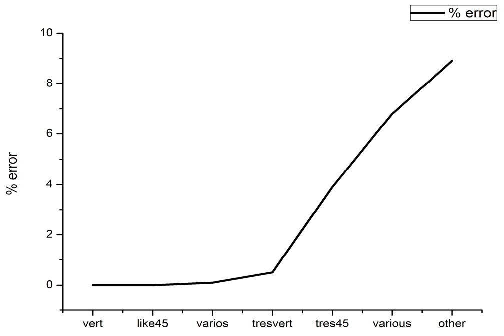

Figure 2. Evolution of the error**.**

4. CONCLUSIONS

As conclusions we see that there is a small increase in error as we have increased the complexity of the images of the fibers.

While working with images with the fibers perfectly defined, the errors have been somewhat negligible. Have begun to run when crossing fibers is when the system has been a bit unstable, especially when he had to calculate the value of a11 of the matrix operator of the vector orientation. As they have grown junctions have been achieved deviations of 8%, which can be considered an acceptable error in the implementation of the algorithms included in the macro.

It is therefore considered feasible to use the macro programmed algorithms for calculating various fiber orientations that were developed in later chapters, and various processes of plastics reinforced with long glass fiber.

REFERENCES

ADVANI, TUCKER III. “The use of tensors to describe and predict fibre orientation in short fibre composites”,. Jour. Of Reol. 31, 1987

FERRÁNDIZ. “Aplicación del análisis de imágenes a la determinación de la orientación de la fibra larga de vidrio en diferentes condiciones de proceso. PH.D. Thesis 2007.

KUMAR, MURTHY. “Hough transform for region extraction in color images”, 2001.

LOVING, TUCKER III, “Automated measurements of fiber orientation in short-fiber composites”. Antec, 1985.

THOMASON, J.L. “The influence of fibre length and concentration on the properties of glass fibre reinforced polypropylene: 5. Injection moulded long and short fibre PP”. Composites A., 33, 1641, 2002.

VAHLUND, “fibre orientation, rheological behaviour and simulation of the compression moulding process for composite material”. Ph.D. Thesis. 2001.

WETHERHOLD, SCOUT. “Prediction of thermoplastic properties in short-fiber composites using image analysis techniques”. Comp. Sci. Tech. 37. 1990

RUSS, J.C. “The image processing handbook”. Ed. CRC, Boca Raton, 2002.

YASUDA K, KYOTO T, MORI N. “An experimental study of flow-induced fiber orientation and concentration distributions in a concentrated suspension flow through a slit channel containing a cylinder”. Reol. Acta. 43, 2004

Nath, SKD . Afsar, AM.” Analysis of the Effect of Fiber Orientation on the Elastic Field in a Stiffened Orthotropic Panel under Uniform Tension using Displacement Potential Approach”. MECHANICS OF ADVANCED MATERIALS AND STRUCTURES 16 (4): 300-307, 2009

Phelps, JH , Tucker, CL . “An anisotropic rotary diffusion model for fiber orientation in short- and long-fiber thermoplastics”. JOURNAL OF NON-NEWTONIAN FLUID MECHANICS 156 (3): 165-176 FEB 2009

Effect of chemical modification on mechanical properties of banana fibers/HDPE composites

D.R. Mulinari, K.C.C. Carvalho
Grupo de Fadiga e Materiais Aeronáuticos (DMT/FEG). Universidade Estadual Paulista, Brazil
G.J.M. Rocha, V.A. Pequeno
Departamento de Engenharia de Bioquímica DEBIQ/EEL/USP. Universidade de São Paulo, Brazil

ABSTRACT

Natural fibers have attracted the attention of researchers because of the advantages over traditional reinforcement materials such as glass fiber in terms of cost, density and specific properties. In the work, mechanical properties of banana pseudo-stalk fibers/HDPE composites were studied. Banana fibers from pseudo stem were treated with 10% sulfuric acid solution, followed by centrifugation, to remove impurities such as waxes, pectins and hemicellulosics fibers and analyzed by SEM. These fibers were mixed with the polymeric matrix (HDPE) in a thermokinetic mixer, model MH-50H, with speed rate maintained at 5250 rpm, in which fibers were responsible for 5 wt% in the composition. After the mixture, composites were dried, ground in mill and placed in an injector camera according to ASTM D-638 specification. Results showed the addition of fibers in matrix increased the tensile strength and modulus compared to the matrix polymeric.

1. INTRODUCTION

Over the past decade there has been a growing interest in the use of lignocellulosic fibers as reinforcing elements in polymeric matrix (Satyanarayana *et al*., 2007). The specific properties of this natural product, namely low cost, lightweight, renewable character, high specific strength and modulus, availability in a variety of forms throughout the word, reactive surface and the possibility to generate energy, without residue, after burning at the end of their life-cycle, motivate their association with organic polymers to elaborate composite materials. However, it is well known that different surface properties between the fiber and the matrix, i.e. the former is highly polar and hydrophilic while the latter is, generally, non-polar and relatively hydrophobic, impose the surface modification of the fibers surface, in order to improve the fiber/polymer compatibility and their interfacial adhesion (Li *et al*., 2008; Araújo *et al*., 2008). Without such a treatment, natural fibers embedded in a polymeric matrix generate unstable interfaces and the stress applied to the fibers/polymer composite is not efficiently transferred from the matrix to the fiber and the beneficial reinforcement effect of the fiber remains under exploited. Several strategies of surface modifications aiming at improving the compatibility between cellulose fibers and polymer matrices were recently reviewed (Mulinari *et al*., 2009; Luz *et al*., 2008).

Then objective of this work was to study the effect of chemical modification on mechanical properties of banana fibers from pseudo stem/HDPE composites.

2. EXPERIMENTAL

2.1 Chemical modification banana fibers from pseudo stem

To remove the soluble extractives and to facilitate adhesion between fibers and matrix, the banana fibers from pseudo stem *in nature* (Figure 1A) were modified (Figure 1B) by pre-treatment with 10% sulfuric acid solution, followed by centrifugation.

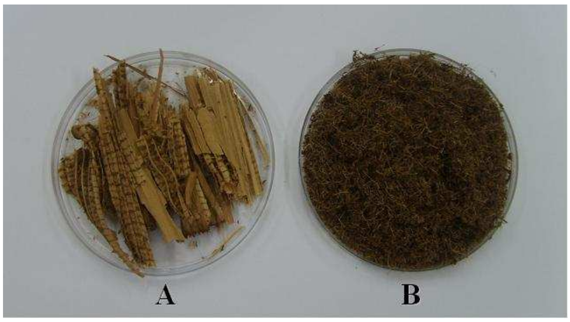

Figure 1. Banana fibers from pseudo stem fibers *in nature* (A) and modified (B).

2.2 Scanning electron microscopy

A JEOL JSM5310 model scanning electron microscope (SEM) was used to observe the banana fibers from pseudo stem fibers *in nature* and modified. The samples to be observed under the SEM were mounted on conductive adhesive tape, sputter coated with gold and observed in the SEM using a voltage of 15 kV.

2.3 Composites preparation

Banana fibers modified were mixed with the HDPE in a thermokinetic mixer, model MH-50H, with speed rate maintained at 5250 rpm, in which fibers were responsible for 5 wt% in the composition. After the mixture, composites were dried and ground in mill, model RONE. Composites and pure HDPE were placed in an injector camera at 165 ^{o}C and 2 °C min^{-1} heating rate in a required dimensions pre-warm mold to obtain tensile specimen.

2.4 Mechanical properties

The mechanical strength of banana fibers reinforced HDPE composites was determined using an INSTRON universal-testing machine (model 8801). Tests were carried out according to ASTM standards D638 with 10 mm.min^{-1} crosshead speed. Tensile strength and modulus values are average results of five tested specimens.

3. RESULTS AND DISCUSSION

3.1 Scanning electron microscopy

SEM provides an excellent technique for examining the surface morphology of banana fibers from pseudo stem *in nature* and modified. The morphology of fibers *in nature* can be observed in Fig. 2. These fibers show a superficial layer with high percentage of extractives. It is also possible to observe in Figure 2A a superficial layer of parenquimas cells.

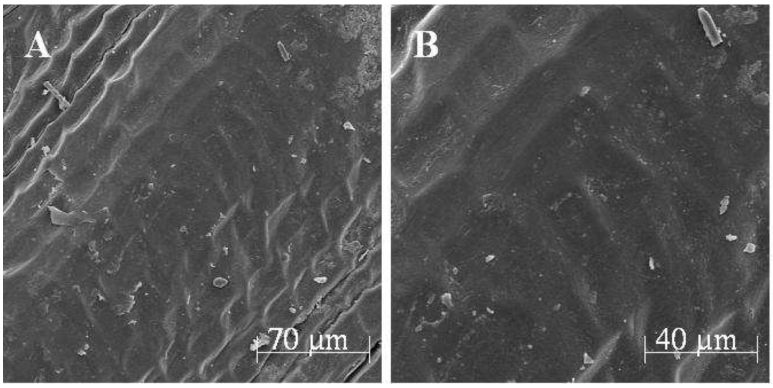

Figure 2. Morphology of banana fibers from pseudo stem *in nature*:
(A) 500X; (B) 1000X.

After the treatment on banana fibers from pseudo stem *in nature* it is observed the removal of the extractives on surface fibers. This image can be observed in Fig.3. It is verified also that with the elimination of superficial layer the contact area for exposition of fibrils (reentrance) and globular marks (salience) increased. As a consequence, it is observed an increase in the roughness of fibers, which contributes with the increase of the adhesion between fiber and matrix. These observations are also obtained with others treated fibers such as sisal, flax, etc (Sreekala and Thomas, 2003), having similar structures.

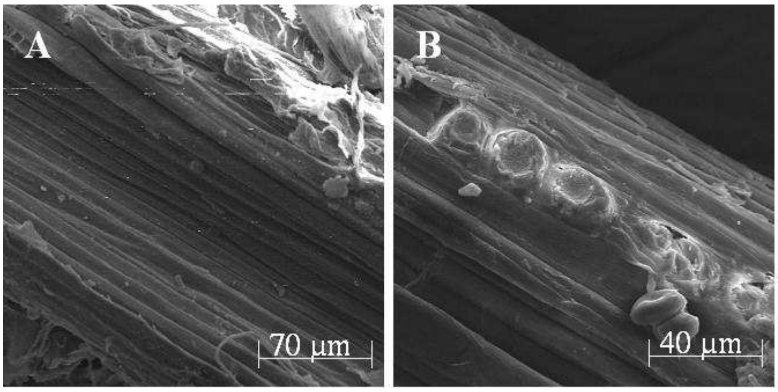

Figure 3. Morphology of banana fibers from pseudo stem modified:
(A) 500X; (B) 1000X.

3.2 Mechanical Properties

Mechanical properties of the composite and pure HDPE are summarized in Table 1. Banana fibers modified/HDPE composites presented higher tensile strength and modulus results compared to pure HDPE. This occurred due to good interaction between fibers and matrix. Fibers insertion can contribute to the modulus increase, which exhibited an increase of 33%, compared to the HDPE.

Table 1. Mechanical properties of the composite.

Samples	*Properties*		
	Elongation at break (%)	*Tensile strength (MPa)*	*Tensile modulus (MPa)*
HDPE	8.9 ± 0.8	15.7 ± 1.1	732.45 ± 90.6
Banana pseudo stem fibers/HDPE 5%	6.4 ± 0.6	22.4 ± 0.1	979.8 ± 34.3

Reinforcement in wt%.

4. CONCLUSIONS

The feasibility of using the banana fibers from pseudo stem as an alternative reinforcement in thermoplastics was verified. Banana fibers modified influenced directly mechanical properties banana fibers/HDPE composites. This modification on fibers increased roughness and caused improve in adhesion between fiber and matrix, which was confirmed by scanning electron microscopy technique.

ACKNOWLEDGEMENTS

The authors are grateful for the research support by CAPES.

REFERENCES

ARAÚJO, J. R., WALDMAN, W. R., DE PAOLI, M. A. (2008). Thermal properties of high density polyethylene composites with natural fibres: Coupling agent effect. *Polym. Degrad. Stab.*, 93, 1170-1175.

LI, Y., HU, C., YU, Y. (2008). Interfacial studies of sisal fiber reinforced high density polyethylene (HDPE) composites. *Compos. Part A*, 39, 570-579.

LUZ, S. M., DEL TIO, J., ROCHA, G. J. R., GONÇALVES, A. R., DEL'ARCO, A. P. (2008). Cellulose and cellulignin from sugarcane bagasse reinforced polypropylene composites: Effect of acetylation on mechanical and thermal properties. *Compos. Part A*, 39, 1362-369.

MULINARI, D.R., VOORWALD, H.J.C., CIOFFI, M.O.H., DA SILVA, M.L.C.P., DA CRUZ, T.G., SARON, C. (2009). Sugarcane bagasse cellulose/HDPE composites obtained by extrusion. *Compos. Sci. Technol.*, 69, 214-219.

SATYANARAYANA, K.G., GUIMARÃES, J.L., WYPYCH, F. (2007). Studies on lignocellulosic fibers of Brazil. Part I: Source, production, morphology, properties and applications. *Compos Part A*, 38, 1694-709.

SREEKALA, M.S., THOMAS, S. (2003). Effect of fibre surface modification on water-sorption characteristics of oil palm fibres. *Compos. Sci. Technol.* 63, 861-69.

Mechanical properties of sugarcane bagasse fibers/HIPS composites

D.R. Mulinari, K.C.C. Carvalho, H.J.C. Voorwald, M.O.H. Cioffi
Grupo de Fadiga e Materiais Aeronáuticos (DMT/FEG). Universidade Estadual Paulista, Brazil

ABSTRACT

In the work, mechanical properties of sugarcane bagasse fibers/HIPS composites were studied. Sugarcane bagasse fibers were treated with 10% sulfuric acid solution, followed by centrifugation, to remove impurities such as waxes, pectins and hemicellulosics fibers and analyzed by SEM. These fibers were mixed with the polymeric matrix (HIPS) in a thermokinetic mixer, model MH-50H, with speed rate maintained at 5250 rpm, in which fibers were responsible for 10 to 30 wt% in the composition. After the mixture, composites were dried, ground in mill and placed in an injector camera according to ASTM D-638 specification. Results showed the addition of fibers in matrix increased the tensile strength and modulus compared to the matrix polymeric.

1. INTRODUCTION

Natural fibers such as sisal, coir, jute, ramie, banana, bagasse, and sapegrass have the potential to be used as a replacement for glass or other traditional reinforcement materials in composites (Zah *et al*., 2008; Lei *et al*., 2007). These fibers offer several advantages including high specific strength and modulus, low cost, low density, renewable nature, biodegradability, easy fiber surface modification, and relative nonabrasiveness.

However certain drawbacks, such as poor compatibility with the hydrophobic polymer matrix, the tendency to form aggregates during processing and the low resistance to moisture, greatly reduce the potential of natural fibres to be used as reinforcement for polymers (Li *et al*., 2008; Araújo *et al*., 2008).

Because of this, several strategies of surface modifications have been used to improve the compatibility between cellulose fibers and polymer matrices. This step is considered critical in the development of these materials. The methods for surface modification can be physical or chemical according to the way they modify the fibre surface. Other frequently used treatments are bleaching, esterification, silane treatment, use of compatibilizer, plasma treatment, acetylation, alkali treatment and treatment with other chemicals (Mulinari *et al*., 2009; GU, 2009; Luz *et al*., 2008; Sreekala and Thomas, 2003).

The objective of this work was to study the effect of chemical modification on mechanical properties of sugarcane bagasse fibers/HIPS composites.

2. EXPERIMENTAL

2.1 Chemical modification sugarcane bagasse fibers

To remove the soluble extractives and to facilitate adhesion between fibers and matrix, the sugarcane bagasse fibers *in nature* (Figure 1A) were modified (Figure 1B) by pre-treatment with 10% sodium hydroxide solution, followed by filtration.

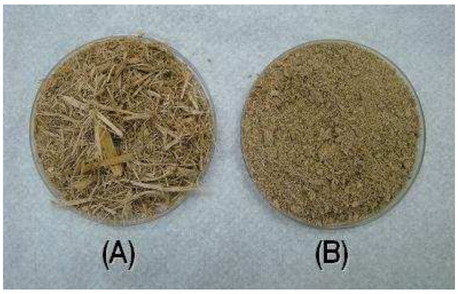

Figure 1. Sugarcane bagasse fibers *in nature* (A) and modified (B).

2.2 Scanning electron microscopy

A JEOL JSM5310 model scanning electron microscope (SEM) was used to observe the sugarcane bagasse fibers *in nature* and modified. The samples to be observed under the SEM were mounted on conductive adhesive tape, sputter coated with gold and observed in the SEM using a voltage of 15 kV.

2.3 Composites preparation

Sugarcane bagasse fibers modified were mixed with the HIPS in a thermokinetic mixer, model MH-50H, with speed rate maintained at 5250 rpm, in which fibers were responsible for 10 to 30 wt% in the composition. After the mixture, composites were dried and ground in mill, model RONE. Composites and pure HIPS were placed in an injector camera at 200 ^{o}C and 2 ºC min^{-1} heating rate in a required dimensions pre-warm mold to obtain tensile specimen.

2.4 Mechanical properties

The mechanical strength of sugarcane bagasse fibers reinforced HIPS composites was determined using a SHIMADZU testing machine (model AG-X 50 kN). Tests were carried out according to ASTM standards D638 with 5 mm.min^{-1} crosshead speed. Tensile strength and modulus values are average results of five tested specimens.

3. RESULTS AND DISCUSSION

3.1 Scanning electron microscopy

SEM provides an excellent technique for examining the surface morphology of sugarcane bagasse fibers *in nature* and modified. The morphology of fibers *in nature* can be observed in Fig. 2. These fibers show a superficial layer with high percentage of extractives. After the treatment on sugarcane bagasse fibers *in nature* it is observed the removal of the extractives on surface fibers. This image can be observed in Fig.3.

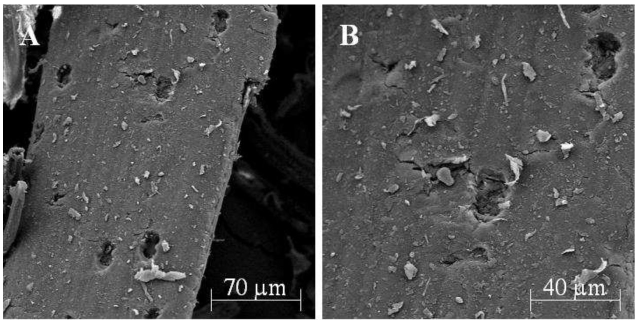

Figure 2. Morphology of sugarcane bagasse *in nature*: (A) 500X; (B) 1000X.

It was verified also that with the elimination of superficial layer the contact area for exposition of fibrils (reentrance) increased. As a consequence, it was observed an increase in the roughness of fibers, which contributes with the increase of the adhesion between fiber and matrix. These observations are also obtained with others treated fibers such as sisal, flax, etc (Sreekala and Thomas, 2003), having similar structures.

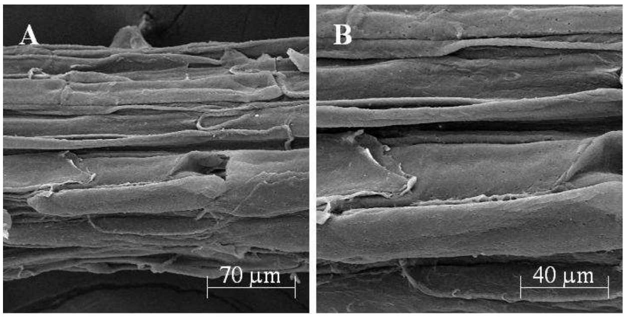

Figure 3. Morphology of sugarcane bagasse fibers modified: (A) 500X; (B) 1000X.

3.2 Mechanical Properties

Mechanical properties of the composite and pure HIPS are summarized in Table 1.

Table 1. Mechanical properties of the composite.

Samples	***Properties***		
	Elongation at break (%)	***Tensile strength (MPa)***	***Tensile modulus (Mpa)***
Pure HIPS	0.8 ± 0.01	24.6 ± 0.07	3045.7 ± 36.4
Sugarcane bagasse fibers/HIPS 10%	0.7 ± 0.006	25.1 ± 0.07	3519.7 ± 42.0
Sugarcane bagasse fibers/HIPS 30%	0.6 ± 0.013	27.7 ± 0.18	4771.5 ± 91.3

Reinforcement in wt%.

Sugarcane bagasse fibers modified/HIPS composites presented higher tensile strength and modulus results compared to pure HIPS. This occurred due to good interaction between fibers and matrix. Fibers insertion can contribute to the modulus increase, which exhibited an increase of 57%, compared to the pure HIPS.

These results may be explained by the good interaction observed between fibers and matrix during the mixture process, confirming that fibers modification improves the fiber and matrix adhesion. This can be observed by the fracture surface. SEM micrograph of the fractured surface for the composite is shown in Fig. 4. However, the addition of fibers in the matrix caused defects.

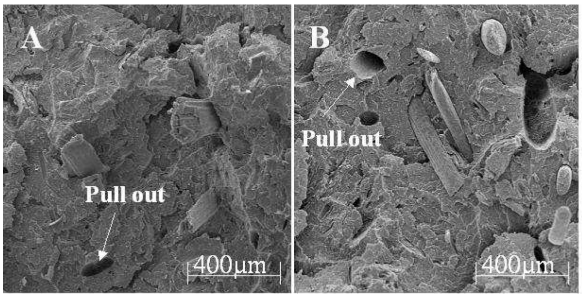

Figure 4. SEM of fractured surfaces of sugarcane bagasse fibers/HIPS composites 100X: (A) 10% wt; (B) 30% wt.

4. CONCLUSIONS

The feasibility of using the sugarcane bagasse fibers as an alternative reinforcement in thermoplastics was verified. Sugarcane bagasse fibers modified influenced directly mechanical properties sugarcane bagasse fibers/HIPS composites. This modification on fibers increased roughness and caused an improve in adhesion between fiber and matrix, which was confirmed by scanning electron microscopy technique.

ACKNOWLEDGEMENTS

The authors are grateful for the research support by CAPES.

REFERENCES

ARAÚJO, J. R., WALDMAN, W. R., DE PAOLI, M. A. (2008). Thermal properties of high density polyethylene composites with natural fibres: Coupling agent effect. *Polym. Degrad. Stab.*, 93, p.1170-1175.

GU, H. (2009). Tensile behaviours of the coir fibre and related composites after NaOH treatment. *Materials & Design*, 30, 3931-3934.

LEI Y, WU Q, YAO F, XU Y. (2007). Preparation and properties of recycled HDPE/natural fiber composites. Compos Part A, 38, 1664–1674.

LI, Y., HU, C., YU, Y. (2008). Interfacial studies of sisal fiber reinforced high density polyethylene (HDPE) composites. *Compos. Part A*, 39, p.570-579.

LUZ, S. M., DEL TIO, J., ROCHA, G. J. R., GONÇALVES, A. R., DEL'ARCO, A. P. (2008). Cellulose and cellulignin from sugarcane bagasse reinforced polypropylene composites: Effect of acetylation on mechanical and thermal properties. *Compos. Part A*, 39, p1362–1369.

MULINARI, D.R., VOORWALD, H.J.C., CIOFFI, M.O.H., DA SILVA, M.L.C.P., DA CRUZ, T.G., SARON, C. (2009). Sugarcane bagasse cellulose/HDPE composites obtained by extrusion. *Compos. Sci. Technol.*, 69, 214-219.

SREEKALA, M.S., THOMAS, S. (2003). Effect of fibre surface modification on water-sorption characteristics of oil palm fibres. *Compos. Sci. Technol*. 63, 861–869.

ZAH R, HISCHIER R, LEÃO AL, BRAUN I. (2007). Curauá fibers in the automobile industry - a sustainability assessment. *J Cleaner Prod*, 15, 1032-40.

Fabricación y caracterización de materiales compuestos CF/epoxi

J. Narciso
Departamento de Química Inorgánica. Instituto Universitario de Materiales de Alicante (IUMA). Universidad de Alicante, España
J.M. Molina
Departamento de Química Inorgánica. Instituto Universitario de Materiales de Alicante (IUMA). Universidad de Alicante, España

RESUMEN

Los materiales poliméricos reforzados con fibra larga son los materiales compuesto más extendidos debido a las buenas propiedades que presentan, su facilidad de preparación, y que se pueden predecir algunas de sus propiedades razonablemente bien. La interfase que es decisiva ya que gobierna las propiedades finales del material, sus propiedades no son fáciles de medir y se suelen medir de manera indirecta en especial en el caso de las propiedades mecánicas. El presente trabajo pretende ilustrar la bondad del análisis dinámico mecánico para medir dicha propiedad de una manera sencilla y fiable.

1. INTRODUCCIÓN

Los materiales compuestos de matriz polimérica reforzados con fibras largas, son los materiales compuestos más extendidos debido a sus excelentes propiedades y su fácil procesado que ha permitido su automatización. Las buenas propiedades unida a su ligereza, le permite ser el material más usado en aeronáutica y en la fabricación de yates y embarcaciones de recreo.

El principal problema de los materiales compuestos en general es su relativo alto coste, que ha limitado su uso a aplicaciones de alta tecnología como las comentadas anteriormente. El alto coste en este caso viene atribuido principalmente al alto coste de los materiales de partida, y en otros casos también la tecnología empleada a su vez representa un alto coste. Muchas de las dificultades del procesado están relacionadas con la mojadura entre el refuerzo y la matriz, y la falta de conocimiento de cómo afecta el enlace interfacial a las propiedades mecánicas del material compuesto. Estos efectos aunque son bien "reconocidos" no se han estudiado en gran extensión y solo existe un limitado número de publicaciones.

Se han ideado un gran número de ensayos para estudiar la interfase, pero en la mayoría de ellos son solos discriminatorios y no nos dicen en realidad la fortaleza del enlace. El ensayo por excelencia es el "pull-out test" . Este ensayo consiste en empujar la fibra hasta que se produzca el desplazamiento a través de la matriz, y medir el esfuerzo necesario para realizarlo. Este método presenta bastantes problemas, solo es válido para fibra larga, el equipamiento es relativamente caro, ya que necesitamos un nano indentador. Desde el punto de vista del ensayo presenta algunas dificultades, ya que debemos tener alineados perfectamente la punta y la fibra, además para que sean válidos los resultados la resistencia de la fibra debe de ser mucho mayor que la de la interfase.

El análisis dinámico mecánico es una técnica muy utilizada en polímeros debido a su naturaleza viscoelástica, aunque también se ha utilizado para estudiar fenómenos de amortiguamiento en metales, algunos autores han propuesto el uso de esta técnica para caracterizar la interfase. Esta técnica presenta un gran número de ventajas, en principio es no destructiva, fácil de realizar, insensible al alineamiento y por lo tanto vale para otros tipos materiales compuestos, y somos capaces de hacer un análisis cuantitativo de la interfase.

El objetivo del presente trabajo es fabricar materiales compuestos epoxi/Cf y caracterizar las propiedades mecánicas e interfaciales de dicho material compuesto.

2. RELACION ENTRE EL ANALISIS DINÁMICO MECÁNICO Y LAS PROPIEDADES INTERFACIALES

La caracterización dinámica mecánica se basa en las diferentes respuestas que puede presentar un material a un estimulo (tensión o deformación) dado en forma sinusoidal. De forma abreviada diremos que si el material es elástico puro no existirá desfase entre el estímulo y la respuesta, mientras que si es viscoso puro el desfase es de pi/2, y por lo tanto toda la energía de deformación es disipada en forma de calor.

En un material compuesto estándar donde el refuerzo es elástico puro y la matriz viscoelástica (polímeros) o inelástica (metales) y una interfase matriz refuerzo, la energía es principalmente disipada en la matriz y en la interfase. En conclusión un material compuesto con una mala unión matriz refuerzo tiende a disipar mayor energía.

2. EXPERIMENTAL

La fibra de carbono seleccionada para el presente trabajo ha sido una de PAN T-300, suministrada por AMOCO, y la resina una resina epoxi suministrada por SHELL. Las propiedades de estos materiales se recogen en la Tabla 1.

Para la fabricación de los materiales compuestos se ha empleado la siguiente técnica: La fibra ha sido alineada usando un bastidor de alambre de acero donde ha sido enrollado el manojo de fibras. Las fibras así dispuestas han sido alojadas en un molde en U, el cual es rellenado por la resina epoxi. Posteriormente se le aplica una presión de 10 MPa y un ciclo de temperatura entre 60 y 120 C para el curado de la resina y consolidación del material compuesto. Las dimensiones finales son 229x12.7x1.6 mm, fabricándose 10 materiales compuestos por condición de trabajo.

Tanto el módulo de flexión como la resistencia a la flexión han sido determinadas usando el método de flexión en cuatro puntos según la norma ASTM D-790.

El análisis dinámico mecánico ha sido realizado en analizador RDS 7700 de la casa Rheometrics, en el modo de torsión con un desplazamiento del 0.1 %, siendo la longitud de la muestra de 64 mm, por lo que se ha podido realizar dos ensayos de cada una de las muestras fabricadas. Obteniéndose G´ (almacenamiento), G´´ (perdida) y la tangente de perdida de cada una de las muestras.

3. RESULTADOS

La figura 1 muestra los resultados obtenidos del módulo de Young donde se puede apreciar claramente una muy buena correlación con las reglas de las mezclas, en especial a las concentraciones de refuerzo menos elevadas. Se observa que con el aumento del volumen de refuerzo se aleja más de las predicciones, esto es debido a que a concentraciones tan alta de refuerzo, el material polimérico tiene mayor dificultad para fluir y hacer una buena unión matriz refuerzo. Respecto a la resistencia a la flexión se observa una mayor dispersión debido principalmente a la influencia de la porosidad que afecta en gran medida y necesita un análisis más detallado.

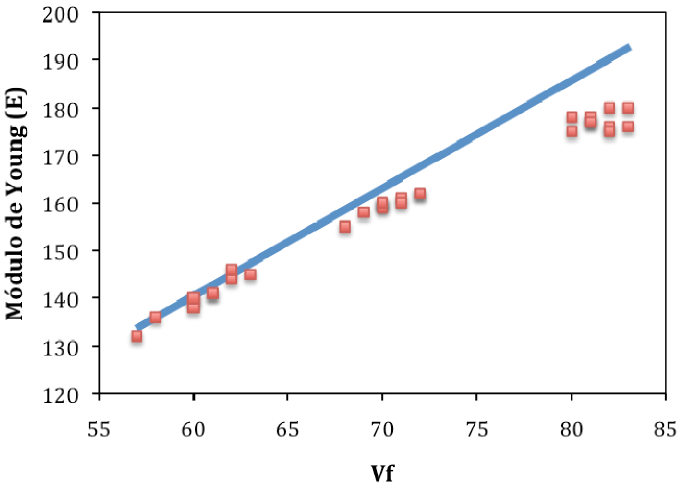

Fig 1. Módulo de Young en función del volumen de refuerzo, la línea en azul representa la regla de las mezclas.

La figura 2 presenta tanto el módulo de almacenamiento como el módulo de perdida, donde se ve claramente el efecto del contenido en fibra, ya que en ambos casos aumenta con el contenido en refuerzo, aunque el paso del 70 al 80% no muestra una mejora ostensible, probablemente debido a que como se comento en el párrafo anterior a la peor unión matriz refuerzo. Este hecho se observa más claramente en la figura 3 donde se presenta la tangente, donde el material reforzado con un 60% de fibras es prácticamente igual que el reforzado con el 70% , ya que la interfase es bastante buena, mientras que el reforzado con el 80% presenta una mayor perdida debido a su mala interfase.

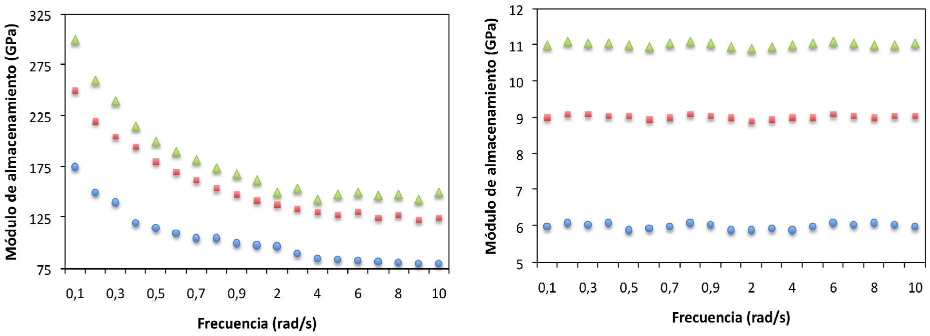

Fig 2. Módulo de almacenamiento y de perdida en función de la frecuencia , donde el color azúl es para el material reforzado con un 60%, el rojo para el del 70 y el verde para el del 80.

Aunque aparentemente las variaciones son muy pequeñas hay que recordar que la matriz en este caso es viscoelástica y por lo tanto el módulo de perdida también viene influenciado por ella

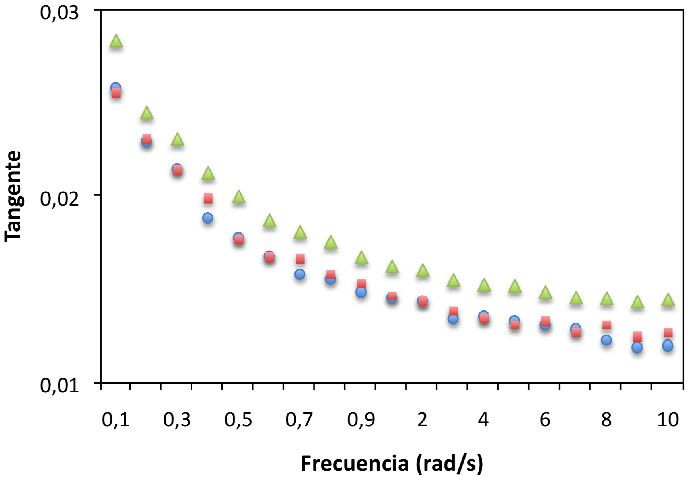

Fig 3. Capacidad de almacenamiento específica (tangente) en función de la frecuencia , donde el color azúl es para el material reforzado con un 60%, el rojo para el del 70 y el verde para el del 80.

3. CONCLUSIONES

El presente trabajo ilustra el uso de la técnica de análisis dinámico mecánico como una herramienta potente y versátil para determinar la fortaleza del enlace en la interfase matriz refuerzo.

PVA/SiO$_2$ and PVA/modified SiO$_2$ nanofiber mats obtained by electrospinning

F.C. Oliveira, A. Barros-Timmons
CICECO, Department of Chemistry, University of Aveiro, 3810-193 Aveiro, Portugal
P.O. Ferreira, C.O. Ferreira, J.A. Lopes-da-Silva
QOPNA Unit, Department of Chemistry, University of Aveiro, 3810-193 Aveiro, Portugal

ABSTRACT

Nanofibers of poly (vinyl alcohol) (PVA) with different amounts of silica (SiO$_2$) and SiO$_2$ modified with 3-aminopropyltrimethoxysilane (APS) (SiO$_2$@APS) have been successfully prepared by electrospinning. SiO$_2$@APS yielded fiber mats with a homogeneous distribution of the fillers along the fibers as opposed to what was obtained with SiO$_2$ without modification. Mechanical properties of PVA/SiO$_2$@APS nanofiber mats revealed a decrease of elongation in comparison to pure PVA nanofibrous mats however, the tensile strength and the Young's modulus have hardly been affected.

1. INTRODUCTION

Despite the existence of the electrospinning technique since the beginning of 20th century, it was only in the last 10 years that this field has received great interest from researchers. This innovative technology allows the production of fibers from a polymer solution or a fluid through the force exerted by electrical induction. These fibers' diameters vary between micrometers to values below 100 nanometers. In comparison with conventional fibers, electrospun fibers have some unique characteristics, such as a high surface-to-volume ratio, high porosity, interconnected three-dimensional porous structures and extremely long length. These properties make them suitable for a variety of applications in such areas as filtration, catalysis, protective textiles, and biomedical engineering including drug delivery, tissue scaffolds, and wound dressing (Subbiah et al., 2005).

The incorporation of metal nanoparticles has shown to provide the polymer nanofibers with distinctive properties like mechanical, thermal, optical, electronic, catalytic and antimicrobial properties (Shao et al., 2003; Wang et al., 2005; Furlan et al., 2007).

The choice of the polymer and solvent plays a crucial role in the characteristics of the nanofibers obtained as well as their interaction with the inorganic nanoparticles. PVA is a polymer that has been studied intensively due to its unique properties, such as good film forming and physical characteristics, high hydrophilicity, processability, biocompatibility, good chemical resistance, and has shown to produce nanofibers by electrospinning with attractive properties. The properties of PVA fibers can be enhanced or modified by incorporation of silica nanoparticles (SiO$_2$) (Shao *et al.*, 2003).

In this work we used the electrospinning technique to prepare fiber mats of PVA/SiO$_2$. To improve the silica dispersion and change polymer-filler interactions, the surface of SiO$_2$ particles was functionalised with 3-aminopropyltrimethoxysilane (APS). The influence of silica surface modification and filler amount on the properties of PVA fibers will be discussed.

2. EXPERIMENTAL

SiO_2 particles with 300 nm average diameter were prepared as previously described by Pinto *et al.* (2008) while SiO_2@APS were prepared following Foschiera *et al.* (2001) method. Previously SiO_2, SiO_2@APS (20% or 60% w/v) suspensions and PVA solutions (20 % w/v) were prepared in 0.1 M CH_3COOH aqueous solution separately. PVA solution was stirred overnight at room temperature, followed by heating at 80 °C during two hours before the addition of silica particles suspensions. PVA/SiO_2 and PVA/SiO_2@APS suspensions were prepared by simple mixture of components (1:1), resulting in a final aqueous suspension of 10 % w/v of PVA and (10 or 30% w/v) of SiO_2 and SiO_2@APS in 0.1 M CH_3COOH. Then, the final suspension was transferred to a glass apparatus, especially made by our group (Scheme 1). This apparatus was adapted to contain a magnetic stirrer in order to maintain the suspension under stirring during the whole experiment to avoid SiO_2 deposition during fiber mat formation.

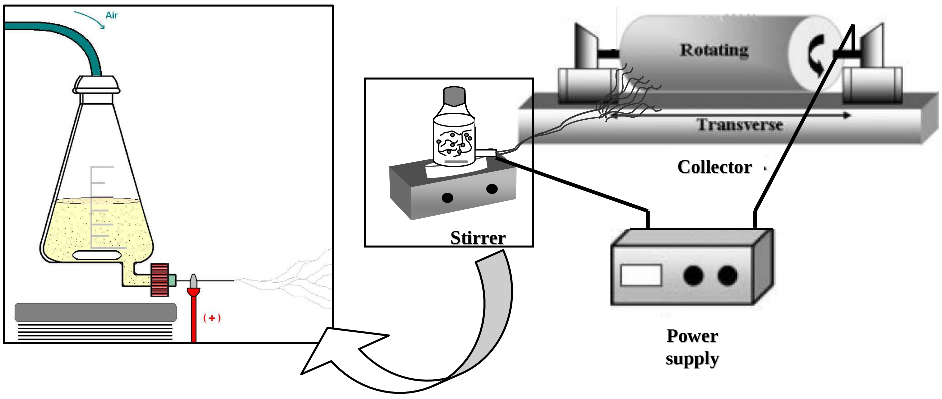

Scheme 1: Experimental apparatus for nanofibers fabrication by electrospinning technique.

3. RESULTS AND DISCUSSION

The fiber mats prepared using PVA, PVA/SiO_2 and PVA/SiO_2@APS were analysed by scanning electron microscopy (SEM) and transmission electron microscopy (TEM) (Fig. 1). As observed in Figure 1, the fiber mats morphologies were different for each sample. For pure PVA sample (Fig. 1a and 1b), the fibers showed a regular size distribution with a reasonable variation in diameter (170-325 nm) as obtained by Ferreira (2008) in his work.

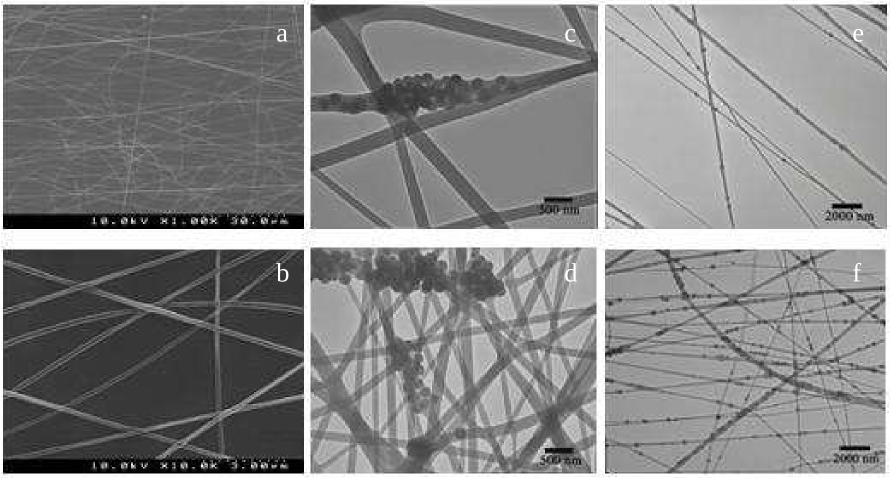

Fig. 1. SEM image of the pure (10% w/v) PVA nanofibers (a and b). TEM images of PVA nanofibers containing (c) SiO_2 (10% w/v), (d) SiO_2 (30% w/v), (e) SiO_2@APS (10% w/v) and (f) SiO_2@APS (30% w/v).

When silica particles were added to the PVA matrix (Fig. 1c-f) the fiber morphologies and diameter were distinct depending of the content and surface characteristics of SiO_2 particles. The use of SiO_2 without modification yielded mats with large aggregates within the PVA fibers, whereas the use of SiO_2@APS yielded mats with the fillers well dispersed along the PVA fibers.

The main reason for this difference is due to the fact that bear silica particles are aggregated at the pH of the CH_3COOH solutions, whilst the modified silica particles are well dispersed due to the repulsions between the terminal protonated amine groups, as can be observed in the graph of average size versus pH (Fig. 2).

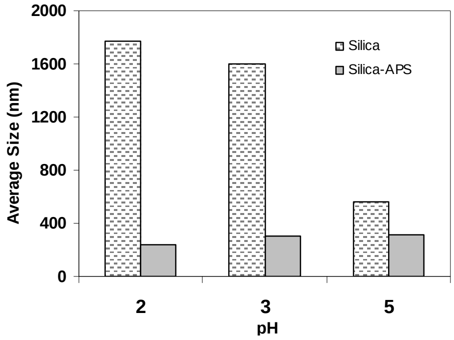

Fig. 2. Average size of SiO_2 and SiO_2@APS in CH_3COOH (aq) solution at different pH values. In general, SiO_2 and SiO_2@APS suspensions were at pH 2,5 – 4,5.

As regards the mechanical properties of nanofibers obtained in this work, only PVA and PVA/SiO_2@APS nanofibers mats were analysed (Fig. 3) since these nanocomposites presented a more homogenous filler distribution and morphology. Clearly the presence of SiO_2@APS in PVA nanofibers reduced the fiber elongation capacity. This effect is essentially observed for PVA/SiO_2@APS nanofibers with higher silica content. However, no important effects were observed on the tensile strength and the Young's modulus.

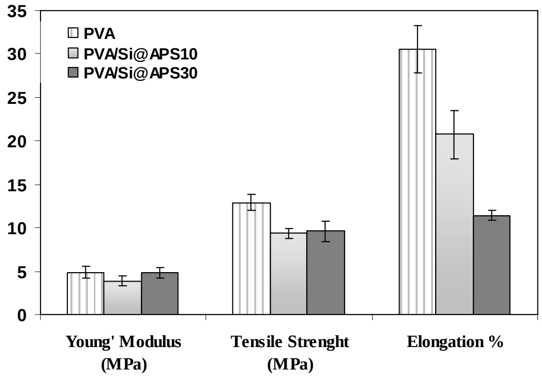

Fig. 3. Mechanical analyses of PVA and PVA/SiO_2@APS nanofibers mats.

4. CONCLUSIONS

PVA/SiO_2@APS nanofibers mats were efficiently prepared by electrospinning. The modified fillers were homogenously distributed along of the nanofibers. The presence of fillers led to a reduction of fiber elongation capacity. Other techniques such as contact angle measurements, dynamical mechanical analyses and solubility tests are being carried out to complete characterization of these materials.

REFERENCES

FERREIRA, P.O. (2008). Matrizes fibrosas de biopolímeros produzidas por electrospinning, Tese de Mestrado, Universidade de Aveiro.

FOSHIERA, J.L., PIZZOLATO, T.M., BENVENUTTI, E.V.J. (2001). FTIR thermal analysis on organofunctionalized silica gel. *J. Braz. Chem. Soc.*, 12, 159-164.

FURLAN, R., SIMÕES, E.W., DA SILVA, M.L.P., RAMOS, I., FACHINI, E. (2007). Modeling of composite fiber production with silica nanoparticles dispersed in polyethyleneoxide. Polymer, 48, 5107-15.

PINTO, R.J.B., MARQUES, P.A.A., BARROS-TIMMONS, A., TRINDADE, T., PASCOAL, C.N. (2008) Novel SiO_2/cellulose nanocomposites obtained by *in situ* synthesis and *via* polyelectrolytes assembly. *Compos. Sci. Technol.*, 68, 1088-1093.

SHAO, C., KIM, H-Y., GONG, J., DING, B., LEE, D-R., PARK, S-J. (2003). Fiber mats of poly(vinyl alcohol)/silica composite via electrospinning. *Mater. Lett.*, 57, 1579-1584.

SUBBIAH, T., BHAT, G.S., TOCK, R.W., PARARNESWARAN, S., RAMKUMAR, S.S. (2005). Electrospinning of nanofibers. *J.Appl. Polym. Sci.*, 96, 557-569.

WANG, Y., YANG, Q., SHAN, G., WANG, C., DU, J., WANG, S., LI, Y., CHEN, X., JING, X., WEI, Y. (2005). Preparation of silver nanoparticles dispersed in polyacrylonitrile nanofiber film spun by electrospinning. *Mater. Lett.*, 3046-49.

Fracture behaviour of PP/ash composites toughened with an olefin block copolymer

S.G. Pardo
Centro Galego do Plástico (CGaP), A Cabana s/n Ferrol, España
Grupo de Polímeros, E.U.P., Univ. A Coruña, Av. 19 de febrero s/n, Ferrol, España
C. Bernal
Grupo de Materiales Avanzados, INTECIN (UBA-CONICET), Dpto. de Ing. Mecánica, Av. Paseo Colón 850, C1063ACV, Buenos Aires, Argentina.
J. Cano, M.J. Abad, L. Barral Losada
Grupo de Polímeros, E.U.P., Univ. A Coruña, Av. 19 de febrero s/n, Ferrol, España

ABSTRACT

The use of fly ash fillers to improve fracture properties of polymer composites as well as to reduce costs and to obtain more environmentally friendly materials was considered in this work. The fracture and failure behaviour of composites based on polypropylene (PP), an olefin block copolymer and ash was studied. Ashes and fly ashes used as fillers are solid industrial wastes produced as the result of the wood industry combustion. During the processing, silane treated ashes with an olefin block copolymer (OBC) were included in a polypropylene matrix. The developed composites exhibited fracture energy values significantly higher than those of the matrix or similar composites without OBC. A fibrillised debonding process was found to be the main deformation mechanism which led to higher energy absorption in both crack initiation and propagation steps. Therefore, it seems to be responsible for the improved fracture behaviour observed in our composites.

1. EXPERIMENTAL

Fly ashes obtained from biomass combustion were used as the filler. They were kindly supplied by Industrias del Tablero S.A. (INTASA). Ashes were separated using a sieve of mesh 400 μm. Isotactic polypropylene (PP 070G2M) delivered by Repsol-YPF, with a melt flow index (MFI) of 12 g/10 min (230 º C, 2.16 kg) and a density of 0.902 g/cm3 was used as the matrix of the composites. The ethylene-octene block copolymer (OBC) INFUSE™ D9507.10 used in this study was supplied by The Dow Chemical Company. The MFI of OBC was 5 g/10 min (190 ºC, 2.16 kg) and density 0.866 g/cm^3. A commercially available polymer processing additive (Dynamar FX 5911, Dyneon, 3M Company) was also added in a proportion of 1 wt.% respect to the mass of PP. The silane coupling agent Geniosil™ GF 96 was supplied by Wacker Chemie Italia S.r.L.
Fracture tests were carried out on single-edge notched bend SENB specimens cut out from compression-moulded thick plaques (thickness, B = 8 mm). Sharp notches were introduced by sliding a fresh razor blade into a machined slot. Crack-to-depth (a/W), thickness-to-depth (B/W) and span-to-depth (S/W) ratios were always kept equal to 0.5, 0.5 and 4, respectively. Three-point-bend tests were performed in an Instron dynamometer 5566 at 1 mm/min. Energy release rate (G_{IQ}) values at initiation were obtained by following ASTM D-5045-92 standard recommendations. Critical energy release rate values at propagation (G_{CP}) were also determined from these tests.

To study the dominant deformation mechanism, some SENB specimens were also tested in three-point bending in the Instron dynamometer 4467, at the same speed used in the fracture tests (1 mm/min). The specimens were tested up to subcritical displacement levels until some deformation was evident. Side surfaces had been previously polished with different abrasive papers of increasing coarseness. Then, they were observed by transmission optical microscopy (TOM) and scanning electron microscopy (SEM) after they had been coated with a thin layer of gold. All tests were carried out at room temperature.

2. DISCUSSION AND RESULTS

2.1 Fracture Behaviour

It has been previously observed (Pardo et al. (2009)) that PP/ash composites displayed higher values of fracture parameters than the matrix as a result of the development of a small particle-induced toughening mechanism. However, fracture properties were also found to decrease with ash content. This result has been attributed to the increase in the number of critical-size flaws that induced premature failure. The incorporation of a silane coupling agent in the formulations led to composites with slightly improved fracture properties due to a better dispersion of ash particles in the matrix and/or changes in the crystallization behaviour of PP.

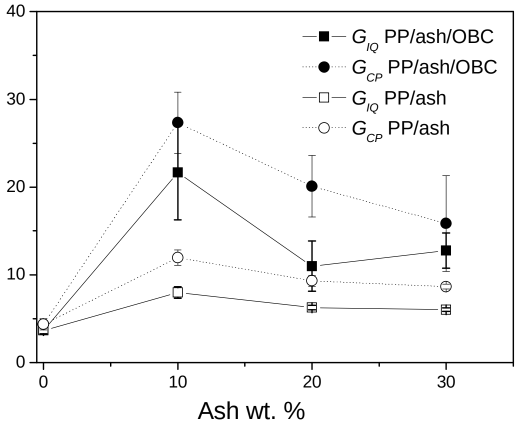

Fig. 1. Energy release rate values at initiation and at propagation for the PP/ash/OBC composites and similar composites without OBC (Pardo et al. (2009)).

In this work, a decreasing trend of the fracture parameters (Figure 1) with increasing ash content was observed for PP/ash/OBC composites, due to the increase in the number of critical-size flaws that induced premature failure in agreement with previous results on similar PP/ash composites. In addition, a significant improvement in the fracture energy values at both initiation and propagation was found for the composites with OBC in comparison to the PP matrix and those without OBC (Pardo et al. (2009)), suggesting that the presence of the olefin block copolymer led to more ductile composites in agreement with previous results on the material tensile response (unpublished results).

2.2 Deformation mechanism

Some composite samples were analysed by optical microscopy (TOM) to study the stress whitening zone developed during deformation (Figure 3).

Fig. 2. Typical side views of composite SENB samples tested up to subcritical displacement levels. Composite: a) 811, b) 712 and c) 613 (10X).

It can be clearly seen in Figure 2, that at lower filler content the stress whitening zone is greater and subsequently more plastic damage occurred. This fact is in accordance with the fracture behaviour observed for the different composites.

In addition, scanning electron microscopy (SEM) observations (Figure 3) revealed that OBC and polypropylene behaved as a unique phase matrix material. The principal aim of the OBC incorporation into PP/ash composite formulations was to achieve increased toughness and improved morphology (a more homogeneous dispersion of ash particles in PP). The main deformation mechanism was found to be a fibrillised debonding process. This mechanism of toughening has been originally proposed by Kim et al. (1998) for particle-filled semicrystalline polymers and later observed by other authors for different polypropylene composites.

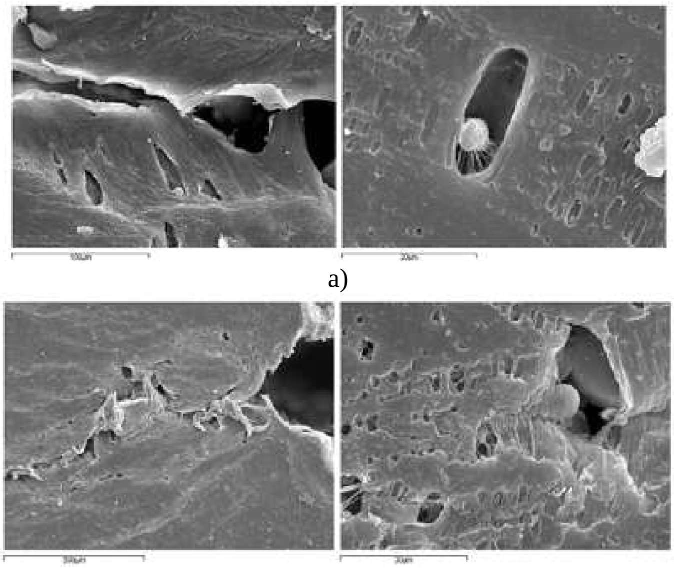

a)

c)

Fig. 3. Side views of composite SENB samples tested up to subcritical displacement levels. Composite: a) 811, b) 712 and c) 613.

Debonding of large particles did not seem to contribute to the deformation mechanism but led to the formation of critical-size flaws in agreement with previous findings on similar composites (Pardo et al. (2009)). Hence, the increase in ash content led to a decrease in the fracture properties due to the greater number of large particles able to induce premature failure.

3. CONCLUSIONS

The fracture behaviour of environmentally friendly composites based on PP, an olefin block copolymer and ash was investigated.

The developed composites exhibited significantly improved fracture behaviour in comparison to the PP matrix or the same composites without OBC.

The main energy-absorption mechanism responsible for the observed fracture behaviour was found to be a fibrillised debonding process.

REFERENCES

AMERICAN SOCIETY FOR TESTING AND MATERIALS (1993). Standard test methods for plane-strain fracture toughness and energy release rate determination of plastics materials; ASTM D5045-93, New York, (USA).

KIM G. M. AND MICHLER G. H. (1998) Micromechanical deformation processes in toughened and particlefilled semicrystalline polymers: Part 1. Characterization of deformation processes in dependence on phase morphology, *Polymer* 39, 5689-5697.

PARDO SG, BERNAL C, ABAD MJ, CANO J, BARRAL L (2009) Deformation and fracture of PP/Ash composites. *Composit Inter.*, 16, 97-114.

Primeros resultados del desarrollo de compuestos híbridos tipo CARALL

J. Rios, G. Kokubu, G. Fernández, G. Porta, E. Chomik, J. Balderrama, N. Fuentes
Comisión Nacional de Energía Atómica GAEN- GIDAT- U. A. Materiales,
Av. Gral. Paz 1499, (B1650KNA) San Martín. Buenos Aires – Argentina.
A. Cambiasso, E. Asta
Universidad Tecnológica Nacional – F. R. Haedo. Grupo Fractomecánica.
París 532 (B1706KNA) Haedo. Buenos Aires – Argentina

RESUMEN

Se ha iniciado un proyecto que comprende el estudio de propiedades mecánicas de compuestos CARALL, que incluye la fabricación de estos compuestos híbridos a escala de laboratorio, la obtención de probetas a partir de ellos y la realización de ensayos. En este trabajo se presentan los primeros resultados de la fabricación de compuestos híbridos a partir de aleaciones de aluminio 1050 y 6061 T0 y fibras de carbono NCT-301 unidireccional.

1. INTRODUCCIÓN

Los materiales compuestos híbridos, laminados fibra-metal, (Fiber Metal Laminates FML) [1], consisten en láminas delgadas de aluminio colaminadas en forma alternada con capas de fibras de carbono unidireccionales embebidas en una matriz de resina epoxy. Los compuestos FML son materiales livianos, con elevada resistencia a la propagación de fisuras, resistencia al daño acumulado y baja absorción de humedad. Tienen por ello un gran potencial de aplicación en la industria naval y aeroespacial [2]. Estos materiales tienen como característica que en ellos la propagación de fisuras tiene lugar mediante el mecanismo “Puenteo de Fibra” (Fiber-Bridging) [3]. Cuando el extremo de una fisura se propaga en forma perpendicular a la fibra tal propagación se realiza preferentemente a través de las láminas de aluminio, y está acompañada por una delaminación controlada, entre las láminas metálicas y la matriz polimérica. Esto causa poco daño en las fibras que permanecen mayoritariamente intactas detrás del extremo de la fisura. Este mecanismo es clave para reducir el factor de intensidad de tensiones en el extremo de la fisura, disminuyendo su velocidad de propagación.

2. PARTE EXPERIMENTAL

Los prototipos se fabricaron a partir de aleaciones de aluminio 1050 y 6061 y fibra de carbono NCT-301 unidireccional, pre-impregnada en una resina epoxy. Las placas de AL 1050 y 6061 se laminaron en frío hasta un espesor de 0,45 mm y se sometieron a un tratamiento térmico de recocido T0 para recuperar la estructura de recristalización. Se decaparon en una solución de hidróxido de sodio al 10% para mejorar el pegado entre la resina de la fibra y la aleación de aluminio en el colaminado. Para las dos aleaciones de Al se fabricaron compuestos híbridos de 120 X 120 mm de dos tipos, según las secuencias de apilamiento: Tipo 4/3: (Al-0-Al-90-Al-0-Al) y tipo 5/4 : (Al-0-Al-90-Al-90-Al-0-Al), donde 0 y 90 indican la orientación de la fibra de carbono con la dirección de laminación de la aleación de aluminio**.** El conformado de los laminados se efectuó en una matriz de aluminio previamente forrada con film desmoldante sobre la que se armó el saco de vacío. El conjunto se sometió a un proceso de curado en autoclave a una presión de 6 bares y a una temperatura de 178 ºC. Los compuestos tipo 5/4 resultaron de 3,6 mm de espesor y los del tipo 4/3 de 3 mm de espesor. Se mecanizaron probetas de tracción de 120 X 20 mm. Los ensayos de tracción se hicieron en una máquina Shimatzu instrumentada con extensómetros. Se determinó el módulo de elasticidad (E) y la tensión de fluencia utilizando el criterio ($\sigma_{0.2}$). Para evaluar la propagación de fisuras, se fabricaron probetas fractomecánicas compactas CT [5], mediante mecanizado por control numérico. Los ensayos de propagación de fisura por fatiga se realizaron en una máquina de tracción servohidráulica MTS.

3. RESULTADOS

Ensayos de tracción

Los ensayos se realizaron en los compuestos base Al 1050. En la Tabla I se muestran los valores del módulo de elasticidad y el valor de la tensión de fluencia en la dirección de laminación del aluminio.

Al	Tipo	E (GPa)	$\sigma_{0.2}$ (MPa)
1050	5/4	71	150
	4/3	80	175

Tabla I. Resultados de los ensayos de tracción.

Ensayo de propagación de fisura

Los parámetros de fisuración por fatiga para cada compuesto ensayado se muestran en la Tabla II. En la tabla III se detalla la velocidad de propagación en la etapa de iniciación de la fisura en probetas CT.

Al	Tipo	ΔK_{th} (MPa $m^{1/2}$)	Ciclos (N)	a (mm)
1050	5/4	5,5	4,4 10^4	2
	4/3	6,8	4,5 10^4	2
6061	5/4	7	1 10^6	1,8

Tabla II. Condiciones de fisuración.
Para R = 0.1

Aluminio	Tipo	ΔK (MPa $m^{1/2}$)	$\Delta a / \Delta N$ (m/ciclos)
1050	5/4	5,5	1,4 10^{-8}
	4/3	6,8	6,3 10^{-8}
6061	5/4	7	2 10^{-9}

Tabla III. Velocidades de Propagación de Fisuras.

Luego de la propagación de la fisura por fatiga se aplicó una carga estática que provocó la apertura de la fisura, la cual se encuentra controlada por la deformación de la resina debido a las tensiones de corte locales entre la fibra y las lámina metálica [3]. En la figura 1 se observa la apertura de la fisura (modo I) en la probeta CT y la zona de deformación plástica en el extremo de la fisura en la lámina de aluminio 1050. Mientras que en la figura 2 se aprecia la apertura de la fisura en el espesor de la probeta CT tipo 5/4 base AL 1050 con apilamiento de la fibra 0-90-90-0.

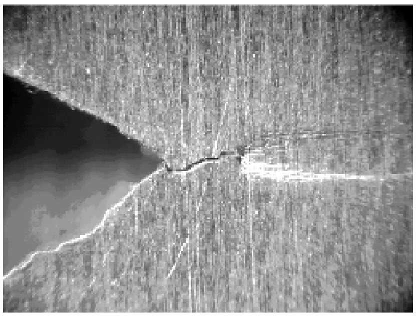

Figura 1. Se observa la entalla, la fisura y la zona deformada en el Al 1050 5/4.

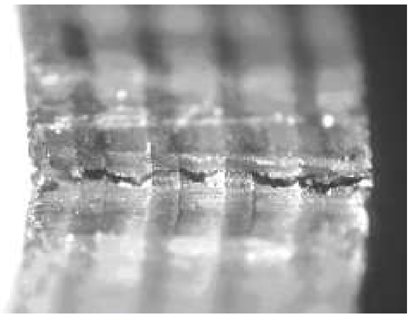

Figura 2. Fisura en el espesor de la probeta CT Al 1050 5/4.

5. DISCUSIÓN

El análisis de la superficie de fractura de la probeta CT tipo 5/4 base Al 1050, figura 2, muestra un menor avance de la fisura en el centro de la sección. Esto marca la diferencia con un material continuo, donde se hubiese esperado un mayor avance de fisura, dado que es allí donde se produce un estado triple de tensiones que favorece el avance de la fisura. El avance de la fisura en la lámina central de aleación aluminio, donde la dirección de las fibras de carbono vecinas es normal al plano de la fisura, es menor que en el resto de las láminas de aluminio próximas a la superficie. Esta forma diferencial del avance de la fisura muestra que en este compuesto híbrido operó el mecanismo de “Puenteo de Fibra” **(**Fiber-Bridging) característico en este tipo de laminados. En la figura 4, en esta misma probeta, se aprecia la morfología de la superficie de fractura como consecuencia de los distintos mecanismos de rotura operantes en las láminas de aleación de aluminio.

Figura 3. Superficie de fisura por fatiga. Probeta CT tipo 5/4 base Al 1050

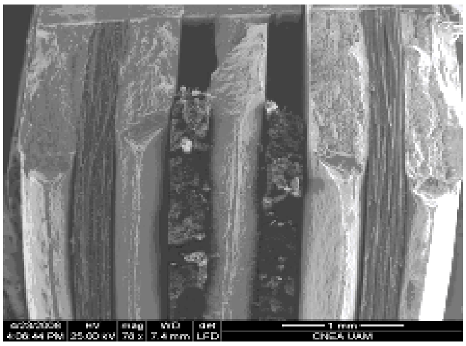

Figura 4. Micrografía SEM de la fisura por fatiga. Probeta CT 5/4 Al 1050.

En la parte superior de la figura 4 las láminas de aluminio presentan una típica superficie de fractura generada por la propagación de la fisura por fatiga. Mientras que en la parte inferior se puede ver la rotura por deformación plástica producida cuando se aplicó una carga estática que provocó la apertura de la fisura. Además se observa claramente la dirección de la fibra de carbono unidireccional. Con respecto a la velocidad de propagación durante la etapa de iniciación de la fisura, en probetas CT, se midieron velocidades de propagación $\Delta a/\Delta N$ de 6,3 10^{-8} en probeta CT tipo 5/4 base Al

1050 y 2 10^{-9} en probeta CT tipo 5/4 base Al 6061. Este último valor está de acuerdo con los valores publicados para un laminado híbrido CARALL base 7075 [6]. Es de notar que estos valores son dos órdenes de magnitud inferior al correspondiente a una lamina de aleación del aluminio de espesor similar, cuyo valor de velocidad de propagación durante la etapa de iniciación de la fisura es de 5 10^{-7} [4]. El retardo en la propagación de la fisura por fatiga, producto del mecanismo de “Puenteo de Fibra” **(**Fiber-Bridging) hizo que fueran necesarios $1x10^{6}$ ciclos para lograr una fisura de 1,8 mm de largo en la probeta CT tipo 5/4 base Al 6061, nuevamente comparables a los mostrados en [6].

6. CONCLUSIÓN

La facilidad experimental de pegado en vacío y curado en autoclave disponibles resultó adecuada para la fabricación de prototipos a escala de laboratorio de materiales compuestos híbridos, laminados fibra-metal con aleaciones de aluminio. Se realizó la caracterización de los compuestos híbridos así obtenidos mediante ensayos de tracción y de propagación de fisuras. Los valores de velocidad de propagación medidos durante la etapa de iniciación de la fisura en probeta CT tipo 5/4 base Al 1050 y tipo 5/4 base Al 6061 son consistentes con los antecedentes que se observan en la bibliografía. En esta muestra se pudo observar que operó el mecanismo el mecanismo Puenteo de Fibra **(**Fiber-Bridging) el cual es típico en este tipo de laminados híbridos.

Si bien no se ha completado la sistemática de ensayos para poder caracterizar completamente el material, los valores obtenidos a partir de los ensayos presentados en este trabajo muestran una buena correlación con los datos existentes en la bibliografía.

REFERENCIAS

[1]. L. B. Vogelesang. "Development of a New Hybrid Material (ARALL) for Aircraft Structure". Delft University of Technology. Ind. Eng. Chem. Dev. 1983, 22, 492-496.
[2] Palkowski H, Lange G. “Creation of tailored high-strength hybrid sandwich structures”, Advanced Materials Research. 2007, 22, 27-36.
[3] Lin C, Kao P. “Effect of fiber bridging on the fatigue crack propagation in carbon fiber-reinforced aluminum laminates”. Mat. Science & Engineering A. 1995; 190:65-72.
[4] W. Brown. “Aerospace Structural Metals Handbook”. Mechanical Properties Nonferrous Alloys. AIWT – 3206. Vol. 2. 1972, pp 1, 22.
[5] Standard Test Method for Measurement of Fracture Toughness. E 1820 – 01. Annual Book of ASTM Standars, Vol. 3.01. American Society for Testing and Materials.
[6] C. T. Lin, P.W. Kao and F.S. Yang. “Fatigue behaviour of carbon fibre-reinforced aluminium laminates”. Composites. Vol. 22. Numer 2. March 1991.

Desarrollo de compuestos de polietileno de alta densidad reforzados con fibras cortas de sisal y cáñamo

V. Amigó, O. Sahuquillo, P. Diaz, C.M. Antolinos
Instituto de Tecnología de Materiales-ITM, Universidad Politécnica de Valencia
R. Llorens, F. Marti
Instituto Tecnológico del Plástico-AIMPLAS, Valencia

RESUMEN

En la actualidad existe una preocupación cada vez mayor con los aspectos que afectan al medioambiente, de ahí que parte de la investigación se dirija hacia el desarrollo de materiales biodegradables y compuestos sostenibles. Dentro de estos compuestos, se está trabajando en la mejora en resistencia de termoplásticos con la incorporación de fibras naturales con el objetivo de ir sustituyendo los refuerzos habituales y permitir la reutilización de residuos de forma que se amplíe la vida útil de estos. El desarrollo de estos materiales supone el reaprovechamiento de residuos agroindustriales con complicada salida comercial y la obtención, de compuestos que permitan mejorar las propiedades de polímeros reciclados. La investigación se lleva a cabo utilizando polietileno reciclado de alta densidad reforzado con fibras de cáñamo y sisal, que provienen de residuos de obtención de cuerdas, reaprovechándolos con un coste relativamente bajo. Las fibras se caracterizan morfológicamente, mediante microscopía óptica y electrónica, y mecánicamente mediante ensayos de tracción. Los compuestos se inyectaron en forma de probetas de tracción y sobre ellas se han realizado ensayos de tracción, flexión e impacto, observando mediante microscopía electrónica las fracturas obtenidas. De acuerdo a lo esperado, la resistencia se incrementa con el contenido de fibra de refuerzo en el compuesto, junto con una reducción en la tenacidad. Los diferentes refuerzos empleados en los compuestos presentan características similares.

1. INTRODUCCIÓN

El desarrollo sostenible es uno de los retos más difíciles a los que se enfrentan las sociedades modernas. En este contexto, la reutilización de los termoplásticos es especialmente urgente debido a sus altos niveles de producción, junto a su larga vida media (Wu, 2007; Singleton, 2003). Curiosamente, este tipo de residuos constituye un potencial de bajo costo de recursos de materias primas para producir componentes estructurales. La pérdida de las propiedades originales en los procesos de reciclaje ha motivado la tendencia a reforzar la matriz termoplástica, mediante fibras sintéticas convencionales, aunque cada vez más se tiende a sustituirlas por fibras vegetales, que cuentan con las ventajas de ser abundantes, resistentes, ligeras, no abrasivas ni peligrosas (Kenny, 2004 a y b). En particular, las fibras cortas son residuos de producción, disponible en grandes cantidades y de bajo costo que son especialmente conveniente para este propósito. Aunque el uso eficiente de fibras vegetales presenta algunas desventajas. Longitud y composición, como corresponde a un recurso natural, están fuertemente condicionadas a su origen. Además, las fibras son difíciles de orientar pues presentan una elevada tendencia a la aglomeración y son muy hidrófilas, por lo que pueden presentar una falta de homogeneidad en su comportamiento mecánico.

Debido a la posibilidad de degradación del componente lignocelulósico (Georgopoulos, 2005), las matrices termoplásticas de polietileno (PE), polipropileno (PP) y poliestireno

(PS) deben procesarse por debajo de 200 ºC (Facca, 2006). Polietileno de alta densidad (HDPE) es el principal componente de plástico reciclado, lo que justifica el creciente interés en la búsqueda de nuevas aplicaciones para este material. En este contexto, el presente trabajo analiza la posibilidad de producción de materiales compuestos y su caracterización térmica y mecánica, sobre la base de materiales reciclados. Se aplican tecnologías de inyección para la producción de materiales compuestos a partir de un polietileno de alta densidad reciclado (rHDPE) reforzado con 30 y 40% en peso de fibras de sisal y cáñamo (Madsen, 2007), procedentes de residuos agroindustriales, por resultando muy económicas pero muy heterogéneas. Se determinarán las propiedades térmicas y mecánicas de los materiales compuestos con especial atención a la influencia de la naturaleza y cantidad de fibras, observándose mediante microscopía electrónica de barrido las secciones transversales de las fracturas producidas por las pruebas mecánicas con el fin de determinar la relación entre las propiedades macroscópicas y las características interfaciales entre la matriz plástica y el refuerzo vegetal (Torres, 2005).

2. MATERIALES Y METODOS

La matriz se compone de plástico reciclado de polietileno de alta densidad (rHDPE) suministrado por Eslava Plásticos (España), mientras que las fibras vegetales son residuos agroindustriales (sisal, de Hilaturas de la Balanza, España; cáñamo de Profillim, Bélgica) con longitudes medias de 200 fibras de 21,16 mm para el sisal y 11,47 mm para el cáñamo. Para mejorar la compatibilidad entre la matriz polimérica y las fibras, se ha utilizado polietileno injertado con anhídrido maleico (Bondyram 5001, Polyram Ram-On Industries, Israel) con una proporción estimada en las mezclas de aproximadamente un 2% en peso. La obtención de los compounds se ha realizado con una extrusora de doble husillo co-rotativa de la marca Leistritz Modelo: 27MAXX 44D. La dosificación de los porcentajes de fibra, 30 y 40% en peso, se realiza utilizando dosificadores gravimétricos, buscando un equilibrio entre el tiempo de residencia y la dispersión de la fibra, para degradar lo menos posible la fibra y obtener las mejores propiedades. Los compounds se han inyectado en una Inyectora ARBURG 420C, modelo ALLROUNDER 1000/350 obteniendo diferentes probetas normalizadas para su ensayo. La morfología de las fibras se ha analizado por microscopía óptica, MO, mediante un microscopio Microphot FX de Nikon Inc., y microscopía electrónica de barrido, MEB, con un equipo JSM 6300 de JEOL Ltd. En la figura 1 se recoge las imágenes de electrones secundarios obtenidas de las fibras analizadas. La degradación de las fibras se ha estudiado mediante un equipo de termogravimetría TGA Q50 de TA Instruments, utilizando Nitrógeno como gas de purga.

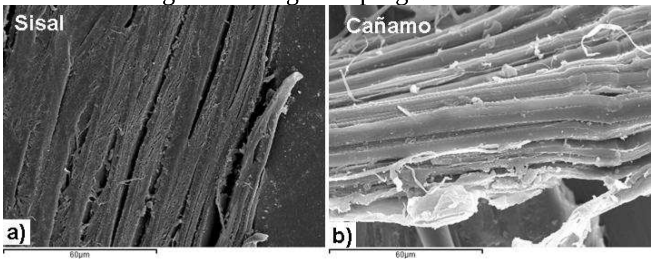

Fig. 1. Aspecto de las fibras naturales investigadas, mediante microscopía electrónica de barrido: a) Sisal y b) Cáñamo.

Los compuestos se han caracterizado obteniendo sus propiedades mecánicas a tracción y flexión mediante una máquina Universal de ensayos INSTRON 4202. Los ensayos de impacto Charpy se han realizado en un péndulo instrumentalizado CEAST mediante martillo de 15 J, en probetas sin entalla con distancia entre apoyos de 64 mm. Las fracturas obtenidas en todos los casos se observan mediante microscopía óptica (Microphot FX) y electrónica de barrido (JEOL JSM6300).

RESULTADOS Y DISCUSIÓN

Las propiedades mecánicas de las fibras resultan bastante diversas y dependen mucho de las condiciones en las que se encuentran, principalmente de su grado de humedad. La Tabla 1 recoge algunos parámetros mecánicos obtenidos en las diferentes fibras.

Tabla 1. Características de fibras empleadas en la modificación de termoplásticos.

Fibra	Densidad (g/cm^3)	Módulo elástico (GPa)	Resistencia tracción (MPa)	Alargamiento a rotura (%)
Cáñamo	1,48		285	1,3
Sisal	1,45	10,40	444-552	2,0-2,5

Durante la extrusión para la obtención de los compounds y en la inyección posterior, las fibras se fraccionan y pierden parte de las posibilidades de refuerzo de acuerdo a su longitud inicial. Sin embargo, uno de los factores de mayor influencia en las propiedades finales del compuesto es la propia degradación térmica de las fibras. Esta degradación, obtenida mediante TGA, presenta unas temperaturas críticas de 320-350ºC en el cáñamo y de 275ºC en el sisal. No obstante, en los ensayos realizados en los diferentes estados del proceso de obtención de los compuestos no se aprecia variaciones significativas, a excepción de una ligera disminución del contenido en humedad por el calentamiento sucesivo en los diferentes procesos para la obtención de las probetas.
Los valores obtenidos con el ensayo de tracción ponen de manifiesto, que la incorporación de las fibras incrementa la resistencia máxima obtenida, Tabla 2, tanto en el cáñamo como en el sisal.

Tabla 2. Propiedades de los compuestos obtenidos a tracción y flexión, junto a los datos del rHDPE para su comparación.

		Tracción			Flexión	
	% Fibra	**Resistencia máxima (MPa)**	**Módulo Elástico (MPa)**	**Alargamiento a rotura (%)**	**Resistencia máxima (MPa)**	**Módulo efectivo (MPa)**
rHDPE	0	26.0 (0.2)*	1218 (91)	192 (51)	25.6 (0.2)*	720 (12)
rHDPE + Sisal	30	34.1 (0.4)	2643 (97)	6 (1)	51.4 (0.5)	2141 (23)
	40	41.5 (0.8)	3678 (144)	4 (0)	65.4 (1.2)	3257 (112)
rHDPE + Cáñamo	30	31.1 (3.1)	2808 (352)	6 (1)	42.8 (0.5)	1689 (34)
	40	33.6 (0.9)	3156 (203)	5 (0)	51.8 (0.4)	2384 (23)

* Entre paréntesis se indican las desviaciones estándar.

Sin embargo, la rigidez de los compuestos obtenidos no parece depender de la naturaleza de las fibras presentando, no obstante, una relación prácticamente lineal con el contenido en fibras e incrementándose sustancialmente en relación a la rigidez del polímero matriz. Al contrario, el alargamiento proporcional de rotura presenta una disminución importante con la incorporación de las fibras de manera que en las mejores condiciones nos encontramos con un 6% frente al 192% del rHDPE. Semejante comportamiento se aprecia en los ensayos de flexión.

Esta semejanza en los resultados a flexión y tracción, coinciden con la tenacidad resultante de los ensayos a impacto en probetas Charpy sin entalla realizados. El polietileno reciclado, utilizado como matriz, no ha presentado fractura, en estas condiciones de ensayo, obteniéndose, no obstante, valores de resiliencia de 145 kJ/m^2, mientras que la introducción de las fibras como refuerzo disminuye sensiblemente la resiliencia, de manera semejante a lo sucedido con el alargamiento proporcional a rotura, hasta valores semejantes para el cáñamo y sisal, alrededor de los 21 kJ/m^2. Las fractografías obtenidas tras los distintos ensayos muestran la falta de plasticidad indicada y confirman el aumento de rigidez en los compuestos por el efecto de extracción de las fibras de la matriz durante el proceso de fractura, así como una mayor rigidez obtenida por el ovillamiento de las propias fibras que depende en gran medida de la cantidad final incorporada al polímero.

3. CONCLUSIONES

- El aprovechamiento de fibras vegetales de desecho es perfectamente viable con la peculiaridad de su disparidad en forma y tamaño que obliga a la peletización previa de las mismas para la obtención de los compounds. Señalar también la necesidad de incluir compatibilizantes en un 2% en peso.
- La degradación de las fibras de sisal y cáñamo, durante los diferentes procesos utilizados en la elaboración de los compuestos, ha sido prácticamente despreciable y tan sólo cabe resaltar la pérdida de agua con los diferentes procesos, por lo que su procesabilidad es perfectamente viable industrialmente.
- La incorporación de fibras aumenta ligeramente las propiedades resistentes del polímero base, HDPE reciclado, pero disminuyen sus propiedades plásticas y tenacidad, aunque todavía mantienen unas resistencias a impacto sobre los 21 kJ/m^2.

AGRADECIMIENTOS

Los autores desean agradecer al Ministerio de Medio Ambiente por su soporte a través del proyecto A581/2007/2-02.2 enmarcado en el Programa Nacional de Ciencias y Tecnologías Medioambientales del Plan Nacional de I+D+i, así como al Programa CYTED por su apoyo en movilidad a través de la Acción de Coordinación de Proyectos de Investigación 307AC0307.

REFERENCIAS

FACCA A. G., KORTSCHOT M. T., YAN N. (2006), *Composites: Part A* 37(10) 1660–1671.
GEORGOPOULOS S. TH., TARANTILI P. A., AVGERINOS E., ANDREOPOULOS A. G., KOUKIOS E. G. (2005), *Polymer Degradation and Stability*, 90, 303-312.
KENNY J.M., PUGLIA D., BIAGIOTTI J. (2004), *Journal of Natural Fibers*, 1(2) 37-68.
KENNY J.M., PUGLIA D., BIAGIOTTI J. (2004), *Journal of Natural Fibers*, 1(3) 23-65.
MADSEN B., HOFFMEYER P., THOMSEN A. B., LILHOLT H. (2007), *Composites: Part A*, 38, 2194–2203.
SINGLETON, A. C. N., BAILLIE, C. A., BEAUMONT, P. W. R., PEIJS, T. (2003), *Composites Part B: Engineering*, 34 (6) 519-526.
TORRES FG, CUBILLAS ML. (2005), *Polymer Testing*, 24, 694–698.
WU Q., LEI Y., YAO F., XU Y. (2007), *Composites Part A* 38, 1664-1674.

Caracterización de *green composites* basados en matrices de polihidroxibutirato y fibra de pita como refuerzo

R. Balart, D. García-Sanoguera, L. Sánchez-Nacher, O. Fenollar
Departamento de Ingeniería Mecánica y de Materiales,
Escuela Politécnica Superior de Alcoy, Universidad Politécnica de Valencia, España

RESUMEN

La utilización de materiales compuestos tradicionales basados en matrices de resinas tipo epoxi, poliéster insaturado, fenólicas,.. con refuerzos de fibras de vidrio, aramida o carbono, está siendo cada vez más cuestionada en sus aplicaciones por los problemas medioambientales y de reciclabilidad que presentan. Este efecto ha motivado el creciente estudio de una nueva generación de materiales compuestos denominados *"green composites"* al no ser agresivos desde el punto de vista medioambiental por sus características de biodegradabilidad. La finalidad del presente trabajo es comparar las características mecánicas de biopolímeros reforzados con fibras naturales para la obtención de *green composites* que sustituyan de forma óptima materiales compuestos tradicionales. Para ello, el objetivo principal es estudiar el comportamiento mecánico, físico, térmico y morfológico de este tipo de biocompuestos. Los materiales utilizados como refuerzo son fibras de pita (Agave Americana) con poli-3hidroxibutirato (PHB) como matriz termoplástica.

1. INTRODUCCIÓN

Actualmente el desarrollo y utilización de materiales respetuosos con el medio ambiente está adquiriendo gran relevancia. Uno de los sectores de materiales técnicos más desfavorecido por estas políticas medioambientales es el de materiales compuestos de matriz polimérica. De forma tradicional, los materiales compuestos de matriz polimérica más extendidos en la industria han sido los formados con fibras de vidrio, aramida o carbono junto con matrices de resinas de poliéster insaturado, epoxi, poliuretanos o fenólicas que cada vez están siendo más cuestionadas por los problemas de reciclabilidad que presentan una vez que han terminado su vida como materiales al servicio de la técnica. Estos hechos han motivado que en la actualidad se estén investigando nuevos sistemas de materiales compuestos medioambientalmente correctos, denominados *"biocomposites"* o *"green composites"*. Para su obtención se utilizan fibras de procedencia natural como refuerzo, entre las que cabe destacar fibra de lino, palma, yute, sisal u otros derivados lignocelulósicos que presentan interesantes propiedades mecánicas, junto con una matriz termoplástica de naturaleza biodegradable, generalmente derivadas de los polialcanoatos, como el ácido poliláctico (PLA), policaprolactona, polihidroxibutirato (PHB), polidroxibutirato-valerato (PHBV), (Bodros 2007, Coats 2008, Petersen 2001, Shibata 2002, Zini et al 2004)

A este respecto, hay que tener en cuenta que en los últimos años se ha producido un gran avance en el desarrollo de polímeros biodegradables para aplicaciones en diversos campos de la tecnología. En este sentido, el desarrollo de poliésteres biodegradables (policaprolactona, copoliésteres alifático, copoliésteres aromáticos, poliésteramidas,

…), polialcanoatos, almidones, … representan una importante línea de investigación y de trabajo de gran interés y con muchas posibilidades de transferencia a aplicaciones industriales. Algunos sectores como el envase y embalaje son pioneros en el desarrollo de polímeros biodegradables debido a la fuerte presión social relacionada con el deterioro del medio ambiente y el desarrollo sostenible.

El presente trabajo se desarrolla dentro de este ámbito, centrado en el estudio de “*green composites*” formulados para el sistema formado por el polímero polihidróxidobutirato (PHB) como matriz junto con una fibra de procedencia natural: pita *(agave americana)* que en conjunto presentan interesantes características de biodegradabilidad para el estudio de materiales con aplicaciones estructurales sustitutivos de los materiales compuestos tradicionales difíciles de reciclar y por lo tanto agresivos con el medioambiente.

El polihidroxibutirato es un poliéster termoplástico producido mediante biosíntesis en una fermentación bacteriológica. Su estructura química se caracteriza por ser un homopoliester termoplástico totalmente lineal e isotáctico formulado a partir del ácido 3-hidroxibutirato, y cuya fórmula se observa en la figura 1. El PHB se caracteriza por ser un poliéster altamente cristalino con una temperatura de fusión alrededor de 180ºC, es muy frágil y presenta un grado de biodegradación muy lento.

$$\text{-[O-CH(CH}_3\text{)-CH}_2\text{-CO]-}$$

Fig. 1. Estructura química del polihidroxibutirato PHB.

2. EXPERIMENTAL

El biopolímero empleado es PHB P226 fabricado por la empresa Biomer (Krailing, Alemania), poliéster termoplástico suministrado en forma de granza para poder ser procesado de forma tradicional como cualquier polímero termoplástico. La fibra utilizada como refuerzo es fibra de pita natural, seca y de 5 mm de longitud que formará parte del *“green composite”* en forma de mat o con disposición espacial isotrópica.

La elaboración del composite se realiza a partir de film de PHB obtenido mediante prensa de platos calientes procedente de granza de PHB procesada a 160ºC y 4 T de presión durante 5 min. Una vez obtenidos los films de PHB se superponen 5 capas alternativas de film y de mat, procesándolas en una prensa de platos calientes en condiciones de temperatura de 160ºC, 4 T y 5 min. Con la finalidad de analizar la influencia de la fibra de pita como refuerzo, se estudian diversos contenidos en peso de fibra: 10, 20, 30, 40 y 50%. Una vez obtenida la plancha de *“green composite”* con espesores finales que varían entre 1.6 y 1.8 mm, se troquelan para obtener las probetas normalizadas para su caracterización mecánica según la norma UNE-EN ISO 527-1 y 4. Esta caracterización se realiza siguiendo la norma citada en una máquina universal de ensayos IBERTEST ELIB 30 (S.A.E. Ibertest, Madrid, España) a una velocidad de 5 mm min^{-1} a temperatura ambiente.

Para la caracterización térmica del material se utiliza una estación para la medida de la temperatura de reblandecimiento Vicat/HDT modelo Deflex 687-A2 (Metrotec S.A., San Sebastian, España), siguiendo la norma UNE EN 727, según el método B50, con los parámetros siguientes: carga 50 N y velocidad de calentamiento del fluido de 50ºC h^{-1}, según la norma de ensayo UNE-EN ISO 306. El análisis de las morfologías de fractura se realiza mediante microscopía electrónica de barrido (SEM) para el que se ha empleado un equipo FEI modelo PHENOM (FEI Company, Eindhoven, The Netherlands), con un rango de magnificación 525-24000 aumentos y un voltaje de aceleración de 5 kV.

3. RESULTADOS Y DISCUSIÓN

El proceso de caracterización térmica de los distintos green composites formulados, mediante el ensayo Vicat, pone de manifiesto como el contenido en fibra aumenta de forma considerable la resistencia compuesto a reblandecerse con la temperatura del nuevo material. El PHB como material matriz se caracteriza por presentar una temperatura de reblandecimiento Vicat de 97.8ºC que pasa a adquirir un valor de 138.4ºC con un 50% de contenido en fibra de pita, por lo que prácticamente aumenta un 41% la resistencia térmica que presentará el material compuesto. Respecto a la aplicación técnica de este nuevo material, es un factor muy importante a tener en cuenta puesto que indicará rangos de temperatura en servicio o condiciones óptimas en aplicaciones reales.

Respecto a los parámetros de resistencia, figura 2, hay que destacar un marcado descenso de características desde el material matriz PHB sin fibra hasta el compuesto con un contenido del 10% de fibra refuerzo, concretamente desde 17.2 a 12.7 MPa de tensión de rotura. A partir del 10% de cantidad de fibra de refuerzo, aumenta paulatinamente la resistencia del material compuesto hasta alcanzar un punto máximo para 40% de fibra de pita y alcanzando valores similares a los iniciales de polímero matriz, 17.3 MPa. El alargamiento a la rotura sufre una pérdida de alrededor del 97%, puesto que pasa de valores de 87.8% para el polímero matriz hasta 2.6% para un 10% de cantidad de fibra y que se mantiene prácticamente constante con el aumento de esta. Hay que tener en cuenta que el PHB como polímero termoplástico presenta muy bajo comportamiento dúctil debido a sus altos niveles de cristalinidad desde el punto de vista estructural. El efecto de enfragilización con la adición de la fibra es debido a la falta de interacción fibra-matriz, figura 3. La falta de adhesión entre fibra-matriz es la responsable de que no exista continuidad física entre las mismas, que hace que esta zona actúe como concentradora de tensiones y provoque la rotura del material incluso con tensiones inferiores a las de material sin refuerzo.

No obstante hay que señalar que en el sistema analizado las respuestas mecánicas óptimas se obtienen para contenidos en fibra del 40% con características mecánicas resistentes ligeramente superiores a las del biopolímero utilizado como matriz. Para contenidos mayores de fibra, las características resistentes disminuyen debido a la alta densidad de fibra de pita que acentúa la enfragilización del material por lo fenómenos anteriormente analizados de falta de adhesión fibra-matriz.

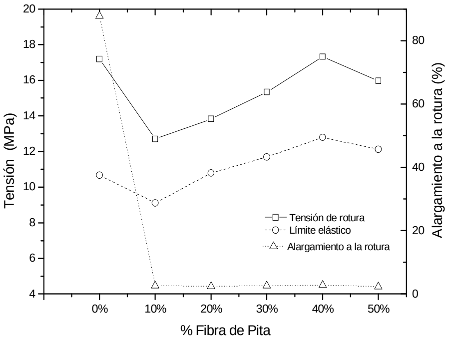

Fig. 2. Variación de las características mecánicas del sistema de material compuesto PHB/fibra de pita respecto al porcentaje de fibra.

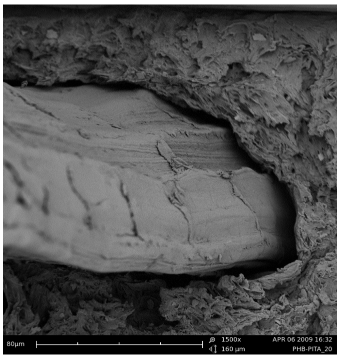

Fig. 3. Micrografías MEB de la morfología de la superficie de rotura por tracción de PHB/fibra de pita 20% (1500x)

4. CONCLUSIONES

En el sistema analizado de *green composite* formado por el polímero polihidróxidobutirato (PHB) como matriz junto con una fibra de procedencia natural: pita *(agave americana)* las respuestas mecánicas óptimas se obtienen para contenidos en fibra del 40% con características mecánicas resistentes ligeramente superiores a las del biopolímero utilizado como matriz. Para esta composición optimizada, la temperatura de reblandecimiento mejora de forma considerable hasta 127ºC ampliando las posibilidades de aplicación de estos materiales bajo solicitaciones más específicas. Además, esta composición es la que presenta mejor dureza superficial al combinar de forma correcta la cantidad de fibra de pita añadida a la matriz de PHB, que en conjunto presentan interesantes características de biodegradabilidad, para el estudio de materiales biodegradables con aplicaciones estructurales sustitutivos de los materiales compuestos tradicionales.

AGRADECIMIENTOS

Los autores agradecen al “Ministerio de Ciencia y Tecnología” Ref: DPI2007-66849-C02-02 por la financiación recibida para el desarrollo de este trabajo de investigación.

REFERENCIAS

BODROS, E., PILLIN, I., MONTRELAY, N. (2007) Comp. Sc. and Tech., 67, 462-470
COATS, E., LOGE, F., (2008) Bioreource Technology, 99, 2680-2686
PETERSEN, K., NIELSEN, P. V. Y OLSEN M. B. (2001), Starch/Stärke, 53, 356-361
SHIBATA, M., OZAWA, K. (2002) Jour. Appl. Polymer Science, 85, 129-138
ZINI, E., BIARDO, M. Y ARMELANO, M. (2004) Macromol. Bioscien., 4, 286-295

Análisis del reemplazamiento de la resina fenol-formaldehido por lignosulfonato en compuestos utilizados en materiales de fricción automovilística

J.V.W. Silveira, E. Bittencourt, Z.J. Águila
Departamento de Tecnología de Polímeros. Facultad de Ingeniería Química.
Universidad Estatal de Campinas, Brasil
N. Gabilondo
'Materials + Technologies', Departamento Ingeniería Química y del Medio Ambiente,
Escuela Politécnica. Universidad del País Vasco/Euskal Herriko Unibertsitatea

ABSTRACT

As the result of the search on renewable sources materials to increase its participation in industrial processes derivatives of lignin, a natural macromolecule found in wood, become a viable alternative for the application in friction elements. Break pads are composite materials which have been constantly improved, mainly by incorporating materials which replace undesirable materials like asbestos, and upgrade the performance of these elements while reducing environmental damage. The purpose of this work is to study the thermal behavior and performance of brake pads manufactured with the phenol-formaldehyde resin partial substitution with different contents of ammonium lignosulfonate, and reinforced with alternative fibers in substitution of asbestos. Our objective is to contribute to the development of alternative technologies of fabrication of different friction materials. Laboratory researches already indicate a potential of application in the automobilist industry, with desirable thermal performance. The lignosulfonate material, despite containing fewer amounts of reacting groups available to the crosslinking polymerization, still can effectively react and form a polymeric matrix with promising tribologic properties.

1. INTRODUCCIÓN

El empleo de materiales naturales en la fabricación de gran diversidad de productos comerciales viene atrayendo la atención de la industria de bienes y consumo. Uno de los polímero naturales mas abundante después de la celulosa es la lignina, que forma parte de todos los vegetales en una proporción considerable constituyendo aproximadamente de 20 a 30% de la madera y plantas vasculares (Khan et al. 2007). La lignina que se utiliza para fines comerciales es derivada de la fabricación del papel. Con la retirada de la celulosa el subproducto obtenido puede ser uno de los diversos compuestos de lignina, entre estos los lignosulfonatos (LS). Los lignosulfonatos tienen estructura reticulada con anillos fenólicos Esta estructura es muy similar a la encontrada en resinas de fenol-formaldehidos (PF), de ahí su compatibilidad y posible utilización como sustitución de los PF, considerando que los costos de adquisición de la misma son muy inferior a los del fenol. Hay una limitación en la utilización de resinas a base de lignina relacionada con las pocas propiedades de adhesión y variabilidad en su desempeño. (Park et al. 2008). Este trabajo consiste en un estudio para verificar la concentración óptima de lignosulfonato de amonio que podrá ser usado como sustituto de la resina fenol-formaldehido en la confección de pastillas de freno para automóviles reforzadas con fibras de aramida, cuyos resultados sean comparables a los obtenidos con los materiales comerciales disponibles.

2. PARTE EXPERIMENTAL

2.1 Preparación de la resina

Fue utilizado el lignosulfonato de amonio sin hierro, conocido comercialmente como VIXILTAN® y resina fenol formaldehído del tipo Novolaca, ambas en forma de polvo fino. Fueron pesadas muestras de 0,05g de mixtura, variándose las concentraciones de cada componente de 0 a 50% de LS. La masa total de cada una fue diluida en 10-15 mL de agua destilada en un erlenmeyer y posteriormente liofilizadas a -60°C por 24 horas. .Las resinas fueron caracterizadas por DSC (25-250°C con una rampa de 10°C/min) y TGA (25-900°C con rampa de 20°/min.).

2.2 Preparación del compuesto

La pastilla fue fabricada siguiendo el proceso de fabricación empleado actualmente en la industria. Comúnmente una formulación comercial posee mas de diez constituyentes, no obstante, para reducir el número de variables que interactúan significativamente en el comportamiento del material, se utilizó una formulación básica que tiene como referencia el trabajo desarrollado por Águila (1999).

Componentes	*% en masa*
Barita	65,0
Resina fenol-formaldehido	6,0 – 10,0
Lignosulfonato de amónio	0,0 – 4,0
Grafito	7,5
Aluminio	7,5
Fibra de aramida	10,0

Tabla 1. Formulación del compuesto.

Se preparo 1 kg de cada formulación variándose la concentración de lignina de 0 a 40% peso en sustitución del fenol-formaldehido. El modelo de pastilla usado como prototipo corresponde al modelo geométrico usado en la fabricación de pastillas para carros de la Volkswagen modelo Gol 1.0 año 01/01. Este compuesto fue caracterizado en un goniómetro a través del método de la gota sésil para verificar su carácter hidrófobo.

3. RESULTADOS Y DISCUSIÓN

En los compuestos puros fue posible verificar que la lignina es mucho mas estable térmicamente que la resina fenol-formaldehido la cual presenta una disminución acentuada cerca de los 400°C como muestran los ensayos termogravimétricos (Fig. 1). La estabilidad del lignosulfonato se debe a la presencia de nitrógeno en los grupos NH_4^+, que forman enlaces de hidrógeno con los átomos del retículo. A partir de los resultados de los análisis de TGA y DTA queda demostrado que las resinas liofilizadas tienen un comportamiento muy similar entre si. Las formulaciones con 20 y 30% de resina pueden ser utilizadas, efectivamente, en materiales de fricción, considerando que con la aplicación del freno la temperatura del sistema (pastilla-disco) puede llegar a alcanzar temperaturas próximas a los 800°C.

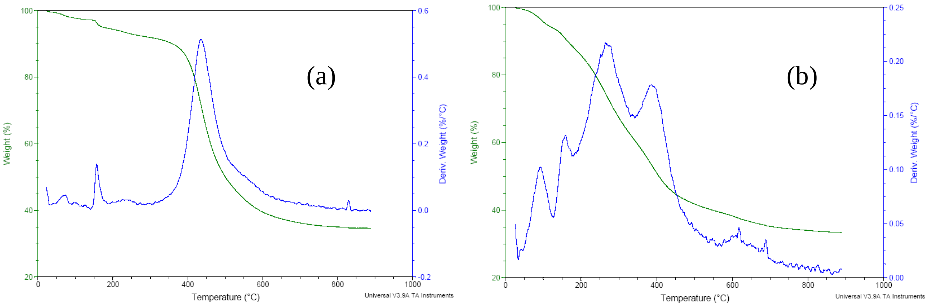

Fig. 1. Análisis de TGA y DTA para la resina fenol-formaldehido (a) y LS (b).

A partir de los resultados de DSC (calorimetria diferencial exploratoria) se observan tres procesos térmicos, el primero es un pico endotérmico entre 50 e 75°C referente a la volatilización de componentes libres, principalmente el fenol y el formaldehído residual. El segundo pico (Tabla 2) aparece entre 110 e 160°C, en este caso es exotérmico y corresponde a la reacción de formación del polímero reticulado. Este es un evento muy significativo a llevar en consideración pues ocurre la reacción de un grupo –C_2OH– y un carbono reactivo de un anillo aromático o entre dos grupos hidroximetil con formación de puentes de metileno entre las unidades estructurales. El último pico aparece entre 160 e 200°C y está asociado a eliminación de agua, principalmente, así como a la presencia de otros compuestos formados a partir de la reacción de reticulación, pues como se trata de una reacción de condensación, existe la liberación de moléculas menores como la de agua. Esto también, puede estar relacionado con la humedad del lignosulfonato inherente a los iones de su estructura. En la medida que la concentración de agua es mayor, mayor será la cantidad de energía necesaria para removerla. Este proceso influencia directamente en la etapa de pos cura de las pastillas.

Muestras	Concentración de lignina en la resina (%)	2º Pico – Exotérmico		3° Pico – Endotérmico	
		T (°C)	ΔH (J/g)	T (°C)	ΔH (J/g)
LS00	0	138,8	38,12	163,1	36,98
LS10	10	142,6	44,53	168,3	28,85
LS20	20	143,1	80,89	173,7	41,50
LS30	30	**143,2**	76,51	**174,0**	51,44
LS40	40	140,6	81,50	169,2	80,35
LS50	50	141,2	71,54	172,4	70,78

Tabla 2. Temperaturas de los picos y variación de la entalpía de las resinas.

Estos datos sirvieron como referencia para la preparación de una muestra de compuesto curado. Las muestras de 3g segregadas fueron sometidas a un tratamiento térmico en un horno estacionario a 65°C por 2h y posteriormente prensadas a una temperatura 145°C, aproximadamente, con el objetivo de completar o proceso de cura las pastillas son colocadas en una estufa a una temperatura de 175°C. El método de ángulo de contacto fue conducido utilizando agua destilada y etileno glicol. La energía libre superficial (γs) fue determinada a través de la ecuación de la ley de Young modificada (Ecuación 1). Cuanto menor es el valor de la energía, mayor es su hidrofobicidad.

$$\gamma_{lv}(1+\cos\theta) = 2\sqrt{\gamma_{sv}^{d} + \gamma_{lv}^{d}} + 2\sqrt{\gamma_{sv}^{p} + \gamma_{lv}^{p}} \qquad (1)$$

Para los compuestos curados se ha observado que con el aumento del contenido de lignina, se tornan más hidrófobos (Fig. 2). Ese resultado concuerda con los resultados esperados, porque cuanto más hidrófobo es el material, menos interacción tendrá con la humedad, evitando algunos problemas de corrosión en el disco de freno (Limpert 1999).

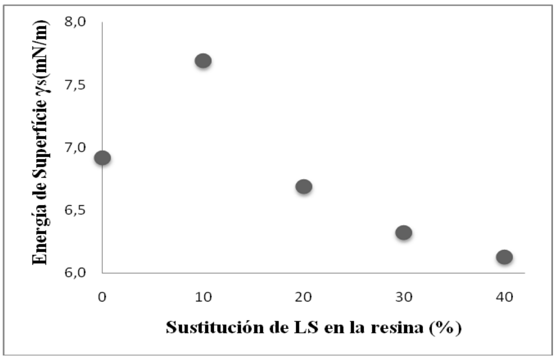

Fig. 2. Energía de superficie de los compuestos con diversas cantidades de LS.

4. CONCLUSIONES

La estabilidad térmica de las mezclas es menor que la resina pura, siendo que las resinas tienen comportamiento semejante. Las sustituciones de 20 y 30% se mostraron más estables en altas temperaturas. Se verificó la necesidad de más energía de pos-cura y también más hidrofobia de los compuestos con mayor cantidad de lignosulfonato. Estos resultados son preliminares para la confección de las pastillas de freno, que serán analizadas por ensayos de fricción (Método Krauss) y desgaste además de análisis de DMA y MEV para verificar su comportamiento mecánico y analizar su estructura morfológica y comprobar resultados.

AGRADECIMIENTOS

Se agradece al CNPq pela beca, al Grupo Inbra por su contribución y al Melbar Ind.

REFERENCIAS

ÁGUILA, Z. J. (1999) *Formulação de compósitos reforçados com fibras de PANOX e polpa de aramida utilizados em materiais de fricção***.** Dissertação, Campinas, Brasil.
KHAN, M. A., ASHRAF, S. M. (2007) Studies on thermal characterization of lignin. *Journal of Thermal Analysis and Calorimetry*,89, 993-1000.
LIMPERT, R. (1999) *Brake design and safety*. 2nd ed. Warrendale: SAE International.
NEHEZ, N. J. (1997) *Lignin-based friction material*. Montreal, Canada, WO 97/14747 PCT95/US95/13286.
PARK, Y.; DOHERTY, W. O. S.; HALLEY, P. J. (2008) Developing lignin-based resin coatings and composites. *Industrial Crops and Products*, 27, 163-167.
TEJADO, A., PEÑA, C., LABIDI, J., ECHEVERRIA, J. M., MONDRAGON, I. (2007) Physico-chemical characterization of lignins from different sources for use in phenol-formaldehyde resin synthesis. *Bioresource Technology*, 98, 1655-1663.

Dynamic-mechanical properties of syntactic foams based on epoxidized soybean oil-epoxy copolymers

F.I. Altuna, R.A. Ruseckaite, P.M. Stefani
Research Institute of Material Science and Technology (INTEMA). National Research Council. Engineering Faculty, Mar del Plata University. Argentina
L. Espósito, I. Mondragon
'Materials+Technologies' Group, Dept of Chemical and Environmental Engineering, Polytechnic School, Universidad País Vasco/Euskal Herriko Unibertsitatea, Pza. Europa 1, 20018 Donostia-San Sebastián, Spain

ABSTRACT

Bio-based syntactic foams were produced by partial substitution of diglycidyl ether of bisphenol A (DGEBA) with epoxidized soybean oil (ESO). Dynamic-mechanical properties of the matrices with different ESO content were evaluated. The glass transition temperature (Tg) values of the matrix were shifted to lower temperatures with increasing ESO content, indicating an increased chain mobility of the matrix due to the contribution of the more flexible long-chain aliphatic fatty acids present in ESO structure. Syntactic foams were prepared by the vacuum – assisted mixing method and the volume fraction of glass microbaloons was 0.55 for all formulations. The Tg values of the syntactic foams did not show significant differences with those of parent matrix. The values of the storage modulus of the foams in the glassy state were lower than those of the corresponding copolymers due to lower density of the foams. In the rubbery state, the moduli of the foams were about one order of magnitude higher than those of the matrices, mainly due to the presence of rigid glass microbaloons in the foams. Results reported herein suggest that large fractions of DGEBA can be replaced by ESO with minor effect on their properties.

1. INTRODUCTION

Syntactic foams are two-phase closed cell foams which are usually made by dispersing mechanically low density hollow particles (microballoons) in a polymeric matrix. The presence of strong but lightweight particles leads to syntactic foams with higher strength compared to single-phase closed cell foams (Shutov, 1991).

Epoxy systems had been widely used to make syntactic foams, owing to their low initial viscosity, easily controlled gelation times, small curing shrinkages, and good adhesion and wetability to the microballoons (Shutov, 1991). Despite that syntactic foams based on epoxy resins have good final properties, the increasing concern about the environmental protection have rise to the search of epoxidized substitutes derived from renewable resources. In this sense, functionalized vegetable oils (FVO) such as epoxidized soybean oil (ESO) are considered attractive candidates to replace at least a proportion of the traditional epoxy resins in thermosetting formulations (Wool and Sun, 2005). Commercially available ESO may be copolymerized with epoxy resin using amines or anhydrides as cross-linking agents (Miyagawa et al, 2004).

The present work focuses on the effect of substituting different amounts of epoxy resin by ESO on the dynamic mechanical properties of copolymers and syntactic foams based on these copolymers.

2. EXPERIMENTAL

Materials

Diglycidyl ether of bisphenol A (DGEBA, Araldite GY250) and methyltetrahydrophthalic anhydride (MTHPA) were supplied by Distraltec (Buenos Aires, Argentina). Epoxidized soybean oil (ESO) was provided by Unipox S.A. (Buenos Aires, Argentina). Both, DGEBA and ESO were dried under vacuum overnight before use. Some physical and chemical properties of the reactants used are listed in Table 1. 1-methylimidazole (1-MI,) was purchased from Huntsman (Buenos Aires, Argentina) and used as initiator without any further treatment. For the preparation of the syntactic foams, Scochlite glass microballoons (K15, density of 0.161 g/cm^3 and average diameter of 60 μm), supplied by 3M (Buenos Aires, Argentina), were used without any further treatment.

Material	Density, g/cm^3	Equivalent weight, g/eq	Iodine value, % Iodine
DGEBA	1.17	91	-
ESO	0.995	121	2.40
MTHPA	1.16	83	-

Table 1. Physical and chemical properties of the reactants.

Preparation of the foams and copolymers

ESO was used to replace 20 to 100 wt.% of DGEBA, and the obtained mixtures were then processed with a stoichiometric amount of MTHPA, and 1-MI (3wt% based on anhydride weight). Volume fraction of glass microballoons for all formulations was kept at 0.55. The mixing process was performed under reduced pressure (10 mm Hg) in order to restrict the volume of air bubbles entrapped in the bulk. Subsequently, the reactive systems were poured into anti-adherent steel molds which were placed into a convection oven (Yamato DKN400, Japan). Based on previous calorimetric studies (Altuna et al. 2009) a two-step curing cycle was used to ensure final conversion: 1h at 130ºC followed by 3h at 190ºC. Copolymer samples were prepared using the same procedure described for the syntactic foams, without the addition of microballoons.

Methods

Dynamic mechanical analysis was performed on a dynamic-mechanical analyzer (DMA) Perkin Elmer UNIX DMA 7 (Connecticut, USA) operating in a three-point-bending mode. Storage modulus (E’), loss modulus (E’’) and loss factor (tan δ) as a function of the temperature were obtained at a heating rate of 10 °C/min from -25 to 190 °C and a fixed frequency of 1 Hz. Samples of 1.5 x 4.5 x 60 mm^3 were used for the tests. Density of the copolymers and foams were determined by measuring the weight and volume of at least five specimens for each formulation. The glass transition temperature (Tg) was determined from the maximum in the loss factor curve. The crosslinking density (ν) and mass between cross-linking points (Mc) was calculated according to the rubber elasticity theory using the storage modulus values at T_g +50ºC (Miyagawa et al. 2004).

3. RESULTS AND DISCUSSION

The density values of DGEBA-ESO matrices decreased with increasing ESO content (Table 2). Similar tendency was reported for copolymers based on epoxidized linseed oil and epoxy resins using anhydrides as cross-linking agents (Miyagawa et al. 2005), and it was mainly attributed to the lower density of the vegetal oil compared with that of the epoxy resin (Table 2). Correspondingly, the foam density slightly decreased with the content of ESO. Since the volume fraction of microballoons was constant for all samples (about 0.55), variations in foam density were mainly ascribed to differences in the matrix density.

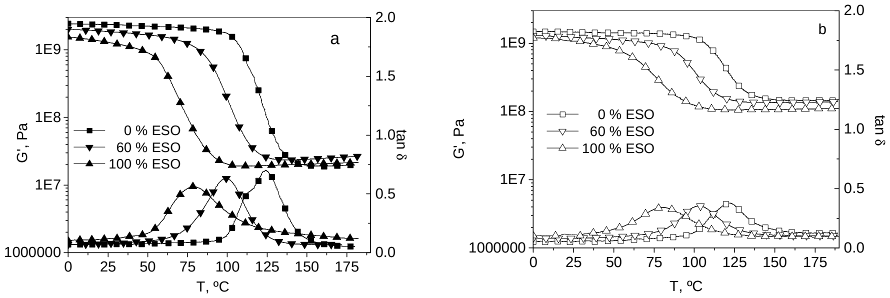

Fig. 1. Storage modulus E' and loss factor tan δ as a function of temperature for copolymers (a) and foams (b) with 0, 60 and 100 wt%ESO.

DMA information was used to evaluate the dynamic-mechanical properties of the DGEBA-ESO matrices as well as to estimate some network parameters. The dynamic mechanical relaxation behavior of the copolymers and foams samples (0, 60 and 100%ESO) was represented by the temperature dependence of storage modulus (E’) and loss factor (tanδ) (Fig. 1a). For a given ESO concentration, the storage modulus in the glassy region remained almost constant and started to decrease near room temperature, showing a drop followed by a plateau as the temperature increased. The appearance of such plateau at high temperature evidences the presence of stable cross-linking points. The values of E´ at 30 °C decreased with ESO content from 2.43 ± 0.13 MPa to 1.34 ± 0.16 MPa for 0% and 100% ESO, respectively. The incorporation of increasing amounts of ESO enhanced the chain mobility of the matrix, and consequently its flexibility, leading to a reduction in T_g and E´ (Table 2). The cross-linking densities did not show significant differences with increasing ESO percentage. It is interesting to point out that neat DGEBA and neat ESO systems displayed similar E´ at T_g + 50 °C, suggesting that values of mass between cross-linking points are similar (Table 2). All the tan δ peaks for

ESO %	Matrix						Foams	
	ρ g/cm^3	Tg ºC	E’ (30ºC) GPa	E’ (Tg+50ºC) MPa	ν mol/cm^3	M$_c$ g/mol	ρ g/cm^3	E’ (30ºC) GPa
0	1.212	124	2.43	19.4	$1.8\ 10^3$	664	0.597	1.46
20	1.197	113	2.41	22.6	$2.2\ 10^3$	551	0.590	1.40
40	1.165	109	2.26	22.2	$2.2\ 10^3$	538	0.586	1.36
60	1.150	99	1.82	24.3	$2.4\ 10^3$	475	0.580	1.33
80	1.127	88	1.48	20.7	$2.1\ 10^3$	530	0.577	1.18
100	1.110	79	1.23	19.1	$2.0\ 10^3$	554	0.573	1.05

Table 2. Matrix and foams properties.

the DGEBA-ESO/MTHPA resin has broadened and decreased in height compared to the tan δ peak for the pure DGEBA/MTHPA. A broadening of the tan δ peak will indicate that the temperature span needed for the transition has increased. It has been noted before that the tan δ peak broadens and shifts to lower temperatures indicating an increment in the segmental motions of the polymer matrix. ESO can introduce irregularities at molecular level within the DGEBA network (Miyagawa et al. 2004). This could be accounted for the inherent characteristics of the aliphatic fatty acids (saturated, unsaturated, functionalized, etc), their length and distribution (Wool and Sun, 2005).

No significant differences between T_g values of the syntactic foams and those of the parent matrices were observed (Fig. 1b; Table 2), evidencing that the presence of microballoons did not restrict molecular motions of the matrix. The values of E' of the foams in the glassy state were lower than those of the corresponding copolymers due to lower density of the foams (Table 2). Glassy state modulus exhibited a monotonic decrease with the ESO content, showing an agreement with the tendency found for the copolymers. However, the foams with 60 wt.% of ESO still showed a high value, being its modulus only 7% lower than that of the DGEBA-based foam. On the other hand, the values of storage modulus in rubbery state were one order of magnitude higher than those obtained for the neat matrix, whatever the ESO content. This was ascribed to the contribution of the rigid microballoons to the storage modulus which preserve their stiffness even at high temperatures.

4. CONCLUSIONS

DMA performed to bio-based syntactic foams showed that for ESO contents up to 60 wt.% neither the storage modulus nor the glass transition temperature are substantially reduced, being their values comparable to those found for foams based on neat DGEBA/MTHPA. These results suggest that an important amount of the synthetic resin can be substituted by a material derived from a renewable resource.

ACKNOWLEDGEMENTS

Authors are grateful to National Research Council, Argentina (CONICET), contract grant number PIP 112-200801-0183 and ANPCYT contract grant number PICT-2006-01560, and National University of Mar del Plata for their financial support.

REFERENCES

- Altuna, F.I., Espósito L., Ruseckaite R.A., Stefani, P.M. (2009) Syntactic Foams from Copolymers based on Epoxidized Soybean Oil. *Comp. Part A, submitted*.
- Miyagawa H, Mohanty AK, Misra M, Drzal LT. Thermo-Physical and Impact Properties of Epoxy Containing Epoxidized Linseed Oil, 1. Anhydride-Cured Epoxy. *Macromol Mater Eng 2004; 289: 629–635*.
- Miyagawa H., Misra M., Drzal L.T., Mohanty A.K. (2005). Novel biobased nanocomposites from functionalized vegetable oil and organically-modified layered silicate clay. *Polymer; 46: 445–453.*
- Shutov F.A. (1991) Syntatic polymeric foams *in Handbook of polymeric foam and foam technology* (Ed. Klempner, D., Frish K.C.), 335-374, Hanser Publisher, New York (USA).
- Wool R.P., Sun X.S. (2005). *Bio-based Polymers and Composites.* Elsevier Academic Press, London (United Kingdom).

Particleboards from chemically modified rice husks and soybean protein concentrate - based adhesives

E.M. Ciannamea, P.M. Stefani, R.A. Ruseckaite
Research Institute of Material Science and Technology, National Research Council,
University of Mar del Plata, Juan B. Justo 4302, 7600 - Mar del Plata, Argentina
A. Jimenez
University of Alicante. Dep. of Analytical Chemistry. PO Box 99, 03080, Alicante,
Spain

ABSTRACT

The technical feasibility of using rice husk (RH) as wood substitute in the production of environmentally sound medium-density particleboards using modified soybean protein concentrate (SPC) as adhesive was evaluated. Chemical modification of RH with NaOH and NaOH followed by H_2O_2 were undertaken to evaluate the effect on the composition and topology of RH. Both treatments were efficient in partially eliminate hemicelluloses, lignin and silica from RH, as evidenced by thermogravimetric analysis (TGA). Scanning electronic microscopy (SEM) observations suggested that alkaline treatment resulted in a more damaged RH substrate than bleaching. Bleached RH – based panels displayed the best set of final properties. Particleboards with this formulation met the minimum requirements of internal bond (IB), modulus of rupture (MOE) and modulus of elasticity (MOR) recommended by the U.S. Standard ANSI/A208.1 specifications for M1, MS and M2-grade medium density particleboards, but resulted in high thickness swelling (TS) values. This limitation was counterbalance by the advantage of being formaldehyde-free which makes them suitable for indoor applications.

1. INTRODUCTION

The use of alternative resources to substitute wood in the particleboard industry has increased in the last years mainly due to the depletion of the forest resources. rice husks (RHs), which are the main by-products of the rice milling process, are available in large quantities, and has the same basic components as wood but in different proportions (25-35% cellulose, 8-21% hemicelluloses, 26-31% lignin, 15-17% amorphous silica and waxes, and 2-5% of other soluble substances) (Stefani et al., 2005). Therefore, it would be expected that RH behave similarly to wood in particleboard production. However, the presence of abundant silica and waxes affects RH interactions with polar adhesives (Leiva et al., 2007). Different strategies have been applied to improve RH adhesion. Among them alkaline treatment facilitates the adhesive nature of the fiber surface by removing impurities, and causes the separation of structural linkages between lignin and carbohydrate and the disruption of lignin structure (Ndazi et al, 2007). The combination of alkaline treatment with H_2O_2 (bleaching), is commonly used to remove the lignin left after the alkaline treatment (Wang et al., 2007). Soy proteins can be used as substitutes for the traditional synthetic adhesives in particleboard manufacturing (Mo et al, 2001). In our previous work we have successfully produced medium-density particle boards based on RHs and un-treated and alkali-treated SPC adhesives. The resultant boards showed comparable mechanical and water resistance properties than UF-bonded ones (Leiva et al, 2007). The main goal of the present work was to upgrade the final mechanical properties and water resistance of RH-SPC particleboards by modifying RH through alkaline and bleaching treatments, using alkali-treated SPC as adhesive.

2. EXPERIMENTAL

2.1 Chemical treatments on RH and SPC modification

RH (Don Juan variety, Entre Ríos, Argentina) was washed at room temperature under vigorous stirring with distilled water and dried at 100 ± 2ºC (control RH, **CRH**)

CRH was soaked in 1M NaOH (mass ratio 1:10), for 30 min at room temperature followed by washing with water to leach out the absorbed alkali (**ARH**)

CRH was first treated with 1M NaOH during 15 min. The alkali-treated RH was washed, filtered and soaked in 0.02 wt% H_2O_2 under stirring for 15 min. After chemical bleaching, RH was washed with water, filtered and dried (**BRH**).

Alkali-treated SPC (**ASPC**) was prepared according to the procedure previously reported (Leiva et al, 2007)

2.2. Particleboard processing and evaluation (Leiva et al., 2007).

RHs were blended with the SPC-adhesive (10wt.% solids) in an orbital paddle mixer for 10 min at room temperature. The mixtures were dried at 70ºC until 40% moisture, and subsequently hot-pressed into particleboards in a 30cm x 30cm steel mould equipped with stops to achieve the same thickness (0.55cm), at 140ºC, 2.9 MPa for 10 min. Target bulk density was 0.80±0.05 g/cm^3. Three replicates for each kind of RH were produced. Particleboards were conditioned at 65% relative humidity at 20ºC for 7 days and evaluated according to the ASTM D1037-93 standard procedure, in an Instron 4467 universal test machine. Nine specimens were prepared MOR, MOE and IB test, and six for 24 hs water absorption (WA) and TS. The analysis of variance (ANOVA) was used (α=0.05) and comparison of means was done employing Tukey test ($P<0.05$).

3. RESULTS AND DISCUSSION

TGA was used to determine qualitatively the effect of chemical treatments on RH composition (Fig.1a). The removal of hemicelluloses could be confirmed by the disappearance of the shoulder at 301º C in DTG curve (Ciannamea et al., 2008). Hemicelluloses and lignin are associated through covalent bonds. Therefore, since hemicelluloses seemed to be efficiently removed, the extraction of lignin is also assumed. Alkaline treatment simultaneously causes the polymorphic transformation of cellulose I into cellulose II within the crystalline cellulose domains (Teh and Rudin, 1990). This fact is accompanied by an increment in the amorphous phase that might decrease the thermal stability of the cellulose fraction. This was evidenced by the shifting in the initial decomposition temperatures and a maximum degradation rate of cellulose peak toward lower temperatures compared to CRH. The reduction of lipids and waxes was also assumed due to the efficiency of H_2O_2 in the oxidation of fatty acids (Larrea et al., 1997), generating products that were not detected by the method of analysis. Chemically treated RHs were stable up to temperatures higher than the one used in processing particleboards (140ºC). So, the thermal degradation of RHs during processing operations is expected to be minor. SEM observations gave further insight on the modification during the treatments of RH morphology. The outer surface of CRH appeared highly undulated due to the presence of regularly spaced conical protrusions, while the inner one appeared to be smoother (Fig. 2a).

Treatment with NaOH induced the cracking of the conical protrusions of the outer surface (Fig. 2b), and increased the roughness of the inner surface which was accompanied with some defibrillation. This could be a consequence of the elimination of the cementing materials of the interfibrillar region. The outer surface of bleached RH showed the conical protrusions broken at the top. The inner surface also showed topological changes including higher roughness and cracks (Fig. 2c).

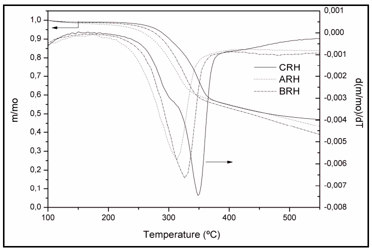

Fig. 1. TG/DTG curves of CRH, ARH and BRH.

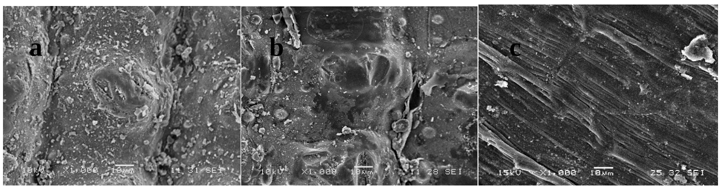

Fig. 2. a) CRH external surface; b) ARH external surface; c) BRH internal surface.

Chemical treatments induced changes which possibly favor chemical interactions, such as hydrogen bonds, between the more exposed hydroxyl groups of RHs and the polar groups of soy proteins. Additionally, mechanical bonding may take place because protein-based adhesives could penetrate more easily into RH microstructure (Mo et al., 2001). However, the elimination of cementing materials may lead to an increase in the substrate brittleness, associated to the increased rigidity of the treated fibers (Ciannamea et al., 2008). The effect of the chemical treatments performed on RH on the mechanical properties will be the result of the competition between the increased adhesion and the damage caused by the chemical agents used. The MOR and MOE values (Table 1) showed that chemical treatments on RH induced better performance on the obtained panels.

RH treatment	MOR (MPa)	MOE (MPa)	IB (Mpa)	WA 24hs (%)	TS 24hs (%)
CRH	11,18 ± 1,13a	2307 ± 300a	0,43 ± 0,15a	73,39 ± 6,88b	28,57 ± 1,76b
ARH	15,37 ± 3,16b	2665 ± 404ab	0,37 ± 0,12a	94,16 ± 8,71cg	60,49 ± 5,81c
BRH	18,45 ± 2,07c	2844 ± 420b	0,45 ± 0,15a	81,95 ± 3,56eg	48,03 ± 4,89e
M-1	11.0	1725	0.4	-	-
M-S	12.5	1900	0.4	-	-
M-2	14.5	2225	0.45	-	-
M-3	16.5	2750	0.55	-	-

Means followed by the same letter are not significantly different (P>0.05).
M-1 and M-S are for commercial usage and M-2 and M-3 are for industrial usage.

Table 1. Properties of RH board and ANSI specifications

It is believed that the changes produced in RH surface by bleaching favor the adhesion by mechanical anchorage, with minor reduction in RH stiffness. The values of MOR and MOE for ARH – based boards were between of those determined for panels based on CRH and BRH. This could be attributed to the higher physical and chemical deterioration of RH provoked by soaking in NaOH during 30 min. On the other hand, IB values were not significantly different. The higher WA and TS (Table 1) for chemically treated RHs, might be caused by the elimination of hydrophobic substances still present in CRH (Ciannamea et al., 2008). According to the tests results, ASPC-BRH particleboards reached the minimum requirements of MOE, MOR and IB to satisfy the U.S. Standard ANSI /A208.1 requirements for M1, MS and M2-grade medium density particleboards. However, particleboards presented high TS and WA values.

4. CONCLUSIONS

Properties of SPC-RH particleboards were upgraded by bleaching of RHs. ASPC-BRH particleboards met the minimum standard requirements recommended by the U.S. Standard ANSI/A208.1 specifications for M1, MS and M2-grade medium density particleboards. The lower water resistance is counterbalanced by the advantage of the adhesive of being formaldehyde-free and the fact of using entire RHs for particleboard manufacture which saves milling and screening operations. The ASCP-BRH particleboards were found to be an environmentally sound option for applications for which the requirements for water resistance are not stringent.

ACKNOWLEDGEMENTS

Authors wish to express their gratitude to CONICET of Argentina and to Universia-Banco Río (Santander Group) for their financial support.

REFERENCES

CIANNAMEA, E.M., STEFANI P.M., RUSECKAITE R. A. (2008) Medium-density particleboards from chemically modified rice husks and soybean protein concentrate-based adhesives, *Bioresource Technology*, under revision.

LARREA, M.A., GROSSMANN, M.V., BELÉIA, A.P., TAVARES, D.Q. (1997) Changes in water absorption and swollen volume in extruded alkaline peroxide pretreated rice hulls. *Cereal Chem.* 74, 98-101

LEIVA, P., CIANNAMEA E.M., RUSECKAITE, R.A., STEFANI, P.M. (2007) Medium-density particleboards from rice husks and soybean protein concentrate. *J. App. Polym. Sci.* 106, 1301-1306

MO, X., HU J., SUN X.S., RATTO J.A. (2001) Compression and tensile strength of low-density straw – protein particleboard. *Ind Crops. Prod.* 14, 1-9

NDAZI, B., KARLSSON, S., TESHA, J., NYANUMWA (2007) Chemical and physical modifications of rice husks for use as composites. *Comp.Part A* 38,925-935

NEMLI, G., KIRCI, H., TEMIZ (2004) Influence of impregnating wood particles with mimosa bark extract on some properties of particleboards, *Ind Crops Prod* 20 339-344

STEFANI, P.M., GARCIA, D., LOPEZ, J., JIMENEZ A. (2005) Thermogravimetric analysis of composites obtained from sintering of rice husk–scrap tire mixtures. *J. Therm. Anal. Calorim.* 81, 315-320.

TEH, J. W., RUDIN, A. J. (1990) Mechanism of adhesion of resole phenolics to cellulosic materials. *Polym Sci Part C: Polym Lett* , 28,363-371

WANG, B., SAIN, M., OKSMAN, K. (2007) Study of structural morphology of hemp fiber from the micro to the nanoscale. *Appl. Compos. Mater* 14, 89-103.

Propiedades de impacto en aleaciones PA6/PP

A.Valea, I. Mondragon, B.González, M.L. González
Departamento de Ingeniería Química y del Medio Ambiente,
Escuela Universitaria de Ingeniería Técnica Industrial,
Universidad del País Vasco UPV/EHU
Plaza de la Casilla, 3, 48012 Bilbao
iapvapea@lg.ehu.es

RESUMEN

Han sido preparados por extrusión, seguido de moldeo por inyección una serie de blends de polipropileno- poliamida 6 de diferentes composiciones, utilizando polipropileno injertado con anhídrido maleico como compatibilizante. Se han ensayado probetas normativas mediante ensayos estáticos mecánicos y mediante ensayos de impacto. Las superficies de fractura procedentes de los ensayos de impacto se han observado después mediante microscopía electrónica de barrido (SEM). Como resultado del estudio se ha podido comprobar que las propiedades mecánicas de las aleaciones dependen mucho de las relaciones PP/PA6. El módulo elástico, la resistencia en tracción y la energía de impacto parecen crecer al hacerlo la concentración de PA6. La resistencia a impacto resultó más elevada para las aleaciones que contienen alrededor de 80% wt. de PA6. La observación de las micrografías electrónicas (SEM) indica que la adición del compatibilizante tiene como resultado una mejor adherencia entre los dominios dispersos de PP y la matriz de PA6 en la aleación PP/PA6 = 20/80.

1. INTRODUCCIÓN

La preparación de mezclas y aleaciones de polímeros implica generalmente el uso de matrices poliméricas que sean fácilmente asequibles comercialmente, primero por suponer materiales plásticos de consumo y por tanto de precio reducido, y por otro lado, por abrir la posibilidad a la incorporación de materiales procedente de recuperación o reciclados. El PP y la PA son termoplásticos fácilmente disponibles y que se fabrican en grandes cantidades. El PP se caracteriza por su relativamente alta temperatura de fusión, entre los commodities, elevado alargamiento a rotura, buena resistencia a humedad y bajo costo, pero tiene relativamente baja resistencia mecánica y a los agresivos químicos y al calor. Por otro lado, la PA posee una mayor resistencia en tracción y es resistente a muchos disolventes. Las PA tienen una gran afinidad por el agua y sus propiedades mecánicas se encuentran a menudo significativamente afectadas por esa absorción de agua. Por este conjunto de características las PA se mezclan con polímeros de bajo módulo, tales como las poliolefinas, para mejorar las propiedades de los materiales (Lamantia, F.P et al 1993, Nobel, B.K et al 1994). La adición de PP disminuye la absorción de agua y reduce los costos de los materiales.

Las mezclas PP-PA se ha demostrado que son inmiscibles. El tamaño y la forma de la fase dispersada son factores importantes que determinan las propiedades mecánicas de las aleaciones. La morfología de las aleaciones depende de cierto número de factores tales como la composición, relación de viscosidad, tensión interfacial y condiciones de procesado. Estos factores pueden determinar cuál de los componentes es la fase dispersada y cuándo puede ocurrir la inversión de fase. La incompatibilidad inherente entre PP y PA6 ha sido un factor limitante a la hora de obtener buenas características en impacto y alta resistencia en tracción de las aleaciones. Se pueden obtener mejoras significativas en las propiedades de las aleaciones por adición de agentes compatibilizantes que son, en su mayoría, poliolefinas funcionalizadas con anhídrido maleico o ácido acrílico y sus derivados. Estos grupos funcionales reaccionan con los grupos amina de la poliamida, dando lugar a intensos enlaces entre las dos fases. La morfología, propiedades estáticas en tracción para diferentes tipos de mezclas y aleaciones ha sido estudiada por varios grupos investigadores, entre ellos el nuestro (A.Valea et al 2007). Las conclusiones comunes son que los compatibilizantes tienden a promover la adhesión interfacial y a producir una fase dispersa con dominios de menor tamaño en los blends PP-PA. Por tanto, la incorporación de agentes compatibilizantes tiene como resultado una mejora en las propiedades en tracción y en impacto de las aleaciones PP-PA.

2. PROCEDIMIENTO EXPERIMENTAL

El polipropileno utilizado en el trabajo corresponde a un Isplen T5, suministrado por Repsol YPF. El copolímero de anhídrido maleico injertado sobre PP utilizado fue un E-43, suministrado por Eastman en concentración de 2,0% wt. La PA6 (K4008) utilizada fue suministrada por Repol. Las composiciones se han preparado secando en primer lugar la granza en una estufa de vacío a 80ºC durante no menos de 24h, seguidamente se ha mezclado en frío mediante un volteador seguido de mezclado en una extrusora Davies Standard Co., de husillo sencillo de 18 mm, con tres zonas reguladas de temperatura aparte de la boquilla y con baño de enfriamiento. El proceso de mezclado se llevó a cabo regulando la temperatura (270 ± 10 ºC y 231,5 ± 3,5 ºC) y a la velocidad (11 ó 19 rpm), de acuerdo con las diferentes composiciones de estos materiales y se determina cuál es el porcentaje de compatibilizante adecuado para el que los valores de las propiedades mecánicas y térmicas resulten óptimas para las probetas ensayadas. Las probetas se han preparado a una presión de $(1070 \pm 70)\cdot 10^5$ Pa y (277,5 ± 7,5) ºC, en una prensa de inyección Arburg que posee moldes diseñados de acuerdo a la geometría establecida por la norma UNE 53021 y ASTM D-256). Se ha tomado en consideración la norma UNE 53003- ISO 291 referente al acondicionamiento de probetas y atmósferas relativas a los ensayos.

El módulo y la resistencia en tracción se ha medido en una máquina universal de ensayos Ibertest mod. ELIB 50W (cf. UNE 53023) a una velocidad de 5 mm/min, con un extensómetro de 25 mm y en un recinto debidamente dispuesto para ensayos de este tipo. Los resultados de impacto Charpy por caída de peso, se llevó a cabo sobre probetas entalladas. La morfología de las superficies de fractura ha sido estudiada por microscopía electrónica de barrido (SEM), con un equipo JEOL 5510. La superficie de las muestras de rotura fueron metalizadas con Au/Pd para mejorar la conducción del haz de electrones en las matrices de PA6/PP/AM.

3. RESULTADOS Y DISCUSIÓN

La Figura 1 muestra la variación del módulo en tracción y de la resistencia en tracción para las aleaciones (PP-PA6) en función del contenido en PA6, respectivamente. Estas Figuras indican que ambos, módulo y resistencia en tracción de las aleaciones aumentan al hacerlo el % PA6. Así parece haber mejoras en las propiedades en tracción a medida que la fase continua PP se sustituye por la fase continua PA.

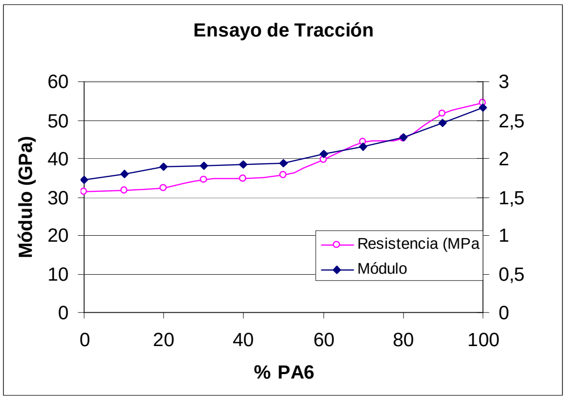

Figura 1. Resultados de los ensayos tracción para mezclas PP-PA6.

La Figura 2 muestra las curvas de impacto por caída de peso, para especimenes PA6-PP en función de su velocidad. Puede verse que la resistencia a impacto de la PA6, ensayada a varias velocidades de impacto es mayor que para el PP en todo el ámbito de velocidades de impacto medidas. En el ámbito medido de 1 m·s^{-1} a 5 m·s^{-1} la resistencia a impacto disminuye un 50 %.

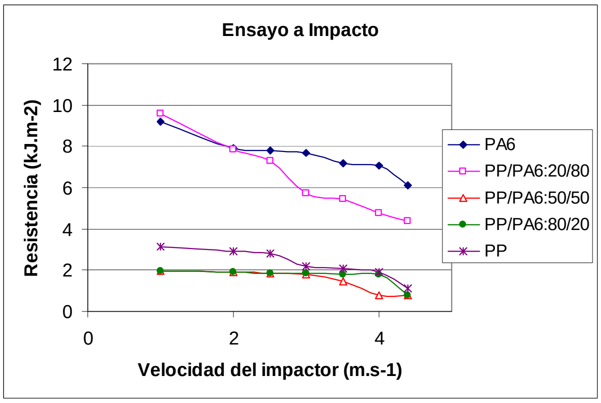

Figura 2. Resultados de resistencia a impacto por caída de peso mezclas PP-PA6.

La Figura 2 indica que aleaciones de PP/PA6 conteniendo hasta 50 % PA6 tienen relativamente baja resistencia a impacto. Sin embargo, la resistencia a impacto es mejor en aleaciones para las que la fracción en peso de PA6 es 80 % tal como ya habíamos evidenciado anteriormente. Puede verse que en todo el ámbito de velocidades de impacto (solicitación) los valores de resistencia a impacto aumentan al hacerlo la concentración de PA6 y se confirma igualmente que para cualquier velocidad de solicitación los valores de resistencia impacto son bajos para composiciones con menos del 50 % en PA6 y aumenta rápidamente la resistencia a impacto en el ámbito de composiciones entre 50 % y 80 % wt en PA6 multiplicándose por un factor superior a cuatro su valor.

La morfología de la aleación influye notablemente en las propiedades mecánicas de las aleaciones PA6-PP, por lo que se ha procedido a estudiar las superficies de fractura de los especimenes después del ensayo de impacto. Se ha podido apreciar una zona de inducción de fractura semicircular como una zona de deformación plástica localizada de la matriz, que ocurre especialmente en las regiones próximas a la entalla. El tamaño de esta zona aparentemente disminuye con la velocidad de impacto. Cuando la velocidad de impacto aumenta hasta 4,0 $m \cdot s^{-1}$ la zona de inducción de fractura en la probeta desaparece, y la fractografía aparentemente muestra solo una zona de rotura frágil, debido a que la formación de la zona de inducción está asociada con la absorción de energía durante el ensayo de impacto. Así, cuanto mayor sea el área de la zona de inducción mayor será la resistencia a impacto del material. Aparece una correlación buena entre la fractografía SEM y los resultados del ensayo de impacto, es decir, la resistencia a impacto de la muestra PA6-PP tiende a aumentar con la disminución en la velocidad de impacto, tal como se muestra en la Figura 2.

Cuando se estudian las micrografías de las aleaciones PP/PA6 = 20/80 (alto contenido en PA6) puede observarse una zona de cizallamiento en el área externa de la piel. La superficie de fractura es muy rugosa cerca de la zona de inicio del crack. Los dominios de pequeño tamaño del PP (en el ámbito de 0,5-1,0 µm) parecen estar bien dispersados en la matriz continua de la PA6, indicando que hay una buena adhesión entre ambas fases. Así el anhídrido maleico injertado en el PP parece ser un buen compatibilizante en cuanto a su eficacia para reducir de tamaño las partículas de PP dispersadas en esta aleación Las micrografías SEM de las aleaciones PA6-PP = 50/50 nos indican que hay gotitas dispersadas bien delimitadas en los bordes, resultando que los bordes son casi indiferenciables en esta aleación. Podemos asignar las gotitas dispersadas como dominios de PP en una matriz continua formada por la fase PA6, de acuerdo con la teoría de Taylor que establece que las partículas dispersadas pueden deformarse solo cuando su viscosidad no excede la de la matriz, que es precisamente el caso en estos sistemas.

AGRADECIMIENTOS

Los autores desean agradecer la ayuda económica recibida del MICINN (Proyecto MAT- 2006, a la UPV- EHU (por su ayuda a Grupos de Investigación) y UNESCO

REFERENCIAS

LAMANTIA, F.P.; Adv. Polym. Technolog., 12 , 47 (1993)
DUBALL, J.; SELLITTI,C.; MYERS, C.; HILTNER, A.; BAER, E.; Appl. Polym. Sci., 52, 195 (1992)
NOBEL, B.K.; VILLEMAIRE, J.P.; AGASSANT, J.F.; Int. Polym. Processing, 9, 119 (1994)
PADWA, A.R.; Polym. Eng. Sci., 32, 1703 (1992)
VALEA, A.; SALAS, P.F.; MONDRAGO, I.; JUANES, F.J.; GONZÁLEZ, M.L.; “Efecto de la incorporación de microesferas sobre las propiedades de aleaciones de PA/PP”. Proceed. GEF-2007 (2007)

Deformation and fracture behaviour of vinylester/fly ash composites

A. Stocchi, E. Rodríguez
Materials Science and Technology Research Institute (INTEMA)
University of Mar del Plata - National Research Council (CONICET),
Av. Juan B. Justo 4302 - B7608FDQ - Mar del Plata, Argentina
A. Vázquez
Laboratorio de Polímeros y Materiales Compuestos. Instituto de Tecnologías y Ciencias de la Ingeniería (INTECIN). Facultad de Ingeniería. Universidad de Buenos Aires, Argentina
C. Bernal
Advanced Materials Group (GMA). INTECIN (UBA-CONICET)
Department of Mechanical Engineering– Engineering Faculty, University of Buenos Aires, Av. Paseo Colón 850 – 1063 – Buenos Aires, Argentina

ABSTRACT

In the present work, the deformation and fracture behaviour of a commercial vinylester resin reinforced with fly ash was investigated. Uniaxial compression tests and fracture tests on SENB specimens were performed on composites with different ash content. Composites fracture surfaces were analysed by SEM and the toughening mechanisms were identified. Under uniaxial compression, all materials exhibited ductile behaviour and the composites were stiffer than the vinylester matrix. In fracture tests, the composites behaved brittlely with improved fracture properties in comparison to the matrix. Different toughening mechanisms such as crack bowing, crack deflection and debonding of ash particles from the matrix followed by plastic void growth were found to be operative in these composites.

1. INTRODUCTION

Nowadays, there is an increasing interest of technical and scientific community to obtain new materials with improved properties and processability at relatively low cost. This is commonly achieved through the incorporation of inorganic fillers to polymers. In addition, mainly as a result of existing environmental rules and regulations; there is also a need of current industries to re-use their wastes. A very attractive alternative to achieve both above commercial and environmental goals seems to be the use of ash and fly ash produced from carbon and other fossil fuels combustion, as reinforcement of polymers (Bose et. al., 2004). They are cheaper and more environmentally friendly than conventional inorganic fillers. On the other side, vinylester is a thermosetting polymer with very high chemical resistance, thermal stability and mechanical strength. However, its low ductility and poor fracture toughness limits its applications as engineering material (Robinette et. al., 2004).

In the present work, the deformation and fracture behaviour of a commercial vinylester resin reinforced with fly ash was investigated. The effect of ash content was studied. The results obtained were compared with the results for the same resin reinforced with commercially available glass beads.

2. EXPERIMENTAL

Fly ashes kindly supplied by Industrias del Tablero S.A. (INTASA, Spain) were used as reinforcement. Commercially available glass beads (Pecinelec, Argentina) with nominal diameter of 80 μm were also used as reinforcement for comparison purposes.

The matrix material was a commercial vinylester resin (Derakane Momentum 411-350 from Dow). Composites with different ash content: 10 wt.%, 20 wt.%, 30 wt.% and 40 wt.% or with 20 wt.% glass beads were prepared.

Uniaxial compression tests were performed on cylindrical specimens in an Instron dynamometer 4467 at 1 mm/min following ASTM D695M-91 standard recommendations.

Fracture characterization was carried out on SENB specimens in accordance with ASTM 5045-93 Standard recommendations.

Fracture surfaces of specimens broken in fracture tests were also analysed by scanning electron microscopy (SEM) to identify the toughening mechanisms.

Contact angle measurements were performed using the sessile drop technique in open air at room temperature. The subtract (disks of compacted fly ash) were moulded in a hydraulic press (9.8 MPa). Static contact angles were determined from image analysis. Optical lens (Navitar 7000) coupled with a CCD camera (JAI) were used to obtain the images. The images were analyzed with a commercial imaging software.

3. RESULTS AND DISCUSSION

Figure 1 shows compressive modulus values for the vinylester/ash composites with different ash content and with 20 wt.% glass spheres. An increase in the material stiffness with ash content was observed up to 30 wt.% ash. This is the expected result from the incorporation of a stiffer second phase in the vinylester matrix. Further increase in the ash content led to a slight decrease in stiffness, probably as a result of poorer particle dispersion in the matrix and/the presence of increased porosity in the samples. However, all composites exhibited higher stiffness values than the matrix. The incorporation of 20 wt.% glass beads into vinylester also led to a slight improvement in the material modulus in agreement with expectations.

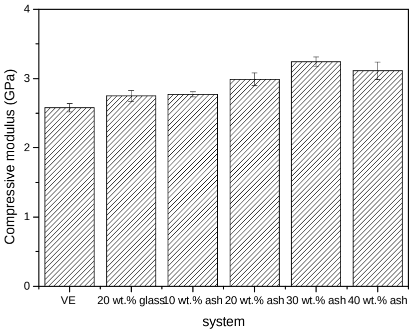

Figure 1. Compressive modulus values for the different composites investigated.

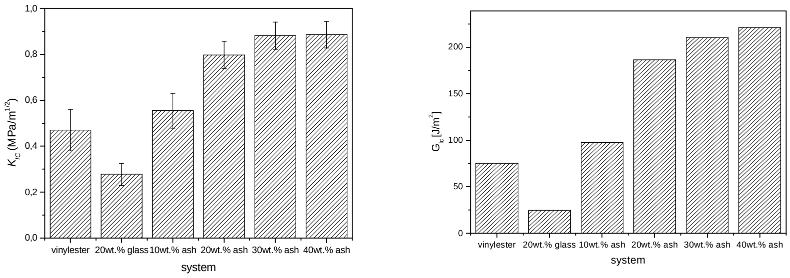

Figure 2. Critical stress intensity factor and energy release rate values for the different composites investigated.

Critical stress intensity factor (K_{IC}) and energy release rate (G_{IC}) values are presented in Figure 2 a and b, respectively. It can be observed that K_{IC} and G_{IC} increased with ash content up to 30 wt.% ash, as the number of sites inducing toughening mechanisms increased. Further increase in filler loading, did not lead to any improvement in fracture properties probably as a result of the higher number of microcracks able to facilitate crack propagation (Lee and Yee, 2000).

On the other hand, the incorporation of 20 wt.% glass beads led to a material with values of K_{IC} and G_{IC} significantly lower than those of the matrix, probably due to the presence of critical-size flaws derived from debonding of the large glass particles (nominal diameter of 80 μm) that induced premature failure (Wong et. al., 1999).

Figure 3 a-f shows SEM micrographs of fracture surfaces. All particles appear clean of the matrix material suggesting relatively poor adhesion between both phases. In the case of micrometer-sized filler particles which are much larger than the plastic zone size, the crack pinning mechanism is expected to occur (Johnsen et. al., 2007). In the SEM micrographs of Figure 3, the bowing marks characteristic of the crack pinning toughening mechanism are clearly observed. Hence, this energy absorption mechanism was present in the composites investigated here.

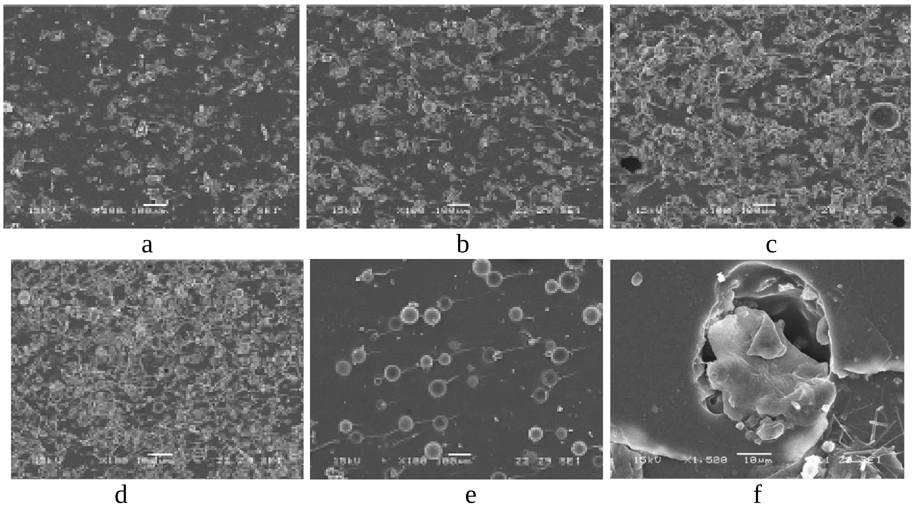

Figure 3. SEM micrographs of the fracture surfaces of SENB specimens (X100) for the composites with different filler content. a) 10 wt.% ash. b) 20 wt.% ash. c) 30 wt.% ash. d) 40 wt.% ash. e) 20 wt.% glass beads. f) Closer view of micrograph a.

Debonding at the matrix-particle interface promoted by the poor matrix-particle adhesion and the subsequent plastic void growth are also observed (Figure 3 f).
Crack deflection should be also taken into account. In this toughening mechanism, the crack front tilts and twists when it founds rigid particles and passes around them. Thus, it leads to an increase in the total fracture surface area and makes the crack to grow locally under mixed-mode conditions (Johnsen et. al., 2007).

Figure 4. Picture of a drop of VE resin in a fly ash substrate.

A low contact angle between a solid and a liquid indicates a tendency of the liquid to wet the solid. In general, for contacts angles lower than 90º it is said that there is a "wetting behaviour" (a complete wetting is achieved at an angle $\theta = 0$), while contacts angles higher than 90º are associated with a "non-wetting behaviour". A good wetting is achieved for contacts angles lower than 45º (Wim et. al., 2005). In our case (Figure 4), a contact angle between vinylester and flyash of 51.23º ± 6.3º was obtained, suggesting intermediate wettability.

4. CONCLUSIONS

The deformation and fracture behaviour of a commercial vinylester resin reinforced with fly ash was investigated.
In uniaxial compression tests, all composites displayed ductile behaviour. An increase in the compressive modulus with the incorporation of ash or glass beads and also with the increase of ash content, was observed. However, for the composite with the highest ash content (40 wt.%) as a result of an increase in the number of voids and/or poorer dispersion of ash into vinylester, a slight decrease in the modulus was found.
The incorporation of ash to vinylester led to composites with improved fracture properties as both the critical stress intensity factor and energy release rate values are higher that those of the matrix. They also increased with filler content. From SEM observations of the fracture surfaces, the toughening mechanisms responsible of the improvement of fracture properties were found to be crack bowing, crack deflection and debonding at the matrix-particle interface followed by plastic void growth. Particle debonding from the matrix was the result of a relatively poor adhesion between vinylester and ash as confirmed from SEM observations and contact angle measurements.

REFERENCES

BOSE S. AND. MAHANWAR P.A, (2004) Effect of Particle Size of Filler on Properties of Nylon-6 *J. of Minerals & Mat. Characterization & Eng.*, 3, 65 .
JOHNSEN B.B., KINLOCH A.J., MOHAMMED R.D., TAYLOR A.C. and SPRENGER. S. (2007) Toughening mechanisms of nanoparticle-modified epoxy polymers *Polym.*, 48, 530.
LEE J. and YEE A. F. (2000), Role of inherent matrix toughness on fracture of glass bead filled epoxies *Polym.,* 41, 8375.
ROBINETTE E.J., ZIAEE S.AND. PALMESE G.R (2004) Toughening of vinyl ester resin using butadiene-acrylonitrile rubber modifiers, *Polym.*, 45, 6143.
WIM F., MERTENS P.(2005) . "Method for coating substrates" *Us Patent 2005/0079291A1*
WONG S.C., MAI Y.W, (1999) Effect of rubber functionality on microstructures and fracture toughness of impact-modified nylon 6,6/polypropylene blends: 1. Structure–property relationships *Polym.,* 40, 1553.

Effect of chemical modification on mechanical and thermal properties of coconut fibres/ HDPE composites

J.O.G. Figueiredo[1*], D.R. Mulinari[1], H.J.C. Voorwald[1], M.O.H. Cioffi[1],
G.M. Rocha[2]
[1]Fatigue and Aeronautic Materials Research Group, DMT/UNESP – Av. Dr. Ariberto Pereira da Cunha, 133 Pedregulho –12516-410, Guaratinguetá/SP, Brazil
[2]Department Biochemical, EEL/USP – Rodovia Itajubá-Lorena km 74,5 –12600-000, Lorena/SP, Brazil

ABSTRACT

The use of natural fibers as reinforcement for thermoplastics has generated much interest due to the low cost, low density, high specific properties characteristics and also due to the environmental protection. Another important advantage is that natural fibers are biodegradable and nonabrasive, readily available and present specific properties comparable to traditional fibers used as reinforcements into the composites.

However some drawbacks, such as the incompatibility between fibers and polymer matrices, the tendency to form aggregates during processing and the poor resistance to moisture, reduce the use of natural fibers as reinforcements in polymers. Incompatibility of components is responsible for poor thermal and mechanical properties. Because of this, various treatments are being used to improve fibers/matrix compatibility, such as bleaching, acetylation and alkali treatment.

In the work, the effect the chemical modification on mechanical and properties of coconut fibres/HDPE composites were studied.

Coconut fibres were treated with 10% sulfuric acid solution, to remove impurities such as waxes, pectins and hemicellulosics fibers. These fibers were mixed with the polymeric matrix (HDPE) in a thermokinetic mixer, model MH-50H, with speed rate maintained at 5250 rpm, in which fibers were responsible for 5 to 15 wt% in the composition. After the mixture, composites were dried, ground in mill and placed in an injector camera according to ASTM D-638 specification. Five specimens were tested in an INSTRON universal-testing machine (model-8801). TGA was carried out using a SEIKO instrument, in N_2 atmosphere at 10 ^{0}C min^{-1} heating rate, from 30 to 650 ^{0}C.

Results showed that, the addition of fibers in matrix increased the tensile strength and modulus as well as thermal stability of composites compared to the matrix polymeric.

Electrical properties and study of microstructure of polymer composites filled with dispersed iron particles

H. Zois
Department of Physics, National Technical University of Athens, Greece
A. Kanapitsas
Department of Electronics, Technological Educational Institute (TEI) of Lamia, Greece
Y.P. Mamunya
Institute of Macromolecular Chemistry, National Academy of Sciences of Ukraine

SUMMARY

The objective of this work is to study structure-electrical properties relationship of composites based on polypropylene (PP), co-polyamide (cPA) or polymer blend PP/cPA filled with dispersed iron (Fe) particles. Dielectric spectroscopy measurements reveal with accuracy the secondary relaxations as well as percolation phenomena. The dependence of electrical conductivity on the filler content shows percolation behavior. The values of the percolation threshold are equal to 20 vol. % for PP-Fe, 28 vol. % for cPA-Fe system and 5 vol. % for the composites based on the PP/cPA blend. The lower value for the PP/cPA-Fe composites is attributed to the peculiar morphology of such composites. In the systems having the polymer blend as a matrix and, as a result of the preparation procedure, the dispersed iron particles are localized only within cPA. So, an interpenetrating network with two distinct phases (PP and cPA-Fe) is formed.

1. INTRODUCTION

Polymer composites filled with metal inclusions are of intense interest for many fields of engineering. This interest arises from the fact that the electrical characteristics of such composites are close to the properties of metals, whereas the mechanical properties and processing methods are typical for plastics. Such composites consist of a thermoplastic or thermosetting matrix filled with dispersed fillers, such as metals, carbon black, or intrinsically conductive polymers. The applications of such composites include temperature sensors, self-regulating heaters, antistatic materials, EMI/RFI shielding, electronic devices, etc.

A specific feature of composites with conductive dispersed fillers is the presence of the so-called percolation threshold, i.e. the value of the filler content where a sharp transition from insulting to conductive state occurs (Stauffer, 1985). Dielectric relaxation spectroscopy (DRS) measurements, in wide frequency and temperature range, filler content dependence of electrical conductivity and optical microscopy investigations were used to study electrical and dielectric properties of these composites, in close relation to their microstructure.

2. EXPERIMENTAL

For the preparation of the composites the following materials were used: a copolymer of polyamide (cPA) PA6/PA6.6/PA6.10 with melt flow index (MFI) 11.9 g/10 min, polypropylene (PP) with MFI= 2.0 g/10 min and iron (Fe) powder with an average size of 3 μm and shape close to spherical one. The PP-Fe and cPA-Fe composites were prepared by mixing the two components in a screw extruder and the filler particles are homogeneously distributed within the polymer matrix. On the contrary, the composites based on the PP/cPA-Fe blend were prepared in a two-step procedure. In the first step, a master batch cPA-Fe with 35 vol. % of Fe powder was prepared. In the second step, the master batch is mixed with the necessary amount of PP. During this step, due to the significant difference of the viscosities of PP and cPA, the filler particles are localized within the polymer phase with the lower viscosity, ie. in cPA (Boiteux et al., 2007). A change to the composite composition leads to a dramatic alteration of its microstructure.

Investigations of the composite structure were carried out by an optical microscope BIOLAR in the transmission light, the slides of the samples being cut at a thickness of about 10 μm. A Novocontrol Alpha Analyser, in combination with the Novocontrol Quatro Cryosystem, was used for broadband DRS measurements in the frequency range 10^{-1}–10^{6} Hz and the temperature range from -150 to 220 ^{o}C.

3. RESULTS AND DISCUSSION

3.1 Dielectric properties and molecular mobility

The PP-Fe, CPA-Fe and PP/CPA-Fe composites were examined with DRS to evaluate the effects of the filler on the molecular mobility of the polymeric chains. Fig. 1 shows representative isochronal plots obtained by DRS measurements: imaginary, ε΄΄, part of dielectric permittivity as a function of temperature for cPA-Fe composites at a fixed frequency f= 1 kHz and for four different iron concentrations, shown on the diagram. This plot is similar for all composite systems studied. The data have been recorded isothermally by frequency scanning, but they have been replotted here to facilitate a comparison with other experimental techniques (DMA, DSC and TSDC).

Two dipolar relaxations, a secondary γ-relaxation at T≈ -110 ^{o}C and a secondary β-relaxation at T≈ -40 ^{o}C are observed, in agreement with DMA and DSC measurements, not shown here. No significant shifting of the peak temperature with increasing filler content is observed. The dynamics of these relaxations is studied on the basis of Arrhenius plots. Typical calculated values of the activation energies are: $E_{act.}$= 0.62 eV for β relaxation of cPA-20 % Fe, $E_{act.}$= 0.33 eV for γ relaxation of cPA-20 % Fe and

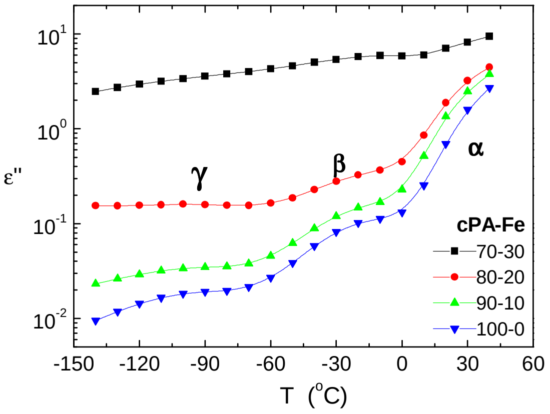

Fig. 1. Isochronal plots for cPA-Fe composite.

$E_{act.}$= 0.36 eV for β relaxation of cPA-5 % Fe composite.

The increase of the ε'' values at higher temperatures is a clear indication for the existence of conductivity effects. Conductivity effects dominate the $\varepsilon''(T)$ behaviour and masks the α-relaxation peak, associated to the glass transition. The contribution of conductivity effects is more significant for the sample with 30 vol. % Fe. It is remarkable that the percolation threshold values obtained from dielectric measurements are in very good agreement with the calculated ones for each composite system.

3.2 Electrical conductivity, percolation and microstructure of the composites

The dependence of electrical conductivity of the composites on the filler volume content, ϕ, has been studied by Boiteux et al. (2007). The percolation threshold, ϕ_c, values for PP-Fe, cPA-Fe and PP/cPA-Fe composites are 20, 28 and 5 vol. %, respectively. The much lower value of the percolation threshold for the blended PP/cPA-Fe composite system is attributed to the presence of the branched conductive cPA-Fe network.

As mentioned above, due to the preparation procedure, the PP/cPA-Fe composites the iron particles are dispersed only within cPA and two distinct phases (PP and cPA-Fe) are formed. So, Fe particles interact only with cPA, whereas PP interacts with the filled phase of cPA-Fe. The filler concentration within cPA is always kept constant, equal to 35 vol. %. It is worth notice that this value is higher than the percolation threshold of cPA-Fe composite (28 vol. %) and, consequently, the cPA-Fe master batch is conductive. A change to the composite composition leads to a dramatic alteration of the structure. This change of composites structure is presented in the micrographs of Fig. 2.

The addition of small amount of PP in the cPA-Fe master batch, or, for high Fe content, demonstrates the structure of the matrix of Fe-filled cPA with isolated inclusions of PP (see, for example, 30Fe). Increase of PP content in the composite results in incorporation of the PP particles and creation of extended inclusions of the PP phase within the cPA-Fe matrix (see 15Fe).

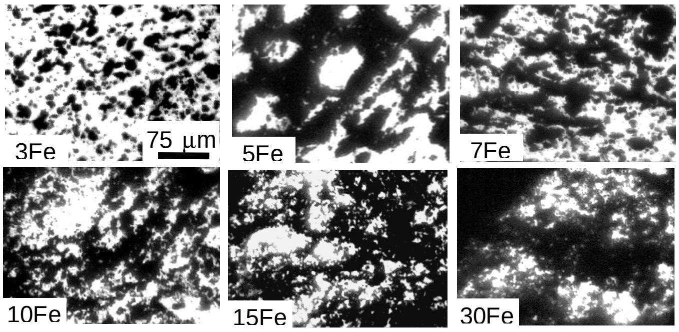

Fig. 2. Evolution of the structure of PP/cPA-Fe composites.

Further increase of the PP content leads to merging of the PP inclusions and to creation of interpenetrating networks of two distinct phases: the insulating PP and the conductive cPA-Fe phase (see 7Fe and 10Fe). In this case, conductive and non-conductive phase are co-continuous. Further increase of PP content results in the collapse of the cPA-Fe network and the composite exhibits the structure of a matrix of PP with the isolated inclusions of cPA-Fe, i.e. island structure is formed (see 5Fe). In this case, the conductive cPA-Fe phase is in the form of separated inclusion in a non-conductive matrix. High predominance of PP in the composite (that corresponds to low content of Fe) decreases the size of the inclusions of Fe-filled cPA (see 3Fe).

Such an evolution of the structure demonstrates a phase inversion, namely the cPA-Fe matrix with insulating inclusions of PP transforms into PP matrix with conductive inclusions of cPA-Fe (compare 3Fe and 15Fe with each other). Such peculiarity of the structure of PP/cPA-Fe composites allows us to accept a structural model with two co-existing phases, ie. cPA-Fe and pure PP, in the interval of the filler content 7-10 vol. %. This description explains the much lower percolation threshold value for the PP/cPA-Fe composites, compared to PP-Fe and cPA-Fe systems. Similar results have been found and schematic models for the interpenetrating microstructure of composites based on PE/POM blend have been proposed by Zois et al (2003).

In such case, conductivity can exist under the conditions of double percolation, (Zois et al., 2003). Two conditions should fulfill, so that the PP/cPA-Fe composites become conductive: first the continuity of the conductive filled cPA-Fe phase is necessary and, second, the conductive iron particles inside the cPA polymer component should create a conductive network.

4. CONCLUSIONS

The blended PP/cPA-Fe composite system has much lower percolation threshold value, which is attributed to the branched structure and the peculiar morphology of such composites. A transition from the structure of nonconductive matrix with conductive inclusions to the structure of conductive matrix with nonconductive inclusions is realized through phase inversion with co-continuous conductive and nonconductive phases. The transition from nonconductive to conductive phase is revealed from dielectric measurements. In addition, DRS measurements show secondary β and γ relaxations for pure cPA and cPA-Fe composites, while α relaxation is masked from conductivity effects. The temperature positions of the above peaks are not affected by the filler composition.

REFERENCES

BOITEUX, G., MAMUNYA, YE.P., LEBEDEV, E.V., ADAMCZEWSKI, A., BOULLANGER, C., CASSAGNAU, P., SEYTRE, G. (2007). From conductive polymer composites with controlled morphology to smart materials, *Synthetic Metals*, 157, 1071-1073.

STAUFFER, D. (1985) *Introduction to percolation theory*, Taylor and Francis, London.

ZOIS, H., APEKIS, L., MAMUNYA Y.P. (2003) Dielectric properties and morphology of polymer composites filled with dispersed iron. *J. Appl. Polym. Sci.*, 88, 3013-3020.

T2. ADVANCED COMPOSITES FOR INDUSTRIAL APPLICATIONS

MATERIALES COMPUESTOS AVANZADOS EN APLICACIONES INDUSTRIALES

Structural loads monitoring of an unmanned air vehicle

M. Frövel, G. Carrión, J.M. Pintado
INTA, Área de Materiales Compuestos, Torrejón de Ardoz, España

ABSTRACT

An Unmanned Air Vehicle, UAV, named SIVA developed by INTA, has been instrumented with several fiber Bragg grating sensors, FBGS, that measures strain and temperature in one outer composite wing and enable to calculate flexural and torsion flight loads. The FBGSs are components of the shelf, COTS, from INSENSYS Company, and are pre-mounted in sensor patches that include in one sensor line two strain sensors in 0º and 90º direction and one temperature sensor. The on-board FBGS interrogator equipment is a robust two channel COTS from the company INSENSYS, called FSI, that uses time-domain sensor identification at 500Hz sampling frequency. The FSI is equipped with a memory card that allows 3 h of autonomous in flight data acquisition. After the flight, the memory card can be easily extracted and the flight data can be evaluated on ground. Real time in flight data transmission to the ground station is also foreseen.

The paper describes the integrated equipments and sensors, and explains the used data evaluation techniques. Flight data of the performed flight campaign will be discussed.

1. INTRODUCTION

UAVs are of big and increment interest for multiple civil and military applications. Structural load monitoring of such UAVs is of certain need not only to evaluate the flight loads and estimate with this data the remaining life time of the structure, but also for a fast and reliable assessment of structural impacts due to unexpected events like hard landings, that can produce significant loads on the structure. This is of especial interest for composite structures where damage is quite often barely visible. In-flight monitoring enables fast turn around times and increases the availability of the UAV.

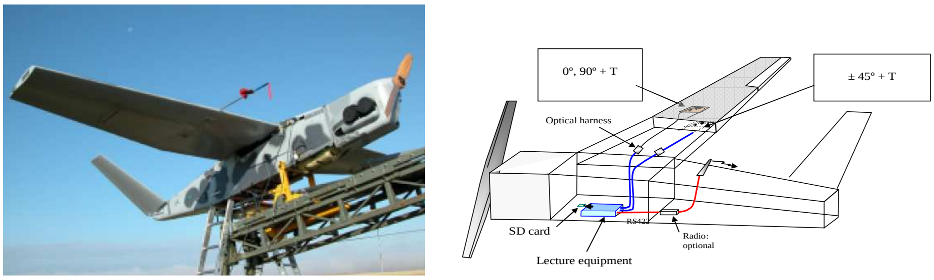

Fig. 1. Left: UAV SIVA in a pneumatic launch ramp. Right: sketch of the installed monitoring system.

SIVA (Sistema Integrado de Vigilancia Aérea) is a complete aerial robotic electro-optic surveillance system developed and integrated at INTA. The UAV is equipped with a sophisticated navigation, guidance mission and flight control system. Its payload is retractable, located in the centre fuselage. It consists of a gimbaled steerable platform upon which a forward looking infrared camera and a CCD TV camera are mounted. The structure of the UAV is made of high strength carbon fibre reinforcing toughened epoxy matrix. The fuselage is a monolithic design and the central wing and the outer, foldable, wings are combined monolithic and sandwich constructions. The wingspan is about 6 m.

Fiber optic sensors have a very high potential for the loads and usage monitoring of UAVs. They are lightweight and can be integrated in the composite structures without a significant decrease of the material properties. Optical fibre FBGS sensors can be highly multiplexed and different types of sensors like strain, temperature, pressure and acceleration can be integrated in the same optical fibre. The optical fibre role is twofold: sensor in the zones where the FBGSs are integrated in the fibre core, and transporting medium, so that a multiple sensors system can be operated with only one single 250 microns optical fibre. Being light the measuring medium, FBGS are completely insensitive to electromagnetic interferences.

2. INTEGRATED LOAD MONITORING SYSTEM

A SIVA UAV has been equipped with an autonomous fibre optic load monitoring system that consists of a lecture equipment, optical fiber harness and strain and temperature sensors located in the outer left hand wing. In this first step of the evaluation, the optical sensors have been surface bonded, not embedded. The system can store the flight data locally and can send the data online to the ground station via radio, although in these first tests only the onboard data storage has been tested.

The used FBGS lecture equipment (FSI) is an all solid state device with no moving parts and that is suited for harsh environments. It works in time division, multiplexing for the sensor identification. Every sensor is identical and can work in a strain range of ± 4500 microstrain. The sensors need to be placed at a minimum distance of 2,5 m to each other. Up to 100 FBGSs can be read simultaneously at 5 Hz. The sampling rate depends on the sensor quantity and is 500 Hz with only one sensor and about 80Hz when the six sensors that are installed in the SIVA. The equipment is completely autonomous with a battery pack and data storage system and weights about 3 kg. Once switched on, the measured data stream on a miniature extractable card type SD in parallel the data stream also and through a RS422 serial interface that can be used to send the measured data directly via radio to the ground station. The equipment can store more than 3 h of flight data. The SD card can be extracted after the flight and the data can be analyzed in a laptop computer. The equipment is integrated in the centre of the fuselage.

The SIVA has been instrumented with two sensor patches from INSENSYS company located one in the upper and the other in the lower wing skin of the foldable outer wing, Fig. 1 and Fig. 2. The patches contain two strain sensors locate at 90º to each other and one temperature sensor. The patches can be serial multiplexed with other patches. In the upper wing skin, the strain sensors have been located in longitudinal and transversal orientation so that they measure wing flexure and transverse strain plus temperature. In the lower wing skin, at ±45º orientation, sensors measure torsion and temperature. The patches have been bonded to the wing skins with epoxy adhesive and vacuum bag cured at room temperature.

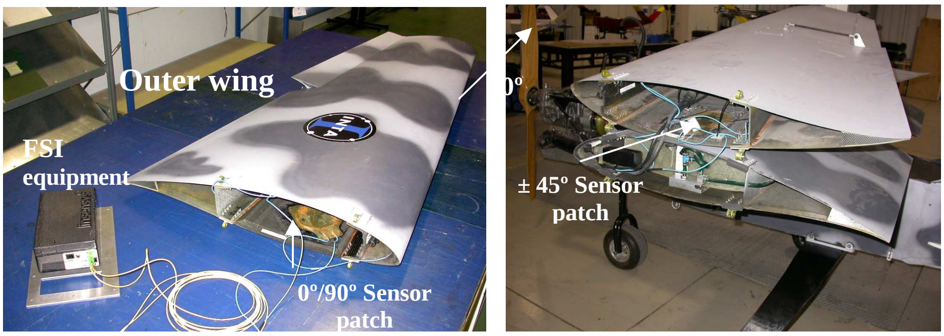

Fig. 2. Left: Outer wing with bonded sensor patches inside the wing on the upper and the lower wing skin and lecture equipment. Right: integrated outer wing.

The data evaluation is performed on ground after flight with the data that are extracted from the SD card. The temperature effect on the strain measurement is compensated with the measurements of the temperature sensors and calibration curves of the temperature sensors and the bonded strain sensor patches that have been measured on ground before the flights in controlled thermal conditions. The temperature compensation is a very important point because the FBGS have the same temperature sensitivity as strain sensitivity and temperature changes can produce more thermal induced strain than the mechanical induced strain due to flight loads.

3. FLIGHT TEST

Flight tests are being actually performed with the integrated monitoring system. The flight tests aim to demonstrate the reliable performance of the equipment, the sensors, their harness and the posterior data evaluation under real in service conditions. The flight test, which is explained in the following paragraph, was a 20 minutes flight with "smooth" flight conditions. The flight test data from the four strain and the two temperature sensors can be seen in Fig. 3. The strain data can be seen on the upper part of the graph corresponding to the left ordinate in microstrain, whilst the temperature data are shown down in the graph and correspond to the left ordinate. The x-axis represents the flight time in 1/10 seconds.

The take off can be seen at about 100 s. The wing is under flexural load and the 0º strain sensor is under compression. The differences between the ± 45º sensors indicate the torsion of the wing. The lower two curves dotted and continue line represent the temperature measurement of the lower and the upper skin respectively. Just before take-off, the temperature of the upper wing skin is about 54ºC due to the intense sunlight, whilst the lower skin, in shadow, is about 46ºC. After take-off, the upper wing cools down faster than the lower one due to the higher air stream. Just after landing, the temperate increases again on the upper skin.

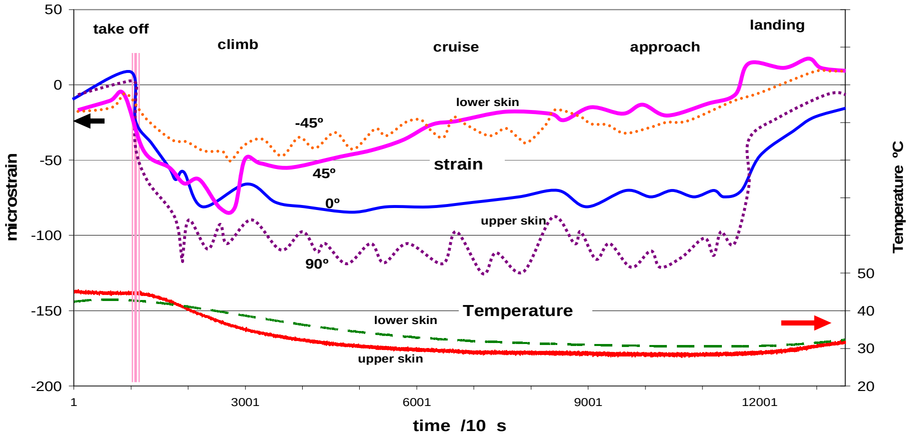

Fig. 3. Flight test data.

The upper skin has suffered a temperature change of more than 20ºC and, due to this, both the thermal induced structural deformations and the wavelength shift due to the thermooptic coefficient of the FBGS, produce a significant apparent strain that needed to be subtracted from the measured total strain value to get the real mechanical strain.

4. CONCLUSIONS

The integrated optical system for strain and temperature measurement showed a satisfying performance in the flight and ground tests. The integrated sensors inside the prefabricated sensor patches and their harness are robust enough to stand the harsh flight environment. The sensor positions in these first trials are not optimal, but the integration of prefabricated patches on the wing skins offered a fast and easy possibility for sensor integration. The integrated temperature sensors enable the necessary temperature compensation of the measured strain data because high temperature changes can be produced in flight and significant temperature gradients occur between the upper and the lower wing skin.

A drawback of the used sensor system is the need to have a distance of 2,5 m between the individual sensors so optical fiber loops are necessary if more than one sensor is needed in one point. The advantage of the integrated system is that it is precise, reliable and ruggidized to stand the flight conditions and enables to measure up to 100 sensors completely autonomous during flight.

ACKNOWLEDGEMENTS

Authors acknowledge the support of the leader of the SIVA project at INTA, Mr. Jaime Cabezas Carrasco, and his team.

REFERENCES

INSENSYS company product information: www.insensys.com
INTA information: http://www.inta.es/programasAltaTecnologia.aspx?Id=1&SubId=3

One single composite for chemical sensor or heating purposes

M. Bouhadid, J. Desbrières, C. Pillon, S. Reynaud
IPREM-EPCP, UMR 5254 (CNRS/UPPA), Hélioparc, 2 avenue du président Angot,
64053 Pau cedex 9, France
N. Redon
Ecole des Mines de Douai, 941 rue Charles Bourseul, BP 10838, 59508 Douai cedex,
France

SUMMARY

The aim of this study was to first optimize the synthesis of a conducting polymer composite. In order to make the process transferable, one step synthesis, aqueous phase dispersion with no use of organic solvent, no post-formulations have been chosen. Tunable formulation was obtained in terms of polymer matrix nature, conducting polymer content, and solid content in order to obtain conducting films with various mechanical and conducting properties.

Sensor and heating surfaces were the target application and both of them have been studied. To do so, the same composite film was studied either in climatic chamber under corrosive gas pollution or as heating soft and stretchable device. Both developments are based on the unique polyaniline properties: pH responsive and resistive.

Both applications have been again developed by keeping in mind future industrial transfer.

INTRODUCTION

The major target of intrinsic conducting polymer (ICP) development is to combine the electrical properties of these materials with the mechanical and processability properties of bulk polymers. Among ICPs, polyaniline (PAni) received a great deal of attention because of its easy preparation with low cost and its stability under environmental atmosphere. Moreover, the electrical conductivity of PAni can be closely controlled over a wide range coming from 10^{-4} to 10 $S.cm^{-1}$ which makes PAni a good candidate for many applications[1-4] as antistatic films, electromagnetic shielding layers, sensors, technical packaging and anticorrosion.

RESULTS AND DISCUSSION

The IPREM-EPCP group focused on the optimization of a simple way of synthesis to yield to a conducting composite in one-step[5,6]. The final aqueous dispersion contains composite particles made of polymer matrix and polyaniline to be used without post formulation. Conducting films are obtained by spaying or automatic film applicator methods. The conductivity and the chemical composition of the final composite may be adapted to the target application.

The same conducting composite was then successfully used as chemical sensor and heating surface. The whole process, *i.e.* from the synthesis to the film forming, remains as simple as possible and is carried out in soft experimental conditions, that is, without external acid or organic solvent.

The study of chemical sensor demonstrated the feasibility of whole polymer sensors to detect ammonia[7,8]. Moreover, all performances of this new chemical sensor are in line with the market needs in terms of response time, sensitivity, reproducibility. At last, these sensors introduced a breakthrough technology since their response is reversible with no need of servicing or calibration between two exposures. This feature is very interesting in terms of time-life and cost.

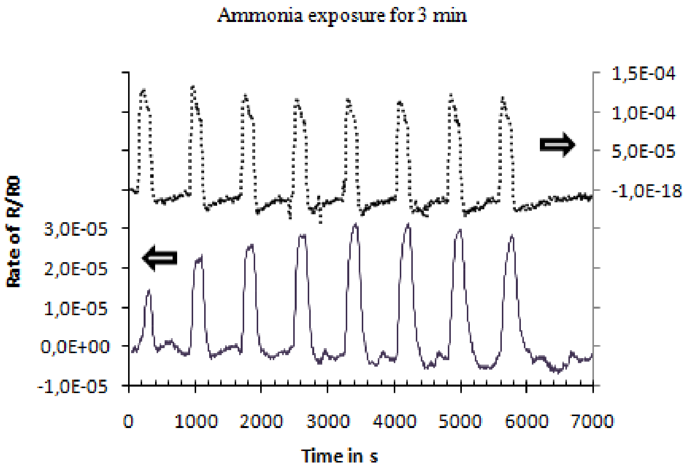

Figure 4. Sensor performances under several exposures to ammonia. Resistance evolution vs. time for composite film containing HCl doped PAni (plain line) et H_3PO_4 doped PAni (dashed line).

The same composite films have been successfully tested as heating surface. The temperature of the films is measured via an Infra-Red camcorder and the results are reported.

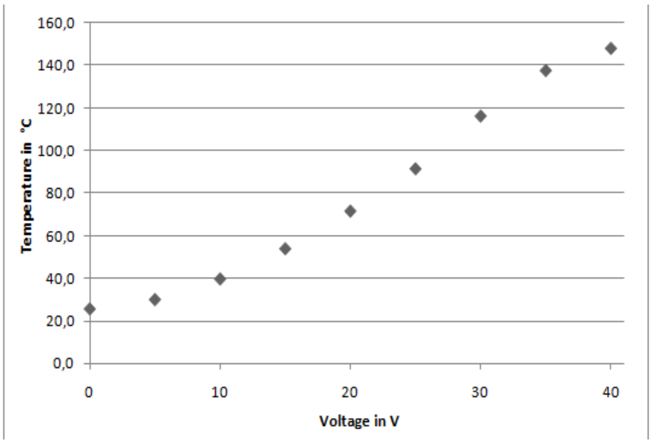

Figure 5. Heating performances of a composite film (50µm) containing HCl doped PAni.

Its heating performances and its processability (soft final material, easy to cut and pattern) allow considering its development as heating devices suitable for low energy building (tunable size, thin film, easy to handle).

REFERENCES

[1]. Stejskal, J.; Trchova, M.; Blinova, N. V.; Konyushenko, E. N.; Reynaud, S.; Prokes, J. Polymer 2008, 49, 180-185.
[2]. Koul, S.; Chandra, R.; Dhawan, S. K. Polymer Guildford 2000, 41, 9305-9310.
[3]. Wessling, B. Synthetic Metals 1998, 93, 143-154.
[4]. Kang, E. T.; Neoh, K. G.; Tan, K. L. Progress in Polymer Science 1998, 23, 277-324.
[5]. Kohut-Svelko, N.; Dinant, F.; Magana, S.; Clisson, G.; François, J.; Dagron-Lartigau, C.; Reynaud, S. Polymer International 2006, 55, 1184-1190.
[6]. Kohut-Svelko, N.; Joubert, M.; Reynaud, S.; FR 05 08172: PCT, 2005.
[7]. Bouhadid, M.; Redon, N.; Plaisance, H.; Desbrières, J.; Reynaud, S. Macromolecular Symposia 2008, 268, 9-13.
[8]. Bouhadid, M.; Thévenot, C.; Ehrenfeld, F.; Redon, N.; Desbrières, J.; Grassl, B.; Reynaud, S. Sensor Letters 2008, 6, 548-557.

Lap shear behavior of carbon fiber/epoxy composite with rivet for aeronautical applications

A.P. da Costa, K.B. Oushiro, G.P. Motta, E.C. Botelho
Depto de Materiais e Tecnologia, Engineering Faculty – São Paulo State University - UNESP, Av. Dr. Ariberto Pereira da Cunha, 333, Guaratinguetá, 12.516-410, Brasil
M.C. Rezende
Divisão de Materiais/AMR, Comando Técnico Aeroespacial - Instituto de Aeronáutica e Espaço (IAE), Avenida Brigadeiro Faria Lima, 1.941, São José dos Campos, 12.227-000, Brasil

SUMMARY

Polymeric composite materials reinforced with continuous fiber have a differential place in aerospace applications as substitute of metallic materials in structural components. Inside of this concept, one of the challenges to practical applications in structural components is the fixing and the joining of polymeric composite structures. In this case, the rivet use to join the composite material usually is better than the composite bonding, because of practice to make the join considering the cure time and the possibility to heat the component to cure the bonding agent in the composite bonding process that can change the structure properties. However, the rivets can originate stress concentration increasing the crack propagation. Another important aspect to practical applications of polymeric composites is the environmental effects that can interfere on the mechanical properties. The present work presents the environmental effect on the mechanical properties in rivet areas of carbon fiber /epoxy composites. The laminates with rivet materials have been supplied by Embraer (Aeronautical Brazilian Company) and they have been submitted to hygrothermal and the UV light conditioning. After the conditioning the specimens have been tested by the lap shear test in order to evaluate the rivet resistance and the fracture propagation. The lap shear results obtained by the conditioned specimens have been compared to the dry specimen's values. The results have shown a relevant change when compared both situations (conditioned and non-conditioned specimens).

1. INTRODUCTION

Polymeric composites have been used in structural components by the aerospace industry due mainly to its search of weight reduction allied to better mechanical properties. Among these materials, the thermoset matrix composites reinforced with tissue fibers are the most commonly used because they are easily processed, they provide a good impregnation of the fiber by the resin and also because they offer good strength, thermal dimensional stability and chemical, electric and solvent resistance (Mazumdar, 2002). The utilization of this material is determined by the joint of thermoset composites, mainly the complexity of this process, and the structural implications on the whole component. The mechanical joint by using rivets is still the most commonly used process, due to the need of disassembly, inspection and repairing of pieces of the components (Gay, et al., 2003). However, the inclusion of rivets and the existence of holes create a state of stress concentration that reduce the resistance to fracture by 40 to 60% of strength and 15% of compression, comparing to structures without hole (Gay, et al., 2003). There are five kinds of failure modes for riveting composites, namely tension, shear-out, bearing, cleavage and pull-out (V.P. Lawlor), and the occurrence of these failure modes depends of material, volumetric fraction and rivets design. The aeronautic composites are designed to fail in bearing or namely tension (V.P. Lawlor). In service, failures of continuous fiber-reinforced composites are commonly attributed to ageing of the material in its particular environment, brought about by a combination of the effects of heat, light, water and mechanical stresses on the material (Botelho, et al., 2005). Several studies have shown the important effects of absorbed water and ageing temperature on the physical and mechanical properties of composite materials. It has been observed that, above a threshold defined for a given temperature and a given ageing time, mechanisms other than simple diffusion can take place within the material (Hough, et al., 2005). Both UV radiation and moisture have adverse effects on the mechanical properties of polymeric matrix, while the ceramic continuous fibers are not affected significantly by either environment. The polymer matrix in a fiber-reinforced composite serves to transfer applied loads to the reinforcing fibers and provide interlaminar shear strength, whereas the fiber-matrix interface governs the load transfer characteristics and damage tolerance. Thus, both these components represent weak links in fiber-reinforced composites and upon degradation, lead to reduced damage tolerance, and thus, lack of long-term durability (Tarnopol'skii, et al., 1999). The objective of this paper is to evaluate the influence of hygrothermal and UV light conditioning on the lap shear properties of the riveted thermoset composites. The material was submitted to the conditioning in a hygrothermic chamber and UV light emission chamber, and then submitted to the lap shear test method. The results of the material under conditioning were then compared to the non-conditioned one.

1. EXPERIMENTAL PROCEDURE

Carbon fiber/epoxy specimens riveted in the double-fastener test mode were machined and donated by EMBRAER.The specimens were conditioned in the UV chamber for nearly 800 hours. The degradation mechanisms caused by UV radiation were determined in conformity with ASTM G154 standard to test methodology for QUV/Se weathering chamber (Q-Panel Lab Products, Cleveland, Ohio). According to this standard, damages caused by sunlight, rain and dew was reproduced by cycles of period of eight hours under UV-B light and eight hours under water condensation provided by the generation of vapor from a water bath. For the hygrothermic conditioning, the specimens were firstly dried in vacuum oven at 60ºC for at least 24 hours before testing. After this procedure, the specimens were weighed and conditioned in the hygrothermic chamber at the temperature of 80ºC and 90% moisture. The conditions selected to saturate the specimens were based on Procedure B of ASTM Standard D 5229 M-92 During this test, the moisture level in the laminates was periodically monitored until the moisture equilibrium state reached a plateau. The material was weighed every three-day period.The conditioned specimens were tested with the Lap shear test methodology of the ASTM D 5861-08 standart, in order to evaluate the influence of different environmental conditionings on the damage tolerance of the riveted material.Before and after the mechanical tests, the laminates were submitted to ultrasound analysis to the morphological evaluation. With this objective was used a ultrasonic inspection instrument (Matec system MU1532) by echo pulse method with 10 MHz and a concave transducer.

2. RESULTS AND DISCUSSION

Figure 1. (a) shows the absorption of moisture retained in the conditioned material after 2 months inside the climatic chamber. The graphic shows that the material absorbed around 0,37% of moisture in this 2 months of conditioning. The absorption process goes on until reaching a pseudo-equilibrium state, after 800 hours, which is a characteristic of the absorption behavior, according to Fick´s diffusion law. This happened easily because of the capillarity provided by the presence of micro-cavity in the structure of the material. After this process, the absorption became slower, due to process of the polymeric chains relaxation and to a void filling process.


(a) (b)

Figure 1 (a) Absorption of moisture of the composite in hygrothermal chamber; (b) Loss of weight by UV light degradation.

Figure 1 (b) also shows the loss of material (around 0,15%) occurred due to a degradation process when it is exposed to UV conditioning. The degradation process happens due to the combined effects of UV radiation and water condensation. UV radiation causes a superficial chemical change of the epoxy and the following water condensation removes the damaged superficial layer and a new layer gets exposed to the UV degradation, creating a cyclic exposition that damages the material after each process. Besides, the presence of UV light might break the water molecule and cause the liberation of free radicals OH- and H+ that contribute to the degradation process of the surface of the material.

Table 1 shows the maximum strength results of the riveted laminates, tested by the lap shear method in dry environment and in materials exposed to hygrothermic and UV conditioning. The results show a degradation of the conditioned specimens properties, comparing to the non-conditioned specimens. According to this Table can be observed a decrease of 3% for the conditioned material in hygrothermal chamber and 5% in ultraviolet light chamber. The reduction of mechanical properties after the hygrothermal conditioning can be explained by the action of moisture and temperature in the fiber matrix interface and the polymer matrix.

Table 1. Mechanical properties to joint carbon fiber/epoxy laminates.

Environmental conditioning	Lap shear stress
Dry specimens	140.41 ±5.9
UV conditioning	136.06 ±3.1
Hygrothermal conditioning	132.62 ±6.7

In the UV chamber, the cyclic process of exposing the material to radiation and to water condensation cause matrix erosion, voids and detachment of the fiber-matrix and microcracks in the epoxy matrix, damaging its structure. Once this is not a catastrophic failure mode, it is not possible to obtain a significant microscopic evaluation of material failures, because any try to remove the rivets would lead to a destruction of the characteristics failures of the material. In this case, the ultrasound was used to provide a better perception of the region affected by the tests performed.

Figure 2 (a) and (b) presents the ultrasound images, comparing no tested and tested specimens by lap shear test. Figure 2 (a) shows the riveting laminate configuration. It can be observed the two rivet that bonding the laminates piece. Figure 2 (b) shows the affected area by bearing failure mode verified in conditioned and non conditioned specimens. This kind of failure is not-catastrophic and occur because of compression in the holes and crushing strength.

Figure 6. Ultrasound images of riveting in no tested (a) and tested (b) laminates carbon fiber/epoxy.

3. CONCLUSION

The influence of hygrothermal conditionings and UV light in riveting strength of carbon fiber/epoxy composites has been investigated. In this work, it was observed that this laminate absorbed 0.37% of moisture after the saturation point, when submitted to hygrothermal conditioning and loss 0.15% of weight mass in the UV light conditioning. For all specimens studied the lap-shear values decrease when exposed to environment conditioning. It is because the humidity associated with the temperature induces resin plasticization and, consequently, reduces strength values of the laminates. In this work also could be observed that the UV light radiation cause the matrix degradation due to the photo-oxidation and all laminates (conditioned and no conditioned) exhibit a similar bearing mode after the shear test.

4. ACKNOWLEDGEMENTS

The authors acknowledge the financial support received from FAPESP and CNPq and the assistance with the ultrasound analysis from Dr. Maria Odila H. Cioffi and Mr. Marcos Y. Shiino.

5. REFERENCES

Botelho E. C., Pardin L. C. and Rezende M. C. Hygrothermal Effects on Damping Behavior of Metal/Glass Fiber/Epoxy Hybrid Composites [Article] // Materials Science and Engineering A. - 2005. - Vol. 399.

Shear flow evaluation in composite thin-walled blades

J.C. Marín, G. Fernandes da Silva
Group of Elasticity and Strength of Materials, School of Engineering, University of Seville. Camino de los Descubrimientos s/n, 41092 Seville, Spain.

ABSTRACT

The present work addresses the evaluation of the shear flow as an extension of the Jourawski's formula. This idea is developed here for the case of multi-celled composite thin-walled section. First it will obtain the explicit formulation of the shear flow due to shear forces and torsion, noting the simplifications adopted. Then the obtained model is verified by means of a problem with analytical solution known. Finally, this model will be applied to the evaluation of the shear flow on an actual configuration of a blade, comparing the results with those of a Finite Element model of the same blade, with a similar discretization.

1. INTRODUCTION

In literature we can find many works devoted to anisotropic thin-walled beam models. The common object of this works is the displacements evaluation. They are rigorous theories with the following basic assumptions: kinematic assumptions consistent with the Timoshenko beam theory, use of Classical Lamination Theory (CLT) to account for the different stiffness of each laminate, and consideration that cross section divides in segments corresponding to the different laminates.

The structural design of wind turbine blades usually takes as a starting point the configuration of the outer surface defined by the aerodynamic design, analysing the elastic problem uncoupled. Therefore the knowledge of approximate displacements (axis displacement, and rotation of section) can be sufficient. Conversely, knowledge of stress and strain, at all points of the section, is essential for an accurate blade design.

Following the basic assumptions above mentioned, Paluch (1993) developed an explicit formulation for the longitudinal normal strain and stress. Cañas et al. (1999) carry out a comparison between stress results calculated by this model and by a Finite Element (FE) model with similar discretization. Taking into account the good agreement shown by the model in the calculation of normal longitudinal stresses, the present work addresses the evaluation of the shear flow as an extension of the Jourawski's formula. This idea, suggested by Massa and Barbero (1998) is developed here for the case of multi-celled composite thin-walled section. First it will obtain the explicit formulation of the shear flow due to shear forces and torsion, noting the simplifications adopted. Then the obtained model is verified by means of a problem with analytical solution known. Finally, this Strength of Material (SM) model will be applied to the evaluation of the shear flow on an actual configuration of a blade, comparing the results with those of a FE model of the same blade, with a similar discretization.

2. SHEAR FLOW EVALUATION

Consider a slice, from a composite laminate thin-walled beam, of size dx along the beam direction, thickness e(s) and distance s along the shape of the cross-section. Now, let us consider a portion of this slice with cross-sectional area A^*. The forces acting on this element have been represented in figure 1. Therefore, we can derive an equilibrium equation:

$$q_c(s).dx - q_c(0).dx + F_\sigma + \frac{\partial F_\sigma}{\partial x}dx - F_\sigma = 0 \quad \Rightarrow \quad q_c(s) = q_c(0) - \frac{\partial F_\sigma}{\partial x} \tag{1}$$

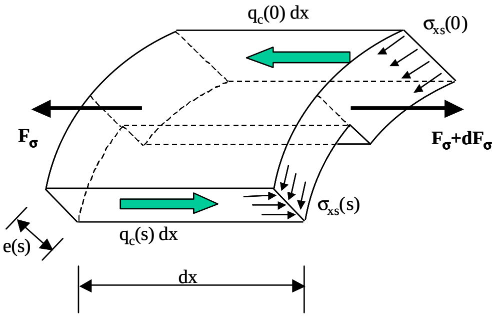

Fig. 1. Force equilibrium diagram.

where q_c is the shear flow (summation of σ_{xs} on the thickness), and F_σ is the resultant normal force in the area A^*. Mathematically, both variables can be expressed as:

$$q_c(s) = \int_{e(s)} \sigma_{xs}(x,s)\cdot de \quad ; \quad F_\sigma = \int_{A^*(s)} \sigma_x(x,y,z)\cdot dA \tag{2}$$

Expression (1) indicates that the total shear flow q_c is composed by two terms, $q_c(0)$ and the derivative of F_σ. The first term $q_c(0)$ for a typical blade cross-section represent the closed section shear flow, and the last term correspond to the open section shear flow.

2.1 Open section shear flow

The derivative of F_σ can be evaluated in a discrete manner taking into account the stress discontinuity between the different laminates present in area A*. The number of elements included in this area A* has been denoted by n*.

$$\begin{aligned}\frac{\partial F_\sigma}{\partial x} &= \left(-\frac{P_x}{E.A}\right)\sum_{i=1}^{n^*} E_i A_i + \\ &+ \frac{1}{k_{yz}}\left[\left(V_z.\sum_{i=1}^{N} E_i.I_{yzi} - V_y.\sum_{i=1}^{N} E_i.I_{yyi}\right).\sum_{i=1}^{n*} E_i.m_{zi} + \left(V_y.\sum_{i=1}^{N} E_i.I_{yzi} - V_z.\sum_{i=1}^{N} E_i.I_{zzi}\right).\sum_{i=1}^{n*} E_i.m_{yi}\right]\end{aligned} \tag{3}$$

where V_y and V_z are the resultant shear forces in section, and EA, k_{yz} is defined by:

$$E\cdot A=\sum_{i=1}^{n}E_i\cdot A_i \qquad k_{yz}=\left(\sum_{i=1}^{n}E_i\cdot I_{yzi}\right)^2-\sum_{i=1}^{n}E_i\cdot I_{yyi}\cdot\sum_{i=1}^{n}E_i\cdot I_{zzi} \tag{4}$$

Following the generalized assumption made for isotropic beams, that the term associated with the distribution of axial load P_x is negligible, the first term of the equation (3) is ignored.

2.2 Closed section shear flow

Considering an arbitrary multi-cell thin-walled section, the requirement of single-valued displacement for an anisotropic beam cross-section is defined by:

$$\int_0^S \gamma_{xs}^{o}\,ds=\int_0^S\left(\left[a_{31}^{-1}\right]N_x+\left[a_{33}^{-1}\right]N_{xy}\right)ds\cong\int_0^S\left[a_{33}^{-1}\right]\cdot q_c(s)ds=\int_0^S\frac{q_c(s)}{G_{xs}(s)e(s)}ds=0 \tag{5}$$

In the above equation we have assumed that the coupling of the normal and tangential flows (that appear according to CLT) will not be taken into account in order to simplify the formulation. Therefore, the term with the normal flow was ignored as an initial approximation. In the same way as for the closed section shear flow due to shear forces, it is possible to derive an expression for the shear flow induced by the torsion for a beam made of a composite laminate material i.e. an anisotropic section.

3. MODEL VERIFICATION

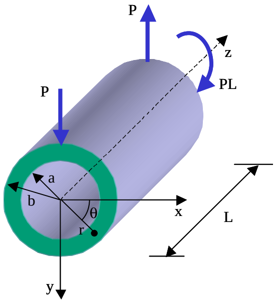

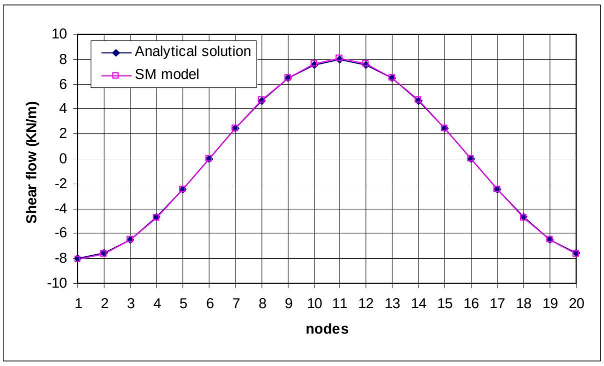

Fig. 2. Verification problem. Fig. 3. Comparison of the shear flow distributions.

As a verification of the developed model, the results for a problem with analytical solution (Lekhnitskii 1981) has been compared. Consider a solid in the form of a hollow cylinder whose material possesses cylindrical orthotropy, subjected to a vertical shear force at one end and a vertical shear force and bending moment at the other end, as is shown in figure 2. The comparison between the model results and the analytical solution are represented in figure 3, showing a good agreement.

4. ANALYSIS OF A BLADE CONFIGURATION

As object for application of the developed SM model an actual blade configuration (from Marin et al. (2008)) has been considered. This configuration has been chosen because we have a FE model for such a blade, which was verified by experimental measurements (Cañas et al. 1999). The results of this FE model will be compared with the results of SM model. As can be seen in figure 4, both models present similar variation and magnitude, although the maximum values of the SM model are higher than those of the FE model.

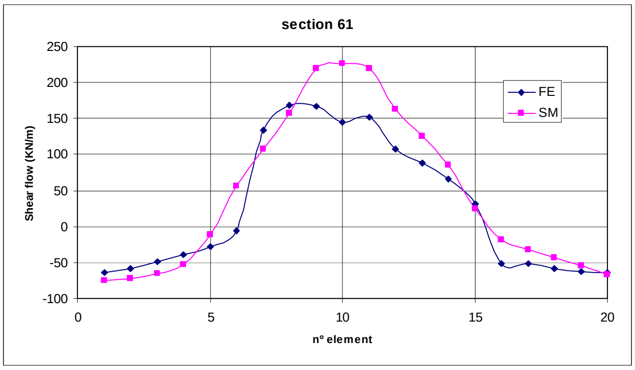

Fig. 4. Shear flow distribution for section 61.

5. CONCLUSIONS

An explicit formulation of the shear flow in a thin walled laminate composite beam of multi-celled cross-section was developed. This formulation was verified by means of a problem with analytical solution known. As an application the SM model was used for the analysis of an actual blade configuration. For comparison purpose the same blade was analysed by a FE model. The results show that both model present similar variation and magnitude.

REFERENCES

PALUCH, B. (1993) A software for design and calculation of wind turbine composite rotor blades, *European Community Wind Energy Conf.*, 8-12 March, 559-562.

CAÑAS, J., MARIN, J.C., BARROSO, A., PARIS, F. (1999) Sobre el uso de modelos de resistencia de materiales y modelos de elementos finitos en el diseño de palas de aerogenerador, *Proceeding of MATCOMP-99, Benalmádena, Spain*, 271-278.

MASSA, J.C. and BARBERO, E.J. (1998) A strength of materials formulation for thin walled composite beams with torsion, *Journal of Composite Materials*, 32(17), 1560-1594.

LEKHNITSKII, S.G. (1981) Theory of Elasticity of an Anisotropic Body, Mir Publishers, Moscú, URSS.

MARIN, J.C., BARROSO, A., PARIS, F., CAÑAS, J. (2008) Study of damage and repair of blades of a 300 kW wind turbine, *Energy*, 33(7), 1068-1083.

Thermal ageing kinetics of PETI 330

M. Ratsimbazafy, G. Minard, X. Colin
ARTS ET METIERS ParisTech, LIM, 151 Boulevard de l'Hôpital, 75013 Paris, France
B. Laine, D. Lévêque
ONERA, DMSC, BP 72, 29 avenue de la Division Leclerc,
92322 Châtillon, Cedex, France

SUMMARY

Thermal ageing of thin films (typically 100 µm thick) of neat polyimide matrix PETI 330 has been evaluated by IR spectrophotometry and gravimetry at 320, 340, 360 and 380°C in various atmospheres (nitrogen, atmospheric air and pure oxygen). As expected, at such levels of temperature, thermal oxidation is the main degradation process, leading rapidly to strong mass losses. However, a thermolysis also proceeds, leading to smaller, but significant, mass losses in the absence of oxygen. A non empirical kinetic model has been derived from a radical chain oxidation mechanism, initiated by the thermal decomposition of both hydroperoxides and the weakest C−C covalent bonds of polymer network, in order to tentatively predict these mass changes. It is found a satisfying agreement between theory and experiment.

1. INTRODUCTION

Europe has a significant delay in the field composite materials dedicated to aeronautic and space applications at moderate temperature (typically between 250 and 700°C). Indeed, organic matrix composite structures are currently used at low temperature but rarely beyond 250°C, because of their low temperature resistance, whereas ceramic and metallic ones are used at significantly higher temperatures, typically beyond 700°C. In US, in the early 1970's, the Lewis Research Centre of NASA developed a family of thermosetting polyimides called "Polymerization of Monomer Reactants" (PMR) (Serafini et al. 1972) to tentatively fill this gap. But, the dangerousness of one of its constitutive monomers (the 4,4'-methylene dianiline (MDA)) was a major obstacle for its commercialisation. In the early 1990s, the Langley Research Centre of NASA proposed an alternative to PMR resins (Hergenrother et al. 1994): the "Phenyl Ethynyl Terminated Imid" (PETI) resins would present a wider processing window (Lincoln et al. 2001) and higher ultimate mechanical properties than PMR (Bryant et al. 1996). Today, the PETI resins appear as serious candidates for the production, at low cost, of light and high mechanical performance composite structures dedicated to aeronautic and space applications up to temperatures of about 300°C. However, these latter will be used by airline companies only if their long-term durability is clearly demonstrated.

The present communication is devoted to the study of thermal oxidative ageing of a PETI 330 polyimide network.

2. EXPERIMENTAL

2.1 Materials

The PETI 330 powder was supplied by UBE Industries. It is a linear oligoimide of low molar mass (2500 g.mol^{-1}) resulting from the reaction of three monomers: 2,3,3',4'-biphenyl tetracarboxylic dianhydride (a-BPDA), 4-phenylethynylphthatic anhydride (4-

PEPA) and 4,4’ oxydianiline (ODA). It is terminated by reactive phenylethynyl groups, of which the crosslinking between 300 and 350°C (according to a complex two-step reaction) would lead successively to polydienic sequences (Takeichi et al. 1980) and then, to aliphatic polycyclic structures (Fang et al. 1998).

Thin PETI 330 films of about 100 µm thick were obtained by press moulding at 320°C during 4 hours. The mould was kept open during the first 20 minutes, in order to enable the removal of eventual volatile products (air bubbles, sorbed water, etc …), and then closed and maintained under a pressure of 40 bars until the end of the moulding operation. Then, films were post-cured at 350°C during 16 hours under primary vacuum in order to reach the maximum crosslinking density (see Fig. 1) while taking care to prevent any polymer pre-oxidation before thermal ageing.

All the samples were characterized by Differential Scanning Calorimetry at a 20°C/min heating rate in nitrogen prior to testing. Their glass transition temperature T_g is close to 350°C.

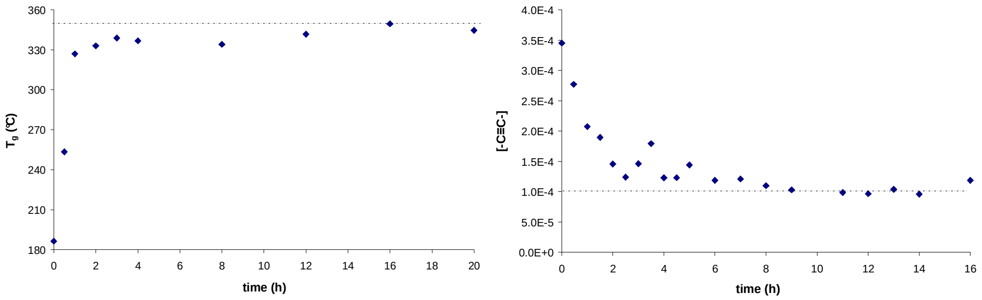

Fig. 1. Determination of optimum post-curing conditions by IR spectrophotometry (left) and differential calorimetry (right).

2.2 Test methods

All the films were stored in the dry atmosphere of a desiccator prior to testing.

Some of them were subjected to isothermal exposure at 320, 340, 360 and 380°C in air-circulating ovens and were removed intermittently to be examined by a Brucker IFS 28 IR spectrophotometer, of minimal resolution of 4 cm^{-1}, in a transmission mode. A peculiar attention was paid on two changes of IR spectra: the consumption of triple bonds, at 2215−2220 cm^{-1}, resulting from the continuation of post-cure reactions, and the build-up of hydroxyl groups, at 3400–3600 cm^{-1}, coming from polymer oxidation. Unfortunately, the initial presence of strong absorption bands of imide groups, at 1650–1800 cm^{-1}, did not permit the detection of carbonyl groups.

Other films were placed on the plateau of a TA Instruments TGA Q500 microbalance and exposed at 320, 340, 360 and 380°C in nitrogen or pure oxygen. Gravimetric curves were recorded continuously versus exposure time.

3. RESULTS AND DISCUSSION

3.1 Analysis of degradation mechanisms

IR analyses reveal that, in air, thermal oxidation starts from the beginning of exposure whatever the temperature under study. On the contrary, there is no evidence of an eventual continuation of post-cure reactions since the concentration of triple bonds remains constant during all the exposure.

Thermal oxidation leads rapidly to strong mass losses, as shown in Figure 2. No doubt, the main part of volatile compounds comes from the thermal decomposition of the main propagation product of the radical chain oxidation mechanism: the hydroperoxide groups. But, the fact that, in absence of oxygen, a smaller, but significant mass loss is detected, suggests that there are other sources of volatile compounds.

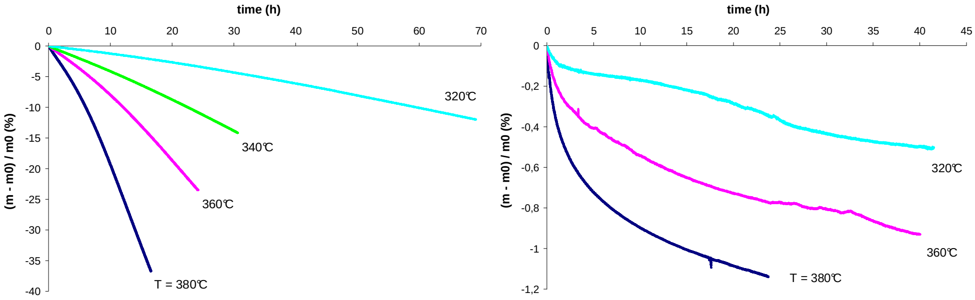

Fig. 2. Mass changes of PETI 330 between 320 and 380°C in pure oxygen (left) and in nitrogen (right).

Looking at the theoretical structure of the fully crosslinked network, one can remark that aliphatic polycyclic structures are essentially composed of tetrasubstituted carbon atoms. The corresponding C−C covalent bonds present a relatively low dissociation energy (typically 300 $kJ.mol^{-1}$, against more than 330 $kJ.mol^{-1}$ for other aliphatic C−C bonds). One can thus suspect that they decompose easily in the temperature range under study. The resulting tertiary radicals are also very unstable. Their rearrangement by β scission can lead to volatile compounds, for instance benzene molecules. This assumption is under investigation at the laboratory: real time analyses of volatile compounds are being performed using ionization Fourier transform Ion Cyclotron Resonance Mass Spectrometry (Sarrabi et al. 2009).

3.2 Kinetic modelling of mass changes

Finally, the following mechanistic scheme has been chosen to describe the general trends of the thermal oxidation kinetics of PETI 330:

0) $PP \rightarrow 2P° + 2\alpha\varphi$ (k_0)
I) $POOH \rightarrow 2P° + H_2O + \upsilon V$ (k_1)
II) $P° + O_2 \rightarrow PO_2°$ (k_2)
III) $PO_2° + PH \rightarrow POOH + P°$ (k_3)
IV) $P° + P° \rightarrow$ inactive products (k_4)
V) $P° + PO_2° \rightarrow$ inactive products (k_5)
VI) $PO_2° + PO_2° \rightarrow$ inactive products $+ O_2$ (k_6)

The main characteristics of this scheme is that it involves two distinct initiations: the thermal decomposition of hydroperoxides (I) leading to an average volatile molecule (noted V, formed with a yield υ, of molar mass M_V) voluntary distinguished from water; and the thermal decomposition of the weakest C−C covalent bonds of polymer network leading to benzene molecules (noted φ, formed with a yield α, of molar mass M_φ).

A system of differential equations (SED) has been derived from this scheme. Remarking that the concentrations of the main reactive species ([POOH], [P°] and [PO_2°]) varies proportionally during exposure, it has been possible to solve the SED without making the classical simplifying assumptions (steady state, long kinetic chain or even, the existence of an interrelationship between termination rate constants).

Then, mass changes can be determined from a balance equation between weight gain due to oxygen consumption and weight loss due to volatile emission:

$$\frac{\Delta m}{m_0} = v_{\infty 1}\left[t - \frac{4}{k_1}\left(1 - \exp - \frac{k_1 t}{2}\right) + \frac{1}{k_1}\left(1 - \exp - k_1 t\right)\right] + v_{\infty 2} t \qquad (1)$$

where $v_{\infty 1}$ and $v_{\infty 2}$ are the maximum mass loss rates (in steady state) for thermal oxidation and thermolysis respectively, which express in function of the different rate constants of the previous mechanistic scheme, oxygen concentration and initial substrate concentrations ([PH] and [PP]).

Such a non empirical model has been used to tentatively simulate the mass changes during the whole course of thermal oxidation. A satisfying agreement has been obtained between theory and experiment whatever the temperature under study. As an example, the simulation obtained at 380°C is reported in Figure 3.

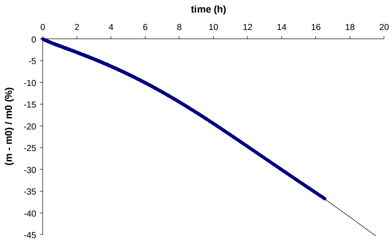

Fig. 3. Comparison between simulation (thin line) and experimental data (thick line) at 380°C in pure oxygen.

4. CONCLUSION

A non empirical kinetic model has been elaborated to describe the thermal ageing of PETI 330 in the absence and the absence of oxygen. It is derived from a realistic mechanistic scheme of which some elementary reactions are being checked at the laboratory yet. However, the satisfying agreement obtained between theory and experimental data indicates clearly all the merits of such an approach.

REFERENCES

BRYANT, R.G., JENSEN, B.J., HERGENROTHER, P.M. (1996) *J. Appl. Polym. Sci.*, 59, 1249-1254.

FANG, X., ROGERS, D.F., SCOLA, D.A., STEVENS, M.P. (1998) *J. Polym. Sci.: Part A: Polym. Chem.*, 36, 461.

HERGENROTHER, P.M., SMITH, J.G. (1994) *Polymer*, 35, 4857-4864.

LINCOLN, J.E., MORGAN, R.J., SHIN, E.E. (2001) *J. Polym. Sci.: Part B: Polym. Phys.*, 39, 2947-2959.

SARRABI, S., COLIN, X., TCHARKHTCHI, A., HENINGER, M., LEPROVOST, J., MESTDAGH, H. (2009) *Anal. Chem.*, in press.

SERAFINI, T.T., DELVIGS, P., LIGHTSEY, G.R. (1972) *J. Appl. Polym. Sci.*, 16, 905-915.

TAKEICHI, T., STILLE, J. (1980) *Macromolecules*, 19, 2103.

Determinación del comportamiento a tracción de sensores de fibra óptica libres y embebidos en material compuesto en el rango de temperaturas entre -150ºC y 160ºC para aplicaciones aeroespaciales

C. Moravec, C. Gutiérrez, M. Frövel, J.G. Carrión
INTA (Instituto Nacional de Técnica Aeroespacial “Esteban Terradas”), Área de Materiales Compuestos; Crta. Ajalvir, P.K. 4; 28850 Torrejón de Ardoz (Madrid, España)

RESUMEN

Con el objetivo de estudiar el comportamiento a tracción de sensores de fibra óptica tipo red de Bragg (FBGS) en el rango de temperaturas entre -150ºC y +160ºC, se han determinado los factores de conversión K(T) para dos tipos distintos de fibras ópticas: unas con recubrimiento acrílico (AC) y otras de poliimida (PI), comprobando, además, si el recubrimiento afecta al valor de K(T). Para ello se ha realizado una preparación previa de las fibras ópticas que poseen grabado el sensor, acondicionándolas para llevar a cabo las medidas ópticas y mecánicas.

Una vez preparadas las fibras, se han realizado los ensayos de las fibras libres para tomar los valores de las mismas como datos de partida en los ensayos de las fibras embebidas en probetas de material compuesto, a modo de calibración de los sensores antes su integración. Posteriormente, con los mismos sensores dentro de los laminados curados de material compuesto, se han efectuado ensayos de tracción, comprobando las lecturas de los sensores a medida que se introducía deformación mecánica.

Finalmente, con los datos obtenidos en ambos casos (sensor libre y embebido), se han calculado los coeficientes de conversión K(T) y se ha efectuado una comparación de los resultados obtenidos, encontrándose que la dependencia, medida mediante K(T), entre el esfuerzo mecánico aplicado y la respuesta óptica con la temperatura, es distinta entre sensores libres y embebidos. En cuanto a la influencia del tipo de recubrimiento, se ha observado que el uso de poliimida da lugar a una mayor sensibilidad con la temperatura.

1. INTRODUCCIÓN

Los sensores FBGS permiten relacionar un fenómeno de tipo óptico con deformaciones de carácter mecánico, por lo que poseen una clara aplicabilidad en la monitorización de deformaciones en sistemas estructurales. Del estudio en profundidad del comportamiento de estos sensores se puede determinar el parámetro del sensor óptico de mayor importancia para dicha aplicación, como es la sensibilidad opto-mecánica del sensor, K(T), también denominado coeficiente de conversión, que transforma resultados ópticos en resultados de deformación mecánica (pm/$\mu\varepsilon$) y que depende de la temperatura, puesto que la variación en la longitud de onda del FBGS puede deberse a la acción conjunta de la temperatura y la carga mecánica actuando sobre la fibra.

Los sensores de fibra óptica basados en la ley de difracción de Bragg son, por sus características, los sensores de deformación mas idóneos para la extensometría en materiales compuestos, con los que se fabrican numerosas estructuras aeroespaciales, presentando una serie de ventajas frente a las galgas extensométricas, como la

multiplexación de sensores, reduciendo el cableado de la red sensora, la estabilidad temporal de la medida o su inmunidad a las interferencias electromagnéticas. En el caso de los materiales compuestos, es posible embeber los sensores de manera sencilla durante el proceso de fabricación, debido a su reducido tamaño, creando redes sensoras integradas en la propia estructura fabricada.
La mayor aportación del estudio realizado reside en que se ha ampliado notablemente la caracterización de este tipo de sensores en el rango de temperaturas de aplicación, obteniéndose una determinación mas fiable del coeficiente de conversión K(T) que transforma una señal óptica en un valor mecánico. Por otra parte, es la primera vez que se caracteriza el mismo sensor, primero libre y luego embebido en material compuesto, permitiendo constatar las diferencias de comportamiento.

2. METODOLOGÍA

Para la realización de los ensayos con los FBGS libres se diseñó y fabricó un dispositivo experimental, constituido por un tubo cilíndrico fabricado de material compuesto con orientación longitudinal (0º) y reforzado en la parte exterior con tiras a ± 45ºC. Se fabricó, igualmente, una tapa que fijaba la fibra al extremo inferior del dispositivo y, finalmente, el tubo se unió a una mesa, anexa a un tornillo micrométrico, con el que se realizaron las deformaciones de la fibra libre de manera controlada.

Fig. 1. Dispositivo diseñado para realizar los ensayos con fibras libres.

Tras el acondicionamiento de las fibras libres, se iniciaron los ensayos de deformación mecánica a diferentes temperaturas utilizando el dispositivo descrito. Mientras se producía la deformación de manera controlada, se obtuvieron los datos de variación de longitud de onda de los sensores, lo que permitió, con posterioridad, la determinación de K(T) para cada uno de los casos.

Finalizados los ensayos con los FBGS libres, se embebieron los sensores en un laminado de material compuesto cuya secuencia de apilamiento fue $[0_8/FO/0_8]$. Tras el curado del laminado y la obtención de las probetas necesarias, se llevaron a cabo los ensayos de tracción a diversas temperaturas, obteniéndose directamente los valores de K(T) en cada caso.

3. RESULTADOS

Una vez finalizados los ensayos, la evaluación de los datos obtenidos para la determinación de K(T) ha permitido comparar los valores obtenidos entre sensores libres y embebidos. La Figura 1 muestra agrupados todos los valores comparados.

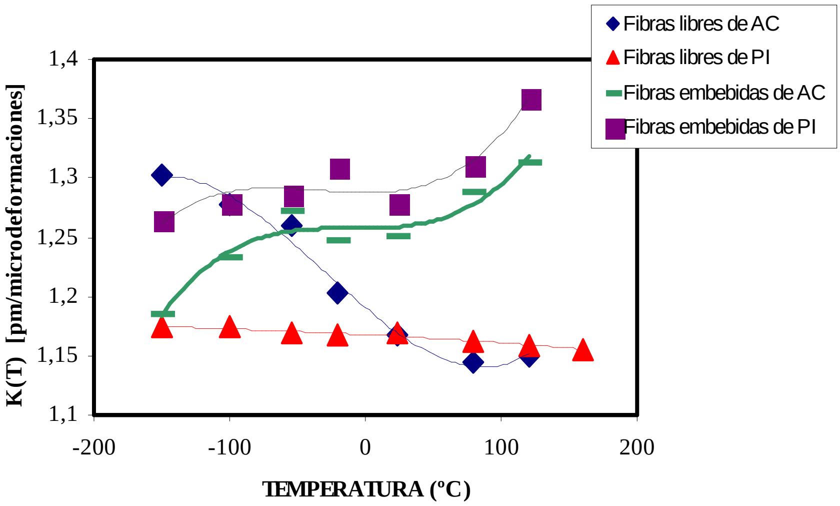

Fig. 1. Variación de K(T) con la temperatura para fibras de acrílico y poliimida.

3.1 Determinación de K(T) para los sensores en fibras libres

Con los datos medidos de variación de longitud de onda y conociendo la deformación introducida en cada caso, el coeficiente K(T) se dedujo de la pendiente de las rectas que se originan de acuerdo con la expresión (1)

$$\frac{\Delta\lambda}{\varepsilon} = \lambda_{B0} \cdot \left(1 - p_{eff}\right) = K\left(T\right)\left[\frac{pm}{\mu\varepsilon}\right] \qquad (1)$$

3.2 Determinación de K(T) para los sensores en fibras embebidas en material compuesto

En este caso, de cada ensayo de tracción, se obtuvieron directamente las gráficas □□ frente a □, de cuyas pendientes se extrajeron los valores de K(T), para cada tipo de recubrimiento y temperatura de ensayo.

3.3 Variación de K(T) comparando fibras libres y embebidas con los distintos recubrimientos.

Para las fibras libres la tendencia general es de disminución de K(T) con la temperatura, mientras que cuando las fibras se encuentran embebidas en material compuesto se produce un aumento de K(T) con la temperatura.

Con respecto al tipo de recubrimiento, para los sensores en estado libre, la variación de K(T) en las fibras de acrílico es mucho más pronunciada que para las fibras de poliimida. Sin embargo, cuando las fibras están integradas en el material compuesto, el comportamiento es muy similar.

4. CONCLUSIONES

Se ha constatado que el coeficiente de conversión K, que relaciona en los FBGS el desplazamiento de longitudes de onda con deformaciones mecánicas, depende de la temperatura, debiendo expresarse como K(T). La dependencia con la temperatura es distinta si los sensores están en estado libre o se encuentran embebidos en láminas de material compuesto.

En los valores de K(T) obtenidos con sensores en fibras libres, se ha observado una respuesta muy diferente entre los usados con recubrimiento acrílico y los que poseen recubrimiento de poliimida. Para los sensores embebidos, los valores de K(T) muestran un comportamiento muy similar para ambos tipos de recubrimiento.

El comportamiento de los sensores embebidos en el material compuesto, si bien muestra una tendencia global a crecer con la temperatura, resulta ser prácticamente lineal para el rango de temperaturas entre -100ºC y +50ºC.

Se comprueba que no es riguroso adoptar el valor de K(T) del sensor libre y aplicarlo cuando está embebido, ya que el comportamiento con la temperatura es claramente dispar. Esto implica realizar siempre una “calibración” del sensor con la temperatura.

REFERENCIAS

FRÖVEL, M., BARÁIBAR, I., PINTADO, J.M., STELZL, D., GÜEMES, A. (2005) Performance evaluation of fiber Bragg gratings over a large temperature range, 5th International workshop on Structural Health Monitoring, 5th IWSHM, Stanford, CA, USA.

FRÖVEL, M. (2006) Sensores de Fibra Óptica tipo redes de Bragg embebidos en material compuesto para medir deformaciones y temperaturas criogénicas. Tesis Doctoral. Escuela Técnica Superior de Ingenieros Aeronáuticos, Universidad Politécnica de Madrid.

MANFRED KREUZER. (2007) Strain Measurement with Fiber Bragg Grating Sensors; Technical Articles, HBM, Darmstadt, Alemania, 2007.

O´DWYER, M., YE CHEN-CHUN, JAMES, S.W., TATAM, R. (2004) Thermal dependence of the strain response of optical fiber Bragg gratings, Measurement Science and Technology 15, pp1607-1613, Institute of Physics Publising Ltd, UK.

Comportamiento a fatiga de reparaciones de estructuras aeronáuticas mediante adhesión de parches de material compuesto

J. Sierra
Grupo de Investigación en Ingenieria Aeroespacial GIIA. Universidad Pontificia Bolivariana, Colombia
A. Güemes
Departamento de Materiales y Producción Aeroespacial. Universidad Politécnica de Madrid, España

RESUMEN

Se realizó un análisis experimental apoyado de validación numérica con el código AFGROW de la Fuerza Aérea Norteamericana para estudiar el comportamiento a fatiga de reparaciones de estructuras metálicas mediante la adhesión de parches de material compuesto. El análisis experimental incluyó ensayos de fatiga en probetas entalladas y pre-agrietadas provistas y desprovistas de reparación. Se encontró que para el caso de los especímenes pre-agrietados, la vida esperada incrementa hasta 32.7 veces. Los resultados experimentales se ajustan en gran medida a los resultados numéricos para la mayoría de los casos de estudio.

1. INTRODUCCIÓN

Uno de los mayores problemas en estructuras aeronáuticas ligeras es el envejecimiento y la corrosión. Los largos ciclos de carga durante la operación de las aeronaves y la interacción con el medio ambiente causan defectos en las estructuras que actúan como sitios ideales para la concentración de esfuerzos. Dichos lugares son los sitios donde típicamente inicia la fatiga del material, reduciendo la vida útil de los componentes.

Mediante la aplicación de parches de material compuesto adheridos a las estructuras o componentes agrietados o desgastados es posible restaurar la integridad estructural de dichos elementos. En la estructura reparada, la fatiga prosigue siempre que cargas cíclicas estén presentes. Por esta razón es importante validar modelos analíticos y numéricos para el cálculo de parches con capacidad de predecir el comportamiento a fatiga de una reparación en una estructura metálica con este tipo de parches.

El propósito de este artículo es validar por medio de un análisis experimental nuevos modelos propuestos por AFGROW (desarrolladores del software del mismo nombre propiedad de la USAF para predicción de crecimiento de grietas) para caracterizar el comportamiento a fatiga de parches adheridos.

El análisis se aplica al espécimen mostrado en la Figura 1. La placa base está fabricada en aluminio 7075-T6 de 1.6 mm de espesor, el parche está fabricado en fibra de carbono/epóxico Hexcel 8552/AS4 y se diseñó para que cumpliera con una relación de rigidez igual a 1. El laminado posee una secuencia de apilamiento $(0,+45,-45,0)_s$. El parche está conformado en forma de medio octágono que se tapera linealmente entre la primera y la última capa del mismo. La primera capa del parche posee una relación de aspecto igual a uno (emula una elipse con relación de aspecto igual a uno o, lo que es lo mismo, una circunferencia) y la última capa del parche posee una relación de aspecto de

4.2 aproximadamente. El film adhesivo utilizado es Cytec 15425D. El ciclo de curado se realizó mediante una sicoteva de la siguiente manera: rampa de calentamiento de 40 minutos desde temperatura ambiente hasta 175°C, sostenimiento de esta temperatura por dos horas y rampa de enfriamiento de 30 minutos hasta temperatura ambiente.

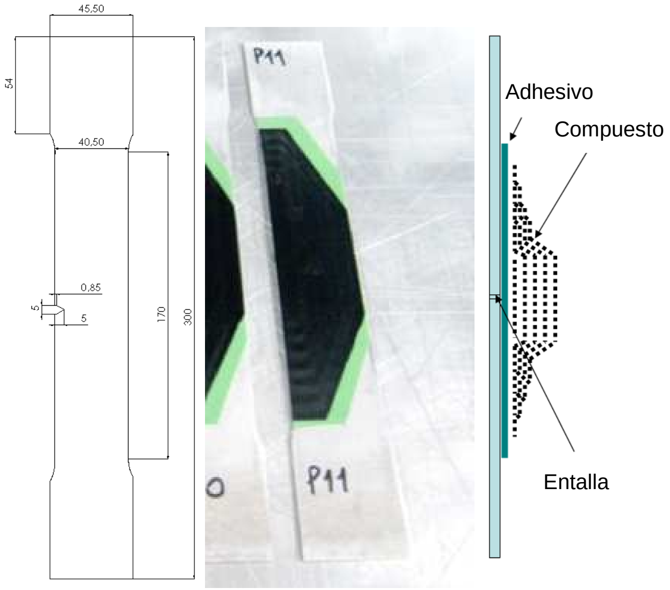

a) b) c)

Figura 1. Espécimen fabricado. a) dimensiones de la placa de aluminio. b) Imagen de espécimen sin curar. c) Esquema de parche fabricado.

Los ensayos realizados consistieron en la aplicación dinámica de cargas al espécimen bajo diferentes condiciones. El crecimiento de las grietas por fatiga se estimó mediante inspecciones visuales y las curvas de longitud de grieta vs. Ciclos se construyeron para la configuración parchada y se compararon contra las curvas de crecimiento de grietas experimentales y teóricas para el espécimen no parchado. Los datos experimentales fueron comparados con predicciones numéricas usando el código AFGROW.

2. RESULTADOS EXPERIMENTALES Y NUMÉRICOS

Se llevaron a cabo 5 ensayos de cada tipo: a) fatiga en especímenes entallados sin reparación, b) fatiga en especímenes preagrietados y reparados, c) fatiga en especímenes entallados y reparados. Cada caso de estudio se modeló con el código AFGROW emulando las condiciones experimentales. Los ensayos de fatiga se realizaron según el MIL-HDBK-5J. Se aplicó un esfuerzo medio de 70.415 MPa con una semi amplitud de 52.815 MPa, de forma que realizara un ciclo sinusoidal entre 17.6 MPa y 123.23 MPa (La carga máxima es aproximadamente del 50% de la carga máxima a tracción estática) a una frecuencia de 20 Hz. La figura siguiente muestra los resultados experimentales y predicción teorica con el código AFGROW, para las tres condiciones indicadas.

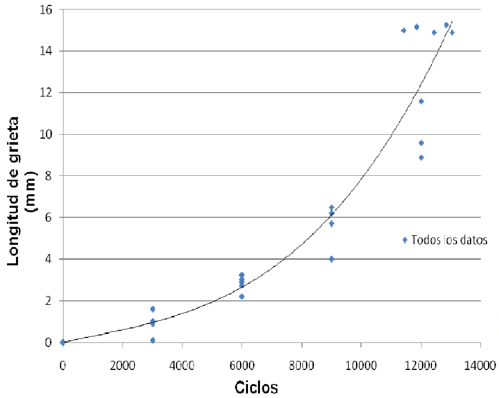
Longitud de grieta (mm)
16
14
12
10
8
6
4
2
0
0
2000
4000
6000
8000
10000
12000
14000
Ciclos
Todos los datos

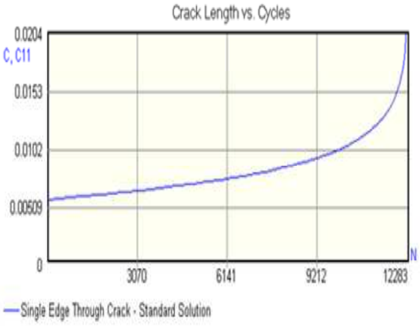
Crack Length vs. Cycles
C, C11
0.0204
0.0153
0.0102
0.00509
0
3070
6141
9212
12283
N
Single Edge Through Crack - Standard Solution

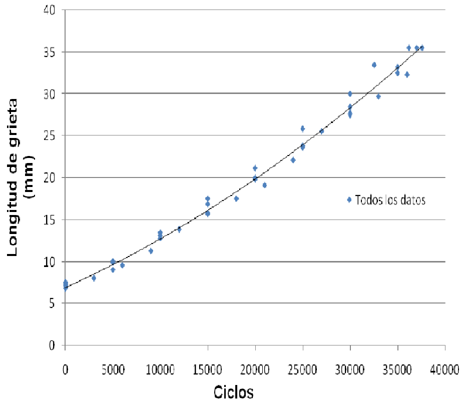
Longitud de grieta (mm)
40
35
30
25
20
15
10
5
0
0
5000
10000
15000
20000
25000
30000
35000
40000
Ciclos
Todos los datos

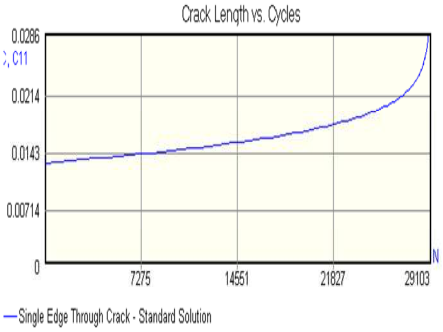
Crack Length vs. Cycles
C, C11
0.0286
0.0214
0.0143
0.00714
0
7275
14551
21827
29103
N
Single Edge Through Crack - Standard Solution

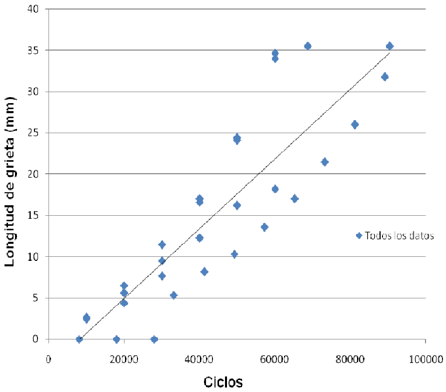
Longitud de grieta (mm)
40
35
30
25
20
15
10
5
0
0
20000
40000
60000
80000
100000
Ciclos
Todos los datos

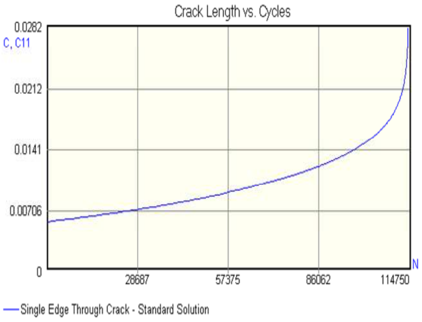
Crack Length vs. Cycles
C, C11
0.0282
0.0212
0.0141
0.00706
0
28687
57375
86062
114750
N
Single Edge Through Crack - Standard Solution

3. CONCLUSIONES

Para las probetas sin reparar, los resultados obtenidos experimentalmente mostraron una vida esperada promedio de 12318.8 ciclos con una desviación estándar de 676.5 ciclos para una longitud promedio de grieta de 15.04 mm. Los resultados numéricos estiman una vida de 12283 ciclos para una longitud de grieta propagada de 15.25 mm. Para el espécimen preagrietado y reparado, los resultados obtenidos experimentalmente mostraron una vida esperada promedio de 35840.75 ciclos con una desviación estándar de 2267 ciclos para una longitud promedio de grieta de 35.98 mm, y para los especímenes solo con entalla y reparados, los resultados obtenidos experimentalmente mostraron una vida esperada promedio de 73073.33 ciclos con una desviación estándar de 14364.3 ciclos para una longitud promedio de grieta de 35.21 mm

El error entre los resultados experimentales y los resultados numéricos para el caso de estudio de fatiga en especímenes entallados desprovistos de reparación es inferior al 1% (0.3%), lo que valida el uso de los modelos numéricos empleados para estimar la vida útil de componentes metálicos bajo fatiga.

Para el caso de fatiga en especímenes preagrietados y reparados el error es del 3.08%, lo que permite de forma análoga validar los modelos numéricos para predecir el comportamiento a fatiga de los especímenes preagrietados. Según el mismo modelo numérico, la vida útil de los especímenes incrementa 32.7 veces por la adición del parche.

Si se tiene en cuenta que la resistencia global de la sección transversal de la zona reparada solo se duplica (para una relación de rigidez igual a uno, el espesor del parche de carbono posee la misma resistencia mecánica que el espesor de la placa de aluminio), es interesante apreciar cómo se logra un incremento de hasta 32.7 veces en la vida útil de los especímenes. No obstante, se requiere más experimentación y técnicas de monitorización en tiempo real que permitan estimar la integridad de las reparaciones.

Los parches de material compuesto son una opción viable para generar reparaciones estructurales de componentes aeronáuticos con un bajo coste, relativa facilidad y adaptabilidad. Como se pudo apreciar, los modelos numéricos pueden generar aproximaciones bastante acertadas a los resultados experimentales obtenidos en este trabajo, no obstante, se deben usar con cuidado ya que como pudo apreciarse, la existencia de algunos fenómenos (como los concentradores de esfuerzos y retardadores) pueden modificar los resultados obtenidos.

REFERENCIAS

ASM INTERNATIONAL. (1990) *ASM Handbook Volume 2. Properties and selection: Nonferrous Alloys and Special-Purpose Materials.* ASM International. (USA)

BAKER, A. (1999) Bonded composite repair of fatigue-cracked primary aircraft structure, en *Composites Structures* (Elsevier), Airframes and Engines Division, Defence Science and Technology Organisation, Fishermen´s Bend, Aeronautical and Maritime Research Laboratory, Melbourne, Australia

Simulation and experimentation with CNTs for health monitoring of composite structures

A. Iriarte, N. Markaide, H. Vallejo, I. Garmendia
Inasmet-Tecnalia, San Sebastian, Spain

ABSTRACT

In the last years condition monitoring of composite structures has gained importance and different types of sensors for load and damage sensing have been developed. The carbon nanotubes CNTs have acquired a big interest due to the exceptional electrical and mechanical properties that can offer for sensor applications. In this paper computer simulations for the composite materials are described and compared with experimental observations. The influencing parameters of the sensing behaviour such as resistance measurement methods have been investigated. The computer simulations are carried out via an in-house developed program called PIEZOELAS, which is a simulation code based on the Finite Element Method to carry out piezoresistive analyses via three-dimensional mechanical and electrical simulations. Finally, a comparison between the theoretical and the experimental investigations has been conducted. The results presented in this work show a high potential for load detection of composite structures via electrical conductivity methods.

1. INTRODUCTION

The objective of the present work has been to evaluate the piezoresistive behaviour of a carbon/epoxy laminate doped with CNTs via electromechanical tests. These results have been compared with computer simulations via an in-house developed program called PIEZOELAS. An interesting potential for the self-sensing has been observed.

2. EXPERIMENTAL PART

2.1. Materials

The materials selected for the laminate manufacturing have been:

- A low viscosity system based on a Bisphenol A epoxy resin and an amine curing agent: Araldite LY564 / Aradur HY2954 from Huntsman.
- As grown Multiwall Carbon Nanotubes (MWCNT) from Arkema: Graphistrength C100
- Unidirectional carbon fibre fabric: Tenax HTA 5131 3K, 150 g/m^2

2.2. Manufacturing

Firstly the MWCNTs were dispersed in the resin by a grinding system (TORUSMILL 5 from VMA Getzmann), in a quantity that represented a 0.5% wt of the total resins system. Next, the corresponding hardener was added and mixed by mechanical stirring during 10 minutes, keeping the mixture under vacuum. The carbon fibre fabrics were then impregnated manually with the doped resin and cured in autoclave under vacuum and 20 bars of pressure at 140ºC during 8 hours. The final laminate consisted of 16 layers oriented in a quasi-isotropic lay-up.

2.3. Characterization

For the measurement of the resistance variation with load, different specimens were tested under tensile load in the elastic regime of the material. In these tests the two probe and four probe resistance measurement methods were used (Fig. 1). The two-probe method has two electrodes to measure electrical resistance: the same probe applies an electric current and measure resistance via the corresponding change in voltage. The four-probe method uses an outer pair of electrodes to apply electric current and uses an inner pair of electrodes to measure resistance from the voltage drop between them.

Fig. 1. Different electrode configurations: (a) two probes, (b) four probes.

Different combinations of electrodes were used for the four probe method resistance measurement that can be seen in Fig.2.

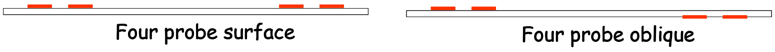

Fig. 2. Different electrodes locations for the four probe method measurements.

The tensile test over a constant section of the specimen results in a constant stress in the entire specimen. However, under the PIEZOELAS program validation point of view, it was decided to machine a non-constant section over the specimen in order to have different stress values along the specimen length.

The current application and voltage measurement were carried out using a KEITHLEY 2410 equipment. The time, current, voltage and load were registered in an acquisition system software (Labview). To register the load from the testing machine (general view in Fig. 3) in Labview a voltage output calibrated wire was connected to the PC.

Fig. 3. General view of the tensile test set up.

3. PIEZOELAS MODELLING

PIEZOELAS is an in-house developed simulation code based on the Finite Element Method to carry out linear and non-linear three dimensional piezoresistive analyses.

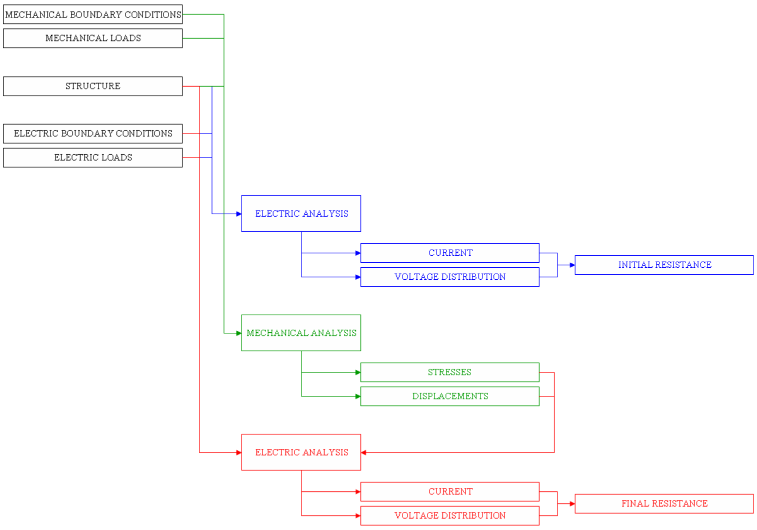

Fig. 4. Flow diagram of the analysis procedure of PIEZOELAS.

The analysis procedure starts by creating an input file that contains a 3D finite element mesh, mechanical and electrical properties, load cases and boundary conditions. First, a 3D electrical analysis is performed to obtain the original electric resistance of the system. Then, taking the mechanical loads and boundary conditions into account, a 3D mechanical analysis is carried out and the stresses and displacements of the system are determined. Finally, considering the tensile state and the deformed geometry of the system (piezoresistive and geometric effects are thus taken into account), a second 3D electric analysis is conducted and as a result, the final electric resistance is calculated. The changes in the resistance determine the piezoresistive response of the system.

3.1. Piezoresistive characterization

A procedure based on the linear piezoresistance equation (C. Smith, 1.954) was developed to determine the needed piezoresistive properties from real tensile tests.

Regarding obtained data, although a high dispersion exists in a low-loaded region, it was clearly observed that the piezoresistive properties of the characterized CNT doped composite materials are not constant values but stress-dependent variables.

4. RESULTS AND DISCUSSION

Results from experimental tests and simulations with PIEZOELAS are presented next. The experimental results presented in section 4.1 are related to tensile tests of samples with variable cross sections. On the other hand, in section 4.2 the reproduction with PIEZOELAS of a particular tensile test of a sample with constant cross section and the real experimental results are shown.

4.1. Experimental tests

Fig. 5 shows the percentage of electrical resistance variation with applied load via two probe and four probe resistance measurement method for the laminate doped with

CNTs. Piezoresistive behaviour of the specimen is appreciated and no significant variation of the resistance change with resistance measurement method is appreciated.

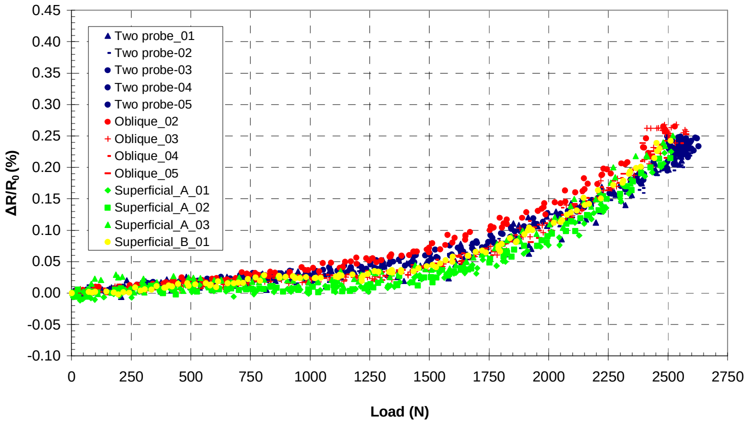

Fig. 5. Results from tensile tests (two and four probe method)

4.2. Correlation with PIEZOELAS

The resistance changes calculated with PIEZOELAS for a tensile test of a sample with constant cross section together with the original experimental results are shown in Fig.6.

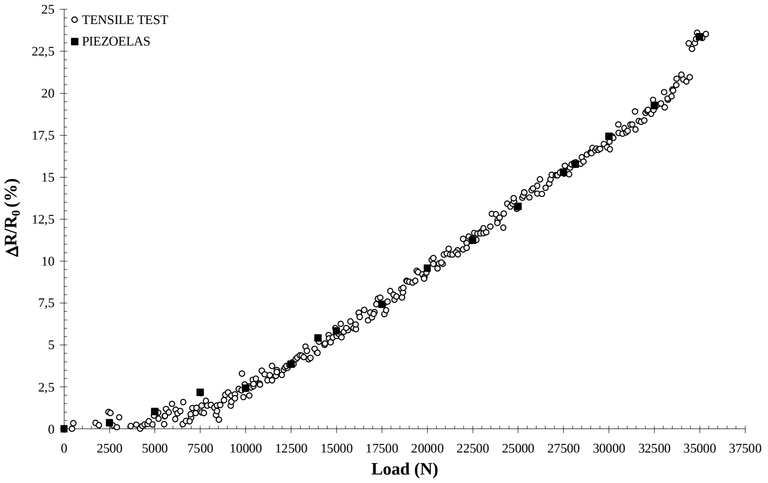

Fig. 6. Resistance changes calculated with PIEZOELAS and real experimental data

5. CONCLUSIONS

An interesting potential for the self-sensing has been observed. The simulation with PIEZOELAS of the specimen with CNTs is in progress and the results will be included in the oral communication of the present work.

ACKNOWLEDGEMENTS

The authors want to thank the economical support received by the European Commission though the NOESIS project, “Aerospace nanotube hybrid composite structures with sensing and actuating capabilities”, Contract number 516150.

Experimental tests on GFRP truss beam for dismountable bridge

A.M.A.J. Teixeira
Civil Engineering Department Instituto Militar de Engenharia
(IME), Rio de Janeiro, Brazil
M.S. Pfeil
COPPE/UFRJ Univ. Federal do Rio de Janeiro, Rio de Janeiro, Brazil
R.C. Battista
COPPE/UFRJ Univ. Federal do Rio de Janeiro, Rio de Janeiro, Brazil

SUMMARY

Lightweight for transport facility and reduced erection and disassembling time are the main requirements of dismountable bridges for emergency purposes which can be favourably satisfied by using GFRP products. A thirty meters span dismountable bridge is being designed and tested as a reduced model at COPPE´s Laboratory of Structures. The bridge is composed of a deck supported by prestressed trussed girders which are mounted by assembling GFRP tubular profiles and steel joints with bearing type connections. Structural tests were first focused on the behaviour of the trussed girder

1:2.3 reduced model in two structural schemes: a 1.3m long cantilever beam and a 13m span simple supported beam. This paper presents the results of the experimental tests performed on a 13m span simple supported beam with two connection details between GFRP tubes and steel joints. The improvement of some connections in the second test enabled the increase of collapse load of the structure.

1. INTRODUCTION

Composite materials have several attractive characteristics such as high resistance, low specific weight, corrosion resistance and dimensional stability (Keller at to. 2003), which make its application interesting in civil engineering, such as buildings, bridges and footbridges. Particularly in the case of dismountable bridges for emergency purposes, whose main requirements are lightweight for transport facility, reduced erection time and maintenance costs, composite materials seem to be very suitable. A composite dismountable bridge has been designed and a reduced model of its main trussed beam is being tested at COPPE’s Laboratory of Structures (Teixeira *et al*. 2007 and Pfeil *et al*. 2009). The thirty meters span bridge whose cross section is illustrated in Fig.1 is composed of a deck supported by prestressed main trussed beam. The trussed girders are mounted by assembling GFRP tubular profiles and steel joints. Bearing type connections between tubular profiles and steel joints are activated by prestressing all elements. To increase the compressive strength of the bearing connections the tubular profiles had their ends reinforced by composite hand lay-up. The structural tests focused on the behaviour of a trussed girder reduced model fabricated in a 1:2.3 geometric scale and assembled in a simple supported thirteen meters span complete model as shown in Fig.2. The work done was very useful to verify the serviceability and collapse structure behaviour and to improve connection details and construction. This paper presents the experimental results obtained from the test of the reduced model of the main trussed beam. The results showed that the tube – joint connection detail plays an important role in the collapse load of the structure.

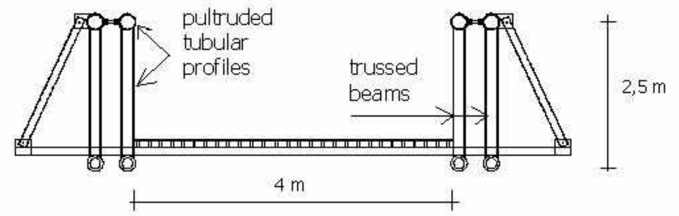

Fig. 1 Bridge cross-section.

Fig. 2. Simple supported trussed beam.

2. SIMPLE SUPPORTED BEAM TESTS

2.1. Structures Mounting and Tests Setup

Two tests were performed on a 13 meters span simple supported beam. The beams were composed of sixteen trussed panels (Fig. 2), which were mounted by assembling pultruded circular tubes with end reinforcement and steel joints with the aid of interior tube splices (Fig. 3). Steel 8mm wires were placed inside the tubes along the truss elements and prestressed in order to impose an overall compressive state of stress. Table 1 presents the geometrical and mechanical properties of the circular tubes used to compose the trussed beam. The notation for the truss elements is shown in Fig. 4 which also illustrates the structural scheme, the load points and the types of tube end reinforcement. In Test 1 all tube ends were reinforced by composite hand lay-up and the tube – joint assemblage was made with the aid of composite tube splices (Fig. 3a). In Test 2, the composite tube splices of the upper chord and of some connections of the lower chord were substituted by steel tube splices as shown in Fig. 4. For the tube –

joint connections of the two central panels the detail with steel jackets was adopted as illustrated in Fig. 3b. The structure was assembled on a table where the initial prestress of the truss elements were applied. Then the structure was lifted and placed on a support frame which also provides lateral bracing, as can be seen in Fig. 2. At this stage the trussed beam is subjected to the initial prestress and self-weight. The next steps were: to increase the prestress load to the lower chord, install the load setup and finally apply the full prestress load to the lower chord. The beams were subjected to two symmetric concentrated loads (see Fig. 4). Tubes axial deformations were measured by strain gages, as well as the loads applied through two hydraulic jacks.

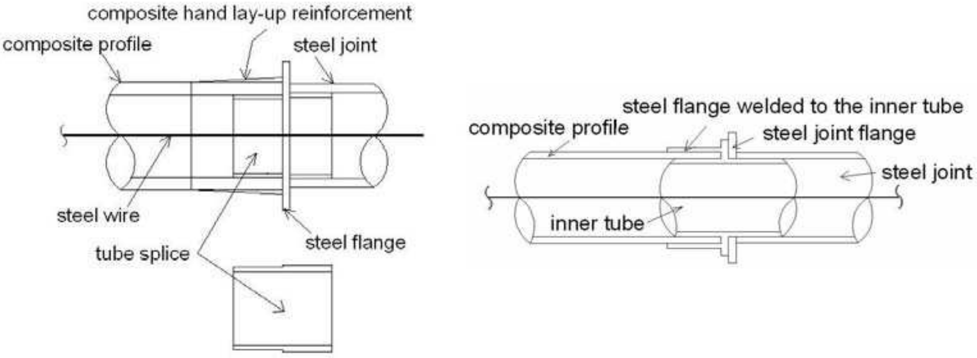

(a) (b)

Fig. 3. Bearing connections: (a) tube ends reinforced by composite hand lay-up and the tube – joint assemblage with the aid of composite tube splices; (b) steel jacket.

Tube	Lower chord (BI)	Upper chord (BS), diagonal (D), vertical member (M)
Diameter (mm)	76	59
Thickness (mm)	9.1	4.5
Young’s Modulus (GPa)	28.2	24.1
Compression strength (MPa)	218	192

Table 1. Properties of the composite circular tubes.

2.2. Experimental Results

In Test 1, upper chord tube BS2 exhibited a compression collapse close to the end reinforcement. The collapse axial force was equal to 57kN while the vertical load P (see Fig. 4) was equal to 24.2 kN. The collapse occurred at a lower than expected load. It was noted that the composite splice tubes are very flexible and do not restrain the rotation between the pultruded tube and the steel joint. As the trussed beam is loaded, the internal forces at the contact faces change from uniform compression (prestressing stage) to non-uniform compression (loading stage). At this stage a partial loss of contact in the joint can occur and lead to a premature collapse. For Test 2 the failed upper chord BS2 was removed and substituted by a new one and new tube-joint connection details were adopted (Fig. 4). In this test, the upper chord BS3 exhibited a compression collapse. This tube was not instrumented with strain gages, so the axial force was not measured. The collapse load P was equal to 32,9 kN, which is 36% higher than the collapse force in Test 1, demonstrating the efficiency of the steel jackets and the steel splices in preventing loss of contact and restraining relative rotation in the connection.

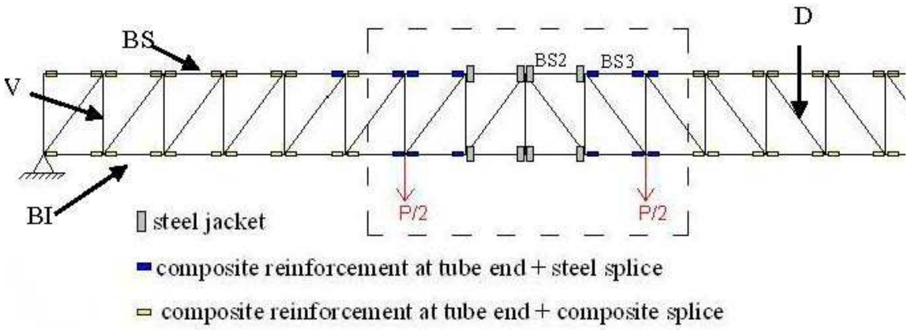

Fig. 4. Structural scheme of the simple supported beam and joint details in test 2.

3. CONCLUSIONS

A composite dismountable bridge has been designed and a reduced model of its main trussed beam was tested. The bridge is composed of a deck supported by prestressed trussed girders erected by assembling GFRP tubular profiles and steel joints. Two assemblages of the trussed beam were performed. In Test 1 the collapse occurred at a lower than expected load. It was noted the sensitivity of the structure to the eccentric compression forces eventually leading to a partial loss of contact at the connections. To prevent this precocious failure, a new connection detail was adopted in Test 2 for the more stressed elements. The results indicated that this particular connection should be extended to all elements for higher resistance to be achieved.

ACKNOWLEDGMENT

The sponsors of the research reported in this paper were *Instituto Militar de Engenharia* and *Conselho Nacional de Desenvolvimento Científico e Tecnológico – CNPq*, the brazilian agency for scientific and technologic development. The authors wish to be grateful to Industries *Cogumelo – Pultrudados em Fibra de Vidro* for the hand lay-up solution and execution and to *Belgo – Arcelor Group* for the donation of the steel wires.

REFERENCES

KELLER, T. (2003) Use of fibre reinforced polymers in bridge construction, in *Structural Engineering Documents, IABSE*. PFEIL, M. S., TEIXEIRA, A. M. A. J., BATTISTA, R. C. (2009). Experimental tests on GFRP truss modules for dismountable bridges, *Composite Structures*, 89, 70-76. TEIXEIRA, A.M.A.J. (2007) Glass fiber reinforced polymer dismountable bridge, *D.Sc. Thesis, COPPE/UFRJ*, Rio de Janeiro, Brasil, November 2007 (in protuguese). TEIXEIRA, A. M. A. J., PFEIL, M. S., BATTISTA, R. C. (2007). Experimental Tests on GFRP tubular truss module for dismountable bridges, *Proceedings of the IV International Conference on Science and Technology of Composite Materials, Rio de Janeiro, Brazil.*

Inhomogeneidades en el campo local de deformaciones en laminados realizados con tejidos de fibra de carbono/epoxi

A. Güemes, A. Fernández-López, C. Dominguez, C. de Miguel
Departamento de Materiales y Producción Aeroespacial. Universidad Politécnica de Madrid, España

RESUMEN

A pesar de que es bien conocida la influencia de la geometría del tejido en el campo de deformaciones, la medida de las deformaciones en la superficie de los materiales compuestos fabricados con tejido se realiza de forma tradicional. La influencia de las inhomogeneidades debidas al tejido se manifiesta en el caso de sensores de fibra óptica basados en la ley de difracción de Bragg (FBG) en distorsiones en el espectro de la red. La posibilidad de disponer sensores FBG de pequeño tamaño se va a utilizar para medir experimentalmente las variaciones del campo de deformación en la superficie, en comparación con las medidas obtenidas por sensores de deformación de tamaño normal.

1. INTRODUCCIÓN

Es posible encontrar infinidad de ejemplos en la bibliografía de sensores de fibra óptica para la medida de deformaciones. Los sensores de fibra óptica más prometedores son las redes de Bragg, debido a la posibilidad de multiplexar diferentes sensores a lo largo de una misma fibra óptica, siendo equivalente cada uno de los sensores a los picos del espectro en reflexión. Las variaciones en la longitud de onda de cada uno de los sensores será proporcional a las deformaciones sufridas por cada sensor, en caso de que fueran uniformes.

Si una FBG está sometida a un gradiente de deformaciones, la variación de la longitud de onda del sensor no será uniforme, lo que provocará variaciones en el espectro. De esta forma, viendo las variaciones sobre el espectro es posible determinar si el campo de deformaciones es uniforme o no, mientras una galga extensométrica no nos proporciona esta información. La perturbación del espectro es un fenómeno frecuente en la bibliografía cuando se realizan medidas sobre tejido, bien con fibra embebida o con fibra pegada sobre el material.

2. MEDIDAS EXPERIMENTALES

Para las medidas se realizaron probetas cuasiisótropas de 3 mm de espesor y 40 mm de ancho, fabricadas con preimpregnados de grafito epoxi AS4/8552. En la superficie de la probeta se pegaron 5 redes. En la probeta se pegaron sobre la superficie 5 redes diferentes, la FBG5 de 10 mm abarcando varias tramas, rodeada de redes de 2 mm, cada una sobre una única trama (ver figura 1).

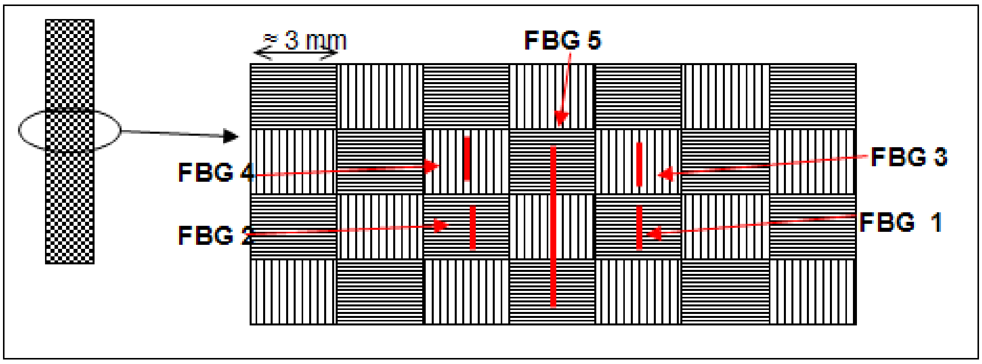

Fig. 1. Localización de los sensores en la probeta ensayada.

Bajo condiciones de tracción pura, se realizaron diferentes medidas del espectro a niveles de carga crecientes.

La FBG 5, correspondiente a una red de 10 mm de longitud que abarca varias tramas del tejido, se ve sometida a un gradiente de deformaciones inducido por las diferentes orientaciones del material. En la figura 2 podemos observar la variación del espectro frente a dos niveles de cargas. Para altos niveles de carga, el gradiente de deformaciones se hace tan intenso que provoca la distorsión del pico inicial en dos picos independientes.

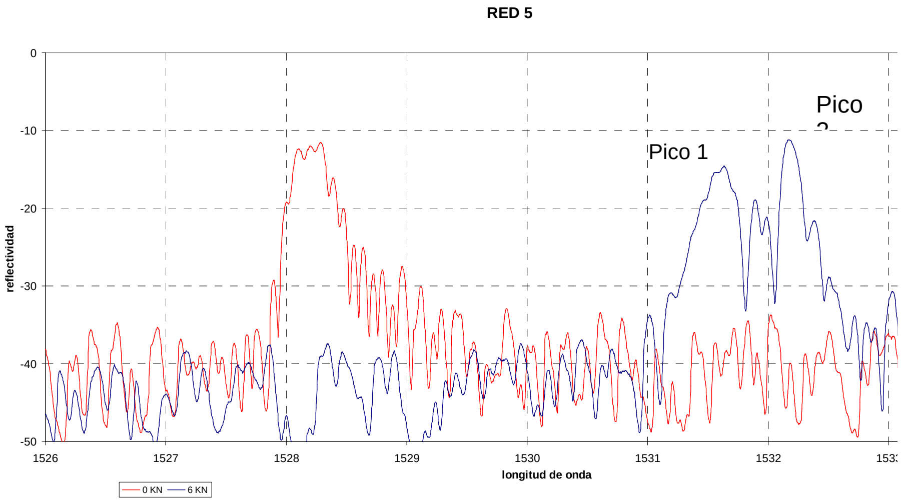

Fig. 2. Espectro de una FBG de 10mm sometida a dos niveles de carga.

Las otras cuatro redes de 2 mm., montadas sobre tramas diferentes de tejido, no presentan ninguna distorsión para el mismo nivel de cargas. Es posible seguir el máximo de su espectro y establecer una relación clara con las deformaciones.

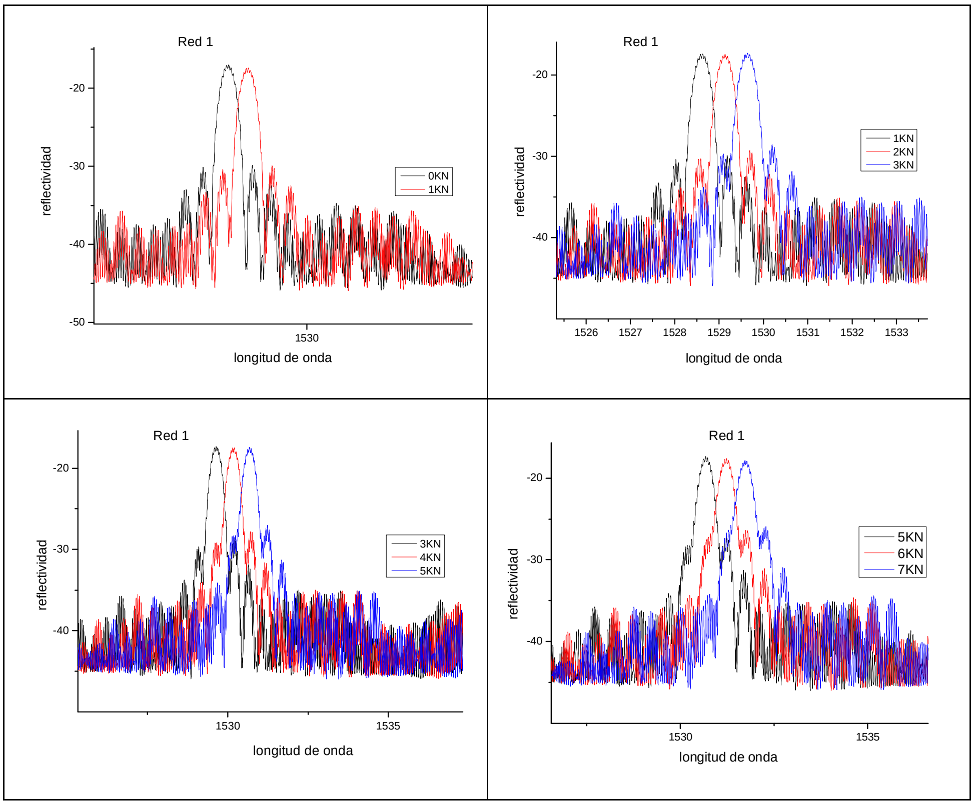

Fig. 3. Espectro de las FBG de 2 mm de longitud pegadas sobre diferentes tramas de tejido bajo diferentes cargas aplicadas.

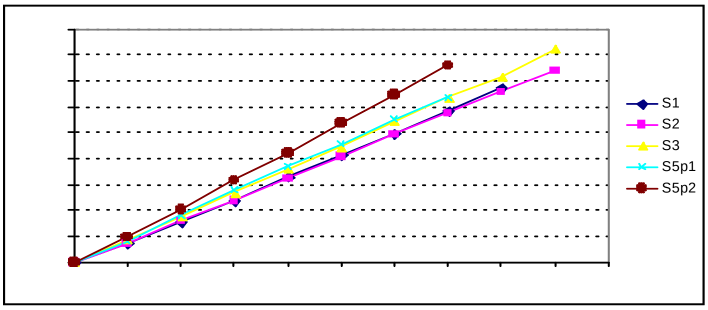

Fig. 4. Medida de deformaciones de los diferentes sensores frente a carga aplicada.

La variación de los máximos de los picos correspondientes a las redes sobre las dos tramas del tejido presentará variaciones de hasta un 10% para el mismo valor de carga aplicada. Las variaciones de deformaciones correspondientes a los dos picos en los que se desdobla la red de 10 mm presentan variaciones de hasta un 15% (ver figura 4).

3. CONCLUSIONES

La textura del tejido provoca significativas diferencias en el campo de deformaciones. Este gradiente de deformaciones tiene una influencia significativa en los sensores de deformación normales, como se puede ver en el espectro de una red de Bragg de 10 mm de longitud que abarque diferentes tramas del tejido.

Mediante FBG de pequeña longitud es posible estudiar la diferencia de deformaciones inducida por las diferentes tramas del tejido, y establecer una relación entre las deformaciones de cada trama con la perturbación del espectro. Solo sensores de deformación de longitudes inferiores al tamaño de las tramas ofrecerán valores de deformación significativos.

REFERENCIAS

DAVOL, KATY; UDD, ERIC; KREGER, STEVE; KUNZLER, MARLEY; LAYLOR, MARTY; HEIDER, DIRK; YU, ZHICHENG (2003) Monitoring of Advanced Composite Weave Structures Using Multi-Axis Fiber Grating Strain Sensors. *Proceedings of SPIE - The International Society for Optical Engineering, v 5278, p 128-134*

LOMOV, S. V.; IVANOV, D.S.; VERPOEST, I.; ZAKO, M.; KURASHIKI, T.; NAKAI, H.; MOLIMARD, J.; VAUTRIN, A. (2008), Full-field strain measurements for validation of meso-FE analysis of textile composites. *Composites Part A: Applied Science and Manufacturing, v 39, n 8, p 1218-1231*

SILVA-MUÑOZ, RODRIGO A.; LOPEZ-ANIDO, ROBERTO A .(2009) Structural health monitoring of marine composite structural joints using embedded fiber Bragg grating strain sensors. *Composite Structures, v 89, n 2, p 224-234*

Eficiencia estructural y coste relativo de materiales híbridos fibra-metal

J.C. Suárez, M.A. Herreros, F. López, P. Pinilla, S. Miguel
Grupo de Investigación en Materiales Híbridos, Universidad Politécnica de Madrid
M.V. Biezma
Departamento de Ciencia e Ingeniería, Universidad de Cantabria

RESUMEN

Los materiales híbridos fibra-metal pretender aunar las ventajas de ambos tipos de materiales evitando, en lo posible, sus inconvenientes. Así, se pretende combinar la elevada resistencia al impacto y durabilidad, junto con facilidad de mecanización y fabricación típicas de los materiales metálicos, con una elevada resistencia y rigidez específicas en la dirección de la fibra, así como una buena resistencia a la fatiga, características de los materiales compuestos. Los materiales híbridos abren nuevas posibilidades a la hora de conseguir prestaciones inalcanzables para los materiales tradicionales. Se considera en este trabajo la eficiencia estructural de paneles de material híbrido constituidos por acero y compuesto de matriz viniléster con refuerzo de fibra de vidrio, comparándolo con la sección equivalente en acero. Asimismo, y en base a un análisis de los costes de las materias primas y los procesos de fabricación, se estudia el coste de los paneles híbridos para distintas configuraciones y bajo qué condiciones su fabricación es competitiva frente a la alternativa en acero.

1. INTRODUCCIÓN

Los paneles sándwich son el epítome del concepto de material híbrido. En ellos se combinan dos o más materiales con una geometría y escala específicas (conformando las caras y el núcleo) para proporcionar a la estructura una rigidez y resistencia elevadas con un peso lo más liviano posible. Es posible considerar a un panel sándwich como una material con su conjunto característico de propiedades, y esto resulta útil para comparar este material híbrido con materiales monolíticos más convencionales. Para hacerlo debemos analizar las prestaciones del sándwich. Usaremos como criterio de excelencia la rigidez a flexión por unidad de anchura, S_w, dividida por la masa por unidad de área, m_a. La rigidez a flexión del panel por unidad de anchura, S_w, viene dado por la ecuación 1, donde las dimensiones, d, c, t y L corresponden a las indicadas en la figura 1, E_c es el módulo de Young del material de las caras y G_n es el módulo de rigidez a cortadura del núcleo.

La constante numérica B depende únicamente del caso de carga considerado. La ecuación (1) tiene dos términos. El primero, entre corchetes, es lo que se obtendría si la rigidez a flexión fuera el único modo de deformación considerado. El segundo término, entre llaves, es un factor de penalización de la rigidez debido al efecto de la cortadura en el núcleo. Si el núcleo resiste de manera adecuada las tensiones de cortadura, el segundo término puede ser despreciado.

$$S_w = (EI)_{sand} = \left[\frac{1}{12}\left(d^3 - c^3\right)E_c\right]\left\{\frac{1}{1+\frac{BE_c tc}{2G_n L^2}}\right\} \quad (1)$$

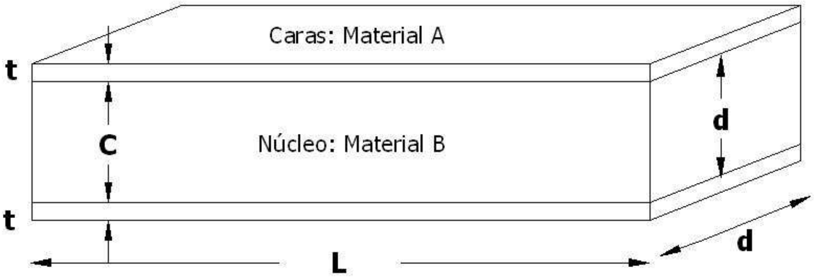

Figura 1. Geometría del panel sándwich.

Considerando el panel sándwich como un material híbrido, se puede definir un módulo aparente $\tilde{E}$ (el módulo de un material homogéneo con la misma rigidez a flexión que el sándwich), esto es

$$\left(EI\right)_{sand} = \frac{1}{12}\left(d^3 - c^3\right)E_c = \frac{1}{2}td^2E_c = \tilde{E}\frac{d^3}{12} \quad (2)$$

donde $d^3/12$ es el segundo momento de inercia de un panel homogéneo de espesor d, y suponiendo que t<<d, entonces

$$\tilde{E} = \frac{6t}{d}E_c \quad (3)$$

El panel tiene una densidad, ρ, que es la media ponderada de las densidades del material de las caras y del núcleo

$$\rho = \frac{2t}{d}\rho_c + (1-\frac{2t}{d})\rho_n \quad (4)$$

Si el núcleo es lo suficientemente ligero el segundo término es pequeño frente al primero. Despreciando el segundo término de (4) y combinando con la ecuación (3), se obtiene

$$\tilde{E} \approx 3\left(\frac{\rho}{\rho_c}\right)E_c \qquad (5)$$

Si el material de las caras es mucho más pesado que el material del núcleo, la relación de densidades en (5) es prácticamente la unidad, de manera que la rigidez aparente resulta estar relacionada con la rigidez de las caras por un factor 3. Dicho de otra manera, el panel sándwich a flexión es aproximadamente tres veces más eficiente que el más eficiente de los materiales compuestos con refuerzo de fibras, incluso cuando las fibras están alineadas en dirección normal al eje de flexión.

Esto es, por supuesto, una idealización. El núcleo siempre se deforma algo a cortadura y tiene una cierta masa. La conclusión más relevante es que el criterio de excelencia para un diseño de peso mínimo para una rigidez impuesta viene dado por la relación de propiedades $E^{1/3}/\rho$, y en esta situación la disposición de los materiales A y B formando un panel sándwich sobrepasa en prestaciones a cualquier otra geometría de híbrido A+B.

2. EFICIENCIA ESTRUCTURAL DE PANELES HÍBRIDOS

Se define la Fracción en Volumen de Metal (FVM) como la proporción de acero respecto a la de material compuesto que hay en el híbrido, obteniéndose mediante la ecuación (6):

$$FVM = \frac{\sum_{1}^{p} t_{ac}}{t_{lam}} \qquad (6)$$

donde: t_{ac} es el espesor de cada lámina de acero; t_{lam} el espesor total del laminado y p el número de chapas de acero. Las probetas sólo de acero, basándonos en (6), tienen una FVM=1. Las probetas sólo de material compuesto (resina y tejido de fibra de vidrio) tienen una FVM=0.

La densidad de los paneles híbridos varía linealmente con FVM y es, lógicamente, independiente del espesor del laminado híbrido. Sin embargo, el peso por metro cuadrado sí que depende del espesor del laminado híbrido. El módulo equivalente del metal puede obtenerse a partir de la ecuación (1), siendo su variación no lineal en función de la FVM del laminado híbrido. La corrección por cortadura en el núcleo es pequeña, pero no ha sido despreciada a la hora de obtener el módulo equivalente.

Aplicando el criterio de excelencia a flexión dado por el índice de prestaciones M1= $E^{1/3}/\rho$, se puede observar en la Figura 2 que cualquier composición del laminado híbrido es más eficiente a flexión que la plancha correspondiente de acero, aunque el óptimo se obtiene para FVM=0,15 aproximadamente. A partir de los resultados anteriores es posible calcular el espesor de un material híbrido equivalente a una plancha de acero de espesor dado, para un valor cierto valor del FVM,. De manera análoga, se puede representar la variación del espesor equivalente del laminado híbrido en función de la FVM. Obviamente, a medida que aumenta el contenido en acero del híbrido (valores de FVM crecientes) el espesor equivalente del laminado híbrido va disminuyendo, pero de forma no lineal.

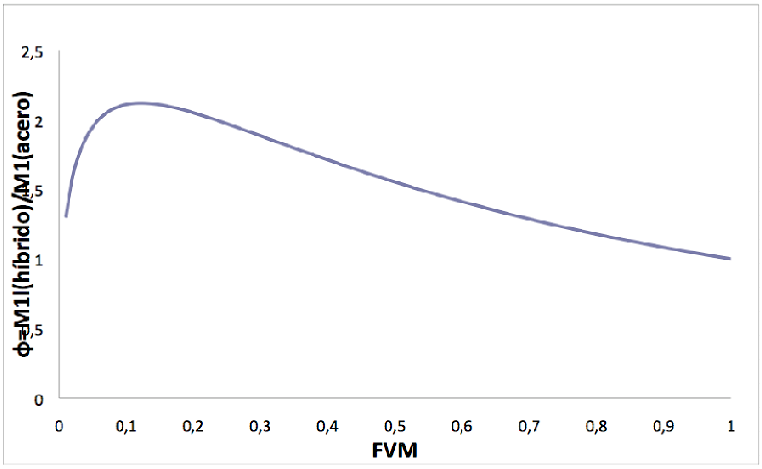

Figura 2. Eficiencia a flexión del laminado híbrido.

El espesor de los laminados equivalentes a un cierto espesor de acero depende de la FVM de cada uno de ellos. Se puede construir un laminado híbrido con un comportamiento a flexión equivalente a una plancha de acero de un cierto espesor y hacerlo de manera que podamos elegir su peso por unidad de superficie. No obstante, no siempre se puede elegir el laminado híbrido con rigidez equivalente de menor peso aéreo, pues existen otros requerimientos (tales como la resistencia en el propio plano o el intervalo de espesores admisibles) que hace necesario elegir paneles sándwich de peso intermedio.

REFERENCIAS

ALLEN HG. Analysis and design of structural sándwich panels. Oxford, UK: Pergamon Press, 1969.

ASHBY MF, EVANS AG, FLECK NA, GIBSON LJ, HUTCHINSON JW, WADLEY HNG. Metal foams, a design guide. Oxford, UK: Butterworth Heinemann, 2000.

CORDON J. Honeycomb structure. In: Dostal CA, editor. Engineered materials handbook. Metals Park, Ohio, USA: ASM International; 1990:721–8.

GIBSON LJ, ASHBY MF. Cellular solids, structure and properties, 2nd ed. Cambridge, UK: Cambridge University Press, 1997.

ZENKERT D. In: An introduction to sandwich construction. Solihull, London, UK: Engineering Advisory Services Ltd., Chameleon Press Ltd, 1995, ISBN 0 947817778.

Sensores de fibra óptica grabados con redes de Bragg embebidos en un laminado carbono/epoxi: Estudio numérico del comportamiento micromecánico

D. Sans, J.A. Mayugo, N. Gascons
AMADE, Escuela Politécnica Superior, Universidad de Girona, España
M. Frövel
INTA, Área de Materiales Compuestos, Torrejón de Ardoz (Madrid), España
C. Gutierrez
Departamento de Ciencia e Ingeniería de Materiales, Univ Rey Juan Carlos, España

RESUMEN

El presente trabajo se centra en el estudio del comportamiento micromecánico de sensores de fibra óptica tipo Bragg (FBGS) para la monitorización del estado de deformaciones y temperatura en un laminado de material compuesto carbono/epoxi. La lectura óptica del sensor se suele relacionar con la deformación longitudinal que recibe el material mediante un parámetro efectivo (llamado K_{norm}).

Se ha realizado un análisis de sensibilidad del citado parámetro frente a las propiedades mecánicas y geométricas introducidas en el modelo (material, fibra óptica y recubrimiento). Para ello, se ha desarrollado un modelo micromecánico en elementos finitos de un FBGS embebido para poder determinar numéricamente el parámetro efectivo $K_{norm.}$ Con el modelo se ha analizado inicialmente la influencia de los resultados frente a variaciones como el tamaño del espécimen, la densidad de mallado o las condiciones de contorno aplicadas, comprobando la robustez del modelo micromecánico. El análisis de sensibilidad del modelo frente a las propiedades mecánicas distintas del laminado en ensayos simétricos a tracción y compresión no ha dado variaciones significativas del parámetro K_{norm} como si se obtuvieron en ensayos experimentales. El presente estudio numérico a nivel micromecánico muestra la importancia de la distancia de transmisión de la deformación por cortante a la hora de inscribir la zona grabada en el sensor.

1. INTRODUCCIÓN

Un sensor de Bragg es una fibra óptica en la cuál una pequeña longitud (10 mm) ha sido grabada con redes de difracción de Bragg mediante exposición UV. Una fibra de determinada longitud permite tener varios sensores multiplexados ya que varias redes pueden ser inscritas cada cierta distancia. Dichos sensores, cuando se embeben, deben estar recubiertos con un recubrimiento suficientemente flexible para evitar discontinuidades y campos no homogéneos de deformación que pueden inducir una respuesta no deseada del sensor debido a cambios significantes en la birrefringencia según demostró Eaton et al. (1995). Cuando el sensor está embebido sufre cambios en los campos de deformación y temperatura del sensor que se pueden relacionar con las variaciones en la zona del material huésped (campo lejano). Las ya comentadas variaciones guardan relación directa con los cambios en la longitud de onda reflejada que a su vez van a guardar relación con determinados campos de deformación dependiendo de la configuración sensor-material y de las propiedades de los mismos. El presente trabajo considera un sensor con recubrimiento, ambos isótropos, embebido en una lamina de material compuesto carbono/epoxi transversalmente isótropa. Dicha lámina tiene las fibras orientadas a 0º con el sensor embebido alineado con las fibras y la secuencia de apilamiento genera dos casos distintos. Uno en apilamiento quasi-isótropo ($[(45/90/-45/0)_3/FO]_s$) y otro en apilamiento transversalmente isótropo ($[0_{10}/FO/0_{10}]$) dónde FO es la fibra óptica embebida.

2. DETERMINACIÓN NUMÉRICA DE k_{norm}

La respuesta del sensor, expresada como el cociente entre los cambios en la longitud de onda reflejada y su longitud de onda aplicada, se expresa en función de los campos de deformación del sensor y lejanos (considerando temperatura constante y la configuración del problema explicada en el anterior punto) según desarrolló Van Steenkiste et al. (1997). Desarrollando dichas expresiones Frövel et al. (2009) propone un parámetro efectivo de relación lineal entre la deformación longitudinal en el campo lejano y la respuesta del sensor conocido como K_{norm}. Dicho parámetro es propuesto por otros autores como Liu et al. (2001) o Kuang et al. (2005), como la diferencia entre la unidad y el coeficiente fotoelástico efectivo ($1-P_{eff}$), y guarda la misma relación entre la deformación longitudinal y la respuesta del sensor. Frövel contempla dos formas de hallar el parámetro, una experimental y una analítica, ambas presentadas en las ecuaciones (1) y (2) respectivamente,

$$K_{norm}^{EXP} = \frac{\left(\Delta\lambda_{avg} / e_1^{\infty}\right)}{\lambda_{B_0}} \tag{1}$$

$$K_{norm}^{AN} = K_1^{'} - \upsilon_{12} K_h^{'} \tag{2}$$

donde υ_{12} es el coeficiente de Poisson entre la dirección de la fibra y el plano y las constantes *K'* las sensibilidades del sensor a los campos lejanos de deformación en la dirección que corresponda al subíndice (*1* es la dirección longitudinal de la fibra y *h* la media en el plano 2-3). En el presente trabajo se propone un modo numérico de hallar K_{norm}, para así usarlo como parámetro comparativo con los resultados experimentales y analíticos para verificar su comportamiento a nivel micromecánico. Dicho parámetro se halla numéricamente como sigue en (3),

$$K_{norm}^{NUM} = \frac{1}{e_1^{\infty}}\left(K_1^s e_1^s + K_h^s e_h^s\right) \tag{3}$$

donde e^s son las deformaciones en la zona del sensor en la dirección que corresponda al subíndice, e^{∞} la deformación en el campo lejano en la dirección que corresponda y K^s las sensibilidades del sensor al campo de deformación del sensor.

3. MODELO MICROMECÁNICO

Se ha desarrollado un modelo numérico de un sensor de Bragg embebido en un laminado de material compuesto. El sensor ha sido modelado a nivel micromecánico mientras que el laminado se ha modelado a nivel meso mecánico orientando las propiedades en función de la secuencia de apilamiento para el laminado ($[(45/90/-45/0)_3/FO]_s$). Se han usado tres materiales distintos para el modelado del sensor, el recubrimiento y el material huésped. Ambas características pueden observarse en la figura 1, en la que sólo se muestra 1/8 de pieza habiendo sido modelada en realidad una mitad en su totalidad aplicando simetría en la mitad de la pieza respecto el plano XZ.

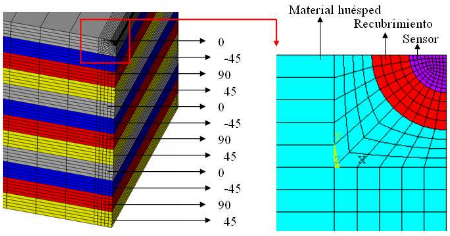

Fig. 1. Modelado numérico de 1/8 de pieza.

El modelo numérico mostrado en la figura 1 ha permitido conocer los campos de deformación tanto del sensor como los lejanos (2-3 diámetros lejos del sensor según Van Steenkiste et al. (1997)), de modo que se han podido calcular los resultados de K_{norm} tanto analíticos como numéricos y compararlos con los experimentales obtenidos por Frövel et al. (2009). Dichas comparaciones se muestran en la tabla 1.

	$K_{norm}^{NUM} x10^{-7}$ (pm/usn/pm)					
ESPECIMEN	EXP [T]	EXP [C]	NUM [T]	NUM [C]	AN [T]	AN [C]
UD [0_{10}/FO/0_{10}]	8.080	8.100	7.955	7.955	7.966	7.975
MD [$(45/90/-45/0)_3$,FO]$_s$	8.086	7.989	7.932	7.934	7.983	7.983

Tabla 1. K_{norm} obtenidos por los tres métodos. (T: tracción; C: compresión).

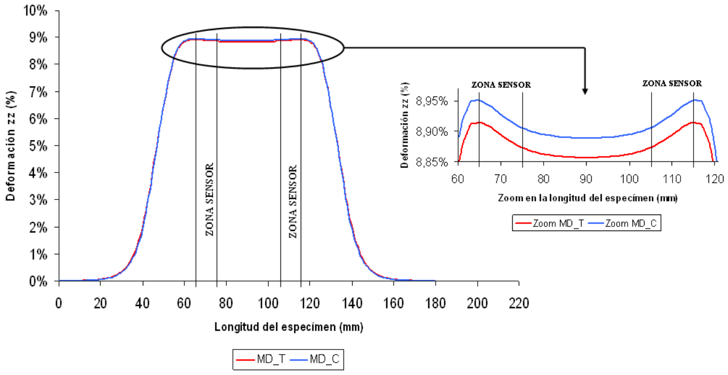

Fig. 2. Evolución de la deformación longitudinal en la zona del sensor.

Experimentalmente se detectan ciertas diferencias en ensayos simétricos a tracción y a compresión que también aparecen en menor medida en los modelos numéricos que tienen en cuenta las distintas propiedades del material a tracción y a compresión. Sin embargo, es importante reseñar que los modelos si han detectado un campo de deformaciones no uniforme en la zona de embebido del sensor que se acentúa en los modelos en apilamiento quasi-isótropo como se muestra en la figura 2. Esto implica que el sensor esté trabajando en una zona no estable de deformación y que por lo tanto su respuesta experimental difiera de la respuesta analítica presentada en la formulación previa por Van Steenkiste (1997).

4. CONCLUSIONES

El presente trabajo ha definido un modo numérico de hallar K_{norm}, parámetro que relaciona la deformación longitudinal del campo lejano de deformación con el output del sensor. También se ha mostrado la importancia de establecer correctamente la posición de embebido del sensor para evitar campos de deformación no uniformes, debidos a la incompleta transmisión de deformación por cortante.

AGRADECIMIENTOS

El primer autor desea agradecer al Ministerio de Educación y Ciencia su aportación económica al presente trabajo en forma de ayuda predoctoral asociada al proyecto de investigación EVISER codificado como TRA2006-15718-C02-01.

REFERENCIAS

Eaton N.C., Drew R.C., Geiger H. (1995). Finite element stress and strain analysis in composites with embedded optical fibre sensors. *Smart Materials & Structures 4:113-117*.

Frövel M., Carrión G., Gutiérrez C., Moravec C., Pintado J.M. (2009). Temperature and humidity dependent performance of FBG-strain sensors embedded in carbon/epoxy composites *en Proceedings of the SPIE Smart Structures/NDE 16th annual international symposium, San Diego, USA*

Frövel M., Cabrerizo F., Pintado J.M. (2009). Influencia de cargas combinadas de tracción/compresión y temperatura en la sensibilidad de los sensores ópticos embebidos y en el coeficiente de Poisson y modulo elático del material compuesto carbono/epoxi T800/M21 *en informe interno del proyecto EVISER, edición inicial.*

Kuang K.S.C., Kenny R., Whelan M.P., Cantwell W.J., Chalker P.R. (2005). Embedded fibre Bragg grating sensors in advanced composite materials. *Optical Communications 251:37-43*

Liu H.Y., Liu H.B., Peng G.D. (2001). Tensile strain characterization of polymer optical fibre Bragg gratings. *Composite Science and Technology 61:1379-87.*

Van Steenkiste R.J., Springer G.S. (1997). Strain and Temperature Measurement with Fibre Optic Sensors, *Technomic publishing company, ISBN Nº:1-56676-480-7*, Lancaster, Pennsylvania (USA).

Influencia del buje en el comportamiento estructural de un acumulador cinético de material compuesto

L. Ripoll
Departament d’Enginyeria Mecànica i de Construcció Industrial
Universitat de Girona, España.
J.L. Pérez-Aparicio
Departamento de Mecánica de Medios Continuos y Teoría de Estructuras
Universidad Politécnica de Valencia, España.

RESUMEN

En un acumulador cinético el buje de unión del rotor con eje central influye en su comportamiento estructural. En el presente trabajo se cuantifican las tensiones generadas y se determina las variaciones del límite de velocidad y de la energía máxima almacenada. Se comprueba que los bujes de geometría maciza son en general perjudiciales, en cambio los de estructura más compleja, hábilmente diseñada, pueden ser indiferentes o incluso favorables.

1. INTRODUCCIÓN

Es sabido que los acumuladores cinéticos con rotor fabricado de material compuesto tienen mayor capacidad de almacenamiento que los metálicos. El material compuesto tiene menor densidad, pero su elevada resistencia permite que la velocidad de giro sea superior y alcanzan mayor energía almacenada por unidad de peso.

Otra diferencia respecto de los metálicos es su mayor elasticidad. Un rotor de material compuesto sometido a una elevada velocidad de giro ω sufre un desplazamiento radial u notablemente superior (fig. 1a). El rotor cilíndrico, en su conjunto, tiende a separarse del eje central, pero en su interior también las fibras externas tienden a separarse de las internas. Se crean tensiones radiales internas de tracción, que al ser transversales a las fibras son muy perjudiciales para el material compuesto. Esta deformación constituye la principal causa de rotura y ha sido ampliamente estudiada en la bibliografía.

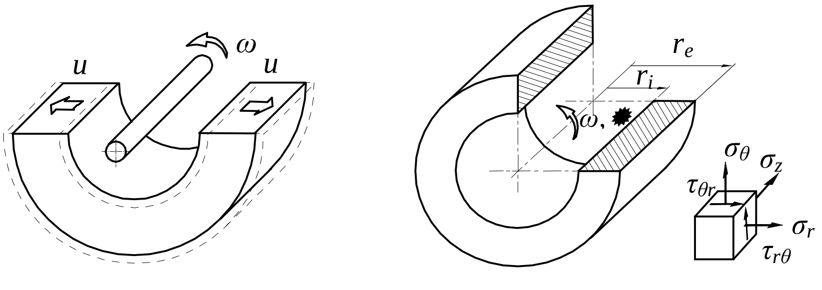

Fig. 1. (a) Desplazamiento radial, superior al rotor de metal (b) Nomenclatura.

En cambio, el desplazamiento del rotor respecto del eje, aunque aparentemente es un fenómeno más simple, ha sido menos estudiado. Requiere analizar el comportamiento tanto del rotor como del buje. El rotor, que debe resistir la fuerza centrífuga, suele tener una forma cilíndrica simple, pero el buje, que ha permitir el desplazamiento radial, se suele construir con formas estructurales más complejas. A continuación se presenta un estudio generalizado para calcular cualquier tipo de fabricación de rotor y buje.

2. FORMULACIÓN

Para determinar las deformaciones y las tensiones en el rotor se aplican las ecuaciones de equilibrio en el plano radial-tangencial (velocidad de giro ω y aceleración angular α)

$$\frac{\partial\sigma_r}{\partial r}+\frac{1}{r}(\sigma_r-\sigma_\theta) = -\rho\omega^2 r \quad ; \quad \frac{\partial\tau_{r\theta}}{\partial r}+\frac{2}{r}\tau_{r\theta}=-\rho\,\alpha\, r \tag{1}$$

siendo, ρ la densidad. También se aplican las ecuaciones cinéticas del desplazamiento radial u y angular υ propias de una estructura cilíndrica

$$\varepsilon_\theta=\frac{u}{r} \quad ; \quad \varepsilon_r=\frac{\partial u}{\partial r} \quad ; \quad \gamma_{r\theta}=\frac{\partial\upsilon}{\partial r}-\frac{\upsilon}{r} \tag{3}$$

Por tratarse de un material compuesto se considera la deformación residual generada por la variación de temperatura ΔT después del curado (coeficientes de dilatación α_θ, α_r y α_z), en cambio se omite la originada por la hidratación para simplificar el sistema de cálculo. Las ecuaciones constitutivas se generalizan mediante el parámetro φ aplicado a la tensión axial (φ=1 para deformación plana generalizado, φ=0 para tensión plana), según Pérez-Aparicio et al. (2003). La deformación axial ε_z^u es el valor constante necesario para que la fuerza axial F_z sea nula.

$$\sigma_z(r)=\varphi\left[E_z\left(\frac{\nu_{\theta z}}{E_\theta}\sigma_\theta+\frac{\nu_{rz}}{E_r}\sigma_r+\varepsilon_z^u-\alpha_z\Delta T\right)\right] \quad ; \quad F_z=\int_{r_i}^{r_e}\sigma_z\,2\pi r\,\mathrm{d}r=0 \tag{4}$$

Los desplazamientos y las tensiones (Pérez-Aparicio et al. (2003)) son

$$\begin{aligned} &u=Ar^{-k}+Br^{k}+U_b\,r^3+U_{d1}\,r+U_{e1}\,r \quad ; \quad \upsilon=Cr^{-1}+Dr+\frac{a}{8}r^3\\ &\sigma_\theta=H_A\,r^{-(k-1)}+H_B\,r^{k-1}+H_b\,r^2+H_{d1}+H_{e1}\\ &\sigma_r=R_A\,r^{-(k-1)}+R_B\,r^{k-1}+R_b\,r^2+R_{d1}+R_{e1} \quad ; \quad \tau_{r\theta}=G_{r\theta}\left(\frac{2C}{r^2}+\frac{a}{4}r^2\right)\end{aligned} \tag{5}$$

en donde, k es el ratio de anisotropía del material y U, H y R son coeficientes que dependen de los distintos efectos: b fuerza centrífuga, d deformación axial y e tensiones residuales térmicas (Ripoll et al. (2007)). Los coeficientes de contorno A, B, C y D se determinan en las ecuaciones (15) i (16), para el caso de un rotor formado n capas y un buje genérico de la Fig. 2a. El buje está modelizado mediante dos constantes elásticas (radial k_r, tangencial k_θ) y una masa de inercia equivalente m_e.

$$\sigma_r^{\,1}(r_1)=\frac{k_r u^1(r_1)\text{ - }m_e r_1\quad{}^{2}}{2\pi r_1}\quad;\qquad \sigma_r^{\,n}(r_{n+1})=0 \qquad (15)$$
$$\sigma_r^{\,j}(r_j)=\sigma_r^{\,j\text{-}1}(r_j)\quad;\qquad u^j(r_j)=u^{j\text{-}1}(r_j)\,;\qquad j=2...n$$

$$\tau_{r\theta}^{\,1}(r_1)=\frac{k_\theta\ \upsilon^1(r_1)}{2\pi r_1}\quad;\qquad \tau_{r\theta}^{\,n}(r_{n+1})=0 \qquad (16)$$
$$\tau_{r\theta}^{\,j}(r_j)=\tau_{r\theta}^{\,j\text{-}1}(r_j)\quad;\qquad \upsilon^j(r_j)=\upsilon^{j\text{-}1}(r_j)\ ;\qquad j=2...n$$

Finalmente, la velocidad límite se determina mediante el criterio de fallo de Christensen (1997), aplicando un factor de rotura igual a la unidad.

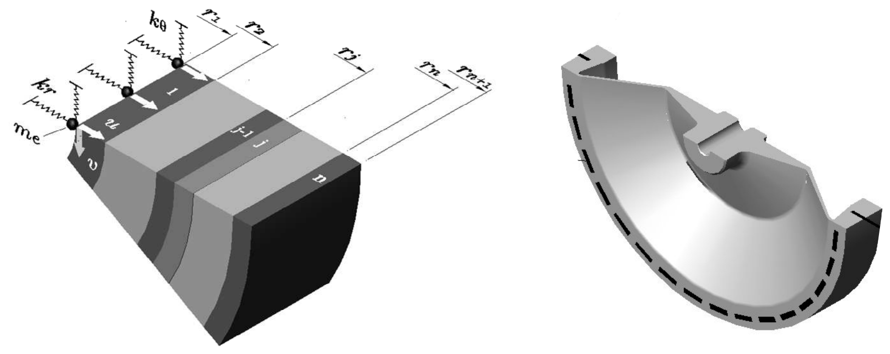

Fig. 2. (a) Rotor multicapa con buje modelizado, (b) Volante con buje Z elástico.

3. MODELOS DE BUJE

Antes de analizar las distintas configuraciones de buje se estudia un rotor libre, aislado de perturbaciones exteriores. Un ejemplo es el volante con buje elástico tipo Z (Fig. 2b). Se ha elegido un rotor de una sola capa de fibra de vidrio, de 0.2 m de radio exterior r_e y 0.06m de longitud, y un decremento de temperatura de curado: de 120 a 20ºC. En la Fig. 4 se presenta la velocidad máxima y la energía almacenada para distintos radios interior r_i. Se observa que los valores tienen un máximo en r_i/r_e =0.73, que separa dos zonas con tendencias claramente distintas: a la derecha, donde espesor de pared es pequeño, rompe por tensión circunferencial, y a la izquierda rompe por tensión radial.

Las configuraciones de buje macizo son las más simples (Fig 3a) y su influencia sobre el rotor depende de la elasticidad del material. Se han aplicado a tres tipos: más rígido que el rotor (aluminio), de rigidez similar (nylon) y más elástico (uretano). En la Fig. 4 se observa que el aluminio es perjudicial, excepto en r_i cercanos a r_e. El nylon y el uretano son perjudiciales en r_i/r_e superiores a 0.65, e indiferente en r_i/r_e inferiores.

Para las configuraciones estructurales se estudia un buje cilíndrico de acero ranurado, con extremos semiesféricos, propuesto por Ha y al.(2006). Las barras ejercen presión radial sobre el rotor y permite velocidades más elevadas en rotores de pared gruesa.

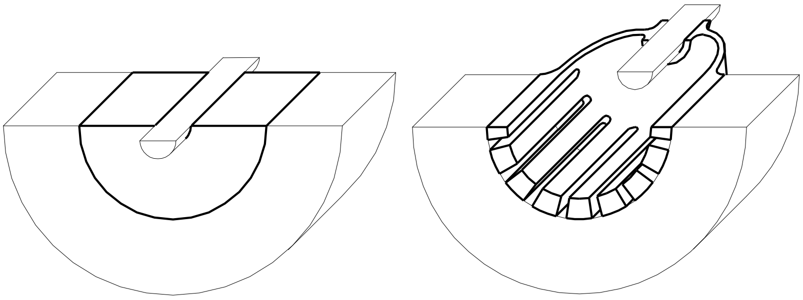

Fig. 3. (a) Buje macizo, (b) Buje metálico de barras flexibles.

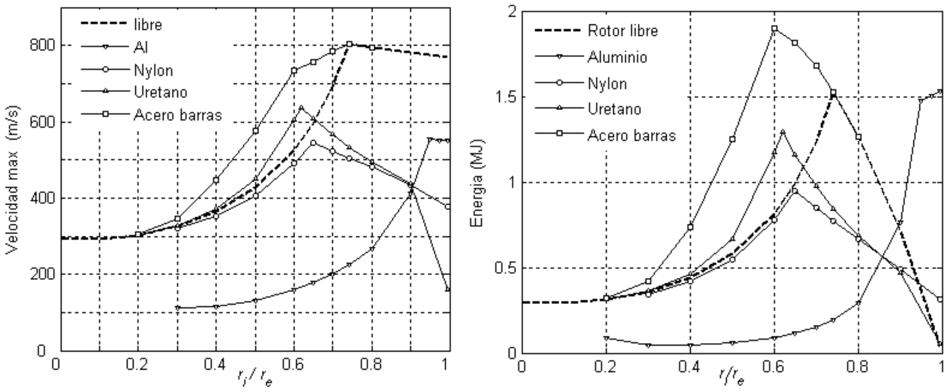

Fig. 4. Velocidad máxima y energía en función del radio interior del rotor.

4. CONCLUSIONES

1. Los bujes de geometría maciza disminuyen el límite de velocidad del rotor, excepto los de material muy elástico cuando el espesor de pared del rotor es grande.
2. Los bujes de configuración estructural compleja suficientemente elásticos no perjudican el rotor, incluso son favorables si ejercen presión radial sobre el rotor.

REFERENCIAS

CHRISTENSEN, R.M. (1997). Stress based Yield/Failure criteria for fiber composites. *Int. J. Solids & Struc., 34,* 529-543.

HA S. K., KIM M. H., HAN S. C., SUNG T. H. (2006) Design and spin test of a hybrid composite flywheel rotor with a split type hub. *J. Composite Materials* 40 (23) 2113-30.

PEREZ-APARICIO J.L., RIPOLL L. (2003). Solución Generalizada para Piezas Cilíndricas de Material Compuesto. *V Congreso AEMAC, Julio 2003,* Zaragoza.

RIPOLL L., PEREZ-APARICIO J.L. (2007). Efecto perjudicial del transitorio en la hidratación del material compuesto aplicado volantes de inercia. *VI Congreso AEMAC,* Valladolid.

Sensores de fibra óptica grabados con redes de Bragg embebidos en un laminado carbono/epoxi: estudio e implementación de un modelo opto-mecánico

C. Gutiérrez, J. Rams
Departamento de Ciencia e Ingeniería de Materiales. Universidad Rey Juan Carlos, España
M. Frövel
Área de Materiales Compuestos. Instituto Nacional de Técnica Aeroespacial (INTA), España
D. Sans, J.A. Mayugo
AMADE, Escuela Politécnica Superior, Universidad de Girona, España

RESUMEN

Se ha observado que existen variaciones significativas en la sensibilidad de los sensores de fibra óptica tipo Bragg (Fiber Bragg Grating Sensor, FBGS) cuando éstos son sometido a tracción o a compresión. Los distintos modelos analíticos no son capaces de explicar estas diferencias de comportamiento, por lo que resulta conveniente estudiar estos sistemas a través de métodos numéricos. Los modelos numéricos basados en la aplicación del método de los elementos finitos permiten estudiar con precisión la variación de los parámetros ópticos ante deformaciones en la fibra óptica, pudiendo tener en cuenta tanto heterogeneidades ópticas como geometrías arbitrarias en cada sección transversal. En este trabajo se estudia el desarrollo de un modelo opto-mecánico de un FBGS, basado en el método de los elementos finitos en combinación con el método de las matrices de transferencia.

1. INTRODUCCIÓN

Se ha comprobado experimentalmente mediante distintos ensayos de caracterización de FBGS embebidos en laminados de material compuesto de carbono/epoxi, que se producen variaciones significativas en la sensibilidad del sensor cuando éste es sometido a tracción o a compresión (Frövel et al. 2009). Por lo tanto la utilización en servicio de este tipo de sensores exige que su comportamiento deba ser caracterizado y comprendido, tanto desde el punto de vista mecánico como desde el óptico. Los distintos modelos analíticos, entre los cuales es especialmente importante el desarrollado por Van Steenkiste et al. (1997), no pueden explicar estas diferencias observadas a tracción y compresión. Los métodos numéricos basados en la aplicación del método de los elementos finitos, para el estudio del comportamiento óptico en la fibra óptica, estudiados por Koshiba et al. (1992) y Kawano et al. (2001), entre otros, permiten estudiar con precisión los modos de propagación en la fibra óptica ante campos de deformaciones no uniformes, pudiendo tener en cuenta, además, heterogeneidades ópticas y geometrías arbitrarias en cada sección transversal de la fibra óptica. Prabhugoud et al. 2006 utilizaron estos métodos en combinación con el método de las matrices de transferencia, introducido por primera vez por Yamada et al.1987, para obtener la respuesta óptica del sensor óptico.

El objetivo de este trabajo es el desarrollo de una herramienta que permita calcular la respuesta óptica de un modelo de elementos finitos de un FBGS embebido en una estructura sometida a cargas en principio arbitrarias, y que ha sido previamente definido a través de una herramienta comercial de análisis de elementos finitos (en este trabajo se ha utilizado ANSYS). El cálculo de los modos de propagación en la fibra óptica y de la respuesta espectral de la red de Bragg se ha se ha desarrollado en Matlab. Este modelo puede ser aplicado a FBGSs embebidos en una gran variedad de materiales huésped, y a diferentes tipos de fibras ópticas. Este modelo también puede tener en cuenta el efecto de la rotación de los ejes de polarización que se produce cuando existen campos de deformaciones no uniformes, lo que ocurre en zonas de concentraciones de tensiones o de avance de grietas. Esta característica resulta de gran importancia en el estudio de la detección de daños en estructuras empleando este tipo de sensores.

2. DESCRIPCIÓN DEL MODELO

Los modelos de elementos finitos para guías de ondas ópticas se clasifican según utilicen una formulación vectorial o escalar. La formulación vectorial puede aplicarse a guías de ondas con cualquier valor de índice de refracción en el núcleo y en la cubierta, también denominada corteza. La aproximación escalar se utiliza en las guías de onda ópticas de guiado débil, en las que los índices de refracción del núcleo y de la cubierta son muy parecidos. Esta aproximación resulta razonable para la mayoría de las fibras ópticas con FBGSs sometidas a un rango de deformaciones dentro de su límite elástico. La ventaja de la formulación escalar es que es más sencilla, más eficiente desde el punto de vista computacional, y no produce soluciones espurias.

El método de las matrices de transferencia divide el FBGS en segmentos a lo largo del eje de la fibra óptica, entre los cuales las propiedades ópticas del sensor permanecen constantes. Por lo tanto, aunque el problema originalmente es de tipo tridimensional, se aborda calculando las constantes de propagación en cada sección del sensor, empleando para ello elementos y ecuaciones bidimensionales, y obteniendo la respuesta espectral de la red de Bragg a lo largo del eje de la fibra óptica. De forma simplificada, el procedimiento de cálculo del modelo sigue los siguientes pasos:

I. Definición de la geometría, las propiedades de los materiales y las condiciones de contorno del FBGS embebido. Los desplazamientos de los nodos y las deformaciones en cada elemento del FBGS son utilizados para la parte óptica del modelo.

II. Para cada elemento de cada sección transversal del FBGS, se aplica una ley fotoelástica para calcular la variación del valor del índice de refracción como consecuencia de la aplicación de una carga, asumiendo que cada elemento es ópticamente isótropo con un único valor de índice de refracción en reposo. Los ejes ópticos p y q coinciden con las direcciones principales de la carga en cada elemento (Fig. 1).

III. La formulación de la ecuación de onda por el método de los elementos finitos, para una fibra óptica de salto de índice, da lugar a una ecuación de autovalores cuyo resultado son los índices de refracción efectivos (n_{eff}) para cada sección de la fibra óptica, y para una longitud de onda dada.

IV. Una vez conocidos los índices de refracción efectivos en cada segmento de la fibra óptica, se calcula la respuesta espectral del FBGS aplicando el método de las matrices de transferencia, y que resulta apropiado para calcular la respuesta espectral en redes de Bragg con propiedades ópticas no homogéneas. El número de segmentos en que se divide el sensor está determinado por la complejidad de las cargas a las que está sometido.

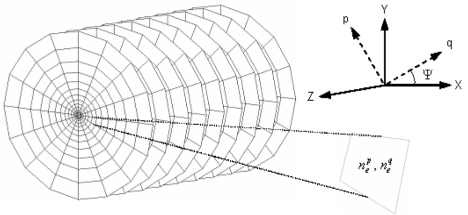

Fig. 1. Modelo de FBGS dividido en secciones a lo largo del eje de la fibra óptica, cada una de ellas discretizada en elementos bidimensionales. Los ejes de polarización de cada elemento son p y q y los ejes de coordenadas globales son X-Y-Z. El eje de la fibra óptica coincide con el eje Z.

3. EVALUACIÓN DEL MODELO

Para comprobar la validez de este modelo, se han planteado distintos casos de prueba que permitan comparar los resultados obtenidos con las soluciones de los modelos analíticos, para diferentes tipos de fibra óptica.

- Comparación de la solución analítica de la ecuación característica de la fibra óptica (representación del índice efectivo n_{eff} de los distintos modos de propagación linealmente polarizados, frente a la frecuencia normalizada V), con los valores obtenidos por el modelo de elementos finitos (Fig. 2).
- Análisis del comportamiento del modelo en los casos de tracción y compresión simples.
- Estudio de la birrefringencia producida en la fibra óptica sometida a carga, a través de la simulación de un FGBS sometido a compresión diagonal (Fig. 3).
- Estudio de casos de distribución de carga no uniforme y de la rotación de los ejes de polarización producida a lo largo del sensor óptico.

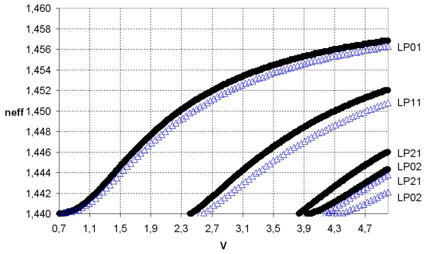

Fig. 2. Solución analítica (círculos) y del modelo de elementos finitos (triángulos, 48 elementos en el núcleo y 160 en la cubierta) de la ecuación característica.

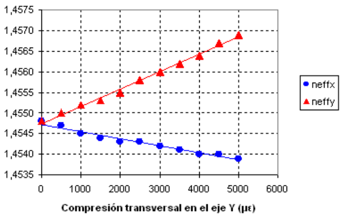

Fig. 3. Variación de n_{eff} para una fibra óptica sometida a compresión transversal en el eje Y, para λ = 1550 nm (V = 4).

En los distintos casos probados, se ha comprobado una excelente correlación entre los modelos más establecidos y el modelo puesto a punto en este trabajo. Esta aproximación es mayor en el caso de que se trabaje con fibras ópticas con un bajo número de modos.

En los otros casos, las tendencias son idénticas a las de la solución analítica. De esta manera, se cuenta con una herramienta de simulación que se puede emplear en la validación y análisis de resultados experimentales, en especial en el caso de sensores sometidos a condiciones de cargas complicadas.

4. CONCLUSIONES

Se ha comprobado la importancia de ajustar adecuadamente el modelo para obtener una precisión suficiente en la resolución de las ecuaciones sin excederse en el tiempo de cálculo. Las simulaciones de un FBGS en estado libre sometido a distintas condiciones de carga muestran el comportamiento esperado según los modelos analíticos, por lo que se trata de un modelo útil en simulación y para el análisis de datos experimentales.

REFERENCIAS

Frövel M., Carrión G., Gutiérrez C., Moravec C., Pintado J.M.; “Temperature and humidity dependent performance of FBG- strain sensors embedded in carbon/epoxy composites”; Proceedings of SPIE Smart Structures/NDE, 16th annual international symposium, San Diego, USA, 2009.
Kawano K., Tsutomu K., “Introduction to Optical Waveguide Analysis”; John Wiley & Sons, Inc, ISBN Nº: 0-471-22160-0, NY, USA, 2001.
Koshiba M., “Optical Waveguide Theory by the Finite Element Method”; MA: Kluwer-Scientific, ISBN Nº: 0-7923-2080-8, Tokyo, Japan, 1992.
Prabhugoud M., Peters K.; “Finite element model for embedded fiber Bragg grating sensor”; Smart Materials and Structures 15, pp 550-562, 2006.
Van Steenkiste R.J., Springer G.S., “Strain and temperature measurement with fibre optic sensors”; Technomic publishing company, ISBN Nº: 1-56676-480-7, Lancaster, Pennsylvania, USA, 1997.
Yamada M., Sakuda K.; “Analysis of almost-periodic distributed feedback slab waveguides via a fundamental matrix approach”; Applied Optics 26, pp 3474-3478, 1987

.

Lightcarboncars: puesta a punto y monitorizado con fibra óptica del procesado mediante RTM de compuestos de matriz termoplástica

A. Agirregomezkorta, M. Sarrionandia, J. Aurrekoetxea
Departamento de Mecánica y Producción Industrial, Mondragón Unibertsitatea, España
A. Fernández-López, A. Güemes
Departamento de Materiales y Producción Aeroespacial. Universidad Politécnica de Madrid, España

RESUMEN

En el presente trabajo se ha monitorizado el proceso de TP-RTM mediante sensores de fibra óptica. La medida distribuida mediante la técnica de la dispersión de Rayleigh se ha mostrado como una herramienta eficaz para la monitorización del proceso de llenado para RTM, ya que se ha detectado con éxito la falta de impregnación de las fibras. La monitorización del proceso de polimerización y cristalización no ha sido posible debido al ciclo térmico utilizado durante el proceso. La técnica también es sensible a la contracción durante el enfriamiento, si bien el efecto del tejido de fibras de carbono limita la realización de medidas al comienzo del enfriamiento.

1. INTRODUCCIÓN

En los últimos años se han desarrollado matrices termoplásticas de muy baja viscosidad (20 mPa.s para el CBT® a 180 °C, la viscosidad en fundido del PBT para inyección es 5000 veces mayor) que se pueden transformar mediante RTM (*ThermoPlastic-RTM*, TP-RTM) (van Rijswijk et al. 2007). A diferencia del procesado tradicional basado en la fusión/cristalización de los termoplásticos, en el procesado en fase líquida también existe la polimerización. Además, la polimerización y la cristalización pueden ocurrir simultáneamente (Parton et al. 2005).

La puesta a punto del TP-RTM requiere de la comprensión de los procesos de llenado, polimerización y cristalización, por lo que resulta imprescindible monitorizar dichos fenómenos durante el procesado. Existen diferentes técnicas para monitorizar los procesos, entre los que destacan las medidas dieléctricas, los ultrasonidos, los termopares, los sensores de voltaje puntual y lineal, y los sensores de fibra óptica (Dunkers et al. 2001). En el presente trabajo se evalúa la viabilidad de monitorizar el proceso de TP-RTM mediante sensores de fibra óptica debido a que esta técnica es mínimamente invasiva y no compromete la integridad estructural del componente, además de ser extremadamente sensible a las deformaciones y variaciones de temperatura [AFL1].

2. MATERIALES Y MÉTODOS EXPERIMENTALES

2.1. Materiales

El prepolímero utilizado en este estudio fue el oligómero CBT160® suministrado por Cyclics. Como refuerzo se utilizó un tejido plano equilibrado [0º/90º] de fibra de carbono de alta resistencia con un gramaje de 200 g/m^2 (Suministrado por Hexcel, ref. 43199). En cada laminado se han utilizado 10 capas.

2.2. Fabricación del compuesto mediante TP-RTM

Se moldearon dos laminados mediante TP-RTM, una sin defectos y otra induciendo voluntariamente un fallo en el llenado. El oligómero fundido (230 ºC) se inyectó mediante vacío en un molde cerrado (calentado a 230 ºC), donde previamente se acomodó el refuerzo. Posteriormente, se enfrió a 190 ºC, manteniendo esta temperatura durante 30 minutos, y finalmente se enfrió fuera del horno durante 120 minutos hasta temperatura ambiente, antes de ser desmoldeado. Se fabricaron dos placas de 250 x 250 x 3,5 mm^3 de CF-pCBT.

2.3. Monitorizado del proceso mediante fibra óptica

Existen multitud de ejemplos en la bibliografía sobre la monitorización de procesos de curado e inyección de resina con sensores de fibra óptica, mayoritariamente redes de Bragg y sensores basados en el efecto Fresnel. En esta ocasión se ha planteado utilizar una técnica basada en sensores distribuidos basada en la medida espectral de la dispersión de Rayleigh. Por medio de esta técnica es posible medir en cada punto de la fibra el paso espectral, que es proporcional a las variaciones de temperatura y deformación según la siguiente relación:

$$\frac{\Delta\lambda}{\lambda} = -\frac{\Delta\gamma}{\gamma} = K_T \Delta T + K_\varepsilon \varepsilon$$

La relación que existe entre la variación de temperatura y deformación con el desplazamiento espectral es idéntica al comportamiento de una red de Bragg, que es una perturbación local en la fibra de periodo constante, relacionado con su longitud de onda en reflexión. Durante la fabricación de la fibra se producen unas imperfecciones en su núcleo, que se pueden modelizar como una red de Bragg distribuida de periodo aleatorio. El espectro de una sección de la fibra es estable en ausencia de perturbaciones exteriores, y se puede asemejar a una “huella dactilar” de la fibra, de forma que cualquier perturbación (normalmente deformaciones y temperatura) sobre ella se ve reflejada en el espectro de la misma. El paso espectral va a ser la magnitud empleada para la monitorización, al tener tanto la temperatura como la deformación una influencia importante, y no existir ninguna medida independiente de la temperatura.

3. RESULTADOS Y DISCUSION

3.1. Monitorizado del llenado del molde

El monitorizar del proceso resulta efectivo para controlar el sistema y permite mejorar los modelos de simulación. Como se observa en la figura 1.a el proceso de llenado no se ha completado satisfactoriamente, ya que entre los pliegues 4 y 7 se encuentra una zona que no se ha rellenado. En los espectros obtenidos con la fibra óptica durante el proceso de inyección se pueden interpretar dos aspectos fundamentales; i) que el sistema ha sido capaz de detectar el punto de entrada y de salida del flujo, y ii) que no ha sido capaz de detectar las zonas defectuosas. Esta falta de sensibilidad se atribuye en parte a la baja viscosidad de la resina, un orden de magnitud menor que las termoestables convencionales (van Rijswijk et al. 2007), lo que induce deformaciones despreciables de la fibra óptica durante el llenado. Por otro lado, la fibra óptica, el molde y el polímero se encuentran a la misma temperatura durante el llenado, por lo que la variación de temperatura tampoco es significativa como para generar distorsiones detectables por el sistema de monitorizado. En trabajos futuros se estudiarán rutas de procesado de TP-RTM en las que el polímero durante el llenado estará más caliente que el molde, y por ende que la fibra óptica, por lo que se prevé que en estas condiciones el sistema sí será válido para monitorizar el llenado.

3.2. Monitorización de la fase de polimerización y cristalización

En la Figura 1.b se muestran las variaciones del paso espectral a lo largo de la fibra óptica embebida durante el proceso de polimerización-cristalización llevado a cabo a 190 ºC durante 30 minutos. Se realizaron 5 mediciones durante dicho proceso. En los espectros no se monitoriza la polimerización, lo que probablemente se justifique por tratarse de un proceso entrópicamente conducido y a temperatura constante, en el que no se produce cambios dimensionales (Karger-Kocsis et a1. 2007). Al ser el paso espectral proporcional a las variaciones de temperatura y deformación, durante esta etapa no se produce una variación significativa, y las pequeñas desviaciones respecto a la medida inicial se pueden explicar por las variaciones térmicas asociadas al proceso. Esto implica que las contracciones generadas durante la cristalización isotérmica son despreciables.

3.3 Monitorización del enfriamiento

En la figura 1.b se observa la variación del paso espectral de una medida realizada a los 10 minutos de comenzar el proceso de enfriamiento desde 190 ºC. Existe una clara diferencia entre las zonas con resina y sin ella, debida a las deformaciones inducidas durante el enfriamiento, y, en menor medida, a la diferente conducción del calor entre las zonas en las que se ha inyectado la resina y en las que no. Debido al alto coeficiente de expansión térmico de la resina, (casi 100 με/K), que al enfriarse generan fuerzas de compresión transversales sobre la fibra, se inducen pérdidas en la fibra, que unidas a las pérdidas debidas a la microflexión provocada por la geometría del tejido, impidieron realizar más medidas durante el enfriamiento.

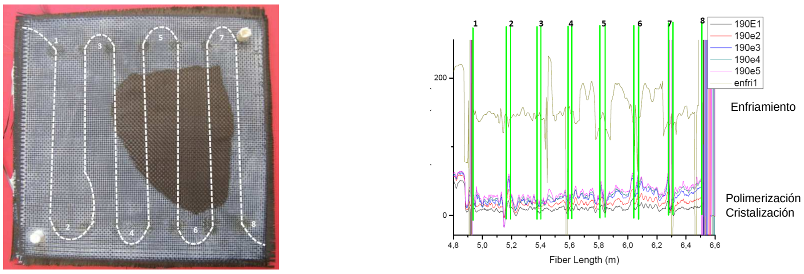

(a) (b)

Fig. 1. Fotografía de la placa con defectos de llenado (a) y paso de la dispersión espectral a lo largo de la fibra (b).

4. CONCLUSIONES

Si bien el sistema ha sido capaz de detectar la entrada y salida de la resina, los defectos de llenado no se detectan durante la fase de inyección debido a que la viscosidad es muy baja y la temperatura de la resina es similar a la del molde. Sin embargo, en el enfriamiento se producen contracciones diferenciales entre las zonas con resina y las mal impregnadas, permitiendo identificar las zonas defectuosas. La naturaleza atérmica del proceso de polimerización del CBT en pCBT, y la ausencia de contracción durante la polimerización, son las razones por las que el sistema de monitorización mediante fibra óptica no ha sido válido. La cristalización isotérmica del pCBT se produce con niveles de contracciones muy bajas, ya que han sido inferiores a la sensibilidad de la fibra óptica. Finalmente, las contracciones asociadas al enfriamiento de la matriz han sido tan grandes que han inducido deformaciones transversales y microflexiones de la fibra que disminuyen la calidad de la señal llegando a impedir cualquier interpretación.

AGRADECIMIENTOS

Los autores desean agradecer a Iñigo Ortiz de Mendivil por su colaboración en el procesado mediante TP-RTM. Se agradece también al Ministerio de Ciencia e Innovación (PSE-370000-2008-4 proyecto LIGHTCARBONCARS) y al Departamento de Educación, Universidades e Investigación del Gobierno Vasco (PI2008-07) por la financiación del presente trabajo.

REFERENCIAS

DUNKERS, J.P., LENHART, J.L., KUEH, S.R., van ZANTEN, J.H., ADVANI, S.G., PARNAS, R.S. (2001). Fiber-optic flow and cure sensing for liquid composite molding. *Opt. Lasers Eng.*, 35, 91–104.

KARGER-KOCSIS, J., SHANG, P.P., MOHD ISHAK, Z.A. RÖSCH, M. (2007). Melting and crystallization of in-situ polymerized cyclic butylene terephthalates with and without organoclay a modulated DSC study. *Express Polymer Letters*, 1, 60–68.

PARTON, H., BAETS, J., LIPNIK, P., GODERIS, B., DEVAUX, J., VERPOEST, I. (2005). Properties of poly(butylene terephthatlate) polymerized from cyclic oligomers and its composites. *Polymer*, 46, 9871-9880.

van RIJSWIJK, K., BERSEE, H.E.N. (2007). Reactive processing of textile fiber-reinforced thermoplastic composites – An overview. *Compos. A: Appl. Sci. Manuf.*, 38, 666-681.

KREGER, S., GILFORD, D., SOLLER, B., WOLFER, M., FROGATT, M. (2004). Fiber Calibration for distributed fiber optic strain and temperature measurements using the optical backscatter reflectometer“, Proc, SPIE, 5502

Use of nanocomposites for the production of RTM structural parts in auto motive applications

J.M. Kenny*, A. Terenzi
Università degli Studi di Perugia, Loc. Pentima Bassa, 21 05100 Terni (TR), ITALY
*Current address: ICTP-CSIC, Juan de la Cierva 3, 28006 Madrid, SPAIN
D.R. Angulo
Sistemas y Procesos Avanzados S.L., C/ María de Luna 11, nave 5 - CEEI Aragón
50.018 Zaragoza, SPAIN
D. Wilde
Alcan Composite Structures, Park Altenrhein CH-9423 Altenrhein, SWITZERLAND
D. Bassan
Centro Ricerche Fiat S.C.p.A., Strada Torino, 50 10043 Orbassano (TO), ITALY

SUMMARY

The work reported in this paper was developed in the framework of the European Project SuperLIGHT-CAR. The overall objective of the project is the realization of advanced multi-material lightweight vehicle structures achieving: 30% weight reduced vehicle structure (Body-In-White), Reduction of manufacturing costs and cycle times, Technologies suitable for large series production (approx. 1000 cars/day), Equivalent performance (C-class segment): e.g. crash, fatigue, etc., Reduced raw material consumption.

In order to fulfil the previous objectives a research work based on a multi-materials approach was addressed in the project.

In order to improve important material properties as mechanical performance, thermal stability and electrical properties, different kind of nanoparticles have been selected and added to the matrix used for the production of structural composites.

The analysis of the rheological properties and cure kinetics was performed in order to analyse the processing ability of the nanofilled system in comparison to the neat resin. The results show an important influence of the nanoparticles on the rheological properties at very low shear rate, whereas at higher shear rates no particular deviations are observed. This is very good in terms of processing ability because the RTM processes involve very high shear rates.

The analysis of the final properties show an important contribution of the nanoparticles. In particular, CSR are very effective in terms of material toughness improvement, whereas CNF give a contribution on the electrical properties, finally the layered silicates are more effective in terms of material modulus.

In general the results of the work show that the use of nanocomposites in the composites produced by RTM technology imply important advantages in terms of final properties with a very low influence on the processing ability.

1. INTRODUCTION

This work is a basic research targeted to evaluate the application possibilities of Nanotechnologies for matrix properties improvements, in RTM structural composites.

Currently there are several possibilities to implement nanotechnologies in polymeric systems, however in this framework only the technologies compatible with industrial applications were investigated. More in detail the costs of the materials used and the processing ability was taken into primary consideration during the research work.

Several work published in literature show that there are good possibilities to improve materials properties such us mechanical performance, thermal resistance, electrical behaviour, etc. of polymeric systems with the application of specific nanofiller dispersed into the polymer matrix. On the bases of these work a specific research activities was addressed on the materials used for RTM processes for the production of structural components for in the automotive field.

The research work started with a preliminary technological screening, after that the materials and the processing conditions was studied and defined, the samples for the testing was produced and tested and finally some injection trials was performed in order to verify the possibility to produce structural composites and to analyse the influence on their final properties.

2. EXPERIMENTAL

The following nanofillers have been considered in this work: Nanoclays (Southern Clays Cloisite 30B), Core shell rubber (Kaneka), Carbon nanofibres (CNF) (Euroguarco). Rheological tests were done in a rotational rheometer ARES with parallel plate geometry (ϕ 25mm). Electrical and mechanical measurements have been performed in order to analyse the effect of the nanofiller on the material performance. Finally some DSC experiments have been performed in order to analyse the cure kinetics of the systems produced. Some injection trials with the nanofilled systems and carbon fibres have been done and the materials produced have been tested.

3. RESULTS AND DISCUSSION

3.1 Rheological and calorimetric analysis

In the following figure 1 the rheological measurements in dynamic conditions at 60°C are reported for the system epoxy/cloisite 30B, filled with different content and processed with different stirring time.

By observing the previous curves it is possible to see that the effect of the filler in the matrix is higher at low shear rate. This is very important and it is very positive in terms of the utilization of the system in RTM process. In fact, the shear rate during the RTM are higher than the maximum shear rate achieved during the test, therefore at those levels of shear rate the difference of the viscosity between filled and pure resin do not compromise the processing ability of the system.

By the previous curves is also important to observe that the stirring time is an important parameter for the dispersion level. Higher is the slope of the curve in the low shear region, higher is the dispersion level of the filler.

The system filled with CSR and CNF show a behaviour quite similar to that observed in silicate filled system.

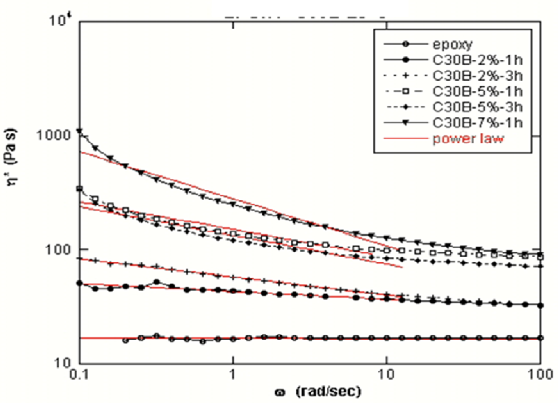

Fig. 1. Rheological measurements in dynamic conditions for epoxy/Cloisite 30B system at 60°C.

The analysis of the cure kinetic of the filled resin performed with calorimetric and rheological measurements show that no particular influences are observed by adding the different kind of nanofiller tested. By observing these curves it is possible to note that the presence of the nanofiller with different content is not particularly significant in terms of curing kinetics. The gelation time and the onset time are practically unchanged with the presence of the nanofiller. Similar results can be observed for system filled with CSR and for system with CNF; moreover the calorimetric analysis confirm this behaviour

3.2 Electrical analysis

In figure 2 the electrical characterization of CNF filled systems is reported.

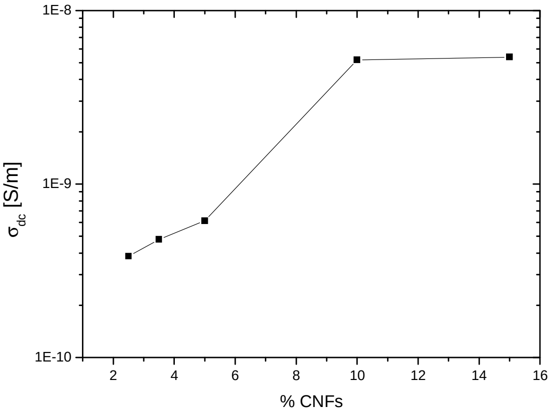

Fig. 2. DC conductivity measurement on the CNF filled epoxy with different concentrations.

It is possible to observe that the percolation threshold is achieved with a content of 10%; in fact, further increase in the concentration does not imply increase in electrical conductivity.

3.3 Mechanical analysis, injection trials and composite characterization

The results of the mechanical analysis of nanofilled resin show important improvements in terms of tensile properties (MMT reinforced materials) and toughness (CSR filled materials.

The first injection trials with a V-RTM technique was performed with the epoxy Cloisite 30B system with a concentration of 2 wt% of nanofiller. This concentration was chosen because the variation of the rheological properties is very low. The carbon fibre volume content is 50%. In this injection trials, relatively slow conditions have been used in order to have a better control of the process. The injection pressure is 2 bar, the vacuum level is 0,4 bar the resin was pre-heated at 40°C in order to have enough time for the injection. The results of the mechanical test are reported in the following table 1.

Materials	**Flex. Young Modulus [GPa]**	**Flex. Strength [MPa]**
Composites	45,85 ± 2,04	502 ± 94
Nano-filled composites	48,63 ± 0,62	680 ± 25

Table 1: Flexural properties of composites with and without nanofiller

By observing these results it is possible to note that the presence of nanofiller has an important effect both on modulus and on strength in flexural conditions. The modulus increase is around 6% and the strength of 35%.

4. CONCLUSIONS

The results achieved in this work show that in some case the nanoparticles can improve significantly the performance of the material used as matrix in RTM process.

It is important to achieve a very good dispersion of the nanoparticles and in several cases the support of ultrasonic technology has to be used to improve this parameter.

The viscosity of the matrix is affected by the presence of nanoparticles, however in several case it is still possible to perform injection with different fabrics typology.

ACKNOWLEDGMENT

The authors want to be grateful to EC for founding SLC project in the 6th framework program.

REFERENCES

DAY R.J., LOVELL P. A., WAZZAN A. A. (2001) Toughened carbon/epoxy composites made by using core/shell particles, *Composites Science and Technology 61, Elsevier.*

FIDELUSA J. D., WIESELA E., GOJNYB F. H., SCHULTEB K., WAGNER H.D. (2005) Thermo-mechanical properties of randomly oriented carbon/epoxy nanocomposites, *Composites: Part A 36, Elsevier*

KICKELBICK G. (2003) Concepts for the incorporation of inorganic building blocks into organic polymers on a nanoscale, *Prog. Polym. Sci. 28, Elsevier*

KÖHLER M., FRITZSCHE W. (2004) Nanotechnology An Introduction to Nanostructuring Techniques, *VCH Verlag GmbH & Co. KGaA, Weinheim Wiley*

NALWA H. S. (2002) Nanostructured Materials and Nanotechnology, *Academic Press A Harcourt Science and Technology Company, San Diego*

Lightcarboncars: reducción del impacto ambiental de automoviles mediante el aligeramiento estructural basado en composites de carbono de bajo coste, sin comprometer la seguridad y el confort

G. Castillo
Departamento de Mecánica y Producción Industrial, Escuela Politécnica Superior de Mondragón Unibertsitatea. Coordinador Proyecto Singular Estratégico Lightcarboncars

RESUMEN

La necesidad de reducir el consumo energético de los vehículos así como sus emisiones de CO_2 implica el desarrollo de motores más eficientes y un drástico aligeramiento de las estructuras de los vehículos sin perjuicio de la seguridad o del confort. Los materiales compuestos han demostrado, mediante su utilización en automóviles de alta gama o de competición, la bondad de su utilización. Sin embargo, el alto costo del material, los bajos ratios de producción, y en menor grado, los problemas de reciclabilidad han limitado, por no decir impedido su implantación en el sector del automóvil de gran producción, gran consumidor energético y fuente de una elevada contaminación. Es por tanto necesario abaratar las materias primas y aumentar las cadencias de fabricación de los componentes de composite, manteniendo los estándares de seguridad y confort. En este artículo se presentan los objetivos y estructuración del Proyecto Singular Estratégico LIGHTCARBONCARS.

1. INTRODUCCIÓN

El calentamiento global es hoy en día indiscutible y puede tener efectos dramáticos sobre la vida individual, colectiva y la seguridad global. Sobre las razones, dejan muy poco lugar a las dudas al señalar que las emisiones de dióxido de carbono (CO_2) se han acelerado en el periodo de 1995-2005. Cabe recordar que el informe de Nicholas Stern (2007) concluía de no hacer nada, se perderá entre un 5% y un 20% del PIB.

En lo que a la contaminación generada por el transporte por carretera se refiere, la nueva Legislación Medioambiental Europea, aprobada el pasado 7 de febrero del 2007, obligará a reducir las emisiones de CO_2 pasando de los 140 g/km actuales a 120 g/km para el año 2012 una medida destinada a paliar en lo posible los efectos del cambio climático. El panorama a nivel del Estado Español es parecido. Informes del Ministerio de Medio Ambiente (MMA 2006), advierten que el transporte continúa siendo “insostenible” ,de ahí que la reducción de emisiones debidas al aligeramiento se alinee con las medidas y herramientas que está impulsando el Gobierno Español para reducir los contaminantes atmosféricos producidos por el transporte, y en concreto por el transporte privado por carretera por ser el modo que más emisiones genera dentro del cómputo de las emisiones debidas al transporte en todos sus modos (TRAMA-2005).
Existen tres estrategias principales para reducir las emisiones de CO_2 de los motores de combustión: 1) la mejora de los motores, 2) la mejora de la aerodinámica y 3) el

aligeramiento del peso del automóvil. En el presente proyecto se abordará este problema desde el aligeramiento estructural.

2. ¿SON LOS CFRP LA MEJOR SOLUCIÓN PARA ALIGERAR LAS ESTRUCTURAS DE LOS VEHÍCULOS?

El aligeramiento de una estructura es el resultado de las buenas propiedades intrínsecas del material (relación rigidez/densidad, resistencia/densidad, absorción de energía específica, etc.), pero también del diseño del componente/material (Fig. 1).

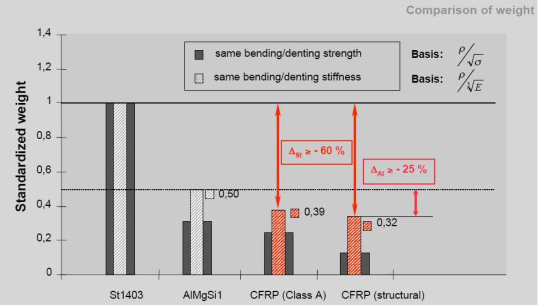

Fig. 1. Comparación de la masa entre el acero (St1403), el aluminio (AlMgSi1) y los CFRP para una rigidez/resistencia a flexión equivalente.

Según datos del proyecto Automotive Lightweighting Materials (Wall, 2004) financiado por el Departamento de Energía de EEUU y el United States Council for Automotive Research (USCAR), una reducción del 10% de masa del vehículo implicaría una reducción del 7% de consumo de combustible y en consecuencia una reducción importante de las emisiones a la atmósfera. Utilizando aceros avanzados de alta resistencia (AHSS) y optimizando los procesos de fabricación, se reduciría entre un 15 y un 25% de la masa del vehículo. Si se utilizan CFRP dicha reducción estaría en el 25-70% de masa total. Para cumplir la Legislación, se deben disminuir en un 14% las emisiones de CO_2, lo que corresponde a una reducción de masa del vehículo del 20%. Si estimamos la masa de un coche en 1600 kg, de los cuales 450 kg corresponden al Body In White (BIW) esto equivaldría a una reducción de 320 kg. La estructura del automóvil debe diseñarse para absorber de forma controlada la energía cinética en el momento del impacto sin dañar a los ocupantes del vehículo (fig.2). Este criterio penaliza sustancialmente la masa del vehículo si se utilizan metales. Sin embargo, los materiales compuestos son muy efectivos para diseñar estructuras con gran capacidad de absorción de energía (Jacob 2004).

Fig. 2. Accidente de Kubika en el Gran Premio de Canada 2007.

3. EL PROYECTO SINGULAR ESTRATÉGICO LIGHTCARBONCARS

En septiembre de 2007, nace con el apoyo del actual Ministerio de Ciencia e Innovación, el PSE-LIGHTCARBONCARS (2007-2011) (PSE-370100-2007-1) (www.gid.uji.es/lightcarboncars/). El objetivo prioritario del presente proyecto es la reducción del impacto ambiental de automóviles mediante el aligeramiento estructural basado en composites de fibra de carbono de bajo coste, sin comprometer la seguridad y el confort. El proyecto se ha estructurado en 6 subproyectos, abarcando todo el ciclo de vida (desde la obtención de materias primas hasta el reciclado, pasando por el procesado y la optimización del diseño). Los objetivos y tecnologías a desarrollar son:

1. Materiales: Se pretende obtener fibras de carbono de bajo coste procedentes de breas, polímeros reforzados con nanopartículas y materiales inteligentes que mejoren sustancialmente las prestaciones mecánicas de los materiales composites y su procesabilidad.
2. Procesos: El objetivo es reducir un 50% los costes con respecto a los procesos de fabricación de compuestos actuales. Se analizarán dos tipos de procesos; el moldeo por compresión y la inyección de polímeros de baja viscosidad (RTM). Además se desarrollarán técnicas de monitorizado de procesos que permitan controlar la calidad de las piezas durante el propio proceso de fabricación.
3. Diseños estructurales: En este subproyecto se pondrán a punto los conceptos estructurales y las herramientas de simulación para optimizar el peso de la estructura, la seguridad ante impactos, fatiga y el confort vibroacústico.
4. Impacto ambiental: El objetivo consiste en reducir el impacto ambiental del automóvil una vez que este haya llegado a su fin de vida útil. Para ello se analizarán las diferentes soluciones de ensamblaje/desensamblaje y reciclaje de la estructura.
5. Diseño, fabricación y ensayo de prototipos: El objetivo de este subproyecto es doble. Por una parte debe de alimentar a los otros cuatro en lo que a especificaciones técnicas y económicas se refiere, y por otra debe de validar los materiales-procesos-diseños desarrollados a nivel de prototipos.
6. Gestión, Vigilancia tecnológica y difusión de resultados.

3.1 Objetivos socio-económicos

Los objetivos socio-económicos del proyecto son:

- Ser capaces de fabricar fibra de carbono de bajo coste.
- Mejorar los procesos productivos para acercarse a los estándares exigidos por la industria del automóvil.

- Optimizar las estructuras del vehículo de forma que su extrapolación a otros componentes permita pensar en una reducción de cómo mínimo un 20%.
- Igualar y si es posible mejorar (sin incremento de costo) la seguridad y el confort vibroacústico.
- Disminuir los costes asociados a la inspección y reparación debido a la vida útil más larga de la estructura.
- Disminuir los residuos generados tras el fin de vida del automóvil.
- Posicionar a la industria del Estado Español en una posición preferencial en tecnologías estratégicas en lo que a diseño/proceso/materiales composites de fibra de carbono se refiere.

4. CONCLUSIONES

Un estudio realizado por Lucintel (2007) prevé que la demanda de carbono aumente un 10% anual en los próximos 5 años. Por ello, múltiples esfuerzos se están realizando en todo el mundo para producir masivamente fibra de carbono. Por otro lado, y especialmente en Japón, se están haciendo importantes esfuerzos en el aligeramiento de vehículos mediante CFRP. Así, Toyota ha fabricado un concept car hibrido a escala, utilizando fibras de carbono en la estructura del vehículo, consiguiendo una reducción del 67% del peso con respecto al modelo Prius. Toray y Nissan han trabajado en el proyecto NEDO (Goichi, 2007) aplicando fibras de carbono para el aligeramiento de vehículos. Finalmente, Toray, fabricante de fibra de carbono, prevé triplicar sus ventas en el sector automoción de aquí al 2016, ya que considera realista su utilización en estructuras de automóviles. Es por ello cuestión de tiempo que se pida a los proveedores de componentes estructurales soluciones en composite.

AGRADECIMIENTOS

El autor desea agradecer por un lado al Ministerio de Ciencia e Innovación, el haber dado su apoyo a este proyecto mediante su aprobación (PSE-370100-2007-1).
Así mismo, mi agradecimiento a todos los participantes en el proyecto, por su labor, sin la cual este proyecto no podría llevarse a cabo: CEI-MONDRAGON, CONDEPOLS, CTAG, EASY, EPS-MU, FIDAMC, FPK, GAIKER, INCAR-CSIC, PEUGEOT CITROËN ESPAÑA, REPSOL-YPF, SERNAUTO, TEAMS, Universidades DA CORUÑA, JAUME I, OVIEDO, SEVILLA, UPM-ETSIA, UPC-CCP, VFUS Armonia.

REFERENCIAS

Goichi, Ben (2007), What we have accomplished in NEDO project for automotive structures, 16th International Conference on Composite Materials, Kyoto 2007.
Jacob G. C., et al. J Appl Polym Sci 92 (2004) 3218-3225.
Lucintel (2007), Worldwide Carbon Fiber Competitive Análisis and Leadership Study.
MMA (2006), Perfil Ambiental de España 2005. Informe basado en indicadores, Ministerio de Medio Ambiente, Dirección General de Calidad y Evaluación Ambiental.
TRAMA (2005), Informe sobre transporte y medio ambiente, TRANSYT (Centro de Investigación del Transporte) y Ministerio de Medio Ambiente.
STERN N. (2007), The economics of the climate change. The Stern review. Cambridge Univ. press.
WALL et al (2005), Progress Report for Automotive Lightweighting Materials.

Lightcarboncars: Nanocompuestos CBT/POSS obtenidos por polimerización in-situ

T. Abt, M. Sánchez-Soto, S. Illescas, J. Gámez-Pérez, M. Ll. Maspoch
Centre Catalá del Plástic. Universitat Politécnica de Catalunya. Terrassa. España

RESUMEN

En este trabajo se han preparado e investigado nanocompuestos formados por CBT® y tres tipos diferentes de nanocargas de tipo oligómerico poliédrico (POSS), dos con funcionalidad reactiva -Trisilanolfenil POSS (T-POSS) y Glicidil POSS (G-POSS)- y uno no reactivo -Isooctil POSS (I-POSS)-. Los POSS fueron mezclados con el CBT en cantidades del 2.5, 5 y 10% previamente a su polimerización, que fue llevada a cabo en una prensa de platos calientes. El análisis micrográfico reveló, en general, una buena miscibilidad del POSS en el CBT. El I-POSS se dispersó a nivel nanométrico en la matriz mientras que tanto el T-POSS como el G-POSS formaron pequeños aglomerados de rango micrométrico. Finalmente, se ha encontrado que el T-POSS interacciona con el proceso de polimerización del CBT inhibiendo la cristalización, mientras que el G-POSS puede inducir la formación de reticulación del CBT durante el procesado siendo posible de este modo aumentar la resistencia térmica del material.

1. INTRODUCCIÓN

Los oligómeros cíclicos son moléculas de bajo peso molecular y estructura de anillo precursoras de polímeros lineales de alto peso molecular. El CBT es una forma cíclica de butilén tereftalato. Tras un calentamiento y en presencia de un catalizador, polimeriza rápidamente por apertura de anillo para dar un PBT (Pang et al. 2006). La reacción de polimerización es atérmica y suele ocurrir simultáneamente a la cristalización entorno de 170 ºC. Estudios previos han demostrado que el CBT polimerizado (pCBT) presenta una mayor fragilidad que el PBT convencional (Abt 2008) El origen de dicha fragilidad se atribuye al desarrollo de estructuras cristalinas de alta perfección combinado con la presencia de pocas moléculas de unión entre ellas. Aunque un enfriamiento severo puede ser capaz de aumentar la tenacidad del pCBT, la máxima deformación alcanzada bajo estas condiciones es del 8% aún muy por debajo de la del PBT (Parton et al. 2006). Una vía para modificar y mejorar las propiedades de los polímeros es mediante el uso de nanorefuerzos. Los POSS son moléculas caracterizadas por una estructura de celda tridimensional que esta formada por un esqueleto inorgánico $(SiO_{3/2})_n$ con n=8,10,12 rodeado por grupos orgánicos ligados covalentemente a los átomos de silicio. Así es posible cambiar la reactividad, compatibilidad o polaridad de la estructura modificando el tipo o número de los grupos funcionales que cuelgan de la celda. Normalmente con estas moléculas se consigue una mejora de la estabilidad térmica del polímero (Illescas et al. 2009), si bien las propiedades mecánicas o fisico-químicas también pueden verse afectadas (Sanchez-Soto et al. 2009). Siguiendo esta línea, se ha estudiado el efecto de los POSS sobre la morfología y propiedades de diferentes nanocompuestos CBT-POSS obtenidos por polimerización in-situ.

2. EXPERIMENTAL

Se usó el CBT-XB3 con un 0.3% de catalizador Fascat que fue suministrado por Cyclics Europe. El pre-polímero fue secado en vacío por 8 horas previo a su uso. Se añdieron tres tipos de POSS, dos con funcionalidad reactiva, Trisilanolfenil POSS (T-POSS) y Glicidil POSS (G-POSS); y uno no reactivo Isooctil POSS (I-POSS) siendo mezclados con el CBT previo a la polimerización en cantidades del 2.5, 5 y 10 % peso. Todas las muestras fueron fundidas y polimerizadas en una prensa de platos calientes a 250ºC realizándose una etapa isotérmica de 5 minutos para asegurar la completa polimerización. Se obtuvieron láminas por prensado que se enfriaron rápidamente. El pCBT fue investigado por espectroscopía infrarroja (FTIR-ATR) comparando los espectros obtenidos con los del PBT y CBT sin polimerizar. La morfología de los compuestos CBT-POSS se analizó por microscopía electrónica de barrido en un aparato JEOL 5610. El análisis calorimétrico se realizó en un equipo Perkin Elmer Pyris 1 usando rampas de calentamiento de 5ºC/min. La entalpía para un PBT 100 % cristalino en fase α se tomo de 132 J/g.

3. RESULTADOS

Los espectros de absorción de CBT y pCBT a diferentes tiempos de polimerización se muestran en la figura 1. Dado que las estructuras químicas de pre-polímero y polímero son muy similares, solo se observan pequeñas diferencias en las bandas de absorción. Sin embargo pueden apreciarse dos bandas (λ= 915 cm^{-1} y λ= 751 cm^{-1}) que crecen conforme lo hace el tiempo de polimerización. La banda a 915 cm-1 se puede adscribir a la vibración del grupo CH_2 y se atribuye a la aparición de cristales de fase α, que evidenciaría el avance de la polimerización con el tiempo. Los espectros de los compuestos pCBT/POSS mostraron en general las señales características del pCBT y de cada uno de los POSS usados. Sin embargo, en el espectro del sistema pCBT/T-POSS se observó la ausencia de la banda de cristalización de fase α, indicando que la estructura de este sistema es amorfa y que por tanto la presencia del T-POSS inhibe la cristalinidad del polímero.

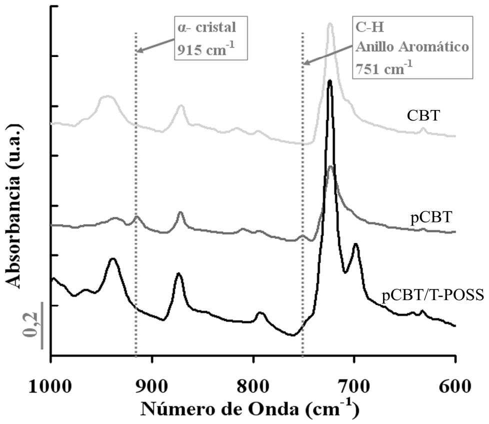

Figura 1. Espectros ATR-FTIR del CBT, pCBT (30min,190ºC) y pCBT/T-POSS.

En la figura 2 se representan las señales de DSC del CBT tras ser polimerizado in-situ. La zona de fusión de los oligómeros cíclicos queda representada por la señal entre 120 y 160 ºC. La polimerización empieza a 160 ºC y es atérmica, por lo que la señal exotérmica siguiente se atribuye a cristalización en frío del pCBT. Por encima de 210 ºC los cristales imperfectos de pCBT (fase β) comienzan a fundir recristalizando inmediatamente en la estructura más estable (fase α). La presencia de los POSS cambia la señal inhibiendo la cristalización en frío, así el pico de fusión del pCBT se transforma en una señal de menor intensidad que llega a desaparecer a altos contenidos de POSS (10%wt.). Para el caso de los compuestos conteniendo G-POSS se observó la imposibilidad de fundir completamente el material polimerizado, indicando que el G-POSS actúa como agente reticulante para el CBT.

En la tabla 1 se recogen los resultados de la caracterización calorimétrica del CBT y los nanocompuestos realizados.

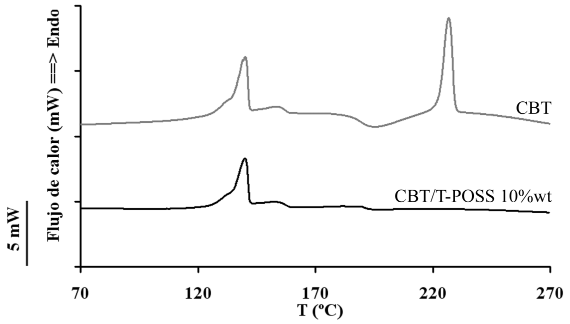

Figura 2. Termogramas DSC de calentamiento correspondientes a CBT y CBT/T-POSS 10%wt.

La morfología de los nanocompuestos fue muy dependiente del tipo de POSS usado. El pCBT/T-POSS mostró una estructura globular en la que pude verse (figura 3a) que el polímero base está poco consolidado mientras que el POSS parece quedar segregado en la superficie. Usando el G-POSS el aspecto de la fractura fue similar al material sin modificar sin notarse la presencia de agregados, hecho indicativo de una buena compatibilidad hasta concentraciones del 5% en peso (figura 3b).

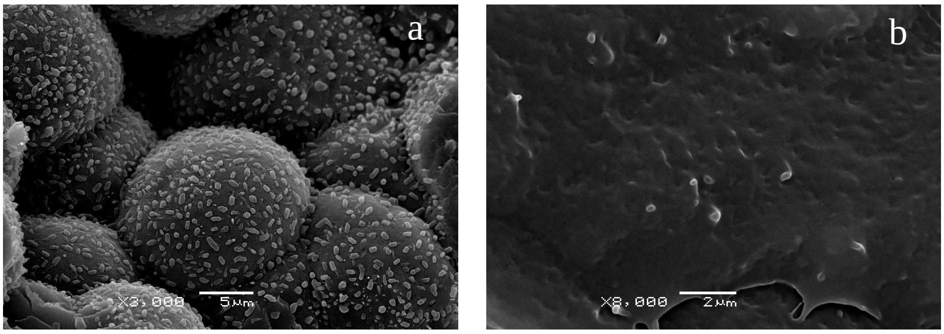

Figura 3. Micrografías de los sistemas a) pCBT/T-POSS y b) pCBT/G-POSS a 2.5% y 5% de nanocarga respectivamente.

A mayores contenidos se aprecian partículas de tamaño entorno a 1 μm posiblemente resultado de interacciones POSS-POSS. Por su parte el I-POSS se dispersa a nivel nanométrico en la matriz hasta contenidos del 5% en peso. No obstante las muestras con 10% de I-POSS mostraron una superficie oleosa indicativa de baja miscibilidad por migración del POSS a la superficie libre.

Tabla 1. Resultados de la caracterización térmica del CBT, pCBT y nanocompuestos polimerizados in-situ.

Compuesto	1er Calentamiento[2]		2º Calentamiento[3]		Cristalinidad Xc (%)
	Tm [ºC]	ΔH_m[J/g]	Tm [ºC]	ΔH_m	
CBT	141.1	41.9	225.7	53.1	28.2
BT190-30[1]	159.8	1.3	230.6	51.5	34.7
pCBT230-20	-	-	225.1	56.7	34.6
CBT/T-POSS 2.5 %w	140.5	43.0	-	-	29.4
CBT/T-POSS 5 %w	140.4	39.6	-	-	23.4
CBT/T-POSS 10 %w	140.5	42.6	-	-	0.6
CBT/G-POSS 2.5 %w	139.5	39.4	228.6	8.3	25.3
CBT/G-POSS 5 %w	139.6	39.2	226.8	6.3	26.6
CBT/G-POSS 10 %w	143.1	30.8	-	-	22.1
CBT/I-POSS 2.5 %w	140.5	41.4	228.5	22.2	27.1
CBT/I-POSS 5 %w	141.9	37.1	232.7	20.9	26.0
CBT/I-POSS 10 %w	144.0	25.1	-	-	27.7

1:pCBT190-30 (polimerizado a 190ºC por 30 minutos . 2: Oligómero. 3: Polímero

4. CONCLUSIONES

Los nanocompuestos CBT/POSS se han sintetizado por polimerización in-situ. El avance de la reacción del CBT se ha podido seguir por FTIR. La adición de POSS inhibe la cristalización en frío y reduce la cristalinidad del polímero. El T-POSS interfiere con la polimerización mientras que el G-POSS actúa como agente reticulante.

5. AGRADECIMIENTOS

Los autores desean agradecer al Ministerio de Ciencia e Innovación el apoyo recibido a través del proyecto LIGHTCARBONCARS PSE-370100-2007-1 y PSS-37100-2008-13

6. REFERENCIAS

ABT, T. (2008) Study of the properties of Polyhedral Oligomeric Sislsesquioxane/polymer nanocomposites. *Master Thesis. Universidad Politécnica de Catalunya.*

ILLESCAS, S., AROSTEGUI, A., SCHIRALDI, D.A, et al (2009). *The role of POSS on the thermo-mechanical properties of polyoxymethylene copolymer based nanocomposites. J. Nanoscience & Nanotechnology. Aceptado, In press.*

SÁNCHEZ-SOTO, M., ILLESCAS, S., SCHIRALDI, D.A. (2008) Study of the morphology and properties of melt-mixed polycarbonate-POSS composites. *Eur. Pol. J. . 45, 345-352*

PANG, K., KOTEK, R., TONELLI A., (2006). Review of conventional and novel polymerization processes for polyesters. *Progr. in Pol. Sci., 31,1009-1037.*

PARTON, H., BAETS, H., LIPNIK, P. et al. (2006). *Properties of poly(butylene terphthalate) polymerized from cyclic oligomers and its composites. Polymer 46, 9871-9880.*

Continuum fracture mechanics approach to prevent type VI cracking of Mod.9Cr-1Mo steel weldment

Y. Monma[1], Y. Li[2], H. Hongo[3], M. Tabuchi[3]
[1]Kochi University of Technology, Japan
[2]Japan Atomic Energy Agency, Japan
[3]National Institute for materials Science, Japan

ABSTRACT

In the advanced ultra-super critical (USC) power plant there has been some severe accidents known as the Type VI cracking in the welded joints (WJ) of modified 9Cr-1Mo steel. The weldment is a heterogeneous material and is composed of three different components: base metal (BM), weld metal (WM) and heat-affected zone (HAZ). The cracking is caused under creep loading by the accumulation of voids in fine-grained part of the HAZ.

Because of the rapid cooling from liquidus to solidus states in welding process it is unavoidable to contain these constituents and their mechanical properties are considerably different. On the basis of creep-rupture tests we conducted at 600 ℃ we have done the FEM calculation of creep deformation and found the local variability.

Starting from the Kachanov-Rabotnov and Hayhurst approach of the continuum fracture mechanics (CDM) we have developed a modification of the CDM equation. In order to correlate the macroscopic model of CDM to microscopic void nucleation-growth model we needed to introduce nonhomogeneous stress-strain distribution in the welded joint.

We discuss two-sided effects of the stress triaxial factor on the creep-rupture time of material were discussed in the study. The role of constraints due to the multiaxial stress state keeps the weak zone of the WJ in the lower equivalent creep stress, thus it greatly improves the creep-rupture time under high stress levels. In the same time it might also contributes the sliding of grain boundaries during creep. The growth of voids is accelerated by the strain imbalance. The stress concentration in the tip zone should be responsible for the growth of Type Ⅳ cracking.

An innovative energy-absorbing structure with double-layered composite keel beam for aircraft fuselage

S.T. Taher[a], S. Ataollahi[b]
[a] Department of Mechanical Engineeing, Curtin University of Technology, Sarawak Campus, CDT 250, 98009 Miri, Sarawak, Malaysia
[b] Mechanical and Materials Engineering Department, Universiti Kebangsaan Malaysia, 43600 UKM Bangi, Selangor, Malaysia

ABSTRACT

It is well-known that the primary design goal for crashworthiness in aerospace and automotive vehicles is to minimize the impact forces transmitted to the occupants and maximize the energy absorption during the crash events. In present study, an innovative double-layered composite energy-absorber system has been successfully developed to retrofit in airplane and helicopter in order to improve their crashworthiness performance. A novel structure of lightweight double-layered composite energy-absorber keel beam has been developed and retrofitted in aircraft sub-floors. Crushable elements of keel beam encompassed of fibreglass fabric wrapped around two foam layer cores. This technique eventually prevented from core-to-facing debonding, especially during axial crashing, whereby the debonding tendency is controlled by a hoop stresses in fibreglass layers. Manufactured block can be used alone as an energy-absorber element in structure or a series of blocks integrate in the form of beam. Inline assembly of the fibre-reinforced blocks is covered with fabric glass fibre reinforcement in order to integrate the blocks in a beam configuration. Two types of triggering modifications had been applied to the developed composite structures and they are “bevel trigger” and “groove trigger”. Quasi-static axial crushing behaviour of the composite structures is investigated experimentally. The design, manufacturing and crush testing of keel beams fabricated are described. Special attention is focused on the analysis of the mechanics of the beam axial collapse, emphasizing on the mechanisms related to the crash energy absorption during the compression of the composite beams with and without use of two types collapse trigger mechanism. Experimental results show that the double-layered composite beam concept is a practical means of producing cost-effective sandwich structures that crush in a stable, progressive manner with high crush force efficiency.

This paper describes an experimental evaluation of the crashworthiness characteristics of a novel design for cost-effective crashworthy composite glass fibre reinforced plastic (GFRP) sandwich structure. All the samples are based on the concept of the ‘‘double-layered” foam-filled block, i.e. two foam core sheets which are wrapped by reinforcement woven fabric, that acts as the reinforcement face and meanwhile tie the core layers and faces together, thus preventing catastrophic failure under axial loading condition. The design, manufacturing and crush testing of rectangular blocks fabricated are described. Special attention is focused on the analysis of the mechanics of the block axial collapse, emphasizing on the mechanisms related to the crash energy absorption during the compression of the composite blocks with and without use of two types collapse trigger mechanism. Experimental results indicated high crushing force efficiency was achieved up to 80%. t is known in the automotive industry to provide a bumper on the front and rear of an automotive vehicle to absorb impact energy and prevent damage to other vehicle components such as fenders, frames, and the like. A new cost-effective lightweight composite energy-absorbing structure has been developed in order to obtain a high degree of crashworthiness in automotive bumper. Assembly system includes a crushable beam cut to desired form of bumper and retrofitted between front and back composite cover/flange of bumper. Crushable energy-absorber beam was consisted of a rectangular multi-celled thin wall composite structure and internal polyurethane foam cores. Polyurethane foam was employed to fill the cells of the structure to eliminate any hypothesis of global buckling. The design, manufacturing and crush testing of multi-celled beam fabricated are described. Quasi-static axial crushing behaviour of the composite structures is investigated experimentally. Special attention is focused on the analysis of the mechanics of the beam collapse during the compression of the composite beams with and without use of two types collapse trigger mechanism. Experimental results show that the multi-celled composite beam concept is a practical means of producing cost-effective sandwich structures that crush in a stable, progressive manner with high crush force efficiency.

Composite Structures for Naval Ships

L. Batista Rosa, F.D. Rico Amado
UESC – Universidade Estadual de Santa Cruz, Manufacturing Engineering
Rodovia Ilhéus-Itabuna, km 16, CEP 45662-000, Ilhéus, BA, Brazil

ABSTRACT

When composite materials are chosen for naval structures, it is generally because they can offer properties, which are particularly attractive for that specific application. These advantages include: reduced weight, better corrosion resistance, lower life cycle costs and better thermal, acoustic and vibration properties.

The weight reduction alone can motivate the use of composites in smaller fast vessels, where the light weight allows operational capabilities that would not be possible with traditional construction. However, larger ships can be developed using traditional materials. This is expected to explain why composites are still not much used in major warships. Other advantages of composites, compared to steel, include reduced maintenance and life cycle costs.

Despite the possibilities above, the use of composites in naval shipbuilding is still limited. Conservatism among naval ship designers favors the use of traditional materials and solutions. Lack of understanding on how composites are used may mean poor designs and poor quality.

This paper discusses composite material structures for naval ships. Those materials offer properties that provide advantages in specific cases. This work also compares the advantages of steel structures. Due to lack of confidence in bonded joints, the joining of a composite superstructure module to a steel hull represents particular challenges. Bolted ones are often chosen in practical designs. But the most important point to make a successful composite structure is the poor mechanical properties in perpendicular direction to that of the reinforcement fibers. For example, the fatigue resistance of a composite structure can hardly match that of a welldesigned steel structure.

The need for increased operational performance and reduced costs has driven the development of composite materials for naval structures. Improvements to warships and submarines are sought in numerous areas such as stability, corrosion resistance, payload and resistance to impact and explosive shock, where composite materials are advantageous.

Caracterización de materiales compuestos mediante modelos micromecánicos y técnicas no destructivas

M. Acebes, A. Corrales
'Fundación CARTIF Parque Tecnológico de Boecillo, Valladolid. España
M.G. Hernández, J.J. Anaya
Instituto de Automática Industrial. CSIC. Arganda de Rey, Madrid. España

RESUMEN

La estructura porosa de los materiales cementicios es la responsable del transporte de sustancias hacia el interior y por consiguiente de los procesos de deterioro. En diversos trabajos se ha demostrado que el grado de saturación provoca una reducción de las propiedades, por lo cual es necesario desarrollar metodologías de ensayos que permitan predecir el comportamiento del material con respecto al volumen de agua presente.

En este trabajo se estudia el efecto del agua en las propiedades elásticas de los materiales cementicios mediante técnicas no destructivas (ultrasonidos y termografía infrarroja activa) y modelos multifásicos. La comparación de los resultados experimentales obtenidos por los dos métodos de ensayos ponen de manifiesto que existe una dependencia, tanto de la difusividad como de la velocidad ultrasónica con la cantidad de agua presente en los poros, existiendo una correlación entre ambos métodos. Igualmente existe concordancia entre el comportamiento teórico a partir de los modelos micromecánicos y la medida de la velocidad ultrasónica.

1. INTRODUCCIÓN

El contenido de agua en la estructura porosa de los materiales de construcción tiene importantes consecuencias en las estructuras edificadas. Las variaciones en la cantidad de agua en los poros inciden en el comportamiento mecánico del material produciendo modificaciones locales y estructurales que pueden ser irreversibles y negativas desde el punto de vista de la estabilidad dimensional.

En diversas investigaciones se ha estudiado la influencia del contenido de agua en las propiedades mecánicas y durables del hormigón mediante ensayos destructivos (Yurtdas et al 2004) y no destructivos (Ohdaira et al. 2000 y Rodríguez et al. 2002). La precisión de estas medidas puede estar influenciada por un amplio conjunto de factores por lo que en este trabajo junto al estudio experimental, se han desarrollado y aplicado modelos micromecánicos que nos permitan valorar la influencia de los diferentes factores. La aplicación de modelos micromecánicos nos permite obtener información del compuesto en función de las características microestructurales de las fases constituyentes, tales como propiedades elásticas, fracciones de volumen, geometría y función de distribución de orientaciones de las inclusiones dentro de la matriz.

2. CARACTERIZACIÓN DE LA ESTRUCTURA POROSA

2.1 Modelos micromecánicos

Supongamos un material heterogéneo formado por una matriz y n-tipos de inclusiones, al cual se le aplica una fuerza o deformación. A partir de las formulaciones de los modelos bifásico y trifásico expuestos en (Hernández et al 2004 y Hernández et al

2006), y si consideramos que no hay interacción entre los tipos de inclusiones y que la interacción sólo se produce entre la matriz y las inclusiones, el modelo micromecánico para materiales con N-fases queda expresado como (Acebes, 2007):

$$C = C^m + \sum_{i=1}^{N-1} \nu^p \left(C^i - C^m\right)\left\langle T^i \right\rangle \left[\nu^m I + \sum_{i=1}^{N-1} \nu^i \left\langle T^i \right\rangle \right]^{-1} \qquad (1)$$

donde C representa el tensor de constantes elásticas, *v* la fracción de volumen, i los tipos de inclusiones y T es el Tensor de Wu (Wu, T. 1966) de cuarto orden, el cual tiene en cuenta la geometría, distribución y orientación de cada uno de los tipos de inclusiones. Si suponemos que las fases son isotrópicas el tensor C queda reducido a dos constantes elásticas independientes C_{11} y C_{44} que a su vez están relacionadas con la velocidad longitudinal y transversal y la densidad (ρ) a través de las expresiones (2):

$$V_l = \sqrt{\frac{C_{11}}{\rho}}; \quad V_t = \sqrt{\frac{C_{44}}{\rho}}\ ; \quad \rho = \sum_{i=1}^{N} \rho_i \cdot v_i \qquad (2)$$

2.2 Ensayos por ultrasonidos

Para la caracterización de los compuestos de cemento mediante técnicas ultrasónicas utilizaremos la medida de la velocidad. La técnica de inspección seleccionada es la transmisión por contacto, mediante dos transductores de 500 kHz colocados en el centro de las caras laterales y utilizando gel como acoplante. Las señales se han procesado digitalmente obteniéndose el tiempo de transmisión utilizando el primer cruce por cero. La velocidad V_l se ha calculado según (3):

$$V_l = \frac{X_c}{t_c - t_e} \qquad (3)$$

siendo X_c el espesor de mortero atravesado, t_c el tiempo cuando la señal atraviesa el centro de la probeta y t_e el error de medida debido a problemas de acoplamiento.

2.3 Ensayos por termografía

La termografía infrarroja es un método de medición de la temperatura sin contacto, basado en detectar la radiación infrarroja que emite todo cuerpo, y a través de las leyes físicas obtener una relación entre esa radiación y la temperatura de la superficie emisora.

Como parámetros característicos pueden definirse emisividad y difusividad. La emisividad es una característica del material que indica la facilidad para emitir energía y la difusividad es un valor único para cada material que indica la relación entre los componentes y las características estructurales. Dentro de las técnicas termográficas, se ha empleado la termografía activa continuada, la cual, es un método rápido aplicable en el análisis de materiales. La variación temporal de la temperatura se puede relacionar, mediante la ley de Fourier, con la difusividad del material según (4):

$$\frac{\partial T}{\partial t} = \alpha \nabla^2 T \qquad (4)$$

3. RESULTADOS OBTENIDOS

Para los ensayos experimentales se ha utilizado un juego de probetas normalizadas de mortero, con diferentes relaciones agua/cemento (a/c). Las medidas de porosidad, junto con las proporciones de fabricación, nos permitieron obtener las fracciones de volumen de las fases. La variación de la velocidad longitudinal (Vl), medida y estimada, a medida que varía el grado de saturación, se muestra en la figura 1. Cuando los poros se llenan de agua Vl disminuye, siendo este descenso mayor en las probetas con una relación a/c más alta. En ninguno de los grupos la estructura porosa se llena completamente, lo cual es debido al aire que queda atrapado durante el proceso de absorción de agua y a las características reales de la estructura porosa (Wilson, M.A. 1991).

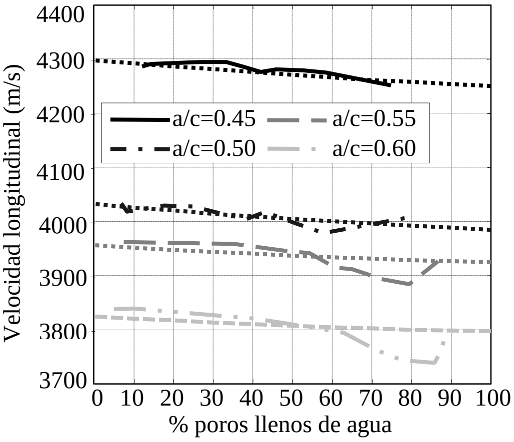

Figura 1. Resultados teóricos y experimentales a medida que el poro se llena de agua.

Para los ensayos termográficos se han introducido las probetas en un horno y se ha estudiado la variación temporal de la temperatura. De esta forma la muestra evoluciona desde un estado transitorio hasta un estado estacionario, de temperatura constante. Teniendo en cuenta sólo el estado transitorio se ha realizado un estudio cualitativo (tabla 1), observándose que las muestras más porosas tienen una variación de temperatura más lenta. A mayor porosidad menor difusividad.

Rel. a/c	0,45	0,50	0,55
$\partial T/\partial t$	0,0279	0,0200	0,0134

Tabla 1. Valores de difusividad para distintas relaciones a/c.

Los resultados se han comparado con un estudio anterior, donde se aplicaba la termografía activa por pulso de tiempo controlado para calcular la difusividad (Poblete, A. et al 2005) cuyos resultado pusieron de manifiesto que existe una correlación entre difusividad y velocidad de transmisión.

4. CONCLUSIONES

Se ha comprobado teórica y experimentalmente que la variación de la velocidad ultrasónica, a medida que los poros se llenan de agua, es muy dependiente de la porosidad y de las características elásticas de la matriz no porosa, que vienen dadas por la relación agua/cemento. Este comportamiento concuerda con el observado por (Yurtdas, I. et al 2006). Los errores relativos cometidos en la predicción de la velocidad longitudinal, son en para todas las relaciones a/c menores de 1%.

Igualmente, se ha comprobado que la difusividad depende de la cantidad de agua presente en los poros, y que pueden complementarse los dos métodos de medida con resultados satisfactorios.

5. AGRADECIMIENTOS

Esta investigación ha sido subvencionada por el Ministerio de Educación y Ciencia y el Ministerio de Fomento dentro de los proyectos BIA 2006-15188-C03-01 y C14/2006, respectivamente.

6. REFERENCIAS

ACEBES, M. (2007) "Estudio y extensión de un modelo micromecánico trifásico para la caracterización ultrasónica de materiales compuestos" *Tesis Doctoral*, 252pp. UPM.

HERNÁNDEZ, M.G. et al (2006). “Formulation of a new micromechanic model of three phases for ultrasonic characterization of cement based materials”, *Cement and Concrete Research*, Vol. 36, pp. 609-616.

HERNÁNDEZ, M.G. et al (2004). “Effect of the fluid in the inclusions of cement paste on the ultrasonic velocity”, *Ultrasonics*, Vol. 42, pp. 865-869.

OHDAIRA, E. et al. (2000) “Water content and its effect on ultrasound propagation in concrete – the possibility of NDE”, *Ultrasonics*, Vol. 38, pp. 546-552.

POBLETE, A. el al (2005) "Thermographic measurement of the effect of humidity in mortar porosity", *Infrared physics & technology*, Vol49 n 3 pp224-227

RODRÍGUEZ, M. et al. (2002) “El contenido de agua en el concreto y su incidencia sobre el valor de la velocidad del pulso ultrasónico”, *XXI Congreso Nacional De Ensayos Nao Destructivos_CONAEND 2002*, Salvador, Brasil.

WILSON, M.A. (1991) “Water movement in Porous Building Materials-X. Absorption from a Small Cylindrical Cavity”, *Building and Environment*, Vol. 26, pp. 143-152.

WU, T. (1966) “The effect on inclusion shape on the elastic moduli of a two place material”, *International Journal of Solids Structure*, Vol. 2, pp. 1-8.

YURTDAS, I. et al. (2004) “Experimental characterisation of the drying effect on uniaxial mechanical behaviour of mortar”, *Materials and Structures*, V.37, pp. 170-176.

YURTDAS, I. et al. (2006) Influences of water by cement ratio on mechanical properties of mortars submitted to drying. *Cement and Concrete Research*, Volume 36, Issue 7, pp. 1286-1293, 2006

Composite materials in marine construction: offshore applications

C. Bao, L. Celorrio, E. Martínez de Pisón, M.A. Martínez, L. López,
Mechanical Engineering Department, La Rioja University, Logroño, La Rioja
J. M. Castresana
Chemical Engineering, País Vasco University / Euskal Herriko Unibertsitatea

ABSTRACT

Composites are fast taking over as superior alternative to other traditional materials even in high pressure and aggressive environmental situations. Applications of composite are increasing tremendously along with the concurrent need for knowledge generation in the area. With technology innovations and developments in processes and products, composites have become attractive candidates for applications in oil gas, piping system, topside applications, down-hole tubing in sub-sea, and others.

1. INTRODUCTION

Composites meet diverse design requirements with significant weight savings and exhibit high strength-to-weight ratio compared to conventional materials. Composites have proved to be a worthy alternative to other traditional materials even in the high-pressure & aggressive environmental situations. Besides superior corrosion resistance, composite materials exhibit excellent fatigue performance, good resistance to temperature extremes and wear, especially in industrial sectors. The **tailorability** of composites to suit specific applications has been one of its greater advantages such as imparting low thermal conductivity & low coefficient of thermal expansion, high axial strength & stiffness etc. Composites have found extensive applications in the oil & gas industry since last two decades.

In the offshore oil and gas industry, the cost of manufacturing and erecting oil rigs could be reduced significantly if heavy metal pipelines could be replaced with lighter ones made of composites. Composite pipes also could be used for fire water piping, sea water cooling, draining systems and sewerage. The cost advantages of composite products are much greater when they replace expensive corrosion-resistant metals such as copper-nickel alloys, duplex / super duplex stainless steel, titanium etc. used in offshore platforms for various applications. Their resistance to corrosion helps in improving reliability and safety & also leads to lower life cycle costs, reduce problems with corrosion and blockage of fire lines, reduction in structural support sizes & material handling during construction.

2. STUDIED OBJETIVES: OFF-SHORE COMPOSITE APPLICATIONS

Applications of composite for off-shore applications are increasing tremendously along with the concurrent need for knowledge generation in the area. The selection of suitable materials plays an important role for imparting durability of the composites when exposed to aqueous fluids. The important issues relating to materials selection are smoke & toxicity in fires, mechanical properties including resistance to impact and adverse environments **(Bao et al. 1991).**

A few current studied applications of composites for off-shore are listed in **Table 1.**

SI.No	**Application**
1	Composite Grids/ Gratings
2	Hand rails & Ladder Components
3	Aqueous Piping System
4	Water & fuel storage tanks, Vessels
5	Low pressure composite valves
6	Spoolable type thermosetting tubes
7	Sump Caissons and pull tubes
8	Cable support systems
9	Modular paneling for partition walls
10	High pressure accumulator bottles
11	Flexible & Floating Risers, Drill pipe
12	Sub – sea structural components
13	Boxes, housings and shelters
14	Fire water pump casing & sea water lift pump casing
15	Tendons
16	Offshore bride connecting between platforms
17	Blast & Fire protection

Table 1. Current applications of composites.

◣**Composite Piping System-** Glass Reinforced Epoxy (GRE) piping system offers complete solution for offshore environment against highly corrosive fluids at various pressures, temperatures, adverse soil and weather conditions (especially in oil exploration, desalination, chemical plants, fire mains, dredging, portable water etc.) GRE pipes are commonly used in oil transportation where resistance to crude oil, paraffin build-up as well as ability to withstand relatively high pressures is required. GRE piping system is also being used on offshore rigs for sea water cooling lines, air vent systems, drilling fluids, fire fighting, ballasts and drinking water lines in offshore application. Standards for the use of composite piping and qualification procedures are being facilitated by various certifying agencies.

◣ **Top Side Applications-** Composite *grids/gratings, hand rails, cable trays, ladders, decking, flooring* have been used on fixed and floating off-shore platforms world over for more than two decades. In topside applications, the inherent corrosion resistance of composite materials reduces life cycle costs by minimizing its maintenance. Low cost, minimum topside weight and ease of transport were important features.

◥ **Composite Grids/Gratings-** Conventionally, grids/gratings are made of mild steel/cast iron. Due to the limitations on corrosion resistance, weight, durability, lifecycle costs etc. for the metallic gratings, composite grids/gratings perform much better due to their superior properties under aggressive environments as in chemical process industry. Worldwide many industries are manufacturing pultruded or compression moulded composite grids/gratings for their applications as *industrial walkways, hand rails, ladders, cable trays*, etc. in chemical/pharmaceutical, transportation & infrastructural sectors. These types of gratings are used mainly at splash zones in offshore platforms.

- **Composite Ladder & Handrail Components.-** Composites enjoy a significant market share of industrial ladders in replacing aluminium and wood in residential ladders. The ladders were originally developed for electrical utilities but have increasingly gained acceptance for general industry & residential uses. Composite ladders are stronger than wood or aluminium and do not absorb water, rot or corrode. Unlike aluminium, fibreglass has excellent insulation properties which substantially reduce the hazard of electrocution by contacting high voltage power lines.
- **Flexible Thermosetting Tube.-** Composite coil tube replaces the existing steel coil tubing for high pressure down-hole applications in offshore platforms. The tube can be coiled or uncoiled on a drum and can easily be transported to the desired location of the wells.. Flexible thermoset coil tubing can withstand high pressure rating up to 500 bars. In general, E-glass is used as the reinforcement but for specific applications carbon fibres could be used.
- **Composite Pressure Risers.-**Composite riser is the pipeline that connects the rig of the water surface to the well bore at the seabed. They must separate the oil, gas and drilling fluids from seawater.. The composite risers could be designed to withstand highly corrosive chemicals, salts and fluids under different environmental conditions..
- **High Pressure Accumulator Bottles.-**. The composite bottles offer significant weight and cost saving being less than 1/3 of the weight of equivalent steel bottles. These bottles can withstand very high internal pressures.
- **Composite Caissons & Pull tubes.-** Caissons are attractive applications for composites as an offshoot of GRE piping technology. Caissons are designed to withstand flexural fatigue loads created by waving loads and corrosion.
- **Composite Pressure Vessels-**The project aimed at developing filament wound pressure vessels for the following applications
- **Composite Pultruded Profiles-** The profiles like gratings, solid rods for electrical insulation, cable trays, ladders etc. were developed successfully with excellent surface finish and flame retardancy as per international standards. The comparison chart of the properties of FRP pultruded sections and structural materials are listed in table 2 & 3.

Properties	**Pultruded FRP**	**Rigid PVC**	**Mild Steel**	**Stainless Steel**	**Wood**
Tensile(N/mm^2) Strength	382	44	340	340	80
Flexural (N/mm^2) Strength	468.3	70	380	380	12
Flexural (N/mm^2) Modulus	22489	2400	196000	196000	700
Izod (Kg.m/cm) Impact	2.15	0.09	1.5	0.53	-

Table 2. Mechanical Properties of Pultruded Profiles Vs. Structural Materials.

Properties	**Pultruded FRP**	**Rigid PVC**	**Mild Steel**	**Stainless Steel**	**Wood**
Specific Gravity	1.8	1.38	7.8	7.92	0.52
Thermal Conductivity (Kcal/hr/m^2/° C)	24.4	6.4	1220	732.00	0.4
Coeff. of Linear Expansion (cm/cm° C) x 10^{-6}	5.2	37	8	10	1.7
Safe Working Temp. (° C)	130	55	600	600	160
Flame Resistance	Good*	Poor	Excellent	Excellent	Poor
Corrosion Resistance					
a. Acidic	Excellent	Good	Poor	Excellent	Poor
b. Alkaline	Good	Fair	Good	Excellent	Poor
c. Solvents	Fair	Poor	Good	Excellent	Fair
d. Coastal Environment	Excellent	Good	Poor	Excellent	Fair
e. Outdoor Exposure	Excellent	Poor	Fair	Excellent	Fair
f. Effluent Water	Excellent	Good	Poor	Excellent	Fair
g. Steam	Good	Poor	Fair	Excellent	Fair

Table 3. Properties of Pultruded Profiles Vs. Other Structural Materials.

CONCLUSIONS

Efficient and economical adaptation of composite materials to offshore applications is becoming an attractive research area. With the growth in petroleum sector, the demand for fibreglass products have increased manifold. Also the amount of energy required for fabricating composite materials for structural applications with respect to conventional materials such as steel & aluminium is lower and it thus works for its economic advantage.

ACNOWLEDGEMENTS

To Plan Nacional I+D+i, Project DPI 2007-61090

REFERENCES

BAO, C., “Materials selection for industrial applications”, Ph. D., UPV/EHU, 1991

Composite materials in marine construction: reasons for use, materials testing and evaluation

C. Bao, L. Celorrio, A. González, A.V. Pernía
Mechanical Engineering Departrment., La Rioja University, Logroño, La Rioja
J.M. Castresana
Chemical Engineering Departrment, País Vasco University/Euskal Herriko Unibertsitatea

ABSTRACT

Composites are fast taking over as superior alternative to other traditional materials even in high pressure and aggressive environmental situations. Applications of composite are increasing tremendously along with the concurrent need for knowledge generation in the area. With technology innovations and developments in processes and products, composites have become attractive candidates for applications in oil gas, piping system, topside applications, down-hole tubing in sub-sea, and others. In fact, composite materials are being used more extensively in the construction of ships and marine structures off shore than ever before. Composites have a higher stiffness and strength by weight than most other materials, including metals such as steel and aluminium. Used in various parts of a commercial or pleasure craft, the result is a far lighter boat that can achieve a higher rate of speed than the same type of boat constructed of aluminium or steel. What's more, the lighter weight keeps fuel costs down – a significant savings for a boat that may hold hundreds or even thousands of gallons of fuel. Nevertheless, their industrial use need reliable methods of Evaluation testing based in standards and regulations such as those in this paper are been described.

1. INTRODUCTION

Due to their characteristics, advanced composite materials have been making steady inroads into military systems for the last 40 years. Principle advantages of composites include higher stiffness to weight ratio (much better than steel or aluminium), endurance under cyclic loading, and resistance to chemical attack (e.g. corrosion resistance). The maritime industry, historically not constrained by weight issues, has used steel as its primary structural material. As a result of recent requirements for faster and more agile ships, the marine applications has been developing and is now starting to use PMCs in primary and secondary structures. Some examples include lightweight foundations, deckhouses, and masts; machinery components, such as composite piping, valves, centrifugal pumps and heat exchangers; and auxiliary or support items, such as gratings, stanchions, vent screens, ventilation ducts, and louvers. The growing interest in composite materials is also driven by the directives to reduce maintenance, save weight, increase covertness and provide affordable alternatives to metallic components with lower life cycle costs.

2. OBJECTIVES COMPOSITES IN SHIPS AND MARINE STRUCTURES: MATERIALS TESTING, EVALUATION AND PROPERTIES SIMULATION

In fact, composite materials are being used more extensively in the construction of ships and marine structures off shore than ever before. Composites have a higher stiffness and strength by weight than most other materials, including metals such as steel and aluminium. Used in various parts of a commercial or pleasure craft, the result is a far lighter boat that can achieve a higher rate of speed than the same type of boat constructed of aluminium or steel.

Weight Advantages: Aside from decreased fuel use, there is another factor associated with the lighter weight: speed. A perfect example is the high-speed passenger ferry, Jet Rider, which operates in Norway and carries 244 passengers at 42 kts (48 mph). With composites making up a large percentage of it's structure, the lightweight craft is not only more cost efficient to build than a comparable metal craft, but also able to move quickly. Other composite-hull vessels include a 259 foot ferry that can carry 570 passengers and 137 cars at speeds up to 47 knots (54 mph).

Corrosion Resistance of Composites: Another reason that composites are being used in shipbuilding and various marine applications is because composites are non-corrosive. Unlike metals that corrode and decay, composites last for many years. Consequently, composites are ideal for combating non-ambient environments like extreme temperatures and seawater. And with some marine apparatus like propeller shafts, buoys and light stations that are designed to remain in the water at all times, use of composite materials ensures long life.

➢ Applications:

✚ Composites in Boat Hulls:

The use of composites, while obviously advantageous, is a relatively recent phenomenon. About 20 years ago, composite hulls were limited to smaller vessels, such as pleasure yachts and small commercial fishing boats. Composites were too new and expensive to incorporate into larger vessels.

✚ Composites in Minesweepers:

The most common early composite application for larger vessels were military minesweeper hulls made from fibreglass. Today many larger vessels are made from composites, with these materials being used in a variety of areas, including hulls, floor and wall panels, decks and bulkheads, as well as ducting systems, oil tanks and waste water tanks, sonar domes, piping, pumps, valves and superstructures.

✚ Composites in Ship Superstructures:

In particular, composites are being employed more extensively in a ship's superstructure (anything above a ship's deck). Use of composite materials reduces weight, which means that more equipment can be installed above the waterline without sacrificing roll stability. Although boats are designed to sustain a certain amount of roll without capsizing, a strong enough force against a top-heavy structure will cause it to capsize. Larger superstructures can be fabricated from composites without proportionally increasing the risk of capsizing.

2. MATERIALS TESTING FOR COMPOSITES IN MARINE APPLICATIONS

However, even with all their favourable properties, composites must withstand the same rigorous testing as steel and metal parts. To ensure that composites meet the demands needed for a seaworthy, strong ship, a variety of tests are performed to simulate the effects of the ocean. By and large, ships have a very long service life, and are expected to perform for 20 years or more. Testing becomes essential in determining how composites used in a ship's and off shore construction will perform many years down the road.

- **Impact Testing**

Impact testing can be done to predict how composites will respond to collisions with piers, loads from breaking waves, damage from running aground and debris from underwater explosions. Having the material undergo impact testing reveals important data, such as the ductile-to-brittle transition point and residual strength after contact with great forces.

- **Fatigue, Compression and Bend Testing**

The action of a ship moving through waves is akin to bending, twisting and wrenching thousands of times each voyage. Fatigue, compression and bending tests must be performed to ensure materials will not fail under these conditions. Fatigue testing measures the durability of composites in cyclic loading applications and establishes when they will deteriorate. Compression tests reveal failure modes, such as delamination and buckling, and measure compression strength. Bending and torsional tests identify when composites will "break."

- **Adhesive Testing**

Similarly, because composite structures and components are often bonded together with adhesives, the bonded joints must be tested as well. Static and cyclic tests measure and detect bond strength, de-bonding modes, peel failure, and fatigue life.

- **Damage Tolerance**

Testing also helps shed light on damage tolerance. Test results establish if one extreme event will cause catastrophic damage or if it will take many years of cumulative damage use to render a ship unsafe.

- **Fire resistance. Passive Fire Protection**

The major difference between metallic and composite structures is that enclosed spaces consisting of PMC structures may be driven to flashover by small fires. Suppression of this demands either preventing a fire's heat from getting to the surface of a composite, or dampening the resin's inherent response to heat.

Fire suppression systems can be active (sprinklers, chemical dispersion) and/or passive (inherently non-combustible materials, fire insulation); this article focuses on passive fire suppression systems. Fire insulation provides a solution for both the hazard of fire involvement of the composite (combustible) structure, and forthe threat of structural collapse.. This reduces the hazard of fire involvement, as well as keeping temperatures on the material’s backside below its glass transition temperature for up to 30 minutes (reducing threat of structural collapse).

For military applications, fire insulation attachment methods for composite structures should be robust enough to withstand the effects of blast and shock in addition to rigorous wear and tear of use in hostile environments.

Assembly of insulation to composite structures is a labour intensive process, with total costs (both material and labour) estimated at about $35-50 per sq ft The insulation must also be shock qualified as Grade A, meaning it must remain intact and functional.

3. SIMULATION PROPERTIES

We can use simulator programs to evaluate previously the materials properties. Such as Laminator program. The Laminator is an engineering program written for Windows 95/98/Me/NT4/2000/XP/Vista that analyzes laminated composite plates according to classical laminated plate theory. Input consists of ply material properties, material strengths, ply fiber orientation and stacking sequence, mechanical loads and/or strains, and temperature and moisture loads. **Output** consists of apparent laminate material properties, ply stiffness and compliance matrices, laminate "ABD" matrices, laminate loads and mid-plane strains, ply stresses and strains in global and material axes, and load factors for ply failure based on Maximum Stress, Maximum Strain, Tsai-Hill, Hoffman, and Tsai-Wu failure theories. A micromechanics calculator is also included for estimating lamina properties for given fiber and matrix properties. The program can also be run from the command line for batch processing.

4. CONCLUSIONS

Composites have a higher stiffness and strength by weight than most other materials, including metals such as steel and aluminium. Used in various parts of a commercial or pleasure craft, the result is a far lighter boat that can achieve a higher rate of speed than the same type of boat constructed of aluminium or steel. , their industrial use need reliable methods of Evaluation testing based in standards and regulations such as those in this paper are been described.

ACNOWLEDGEMENTS

To Plan Nacional I+D+i, Project DPI 2007-61090

REFERENCES

BAO, C., “Materials selection for industrial applications”, Ph. D., UPV/EHU, 1991

Composite materials in marine construction: the cost effective use of fibre reinforced composites offshore

C. Bao
Mechanical Engineering Departrment., La Rioja University, Logroño, La Rioja
J. M. Castresana
Chemical Engineering Departrment, País Vasco University / Euskal Herriko Unibertsitatea
A. Basterretxea, I. Loroño, L. Martin
Machines and Heat Engines Department, País Vasco University / Euskal Herriko Unibertsitatea

ABSTRACT

Composites materials of fiber-reinforced polymer matrix (PRF)s are currently used as construction materials due to their physical and chemical characteristics to replace other traditional materials such as wood, plastics or metals. In marine construction industry, the use of reinforced polymer composites fiberglass, GRP, has rice in recently years. Nevertheless, some factors (such as price, rules, lack of information, ..) have delayed the deployments. So solve this problem, this Study is a useful industrial tool, tha permit to compare graphically some mechanical properties obtained in laboratory test of some GRP composite materials with different percentage of glass fiber in order to be used in marine construction.

1. INTRODUCTION

This initiative began life as a highly academic approach to the problem associated with the behaviour of fibre reinforced polymer composite materials in the offshore environment, but evolved over the years into a model collaboration research initiative between universities, oil companies, manufacturers, material suppliers, designers and government agencies. Beyond considerable amounts of funding, industrial support has included the provision of equipment, the supply of materials, the execution of field trials and the provision of expert advice.

2 AIMS AND OBJECTIVES

The initial documentation prepared for the launch of the Programme in 1988, drew attention to the significant savings that composite materials could offer to the offshore industry in terms of reductions in platform weight, installation and through life costs, as well as the enhanced safety that could be achieved as a result of demanning opportunities and the increased corrosion resistance of vital systems. This was contrasted with the low rate of penetration of composite materials into the offshore markets. Three major barriers were identified to a wider use of composites offshore:
The existing regulatory requirements on the combustibility of materials for use offshore;
The lack of reliable experimental and analytical data on the performance of composite materials in hostile offshore environments; The lack of efficient design methods and working standards for the structural use of composites and the unfamiliarity of offshore designers with such materials.

Impact behaviour of pultruded gratings

The work investigated the following:

1. The effect of load distribution across the beams.

2. Failure mode.
3. Critical energy to cause onset of failure.
4. The effect of span.
5. Residual strength.
6. The effect of fire.

Experimental details*:* The gratings were made from assemblies of pultruded T (Pedwalk 38mm and Duradek 50 mm), and I-beam (Duradek - I, 38 mm) sections connected by transversely running composite dowels. The polyester and vinyl ester resin matrices contained appropriate fire retardents and fillers.

Results: The results of testing showed that the static strength underestimates impact performance and that the load distribution has practical implications on performance. The transverse dowels are very effective at sharing load and the grating panel retains significant strength even when individual beams have been taken past the critical energy of failure. The critical energy for the panel may be of the order of 1000 J for 1000 mm span and under such circumstances beams exhibit visible damage on the top compression surface. ***Significance:*** The work provides important performance information with regard to the safe use of GRP gratings offshore and in particular it addresses possible concerns about the post impact strength capability of GRP gratings. The work suggests that static strength can be used to provide a conservative estimate of impact performance. However the results relate to pultruded sections and caution should be applied when considering moulded gratings. The work demonstrated that visibly charred GRP grating that appears to be essentially intact after exposure to fire can support the weight of evacuating personnel after it has been exposed to heat radiation from a fire.

Composite cylinders subjected to axial compression and external pressure: This work describes an experimental and theoretical investigation into the buckling and material strength of filament wound (55 degree) GRP cylinders when subject to external pressure and axial compression loading.
Experimental details:The test cylinders were 500 to 2000 mm in length, with 100 and 200 mm internal diameter and 5 to 6.5 mm wall thickness. ***Modelling and results****:* A finite element computer code was written to calculate the theoretical bifurcation buckling and first ply to failure of the pipe subject to different combinations of loading conditions. The results are summarised as follows: Very good agreement was achieved between theory and practice; The majority of the experimental results of critical loads lay within 0.9 to 1.03 of the theoretical prediction; For the geometries tested the buckling mode of failure is dominant for external pressure : axial compression ratios greater than 0.25. ***Significance:*** While the characteristics of GRP cylinders subject to internal pressure and tensile loading is reasonably well covered in the literature little information is available for the compressive stress conditions investigated in this work. The work validates the use of appropriate theoretical methods to predict external collapse loads of composite tubular elements, the testing of which may be difficult or expensive to carry out in practice.

The Behaviour of Composites in Production Fluids
This work investigated the effect of production fluids on high pressure GRP piping and includes a useful literature survey.

Experimental details*:* Anhydride epoxy 97 mm internal diameter, 8 to 9 mm thick GRP tubes were supplied by ABB of Sweden. These were filled with either Gulfaks ‘A’ crude oil or brine. Both media were topped with a 90/10 mixture of methane and carbon dioxide at a pressure ranging between 90 and 130 bar. The test temperature was 80°C. The original intention had been to expose the tubes for a period up to 18 months but due to an oversight in the design of the end closure (which resulted in premature failure of the end closure), the test period had to be restricted to 6 months. The test samples were also strain gauged. Diametral compression tests were carried out on ring specimens cut from the tube. Visual, SEM and Dynamic Mechanical Thermal Analysis (DMTA) examinations were also performed. ***Results****:* No reduction in burst strength or mechanical properties could be detected after 6 months exposure to either environment. Visual examination showed a “whitening” of the resin on the surface exposed to brine after 6 months. This intensified with increasing pressure. This was believed to be due to hydrolytic degradation of the surface resin, which exposed the glass fibres. ***Significance****:* While the work demonstrates the ability of glass/epoxy tubulars to contain high pressure production fluids at 80°C in the short and medium term, it confirmed previously identified concerns about the suitability of anhydride cured epoxies for this service.

Characteristic Base line Optimum conforming Solution Optimum radical solution
For both solutions it was found that closed hollow sections and cellular panels afford the most cost effective structural performance and offered better impact and fire performance than open sections such as I beams. Pultrusion and filament winding were generally found to be the most cost effective manufacturing processes. Generally polyester resin and E glass fibre were the preferred constituent materials for primary structural components in a ventilated environment. Phenolic resins were preferred for lighter structural elements and non-structural panels where low smoke and toxicity emissions in a fire were required. The optimum radical solution was found to be best in terms of weight and fabricated cost, and was recommended to be carried forward for more detailed evaluation in CP 453..

Detailed conceptual design and cost assessment of composites topsides: This is followed by a section that identifies methods for predicting composite properties and behaviour of composite materials, including hydrothermal and fire behaviour, impact and damage tolerance, where the composition is defined in terms of matrix and fibre configuration. The structural design methodology was based on a limit state approach and the report describes how criteria can be arrived at for partial factors, ultimate strength, serviceability, fatigue life and durability. However the extent to which this information was actively applied in the study is not clear. The general design approach is described where it is explained that the shape and size of components are dictated by the capability of the processing method and the connectivity of the structural system. Further work was carried out to optimise both the composite structure and the space. More detailed assessments were carried out on the stress distribution of the cylindrical shell, the production deck, and the effect of blast overpressure. The key areas examined in the conforming solution were the beam connections, the structural behaviour of decks, and the impact resistance of the helideck. The more detailed analysis investigated the effect of long term creep in primary beams, viability of tubular beam options, the stresses at a beam to column connection and elastic resilience of the helideck to impact. The latter includes comment about health and safety issues, handling, workforce training and inspection and repair. The requirements for platform installation are discussed where it is noted that the lower weight of a composite structure would afford no appreciable advantage for most practical situations. This is because of the ample lift capacity of vessels general available for installation. However the effect of weight reduction on the installed cost of floating facilities such as TLP's and semisubmersibles was shown to be significant. Comment is given about the factors dictating the process which would enable composites to be implemented in structural applications offshore. It is suggested this would require close cooperation between one or more operators, a main contractor and a number of specialist designers and product suppliers. The cost of carrying out a comprehensive testing program to validate the design was identified as likely to be significant. There is a need to educate personnel concerned with the design, fabrication and certification of composite structures and to encourage the development of suitable design codes. Significant effort was applied comparing the construction costs, in terms of material and fabrication cost, for the base line and radical solutions on a like-for-like basis. Just the production deck was costed for the Conforming option to enable an estimate of the complete platform to be obtained. The claimed weight and cost savings for both composite designs were dependent on the choice of these factors.

Significance: This was the first major study carried out to investigate the practicalities of constructing primary structures using composite materials on offshore platforms. The study found that it was technically and economically viable to construct primary structures for the topside of minimum facilities production platform almost entirely out of composite materials given a large enough order base to limit the effect of one off-costs.

Recommended Standard Composite Components

The philosophy behind the guideline is material independent. The Limit State design method recognises the different modes of failure of each functional requirement and the need to associate each mode of failure with a specific limit state beyond which the structure would no longer satisfy the functional requirement. Different limit states are defined, each limit state being related to the kind of failure mode and its anticipated consequences. Both ultimate limit state (ULS) and serviceability limit state (SLS) are required to be considered in the design of the structure. Safety classes are determined based on the consequences of failure when the mode of failure is related to the ultimate limit state. Service classes are based on the frequency of service interruptions or restrictions caused by modes of failure related to the serviceability limit state.

CONCLUSIONS

This work has shown that there were no insurmountable technical or economic barriers to the increased, and safe, usage of composite materials offshore. It has provided a sound and scientific basis upon which regulatory changes can be based and introduced. It has also contributed to substantial changes in the attitude of both the offshore industry and its regulators towards the use of composite materials in offshore environments.

ACNOWLEDGEMENTS: to Plan Nacional I+D+i, Project DPI 2007-61090

REFERENCES

BAO, C., “Materials selection for industrial applications”, Ph. D., UPV/EHU, 1991

Determination of the overall heat transfer coefficient "U" in heat insulation sandwich panels

A.P. Sartori
Randon Implementos Rodoviários, Brazil
P.R. Wander, M. Giovanela, J.S. Crespo
Centro de Ciências Exatas e Tecnologia, Universidade de Caxias do Sul, Brazil
R.C.R. Nunes
Universidade Federal do Rio de Janeiro, Instituto de Macromoléculas, Brazil

SUMMARY

A sandwich panel consists essentially of two face sheets and may even have metal reinforcements and a core formed, usually by a cellular polymer. The faces of this type of panel may be joined by a structural adhesive or in cases where the core is a rigid polyurethane foam injected directly on the substrates the union will occur naturally. The most relevant property of the sandwich panels for the transport of frozen or chilled cargo is thermal conductivity (k). Within this context the objective of this work is to obtain and characterize sandwich panels which can be used in refrigerated chambers. This work presents four alternatives for composite sandwich, sample 1 (PRFV/PU/PRFV), sample 2 (AG/PU/AG), sample 3 (Al Crimpy/PU/PRFV) and sample 4 (Al /PU/Al) on which thermal analyses were performed and the overall heat transfer coefficient (U) of the system determined. It could be concluded that the value of U of the system currently used is at the limit specified by the standard.

1. INTRODUCTION

The transportation of perishable and fragile foods has increased considerably in the last years. Sandwich panels are used in the construction of stationary refrigerated chambers, civil construction, vehicles for the transport of frozen and refrigerated goods. The most important and desired characteristics of the sandwich panels are the structural properties combined with the low density and the exceptional thermal isolation (TORREIRA et to. 1980, ANONYMOUS et to. 2006). In this sense, this work had as objective to evaluate different kinds of composites as to their effectiveness to the thermal isolation.

2. EXPERIMENTAL

2.1. Sandwich panels injection

For each proposed alternative (samples 1 to 4) six specimens were made. Each panel was submitted to the process of rigid polyurethane foam injection with a low pressure equipment and a fixing mold system at the temperature of 45°C. The mass of PU injected in the panels was calculated through the volume of each panel and the desired density of 42 kg/m³.

2.2. Assembling of the cubes (specimens) to the conductance test

Six specimens were assembled in the shape of cubes to the accomplishment of the thermal conductance test for determined the U parameter. During the assembling of the specimens a PU adhesive was used.

2.3. Experiment

The systematic of the specimen assembling (cubes) was maintained constant for each one of the four configurations of panels exposed in this work. Initially, the thermocouple (TP1 to TP6) were positioned and fixed inside the specimens. After, a period of stabilization of the internal specimens temperature was waited, the data collection (current and voltage) begun, every 15 minutes during a period of 2 hours. The difference of the internal medium temperature was maintained at 45ºC during the test (ABNT NBR 2006, ATP 2008).

2.4. Thermography

All the sandwich composites that composed the 4 configurations of the test cube were submitted to the thermographical analysis. Initially, the thermographic chamber had its emissibility was calibrated through the external termopar (ambient temperature). Immediately after the data collection (equalizes internal temperature), thermographic images were obtained and afterward were submitted to analysis in a specific software (Quick Report 1.1.).

2.5. Calculation for the Determination of the overall heat transfer coefficient

The calculation for the U determination is based on the experimental data collected. To obtain this coefficient, the system temperatures were collect (internal and external ambient, internal and external walls) and the tension and current data that are the product of the dissipated potency for each system in the maintenance of the internal temperature. After the conclusion of the data collection, analyses in the external and internal dimensions of the test cubes were made. To calculate this coefficient (equation 1), the theoretical value of h (air heat transfer coefficient) of internal and external convection and the density and viscosity of the air in the obtained temperatures were used. The equations below were used for the achievement of the overall heat transfer coefficient (PARSONS, 1997). The Table 1 shows the used equations.

$U_i = \dfrac{\dfrac{1}{(\mathrm{h_{ext}} \times \mathrm{A_{ext}})} + \mathrm{R} + \dfrac{1}{(\mathrm{h_{int}}\ \mathrm{x}\ \mathrm{A_{int}})}}{A_{int}}$	Global heat transfer coefficient	**Equation 1**
$h_{ext} = \dfrac{(Nu \times k)}{L}$	Internal and external air heat transfer coefficient	**Equation 2**
$\mathrm{Nu} = 0{,}13\,(\mathrm{Gr} \times \mathrm{Pr})^{0{,}33}$	Nusselt number	**Equation 3**
$GR = \dfrac{(\mathrm{g}.\beta.\Delta\mathrm{T}.\mathrm{L}^3)}{(\mu/\delta)^2}$	Grashof number	**Equation 4**
$Pr = \left(\dfrac{\mu.\mathrm{cp}}{k}\right)$	Prandlt number	**Equation 5**
$R = \left(\dfrac{\Delta\mathrm{T}}{Q}\right)$	Composite resistance	**Equation 6**

Table 1. Equations for the calculation of the global heat transfer coefficient.

where, U_i (global heat transfer coefficient), h_{ext} (heat transfer coefficient external air), h_{int} (heat transfer coefficient internal air), A_{ext} (external area), A_{int} (internal area), R (composite resistance), Nu (Nusselt number (turbulent system)), k (thermal condutivity of the air), L (length), Gr (Grashof number), Pr (Prandlt number), g (gravity), β (1/average temperature), ΔT (variation temperature), μ (viscosity), ρ (density), Cp (specific heat), k (thermal condutivity) and Q (average power).

For the achievement of the global U of the system, it is necessary the calculation for the values of h_{ext} and h_{int}, and the resistance of the composite being evaluated. For natural convection heat transfer coefficients the equation 2 is used. The Nusselt number (equation 3) considers a laminar range when the Prandlt number is between 10^4 and 10^8 and a turbulent range when this number is between 10^8 and 10^{12}. In this experiment the turbulent band was used to obtain h_{ext} and h_{int}. For the 4 composites proposals (PRFV/PU/PRFV, AG/PU/AG, Al Crimpy/PU/Al e Al/PU/Al), the calculations used to obtains the global coefficient were the constants in the equations from 1 to 6 (PARSONS 1997).

3. RESULTS AND DISCUSSION

The composites alternatives exposed in this work were submitted to thermographic analysis during the global heat transfer coefficient determination. Also, after the tests, samples of the PU rigid foam used as the core of the panels in study were collected and submitted to the verification of their thermal conductivity (k). Table 2 shows the results obtained in the thermographic analysis of the different composites, the overall heat transfer coefficient for the different materials, the factor of thermal conductivity of the PU rigid foam, and the cost per m² of the materials.

Composite	External temperature (°C)	Internal temperature (°C)	Global coefficient (W/m²K)	PU thermal conductivity (W/mK)	Cost* (US$/m²)
PRFV/PU/PRFV	23.5 ± 0.5	72.2 ± 1.0	0.2015	0.02348	37.65
AG/PU/AG	22.1 ± 1.2	64.5 ± 0.6	0.2688	0.02458	19.65
Al Crimpy/PU/PRFV	28.1 ± 0.7	68.3 ± 0.3	0.3211	0.02440	39.28
Al/PU/Al	27.1 ± 1.5	66.6 ± 0.4	0.3468	0.02333	27.06

Table 2. Results of the composites.

In Table 2, it is possible to verify that the average temperature obtained from the 76.800 points of each thermographic image collected, shown a small standard deviation. This allows a trustful evaluation of the system, showing that there was stabilization and small loss of internal temperature through the union elements of the test cube (adhesive). The material that shown less external temperature was the composite AG/PU/AG, however the average internal temperature was smaller than the obtained for the composite PRFV/PU/PRFV that had an external temperature just 1.4ºC higher than the alternative with AG (ALVARADO et to. 2009). For the composite PRFV/PU/PRFV, the ΔT between the internal temperature and the external wall was 48.63ºC, at the same time as for the composite AG/PU/AG, the value obtained was 42.40ºC. This happens because the face materials from the PRFV/PU/PRFV alternative are polymeric and have a smaller thermal conductivity than the others face materials from the AG/PU/AG alternative, which are metallic and have a higher thermal conductivity than the polymeric materials. The alternatives with aluminum faces showed a higher thermal loss between the internal temperature and the external walls of the system. In figure 1 the obtained external temperatures can be observed, as well as the region where the panels where united with adhesive for the assembling of the test cubes.

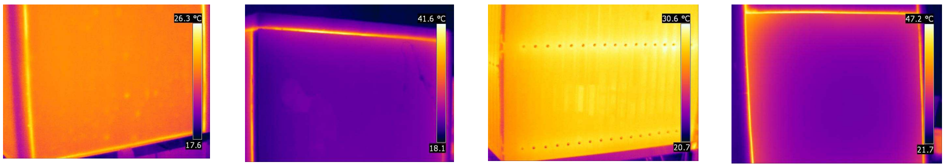

(a) PRFV/PU/PRFV (b) AG/PU/AG (c) Al Crimpy/PU/PRFV (d) Al/PU/Al

Figure 1. Thermographic analysis of the sandwich panels.

It is possible to identify that the spots where the temperature is higher are located in the joint region, that is, where the polyurethane adhesive is in evaluation and not the composite. Generally speaking, this kind of analysis allows observing the uniformity of the PU rigid foam injection. This information is related with the values obtained for the thermal conductivity of the foam in Table 2. For the Figure 1c, it is possible to identify through the image that the higher thermal loss can be located in the region of the clinches, where a thermal bridge exists. The obtained experimental data that is more relevant and was the reason of this work is the overall heat transfer coefficient, which considers the composite resistance, the area for each specimen and the thermal conductivity coefficient of the internal and external air. For the PRFV/PU/PRFV composite the smallest coefficient was found, that is, 43% less than obtained for the traditional composite used in road equipment and specified in the NBR 14701. Another option that showed a coefficient approved by the NBR 14701 was the composite AG/PU/AG whose coefficient was 23% lower. The composites with aluminum face showed values in the edge of the allowed by the NBR 14701 or 12.5% higher than the maximum value allowed. In this research, the cost per m² was also considered for each proposed alternative, being that for the most efficient alternative, concerning thermal isolation, the cost was 4% lower than the actual system.

3. CONCLUSIONS

All the studied alternatives are in agreement with the ABNT NBR 14701. The results of U, allow the concerning performance: PRFV/PU/PRFV, AG/PU/AG, Al Crimpy/PU/PRFV e Al/PU/Al. Concerning the cost of the panels in a decreasing form: AG/PU/AG, Al/PU/Al; Al Crimpy/PU/PRFV e PRFV/PU/PRFV. As a final conclusion the alternative AG/PU/AG has the best relation cost/performance.

REFERENCES

ABNT NBR 14701 (2006) Associação Brasileira de Normas Técnicas - Implemento Rodoviário Carroceria Termicamente Isolada – Desempenho Térmico (Rio de Janeiro, Brazil).

ALVARADO J.L., TERRELL W.JR., JOHNSON M. (2009). Passive cooling systems GNfor cement-based roofs. *J. Building and Environment.*, 44, 1869-1875.

ANONYMOUS (2006) Sandwich Panels in Vehicle Construction (Ed. Verlag Moderne Industrie, Germany).

ATP Handbook (2008) - Agreement on the International Carriage of perishable foodstuffs and on the special equipment to be used for such carriage (England).

PARSONS R.A. (1997) Fundamentals Handbook (Ed.ASHRAE, USA).

TORREIRA R.P. (1980) Isolamento Térmico – Calor e Frio, (Ed. Fulton Editora Técnica, Ltda - São Paulo, Brazil).

Lightcarboncars: estudio reólogico del reciclado de pCBT/CF obtenido mediante RTM

S. Neira, L. German, K. Gondra, G. Pardo
GAIKER-IK4
A. Agirregomezkorta, M. Sarrionandia, A. Arostegui, J. Aurrekoexea
Departamento de Mecánica y Producción Industrial. Mondragón Unibertsitatea, España.

RESUMEN

En el presente trabajo se ha estudiado el comportamiento reológico del pCBT/CF obtenido mediante RTM. Los resultados han demostrado que la viscosidad del compuesto reciclado es entre dos y cuatro veces menor, dependiendo de la velocidad de cizalla. En el rango estudiado la granulometría del reciclado no tiene efecto sobre la viscosidad. La baja viscosidad dificulta su procesado en equipos convencionales de termoplásticos, por lo que deberá forzosamente reutilizarse mezclado con PBT de grado inyección. La adición de tan solo un 2% de pCBT/CF al PBT de inyección reduce su viscosidad hasta la mitad. Añadiendo porcentajes mayores (20 y 40%) disminuyen aún más la viscosidad pero de forma menos pronunciada.

1. INTRODUCCIÓN

Las principales ventajas funcionales de los materiales compuestos de matriz termoplástica frente a las termoendurecibles son; la mayor resistencia al impacto y a la fatiga, la adecuada reparabilidad, la posibilidad de ensamblar estructuras por soldadura, la ausencia de emisiones volátiles orgánicas durante el procesado y la reciclabilidad. Lo más habitual en el procesado por RTM es que la matriz empleada sea de carácter termoendurecible, pero en los últimos años se han desarrollado matrices termoplásticas de muy baja viscosidad (20 mPa.s para el CBT® a 180 °C, la viscosidad en fundido del PBT para inyección es 5000 veces mayor) que se pueden transformar mediante RTM (van Rijswijk et al. 2007).

Estas matrices termoplásticas que se pueden procesar en vía líquida son de reciente aparición, por lo que aún quedan muchos interrogantes sobre su estructura, sus propiedades y su reciclabilidad. En la bibliografía existe una sola referencia a la reciclabilidad de este tipo de materiales, y además se centra en el estudio de la matriz sin ningún tipo de refuerzo (Parton et al. 2005).

Por lo tanto, el presente trabajo viene a cubrir el vacío que existe sobre la reciclabilidad del compuesto de pCBT reforzado con tejido de fibra de carbono obtenido por RTM. La información obtenida será de utilidad a la hora de evaluar las diferentes vías de revalorización, y de buscar aplicaciones del compuesto reciclado. En este estudio preliminar se analiza la reología de diferentes triturados y de la mezcla de dicho compuesto triturado con un grado de inyección de PBT. En futuros trabajos se determinarán las propiedades mecánicas de dichos compuestos reciclados y revalorizados.

2. MATERIALES Y MÉTODOS EXPERIMENTALES

2.1. Materiales

Los materiales que se ha utilizado en este trabajo son el CBT160® de la casa Cyclics Corporation, material que se suministra en forma de granza y que incorpora el catalizador. En lo que a las fibras de carbono se refiere, se ha utilizado tejido de carbono de alta resistencia HR con arquitectura de tipo tafetán de 193 g/m^2 (ref. 43194 Axson). El compuesto se ha obtenido por el proceso de transformación TP-RTM. La densidad del pCBT/CF es de 1,47 g/cm^3 y su porcentaje de fibra en volumen es del 31,86 %. Se ha seleccionado un PBT de grado inyección (Pocan®) como material de referencia a la hora de comparar la viscosidad del pCBT/CF reciclado, y para revalorizar el compuesto introduciéndolo como refuerzo en el PBT de grado de inyección.

2.2. Reciclaje del compuesto pCBT/CF

En la primera etapa del proceso de reciclaje se trituran las placas de compuesto, pero no posee una granulometría definida (figura 1.a), ya que este tipo de equipo simplemente desintegra aleatoriamente la morfología inicial del material.

Con objeto de obtener un triturado final del producto, con tamaño de partícula homogéneo, se introduce este último en el molino de martillos (figura 1.b). Los productos de partida pasan a la zona de acción, donde los martillos los empujan contra la malla (8 mm). La reducción del tamaño del material (figura 1.c) es producida principalmente por fuerzas de impacto, aunque si las condiciones de alimentación son obturantes las fuerzas de rozamiento pueden también tomar parte en la reducción de tamaño. Finalmente, el residuo obtenido se introduce en un molino criogénico (figura 1.d) donde se define la granulometría deseada mediante el intercambio de mallas (figura 1.e), que en el presente estudio se han fijado en tres tamaños 0,08-0,25 y 0,5 mm (figura 1.f).

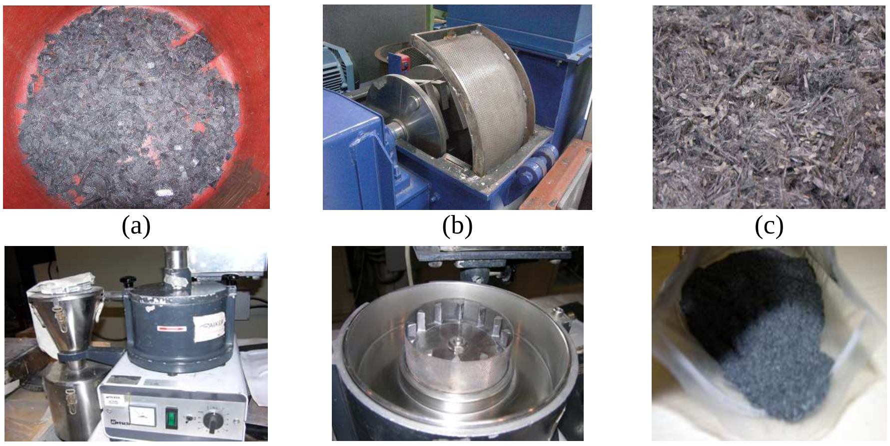

(a) (b) (c)

(d) (e) (f)

Fig. 1. Triturado inicial del compuesto pCBT/CF (a), detalles del martillo y malla utilizados en la molienda (b), triturado tras la molienda (c), molino criogénico (d), detalle de la malla (e) y triturado de 0,5 mm (f).

2.3. Medidas reológicas

Para el análisis reológico del compuesto se utilizó el equipo de MINILAB. El sistema esta basado en dos husillos cónicos con un canal reológico integrado, mediante una válvula que puede controlar que el material este recirculando. En el canal reológico hay dos sensores de presión que permiten medir la viscosidad del material. Los parámetros fijados son la temperatura (260 ºC), el número de medidas a tomar durante el ensayo (10) y el intervalo de revoluciones de los husillos para las que se va a realizar el ensayo reológico (30-360 r.p.m), obteniéndose finalmente una curva de par de torsión en función de la velocidad de giro de los husillos.

3. RESULTADOS Y DISCUSION

3.1. Reología de los compuestos pCBT/CF

En el estudio reológico, dada la baja viscosidad de los compoundings analizados, ha sido imposible determinar valores de viscosidad y el análisis se ha centrado sobre datos de par de torsión (*M*) determinados por la resistencia que opone el material al giro de los husillos en función de la velocidad. Este valor de *M* se puede interpretar como una medida indirecta de la viscosidad, a mayor par mayor es la viscosidad del fundido. En la figura 2 se pueden observar las diferencias obtenidas para las granulometrías de triturado de pCBT/fibra de carbono de 0,08-0,25 y 0,5 mm, así como el pCBT sin refuerzo y el PBT, ambos pulverizados a 0,5 mm. Las tres principales lecturas que se pueden realizar son; 1) la viscosidad de los materiales obtenidos por RTM, tanto el pCBT sin reforzar como sus composites, es entre dos y cuatro veces inferior al del PBT de grado inyección; 2) la presencia de la fibra de carbono triturada reduce ligeramente la viscosidad; y 3) la granulometría del compuesto reciclado no parece tener influencia en las condiciones de estudio realizadas.

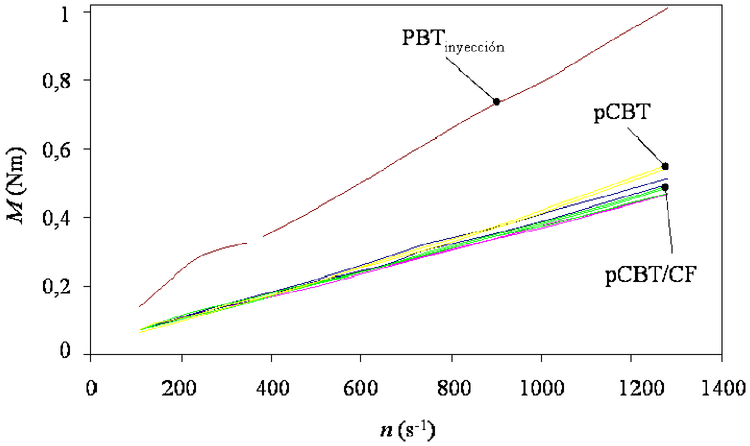

Fig. 2. Par de torsión (*M*) frente a velocidades de cizalla (*n*) para los triturados del compuesto en función de la granulometría.

3.2. Reología de las mezclas de PBT virgen de grado de inyección con compuestos pCBT/CF reciclado

Visto que en el rango estudiado la granulometría no influye sobre el comportamiento reológico del compuesto, y que las propiedades mecánicas dependen de la longitud de fibra, se ha elegido el triturado de mayor tamaño (0,5 mm). Lo resultados (figura 3) muestran que la incorporación de un 2 % de reciclado reduce la viscosidad de la mezcla, y que esta reducción aumenta con el contenido de reciclado, si bien lo hace en menor medida.

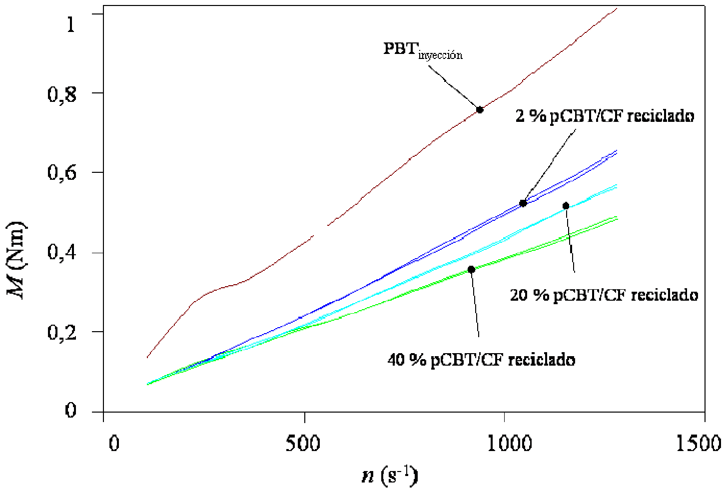

Fig. 3. Par de torsión (*M*) frente a velocidades de cizalla (*n*) para las mezclas con 2, 20 y 40 % de pCBT/CF reciclado.

4. CONCLUSIONES

El compuesto reciclado de pCBT/CF presenta una viscosidad muy baja, lo que imposibilita la utilización del mismo directamente en máquinas de procesado de termoplásticos adaptadas a viscosidades mucho mayores. La granulometría, en el rango estudiado, no influye sobre la reología del compuesto reciclado. La incorporación de un 2 % de compuesto reciclado en le PBT de grado de inyección disminuye fuertemente la viscosidad, pero porcentajes mayores de reciclado (20 y 40 %) reducen la viscosidad proporcionalmente menos.

5. AGRADECIMIENTOS

Los autores desean agradecer al Ministerio de Ciencia e Innovación (PSE-370000-2008-4) y al Gobierno Vasco (PI2008-07) la financiación.

6. REFERENCIAS

PARTON, H., BAETS, J., LIPNIK, P., GODERIS, B., DEVAUX, J., VERPOEST, I. (2005). Properties of poly(butylene terephthatlate) polymerized from cyclic oligomers and its composites. *Polymer*, 46, 9871-9880.

van RIJSWIJK, K., BERSEE, H.E.N. (2007). Reactive processing of textile fiber-reinforced thermoplastic composites – An overview. *Compos. A: Appl. Sci. Manuf.*, 38, 666-681.

Effect of temperature, moisture and UV radiation on viscoelastic properties of glass fiber/epoxy laminates for structural pipeline

A.P. da Costa, M.L. Costa, E.C. Botelho
Depto de Materiais e Tecnologia, Engineering Faculty – São Paulo State University - UNESP, Av. Dr. Ariberto Pereira da Cunha, 333, Guaratinguetá, 12.516-410, Brasil
L.C. Pardini
Divisão de Materiais/AMR , Comando Geral de Tecnologia Aeroespacial - Instituto de Aeronáutica e Espaço (IAE), praça Mal-do-Ar, 50, São José dos Campos, 12.228-905, Brasil

SUMMARY

Filament-wound polymer-matrix composite tubes find uses as pressure vessels, rocket launchers, etc., where internal pressure is the primary constraint. Increasing use of these structural parts has given rise to the need for tests to identify characteristics of their mechanical and viscoelastic behavior. Among these polymeric composites, the glass fiber/epoxy laminates are the most used due to low processing cost, flexibility, great service life and excellent insulation and corrosion properties. The main objective of this experimental investigation was to study the effects of moisture absorption, UV light and sea water conditioning and exposure to elevated temperature on the viscoelastic properties of glass fiber reinforced epoxy composite tubes. For this purpose, parts of the filament wound tubular composite specimens were immersed in distilled water at two different temperatures for approximately two months and their moisture absorption was recorded. The rate of moisture absorption was greater for the group of specimens immersed in distilled water at an elevated temperature (60°C) than those at room temperature (~20 °C). In this work, this laminate also was submitted to UV and in saline solution substitute to sea water during around 60 days. The viscoelastic behavior of a glass fiber/epoxy matrix composite material system used for pipeline has been evaluated though dynamic mechanical analysis. The effects of the heating rate, frequency, and measurement method on the glass transition temperature (Tg) were studied.

INTRODUCTION

Damage caused by corrosion are almost inevitable in pipelines transporting oil and derivatives over time. When they are present, it is necessary to evaluate the damage extent and so apply the repair procedure. Pipelines composites repairs have advantages due to simplicity in application of this material, that involve the damage pipe with layers of polymer material reinforced by oriented fibers, which should be directed to circumferential tension (Marcelino, et al. 2003).

The use of composite material is very attractive in pipes uses due to properties such as higher chemical and cathodic corrosion resistance and low weight and flexibility (Laney, 2002). Among the polymer composites, the glass fiber / epoxy composites are the most studied class of materials and provide good technical and economical benefits for most applications (Barton Jr., et al., 2006) (Srihari, et al., 2002).

The presence of environmental variables must always be considered in the design and installation of pipes, since these one can influence the life of the metal and the composite used in repair, especially the presence of moisture, salinity and ultraviolet light (Alkazraji, 2008). The presence of moisture causes plasticization of the matrix, with the consequently reduction in the creep of the matrix as well as modulus of the matrix toughening (Cunha, et al., 2006). The ultraviolet light radiation causes degradation of the matrix surface and by photo-oxidation of the matrix (Kumar, et al., 2002).

This work presents the evaluation of the environmental condition on the viscoelastic properties by using dynamic mechanical analysis. The effects of the temperature, moisture and UV radiation on the glass transition temperature (Tg) were studied.

EXPERIMENTAL PROCEDURE

In the present work epoxy/glass fiber composites specimens used in repaired pipelines were used. Samples of this material were conditioned in QUV/Se weathering chamber (Q-Panel Lab Products, Cleveland, Ohio) that induces degradation mechanisms from UV radiation and water condensation. The laminate was conditioned for 900 hours under a cycle of 8 hours of exposure to UV light and 8 hours of exposure to water spray.

In order to evaluate the moisture effect on the viscoelastic properties, epoxy/glass fiber specimens were conditioned in a distilled water bath (at 25°C and 60 ° C) and in a saline solution bath. Before these procedures, the specimens were dried in a vacuum oven at 60 ° C for at least 24 h before testing.

The saline solution bath was used in order to simulate the seawater environment. In this conditioning, the specimens were weighed and immersed in salt solution water bath prepared according to ASTM D 1144-98 standard, that covers the preparation of solutions containing inorganic salts in proportions and concentrations representative of ocean water.

For both moisture conditioning (water and salt solution baths) the moisture level in the laminates was periodically monitored as a function of time by measuring the mass of traveller specimens until the moisture equilibrium state reach a plateau.

After the environmental conditionings, the composite glass transition temperatures were evaluated by dynamic mechanical analysis. For this test were used: range temperature from 20 º C to 250°C, heating rate of 3^{o}C/min, under ambient atmosphere and frequency of 2 Hz.

RESULTS AND DISCUSSION

(a) shows the moisture absorption of the conditioned materials in distilled water bath at 25^{o}C and the seawater bath at 25^{o}C, both after to be submitted in these conditionings during one month and in heated bath conditioning at 60^{o}C for two months. According to the graphs, can be observed that the composite material absorbed 0.60% of moisture during the hygrothermal conditioning, and 0.35% during the distilled water and saline conditioning. The process of absorption, characterized by the growth curve was followed in a linear fashion to reach a state of pseudo-equilibriumat a time of 200 hours for distilled water and saline conditioning and 500 hours for hygrothermal conditioning. As shown, starting from this point the absorption becomes slower due to a polymer chains relaxation process and filling empty. The moisture absorption had a behavior according to the Fick's diffusion law and was facilitated by the capillarity effect due to micropores in the structure from the processing of the material.

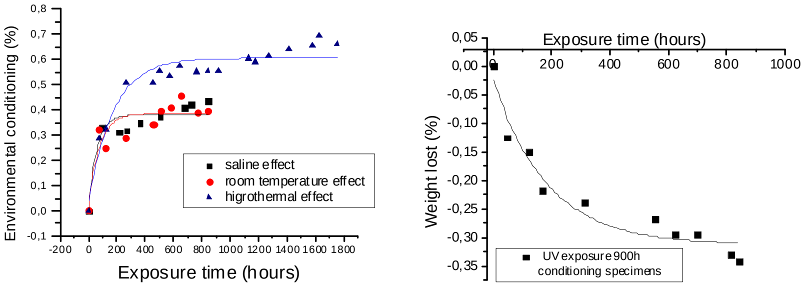

Figure 1. Gain (a) and loss (b) of weight for different environmental conditionings.

By using Figure 1a, can be observed that in both conditioning, saline bath and distilled water bath, the saturation point was the same, in around 200 exposure hours with the weight increase of around 0.35%. However, when submitted to heated bath (60°C) was observed an increase of absorbed moisture and time to reach the saturation point. This difference can be explained due to the high temperature induces the moisture diffusion processes.

(b), presents the weight loss as a result of the degradation process when the material was exposed on UV conditioning. This loss was approximately 0.30% and happens due to cycling between the factors of UV radiation and condensation of water. It can be explained by the UV radiation that causes a chemical change in the epoxy surface and by the sequential water condensation that causes the removal of the degraded surface layer and the exposure a new material layer to UV degradation. Besides this factor, the ultraviolet light radiation presence can cause the water molecule fission in free radicals OH- and H+ that contribute to the degradation process in the surface material.

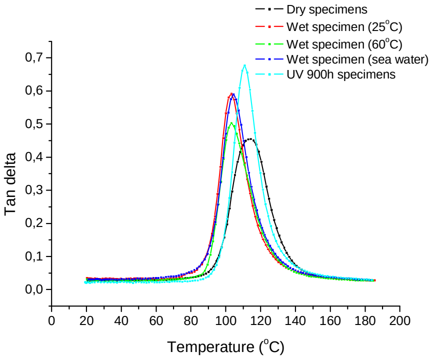

Figure 2. Glass transition temperature for glass fiber/epoxy.

Figure 2 shows the chain relaxation in tan δ curve obtained by the dynamic-mechanical

analysis for laminates of epoxy/glass fiber. By this curve can obtained the glass transition temperature for the studied laminates. According to this results can be observed that the values decrease with the environmental conditioning: Tg (dry specimens) = 114,37oC, Tg (UV 900 h specimens) = 110.85°C, Tg (60^{o}C wet specimens) = 103.14^{o}C, Tg (25^{o}C wet specimens) = 103.15^{o}C, Tg (seawater wet specimens) = 104.41°C. The decrease of glass transition temperature is more intense in composites immersed in bath when compared to the material exposed to ultraviolet light radiation. The lower Tg for immerged materials is due to the higher polymer chains mobility facilitated by humidity. However, the glass fiber/epoxy Tg was almost the same for all conditioned by immersion, demonstrate that the temperature did not chain relaxation affect the chain relaxation final properties. This is because the laminate has reached a balance in the plasticization level which was maximum and equal for all immersed specimens.

As can be observed in Figure 2, specimens after to be submitted to ultraviolet light radiation conditioning presented low degradation effects on glass transition temperature values when compared with specimens submitted to bath conditioning. This behavior happened due to the degradation process under ultraviolet light occurs preferentially on the surface, breaking the chains and causing pores and microcrack in more external layers of the laminate.

The glass transition study for polymeric composites is an important property to be measured when these materials are used in structural repairs. These glass transition decreases are a directly interference in material mechanical properties and they can make failures in interfacial bond.

CONCLUSION

The influence of distilled water and seawater baths, at room service temperature (25°C), hot water bath at 60^{o}C and UV light exposure have been investigated for the glass fiber/epoxy laminates. In this work, it was observed that this laminate absorbed 0.35% of moisture after the saturation point, when submitted to seawater and distilled water conditionings and 0.60% in hygrothermal conditioning by using 60°C. Therefore, after UV light radiation conditioning, this laminate presents 0.30% of loss weight.

Dynamic-mechanical analyses were done in all conditioned specimens and the glass transition temperatures were evaluated. These analyses show that the Tg decrease when exposed to environment conditioning. This behavior happened because the humidity always induced resin plasticization and, consequently, increase the polymer chain relaxation. The small glass transition temperature decrease induced by UV radiation is due to a surface phenomena degradation.

ACKNOWLEDGEMENTS

The authors acknowledge financial support received from FAPESP and CNPq.

REFERENCES

Alkazraji, Duraid. 2008. *A quick guide to pipeline engineering.* Cambridge England : Qoodhead publishing limited, 2008.

Barton Jr., Oscar and Mouring, Sarah. 2006. On the moisture-related buckling of marine composite panels using approximate analysis. 2006.

Irradiated microwave synthesis: a new way to obtain conducting copolymers

P. Marcasuzaa, J. Desbrières, S. Reynaud
IPREM-EPCP, UMR 5254 (CNRS/UPPA), Hélioparc, 2 avenue du président Angot,
64053 Pau cedex 9, France
O. Donard
IPREM-LCABIE, UMR 5254 (CNRS/UPPA), Hélioparc, 2 avenue du président Angot,
64053 Pau cedex 9, France

SUMMARY

The present study describes a new of synthesis of intrinsic block copolymer synthesis using microwave irradiation. This new process in not dependent upon the thermal conductivity of the vessel materials, leads to a rapid rise in temperature directly related to the rotational motion of the molecules induced by microwave irradiation. As a result, the heating rate and efficiency of MW heating strongly depends on the dielectric properties of the reactant and/or solvent. Microwave mode of irradiation has been deeply studied in order to obtain best irradiation conditions to discriminate thermal from microwave effect. Experimental conditions in terms of irradiation power, temperature, and reaction time have been then optimize to obtain perfect control of the polymerization when using ATRP. Special attention is given to the comparison between conventional (oil bath) and microwave heating. The telechelic polyaniline end-capped polymers were synthesized through ATRP followed by coupling reaction and the complete procedure was successfully carried out under microwave irradiation allowing decreasing significantly the reaction time from days to hours.

INTRODUCTION

Microwave synthesis represents a major breakthrough in synthetic chemistry versus conventional heating sometimes known to be time consuming because of its low efficiency. If the microwave energy was developed for industrial application from the middle of the 20th century, first microwave-enhanced organic chemistry was not explored until the mid 1980s[1,2]. Because of the nearness of step growth polymerization and organic chemistry, this polymerization type was first reported under microwave irradiation. In current polymer science, the use of microwave-assisted polymer synthesis has been widely investigated by several research groups and some reviews have already appeared[3-7]. Until recently, most of the researches were performed in multi-mode domestic microwave ovens which are proven to be problematic. These apparatus are not designed for the requirements of laboratory usage and most of them concern the experimental condition accuracy (temperature and pressure monitoring). This lack of experimental condition control leads to many controversy within published results in the area of controlled radical polymerization.

Even if the occurrence of any microwave effect is still to be demonstrated, the use of microwave energy remains promising due to shorter reaction time and greater yield, improved energy utilization, less environmental pollution method and better selectivity.

Encouraged by the above results, as a part of our research to prepare conducting composite with architecture control[8,9],in this work, we report the synthesis of conducting block copolymers by using controlled radical polymerization under microwave irradiation. Special attention is given to the comparison between conventional (oil bath) and microwave heating in terms of reaction time, molecular weight control and selectivity.

RESULTS AND DISCUSSION

In comparison to the impressive development of the MW technique in organic synthesis during the last decades, microwave-assisted polymer synthesis is rather new emerging field and mainly reported from the late of 1990's[3,7,10] (see).

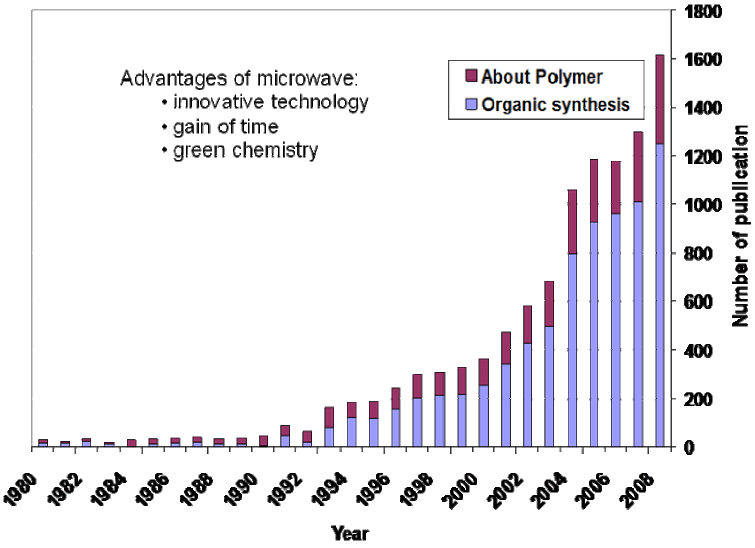

Scopus keywords: Microwave, organic synthesis, microwave, polymer

Figure 7. Evolution of interest of microwave synthesis.

The synthesis of block copolymers containing one block of intrinsic conducting polymer[11] has already been reported. The strategies involved fastidious synthesis as multi-step syntheses and drastic experimental conditions. However the synthesis of these kind of polymer are still of interest because these materials are used as models to study the conduction phenomena and interface organization[11], and they also may be used as conducting additives in insulating matrices[12].

The aim of our work is to study the use of MW synthesis to obtain conducting block copolymers while controlling the molecular weights and polydispersity index. The telechelic polyaniline end-capped polymers were synthesized through ATRP in bulk. The precursor polymers were subsequently functionalized with oligoaniline to obtain the final conducting copolymer as described in.

Figure 8. Scheme of synthesis

The objectives are at the same time to reduce the duration of the synthesis while keeping the process as simple as possible. Special attention is also given to the comparison with the results obtained under conventional heating to determine the occurrence of non-thermal MW effects which is still a controversial topic.

After a brief presentation of the MW irradiation methods *i.e.* dynamic and pulsed modes, kinetic results will be shown and evidence of living/controlled nature of the polymer will be given. The occurrence of a “microwave effect” is discussed. The block copolymers containing a conducting block of poly- or oligo-aniline were characterized to confirm their morphology and intrinsic properties.

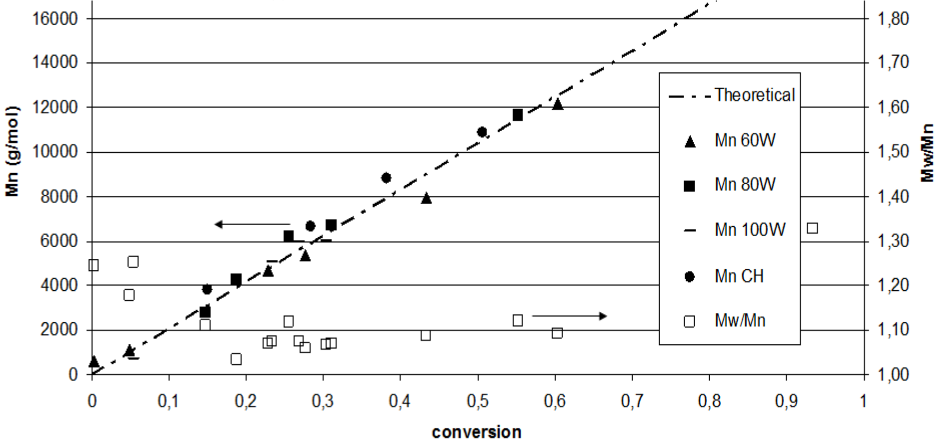

Figure 9. Dependence of Mn and polydispersity on the monomer conversion under conventional heating (CH) at 95°C and microwave irradiation (60, 80 and 100W) for ATRP of styrene with [styr]/[EBP]/[CuBr]/[PMDETA] = 200/1/1/1.

REFERENCES

1. Giguere, R. J.; Bray, T. L.; Duncan, S. M.; Majetich, G. Tetrahedron Letters 1986, 27, 4945-4948.
2. Gedye, R.; Smith, F.; Westaway, K.; Ali, H.; Baldisera, L.; Laberge, L.; Rousell, J. Tetrahedron Letters 1986, 27, 279-282.
3. Bardts, M.; Gonsior, N.; Ritter, H. Macromolecular Chemistry and Physics 2008, 209, 25-31.
4. Hoogenboom, R.; Schubert, U. S. Australian Journal of Chemistry 2009, 62, 181-183.
5. Hoogenboom, R.; Schubert, U. S. Macromolecular Rapid Communications 2007, 28, 368-386.
6. Sinnwell, S.; Ritter, H. Australian Journal of Chemistry 2007, 60, 729-743.
7. Wiesbrock, F.; Hoogenboom, R.; Schubert, U. S. Macromolecular Rapid Communications 2004, 25, 1739-1764.
8. Kohut-Svelko, N.; Reynaud, S.; Martinez, H.; Dedryvère, R.; Gonbeau, D.; François, J. Langmuir 2005, 21, 1575-1583.
9. Kohut-Svelko, N.; Dinant, F.; Magana, S.; Clisson, G.; François, J.; Dagron-Lartigau, C.; Reynaud, S. Polymer International 2006, 55, 1184-1190.

10. Bogdal, D.; Penczek, P.; Pielichowski, J.; Prociak, A. Advances in Polymer Science 2003, 163, 193-263.
11. Hanfu Wang, Y. H. Macromolecular Rapid Communications 2009, 30, 521-527.
12. Laska, J.; Zak, K.; Pron, A. Synthetic Metals 1997, 84, 117-118.

Fibras de carbono de uso general a partir de derivados del petróleo

D. Barreda, B. Lobato, C. Blanco, M. Granda, R. Menéndez, R. Santamaría
Departamento de Química de Materiales, Instituto Nacional del Carbón, CSIC, Apdo. 73, 33080-Oviedo

RESUMEN

En este trabajo se estudia la preparación de breas de petróleo para la obtención de fibras de carbono de uso general (FCUG). Las breas se prepararon partiendo de distintos tipos de residuos de petróleo: aceite decantado (DO), fuelóleo de pirólisis (FOP) y residuo de vacío (VR). Tras su caracterización se seleccionaron dos de las breas obtenidas para el estudio de su comportamiento durante el hilado. Finalmente se optimizaron las condiciones de estabilización y carbonización de las fibras verdes.

1. INTRODUCCIÓN

Las breas son utilizadas en la industria para la fabricación de diversos tipos de materiales, como ánodos, electrodos de grafito y, más recientemente, materiales de carbono más avanzados, como composites o fibras de carbono. La complejidad de las breas requiere de una adecuada caracterización, que nos permita predecir su comportamiento ante un tipo de aplicación determinado. Algunos de los parámetros más empleados para su caracterización son la fracción de insolubles en tolueno, el punto de reblandecimiento, el análisis térmico (termobalanza) y el índice de aromaticidad. Estos parámetros son indicativos de las propiedades de las breas, pero no suficientes para tener una caracterización completa de estas. Aunque dos breas tengan parámetros similares pueden tener un comportamiento térmico distinto (Alcañiz et al. 2001).

Las fibras de carbono presentan una amplia gama de propiedades dependiendo del precursor utilizado en su preparación y de las aplicaciones a que son orientadas. En el mercado existen fibras de carbono de alto módulo (FCAM), obtenidas a partir de breas de alquitrán de hulla o de petróleo. Pero también se pueden preparar fibras de más bajo coste, conocidas como fibras de carbono de uso general (FCUG), que presentan prestaciones inferiores pero suficientes para su utilización en aplicaciones convencionales (refuerzo de diferentes materiales compuestos, fibras de carbono activadas para sistemas de purificación).

2. EXPERIMENTAL

Las breas se obtuvieron en un autoclave de acero inoxidable de 1 L de capacidad mediante tratamientos oxidativos. Todos los tratamientos tuvieron lugar a 350ºC de temperatura y bajo una presión gaseosa de 5 bar. La presión gaseosa se aplica con el objeto de evitar la masiva eliminación de volátiles durante la reacción. Se obtuvieron varios tipos de breas isótropas en función del tipo de residuo de petróleo utilizado, del tiempo de reacción y del flujo de aire utilizado durante la reacción. Hasta alcanzar la temperatura de reacción y, tras la finalización de la misma hasta su enfriamiento a temperatura ambiente, se mantuvo un flujo continuo de nitrógeno de 100 ml/min con el objeto de arrastrar los volátiles generados.

Los materiales obtenidos se caracterizaron atendiendo a su punto de reblandecimiento, análisis elemental, comportamiento en pirólisis (termobalanza), espectro infrarrojo y solubilidad en tolueno.

Por otra parte se seleccionaron dos de las breas obtenidas (una preparada a partir de FOP y otra a partir de DO) para la preparación de fibras de carbono. El hilado se llevo a cabo en una hiladora monofilamento de acero inoxidable, recubierta con un horno eléctrico cuya temperatura se controló con un termopar conectado a un programador de temperatura. La extrusión de la brea se realizó por aplicación de presión gaseosa de nitrógeno, a una temperatura ligeramente superior a la del punto de reblandecimiento de la brea, y tuvo lugar a través de un spinerette de grafito de un solo orificio.

Finalmente se optimizaron los procesos de estabilización oxidativa y carbonización de las fibras en función de las características del precursor utilizado.

3. RESULTADOS Y DISCUSIÓN

Todos los tratamientos con aire se llevaron a cabo a 350ºC y bajo una presión gaseosa de 5 bar. En las tablas 1 y 2 aparecen los flujos de aire utilizados con los correspondientes tiempos de reacción para cada brea. También aparecen reflejados tres de los parámetros utilizados para la caracterización de las mismas: el punto de reblandecimiento (P.R.), la fracción de insolubles en tolueno (I.T.) y el índice de aromaticidad (Iar), obtenido a partir de la región de los enlaces C-H aromáticos (3000-3100 cm^{-1}) y alifáticos (2800-2980 cm^{-1}) en el espectro infrarrojo de las muestras.

Tabla 1. Propiedades de los materiales obtenidos.

	FOP_1	**FOP_2**	**FOP_3**	**FOP_4**	**FOP_5**
Flujo Aire (L/h)	60	60	60	80	100
tiempo reacción (h)	4	4.5	5	4	4
P.R. (ºC)	234.5	257.4	261.9	254.8	327.9
I.T. (%)	52.7	59.0	59.2	59.6	71.2
Iar	45.6	47.5	46.0	45.5	47.1

Tabla 2. Propiedades de los materiales obtenidos.

	DO_1	**DO_2**	**VR_1**	**VR_2**
Flujo Aire (L/h)	80	80	60	60
tiempo reacción (h)	6	6.5	5	5.5
P.R. (ºC)	211.4	239.2	192.4	242.4
I.T. (%)	49.5	55.4	20.5	35.6
Iar	37.7	42.9	13.9	10.5

A medida que aumenta la severidad del tratamiento (mayores tiempos de reacción y flujos de aire mayores) se obtienen breas más polimerizadas, como refleja su mayor punto de reblandecimiento y su mayor contenido en insolubles en tolueno.

En la Figura 1 se representa la pérdida de peso de tres de las muestras seleccionadas frente al aumento de temperatura bajo condiciones de atmósfera inerte (N_2). Las muestras preparadas a partir de fuelóleo de pirólisis presentan una marcada pérdida de volátiles en la región de los 150-350ºC.

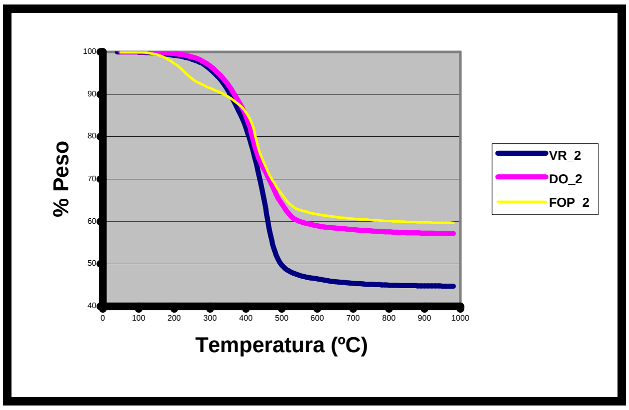

Fig. 1. Termogravimetría en atmósfera de N_2.

En el espectro infrarrojo (Figura 2) se aprecia que, en el caso del residuo de vacío, la proporción de hidrógenos aromáticos (3000-3100 cm^{-1}) es muy pequeña en comparación con los hidrógenos alifáticos (2800-2980 cm^{-1}). Sin embargo, en el caso del fuelóleo de pirólisis y del aceite decantado esta proporción se mantiene muy similar.

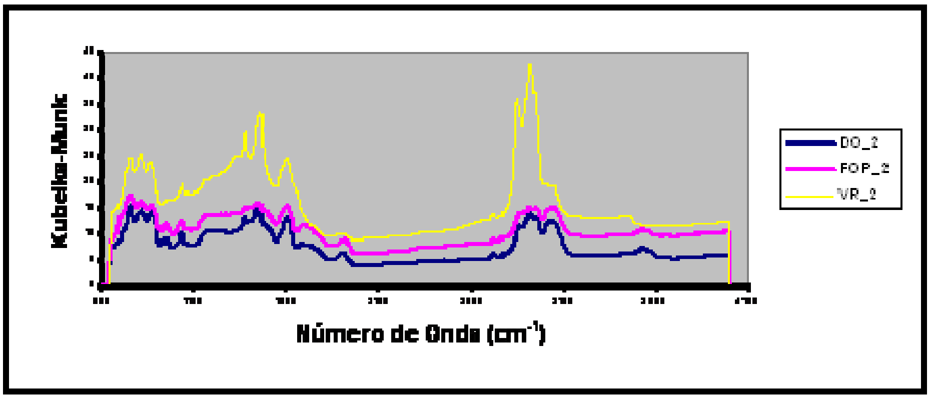

Fig. 2. Espectro infrarrojo de tres de las muestras.

A partir de las muestras DO_2 y FOP_2 se obtuvieron fibras de carbono. Las fibras se estabilizaron con aire siguiendo el siguiente programa de calentamiento: de 25 a 190°C a 3°C/min; 10 min a 190°C; de 190ºC a 200°C a 3°C/min; 10 min a 200°C; de 200 a 220°C a 3°C/min; 5 min a 220°C; de 220ºC a 260°C a 3°C/min; 5 min a 260°C; de

260ºC a 310°C a 3°C/min; 5 min a 310°C. El tiempo total de estabilización es de 2 horas y 10 minutos. Tras la estabilización, el material se carbonizó a 900°C en nitrógeno durante 30 minutos.
En la Figura 3 se muestran las fibras verdes obtenidas a partir de la brea FOP_2.

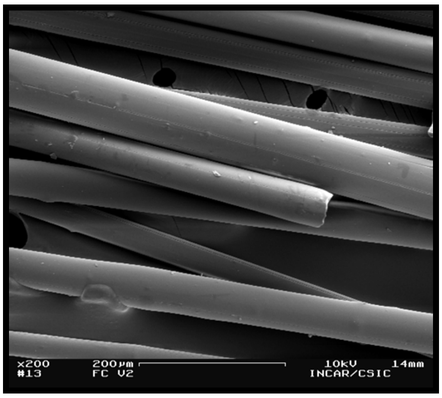

Fig. 3. Imagen de SEM de las fibras a 200 aumentos.

4. CONCLUSIONES

Se han desarrollado diferentes breas a partir de distintos residuos de petróleo. Su caracterización nos permite escoger el precursor más adecuado a la hora de proceder al hilado. Las breas con puntos de reblandecimiento entorno a los 250ºC facilitan el posterior proceso de estabilización oxidativa de las fibras, reduciendo notablemente el tiempo del proceso.

REFERENCIAS

ALCAÑIZ-MONGE, J., CAZORLA-AMORÓS, D., LINARES-SOLANO, A. (2001). Characterisation of coal tar pitches by thermal analysis, infrared spectroscopy and solvent fractionation. Fuel 41-48.

Lightcarboncars: caracterización del comportamiento dinámico (vibratorio y de impacto) de laminados de fibra de carbono para su utilización en simulación

L. Aretxabaleta, M. Mateos, M.J. Elejabarrieta, G. Castillo
Departamento de Mecánica y Producción Industrial. Mondragon Unibertsitatea

RESUMEN

El aligeramiento de los automóviles es uno de los medios para reducir las emisiones de CO_2. La estructura del automóvil debe diseñarse para absorber la energía cinética en el momento del impacto, y además hacerlo de forma controlada. Los materiales compuestos son muy efectivos para diseñar estructuras con gran capacidad de absorción de energía, pero implican dificultades (decidir qué composite, cuánto, y dónde hay que ponerlo) que no se pueden superar sin potentes herramientas de cálculo.

Por otro lado, la reducción del ruido y de las vibraciones en el interior del vehículo es un requerimiento esencial para obtener una buena calidad del mismo y la satisfacción del viajero. Para solventarlo, se utilizan gran cantidad de materiales amortiguadores y absorbentes, con el consiguiente incremento del peso global del vehículo.

En este artículo, se presentan las técnicas y métodos de análisis experimentales de comportamiento vibroacústico e impacto necesarios para caracterizar laminados. Los resultados obtenidos de la caracterización permitirán obtener las leyes de comportamiento de los composites y los modelos de material que posteriormente se implementen en las simulaciones vibratorias y a impacto.

1. INTRODUCCIÓN

Según datos del proyecto *ALM* (Automotive Lightweighting Materials), el empleo de materiales composites de fibra de carbono en la construcción de vehículos permitiría reducir su peso en un porcentaje comprendido entre 25-70%. El empleo de composites también permite diseñar estructuras que disipen una gran cantidad de energía y además de manera controlada, para no comprometer la seguridad de los ocupantes.

Por otra parte, el control de las vibraciones estructurales permite alargar la vida de los componentes y aumentar el confort. Existen diferentes metodologías para introducir amortiguamiento y controlar las vibraciones estructurales (Ewins et al. (2001), y Martínez et al. (2007)), destacando el empleo de composites reforzados con fibra debido a su rigidez y resistencia específicas, y a su capacidad de amortiguamiento.

Por ello, el reto de la optimización del diseño estructural tiende hacia el desarrollo de materiales compuestos de mayor rigidez y ligereza, y una mayor capacidad interna de amortiguamiento y absorción. Las herramientas de simulación numérica permiten predecir estos comportamientos sin necesidad de realizar ensayos sobre prototipos. Sin embargo, la obtención de un resultado satisfactorio está condicionada a una adecuada caracterización de los materiales que permitan poner a punto los modelos numéricos.

A continuación se presenta la caracterización experimental vibroacústica de composites con fibra de carbono (GG200P) y matriz de pCBT. Por una parte se aborda la caracterización vibroacústica, y por otra, se propone un protocolo de caracterización a impacto del material analizado para su empleo en simulaciones numéricas mediante el método de elementos finitos.

2. COMPORTAMIENTO VIBROACÚSTICO

Los materiales compuestos de matriz polimérica reforzada con fibra exhiben un comportamiento viscoelástico y pueden disipar energía bajo una carga periódica (Yin-Tao *et al.* 2001). Estos materiales ante un estado de carga armónico, presentan un comportamiento que se puede representar mediante el modelo de amortiguamiento estructural:

$$\sigma(t) = E^{*}\varepsilon(t) = (E' + \mathrm{i}E'')\varepsilon(t) = E(1 + \mathrm{i}\eta)\varepsilon(t)\,, \tag{1}$$

donde E^{*} es el módulo complejo, $E' = E$ es el módulo elástico, E'' es el módulo de pérdida y η es el factor de pérdida definido por el cociente entre E'' y E'

La capacidad de amortiguamiento del composite, η, depende de diversos factores relacionados tanto con la carga como con el material (Ewins et al. 2001 y Gibson 1976). Teniendo en cuenta la dependencia del módulo complejo con la frecuencia se obtiene,

$$E^{*}(\omega) = E'(\omega) + \mathrm{i}E''(\omega) = E(\omega)(1 + \mathrm{i}\eta(\omega))\,. \tag{2}$$

En este trabajo se ha caracterizado el material en frecuencia a temperatura ambiente (22 ± 1ºC) y dentro del rango de la viscoelasticidad lineal mediante ensayos dinámicos.

Estructuras analizadas

Se ha analizado el comportamiento dinámico a flexión de vigas empotradas-libres de sección rectangular. Se han analizado cinco materiales: pCBT sin fibra; con 34% en volumen de fibra en laminados $[0/90]_{10s}$ y $[45/\text{-}45]_{10s}$, y laminados $[0/90]_{8s}$ y $[45/\text{-}45]_{8s}$ con un 45% en volumen de fibra. En la Tabla **1** se detallan las propiedades geométricas y la densidad de los diferentes materiales analizados.

	PCBT	CFC34% 0-90	CFC34% ± 45	CFC45% 0-90	CFC45% ± 45
b (± 0.05 mm)	10.00	10.00	10.00	10.00	10.00
H (± 0.005 mm)	3.150	1.885	1.864	3.050	3.132
ρ (± 5 kg/m^3)	1324	1397	1414	1433	1320

Tabla 1. Datos geométricos y densidad de las probetas, donde *b* es la anchura, *H* el espesor y ρ la densidad del conjunto.

Técnica experimental

El módulo complejo se ha caracterizado según la norma ASTM E 756 – 05 (2009). Se han ensayado cinco probetas de cada material, con diferentes longitudes libres.. De las funciones de transmisibilidad cruzada medidas en la viga composite empotrada-libre, se deduce el módulo de almacenamiento E . El factor de pérdida η, se obtiene aplicando el método HPB (*Half Power Bandwidth*). La excitación empleada en este trabajo ha sido de tipo sísmico en el empotramiento (Cortés *et al.* 2008).

En la Figura 1 se muestra el módulo elástico y el factor de pérdida en función de la frecuencia para los cinco materiales analizados.

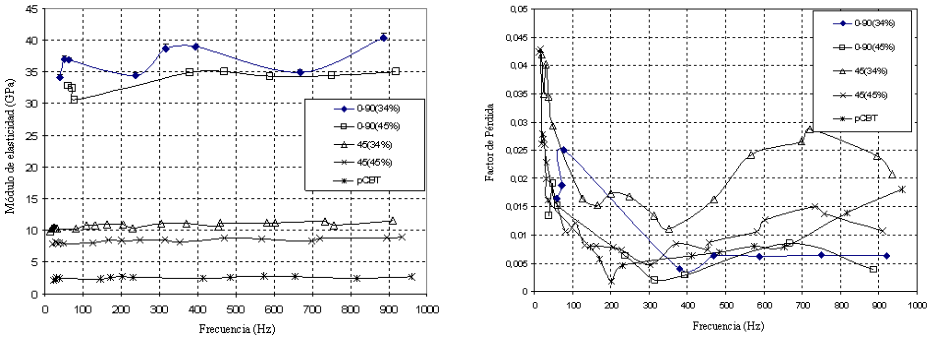

Fig. 1. Módulo elástico (GPa) y factor de pérdida de los compuestos.

El módulo elástico de los materiales analizados se mantiene prácticamente constante en la banda de 0 Hz a 1kHz, siendo más sensible a esta variable los compuestos con fibra a ±45. Así mismo, la rigidez es máxima con un 45% de fibra orientada a ±45. El factor de pérdida máximo se da a bajas frecuencias, entre 100 Hz y 400 Hz decrece, y se incrementa de nuevo a altas frecuencias. Se observa que el compuesto con mayor amortiguamiento es el de la fibra orientada a ±45 con la menor concentración de fibra.

3. COMPORTAMIENTO A IMPACTO

Los composites suelen considerarse como elástico lineales a la hora de simular su comportamiento estructural. Esto puede resultar correcto cargas estáticas y pequeñas deformaciones. Sin embargo, cuando se trata de simular el comportamiento a impacto, las diferencias entre los resultados numéricos y experimentales puede ser importantes. En la figura 2 se muestra la correlación numérico-experimental de la curva fuerza-tiempo para un ensayo de impacto por caída de dardo, llevado a cabo con un proyectil semiesférico de diámetro 12,7 mm, masa 1,803 kg y velocidad de impacto 1 m/s.

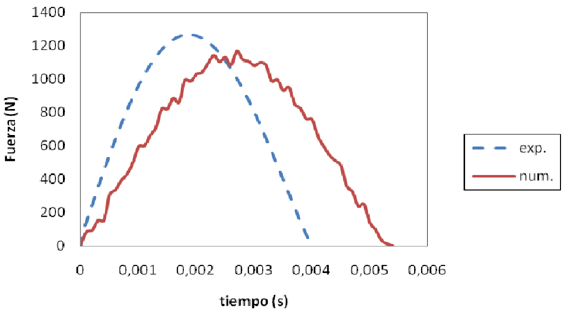

Fig. 2. Correlación numérico-experimental.

En la simulación, el material se ha modelizado con elementos placa y como un laminado de 10 capas de material ortótropo elástico lineal, de módulo 14,7 GPa obtenido en condiciones cuasi-estáticas. Se observa que ambas curvas presentan un valor máximo similar, aunque la pendiente inicial es notablemente inferior en la numérica. Esto puede asociarse a la variación de propiedades del material con la velocidad de deformación

(Zukas et al. 1992). Como resultado preliminar, se ha obtenido el módulo de elasticidad a flexión a partir del ensayo de impacto por caída de dardo (Martínez et al. 2006), obteniéndose un valor de 23 GPa (56% mayor que el módulo cuasi-estático). Por tanto, resulta necesario caracterizar el material a diferentes velocidades de deformación. Para ello, se propone el empleo de una máquina de tracción servo-hidráulica para velocidades medias, e impacto-tracción instrumentado para velocidades (Aretxabaleta et al. 2005).

4. CONCLUSIONES

Se ha determinado el comportamiento dinámico de compuestos con fibra de carbono con volúmenes y orientaciones de fibra diferentes, en función de la frecuencia. Se ha observado que el módulo elástico se mantiene constante en la banda analizada, aunque el amortiguamiento aumenta con la frecuencia. En cuanto al comportamiento frente a impacto, se ha comprobado que en condiciones de impacto la rigidez del material aumenta considerablemente, destacándose la necesidad de caracterizar el material a esas velocidades de deformación .A partir de la caracterización será posible simular el comportamiento vibroacústico y de impacto de estructuras composites.

AGRADECIMIENTOS

Este trabajo ha sido subvencionado por el Ministerio de Educación y Ciencia, PSE-370100-2007-1.

REFERENCIAS

ASTM E 756-05 (2009). Standard test method for measuring vibration-damping properties of materials. *American Society for Testing*.

CORTÉS, F., ELEJABARRIETA, M.J. (2007) Viscoelastic materials characterisation using the seismic response, *Materials and Design*, Vol. 28(7); 2054-2062.

EWINS, D.J., INMAN, D.J. (2001) *Structural Dynamics @ 2000: current status and future directions.* Philadelpia: Research Studies Press.

GIBSON, RF. (1976) Dynamic mechanical behaviour of fiber-reinford composites: measurement and analysis. *Journal Composite Material* Vol. 10, 325-41.

MARTINEZ, M., CORTÉS, F., ELEJABARRIETA, M.J. (2007), Experimental and numerical analysis of vibroacoustic attenuation in sandwich structures, *19th International Congress on Acoustics (ICA),* Madrid.

MARTINEZ, A..B., MASPOCH, M.Ll., SANTANA, O., NAVAS, J.A. (2006). Impacto de baja energía de poliésteres lineales. *IX Congreso Nacional de Materiales* –Vigo 06.

YIN-TAO, W., LIANG-JIN, G., TING-QING, Y. (2001) Prediction of the 3-D effective damping matrix and energy dissipation of viscoelastic fiber composites, *Composite Structures* Vol. 54, 49-55.

ZUKAS, J.A., NICHOLAS, T., SWIFT, H.F., GRESZCZUK, L.B., CURRAN, D.R. (1992) *Impact dynamics*, Krieger Publishing Company, Malabar, Florida (USA).

ARETXABALETA, L., AURREKOETXEA, J., URRUTIBEASCOA, I., SÁNCHEZ-SOTO, M. Characterization of the impact behaviour of polymer thermoplastics. *Polymer Testing*, 2005b, 24, 145-151.

T3. METAL-MATRIX COMPOSITES
MATERIALES COMPUESTOS DE MATRIZ METÁLICA

Influencia de recubrimientos Al-Si/SiCp en el comportamiento a la corrosión de la aleación AZ31 en 3,5% NaCl

A. Pardo[a], M.C. Merino[a], M. Mohedano[a], J. Rams[b], P. Casajús[a], R. Arrabal[a] , E. Matykina[c]
[a]Departamento de Ciencia de Materiales, Facultad de Química, Universidad Complutense, 28040, Madrid, España
[b]Departamento de Ciencia e Ingeniería de Materiales, ESCET, Universidad Rey Juan Carlos, 28933, Móstoles, Madrid, España
[c]Corrosion and Protection Centre, School of Materials, The University of Manchester, P.O. Box 88, Sackville Steet, Manchester, M60 1 QD, United Kingdom

RESUMEN

Se ha estudiado el comportamiento a la corrosión en 3,5% NaCl de la aleación Mg/Al AZ31 protegida con recubrimientos de materiales compuestos de matriz de Al-11Si reforzadas con partículas de SiC (SiCp). Así mismo, se ha estudiado la influencia de la proporción de refuerzo mediante medidas tanto gravimétricas como electroquímicas de corriente continua y alterna. La naturaleza de los productos de corrosión ha sido analizada mediante microscopía electrónica de barrido (MEB) y difracción de rayos X de incidencia rasante (DRX). Los recubrimientos efectuados por proyección térmica, con elevado grado de porosidad no aportan protección suficiente a la aleación AZ31, observándose corrosión galvánica del substrato. La aplicación de un proceso posterior de presión en frío mediante la aplicación de una tensión de 32 MPa favorece la consolidación de los recubrimientos mejorando significativamente su comportamiento a la corrosión y aumentando la dureza superficial de la aleación de Mg ensayada.

1. INTRODUCCIÓN

Las aleaciones de Mg presentan una buena combinación resistencia/peso y fácil mecanizado y reciclado. Sin embargo, su aplicación industrial como materiales estructurales presenta dos problemas básicos; baja resistencia al desgaste y a la corrosión (Pardo 2008). La proyección térmica es un método eficiente y flexible para la deposición de recubrimientos protectores y que está siendo ampliamente usado para la protección de materiales frente a la corrosión y desgaste (Pokhmurska 2008).

En el presente trabajo se avalúa la eficiencia frente a la corrosión de recubrimientos Al-11Si/SiCp y la posterior consolidación de los recubrimientos por aplicación de una presión en frío de 32 MPa.

2. PROCEDIMIENTO EXPERIMENTAL

Se utilizaron la aleación AZ31 (3,1Al; 0,73Zn; 0,25Mn; 0,002Si; 0,005Fe; bal. Mg) y Mg de pureza comercial (0,006Al; 0,0014Zn; 0,05Mn; 0,019Si; 0,001Cu; 0,004Fe; bal. Mg) como substratos, los cuales fueron chorreados con arena y recubiertos con Al-11Si/SiCp mediante proyección térmica con una pistola Castolin DS8000 con llama neutra de oxígeno-acetileno. La distancia y velocidad de proyección fueron de 20 cm y

300 m/s respectivamente, con una velocidad transversal de 150 cm/min. Se utilizó polvo de Al-11Si (99,5%- 75 μm) mezclado en un molino de bolas (225 rpm-30 min) con polvo de SiCp (99%-52 μm) con estructura α-SiC 6H. Se ensayaron tres recubrimientos con un contenido de SiCp de 5, 15 y 30 % en volumen y se evaluó el efecto de un post-tratamiento en frío consistente en la aplicación de una presión de 32 MPa durante 3 min. Se realizaron ensayos gravimétricos y electroquímicos en 3,5% NaCl a 25 ºC y pH inicial de 5,6. Se utilizó un potenciostato AUTOLAB PGSTAT 30 con montaje de tres electrodos, utilizando grafito como contraelectrodo y Ag/AgCl (3M KCl, 0,197 V vs. electrodo de hidrógeno) como electrodo de referencia. La superficie de ensayo se fijó en 0,28 cm^2. La naturaleza de los productos de corrosión fue estudiada mediante MEB y DRX de incidencia rasante. Se realizaron ensayos de dureza Vickers (AKASHI modelo AVK-AII) para evaluar la influencia de la modificación superficial en esta variable.

3. RESULTADOS Y DISCUSIÓN

3.1 Microestructura

Los recubrimientos Al-Si/SiC/30p por proyección térmica (PT) presentan un espesor de 500 ± 100 μm con un elevado grado de porosidad, rugosidad superficial y bajo grado de adherencia entre las partículas de Al-11Si y las partículas reforzantes SiCp. La intercara substrato/recubrimiento presenta irregularidades originadas durante el tratamiento de preparación superficial y zonas con bajo grado de adherencia (Fig. 1a,b). El post-tratamiento en frío (PT + PF) consolida el recubrimiento (360 ± 30 μm), reduciendo drásticamente la porosidad y mejorando el contacto en las intercaras Al-11Si/SiCp y substrato/recubrimiento (Fig. 1c,d). Los recubrimientos efectuados por proyección térmica, con elevado grado de porosidad, no mejoran sustancialmente la dureza de la aleación base (<40HV). Sin embargo, la consolidación de los recubrimientos y la adición de SiCp mejoran significativamente la dureza superficial tanto de la aleación AZ31 (entre 1,4 y 3 veces) como del Mg (entre 2 y 4,5 veces), lo que induce a pensar que los recubrimientos efectuados pueden mejorar la resistencia al desgaste de ambos materiales. (Recubrimientos PT + PF: AlSi/SiC/5p 90 HV, AlSi/SiC/15p 125 HV, AlSi/SiC/30p 195 HV).

3.2 Ensayos gravimétricos

La aleación AZ31 presenta una pérdida significativa de masa después de 10 días en 3,5% NaCl (-54 mg cm^{-2}) debido a un severo proceso de corrosión. Para los recubrimientos Al-11Si/SiCp PT con un elevado grado de porosidad, se observa un aumento de masa (120 mg cm^{-2}), que aumenta ligeramente con la adición de SiCp, asociada a la nucleación y crecimiento de una capa de productos de corrosión. Las muestras con recubrimientos Al-11Si/SiCp PT + PF presentan menor ganancia en masa (80 mg cm^{-2}) y por tanto un mejor comportamiento a la corrosión.

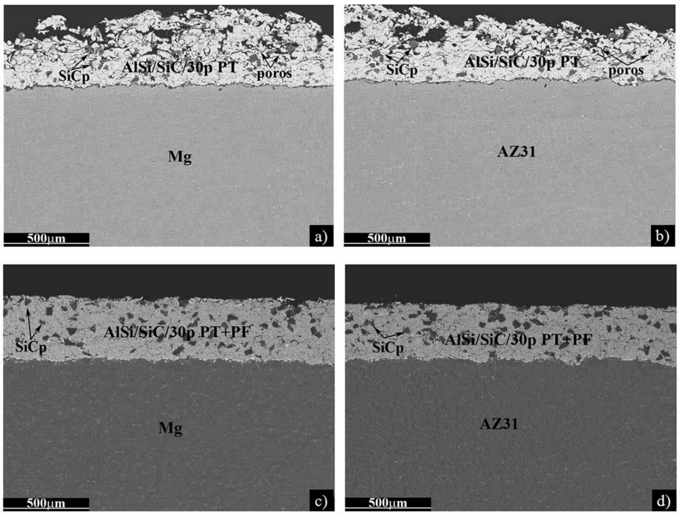

Fig. 1. Micrografías MEB del recubrimiento Al-Si/SiC/30p: a,b) PT y c,d) PT+PF.

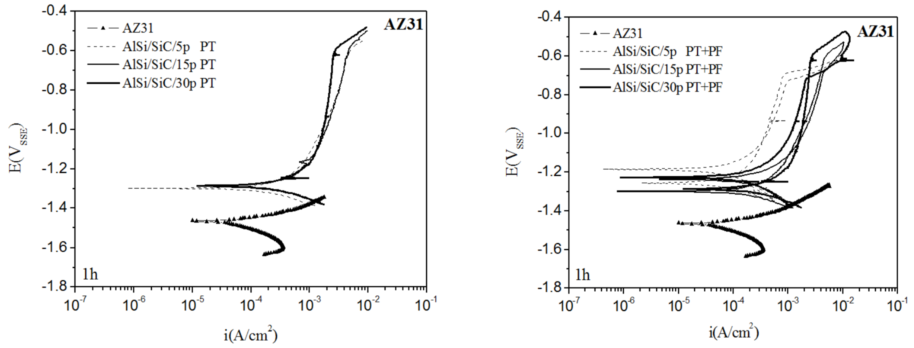

Fig. 2. Curvas de polarización después de 1 h de inmersión en 3,5% NaCl.

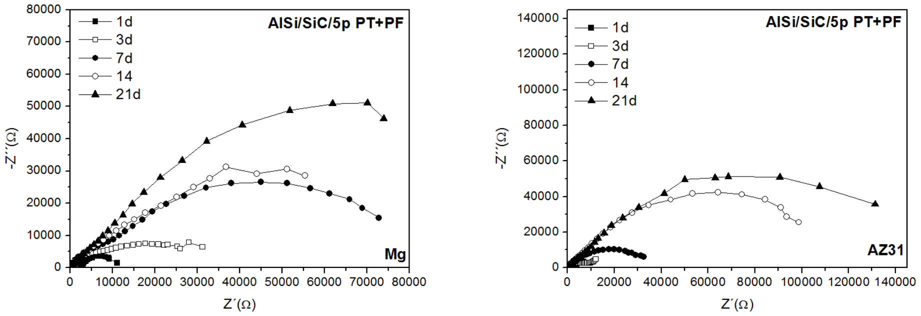

Fig. 3. Diagramas de Nyquist en función del tiempo de inmersión en 3,5% NaCl.

3.3 Ensayos electroquímicos

El valor de E_{corr} de los materiales de partida se localiza en -1,5 V. Para los recubrimientos Al-11Si/SiCp PT, E_{corr} se desplaza hasta -1,40 V y no se modifica demasiado la i_{corr}, mientras que para los recubrimientos con post-tratamiento, E_{corr} se sitúa en -1,0 V y la i_{corr} disminuye un orden de magnitud, apareciendo un intervalo de pasivación de 0,45/0,55 V con un potencial de picadura bien definido a -0,59/-0,65 V (Fig. 2). Los diagramas Nyquist muestran un arco capacitivo a altas y medias frecuencias cuyo diámetro se asocia con la resistencia a la transferencia de carga de la corrosión del metal (Fig. 3). La adición de 3.1% Al reduce la velocidad de corrosión del Mg, pero el nivel de corrosión sigue siendo elevado al igual que con los recubrimientos PT. Para los recubrimientos Al-Si/SiCp PT+PF, el diámetro del arco aumenta con el tiempo de inmersión, lo que sugiere formación de una película de productos de corrosión ligeramente protectora. El nivel de protección disminuye con el aumento de la proporción de refuerzo y el tiempo de inmersión en el medio de ensayo.

3.4 Caracterización de los productos de corrosión.

Se produce desprendimiento de los recubrimientos PT debido a la penetración de la disolución a través de los poros y corrosión galvánica del substrato con formación de $Mg(OH)_2$ de acuerdo con los análisis DRX. Los recubrimientos PT + PF muestran menor corrosión aunque son susceptibles de corrosión galvánica a tiempos largos, siendo necesaria una optimización del proceso de consolidación (Fig. 4).

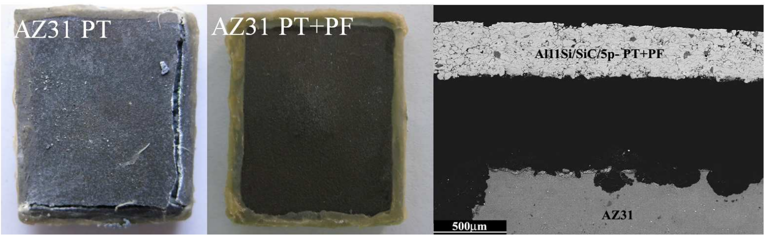

Fig. 4. Morfología de las muestras después de 10 días en 3,5% NaCl.

4. CONCLUSIONES

Los recubrimientos Al-Si/SiCp PT no aportan suficiente protección en 3,5% NaCl debido a su elevada porosidad que favorece fenómenos de corrosión galvánica de los substratos Mg y AZ31. La consolidación de los recubrimientos mediante presión en frío suministra un mayor grado de protección y mayor dureza superficial.

REFERENCIAS

PARDO, A., MERINO, M.C., COY, A.E., VIEJO, F. ARRABAL, R. y FELIÚ S.Jr. (2008). Influence of microstructure and composition on corrosion behaviour of Mg/Al alloys in chloride media. *Electroch. Acta. 53, 7890-7902.*

POKHMURSKA, H., WIELAGE, B., LAMPKE, T., GRUND, T., STUDENT, M., y CHERVINSKA, N. (2008). Post-treatment of thermal spray coatings on magnesium. *Sur. Coat. Technol. 202, 4515-4524.*

Agradecimientos

Los autores expresan su gratitud al MCYT (Proyecto MAT2006-13179-C02-01-02) y a la CAM. ESTRUMAT_CM (reference MAT/77) por la financiación de este trabajo.

Metal coated powders by the electroless plating method: application to advanced composite materials

J. Barcena, N. Markaide, S. Florez, R. Rodriguez, J. Coleto
INASMET-Tecnalia, Mikeletegi Pasealekua 2, E-2009 Donostia

ABSTRACT

In the present study, the electroless plating was used for the coating of reinforcements (particles and fibres) with a thin metal layer. This is of quite interest regarding metal matrix and polymer matrix composites. In the first case, the electroless technique has helped to design a proper metal/ceramic interface by the incorporation of a thin layer of metal (Ni, Co and Cu) on ceramic substrates at micrometric and nanometric level (carbon, silicon carbide). Moreover it allowed the incorporation of the metal matrix and a homogeneous distribution at high volume percent of ceramic reinforcements. In the second case, we have envisaged the enhancement of the electrical properties of polymer composites by the incorporation of metallised (copper) carbon nanotubes and nanofibers. Finally, this technique has been successfully used to deposit Cu and Ni on the shell of active polymeric microcapsules which embebbed in a polymeric matrix respond to external activation sources.

1. INTRODUCTION

Composite materials can be tailor made to provide a huge range of properties required in multiple applications. Densification and homogeneity are two of the most important driving issues to be accomplished in order to achieve the required properties. However, when using the conventional Powder Metallurgy route the interfacial bonding between the metal matrix and the reinforcement is weak, especially when insolubility or no wetting is present. (Daoush et al. 2008).

One smart way to overcome this problem is the coating of the reinforcement with metal layers. This allows placing the metal in the “right” place, being this deposited on the surface of the reinforcement. This metal layer can serve as an interfacial element (Valencia et al. 2007) of later the metal matrix after consolidation (Barcena et al. 2007).

The electroless plating method began with its discovery in the forties decade by chance (Brenner et al. 1946) and opened the door for another level of advanced materials due to its cost effectiveness. Nowadays is widely used in printed circuit industry and the automotive sector The electroless plating permits the deposition of metals from its ionic states in the solution by means of a chemical reducing agent rather than electrical current (Sharma et al. 2006). This, as a smart technique, allows placing metals on different substrates: ceramics, metals and polymers (Paunovic et al. 2000). In the case of non-metallic substrates a previous treatment is required in order to activate the surface and make the coating possible.

The main advantages of coated particles or fibres are the following:

- Better distribution of reinforcements (to avid the presence of agglomerates).
- Reduced fracture of reinforcement (due to a protective ductile matrix).
- Improved adhesion between the metal matrix and the reinforcement.
- Improved thermal/electrical contact between reinforcement and matrix.

- Higher packaging is possible (higher volume fraction).

2. EXPERIMENTAL

Prior to the coating process it is necessary to catalyse the surface of the substrate. The activation is carried out by adsorbing Sn and Pd ions on the substrate surface. Thus, the fibre is immersed in two catalysing baths composed by hydrochloric acid and Tin (sensitizing bath), followed by a bath containing hydrochloric acid and Palladium (activation bath). The distribution of the Pd nuclei has a major effect on the coating homogeneity. After catalysing, nanofibers are soaked into the coating solution, in which the red-ox reaction is carried-out.

The plating bath is generally composed of the five agents: Solvent (Water is commonly used), a metallic salt (as the source of the metallic ions), complexing agent (in order to improve the solubility of metal salt in the solution), the buffering agent (to control the pH of the plating solution) and the reducing agent (which reduces the metallic ions to metal on the substrate surface).

The electroless coating process has been carried-out in order to deposit Copper, Nickel and Cobalt. The details of the formulations are shown in

Table 1. It is of high importance to control the pH and the temperature of the plating bath. Each kind of plating bath possesses its optimal plating conditions.

Agents	**Copper**		**Nickel**		**Cobalt**	
	Products	Parameters	Products	Parameters	Products	Parameters
Metallic Salt	CuSO4	10 g/l	NiSO4▪6H2O	14 g/l	CoSO4▪7H2O	10 g/l
Complexing A.	Rochelle Salt	50 g/l	C6H5Na3O7	12 g/l	(NH4)3C5H	24 g/l
Buffering A	NaOH	10 g/l	NH3	10 ml/l	NH3	10 ml/l
Reducing A.	HCHO	15 ml/l	NaPH2O2H2O	10 g/l	NaPH2O2H2O	25 g/l
pH	12.5-13		9		9	
Temperature	25 ºC		35		35-80	

Table 1. Details of the selected electroless plating formulations.

3. RESULTS AND DISCUSSION

3.1. Nanometric materials

Different particles at nanometric level have been successfully coated with copper in view of a thermal management application. In this case the idea is to reduce the coefficient of thermal expansion of the metals matrix, while maintaining or even increasing the thermal conductivity. Carbon nanofibres (CNFs) and silicon carbide nanoparticles have been coated (see Fig. 1).

Furthermore, a thin layer of nickel and cobalt have been also place by the electroless technique in order to enhance the interfacial adhesion.

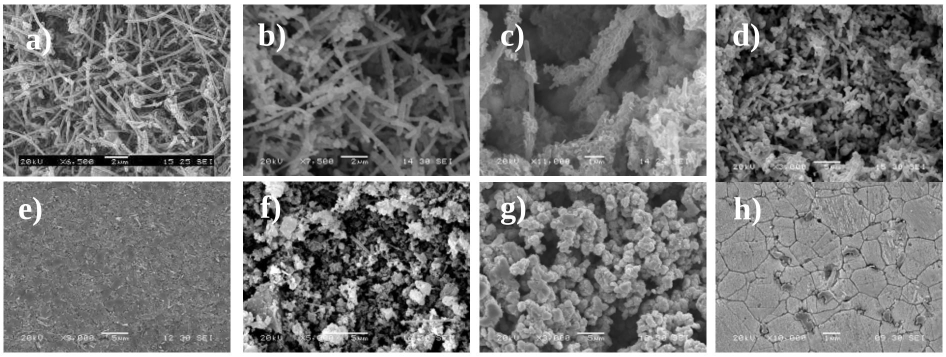

Fig. 1. Coating of nanoparticles: Carbon nanofibres (a-e) and silicon carbide (f-h). a) As received CNFs, b) Nickel plating, c) Cobalt Plating, d) Copper plating, e) Consolidated Cu/CNFs composite, f) As received SiC nanoparticles, g) Copper plating and h) Consolidated Cu/SiC composite.

The consolidation by hot pressing shows an excellent distribution of the nanoreinforcement in the copper matrix, even at very high volume fractions of reinforcements (up to 60 vol. %).

In addition, the copper coating of carbon nanotubes (CNTs) has been carried out and afterwards incorporated into an epoxy matrix in order to assess the enhancement of the electrical conductivity (see

Fig. **2**). The coating and the dispersion seemed to be homogeneous. A good adhesion of the coated CNT with the epoxy is observed.

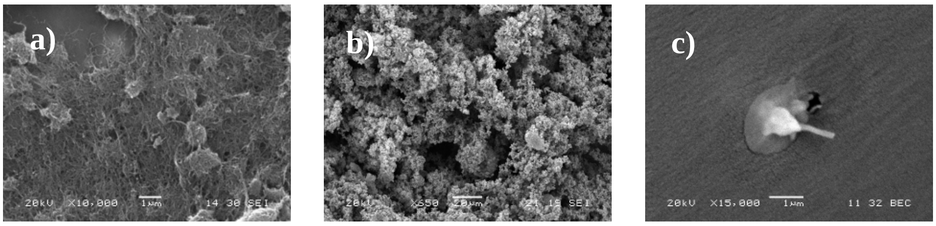

Fig. 2. Coating of CNTs: a) pristine CNTs, b) copper plating and c) incorporation into epoxy.

3.2. Micrometric Materials

The electroless technique has also been used for the coating of micrometric materials. The first envisaged system has been the Cu/Diamond composite material, aslo in view of a thermal management application.

Fig. **3**b shows the homogeneous copper coating placed on the surface of the diamond particles. This allows an excellent and adhesion of the particles in the copper matrix after the consolidation as seen in

Fig. **3**c.

Finally, this technique has been successfully used to deposit Cu and Ni (see

Fig. **3**e and f respectively on the surface of active polymeric microcapsules which embebbed in a polymeric matrix respond to external activation sources.

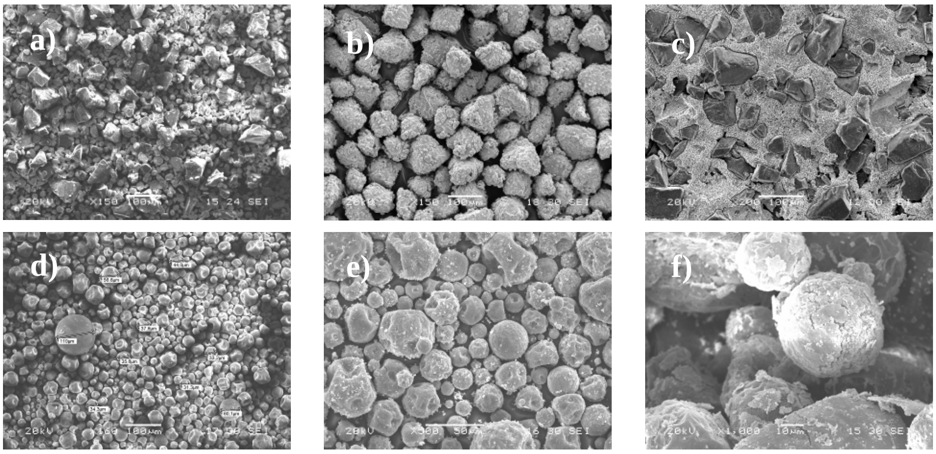

Fig. 3. Coating of micrometric particles: Cu/Diamond composites (a-c), Metal/Polymer capsules (d-f). a) As received diamond particles, b) Copper plating, c) Nickel plating, d) As received microcapsules, e) Copper plating and f) Nickel plating

4. CONCLUSIONS

A range of different metals (Cu, Ni, Co) have been successfully placed on the surface of different substrates (ceramics and polymers) by the electroless plating method. This has allowed the homogeneous deposition of a thin metal layer in order to obtain tailorable composite powders at the micrometric and nanometric level. Different applications have been envisaged for these materials, from the thermal and electrical conductivity enhancement in aerospace systems to active materials.

ACKNOWLEDMENTS

The authors would like to thank the Spanish Ministry of Science (Project Ref. TEC2005-07937-C02-02/MIC).

REFERENCES

BARCENA, J.; MAUDES, J., SARRIÉS, J.I., MARTÍNEZ, R., COLETO, J. (2007) Nuevos avances en la fabricación de composites cobre/nanofibras de carbono con altos volúmenes de refuerzo para aplicaciones de gestión térmica, en Actas de *MATCOMP'07*, Valladolid, Spain, 415-422.

BRENNER, A, RIDDELL G.E. (1946) Nickel plating on steel by chemical reduction. J *Res Natl Bur Stand*, 37, 32-34.

DAOUSH, W.M., MAOUSTAFA, S.F, (2008) Coated powders "a good base" for intermetallics. *Metal Powder Report*, December, 16-18**.**

PAUNOVIC, M. (2000) Electroless deposition of copper. in *Modern Electroplating*. (Ed. Mordechay, S., Paunovic, M.) John Willey and Sons, New York (USA).

SHARMA, R., AGARWALA, R.C., AGARWALA, V. (2006) Development of copper coatings on ceramic powder by electroless technqiue, *Applied Surface Science*, 252, 8487-8493.

VALENCIA, M.F., MARTINEZ, H.V., MORALES, A., DUQUE, A., CRUZ, L.J. (2007) Materiales compuestos Al-Si/β-SiC$_p$ procesados por compoforjado, en Actas de *MATCOMP'07*, Spain, 373-381.

Electrodeposición y caracterización de recubrimientos micro y nanocomposites de Ni/Al_2O_3

I. García-Urrutia, E. García-Lecina, M. Díaz-Fuentes, J.A. Díez
Departamento de Tratamiento de Superficies, CIDETEC, Pº Miramón 196, 20009 San Sebastián (España). igarcia@cidetec.es

RESUMEN

En este trabajo, se han generado por electrodeposición recubrimientos composite de Ni/Al_2O_3 empleando diferentes concentraciones en disolución de partículas de tamaño micro (1 µm) y de tamaño nano (50 nm), con el objetivo de analizar diferencias en su comportamiento. Previamente, se analizaron mediante métodos electroacústicos las suspensiones formadas por las partículas de Al_2O_3 en el electrolito de níquel con el fin de determinar el tamaño de partícula en el medio. Los recubrimientos micro y nanocomposite obtenidos fueron caracterizados en cuanto a composición (EDX) y morfología (SEM). Además, se evaluaron propiedades mecánicas como la dureza, observándose importantes cambios de comportamiento entre el empleo de partículas nano y de partículas micro.

1. INTRODUCCIÓN

La electrodeposición de composites consiste en la inclusión de partículas cerámicas, metálicas o poliméricas, de tamaño micrométrico o nanométrico, en una matriz metálica electrodepositada. Estos recubrimientos combinan sinérgicamente las propiedades de los dos materiales, de manera que se obtiene un recubrimiento con propiedades superiores a cada uno de sus componentes, mejorando propiedades como dureza, resistencia al desgaste, lubricación o resistencia a la corrosión (Hovestad et al. 1995). A la hora de definir un recubrimiento composite no sólo es importante la elección de la naturaleza de la matriz metálica y de las partículas, sino también el tamaño de estas últimas. La mayor parte de los estudios realizados en este campo, se han centrado en el empleo de partículas de tamaño micrométrico. Sin embargo, en los últimos años se ha producido un cambio importante tras la constatación de que la disminución del tamaño de partícula a nivel nano (entre 1 y 100 nm) permitía obtener materiales con propiedades mejoradas a las obtenidas previamente con partículas micrométricas, gracias a su reducido tamaño y a su elevada relación superficie-volumen (Low et al. 2006).
Por tanto, el objetivo del presente trabajo se ha centrado en el estudio del comportamiento de partículas de Al_2O_3 de tamaño micro y nanométrico, empleadas en la electrodeposición de recubrimientos composite de matriz de níquel. Las suspensiones formadas por las partículas de Al_2O_3 en el electrolito de níquel se analizaron mediante métodos electroacústicos con el fin de determinar el tamaño de partícula real en el medio. Asimismo, los recubrimientos micro y nanocomposite obtenidos fueron caracterizados en cuanto a contenido en partículas, morfología y dureza.

2. EXPERIMENTAL

Los recubrimientos composite de Ni/Al_2O_3 fueron generados por electrodeposición a partir de un electrolito de níquel Watts sin aditivos formado por 250 g L^{-1} de

$NiSO_4 \cdot 6H_2O$, 45 g L^{-1} de $NiCl_2 \cdot 6H_2O$ y 40 g L^{-1} de H_3BO_3, donde se añadieron las partículas de Al_2O_3 en concentraciones entre 25 y 100 g L^{-1}. Se emplearon dos tipos de partículas, α-Al_2O_3 (Alfa Aesar) de tamaño medio 1μm y γ-Al_2O_3 (Sigma-Aldrich) de tamaño medio <50 nm.

Para la electrodeposición se empleó una celda de 200 mL de capacidad. El pH de la disolución fue de 4, y la temperatura se mantuvo a 55ºC mediante un controlador automático. Los recubrimientos fueron depositados sobre un cátodo de acero de bajo contenido en carbono de 3 cm^2. Como ánodo se empleó una lámina de níquel puro. Las partículas de alúmina se añadieron al electrolito de níquel Watts, manteniéndolas en suspensión mediante agitación magnética durante 24 horas antes de realizar la electrodeposición. El proceso de electrodeposición se llevó a cabo a una densidad de corriente constante de 5.0 A dm^{-2}, manteniendo la agitación magnética en la celda. Después de la electrolisis, las muestras se limpiaron en etanol con ultrasonidos para eliminar las partículas adsorbidas sobre la superficie.

El potencial Z y la distribución de tamaño de partícula en el electrolito fueron determinados empleando métodos electroacústicos (DT1200, dispersión Technology) (Dukhin et al. 2002). La morfología de la superficie y de los recubrimientos en sección fue analizada mediante microscopia electrónica de barrido (SEM). El porcentaje en peso de Al_2O_3 incorporado en el recubrimiento se determinó empleando un microanalizador de energía dispersiva de rayos-X (EDX) acoplado al SEM. Para determinar la dureza de los recubrimientos composite de Ni/Al_2O_3 se utilizó un microdurómetro Fischerscope H100 con una carga de 30 mN.

3. RESULTADOS Y DISCUSIÓN

3.1. Caracterización de las suspensiones

El potencial Z y la distribución de tamaño de partícula en el electrolito fueron determinados empleando métodos electroacústicos. Esta técnica permite realizar medidas sobre suspensiones concentradas con elevada fuerza iónica, lo que permitió llevar a cabo mediciones en condiciones reales de trabajo. Los resultados obtenidos mostraron que el potencial Z se desplaza hacia valores más cercanos a cero al aumentar la concentración de partículas en el electrolito. Por otro lado, se observó que el tamaño de partícula en el medio se mantenía para la alúmina de tamaño micrométrico, mientras que para la alúmina nano se observaban aglomeraciones (el tamaño de partícula obtenido en el medio era mayor que el medido a partir de las partículas en polvo).

3.2. Electrodeposición de micro y nanocomposites de Ni/Al_2O_3

Con el fin de analizar el efecto tanto del tamaño como de la concentración de partículas en el electrolito sobre el contenido de partículas en el depósito, se generaron recubrimientos con los dos tipos de alúmina a diferentes concentraciones. En la figura 1 se puede observar que en los dos casos se produce un aumento de la cantidad de partículas incorporadas en el depósito al aumentar la concentración de partículas en el baño, siendo este aumento más acusado para las partículas micro. Además, se puede observar que para la misma concentración de partículas en el electrolito, hay una mayor incorporación de partículas micro que nano al depósito.

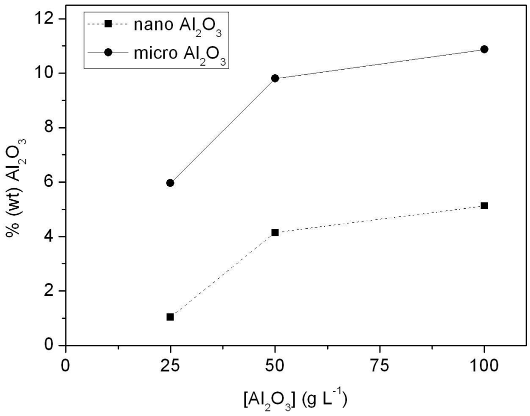

Fig. 1. Efecto de la concentración de Al_2O_3 en el electrolito sobre el porcentaje en peso de Al_2O_3 en el depósito, para partículas micro y nanométricas.

3.3. Caracterización de los recubrimientos de Ni/Al_2O_3

3.3.1. Morfología

La morfología de los recubrimientos micro y nanocomposite fue analizada por SEM.

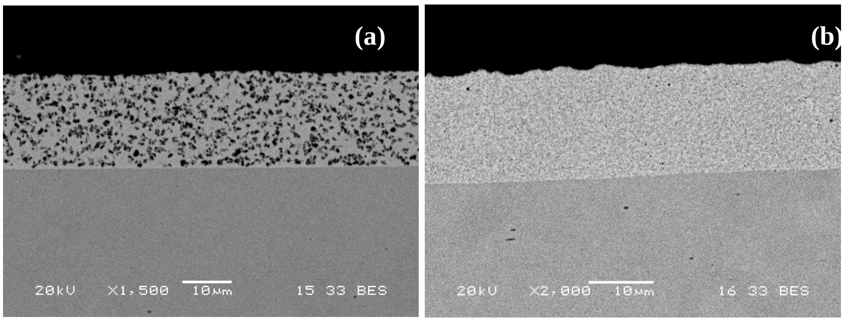

Fig. 2. Imagen SEM en sección de los recubrimientos micro(a) y nanocomposite (b) de Ni/Al_2O_3.

El análisis en sección de las capas (Figura 2) nos permite observar que los recubrimientos son compactos, homogéneos y con buena adherencia con el material base. Las partículas de Al_2O_3 están codepositadas uniformemente en la matriz de níquel. En el caso del micro, el tamaño de partícula en el recubrimiento se mantiene alrededor de 1 μm, mientras que en el nano se observan algunas aglomeraciones.

3.3.2. Dureza

En la figura 3 se puede observar que para un mismo tipo de partícula hay un aumento de la dureza al aumentar el porcentaje de alúmina en el depósito. Esta dureza es en todos los casos superior a la de un recubrimiento de níquel puro (≈250 HV), lo que nos indica que la introducción de partículas de Al_2O_3 mejora dicha propiedad. Además, se puede observar que el efecto de las partículas nano sobre la dureza es mayor que en las micro, ya que con porcentajes inferiores de partículas en el recubrimiento se obtienen durezas considerablemente superiores.

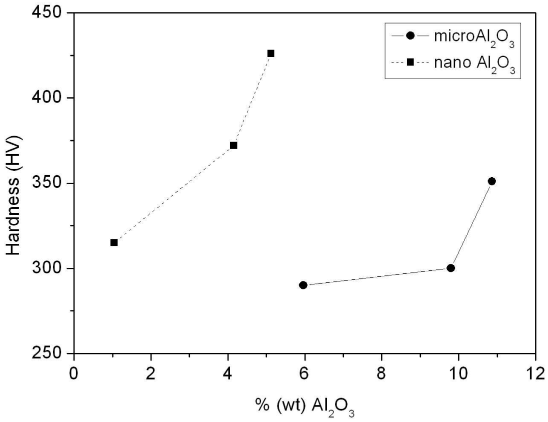

Fig. 3. Durezas de los recubrimientos composite de Ni/Al_2O_3 en función del tamaño de partícula y del porcentaje de alúmina incluida en el depósito.

4. CONCLUSIONES

En este trabajo, se ha comprobado que un aumento de la cantidad de partículas en el electrolito provoca un aumento en el porcentaje de partículas en el depósito. Además, se ha podido constatar que, a pesar de obtenerse menores porcentajes de partículas al emplear partículas nano, propiedades como la dureza se mejoran considerablemente.

REFERENCIAS

DUKHIN, A.S., GOETZ, P.J. (2002) Ultrasound for Characterizing Colloids, Elsevier Science B.V., Amsterdam.

HOVESTAD, A., JANSSEN, L.J.J. (1995) Electrochemical codeposition of inert particles in a metallic matrix, *en Journal of Applied Electrochemistry*, 25, 519-527.

LOW C.T.J., WILLS, R.G.A., WALSH F.C. (2006) Electrodeposition of composite coatings containing nanoparticles in a metal deposit, *en Surface & Coating Technology*, 201, 371-383.

Properties of Al-20vol.%TiB_2 composites manufactured by underwater shock consolidation

H. Eskandari
Department of Mechanical Engineering, Persian Gulf University, Bushehr, Iran
H.M. Ghasemi
Department of Metallurgy and Materials Engineering, University of Tehran, P.O. Box 11365-4563, Tehran, Iran
K. Hokamoto
Shock Wave and Condensed Matter Research Center, Kumamoto University, Kurokami, Kumamoto 860-8555, Japan

SUMMARY

Aluminum matrix composites containing 20vol%TiB_2 particles were manufactured by underwater shock consolidation method. Underwater shock consolidation is a one-stage densification process, which involves a very rapid and intense deposition of shock energy on powder particle surfaces. Microstructure of recovered compacts were examined by optical microscope. Density, hardness and bending strength of the compacts were measured before and after sintering treatment. SEM fractography examination was used for analysis of fracture surfaces of the compact. The sintered composite samples showed better improvement in the bending strength and deflection.

1. INTRODUCTION

Aluminium metal matrix composites are being considered as a group of new advanced materials for its light weight, high strength, high specific modulus, low coefficient of thermal expansion and good wear resistance properties. Combination of these properties are not available in a conventional material (Surappa et.al. 1981, Zhao et.al. 2004, Odonnel et.al. 2001, Lioyd et.al. 1994). Shock consolidation such as underwater explosive compaction is a process which shows characteristics that differentiate it from the traditional powder metallurgy. These characteristics are: partial or total elimination of sintering operation, the ability to compact alloys or powder mixtures that in conventional techniques would undergo chemical reaction during sintering, and the treatment of amorphous powders without degradation of original microstructure. Underwater shock consolidation is a one-stage densification process, which involves a very rapid and intense deposition of shock energy on powder particle surfaces. Shock synthesis of the aluminum and aluminum alloy matrix system (by axisymmetric and underwater methods) and studies of the effects of process parameters and micro structural variations with respect to the processing conditions have been investigated by some researchers(Hokamoto et.al. 1997, Sivakumar et. al, a,b,c, 1996, 2000, 2001). Some of the results have indicated that subsequent mechanical working or heat treatment is required to improve the mechanical properties of the composites. In the present investigation an attempt has been made to manufacture Al reinforced with 20vol% TiB_2 particulates using one dimensional underwater shock consolidation. The effect of sintering on mechanical properties has been studied.

2. MATERIALS AND EXPERIMENTAL PROCEDURES

The Al powder used for this research was commercially atomized pure aluminum (99%). The particles were spherically shaped with a mean size of about 45 μm. Pure TiB_2 powder (>99%) with a mean size of about 15 μm was used as reinforcing material. The experiments were conducted in experimental set up for underwater explosive compaction, which was described previously by Hokamoto et al.(1997). The powders were mixed for 90 minutes in a conventional ball mill and then they were mechanically packed into a mild steel container having 30 mm inner diameter and 22.5 mm wall thickness. The prepared powders were found to be almost 0.6 of the theoretical density. Aluminum powder was used in the bottom of the container to act as a shock absorber. A SEP explosive produced by Asahi-kasei Corporation was employed (Detonation velocity = 7000 m/s and Density = 1.3 g/cm^3). The height of water column was 5 mm. The underwater shock pressure applied on the powders was estimated as 12.5 GPa through numerical simulation (Itoh et. al. 1994) Explosively compacted specimens were studied by optical microscopy. The average micro-Vickers hardness was calculated for ten measurements on each sample under a load of 300g in as-compacted and also in sintered conditions. Sintering operation carried out in an electric furnace under controlled argon atmosphere at 400 ^{0}C for 70 minutes. The bending samples prepared from center region of the compact specimens. The density of the compacts after explosive compaction has been measured by Archimedes method. Observations of the composite microstructure were carried out using optical microscopy and also scanning electron microscopy. Crystallographic structures of the interfacial reaction products were identified using X-ray diffraction (XRD) with CuK_α radiation.

3. RESULTS AND DISCUSSION

Table 1 shows the variation of hardness, bending strength, deflection and density in the as-compacted and sintered specimens. It can be seen that the sintering decreases the hardness of the samples due to softening effect of the Al-matrix. The variations in hardness were almost uniform from center to periphery and top to down in each specimens. Fig. 1(a) shows SEM micrographs of the distribution of TiB_2 particles within the Al-20vol.%TiB_2 composite. compacts produced by underwater explosive compaction. No significant variations were observed in the microstructure across the cross section of the Al matrix completely different from the microstructures of the

No	**Properties**	**Al-20vol.%TiB_2 composite compact conditions**	
		As-Compacted	**After Sintering**
1	**Bending strength (MPa)**	**334**	**363**
2	**Deflection (mm)**	**0.2**	**0.9**
3	**(VHN_{300gr})**	**75**	**66**
4	**Density (%TD)**	**98.7**	**99.8**

Table 1. Experimental data.

composites produced by axisymmetric geometry (Eskandari et.al. 2004). This uniformity in the microstructure could be due to the applied uniform shock pressure on the surface of the powders across the cross section. The variation of shock pressure through the water column are negligible resulting in uniform microstructure along top to bottom of the sample. SEM studies conducted on the bending fracture surface of the as-compacted and Sintered composite are shown in Fig. 1(b,c). The fractured face of the as-compacted sample shows a crack generated by decohesion at the interface between Al matrix and TiB_2 particle, Fig. 1(b), while fracture surface of the sintered composite showed no debonding at the interface Fig. 1(c). The well-bonded interface facilitates the efficient transfer and distribution of load from the matrix to the reinforcing phase, which leads to Improvment in composite strengths. Therefore, a strengthened interfacial bond between Al/Al and Al/TiB_2 is predicted to be responsible for the improvement in bending strength and deflection of the Al-20vol%TiB_2 composite compact after a partial sintering operation. The x-ray diffraction pattern for the sintered composite is shown in Fig. 2. As seen in the graph, the X-ray profile shows only aluminum and TiB_2 diffraction peaks and no evidence for the presence of interfacial reaction prouducts could be seen in the sintered composite. Due to the extremely short processing time in the underwater

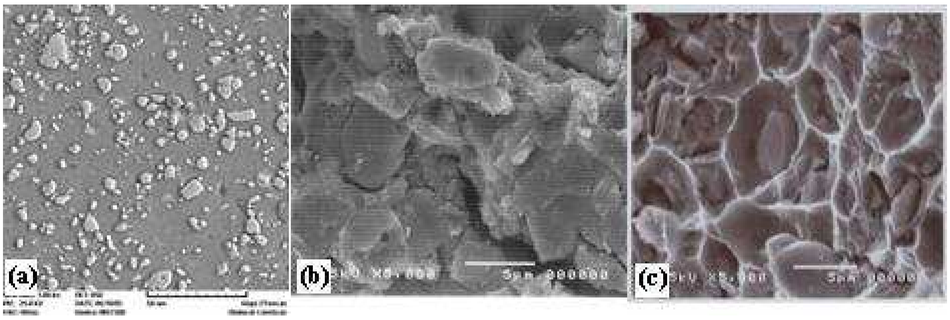

Fig. 1. SEM microstructure of the Al-20vol%TiB_2 composite compacts produced by underwater explosive compaction (a), and bending fracture surfaces for (b) As-compactedand, (c) After partial sintering.

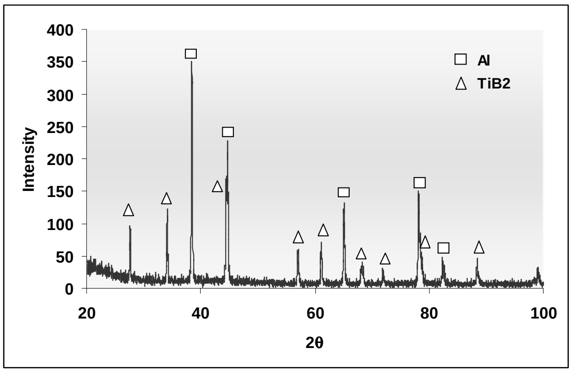

Fig. 2. XRD spectra of sintered Al-20vol%TiB_2 composite

explosive compaction, the reaction between the aluminum matrix and the TiB_2 particles could be inhibited and interfacial reaction products such as Al_3Ti at the interface may not be detected.

3. CONCLUSIONS

Al-20vol.%TiB_2 composite compacts successfully manufactured by underwater explosive compaction method. The results showed that the density of the composite compact increased by partial sintering treatment. The bending strength and bending deflection of the composite increased after partial sintering. X-ray diffraction pattern showed only diffraction peaks observed are from the Al matrix and the TiB_2 particles.

REFERENCES

ESKANDARI, H., GHASEMI, H. M., EMAMY, M. (2004). Microstructure and interface studies of Al/SiC_p composites produced by dynamic compaction, Mater. Sci. Forum, 465-466, 213-219

ESKANDARI, H., HOKAMOTO, K. (2004). Comparative Study of Al/SiC_p composites manufactured by Direct and Underwater Explosive Compaction Mater. Sci. Forum, 465-466(2004), p. 433.

HOKAMOTO, K., RAGHUKANDAN, LEE, J. S., FUJITA, M., TOMOSHIGE, M., (2003). Mater. Sci. Forum. 437-438, 169-173

HOKAMOTO, K., FUJITA, M. (1997). Shock-wave research on condensed matter at High Energy Rate Laboratory of Kumamoto University-An introduction Physica B: Condensed Matter. 239, 187-190

HOKAMOTO, K., TANAKA, S., ITOH, S., MEYERS, M. A., CHEN, H. C. (1997). High temperature shock consolidation of hard ceramic powders, *Physica B: Condensed Matter, 239, Issues 1-2, 1-5*

ITOH, S., KUBOTA, S., KIRA, A., FUJITA, M. (1994). J. Japan Explosives Soc., 55, 71-75

LIOYD, D. J. (1994). Particle reinforced aluminium matrix composite, Intern. Mater. Reviews., 39, 1-23

ODONNELL, G., LOONY, L. (2001). Production of aluminum matrix composites using conventional PM technology, Material Science and Engineering A303, 292-301

SIVAKUMAR, K, BALAKRISHNA, T. (1996). Dynamic consolidation of Al and Al-20vol.%SiC_p composite powders., J. Mater. Processing Technol., 62 , 191-198

SIVAKUMAR, K. SOLOMAN RAJ, P. HOKAMOTO, (2000). J. Mater. Sci., 35, 5823-5827

SIVAKUMAR, K. SOLOMAN RAJ, P. HOKAMOTO, K. (2001). Studies on shock consolidation 2124 Al-40vol.%SiC_p composite, J. Mater. Process. Technol., 396-401

SURAPPA, M.K., ROHATGI, R. K. (1981). Preparation and properties of cast aluminium–ceramic particle composites, J. Mater. Sci. 16, 983–993.

ZHAO M.N., (2004). TiB_{2p} /Al composite fabricated by squeeze casting technology, Materials science and engineering A 374, 303-306

Influencia de la distribución de partículas de refuerzo en el endurecimiento por deformación del material compuesto AA6061/$MoSi_2$/15p

J. Corrochano, J. Ibáñez, M. Lieblich,
Centro Nacional de Investigaciones Metalúrgicas, CENIM-CSIC, Madrid
P. Barkoczy
Institut of Materials Science, University of Miskolc, 3515, Miskolc, Hungary
J.M. Badía
Departamento de Materiales y Producción Aeroespacial. Escuela Técnica Superior de Ingenieros Aeronáuticos, UPM, Madrid

RESUMEN

Es bien conocido que la distribución espacial de las partículas de refuerzo juega un importante papel en las propiedades mecánicas de los materiales compuestos de matriz metálica. No obstante, apenas existen trabajos que correlacionen dicha distribución con las propiedades mecánicas de manera cuantitativa. En el presente estudio se realiza esta correlación para seis materiales compuestos de matriz aleación de aluminio 6061 reforzados con 15 % en volumen de partículas de $MoSi_2$ con diferentes tamaños y distribuciones del refuerzo. La cuantificación de la homogeneidad de la distribución se hace a través del coeficiente de variación de la media de las distancias a los primeros vecinos, COV_λ. Las propiedades mecánicas se obtuvieron de ensayos de tracción a temperatura ambiente, sobre muestras en estado solubilizado. Se observó que los valores del COV_λ son proporcionales a los del exponente del endurecimiento por deformación para aquellos materiales con tamaño de partículas parecido.

1. INTRODUCCIÓN

En general los materiales compuestos (MC) de matriz metálica reforzados con partículas tienen mayores valores de resistencia mecánica y módulo elástico que la matriz correspondiente, aunque una menor ductilidad. Las características geométricas de las partículas tienen gran importancia en las propiedades mecánicas de los materiales compuestos. En relación a la distribución de las partículas, y a falta de definiciones precisas de términos como homogeneidad, aglomeración y azar, está demostrado en diversos trabajos (Corbin et al. 1994, Segurado et al. 2003, Gammage et al. 2004, Zhang et al. 2008) que distribuciones heterogéneas dan lugar a bajas propiedades mecánicas. En estos y otros estudios se utilizan diversos criterios a la hora de cuantificar el grado de aglomeración de las partículas. Uno de los más útiles es el coeficiente de variación de la media de la distancia entre próximos vecinos, $COV_\lambda=\sigma_d/\lambda_m$, siendo σ_d la desviación estándar en la distancia media de los próximos vecinos, y λ_m el valor medio de la distancia media de los próximos vecinos para todas las partículas (Yang et al. 2001). Este parámetro es esencialmente independiente de la forma, tamaño, orientación y fracción de volumen de las partículas, pero muy sensible a la inhomogeneidad de la distribución. Varía entre 0 y 1, de manera que los valores cercanos a 1 corresponden a las distribuciones menos homogéneas, y toma el valor de 0,36 para una distribución al azar. El objetivo de este trabajo es estudiar la posible correlación entre COV_λ y las propiedades mecánicas a tracción de seis materiales compuestos AA6061/$MoSi_2$/15p.

2. EXPERIMENTAL

Se fabricaron seis materiales compuestos por vía pulvimetalúrgica. Como matriz se usó polvo de la aleación de aluminio 6061, con tamaño medio de partículas de 50 μm, que se mezclaron con 15% en volumen de polvo de $MoSi_2$ utilizando diferentes métodos: cubo de rotación, molino planetario de bolas durante 4 y 10 horas, y mezcla húmeda. Se usaron dos tamaños iniciales de partículas de $MoSi_2$: < 3 μm y 10-45 μm. Una vez mezclados, los polvos se consolidaron por extrusión en caliente en una prensa horizontal a 450ºC a 0,3 mm/s de velocidad y relación de extrusión de 27:1. Como material de referencia se preparó, con el mismo procesado, la aleación 6061 monolítica (MM). En la tabla 1 se muestra el código, los métodos de mezcla y los tamaños de partícula de $MoSi_2$ antes y después de la mezcla, de todos los materiales procesados. Justo antes de la realización de los ensayos mecánicos, los materiales consolidados se solubilizaron a 520ºC durante 30 minutos, seguido de enfriamiento en agua. Los ensayos de tracción se llevaron a cabo sobre probetas cilíndricas de 3 mm de diámetro y 20 mm de longitud útil a temperatura ambiente con una velocidad de deformación de $5x10^{-4}$ s^{-1}.

Material	D_{ri} μm	D_{rf} μm	Método de Mezcla	Código
AA6061			Recepción	0AR
AA6061			Molino 4 h	0M(4h)
AA6061			Molino 10h	0M(10h)
AA6061/MoSi2 Grupo 1	<3	1,36	Húmeda	1W
AA6061/MoSi2 Grupo 1	<3	0,58	Molino 4 h	1M(4h)
AA6061/MoSi2 Grupo 1	<3	0,35	Molino 10h	1M(10h)
AA6061/MoSi2 Grupo 2	10-45	17,01	Cubo de rotación	2C
AA6061/MoSi2 Grupo 2	10-45	1,38	Molino 4 h	2M(4h)
AA6061/MoSi2 Grupo 2	10-45	0,59	Molino 10h	2M(10h)

Tabla 1. Materiales, tamaño inicial (D_{ri}) y final (D_{rf}) de las partículas de $MoSi_2$, métodos de mezcla y código.

3. RESULTADOS Y DISCUSIÓN

En la tabla 2 se muestran los valores numéricos del exponente de la deformación, N en la ecuación de Hollomon, $\sigma_r=K\varepsilon_r^N$, extraídos a partir de las pendientes de la función $\log\sigma_r$-$\log\varepsilon_r$. Dicha función no es una recta, habiéndose calculado la pendiente en dos tramos, uno en las proximidades del límite elástico (Ni) y otro para deformaciones más altas, pero diferente según se trate de los MC (N_{MC} con $0.01<\varepsilon_r<0.04$) o de los MM (N_{MM} con $0.01<\varepsilon_r<0.08$). En dicha tabla se aprecia que el comportamiento del exponente de la deformación es muy diferente entre los materiales reforzados y sin reforzar. Para pequeñas deformaciones el endurecimiento por deformación de los MC es muy superior al de los MM, excepto para el material 2C. Para deformaciones superiores al 1% la tendencia se invierte, con $N_{MC}<N_{MM}$, efecto observado por Varma et al. (2001).

Código	λ_m µm	COV$_\lambda$	N_i 0,1-0,3%	N_{MM} 1-8%	N_{MC} 1-4%	ε_f %	ε_u %
0AR			0,040	0,281		24,0	15,9
0M(4h)			0,048	0,215		14,5	10,7
0M(10h)			0,046	0,179		11,0	8,7
1W	1,97	0,56	0,115		0,173	7,2	6,9
1M(4h)	0,96	0,51	0,136		0,149	7,7	6,5
1M(10h)	0,83	0,41	0,083		0,096	9,6	5,8
2C	19,99	0,41	0,038		0,160	8,4	7,4
2M(4h)	1,47	0,46	0,116		0,125	10,3	7,5
2M(10h)	0,98	0,41	0,091		0,094	9,4	5,4

Tabla 2. Parámetros λ_m y COV$_\lambda$ de la distribución de partículas, exponentes de la deformación N_i, N_{MM}, y N_{MC}, y alargamientos a fractura, ε_f y uniforme, ε_u.

El efecto de las partículas de $MoSi_2$ sobre el endurecimiento por deformación depende de su tamaño, distancia interparticular, distribución, fracción de volumen y factor de forma, y puede ser analizado en términos del movimiento de las dislocaciones y por la presencia de tensiones internas. Las marañas de dislocaciones que se encuentran en torno a las partículas generadas por incompatibilidad plástica con la matriz, debido a diferencias en el coeficiente de expansión térmica, evolucionan con la deformación para formar celdas, cuyo tamaño está asociado a la distancia interparticular, λ. Por debajo de una λ crítica, en torno a 1µm (Gammage et al 2004) se desarrolla un estado de tensiones triaxial elevado que conduce al aumento de N a pequeñas deformaciones. Por tanto, N_i será mayor en los MC que en los MM. Asociado a λ, se halla el tamaño de las partículas de refuerzo, que influye en el inicio y evolución del daño por fractura y por nucleación y crecimiento de microcavidades. Cuanto mayor es el tamaño de una partícula, o menor es λ para una fracción de volumen fija, el daño se inicia para deformaciones menores, de modo que la resistencia mecánica, crece con $1/\lambda$. Está demostrado, tanto en trabajos teóricos (Corbin 1996, Segurado et al 2003, Gammage 2004) como experimentales (Zhang 2007), que el grado de aglomeración de las partículas influye en el endurecimiento, de manera que a mayor aglomeración mayor es el endurecimiento por un aumento de la concentración de tensiones en las partículas aglomeradas.

En nuestro caso, la fracción de volumen es fija y el factor de forma es similar por lo que las variables serían λ_m y COV$_{\lambda m}$. En la fig. 1a se representa N_{MC} en función de $1/\lambda_m$, y en la 1b en función del COV$_{\lambda m}$. Se aprecia que COV$_{\lambda m}$ presenta mejor correlación que $1/\lambda_m$, pues agrupa en una sola recta a todos los MC excepto el 2C. En este material, al tener partículas de refuerzo con λ muy superior al valor crítico, la densidad inicial de dislocaciones sería menor que en los otros MC, lo que unido a que son más propicias a sufrir daño en las primeras etapas de la deformación, darían lugar a un N_i menor.

La razón de esta mejor correlación podría residir en que COV$_{\lambda m}$ tiene en cuenta el grado de aglomeración. Por tanto, la comparación de estas dos gráficas pone de manifiesto la importancia que tiene distribución de las partículas de refuerzo en el endurecimiento. El hecho de que en la fig.1b el material 2C se aparte del ajuste en la recta podría interpretarse como que los mecanismos que operan en su deformación plástica son diferentes a los del resto de los MC. Esta interpretación vendría avalada por tener además un N_i sensiblemente inferior a los demás MC.

Una característica importante de la figura 1b es que se muestra por primera vez en forma cuantitativa que el grado de aglomeración (clustering) medido a partir del $COV_{\lambda m}$ es proporcional al exponente de la deformación para tamaños de partícula en torno a 1µm.

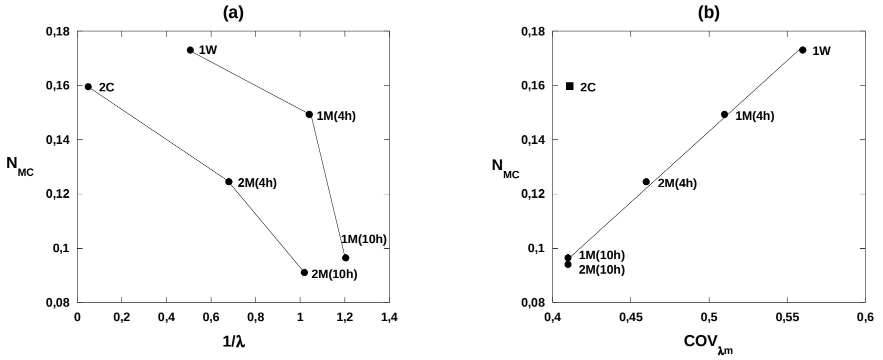

Fig. 1. Variación del exponente de la deformación del material compuesto para deformaciones superiores al 1%, N_{MC}, con $1/\lambda_m$ (a) y con el $COV_{\lambda m}$ (b).

4. CONCLUSIONES

.- Para un análisis correcto del proceso de deformación de los MC resulta fundamental estudiar las primeras etapas de la deformación plástica, incluso antes del $\sigma_{0,2}$.

.- En los MC con tamaño de partícula de refuerzo del orden de 1 µm, conforme aumenta la homogeneidad de la distribución (o sea, conforme disminuye $COV_{\lambda m}$) disminuye el exponente de la deformación para ε>1% según la ecuación $N_{MC} = 0,12 + 0,52$ COV.

AGRADECIMIENTOS

Se agradece la financiación del proyecto CICYT MAT2006-01251.

REFERENCIAS

CORBIN SF, WILKINSON DS (1994) The influence of particle distribution on the mechanical response of a particulate metal matrix composite. *Acta Metall* 42 1311-1318.

GAMMAGE J, WILKINSON D, BRECHET Y, EMBURY D (2004) A model for damage coalescence in heterogeneous multi-phase materials, *Acta Mater*, 52, 5255–5263

SEGURADO J, GONZÁLEZ C, LLORCA J (2003) A numerical investigation of the effect of particle clustering on the mechanical properties of composites, *Acta Mater.* 51, 2355-2369.

VARMA VK, KAMAT SV, MAHAJAN YR, KUTUMBARAO VV (2001), Effect of reinforcement size on low strain yielding behaviour in Al–Cu–Mg/SiC_P composite, *Mater Sci Eng* A318, 57-64

YANG N, BOSELLI J, SINCLAIR I. (2001) Simulation and quantitative assessment of homogeneous and inhomogeneous particle distributions in particulate metal matrix composites. *J. of Microscopy*, 201(2), 189-200.

ZHANG D, SUGIO K, SAKAI K, FUKUSHIMA H, YANAGISAWA O (2008) Effect of volume fraction on the flow behavior of Al-SiC composites considering the spatial distribution of delaminated particles, *Mater Trans*, 49, 661-670.

Residual stress and microstructural characterization of friction stir welded metal matrix composite

S. Ferreira-Barragáns, R. Fernández, G. González-Doncel
Dpto. de Metalurgia Física, Centro Nacional de Investigaciones Metalúrgicas CENIM, C.S.I.C., Av. de Gregorio del Amo 8, 28040 Madrid, Spain
D. Gesto, P. Rey
AIMEN Centro Tecnológico, C/ Relva 27A, Porriño, 36410 Pontevedra, Spain

SUMMARY

The microstructure and the mechanical properties of a joint conducted by friction stir welding, FSW, in 2124Al-25vol%SiCp composite has been investigated. For comparison FSW made in un-reinforced 2024Al alloy has been also studied. Special attention was paid to the characterization of the residual stress, RS, state by synchrotron x-ray radiation diffraction. The welds were conducted in a T6 condition. FSW leads to a fine microstructure in the nugget region and to over-ageing in the heat affected zone. The typical "M" profile of the RS through the welds is obtained. This stress is higher and more isotropic in the composite than in the alloy.

1. INTRODUCTION

Metal matrix composites, MMCs, with discontinuous reinforcement are well known because they improve several properties of the un-reinforced alloys, such as the elastic modulus and yield stress, creep resistance, or wear properties (Christman *et al.* 1989). Furthermore, these improvements involve a very little increase in weight, which make these composites very attractive structural materials in the transportation sector (Rohatgi 1991). A massive use of these composites with the accompanying reduction in vehicles weight would imply a substantial diminution in fuel consumption and to a reduction in green house effects emissions. However, their use is still limited to very specific applications. This is surprising considering the immediate environmental benefits. This limitation is mainly due to the fact that processes such as machining, forging or welding, are not yet fully implemented in these materials. A lot of effort is, therefore, needed to overcome this problem.

This study is framed in an ongoing research oriented to improve the mechanical performance of joints in MMCs obtained by FSW. To achieve this objective, it is necessary, among other factors, to know the magnitude and distribution of the residual stress, RS, generated during welding. This stress influences the "quality" of the resulting unions and, hence, their mechanical performance (James et al. 2007). In this research, the RS state resulting from FSW conducted in 2124Al-25%SiCp composite and 2024Al alloy is presented.

2. MATERIALS AND EXPERIMENTAL PROCEDURE

2124Al-25vol%SiCp composite (AMC225xe) obtained by a powder metallurgical route (AMC, UK) and 2024Al (Alustock) in the form of plates of 15 mm in thickness were used. It was not possible to obtain 2124Al alloy plate of this thickness. The pieces to be joined were first heat treated to a T6 or fully hardened condition. This consists on a solution treatment at 530ºC during 2h followed by quenching in oil bath at 20ºC and subsequent annealing at 160ºC during 18h for the composite and 20h for the alloy.

2.1 Description of the FSW process

After the T6 treatment, butt joints were conducted in two passes, on both sides of the plates, without any previous surface preparation. The FSW tool had a fixed threaded pin of truncated cone geometry and three grind flats at 120º. The tool was fabricated from H13 (Q&T, 49 HRc) material except for the pin, which was fabricated from multiphase MP159 alloy. The welding conditions are summarized in Table 1.

Material	Rotation speed (rpm)*	Welding speed (mm/min)	Force (kN)**
2024Al-T6	**400**	**100**	**23**
2124Al-25vol%SiCp-T6	**300**	**75**	**8.5**

* CCW (counter-clock wise). ** Position control.

Table 1: Parameters employed in the FSW process.

2.2 Microstructural and mechanical characterization

The microstructure was studied by optical and scanning microscopy on samples prepared by conventional metallographical procedures. Vickers hardness tests, HV5, were made on an EMCOTEST M10 010 hardness testing machine. Hardness maps of the welds were obtained by indenting on different positions along several lines, such that a grid of 5x5 mm^2 in size was completed.

2.3 Determination of the residual stress in the welds

Near surface RS values across the welds (first pass) have been obtained by synchrotron radiation diffraction in energy dispersive mode (in reflection) in the range of 10-150 keV, at EDDI line of BESSY, Berlin, Germany. This mode allows obtaining many diffraction peaks simultaneously. Here, only the results from the 311 reflection will be presented. This peak presents a low plastic anisotropy and, hence, the relationship between the lattice parameter and the stress is approximately linear. The analysis of the remaining peaks is being the subject of an ongoing study. The Bragg's angle was $\theta = 4º$. The primary slit was of 1x1 mm^2 and the secondary one was of 1x0.03 mm^2 (gage volume: 1x1x0.03 mm^3). Both the longitudinal, σ_L (along the welding), and transverse, σ_L (across the welding), components of the RS were determined from the strains assuming a biaxial stress state (σ_N = 0, sub-index N indicates normal direction to the sample surface).

$$\sigma_{L,T} = \frac{E}{1+\upsilon}\left(\varepsilon_{L,T} + \frac{\upsilon}{1-2\upsilon}\varepsilon_{T,L}\right) \tag{1}$$

where ε_L y ε_T are the strains along the longitudinal and transverse directions, respectively, E is the Young's modulus, and ν is the Poisson's ratio. The sen$^2\Psi$ method, where Ψ is the angle between the scattering vector and the sample axis direction, was employed for this purpose.

The un-stressed lattice parameter, d_0,, was measured on comb type of samples to take into account the possible microstructural and chemical changes introduced by the FSW process (Pratihar *et al*. 2006).

3. RESULTS AND DISCUSSION

Macrographs of the resulting welds (cross section) are shown in fig. 1. Welding "quality" is better in the alloy than in the composite. The welding in the composite is not as good as expected due to the presence of tunnel defects (fig. 1b). This suggests that the welding parameters are more critical in the composite than in the alloy and that these parameters must be optimized. The grains size in both cases in clearly reduced. Hardness is higher in the composite (~170 HV) than in the alloy (~110 HV), and in both materials hardness decreases in the welding region due to over-ageing associated to heating produced by the FSW process.

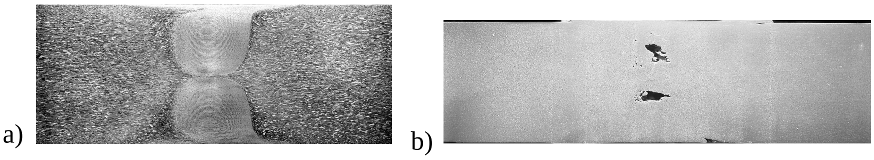

Fig. 1. Macrographs of the FSW samples. a) 2024Al Alloy, b) 2124Al-25vol%SiCp composite.

The variation of d_0 is summarized in fig. 2. This variation indicates structural changes introduced by the FSW process: These are more pronounced in the composite than in the alloy. It is also seen that d_0 is, in average, higher in the composite. This result points out the strong dependency of this parameter on the alloying elements.

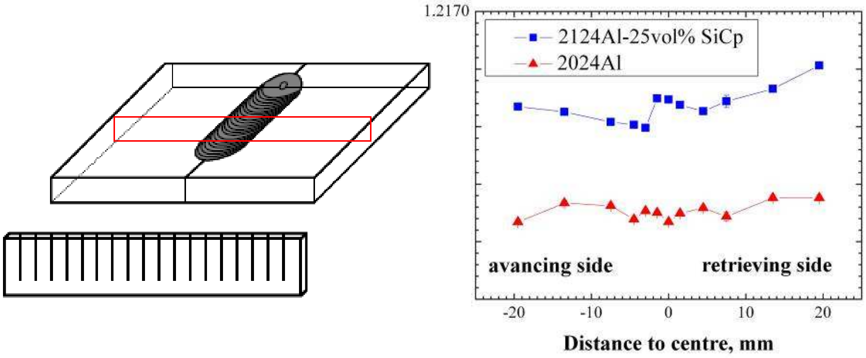

Fig. 2. Typical "comb" sample used to measure the un-stressed lattice parameter, d_0. Variation of d_0, across the weld, in the alloy and the composite.

The results of the RS analysis are shown in fig. 3. It is seen the typical "M" variation of the RS across the welds (Mishra *et al*. 2005). The RS state is more isotropic in the composite than in the alloy. In the latter one, the longitudinal component is clearly higher than the transverse one. The RS gradient is also higher in the composite than in the alloy. The isotropic character of the stress in the composite could be attributed to the tunnel defects arising during the FSW process. In turn, these defects could be a consequence of the high stress level achieved during FSW, associated to the microscopic RS state in the composite. This stress is due to the presence of the ceramic reinforcing particles in this material. The imperfections in the composite may have released partially the RS in this material.

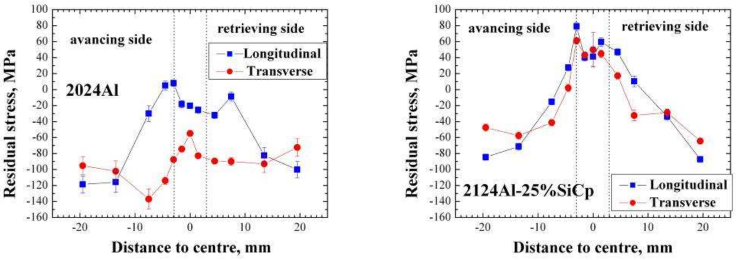

Fig. 3 Residual stress profiles resulting from the FSW process in the alloy and the composite.

4. CONCLUSIONS

1. The weld quality is better in the alloy than in the composite due to the presence of tunnel defects in the latter one. This result reveals the present difficulty of joining plates from metal matrix composites of several mm in thickness by FSW.
2. Variations of d_0 across the welds reveals structural changes during the FSW process.
3. The RS follows the typical "M" profile. This stress is higher and more isotropic in the composite than in the alloy. The RS gradient is also higher in the composite, possibly due to the additional contribution of a microscopic RS associated to the presence of the ceramic particles.

ACKNOWLEDGEMENTS

Projects MAT-05-0527 and PTR95-1007-OP from MICINN (Ministerio de Ciencia e Innovación), Spain, and contract nº RII 3CT-2004-506008 from BESSY, Germany.

REFERENCES

CHRISTMAN T., NEEDLEMAN A., SURESH S. (1989) An experimental and numerical study of deformation in metal-ceramic composites, *Acta Metall.*, 37, 3029-3050.

ROHATGI P. (1991) Cast aluminum-matrix composites for automotive applications, *JOM*, 43, 10-15.

JAMES M.N., HUGES D.J., CHEN Z., LOMBARD H., HATTINGH D.G., ASQUITH D., YATES J.R., WEBSTER P.J. (2007) Residual stresses and fatigue performance, *Engineering Failure Analysis* 14, 384-395.

PRATIHAR S., STELMUSKH V., HUTCHINGS M.T, FITZPATRICK M.E., STUHR U., EDWARDS L. (2006) Measurement of the residual stress field in MIG-welded Al-2024 and Al-7150 aluminium alloy compact tension specimens, *Materials Science and Engineering A* 437, 46-53.

MISHRA R.S., Ma Z.Y. (2005) Friction stir welding and processing, *Materials Science and Engineering R* 50, 1-78.

Microstructure strengthening analysis of hybrid metal matrix composites

A. Riaz Ahamed
Department of Aeronautical Engineering, Park College of Engineering and Technology,
Coimbatore 641 659. Tamil Nadu, India
P. Asokan
Department of Production Engineering, National Institute of Technology
Trichy 620 015. Tamil Nadu, India
S. Aravindan
Department of Mechanical Engineering, Indian Institute of Technology
New Delhi 110 016. India

SUMMARY

Hybrid metal matrix composites with SiC and B_4C particles dispersed in aluminum matrix, prepared by stir casting were tested for their yield strength. It is understood that the strength of the composite increased with the addition of discontinuous reinforcements. The increase in strength is due to an increase in dislocation density and a reduction of the subgrain size. A microstructural strengthening analysis was carried out to predict the yield strength. The results were compared with experimental values.

1. INTRODUCTION

Microstructural effects arising out of the presence of particles modify the *in situ* behaviour of the matrix and the composite. Various dislocation strengthening mechanisms contribute to the increase in yield stress of the composite. The generation of dislocations is due to a difference in thermal coefficient of expansion between the matrix and the reinforcement (ΔCTE) according to Wang, L., Shi, N., Arsenault, R.J. (1991). T. W. Clyne, T. W., Withers P. J. (1993) and Kainer, K. U. (2006) have separately discussed various micromechanical models to enunciate the influence of induced dislocations, grain size and strain hardening on the strength of the composite. Hideki Sekine, Rong Chen (1994) reported on a microstructural strengthening analysis with low strength aluminium matrix. Hybrid composites having two or more particulate reinforcement types can be manufactured by conventional metal methods. The objective of the present work is to apply the models to predict the yield strength of Al-5vol%-SiC-5vol%B_4C composites.

2. RESULTS AND DISCUSSION

Samples of the hybrid composites were prepared by stir casting route as done by Zhou, W., Xu, Z.M. (1997) and Riaz Ahamed, A., Asokan, P., Aravindan, S. (2008). Figure 1 shows the microstructure of sample. Table 1 shows properties of the matrix and reinforcements.

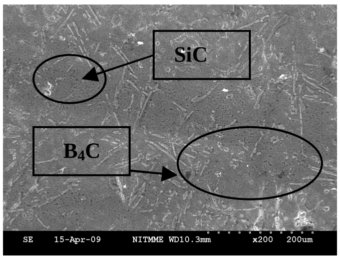

Figure 1. SEM Micrograph of Al-SiC$_p$-B$_4$C$_p$ composite.

Table 1. Some properties of the constituents of the Al-SiCp-B4Cp composite.

Mtl.	**Particle Dia (µm)**	**Young's Mod (GPa)**	**Shear Mod (GPa)**	**Poisson's ratio**	**Coeff. of therm. expn (x 10^{-6} C^{-1})**	**Burgers vector (nm)**
SiC$_p$	10	427	-	0.17	4.3	-
B$_4$C	70	445	-	-	5.0	-
Al	-	69.85	26.2	0.33	23.2	0.282

2.1 Yield strength of the composite

The modified shear lag model which is suitable for small aspect ratio particles predicts yield stress as

$$\sigma_{cy} = \sigma_{my}[V_f(\frac{S+2}{2}) + V_m] \tag{1}$$

where σ_{cy} and σ_{my} are the composite and matrix yield strengths respectively, V_f and V_m denote fibre and matrix volume fractions respectively and S the mean aspect ratio.

2.2 Strengthening by silicon carbide and boron carbide particles

The influence of ceramic particles can be described by

$$\sigma_{cy} = \Delta\sigma_{dis} + \Delta\sigma_{gb1} + \Delta\sigma_{gb2} + \Delta\sigma_{wh1} + \Delta\sigma_{wh2} \tag{2}$$

where $\Delta\sigma_{dis}$ is the incremental increase in yield strength due to geometrically necessary dislocations, $\Delta\sigma_{gb1}$ is the incremental increase due to smaller grain size resulting from recrystallization during thermomechanical treatment of the composite, $\Delta\sigma_{gb2}$ is the incremental increase due to the changes in subgrain size as in a relaxation process, $\Delta\sigma_{wh1}$ is the incremental increase due to strain hardening and $\Delta\sigma_{wh2}$ is the increment of the average principal stress at the particle surface.

The effect of dislocations $\Delta\sigma_{dis}$ is given by

$$\Delta\sigma_{dis} = \alpha.G.b.\rho^{\frac{1}{2}} \tag{3}$$

where G is the shear modulus of the matrix material, α is the dislocation strengthening efficiency and ρ is the dislocation density.

$$\rho = 12\frac{\Delta C \Delta T V_f}{bd} \tag{4}$$

where ΔC is the difference in thermal expansion coefficients between the matrix and the reinforcements, ΔT is the temperature difference, V_f is the volume fraction of the reinforcement, b is the Burger's vector and d the particle size. The dislocation strengthening efficiency α is taken as 1.4. Since two reinforcements are present the incremental increase due to both the reinforcing phases are superposed linearly as

$$\Delta\sigma_{dis} = \sqrt{{}^{1}\Delta\sigma_{dis}^{2} + {}^{2}\Delta\sigma_{dis}^{2}} \qquad (5)$$

The effect of recrystallization on grain size $\Delta\sigma_{gb1}$ is estimated from the Hall-Petch equation as

$$\Delta_{gb1} = k_{Y1} D^{\frac{-1}{2}} \qquad (6)$$

where $\Delta\sigma_{gb1}$ is the yield strength contribution from changes in grain size during recrystallization during thermomechanical treatment. As a result, the grain size in the matrix becomes smaller than that in the reinforcement. k_{Y1} is a constant and is equal to 0.1 $MNm^{-3/2}$. The yield strength of a matrix with smaller grain size is larger than that with larger grain size. The grain size D is given by the following relation

$$D = d\,[(\frac{1 - V_f}{V_f})]^{1/3} \qquad (7)$$

where D is the resultant grain size and d the particle size. The combined effect is taken. The effect of relaxation on the grain size $\Delta\sigma_{gb2}$ is given by

$$\Delta_{gb2} = k_{Y2} D_s^{\frac{-1}{2}} \qquad (8)$$

where $\Delta\sigma_{gb2}$ is the yield strength contribution due to changes in subgrain size as during relaxation process, k_{Y2} is a constant equal to 0.05 $MNm^{-3/2}$, D_s is the resulting grain size

$$D_s = d\left(\frac{\pi d^2}{6V_f}\right)^{\frac{1}{2}} \qquad (9)$$

where d is the particle size.

The strain hardening contribution $\Delta\sigma_{wh1}$ is given by

$$\Delta\sigma_{wh1} = KG\left(V_f b / d\right)^{\frac{1}{2}} \varepsilon^{\frac{1}{2}} \qquad (10)$$

where K is a constant and ε is the tensile strain. The value of K is taken as 0.4 and the tensile strain ε is taken to be the matrix strain, 0.002. The density of secondary dislocation rises steeply with the increase of strain, and acts as a forest to impede the movement of the primary glide dislocations.

$$\Delta\sigma_{wh2} = \frac{2G(1-\nu)}{(1-2\nu)} V_f \varepsilon \qquad (11)$$

where ν is the Poisson's ratio

3. Microstructure strengthening

The yield strength of the matrix may be equal to that of the original matrix plus the increments of the matrix yield strength due to microstructure strengthening mechanisms

$$\sigma_{my}^{*} = \sigma_{my} + \Delta\sigma_{dis} + \Delta\sigma_{gb1} + \Delta\sigma_{gb2} + \Delta\sigma_{wh1} + \Delta\sigma_{wh2} \qquad (12)$$

Substituting equation (12) in (1) gives the yield strength as

$$\sigma_{cy} = \sigma *_{my}[V_f(\frac{S+2}{2}) + V_m]$$

(13)

The result of the combined microstructure strengthening analysis is compared with the experimental results. Table 2 shows the results.

Table 2 Experimental and predicted results of the hybrid composite

Property	**Values MPa**	**Property**	**Values MPa**
Al. alloy YS	35	Subgrain strengthening	20.7
Al-SiCp-B4Cp comp. YS	81.4	Subgrain strengthening	0.026
Stren by SiC & B4C particles	73.6	Secy. dislo. strengthening	0.59
Ther. expn. dislo. strengthening	6.95	Geom. neces. dislocation	10.33

4. CONCLUSIONS

Theoretical strength analysis based on the modified shear lag theory and other strengthening mechanisms were applied to predict the yield stress of aluminum matrix composites. The difference in the yield stress values is due to factors such as voids, inclusions, non-uniform particle distribution and interfacial chemical reactions.

REFERENCES

CLYNE, T.W., WITHERS, P.J. (1991) Introduction to metal matrix composites, 84-86, Cambridge University Press, Cambridge.

HIDEKI SEKINE, RONG CHEN (1994) A combined microstructure strengthening analysis of SiC_p/Al metal matrix composites, *Composites*, 26, 183-188

KARL U. KAINER (2006) Basics of metal matrix composites, in *Metal Matrix Composites. Custom-made Materials for Automotive and Aerospace Engineering* (Ed. Karl U. Kainer), 20-23, Wiley-VCH Verlag GmbH & Co. KGaA, Weinheim.

RIAZ AHAMED, A., ASOKAN, P., ARAVINDAN,S. (2008) EDM of Hybrid Al-SiC_p-$B4C_p$ and Al-SiC_p-Glass metal matrix composites, *International Journal of Advanced Manufacturing Technology,* DOI: 10.1007/s00170-008-1839-0

WANG, L., SHI, N., ARSENAULT, R.J. (1991) The strengthening mechanisms of discontinuous metal matrix composites, in *Morris E. Fine Symposium* (Ed. Peter K. Liaw et al), 129, The Minerals, Metals & Materials Society

ZHOU, W., XU, Z.M. (1997) Casting of SiC reinforced metal matrix composites, *J Mater Process Technol,* 63, 358-363

Quantitative estimation of microstructure homogeneity of mechanical alloyed composite materials

P. Bryantsev, M. Samoshina, A. Aksenov
State Technological University «Moscow Institute of Steel and Alloys», Russia

SUMMARY

The most promising method of dispersion-strengthened composite materials obtaining is mechanical alloying. In dispersion-strengthened composite materials especially based on heterogeneous matrix it is important to achieve the homogeneous structure to support the isotropic mechanical properties. This is reaching by uniformly distribution of strengthening particles in composite matrix.

1. INTRODUCTION

Qualitative assessment of homogeneity of phase constituents in composite materials is probably by microstructure estimation (Fogagnolo J.B. et al. 2003). In our work the method of quantitative estimation of microstructure homogeneity of mechanical alloyed composite materials is suggested.

2. EXPERIMENTAL

Dispersion-strengthened materials obtained by mechanical alloying from commercial chips of aluminium alloys Al4Cu1.5Mg and Al12Si2Cu0.8Fe (Table 1). The chips used were free of moisture and grease. Powdered α-SiC (particle size, 10 μm) in the amount of 20 wt. % was used as strengthening particles. Mechanical alloying was carried out in a Gefest 11-3 planetary mill in sealed containers with quasi-cylindrical milling bodies in an argon atmosphere for 1–2 h. The ratio of the weight of the milling body to that of the mixture was 6:1.

№	Alloy	Chemical composition, wt. %				
		Si	Cu	Mg	Mn	Fe
1	Al12Si2Cu0.8Fe	12	2.2	0.2	0.3	0.8
2	Al4Cu1.5Mg	–	4.4	1.5	0.7	–

Table 1. Compositions of the initial aluminium alloys.

Granules of the composite materials (Al4Cu1.5Mg+Al12Si2Cu0.8Fe)–20% SiC were used to produce consolidated cylindrical specimens 15 mm in diameter and 10 mm in height by double-action compaction at a temperature of 400°C.

3. RESULTS AND DISCUSSION

Quantitative estimation of homogeneity of the most specific phase constituents' distribution subject to time of treatment in planetary mill was carrying out on consolidated specimens of composite material (Al4Cu1.5Mg+Al12Si2Cu0.8Fe) – 20 vol.% SiC. Assessment of degree of mechanical alloying completing realizes by redistribution of particles of S (Al_2CuMg) and θ ($CuAl_2$) phases presented mainly in matrix alloy Al4Cu1.5Mg. In addition the estimation of homogeneity of strengthened particles SiC distribution is carried out. The digital images of microstructure of consolidated specimens after every experimental milling time were counted by quantitative metallographic software ImagescopeM. In SEM image of composite material microstructure particles of S and θ phase looked white, SiC particles are looked dark-grey on light-grey background of aluminium solid solution (Fig. 1).

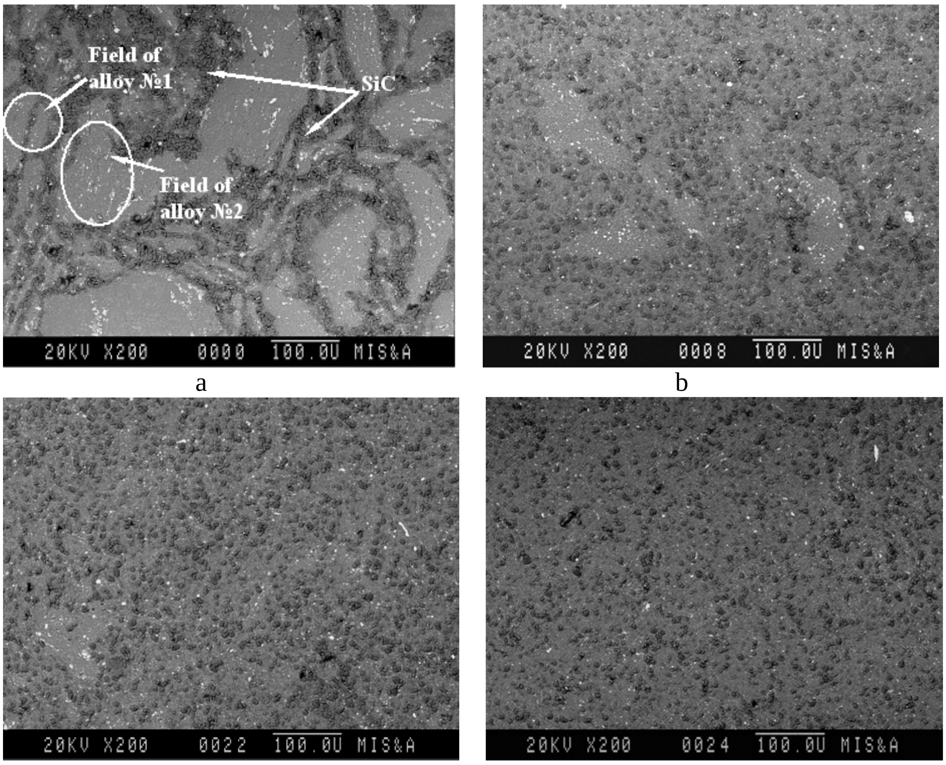

a b

c d

Fig. 1. Microstructure of consolidated specimens of composite material (Al4Cu1.5Mg+Al12Si2Cu0.8Fe) – 20 vol.% SiC after milling in planetary mill at 16 min (a), 60 min (b), 90 min (c), 120 min (d).

For every image the common coefficient of charge is defined:

$$K_{ch}^{com} = \frac{\sum_{k=1}^{N} F_k}{F_{im}}, \qquad (1)$$

where N – number of particles;
F – area of particle;
F_{im} – area of image.

Then each image is disrupted to certain number of fields as shown in Fig. 2 and coefficient of charge K_{ch} is defined for each field:

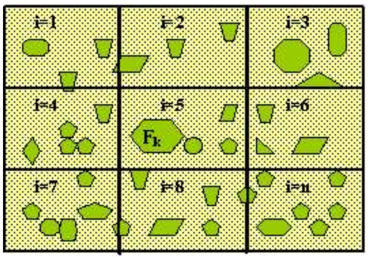

Fig. 2. The scheme of composite material microstructure.

$$K_{ch} = \frac{\sum_{l=1}^{B} F_l}{F_f}, \tag{2}$$

where B – number of particles in field;
F_f – area of field.

The measure of data scattering is the standard deviation S:

$$S = \sqrt{\frac{\sum_{i=1}^{n} (K_{ch_i} - K_{ch}^{com})^2}{n}}, \tag{3}$$

where n – number of fields that image was disrupted.

Then combination of data selections obtained from images of specimen is performed and standard deviation of combined data selection is:

$$S_{com} = \sqrt{\frac{\sum_{j=1}^{m} n_j S_j^2}{\sum_{j=1}^{m} n_j}}, \tag{4}$$

where m – number of images of specimen.

Characteristic of structure homogeneity is the variation coefficient. This quantity shows degree of deviation of analyzable phase distribution from uniform distribution (S = 0):

$$K_{\text{var}} = \frac{S_{com}}{\overline{K}_{ch}^{com}} \cdot 100\%, \tag{5}$$

where $\overline{K}_{ch}^{com}$ - the average common coefficient of charge for m images defined as:

$$\overline{K}_{ch}^{com} = \frac{\sum_{j=1}^{m} K_{ch\ j}^{com}}{m} \tag{6}$$

The lower variation coefficient results more structure homogeneity, particles have more uniform distribution. Increasing of milling time results more refining of particles, the finest particles become undistinguished from matrix background and it decrease the coefficient of charge. For comparability of results the reduction coefficient is needed:

$$K_{red} = \frac{\overline{K}_{ch}^{com}}{\overline{K}_{ch}^{\overset{com}{true}}}\,, \tag{7}$$

where $\overline{K}_{ch}^{\overset{com}{true}}$ - the average common «true» coefficient of charge.

It equals the average common coefficient of charge for specimen after minimal milling time (in structure of this specimen there are coarse particles which marked by software with maximal accuracy).

Then «true» variation coefficient is:

$$K_{\text{var}}^{true} = K_{red} \cdot K_{\text{var}} \tag{8}$$

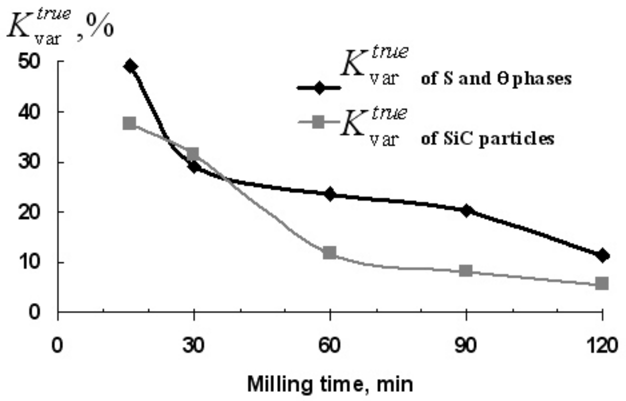

Fig. 3. The milling time dependence of variation coefficient of particles distribution in composite material (Al4Cu1.5Mg+Al12Si2Cu0.8Fe) – 20 vol.% SiC

The milling time dependence of variation coefficient of S and θ phase's distribution as well as SiC distribution was plotted. In Fig. 3 regular decreasing of variation coefficient with time of mechanical alloying is shown and decreasing is passed with decay.

At final time of mechanical alloying (120 min) value of variation coefficient of S and θ phases distribution reaches 10 %. For the reason of qualitative analysis of microstructure homogeneity value K_{var}=10% was accept as index of satisfactory homogeneity of composite material microstructure. K_{var} for SiC distribution reaches value lower 10 % after 90 min of milling time but «mixing» of matrix alloys not occurs in full (see Fig. 1c).

4. CONCLUSION

In work the technique of quantitative estimation of microstructure homogeneity of mechanical alloyed composite materials is offered. As an indicator of satisfactory degree of microstructure homogeneity value of variation coefficient of 10 % is accepted. It is shown that such value is reached in a material (Al4Cu1.5Mg+Al12Si2Cu0.8Fe) – 20 vol. % SiC after 120 min of mechanical alloying.

REFERENCES

FOGAGNOLO J.B., VELASCO F., ROBERT M.H., TORRALBA J.M. (2003). Effect of mechanical alloying on the morphology, microstructure and properties of aluminium matrix composite powders. *Mater. Sci. and Eng. A, 342, 131-143*.

Nuevos materiales de alta conductividad térmica basados en diamante para micro y opto-electrónica

R. Prieto
Instituto Universitario de Materiales de Alicante, Universidad de Alicante, Apto 99, E-03080, Alicante, Spain
J.M. Molina
Instituto Universitario de Materiales de Alicante, Universidad de Alicante, Apto 99, E-03080, Alicante, Spain
Departamento de Química Inorgánica, Universidad de Alicante, Apto 99, E-03080, Alicante, Spain

RESUMEN

Se presentan diversos aspectos de la fabricación (mediante infiltración a baja presión), procesado y propiedades de una nueva clase de materiales con muchas posibilidades de comercialización en el competitivo campo de los disipadores de calor para micro y opto-electrónica: materiales compuestos con matrices de Al-Si y Ag-Si y refuerzo de diamante interconectado por una fase ligante de silicio.

1. INTRODUCCIÓN

Algunas de las aplicaciones más recientes de un sector en creciente demanda como el de la electrónica han alcanzado su límite tecnológico por la imposibilidad de encontrar materiales capaces de extraer el excesivo calor generado en el funcionamiento de sus equipos. Hoy en día se plantea como estrictamente necesario encontrar nuevos materiales que combinen altas conductividades térmicas con bajos coeficientes de expansión y que cumplan además con otros requisitos propios de cada aplicación.

En micro y opto-electrónica (que son las ramas de la electrónica más exigentes en cuanto a disipación térmica) se requieren materiales disipadores de calor con un mínimo de conductividad térmica (CT) de 400 W/mK y un coeficiente térmico de expansión (CTE) máximo de 3-8 $x10^{-6}$ K^{-1}. En este trabajo se propone la fabricación de una nueva generación de disipadores de calor que cumplen tales requisitos y que se basan en el uso de materiales compuestos de matriz metálica con refuerzos discretos de diamante interconectados mediante puentes de silicio. El diamante aporta conductividad térmica al material, mientras que el silicio controla su expansión térmica dimensional.

2. PROCEDIMIENTO EXPERIMENTAL

2.1 Fabricación de las preformas de diamante

Se han utilizado partículas de diamante de calidad ISD (ILJIN Diamond GmbH, Nuremberg, Germany; con una conductividad intrínseca de alrededor de 1800 W/mK) de tamaño medio de 200 μm. El polvo de silicio (Alfa Aesar GmbH, Karlsruhe, Germany) que formará los puentes de interconexión entre partículas tiene un tamaño promedio de alrededor de 20 μm. El calentamiento de los compactados de mezclas de polvos se ha realizado con un equipo de la casa Leybold-Heraeus (modelo UNIVEX 300), que permite imponer una diferencia de potencial entre los extremos del crisol que contienen la muestra y aumentar así la temperatura por efecto Joule. La corriente impuesta a las muestras fue de 6 amperios y el vacío utilizado fue de 10^{-5} mbar.

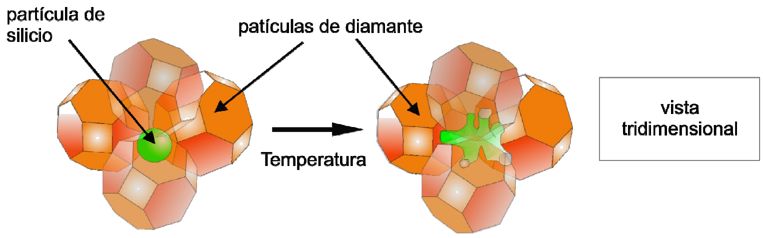

Figura 1. Dibujo que muestra la unión de las partículas de diamante con silicio por el método de sinterización con agente ligante.

2.2 Infiltración de las preformas de diamante con aleación Al-12%Si y Ag-3%Si

Se ha utilizado un equipo de infiltración convencional por presión de gas que consta de una cámara de acero inoxidable en cuyo interior se encuentra un horno eléctrico ($T_{máx}$= 1200 ºC). Los metales utilizados son aleaciones de Al y Ag con Si en composición eutéctica.

2.3 Evaluación de las propiedades térmicas de los materiales fabricados

Se han medido dos propiedades en los materiales fabricados: la conductividad térmica (CT) y su coeficiente térmico de expansión (CTE). La medida de CTE se ha realizado con un analizador termomecánico TMA 2940-TA Instruments, en el intervalo de temperatura de 20-300ºC. La conductividad térmica se ha medido mediante un método relativo de estado estacionario cuyo error absoluto asociado es de ±2%, con una reproducibilidad mayor al 99%.

3. RESULTADOS Y DISCUSIÓN

La figura 2 muestra los valores de compactación conseguidos con las mezclas bimodales de partículas de diamante (partículas grandes de 200 µm) y silicio (partículas pequeñas de 20 µm). Las preformas elegidas para su procesado en caliente fueron las de máxima compactación (0.73) que se consigue para una mezcla de 80% de diamante y 20% de silicio.

Las preformas obtenidas después del calentamiento por corriente eléctrica presentan una microestructura de partículas de diamante unidas por una fase silicio que dada su forma se entiende que ha pasado por estado fundido (Figura 3). La microestructura de esta fase ligante de silicio varía en función de las condiciones de calentamiento. Para calentamientos muy rápidos (de 5ºC/s) y tiempos de espera cortos (1min a 1500ºC) se tiene que el silicio forma puentes de unión entre las partículas de diamante (Figura 3a). Sin embargo, si la velocidad de calentamiento decrece o el tiempo a máxima temperatura se alarga las partículas de diamante quedan cubiertas en su totalidad por una capa fina de silicio debido a que el silicio a esta temperatura moja perfectamente el diamante con el tiempo (Figura 3b).

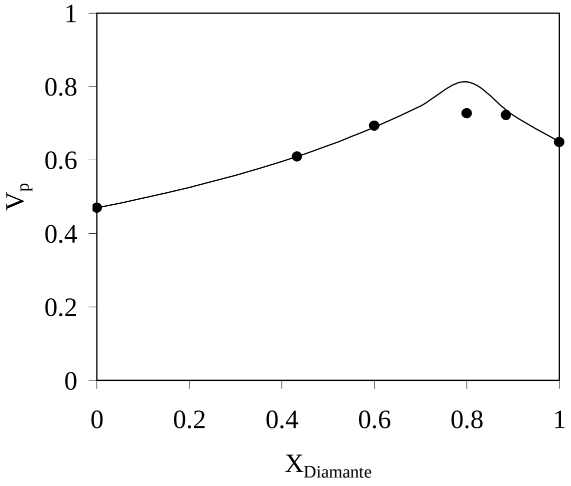

Figura 2. Fracción de volumen de los compactos formados por partículas de diamante de 200 μm y silicio de 20 μm. Los puntos son resultados experimentales. La línea representa la predicción realizada con un modelo sencillo presentado en (Molina et al. 2002).

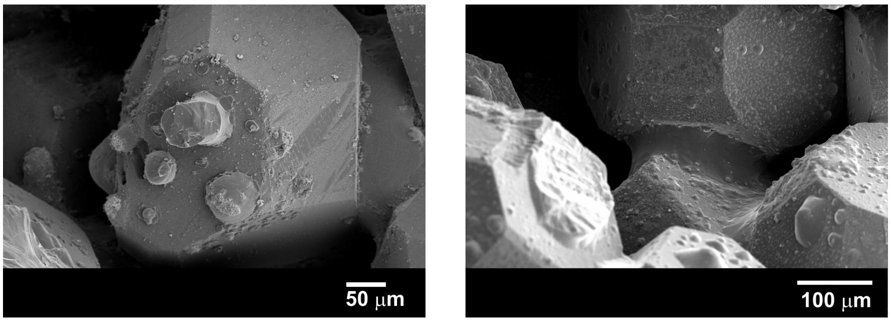

(a) (b)

Figura 3. Microestructuras de las preformas obtenidas para calentamientos rápidos y tiempos de espera cortos (a) y para calentamientos lentos y tiempos de espera largos (b).

La tabla 1 muestra las preformas que han sido infiltradas con metal y sus condiciones de procesado e infiltración, así como también su caracterización térmica y termomecánica a través de las medidas de conductividad térmica y coeficiente térmico de expansión.

La interpretación de los resultados obtenidos es muy clara. Las preformas que contienen mezclas de diamante-silicio aumentan su fracción de volumen debido a que las partículas de menor tamaño de silicio se sitúan entre los huecos que dejan entre sí las de diamante. La fracción de volumen de diamante en todos los casos es, por tanto, constante e igual al 65% del total del volumen del material. El silicio presente, que sirve de fase ligante entre el diamante, posee un valor de conductividad térmica menor al del metal y por ello los materiales con silicio presentan una ligeramente menor conductividad térmica que aquellos sin silicio. Sin embargo, su coeficiente de dilatación térmica decrece debido al bajo CTE del silicio (≈ 2-4 $\times 10^{-6}$ K^{-1}).

preforma	metal	V_p total	Velocidad calentamiento*	Tiempo a T máxima*	CTE ($\times 10^{-6}$ K^{-1})	CT (W/mK)
D	Al-Si	0.65	---	--	11.3	475
D + Si	Al-Si	0.73	5ºC/s	1min	8.4	468
D + Si	Al-Si	0.73	1.5ºC/s	3 min	14	380
D	Ag-Si	0.65	---	---	6.2	660
D + Si	Ag-Si	0.73	5ºC/s	1 min	5.5	655
D + Si	Ag-Si	0.73	1.5ºC/s	3 min	7.2	490

* Ambas condiciones se refieren al procesado de las preformas durante el proceso de sinterización.

Tabla 1. Características de los materiales fabricados (D se refiere a diamante; V_p es la fracción de volumen total de refuerzo; CTE y CT con el coeficiente térmico de expansión y la conductividad térmica respectivamente).

Los valores menos competitivos de las muestras procesadas a baja velocidad de calentamiento y más largos períodos de estancia a alta temperatura se deben a que el silicio recubre la superficie de las partículas de diamante aislando éste último de su contacto con el metal y separando ambas fases térmicamente conductoras. El resultado se puede entender como la respuesta de un material formado por una fase metálica continua y una fase refuerzo discreta con una elevada resistencia interfacial. En este caso, las propiedades térmicas interesantes de la combinación de metal y diamante desaparecen debido a la capa de baja conductividad térmica que separa ambas fases.

4. CONCLUSIONES

El método de fabricación de preformas de diamante por sinterización con fase ligante de silicio resulta ser un método atractivo y eficiente. Las preformas obtenidas pueden ser infiltradas con un metal líquido como Al-Si o Ag-Si y dan como resultado materiales con unas muy interesantes propiedades térmicas para aplicaciones en micro y optoelectrónica. Las condiciones de procesado de la preforma y del material son extremadamente importantes y determinan las propiedades finales y por tanto el uso del material como disipador de calor para las mencionadas aplicaciones.

AGRADECIMIENTOS

Los autores agradecen la financiación obtenida a través de la Generalitat Valenciana (proyecto GVPRE/2008/244) y la Universidad de Alicante (proyecto GRE08-P13). J.M. Molina queda también agradecido al Ministerio de Educación y Cultura por su contrato “Juan de la Cierva”.

REFERENCIAS

MOLINA, J.M., SARAVANAN, R.A., ARPON, R., GARCÍA-CORDOVILLA, C., LOUIS, E., NARCISO, J. (2002). Pressure infiltration of liquid aluminium into packed SiC particulate with a bimodal size distribution, *Acta Mater.*, 50, 247-257.

Análisis numérico de la propagación de grietas por fatiga en materiales compuestos de matriz metálica

J.E. Ortiz
Grupo de Elasticidad y Resistencia de Materiales.
Escuela Técnica Superior de Ingenieros. Universidad de Sevilla.
Av. De los Descubrimientos s/n. Sevilla. España
jortiz@esi.us.es

RESUMEN

El presente trabajo es un estudio numérico de la propagación de grietas por fatiga en materiales compuestos de matriz metálica. Se estudia la propagación e interacción de grietas en materiales de matriz metálica austemperizada con agregados de nódulos de grafito. La propagación de grietas es desarrollado mediante de un análisis incremental usando la formulación mixta del método de elementos de contorno. Se evalúa la influencia del término finito del campo de tensiones conocido como “T-stress” sobre la dirección de la propagación. Este término dependiendo de su magnitud y orientación puede influenciar la dirección de la propagación. A su vez la interacción de grietas puede ejercer una fuerte influencia sobre estas dos características. Se modelan ejemplos que ilustran dicha influencia durante la interacción de grietas y se modela la propagación de macro y micro grietas en medios típicos de estos materiales. Los resultados concuerdan con las observaciones experimentales y se validan algunos mecanismos de fractura propuestos en la literatura.

1. INTRODUCCIÓN

Los materiales de matriz metálica austemperizada con nódulos de grafito son materiales relativamente nuevos y aptos para una gran variedad de aplicaciones, Stokes et al. (2007). Las buenas propiedades de la tenacidad a la fractura están asociadas al proceso de microfisurado que se desarrolla y que se propaga simultáneamente acompañando a la grieta principal en su avance. Existe evidencia de que el agrietamiento redistribuye y reduce la tensión promedio cerca del vértice de la grieta principal disminuyendo a la vez la energía elástica disponible debido a las nuevas superficies de fractura creadas, Stokes et al. (2007). Este mecanismo explica la baja velocidad de propagación de grietas y altos valores ΔK_{th} umbral en comparación a los materiales metálicos. El proceso se acentúa cuando $\Delta K/\Delta K_{th}>>1$ (ΔK_{th} es el valor umbral de propagación en fatiga) a estos niveles la macrogrieta “busca” a los nódulos a lo largo de su propagación trazando un camino de mayor superficie debido a la interacción con las microgrietas que se originan desde las superficies irregulares de los nódulos, Stokes et al. (2007). Un segundo factor que puede incidir en la dirección de la propagación es la tensión finita conocida como “T-stress” tensión paralela a la grieta, Ayatollahi et al. (2002). Esta tensión es de particular interés durante el proceso de interacción de grietas ya que su módulo y orientación son fuertemente influenciados, Chen et al. (2009). En el presente trabajo se estudia la propagación de grietas en materiales de matriz metálica autemperizada usando la formulación mixta de los elementos de contorno. Se calculan parámetros de primer y segundo orden y se evalúa su incidencia en la dirección de la propagación.

2. DIRECCION DE LA PROPAGACION DE GRIETAS.

Las tensiones en la vecindad del vértice de una grieta se pueden aproximar mediante el siguiente desarrollo en serie

$$\underline{\underline{\sigma}}(r,\theta)=\frac{K_I}{\sqrt{r}}(\underline{\underline{s}}_I(\theta)+m\underline{\underline{s}}_{II}(\theta)+M(r)\underline{\underline{\tau}}_I(\theta)+.....) \qquad (1)$$

donde r y θ son las coordenadas polares con origen en el vértice de la grieta, $m=K_{II}/K_I$ y $M(r)=T\sqrt{r}/K_I$. Los coeficientes K_i ($i=I, II$) son los factores de intensidad de tensiones y T es la tensión no singular paralela a la dirección de la grieta conocida en ingles como *T-stress*. Las funciones angulares $\underline{\underline{s}}_I$, $\underline{\underline{s}}_{II}$ y $\underline{\underline{\tau}}$ están normalizadas con $s_{I\theta\theta}(\theta=0)=1$, $s_{IIr\theta}(\theta=0)=1$ y $\tau_{rr}(\theta=0)=1$. La estabilidad direccional de la propagación de grietas está gobernada por la tensión *T-stress*. En general la influencia de este término sobre el ángulo de propagación se puede estimar aplicando el criterio de tensión circunferencial máxima (TCM), $\partial\sigma_{\theta\theta}/\partial\theta=0$. En la Fig. 1 se puede apreciar el ángulo de propagación para distintos valores de $B.\alpha$ ($B=T(\pi a)^{1/2}/K_I$ y $\alpha=(2r_c/a)^{1/2}$), r_c es una distancia critica donde la contribución de los términos de orden superior a $O(r^{1/2})$ en la Ec. (1) pueden ser ignorados. En modo I la propagación es direccionalmente estable cuando la tensión *T-stress* es negativa (compresión) en cambio si esta es positiva la propagación se torna inestable.

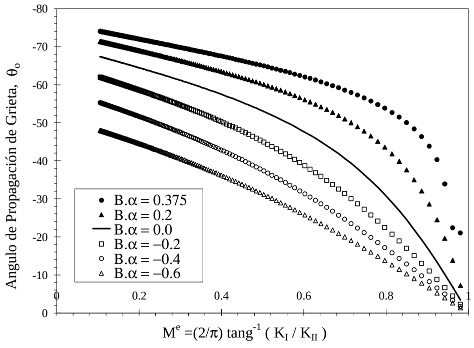

Fig 1. Efecto de T-stress sobre la dirección de la propagación basado en el criterio TCM.

3. CÁLCULO DE *T-STRESS* E INTERACCIÓN DE GRIETAS

En el presente trabajo se ha adaptado la integral de interacción presentada por Cisilino y Ortiz (2003) para el cálculo de la tensión *T-stress* y K_I. El problema elástico es resuelto usando la formulación mixta del método de los elementos de contorno. En la Tabla 1 se presenta los valores K_I, T y B para probetas con grieta central y grieta lateral bajo tensión y probeta con grieta lateral a flexión pura (siglas en ingles MT, SENT y SENB, respectivamente). Los resultados se comparan con los obtenidos por Cheng et al. (2001).

PROBETAS	$K_I/\sigma\sqrt{\pi a}$		T/σ		$B=T\sqrt{\pi a}/K_I$	
	Ortiz	**Chen[1]**	**Ortiz**	**Chen[1]**	**Ortiz**	**Chen[1]**
MT (2a/w=0.3, h/w=1.0)	1.1293	1.1232	-1.1588	-1.1553	-1.0261	-1.0286
SENT(a/w=0.3, h/w=12.0)	1.6130	1.6598	-0.5969	-0.6103	-0.3700	-0.3677
SEMB(a/w=0.3, h/w=12.0)	1.0762	1.1241	-0.0796	-0.0791	-0.0739	-0.0704

Tabla 1. Cálculo de valores de K_I, T y B para distintos tipos de probetas.

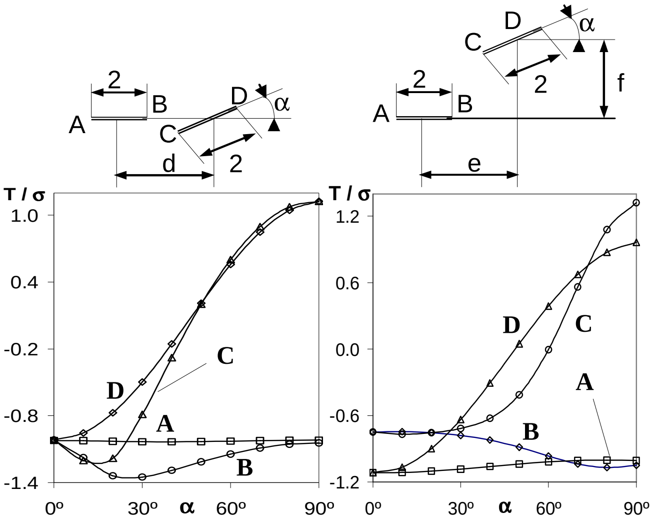

Fig. 2. T-stress en interacción de grietas en distintas posiciones.

En la Fig. 2 se presentan los valores de *T-stress* para dos grietas de igual longitud en un primer caso alineadas con a/d=2/5 y en un segundo caso con posiciones relativas a/e=2/3 y e/f=3/4. En ambos casos se ha considerado que la grieta de la derecha tiene una inclinación α entre 0º y 90º. Se observa claramente la incidencia de la interacción sobre el valor y orientación (signo) de la tensión *T-stress* correspondientes a los vértices de ambas grietas.

4. PROPAGACION DE GRIETAS POR FATIGA EN MATERIALES COMPUESTOS DE MATRIZ METÁLICA

Usando la formulación mixta del método de los elementos de contorno se ha modelado una disposición típica de nódulos de grafito en fundiciones nodulares considerando microgrietas en los puntos ecuatoriales de los nódulos la longitud de la grieta principal en 40 veces la longitud de las microgrietas, ver Fig. 3. Las constantes del material para la ley de propagación $da/dn = C(\Delta K^m - \Delta K_{th}^m)$ son C=4.43x10^{-10}, m=1.85 y ΔK_{th}=5MPa√m. La evolución del $\Delta K/\Delta K_{th}$ a lo largo de la propagación de la grieta principal y microgrietas se puede apreciar en la Fig. 4.

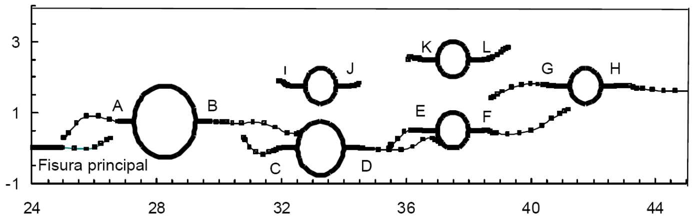

Fig. 3. Propagación de grietas por fatiga en materiales con matriz metálica.

Se observa claramente que existe una fuerte interacción o “atracción” entre ambos tipos de grietas. La presencia de la grieta principal activa el “microfisurado” siguiendo esta el

de ΔK en ambas grietas son del
valores superiores al de la grieta

ón principal corresponde al de la
to. Este proceso de interacción se
de mayor longitud que el camino
K siendo así que para valores
ismo antes descripto gobierna el
ores ΔK cercanos a ΔK_{th} la grieta
ado dado que estas se encuentran

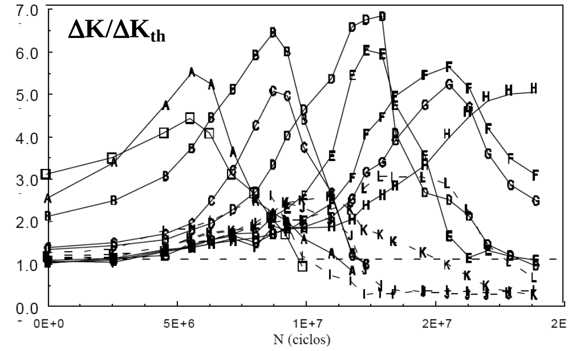

Fig. 4. Evolución de ΔK para las grietas de la Fig. 3.

5. CONCLUSIONES

En este trabajo se presentó un estudio numérico y fractomecánico de propagación de grietas por fatiga en fundiciones nodulares austemperizadas. Se cálculo los parámetros de fractura de primer y segundo orden para una grieta e interacción de grietas. Se ha establecido que el *T-stress* gobierna el ángulo de propagación de una grieta. Usando la formulación mixta de los elementos de contorno se ha identificado el proceso de interacción entre grietas, microgrietas y nódulos de grafitos. Los resultados obtenidos concuerdan con las observaciones experimentales y permiten validar los modelos de mecanismos de fractura propuestos en la literatura así cómo llegar a un mejor entendimiento del problema en estudio.

AGRADECIMIENTOS

Estudio financiado por el Programa Ramón y Cajal del Ministerio de Ciencia e Innovación del Gobierno Español.

REFERENCIAS

STOKES B., GAO N., REED P.A.S. (2007). Effects of graphite nodules on crack growth behaviour of austempered ductile iron. Materials Science and Engineering A (445-446), 374-385.

AYATOLLAHI M.R., PAVIER M.J., SMITH D.J. (2002). Mode I cracks subjected to large T-stresses. Int. J. of Fract. 117, 159-174.

CHEN Y.Z., WANG Z.X., LIN X.Y. (2009). Evaluation of the T-stress for interacting cracks. Computational Materials Science 45, 349-357.

CHEN C., KRAUSE R., PETTIT R.G., BANKS-SILLS L., INGRAFFEA A. (2001). Numerical assessment of T-stress computation using a p-version finite element method. Int. J. of Fract. 107, 177-199.

CISILINO A.P., ORTIZ J.E., (2005). Boundary element analysis of three-dimensional mixed-mode cracks via the interaction integral. Comp. Meth. Ap. Mech. Engrg. 194, 935-956.

Free-sintering of low-Co metal matrix composites segments for diamond tools

P. Rey, **A. Fernández**
Departamento de Materiales y Procesos de Fabricación, Centro Tecnológico AIMEN,
C/ Relva 27A, Porriño, 36410 Pontevedra, España
M. Fernández
DIAMANCENTER S. L., Queimadiña-Leirado, 36457, Salvaterra do Miño, España

SUMMARY

Diamond tools have been developed to satisfy all possible requirements of the natural stone industry. Improvements in processing technologies can have a significant effect on reducing the cost and enhancing the quality of the processed stone. Free-sintering is a competing technology to obtain diamond-MMCs with a substantial cost saving. The aim of this work is to produce composites segments with low-Co metal matrices for using in saw blades by free-sintering. They were characterized by means of their physical and mechanical properties. A study by electron microscopy coupled with electron dispersive X- ray was also performed to evaluate the matrix microstructure and the integrity of the diamond grits. In general, the results show that the sintered segments under vacuum presented good properties of density and hardness but the diamond grits were damaged.

1. INTRODUCTION

Natural stones have a large potential market worldwide due to their ornamental and structural properties. Processing techniques add considerable value to the stone materials so it is necessary to find competing alternatives. Nowadays the preferred route for fabrication of composite segments is by hot-pressing powder preforms of metallic matrices and diamond grits in a protective atmosphere. Co is almost the preferred element for metal matrices. Hot pressing technique has several disadvantages (Spriano *et al*, 2005). On the one hand, graphite dies last only several cycles and are expensive. On the other hand, dies must be re-machining because of dimensional tolerances causing graphite dust and an unsafe work environment. Co powder is technically a very good product for diamond tools but undesirable due to his high and instable price. Therefore, replacement with low Co content alloys or preferably Co free ones is the main focus of interest within the diamond tool industry (M. Żak-Szwed *et al.* 2008). New products such as pre-alloyed powders are an ideal alternative to Co, combining both technical and economical advantages. Lowering Co content in segments also has health benefits, since exposure to very high levels of Co can cause illnesses (Kim, J.H. *et al.* 2006). In fact, most cases of Co toxicity relate to occupational skin contact or inhalation producing dermatitis, Co sensitization, eczema, pneumoconiosis and bronchial asthma. Sintering without pressure or free-sintering is a competitive method to obtain low Co metal bonded diamond composites for saw blades. Free-sintering is a cost effective technique both because of raw powders and equipment. Without graphite moulds, the production rate can be increased due to the high number of segments that can be sintered simultaneously in each cycle. In this paper we present the results based on the need for new, economic and ecological diamond cutting tools. Free-sintered segments present good quality and properties and the cost saving is substantial.

2. EXPERIMENTAL PROCEDURE

The metallic powder for the matrices consists of agglomerates of individual pre-alloyed bond powders, consisting of a Fe/Co phase and a Cu phase. A 15% of FeP particles are added as sintering additive (MX4885, Eurotungstene) (see fig. 1-A). Diamond grits used are industrial synthetic diamonds with a grain size 30/40 mesh. The crystals are well defined cuboctahedron with minimized internal impurities (fig. 1-B). Table 1 shows the exact composition of the metallic powders analyzed by ICP.

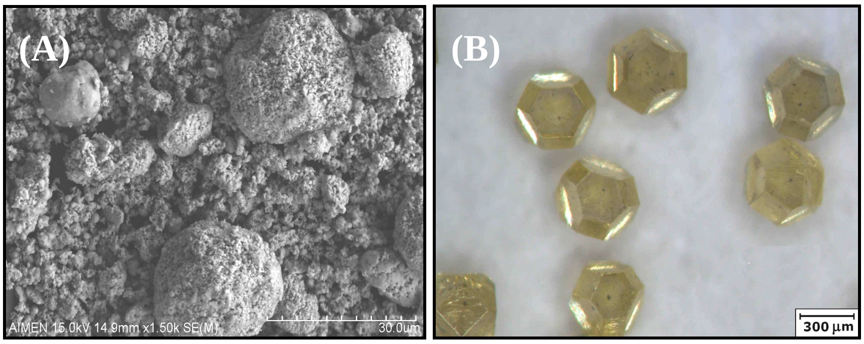

Fig. 1. Pre-alloyed powders composed of Fe, Co, Cu and P (A) and industrial diamond grits used for free-sintering experiments (B).

%Fe	%Cu	%Co	%P
48	35	15	2

Table 1. Chemical composition of pre-alloyed powders.

The production of diamonds segments consists of 3 main steps: powder mixing, cold pressing and free-sintering of the segment.

2.1. Powder mixing

The powder components were placed in a turbular mixer inside a small container. A binding compound, a mixture of ethanol and ethylene glycol (2% wt) was added to the powder to reduce the friction between the particles. After a prefixed time, the synthetic diamonds were added and mixed together with the powder in a concentration of 0.026% (wt). Depending on the powder quantity mixing time lied between 20 min. and 1 hour.

.2.2. Cold pressing

In this stage the powder with diamond grits was filled in a mould, which has the requested shape and dimension of the segment. After the mould was filled, pressure (P) was applied in one direction from the top of the press and then the compacted powder was pushed out by a punch. Powders were compacted at different P, between 6 and 34 Tn. The area of the segments was 29cm^2. Between 46% and 83% of the theoretical density was reached.

2.3. Free-sintering

The cold pressed segments were placed on a ceramic plate inside a TAV vacuum furnace. Free-sintering experiments were carried out at different times (t) and temperatures (T) under vacuum. A typical free-sintering cycle consists on heating up to about 890° C at 3.5ºC/min. Then, heating up at 0.4ºC/min until the final T is reached. Holding at T for different t followed by cooling down to room temperature.

3. RESULTS AND DISCUSSION

The effect of P, T and t on the properties of segments is shown in figs. 2 and 3.

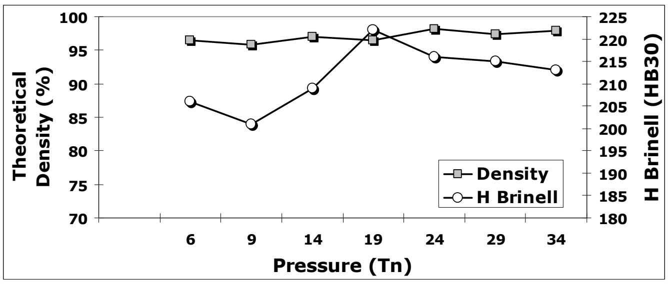

Fig. 2. Effect of consolidation pressure on density and hardness of the segments (Thermal cycle 940ºC/40 min).

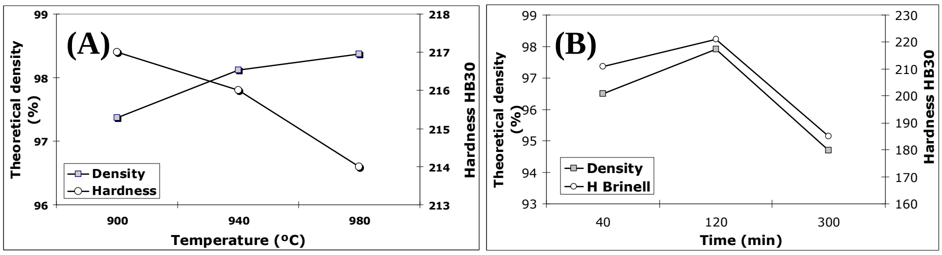

Fig. 3. Effect of T (A) and t (B) on density and hardness of the segments (P=19 Tn)

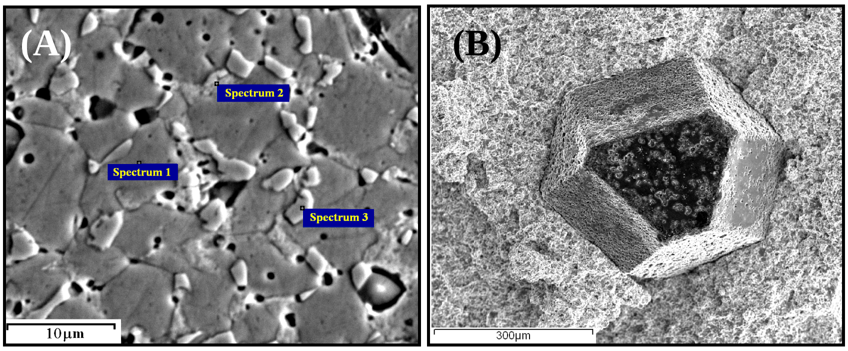

Fig. 4. Microstructure corresponding to segment after free-sintering in vacuum, 940ºC-40 min (A); appearance of diamond grit after vacuum sintering (B).

The densification curve shows an excellent sintering behaviour of the powders. However the hardness reaches the maximum value at 19 Tn. For higher pressures, the hardness drops and an excessive wear of the press dies and punches occur. The softening produced at higher T and t sintering conditions is related to grain growth and can be explained by the Hall-Petch relationship between hardness and grain size in metallic matrices. On the other hand, excessive t produces a diminution of density as a consequence of the copper loss on the surface of the segments. The polished cross-section microstructure of a segment is shown in fig. 4-A. EDS analyses in the different zones are also shown (Table 2). Fig. 4-B shows the damage of a diamond grit showing pitting and rounded edges.

	C	**P**	**Fe**	**Co**	**Cu**
Spectrum 1	7.96	0.58	71.61	18.14	1.71
Spectrum 2	6.20	1.03	8.63	1.86	82.29
Spectrum 3	8.68	7.778	66.54	15.12	1.89

Table 2. EDS analyses of the corresponding zones of fig. 4-A.

The fracture surface reveals that the diamond crystals had a black appearance as a consequence of graphitization at high temperatures, vacuum atmosphere and catalytic metals (Fe, Co). Vacuum seems to be not effective as reducing atmosphere for oxide elimination. SEM/EDS observations of microstructure show dark-grey grains correspond to Fe/Co solid solution and a light-grey phase corresponding to Cu. There is another phase at the grain boundaries having high quantities of P, which has been formed during cooling because of the lower solubility of P in αFe at room T. These results are consistent with the Fe-Co-Cu, Fe-P and Cu-P phase diagrams.

4. CONCLUSIONS

Free-Sintering is an adequate and reliable route for fabrication of low-Co segments for diamond tools. Good results of hardness and density can be achieved for the processing conditions considered in the present paper, but excessive time and temperature promotes loss of density and grain growth. On the other hand, vacuum sintering produces diamond grits degradation as a consequence of the presence of metallic oxides.

ACKNOWLEDGMENTS

The authors gratefully acknowledge financial support from Galician government under the contract 07MT019E

REFERENCES

KIM J. H., GIBB H. J., HOWE P. D (2006) Co and Inorganic Co Compounds, *Concise international chemical assessment document*, 69, WHO Publications, Switzerland.
SPRIANO, S., CHEN, Q., SETTINERI, L., BUGLIOSI, S. (2005) Low content and free cobalt matrixes for diamond tools, *Wear*, 259, 7-12,1190-96.
ŻAK-SWED, M., KONSTANTY, J., RATUSZEK, W. (2008) Properties of Fe-Cu matrices for diamond impregnated tools, *Industrial Diamond Review*, 2, 29-34.

Structure and properties of dispersion-strengthened composite materials on the basis of Al-Fe-Si-Cu system obtained by mechanical milling

M. Samoshina, A. Aksenov, P. Bryantsev
State Technological University «Moscow Institute of Steel and Alloys», Russia

SUMMARY

During production of high-purity aluminum by electrolytic refining are formed so-called anodic sludges. Inherently such waste represents an alloy, which chemical compound is within the limits of: 50-60 % Al, 25-35 % Cu, ~10 % Fe and 5-10 % Si. The effective way of anodic sludges recycling does not exist. Such waste can be inexpensive initial raw material for obtaining dispersion strengthened composite materials by mechanical alloying. This method is the perspective technology allowing in a wide range of opportunities to influence materials structure and as a result to receive dispersion strengthened composites with a unique complex of properties.

1. INTRODUCTION

Anodic sludge structure contains more than 75 % refractory intermetallic phases. The size of intermetallic particles reaches hundreds and thousands micrometers. Processing in a high-energy mill probably to achieve significant refinement of such particles. The material with such disperse structure possesses a unique complex of properties: a high level of thermal stability and wear resistance in a combination to low level of thermal expansion coefficient.

2. EXPERIMENTAL

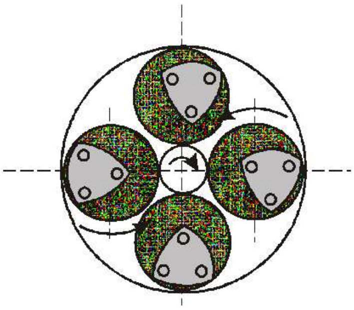

Fig. 1. The basic scheme of a planetary mill with quasi-cylindrical milling bodies.

The alloy Al - 25 % Cu - 10 % Fe - 10 % Si with composition typical for industrial anodic sludges have prepared in laboratory conditions. For imitation of industrial conditions an alloy cast in steel mold 50 mm in diameter, 250 mm in height. Before mechanical alloying castings were splited by shock influence till the size of parts about 5-10 mm. Efficiency of all processes at mechanical alloying is defined by the type of aggregate providing mechanical energy transmission in a material. In work it has been preferred a planetary mill with massive quasi-cylindrical milling bodies (fig. 1). Mechanical alloying process with use milling bodies of this kind is characterized by more rare and powerful single impacts in comparison with use of traditional ball load (Tikhomirov et al. 2006). Before milling containers with an initial material were vacuumized and then filled with argon for exception of material oxidation. During work containers were cooled by flowing water. The ratio of the weight of the milling body to that of the mixture was 6:1. Time of milling changed from 1 up to 6 h.

The compacted cylindrical samples 15 mm in diameter and 10 mm in height obtained by double-action compaction at a temperature 480 ^{0}C. The major characteristic of consolidated samples quality is density (or porosity) which estimated by a technique of hydrostatic weighing.

Calculation of the equilibrium multicomponent phase diagrams Al - Cu - Fe - Si was carried by TCW4 Thermocalc software with thermodynamic database TTAL5. Phase structure was investigated by X-ray diffraction analysis on diffractometer D8 ADVANCE. Metallographic researches spent on scanning electronic microscope JSM-35 CF.

Hardness and microhardness of a material was assessed in the Vickers hardness test. Hot hardness tests of compact samples was carried on Brinell hardness tester with the electroresistance furnace. The test temperature was 350±2 ^{0}C. The tested sample held under loading for1 h. Researches of wear resistance of compact samples under the scheme "pin-on-disk" were spent on Tribometer, CSM Instr without greasing. Thermal expansion coefficient (CTE) was estimated on dilatometer LINSEIS 76/1000. Measurements spent in an air atmosphere in 20-400 ^{0}C, with heating rate 10 K/min. By results of measurements counted average in temperatures range coefficient of thermal expansion.

3. RESULTS AND DISCUSSION

To know phase composition of industrial anodic sludges series of polythermal sections of the equilibrium phase diagram Al - Cu - Fe - Si has been plotted with use of TCW4 Thermocalc software. The analysis of the constructed sections has shown that solidus temperature of alloys of system Al-Fe-Si-Cu which are being in the field of interest (50-60 % Al-25-35 % Cu-10 % Fe-5-10 % Si) is similar and makes ~ 525 ^{0}C. In these alloys there are no phase transformations at temperatures below solidus and their phase structure is similar in conditions of equilibrium crystallization: (Al) +Si+Al_7Cu_2Fe+$CuAl_2$. These data allow counting on reception of a composite material with the fixed phase structure in independence of variation on a chemical composition of initial raw material (anodic sludges). In this connection there will be no necessity for additional operation of sorting of raw material on a chemical compound that will reduce expenses for production of new materials.

However, industrial anodic sludges formed in conditions of non-equilibrium crystallization can have the phase structure differing from calculated. X-ray and structure analysis of alloy Al-25% Cu-10% Fe-10% Si close to composition of industrial anodic sludges and received in the conditions approached to industrial has shown that besides equilibrium phases in structure of a material there are large needles of phase β-(AlFeSi), obviously not dissolved during peritectic reactions (fig. 2). The size of intermetallic particles in this material reach hundreds and thousands microns, and their volume fraction makes ~ 75 %. Presence in anodic sludges structure of the large volume fraction refractory intermetallic particles allows counting on obtainment on their basis of a heat resisting wear proof material by mechanical alloying.

Refining kinetics of material Al-25% Cu-10% Fe-10% Si during mechanical alloying in planetary mill it is possible to observe on fig. 3. During 6 h of mechanical alloying granules of a material are continuously reduced meanwhile their hardness is increased.

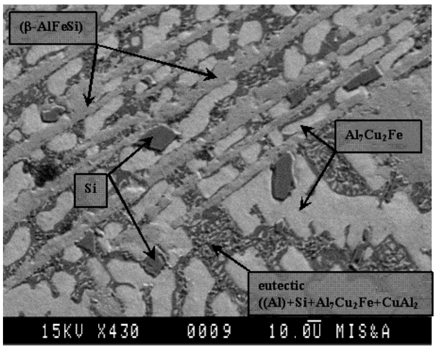

Fig. 2. Microstructure of alloy Al-25% Cu-10% Fe-10% Si (SEM).

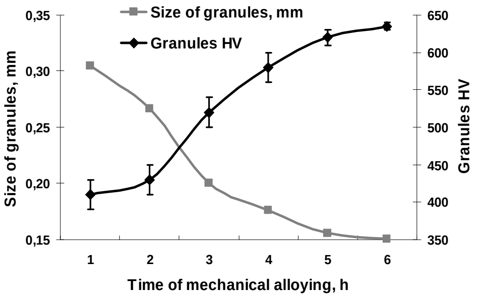

Fig. 3. Average size and hardness of granules of material Al-25% Cu-10% Fe-10% Si vs time of mechanical alloying.

After mechanical alloying granules of material Al-25% Cu-10% Fe-10% Si were consolidated. The density of the consolidated samples has made 3,46 - 3,49 g/cm^3 that corresponds to residual porosity 0,8 - 0 %. Microstructures of the consolidated samples are presented on fig. 4. Within the first hour of milling it is observed only fracturing of large intermetallic particles and as a whole the structure of a material remains coarse. During the further millng there is a refining and redistribution of these particles. After 6 h of milling identification phases are fined in the strongest degree and become practically not distinguishable from a matrix background.

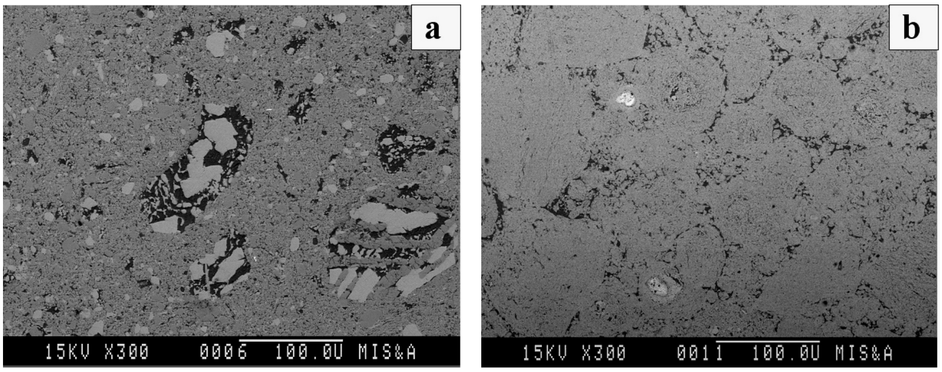

Fig. 4. Microstructure of consolidated samples of mechanicaly alloyed material Al-25% Cu-10% Fe-10% Si (SEM): a – after 1 h; b - after 6 h of mechanical alloying.

The consolidated samples with such disperse structure possess a high level of hardness, both at room and at the higher temperature, low level of thermal expansion coefficient, and also a high level of wear resistance. The properties of a composite in comparison with traditional piston silumin (Al – 12% Si – 2% Cu – 1% Mg – 1% Ni – 0.4% Mn – 0.1% Ti) are presented in tab. 1.

Material	HV	Hot hardness ($350\ ^0C$)	CTE·10^6, 1/K ($20\text{-}400\ ^0C$)	Wear, $mm^3/N \cdot m$
Al-25%Cu-10%Fe-10%Si	430±20	39±6	14,2	$2{,}8 \cdot 10^{-4}$
piston silumin	120±5	12±2	23,0	$6{,}4 \cdot 10^{-3}$

Table 1. The properties of consolidated composite material Al-25% Cu-10% Fe-10% Si and traditional piston silumin (Al – 12% Si – 2% Cu – 1% Mg – 1% Ni – 0.4% Mn – 0.1% Ti).

4. CONCLUSION

1. Series of polythermal sections for system Al-Cu-Fe-Si is constructed to define temperatures of phase transformations and research of phase composition of industrial anodic sludges. Alloys of system Al-Fe-Si-Cu in the field of interest have similar solidus temperature ~ 525 ^0C. In these alloys there are no phase transformations at temperatures below solidus and their phase composition is similar in conditions of equilibrium crystallization: (Al) +Si+Al_7Cu_2Fe+$CuAl_2$.
2. Structure and phase composition of alloy Al-25% Cu-10% Fe-10% Si close to composition of industrial anodic sludges and received in the conditions approached to industrial have been studied by methods of scanning microscopy, quantitative metallography and X-ray analysis. Presence at structure of a material of following phases is identificated: aluminium solid solution (Al), Si, $CuAl_2$, Al_7Cu_2Fe and β-(AlFeSi). The sizes of intermetallic particles in this material achieve 1000 microns and their volume fraction makes ~ 75 %.
3. After mechanical alloying in the planetary mill during 6 h there is a refining and redistribution of large intermetallic particles and formation of homogeneous structure of material Al-25% Cu-10% Fe-10% Si.
4. The consolidated composite material on the basis of Al-25% Cu-10% Fe-10% Si surpasses traditionally used piston silumin (Al – 12% Si – 2% Cu – 1% Mg – 1% Ni – 0.4% Mn – 0.1% Ti) on all complex of the major working properties. Characteristic of thermal stability is higher more than three times, wear resistance is higher more than degree, and thermal expansion coefficient is lower twice.

REFERENCES

TIKHOMIROV A.V., AKSENOV A.A., SHELEKHOV E.V., KALOSHKIN S.D. (2006). Mechanical alloying of Al-Mg alloys and composite materials applying planetary mill equipped with ball charge and quasi-cylindrical milling body. *In book of abstracts of V International Conference on Mechanochemistry and Mechanical Alloying, Novosibirsk, Russia,* 188.

Fabricación y caracterización de recubrimientos de material compuesto de matriz de aluminio reforzado con $MoSi_2$ fabricados por proyección térmica

B. Torres, M. Campo, J. Rams
Departamento de Ciencia e Ingeniería de Materiales, Escuela Superior de Ciencias Experimentales y Tecnología, Universidad Rey Juan Carlos, 28933 Móstoles, Madrid, Spain
M. Lieblich
Departamento de Metalurgia Física, Centro Nacional de Investigaciones Metalúrgicas, CENIM, CSIC, Avda. Gregorio del Amo 8, 28040 Madrid, Spain

RESUMEN

En este trabajo se plantea el desarrollo de recubrimientos de material compuesto de matriz de aluminio reforzado con intermetálicos como alternativa a los materiales compuestos reforzados con cerámicos. Para ello se han optimizado los parámetros que influyen en el proceso de proyección térmica: distancia de proyección, velocidad de alimentación del polvo y número de capas proyectadas. También se ha estudiado cómo influye el tamaño de las partículas de $MoSi_2$ (100 y 25 µm), en la calidad del recubrimiento obtenido. En ambos casos se ha evaluado el grado de refuerzo y la porosidad mediante técnicas de caracterización microestructural (microscopía óptica y MEB) y microanalíticas (EDX), obteniéndose recubrimientos con un 8 % de refuerzo y un 2 % de porosidad.

1. INTRODUCCIÓN

La fabricación de recubrimientos de materiales compuestos de matriz de aluminio reforzados con cerámicos sigue siendo investigada, no existiendo información con refuerzo intermetálico. Las técnicas de fabricación de los recubrimientos son múltiples siendo la proyección térmica la más muy utilizada industrialmente dado que permite obtener buenos recubrimientos con un coste muy inferior al que se tiene con otras técnicas. Torres et al. (2007 y 2009), Rams et al. (2008) fabrican con éxito por este medio recubrimientos de materiales compuestos de matriz de aluminio reforzados con cerámicos Estos recubrimientos tienen algunos inconvenientes que podrían reducirse sustituyéndolos por intermetálicos. Una de las desventajas del refuerzo cerámico es la gran diferencia en el coeficiente de expansión térmica entre matriz y reforzante cerámico que debilita el material cuando las condiciones de servicio incluyen ciclos térmicos. El hecho de que los intermetálicos tengan un coeficiente de expansión térmica más cercano al del aluminio hace que disminuyan las tensiones residuales en las intercaras, consiguiendo así una menor incidencia de fatiga térmica. Otra desventaja de los materiales reforzados con cerámicos es que su abrasividad es mucho mayor, de manera que la sustitución implicaría un aumento de la vida de la superficie antagonista, si van a ser utilizados para desgaste Wang et al. (2002), así como un aumento en la vida en servicio de las herramientas y las máquinas utilizadas en la mecanización de las distintas partes. Otro beneficio del refuerzo intermetálico es que el material compuesto se puede reciclar fácilmente, ya que el intermetálico se recicla a la vez que la matriz, mientras que con los cerámicos es necesario separarlos previamente, encareciendo el proceso.

Se ha demostrado que la calidad de los recubrimientos obtenidos por esta técnica: baja porosidad, adecuado grado de refuerzo, buena unión refuerzo-matriz y buena adhesión sustrato-recubrimiento, depende del tipo de material que se proyecta y del tipo de sustrato. Por esto en este trabajo se han optimizado los parámetros que influyen en el proceso de proyección térmica: distancia de proyección, cantidad de polvo proyectado y número de capas depositadas para dos tamaños de refuerzo intermetálico.

2. PROCEDIMIENTO EXPERIMENTAL

2.1. Materiales de partida

Se ha empleado un polvo de proyección de aluminio (pureza del 99,8 %) suministrado por CASTOLIN que tiene un tamaño medio de partícula de 125 µm.

Las partículas de intermetálico $MoSi_2$ fueron suministrados por INASMET y se obtuvieron por síntesis autopropagada a temperatura elevada SHS. Se han utilizado dos tamaños de partículas muy diferentes < 125 µm y < 25 µm.

Estas partículas se mezclaron durante 15 minutos en un molino de bolas, con una relación del 20 % en volumen con el aluminio, para obtener las mezclas de proyección.

2.2 Condiciones de proyección de los recubrimientos

El equipo de proyección térmica empleado ha sido el DS8000 de CASTOLIN. Las condiciones que se emplearon fueron las siguientes: llama neutra, boquilla muy energética (SS40, típica de cerámicos) y no se impulsó el polvo con aire.

Las condiciones de proyección se variaron para optimizar la calidad de los recubrimientos según se observa en la Tabla 1. Se emplearon 2 distancias (15 y 20 cm), dos alimentaciones del polvo (0,56 y 1,1 g/s) y una o dos capas de proyección.

El material compuesto se proyectó sobre un sustrato de aluminio granallado con corindón de 1 mm, limpieza con acetona en un baño de ultrasonidos y secado con aire a presión.

En algunos casos (Tabla 1) las muestras se precalentaron durante 15 minutos a 200 ºC para mejorar la calidad y adherencia del recubrimiento.

Tabla 1. Variables de proyección estudiadas

Tamaño $MoSi_2$ (µm)	Precalentamiento	Condiciones de proyección			% Refuerzo	% Porosidad
		Distancia (cm)	Alimentación (g/s)	Capas		
< 125	No	15	0,6	1	1,2 ± 1,0	10 ± 3,1
				2	6,3 ± 2,3	2,6 ± 0,6
			1,1	1	3,9 ± 1,2	7,1 ± 1,8
				2	4,7 ± 0,2	6,7 ± 2,0
		20	0,6	1	4,9 ± 0,5	6,1 ± 1,9
			1,1	2	6,7 ± 2,3	6,6 ± 1,1
	Si	15	1,1	2	7,8 ± 2,4	2,3 ± 1,5
		20			6,2 ± 2,2	4,9 ± 1,5
< 25	No	15	1,1	1	2,1 ± 0,3	3,6 ± 2,7
		20		1	1,6 ± 0,5	3,4 ± 0,9
				2	0,8 ± 0,2	8,6 ± 1,6
	Si	15		2	1,1 ± 0,1	3,5 ± 0,8

2.3. Caracterización de los recubrimientos

La evaluación de la calidad de los recubrimientos de material compuesto fabricados se ha realizado mediante técnicas de caracterización microestructural (microscopía óptica y electrónica de barrido, en este caso se utilizó un microscopio Philips ESEM XL-30) y microanalíticas (EDX). Las medidas de porosidad y el grado de refuerzo se realizaron mediante análisis de imagen sobre secciones transversales en al menos cinco zonas diferentes.

Las medidas de rugosidad tanto del sustrato antes de proyectar, como del recubrimiento proyectado se han realizado en un rugosímetro Mitutoyo Surftest SJ-301.

3. RESULTADOS Y DISCUSIÓN

A la vista de los resultados de porosidad y grado de refuerzo de la tabla 1 se puede concluir que para conseguir recubrimientos de baja porosidad (2 %) y razonable grado de refuerzo (8 %), Figura 1a, las variables de proyección mejores son 15 cm y 2 capas, es decir, condiciones donde la temperatura es más elevada y por tanto la unión entre las gotas de aluminio es mejor.

Al realizar un precalentamiento al sustrato antes de proyectar se consigue una mejor unión sustrato-recubrimiento así como un aumento del grado de refuerzo y disminución de la porosidad que con el sustrato frío, Figura 1b. Esto es debido a que el aluminio al chocar contra el sustrato tarda más en enfriar produciendo una mejor unión de la intercara así como entre las gotas de aluminio. El aumento del grado de refuerzo se debe a que para que las partículas de $MoSi_2$ se adhieran al sustrato necesitamos que previamente se haya pegado aluminio y que éste tenga una fluidez suficiente cuando las partículas choquen no permitiendo que reboten.

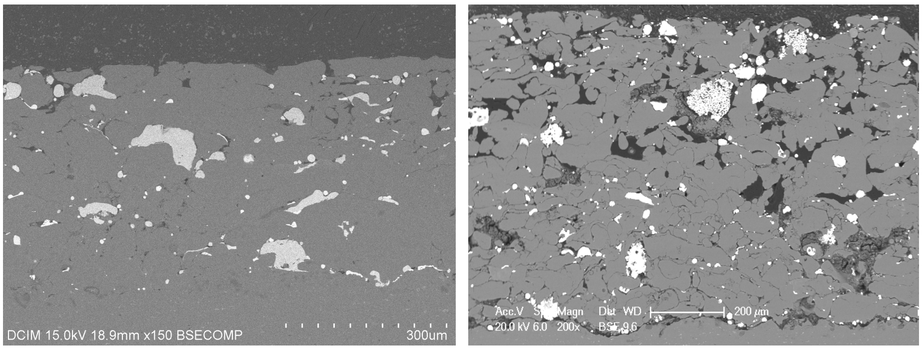

Fig. 1. Imágenes de SEM de la sección transversal del recubrimiento con partículas de $MoSi_2$ < 125 μm proyectado a 15 cm, alimentación del polvo de 1,1 g/s, dos capas, a) con y b) sin precalentamiento.

Para el menor tamaño de partícula empleado, el grado de refuerzo que se obtiene es muy bajo (1,6 %) y porosidades medias de un 3,5 %. Estos valores de porosidad son muy similares a los obtenidos por estos autores en trabajos anteriores cuando se proyecta aluminio sin refuerzo. El bajo rendimiento obtenido con las partículas de pequeño tamaño se debe a que éstas se aglomeran y no se mezclan adecuadamente con el aluminio, proyectándose en muchas ocasiones aluminio sin reforzar. Con las partículas de menor tamaño pequeño no se ha conseguido mejorar la calidad del recubrimiento que varia poco con los parámetros de proyección.

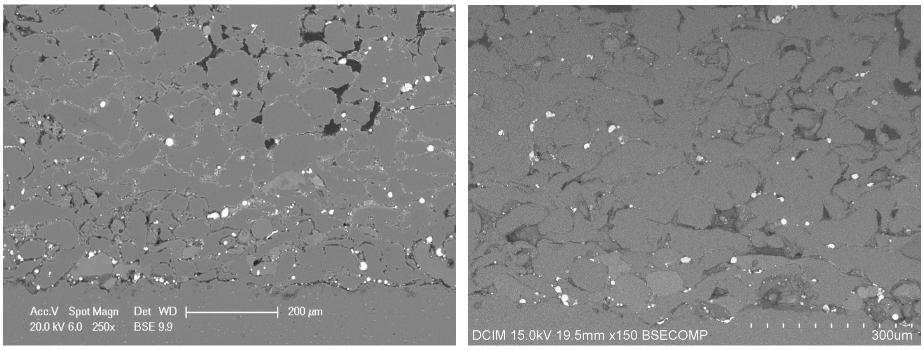

Fig. 2. Imágenes de SEM de la sección transversal del recubrimiento con partículas de $MoSi_2$ < 25 µm, proyectado a 15 cm, alimentación del polvo de 1,1 g/s, dos capas, a) sin y b) con precalentamiento.

4. CONCLUSIONES

Mediante la técnica de proyección térmica con llama oxiacetilénica se pueden fabricar recubrimientos de material compuesto reforzado con el intermetálico $MoSi_2$ con al menos un 8% de refuerzo y un 2% de porosidad.

El precalentamiento antes de la proyección térmica es un parámetro clave para conseguir recubrimientos bien adheridos con mayor grado de refuerzo y menor porosidad.

El tamaño de partícula de refuerzo afecta mucho al grado de refuerzo real obtenido en los recubrimientos.

Los recubrimientos de mayor calidad se consiguen con partícula de tamaño 125 µm distancias de proyección de 15 cm, alimentación del polvo alta (1,1 g/s) y dos capas de proyección.

AGRADECIMIENTOS

Los autores quieren agradecer al MEC los proyectos MAT2006-13179-C02-01, MAT2006-01251 y a la CAM el proyecto (S-0505/MAT/0077).

REFERENCIAS

RAMS J., CAMPO M., TORRES B., UREÑA A. (2008). Al/SiC composite coatings of steels by thermal spraying, Materials Letters 62, 2114-2117.

TORRES B., CAMPO M., UREÑA A., RAMS J. (2007). Thermal spray coatings of highly reinforced aluminium matrix composites with sol–gel silica coated SiC particles, Surface & Coatings Technology 201, 7552-7559.

TORRES B., CAMPO M., RAMS J. (2009). Properties and microstructure of Al–11Si/SiCp composite coatings fabricated by thermal spray. Surface & Coatings Technology 203, 1947-1955.

WANG Y., RAINFORTH WM., JONES H., LIEBLICH M. (2001). Dry wear behaviour and its relation to microstructure of novel 6092 aluminium alloy–Ni_3Al powder metallurgy composite. Wear, 250, 1421-1432.

Ferromagnetic Microwires Composite Metamaterials with Tunable Microwave Electromagnetic Parameters

M. Ipatov, L.V. Panina, V. Zhukova, J. Gonzalez, A. Zhukov
Dpto. de Física de Materiales, Fac. Químicas, UPV/EHU San Sebastián 20009, Spain
J.M. Blanco
Dpto. de Física Aplicada I, EUPDS, UPV/EHU San Sebastián 20009, Spain

ABSTRACT
The effect of the external magnetic field on microwave response from composites containing CoFeSiBCr amorphous wires has been demonstrated by measuring S-parameters in free space in the frequency band of 0.9-17 GHz. Two types of composites made of lattices of continuous and short –cut wires are measured. Application of the field results in increasing of the dielectric losses owing to increase in the wire impedance. The results are analyzed in terms of the effective permittivity.

1. INTRODUCTION

Composites with embedded metallic wires may demonstrate a strong dispersion of the effective permittivity ε_{ef} in the microwave range [1,2]. The use of ferromagnetic wires allows tuning this dispersion by changing the magnetic structure with external magnetic, mechanical or thermal stimuli. The possibility to control or monitor the electromagnetic parameters (and therefore scattering and absorption) of composite metamaterials is of great interest for like remote non-destructive testing, structural health monitoring, tuneable coatings and absorbers. The magnetic tunability of microwave response was reported earlier for different types of wire media demonstrating that underlying physics is related with the magnetoimpedance (MI) effect in wires [3]. In this work, we consider two types of magnetic wire composites: arrays of continuous wires and of short-cut CoFeSiBCr glass coated amorphous wires showing large MI [4].

2. EFFECTIVE PERMITTIVITY OF WIRE MEDIA

Composites containing long parallel wires can be characterised by plasma-like dispersion of ε_{ef} [1-2] with a negative value of the real part of the permittivity below the characteristic plasma frequency, f_p :

$$\varepsilon_{ef}^2 = 1 - \frac{\omega_p^2}{\omega^2 (1 + i\gamma)}, \quad \omega_p = 2\pi f_p, \quad f_P^2 = \frac{c^2}{2\pi b^2 \ln(b/a)} \tag{1}$$

Here, γ is the relaxation parameter and c is the velocity of light. For wire radius a in the micron range and spacing b between them of about 1cm the characteristic plasma frequency is about 4 GHz. A number of experimental studies confirmed a negative permittivity in the GHz region for wire media. We have demonstrated that in general γ is defined by the wire surface impedance ς_{zz} :

$$\gamma = \frac{c\varsigma_{zz}}{\omega a \ln(b/a)} \tag{2}$$

This parameter may change under applied magnetic field, H_{ex}, as a result of the MI effect. Then, the permittivity spectra will depend on H_{ex} (see Fig. 1a). The composites with short-cut wire inclusions are characterized by a resonance type of ε_{ef} where wires behave as dipole antennas with the resonance at half wave length condition: $F_{res} = c/2l\sqrt{\varepsilon_d}$, where ε_d - permittivity of the matrix. If the interaction between the wires is small, ε_{ef} is composed of the averaged dipole polarization χ and may be expressed analytically for the case of not very strong skin effect [3]:

$$\varepsilon_{eff} = \varepsilon + 4\pi p\chi\,,\ \chi = \frac{1}{2\pi \ln(l/a)(\tilde{k}a)^2}\left(\frac{2}{\tilde{k}l}\tan(\tilde{k}l/2) - 1\right), \tag{3}$$

$$\tilde{k} = k\left(1 + \frac{ic\varsigma_{zz}}{\omega a \ln(l/a)}\right)^{1/2},\ k = \omega\sqrt{\varepsilon}/c \tag{4}$$

Here p is the wire volume concentration and, $\tilde{k}$ is the renormalized wave number. Comparing equations (2) and (4) it is seen, that in both cases the dependence on the wire surface impedance occurs in a similar way, controlling the dielectric losses in the case of a moderate skin effect. The permittivity spectra for short-cut wire composites are given in Fig. 1b. It is seen that applying a magnetic field which increases the wire impedance suppresses the resonance behavior due to increased losses.

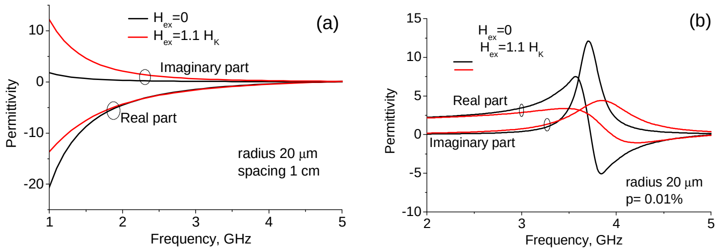

Fig. 1. Effective permittivity spectra in composites depicted in Figs.1a,b, respectively, with H_{ex} as a parameter. Modelling is performed for wires with a circumferential anisotropy (anisotropy field H_k=500A/m). The other parameters are: resistivity 130μΩcm, magnetisation 0.05T, wire radius 20 μm. For (a), b=1cm. For (b), l=4cm, p=0.01%.

Amorphous ferromagnetic microwires exhibit large MI effect even at GHz frequencies. This makes them very promising for engineering artificial dielectrics with tuneable microwave properties. It is expected that any physical effect (magnetic field, mechanical stress, temperature) that results in change in the magnetic structure (whilst the ac permeability remains high) will affect the dispersion of the effective permittivity.

3. EXPERIMENTAL

The microwave properties of wire composites were investigated by free space methods. $Co_{66}Fe_{3.5}B_{16}Si_{11}Cr_{3.5}$ glass coated amorphous wires with radius of 20 μm were glued in paper to form wire-lattices of 50x50 cm^2 with separation b of 10 mm. After measurements, such wire-lattice was sequentially cut in stripes of 40, 20 and 10 mm wide to form the composites with short dipole wires. The S-parameters were measured at 0.9-17 GHz in the presence of external field ranging up to 3000A/m applied through a plane coil with turns perpendicular to the electrical field in the incident wave. The effective permittivity spectra were deduced from S-parameters with the help of Reflection/Transmission Epsilon Fast Model. The MI was measured in the frequency range up to 500MHz.

4. RESULTS AND DISCUSSION

The impedance plots vs. field seen in Fig. 2 have two symmetrical peaks, typical of circumferential anisotropy and the impedance change ratio up to 300% at 500 MHz.

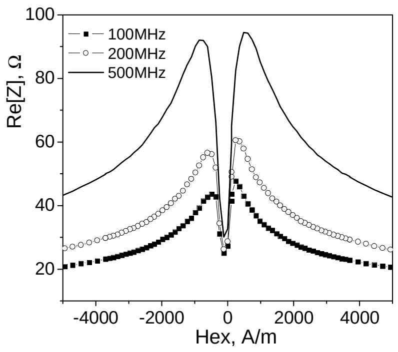

Fig. 2. Wire impedance vs. field for different frequencies.

The relative change in *R* and *T* is about 10% at lower frequencies while the phase of transmission shifts about 40 degrees at 1 GHz with the change of the field (Fig.3). The permittivity spectra deduced from *R* and *T* plots are consistent with the theoretical plots seen in Fig. 1a. The effective thickness was taken equal to the lattice period of 1 cm. The imaginary part of the permittivity increases with the field due to the increase in the wire impedance resulting in decrease in the transmission amplitude (although the reflection amplitude also decreases).

Figure 4 shows the spectra for cut-wire composites with different wire length of 40, 20 and 10 mm and with the field as a parameter.

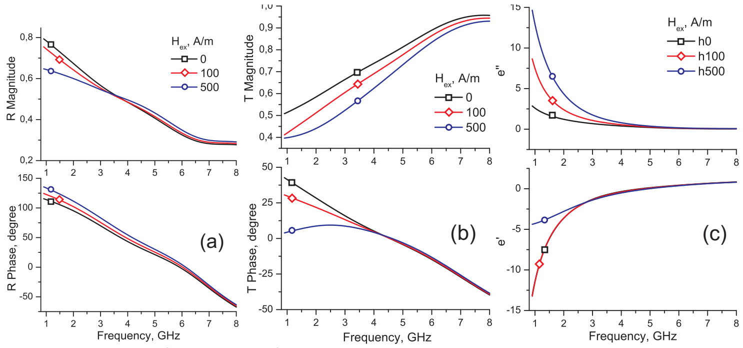

Figure 3. Spectra of *R*, *T* and ε_{ef} for composites with long wires with H_{ex} as a parameter (H_{ex}=0,100, 500A/m).

The transmission spectra have a deep minimum near a resonance demonstrating a stop filter behaviour. The magnitude of this minimum depends strongly on the field for longer wires with lower resonance frequency, F_{res}. For shorter wires the field dependence is not noticeable since the wire ac permeability is nearly unity and the impedance becomes insensitive to the magnetic properties. The phase of the transmitted wave shows reversal behaviour near F_{res} which sensitively shifts with the field.

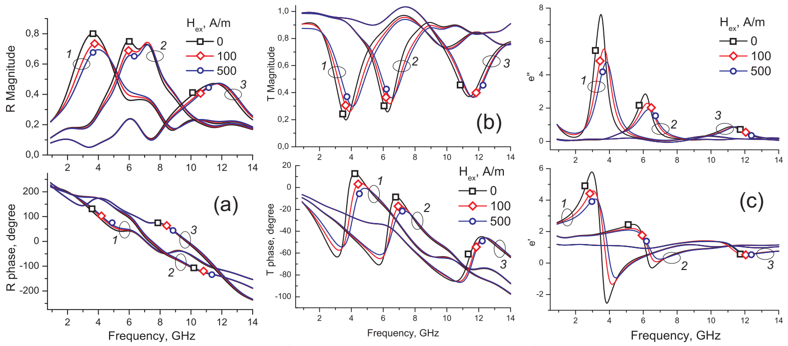

Figure 4. Spectra of *R*, *T* and ε_{ef} of composites with cut wires of length 40 (1), 20 (2) and 10 (3) mm with the field as a parameter.

Fig. 5 shows the $F_{res}(H_{ex})$ dependence of the resonance frequency F_r on magnetic field for composite with 40 mm inclusions. The similar form has the minimum of transmission magnitude T_{min} that is a result of a dumping increasing with magnetic field.

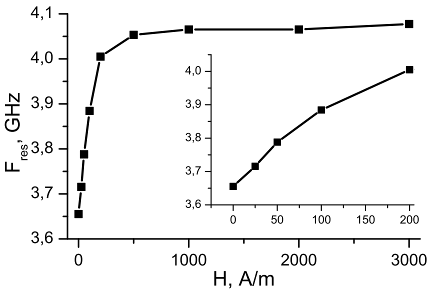

Figure 5. $F_{res}(H_{ex})$ dependence for composite with 40 mm long wires.

5. CONCLUSIONS

We report on magnetic field dependence of the dielectric response in composites with arrays of parallel magnetic wires, continuous and short-cut, in the frequency region of 0.9-17 GHz. Both the real and imaginary parts of ε_{ef} show strong variations with increasing H_{ex} owing to the MI effect which controls the losses in the dielectric response. Long-wire composite has a plasmonic type dispersion of ε_{ef} with negative values of its real part below the plasma frequency (GHz range) for wire spacing of about 1 cm and wire diameter of few microns. The presence of H_{ex} suppresses low-frequency plasmons increasing the value of the real part of the permittivity. For cut-wire composites we confirmed a resonance type of ε_{ef} dispersion due to the dipole resonance in wires at half wavelength condition. Application of H_{ex} broadens the resonance and shifts it towards the higher frequencies. Therefore, both types of wire composites exhibit strong ε_{ef} (H_{ex}) dependence suitable for applications.

We acknowledge support under projects MAT2007-66798-CO3-01 (MEC) and Saiotek 08 METAMAT (SPRI).

REFERENCES

1. Rotman W., “Plasma simulation by artificial dielectrics and parallel plate media,” *IRE Trans. Antennas Propagat.*, vol. 10, 82–95, 1962.
2. Pendry, J. B., A. J. Holden, W. J. Stewart, and I. Youngs, “Extremely Low Frequency Plasmons in Metallic Mesostructures,” *Phys. Rev. Lett.*, Vol. 76, No. 25, 4773-4776, 1996.
3. Makhnovskiy D. P., L. V. Panina, “Field dependent permittivity of composite materials containing ferromagnetic wires,” *J. Appl. Phys.* **93** 4120, 2003.
4. Zhukova V., M. Ipatov, A. Zhukov, J. Gonzalez, J.M. Blanco “GMI effect in ultra-thin glass-coated Co-rich amorphous wires,” *Sens. Acruators B-Chem.* Vol. 126, 318-323, 2007.

T4. OTHER MATRIX COMPOSITES
MATERIALES COMPUESTOS DE OTRAS MATRICES

Environmental electron microscopy (ESEM) and energy dispersive microanalysis (EDS) in a FPP/cement matrix composite

J.M. Rincón, M. Romero, Mª.S. Hernández-Crespo,
R. Talero
Departamento de Sistemas Constructivos,
Instº. E.Torroja de Ciencias de la Construcción,
CSIC, Madrid, Spain
A. García- Santos
Departamento de Construcción y Tecnología Arquitectónica,
Escuela Superior de Arquitectura, Universidad Politécnica de Madrid, Spain

ABSTRACT

A cementicious composite of polypropilene fibers (FPP) embedded into cement matrix has been full characterized by ESEM , FESEM (field emission electron microscopy) and X- rays energy dispersive analysis (EDX). The bulk microstructure is very homogeneous depicting an uniform distribution of fibers into the matrix ; however, the final surface of sample after solidification is different according to the contacts areas of mold, giving rise to layered surface in some cases. Interfaces among crystalline phases of cement matrix. From the mechanical testing of this material it is considered suitable the content of 2.5% of polypropilene. In this paper are presented and discussed the microanalytical results showing a high degree of local heterogeneity in the composition of the C –S -H amorphous phase.

1. INTRODUCTION

Since time it is well known that growing of crystals from ionic solutions such as the water content, the cement phases are affected by the presence o heterogeneous phases as is the case of fiber/ cement matrix composites (Egli et al, 1963). Cements and fibers are compatible, because the adhesion force of cement matrix composites is reached from the forces due to the secondary connections and to the mechanical interconnection among fibers, as well as the irregularities of contact surfaces (Sanders,1982). The additions of fibers to cement matrices facilitate the absorption of internal tensions in the bending strength of fibered dispersion phase and the compressive strength in the cement matrix, as was demonstrated in previous work by introduction of polypropylene short fibers into a standard type mortar cement (García- Santos et al, 2004) (Rincón et al., 2005). The aim of this research was to characterize and discuss the microstructure and microanalytical composition of this type of composite by ESEM and EDS.

2. MATERIALS AND METHODS

2.1. Materials

As matrix for the composite was used a cement CEM-II-32.5B, which was prepared by following the spanish cement standards UNE 80301 and UNE- ENV 197-1-IN. The initial composite formulation was: 68% of Portland clinker, 20 % of natural puzolane, 12% of limestone and 3.07 of sulphates without chlorides as inorganic addition. After experimental determination of fractions, this composite contains (wt%): aggregates = 82.77 %, cement = 15.11% and fibers = 2.12% with a ratio cement/ aggregate = 1/5.5. The polypropylene fibers (FPP) were 20 mm average lengh.

The media for aggregation of FPP was melamine formaldehyde (MF) (Melment F-10) and percentages in the 0.1-0.3 % volume fraction range. The ratio cement/ aggregate of 1/ 3/ 0.5 with pH = 7 for water and curing dates of 7 and 28 days.

2. 2. Methods

The mechanical resistance testing was determined by the UNE EN 196-1 standard method and detailed microstructure observations have been carried out in the sample 25-115-3 (2% FPP addition with 0.5 % MF and 28 days of curing). Electron microscopy with analytical spectrometers have demonstrated is a very valuable method for knowledgment of inorganic materials (Rincon et al, 1998, 2001). More recently, the Environmental Scanning Electron Microscopes (ESEM) have been very useful for observation of hydrated specimens (Cameron,1994). In this case it has been used a Philips XL- 30 instrument with EDS Edax spectrometer. ESEM allows the observation of samples with different content of water phase without inherent damage and conduction problems coming from electron irradiation or lack of conductivity. The imaging from secondary electrons in this case is possible due to a gas secondary electron detector (GSE) working in water pressure of 2.0 Torr and was used at 20 kV acceleration voltage, 20 mA current intensity

3. RESULTS AND DISCUSSION

From electron microscopy observations the presence of phases were: portlandite, calcium aluminate hydrates, calcium silicate hydrates (C-S-H gel) and small content of ettringite (García- Santos et al., 2005) (Rincón et al., 2004). Amorphous areas which contain a few fine acicular crystallites (3-7 microns length by 0.5 microns width) of ettringite were seen, as well as globular high contrast in several zones. Calcium silicate hydrates ($x\mathrm{CaO} \cdot y\mathrm{SiO_2} \cdot m\mathrm{H_2O}$ gel, which usually is written as C–S–H (Bentur et al., 1979) has not exact chemical composition. Thus this amorphous gel usually is (wt.%): $40–48\mathrm{SiO_2} \cdot 20–42\mathrm{CaO} \cdot 5–13\mathrm{Al_2O_3} \cdot 2–9\mathrm{MgO} \cdot 2–5\mathrm{Na_2O} \cdot 5–6\mathrm{K_2O} \cdot 4.8–5.1\mathrm{Fe_2O_3}$, with a $\mathrm{CaO/SiO_2}$ ratio of 0.5–0.9.

The ettringite ($6\mathrm{CaO} \cdot \mathrm{Al_2O_3} \cdot 3\mathrm{SiO_2} \cdot 32\mathrm{H_2O}$), also named in the literature usually with the abbreviation: AF_t^{19} is an expansive phase. The Figure 1 shows a drawing of the composite specimen where the detailed microstructure investigation was carried out depicting the several surface areas observed by ESEM. The area A corresponds to a removed sheet layer of the superior surface (compression zone); area B corresponds to the fracture surface produced as a consequence of the rupture after the bending testing showing the edges of fibers. The C area corresponds to a relatively smooth surface in contact with the mold; the D area corresponds to an inferior area (tensile zone) that appears lifted or swollen. The E area is an interface area of an almost cubic type break block produced along the test specimen by shear effect in this area.

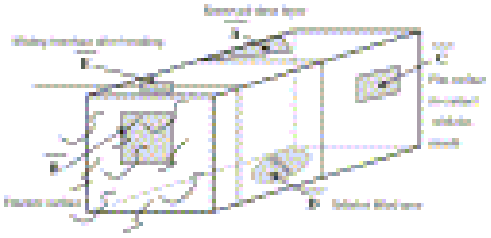

Fig. 1. Sample of FPP/ cement composite showing the areas of observations and microanalysis by ESEM (Rincón et al, 2004 y García Santos et al., 2005).

Oxide (wt%)	sample surface	Surface slided	Fractured surface 1 (bending test)	Fractured surface 2 (bending test)	Interface (fractured and slided surfaces)	EDS average
SiO_2	48.19	40.82	18.89	44.38	11.82	79.92
CaO	41.79	31.71	56.40	20.05	43.89	14.37
Al_2O_3	4.61	12.66	14.51	10.78	13.11	2.76
MgO	3.93	2.68	5.28	9.02	10.30	0.49
Na_2O	1.47	1.55	-	4.71	-	1.01
K_2O	-	5.14	-	5.92	-	0.79
Fe_2O_3	-	4.78	4.93	5.14	15.44	0.15
SO_3	-		-	-	3.95	0.48
Cl^-	-	0.66	-	-	-	0.005
Ca/ Si	1.31	1.20	4.55	0.69	5.65	0.18

Table 1. EDS microanalysis from different areas showed in Figure 1 from the FPP/ cement composite.

The Table 1 shows the EDS microanalysis from several C-S-H gel areas of prismatic fractured sample of the FPP/ cement composite here investigated. The CaO/ SiO_2 ratios are given in order to evaluate the different C-S-H gels detected in this composite. It has been observed that composition of C-S-H gel differs from different areas. It is well known when Ca/ Si ratios are 1.1 the gel is considered puzolanic and when this ratio is 1.7 it is considered primary origin. Lower ratios decrease the chloride diffusivity in cements and protect from corrosion as is the case of cements with silica fume additions. As is well known this gel has not constant composition.

4. CONCLUSION

A composite material with addition of MF and single addition of synthetic fibres of polypropylene as element of reinforcement for a cement matrix produces an increment of the bending mechanical resistance in the face of tensions according to the percentage of fibre addition. This improvement in strength is higher with the addition of MF. From the analysis of the mechanical behaviour, it is considered suitable the proportion of single addition of 2.0% of fibre of polypropylene giving the best values simultaneously for the bending and the compressive strength. A high degree of compatibility has been observed between the polypropylene fibres and the mentioned matrix with precipitation of crystallites over the fibres surface. However, the composition of C-S-H gel matrix phase is very heterogeneous with strong variations on spot analysis made by ESEM /EDS microanalysis, due to the high diffusion of components which takes place in this gel phase.

ACKNOWLEDGEMENT

This cooperative research has been made in the frame of the Cooperation Agreement between the Madrid Polytechnic University (UPM) and the CSIC (Consejo Superior de Investigaciones Científicas).

REFERENCES

BENTUR, A. and BERGER, R. L. (1979). Chemical composition of C-S-H gel formed in the hydration of calcium silicate pastes. *J. Amer. Ceram. Soc*, 117-125.

EGLI, P.H. and JOHNSON, L.R. (1963) The art of science of growing crystals (Ed. Gilman J. J.), Wiley, New York, p. 194.

GARCIA SANTOS, A., Rincón, J. Ma., Romero, M. and Talero, R. (2005).Characterization of a FPP cement composite using ESEM, FESEM and mechanical testing. Constr. Build. Mater. 19, 396-403.

RINCON J. Ma. and ROMERO, M. (1996) Microstructural Charact. by Electron Microscopy of Ceramics and Glasses. *Microscopy and Analysis*, nov. 23-25.

RINCON J. Ma. and ROMERO, M. (1998) Characterization Techniques of Glasses and Ceramics (Ed. Springer- Verlag), Heidelberg, Berlin.

RINCON, J. Ma., ROMERO, M., HERNÁNDEZ- CRESPO M., TALERO, R. and GARCIA SANTOS, A. (2004). Microestructura y propiedades mecánicas de un composite de fibras de polipropileno en matriz de cemento. Mater. Construcc. 54 (274), 73-82.

SANDERS B.A. (1982) Short fiber reinforced composite materials (Ed. ASTM).

TAYLOR, H.F.W. (1986). Proposed structure for calcium silicate hydrate. *J. Amer. Ceram. Soc.* 28, 265-277.

Mechanical properties of plaster reinforced with polyamide fibres obtained from shredded tires

F. Parres, J.E. Crespo-Amorós, A. Nadal-Gisbert
Department of Mechanical and Materials Engineering, Polytechnic University of
Valencia, Plaza Ferrandiz y Carbonell, 2; 03801; Alcoy – Alicante (Spain)

ABSTRACT

The importance of recovering waste materials generated by industrialised societies is mainly due to the environmental impact they have, and one of the principal problem areas is tires. In recent years, an enormous amount of tires has been recycled. The metals they contained have been recovered and the tire particles have been used in several applications. Fibres acting as reinforcement are another material that appear in the recovery process. Before addressing the possible re-use of these fibres, they have to be characterised and identified. Several techniques of thermal analysis allow these fibres to be identified through melt point analysis, whose results show the presence of polyamide 6 and 6.6. Polyamide fibres have been frequently used as a ceramic reinforcement and polymer matrix, and the most important benefit they contribute to is to avoid a catastrophic failure of the ceramic material in two pieces. The compression and bending test show differences between samples prepared with different percentages of fibre.

1. INTRODUCTION

In recent years, the re-use of waste materials has become extremely important for two main reasons: economic and environmental. With the first of these, the recovery of material often means a reduction in manufacturing costs of certain products which enables them to compete with virgin products. However, it is the second reason, the environmental impact factor, which is assuming greater importance nowadays. Over the last decade many governments have imposed legislation to deal with this problem. In the case of thermoplastics, recovery processes are generally not very complicated and the simple use of heating allows new products with similar characteristics to be obtained. On the other hand the recovery of other materials such as tires is more complicated as new tires cannot be manufactured by recycling old ones. One of the solutions adopted has been the use of recycled tires in other applications such as acoustic insulation, flooring for children's parks and other products obtained from shredded tires. In the tire recovery process several types of fibres are also obtained, including fibres incorporated in the tires for reinforcement.

Fibres, in general, have been used by several authors in order to improve mechanical properties of fragile materials. In ceramic materials, fibres help prevent the crack from advancing from its origin and also avoid the piece breaking completely in two. Plaster, traditionally, has traditionally used glass fibre as reinforcing agent, but recently there are some papers where they study the properties of ceramic materials reinforced with polymer fibres (Camli, U.S., et al. 2007,Xiao, J.Z., et al. 2004). The aim of this research has been the use of fibres from shredded tires that act as plaster reinforcement.

2. EXPERIMENTAL

Materials

Fibres derived from the tire shredding process, were supplied by Industrias del Neumatico, S.A., Aspe (Alicante) - Spain. Plaster prepared by hydration with a water ratio of 0.8 is the material used in this research.

Mechanical properties measurements

The mechanical properties of the samples were evaluated using an ELIB 30 electromechanical universal testing machine by Ibertest (S.A.E. Ibertest, Madrid, Spain), with two load cells (5 and 50 kN) to determine the flexion resistance and compression strength of the test pieces.

3. RESULTS AND DISCUSSION

Mechanical properties

The addition of fibres in the plaster mold causes important differences as far as its mechanical performance under different load stages (flexural and compression) is concerned. The flexure test with a lack of fibre is characterized by a lineal performance until the maximum flexure value (σ_r); once this value has been reached, the rupture of piece is completed and the flexure decreases sharply until zero. Nevertheless, the existence of fibre causes variations in the rupture process, because once the maximum flexure value has been reached, it decreases sharply until the fibre starts to act and the tension (σ_s) is stabilized by the interaction of the fibre with the mold phase (plaster).

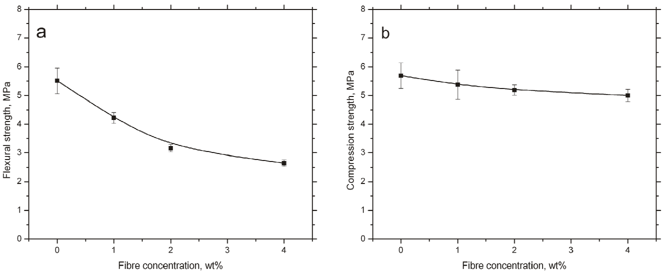

Fig. 1. Evolutions of the flexural strength and compression strength of plaster reinforced with PA recycled fibres.

The connection between σ_r and σ_s is known as fibre efficiency factor (FEF) and its value is between 0 and 1, being the highest values indicative of the early performance of the fibre. The performance of plaster with fibre is very different depending on the type of effort applied. In the case of the test failure, the addition of fibre causes a sharp decrease in the flexural strength until reaching a loss of 50% for a fibre contents of 4% (Fig. 1-a). Nevertheless, the addition of fibre in plaster causes a different effect on properties obtained after the compression test. In this case, the value evolution shows a slight decrease which represents a loss of only 12% (Fig. 1-b).

The major benefit of the presence of fibres is to avoid a catastrophic failure of the material in two pieces. In this case, and as has been repeated in other research, the fibre efficiency factor (FEF) value increases with the fibre percentage, and reaches a value of 0,5 for contents of 4% of fibre (Eve, S., et al. 2002,Eve, S., et al. 2006,Eve, S., et al. 2004) (Fig. 2). Given that microfibre is 86% of the total weight of fibre and that fibres smaller than 20 mm represent the biggest percentage (98%) of the fibre obtained after the tire´s recovery process, the mixture of plaster with separate fibre, plaster with microfibre (1, 2, and 4 wt%) and plaster with fibre less than 20 mm (1, 2, and 4 wt%) is considered.

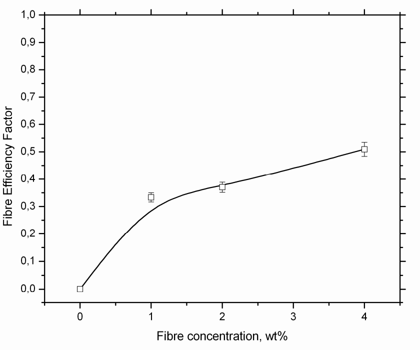

Fig. 2. Evolution of the fibre efficiency factor of plaster reinforced with PA recycled fibres.

In both cases, results show a very similar evolution in flexural strength to that of compression strength, where the increase of the fibre percentage causes a decrease of the flexural strength while the compression strength values remain practically constant (Fig. 3).

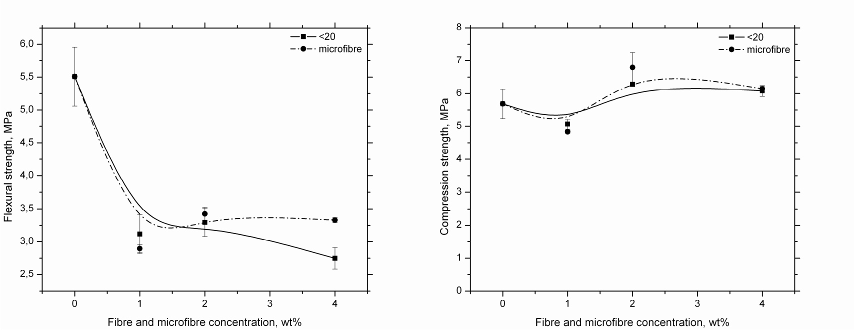

Fig. 3. Evolution of the flexural and compression strength of plaster reinforced with PA microfibres and fibres <20 mm.

Nevertheless, the fibre efficiency factor values show some important differences. The plaster mixtures with microfibre show higher values than the ones with fibre.

Results show also more efficiency in microfibre, since for low percentages of this (1%), FEF show positive values (0.25). But, with the same percentage, the fibre isn´t able to act and its FEF is zero. This effect is due to a greater level of dispersion of the microfibre in the plaster mold (Fig. 4).

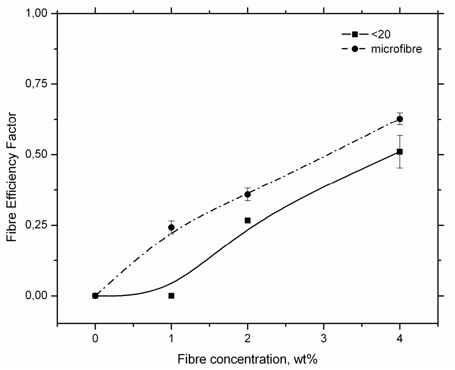

Fig. 4. Evolution of the fibre efficiency factor of PA microfibres and fibres (<20mm).

4. CONCLUSION

The results obtained by the mechanical characterization of mixtures of plaster with fibre and of plaster with microfibre do not differ from the ones obtained with the non-divided fibre. Despite the results obtained with the microfibre being slightly higher than the others due to its greater dispersion, the difficult process of division of fibres in two pieces (fibre and microfibre) doesn't compensate for the improvement obtained in the results. To sum up, the direct use of fibres obtained from shredded tires as plaster reinforcement is viable.

REFERENCES

Camli, U.S., Binici, B. (2007) Strength of carbon fiber reinforced polymers bonded to concrete and masonry.21:1431-1446.
Eve, S., et al. (2002) Microstructural and mechanical behaviour of polyamide fibre-reinforced plaster composites. *J. European Ceram. Soc.*;22:2269-2275.
Eve, S., et al. (2006) Investigation of the setting of polyamide fibre/latex-filled plaster composites. *J. European Ceram. Soc.*;26:2541 - 2546.
Eve, S., et al., *Euro Ceramics VIII: Effects of polyamide and polypropylene fibres on the setting and the mechanical properties of plaster*, 264-268, 2531-2535.
Xiao, J.Z., et al. (2004) Experimental study on bond behavior between FRP and concrete.18:745-752.

Nuevos materiales compuestos carbono-carbono 3D para aplicaciones en fusión

A. Centeno, C. Blanco, R. Santamaría, M. Granda, R. Menéndez
Instituto Nacional del Carbón, CSIC, Apdo. 73, 33080-Oviedo, España
G. Pintsuk, J. Linke
Forschungszentrum Jülich, EURATOM Association, 52425, Jülich, Alemania
C. Gualco
Ansaldo Ricerche S.p.A., I-16152, Genova, Italia

RESUMEN

En este trabajo se desarrollaron materiales compuestos carbono-carbono 3D dopados con nanopartículas de carburo de titanio, estudiando la influencia del dopante en la estructura y propiedades de los materiales resultantes, así como su comportamiento bajo flujos de alta energía. Con el material de mejor comportamiento se diseñó un módulo del cual se estudió su respuesta a fatiga térmica.

1. INTRODUCCIÓN

Los materiales compuestos carbono-carbono (CFCs) se han propuesto como materiales para la zona de la primera pared que contiene el plasma en el ITER, primer prototipo de reactor termonuclear de fusión para demostrar la viabilidad de esta forma de energía, debido a sus excelentes propiedades termomecánicas (Barabash et al., 1998). Sin embargo, es necesario mejorar aún propiedades como conductividad térmica, resistencia al choque térmico y erosión química, directamente relacionadas con la destrucción del material (Würz et al., 2002).

Se ha demostrado que la adición de TiC a grafitos contribuye eficazmente a un aumento de la conductividad térmica de los mismos, junto con la mejora de la resistencia a la erosión química por bombardeo de hidrógeno (García-Rosales et al., 2009). Por ello, en este trabajo se aborda el desarrollo de CFCs dopados con TiC, para conseguir mejorar sus propiedades. Los materiales desarrollados fueron caracterizados y finalmente se estudió su comportamiento en ensayos de fatiga térmica.

2. EXPERIMENTAL

Una brea de mesofase (AR) comercializada por *Mitsubishi Gas Chemical* se utilizó como precursor de matriz para densificar una preforma 3D con tejido ortogonal suministrada por *SGL Carbon Group, y* compuesta de haces de fibras de carbono de brea (eje-*x*) y PAN (eje-*y* y *z*). Las preformas se densificaron mediante impregnación líquida con el precursor de matriz, bien AR o el precursor dopado (AR con 10 % en peso de nanopartículas de TiC) (Centeno et al., 2009). Tras varios ciclos de densificación, los materiales se grafitizaron a 2700°C. El material no dopado se denominó CFC y el dopado Ti-CFC. Ambos se caracterizaron atendiendo a su microestructura y propiedades termo-físicas.

Los materiales se expusieron a cargas térmicas transitorias en el equipo de haz de electrones JUDITH, para simular condiciones de operación en un reactor de fusión. Los ensayos de choque térmico se llevaron a cabo en muestras con los haces de fibra de brea dispuestos paralelamente a la dirección de transferencia de calor. Los materiales se expusieron a cargas térmicas de 1, 1,6 y 2,4 GW/m^2 durante pulsos de 5 ms y aplicando múltiples disparos. Varios diagnósticos fueron utilizados para seguir el comportamiento del material y la microscopía electrónica de barrido se utilizó para comprobar la integridad del mismo.

El módulo final para su ensayo a fatiga térmica fué desarrollado con Ti-CFC. Se utilizaron 3 piezas del material de 20x27x5 mm unidas a un bloque de CuCrZr (disipador de calor), utilizando una interlámina de molibdeno. La unión de los componentes se llevó a cabo bajo tratamiento térmico a 1035ºC a vacío durante 18 minutos, utilizando una aleación Cu-ABA en la unión con el CFC y una aleación Gemco en la parte de unión al CuCrZr. El módulo se sometió a ensayos de “choque térmico” consistentes en el calentamiento hasta 450ºC seguido de un rápido enfriamiento en agua hasta temperatura ambiente para comprobar la unión de los componentes. Adicionalmente, se llevaron a cabo estudios de microscopía óptica y SEM para comprobar la calidad de la unión. El módulo fue expuesto a ensayos de fatiga témica en JUDITH aplicando múltiples ciclos de cargas térmicas a 15 MW/m^2 y 20 MW/m^2. Durante los ensayos se utilizó una cámara de infrarrojos para detectar la formación de puntos de sobrecalentamiento y erosión en el material. Tras los ensayos el modulo se analizó mediante microscopía óptica para identificar dónde se produjo el fallo.

3. RESULTADOS Y DISCUSIÓN

La Tabla 1 muestra algunas de las propiedades de los materiales desarrollados. Ambos materiales presentan una conductividad térmica muy elevada (>200 W/mK), que es significativamente mayor en el caso del material dopado (288 W/mK), como consecuencia del efecto catalítico que tiene el titanio sobre la grafitización.

Materiales	Porosidad abierta (%)	Porosidad cerrada (%)	Densidad geométrica (g/cm^3)	Ti en matriz (at.%)	Ti en CFC (at.%)	C. térmica (dirección-x) (W/mK)
CFC	17	0	1,70	-	-	220
Ti-CFC	17	0	1,74	~3	0,6	288

Tabla 1. Propiedades termo-físicas de los materiales.

En la Figura 1 se muestran imágenes de SEM del material Ti-CFC tomadas en la dirección del eje-x. La imagen (b) muestra la buena dispersión del TiC en la matriz, con tamaños de partícula sub-micrométricos.

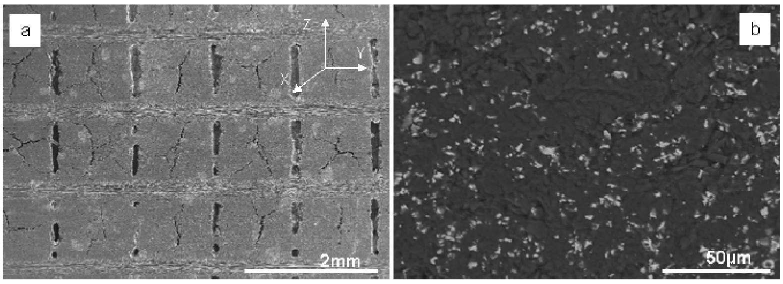

Fig. 1. Imágenes SEM de Ti-CFC.

3.1 Comportamiento del material expuesto a intensas cargas térmicas

Tras la aplicación de las cargas térmicas, las zonas más erosionadas se corresponden con los haces de fibra PAN orientados en dirección perpendicular a la carga aplicada. Esto es debido a la baja conductividad térmica que presentan en dicha dirección y que por tanto, hace que no sean capaces de evacuar eficazmente la energía depositada en ellas. En el caso de las fibras de mesofase la conductividad térmica es muy superior, lo que permite una buena disipación del calor y una erosión prácticamente insignificante. A pesar de ello, como consecuencia del sobrecalentamiento que ocurre en las fibras PAN, las fibras de brea que se encuentran próximas a ellas (en la interfase entre ambos haces), también son erosionadas. En último término lo serán las fibras del centro del haz.

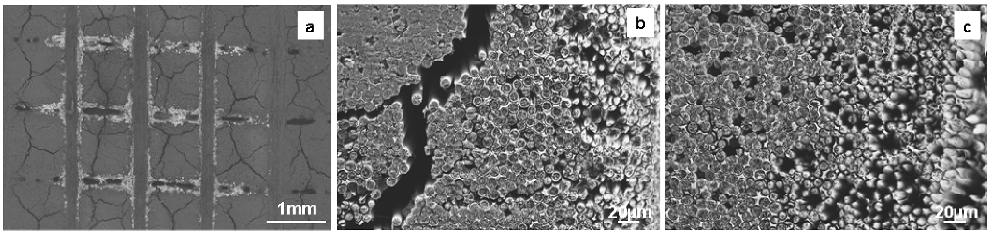

Fig. 2. Imágenes de SEM: a) Ti-CFC ensayado a 1,6 GW/m^2, 5 ms, 10 x b) Ti-CFC y c) CFC, fibras de brea próximas a la interfase haces de fibras PAN/brea sometidos 1,6 GW/m^2, 5 ms, 100 x.

El análisis de la superficie erosionada muestra en Ti-CFC un enriquecimiento de carburo en la superficie (imagen a) y en general una erosión menor del material. CFC mostró un mayor número de fibras afectadas en la interfase (hasta ~ 120 µm de distancia a la interfase frente a ~ 60 µm en el material dopado, imágenes b y c). La erosión en las fibras del centro del haz también fue muy inferior en los materiales dopados.

3.2 Ensayo de fatiga térmica

El material mostró un buen comportamiento a fatiga térmica. Una de las piezas soportó 100 ciclos a 15 MW/m^2 seguidos de 62 ciclos a 20 MW/m^2, mientras que en las otras dos se observaron puntos de sobrecalentamiento en ciertas áreas. Para comprobar porqué ocurrió el fallo en esas zonas concretas del material se comprobó mediante microscopía óptica que el sobrecalentamiento fue debido a un fallo en la unión de los componentes.

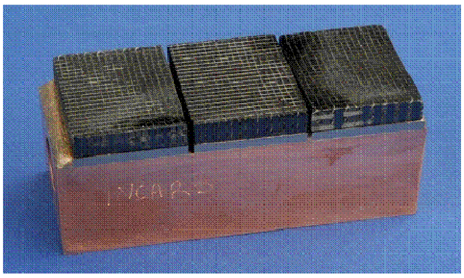

Fig 3. Módulo tras el ensayo de fatiga térmico.

4. CONCLUSIONES

Los materiales desarrollados tienen una conductividad térmica muy elevada, especialmente el que contiene TiC, presentando una mejora significativa en la resistencia al choque térmico. El módulo preparado con dicho material mostró un buen comportamiento en ensayos de fatiga térmica y por ello es prometedor como material de revestimiento de la primera pared en reactores termonucleares de fusión.

AGRADECIMIENTOS

Este trabajo ha sido desarrollado en el marco del proyecto europeo “EXTREMAT” (NMP-CT-2004-500253) financiado por la Unión Europea y por el Programa Nacional de Cooperación Internacional de Ciencia y Tecnología (MAT2004-22787-E).

REFERENCIAS

BARABASH, V. et al. (1998). Carbon fiber composites application in ITER plasma facing components. *Journal of Nuclear Materials* 258-263 (Part 1): 149-159.
CENTENO, A. et al. (2009). Development of titanium-doped carbon-carbon composites. *Journal Materials Science*, DOI 10.1007/s10853-009-3327-9.A.
WÜRZ, H. et al. (2002). Macroscopic erosion of divertor and first wall armour in future tokamaks. *Journal of Nuclear Materials* 307-311(Part 1): 60-68.
GARCIA-ROSALES, C. et al. (2009). Ti-doped isotropic graphite: A promising armour material for plasma-facing components. *Journal of Nuclear Materials* 386-388: 801-804.

Comparative study on the thermal stability of modified asphalt by styrene-butadiene-styrene (SBS) and ethylene-vinyl acetate (EVA) copolymers

M. Kaci[1], N. Dehouche[1], K. Ait Mokhtar[2]
[1]Laboratoire des Matériaux Organiques, Faculté de la Technologie, Université de Bejaia, Algeria
[2]Laboratoire des Routes et Aérodromes, Faculté de Génie Civil, USTHB, Alger, Algeria

ABSTRACT

One of the primary uses for asphalt is in road construction. Even though, asphalt constitutes only a small fraction of the complex construction composite, it has a significant impact on the performance of pavements. Asphalt concrete pavements, however, suffers from different kinds of distresses like low temperature cracking, rutting, fatigue, etc. Indeed, at elevated temperatures (40-60°C), asphalt exhibits a viscous liquid-like behaviour, whereas at low temperatures (0 to -30°C), asphalt is glassy and brittle. Hence, modified asphalt is needed. Among the different types of asphalt modification, polymer modification is the most common one.

Therefore, this paper reports a comparative study between styrene-butadiene-styrene (SBS) and ethylene vinyl acetate (EVA) copolymers used as polymer modifier agents in bitumen at various concentrations (3, 5 and 7 wt %). The effects of both the type and concentration of polymers on the morphology and the thermal and mechanical properties of the modified bitumen were investigated before and after accelerated ageing with rolling thin film oven test (R.T.F.O.T).

The study showed that before R.T.F.O.T, all the modified asphalts exhibited an improvement in the softening point, whereas the penetration, the thermal susceptibility and the ductility decreased. Further, the modified bitumen with 5 wt % SBS exhibited better results.

After R.T.F.O.T, The results clearly indicated that the samples prepared with 5 wt % SBS modified bitumen are less susceptible to temperature changes than the other modified samples.

Aplicación de electrodos transparentes de ITO y Al:ZnO en nuevos dispositivos electroópticos

C. Guillén, J. Herrero
Departamento de Energía. Centro de Investigaciones Energéticas, Medioambientales y Tecnológicas (CIEMAT). Madrid, España
C. Pozo-Gonzalo, J. Pomposo
Departamento de Nuevos Materiales. Centro de Tecnologías Electroquímicas (CIDETEC). San Sebastián, España

RESUMEN

Se han preparado láminas delgadas de ITO (óxido de indio dopado con estaño) y de AZO (óxido de zinc dopado con aluminio) sobre vidrio mediante pulverización catódica a partir de blancos cerámicos, ajustando la potencia y el tiempo de depósito en cada caso para obtener transmisión óptica en el visible superior a 80 % y resistencia eléctrica del orden de 10^3 S/cm, lo que permite su aplicación como electrodos transparentes. Para dicha aplicación se han ensamblado y ensayado distintas láminas de ITO y de AZO en dispositivos electroópticos, aplicando sobre estos sustratos conductores una mezcla electrocrómica en base polimérica mediante técnicas del tipo doctor-blade. El análisis comparativo de las características electroópticas de los dispositivos desarrollados hace posible adecuar los electrodos utilizados para esta nueva aplicación.

1. INTRODUCCIÓN

Los óxidos conductores transparentes (OCT) son ampliamente utilizados como electrodos en una gran variedad de dispositivos electroópticos, desde pantallas planas a células solares o dispositivos electrocrómicos (Granqvist 2007). Concretamente, los electrodos de ITO son hoy día los más desarrollados, y su alta demanda junto a la limitación en las reservas de indio han llevado a un considerable aumento de su precio en los últimos años. Por ello, la investigación en OCT alternativos está ganando importancia, y entre éstos destaca el Al:ZnO ó AZO como una opción de calidad aceptable y económica (Minami et al. 2008). Una de las tecnologías más utilizadas en la preparación de diversos OCT en lámina delgada es la pulverización catódica (Exarhos 2007), destacando un creciente interés en la reducción de la temperatura de preparación, para disminuir el consumo energético del sistema de producción y para permitir su aplicación sobre materiales sensibles, así como el reemplazo de los sustratos rígidos de vidrio por sustratos flexibles de plástico (Logothetidis 2008). No obstante, el aumento de la temperatura de preparación o un tratamiento térmico posterior permiten mejorar la transparencia y la conductividad eléctrica de las láminas de OCT, por lo que resulta interesante conocer y evaluar la influencia del calentamiento sobre estas características.

Nosotros hemos preparado láminas de ITO y de AZO sobre sustratos de vidrio a temperatura ambiente y algunas se han calentado posteriormente, con el propósito de establecer la influencia del material utilizado y el calentamiento sobre sus propiedades ópticas y eléctricas. Posteriormente se les ha aplicado una mezcla electrocrómica de base polimérica, para evaluar comparativamente los distintos electrodos desarrollados en función de las características electroópticas de estos dispositivos.

2. PROCEDIMIENTO EXPERIMENTAL

Los electrodos de ITO y de AZO se han preparado sobre sustratos de vidrio a temperatura ambiente, mediante la técnica de pulverización catódica, a partir de blancos cerámicos. Como gases de proceso y reactivo se han utilizado flujos controlados de argon y oxígeno, ajustando la potencia y el tiempo de acuerdo a los resultados obtenidos en anteriores trabajos (Guillén et al. 2007 y 2009). Tras la preparación se han calentado en vacío algunas de las muestras, a 350 ºC durante 20 minutos. Se han realizado medidas de transmisión óptica en el rango de longitudes de onda entre 300 y 1200 nm, y de resistencia eléctrica laminar por el método de las cuatro puntas.

Los dispositivos se han elaborado aplicando sobre los distintos electrodos una mezcla electrocrómica en base polimérica mediante el procedimiento ya descrito anteriormente (Pozo-Gonzalo et al. 2008). Las características electroópticas de estos dispositivos se han analizado mediante técnicas de espectroelectroquímica.

3. RESULTADOS Y DISCUSIÓN

En la figura 1 se representan los datos de transmitancia para los vidrios recubiertos con láminas de ITO y de AZO preparadas a temperatura ambiente y después de recibir tratamiento térmico. Se observa que la absorción óptica tiene lugar a longitudes de onda inferiores a 400 nm, mientras que se mantiene una transmisión media superior al 80 % entre 400 y 800 nm, con máximos de transmisión que llegan a superar el 90 % localizados a longitudes de onda que dependen del material concreto y el calentamiento. Así puede verse que el máximo se sitúa a 496 nm para el ITO y a 467 nm para el AZO tal y como son preparados, desplazándose tras el tratamiento térmico a 466 nm y 459 nm respectivamente. En cuanto a las características eléctricas de los recubrimientos, presentaron valores medios de la resistencia laminar inferiores a 60 Ω/sq, disminuyendo por debajo de 30 Ω/sq después de ser calentados.

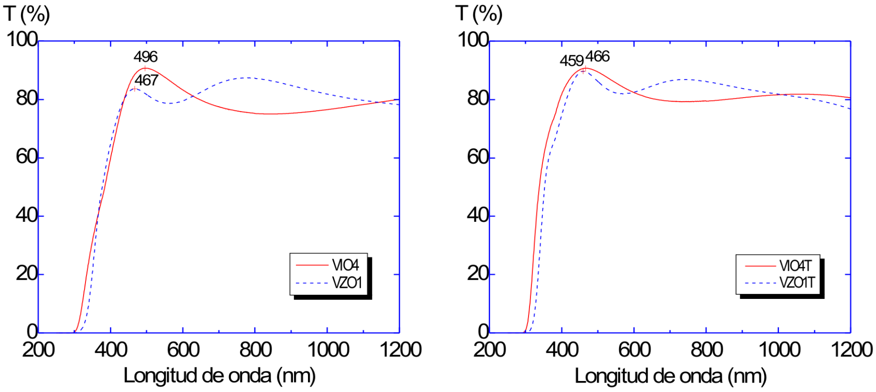

Fig. 1. Datos de transmitancia de vidrios recubiertos con ITO y AZO depositados a temperatura ambiente (VIO4, VZO1) y después de calentados (VIO4T, VZO1T).

En las figuras 2 y 3 se ilustran los datos de transmitancia en función del voltaje de polarización correspondientes a los dispositivos construidos sobre los distintos electrodos ya analizados. Para evaluar el comportamiento de las láminas de ITO y de

AZO utilizadas se ha medido el contraste óptico de los dispositivos, que se calcula como la máxima diferencia en transmitancia entre el proceso de oxidación y reducción a una longitud de onda determinada. Los resultados obtenidos se resumen en la tabla 1, donde puede verse que los valores de contraste más altos se alcanzan con los electrodos sin calentamiento, siendo el contraste superior a 83 % con láminas de ITO (referencia VIO4) y próximo a 78 % con las de AZO (referencia VZO1). Estudios similares se llevaron a cabo sobre electrodos de ITO comerciales con resultados análogos (contraste del 80 %) que corroboran la adecuada actuación de las láminas preparadas en el presente trabajo como electrodos en los dispositivos desarrollados.

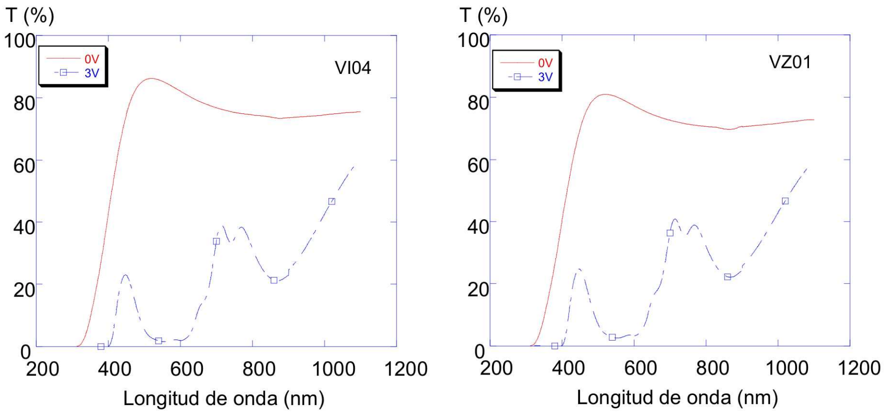

Fig. 2. Datos de transmitancia a 0V y 3V para dispositivos construidos sobre las láminas de ITO y de AZO depositadas a temperatura ambiente (VIO4 y VZO1).

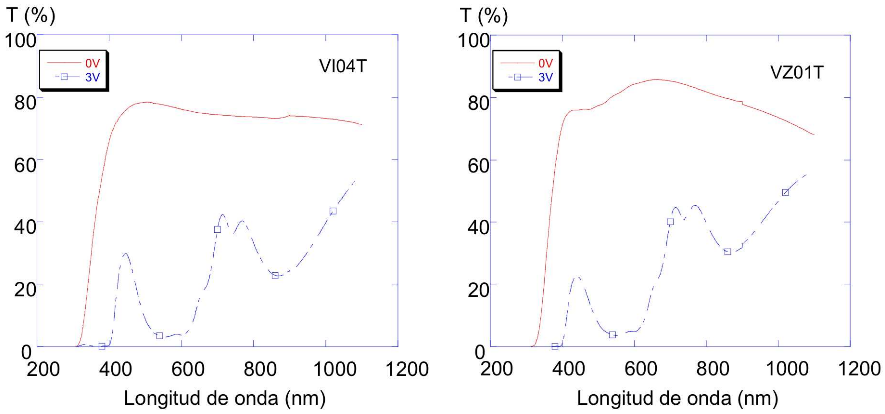

Fig. 3. Datos de transmitancia a 0V y 3V para dispositivos construidos sobre las láminas de ITO y de AZO que recibieron calentamiento (VIO4T y VZO1T).

No se observa un cambio significativo en el comportamiento de los dispositivos construidos sobre los electrodos que han recibido tratamiento térmico (referencias

VIO4T, VZO1T), salvo una cierta disminución del contraste a 550 nm que puede relacionarse con el desplazamiento hacia longitudes de onda inferiores del máximo de transmisión de dichos electrodos tras el calentamiento.

Electrodos	Tmáx.	Tmin.	Contraste Óptico
VIO4	86.0 %	2.6 %	83.4 % (a 536 nm)
VZO1	80.4 %	2.7 %	77.7 % (a 545 nm)
VIO4T	77.5 %	3.1 %	74.4 % (a 553 nm)
VZO1T	81.2 %	3.6 %	77.6 % (a 553 nm)

Tabla 1. Datos de transmisión y contraste óptico de los dispositivos.

4. CONCLUSIONES

Se han obtenido mediante pulverización catódica láminas delgadas conductoras de ITO y de AZO sobre vidrio, con una transmisión media del 80 % en la región espectral del visible, y máximos de transmisión próximos al 90 % localizados entre 450 y 500 nm. La aplicación de estas láminas como electrodos transparentes en dispositivos electrocrómicos ha resultado eficiente, consiguiendo alcanzar alrededor de 550 nm valores de contraste óptico superior al 83 % con láminas de ITO y próximo a 78 % con láminas de AZO, tal como son preparadas a temperatura ambiente y sin que se requiera un tratamiento térmico adicional.

AGRADECIMIENTOS

Se agradece la financiación del Programa Nacional de I+D del Ministerio de Ciencia e Innovación a través del proyecto ELECTRODOS DE ALTA EFICIENCIA PARA NUEVOS DISPOSITIVOS ELECTROOPTICOS (TEC2007-66506-C02-00), donde se coordinan las actividades realizadas por los respectivos grupos de investigación del CIEMAT (TEC2007-66506-C02-01) y de CIDETEC (TEC2007-66506-C02-02).

REFERENCIAS

EXARHOS, G.J., ZHOU, X.D. (2007). Discovery-based design of transparent conducting oxide films. *Thin Solid Films*, 515, 7025-7052.

GRANQVIST, C.G. (2007). Transparent conductors as solar energy materials: A panoramic review. *Sol. Energy Mater. & Sol. Cells*, 91, 1529-1598.

GUILLÉN, C., HERRERO, J. (2007). Structure, optical, and electrical properties of indium tin oxide thin films prepared by sputtering at room temperature and annealed in air or nitrogen. *J. Appl. Phys.*, 101, 073514.

GUILLÉN, C., HERRERO, J. (2009). Structure, optical and electrical properties of Al:ZnO thin films deposited by DC sputtering at room temperature on glass and plastic substrates. *Phys. Status Solidi A*, DOI 10.1002/pssa.200925061.

LOGOTHETIDIS, S. (2008). Flexible organic electronic devices: Materials, process and applications. *Mater. Sci. Eng. B*, 152, 96-104.

MINAMI, T., MIYATA, T. (2008). Present status and future prospects for development of non- or reduced-indium transparent conducting oxide thin films. *Thin Solid Films*, 517, 1474-1477.

POZO-GONZALO, C., POMPOSO, J., GRANDE, H., SALSAMENDI, M., MARCILLA, R. (2008). Patent PCT200800258.

Incorporación de subproductos industriales de carácter puzolánico en la elaboración de tejas de microhormigón para uso preferente en países en vías de desarrollo

J. Monzó[1], M.V. Borrachero[1], J. Payá[1], M. Ospina[2], R. Méndez[1], D. Martínez-Velandia[1]
[1]Instituto de Ciencia y Tecnología del Hormigón. Universidad Politécnica de Valencia. Camino de Vera s/n. 46022 Valencia, España
[2]Arrocera La Esmeralda S.A. Jamundi. Colombia

RESUMEN

En el presente trabajo, se han utilizado dos puzolanas; la ceniza volante de central térmica (CV) y el catalizador de craqueo catalítico usado (FCC), para la elaboración de tejas de microhormigón, con sustituciones de cemento por las mencionadas puzolanas de hasta un 30% en peso, constituyendo de esta forma mezclas ternarias cemento-CV-FCC. Los resultados preliminares ponen de manifiesto la bondad de estos materiales compuestos y confirman que sería posible reducir el coste de las tejas, sustituyendo parcialmente cemento por los residuos puzolánicos mencionados anteriormente.

1. INTRODUCCIÓN

En los países en vías desarrollo, el coste de los materiales de construcción supone en la mayoría de los casos, la partida más importante del coste total de una vivienda. Este hecho todavía se acentúa más cuando hablamos de vivienda para población con bajos ingresos (Salas, 1992). En estos países, el cemento Pórtland es uno de los materiales más costosos sobretodo para este segmento mayoritario de la población. Por este motivo, en los últimos años se han realizado investigaciones en dos sentidos, por un lado utilizando materiales no cementicios (adobe, tapial, quincha, bagazo, azufre, guadua, madera, etc) según la disponibilidad de los mismos en cada país, y por otro lado, se ha tratado de optimizar los contenidos de cemento Pórtland en morteros y hormigones mediante la adición de puzolanas, consiguiendo en muchos casos mejorar las propiedades de los morteros y hormigones originales (Payá et al. (a), 1999; Payá et al (b), 1999). La utilización de este tipo de materiales permitiría obtener morteros y hormigones de buena calidad a un precio reducido, lo que facilitaría su uso por los sectores de la población con escasos recursos

En el presente trabajo, se han utilizado dos puzolanas; la ceniza volante de central térmica (CV) y el catalizador de craqueo catalítico usado (FCC), para la elaboración de tejas de microhormigón, con sustituciones de cemento por las mencionadas puzolanas de hasta un 30% en peso, constituyendo de esta forma mezclas ternarias cemento-CV-FCC. La producción de tejas, basada en el vibrado suave del microhormigón, material compuesto de árido fino como refuerzo y matriz conglomerante hidráulica, y su colocación posterior sobre un molde curvado hasta su endurecimiento, es una tecnología muy utilizada en los países en vías de desarrollo, debido a su fácil implementación y a los bajos costes de inversión, además de manejabilidad del equipo que permite fácilmente su desplazamiento a la zona de utilización de las tejas, (Lorenzo et al., 2005).

2. MATERIALES Y MÉTODOS

El cemento utilizado es un cemento Portland CEM II/A-L 32.5N suministrado por CEMEX (Buñol). El catalizador de craqueo catalítico usado (FCC), fue suministrado por la empresa BP OIL España S.A. (Castellón). La ceniza volante utilizada es de tipo F y fue suministrada por la Central Térmica de Andorra (Teruel). Se utilizó un árido silíceo suministrado por la empresa Caolines Lapiedra (Liria-Valencia) y cuando fue necesario el fluidificante Melment L240 de la empresa Degussa S.L

Para la molienda del FCC se utilizó un molino de bolas Gabrielli Mill-2, obteniendo después del proceso de molienda un material con un diámetro de medio de 19.73µm. Las tejas se elaboraron utilizando una máquina Tevi construida por el Centro de Estudios de Construcción y Arquitectura Tropical. ISPAJAE. Cuba (Figura 1). Para el ensayo a flexión de la tejas se utilizó una prensa universal INSTRON 3382, diseñando una pieza específica para conseguir un reparto homogéneo de la carga a lo largo de la superficie de la teja (Figura 2). La elaboración de las probetas prismáticas de 4x4x16 cm se realizó utilizando una amasadora y compactadora de mortero IBERTEST según la norma UNE-EN 196-1:1996. Dichas probetas fueron ensayadas a flexotracción y compresión después de estar sumergidas en agua durante 28 días de curado a 20°C. La trabajabililidad se midió utilizando una mesa de sacudidas según la norma UNE 83-811-92

Se fabricaron tejas tipo romana con una mezcla de microhormigón con relación agua/cemento de 0,5 y árido/material cementante de 3. Se estudiaron diferentes sustituciones de cemento por mezclas de FCC y CV de hasta el 30% en peso. En la tabla 1 se indican las diferentes mezclas estudiadas. La resistencia a flexión transversal de las tejas se realiza aplicando la norma UNE-EN 491 de julio de 2005. En este ensayo la teja es colocada sobre dos apoyos metálicos redondeados, ubicados con una amplitud de 311mm, a 2/3 de la distancia de cuelgue (ver figura 2).

% Cemento	100	90	90	80	80	80	70	70	70	70
% CV	-	10	-	20	10	-	30	20	10	-
% FCC	-	-	10	-	10	20	-	10	20	30
Fluidez (mm)	129	135	126	138	136	131*	140	139	137	127*

***A estas mezclas se les ha adicionado superplastificante en su preparación**

Tabla 1. Mezclas ternarias estudiadas y trabajabilidad de dichas mezclas.

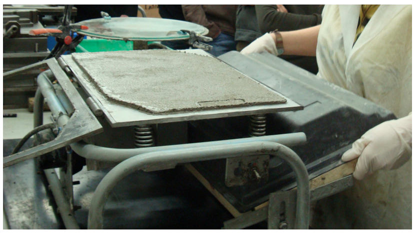

Figura 1. Maquina de fabricación de tejas.

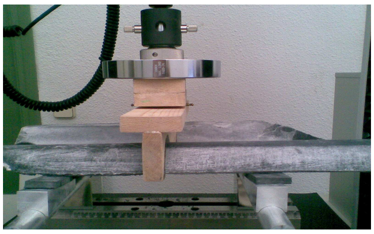

Figura 2. Ensayo de tejas a flexión.

2. RESULTADOS Y DISCUSIÓN

En el proceso de fabricación de tejas, mediante la tecnología expuesta anteriormente, la trabajabilidad de las mezclas es un factor clave, ya que valores muy altos de la misma, producen segregación y por el contrario valores excesivamente bajos dificultan una compactación adecuada de la mezcla, generando aumentos de permeabilidad, no deseados en la tejas. En la tabla 1 se recogen los valores de fluidez en función del porcentaje de FCC y CV usados. Hay que señalar que en el caso de las mezclas con un 20 y 30% de FCC y sin CV, se les adicionó un 0.75 y un 1% de superfluidificante, respectivamente, para obtener una trabajabilidad adecuada. Se observa en todos los casos, un aumento de la fluidez del mortero conforme aumenta el porcentaje de CV, como cabría esperar teniendo en cuenta la forma esférica de las partículas de CV, que actúan como lubricante sólido (Malhotra et al, 1994). La presencia de FCC en las mezclas produce una disminución de la fluidez (Payá et al, 1999b), ya que las partículas de éste presentan formas irregulares, además de tratarse de un compuesto con una gran superficie específica que retiene parte del agua de amasado, lo que obliga a añadir superplastificante en dichas mezclas para aumentar la fluidez y hacerlas trabajables. En las mezclas que contienen las dos puzolanas, el efecto lubricante de la ceniza compensa la disminución de fluidez que produce el FCC (ver tabla 1). Así pues se constata el carácter complementario, en lo que a fluidez se refiere, de ambos residuos.

En las figuras 3 y 4 se representan la resistencia a flexotracción y compresión respectivamente de las probetas prismáticas, frente al porcentaje de FCC, para distintos contenidos de CV a 28 días de curado. Las tendencias observadas en ambos casos son prácticamente similares: se aprecia un aumento de ambas resistencias, para un porcentaje determinado de FCC, conforme es mayor el porcentaje de CV. Los resultados preliminares, ponen de manifiesto el carácter puzolánico de ambos residuos.

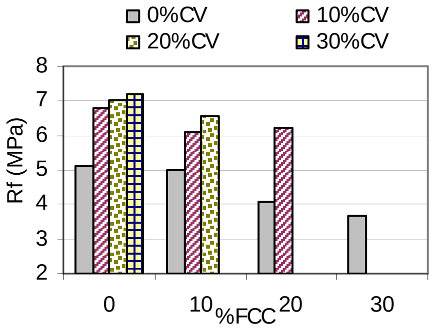

Figura 3. Resistencias a flexotracción de morteros cemento/CV/FCC.

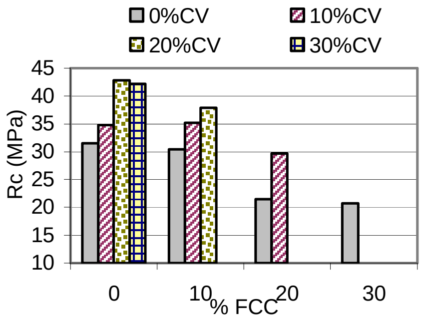

Figura 4. Resistencia a compresión de morteros cemento/CV/FCC.

En la figura 5 se representa la carga máxima aplicada sobre la teja frente al porcentaje de FCC, para distintos porcentajes de CV. Las tendencias obtenidas son parecidas a las obtenidas para las resistencias a flexotracción de los prismas, si bien en este caso, se pone de manifiesto la existencia de valores superiores para los morteros que contienen porcentajes mayores de FCC. Este hecho podría tener su explicación en la mayor facilidad de compactación de las tejas frente a las probetas, ya que estas últimas tienen un espesor netamente superior (4 cm frente a 1 cm para las tejas). Se constata en todos los casos que cualquier sustitución de cemento por puzolana (CV y/o FCC) produjo valores de carga máxima en las tejas superior a la teja control que no contenía puzolana.

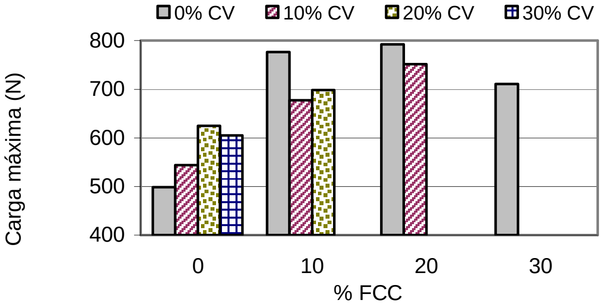

Figura 5. Carga máxima aplicada sobre tejas de microhormigón con mezclas ternarias cemento/CV/FCC, curadas a 28 días.

3. CONCLUSIONES

Los resultados preliminares ponen de manifiesto la bondad de la sustitución de hasta un 30% en peso de cemento por mezclas CV-FCC, en la elaboración de tejas de microhormigón. En todos los casos la carga máxima que soportó la teja que contenía puzolana (CV y/o FCC) fue superior a la carga máxima soportada por la teja control que no contenía puzolana. Estos resultados confirman que sería posible reducir el coste de las tejas, sustituyendo parcialmente cemento por los residuos puzolánicos ensayados en este trabajo de investigación.

REFERENCIAS

LORENZO P. et al.(2005) Un techo para vivir. Tecnologías para viviendas de producción social en América Latina. Teja Tevi. Ficha 7.5, *Centro de Estudios de Construcción y Arquitectura Tropical.* ISPAJAE. Cuba, (Ediciones UPC).

MALHOTRA V.M., RAMEZANIANPOUR A.A.(1994) Fly ash in concrete. 50-54 (Ed CANMET). Canadá.

PAYÁ J. BORRACHERO MV., MONZÓ J., ORDÓÑEZ LM., BONILLA M., MELLADO A. (1999) (a). Cenizas de cáscara de arroz (CCA) obtenidas en condiciones de combustión no-controladas. Posibilidades de uso en hormigones In *Proceedings of III Congreso Nacional de Materiales Compuestos MATCOMP99*, 501-508

PAYÁ J., MONZÓ J., BORRACHERO MV., (1999) (b). Fluid catalytic cracking catalyst residue (FC3R), an excellent mineral by-product for improving early strength development of cement mixtures. *Cem Concr Res*, 29 1773-1779

SALAS J. (1992). Contra el hambre de vivienda. Soluciones tecnológicas latinoamericanas. 55-107. En *Tecnologías para viviendas de interés social,* (Ed Escala) 55-107. Bogotá (Colombia).

Nuevos materiales compuestos con matriz activada alcalinamente

M.M. Tashima, M.V. Borrachero, J.Monzó, L. Soriano, J. Payá.
Instituto de Ciencia y tecnología del Hormigón ICITECH
Universidad Politécnica de Valencia - UPV
Edificio Caminos 2, Camino de Vera s/n, 46022 Valencia, España

RESUMEN

El desarrollo de nuevos materiales conglomerantes sin el uso de cemento es un reto que permite acercarnos hacia la reducción de emisiones de CO_2. Estos materiales requieren habitualmente de un material mineral activable que tenga propiedades conglomerantes en ambientes fuertemente alcalinos. En este trabajo, se estudia la preparación de morteros activados alcalinamente con el uso de un residuo procedente del vidrio (VSAC), de composición SiO_2-Al_2O_3-CaO. Se prepararon morteros con árido silíceo, con una matriz fabricada a partir de mezclas VSAC/NaOH en diferentes proporciones y curada a 65ºC durante 3 días. Estos morteros, materiales compuestos árido-conglomerante, fueron ensayados mecánicamente a flexotracción y a compresión, obteniéndose valores de resistencia mecánicas comparables, y, en algunos casos superiores, a los morteros convencionales de cemento Portland. Asimismo, se caracterizó la matriz conglomerante por medio de SEM, análisis termogravimétrico y DRX, así como se evaluó la alcalinidad de la matriz resultante del tratamiento térmico.

1. INTRODUCCIÓN

Las primeras investigaciones para el desarrollo de materiales activados alcalinamente empezaron en 1940 donde Purdon presenta un estudio muy detallado sobre la utilización de conglomerantes sin cementos a partir de escoria activadas con hidróxido sódico (Shi, 2006). Desde entonces, muchos trabajos vienen siendo realizados con el propósito de encontrar nuevos materiales conglomerantes que puedan reemplazar el cemento Portland disminuyendo así, las emisiones de CO_2 derivadas del proceso de fabricación del mismo (Fernández-Jiménez, 2005).

En el desarrollo de materiales activados alcalinamente es necesario el uso de un material mineral activable y ambientes alcalinos. En lo que se refiere a los activadores alcalinos, las soluciones más comúnmente utilizadas son NaOH, KOH, silicato sódico + NaOH, Na_2CO_3. Entre los materiales conglomerantes se pueden destacar la escoria de alto horno, la ceniza volante y el metacaolín. Todos estos materiales son de origen silicoaluminoso (Al_2O_3-SiO_2) y presentan un elevado porcentaje de material amorfo. Según el estudio presentado por Xu (2000), diversos materiales naturales de esa composición también pueden ser activados alcalinamente presentando valores de resistencia a compresión aceptables.

El presente trabajo muestra los resultados preliminares del estudio sobre la preparación de morteros con el uso de un residuo procedente del vidrio (VSAC) activado alcalinamente con soluciones de NaOH y curado a 65ºC durante 3 días. Hasta el presente momento no se ha encontrado ninguna referencia sobre el uso del VSAC en morteros activados alcalinamente. Los morteros fueron ensayados mecánicamente a flexotracción y compresión, y además, las matrices conglomerantes fueron analizadas por DRX, análisis termogravimétrico, SEM y también se evaluó la alcalinidad de la matriz.

2. PROGRAMA EXPERIMENTAL

Para la fabricación de los morteros activados alcalinamente fue utilizado árido silíceo equivalente al árido especificado en la UNE-EN 196-1 (1996). El reactivo utilizado para la preparación de las soluciones fue NaOH 98% en pellets suministrado por Panreac S.A. El VSAC presenta en su composición un 57,9% de SiO_2, 12,93% Al_2O_3, 23,51% de CaO, 2,88% MgO y otras impurezas. En los morteros se adoptó una relación árido/VSAC 3:1 y la relación solución activante/VSAC fue la variable estudiada. Las probetas fueron curadas a 65ºC durante 3 días y luego ensayadas mecánicamente a flexotracción y a compresión. La relación solución activante/VSAC se varió entre 0,5 y 0,68.

En el análisis de la matriz conglomerante por termogravimetria se utilizó una termobalanza TGA 850 Mettler-Toledo con atmósfera de nitrógeno con flujo de 75ml/min y una velocidad de calentamiento de 10ºC/min. Este ensayo se realizó con el objetivo de verificar la formación de productos hidratados y, que fue comprobada con los ensayos de DRX y SEM. La alcalinidad de la matriz también fue medida para todas las relaciones solución activante/VSAC estudiadas.

3. RESULTADOS Y DISCUSIONES

En la Figura 1 se muestra los valores de pH obtenidos para cada relación solución activante/VSAC estudiada. Como se puede notar, cuanto mayor es la relación, mayor es el valor del pH de la matriz conglomerante. Las matrices conglomerantes presentan valores de pH alrededor de 12,0-12,5. Estos valores son similares a los que se obtienen en matrices de cemento Portland.

En el análisis termogravimétrico se observa la formación de productos hidratados en las matrices conglomerantes. Cuanto mayor es la relación sol.activante/VSAC, mayor es la formación de hidratos, excepto para la relación 0,68 donde ocurre una reducción. Los porcentajes de hidratos formados pueden ser observados en la Tabla 1.

Sol. Activante/VSAC	0,50	0,54	0,59	0,63	0,68
hidratos (%)	6,95	11,12	14,27	19,20	17,79

Tabla 1. Porcentaje de hidratos en función de la relación sol. activante/VSAC.

Cuando se observa una reducción en la formación de los hidratos es de esperar que los valores de resistencia también disminuyan, ya que se tiene una menor cantidad de productos resistentes (hidratos).

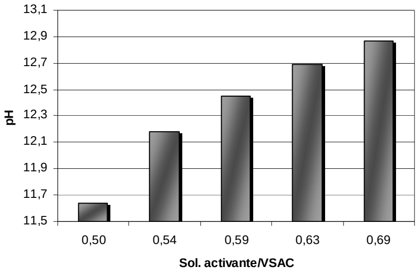

Fig. 1. Valores de pH para las distintas matrices conglomerantes.

En la Fig. 2 se muestran los valores de resistencia mecánica obtenidos para los morteros activados alcalinamente curados a 65ºC durante 3 días. Se puede notar claramente que para la flexotracción existe un valor máximo que está entre las relaciones 0,59 y 0,63. Precisamente, para estas dosificaciones se obtienen valores similares a los obtenidos para morteros de cemento Pórtland convencionales. Para la resistencia a compresión se observa una tendencia muy similar a presentada para la flexotracción, observándose un óptimo para la relación 0,63. Fueron obtenidos valores de resistencia comparables e incluso superiores a los que se obtienen en morteros de cemento Pórtland curados a 28 días a temperatura ambiente. Según lo que se ha visto en la bibliografía, los valores de resistencia están dentro de lo que se espera para un mortero activado alcalinamente. Por todo ello, se puede considerar que el VSAC es un material con características adecuadas para ser activado alcalinamente.

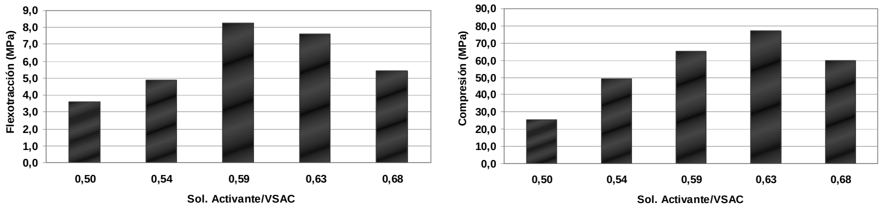

Fig. 2. Resistencia a flexotracción y compresión para los morteros activados alcalinamente.

A continuación son presentados los difractogramas de RX obtenidos para las distintas relaciones de sol.activante/VSAC estudiadas y también para el VSAC (Fig.3). Los resultados muestran que, independientemente de la relación sol. activante/VSAC, las matrices conglomerantes presentan un carácter predominantemente amorfo y también presentan algunos picos referentes a $CaCO_3$, silicoaluminato sódico y C-S-H.

En la Fig. 4 se observa los productos formados en la matriz conglomerante. Son productos de carácter predominantemente amorfo, y se presentan como una matriz muy densa y compacta.

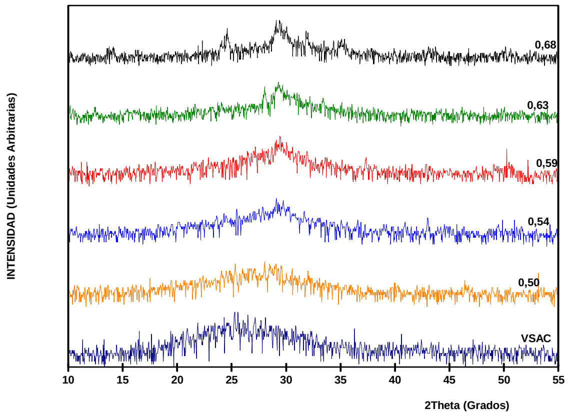

Fig. 3. DRX para las distintas relaciones sol. activante/VSAC.

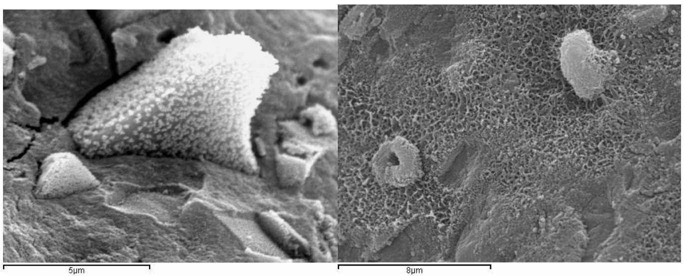

Fig. 4. SEM del conglomerante con relación sol. activante/VSAC 0,63.

4. CONCLUSIONES

La utilización del VSAC en morteros activados alcalinamente parece ser una alternativa viable en la fabricación de nuevos materiales compuestos ya que se puede obtener valores considerables de resistencia. Parece existir una relación óptima sol.activante/VSAC para este tipo de matriz conglomerante donde se obtienen resistencias a compresión superiores a las que se obtienen en morteros de cemento Portland. Los productos hidratados formados en estos materiales compuestos presentan carácter predominantemente amorfo y la formación de hidratos está directamente relacionada con la resistencia a compresión.

REFERENCIAS

Fernádez-Jiménez A; Palomo A. Composition and microstructure of alkali activated fly ash binder: Effect of activator. Cem Conc Res 2005; 35:1984-1992.

Shi C; Roy D; Krivenko P. Alkali-activated cements and concrete. London: Taylor& Francis Ltd.; 2006.

Xu H; Deventer JSJ. The geoplymerization of alumino-silicate minerals. Min Processing 2000; 59:247-266.

Propiedades ópticas de láminas delgadas de composites preparados con nanofibras de carbono y partículas de vidrio

F. Rubio, C. Palencia, J. Rubio, J.L. Oteo
Departamento de Química-Física de Superficies y Procesos. Instituto de Cerámica y Vidrio. CSIC. Madrid, España
A.H. Tamayo
Fachbereich Materialwissenschaft. Fachgebiet Disperse Feststoffe
Petersenstr. 23, 64287 Darmstadt. Deutschland
C. Merino
Grupo Antolín Ingeniería. Ctra. Madrid-Irún, km. 244,8. 09007. Burgos

RESUMEN

En el presente trabajo se han estudiado las propiedades ópticas visible y ultravioleta de nanocomposites de matriz vítrea reforzados con nanofibras de carbono Ganf. Se ha observado que los cambios más importantes se producen en la trasmisión ultravioleta y en la reflexión visible. Así se ha observado que cualquiera que sea la concentración de nanofibras Ganf la incorporación de éstas elimina la absorción ultravioleta del vidrio a la vez que modifica la reflexión visible produciendo una variación no lineal para la concentración del 1% en nanofibras.

1. INTRODUCCIÓN

No cabe ninguna duda de la importancia de los materiales compuestos de matriz vítrea o cerámica en aplicaciones a elevadas temperaturas. En este sentido, la incorporación de nanofibras de carbono puede dar lugar a avances importantes en este tipo de materiales. Sin embargo, una de las desventajas de las nanofibras está en su baja resistencia térmica por encima de 600 ºC (Tamayo et al. 2009), lo que da lugar a que durante el procesado del composite gran parte de ellas se pierda por degradación. A pesar de ello la incorporación de nanofibras de carbono en matrices vítreas no tiene por qué estar dirigida solamente hacia composites con propiedades mecánicas mejoradas sino que es posible su utilización en composites con propiedades ópticas modificadas, lo que les hace ser unos materiales muy interesantes en aplicaciones fotónicas tales como óptica no lineal, dispositivos ópticos, protecciones ópticas, filtros espaciales y temporales, etc. [Dimaio et al. 2003]. Estas propiedades hace que los vidrios reforzados con nanofibras de carbono sean materiales compuestos de un alto interés tecnológico. En este trabajo se han preparado láminas delgadas de composites a base de nanofibras de carbono y partículas de vidrio, y se ha estudiado el cambio en su transmisión-reflexión luminosa.

2. EXPERIMENTAL

2.1 Materiales y composites

Las NFC utilizadas en este trabajo han sido proporcionadas por el Grupo Antolín Ingeniería, S. A. y son conocidas como Ganf. Estas tienen un diámetro medio entre 20 y 80 nm, índice de grafitización del 70% y una densidad próxima a 2 g.cm^{-3}. El vidrio utilizado ha sido uno comercial sodocálcico conteniendo un 70% de SiO_2, 16% Na_2O y 7 % CaO. El 5% restante lo aportan los óxidos MgO, B_2O_3 y Al_2O_3. El vidrio fue molido primero en mortero de ágata y luego por atrición hasta alcanzar un tamaño comprendido entre 5 y 10 μm, y el final de 1 μm. Los composites se prepararon por molturación de las NFC y polvos de vidrio en porcentajes del 1, 10 y 90 % en peso respecto al vidrio. Posteriormente se aplicaron capas delgadas sobre piezas de vidrio y se trataron térmicamente a 1000 ºC en horno de atmósfera neutra durante 1 hora, tiempo suficiente para alcanzar la fluidez de las partículas de vidrio y consolidad la capa nanocomposite.

2.1 Caracterización de la interacción. Raman.

Las propiedades ópticas de los nanocomposites Ganf-vidrio se determinaron mediante espectroscopía UV-vis (Perkin-Elmer, Lambda 40) en el intervalo 190 – 1100 nm. Se obtuvieron espectros tanto en modo transmisión como en reflexión. Las propiedades ópticas se determinaron utilizando en sistema CIELab [Nassau. 1983] según la Comisión Internacional de la Iluminación (CIE) utilizando el iluminante C correspondiente a la distribución espectral de la luz solar media en cielo nublado, y Observador de 10 º.

3. RESULTADOS Y DISCUSIÓN

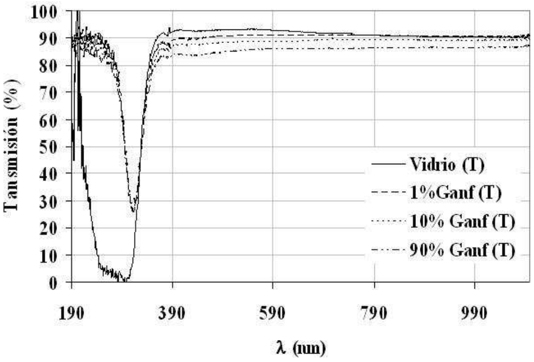

Fig. 1. Espectros UV-vis (Transmisión) de los nanocomposites Ganf-Vidrio.

En la Figura 1 se muestran los espectros de transmisión UV-vis de los nanocomposites preparados con diferentes contenidos en Ganf. Y en la Figura 2 se muestran los correspondientes al modo de reflexión. Uno de los primeros efectos observados por la incorporación de nanofibras Ganf a la matriz vítrea es la eliminación de la transmisión UV (entre 190 y 300 nm) respecto al vidrio sin nanofibras (Fig. 1). Este efecto no se produce en los espectros de reflexión (Fig. 2) en donde el % de reflexión depende de la concentración de nanofibras. En las Figuras 3 y 4 se muestran los mismos espectros en la región visible (370-950 nm), en los que ya se pueden comparar más los efectos producidos por las nanofibras en la matriz vítrea. Ahora, en los espectros de transmisión se observa claramente que la incorporación de nanofibras de carbono reduce la transmisión luminosa del vidrio, desde el 93 % al 85 %. No obstante, los vidrios continúan siendo transparentes a pesar de que

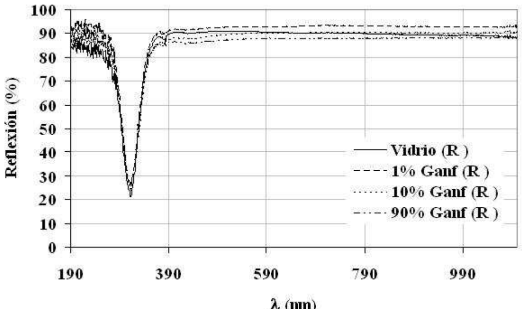

Fig. 2. Espectros UV-vis (Reflexión) de los nanocomposites Ganf-Vidrio.

contienen un 90 % de nanofibras.

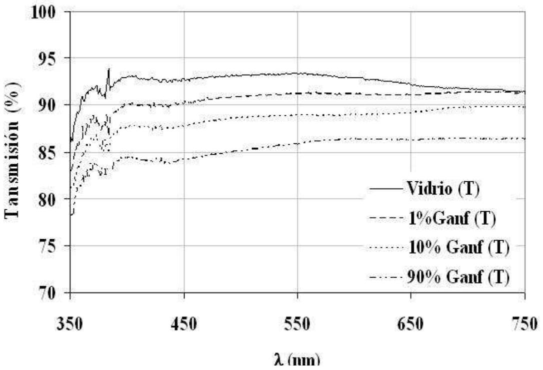

Fig. 3. Espectros de Transmisión en la región visible de nanocomposites Ganf-Vidrio.

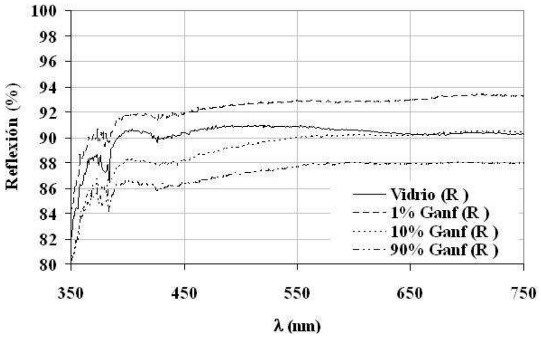

Fig. 4. Espectros de Reflexión en la región visible de nanocomposites Ganf-Vidrio.

Por otro lado, los espectros de reflexión muestran que el nanocomposite del 1% de Ganf posee mayor reflexión óptica que vidrio base. El que contiene el 90 % de Ganf da la menor reflexión óptica visible.

A partir de estos espectros se han calculado las coordenadas cromáticas L, a* , b*. L indica la luminosidad o transmisión luminosa (100 = transparente; 0 = opaco negro). a* varía de positivo (+) color rojo, a negativo (-) color verde, mientras que b* es positivo (+) amarillo o negativo (-) color azul. En la Tabla 1 se recogen los valores obtenidos para cada nanocomposite.

Según los datos de esta Tabla 1 los nanocomposites son transparentes, con valores de L superiores a 90. Según las medidas de transmisión se observa que al aumentar el contenido en nanofibras Ganf disminuye el valor de la luminosidad, debido al marcado color negro de las nanofibras. Sin embargo, según los valores de L determinados por reflexión se observa que para una capa de nanocomposite con un 1% de nanofibras Ganf, la reflexión aumenta desde 96.28 (vidrio matriz) a 97.13, es decir las nanofibras producen una mayor reflexión óptica visible que la que tiene el vidrio original. Esta propiedad es indicativa del efecto que producen los nanomateriales en matrices vítreas. No obstante, a medida que la concentración de nanofibras aumenta al 10 y al 90 % la reflexión disminuye hasta 95. Es de tener en cuenta también que los valores alcanzados mediante reflexión son menores que los de transmisión, lo que de nuevo es un hecho importante a tener en cuenta en matrices vítreas modificadas ópticamente por nanofibras de carbono.

En cuanto a los valores de a* y b*, se observa tanto por transmisión como por reflexión como al aumentar el contenido en nanofibras Ganf el vidrio inicial con una leve tonalidad verde alcanza la tonalidad roja, a la vez que la tonalidad amarilla se ve reforzada. En estos casos no se observan variaciones no lineales con la concentración de nanofibras en el composite de matriz vítrea.

	L	**a***	**b***
TRANSMISIÓN			
Vidrio	97.27	- 0.37	0.23
Capa 1%	96.47	- 0.18	0.61
Capa 10%	95.53	- 0.11	0.68
Capa doble 90%	94.23	+ 0.07	1.08
	Transparente	Verde (-) → rojo (+)	Amarillo (+)
REFLEXIÓN			
Vidrio	96.28	- 0.28	0.18
Capa 1%	97.13	- 0.10	0.49
Capa 10%	95.93	- 0.09	1.03
Capa doble 90%	95.00	+ 0.002	0.82
	Transparente	Verde (-) → rojo (+)	Amarillo (+)

Tabla 1. Propiedades ópticas en la región visible de nanocomposites Ganf- vidrio.

4. CONCLUSIONES

En este trabajo se ha estudiado por espectroscopía UV-vis las propiedades ópticas de nanocomposites de matriz vítrea reforzados con nanofibras de carbono Ganf. Se ha observado que la presencia de nanofibras modifica las propiedades ópticas de transmisión y reflexión, si bien la segunda la variación no es lineal con la concentración de nanofibras. Este resultado es importante a la hora de emplear estos nanocomposites en aplicaciones ópticas especiales.

AGRADECIMIENTOS

Los autores desean agradecer el presente trabajo al proyecto CENIT DOMINO financiado por el CDTI.

REFERENCIAS

DIMAIO, J., RHYNE, S., YANG, Z., FU, K., CZERW, R., XU, J., WEBSTER, S., SUN, Y-P., CARROLL, D.L., BALLATO, J. 2003. Transparent silica glasses containing single walled carbon nanotubes. *Inf. Sci.* 149, 69–73

TAMAYO, A. H., RUBIO, F., PALENCIA, C., RUBIO, J., OTEO, J.L., MERINO, C. (2009). Interacción entre nanofibras de carbono y partículas de vidrio en la preparación de composites de matriz vítrea. *Publicado en este mismo volumen*.

NASSAU, K. (1983). The Physics and Chemistry of Color: The Fifteen Causes of Color. John Wiley and Sond (USA).

Interacción entre nanofibras de carbono y partículas de vidrio en la preparación de composites de matriz vítrea

A.H. Tamayo
Fachbereich Materialwissenschaft. Fachgebiet Disperse Feststoffe
Petersenstr. 23, 64287 Darmstadt. Deutschland
F. Rubio, C. Palencia, J. Rubio, J.L. Oteo
Departamento de Química-Física de Superficies y Procesos. Instituto de Cerámica y Vidrio. CSIC. Madrid, España
C. Merino
Grupo Antolín Ingeniería. Ctra. Madrid-Irún, km. 244,8. 09007. Burgos

RESUMEN

El presente trabajo estudia las interacciones entre nanofibras de carbono y partículas de vidrio durante el proceso de consolidación hasta una temperatura de 600 ºC para obtener composites de matriz vítrea. El estudio se ha basado en las bandas situadas a 1080 cm^{-1}, 1385 cm^{-1} y 1590 cm^{-1}, asignadas a los enlaces C-O y C-C de los planos grafíticos, respectivamente. Se ha comprobado como entre 300 y 400 ºC las nanofibras se oxidan y entre 500 y 600 ºC se degradan, sin embargo la estructura grafítica no solo se mantiene sino que aumenta, lo que indica que el ataque a la nanofibra tiene lugar por aquellas zonas de la misma menos graníticas.

1. INTRODUCCIÓN

En los últimos años, el desarrollo tanto de nanotubos como de nanofibras de carbono (NTC, NFC), ha dado lugar a grandes expectativas en el campo de los materiales compuestos (composites) de elevadas prestaciones mecánicas (Balazsi et al. 2005). En materiales compuestos para aplicaciones a elevadas temperaturas, es necesario poseer matrices y fibras capaces de mantener sus propiedades en tales condiciones. En este sentido, aunque la utilización de NFC permitiría alcanzar buenas propiedades mecánicas, sin embargo su interacción con la matriz a elevada temperatura hace inviable su utilización. Durante la preparación de materiales compuestos de matriz vítrea, la interacción entre una NFC y una partícula de vidrio tiene lugar no solo por la presencia de aire en el medio de reacción sino también por la diferente naturaleza química existente entre ambos materiales. En este sentido la mayoría de las investigaciones realizadas se basan en la preparación de los materiales compuestos en atmósferas neutras o bien mediante nuevos sistemas de procesado como el Spark Plasma Sintering (SPS) [Balazsi et al. 2005]. Sin embargo, a pesar de eliminar el aire antes de llevar a cabo el procesado del composite así como a pesar de utilizar atmósferas neutras, la interacción NFC-vidrio siempre va a tener lugar debido sobre todo al fuerte carácter oxidante de una partícula vítrea, carácter que no solo se debe a su composición de óxidos inorgánicos sino también a la rotura de enlaces Si-O-Si durante la molienda necesaria para obtener las partículas [Pérez-Villar et al. 2008]

En este trabajo se ha estudiado la interacción entre nanofibras de carbono y partículas de vidrio con el fin de conocer las reacciones que tienen lugar en función de la temperatura o, lo que es lo mismo, durante el procesado del composite. Para ello se ha utilizado la espectroscopía Raman y se han realizado los espectros *in situ* a diferentes temperaturas de tratamiento.

2. EXPERIMENTAL

2.1 Materiales y composites "en verde"

Las NFC utilizadas en este trabajo han sido proporcionadas por el Grupo Antolín Ingeniería, S. A. y son conocidas como Ganf. Las NFC Ganf poseen un diámetro medio comprendido entre 20 y 80 nm, un grado de grafitización del 70% y una densidad próxima a 2 g.cm^{-3}. El vidrio utilizado ha sido uno comercial sodocálcico conteniendo un 70% de SiO_2, 16% Na_2O y 7 % CaO. El 5% restante lo aportan los óxidos MgO, B_2O_3 y Al_2O_3. El vidrio fue molido primero en mortero de ágata y luego por atrición hasta alcanzar un tamaño comprendido entre 5 y 10 μm, y el final de 1 μm. Los composites en verde se prepararon por molturación de las NFC y polvos de vidrio al 50% en peso en molino de ágata durante 10 minutos. Posteriormente se tomó una punta de espátula de la mezcla (composite en verde) y se llevó a una cámara Linkam de calentamiento donde se realizaron los ensayos de interacción vidrio-NFC.

2.1 Caracterización de la interacción. Raman

La interacción NFC-vidrio se estudió mediante un equipo Raman in Vía (Renishaw) utilizando un láser de 514 nm y una potencia de 10 mW. Los espectros Raman fueron realizados in situ sobre una muestra de composite "en verde" para lo cual se utilizó una cámara Linkam con velocidad de calentamiento de 10 ºC.min^{-1} refrigerada por agua. Los espectros se obtuvieron a diferentes temperaturas para lo cual se mantuvo cada una de ellas el tiempo necesario hasta que se hubo obtenido el espectro correspondiente. La resolución fue de 2 cm^{-1}.

3. RESULTADOS Y DISCUSIÓN

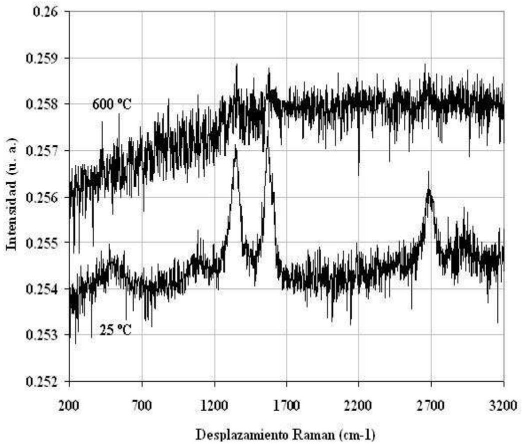

Fig. 1. Espectros Raman de los composites a 25 y 600 ºC entre 200 y 3200 cm-1.

En la Figura 1 se muestran los espectros Raman de los composites a 25 ºC y a 600 ºC. Puede comprobarse como en ellos aparecen las bandas principales correspondientes a las NFC situadas a 1600 y 1370 cm-1 correspondientes a los enlaces C-C en grafitos ordenados y desordenados, repectivamente. También aparece a 2700 cm-1 la banda de segundo orden del grafito, así como una banda de muy pequeña intensidad situada a 1080 cm-1 asignada a los enlaces C-O existentes en la superficie de las NFC [Lespade et al. 1984]. Sobre 470 cm-1 aparece también uma banda amplica debida a la flexión Si-O-Si del vidrio utilizado como matriz. A 600 ºC prácticamente todas las bandas han desaparecido, lo que indica que las NFC han reaccionado con las partículas de vidrio o bien con la atmósfera existente y se ha producido su degradación.

En base a estos resultados e realizaron los espectros Raman a intervalos de 100 ºC (Fig. 2). Así se pude comprobar como a medida que aumenta la temperatura cada una de las bandas mencionadas decrecen en intensidad hasta prácticamente desaparecer a los 600 ºC. Es de destacar que la banda situada sobre los 1600 ºC posee un hombro a 1610 cm^{-1}, mientras que el pico fundamental está situado a 1587 cm^{-1}. Es conocido que dicho hombro se debe a imperfecciones de la red grafítica de tal forma que a medida que aumenta el grado de grafitización del material el hombro desaparece y la banda más intensa se sitúa sobre los 1580 cm^{-1} y decrece su anchura media. Así mismo, la banda de 1380 cm^{-1} debe de decrecer cuanto más grafítico es el material.

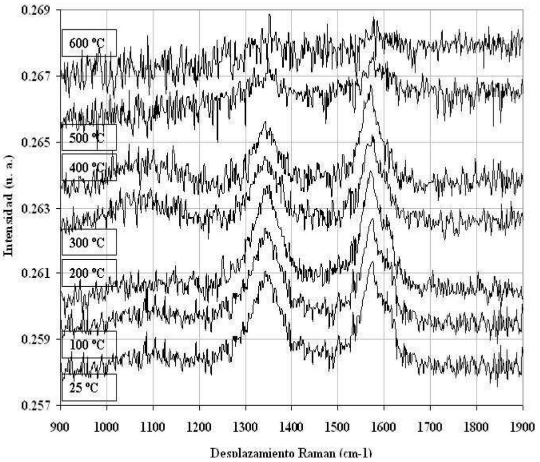

Fig. 2. Espectros Raman *in situ* de los composites tratados a diferentes temperaturas.

En base a estos resultados, en la Tabla 1 se recogen los valores de posición e intensidad de las bandas fundamentales (D, G y enlace C-O), así como la relación entre la D y la G (valor que está relacionado con el índice de grafitización), para las NFC en función de la temperatura de tratamiento de los composites.

T (ºC)	**Banda G**		**Banda D**		**Banda C-O**		**I_D / I_G**
	Posición	Intensidad	Posición	Intensidad	Posición	Intensidad	
	cm^{-1}	u. a.	cm^{-1}	u. a.	cm^{-1}	u. a.	
25	1572.0	3.15	1347.0	2.8	1085.0	0.65	0.89
100	1573.4	3.05	1347.5	2.75	1084.0	0.60	0.90
200	1571.5	3.65	1345.2	3.15	1069.3	0.50	0.86
300	1575.0	2.40	1342.8	1.9	1079.9	0.75	0.79
400	1571.5	2.90	1341.9	1.8	1077.3	0.70	0.62
500	1575.2	1.05	1351.2	0.65	1077.0	0	0.62
600	1583.3	0.80	1351.0	0.43	1077.0	0	0.54

Tabla 1. Parámetros de las bandas Raman de NFC.

Como puede verse en esta Tabla 1, las intensidades de cada una de las bandas disminuyen con la temperatura de tratamiento, lo que indica que las nanofibras de carbono están reaccionando bien con las partículas de vidrio o bien con la atmósfera del medio. Teniendo en cuenta que cualquier oxidación de la superficie de las nanofibras debería conducir a la formación de enlaces C-O en ella, la banda de 1070 cm-1 debería aumentar, hecho que se confirma entre las temperaturas 300 – 400 ºC, mientras que para temperaturas mayores dicha banda desaparece. Este resultado indica que las nanofibras de carbono resisten temperaturas de 200 ºC, entre 300 y 400 ºC se oxidan y a 500 ºC se degradan rápidamente.

En relación con las bandas D y G, se puede comprobar como hasta 200 ºC dicha relación se mantiene, es decir, la estructura grafítica no sufre cambio alguno. A partir de 300 ºC esta relación decrece, lo que indica que las nanofibras se están grafitizando, lo que tiene que ser debido al efecto de la temperatura y a la eliminación de grupos funcionales superficiales. Este resultado está de acuerdo con la desaparición del hombro situado a 1600 cm-1, mencionado anteriormente.

Es de destacar que a 600 ºC aún son observables las bandas D y G con muy pequeña intensidad, lo que parece indicar que aunque se grafiticen las nanofibras, éstas se degradan por la presencia de las partículas de vidrio.

4. CONCLUSIONES

En este trabajo se ha estudiado por espectroscopía Raman la interacción entre nanofibras de carbono y partículas de vidrio durante la obtención de materiales compuestos de matriz vítrea. El estudio se ha realizado in situ a diferentes temperaturas y se ha basado en el análisis de las bandas D, G y C-O de las nanofibras. Se ha observado como entre 300 y 400 ºC las nanofibras se oxidan para formar enlaces C-O y luego, entre 500 y 600 ºC, se degradan. Sin embargo al aumentar la temperatura de tratamiento aumenta el grado de grafitización, ya que las partes más amorfas de las Ganf se oxidan antes que las partes más cristalinas.

AGRADECIMIENTOS

Los autores desean agradecer el presente trabajo al proyecto CENIT DOMINO financiado por el CDTI.

REFERENCIAS

BALAZSI, CS., SHEN, Z., KONYA, Z., KASZTOVSZKY, ZS., WEBER, F., VERTESY, Z., BIRO, LP., KIRICSI, I., ARATO, P. (2005) Processing of carbon nanotube reinforced silicon nitride composites by spark plasma sintering. *Comp. Sci. Tech.* 65, 727–733.

LESPADE, P., MARCHAND, A., COUZI, M., CRUEGE, F. (1984). Caracterisation de materiaux carbones par microspectrometrie Raman. *Carbon*, 22 (415) 375-385.

PÉREZ-VILLAR, S., TAMAYO, A., MAZO, M.A., RUBIO, F., RUBIO, J. (2008). Aplicación de las espectroscopias IR/ATR y Raman al estudio de la superficie de vidrios sometidos a molturación. *Bol. Soc. Esp. Ceram. Vidrio*. 47 (2), 89-94.

Reciclado de residuos de roca en el diseño de soportes para losetas de revestimiento y solado

Mª.A. Rodríguez, J. Cabezas. L. Fernández, S. García
Grupo de Análisis de Recursos Ambientales. Universidad de Extremadura. Badajoz. España
F. Rubio, J. Rubio
Departamento de Química Física de Superficies y Procesos. Instituto de Cerámica y Vidrio (CSIC). Madrid. España

RESUMEN

En este trabajo se han fabricado materiales compuestos de resina de poliéster y residuos de roca procedentes de las plantas transformadoras de roca ornamental. El objetivo del presente trabajo es la utilización del material compuesto obtenido como soporte en los tableros de roca ornamental, lo que facilitará el manejo de las tablas que se comercializan en la actualidad, con la consiguiente reducción del peso y coste en el transporte, así como ahorro de materia prima.

1. INTRODUCCIÓN

El sector de la Piedra Natural se enfrenta actualmente a una importante problemática derivada de la necesidad de compatibilizar las exigencias de la industria con la sostenibilidad del entorno. El desconocimiento, y en ocasiones, el incumplimiento de las normativas medioambientales es un hecho que no se debe obviar y que precisa soluciones inmediatas. Por ello, la importancia que adquiere la investigación y desarrollo de nuevos materiales a base de residuos de rocas ornamentales, es evidente.

Es bien sabido que la cantidad de estériles que se acumulan en las inmediaciones de las explotaciones mineras pueden llegar a alcanzar hasta el 90% de su producción. Liberar a las empresas de este tipo de residuos al mismo tiempo que se les da un valor añadido, al preparar otro tipo de materiales que también podrían ser utilizados en la construcción, sin que resulten competencia alguna para la propia piedra natural, supone un reto importante en el sector de las rocas ornamentales, tanto para las personas que investigan en él como para los propios empresarios.

Algunas empresas transformadoras de piedra natural radicadas en Extremadura apuestan por la investigación, al considerarla como uno de los pilares de su desarrollo y modernización, interesándose en las investigaciones que sobre el aprovechamiento de este tipo de residuos, venimos realizando desde hace más de 10 años. Una empresa comprometida, con la eliminación de escombreras y lodos que generan diariamente y también con el aprovechamiento de la mayoría de ellos, dando valor a un subproducto originalmente residual, es PINASUR (Piedra Natural Asuar, S.L.), situada en Almendralejo (Badajoz).

En este trabajo se han preparado placas de materiales compuestos incorporando lodos procedentes del corte de mármoles y granitos, en matrices poliméricas, que fueron posteriormente utilizadas como soporte en plaquetas de mármol o granito natural, reduciendo así tanto el espesor de las tablas de piedra ornamental empleadas para revestimiento o solado, como el peso de dichas placas.

2. EXPERIMENTAL

Los lodos de mármol y granito empleados fueron suministrados por la empresa PINASUR. Estos lodos se secaron y tamizaron para separar los distintos tamaños de grano. Los resultados que presentamos en este trabajo son los correspondientes a partículas inferiores a 50 micras.

La caracterización textural de los lodos se realizó mediante Adsorción de nitrógeno, Porosimetría de Hg y Microscopía electrónica de barrido (MEB), principalmente.

Los materiales compuestos se prepararon mezclando directamente los lodos con una resina de poliéster, y se caracterizaron mecánicamente mediante flexión a tres puntos. Se utilizaron relaciones residuo/resina de 75/25 en peso.

Las placas de material compuesto se pegaron a plaquetas de mármol comerciales, utilizando distintos adhesivos; pegamento convencional, loctite y la propia resina de poliéster. Los nuevos materiales bi-placa obtenidos, se caracterizaron mediante resistencia a flexión y a tracción para comprobar el grado de adherencia entre el composite y el mármol.

3. RESULTADOS Y DISCUSIÓN

3.1. Caracterización textural del residuo

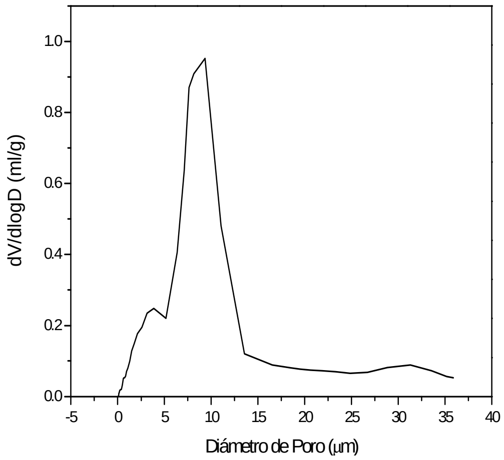

Los resultados correspondientes a la caracterización mediante adsorción de nitrógeno indican que estos lodos tienen una superficie específica aproximada de 0.15 m^2/g. Según la clasificación de la IUPAC, la isoterma obtenida es tipo II, que se corresponde con sólidos no porosos puesto que no presenta ciclo de histéresis. La distribución de poros obtenida a partir de la isoterma de desorción indica cierta tendencia a la presencia de macroporos, corroborado con la curva de distribución de poros obtenida mediante porosimetría de mercurio (figura 1), en la que se aprecia la presencia de tres tamaños de poro bien definidos, situados a 3.9, 8.2 y 9.2 micrómetros, así como otros de mayor tamaño que pueden ser ocasionados por los poros existentes entre las partículas.

Figura 1. Distribución de poros de los lodos utilizados en la fabricación del material compuesto.

3.2. Caracterización mecánica de los materiales

La caracterización del mármol, composite y par mármol-composite (a partir de ahora PMC) se llevó a cabo mediante medidas de flexión y tracción. En la figura 2 se presentan fotografías correspondientes a las medidas de flexión en tres puntos sobre los PMC para las dos situaciones que pueden darse; ejerciendo la presión sobre el mármol (fig.2a) o sobre el material compuesto (fig.2b).

Figura 2. Medidas de flexión en 3 puntos para los nuevos materiales PMC.

La resistencia a la flexión del mármol (Tabla 1) es baja comparada con la del material compuesto, lo que indica que el mármol va a ser el material limitante. Esto se observa mejor cuando se caracteriza mecánicamente el par PMC; al realizar el ensayo ejerciendo presión sobre el mármol el material compuesto es quien actúa como receptor de la carga (fig. 2a), y hasta que éste no se rompe, el par PMC mantiene las propiedades iniciales, mientras que cuando la presión se ejerce sobre el material compuesto, la resistencia a la flexión es prácticamente la de éste. El módulo de Young y la deformación siguen comportamientos similares, en función del material sobre el que se ejerce la presión.

MUESTRA	MARMOL (M)	MAT. COMP. (MC)	M/MC	MC/M
MOR (MPa)	17.87	47.50	47.70	10.92
Mod. Young (GPa)	8.95	15.45	14.20	7.72
L/L0 (%)	2.79	4.92	4.22	2.76

Tabla 1. Propiedades mecánicas obtenidas mediante flexión en 3 putos de los materiales estudiados.

Para determinar el grado de adherencia entre el mármol y el composite con los diferentes adhesivos utilizados (pegamento universal, loctite y la propia resina de poliéster), los nuevos composites se caracterizaron también mediante medidas de tracción. En estos ensayos, la superficie de contacto fue aproximadamente de 50x50 $mm^{2.}$ (Figura 3).

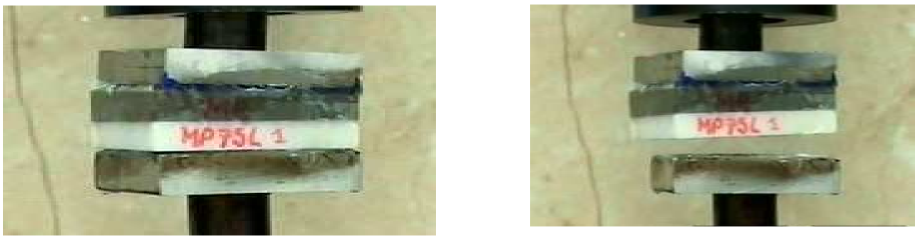

Figura 3. Medidas de tracción para los pares PMC.

Las curvas de tracción para los tres adhesivos utilizados, y los valores de la resistencia a la tracción y el desplazamiento observado hasta rotura se muestran en la figura 4 y Tabla 2, respectivamente.

PEGAMENTO	UNIVERSAL	LOCTITE	RESINA
Resistencia Tracción(MPa)	0.91	1.53	1.87
Desplazamiento (mm)	3.01	3.64	3.93

Tabla 2. Propiedades mecánicas obtenidas mediante medidas de tracción.

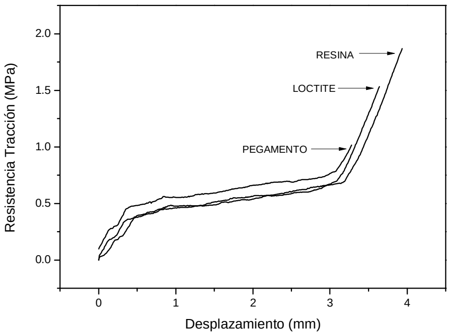

Figura 4. Variación de la resistencia a la tracción en función del adhesivo utilizado.

Se observa un comportamiento similar para los tres adhesivos; la carga se incrementa al inicio muy rápidamente y casi se estabiliza en un amplio rango de desplazamiento, indicando que el composite se comporta elásticamente, ya sea por el adhesivo utilizado para pegar las piezas los útiles metálicos de tracción, o bien por el tipo de adhesivo utilizado para pegar el mármol y el material compuesto entre sí. Finalmente, la carga vuelve a incrementar rápidamente antes de romper. Según los datos de la Tabla 2 y la figura 4, la propia resina de poliéster es el adhesivo que proporciona mejor unión entre el mármol y el composite soporte, reduciéndose la resistencia un 20% en el caso del loctite y casi un 50% para el pegamento universal.

4. CONCLUSIONES

La disminución de peso de las planchas comerciales de piedra natural ha sido posible mediante la reducción del espesor de dichas placas a la mitad y la incorporación en su lugar de una placa de material compuesto en la que se han empleado residuos procedentes de las labores de transformación de mármoles y granitos, con las consiguientes mejoras que esto supone para el transporte y manipulación.

La óptima unión de ambas placas, así como la mejora en propiedades mecánicas con respecto a las exhibidas por el mármol, permitirán utilizar menor cantidad de piedra natural, con el consiguiente ahorro de un recurso no renovable, al mismo tiempo que se minimizan los residuos generados en el sector de las rocas ornamentales.

REFERENCIAS

RODRÍGUEZ, MªA., RUBIO, F., RUBIO, J., MURCIEGO, A. (1999). Preparación y propiedades de MC a partir de residuos de rocas. III Congreso N. de Mat. Compuestos.
SEGADLES, A.M., CARVALHO, M.A., ACCHAR, W. (2005). Using marble and granite rejects to enhance the processing of clay products. APP. Clay Sci, 30,1,42-52.

T5. BIOCOMPOSITES FOR SPECIFIC APPLICATIONS BIOCOMPOSITES PARA APLICACIONES ESPECÍFICAS

Recent research results on natural fiber composites

A. Vázquez
Grupo de Polímeros y Materiales Compuestos, Instituto de Investigaciones en
Tecnología y Ciencias de la Ingeniería (INTECIN)- CONICET
Facultad de Ingeniería- Universidad de Buenos Aires
Las Heras 2214- Buenos Aires- 1127AAR-Argentina
C.R. Bernal
Grupo de Materiales Avanzados, Departamento de Mecánica, Facultad de Ingeniería,
Universidad de Buenos Aires. Paseo Colón 840, Buenos Aires-Argentina
G. Francucci, A. Stocchi, A.N Fraga, J. Doumecq, E.S. Rodríguez
Institute of Material Science and Technology (INTEMA)
University of Mar del Plata - National Research Council (CONICET),
Av. Juan B. Justo 4302 - B7608FDQ - Mar del Plata, ARGENTINA

ABSTRACT

On the World Years of Natural Fibers declared by FAO, their utilization in order to obtain added valuable material is a key factor. Our group is working in the subject since 1994, and recent results on: i) fiber treatment, ii) vacuum infusion technique, iii) dielectric measurement, will be discussed.

A fiber treatment consisting on an alkali treatment superimposed to biaxial tensile stress for woven jute fabric/vinylester laminates was done. The influence of the treatment time on the composites' mechanical properties was also studied.

Resin transfer moulding technique is a processing which permit to obtain a composite material with less content of voids. However their use with natural fibers has some particular characteristics which were analyzed. Untreated and alkali-treated jute fabrics were used and the treatment effect on the mechanical properties of the fiber and composites, as well as on the processing conditions was studied.

In order to correlated the dielectric properties to water absorption in natural fiber composites, gravimetric and dielectric measurements were used to monitor distilled water and artificial seawater uptake in vinylester matrix and natural fiber composites.

1. INTRODUCTION

Natural fibers have several advantages as reinforcement of polymer: biodegradability, low density, high specific properties, low cost, nonabrasive processing characteristics and availability from renewable resources. The disadvantages of natural fibers are moisture absorption leading to fiber swelling, low thermal resistance and fire resistance, local or seasonal variations in quality, lower mechanical properties (impact) than glass fiber composites and low fiber-matrix adhesion (especially with thermoplastic matrices). The mechanical properties of composites based on natural fibers are influenced by different factors. These factors are: i) the high variability of natural fiber strength properties due to their natural nature, ii) non-uniform fiber cross-sections iii) the fibril nature of natural fibers and the possibility to alter their morphology (i.e. change in the spiral angle and increase of molecular orientation, density, fibrillation) by chemical treatment iv) imperfect fiber-matrix interfaces (especially with thermoplastic polymers), and v) processing conditions. The treatments improved the mechanical properties of the composites, but in different degrees in order to the type of treatment.

The aim of the presentation is based on different works developed with natural fibers and thermosetting resins. The presentation includes some of the important subject on these natural fiber composites: fiber treatments, vacuum infusion technique particularities, and the dielectric characterization versus water absorption.

2. FIBER TREATMENT

Several chemical treatments have been proposed in the literature with the aim to improve the tensile properties and water absorption of natural fibers. However, there was not taken into account the increase on the fiber cost and the fact that chemical composition and morphological changes of the technical fibers could be also induced by chemical treatment (**Plackett and Vázquez, 2004; Cyras et al., 2004**).

Commercial woven jute fabrics (Casthanal, Textil CIA, Brazil) were used as reinforcement. The matrix material was prepared from general purpose vinylester resin (Derakane Momentum 411–350 from Dow, kindly provided by Poliresinas San Luis, Buenos Aires, Argentina) and accelerator in a weight ratio of 1 : 0.05, respectively. Jute fabrics were treated with Na(OH) aqueous solution (5% w/v) for different periods of time (1, 2, 4, and 24 h) with continuous shaking at 25°C under biaxial tension.

The compliance of the jute fabrics was evaluated and the results showed that the natural fibers treated during 4 h at room temperature showed the lower compliance. It was attributed to the increase of the crystalline index of the natural fibers obtained by DRX technique.

The increase of their crystallinity is due to the extraction of lignin compound, and the change from cellulose I to II (**Cyras et al 2004**). At 24 h of treatment, the fibers have an increase in crystallinity but the fibers are degraded, and they have lower mechanical properties than 4 h of treatment.

Composite with VE resin and 40 wt.% of jute fibers was fabricated. The Young’s modulus and tensile strength values for the composites with fabrics treated with alkali under stress at different treatment time was: 5,97 GPa for untreated fibers, 7,68 GPa for 4 h alkaline treatment under tension, and 5,96 GPa for 24 h alkaline treatment under tension. The alkaline treatment without tension during 24 h produces a modulus of 5,24 GPa. This results permit to demonstrate that there is an optimum treatment time at room temperature (**Stocchi et al, 2006; Vázquez et al 2009**)

3. VACUUM INFUSION

Woven jute fabric and vinylester resin was used to prepare the composites using the vacuum infusion technique. The fibers were treated with NaOH (5 wt.%) for 24 h at room temperature. The treatment with alkali may modify the crystallographic cell from cellulose I to cellulose II and it may also greatly affect the surface morphology of natural fibers. The alkali treatment produces a rough surface, and the number of anchorage points increases. The injection times increased in the treated jute fabrics as a consequence of the increase in the exposed area and the flow resistance. The fabric permeability decreased, also, in the tubular structure collapse of the fibers, which could reduce the capillary pressure. Flexural and impact properties of the treated-jute composites are lower than untreated-jute composites (**Rodríguez et al 2007**).

From our work, we demonstrated that jute reinforcements absorb great amount of fluid during the infusion process. The fluid absorption affects the permeability value of the fabric, because it removes fluid from the main stream as it travels through the reinforcement, acting as a sink component and thus decreasing flow velocity during the unsaturated flow. Furthermore, saturation of natural fibers can cause swelling, thus reducing the porosity and increasing flow resistance during saturated flow. So both saturated and unsaturated permeability values of the Jute fabric are reduced because of the fluid absorption. Also, in the infusion of composite parts with true resins the swelling of the fibers is still present, as could be demonstrated with swelling test with vinylester and phenolic resins (**Francucci et al 2009**).

4. DIELECTRIC MEASUREMENTS

Natural fibre disadvantage is its mayor capacity of water absorption, which in turn provokes gradual loss of mechanical properties. Then, the rate of ageing will be affected when water diffuses into the polymer composite and causes premature failure. To determine these factors it is very interesting to use a non destructive technique, such as measuring the dielectric properties of the material. Gravimetric and dielectric measurements have been used to monitor water uptake in composites based on unsaturated polyester and glass, jute and washed jute fibers. The results showed that the dielectric constant of jute fiber composites is higher than the composites based on glass fibers. Also, when the frequency increases the permittivity decreases. A Fickian diffusion model was applied and the effective diffusion coefficient was calculated. The results showed that when the sizing is removed in jute fibers washed with hot water, the effective coefficient diffusion increases. Changes in the dielectric permittivity were measured at different frequencies and at different times during water absorption at room temperature. A non-linear behaviour has been found in the changes of the permittivity with water absorption in the range frequency of 200 Hz to 1 MHz (**Fraga et al 2006**). Recently, it was studied the water uptake in vinylester matrix and sisal unidirectional composites. The amount of water absorbed was independent of fiber directionality within the composite. The dielectric constant was measured for 90º, where samples were cut so to place fibers perpendicular to the electric field; and for 0º, with fibers parallel to the field, founding that dielectric constant was greater for 90º, where contact surface between the fiber and the electrode is greater than for 0º composites. It was found that the dielectric constant of the matrix and the composite decreases as the frequency increases and increases as water absorption increases as consequence of their higher polarity.

CONCLUSIONS

An optimum alkaline treatment under tension, based on the mechanical properties of a single natural fiber, was obtained. This result is a consequence of two effects which occur simultaneously: the increase of fiber orientation and the fiber damage due to alkaline medium. The alkali treatment without tension produced a drop in both tensile strength and Young’s modulus of the fibers. This result was attributed to the excessive extraction of lignin and hemicellulose, which play a cementing role in the structure of fibers.

Fluid absorption and swelling are mechanisms present in natural fibers vacuum infusion technique. Fluid absorption removes fluid from the main stream as it travels through the reinforcement, acting as a sink component and thus decreasing flow velocity during the unsaturated flow. Also, the saturation of the natural fibers cause swelling, reducing the porosity and increasing flow resistance during saturated flow. The longer injections times obtained for the treated jute fabric were due to the more compact and rougher fiber surface that produced the treatment. A lower capillary pressure that leads to lower fabric permeability was a consequence of the fiber lumen collapse.

The composites fabricated by vacuum infusion technique and alkaline-treated fibers without tension presented a brittle behavior with lower flexural and impact properties in the case of the composites reinforced with treated jute. The drop in the mechanical properties of the fibers was the main cause of these results.

The dielectric constant decreases when the frequency increases and it increases with water uptake for all composites. The washed jute composite has a higher dependence on water uptake and frequency, and this can be attributed to the effect of a higher interaction of the jute fiber cellulose –OH to water molecules. The relationship between relative permittivity and water uptake is non-linear in the range of frequency 200 Hz to 1 MHz used in the measurements. Dielectric constant value depends on fiber direction in the composite respect to the electric field applied. Dielectric constant is greater for composites where fiber direction is perpendicular to the electric field applied, than for composites where both are parallel.

REFERENCES

CYRAS VP, VALLO C, KENNY JM, VAZQUEZ A. (2004) Effect of Chemical Treatment on the Properties of Short Sisal Fiber-Reinforced PCL/Starch Blend, *Journal of Composite Materials***,** 38, 16, 1387-1400.

FRAGA AN, FRULLONI E, DE LA OSA O, KENNY JM, VAZQUEZ A. (2006) Relationship between Water Absorption and Dielectric Behaviour of Natural Fiber Composite Materials, *Polymer Testing*, 25, 2, 181-187.

FRANCUCCI G., RODRIGUEZ E., VÁZQUEZ (2009) A. Study of saturated and unsaturated permeability in natural fiber fabrics, *Composite Material part A.*, sent 2009

PLACKETT D., VAZQUEZ A. (2004) Biopolymers and Biocomposites in *Green Composites: polymer composite and the environment*, Chapter 5, Woodhead Publishers, CarolineBaille, ISBN 1-85573-739-6

RODRIGUEZ ES, STEFANI PM, VAZQUEZ A. (2007) Effects of Fiber Alkali Treatment on Vacuum Infusion Process and Mechanical Properties of Jute Vinylester Composites, *Journal of Composite Materials*, 41, 14, 1729-1741.

STOCCHI A., LAUKE B., VÁZQUEZ A., BERNAL C. R. (2006) A novel fiber treatment applied to woven jute fabric/vinylester laminates, *Composites: Part A* 38 1337–1343.

VÁZQUEZ A., STOCCHI A., BERNAL C.R, (2009) Recent innovative results on natural fiber composites, *Int. J. Materials and Product Technology*, 36, Nos. 1/2/3/4, 348-357.

Study of the interaction of various liquids with ligno-cellulosic materials using colid-state NMR and DMA

H. Sugimoto, K. Kojiro, T. Miki, K. Kanayama
Materials Research Institute for Sustainable Development, National Institute of
Advanced Industrial Science & Technology (AIST)

SUMMARY

Plastics depend strongly on underground resources such as petroleum. To produce novel wood materials as a substitute for plastics, the fine structure of wood and the interaction between wood and various solvents - ethylene glycol (EG), tri-ethylene glycol (TEG), Methanol (MeOH), dimethyl folmamyde (DMF), dimethyl sulfoxide (DMSO)- were examined using the solid-state nuclear magnetic resonance (NMR), analysis and the Dynamic Mechanical Analysis (DMA). The dynamic Young's modulus and tanδ -frequency curves of every sample indicated that the relaxation process at the temperature range from 20 to 100C due to the glass transition of lignin which is a major component of wood. Another process was observed at the lower temperature due to the reorientation of the solvents. The movement of the solvents confined in wood was slower than that of bulk. This result suggests that the movement of the solvents in wood is confined in the micro pore of wood. This assumption is consistent with the ^{13}C CP/MAS NMR measurement results. Despite being above melting temperature of these solvents, the resonances of solvents in ^{13}C CP/MAS NMR spectra were observed for the wood samples in accordance to EG and MeOH.

1. INTRODUCTION

Plastics depend strongly on underground resources such as petroleum. Therefore, we are trying to produce novel wood materials as a substitute for plastics. Wood and woody biomass is a renewable resource, if forests are controlled appropriately. Recently, we succeeded in transfer molding soft wood, hard wood and some lignocellulosic materials directly without a powdering process to save time and energy. The time of this molding process is short. Moreover, the forming process needs no adhesion, because of a self-bonding effect. However, since the flow process during molding requires a high pressure and temperature and is strongly influenced by sample moisture contents, the sample conditioning is very difficult. Therefore, to obtain an easier method, molding properties of wood impregnated with various organic solvents was examined. As expected, the wood impregnated with some solvents flowed by the pressure and temperature lower than with water. These solvents might adsorb lignin selectively (Nakatani et al. to 2008). But, the influence of those solvents on the fine structure of wood is still unclear. In our previous paper, we studied the dielectric properties of wood and cellulose conditioned at various relative humidities(RH) to clarify the influence of water on the fine structure of wood (Sugimoto et al. to 2007,2008). The structures of adsorbed water in wood and in cellulose are like that of ice. We assumed that these water molecules were hindered by the surrounding wood molecules. Similar results obtain by dynamic viscoeleasticity measurement. In the present study, we evaluate the effect of various solvents to wood from the viewpoint of fine structure using the dynamic viscoelasticity(DMA), dielectric spectroscopy(DES), and nuclear magnetic resonance(NMR) measurements.

2. MATERIALS AND METHODS

Three types of Japanese cypress (*Chamaecyparis obtusa*) sap wood specimens of 30mm(R, radial direction□×4mm(L, longitudinal direction)×1mm(T, tangential direction), 50mm(R, radial direction□×50mm(T, tangential direction)×5mm(L, longitudinal direction), and powder(50mesh pass 100mesh on) for DMA, DES, and NMR, respectively, were prepared. They were impregnated hereinafter with various organic solvents under 8kPa for 1hour and under atmospheric pressure for more than 24hours before the measurements were carried out on them. We used five kinds of organic solvents, ethylene glycol(EG), tri-ethylene glycol(TEG), Methanol (MeOH), dimethyl folmamyde(DMF), dimethyl sulfoxide(DMSO). The storage modulus and the loss tangent along R of the specimens were measured by the ±5μm tensile forced oscillation method using a Dynamic Mechanical Spectrometer (DMA50, Metravib). DMA measurements were conducted at the frequency 0.1, 0.5, 1.0, 5.0, 10Hz over a temperature range from –100˚C to 20˚C at heating rates of less than 1˚C /min. DES measurements were conducted at heating rates of less than 1˚C /min over the temperature range from –150˚C to 20˚C and the frequency range from 20 Hz to 1 MHz. An LCR-meter (Japan Hewlett-Packard Co. Ltd., HP4284A), an electrode (Ando Electric Co. Ltd., SE-3O, effective diameter = 38 mm) and a bath (Ando Electric Co. Ltd., TO-3) were used for DES measurements. CP/MAS ^{13}C Solid-State NMR experiments were performed on a Varian 400-MR spectrometer operating under a static field strength of 400MHz at -50, -20, 0, 20, 40, 60, 80˚C. The contact time for CP was 2ms with a decoupling power of 63kHz. The MAS speed was 16kHz. The delay time after the acquisition of the FID signal was 2s. The chemical shifts were calibrated by using the adamantane resonance at 20.441ppm.

3. RESULTS AND DISCUSSION

Fig. 1 shows Temperature variations of dynamic Young's modulus (*E*') and loss tangent at the various frequencies for wood impregnated with dimethyl sulfoxide. It has been suggested that *E*' slightly drops above -20°C. This indicate that the one relaxation process exists. In connection with the effects of temperature on the mechanical properties of wood, thermal softening properties of wood and wood components have been studied (Goring to 1963, Furuta et al. to 2001). Takamura and Furuta reported that cellulose, hemicellulose and lignin, which are wood components, soften around 230°C, -50°C, 80°C, respectively, in the water-swollen state. Although the method of isolation is considered to affect these results, many studies reported similar results, so, this relaxation may be due to the glass transition of lignin in wood. The apparent activation energies (ΔE) of the relaxation of impregnated wood with water, EG, DMF, DMSO were 423, 291, 128, 80kJ/mol, respectively.

On the otherhand, three processes were observed at the lower temperature. The small relaxation process at around -40°C, is may be due to the glass transition of hemicellulose, because it appeared in the moist wood at near temperature. But we don't have further information, we will be discuss in another paper. The peak observed at -110°C is due to the glass transition of bulk DMSO. It appeared in the glass filter dipped in DMSO. One broad relaxation process was observed at around -80°C. The specimen impregnated in EG has similar relaxation process which is not observed in bulk solvent. The structure of water in wood is similar to that of ice, because water confined in micro-pore of wood (Sugimoto et al. to 2007, 2008). The possibility of the confinement of other solvents in wood is acceptable. If the movement of the solvents confined in wood is slower than that of bulk, ^{13}C CP/MAS NMR measurement is applicable to measure movement of solvent in wood. In fact, despite being above melting temperature, the resonances of EG and MeOH in ^{13}C CP/MAS NMR spectra were observed for the wood samples. These results suggest that the movement of the solvents in wood is confined in the micro pore of wood.

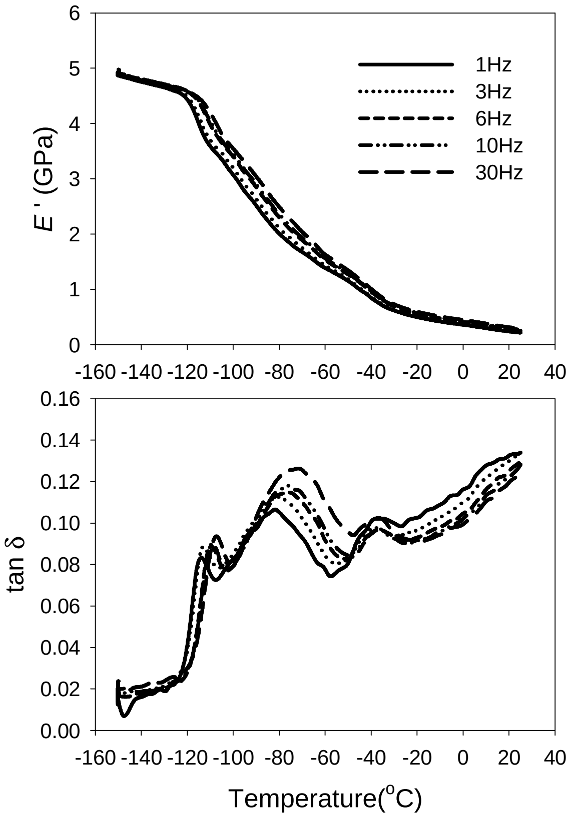

Fig. 1. Temperature variations of dynamic Young's modulus (*E'*) and loss tangent at the various frequencies for wood impregnated with dimethyl sulfoxide.

4. CONCLUSIONS

Rheological (dynamic mechanical and dielectric) properties and CP/MAS spectrums for wood impregnated with various organic solvents - ethylene glycol(EG), tri-ethylene glycol, dimethyl folmamyde(DMF), dimethyl sulfoxide(DMSO) - were examined. The results are summarized as follows: The relaxation process due to the glass transition of lignin in wood exists at the measurement range. The apparent activation energies of the sample impregnated with water and EG were higher than that with DMSO and DMF. These results may be not only due to the hydrogen bonding per volume, but also to the confined effect in wood. In fact, the CP/MAS spectra of EG – Wood sample indicates the existence of the slow movement EG at higher temperatures of the melting point.

ACKNOWLEDGMENT

The authors are sincerely grateful to Dr. Masakazu Nishida, Research Institute of Instrumentation Frontier (AIST), for kindly helping for the measurements of CP/MAS NMR.

REFERENCES

Furuta, Y., Obata, Y., Kanayama, K. (2001) J. materials Science, 36, 4, 887-890.
Goring, D. A, I.,Pulp Paper Mag. Can., 64, 515-527, 1963
Nakatani, T., Ishimaru, Y., Iida, I., Furuta, Y. (2008) *MokuzaiGakkaishi* , 54, 17-23.
Sugimoto, H., Tsunehisa, M., Kanayama, K., and, Norimoto, M. (2007) *Holzforschung*, 61, pp. 89–94.
Sugimoto, H., Tsunehisa, M., Kanayama, K., and, Norimoto, M. (2008) *J. Non-Crystalline Solids* 354 3220–3224

.

Composites made of recycled films reinforced with natural fibers and mineral fillers

A.L. Leão
Dept. of Natural Resources
College of Agricultural Sciences – FCA
UNESP – São Paulo State University
Botucatu, SP, Brazil
S.F. Souza
Dept. of Natural Resources
College of Agricultural Sciences – FCA
UNESP – São Paulo State University
Botucatu, SP, Brazil
E. Frollini
IQSC – Chemical Institute of Sao Carlos
USP –Sao Paulo
São Carlos, SP, Brazil
C.A.F. Correa
College of Forestry
University of Toronto

SUMMARY

There has been a growing interest in polymer composites with lignocellulosic fibres in the latest years for two reasons: the production of composite materials based on lignocellulosics is more economic than the production of thermoplastics, and also the lignocellulosic fibres are an attractive and cheaper alternative to the development of renewable and biodegradable materials. Therefore, new materials are being developed for use in several industrial sectors: construction, packaging, automobile sector among others. The composites with natural fibres (based on renewable resources) are particularly interesting since they can replace traditional materials as wood, mineral and plastics in some applications. The development of these materials has been attracted by the need of durable materials that can be used in outdoor environments without chemical treatments.

It was used in this study film of PP bi-oriented and recycled material (blends of Polyethylene – PP with Polyethylene Terephthalate – PET, which components ratio is unknown). The PP film and the blend were obtained from recycled films.

The wood (pinus) was used as a reinforcement in several systems. The compatibilizing agent MAPP (polypropylene-graft- maleic anhydride) was used to improve the compatibility fibre/matrix and by this way make viable the blends with better mechanical characteristics.

The composites were obtained through processing in a twin screw extruder model ZSK 25, using a temperature profile in which the maximum value is 190ºC to avoid degradation of the fibres. The pellets were dried and after submitted to the injection molding machine to obtain specimens according to the ASTM standards. The several compositions were assessed by melt flow index, tensile mechanical and Izod impact (notched) tests

The results presented in this work showed that the wood is a good filler or reinforced for the production of low cost composites. In addition to this, the use of pos-consumer material also seemed viable.

The composite BOPP58%/wood40%/MAPP2% exhibited excellent value for the TS, but an impact resistance extremely low. Then, it could be used in applications where the Impact Resistance exposition is not so important.

1. INTRODUCTION

There has been a growing interest in polymer composites with lignocellulosic fibres in the latest years for two reasons: the production of composite materials based on lignocellulosics is more economic than the production of thermoplastics, and also the lignocellulosic fibres are an attractive and cheaper alternative to the development of renewable and biodegradable materials. Thus, new materials are being developed for use in several industrial sectors: construction, packaging, automobile sector among others. The composites with natural fibres (based on renewable resources) are particularly interesting since they can replace traditional materials as wood, mineral and plastics in some applications (LEÃO, 2007).

In addition to this fact, the use of natural lignocellulosic fibres has shown several advantages as reinforcement of thermoplastic matrix in relation to the synthetic fibres as: good mechanical properties, environmental friendly, non-abrasive if compared with the traditional inorganic fillers (PP, talc, among others), low cost, non-toxicant (improving the working conditions), low density, etc. Besides, the use of natural fibres will contribute to reduce the request for products based on oil, and the deforestation by the replacement of products based on wood (RAHMAN, et al., 2009; LEÃO, et al., 2007).

2. MATERIALS E METHODS

It was used in this sutdy film of PP bi-oriented and recycled material (blends of Polyethylene – PP with Polyethylene Terephthalate – PET, which components ratio is unknown). The PP film and the blend were obtained from recycled films. The wood (pinus) was used as filler in several systems. The compatibilizing agent MAPP (polypropylene-graft- maleic anhydride) was used to improve the compatibility fibre/matrix and by this way make viable the obtainment of systems with better mechanical characteristics.

The composites were obtained through processing in a twin screw extruder model ZSK 25, using a temperature profile in which the maximum value is 190ºC to avoid degradation of the fibres. The pellets were dried and after submitted to the injection molding machine to obtain specimens according to the ASTM standards. The samples were conditioned at 25ºC for approximately 48 hours before the mechanical characterization. The several compositions were assessed by melt flow index, tensile mechanical and Izod impact (notched) tests.

The tensile test was performed following the ASTM standard (ASTM D638). For each composition, 5 specimens were used. This characterization was performed using a cell load of 3000 N and velocity corresponding to 5 mm/min.. The impact resistance tests were done according to the ASTM D-256 standard. The result is an average value obtained from 8 specimens. The melt flow index values were determined using the conditions by the standard ASTM D-1238.

3. RESULTS AND DISCUSSION

The tensile strength value of a composite can qualitatively indicate the level of adhesion between the phases, that is, if this value were higher than that for the pure polymer, it can be said that the matrix transferred tension to the disperse phase. This tension transference occurs through the interface as a result of longitudinal plastic deformation between the filler and the matrix and also as a result of the friction contact between the components. On the other hand, the lack of compatibility in the system will cause deficiencies during the process of mechanical solicitation transference of the matrix to the particles inducing to failure by delamination in the interface filler/matrix.

The Figure 1 shows the mechanical behavior of the composites BOPP/wood and also the influence that 2% of the compatibilizer agent (MAPP) had on the mechanical behavior of the composites.

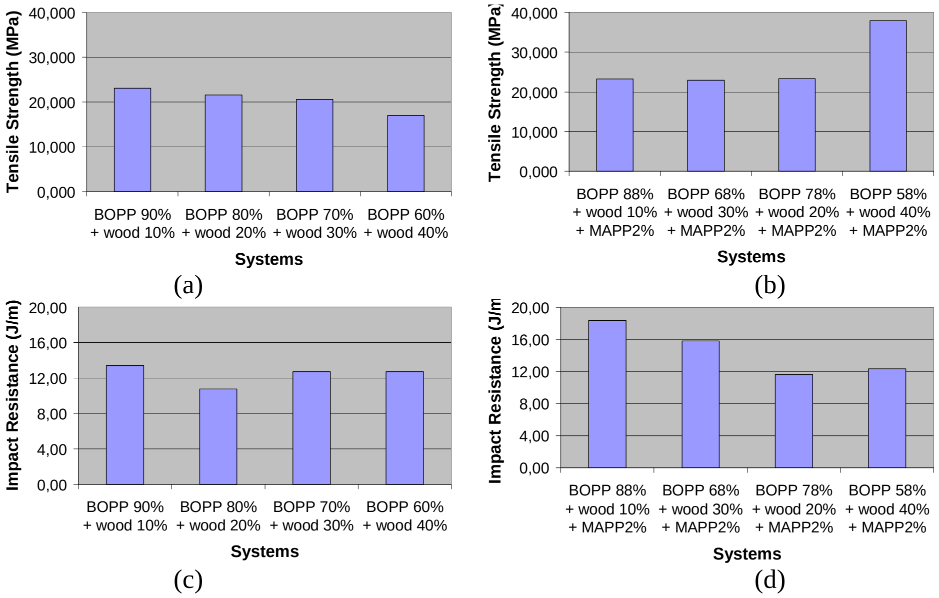

Figure 1 Mechanical properties for the composites BOPP/wood: (a) Tensile Strength, (c) Impact Resistance Izod (notched) – composites BOPP/wood and (b) Tensile Strength, (d) Impact Resistance Izod (notched) - composites BOPP/wood/MAPP.

Comparing the composites with different kinds of fillers but same content (30%), it can be observed that the addition of wood seemed to be more drastic in relation to the drop in TS. However, besides the advantages of using natural fillers, as already mentioned, it is important to emphasize that the wood shows low density (≈1,4 g/cm^3 X ≈2,5 g/cm^3 for the mineral fillers). So, the properties presented by composites based on natural fillers, when considered the weight can be profitable in some applications, as for example, in the automotive and transportation sectors.

5. CONCLUSIONS

The results presented in this work showed that the wood is a good filler or reinforced for the production of low cost composites. In addition to this, the use of pos-consumer material also seemed viable. Then, the results showed that is possible to produce environmental friendly composites with adequate mechanical properties to some applications, as for example. Through the compositions analyzed it was seen that a wide variety of materials with different characteristics were obtained.

The composite BOPP58%/wood40%/MAPP2% exhibited excellent value for the TS, but an impact resistance extremely low. Then, it could be used in applications where the IR is not so important.

ACKNOWLEDGMENTS

Special thanks to Recplast for their financial support and material supply need for this study. The author thanks the CNPq and FAPESP for their support.

REFERENCES

LEÃO, A. L. et al. Thermosetting and thermoplastic composites based on natural fibers: processing, properties, applications and Recyclability.

LEÃO, A. L. et al. State of the art for extrusion and injection molding NFPC – Natural Fiber Plastic Composites in Brazil. In: International Conference on Innovative Natural Fibre Composites for Industrial Applications, 2007, Roma. Proceedings of International Conference on Innovative Natural Fibre Composites for Industrial Applications, 2007.

RAHMAN, d.R. et al. Mechanical properties of polypropylene composites reinforced with chemically treated abacá. Composites: Part A (2009), doi: 10.1016/j.compositesa.2009.01.013

Recent advances on the surface chemical modification of cellulose fibres

M.N. Belgacem
Laboratoire de Génie des Procédés Papetiers (LGP2), UMR CNRS 5518
Grenoble INP - Pagora – Domaine universitaire - 461, rue de la papeterie
38402 Saint-Martin-d'Hères - France

SUMMARY

Several approaches of chemical modification of cellulose fibres' surface have been studied, in order to reduce their hydrophilic character and to improve the strength of their adhesion to the matrix in composite materials. Relevant advances were achieved recently in different modification strategies, namely (i) physical treatments such as plasma; (ii) chemical grafting by click chemistry or by using polyether and polyester grafts and (iii) silanol-cellulose condensation directly or through inorganic-organic hybrid cellulose-based materials. The characterisation of the modified surfaces was performed using elemental analysis, contact angle measurements, Scanning Electron Microscopy, CP-MAS ^{13}C-NMR, FTIR and X-ray photoelectron spectroscopy. The present paper reports the most relevant advances in the field of surface chemical modification of cellulose fibres.

1. INTRODUCTION

The use of natural cellulose fibres as reinforcing elements in macromolecular composite materials is a growing topic of investigation, particularly in view of replacing, at least partly, glass fibre-based composites, which cannot be recycled at the end of their life cycle (Belgacem and Gandini, 2008, Sabu and Pothan, 2009). Lignocellulosic fibres possess major limitations when used in the field of composite materials, since they are highly polar and hydrophilic. As a consequence, they are poorly compatible with commonly used non-polar matrices and they are subjected to a loss of mechanical properties upon atmospheric moisture adsorption. In order to avoid these drawbacks, they are systematically submitted to specific surface modifications in order (i) to provide them with an efficient hydrophobic barrier and (ii) to compatibilize their surface with that of a non-polar polymer matrix. In this context, the chemical moieties exploited are superficial hydroxy functions, which can be converted into esters, ethers, urethanes and siloxanes functions.

This paper reports the most recent and relevant advances in different modification strategies applied to cellulose fibres, namely (i) physical treatments such as plasma; (ii) chemical grafting by through click chemistry or using polyether and polyester grafts and (iii) silanol-cellulose condensation directly or through inorganic-organic hybrids cellulose-based materials.

2. SURFACE TREATMENTS OF CELLULOSE

2.1. Plasma

The treatment of additive-free hand sheet paper samples with cold-plasma showed that cellulose can be chemically linked with either reactive silane coupling agents (Gaiolas el al., 2008) (vinyl trimethoxysilane, **VTS**, and γ-methacrylopropyl trimethoxysilane, **MPS**) or natural products (Gaiolas el al., 2009), such as myrcene, **My** and limonene, **LM**. Contact angle measurement and X-ray Photoelectron Spetroscopy (XPS) were used to ascertain the occurrence of the grafting. In fact, the contact angle value of a drop of water deposited at the surface of paper increased from 30° for unmodified substrate to more than 100° for **VTS**-, **MPS**-, **LM**- and **My**-treated samples. Moreover, the treated surfaces became totally non polar, as their polar contribution to the surface energy decreased from about 23 mJ/m^2, for pristine samples, to practically zero for all the treated surfaces, as summarized in Table 1.

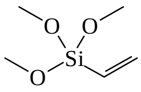

VTS

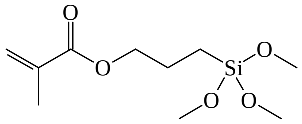

MPS

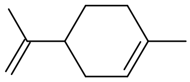

LM

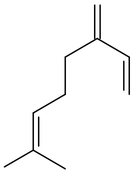

My

Cellulose	Θ_w, °	Surface Energy, mJ/m^2			References
		Dispersive	Polar	Total	
Virgin	40	25.3	25.0	50.3	Gaiolas et al., 2008
VTS-treated	98	27.0	0.6	27.6	Gaiolas et al., 2008
MPS-treated	100	32.0	0.2	32.2	Gaiolas et al., 2008
LM-treated	98	32.8	0.3	33.1	Gaiolas et al., 2009
My-treated	112	27.4	0.8	28.2	Gaiolas et al., 2009

Table 1. Surface energy of cellulose, before and after different grafting.

For **VTS**- and **MPS**-treated samples, the XPS spectra showed the appearance of two new peaks at 102 and 150 eV, relative to the presence of Si atoms and a substantial increase in Cl signal, attributed to the enrichment of the surface by C–H moieties borne by the silanes. SEM confirms the presence of the silane, both in the bulk and at the surface of the treated samples. The treated surfaces displayed water-barrier properties, since the penetration of the liquid was reduced significantly. The XPS spectra showed that the modification with **LM** and **My** gave rise to a very significant change in the O/C ratio, as well as to the intensity of the C1 peak assigned to aliphatic carbon sequences.

2.2. Chemical grafting by click chemistry or using polyether and polyester grafts

Very recently, a new approach of grafting cellulose surface fibres by polycaprolactone macromolecular chains in heterogeneous conditions *via* click-chemistry was reported (Krouit el al., 2009), as illustrates Scheme 1. Cellulose esters were prepared by reacting avicell with undecynoic acid, in order to prepare a cellulose substrate bearing multiple C≡C-terminated hairs. The thus modified avicell samples were first characterised by FTIR and XPS spectroscopy and elemental analyses and showed that the grafting had indeed occurred.

In parallel, polycaprolactone-diol (PCL) was converted into an azido-derivative and the ensuing products characterised by FTIR and ^{13}C-NMR spectroscopy. Both methods confirmed the success of such a modification. Finally, cellulose esters were reacted with azido-PCL grafts, in heterogeneous conditions, through "click chemistry". The resulting modified cellulose substrates were characterized by the same techniques mentioned above. All the three techniques confirmed that the grafting has occurred efficiently, since a weight gain of about 20% was achieved.

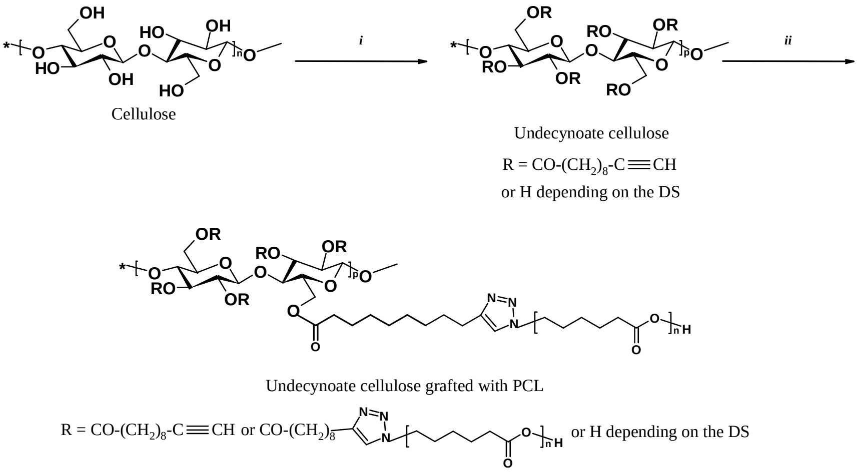

Scheme 1.

2.3. Silanol-cellulose condensation through inorganic-organic hybrids

Hardwood Eucalyptus bleached kraft fibres were used as a cellulosic substrate to produce inorganic-organic hybrids materials, by grating nano-silica particles, using a sol-gel process (Gonçalves el al., 2008). The prepared materials were then chemically modified with two fluorine-bearing alkoxysilane coupling agents, namely: 3,3,3-trifluoropropyl trimethoxysilane (**FPTS**) and 1H,1H,2H,2H,perfluorooctyl trimethoxysilane (**FOTS**), in order to produce super-hydrophobic surfaces (Gonçalves el al., 2008).

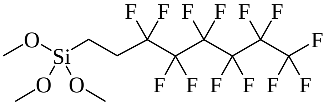

FPTS

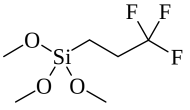

FOTS

Super-hydrophobic cellulose nano-composites were thus prepared using a multi-step nano-engineering process. Different techniques were used to prepare highly rough surfaces with very low surface energy. The first feature was achieved by the presence of amorphous silica particles, whereas the second one was insured by perfluoro moieties, which yielded a surface at which a drop of water formed a contact angle approaching 150°. The modification calls upon an aqueous Layer-by-layer system followed by siloxane hydrolysis. All the reaction steps were conducted at room temperature in air. The modified fibres were examined by scanning electron microscopy (SEM) and atomic force microscope (AFM) (Gonçalves el al., 2008).

2.4. Directly silanol-cellulose condensation

Much more recently, the surface of model cellulose fibres, Avicell (AV), as well as that of Whatman paper (WP) was chemically modified with **FPTS** and **FOTS** (Ly el al., 2009). After modification, the ensuing fibres were submitted to soxhlet extraction, in order to remove all physically adsorbed unbounded molecules. The occurrence of the grafting was confirmed by the presence of silicon and fluorine atoms detected by elemental analysis, X-ray photoelectron spectroscopy and Scanning Electron Microscopy (SEM). The contact angle measurements showed that, after grafting, the cellulose surface became totally hydrophobic. The C1s spectra show that the modification of cellulose with **TFPS** and **TFOS** displayed some substantial changes, namely: (i) the appearance of a C-Si peak at 283 eV, in all the modified substrates; (ii) the appearance of a CF_3 peak at 292 eV, in the **TFPS**-modified AV; (iii) the appearance of CF_2 and CF_3 peaks, respectively at 290 and 292 eV, in the **TFOS**-grafted AV; and (iv) the increase in the C1 signal, in all the spectra. AV seems to be systematically more reactive, which can be related to its higher specific surface area compared with PW.

3. CONCLUSIONS

Cellulose macromolecules can be grafted successfully by natural polymerizable molecules or silane coupling agents and using a solvent-free process, at room temperature. Such a treatment can be considered as a promising new approach, particularly in papermaking and textile applications, where the hydrophobisation of the tissues or paper-based packaging materials is an extremely important issue.

Original cellulose-silica-silane composite materials were prepared and found to have super-hydrophobic surface, which opens new ways of valorising cellulose, a ubiquitous renewable resource. Applications, such as water repellence and self-cleaning, could be envisaged for these fibres.

REFERENCES

BELGACEM M. N., GANDINI A., Editors (2008) *Monomers, Polymers and composites from Renewable Resources*”, Elsevier, Amsterdam, Netherlands.

GAIOLAS C., COSTA A.P., NUNES M., SANTOS SIVA M.J., BELGACEM M. N. (2008). *Plasma Processes Polym.*, **5**, 444-452.

GAIOLAS C., BELGACEM M. N., SILVA L., THIELEMANS W., COSTA A. P., NUNES M., SANTOS SILVA M. J. (2009) *J. Colloid Interface Sci.*, **330**, 298-302.

GONÇALVES G. MARQUES P. A. A. P., TRINDADE T., NETO C. P., GANDINI A. (2008). *J. Colloid Interface Sci.*, **324**, 42-46.

KROUIT M., BRAS J., BELGACEM M. N. (2008) *European Polym. J.*, **44**, 4074-4081.

LY B., BRAS J., BELGACEM M. N. (2009) in preparation.

SABU T., POTHAN L. Editors (2009) *Cellulose Fibre Reinforced Polymer Composites*, Old City Publishing, Philadelphia (USA).

On the evaluation of the cross-section area of lignocellulosic fibers

S. Paciornik, M.H.P. Mauricio, B. Temer, J.R.M. d'Almeida
Materials Engineering Department (DEMa),
Catholic University of Rio de Janeiro (PUC-Rio), Rio de Janeiro, Brazil

SUMMARY

Lignocellulosic fibers have several advantages as reinforcement for polymer-matrix composites as, for example, their biodegradability and neutrality with respect to CO_2 emission. However, they have some disadvantages such as the variability of properties that present large bounds due to several factors. In respect to the determination of fibers properties one issue is the actual measurement of the fiber cross-section. It is usual to measure a "typical" diameter and to assume that the fibers have circular cross-sections, although this is known to be a relatively crude approximation. In the present work, digital microscopy and image analysis were used to measure the actual cross-section of several lignocellulosic fibers. The true area was compared to those calculated from minimum and maximum projected diameters, and the errors were analyzed.

1. INTRODUCTION

Lignocellulosic fibers have been employed since Ancient times, but their engineering importance decreased progressively. By the middle of the 20th century the achievement of large scale production of polymeric fibers reduced even more their use, including the traditional usage niches, as for example in textiles and ropes. The last decades saw a rebirth of the importance of lignocellulosic fibers due to the growing needs for a more sustainable development, and large industries, such as auto making, began to reintroduce fibers, such as coir, to reinforce interior door panels and other non-structural elements. A very important aspect to be highlighted when dealing with lignocellulosic fibers is that they are neutral in respect to CO_2 emission (Mohanty *et al* 2002), being therefore in context with the Kyoto protocol.

Despite several advantages, some characteristics hinder the larger use of lignocellulosic fibers. One can cite the variability of properties, what is an intrinsic characteristic of a naturally growing material. Therefore, it is very common to find very wide ranges for the mechanical properties of lignocellulosic fibers reported in the literature. For example, values ranging from 393 to 773 MPa are reported for the tensile strength of jute (Bledzki and Gassan 1999).

As a matter of fact, since lignocellulosic fibers present a large variability of shape and size of their cross section, inaccurate values of their mechanical properties can be generated if a non-representative cross section is being measured. In fact, it is usual practice to measure a "typical diameter" using calipers or optical microscopy analysis, and to assume that the fibers have a circular cross section. How much error is introduced by these techniques is an open question.

In the present paper, digital optical microscopy was used to analyze a large sample of several lignocellulosic fibers, and to measure their real cross sections. The results were compared to results obtained assuming circularity, the deviations of this assumption were measured and their impact upon the tensile strength of the fibers was discussed.

2. MATERIALS AND EXPERIMENTAL METHODS

The fibers studied were prepared for observation under the optical microscope. During mounting, and prior to surface preparation, an attempt was made to keep the fibers aligned and normal to the plane of observation. Whenever possible, excessive agglomeration of fibers was controlled, to ease fiber discrimination during image processing. The samples were then ground and polished down to 1 µm diamond paste.

The prepared samples were observed with an optical microscope, Zeiss Axioplan 2ie, fully motorized and computer controlled, employing an Axiocam HR digital camera. Image acquisition, microscope control, image processing and analysis were done under Axiovision 4.7 software. Images were acquired in the reflected light mode, at different magnifications. To balance resolution and field size requirements, mosaic images (Paciornik and Maurício 2004) were automatically acquired covering a larger field of the samples, in which a representative number of fibers was imaged.

3. IMAGE ANALYSIS METHODOLOGY

The traditional image processing and analysis sequence was employed. In the pre-processing step an edge enhancement filter was applied to reduce the well-know halo effect. For some samples, residual scratching caused by polishing was reduced using a sigma low-pass filter. This is a tunable blurring filter that can be used to selectively reduce defects at the scale of scratches, while preserving the filter edges.

In the segmentation step fibers were discriminated by intensity thresholding. Given the wide variety of fiber types and shapes, automatic thresholding was not always successful and an appropriate threshold was interactively selected by the user.

Post-processing was used to correct three main segmentation problems: residual particles dispersed in the matrix that could be mistaken as small fibers, residual polishing scratches, and touching fibers. Touching fibers were separated with the traditional watershed method (Gonzalez and Woods 2008). However, because fiber shapes are so irregular and edge defects can arise from the several processing steps, the watershed method could create false boundaries and break fibers in certain cases. Thus, whenever necessary, spurious objects were manually eliminated to avoid biasing the statistical analysis.

The resulting fiber population was measured and 3 parameters were directly obtained from each fiber: True Area (TA), Maximum and Minimum Calipers (F_{max} and F_{min}). These calipers are equivalent to the commonly used diameter measurements from which the fiber area is estimated. Thus, F_{max} and F_{min} were used to calculate two other area estimates: AF_{max} and AF_{min}. Finally, absolute relative errors between TA and the two estimates were obtained (Eq. 1).

$$\Delta F_{max} = 100\left|\frac{TA-AF_{max}}{TA}\right| \text{ and } \Delta F_{min} = 100\left|\frac{TA-AF_{min}}{TA}\right| \qquad (1)$$

4. RESULTS AND DISCUSSION

Typical images of the analyzed fibers (piassava, jute and pupunha) are shown in Fig. 1.

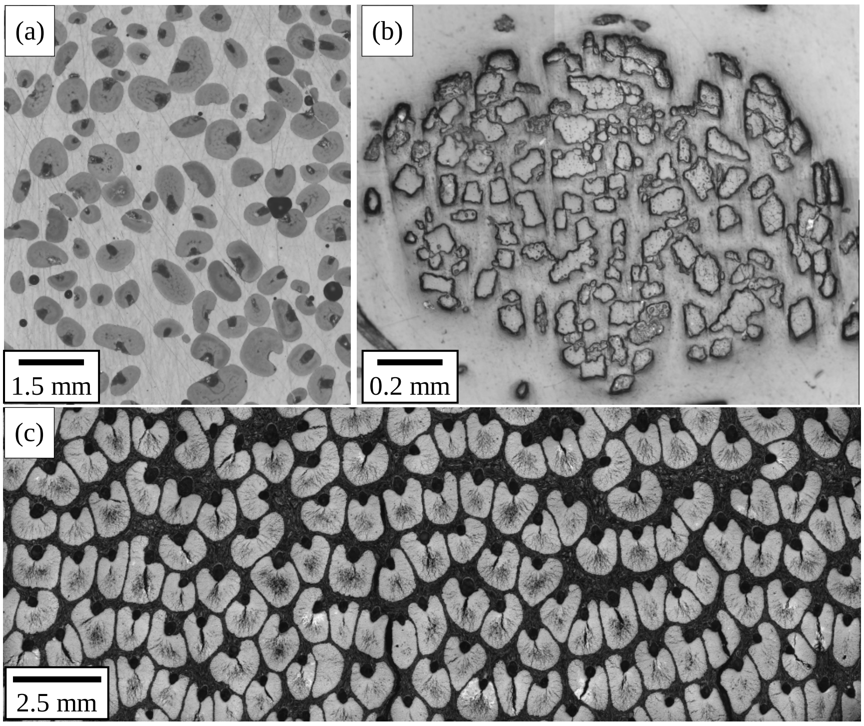

Fig. 1. Typical mosaic images (OM) (a) Piassava; (b) Jute; (c) Pupunha

Using the image processing sequence described above it was possible to measure the TA, F_{max} and F_{min} for the majority of the fibers from the 3 samples. As an example, the TA distribution for pupunha is shown in Fig. 2. The same wide dispersion is found for the other two materials.

Table 1 shows the number of measured fibers and the statistics for relative errors ΔF_{max} and ΔF_{min} for each sample. These numbers show that the errors committed when estimating the area through the calipers can be as high as 400%, depending on which caliper is measured with traditional methods. Clearly, these errors are strongly technique and operator dependent. Piassava and pupunha show similar results and lower error values than jute, mainly due to very different fiber shape of the latter material.

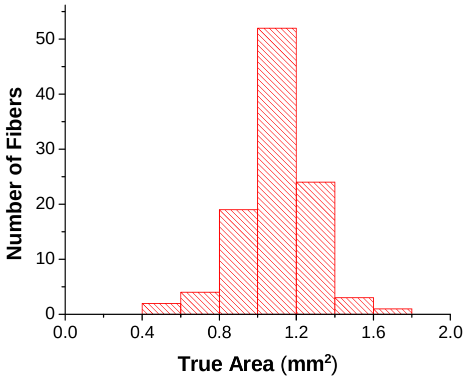

Fig. 2. True area distribution for pupunha fibers.

Table 1. Statistics for measured fibers, ΔF_{max} and ΔF_{min} for the 3 samples.

		Piassava	Jute	Pupunha
# Measured Fibers		80	150	100
ΔF_{max} (%)	Minimum	10	28	18
	Maximum	140	393	213
	Mean	54	124	66
ΔF_{min} (%)	Minimum	3	0	0
	Maximum	55	70	52
	Mean	27	25	20

4. CONCLUSIONS

The well known variability of lignocellulosic fibers was confirmed by True Area measurements. The error in the areas based on calipers was very high. This certainly impacts any mechanical behavior modeling of these materials. Digital microscopy and image analysis were shown to be relevant tools, increasing the accuracy of individual measurements while allowing a representative population of fibers to be evaluated. It also allows the measurement of more sophisticated shape factors which can be, in the future, introduced in the models.

REFERENCES

BLEDZKI, A.K., GASSAN, J. (1999). Composites reinforced with cellulose based fibres. *Prog. Polym. Sci*. 24, 221-274.

MOHANTY, A.K., MISRA, M., DRZAL, L.T. (2002). Sustainable Bio-Composites from Renewable Resources: Opportunities and Challenges in the Green Materials World. *J.Polym.Environ*. 10(1/2),19-26.

PACIORNIK, S., MAURÍCIO, M.H.P. (2004). Digital Imaging, *in ASM Handbook: Metallography and Microstructures*. (Ed. Vander Voort, G.), 368-402. ASM International, Materials Park, Ohio (USA).

GONZALEZ, R.C., WOODS, R.E. (2008). Digital Image Processing, 3rd ed. Upper Saddle River, NJ: Pearson Prentice Hall.

Influence of natural fibres in biocomposites

M. García, I. Garmendia, J. García-Jaca
Fundación CIDEMCO-Tecnalia, área Anardi 5, 20730 Azpeitia (Guipúzcoa), Spain
e-mail: miriam.garcia@cidemco.es, javier.garcia@cidemco.es

SUMMARY

This article summarizes the results obtained in the European research project “Eco-houses based on eco-friendly polymer composite construction materials”. Composites based in poly(lactic acid) and natural fibres, specifically kenaf and rice husks, were developed for the manufacture of constructive elements. Mechanical properties (tensile and flexural) were analysed, as well as fire behaviour before and after the addition of a fire retardant and outdoor durability by means of accelerated ageing.

1. INTRODUCCIÓN

Biocomposites are formed by biopolymers reinforced with natural fibres. These fibres can come from both wood and crops in form of subproducts of non foodstuff cultivation specific for this type of applications. Natural fibre composites (NFC) show performances as good as glass fibre composites (*JEC composites Forum 2006*) but with lower specific weight, machine wear and price, at expense of lower impact strength. This enables the consume of these composites to grow yearly. The blending of biodegradable polymers and natural fibres offer the possibility to obtain a new class of eco-friendly and fully degradable composites.

The automotive industry is the biggest user of NFCs in Europe at the moment, with half the total consumption. However, this amount corresponds to 7% of NFC consumption worldwide. In future, according to *Hackwell Group* it is expected a few European automotive suppliers to be diverted to new natural fibres. On the other hand, there is a great scope for growth in wood-plastic composites (WPC) sales in construction and furniture (*CTBA 2007*). Construction is already the second largest sector after automotive. Few furniture made of NFC are still available in the market, but more and more companies such as Ikea or IPT are developing furniture components made of this material. The industry of infrastructures is also a good potential consumer in applications such as highway sound barriers and waterfront fixtures.

The advantages of NFCs are their good dimensional stability and durability against fungi and insects compared to wood (*Stark 2006 and Schut 2005*). Both aspects make these materials to have a service life of even 25-30 years with very low maintenance requirements. Moreover, even they can content high amounts of fibre, they can be processed like plastics. The aim of this work was to analyse the effect of different fibre types in the performance of biocomposites. Poly(lactic acid) was blended with kenaf and rice husks to prepare the composites which were firstly compounded and then injected and their properties were measured.

2. RESULTS AND DISCUSSION

Figures 1a and b show the results of the tensile tests. Young’s modulus increases dramatically after adding the fibres and increases at increasing the fibre content. On the contrary, tensile strength reduces after the addition of the fibres, especially with the rice husks. Thus, the fibres increase the fragility of the composites. However, the results are very promising because, despite being lower than those of commercial 30% glass fibre-filled polypropylene (PP), kenaf composite results are similar to those of a commercial 20% glass fibre-filled PP and both kenaf and rice husks composites evidence much better performance than 30% glass bead-filled PP.

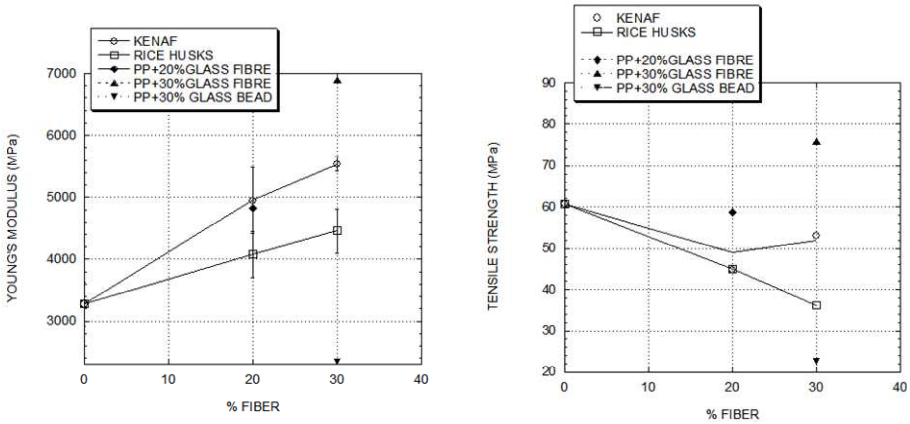

Figure 1. Tensile modulus (a) and strength (b) of biocomposites. PP based composites are commercial grades from RTP.

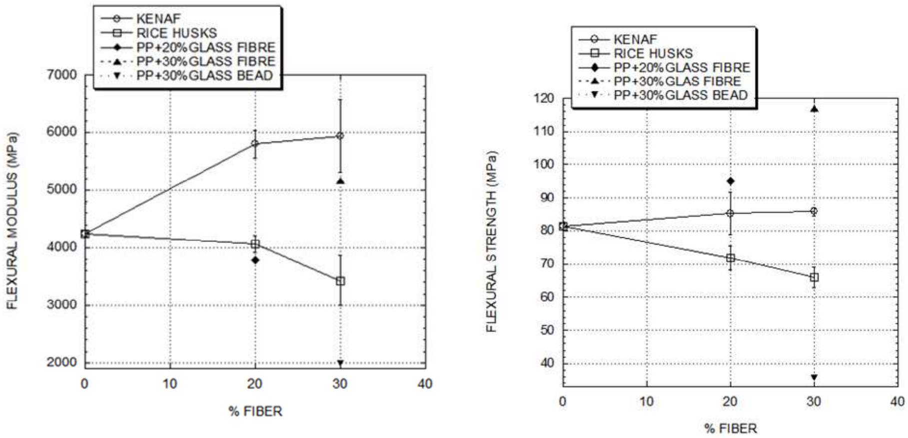

Figure 2. Flexural modulus (a) and strength (b) of biocomposites. PP based composites are commercial grades from RTP.

Figures 2a and b show the results of the flexural tests. As can be seen, increases are observed after the addition of kenaf in both modulus and strength. However, rice husks give rise to decreases in both properties, indicating that they act as a filler rather than a fibre, due to its low aspect ratio (50 for kenaf vs. 3.5 for rice husks). The results are very positive because in both kenaf and rice husks composites, modulus values are much better than that of glass bead-filled PP and even better than those of glass fibre-filled PP. On the contrary, strength values of natural fibre-filled composites are somewhat lower than those of glass fibre-filled PP, despite being much better than glass bead-filled PP.

Thus, the new eco-composites can compete with typical plastics like glass fibre-reinforced polypropylene.

In order to improve the durability and fire resistance of the composites, fire retardant ($Al(OH)_3$) and pigment (iron oxide) was added to composites with 20% fibre (this composition was selected as the most suitable regarding processing and performance). After some preliminary tests, 4% of pigment and 10% of fire retardant were selected as the most suitable contents.

Fire tests showed remarkable enhancements after the addition of the fire retardant as shown in figure 3. PLA did not evidence any value because it lost integrity immediately when coming into contact with the flame. Burning time of both kenaf and rice husks composites was similar prior to the addition of the fire retardant. However, the time required for burning the specimens increased by 30% in kenaf composites and by more than 50% in rice husks composites when the aluminium hydroxide was added. A higher fire retardant content did not lead to greater increases in the burning time, indicating that the selected fire retardant content is the minimum required for the maximum effectiveness in fire performance.

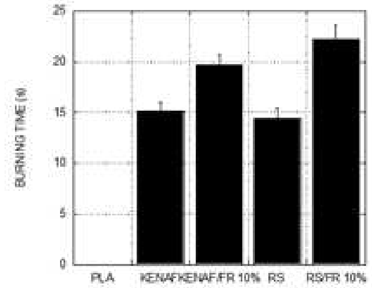

Figure 3. Single flame source tests of the biocomposites with and without fire retardant.

Durability tests showed that composites without pigment evidenced bleaching, cracking and chalking after keeping them for 500 hours in the QUV (cycles consisting on 4h condensation at 50ºC followed by 4h with UV-B light at 60ºC). After 1500 hours, the test bars were completely broken. However, the composites with pigment took on a much better appearance. Pigmented composites did not evidence any bleaching nor chalking - just some cracking in very few bars after 1500 hours.

As regards retaining the properties, it was observed that the addition of the pigment and the fire retardant did not change the flexural properties of the neat composite before ageing. However, as seen in table 1, flexural modulus, strength and strain markedly decreased after maintaining the composites under severe conditions. The decrease in the modulus is not so noteworthy, indicating that the rigidity of the materials at low deformation levels is maintained after ageing. As stated by Stark (2005), this could be due to an increase in crystallinity of the polymer rich surface. However, as usual, ageing gives rise to a decrease in the elasticity of the materials, and, thus, ductility diminishes.

As a consequence, a strong decrease in the flexural strength takes place. This is claimed (Stark 2001) to be because moisture penetration into the composite degrades the fibre-polymer interface, which in turn causes loss of strength as the stress transfer from matrix to fibre becomes less efficient.

Ageing time (h)	Kenaf			Rice husks		
	Modulus (MPa)	Strength (MPa)	Strain (%)	Modulus (MPa)	Strength (MPa)	Strain (%)
0	5797±239	82±9	2.4±0.3	4067±147	77±10	2.9±0.6
500	5249±306	32±6	1.0±0.2	4164±40	29±9	1.0±0.5
1500	4877±503 (	29±7	1.1±0.3	4039±179	12±1	1.0±0.5

Table 1. Flexural properties of aged composites.

3. CONCLUSIONS

The overall conclusion is that kenaf composites give rise to much better mechanical performance than rice husks composites. However, an improvement in the fire resistance of PLA/rice husks composites is even higher than that of kenaf composites. For applications where high performances are not required, such as housing or decorative appliances, PLA/rice husks composites, which show better performance than glass bead-filled PP, are a good choice in order to obtain a completely biodegradable material which is cheaper than usual biopolymers because of the low price of rice husks. On the other hand, the addition of kenaf led to high increases in the tensile and flexural modulus without noticeable changes in the strength. Moreover, fire resistance also increased remarkably. In order to enhance durability of the materials, it is necessary to add a pigment to the composites. 4% iron oxide is enough to maintain the correct appearance of the composites without high loss in terms of rigidity.

ACKNOWLEDGEMENTS

This work was supported by the EU within the framework of an INCO Project. CIDEMCO wishes to thank the EU for the financial support.

REFERENCES

Wood Plastics Composites in Europe: Analysis - Technology - Market Opportunities, Hackwell Group, UK, 2006

“*Natural fibres forum proceddings*” JEC Composites Forums, Paris, 2006

3rd Wood fibre Polymer Composites International Symposium, Innovative Sustainable Materials applied to Building and Furniture, CTBA, Bordeaux, 2007

Schut J. H. “Wood-plastic composites weathering quality issues”, Plas. Tech., 2005

Morrell J. J.; Stark N. M.; Pendleton D. E.; McDonald A. G. “Durability of wood-plastic composites”, Wood Design Focus, 2006, 16, 7-10

Stark N. “Changes in wood flour/HDPE composites after accelerated weathering with and without water spray” 2nd Wood fibre polymer composites symposium, Bordeaux, 2005

Stark N. “Influence of moisture absorption on mechanical properties of woodflour-polypropylene composites” J. Thermoplast. Comp. Mat., 14, 421-432, 2001

Propiedades de materiales compuestos obtenidos a partir de fibras residuales de celulosa y una mezcla de residuos plásticos de RSUs y de invernadero

C. González-Sánchez, A. Martínez-Aguirre, B. Pérez-García
Departamento Ingeniería Química y Tecnología del Medio Ambiente.
Facultad de Química. Universidad de Oviedo, España
C. Fonseca-Valero
Departamento de Química Industrial y Polímeros.
EUITI. Universidad Politécnica de Madrid, España
J. Martínez-Urreaga
Departamento de Ingeniería Química Industrial.
EPSII. Universidad Politécnica de Madrid, España
cgs@uniovi.es

RESUMEN

El objetivo del presente trabajo es la determinación de las principales propiedades mecánicas y térmicas de materiales compuestos de matriz polimérica, constituida por una mezcla de residuos plásticos de origen agrario y del post-consumo, en los que, como refuerzo, se emplean distintos porcentajes de fibras residuales de celulosa (25, 30 y 35%, en peso). También se empleó un agente de acoplamiento para mejorar la adhesión entre la matriz y el refuerzo. Las materias primas fueron sometidas a mezclado y amasado en una extrusora de doble husillo. De las granzas resultantes se obtuvieron, mediante moldeo por inyección, las probetas multipropósito sobre las que se llevaron a cabo los ensayos. Los resultados muestran que, prácticamente, en todos los casos, a medida que se incrementa el contenido de fibras, se ven mejoradas las propiedades mecánicas y térmicas. Del mismo modo, la adición del agente de acoplamiento tiene un efecto positivo, observándose una mejora de las propiedades para los materiales compuestos que lo incorporan en su formulación.

1. INTRODUCCIÓN

El impulso del reciclaje de plásticos residuales de distinto origen depende, en parte, de que se puedan utilizar en la obtención de productos con unas prestaciones y valor añadido que compensen sobradamente los costes de gestión de los residuos de partida. En el presente trabajo se aborda la utilización de mezclas de residuos plásticos como matrices para la obtención de materiales compuestos reforzados con fibras residuales de celulosa, dadas las ventajas inherentes a este tipo de materiales compuestos como son, entre otras, su baja densidad, su bajo coste, su biodegradabilidad y su buena relación propiedades/peso.

2. MATERIALES Y MÉTODOS

Las mezclas de residuos plásticos utilizadas como matrices incluyen residuos plásticos procedentes de los residuos sólidos urbanos (RSU), principalmente PEAD, y plásticos residuales de origen agrario (INV), principalmente PEBD. Como refuerzo se utilizaron fibras residuales de celulosa procedentes de la fabricación de pasta de celulosa. Como agente de acoplamiento se utilizó un polietileno maleado (PEM). También se adicionó un 0,3% de un estabilizante térmico (TS) a todas las formulaciones. Las materias primas se sometieron a mezclado y amasado en una extrusora de doble husillo, obteniéndose granzas con un 25, 30 y 35%, en peso, de refuerzo, así como con un 1,5% de agente de acoplamiento y sin él. Dichas granzas se emplearon para la obtención, mediante moldeo por inyección, de las probetas multipropósito sobre las que se determinaron las propiedades mecánicas y térmicas (tracción, flexión y punto VICAT) siguiendo las normas ISO 527, ISO 178e e ISO 306. Se evaluó así el efecto que producen sobre dichas propiedades tanto el contenido de refuerzo como la adición o no de agente de acoplamiento.

3. RESULTADOS Y DISCUSIÓN

La Tabla 1 recoge los valores obtenidos para las principales propiedades mecánicas: módulos de elasticidad a tracción (E_t) y a flexión (E_f), resistencia máxima a tracción (σ_t) y carga a flecha de 6 mm ($\sigma_{f\ (6\ mm)}$).

Tabla 1. Propiedades mecánicas de los materiales compuestos

INV (%)	**RSU (%)**	**FIBRA (%)**	**PEM (%)**	**TS (%)**	**E_t (GPa)**	**σ_t (MPa)**	**E_f (GPa)**	**$\sigma_{f\ (6\ mm)}$ (MPa)**
59,82	39,88	0	0	0,3	0,33 (0,03)	13,71 (0,17)	0,29 (0,01)	7,48 (0,04)
44,82	29,88	25			0,92 (0,05)	19,25 (0,58)	1,03 (0,02)	17,21 (0,33)
41,82	27,88	30			1,10 (0,02)	22,73 (0,78)	1,35 (0,06)	21,93 (0,62)
38,82	25,88	35			1,21 (0,03)	20,54 (0,46)	1,51 (0,03)	23,54 (0,32)
58,92	39,28	0	1,5		0,31 (0,02)	15,72 (0,51)	0,31 (0,02)	7,91 (0,08)
43,92	29,28	25			0,96 (0,04)	20,56 (0,24)	1,07 (0,03)	17,68 (0,21)
40,92	27,28	30			1,20 (0,06)	22,69 (0,40)	1,52 (0,03)	23,94 (0,20)
37,92	25,28	35			1,23 (0,06)	23,21 (0,64)	1,52 (0,05)	24,43 (0,38)

En la Fig. 1 (a) se representa el efecto del porcentaje de refuerzo sobre la *resistencia máxima a tracción* de los materiales compuestos, pudiendo también apreciarse el efecto de la adición de agente de acoplamiento (en isolíneas). Se observa que, salvo para el caso de los materiales con un 35%, en peso, de refuerzo y sin agente de acoplamiento, el aumento del contenido de refuerzo lleva aparejado el incremento del valor de σ_t. Del mismo modo, se aprecia que la adición de agente de acoplamiento mejora los valores obtenidos para, prácticamente, todos los porcentajes en peso de refuerzo.

La Fig. 1 (b) muestra cómo influye el porcentaje de refuerzo sobre la *carga a flecha de 6 mm* para los materiales con y sin agente de acoplamiento. Al igual que en tracción, el comportamiento a flexión mejora a medida que aumenta el contenido en fibras y cuando se incorpora agente de acoplamiento a los materiales.

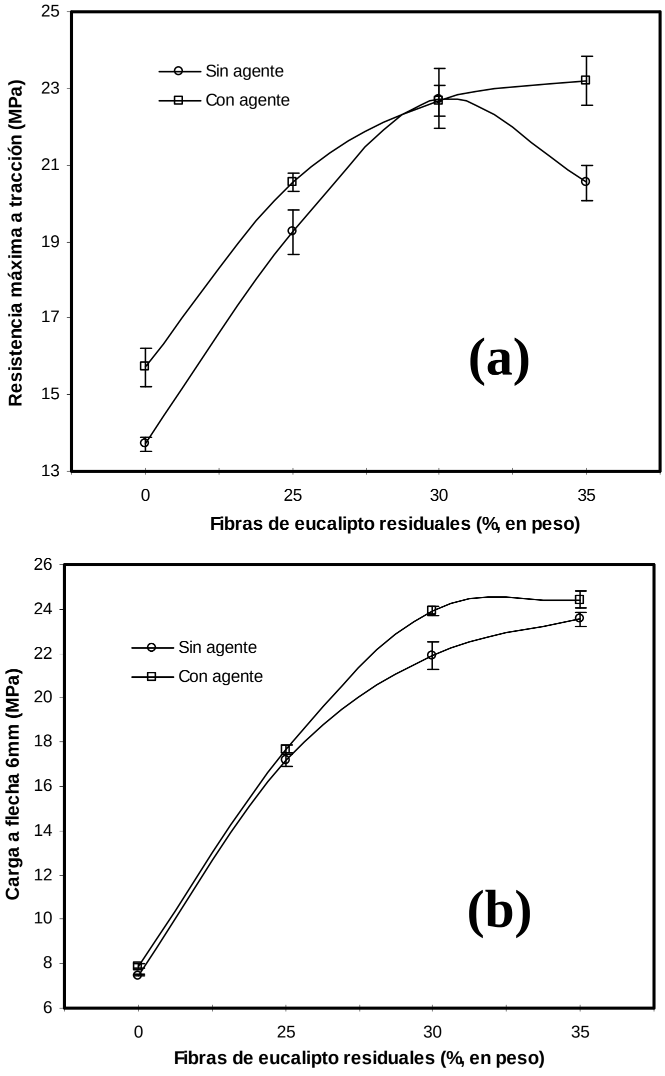

Fig. 1. Efecto del porcentaje de refuerzo y de la adición de PEM sobre la *resistencia máxima a tracción* (a) y sobre la *carga a flecha de 6 mm* (b).

La Fig. 2 pone de manifiesto que tanto el aumento del porcentaje de fibras, como la presencia de agente de acoplamiento producen, generalmente, un aumento de la temperatura VICAT de los materiales compuestos.

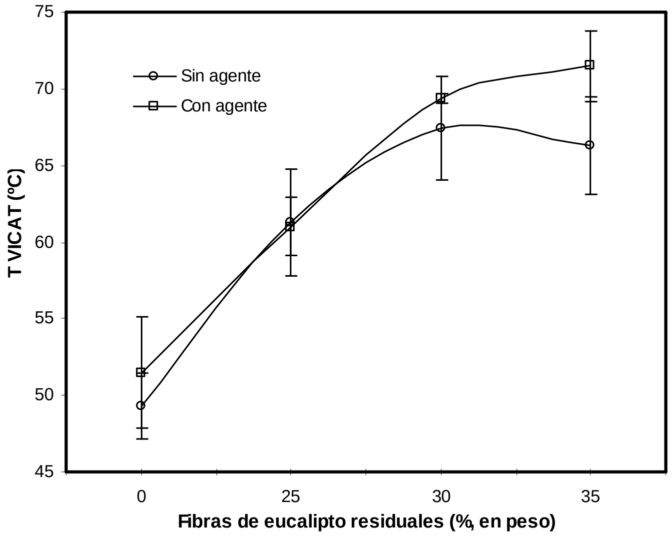

Fig. 2. Efecto del porcentaje de refuerzo sobre la *temperatura VICAT*.

4. CONCLUSIONES

1. El uso de fibras de celulosa residuales permite mejorar las propiedades mecánicas y térmicas de mezclas integradas por residuos de plásticos de RSU y de invernadero, impulsando su necesario reciclaje.
2. Los materiales compuestos reforzados con un 35%, en peso, de fibras residuales de celulosa y que incorporan un 1,5%, en peso, de polietileno maleado presentan las mejores propiedades de todas las formulaciones estudiadas.

AGRADECIMIENTOS

Los autores agradecen profundamente a la *Secretaría General para la Prevención de la Contaminación y el Cambio Climático* del **Ministerio de Medio Ambiente** la financiación del Proyecto de ref. MMA07–A462–2007–2–02.7 en el que se enmarca el presente trabajo, así como a las empresas BEFESA y ENCE-Navia por haber suministrado algunas de las materias primas.

Mechanical and thermal properties of cellulose fibers from sugarcane Bagasse/HDPE composites

D.R. Mulinari; H.J.C. Voorwald; M.O.H. Cioffi
Grupo de Fadiga e Materiais Aeronáuticos (DMT/FEG). Universidade Estadual Paulista, Brazil
G.J.M. Rocha
Departamento de Engenharia de Bioquímica. Universidade de São Paulo, Brazil
M.L.C.P. Da Silva
Departamento de Engenharia de Química. Universidade de São Paulo, Brazil

ABSTRACT

In the work, effect of chemical modification on mechanical and thermal properties of cellulose fibers from sugarcane bagasse/HDPE composites was studied. Cellulose fibers from sugarcane bagasse were mixed with HDPE in a thermokinetic mixer, in which fibers were responsible for 5 to 40 wt% in the composition. After the mixture, composites were dried, ground in mill and placed in an injector camera according to ASTM D-638 specification. The influence of modified fibers content in the composites was studied by mechanical (tensile tests) and thermal analyses (TGA). Results showed that, the addition of fibers in matrix increased the tensile strength and modulus as well as thermal stability of composites compared to the matrix polymeric.

1. INTRODUCTION

Recently the interest in composite materials reinforced with natural fibers increased considerably, because new environmental legislation as well as consumer pressure has forced manufacturing industries to search materials that can substitute conventional non-renewable materials such as glass fibre (Satyanarayana *et al*., 2007). The advantages of natural fibers over traditional glass fibers are acceptable as good specific strengths and modulus, economical viability, low density, reduced tool wear, enhanced energy recovery, reduced dermal and respiratory irritation and good biodegradability (Zah *et al*., 2008).

However, natural fibre reinforced polymeric, also present disadvantages such as the incompatibility between the hydrophilic natural fibers and hydrophobic thermoplastic and thermoset matrices. Incompatibility of components is responsible for poor thermal and mechanical properties. To solve these problems, various treatments are being used to improve fibers/matrix compatibility, such as bleaching, acetylation and alkali treatment (Mulinari *et al*., 2009; Gu, 2009; Sreekala and Thomas, 2003).

The objective of this work was to study the effect of chemical modification on mechanical and thermal properties of cellulose fibers from sugarcane bagasse/HDPE composites.

2. EXPERIMENTAL

2.1 Materials description

Cellulose (CB) from sugarcane bagasse was obtained by pre-treatment with 10% sulfuric acid solution, followed by centrifugation, deslignification with 1% sodium hydroxide solution and bleaching with sodium chloride. Modified cellulose (CM) with zirconium oxychloride was obtained by according to Mulinari and Da Silva (2008).

2.2 Composites preparation

Cellulose fibers from sugarcane bagasse modified and non-modified were mixed with the HDPE in a thermokinetic mixer, model MH-50H, with speed rate maintained at 5250 rpm, in which fibers were responsible for 5 to 40 wt% in the composition. After the mixture, composites were dried and ground in mill, model RONE. Composites and pure HDPE were placed in an injector camera at 165 ^{o}C and 2 ºC min^{-1} heating rate in a required dimensions pre-warm mold to obtain tensile specimen.

2.3 Mechanical and thermal properties

The mechanical strength of sugarcane bagasse cellulose modified and non-modified reinforced HDPE composites was determined using an INSTRON universal-testing machine (model 8801). Tests were carried out according to ASTM standards D638 with 10 mm.min^{-1} crosshead speed. Tensile strength and modulus values are average results of five tested specimens. TGA was carried out using a Perkin Elmer (TGA 7) instrument, in N_2 atmosphere at 10 ^{o}C min^{-1} heating rate, from 30 to 650 ^{o}C.

3. RESULTS AND DISCUSSION

3.1 Mechanical Properties

Mechanical properties of the composites are summarized in Table 1. Cellulose fibers modified with hydrous zirconium oxide presented higher tensile strength and modulus results compared to cellulose fibers non-modified. The amount of added reinforcement contributed to variation of the tensile modulus as indicated in Table 1.

Table 1. Mechanical properties of the composite.

Samples	*Properties*		
	Elongation at break (%)	*Tensile strength (MPa)*	*Tensile modulus (MPa)*
HDPE	8.9 ± 0.8	15.7 ± 1.1	732.45 ± 90.6
CB5%	5.4 ± 0.4	16.2 ± 0.7	942.5 ± 98.6
CB10%	5.5 ± 0.2	15.6 ± 0.3	897.4 ± 27.5
CB20%	5.7 ± 0.3	15.8 ± 0.3	1140.7 ± 62.5
CB30%	6.0 ± 0.7	16.7 ± 0,8	1156.0 ± 179.8
CB40%	5.7 ± 0.5	16.8 ± 1,3	1216.8 ± 191.3
CM5%	7.2 ± 0.1	20.8 ± 0.4	1177.7 ± 25.0
CM10%	7.4 ± 0.4	21.9 ± 0.6	1238.5 ± 41.0
CM20%	6.5 ± 0.2	20.9 ± 0.4	1306.4 ± 26.9
CM30%	5.5 ± 0.2	19.9 ± 0,4	1489.9 ± 71.0
CM40%	5.9 ± 0.4	23.2 ± 0,6	1628.9 ± 109.4

Reinforcement in wt%.

Fibers insertion can contribute to the modulus increase, because the Young’s modulus of the fibers is higher compared to the thermoplastic modulus. However, to obtain a significant increase, a good interfacial bond between fiber and matrix is necessary. The tensile strength exhibited a good interaction between fibers and matrix, with increases of 48%, compared to the HDPE. This increase in tensile modulus occurred as a consequence of the oxide treatment.

3.2 Thermogravimetric analysis

Figs. 2 and 3 show TG curves of HDPE, cellulose fibers (modified and non-modified), and cellulose fibers/HDPE (5 and 40 wt%). HDPE showed a one-step decomposition process, while composites clearly showed a two-step process. In the first and second stages, the fiber and matrix decompositions occurred. Composites presented intermediary thermal stability between fiber and matrix.

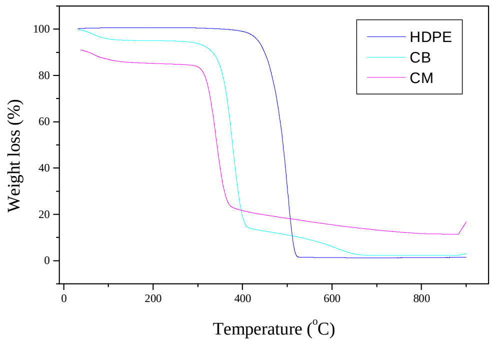

Figure 2. TG curves of HDPE and natural fibres: (CB) and (CM).

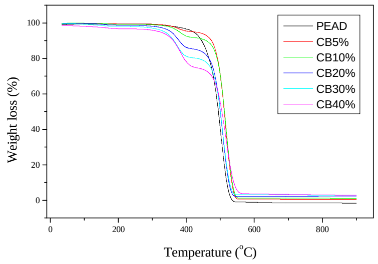

Figure 3a. TG curves of HDPE and CB/HDPE composites.

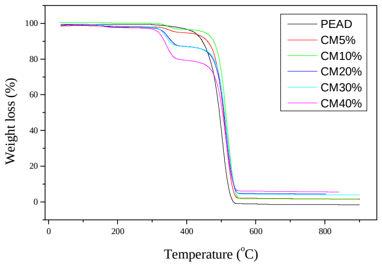

Figure 3b. TG curves of HDPE and CM/HDPE composites.

HDPE started decomposition at about 430 °C, which was higher than fiber. TG curves for cellulose fibers exhibited two degradation stages. The first stage of weight loss occurred between 30 and 100 °C (both fibers), which correspond to the water vaporization heat in the sample. The second stage of weight loss for neat fiber presented thermal degradation peaks around 310 °C. Table 2 shows the weight loss and degradation temperature peak of composites, HDPE and fibers. At 400 °C, HDPE practically did not lose weight, however from 450 °C on, the weight loss was fast and accentuated, resulting in minimum residue.

Table 2. Thermal properties of the materials.

Samples	*Weight loss (%)*						*Degradation temperature (^{o}C)*	
	100 ^{o}C	*200 ^{o}C*	*300 ^{o}C*	*400 ^{o}C*	*500 ^{o}C*	*600 ^{o}C*		
PEAD	0.65	0.65	0.74	3.33	59.7	98.7	---	434
CB	4.3	5.1	6.4	81.2	88.9	93.9	---	335
CM	13.1	14.8	16.3	78.4	81.7	84.5	---	312
CB5%	0.0	0.5	0.6	4.3	26.7	99.4	365.0	476.0
CB10%	0.2	0.65	1.0	7.6	33.4	98.8	376.8	513.7
CB20%	0.3	1.2	1.8	13.4	43.9	97.8	379.3	510.3
CB30%	0.6	1.8	2.7	18.4	45.2	96.8	375.6	511.2
CB40%	1.9	3.2	4.2	22.8	49.1	96.4	377.7	512.7
CM5%	1.3	1.7	19	5.3	39.8	98.0	347.1	510.4
CM10%	0.8	1.0	1.2	4.7	28.2	98.2	345.2	516.6
CM20%	1.05	2.1	2.5	13.0	39.1	95.3	346.4	513.4
CM30%	0.5	1.5	2.0	13.1	35.4	95.7	339.3	515.5
CM40%	0.8	2.4	3.2	20.7	45.6	94.0	340.0	511.8

Table 2 also shows that the composites reinforced with modified fibers presented higher thermal stability than the composites reinforced with non-modified fibers (at 400 ^{o}C) and that the addition of fibers decreased the thermal stability of the composites.

4. CONCLUSIONS

Cellulose fibers modified with zirconium oxychloride influenced directly mechanical properties cellulose fibers/HDPE composites. On the other hand, this modification didn’t influenced thermal properties composites, but compared to the pure HDPE increased thermal stability.

ACKNOWLEDGEMENTS

The authors are grateful for the research support by CAPES.

REFERENCES

GU, H. (2009). Tensile behaviours of the coir fibre and related composites after NaOH treatment. *Materials & Design*, 30, 3931-3934.

MULINARI, D.R., DA SILVA, M.L.C.P. (2008). Adsorption of sulphate ions by modification of sugarcane bagasse cellulose. *Carbohyd Polym*, 74, 617-620.

MULINARI, D.R., VOORWALD, H.J.C., CIOFFI, M.O.H., DA SILVA, M.L.C.P., DA CRUZ, T.G., SARON, C. (2009). Sugarcane bagasse cellulose/HDPE composites obtained by extrusion. *Compos. Sci. Technol.*, 69, 214-219.

SATYANARAYANA, K.G. GUIMARÃES, J.L. WYPYCH, F. (2007). Studies on lignocellulosic fibers of Brazil. Part I: Source, production, morphology, properties and applications. *Compos Part A*, 38, 1694–1709.

SREEKALA, M.S., THOMAS, S. (2003). Effect of fibre surface modification on water-sorption characteristics of oil palm fibres. *Compos. Sci. Technol.* 63, 861–869.

ZAH R, HISCHIER R, LEÃO AL, BRAUN I. (2007). Curauá fibers in the automobile industry - a sustainability assessment. *J Cleaner Prod*, 15, 1032-40.

Propiedades a tracción de composites basados en fibras naturales y matriz de poli(ácido láctico)

A. Arbelaiz, U. Txueka, I. Mezo, A. Eceiza, I. Mondragon
'Materials + Technologies' Group, Dpto. Ingeniería Química y del Medio Ambiente,
Escuela Politécnica. Universidad del País Vasco/Euskal Herriko Unibertsitatea
G. Vargas
Departamento de I+D+i, Alonso Hernández y asociados arquitectos S.L.

RESUMEN

Los composites se prepararon mezclando el termoplástico biodegradable de PLA con fibras naturales en un mezclador interno, tras lo cual se consiguieron probetas de tracción mediante el moldeo por inyección. Para mejorar la adhesión entre la fibra/matriz se sintetizó el copolímero de injerto de poli(ácido láctico)-anhídrido maleico (MAPLA) en un mezclador interno. La reacción de injerto del anhídrido maléico se llevó a cabo en presencia del iniciador peróxido de dicumilo. Se estudiaron las propiedades a tracción en función de la cantidad de MAPLA y se definió una dosis óptima del compatabilizador. Por otra parte, la influencia del contenido de fibra en las propiedades de tracción también ha sido estudiadas.

Para composites de PLA/fibras naturales sin agente de compatibilización, tras la adición de las fibras naturales la resistencia a tracción disminuye o presenta un valor similar a la de la matriz pura. Este comportamiento sugiere que entre la fibra y matriz apenas hay transferencia de tensiones y el valor de resistencia apenas varia con el contenido de las fibras.

En cuanto a composites de PLA/fibras naturales modificados con agente de compatibilización (MAPLA), la resistencia a tracción aumenta con el contenido de fibras en el composite, esta mejora de la resistencia puede deberse a una mejora de adhesión entre las fibras/matriz y a una mejor dispersión de las fibras.

Como era de esperar, a mayor cantidad del contenido de las fibras en el composite, el módulo a tracción observado era mayor.

1. INTRODUCCIÓN

La creciente preocupación y las nuevas leyes medioambientales están forzando a las industrias la busqueda de materiales más ecológicos para la obtención de sus productos (Oksman et al. 2003). La utilización de materiales plásticos desechables hace aumentar la proporción de basura difícil de degradar, por lo que para reducir la cantidad de desechos plásticos se tiene que desarrollar materiales plásticos reciclables y/o biodegradables (Iannace et al. 1999). La mayoría de los polímeros sintéticos se obtienen a partir del petróleo, por lo que no se degradan fácilmente en el medio ambiente (Lee et al. 2003), y crean muchos problemas (Shimao, 2001). Debido a esto, en los últimos años se ha invertido muchos esfuerzos en el desarrollo de materiales biodegradables, los cuales podrían solucionar el problema del desecho que tienen asociados los materiales sintéticos no degradables (Curvelo et al. 2001; Matzinos et al. 2002; Mohanty et al. 2000). Sin embargo, estos nuevos polímeros en general son todavía más caros y por lo tanto no pueden competir económicamente con los plásticos comunes (Amass et al. 1998; Corradini et al. 2004). Las propiedades y el costo de los polímeros biodegradables se pueden modificar y mejorar añadiéndole fibras lignocelulósicas sin modificar su biodegradabilidad (Iannace et al. 1999). Se ha comprobado que las fibras naturales son un material adecuado de refuerzo, ya que combinan buenas propiedades mecánicas y ventajas medioambientales tales como la biodegradabilidad y su abundancia (Bledzki et al. 1999).

El poli(acido láctico) es uno de los polímeros más prometedores ya que se obtiene tras la polimerización del ácido láctico obtenido a partir de la fermentación de los azucares del maíz, caña de azúcar o remolacha. El PLA es un poliéster alifático de origen natural que se puede adquirir a gran escala y aunque el precio es más elevado que el de los polímeros comerciales tradicionales la tendencia del precio va a la baja en los últimos años.

La mayoría de los composites existentes actualmente en el mercado están fabricados con fibras y matrices poliméricas no degradables (Li et al. 2004). El objetivo principal del trabajo es desarrollar un composite basado en materiales totalmente renovables.

2. RESULTADOS Y DISCUSIÓN

Las figura 1a muestra la resistencia a tracción de composites PLA/fibras naturales sin agente de acoplamiento en función del contenido en fibra. La resistencia atracción de los composites es similar o peor que el de la matriz pura, además el valor de resistencia apenas varia con el contenido en fibra. Los resultados obtenidos están de acuerdo con lo observado por otros autores en composites basados en PLA y fibras lignocelulósicas (Pan et al. 2007; Huda et al. 2006. Este comportamiento sugiere que la transferencia de tensiones entre la matriz y las fibras es nula o muy pequeña, además es independiente a la cantidad de fibra que contiene el composite (Sanadi et al. 1995; Rana et al 1998).

Como se esperaba, en la figura 1b se observa que al aumentar el contenido de fibras en el composite aumenta el valor del modulo obtenido. Un comportamiento análogo fue observado por otros autores en composites basados en fibras lignocelulósicas y matriz polimérica (Van den Oever et al. 2000; Bax et al. 2008)

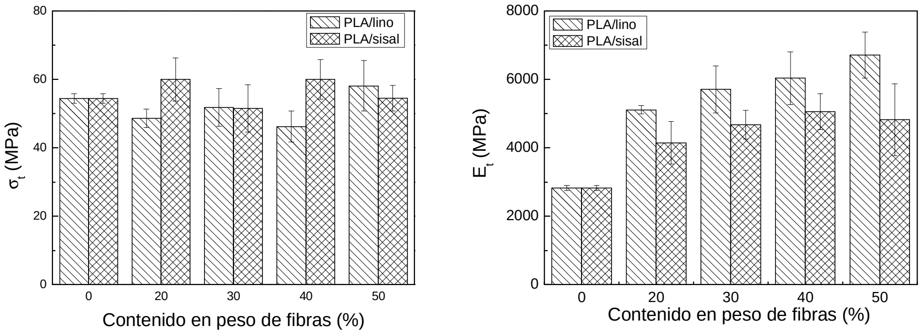

(a) (b)

Fig. 1. Propiedades de tracción de composites basados en PLA/fibras naturales: (a) resistencia, (b) módulo.

Las figuras 2a-b muestran las propiedades mecánicas de los composites de PLA/lino sin modificar y modificados con un 1 % de MAPLA (en peso respecto a la cantidad de fibra). Al añadir un 1 % en peso de MAPLA los composites mejoran considerablemente la resistencia a tracción. Esta mejora de la resistencia puede deberse a una mejora de adhesión entre la fibra y matriz. El módulo apenas se observa diferencias entre los sistemas modificados y sin modificar.

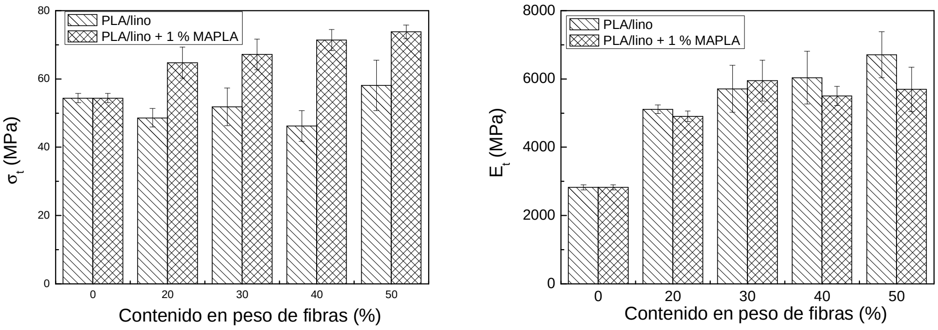

(a) (b)

Fig. 2. Propiedades de tracción de composites basados en PLA/lino sin modificar y modificados con 1% de MAPLA: (a) resistencia, (b) módulo.

3. CONCLUSIONES

Los composites basados en PLA/fibras naturales apenas mejoran la resistencia a tracción de la matriz de partida.

Los composites basados en fibras de lino presentan un valor de módulo mayor que los basados en fibras de sisal.

La adición de una pequeña cantidad de MAPLA mejora sustancialmente el valor de resistencia y apenas varia el valor del módulo.

AGRADECIMIENTOS

Los autores desean agradecer a la Universidad del País Vasco-Euskal Herriko Unibertsitatea y a la empresa Alonso Hernández y asociados arquitectos S.L. por la financiación del proyecto UE07/08 "Desarrollo de composites basados en materiales renovables para su aplicación en la construcción".

También se quiere agradecer al Gobierno Vasco-Eusko Jaurlaritza por el proyecto CIC inanoGUNE-ETORTEK 0911.

REFERENCIAS

AMASS W., AMASS A., TIGHE B.A. (1998), A review of biodegradable polymers: Uses, current developments in the synthesis and characterization of biodegradable polyesters, blends of biodegradable polymers and recent advances in biodegradation studies, *Polymer International* 47, 89-144.

BAX B., MÜSSIG J. (2008), Impact and tensile properties of PLA/Cordenka and PLA/flax composites, C*omposites Science and Technology* 68, 1601-1607.

BLEDZKI A.K., GASSAN J. (1999), Composites reinforced with cellulose based fibres, *Progress in Polymer Science* 24, 221-274.

CORRADINI E., MATTOSO L.H.C., GUEDES C.G.F., ROSA D.S. (2004), Mechanical, thermal and morphological properties of poly(ε-caprolactone)/zein blends, *Polymers for Advanced Technologies* 15, 340-345.

CURVELO A.A.S., DE CARVALHO A.J.F., AGNELLI J.A.M. (2001), Thermoplastic starch-cellulosic fibers composites: Preliminary results, *Carbohydrate Polymers* 45, 183-188.

HUDA M. S., DRZAL L. T., MISRA M., MOHANTY A. K. (2006) *Journal of Applied Polymer Science*, 102, 4856-4869.

IANNACE S., NOCILLA G., NICOLAIS L. (1999), Biocomposites based on sea algae fibres and biodegradable thermoplastic matrices, *Journal of Applied Polymer Science* 73, 583-592.

LEE S.H., OHKITA T. (2003) Mechanical and thermal flow properties of wood flour-biodegradable polymer composites, *Journal of Applied Polymer Science* 90, 1900-1905.

LI X. H., MENG Y. Z., WANG S. J., VARADA RAJULU A., TJONG S. C. (2004), Journal of Polymer Science Part B: Polymer Physics 42, 666-675.

LUO S., NETRAVALI A.N. (1999), Interfacial and mechanical properties of environment-friendly 'green' composites made from pineapple fibres and poly(hydroxybutyrate-co-valerate) resin, *Journal of Materials Science* 34, 3709-3719.

MATZINOS P., TSERKI V., GIANIKOURIS C., PAVLIDOU E., PANAYIOTOU C. (2002) Processing and characterization of LDPE/starch/PCL blends, *European Polymer Journal* 38, 1713-1720.

MOHANTY A.K., KHAN M.A., HINRICHSEN G. (2000), Influence of chemical surface modification on the properties of biodegradable jute fabrics-polyester amide composites, *Composites Part A* 31, 143-150.

OKSMAN K., SKRIFVARS M., SELIN J.F. (2003), Natural fibres as reinforcement in polylactic acid (PLA) composites, *Composites Science and Technology* 63, 1317-1324.

PAN P., ZHU B., KAI W., SERIZAWA S., IJI M., INOUE Y. (2007) *Journal of Applied Polymer Science* 105, 1511-1520.

RANA A.K., MANDAL A., MITRA B.C., JACOBSON R., ROWELL R., BANERJEE A.N. (1998) Short jute fiber-reinforced polypropylene composites: effect of compatibilizer. *Journal of Applied Polymer Science* 69, 329-338.

SANADI A.R., CAULFIELD D.F., JACOBSON R.E., ROWELL R.M. (1995) Renewable agricultural fibres as reinforcing fillers in plastics: mechanical properties of kenaf fibre-polypropylene composites. *Industrial & Engineering Chemistry Research* 34, 1889-96.

SHIMAO M. (2001), Biodegradation of plastics, Biotechnology 12, 242-247.

VAN DEN OEVER M.J.A., BOS H.L., VAN KEMENADE M.J.J.M. (2008) Influence of the physical structure of flax fibres on the mechanical properties of flax fibre reinforced polypropylene composites. *Applied Composite Material* 7, 387-402.

Composites de resinas furánicas y refuerzo de fibras naturales. Efecto de la modificación superficial

M.L. González, J.C. Miguez, F.J. Juanes, B. González, A.Valea
Departamento de Ingeniería Química y del Medio Ambiente,
Escuela Universitaria de Ingeniería Técnica Industrial,
Universidad del País Vasco UPV/EHU
Plaza de la Casilla, 3, 48012 Bilbao
[1] E-mail: marialuz.gonzaleza@ehu.es

RESUMEN

En este estudio se pretende analizar el efecto de diferentes tipos de tratamientos sobre las propiedades de la fibra y sobre las propiedades del material composite elaborado en base a resina furánica y fibra sisal, ambos procedentes de materias primas renovables. Las fibras de sisal se han sometido a los tratamientos de mercerización, silanización, y acetilación. La evaluación de las modificaciones sufridas por la fibra se ha llevado a cabo mediante análisis de grupos funcionales superficiales a través de los espectros FTIR, evaluación de las energías superficiales y análisis DSC y TGA. El tratamiento que ha conducido a mejorar ligeramente las propiedades mecánicas en tracción es la acetilación, debido posiblemente a la presencia de grupos CH_3 en la superficie.

1. INTRODUCCIÓN

La legislación medioambiental actual está presionando, y lo seguirá haciendo en el futuro, para restringir considerablemente los compuestos no degradables y para promover y potenciar la utilización de los recursos renovables. Es necesario, por tanto, recurrir a nuevas estrategias que permitan obtener materiales composites con propiedades similares a los tradicionales pero medioambientalmente más aceptables y económicos. Los composites biodegradables fabricados totalmente a partir de materias primas vegetales parecen ofrecerse como única alternativa para conseguir dichos objetivos.

Las fibras naturales como sisal, yute, caraua, coconut y otras se clasifican dentro de los materiales lignocelulósicos, y constituyen la principal fuente de celulosa, poliosas (hemicelulosa) y lignina. La celulosa es un polisacárido semicristalino natural. Las hemicelulosas son copolímeros de diferentes monosacáridos. A partir de las hemicelulosas se obtiene el alcohol furfurílico promotor de las resinas furánicas. La fibra sisal es una de las más resistentes y se obtiene de la planta denominada “Agave Sisilana”. Es barata, tiene baja densidad, alto módulo elástico y resistencia a tracción, es accesible y biodegradable. Investigar sobre la forma de obtener material composites cuya matriz sea una resina furánica procedente del alcohol furfurílico procedente de la hemicelulosa y el refuerzo sea fibra sisal, resulta de interés en aras a la sostenibilidad.

Como es bien conocido, las buenas propiedades mecánicas de los materiales composites reforzados con fibras dependen fundamentalmente de: 1) el módulo y resistencia de las fibras, 2) de la resistencia y estabilidad química de la matriz y 3) de la efectividad de los enlaces en las interfacies entre la fibra y la matriz para transferir los esfuerzos. La gran cantidad de grupos hidroxilo existentes en la superficie de la fibra le confiere propiedades hidrofílicas, lo cual conduce a una pobre adhesión interfacial entre la fibra sisal y las matrices hidrofóbicas. Sin embargo, la adhesión es normalmente fuerte en composites con matrices preparadas con polímeros polares capaces de formar enlaces con los grupos –OH de la superficie de las fibras. Cuando la matriz es una resina furánica, según J.M. Faulstich de Paiva et al (2006) podrían producirse enlaces involucrando grupos hidroximetilo del polímero y los anillos aromáticos de la lignina durante el proceso de curado.

Para mejorar la adhesión interfacial las fibras sisal se han sometido a diversos tratamientos. La mercerización generalmente mejora las características de la superficie de la fibra desplazando las impurezas naturales o artificiales de la superficie, produce cierta degradación superficial que aumenta el área de la superficie efectiva para el contacto con la matriz pudiendo conducir a mejorar las propiedades del composite. Durante la esterificación y la silanización superficial se producen reacciones químicas con la celulosa de la superficie para sustituir los grupos –OH hidrofílicos por otros grupos menos polares.

En este estudio se pretende analizar el efecto de diferentes tipos de tratamientos sobre las propiedades de la fibra y su efecto sobre las propiedades del material composite elaborado en base a resina furánica y fibra sisal.

2. EXPERIMENTAL

Las fibras de sisal han sido repetidamente lavadas con agua destilada caliente para asegurarnos la retirada de la mayor parte de las sustancias solubles en agua de la superficie y secadas a 105ºC. Sobre estas fibras lavadas con agua se han llevado a cabo los diferentes tratamientos. En la tabla 1 se indican las propiedades básicas de la fibra sisal (Yan Li et al, 2006).

Diámetro (μm)	% agua	Resistencia a tracción (MPa)	Módulo elástico (GPa)	Alargamiento a rotura (%)
100-300	8-10	100-700	25-50	3-6

Tabla 1. Propiedades básicas de la fibra sisal.

Las fibras de sisal se han sometido a los tratamientos de mercerización, silanización, y acetilación. En la mercerización (M) se ha utilizado una disolución de NaOH al 20%. La silanización (S) se ha llevado a cabo con viniltrimetoxisilano al 10% en disolución acuosa a pH ≈ 3,0 con el fin de conseguir mayor formación de silanoles. Para la acetilación (A) se ha utilizado el proceso simplificado desarrollado por Chand et al.

La evaluación de las modificaciones superficiales sufridas por la fibra debido a los tratamientos se ha llevado a cabo mediante análisis de grupos funcionales superficiales a través de los espectros FTIR utilizando un espectrofotómetro de Perkin Elmer Spectrum 1000, con dispositivo ATR y a través de la medida de ángulos de contacto con un tensiómetro Krüss K12 y una columna de adsorción utilizando el método de Washburn.

Los análisis térmicos DSC y TGA se han llevado a cabo con sendos equipos de Mettler.

Las placas de material composite se han elaborado utilizando una resina furánica furolite de Transfurans, modificada con ε-caprolactona (30 phr). Se han moldeado en un molde de compresión, en la condiciones previamente optimizadas (en 3 etapas) utilizando fibra corta (5-6 mm) al 5,0 % distribuída al azar. Se han realizado ensayos de tracción con una máquina universal de ensayos Ibertest Mod. Elib 50W y mecanicodinámicos con un DMA de TA Instruments

3. RESULTADOS

La mercerización es un proceso irreversible que tiende a incrementar la cantidad de celulosa de la fibra mediante el ataque a sus estructuras cristalinas y elimina las impurezas presentes como ceras y pectinas. Los silanos corresponden en general a una estructura del tipo (R´O)$_3$-Si-R donde R es un grupo alquílico que puede presentar reacciones de condensación con los grupos hidroxilo de la superficie de la fibra y una molécula de silano hidrolizada, quedando en el exterior los grupos R´ organofuncionales capaces de establecer enlaces covalentes con el polímero, además, disminuye la higroscopicidad de la fibra. En el tratamiento de acetilación se pretende la sustitución de grupos –OH de la fibra por grupos –CH$_3$. En la figura 1 se presentan los espectros infrarrojos de las fibras sometidas a los diferentes tratamientos. Cabe destacar: a) el desplazamiento de la banda del carbonilo desde 1728 cm^{-1}de la lignina y holocelulosa hasta 1711 cm^{-1} tras la acetilación. b) Tras el tratamiento de silanización disminuye la altura de la banda –OH debido a la disminución del contenido en agua. c) Tras la mercerización desaparece prácticamente la banda del carbonilo de la lignina.

A través de los ángulos de contacto medidos se ha calculado la energía libre superficial, y las componentes polar y dispersiva utilizando la metodología de Owens-Wendt et al . Los resultados obtenidos se reflejan en la tabla 2.

Tratamiento	º agua	º etilenglicol	γ^p (mN.m^{-1})	γ^d (mN.m^{-1})	γ (mN.m^{-1})
-	87,8º	59	25,47	20,66	46,13
Silanización	89º	67	13,19	28,11	41,30
Acetilación	90º	70	18,71	22,86	41,57
Mercerización	90º	74º	10,97	29,32	40,29

Tabla 2. Resultados de las energías superficiales de las fibras sisal.

A través de las curvas DSC, TGA y DTGA de las fibras sometidas de diferentes tratamientos que se presentan en las figura 1 y 2, cabe destacar la práctica desaparición de las formas cristalinas en las fibras sometidas a mercerización, que en los DSC aparecen como dos picos exotérmicos a 300ºC y 340ºC, que se corresponden en las curvas TGA con la pérdida de masa entre 14 -17% en ese rango de temperaturas, excepto en la fibra con tratamiento de mercerización. Cabe destacar también que el mayor contenido en agua se corresponde con las fibra sin tratar (8,6%w) que posee mayores valores en la componente polar de su energía superficial. La fibra tratada por mercerización presenta un solo tramo de degradación que comienza a 195ºC, antes que las sometidas al resto de los tratamientos gracias a las formaciones cristalinas que presentan, cuya morfología cambia ligeramente con los diferentes tratamientos.

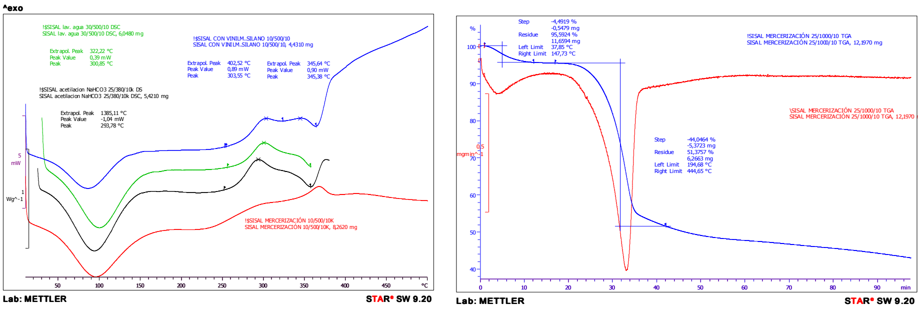

Figuras 1 y 2. Curvas DSC de las fibras lavadas y con los tratamientos A, S y M. curvas TGA y DTGA de la fibra sisal sometida a mercerización.

La evaluación de las propiedades mecánicas servirán para evaluar la eficacia de los diferentes tratamientos en la compatibilización entre fibra y resina. Los resultados de de los ensayos mecánicos realizados en tracción se presentan en la tabla 3.

Tratamiento	E (GPa)	Rmax (MPa)	Alargamiento	
-	2,270	5,0	0,47	
Acetilación	2,367	6,6	0,67	
Mercerización	2,159	3,8	0,4	

Tabla 3. Resultados de los ensayos a tracción.

El tratamiento de acetilación parece conducir a una mejor adhesión entre la matriz y la fibra posiblemente debido a que los grupos CH_3 anclados en la superficie de la fibra son capaces de reaccionar con los grupos –OH de la resina. Sin embargo el tratamiento de silanización no conduce a mejorar las propiedades, respecto a las del composite con fibras sin tratar, posiblemente debido a la presencia de grupos –OH en la resina y en la superficie de la fibra que podrían intervenir en el proceso de curado. Los bajos valores obtenidos pueden deberse a la posible formación de policaprolactona produciéndose una separación de fase, que se ha visualizado por SEM.

AGRADECIMIENTOS

Agradecemos al M.E.C y a la UPV/EHU las ayudas recibidas y a GAIKER-IK4 por su intermediación en la adquisición de la resina.

REFERENCIAS

MARON POMMET et al "Surface Modification os Natural Fibers Using Bactaria: Depositing Bactarial Cellulosa onto Natural Fibers To Create Hierarchical Fiber Reinforced nanocomposites". Biomacromolecules 2008, 9, 1643-1651.
YAN LI, YIU-WING MAI "Interfacial Characteristics of Sisal Fiber and Polymeric Matrices". The Journal of Adhesion, 82. 527-554, 2006.
B.SINGH, M.GUPTA, ANCHAL VERMA AND OS TYAGI. " FT-IR microscopic studies on coupling agents: treated natural fibres". Polym Int 49; 1444-1451 (2000)

Synthesis, characterization, mechanical properties of polymer composite reinforced with banana peel

C.Y. Watashi, P.H.F. Pereira , H.J.C. Voorwald , M.O.H. Cioffi
Department of Materials Group of Fatigue and Aeronautical Materials, Universidade Estadual Paulista – FEG UNESP

SUMMARY

This work presents the results obtained by testing the traction of composites prepared from the polymer matrix of high density polyethylene (HDPE) reinforced with banana peel. The fibers were extracted from banana peel, dried on oven, crushed, washed and sieved with 200 mesh. Than the samples were processed.

1. INTRODUCTION

1.1 Natural Composite

Natural composite is characterized by being formed of polymeric matrix and natural fiber reinforcement The advantages of using vegetable fibers for reinforcement over synthetic fibers, such as glass fibers, and mica, in the reinforcement of composites are: biodegradability, low cost and density, high toughness, good thermal properties, reduced use of instruments for treatment or processing, acceptable specific strength properties, reduced tool wear, reduced dermal and respiratory irritation (TITA, 2002; SILVA, 2003; MOTHÉ, 2004).

Although many advantages, the use of natural fibers has some disadvantages, specially the hydrophilic nature. The major constituents of biofibres are cellulose, hemicellulose and lignin. The amount of cellulose, in lignocellulosic systems, can vary depending on the species and age of plant/species (SANADI). All vegetable fibers are hydrophilic in nature, and their moisture content can reach 3-13% (BLEDZKI).

To improve the properties of composites natural reinforcing fibers can be modified by physical and chemical methods (BLEDZKI).

1.2 Banana peel

Banana is the most consumed fruit in the world. The taste and presence of essential vitamins such as B6, ensure the cultivation in over 120 countries, occupying 10 million hectares (EMBRAPA). Brazil is the world second producer of banana, only behind India, in 2006 brazilian production was 6.956.179 tons in 504.586 ha (IBGE).

Despite the big production, Brazil has the highest rate of wastage, that can reach 60% of the entire crop. This loss occurs during marketing, harvesting and transport. Besides this, there is the loss of peel, which generates large residual biomass (IBE).

For a better destination of banana peel, instead of landfills, studies have been made to reduce waste. One solution is application of banana peels in composite.

2. EXPERIMENTAL PART

Peels were separated, weighed and dried for 48 hours in 50 ºC. After dried peel were crushed on common processor and sieved in 200 mesh. After 10 minutes of immersion in water fibers were vacuum filtered and dried at 50 ºC for 24 hours. Composites were made using high intensity termocinetic mixer for plastic (Dryser) (5 or 10% by weigh of reinforce). After mixing reinforce and matrix material was ground in pellets mill and dried at 80 ºC for 2 hours.

Composites and high density polyethylene (HDPE) were mixed in injection camera at 165 ºC and 2 ºC.min^{-1} of heating rate. Melted material was injected in pre-heated form at 165 °C with desired dimension to obtain the specimens for making mechanical traction specimens. Specimens dimensions were according to ASTM D 638, with 13 mm wide, 160 mm length and 2,7 mm thick. Mechanical properties of tensile resistance, elongation and elasticity modulus in tension were evaluated.

Banana peel washed with water and *in nature* were characterizated by X-ray diffraction (XRD), thermogravimetry (TG) and differential scanning calorimetry (DSC), scanning electron microscopy (SEM). The X-ray difratogram determines the type of physical structure, ie the parameters of networks and the interplanares spacings the network of crystalline material. Thus, they obtained the difratograms X-ray fiber of the banana peel in nature and the fibers of the banana peel washed. To obtain the difratograms, was used radiation CuKα source, voltage 40 kV, current 40 mA, scanning 0,05 (2θ/5s) for values of 2θ between 10° and 70°. The TG studies the variation of mass of a sample after a physical or chemical transformation as a function of time or temperature. The heating rate was 20 ° C min^{-1} in 50 mL.min^{-1} flow of nitrogen in a temperature range between 25 and 900 ° C, to determine the thermal profile of banana peel *in nature* and washed. SEM study physical characteristics of samples, providing information about morphology and composition of analyzed material. The samples were fixed in sample pot with a strip of carbon self-dual side. Micrographs were obtained by SEM on a JEOL JSM5310, with the tungsten filament operating at 10 kV, using secondary electrons, the sample were covered with a thin layer of gold.

3. RESULTS ANS DISCUSSION

The X-Ray diffratograms of crushed banana peel *in nature* and crushed banana peel washed with water (Figure 1) presents semicrystalline peaks with amorphous areas.

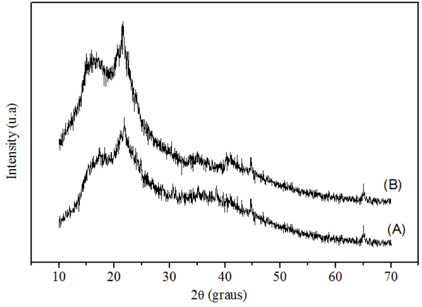

Fig. 1. X-Ray Difratofram: (A) banana peel crushed in nature (B) banana peel washed with H_2O.

Analyzing the intensity of the peaks obtained on diffratograms there was a difference, from this difference was calculated the crystallinity index. The crystallinity index was calculated according to equation 1, using the empirical method of Segal (RODRIGUES).

$$I_c = \frac{I_{(002)} - I_{(am)}}{I_{(002)}} \times 100 \qquad (1)$$

Where: I_c → index of crystallinity in percentage;

$I_{(002)}$ →intensity of diffraction peak representing the crystalline material near 2θ = 22°

$I_{(am)}$ → intensity of diffraction peak that represents amorphous material around 2θ = 16°

The results showed that for banana peel *in nature* was obtained 20,6% of crystallinity, while washed banana peel obtained 14,4% of crystallinity.

The TG was performed in order to verify the thermal stability of fiber *in nature* Figure 2 (A) fiber washed with water Figure 2 (B), so that with other tests may establish the efficiency of treatment of banana peel with distilled water.

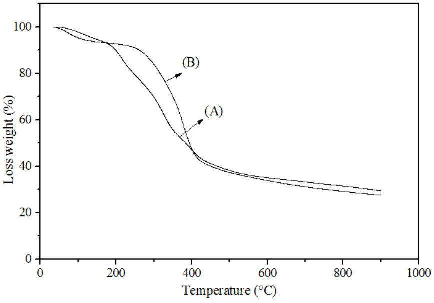

Fig. 2. TG curve: (A) of the banana peel *in nature* (B) banana peel washed with H_2O.

From the thermograms (Figure 2) of fiber *in nature* and washed fiber with distilled H_2O was possible to get the temperatures which occur lost of weight, the amount of residue after temperature treatment and temperature which occurs fiber thermal stability, which provide the limit of temperature that fiber can be subjected and the influence of treatment with distilled water on fiber and the composite characteristics.

The samples didn’t show significant differences on residue amount (%), but washed banana fiber stability was better stable until around 250 °C, while the non-washed around 180° C. So the washing process didn’t remove the amount of residue present in fiber, but rose by 28% the temperature at which the degradation of fiber occurs, ie there was an improvement in stability of the fiber.

Material	m (%)	ΔT (ºC)	dm(ºC)	R (%)
Banana *in nature*	6,109 61,057	25-160 160-800	114,03 283,33 Σ = 397,36	32,834
Washed Banana	6,512 61,768	25-180 180-800	72,30 350,58 Σ = 377,88	31,72

Table 1. Results obtained thermogravimetric curves.

SEM of banana peel fibers *in nature* (Figure 3, 4) and washed fiber with H_2O (Figure 5, 6), with 100 and 1000 times magnification, showed a change on morphology.

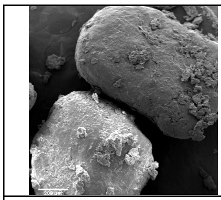	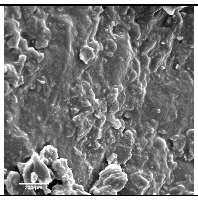	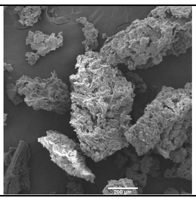	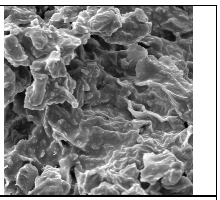
Figure 3 Microscopy of banana peel *in nature* increased 100X	**Figure 4 Microscopy banana pell *in nature* increased 1000X**	**Figure 5 Microscopy of washed banana peel increased 100X**	**Figure 6 Microscopy of washed banana peel increased 1000X**

On 100 times magnification of *in nature* banana peel fiber, the particles have an oval shape, while the unwashed fiber don’t have defined format and size of the particles are smaller. The *in nature* fiber with 1000 times magnification, when compared with the washed fiber, has a surface with less roughness, therefore less surface area.

As higher the surface area as better the possibility of adhesion between fiber and matrix, thus improving the mechanical properties of composite.

The results of tensile strength, modulus of elasticity and elongation obtained from the tensile test for HDPE composites reinforced with different levels of fiber in the banana peel are shown in Table 2.

Analyzing the results of Table 2 it was observed that the composites reinforced with different quantities of fiber had better tensile strength compared to pure HDPE. However, the composites reinforced with 5% (m/m) of fiber showed strength 6,6% higher than the composite reinforced with 10%, which may have occurred because despite the greater amount of fiber, the volume fraction occupied by the reinforce influence on mechanical properties of the composite.

Material	**Elongation (%) – ε**	**Tensile Strenght (MPa) - σ**	**Modulus of Elasticity (MPa) E**
Composite HDPE/banana 5 %	2,3 ± 0,1	19,1 ± 0,6	814,5 ± 8,5
Composite HDPE/banana10%	2,4 ± 0,1	18,2 ± 0,4	760,5 ± 5,3
HDPE	2,1 ± 0,3	15,7 ± 1,1	732,5 ± 90,6

4. CONCLUSIONS

Washed banana peel presented considerable reduction of impurity level and a decrease in crystallinity when compared with natural peel, but the fiber got a better stability on temperatures up to 250 °C (482 ºC) and higher roughness on its surface, which improved the fiber matrix interaction.

REFERENCES

TITA, S. P. S.; PAIVA, J.; FROLLINI, E. Resistência ao impacto e outras propriedades de compósitos lignocelulósicos: matrizes termofixas reforçadas com fibras de bagaço de cana-de-açúcar. *Polímeros: Ciência e Tecnologia*, v. 12, n. 4, p. 228-239, 2002.

SILVA, C.S. et al. Avaliação econômica das perdas de banana no mercado varejista: um estudo de caso. Revista Brasileira de Fritucultura, Jaboticabal, 2003.

MOTHÉ, C. G., AZEVEDO, A. D. de, Análise térmica de materiais, São Paulo, ed. Editora 2002;

SANADI, A. R., ROWELL, R. M., CAULFIELD, D. F., Polym News 20, 7 (1996).

BLEDZKI, A.K., REINMANE, S. and GASSAN, J.J.,Appl. Polym. Sci.,1996, 59, 1329.

EMBRAPA; Embrapa lança publicação sobre cultura da banana; 25/11/2004.

IBGE; Instituto Brasileiro de Geografia e Estatística – Produção Agrícola Municipal. Culturas temporárias e perman. Pesq. agric. munic., Rio de Janeiro, v.33, p.1-133, 2006.

IBE – Instituto Brasileiro de Economia, Balanço e disponibilidade interna de gêneros alimentícios de origem vegetal. Rio de Janeiro, 1988.67p.

RODRIGUES F.G., ASSUNÇÃO R.M.N., VIEIRA J.G., MEIRELES C.S., CERQUEIRA D.A., BARUD H.S., RIBEIRO J.L.R., MESSADDEQ Y. Characterization of methylcellulose produced from sugar cane bagasse cellulose: Crystallinity and thermal properties. Polymer Degradation and Stability2007;92:205-10.

Morfología y propiedades de materiales compuestos reciclados de polipropileno y fibras de celulosa

A. Ochoa, C. Fonseca, T. Aguinaco
Departamento de Química Industrial y Polímeros. Universidad Politécnica de Madrid.,
E.U.I.T.I. Ronda de Valencia 3, 28012 Madrid. España
E-mail almudena.ochoa@qi.upm.es
C. González
Departamento de Ingeniera Química y Tecnología del Medio Ambiente. Universidad de Oviedo. C/ Julián Clavería s/n.33071-Oviedo. España
F. Ania
Departamento de Física Macromolecular. Instituto de Estructura de la Materia, CSIC.
C/ Serrano, 119. 28006-Madrid. España

RESUMEN

El objetivo de este trabajo ha sido analizar la variación de las propiedades térmicas y mecánicas y de la estructura cristalina, de materiales compuestos con matriz de PP y fibras naturales en relación con su reciclado mecánico. Para ello, distintos materiales compuestos con un 50% en peso de fibras de celulosa, tanto refinadas como no refinadas y con un 1,5% de agente de acoplamiento MAPP, fueron sometidos a tres ciclos sucesivos de moldeo por inyección.

Las propiedades térmicas por DSC y los datos de cristalinidad por difracción de rayos X a ángulos grandes (WAXS) muestran para los materiales compuestos originales, así como para los reciclados, una disminución de la cristalinidad con respecto a la de la matriz; indicando que los procesos de nucleación no están favorecidos por la presencia de las fibras. Los cristales formados corresponden a la forma cristalográfica α del polipropileno y no se observan diferencias significativas en las temperaturas de cristalización entre los materiales refinados y no refinados.

Por otra parte, la matriz de polipropileno presenta una menor cristalinidad con el reciclado, coincidiendo con la disminución de los valores obtenidos del módulo de Young. Esta última propiedad disminuye ligeramente en el tercer reciclado de los materiales compuestos en comparación con los originales.

En ninguna de las series se aprecia variación significativa en los valores del tiempo de inducción a la oxidación (TIO) entre los materiales originales y sus correspondientes reciclados.

1. INTRODUCCIÓN

Las propiedades físicas, mecánicas y térmicas de los materiales compuestos están muy influenciadas por el tipo, proporción y morfología de las fibras de refuerzo, así como por la adhesión interfacial entre la matriz y la fibra.

La presencia de refuerzo en estos materiales, aumenta la viscosidad del material fundido. Esa mayor viscosidad implica que, durante las operaciones de procesado, se tenga que aplicar un esfuerzo mecánico mayor, lo que provoca una mayor degradación en el material. Por otra parte, también durante el procesado, la cizalla mecánica puede provocar un cierto grado de rotura de las fibras que se traduce en un deterioro más rápido de las propiedades mecánicas.

Uno de los principales inconvenientes, que limita la utilización de fibras de celulosa como refuerzo de materiales compuestos, es su baja estabilidad térmica, ya que su degradación comienza a partir de los 200ºC, que es una temperatura próxima a la temperatura de fusión de la matriz termoplástica de PP.

2. PROCEDIMIENTO EXPERIMENTAL

2.1 Materiales

Como matriz polimérica termoplástica se empleó un polipropileno (PP) comercial, MOPLEN 648U (BASELL) (ρ=0.90 g/cm^3, ISO 1183) (IF = 120 g/10 min 2.16, ISO 1183), con una proporción del 48.5% en peso en las formulaciones. Parte de las fibras de celulosa (eucalipto globulus crudo blanqueadas), fueron sometidas a un proceso de refino hasta llegar a 45ºSR en suspensión acuosa. A medida que las fibras se refinan, se puede llegar a conseguir un contacto más íntimo entre la fibra y el polímero.

Estos materiales compuestos fueron preparados utilizando una extrusora Berstoff, de doble husillo corrotante de 25 mm, con una proporción de 1,5% en peso de agente de acoplamiento.

2.2 Equipos y Ensayos

Se estudiaron las propiedades térmicas mediante un calorímetro diferencial de barrido, METTLER TOLEDO DSC 823^e. y para los ensayos TIO, se siguió la norma ISO 11357-6. Para la determinación del módulo de Young, se utilizó una máquina de ensayos Hounsfield H10KT siguiendo la norma ISO 527.

También se estudió la estructura cristalina empleando un difractómetro de rayos X Seiffert XRD 3000, con radiación Cu K_α y filtro de Ni, operando a 30 mA y 40 kV. Los difractogramas se recogieron sobre el rango 2θ = 5- 40º.

3. RESULTADOS Y DISCUSIÓN

Las propiedades térmicas por DSC de la matriz indican una disminución de la cristalinidad en el tercer reciclado respecto de los valores iniciales de cristalinidad en el PP original. También en los difractogramas de la Fig. 1 se puede observar una menor cristalinidad del PP con el reciclado, especialmente en el pico de mayor intensidad (2θ = 16,6º). Este resultado coincide con un gradual descenso en los valores obtenidos del Módulo de Young. Ambos fenómenos son debidos probablemente a la rotura de las cadenas, característica de la degradación del polipropileno por reprocesado.

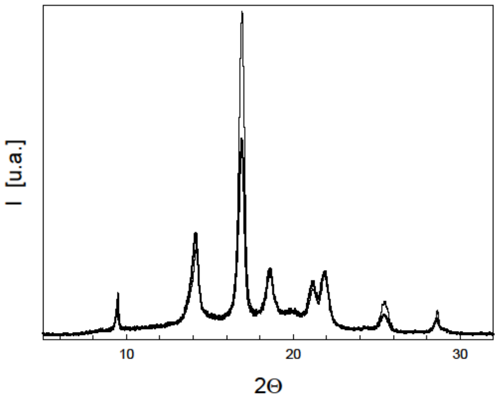

Fig. 1. Difractogramas WAXS de PP original (línea fina) y reciclado (línea gruesa).

Los datos de cristalinidad por difracción de rayos X para los materiales compuestos originales, así como para los reciclados, muestran una disminución de la cristalinidad con respecto a la de la matriz; indicando que las fibras no favorecen los procesos de nucleación. Tampoco se observan diferencias significativas entre los materiales refinados y los no refinados. Sólo cabe destacar un ensanchamiento en el pico de 21,8° para los materiales compuestos, independientemente del tratamiento aplicado. Este ensanchamiento es debido a la contribución del pico de difracción más intenso de las fibras de celulosa.

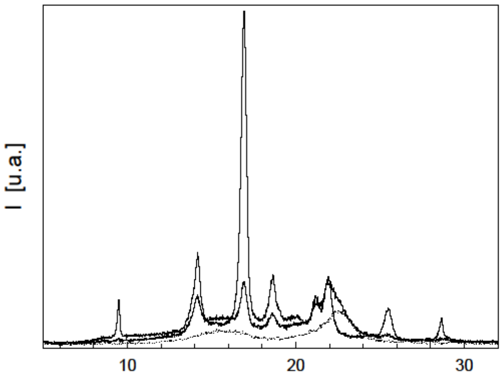

Fig. 2. Difractogramas WAXS de PP (línea fina) y de un material compuesto original (línea gruesa). La celulosa corresponde a la línea de puntos.

Tanto los termogramas, con temperaturas de fusión en torno a 165ºC, como la posición de los picos de difracción, en la matriz y en los materiales compuestos, indican que los cristales formados corresponden a la forma cristalográfica α del polipropileno. No se observa ninguna traza del máximo de intensidad a 16,1° característico de la forma β.

En ninguna de las series se aprecia variación significativa en los valores del TIO entre los materiales originales y sus correspondientes reciclados, tal y como se observa en la Tabla 1. Sin embargo, en los materiales compuestos originales, se observa un pico típico de reacción de degradación alrededor de 200 ºC. Los índices de cristalinidad de los materiales compuestos originales son mayores en los materiales no refinados, resultados que concuerdan con los obtenidos para el módulo de Young.

MATERIAL	**Matriz PP**		**Material Compuesto Refinado**		**Material Compuesto No Refinado**	
	Original	3^{er} Reciclado	Original	3^{er} Reciclado	Original	3^{er} Reciclado
TIO (min)	2,64	2,20	2,25	2,20	2,61	3,45

Tabla 1. Valores del TIO

3. CONCLUSIONES

- El índice de cristalinidad de la matriz disminuye con el número de reciclados.
- No se observan diferencias en las temperaturas de cristalización y fusión, ni en las estructuras cristalinas de los materiales reciclados refinados y no refinados, no favoreciéndose en ninguno de ellos procesos de nucleación en la matriz por parte de las fibras de celulosa.
- Los cristales de PP formados, tanto en los materiales originales como en los reciclados, son del tipo α.
- Los índices de cristalinidad y los valores del módulo de Young son mayores en los materiales originales con fibras no refinadas. Ambas propiedades, tienden a disminuir en el tercer reciclado tanto en los materiales compuestos refinados como en los no refinados.
- No se observa pérdida importante de estabilizantes durante el proceso de reciclado.

AGRADECIMIENTOS

F.A. agradece al Ministerio de Educación y Ciencia (MEC) la financiación del proyecto de investigación FIS2007-60534.

REFERENCIAS

1. KRACHE R., BENAVENTE R., LÓPEZ-MAJADA J.M:, PEREÑA J:M., CERRADA M. L., PÉREZ E. (2007) "Competition between α, β and γ Polymorphs in a β-Nucleated Metallocenic Isotactic Polypropylene". Macromolecules, 40, 6871 – 6878.
2. RABELLO M. S., WHITE J. R (1997). "The role of physical structure and morphology in the photodegradation behaviour of polypropylene". Polym. Degrad. and Stabil. 56; 55-73.

Desarrollo de un material compuesto (plástico-madera) elaborado con material reciclado

J. González
Posgrado de la Facultad de Ingeniería, UNAM, México D.F.
A. Barba
Centro de Ingeniería de Superficies y Acabados (CENISA). Departamento de Materiales y Manufactura. División de Ingeniería Mecánica e Industrial. Facultad de Ingeniería. UNAM. México D.F.

RESUMEN

El presente trabajo pretende dar a conocer las posibilidades de un nuevo material compuesto plástico-madera, para ser aplicado en alguna industria que desarrollo propiamente el diseño de ingeniería. Es bien conocido que los plásticos son materiales ampliamente utilizados en un sinfín de aplicaciones, por sus atractivas características tales como, versatilidad, ligereza, factibilidad de procesamiento y el combinarlo con algún tipo de madera apropiada, puede mejorar diversas propiedades y así ampliar sus campos de aplicación. Si en su momento, como es el caso de este proyecto, se hace uso de material reciclado, el atractivo de los bajos costos se puede agregar cada vez más a las condiciones de obtener un material que cumpla con propiedades específicas para la industria. Por otro lado, se observa que el impacto que ha causado el uso de materiales reciclados, dentro de la ingeniería, se atribuye a que se mejorar propiedades mecánicas que se manejan específicamente para las aplicaciones determinadas.

1. INTRODUCCIÓN

A continuación se señalan algunos casos específicos a través de gráficas en donde se puedo observar el impacto que tiene el consumo de material plástico en el país y por otro lado mencionar que el plástico a utilizar es el polipropileno, ello debido al consumo que se tiene de este material.

Tipo de basura	**2003**	**2004**	**2005**	**2006**	**2007**
Total	**32 916**	**34 603**	**35 383**	**36 135**	**36 865**
Papel, cartón, productos de papel	**4 909**	**5 160**	**5 276**	**5 388**	**5 489**
Textiles	**495**	**520**	**531**	**542**	**552**
Plásticos	**2 013**	**2 116**	**2 162**	**2 208**	**2 223**
Vidrios	**2 158**	**2 210**	**2 261**	**2 309**	**2 341**
Metales a/	**1 048**	**1 160**	**1 185**	**1 210**	**1 298**
Aluminio	**587**	**606**	**619**	**633**	**650**
Ferrosos	**283**	**329**	**336**	**343**	**410**
Otros ferrosos b/	**178**	**225**	**230**	**234**	**238**

Tabla 1. Generación de residuos urbanos (en miles de toneladas)[1]

Además, es necesario mencionar que la distribución de materiales plásticos de acuerdo a los consumos de artículos clasificados como generales y técnicos, tienen una gran diversidad de aplicación, por ello el interés de abordar esta temática con materiales reciclados.

En la tabla 1 se muestra la cantidad de material plástico que se tiene hasta el 2007 en el país de México, y se puede apreciar que el consumo favorece al aprovechamiento de los residuos para este proyecto con materiales reciclados.

Por otro lado, en un párrafo anterior se menciono que se hará uso del polipropileno reciclado como materia prima y ello se debe a que en el país se consumen productos elaborados con este material y lo cual permite aprovechar este factor. Por otro lado, loa madera a utilizar es directamente extraída de las madererías, la materia prima es el aserrín de pino, que se utilizará como refuerzo del material plástico y así obtener el material compuesto.

2. METODOLOGÍA

La metodología a seguir pare generar el material compuesto esta formada por los siguientes pasos:

1. Separación del aserrín
2. Combinación del aserrín con el polipropileno
3. Peletizado (extrusión)
4. Pieza (probetas de tracción, mediante inyección)
5. Observación en microscopio óptico

Dentro de la separación del aserrín es muy importante considerar que el proceso debe tener un cuidado estricto, debido a que en este caso en particular no se esta tratando de ninguna forma el material y ello conlleva a ser muy cuidadosos en el momento de realizar dicho proceso.

Para generar comparativas importantes se realiza la combinación del aserrín con material plástico virgen y reciclado, y con ello tener los parámetros de evaluación más claros.

El peletizado se realiza con una máquina de extrusión para posteriormente utilizar el pelet en una máquina de inyección y generar las piezas a ensayar.

Es necesario mencionar que las piezas obtenidas, probetas de tracción, se encuentran normalizadas, considerando la norma D 638M, en donde se dan las especificaciones de la probeta para su evaluación en los ensayos mecánicos.

Por último, la observación del microscopio permite iniciar el la etapa de la determinación de la geometría para obtener una mejor adhesión de la materia prima reciclada.

3. DESARROLLO EXPERIMENTAL CON MICROSCOPIO

En primer lugar se realizan cortes en secciones diferentes de la probeta para asimismo colocarlas sobre la base del microscopio e ir observando el comportamiento que tiene el aserrín con el material plástico.

En la figura 1 se pueden apreciar los secciones a visualizar, al igual que el microscopio en donde se realiza el ensayo.

Fig. 1. Probetas y microscopia a utilizar para los ensayos.

En la siguiente imagen se observan como se encuentra el aserrín ya unido con el material plástico y su geometría antes de ser combinados.

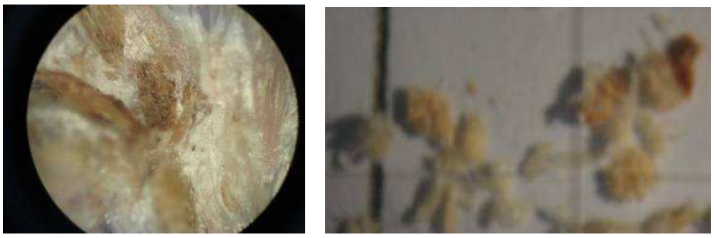

Fig. 2. Observación del aserrín con el material plástico.

Estas observaciones desarrolladas van a permitir describir los resultados que a continuación se mencionan.

4. RESULTADOS

En primera instancia se muestran gráficas que permiten comparar el comportamiento del flujo, la obstrucción, si es que existe, que se da entre el aserrín y el polipropileno.

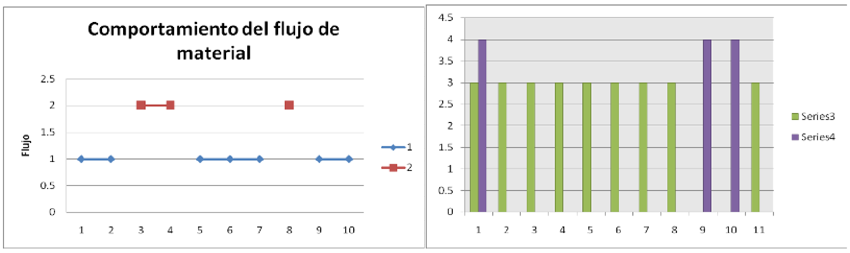

Fig. 3. Comportamineto y obstrucción del aserrín

La siguiente figura da los resultados la existencia deaserrín sobre la superficie del material compuesto.

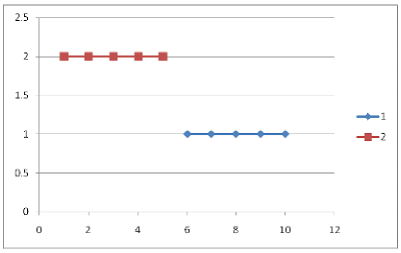

Fig. 4 Visualización del aserrín sobre la superficie.

Hasta el momento son los datos que se han obtenido de este proyecto, y se sigue trabajando para obtener diversos materiales con productos reciclados.

5. CONCLUSIONES

Con los resultados obtenidos hasta el momento se puede concluir que el proyecto va por buen camino ya que se logra comprender que la adherencia del aserrín al polipropileno tiene mucho que ver con el comportamiento y tamaño del aserrín que se vaya a utilizar. Por otro lado, la microscopia óptica permite fusionar más la información y establecer adecuadamente los parámetros que va a generar al materia como una alternativa ´mas de la nueva generación de materiales compuestos.

REFERENCIAS

[1] FUENTE: INEGI. Con base en SEDESOL. Dirección General de Equipamiento e Infraestructura en Zonas Urbano-Marginadas, 2008.
SOLIS, J.M. (2005). Elaboración de productos manunfacturados por moldeo utilizando plásticos de postconsumo y materiales lignocelulósicos. Depto. Ciencias/Química, Universidad Bio-Bio. Chile
Johnson JA, Nearn WT. Theory and design of wood and fiber composite materials. Reinforcement of polymeric systems with Douglas-fir bark fibers, New York: Syracuse University Press; 1972. (chapter 15), p. 371–400.

Materiales termoestables obtenidos por copolimerización del alcohol furfurílico con una lactona. Efecto de la modificación estructural sobre la cinética y las propiedades

M.L González, J.C. Miguez, F.J. Juanes, B.González, A. Valea
Departamento de Ingeniería Química y del Medio Ambiente, Escuela
Universitaria de Ingeniería Técnica Industrial, U.P.V.- E.H.U.
Plaza de la Casilla, 3, 48012 Bilbao
[1] e-mail: marialuz.gonzaleza@ehu.es

RESUMEN

A partir de la biomasa procedente de los residuos vegetales se obtiene el alcohol furfurílico. El alcohol furfurílico en medio ácido (pH < 2-3) y en condiciones controladas puede llevarse en dos etapas el proceso de polimerización. La ε-caprolactona en medio ácido sufre la apertura del anillo y debido a su tendencia a reaccionar con los grupos –OH puede originar modificaciones estructurales que dotan a las cadenas de mayor flexibilidad. Para analizar el efecto de la introducción de la caprolactona sobre la cinética del proceso y las modificaciones estructurales producidas durante la polimerización y curado de la resinas se han realizado estudios cinéticos utilizando el método de Vyazovkin, de cinética libre, espectroscópícos FTIR y reológicos. La apertura del anillo e incorporación en el sistema reaccionantes ocurre desde la primera etapa de la polimerización.

1. INTRODUCCIÓN

En la actualidad, siguiendo criterios de sostenibilidad, existe un creciente interés en encontrar materias primas renovables como alternativa al petróleo para la síntesis de materiales plásticos y composites. A partir de la biomasa procedente de los residuos vegetales se obtiene el alcohol furfurílico. El alcohol furfurílico (FA) en medio ácido (pH < 2-3) reacciona consigo mismo de forma incontrolada dando lugar a un material termoestable totalmente poroso e inservible. Si se utilizan ácidos más débiles o más diluídos el alcohol furfurílico protonado reacciona preferentemente con el agua para recuperar el alcohol o bien lo hace en α para originar un hidroxifurano o lactona del ácido levulínico que, en el medio de la reacción, se hidroliza al ácido. Llevando a cabo la reacción en condiciones controladas puede llevarse a cabo el proceso en dos etapas. En una primera etapa, el alcohol furfurílico resinifica o se homopolimeriza, mediante una metilolación que supone la condensación del grupo metilol de una molécula de FA con el de otra molécula en la posición cinco, originando inicialmente dímeros y trímeros que se conocen como resinas furánicas. En una segunda etapa estas cadenas de prepolímero pueden entrecruzarse por grupos metileno dando a lugar a un material termoestable de color negro que resulta ser demasiado frágil, lo que limita mucho sus posibles aplicaciones. Una vía para modificar estructuralmente la resina y dotarla de tenacidad es la incorporación de comonómeros que se interpongan entre los anillos furánicos aportando flexibilidad al material (G. Jiang et al 2006). Según las investigaciones de Servando González et al (2007) la introducción de lactonas, durante el proceso de curado de una DGEBA, puede originar intermedios de reacción tipo espirortoésteres (SOEs), compuestos bicíclicos que se usan frecuentemente para expandir los monómeros disminuyendo la fragilidad y la contracción de la resina durante el curado. En trabajos anteriores (A. Valea et al 2009) se ha utilizado la ε-caprolactona como comonómero de una resina furánica durante la etapa de curado. La ε-caprolactona en medio ácido sufre la apertura del anillo y debido a su tendencia a reaccionar con los grupos –OH podría incorporarse entre dos anillos furánicos, aumentando el tamaño de la cadena alifática que los une, produciéndose la modificación estructural que se persigue. Pero, durante el proceso de curado se prevé que pueden ocurrir diferentes tipos de reacción: (a) la homopolimerización de la resina furánica, (b) la reacción de la lactona con la resina furánica, c) la reacción entre las especies intermedias formadas, d) la reacción de la resina furánica con la especie intermedia y e) la homopolimerización de la caprolactona. El predominio de unas de estas reacciones sobre las otras condicionará los mecanismos cinéticos del proceso, la estructura y morfología del material obtenido y, por tanto, sus propiedades térmicas y mecánicas. La reactividad de la resina furánica depende de la concentración de grupos funcionales finales, es decir de su peso molecular, de la composición en caprolactona y del tipo de catalizador utilizado.

El objetivo de este estudio es contribuir al conocimiento sobre los procesos de polimerización y curado del FA en presencia de ε-caprolactona, utilizando un catalizador ácido convencional y un catalizador del tipo triflato. Gracias al cual sería posible controlar las modificaciones estructurales de la resina que permitan mejorar sus propiedades mecánicas, y la estabilidad dimensional del material durante el procesado. Los estudios cinéticos se han realizado utilizando el método de cinética libre de Vyazovkin (2006). Los cambios estructurales que ocurren durante el proceso de polimerización y curado se han estudiado por análisis FTIR y mediante los cambios reológicos asociados.

2.EXPERIMENTAL

El monómero alcohol furfurílico (FA) y el catalizador ácido p-toluensulfónico 75% (PTS) han sido suministrados por Foseco. La ε-caprolactona (ε-CL) y el el triflato de erbio (TFE) reactivo suministrados por Alfa Aesar.

Los ensayos DSC se han llevado a cabo con un DSC Mettler-Toledo, equipado con el software “advanced model-free kinetics STAR. La liberación de volátiles durante el proceso de policondensación del FA hace necesario la utilización de crisoles de acero de media presión. Para llevar a cabo el estudio cinético se han realizado varios ensayos dinámicos con diferentes programas de temperaturas. Los ensayos termogravimétricos se han realizado con una TGA Mettler Toledo con programa informático de tratamiento y evaluación de las curvas. Se ha utilizado un FTIR de Perkin Elmer 2000 con un dispositivo ATR Golden para realizar los estudios espectroscópicos. Para estudiar la evolución de la viscosidad durante el proceso de polimerización se ha utilizado un reómetro Haake VT-500 con dispositivo placa-cono.

3. RESULTADOS

En las curvas DSC obtenidas durante el ensayo dinámico de calentamiento (10ºC/min) para la homopolimerización del FA utilizando PTS como catalizador se detecta la aparición de dos picos exotérmicos. El primer pico se asocia con un mecanismo tipo

MA (monómero activo) y el segundo a mecanismos tipos CA (cadena activa) (Milkovic et al 1979). En las curvas de la variación de la Energía de activación efectiva con la conversión deducidas utilizando el método de Vyazovkin, se observan tres tramos, figura 1, lo que indica cambios en los mecanismos de reacción, en el tercer tramo a altas conversiones son los mecanismos de difusión las que gobiernan el proceso.

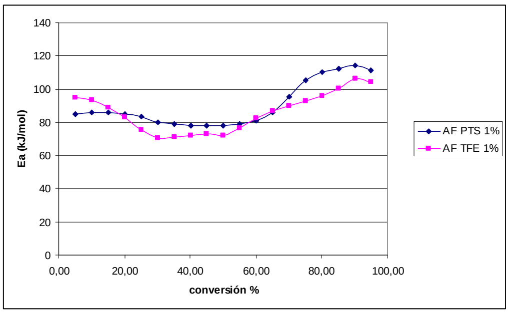

Fig. 1. Efecto del tipo de catalizador.

En la figura 1 se observa que la sustitución del catalizador ácido PTS por el triflato de erbio ejerce un efecto apreciable sobre el primer tramo ($\alpha < 0,25$) que se correspondería con las primera etapas de formación de las especies activas y la polimerización lineal, lo cual conduce a que en la segunda etapa la energía de activación efectiva sea unos 10 kJ/mol menor en el caso de utilizar el TFE como catalizador.

Para analizar el efecto de la introducción de la caprolactona como comonómero desde el comienzo del proceso de polimerización se han estudiado los sistemas con diferentes relación molares AF/ε-CL :1/0; 2/1, 3/2, 2/1 y 0/1 todas ellas al 1% de TFE. Cabe destacar en primer lugar que el pico exotérmico de la curva DSC (a 10ºC/min) para el sistema AF/ECL:0/1 es de 180ºC luego se podría, en principio, considerar que la homopolimerización de la caprolactona es termodinámicamente poco favorable. Algunos de los resultados más destacables se representan en las figuras 2 y 3. A través de las curvas DSC representadas en la figura 2, puede deducirse que cuando aumenta el contenido en caprolactona los picos de reacción se desplazan a mayores temperaturas y disminuye la velocidad de reacción ($d\alpha/dT$), sobre todo en los últimos tramos de reacción; este efecto era esperable debido a la disminución de grupos funcionales alcohol. En la figura 3 se observa que la diferente composición en caprolactona afecta también a los valores de las energías de activación efectiva, lo cual supone cambios en los mecanismos de reacción

En la figura 3 se observa que la mayor diferencia en las curvas de la variación de la Energía de activación efectiva para las diferentes composiciones aparece en el primer tramo ($\alpha < 0,25$), en el que se forman las especies activas intermedias entre ambos componentes y los precursores poliméricos que en la segunda y tercera etapas entrecruzarán. El sistema AF/ECL:1/1 parece no seguir la tendencia que siguen el resto de las composiciones estudiadas, lo cual podría deberse a que a altas concentraciones de caprolactona la homopolimerización no es despreciable.

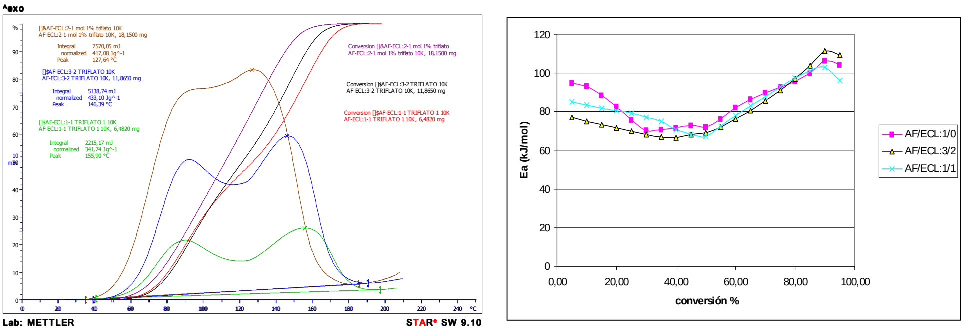

Figuras 2 y 3: Efecto de la adición de la ε-caprolactona como comonómero del AF.

La evolución estructural de la resina durante el proceso de polimerización se ha estudiado por FTIR a través de la variación en la absorbancia de las bandas asociadas a determinados grupos funcionales. Se destaca la del grupo C=O que aparece a 1773 cm^{-1} cuando forma parte de un ciclo y se desplaza a11730 cm^{-1} cuando por apertura del ciclo forma parte de una cadena alifática. Se ha podido comprobar que para conversiones del 20-30% la banda a 1773 cm^{-1} prácticamente ha desaparecido, aumentando la de 1730 cm^{-1}, lo que confirmaría la incorporación de la caprolactona al proceso de polimerización. La incorporación de la caprolactona flexibiliza las cadenas. A través de la medida de la variación de la viscosidad con el tiempo, durante el proceso de polimerización y curado, se ha observado una disminución de la viscosidad a medida que aumenta la composición en ECL, durante el proceso. Se observa un comportamiento anómalo para la composición AF/ECL:1/1

AGRADECIMIENTOS

Agradecemos al M.E.C y a la UPV/EHU las ayudas recibidas, para desarrollar los Proyectos MAT 2006-13313- CO2-02 y UNESCO07/03 (2007) y la Ayuda a grupos de investigación de la UPV-EHU.

REFERENCIAS

G. JIANG, G.S.WALKER, I.A.JONES, C.D.RULD. Journal of Applied Polymer Science, Vol.102, 3900-3906 (2006)
S.VYAZOVKIN “Model-Free Kinetics” Journal of Therrnal Analysis and Calorimetry, Vol 83 (2006) 1, 45-51.
SERVANDO GONZÁLEZ, XABIER FERNANDEZ-FRANCOS, JOSEP MARÍA SALLA, ANGELS SERRA, ANA MANTECÓN, XAVIER RAMIS “New Thermosets obtained by cationic copolymerizacion of DGEBA with γ-caprolactone with improvement in the shrinkage II. Time-Temperature-Transformation (TTT) cure diagram” Journal of Applied Polymer Science, Vol 104, 3406-3416 (2007)
VALEA, A.; MONDRAGÓN, I.; GONZALEZ, B.; JUANES, F.J.; GONZÁLEZ, M.L. (2009). “Mejora de la tenacidad de las resinas furánicas por copolimerizacion con ε-caprolactona”. Anales XXVI Congreso del Grupo Español de Fractura pp.226-231 (2009).

Estudio de las propiedades físico químicas y mecánicas de 4 tipos de Guadua Angustifolia Kunth. Un material compuesto natural

L.A Sánchez[1], M. Contreras[2], Del Real A[1], M. E Rodriguez[1]
[1]Centro de Física Aplicada y Tecnología Avanzada. Universidad Nacional Autónoma de México.
[2]Universidad Autónoma de Querétaro. Querétaro, México.

RESUMEN

La *Guadua Angustifolia Kunth* es un material compuesto natural perteneciente a la familia de las Angiospermas y la cual crece en abundancia en los países tropicales, recientemente se ha convertido en una alternativa económica para la construcción de viviendas y sus fibras han sido utilizadas, recientemente, en refuerzo de materiales compuestos. LA *Guadua* es considerada un material compuesto debido a que su culmo consiste en un manojo de fibras insolubles completamente alineadas en la dirección longitudinal embebidas en una matriz de lignina, y estos a su vez alojadas en un tejido parenquitimoso, las fibras le suministran una buena resistencia a la tensión y una gran rigidez en la dirección en la cual se encuentran alineadas.

Los cuatro especimenes de bambú fueron sometidos a análisis de Difracción de Rayos X con el fin de determinar sus componentes cristalinos, se les realizo un análisis bromatológico completo donde se incluyo determinación de minerales, grasas, cenizas y porcentaje de fibra soluble e insoluble, mediante SEM / EDS se evaluó la morfología de cada uno de los especimenes y se hizo un análisis semicuantittivo de los componentes presentes, por último fueron sometidas a ensayos de compresión y flexión bajo los estándares DIN 52 186 en una maquina universal de pruebas mecánicas.

El objetivo de este trabajo es correlacionar la morfología, composición química y estructural de las cuatro variedades de *Guadua Angustifolia Kunth* con la respuesta mecánica que presenta cada una a los ensayos de flexión y compresión.

Influencia del tipo de soporte celulósico empleado sobre el comportamiento de membranas intercambiadores de iones

N. Escobar
Escuela de Ingeniería, Facultad de Ingeniería Mecánica, Grupo de Investigación sobre Nuevos Materiales, Universidad Pontificia Bolivariana, Medellín, Colombia.
A. Arrieta
Grupo DANM/ Desarrollo y Aplicación de Nuevos Materiales,
Universidad Pontificia Bolivariana, Montería, Colombia.
D. Rendón
Escuela de Ingeniería, Facultad de Ingeniería Agroindustrial,
Universidad Pontificia Bolivariana, Medellín, Colombia.
P. Gañán
Escuela de Ingeniería, Facultad de Ingeniería Mecánica, Grupo de Investigación sobre Nuevos Materiales, Universidad Pontificia Bolivariana, Medellín, Colombia

RESUMEN

El paso de fluidos naturales a través de suelos de rocas sedimentarias como la piedra caliza, provoca la disolución de iones como el calcio y el magnesio. Estos cationes divalentes cuando se encuentran en altas concentraciones son los responsables de la dureza del agua. La eliminación de la dureza y en general la disminución de la cantidad de iones no deseables en el agua se realiza a través de polímeros de intercambio iónico como resinas sulfonadas de fenol-formaldehido y, en los últimos años se ha venido empleando polímeros como el poliestireno sulfonado, materiales todos ellos de alto costo. En general estos sistemas sufren un proceso de saturación y deben ser regenerados o cambiados según sea necesario incrementando el costo del tratamiento de aguas. Toda esta problemática sugiere entonces la importancia que tiene desarrollar un nuevo sistema de ablandamiento de aguas utilizando materiales económicos y de fácil acceso. Para tal fin, diferentes muestras de celulosa bacterial y vegetal han sido empleadas como soporte para la deposición de películas de polímeros conductores como el polipirrol. Las muestras obtenidas han sido empleados como membranas intercambiadoras de iones y evaluadas a través de conductimetría cíclica, ensayos de caracterización del material como ángulo de contacto, análisis termogravimétrico y morfológico que permiten comprobar la apropiada deposición del polímero sobre el sustrato generando resultados que pueden ser opciones viables para la construcción de dispositivos requeridos en el tratamiento de aguas duras.

1. INTRODUCCIÓN

El empleo de agua dura tanto para usos domésticos como industriales, cuando se emplea y no es tratada, genera problemas de formación de incrustaciones en equipos como calderas, tanques de almacenamiento o sistemas de drenaje de uso muy común para métodos de riego en el ámbito agroindustrial debido a las incrustaciones que afectan su - fracción de iones hierro y manganeso, cuya presencia puede manchar los tejidos, formar depósitos en tuberías, u otros elementos, así como inducir su corrosión. (MEJIA et al. 2001) y (CARDENAS, J. et al. 2005).

La eliminación de la dureza o remoción y en general, la disminución de la cantidad de iones no deseables en el agua se realiza a través de la utilización de resinas de intercambio iónico como zeolitas, resinas sulfonadas de fenol-formaldehido y, en los últimos años mediante poliestireno sulfonado, todos ellos materiales muy costosos. Estos polímeros sufren un proceso de saturación y deben ser regeneradas o cambiadas incrementando el costo del tratamiento de aguas. (CARDENAS, J. et al. 2005). Este proceso tiene inconvenientes importantes como la alta generación de residuos, ya que se obtienen disoluciones altamente ácidas o básicas muy concentradas en metales en solución que deben ser tratadas o eliminadas.

Toda esta problemática sugiere entonces desarrollar una membrana o filtro intercambiador de iones, que tenga un soporte o sustrato sobre el cual se realiza la reacción de síntesis o polimerización requerida para recubrirle con el polímero conductor (pirrol) buscando mediante estímulos electroquímicos obtener procesos de intercambio de iones al interior de la matriz polimérica durante la oxidación/reducción de los polímeros conductores. En este trabajo se sintetizaron dos sustratos económicos y de fácil acceso para la preparación de la membrana polimérica de polipirrol, Ellos son esencialmente dos fuentes diferentes de celulosa, una de origen vegetal aislada mediante tratamientos mecánicos y químicos de residuos fibrosos generados por la agroindustria de *Musáceas* comestibles colombiana y otra obtenida mediante la actividad extracelular de bacterias como el *Acetobacter xylium spp.*

2. MATERIALES Y MÉTODOS

Los sustratos celulósicos tanto de naturaleza vegetal como bacterial fueron obtenidos siguiendo procedimientos previos realizados por los autores del presente trabajo (ZULUAGA, R. et al. 2009). Los correspondientes a muestras de celulosa vegetal fueron aislados empleando sucesivas etapas que involucran la utilización de disoluciones de KOH al 5 % y máquinas como el *Waring Blender* para los procesos mecánicos (ZULUAGA, R. et al. 2009). Para el cultivo de celulosa bacterial fueron empleados fuentes económicas de carbohidratos como las correspondientes a desechos de frutas como la piña y la panela. En cuanto a los reactivos empleados para la deposición de la película del polímero sobre las muestras de celulosa se encuentran monómero pirrol de la marca *Aldrich*, además del sodio dodecilbensulfónico y el persulfato de amonio, los cuales actúan como medios dopantes.

El proceso metodológico que se utilizó para la realización del proyecto fue el siguiente:

a) Se realizó la síntesis del polipirrol sobre los sustratos por dos métodos de deposición directa (DD) y en solución con una concentración de 0,5 molar (DS) de monómero, la cual permite garantizar que el film estuviera cubierto totalmente. El comportamiento electroquímico de la membrana se evalúo por medio de voltimetría cíclica utilizando un equipo potenciostato-galvanostato marca PARSTAT modelo 2263. La variable a controlar corresponde al voltaje aplicado sobre la membrana intercambiadora de iones, tomando un valor de – 0,5 V con un tiempo de aplicación de 0 a 6 h y realizando toma de datos cada segundo.

b) Se realizó la caracterización y valoración de las membranas producidas a partir del polímero conductor polipirrol, verificando la conductividad luego de realizar la síntesis con un equipo con un multímetro marca *BK PRESICION* modelo 5491a, ver figura 1.

c) La deposición de la película también fue monitoreada empleando la determinación del ángulo de contacto a través de la técnica de la gota en reposo o sessile drop. El equipo utilizado corresponde a un *Fotomicroscopio OCA15LTH plus HTF1200* que dispone de un software *SCA20*. El líquido de prueba, que corresponde a agua ultrapura y fue dosificado a través de una micropipeta *Transferpette®* de *Brand*. Las mediciones fueron realizadas en períodos de tiempo que oscilaban entre 1,5 - 2 s, y empleando una velocidad de grabación de 25 cuadros/s. En cuanto a la caracterización térmica, esta fue realizada mediante análisis termogravuimétrico empleando un equipo *Metler Toledo TGA/SDTA85IE/lLF/1610.* Los ensayos fueron realizados en atmósfera de nitrógeno a una velocidad de calentamiento de 10 °C min^{-1}. En cuanto a la caracterización morfológica realizaron ensayos de microscopía electrónica de barrido, JEOL JSM 5910 LV. Las muestras fueron incluidas en parafina y cortadas en el microtomo para facilitar su manipulación. La zona gruesa del corte fue cubierta con una delgada capa de oro en un *sputter coater,* mejorando así la conductividad eléctrica. En tanto que los de microscopía óptica fueron realizados con un equipo Leyca modelo DLMN.

Fig. 1. Medición de la conductividad en una membrana de polipirrol y sustrato de celulosa bacterial realizada por deposición directa.

3. RESULTADOS Y ANÁLISIS

Los resultados de conductimetría cíclica realizados sobre las muestras de membranas depositadas sobre ambos tipos de sustratos de celulosa presentaron valores entre 3,74 y 3.91 Ω. Estos valores sugieren una adecuada deposición del polímero para ambos tipos de muestras de celulosa e indican que pueden actuar como potenciales membranas intercambiadoras de iones, lo cual abre la posibilidad de emplear este tipo de materiales para aplicaciones menos convencionales como esta. Con miras a establecer la homogeneidad de la deposición se realizaron ensayos de determinación de ángulo de contacto sobre diferentes puntos del film y empleando en todos los casos agua ultrapura como líquido de prueba. Tal como se aprecia en la Figura 2 en toda la superficie de la membrana recubierta con el polipirrol se alcanzaron valores para los ángulos de contacto de 90°, esto indica que el incremento en la tendencia hidrofóbica se relaciona con la capa depositada o formada de polímero. Así mismo se observó baja dispersión en los resultados a lo largo de las membranas, obteniendo desviaciones menores al 10% sugiriendo que los métodos de deposición directa y en solución pueden ser efectivos al momento de desarrollar estos materiales. Así mismo los ensayos de caracterización térmica y morfológica siguieren presencia del polímero y una adecuada adhesión al sustrato. De otro lado la estabilidad térmica de las membranas se encuentra condicionada tanto por el sustrato como por la película de polímero depositada.

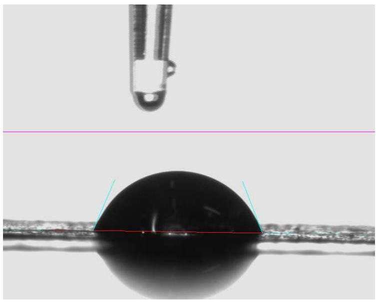

Fig. 2. Interacción entre el líquido de prueba y una membrana de polipirrol y sustrato de celulosa vegetal realizada por deposición directa.

4. CONCLUSIONES

De acuerdo con los resultados obtenidos en este trabajo se indica que es posible realizar membranas intercambiadoras de iones mediante la deposición de películas de polipirrol sobre sustratos de bajo costo como son los elaborados a partir de celulosa vegetal y bacterial. Los ensayos de evaluación del ángulo de contacto, caracterización térmica y microscopía óptica indican que existe una adecuada deposición de la película y que la estabilidad térmica de la membrana es fruto de una contribución tanto del polímero como del sustrato empleado.

REFERENCIAS

CARDENAS, J. A. (2005) Calidad de agua pura para estudiantes de ciencias ambientales. Universidad Distrital Francisco José De Caldas. Capitulo 11 – Dureza Total. Bogotá D.C Colombia.

MEJIA, G.A. GOMES, J.(2000) Los desechos generados por la industria bananera en Colombia. En: Seminario internacional gestión integral de residuos sólidos y peligrosos Siglo XXI. Experiencias Director Cenibanano y Técnico de investigación. Colombia.

Secretaria de Economía. Estados Unidos mexicanos. (2001) Análisis de agua – Determinación de dureza total en aguas naturales, residuales y residuales tratadas – Método de prueba (NMX-AA-072-1981). NMX-AA-072-SCFI.

ZULUAGA, R. (2009) Cellulose microfibrils from banana rachis: Effect of alkaline treatments on structural and morphological features*:* Carbohydrate Polymers, 51-59.

Effect of filler loading and compatibilizer on mechanical and morphological properties of wood polymer composites

B. Kord
Corresponding Author: Scientific Member of Islamic Azad University,
Malayer Branch, P.O. Box 65718/117, Malayer, Iran
behrouzkord@yahoo.com
B. Kord
Scientific Member, Department of Wood and Paper Science and Technology,
Islamic Azad University, Chalous Branch, P.O. Box 46615/397, Chalous, Iran
behzad_k8498@yahoo.com

SUMMARY

In this study, the effect of wood flour and compatabilizer content on mechanical properties and morphological behavior of wood plastic composites were investigated. For this purpose, wood flour-polypropylene composites were made by counter rotating twin-screw extruder. The variable factors were wood flour content (0%, 10%, 20%, 30%, 40% and 50% weight ratios) and MAPP as coupling agent (0%, 1% and 2% weight ratios). Mechanical properties such as: flexural modulus, tensile modulus and notch impact strength were measured. Result indicated that, Increase of wood flour content caused to all mechanical properties of wood polymer composites except notch impact strength increased. Also, in present of coupling agent caused to improve the all mechanical properties of wood polymer composites. The SEM micrographs revealed well-dispersed wood flour on the fracture surfaces of the test samples fabricated using a coupling agent.

1. INTRODUCTION

Wood plastic composites (WPCs), which are defined as composite materials containing wood (in various forms such as wood flour and fiber, kenaf fiber, hemp, sisal etc) and thermoplastic materials (e.g. polyethylene, polypropylene, PVC etc.), are a relatively new family of composite materials. Compared to the traditional synthetic fillers, the natural fibers present lower density, less abrasiveness, lower cost and they are renewable and biodegradable. WPCs are becoming more and more commonplace and are also gaining considerable popularity in the world. A disadvantage of natural fibers are they could not good adhesion with polymer so caused the decrease physical and mechanical properties of WPCs. Therefore, use of compatibilizers can enhance water resistance of the Composites through better encapsulation of the fibers by the plastic. The aim of this study was to investigate the effect of wood flour and coupling agent content on the mechanical and morphological properties wood polymer composites.

2. EXPERIMENTAL

Polypropylene, PI0800 (MFI=3.1 g/10min) was supplied by Bandar Imam Petrochemical Industries, Iran. Beech wood-flour was from Cellulose Aria Co, Iran. Maleic Anhydride Polypropylene (MAPP) provided by Malajchoob Factory, Gorgan, Iran. Oven-dried WF and BF with a moisture content of less than 3%, polypropylene and MAPP were weighed and then physically mixed in a laboratory mixer for 10 min. The mixtures were then extruded using a laboratory twin-screw extruder. The specimens were cut out of for testing. The flexural, tensile and impact tests were measured according to the ASTM D790-03, D638-03 and D256 respectively. The morphology of the interface region of the tensile fractured surfaces of composite specimens was studied using Scanning Electron Microscope (JEOL-JSM5800,Japan).

3. RESULT AND DISCUSSION

The variation of the flextural and tensile modulus versus wood flour content at different levels of MAPP in wood polymer composites shows that in figures 1 and 2. As can be seen, the flextural and tensile modulus of the composites increases with increasing the wood flour loading. As we know the modulus of composites are composed from their constitue materials, so with increasing the wood flour to polymer matriz we are expected that the flextural and tensile modulus will be increase. Also figures 1 and 2 illustrates, the flextural and tensile modulus increases with increase of MAPP at different levels of wood flours. It is well established that presence of the MAPP as coupling agent enhances the interface adhesion between wood flour and pp matrix and brings better encapsulation of wood particles by the plastic which consequently results in higher flextural and tensile modulus.

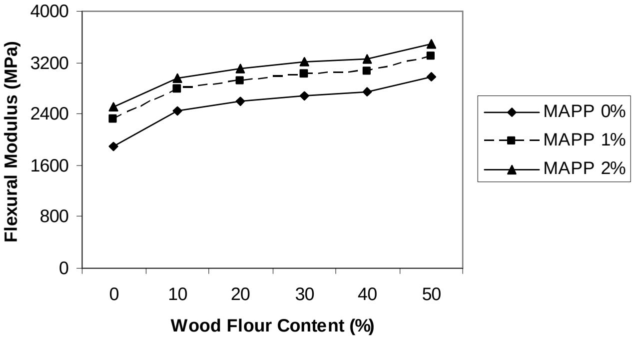

Figure 1. Flexural modulus of samples at different wood flour and coupling agent levels

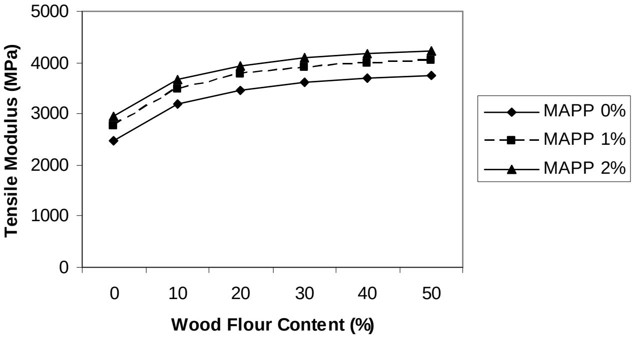

Figure 2. Tensile modulus of samples at different wood flour and coupling agent levels.

Figure 3 shows the variation of the impact strength versus wood flour content at different levels of MAPP in wood polymer composites. As can be seen, the impact strength of the composites decreases with increasing the wood flour loading. The fibers play an important role in the impact resistance of fiber-reinforced composites as they interact with the crack formation and actas stress-transferring medium. Also figure 3 illustrates, the impact strength increases with increase of MAPP at different levels of wood flour. The enhancement in the impact strength could be attributed to the more homogeneous dispersion of the fiber resulting from the increasing wettability of the fiber with increasing concentration of the coupling agent that leads to more uniform distribution of the applied stress and requires more energy for the fiber debonding and subsequent fiber pull out as these are the causes of impact failure of the composites.

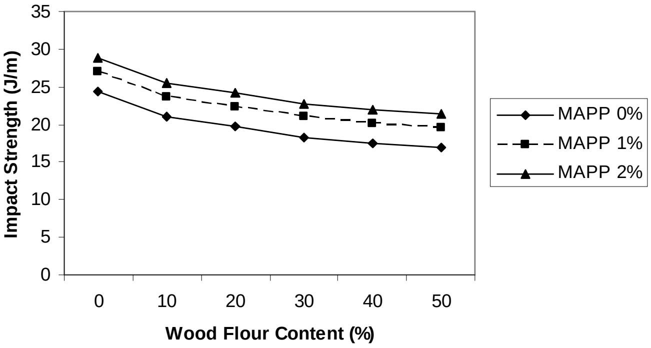

Figure 3. Impact strength of samples at different wood flour and coupling agent levels.

Scanning electron microscopy in figure 4 shows that the insufficent adhesion between wood flour and polypropylene without coupling agent, and with adding the MAPP to polymer matriz caused to enhances the interface adhesion between wood flour and polymer matrix and brings better encapsulation of wood particles by the plastic (figure 5). Also these figures shows that the strong interfacial bonding between the wood flour and polymer matrix caused by the compatibilizing agents. The SEM micrographs revealed well-dispersed wood flour on the fracture surfaces of the test samples fabricated using a coupling agent.

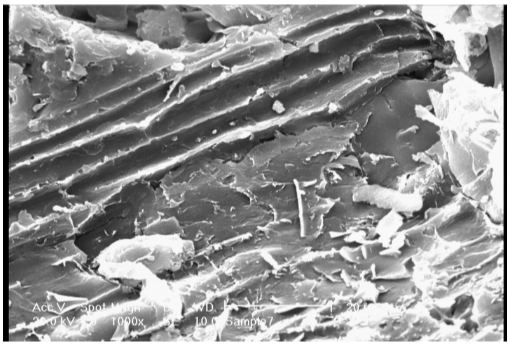

Figure 4. The surface fracture of composite without MAPP

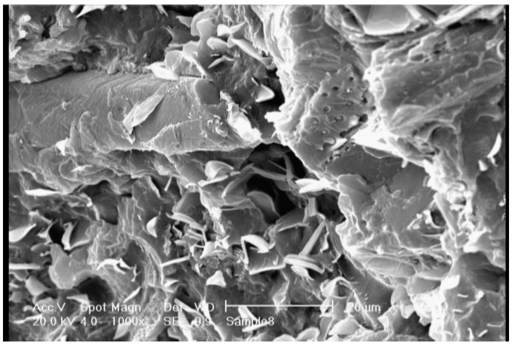

Figure 5. The surface fracture of composite with 2% MAPP

4. CONCLUSION

The following conclusions could be drawn from the results of the present study:

1.The flextural and tensile modulus of wood polymer composites increases with increase of wood flour loading. However, the impact strength decreased with increased wood flour content.

2. all mechanical properties of wood polymer composites improved by in present of coupling agent.

3. The SEM micrographs revealed well-dispersed wood flour on the fracture surfaces of the samples fabricated using a coupling agent.

REFERENCES

Agarwal, B.D and L.j, Broutman, 1980. Analysis and performance of fiber composites, Journal of polymer science 18(10):689-690.

Bataille, P., Richard, L., and Sapieh, S., 1989. Effect of cellulosic fibers in polypropylene composites, Polymer Composites, 10(2): 103-108.

George, J., Sreekala, M.S., and Thomas, S., 2001. A review on interface modification and characterization of natural fiber reinforced plastic composites, Polymer engineering and Science, 41(9):1471-1485.

Hull, D. 1991. Introduction to Composite Material, Cambridge University.

Karnani, R., Krishnan, m., Narayan,R., 1997. Biofiber Reinforced polypropylene composites. Journal of polymer Engineering science, 37(2):476-483.

Kit, L.Y., Binoy, K., Gogot, C. and Selke, S.E., 1990. Composites from compounding wood fibers with recycled HDPE, Polymer Engineering and Science, 30(11): 693-699.

Kokta, B.V., and Maladas, D., 1990. Composites of Polyvinyl Chloride wood fibers. Journal of Polymer Plastic Technology, 20 (1-2) 87-118.

Oksman, K., and Clemon, C. 1998. Mechanical properties and morphology of impact modified polypropylene-wood flour composites, Journal of Applied Polymer Science, 67(9): 503-1513.

Raj, R.G., Kokta, B., Gruleau, G., and Daneault, C., 1990. The influence of coupling agents on mechanical properties of composites containing cellulose fillers, Journal of Polymer Plastic Technology Engineering, 29(4): 339-353.

Stark, N.M., Rowlands, R.E., 2003. Effects of wood fiber characteristics on mechanical properties of wood/polypropylene composites, Wood and Fiber Science 35(2):167-174.

Biocomposites with immobilized enzymes for creation of sensitive elements of biosensor systems

G.A. Bektenova
Laboratory of Synthesis and Physical Chemistry of Polymers.
A.B. Bekturov Institute of Chemical Sciences,
Almaty, Republic of Kazakhstan

SUMMARY

The new method of enzyme-glycoproteins immobilization by means of formation monomolecular (nanosized) layers onto silica surfaces as well as a polymer matrix with the aid of new bifunctional spacers on the basis of boronic acids has been developed. It was shown that the most stable enzyme complexes with carrier are formed in the range of pH values near to pK of boronic acids.

The new biocomposites - immobilized preparations of acetylcholine esterase with high relative catalytic activity and stability at storage as well as in conditions of continuous exploitation have been obtained.

1. INTRODUCTION

Immobilization of a biological material, in particular enzymes, on various carriers is one of the key moments when creating biosensor systems. In the case of a number of enzymes–glycoproteins the binding of enzyme to a carrier surface may be carried out through the carbohydrate content of the enzyme molecule structure with the aid of bifunctional boronic acids, the protein matrix and the enzyme active centre not being touched. This allows to preserve maximally native conformation of enzyme and therefore its biocatalytical activity and also as much as possible to combine spatially the primary molecular sensor (bioreceptor) and the microelectronic amplifier by the way of their integration through a system of covalent bonds or through micro- and/or nanospace that leads to essential increase in sensitivity of a system.

2. RESULTS AND DISSCUSSION

2.1 Investigation of interaction BA with diols

The model theoretical and experimental researches of an interaction of some synthesized by us boronic acids (BA) with diol-containing solid phases in dependence on pH to reveal optimal conditions of stable boronate-diol complex formation at immobilization of enzymes-glycoproteins were carried out in static conditions. Distinctions of the acidity of dihydroxyboryl groups in the synthesized compounds and used as spacers have to result in a variation of immobilization conditions.

The mathematical model for a case of the simplest boronate-diol complex formation when two OH-groups of BA interact with hydroxyl groups of one molecule of diol has preliminary been considered. Expression for optimum pH value at which a stable boronate-diol complex is formed has been received:

$$[H^+] = K_a K_w / K_D \quad (1) \quad \text{or} \quad pH_{opt.} = 1/2\, pK_a - 1/2\, pK_D + 7. \quad (2)$$

The received equation (2) not only confirms our assumption of dependence of pH_{opt} value on boronic acids and diols ionization constants, but also indicates to its shift in more acid area relatively pK_a values of PhBA (phenylboronic acid) (table 1).

Table 1. Dependence of pH value of the maximum interaction of polyvinyl alcohol (PVA) with boronic acids on acidity of $B(OH)_2$-group.

№	Compound	pK_a	$pH_{opt.}$
1	PhBA	8,90	7,70
2	p-TBA	9,26	7,90
3	p-COOH- PhBA	8,56	7,70
4	p-$COOCH_3$- PhBA	7,69	6,35
5	2-NO_2-4-COOH- PhBA	8,79	7,65
6	2-NO_2-4-$COOCH_3$- PhBA	8,36	5,95
7	m-TBA	9,00	8,40
8	m-COOH- PhBA	8,56	6,95
9	m-$COOCH_3$- PhBA	7,56	6,35
10	3-COOH-5-NO_2- PhBA	6,85	5,20
11	3-$COOCH_3$-5-NO_2- PhBA	6,59	5,20
12	3-NO_2-TBA	7,70	6,345
13	3-NO_2-4-Br-TBA	5,52	4,36
14	Benzoic acid	4,12	-

The experimental research of boronic acids complex formation with diols in static conditions was carried out, using a model BA- (PVA), modified with cyclohexanone. Relative change of optical density of a solution before and after interaction was the measure of a complex stability. Results of research are represented in table 1. The received dependences represent one type curves having the maximum, lying in more acid area, than pK_a value of corresponding BA.

Thus, on the basis of the carried out experimental research which basically corresponds to the offered model, it is possible to choose precisely enough optimum conditions of glycoproteins immobilization with the use of derivatives of PhBA as spacers.

2.2 Activation of carriers with boronic acids

Activation of carriers with boronic acids_by formation of bond similar to peptidic between an amino group of the carrier and carboxyl group of spacer or on the contrary is the first stage of the developed immobilization method.

Among all accessible and convenient methods of carboxyl groups activation a chloranhydride method has been appeared the most suitable. We used thionyl chloride for activation of silochrom (Si/Ch) carboxyl groups, and for carboxyl groups spacers - such rigid reagent as phosphorus pentachloride.

All synthesized carboxyl-containing boronic acids possess different reaction ability on COOH-group and they can be rowed:

4-COOH-PhBA<3-COOH-PhBA<2-NO_2-4-COOH-PhBA<3-COOH-5-NO_2-PhBA

This law may be explained by the influence of various constituents and their positions on distribution of electronic density in molecules of boronic acids.

The control over silochrom modifying process with boronic acids carried out by the method of diffusive reflections in the UV-area and allowing to get spectra of solid powdery substances as well as HCl release observed by us at interaction of silochromes with BA and also a quantitative estimation of degree of covalent binding of boronic acids with a carrier matrix carried out by the difference of static exchange capacities on COOH- and NH_2- groups of initial and activated carriers indicate to the chemical bond formation. Moreover, a treatment of silochromes modified with boronic acids by the concentrated solutions of salts (1 M NaCl) and organic solvents does not lead to removal of BA from a surface of carriers that testifies to their stable chemical interaction.

2.3 Immobilization of acetylcholine esterase

Immobilization of acetylcholine esterase (AChE) was carried out at +4 ^{o}C in a phosphatic buffer solution on samples mentioned above. pH of a buffer solution was selected on the basis of results of model studying of optimum conditions of boronate-diol complex formation. For complex stabilization and sorption reduction 1 M NaCl was added. For each sample in the same conditions we carried out the sorption immobilization of glycoprotein on silochromes, not modified with boronic acids. It has allowed to compare the influence of a method of enzymes binding with carriers on catalytical activity.

Quantity of the bound enzyme was determined by a difference of fluorescence of glycoprotein solutions before and after immobilization. Activity of immobilized preparations was analyzed by amperometric method.

Results on degree of filling of a surface of carriers by enzyme depending on a way and conditions of immobilization as well as the loss of catalytic activity in immobilization process are represented in table 2.

Table 2. Immobilization conditions and characteristics of immobilized enzymes.

№	Carrier	Spacer	The method of immobilization	pH of immobilization	The AChE content on the carrier, mg/g,	Relative activity of AChE, %
1	NH_2 -Si\Ch	3-COOH-PhBA	chemical	6,35	2,80	41,5
			sorption	6,35	0,31	38,0
2	NH_2 - Si\Ch	2-NO_2-4-COOH - PhBA	chemical	6,00	3,65	29,0
			sorption	6,00	0	-
3	NH_2 - Si\Ch	3-COOH-5-NO_2- PhBA	chemical	5,40	2,75	30,0
			sorption	5,40	0	-
4	COOH-Si\Ch	3-NH_2- PhBA	chemical	7,90	2,90	49,0
			sorption	7,90	0,78	52,0

Residual activity depends on pH of a solution and is maximal at carrying out «sewing» in the conditions optimal for functioning of enzyme. For AChE the maximum relative activity (41-49 %) was observed at use of the buffer with pH 7,9 and 7,0, corresponding to a pH-optimum of action of AChE. The most suitable spacer in this case is 3-NH_2-

PhBA, and also 3-COOH-PhBA, forming a strong complex with enzyme in alkaline area of pH. Comparison with the literary data has shown that at immobilization of AChE by glutaric aldegyde method the relative activity was about 30 %. It is necessary to underline that for AChE this method has been developed by us for the first time.

Stability of immobilized glycoprotein has been investigated at storage and in operation conditions in comparison with soluble and sorption immobilized forms of enzyme. It was shown that in spite of various relative activity of enzyme immobilized by the chemical method by means of different boronic acids, their stability in all cases is almost identical and in several times exceed that for sorption immobilized samples both at storage and in the conditions of continuous operation. At storage of covalent immobilized glycoproteins their activity is remained twice longer, and the period of semi-inactivation reaches almost 2 months while for sorption immobilized enzymes this time is 17-18 days.

Thus, at immobilization of enzymes-glycoproteins on silica and other carriers activated with boronic acids, the high enough effect of stabilization of enzymes is reached. Comparison of our results with the literary data allows to conclude that the basic contribution to stabilizing effect brings the chemical nature of the sewing agent (boronic acids), carrier surfaces (silochroms) and a way of immobilization (complex formation of dihydroxyboryl groups of the activated carrier with carbohydrate part of an enzyme).

3. CONCLUSIONS

The new method of enzyme-glycoproteins immobilization by means of formation monomolecular (nanosized) layers onto silica surfaces as well as a polymer matrix with the aid of new bifunctional spacers on the basis of boronic acids has been developed. It was shown that the most stable enzyme complexes with carrier are formed in the range of pH values near to pK of boronic acids.

The new biocomposites - immobilized preparations of acetylcholine esterase with high relative catalytic activity and stability at storage as well as in conditions of continuous exploitation have been obtained.

The proposed method combines advantages both of a sorption method by the soft conditions of carrying out and a covalent method of immobilization by the achieved stability of enzyme binding with the carrier that allows to receive immobilized preparations possessing high relative catalytic activity and stability, both at storage, and in the conditions of continuous operation. This method is especially convenient if it is necessary to arrange the enzyme close to a carrier surface, for example, for achievement of effective direct electronic transfer between enzyme and an electrode surface at creation of biosensor systems for clinical diagnostics, bioscreening of new physiologically active compounds and other areas of biotechnology and ecological monitoring of environmental objects. Besides the developed method may be also recommended to receive biocomposites with whole cells and cell components, containing, as it is known, carbohydrates in a composition of the cell walls.

Carbon nanostructures-biodegradable elastomeric polyurethane nanocomposites: synthesis and characterization

B. Fernandez-d´Arlas, I. Mondragon, M.A. Corcuera, A. Eceiza
'Materials + Technologies' Group, Departamento Ingeniería Química y del Medio Ambiente, Escuela Universitaria Politécnica. Donostia- San Sebastián, Universidad del País Vasco/Euskal Herriko Unibertsitatea
U. Khan, J.N. Coleman
'Chemical Physics of 1D-Nanostructures' Group, School of Physics. Trinity College of Dublín. Ireland

ABSTRACT

Carbon nanotubes and graphene are novel carbon nanostructures which are expected to act as very good fillers enhancing mechanical and electrical properties of novel composites. They are also good candidates for preparing different novel elastomeric composites.

A series of biodegradable polyurethanes, with interest for soft tissue engineering, were prepared. Composites of these matrices with carbon nanotubes were prepared using both in-situ polymerization and solvent mixing synthesis pathways with different types of carbon nanotubes functionalisation. The preliminary results show that depending on the polyurethane hard segment content and carbon nanotubes functionalisation different mechanical properties varied in different ways, this being matched to the interactions between functional groups on the carbon nanotubes and either hard or soft segments of polyurethanes composites.

1. INTRODUCTION

1.1 In search of new composites with outstanding properties

Incorporation of carbon nanotubes into elastomers such as polyurethanes could be a new route for preparing high standing biomaterials such as biomedical scaffolds or smart elastomers. But preparation of suitable carbon nanotubes (CNT) composites has been an issue in the last years within the new composites community. While trying to improve some properties such as electrical conductivity, yield stresses, or young modulus, other properties as strain at break or tensile strength did not improve at all, or even trend to worse.

1. 2 Carbon nanotubes/graphene functionalisation

A pursue for a suitable functionalisation of nanotubes before incorporation into the polymer matrix, has been pointed by many authors to be the route to follow in order to improve the materials as a whole. Different attempts to incorporate nanotubes into polyurethanes matrices can be found in the literature, some of which include acid treatment to nanotubes (Sahoo et al. 2006), organic functionalisation followed by in-situ polymerisation (Xia et al. 2006), or incorporation of organically modified nanotubes into polyurethanes by solution mixing (Coleman et al. 2006).

As Liff et al. (2007) have found working with nanoclays/polyurethanes nanocomposites, interaction with polyurethanes hard segments (HS) is crucial to obtain an increase in properties without a decrease in toughness.

In this work an attempt to find the proper functionalisation of multiwalled carbon nanotubes (MWCNT) for the incorporation into newly prepared biomedical grade polyurethane is presented. Polyurethanes HS consisting on 1,6-hexamethylene diisocyanate (HDI) and 1, 4-butanodiol (BD) were grown over acid treated MWCNT to obtain hard segment functionalised nanotubes, MWCNT-g-HDI-BD. In this way a better interaction between nanotubes and polyurethanes hard segments is expected, as depicted in figure 1.

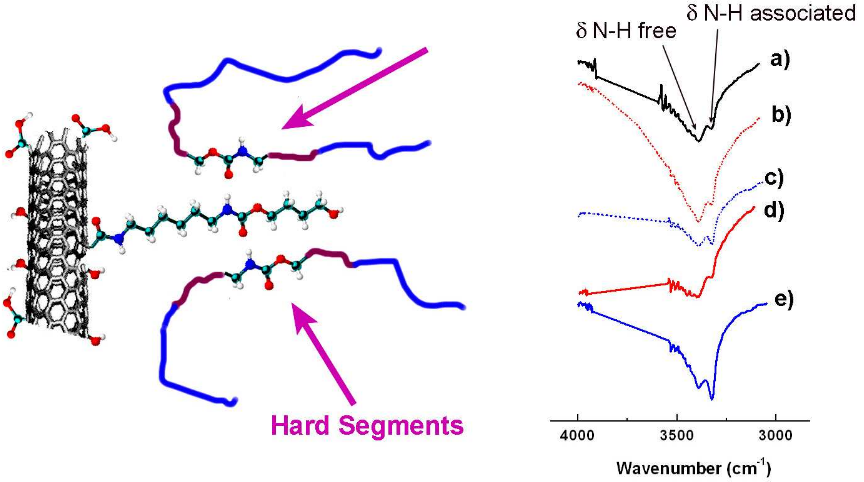

Figure 1. Interaction between functionalised multiwalled carbon nanotubes and polyurethanes hard segments. To the right the infra red spectra in the amide region of a) pristine polyurethane, b) 4 wt % MWCNTCOOH c) 4 wt % MWCNT-g-HDI-BD c, d) 8 wt % MWCNTCOOH and e) 8 wt % MWCNT-g-HDI-BD composites.

2. RESULTS

Polyurethanes HS were grown onto MWCNT surface (figure 1) in order to improve both dispersability of nanotubes in the chosen solvent, tetrahydrofuran (THF), and interaction with polyurethanes HS. Yield of organic modification was around 30 wt % as studied by means of thermo gravimetric analysis (TGA). Although Young´s modulus and plateau region stresses were not better than those composites prepared with solely acid treated nanotubes (MWCNTCOOH), elongation at break and tensile strength were improved (see figure 2). Plateau stresses and young modulus improved for both type of nanotubes. The functionalised nanotubes (MWCNT-g-HDI-BD) provided almost as twice break-toughness as MWCNTCOOH.

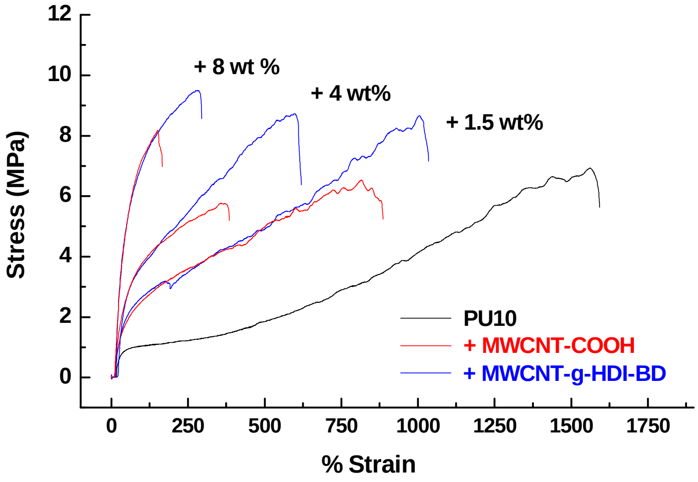

Figure 2. Stress versus strain curves for composites made with a 10 wt% hard segment polyurethane and different loads of nanotubes.

3. CONCLUSIONS

A new functionalisation of nanotubes was undertaken in order to improve dispersion and interactions with polyurethanes hard segment. Composites prepared with functionalised nanotubes containing 30 wt % of polyurethanes hard segments showed improved toughness and tensile strength in comparation with the ones prepared with solely acid treated nanotubes.

ACKNOWLEDGEMENTS

This work was supported by the Basque Government *'Etortek 2005/BiomaGUNE 2005'* (IE05-143), *'Saiotek 2007'* (S-PE07UN02), *'Grupos Consolidados'* (IT-365-07), and also by Ministerio de Ciencia y Tecnología (MAT 2005-06530).

REFERENCES

COLEMAN, J., KHAN, U., GUN´KO, Y.K. (2006) Mechanical Reinforcement of Polymers Using Carbon Nanotubes. *Adv. Mater. 18*, 689-706

LIFF, S.M., KUMAR, N., McKINLEY, G. (2007) High-performance elastomeric nanocomposites via solvent-exchange processing. *Nature*. 6, 76-83

SAHOO, N.G., JUNG, Y.C., YOO, H.J., CHO, J.W. (2006). Effect of Functionalized Carbon Nanotubes on Molecular Interaction and Properties of Polyurethane Composites. *Macromol. Chem. Phys*. 207, 1773-1780

XIA, H., SONG, M. J. (2006) Preparation and characterisation of polyurethane grafted single-walled carbon nanotubes and derived polyurethane nanocomposites. *Mater. Chem*. 16, 1843-1851.

Modificación química de fibras naturales para la obtención de composites biodegradables

R. Llano-Ponte, A. Horrillo, L. Serrano, I. Egües, I. Mondragon, J. Labidi
Grupo de Materiales y Tecnologias
Departamento de Ingeniería Química y del Medio Ambiente
Universidad del País Vasco (UPV/EHU).
Plaza Europa, 1, 20018, Donostia-San Sebastián, Spain
rodrigo.llano-ponte@ehu.es

RESUMEN

En este trabajo se presenta la obtención y caracterización de fibras de yute que han sido modificadas mediante diferentes procesos químicos con el objetivo de ver la influencia de los mismos sobre las características de las fibras obtenidas (contenido en celulosa, hemicelulosa y lignina), así como la influencia de los tratamientos sobre sus propiedades mecánicas y morfológicas.

Para ello se han realizado diversos tipos de tratamientos de fibras de yute: mercerización + hidrólisis (M+H), hidrólisis + mercerización (H+M) e hidrólisis + organo-solv (H+OS). Las fibras obtenidas se han caracterizado tanto químicamente (TAPPI) como por FT-IR y TGA. Las fibras obtenidas serán, posteriormente utilizadas, para obtener composites con PLA como matriz.

1. INTRODUCCIÓN

La idea de usar las fibras de celulosa como elementos de refuerzo en los materiales composites no es nueva. El hombre ha usado esta idea a lo largo del tiempo, desde el comienzo de nuestra civilización se ha utilizado hierba y la paja para fabricar, mezcladas con barro, ladrillos (adobe). Por otra parte, a lo largo de los últimos años diversos investigadores han estudiado la compatibilidad entre diferentes tipos de fibras y matrices biodegradables (Le Digabel and al., 2004; Le Digabel, 2004; Avérous, and al.). El ácido polilactico (PLA) ha sido procesado con residuos de pasta de papel o serrín de madera (Levit and al., 1996), con fibras de kenaf (Nishiro and al., 2003), con fibras de jute (Plackett and al., 2003), con fibras de lino (Oksman and al., 2003; Van de Velde, 2002) [1-9]

2. CARACTERIZACIÓN DE LAS FIBRAS DE YUTE

2.1. Caracterización química

Mediante las normas TAPPI se ha realizado la caracterización de las fibras de yute que se ha utilizado en este trabajo, en la tabla 2.1 se muestra los resultados obtenidos así como los resultados procedentes de otros autores. Los resultados obtenidos de la bibliografía presenta resultados similares en cuanto a la lignina y la holocelulosa, pero el contenido en hemicelulosa presentan desviaciones importantes, esto puede ser debido a factores medioambientales, así como la influencia que sobre la composición de la fibra tiene el tiempo de recogida, almacenamiento, tratamientos, etc.

Propiedad	Yute	Yute [10]	Yute[4]	Yute[11]
Humedad	7,32±0,12			
Cenizas	1,95±0,23			
Solubilidad en agua caliente	9,87±0,28			
Solubilidad en NaOH al 1 %	13,29±1,41			
Extraíbles en etanol y benceno	1,13±0,28			
Lignina	14,76±1,19	12-13	11,8	13
Holocelulosa	79,99±2,58	74,6-91,9	76,4	85
Celulosa	51,99±0,76	61-71,5	64,4	72
Hemicelulosa	28,00±1,67	13,6-20,4	12	13

Tabla 2.1 Caracterización química de la materia prima mediante la utilización de las normas TAPPI.

2.2. Caracterización físico-química

Tanto la materia prima utilizada, como las fibras obtenidas mediante los diferentes tratamientos, fueron estudiadas por ensayos de FTIR y de TGA con el objetivo de compara los resultados obtenidos por los diferentes proceso empleados.

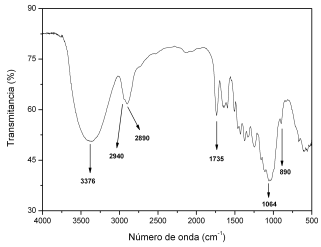

Fig. 2.1. Espectro de infrarrojos de la fibra de Yute.

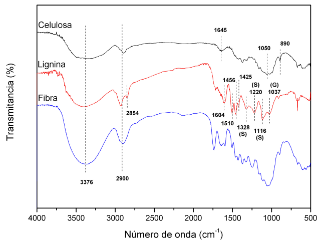

Fig. 2.2. Espectro de infrarrojos de la fibra de Yute, de su celulosa y lignina.

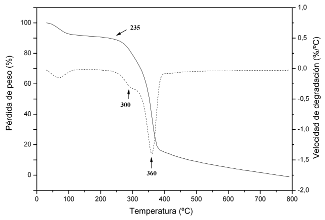

Fig. 2.3. Variación del peso de la fibra en función de la temperatura.

2.3. Las fibras modificadas

Los tratamientos aplicados de mercerización (M) e hidrólisis (H) se han realizado en un reactor de 2 l y el proceso organosolv (OS) se ha realizado en un reacto de 1 litro presurizado, en la tabla 2.2.se muestran las condiciones de proceso.

Proceso	Productos (%w)	Temperatura (ºC)	tiempo (min)
Mercerización	5 (NaOH)	103	70
Hidrólisis	1 (H_2SO_4)	ebullición	70
Organosolv	60 (Etanol)	ebullición	70

Tabla 2.2. Condiciones de procesado.

Como se puede observar en la tabla 2.3, donde se muestran los resultados del análisis químicos de las fibras obtenidas por los diferentes tratamientos, una disminución del contenido en lignina cuando se emplea el proceso de hidrólisis para el tratamiento de las fibras aumentando sustancialmente el contenido en celulosa y una disminución de la hemicelulosa, siendo el tratamiento más adecuado el de H + M.

	M + H	H + M	H + OS
Lignina	15,39±0,72	12,41±1,23	12,57±1,23
Celulosa	42,57±1,70	54,68±4,28	51,55±8,13
Hemicelulosa	35,47±0,18	23,17±3,5	23,03±6,85
Otros	6,61	9,74	12,85

Tabla 2.3. Variación del contenido de celulosa, hemicelulosa y lignina en función del tratamiento empleado.

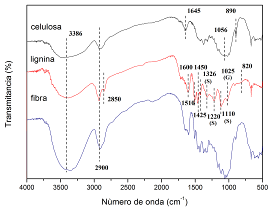

Fig. 2.4. Espectro de infrarrojos de la fibra modificada por proceso (M + H).

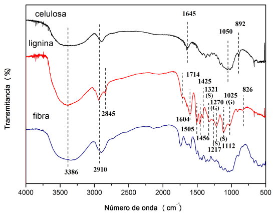

Fig. 2.5. Espectro de infrarrojos de la fibra modificada por proceso (H + M).

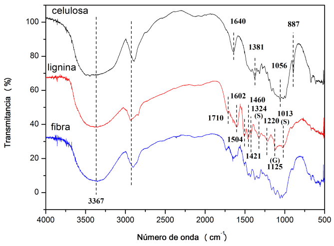

Fig. 2.6. Espectro de infrarrojos de la fibra modificada por proceso (H +OS).

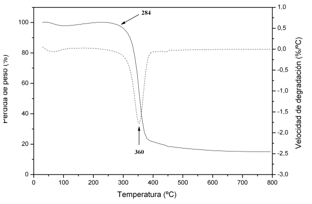

Fig. 27. Variación de la pérdida de peso en función de la temperatura y del proceso de (M + H).

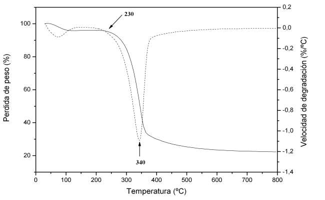

Fig. 2.8. Variación de la pérdida de peso en función de la temperatura (H + M).

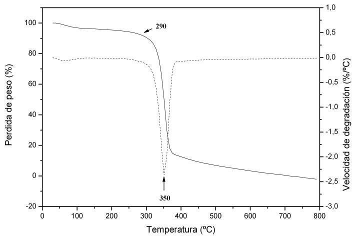

Fig. 2.9. Variación de la pérdida de peso en función de la temperatura (H + OS).

REFERENCIAS

[1] L. H. CARVALHO, (1997)"Chemical Modification of Fibers for Plastics Reinforcement inComposites ", in Lignocellulosic-Plastics Composites, A. L. Leao, F. X. Carvalho, and E. Frollini, Brazil.

[2] LE DIGABEL, F., BOQUILLON, N., DOLE, P., MONTIES, B., AVÉROUS, L. (2004). "Properties of thermoplastic composites on wheat Straw lignocellulosic fillers", Journal of Applied Polymer Science, 93 (1), 428-436.

[3] LE DIGABEL, L. (2006). "Incorporation de co-produits de paille de blé dans le matrices thermoplastiques. Approche de la compatibilité charge-matrice et propriétés des composites", Ph.D. Thesis URCA Reins (France) (2004).

[4] AVEROUS, L., LE DIGABEL, F., "Properties of biocomposites based on lignocellulosic fillers", Carbohydrate Polymers, 66, 4, 450-493.

[5] LEVIT, M. R., FARREL, R. E., GROSS, R. A., MCCARTHY, S. P. (1996). "Composites based on poly(lactic acid) and cellulosic materials: Mechanical properties and biodegradability", Annual Technical Conference – Society of Plastics Engineers", 54 th, vol 2, 1387-1391

[6] NISHINO, T., HIRAO, K., KOTERA, M. NAKAMAE, K., INAGAKI, H. (2003). "Kenaf reinforced biodegradable composites", Composites Science and Thchonology", 63, 1281-1286

[7] PLACKETT, D., LOGSTRUP ANDERSEN, T., BATSBERG PEDERSEN, W., NIELSEN, L. (2003). "Biodegradable composites based on l-polylactide and jute fibres", Composites Science and Technology, 63 (9), 1287-1296.

[8] OKSMAN, K. SKRIFVRS, M., ELIN, J.-F. (2003). "Natural fibres as reinforcement in polylactic acid (PLA) composites". Composites Science and Technology, 63, 9, 1317-1325.

[9] VAN DE VELDE, K., KIEKENS, P. (2002). "Biopolymers: overview of several properties and consequences on their applications", Polymer Testing, 21 (4), 433-422.

[10] CORRALES BARBE, F., "Modificació de fibres de jute per l'elaboració de plástics reforçats reciclables. Tesis doctoral. ISBA 84-689-0991-2.

[11] BLEDZKI, A.K., GASSAN, J. (1999)"Composites reinforced with cellulose based fibres. Prog. Polym. Sci. 24, 221-274.

Modelización de las propiedades a tracción de materiales compuestos de polipropileno y pasta mecánica

J.P. López, F. Vilaseca, J.A. Méndez, L. Peña, M.A. Pèlach, P. Mutjé
Grup LEPAMAP, Escola Politècnica Superior, Universitat de Girona, Avda. Lluís Santaló, 17071 Girona (España). Telf: 972 41 84 63, E-mail: fabiola.vilaseca@udg.edu

RESUMEN

A partir de las propiedades experimentales a tracción en materiales compuestos de pasta mecánica y polipropileno, se determina, mediante la metodología de Bowyer y Bader, la tensión interfacial. La determinación experimental del coeficiente de orientación permite la obtención de la resistencia intrínseca a tracción de las fibras de pasta mecánica y consecuentemente el factor de acoplamiento fibra-matriz.

1. INTRODUCCIÓN

En general la resistencia a tracción de un material compuesto σ_t^c, depende del tipo de refuerzo (propiedades intrínsecas), grado de dispersión, tipo de matriz, grado de orientación del refuerzo en el seno del material (χ_1), de la relación de aspecto del refuerzo (l/Ø) y de la tensión interfacial (τ) entre el refuerzo y la matriz. Mientras que el módulo de Young depende de los mismos parámetros pero es prácticamente independiente de τ. Para un detreminado proceso de inyección-extrusión el parámetro determinante es τ . La determinación experimental de τ es prácticamente imposible para este tipo de refuerzos, debido a las características morfológicas de las fibras de pasta mecánica. La metodología de Bowyer-Bader permite estimar τ a partir de la distribución de longitudes del refuerzo y de su diámetro (metodología Kajaani), del módulo intrínseco de las fibras, y del diagrama esfuerzo deformación experimental del material compuesto y de la matriz. El módulo intrínseco de las fibras, dado que su medida experimental es físicamente imposible, se puede estimar a partir del modelo de Hirsch. De otra parte se ha determinado el coeficiente de orientación de las fibras de acuerdo con la ecuación $\chi_1=\cos^4\phi$.

2. METODOLOGÍA EXPERIMENTAL

Las fibras de pasta mecánica fueron extraídas del material compuesto y las distribuciones de longitud y diámetro se determinaron mediante un analizador de la morfología de fibras Kajaani, modelo FS-200.

El modelo de Hirsch, es una combinación de las regla de las mezclas en serie y en paralelo (Doan et al. 2006). En este estudio el valor de β utilizado fue de 0,4335. Este valor fue determinado en trabajos anteriores del grupo utilizando la misma matriz y otro tipo de refuerzo lignocelulósico.

Metodología de Bowyer – Bader

El método de análisis se basa en el modelo de Kelly-Tyson modificada para la predicción de la resistencia σ_t^c de un material compuesto de matriz polimérica con fibras cortas alineadas (Thomason, 2007). Este modelo se puede simplificar como σ_t^c = $\chi_1(X + Y) + Z$, donde Z es la contribución de la matriz, X es la contribución sub-crítica de fibra, y Y es la contribución súper-crítica de fibra, en referencia a una longitud crítica de fibra definida por $L_c = \sigma_t^f D/2\tau$, donde σ_t^f es la resistencia intrínseca de la fibra, D es el diámetro medio de fibra y τ es la tensión interfacial. El modelo de Kelly-Tyson asume que todas las fibras están alineadas en la dirección en la se aplica la carga y la ecuación no se puede integrar para dar un factor que tenga en cuenta la compleja orientación de las fibras en la mayoría de los materiales compuestos termoplásticos moldeados. La solución más habitual a este problema es ajustar los datos experimentales utilizando un coeficiente de orientación (χ_1). Bowyer y Bader extendieron el concepto original de Kelly-Tyson para modelar la curva esfuerzo – deformación antes de la ruptura. La base de su argumento fue que a cualquier valor de deformación del material compuesto (ε_c) existe una longitud crítica de fibra definida por $L_\varepsilon = \sigma_f \cdot D/2\tau$. Las fibras más cortas que L_ε aportan un esfuerzo medio igual a $L\cdot\tau/D$ y las fibras más largas que L_ε aportan un esfuerzo medio de $E_f\varepsilon_c(1 - (E_f\varepsilon_c D/4L\tau))$. El esfuerzo del material compuesto para cualquier valor de deformación viene dado por:

$$\sigma_c = \chi_1 \left(\sum_i \left[\frac{\tau L_i V_i}{D} \right] + \sum_j \left[E_f \varepsilon_c V_j \left(1 - \frac{E_f \varepsilon_c D}{4\tau L_j} \right) \right] \right. + (1 - V_f) E_m \varepsilon_c \qquad (1)$$

Aunque χ_1 y τ generalmente no sean conocidos, se pueden obtener valores para estos factores si se conoce el esfuerzo (σ_1 y σ_2) del material compuesto a dos valores de deformación diferentes (ε_1 y ε_2). La contribución de la matriz (Z) se puede calcular a partir de la determinación del módulo de la matriz. Z se utiliza para calcular la relación de contribuciones de fibra para las dos deformaciones (R).

$$R = \frac{\sigma_1 - Z_1}{\sigma_2 - Z_2} \qquad\qquad R^* = \frac{X_1 + Y_1}{X_2 + Y_2} \qquad (2 \text{ y } 3)$$

Se utiliza (1) asumiendo un valor de τ para calcular la relación R^* (valor teórico de R). En este punto la relaciones R y R^* son independientes de χ_1. El valor de τ se ajusta hasta que $R^* = R$.

3. RESULTADOS Y DISCUSIÓN

En la tabla I se muestran los resultados experimentales a tracción de los materiales compuestos obtenidos. Tanto la resistencia a tracción como el módulo de Young evolucionan linealmente con el porcentaje de refuerzo.

A partir de la distribución de longitud de las fibras de refuerzo (Figura 1), su diámetro (33.5 µm) y su peso específico (1.33 g/ml), y considerando el módulo estimado mediante el modelo de Hirsch (25.8 GPa), es posible calcular la tensión interfacial fibra-matriz, que resulta ser, respectivamente, de 20.2, 20.8, 21.5, y 19.5 MPa.

Refuerzo (wt%)	**σ_t (MPa) [s.d.]**	**E_t (GPa) [s.d.]**	**ε_t (MPa) [s.d.]**
0	27,6 [0,5]	1,5 [0,1]	9,3 [0,2]
20	40,6 [0,4]	3,4 [0,1]	4,6 [0,1]
30	46,8 [0,6]	4,3 [0,1]	4,4 [4,4]
40	51,2 [0,6]	5,4 [0,1]	3,7 [3,7]
50	56,3 [1,0]	6,5 [0,0]	3,5 [3,5]

Tabla I. Propiedades a tracción de los materiales compuestos.

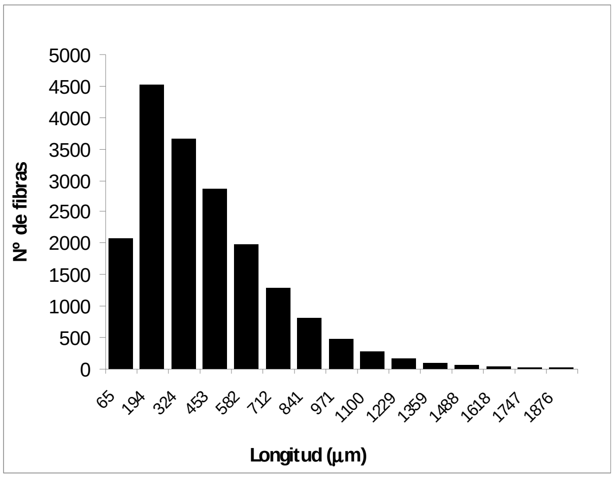

Figura 1. Distribución de longitudes de las fibras en el seno de la matriz.

Para la matriz utilizada en este estudio la contribución al esfuerzo (en MPa) en función de la elongación se puede calcular fácilmente mediante la ecuación 4:

$$\sigma_m = -0.0159\varepsilon^4 + 0.3712\varepsilon^3 - 3.3674\varepsilon^2 + 14.895\varepsilon + 0.0493 \qquad (4)$$

El cálculo experimental del factor de orientación $\chi_1 = \cos^4\phi$ (Templeton, 1990) conduce a valores del factor de orientación, respectivamente, de 0.324, 0.314, 0.307 y 0.305, para los composites reforzados con un 20, 302 40 y 50 % en peso de pasta mecánica. Su sustitución en la ecuación 2 permite estimar la carga intrínseca a tracción de las fibras de pasta mecánica, que resulta ser de 531, 555, 634 y 656 MPa, respectivamente. Finalmente, aplicando la regla de las mezclas modificada (ecuación 5), donde σ_t^{m*} es la carga de la matriz a la elongación de ruptura del material compuesto:

$$\sigma_t^C = f_a V^F \sigma_t^F + (1 - V^F)\sigma_t^{m*} \qquad (5)$$

4. CONCLUSIONES

Del estudio efectuado se puede concluir:

- La tensión interfacial calculada mediante Bowyer-Bader permanece prácticamente constante para los diferentes materiales compuestos estudiados, siendo ésta algo superior a la sugerida por el criterio de Von Misses (Pegoretti et al., 1996).
- Los coeficientes de orientación de las fibras en el seno del material compuesto se sitúan por encima de 0.3, muy por encima del 0.2 sugerido por Sanadi et al. (1994).
- De acuerdo con las resistencias intrínsecas, los factores de acoplamiento decrecen a medida que aumenta el porcentaje de refuerzo.

REFERENCIAS

- DOAN, T.T.L., GAO, S.L., MÄDER, E. (2006). Jute/polypropylene composites I. Effect of matrix modification. *Compos. Sci. Technol.* 66, 952-963.
- PEGORETTI, A., DELLA VOLPE, C., DETASSIS, M., MIGLIARESI, C. (1996). Thermomechanical behaviour of interfacial region in carbon fibre/epoxy composites. *Composites Part A*. 27, 1067-1074.
- SANADI A.R., YOUNG, R.A., CLEMONS, C., ROWELL, R.M. (1994). Recycled newspaper fibers as reinforcing fillers in thermoplastics: Part I – analysis of tensile and impact properties in polypropylene. *J. Reinf. Plas. Comp*. 13, 54-67.
- TEMPLETON, P.A., (1990). Strength predictions of injection moulding compounds. Journal of Reinforced Plastics and Composites, 9, 210-225.
- THOMASON J.L. (2007). The influence of fibre length and concetration on the properties of glass fibre reinforced polypropylene: 7. Interface strength and fibre strain in injection moulded long fibre PP at high fibre content. *Composites: Part A*, 38, 210-216.

Fibras lignocelulósicas recicladas comparativamente con fibras de vidrio-E: competitividad técnico-económica de sus composites de polipropileno

J.P. López, J.A. Méndez, L. Peña, F. Vilaseca, M.A. Pèlach, P. Mutjé
Grup LEPAMAP, Escola Politècnica Superior, Universitat de Girona, Avda. Lluís Santaló, 17071 GIRONA (Spain). Telf: 972 41 84 63, E-mail: fabiola.vilaseca@udg.edu

RESUMEN

Se evalúa desde un punto de vista técnico y económico la competitividad de composites reforzados con fibras lignocelulósicas recuperadas con respecto a los composites reforzados con un 30% en peso de fibra de vidrio E, típicamente aplicado en la industria.

1. INTRODUCCIÓN

Las fibras lignocelulósicas recuperadas son una materia prima que puede ser usada como material de refuerzo de matrices termoplásticas como el polipropileno. En la Unión Europea la tasa de recuperación está incrementándose significativamente debido a la s exigencias legislativas y al creciente interés de las industrias papeleras por las fibras secundarias (recuperadas) en la producción de papel. El coste de las fibras lignocelulósicas recuperadas se sitúa entorno a 0.1 €/kg, frente a los 1.2-1.5 €/kg correspondiente a la fibra de vidrio E. Desde un punto de vista técnico, las propiedades mecánicas de los composites de PP reforzados con fibras lignocelulósicas son inferiores a las conseguidas con composites de PP reforzados con fibra de vidrio E, para un mismo porcentaje de refuerzo, ya que las propiedades intrínsecas de uno y otro refuerzo son obviamente distintas.

En este trabajo se estudian las propiedades a flexión de materiales compuestos de PP reforzados con fibra de vidrio E o con fibras lignocelulósicas procedentes de papel de periódico recuperado.

2. METODOLOGÍA EXPERIMENTAL

Para el presente trabajo se utilizó polipropileno (PP) homopolímero de Repsol (d=0.905 g/ml; y MFI de 30 g/10 min), fibras lignocelulósicas procedentes de papel de periódico recuperado (d=1.43 g/ml) y fibra de vidrio E tratada (d=2.45 g/ml). Para mejorar la adhesión interfacial, se aplicó un 6% en peso, con respecto al porcentaje de refuerzo, de un agente de acoplamiento en base a polipropileno modificado con anhídrido maleico (MAPP). La preparación de los materiales compuestos se llevó a cabo mediante un mezclador Brabender® que operaba a 20 rpm para el caso de los composites con fibra de vidrio E y a 80 rpm para el caso de los composites con fibras lignocelulósicas recuperadas. Se prepararon materiales compuestos con porcentajes de refuerzo en peso de hasta el 30% para la fibra de vidrio E y de hasta el 60% para las fibras lignocelulósicas. Una vez obtenidos los materiales compuestos, se obtuvieron probetas estándar mediante la técnica de moldeo por inyección y se sometieron a ensayos mecánicos a flexión (ISO 178).

3. RESULTADOS

En la Tabla I se muestran los resultados a flexión de los materiales compuestos obtenidos. En ambos casos, tanto la resistencia máxima a flexión como su módulo elástico aumentaron linealmente con el porcentaje de refuerzo incorporado. Cabe destacar también que la aplicación de un 6% de MAPP en los composites con fibra de vidrio E se tradujo en una mejora sustancial de la resistencia máxima de los composites con este tipo de refuerzo. Por otra parte, y de acuerdo con lo que ocurre con los refuerzos vegetales, el módulo elástico de los composites con fibra de vidrio fue independiente de la calidad de la interfase fibra-matriz.

% de refuerzo	**Resistencia máxima (MPa)**	**Módulo elástico (GPa)**
0	40.2 ± 1	1.1 ±0.1
Fibra de vidrio – E tratada		
10	63.1 ± 2	2.3 ±0.2
20	78.3 ± 2.7	3.2 ±0.2
30	88.1 ± 3.1	4.7 ±0.2
Fibra de vidrio – E con un 6% de MAPP		
10	68.3 ± 1.8	2.4 ±0.1
20	94.8 ± 2	3.2 ±0.1
30	109.8 ± 1.5	4.7 ±0.1
Fibra lignocelulósica con un 6% de MAPP		
20	63.8 ±0.9	2.9 ±0.1
30	73.5 ±0.8	3.3 ±0.1
40	79.3 ±1.2	4.2 ±0.1
50	86.8 ±3.8	4.9 ±0.2
60	97.1 ±2.2	5.7 ±0.1

Tabla I. Propiedades mecánicas a flexión.

El objetivo del presente trabajo es establecer comparaciones a nivel técnico y económico entre materiales compuestos reforzados con fibra de vidrio E y materiales compuestos reforzados con fibras lignocelulósicas. Para ello es posible aplicar la regla de las mezclas modificada a la resistencia máxima a flexión de acuerdo con la ecuación (1) (Hull, 1981), en donde σ_f se refiere a la resistencia máxima a flexión, V^F al porcentaje en volumen del refuerzo y f_a al factor de acoplamiento a flexión del material compuesto. Los superíndices C, F y m se refieren al composite, fibra y matriz en el punto de rotura.

$$\sigma_f^C = f_a V^F \sigma_f^F + (1 - V^F)\sigma_f^m \tag{1}$$

A partir de aquí, y para cada caso, se define el factor de esfuerzo a flexión (FSF) según la ecuación (2) (Thomason, 2002):

$$FSF = \sigma_f^C - (1 - \mathrm{V}^{\mathrm{F}})\sigma_f^m = f_a V^F \sigma_f^F \qquad (2)$$

Si se representa el FSF en función del porcentaje en volumen, para cada tipo de material compuesto, se obtiene la gráfica de la figura 1. A partir de la regresión lineal que se obtiene en cada caso, se puede realizar un estudio comparativo entre las distintas formulaciones. Así, se obtiene que la relación entre el FSF de la fibra de vidrio E tratada y las fibras lignocelulósicas recuperadas es de 2.6, y es de 3.61 entre la fibra de vidrio E con MAPP y las mismas fibras lignocelulósicas. Ello significa, por ejemplo, un factor de esfuerzo a flexión de 53 se consigue con un 30% en peso de fibra de vidrio E tratada (típicamente industrial) o con un 40% en peso de fibra lignocelulósica químicamente modificada. O bien, un factor de esfuerzo a flexión de 75 se alcanza con un composite al 30% en peso de fibra de vidrio E con MAPP y un 60% en peso de fibra lignocelulósica acoplada también con MAPP.

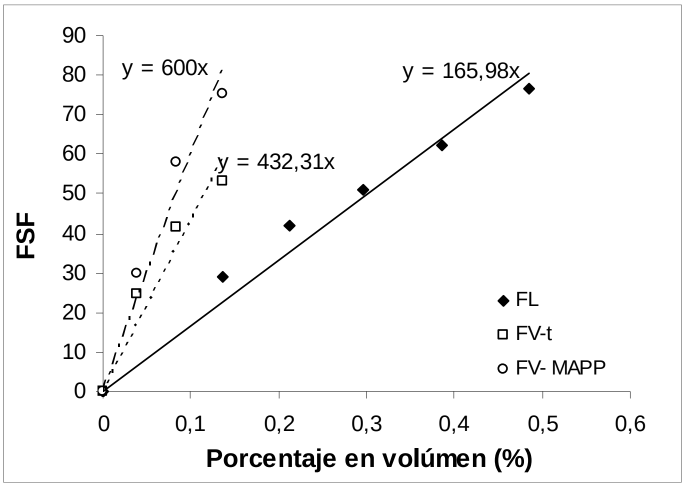

Figura 1: Factor de esfuerzo a flexión en función del porcentaje en volumen de refuerzo.

Por otro lado, es posible realizar la misma aproximación para el módulo elástico a flexión, y se define el factor de módulo a flexión, de acuerdo con la ecuación (3) (Thomason, 2002). En esta ecuación, el parámetro η_e se refiere al factor de eficacia y el resto de los parámetros son análogos a la regla de las mezclas para la resistencia máxima.

$$FMF = E_f^C - (1 - \mathrm{V}^{\mathrm{F}})E_f^m = \eta_e V^F E_f^F \qquad (3)$$

Así, si la función que representa el FMF en función del porcentaje en volumen es FMF=29.792V^{F} para la fibra de vidrio E y FMF=11.054V^{F} para las fibras lignocelulósicas. En este caso la relación del factor de módulo a flexión entre ambos refuerzos es de 2.6, equivalente al obtenido para el esfuerzo a flexión, sin agente de acoplamiento MAPP.

En lo que se refiere a la competitividad económica, es posible evaluar el coste de los materiales, suponiendo constantes los procesos de extrusión e inyección. En este sentido, el precio por kilo de un compuesto de PP reforzado al 30% en peso con fibra de vidrio E y un 6% de MAPP es de 1.159 €/kg. Mientras que el coste por kilo de un material compuesto de PP reforzado al 60% con fibras lignocelulósicas recuperadas y un 6% de MAPP es de 0.568 €/kg. Los precios de las materias primas se han tomado de 1€/kg para el PP, 4 €/kg para el MAPP, de 1.35 €/kg para la fibra de vidrio E y de 0.1 €/kg para las fibras lignocelulósicas recuperadas.

4. CONCLUSIONES

Partiendo como referencia del polipropileno reforzado con fibra de vidrio E anclada químicamente o simplemente tratada, se ha evaluado la competitividad técnica y económica de los materiales de PP reforzados con fibras lignocelulósicas recuperadas. Los resultados muestras que las fibras lignocelulósicas son competitivas, tanto técnicamente como económicamente.

REFERENCIAS

- HULL, D. (1981). An Introduction to Composite Materials, Cambridge University. Cambridge.
- THOMASON, J.L. (2002). The influence of fibre length and concentration on the properties of glass fibre reinforced polypropylene: 5. Injection moulded long and short fibre PP.

Partially bioresorbable PMMA-starch composites for bisphosphonate drug delivery

E. Franco-Marquès, J.A. Méndez, L. Peña, M.A. Pèlach
Lepamap Group, University of Girona. Campus Montilivi, 17071, Girona, Spain
J. Gironès
Institute of Polymer Science and Technology, CSIC. Juan de la Cierva 3, 28006, Madrid, Spain
M.P. Ginebra
Department of Material Science and Metallurgy, Technical University of Catalonia (UPC). Av. Diagonal 647, 08028, Barcelona, Spain

ABSTRACT

The present work is based on the preparation of self-curing acrylic composites for developing a drug delivery carrier for therapeutic treatment of osteoporosis. A common formulation of PMMA beads was modified with two different starch based biopolymers in order to obtain partially bioresorbable. Different properties were characterised: hydrophilicity and particle size. Benzoyl peroxide (BPO)/4,4'-(dimethylamino)difenyl carbinol (BZN) was used as red-ox initiator system. Mechanical behaviour, residual monomer content, *in vitro* behaviour, curing parameters and drug delivery of Ibandronate were evaluated.

INTRODUCTION

Self-curing acrylic formulations based on PMMA are one of the most important polymer systems for bone and prostheses fixation in orthopaedic surgery, being an alternative to non-cemented techniques. First reference of the application of these materials in total hip replacement (THR) was published in 1961 by John Charnley [Charnley 1961]. These composites are materials formulated by a red-ox polymerisation reaction of two phases, one solid (powder, mainly PMMA) and one liquid (monomer, methylmethacrylate).

This work has been focused in the modification of the solid phase by adding two different starch based biopolymers to evaluate the effect of nature of the polymer, particle size distribution and solid:liquid ratio in the mechanical properties, curing parameters, *in vitro* behaviour, biodegradation and drug delivery capacity of Ibandronate, as bisphosphonate for osteoporosis treatment.

MATERIALS & METHODS

Materials

The composites were based on poly(methyl methacrylate) (PMMA) (Degacryl MW 332) and methyl methacrylate (MMA) (Acros Organics). Benzoyl peroxide (BPO) and 4,4'-(dimethylamino)difenyl carbinol (BZN) were acquired from Scharlau and Fluka, respectively. Starch based biopolymers Mater-Bi YI014U/C (TPS1) and Biopar (TPS2) were supplied by Novamont and Avebe, respectively. Ibandronate as supplied by Merck.

Methods

The materials were prepared by means of a red-ox polymerisation reaction reported in a previous work [Méndez et al. 2004]. PMMA beads from solid phase were substituted by an amount of TPS1/TPS2 to obtain a final composition of 2:1 PMMA:starch. Each formulation was named as follows: X-Y-Z, were X: TPS1/TPS2/PMMA, Y: particle size of TPS1/TPS2 and Z: the solid:liquid ratio (S:L). Properties such as curing parameter, residual monomer content, *in vitro* behaviour (water uptake/weight loss), compressive mechanical properties and capacity to deliver Ibandronate were determined.

RESULTS & DISCUSSION

In vitro behaviour

Table I summarises the maximum water uptake values (MWU) and the loss of weight (LW) for composites modified with TPS1 and TPS2. The addition of the biodegradable component with smaller particle size distribution produced higher values of maximum water uptake (MWU) attributed to the increase in the specific surface of the starch. The higher capacity of water absorption of the formulations modified with TPS1, compared with that of TPS2 was related with the different commercial formulation, being TPS1 more hydrophilic than TPS2. Another interesting observation was the loss of weight of the composites upon immersion in PBS related with the leaching of the plasticizers of starch to the external medium.

Table I. Maximum water uptake (MWU) and weight loss (WL).

Fomulation	MWU (wt%) [s.d.]	LW (wt%) [s.d.]
TPS1-300-2	12.0 [0.5]	4.5 [0.5]
TPS1-150-1.5	13.6 [0.4]	6.9 [1.1]
TPS1-75-1	15.3 [1.0]	9.2 [0.4]
TPS2-300-2	8.6 [0.8]	5.8 [0.1]
TPS2-150-1.5	11.2 [1.4]	6.7 [0.4]
TPS2-75-1	13.1 [1.1]	9.1 [1.0]

Curing Parameters and Residual monomer content

Curing parameters and residual monomer content are summarised in table II. Peak temperature reached during the curing process, decreased when compared with the formulation based on PMMA with the same S/L ratio and was lower than 90º C (required by ISO 5833). This result is indeed beneficial, since a minimisation of necrotic phenomena in the implantation surrounding tissue will be derived. Setting time did not exhibited significant changes when part of PMMA from the solid phase was substituted by TPS1/TPS2, compared with PMMA controls. About residual monomer content, this parameter increased due to the use of lower S/L ratios because of the presence of more monomer in the formulation. Larger amounts of monomer during the curing process lead larger amounts of residual monomer content. These values were analogous to those found in previous research works [Weill et al. 1996] [Méndez et al. 2004].

Table II. Curing parameters and residual monomer content.

Formulation	T_{max} (ºC)	$t_{setting}$ (min)	RMC (%)
PMMA-2	75.6	8.9	0.40 [0.02]
PMMA-1.5	87.7	13.7	0.60 [0.02]
PMMA-1	92.3	14.4	1.10 [0.03]
TPS1-300-2	60.3	8.9	2.16 [0.06]
TPS1-150-1.5	55.6	12.1	2.97 [0.05]
TPS1-75-1	54.4	13.4	3.50 [0.06]
TPS2-300-2	65.7	8.4	1.05 [0.04]
TPS2-150-1.5	68.8	10.0	2.51 [0.03]
TPS2-75-1	65.9	14.4	2.86 [0.03]

Mechanical evaluation

Compressive stress was followed at different incubations times. The results are summarised in Figure 1. Both materials, modified with TPS1 and TPS2, suffered a drop of compressive stress at failure (σ_c) with the immersion time as well as with the decrease of the particle size due the leaching of the plasticizers [Azevedo et al. 2003] from thermoplastic starch and the plastifying effect of absorbed water. On the other side, the smaller particle size increased the specific surface of the biodegradable polymer, increasing the no compatible interface between PMMA and starch..

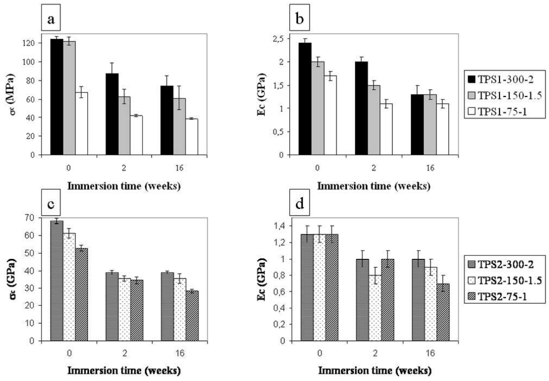

Figure 1. Mechanical properties under compressive stresses. a-b:TPS1; c-d: TPS2.

Compressive modulus showed a decrease with immersion time as well as particle size.

Drug release

Drug release of Ibandronate from composites loaded with TPS1 and TPS 2 are showed in figure 2. There is a high dependence of the release of the medicament with the kind as well as the particle size of the added powder of the thermoplastic starch. TPS1 released a higher concentration of the bisphosphonate for each formulation compared with those formulated with TPS2. Ibandronate has a high solubility in water and TPS1 absorbs a higher amount of water than TPS2 . Both effects induced a higher delivery of the drug in PBS, that reached in the case of the formulation TPS1-75-1 up to 10 mg·ml^{-1} and 6 mg·ml^{-1} in the case of TPS2-75-1.5, 18 and 11 times higher than PMMA-1.5 (control), respectively.

About particle size dependence, the release was higher for the materials formulated with the smaller one. This phenomenon was in agreement with the establishment of interfaces PMMA-starch with low compatibility. The addition of smaller particle sizes increased interface area between PMMA and starch allowing the absorption of higher amounts of water, as mentioned above, to release higher amounts of drug.

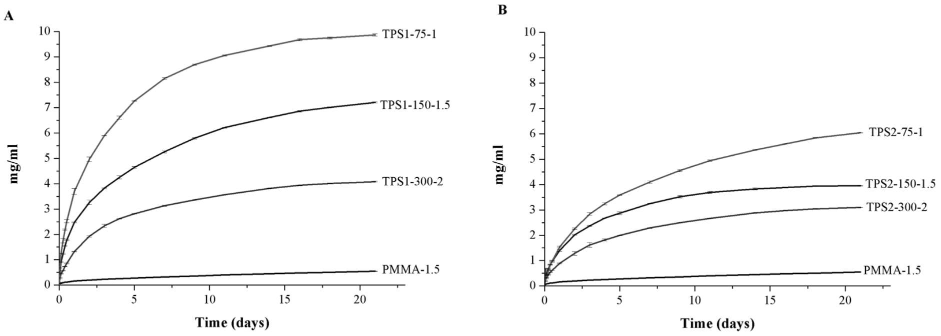

Figure 2. Drug release profiles. Formulations modified with a) TPS1 and b) TPS2.

CONCLUSIONS

In this work, a study of the influence of the addition of two different commercial starch-based biopolymers for the preparation of self-curing composites to be used as acrylic bone cements has been performed. Thermoplastic starches gave rise to formulations with acceptable mechanical properties, although decreased after PBS immersion. This effect focused their use in applications when high bearing loads are not demanded. Thermoplastic starch addition also produced self-curing formulations that modulated the delivery of bisphosphonates depending on its hidrophilicity and its particle size distribution. These results can be of great interest to the field of controlled drug delivery systems in orthopaedic surgery.

ACKNOWLEDGEMENTS

MEC (project MAT2006-11516). *Fundación Maria Francisca de Roviralta.* University of Girona (BR-07/05 doctorate grant).

REFERENCES

AZEVEDO, H.S. et al. (2003). In Vitro Assessment of the Enzymatic Degradation of Several Starch Based Biomaterials. *Biomacromolecules,* 4, 1703-1712.
CHARNLEY, J. (1961). Arthoroplasty of the hip; a new operation., 27, 1129-1132.
MÉNDEZ, J.A et al. (2004). Injectable self-curing bioactive acrylic-glass composites charged with specific anti-inflammatory/analgesic agent. *Biomaterials,* 25, 2381-2392.
WEILL, A., CHIRAS, J., SIMON, J.M., ROSE, M., SOLA-MARTÍNEZ, T., ENKAOUA, E. (1996). Spinal metastases: indications for and results of percutaneous injection of acrylic surgical cement. *Radiology,* 199, 241–247.

Gelatin-poly(lactic acid) multilayer films for hydrophobic applications

C. Peña[1], M.D. Martin[1], A. Retegi[1], R. Ruseckaite[2]
K. de la Caba[1], I. Mondragon[1]
[1]'Materials + Technologies' Group, Departamento Ingeniería Química y M. Ambiente,
Escuela Politécnica. Universidad del País Vasco/Euskal Herriko Unibertsitatea
[2]Research Institute of Material Science and Technology (INTEMA)
Mar de Plata, Argentina

ABSTRACT

Multilayer films were obtained by coating gelatin with poly(lactid acid) by dip-coating technique in order to improve water resistance of neat gelatin film. The surface of obtained materials was analysed by Fourier transform infrared spectroscopy in a single reflection ATR mode and by contact angle determination. Mechanical properties and phase transitions by differential scanning calorimetry were also measured.

1. INTRODUCTION

Renewable resources from animals or plants as proteins can be employed for the development of green polymeric materials that would not involve the use of toxic or noxious component in their manufacture and could be degraded in natural environmental ambience (Sinha et al, 2005). As one kind of protein, gelatin derived from chemical degradation of collagen, has gained more attention as raw material because of its abundance and biodegradability (Cao et al, 2007). The main limitation of gelatin for the preparation of packaging films arises from its rapid dissolution in aqueous environments. In order to avoid these problems chemical cross-linking procedures by reaction with glutaraldehyde, formaldehyde or native and oxidized polysaccharides have been considered (Cortesi et al. 1998).

In this work, the strategy to reduce the solubility has been the manufacture of gelatine based multilayer films containing the non-water soluble poly(lactic acid) (PLA) by dip-coating technique. Several pH have been analysed in order to analyse if it is a variable in the coating process. PLA is industrially obtained from the polymerisation of lactic acid, a fermentation product of low cost polysaccharides. PLA solutions in organic solvents can be employed for transparent film preparation (Rhim et al. 2006).

2. EXPERIMENTAL

Commercial gelatin (G) type A from acid pretreated pigskin (isoelectric point 7) was supplied by Sigma and employed as received without any further treatment. Poly(lactic acid) (PLA) 3051D from NatureWorks has been employed without modification. Films have been prepared in two stages. In the first one, G films were obtained from G aqueous solution (5 wt%) and casting procedure at room temperature in polystyrene Petri plates. G films were obtained at three pHs (pH 5, 7 and 9) by adjusting the pH of the G solutions with sodium hydroxide 1 N. In all cases, thickness of obtained films were around 40-80 µm. These films are named G5, G7 and G9, respectively. In the second stage, PLA was solved in dicloromethane (5, 10 and 15 wt%) and G films were wetted in PLA solution by automatic dip-coating technique (DC Multi-8, Nima Technology). By this technique, films of G were immersed at controlled speed (30 mm/min) during 20 min and then there were taken out also at controlled speed. In order to optimize the coating conditions, two take out rates were evaluated: 10 and 20 mm/min. Obtained films were hang out for solvent evaporation. In order to avoid residual solvent presence in films, they were finally dried under vacuum at 35 ºC during 24 h. The original thickness of G films increased after coating around 10-15 %. Obtained multilayer films are named GPLA5, GPLA7 and GPLA9, being the numbers the pH of G solution after film preparation.

Multilayer films were analysed by Fourier transform infrared spectroscopy (FTIR) (Nicolet Nexus spectrometer) with a single reflection ATR system of ZnSe lenses (MKII Golden Gate, Specac). The acquisition conditions were 1000-4000 cm^{-1} spectral range, 20 scans and a resolution of 4 cm^{-1}. Contact angle (CA) of films were also measurement using ultrapure water from Millipore purification system in a Contact Angle system OCA (Dataphysics). The average values were obtained from 10 measurement for each system. Phase transitions of obtained films were determined by differential scanning calorimetry (DSC) (Mettler DSC822). 3-5 mg of samples were sealed in an aluminium pan. Scanning temperature range from 25-250 ºC was employed and sample crucibles were heated at 10 ºC min^{-1}. Tensile tests were carried out in a Miniature Materials Tester (MiniMat 2000) of Rheometric Scientific. Probes were cut with a pneumatic die cutter. Dimensions of probes and test conditions were set according to D1708-93 standard. Test rate was 1 mm/min. For each composition 5 specimens were tested and the average values were calculated.

3. RESULTS AND DISCUSSION

In order to optimize the coating procedure, two take up rates (10 and 20 mm/min) and three PLA concentrations (5, 10 and 20 wt%) were evaluated. As figure 1 shows, when 20 mm/min was employed, the material was white and with 10 mm/min it was transparent. The white samples were observed by microscopy and bubble presence was confirmed.

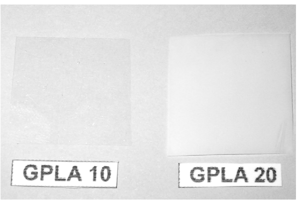

Fig. 1. GPLA films obtained at 10 and 20 mm/min to take up.

The same behaviour was observed for PLA solutions at 10 and 20 % dilution, due to the higher viscosity of solutions. Then, coating procedure was performed with PLA solutions at 5 % and the lower take up rate (10 mm/min) in order to avoid the bubble formation.

FTIR spectroscopy was used to evaluate the chemical groups present in the surface of the films. In figure 2a, spectra of G films are shown. As can be seen, characteristic amide I, II and III bands can be observed at 1630, 1530 and 1230 cm^{-1}. Not important changes can observed when pH was changed. On the other hand, PLA is an aliphatic polyester which shows the characteristic peaks at 1750 and 1180 cm^{-1}, due to the C=O and C-O-C groups (figure 2b). The analysis of the spectra of coated films with PLA reveals that characteristic bands of PLA were in the surface of materials. Nevertheless, when spectra are compared with the one for neat G, it can be observed that in all cases G bands were also in the surface spectra of multilayer films. It could be due to two factors: (1) PLA layer was inhomogeneous, or (2) the employed technique, IR waves could penetrate some µm in the very thin (10 µm) PLA transparent layer.

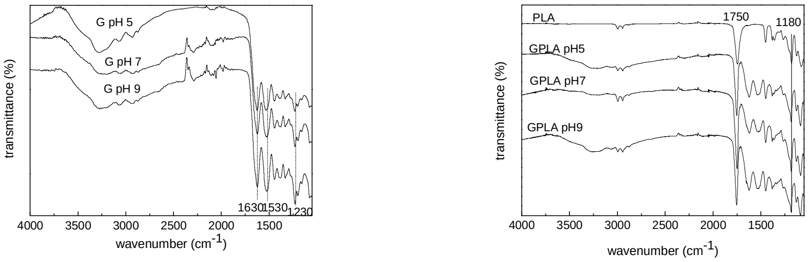

a *b*

Fig. 2. FTIR spectra of *a)* G film from solutions at pH 5, 7 and 9 and *b)* PLA and multilayer films obtained from G film solution at pH 5, 7 and 9.

In order to clarify this fact, contact angle of films were measured (table 1). As can be seen, the CA of G films was higher than 90º at analysed pHs, and for PLA film 74º, similar to the one obtained for this material by Lin et al (2007) (73 º). In the case of modified samples, CA values are similar to the ones for neat PLA. Then, it can envisage that G is not in surface. In addition, pH did not affect the CA value as occurred in G films in which differences could be attributed to the different arrangement of polar groups of the aminoacid chains at each pH and, as consequence, to different interaction level with water.

System	G5	G7	G9	GPLA5	GPLA7	GPLA9	PLA
CA (º)	105±6	97±5	90±6	75±2	74±3	75±3	74±1

Table 1. Contact angle of G films and GPLA multilayer films obtained from G solutions a pH 5, 7 and 9.

t (min)	0	10	20	22
G	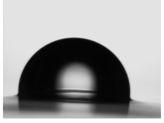		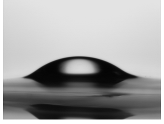	
CA	96º	82º	67º	-
t (min)	0	10	20	30
GPLA	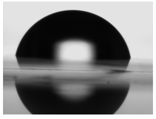	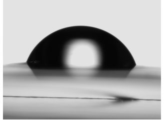	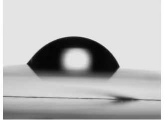	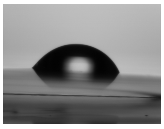
CA	79º	70º	69º	64º

Table 2. Contact angle images and values at several times for G and GPLA films.

To verify this conclusion, CA variation upon time of a drop in G and GPLA films was analyzed. Table 2 shows that G films present a higher initial CA but at around 20 min the drop was not visible because it was absorbed by the film. The GPLA film did not show this behaviour and the drop was visible after 30 min. Figure 3 shows the evolution of CA. As can be seen, the absorption rate is clearly lower for GPLA films than in G films, thus, the lower hydrophility of the multilayer GPLA film can be confirmed.

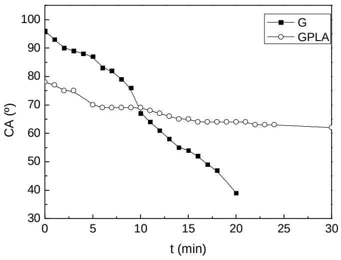

Fig 3. CA evolution for G and GPLA films.

Thermal analysis by DSC showed that neither T_g nor T_m of GPLA films did not vary respect to the ones for neat G. Mechanical properties of GPLA films have been also measured. Both rigidity and strength were the same than for G films.

3. CONCLUSIONS

The hydrophilic nature of G can be reduced by coating with PLA without variations in both critical temperatures and mechanical properties of neat G films. The coated PLA layer protects G film and eliminates the differences upon pH in G-water interactions.

ACKNOWLEDGEMENTS

Financial support from Basque Country Government in the frame of Grupos Consolidados (IT-365-07) and SAIOTEK09 are gratefully acknowledged. C. Peña, thanks University of the Basque Country (Ayudas para la especialización de investigadores doctores en la UPV/EHU) for the grant for this project.

REFERENCES

CAO, N., FU, Y., HE, J. (2007) Mechanical properties of gelatin films cross-linked, respectively by ferulic acid and tannin acid. *Food Hydrocolloids,* 21, 575-584.

CORTESI, R., NASTRUZZI, C., DAVIS, S.S. (1998) Sugar cross-linked gelatin for controlled release: microspheres and disks. *Biomaterials,* 19, 1641-1649.

LIN, Y., CHEN, X., JING, X., JIANG, Y., SU, Z. (2008) Gelatin multilayers assembled on Poly(L-lactic acid) surface for better cytocompatibility. *Journal of Applied Polymer Science,* 109, 530-536.

RHIM, J., MOHANTY, A.K., SINGH, S.P., PERRY, K.W. (2006) Effect of the processing methods on the performance of polylactide films: thermocompression versus solvent casting. *Journal of Applied Polymer Science*, 101, 3736-3742.

SINHA, RAY, S., BOUSMINA, M. (2005) Biodegradable polymers and their layered silicate nanocomposites: In greening the 21st century materials world. *Progress in Materials Science*, 50, 962-1079.

Biocomposites from renewable resources: epoxidized soy bean oil/bacterial cellulose composites

A. Retegi[1], C. Peña[1], N. Gabilondo[1], P. Stefani[2], K. de la Caba[1], C. Castro[3], P. Gañan[3], I. Mondragon[1]
[1] 'Materials + Technologies' Group, Departamento Ingeniería Química y M. Ambiente,
Escuela Politécnica. Universidad del País Vasco/Euskal Herriko Unibertsitatea
[2] Research Institute of Material Science and Technology, National Research Council,
Engineering Faculty, Juan B. Justo 4302, B7608FDQ Mar del Plata, Argentina
[3] New Materials Group, Universidad Pontificia Bolivariana Circular 1 # 70-01,
Medellin, Colombia

ABSTRACT

Transparent biobased composites have been produced from totally renewable resources: bacterial cellulose (BC) nanofibres and epoxidized soy bean oil (ESO). BC nanofibres have been obtained in static culture from *Gluconobacter xylinum*. BC films immersed in ESO solution at different conditions allow achieving ESO/BC biocomposites with different BC contents. Increasing BC content, tensile strength and modulus are enhanced due to BC random in plane network-like structure. Transparency of the samples is maintained even at high BC contents.

1. INTRODUCTION

Bacterial cellulose (BC) is a form of cellulose produced by bacteria such as *Gluconobacter xylinum*. BC high mechanical properties including tensile strength and modulus, high water-holding capacity, high moldability, high crystallinity, and high biocompatibility make them excellent reinforcement for polymeric matrices due to bacterial cellulose nanofibre is a ribbon-shaped fibre of 10-50 nm diameter forming a 3D network (Putra et al. 2008).

Currently novel composites with high plant or bacterial cellulose content and high transparency have been developed (Iwamoto, 2005). However, few works have been developed about composites of bacterial cellulose with matrices from renewable resources.

Triglyceride plant oils represent a major class of such renewable resources. Soybean oil (SBO) is the most readily available and one of the lowest cost vegetable oils in the world. Epoxidized soybean oil (ESO) is manufactured by the epoxidation of the double bonds of the SBO triglycerides and it is industrially available in large volumes at a reasonable cost (Boquillon et al. 2000).

In this study preparation of composites from renewable resources as BC/ESO with high BC content has been developed and their transparency, morphology, thermal properties and mechanical properties have been characterized.

2. EXPERIMENTAL PART

2.1. Materials and composite preparation

ESO has been kindly supplied by Hebron S.A. and cured with hexahydrophthalic anhydride (Fluka) and 1-methyl imidazol (Sigma Aldrich) as catalyst. Acetic acid, perchloric acid (0.1 N), toluene and acetic anhydride (Panreac) have been used for BC acetylation.

BC has been obtained from a *Gluconobacter xylinum* pellicle incubated for 13 days at 28 ºC in a static culture. BC pellicles with a thickness of 0.5-0.7 cm have been boiled in 5 wt % NaOH solution for 90 min at 120 ºC in order to remove cells and then thoroughly washed under running water for 2 days. Then, BC have been suspended in water (0.5 wt %) and stirred for 48 h. The suspensions have been vacuum filtered using nylon membrane filter (0.2 mm mesh) producing 25 mm diameter mats that have been oven dried at 70 ºC for 48 h between glass plats. BC mats have been compressed at 50 MPa in order to increase stiffness of the material obtaining 40-50 μm thickness films.

BC films have been acetylated following Ifuku et al. (2007) proposed procedure. Sample has been placed in a mixture of 40 mL of acetic acid, 40 mL of toluene and 0.2 mL of perchloric acid 0.1 N. Then acetic anhydride (2 mL) has been added with continuous stirring. The mixture has been allowed to stand for 1 h at room temperature and then washed with methanol. Finally modified BC films have been hot-pressed at 10 MPa for 5 min at 80 ºC.

Composite films have been obtained after immersion in ESO/hardener/catalyst diluted in THF at concentrations 1:3, 2:3, 1:1 of acetylated BC films and maintained under vacuum for 24 h. Impregnated films have been taken out from the solutions and maintained at 120 ºC under vacuum to eliminate residual solvent, and finally cured at 120 ºC for 4 h.

2.2. Characterization

Atomic force microscopy (AFM) from Digital Instruments having a NanoScope III controller with a MultiMode head has been used to characterize the morphological distribution of BC and BC/ESO composites.

Transparency of the samples has been measured using a UV-visible (UV-Vis) spectrometer from 200 nm to 1100 nm at 25 ºC.

X-ray diffraction (XRD) patterns have been measured with a X-ray diffractometer PW1710 (Philips) with CuKα radiation (k = 1.54 Å). Samples have been scanned from 10 to 40 2θ.

Thermal stability of ESO/BC composites has been analyzed in a Mettler/Toledo thermogravimetric analyzer. Tests have been carried out in nitrogen atmosphere from 25 to 800 ºC with a scan rate of 10 ºC/min.

Tensile tests have been performed in a Minimat miniature mechanical test machine using a 200 N load cell. The crosshead rate used in the test has been 1 mm/min and distance between grips used has been 22 mm following ASTM D 1708 standard. At least five specimens have been tested for each set of samples being the mean values reported.

3. RESULTS AND DISCUSSION

In Figure 1, photographs of ESO, BC and ESO/BC composite films are shown. As seen, the transparency of ESO resin film is remarkably higher than that of BC film. However ESO/75BC composite film retained the transparency of the resin even at that BC content. These results are confirmed by measuring the transmittance of the films in the UV-visible spectrophotometer.

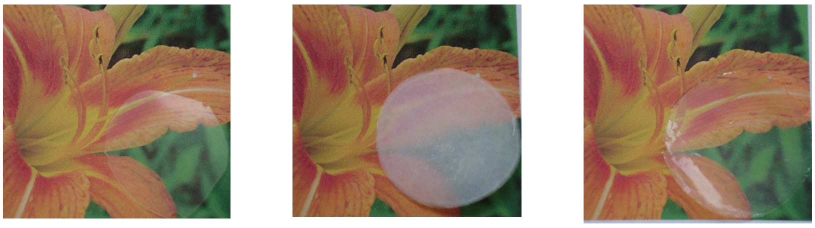

Fig. 1. ESO, BC and ESO/75BC composite films.

As illustrated in Figure 2, BC nanofibrilar films exhibit very low light transmittance (less than 20 %) whereas ESO resin is quite transparent with a transmittance of 75 % at a wavelength of 600 nm. In the case of ESO/BC composites, the transmittance is retained even at high BC content. In order to obtain transparent composite materials there are two main conditions: the similarity between the refractive indices of the components and the size of the reinforcement must be ten times smaller than the wavelength of visible light in order to avoid light scattering. In this case, the refractive index of bacterial cellulose fibres is 1.618 along the fibre, 1.544 in transverse direction and that of ESO resin is 1.470. However, the composite maintains its transparency due to the "size effect" of BC nanofibres (Yano et al. 2005), which makes BC appropriate to combine with optically transparent resins with different refractive indices.

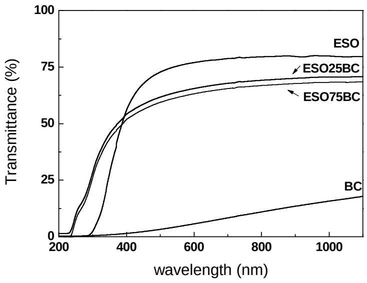

Fig.2. BC, ESO and ESO composites UV-vis transmittance curves.

Finally, mechanical tensile properties of BC, ESO and ESO/BC composites are shown in Table 1. As expected, elastic modulus and tensile strength increase with BC content and elongation is slightly decreased. This improvement is related to the dispersion of high resistance rigid network-like nanofibrillar BC in the composite material (Figure 3)

Sample	**Modulus** (GPa)	**Strength** (MPa)	**Elongation** (%)
ESO	0.5 ± 0.1	5.5 ± 0.4	3.6 ± 0.5
ESO25BC	3.8 ± 0.3	25 ± 0.4	2.5 ± 0.5
ESO75BC	5.9 ± 0.2	88 ± 0.7	2.4 ± 0.4
BC	9.2 ± 0.2	135 ± 8	2.2 ± 0.1

Table 1. Tensile properties of ESO, BC and ESO/BC composites.

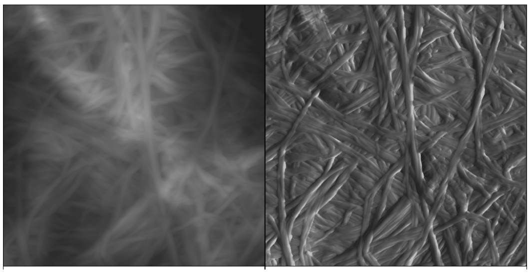

Fig. 3. 3 μmx3μm AFM image of ESO75BC composites, left/right: height/phase.

4. CONCLUSIONS

Composite materials based in bacterial cellulose have been produced demonstrating that BC nanofibres offer promising characteristics as reinforcing material for optical applications due to the size effect.

ACKNOWLEDGEMENTS

Financial support from inanoGUNE and SAIOTEK-2009 projects (funded by Eusko Jaurlaritza) is gratefully acknowledged.

REFERENCES

BOQUILLON, N., FRINGANT, C. (2000). Polymer networks derived from curing of epoxidised linseed oil: influence of different catalysts and anhydride hardeners. *Polymer*, 41, 8603-8613.

IFUKU, S., NOGI, M., ABE, K., HANDA, K., NAKATSUBO, F., YANO, H. (2007). Surface modification of bacterial cellulose canofibres for property enhancement of optically transparent composites: dependence on acetyl-group DS. *Biomacromolecules*, 8, 1973-1978.

IWAMOTO, S., NAKAGAITO, A.N., YANO, H., NOGI, M. (2005). Optically transparent composites reinforced with plant fibre-based nanofibres. *Appl. Phys., A* 81, 1109-1112.

PUTRA A., KAKUGO, A., FURUKAWA, H., GONG, J.P., OSADA, Y. (2008). Tubular bacterial cellulose gel with oriented fibrils on the curved surface. *Polymer*, 49, 1885-1891.

Assessing the viscoelastic behaviour and the thermostabilising effect of adding natural fibres to starch-based matrices to design sustainable biocomposites

R. Moriana[1], F. Vilaplana[1,2], J.D. Badia[1], A Ribes-Greus[1]
[1]Instituto de Tecnología de Materiales (ITM), Universidad Politécnica de Valencia
Camino de Vera s/n, E-46022 Valencia, Spain
[2]Department of Fibre and Polymer Technology, School of Chemical Science and Engineering,KTH - Royal Institute of Technology,Teknikringen 56-58, SE-10044 Stockholm, Sweden

ABSTRACT

Biocomposites based on thermoplastic starch copolymers (Mater-Bi KE03B1) and reinforced with natural fibres (cotton, hemp, and kenaf) were prepared and characterised in terms of their thermo-mechanical properties, in order to assess the influence of biofibre addition on the properties of the matrix. In general, natural fibres can be mixtured with the polymeric matrix, enhancing the mechanical properties. At the same time, natural fibres increase the thermal stability associated to the thermal decomposition processes. Interesting differences between lignocellulosic fibres (hemp and kenaf) and cellulose fibres (cotton) are found when added into the pure Mater-Bi; hemp and kenaf fibres enhance the thermal stability of Mater-Bi more significantly than cotton fibres, whereas the Mater-Bi /cotton biocomposite exhibits the highest mechanical performance.

1. INTRODUCTION

Environmentally-friendly composites (prepared from a biodegradable matrix and natural fibres as reinforcements) are being used as an alternative to traditional reinforced composites. Thermoplastic starch-based polymers have drawn increased attention among other biodegradable materials, due to their raw material availability and low price. Unfortunately, most of these materials still have poor physical properties for load-bearing applications. A broad approach to solve this problem is adding natural fibres into the biodegradable thermoplastic starch.

Natural fibres have advantages from the point of view of fibre-matrix adhesion, especially with polar-matrix materials. This fact opens up further possibilities for using natural fibres as sustainable filler in biocomposites. The challenge is to prove that natural fibres are efficient reinforcements of thermoplastic starch-based materials by not only improving mechanical properties but also by decreasing costs and preserving simultaneously their biodegradability. In this study, three different natural fibres (hemp, kenaf, and cotton) have been used as fillers into a commercial starch-based thermoplastic material and the viscoelastic behaviour and the thermal stability of each designed biocomposite has been studied.

2. EXPERIMENTAL

2.1. Materials and sample preparation

The biocomposites were prepared using a starch-based thermoplasctic commericalized under the Mater-Bi KE03B trade mark (Novamont, Italy) as polymeric matrix. Cotton, hemp and kenaf were the natural fibres employed as reinforcement, provided by Yute S.L. (Spain). The average length and fibre diameter of each kind of natural fibres were determined by optical microscopy over 100 fibres. The chemical composition (lignin, cellulose and hemicellulose content) was analysed using Klason method and carbohydrate analysis, following an experimental protocol described by Theander at to (1986).

The matrix and the pelletisated biofibres were incorporated in a co-rotative twin screw extruder at 438K (Werner & Pfleiderer ZSK25). Bars with dimensions 110x110x2mm were obtained by compression moulding, providing three different kinds of biocomposite with 10% in weight of each biofibre.

2.2. Thermogravimetric measurements

The thermal decomposition of the natural fibres, pure matrix and their biocomposites were evaluated by dynamic thermogravimetric analysis (TGA) using a Mettler-Toledo TGA/SDTA 851 (Columbus, OH). Approximately 8,5 mg of sample was heated between 298K and 775K at different heating rates (3, 5, 10, 20, and 30 K/min) under Ar atmosphere flow (50 mL/min). The values of maximum decomposition temperature and weight loss, as well as the kinetic triplet of each constituent of the studied materials were obtained.

2.3. Dynamic mechanical thermal measurements

The viscoelastic measurements were carried out in a dynamic-mechanical-thermal analyser MARK IV DMTA (Rheometric Scientific, United Kingdom). The sinusoidal deformation was applied to rectangular samples with dimensions of 50x10x2mm in the double clamped cantilever mode. Multifrequency scans were performed between 0,1Hz and 100Hz using 4 frequencies per decade at a temperature region between 173K and 363K; the temperature region from 173K to 298K was scanned with a step rate of 4K/scan, while between 298K and 365K the step rate was set at 2K/scan. The values of loss tangent (tan δ), storage modulus (E’), and loss modulus (E’’) versus temperature and frequency were thus obtained.

3. RESULTS AND DISCUSSION

The pyrolysis of Mater-Bi by TGA shows a complex thermal decomposition with two main weight-loss regions: the first weight-loss region centred on 608K is related to starch; and the second weight-loss region around 707K is associated to the synthetic component present in the pure Mater-Bi. From the pyrolysis of natural fibres, several weight-loss regions can be observed in agreement with other studies (Wang et to 2003). The main weight-loss region (480-830K) shows a complex thermal decomposition process where different overlapped peaks related to hemicellulose, pectins, cellulose and lignin (in the fibres that have lignin content) can be observed. Cotton fibre is the most thermal stable with the higher onset decomposition temperature.

When the pure Mater-Bi is reinforced, the thermal decomposition of the three studied biocomposites presents two main weight-loss regions, similarly to the pure Mater-Bi. The region associated to the synthetic component of this polymeric matrix is not significantly affected by the addition of cotton, kenaf and hemp fibres. Interestingly, the peak corresponding to starch degradation in pure Mater-Bi, which is completely overlapped with hemicellulose/pectine and cellulose degradation in natural fibres, is here displaced to higher temperatures for the studied biocomposites. Although cotton fibre has previously shown the most thermal stability, it is Mater-Bi/kenaf composite which exhibits the highest temperature peak when the different composites are compared.

Moreover, the kinetic parameters (Ea,A,f(α)) have been determined for every decomposition process using different isoconversional methods: the Ozawa (Ozawa et to. 1965) and Friedman (Friedman et to. 1964) methods. Both methods calculate the Ea without considering the decomposition mechanisms. On the other hand, Criado method (Criado et to. 1978) was employed to analyse the reaction mechanism of the different decomposition processes for the pure Mater-Bi and its biocomposite. The average Ea and the A related to the thermal decomposition of starch and synthetic component of the pure Mater-Bi were fixed as 98 kJ/mol and $10^{9.5}$ min^{-1} and 175 KJ/mol and $10^{13.5}$ min^{-1}, respectively. Moreover, the thermal decomposition kinetics for both weight-loss regions follow a (n+m; n) type model, being the algebraic expression $f(\alpha)=\alpha^{0.5}\cdot(1-\alpha)^{1.5}$.

When natural fibres are incorporated into the pure Mater-Bi, the Ea associated to both thermal decomposition regions increase for every studied biocomposites. For Mater-Bi/cotton biocomposites, the major increase of Ea occurs in the decomposition process related to the synthetic biodegradable component. On the other hand, kenaf and hemp fibres enhance the Ea of the thermal decomposition region associated to starch. Regarding the kinetic mechanisms, the results suggest that the actual reaction mechanism related to starch component is not affected by the addition of cotton fibres due to the similarity between the composition of cellulose and starch. However, the addition of kenaf and hemp fibres changes the thermal decomposition mechanisms of both starch and the synthetic component in the Mater-Bi.

The dynamic mechanical spectrum of the pure Mater-Bi presents different characteristic relaxations at a frequency range of 0.1-100 Hz. The relaxation that appears at low temperatures is centred at 219K (labelled as β) and may be attributed to the glass transition of the synthetic component of Mater-Bi; the second relaxation (labelled as α) that appears at 330K may be related to the chain movements prior to the fusion of this synthetic component. The biocomposites show the same viscoelastic transitions as the pure Mater-Bi; an increase in the elastic modulus can be also observed due to the fibre reinforcement. The storage modulus of the reinforced biocomposites is highest for Mater-Bi/cotton composite over the entire range of temperatures.

Modified Fuoss-Kirkwood empirical model (Fouss et to. 1941) and Charlesworth deconvolution procedure (Charlesworth et to. 1993) were applied to the experimental data of pure Mater-Bi and its biocomposites, in order to fit the relaxation functions and obtain the values of the loss modulus maximum and the corresponding temperature for each viscoelastic relaxation at the different frequencies. The Arrhenius maps for the pure Mater-Bi and its biocomposites could be thus obtained by plotting the temperature of the maximum of the loss modulus curves (T_{max}) from the Fuoss-Kirkwood fittings versus the frequency for all the studied relaxations. Arrhenius equation was therefore applied to obtain the activation energies associated to α secondary relaxation for pure Mater-Bi and its biocomposites.

The experimental data from the Arrhenius maps to β relaxation (primary relaxation) could be therefore fitted to the Vogel-Fulcher-Tammann-Hesse (VFTH) equation *(1)* according to the free-volume theory in order to obtain the parameter related to the molecular free volumen (Fulcher et to. 1925).

$$\ln \tau_i = A_0 + \frac{m_v}{T - T_\infty} \quad (1)$$

Here, τ_i is the relaxation time; A_0 is an empirical parameter; T_∞ is the temperature at which the free-volume would be zero were it not for the formation of the glassy state; m_v is a parameter related to the relative free-volume. The addition of natural fibres induces a clear reduction in the molecular free volume parameter associated to the chains of the synthetic component present in the Mater-Bi; these changes may be related to the interfacial adhesion between the lignocellulosic fillers and the polymeric matrix.

4. CONCLUSIONS

Natural fibres can be successfully incorporated into the thermoplastic-starch matrix, enhancing the mechanical properties and reducing the molecular free-volume of the overall biocomposite. At the same time, natural fibres act as suitable fillers for Mater-Bi, by increasing the thermal stability and the activation energy associated to the thermal decomposition processes. Specifically, cotton fibres offer the highest mechanical reinforcement to the biocomposite; hemp biocomposites exhibit the lowest free-volume parameter; and kenaf confers the major thermal stability to the biocomposite. The choice of natural fibre reinforcement constitutes an interesting option to tailor the properties of the resulting materials, and allows broadening the application range of starch-based reinforced biocomposites**.**

ACKNOWLEDGEMENTS

The authors would like to acknowledge the Ministerio de Educación y Ciencia and the Ministerio of Medio Ambiente (Spanish Government) for the economical support through the FPU, FPI predoctoral grants and the ENE2007-67584-C03-01 project.

REFERENCES

CHARLESWORTH JM. (1993) *J Mater Sci***,** 28, 399
CRIADO JM. (1978) *Thermochimic Acta***,** *86,* 24
FRIEDMAN (1964) *Journal.Polym.Sci.C, 6,* 183
FULCHER GS. (1925) *Journal of the American Ceramic Society,* 6, 339
FUOSS RM, KIRKWOOD JG. *J. Am. Chem. Soc,* 2, 385.
OZAWA T (1965) *Bull Chem Soc Jpn*, 88, 6
THEANDER O, WESTERLUND EA (1986) *J.Agric.Food Chem.,* 34, 330
WANG XL, YANG KK, WANG YZ, WU B, LIU Y, YANG B (2003) *Polym Degrad Stab.* 81, 415.

Desarrollo de materiales compuestos con fibras naturales en el espacio económico de Castilla – La Mancha

M.M. Moreno Valencia
Departamento de producción vegetal y tecnología agraria. E.U. Ingeniería Técnica Agrícola, Universidad de Castilla – La Mancha, España
A. Rosa Serradilla
Ingeniero de Materiales, Línea especializada de materiales compuestos, Altran Technologies. Madrid, España

RESUMEN

El presente trabajo es un estudio de viabilidad que tiene como objetivo alcanzar un reto tecnológico a la vez que impulsar el tejido empresarial de la comunidad de Castilla – La Mancha.

El desarrollo de una línea de futuro en el ámbito de los materiales compuestos reforzados con fibras naturales implica muchos beneficios para la comunidad autónoma como son la recuperación de cultivos herbáceos, el impulso de empresas como las de transformación de las plantas, tratamientos de las fibras naturales y fabricantes de equipos originales o subcontratistas de primer nivel.

El estudio se divide en cuatro fases que abarcan desde la producción de fibras naturales, los tratamientos superficiales de las fibras, el estudio de la capacidad manufacturera de la región hasta el diseño de un prototipo.

1. INTRODUCCIÓN

La actual preocupación ambiental por parte de los países industrializados está propiciando una creciente tendencia para el desarrollo de materiales compuestos reforzados con fibras naturales que sustituyan a los materiales compuestos reforzados con fibra de vidrio. Estas fibras naturales pueden ser aprovechadas debido a las excelentes propiedades mecánicas específicas y de reciclabilidad. En comparación con las fibras de vidrio, los costes se reducen y además, disminuyen los peligros en lo que respecta a la salud del personal de fabricación.

Una de las actividades del estudio es seleccionar el cultivo herbáceo de mayor viabilidad en la comunidad autónoma de Castilla – La Mancha. Una vez seleccionada la fibra, se procede a evaluar el tratamiento superficial, físico o químico, más adecuado con el fin de tener la mejor adhesión interfacial con la matriz. La siguiente fase del proyecto es la de la realización de un estudio de la capacidad manufacturera de la región y por último se realiza la fase preliminar de implantación de un producto concreto de la estructura secundaria de una torre de aerogenerador.

Los cultivos herbáceos en la comunidad de Castilla – La Mancha pueden ser recuperados si se les da la aplicación adecuada a las fibras transformadas.

La utilización de las fibras naturales como refuerzo de materiales compuestos cada vez está encontrando más aplicaciones de valor añadido como pueden ser desde piezas del sector de la automoción pasando por raquetas, cascos, piraguas y otras muchas aplicaciones que están en estudio de viabilidad.

2. DESCRIPCIÓN DE LOS TRABAJOS REALIZADOS

Los trabajos se dividen en cuatro fases. Aunque la fase final de este proyecto sea la fase preliminar del desarrollo de una estructura del sector de la energía eólica, la realidad es que el auténtico fruto de este proyecto será la concepción de un área industrial de desarrollo competitivo dentro de Castilla – La Mancha.

2.1 Fase 1: Estudio de producción de fibras naturales

En esta primera fase, atendiendo a las cualidades climatológicas, al histórico de cultivos herbáceos, a las propiedades de las fibras naturales y al procesado de las plantas para la obtención de las fibras, se identifica cual es la planta que tiene mayor posibilidad de prosperar su cultivo en la comunidad autónoma de Castilla – La Mancha.

Atendiendo al histórico de cultivos, se observa como el lino textil y el cáñamo textil fueron los principales cultivos herbáceos de la comunidad autónoma durante la década de los ’90. Siendo el lino textil el cultivo de mayor importancia.

En el año 1999 se dio el máximo de hectáreas cultivadas en la Junta de Castilla – La Mancha para el caso del lino textil (44.703 Ha), coincidiendo con el máximo de hectáreas cultivadas en el territorio de España (126.593 Ha). El peso específico de esta comunidad en relación al cultivo de Lino textil total a nivel nacional fue del 35% para el año 1999 (Base de datos junta de Castilla – La Mancha).

Con estas cifras se refleja el potencial que puede llegar a tener la comunidad de Castilla – La Mancha respecto a una posible recuperación de este tipo de cultivos.

En este estudio se están definiendo los mapas de producto y se propondrán posibles situaciones de plantas de transformación del cultivo.

Los costes de explotación se están estimando para diferentes superficies de explotación en función de la capacidad de generar 1000 ton/año, 2500 ton/año y 5000 ton/año, siendo estas toneladas de pacas.

El estudio de la producción abarca también la evaluación del impacto ambiental así como el personal necesario para explotar un número determinado de hectáreas.

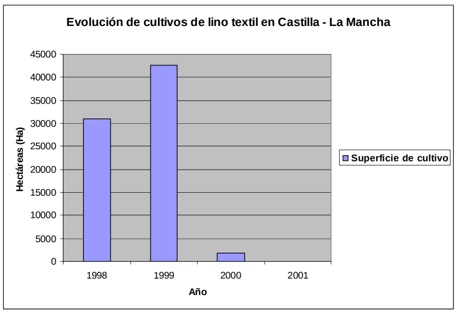

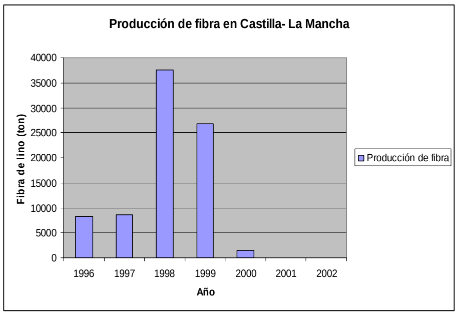

Fig. 1. Superficie de cultivo C-LM.

Fig. 2. Producción de fibras C-LM

2.2 Fase 2: Estudio de los tratamientos superficiales

La adhesión entre las fibras y la matriz en un material compuesto juega un importante papel en las propiedades mecánicas del material, debido a que la transferencia de tensiones entre la matriz y las fibras. Esta adhesión se puede mejorar modificando superficialmente la superficie de las fibras.

Para el caso de las fibras de lino, hay muchos tratamientos posibles, tanto físicos como químicos. La alta hidrofilia de las fibras provoca el hinchamiento de las mismas dando como resultado la inestabilidad dimensional y una pérdida de las propiedades mecánicas.

Hay varios mecanismos para mejorar la adhesión como son los cambios en la energía superficial de la fibra, la impregnación de las fibras y el acoplamiento químico.

Para seleccionar un tratamiento es muy importante conocer la matriz que se va a utilizar, en el caso de utilizar una matriz de polipropileno, la influencia de un tratamiento con anhídrido maleico ve incrementada su resistencia a tracción en un 50% y en un 100% su módulo de Young (J. Gassan et al. 1999) Las mejores propiedades de los materiales compuestos de fibra de lino con matriz de polipropileno son cuando se tratan con el copolímero anhídrido maleico polipropileno. (I. Mondragón et al. 2003)

El tratamiento de alcalinización es de los de mayor utilización debido a su bajo coste y a la ganancia en efectividad de las fibras. Estos tratamientos vienen motivados debido a que el principal componente de la fibra es la celulosa y esta tiene grupos hidroxilo que son capaces de formar puentes de hidrógeno con las moléculas de agua. Estos tratamientos de alcalinización son simples y efectivos cuando se quiere mejorar la adhesión fibra/matriz en una resina epoxídica (I. Verpoest et al 2005).

Los métodos químicos tienen la desventaja de producir una considerable cantidad de sustancias y vapores peligrosos, los cuales contaminan el medio ambiente y tienen que ser eliminados.

Una alternativa para los tratamientos físicos es el método por plasma frío, es una técnica más benévola con el medio ambiente. La mejora viene determinada por la modificación física y química de la superficie, se produce un aumento de la rugosidad superficial de la fibra debido al efecto sputtering. Esto produce un aumento de la superficie de contacto entre la fibra y la matriz. La mejora química viene dada por la implantación de grupos polares en la superficie de la fibra, reduciendo la energía superficial y promoviendo el enlace químico entre la fibra y la matriz polimérica. El éxito del plasma frío en los tratamientos superficiales es debido a su alta temperatura electrónica y una baja temperatura del gas. (Yiu-Wing Mai et al. 1996**)**

Para el caso del cáñamo podemos extrapolar los tratamientos superficiales pues los tratamientos químicos actúan sobre la celulosa y los tratamientos físicos como el plasma actúan físicamente igual que lo hacen en el lino.

2.3 Fase 3: Estudio de la capacidad manufacturera

La agrupación de actividades en una misma área económica beneficia la relación calidad/precio de un producto, haciéndolo más competitivo. El ahorro en los costes de logística y el desarrollo de una nueva industria competitiva en un sector en auge son algunas de las ventajas.

La situación estratégica de la planta de transformación de las fibras debe tener como condición estar rodeada de los cultivos en un radio no mayor de 30 km. Este máximo es para que el balance económico sea favorable.

Se está realizando una prospección de las empresas que actualmente tienen como actividad la transformación de las plantas en fibras naturales y de las empresas con capacidad para hacer un tratamiento superficial de las mismas así como los fabricantes de equipos originales (OEMs) o sus subcontratistas de primer nivel.

2.4 Fase 4: Prototipo. Diseño y fabricación

El diseño de una parte de la estructura de un aerogenerador, spinner o nacelle, es la última fase del proyecto. Se han elegido este tipo de estructuras por ser de frecuente utilización en el área de económica de Castilla – La Mancha. Adicionalmente, su permanente exposición a condiciones medioambientales extremas permitirá la correcta valoración del material compuesto objeto de este estudio. La fabricación de los moldes y de la estructura forma parte de la fase 2 de este proyecto a desarrollar en 2010.

3. CONCLUSIONES

De acuerdo con los resultados obtenidos se obtienen las siguientes conclusiones:

- La planta con mayor probabilidad de éxito en la producción de fibras para su uso como refuerzo de materiales compuestos en Castilla – La Mancha es el lino (*Linum Usitatissimum L),* no solo por sus propiedades mecánicas sino también por la potencialidad de un cultivo eficiente en la comunidad autónoma. La variedad está por determinar.
- El tratamiento superficial de alcalinización es el tratamiento mas eficiente y menos costoso para mejorar la adhesión de las fibras y la matriz y el tratamiento con plasma es el más benévolo con el medio ambiente y de mayor compatibilidad con distintas matrices.
- Existe infraestructura industrial para la transformación de las plantas en las fibras naturales y para su tratamiento superficial además de una importante presencia de empresas relacionadas con la fabricación de materiales compuestos en los sectores aeronáutico y eólico.

REFERENCIAS

BASE DE DATOS DE LA CONSEJERIA DE AGRICULTURA DE LA JUNTA DE CASTILLA – LA MANCHA,
http://www.mapa.es/es/estadistica/pags/anuario/introduccion.htm

GASSAN, J (1999). Composites reinforced with cellulose based fibres. *Progress in polymer science*, 24 (1999) 221-274

MONDRAGÓN, I (2003). Effects of fibre treatment on wettability and mechanical behaviour of flax/polypropylene composites. *Composites science and technology,* 63 (2003) 1247-1254.

VERPOEST, I (2005). Improving the properties of UD flax fibre reinforced composites by applying an alkaline fibre treatment. *Composite: Part A*, 37 (2006) 1368-1376.

YIU-WING MAI (1996). Application of plasma technologies in fibre-reinforced polymer composites: a review of recent developments. *Composites Part A*, 28A (1997) 73-86

Biodegradable composites based on polycaprolactone and natural reinforcements with optimized properties

A. Vazquez
Laboratory of Polymer and Composites (INTECIN). Engineering Faculty, University of Buenos Aires, Argentina
L. Ludueña; M. Casco; R. Ollier and V. Alvarez
Research Institute of Material Science and Technology (INTEMA), Engineering Faculty, National University of Mar del Plata - Mar del Plata - Argentina

ABSTRACT

The main objective of this work was to obtain biodegradable composites from polycaprolactone and natural reinforcement with optimized mechanical properties by the chemical modification of bentonite or surface treatments on cellulose fibers. Ammonium and phosphonium salts were used as clay modifiers at different concentrations and times of reactions whereas alkaline-treatments (5, 10, 15 and 20 wt.% of NaOH and 10 wt.% of KOH); acetylation (with glacial acetic acid 1 or 2 hours followed by catalyzed acetic anhydride) and esterification (treatments with stearic and lauric acids) were applied to cellulose fibers. Modified bentonites and cellulose fibers (TGA; DSC; FTIR; WAXS, water absorption; contact angle; SEM) were characterized and most compatible were used to prepare composites (15 wt.%) and nanocomposites (5 wt.%). Mechanical properties were correlated with chemical modifications.

INTRODUCTION

Due to environmental problems, the development biodegradable polymeric products to be used as packaging, are receiving growing attention (Lepoittevin et.al. 2002). Polycaprolactone (PCL) which is biodegradable and biocompatible polyester with a number of potential applications from agricultural usage to biomedical devices (Dubois et.al. 1991) belongs to this class of synthetic biodegradable polymers. Its performance can be greatly enhanced by incorporation of fillers. One possibility is to add natural fibers giving to the final material the additional benefit of complete biodegradability (Mohanty et al 2000). The use of natural fibers (Roohani et. al. 2008) is based on their low-cost, renewability, low densities and low abrasively. Nevertheless, this kind of reinforcements displayed opposite polar behavior with respect to hydrophobic matrices. So, it is necessary to modify the fibers (Plackett and Vázquez 2004) but especially at the surface in order to prevent the destruction of the integrity and thus, their mechanical properties. Another possibility is to incorporate nano-fillers. The nanoparticles mostly used to reinforce polymeric materials are layered silicates. Among them, the use of bentonite is interesting due to environmental and economic factors, their natural abundance, and their mechanical and chemical resistance. In order to achieve better properties it is necessary to obtain a totally exfoliated structure (where silicate layers are completely and uniformly dispersed in a continuous polymeric matrix) but the tendency of the particles to agglomerate has been difficult to overcome in addition to its hydrophilic character, so it is necessary to make a previous treatment. The most popular one consists on converting these hydrophilic silicates to organophilic ones. The hydrated cations that are in the interlayer can be easily replaced by other positively charged surfactants such as alkyl ammonium or phosphonium cations. The modified clay has less surface energy and is more compatible with hydrophobic polymers whose are able to introduce inside the galleries under defined processing conditions.

The aim of this work was to perform different chemical treatments (alkaline, acetylation and esterification) to cellulose fibers and chemical modification to the bentonite (with ammonium and phosphonium salts) in order to improve the reinforcement/polymer compatibility and to obtain biodegradable composites and nanocomposites with optimized final properties. These final products can be used in food package industry

MATERIALS AND METHODS

Polycaprolactone Mn = 80.000 gr/mol (Sigma Aldrich) was used as a matrix. Bentonite was supplied by Minarmco S.A.. (Neuquén, Argentine). Cellulose was obtained from cotton by following a previously reported procedure: (Moran et.al.).

Modification of bentonites

a) Tributilhexadecylphosphonium bromide (Hedley et al 2007). 2.5 gr of clay were dispersed in 100 ml of deionised water. Then, the aqueous solution of TBHP of the corresponding concentration was added. The mixture was stirred for 4 hours at 70ºC. :

b) Octadecylammonium chloride (Bala et al, 2000). Adequate quantities of octadecyl amine, HCl and distilled water were weighted. The mixture was heated at 80ºC for few minutes in order to protonate the amine. After that, 2.5 gr of clay were dispersed in 100 ml of deionized water at 80ºC and the ammonium solution was added. The mixture was stirred vigorous keeping the temperature constant.

Modification of cellulose

a) Alkaline treatments: cellulose fibers (2.5 g) were treated with (100 ml) of 5, 10, 15 and 20 wt% of NaOH and 10 wt% of KOH 1 h at 30 ºC under continuous stirring.

b) Acetylation: cellulose fibers (2.5 g) were treated with glacial acetic acid (125 ml) at room temperature by using a shaker for 1 or 2 hr. After this process, acetic anhydride (50 ml) with 2 drops of H2SO4 was added for 5 min.

c) Esterification: The reactions were carried out under reflux for 4 hr using 2 g of cellulose, 100 ml of toluene and 0.44 ml of dodecanoyl chloride and 0.5 ml of pyridine or 0.57 g of octadecanoyl chloride and 0.6 ml of pyridine. Then was filtered and the modified cellulose was submitted to a soxhlet extraction with acetone for two days.

Characterization of original and modified reinforcements

X-Ray patterns: PW1710 diffractometer with a CuKα generator at room temperature.

Thermogravimetric Analysis (TGA): Shimadzu TGA-50.(25 to 1000ºC) at 10ºC/min

FTIR measurements: FTIR Genesis II (4000 - 600 cm-^{1}) at room temperature.

Water absorption tests: 90% RH. Before tests, samples were dried under vacuum.

Contact angle measurements: Compacts powders were prepared in a press. Sessile drops of ethylene glycol and diiodomethane were formed on the surface of the solids.

Scanning Electron Microscopy (SEM) JEOL JSM-6460 LV. Diameter of at least 100 fibers of each treatment was measured in order to make a statistical distribution.

Characterization of composites (PCL+ 15wt.% cellulose or PCL + 5 wt.% bentonite)

Differential Scanning Calorimetry (DSC): Shimadzu DSC-50 from 25 to 400ºC at 10ºC/min under nitrogen .The degree of crystallinity was calculated from this curves..

Mechanical properties: Tensile tests in a Instron 4467 at 50 mm/min. Before tests, all specimens were preconditioned at 65% RH (relative humidity).

RESULTS AND DISCUSSION

Modified bentonites. In the case of phosphonium salt, there was a little increase in the interlayer spacing as *f* increased were pristine bentonite was used Comparing the same surfactant amount, by changing the pristine clay for saturated one ; the difference between is negligible (the same as the saturated respect to pristine one). Regarding the octadecylamomniumm modifications, all of them produced and increase on the interlaminar spacing. By using 1.5 CEC it is clear that the stirring time had not an important effect on d001 (average 1.74 nm). On the other hand increasing f (from 1.5 to 3.0), only a marginal augment on this parameter was observed. It is interesting to note that for the lower f (1.5 CEC), there were no important effect of saturation but for higher f (3.0 CEC) the differences are quite notable being d_{001} superior for Na+ saturated bentonite.. One interesting result from TGA experiments is that the water content (obtained from residual mass curve until 130ºC); it is understandable that all modifications produced an undoubtly decrease on the absorbed water which in turns indicates enhance on the hydrophobicity. By comparing TBDP clays it is possible to observe that the increment on the modifier concentration has a direct effect on the organic content, as it was expected. On the other hand, it is also clear that the effectively of the modifier is improved for saturated bentonite. In the case of ODAC, no important changes were observed as a function neither of time; nor in the TGA curves neither in the organic content (around 2.8 ± 0.7% in this three cases). This is also coherent with the behavior observed for d001. On the other hand, by increasing the modifier concentration for a fixed time, an important increase on the organic content was detected. (from 3 to 12%) whereas the changes in the interlayer spacing was not so high, so that, it is quite possible that some part of the organic modifier did not enter in the clay galleries. For the same time and modifier concentration, the organic content was higher in the case of saturated clay in this case also the interlayer space was higher, specially in the case of the higher modifier concentration giving the idea that the introduction of the modifier inside the clay was effective. The thermal stability of phosphonium modified clays is higher than that of the ammonium modified ones. It is interesting to note that the temperature for maximum rate of mass loss decreased for saturated clay and also for higher quantities of surfactant. Polarity was really low in all cases but especially when high surfactant amounts were employed. This result is also interesting because the water absorption (which was also reduced) gives idea about the complete clay and this latter about the external hidrophobicity which became important to interact with the hydrophobic thermoplastic polymers.

Modified cellulose fibers. Alkaline treatment produced a decrease on the crystallinity index (FTIR and DRX) accompanied by the change of cellulose arrangement (from I to II); an increase on the water uptake (water absorption test) due to a higher polarity (contact angle test) and the exposition of free hydroxyl groups on the surface. On the other hand, acetylation generated fibers with higher crystallinity, without changing the cellulose (I), and lower polarity degree and water absorption (according to the surface groups). In the case of esterification, the crystallinity did not show important variations (being always cellulose I) but the water absorption and the polarity decreased until zero; and a strong reduction on the fibers aspect ratio with respect to untreated cellulose was observed. The esterification indexes confirmed that these treatments took place only at the surface.

Composites: 15 wt.% of celluloses (untreated; Cel10KOH; Cel20KOH; CelAc2h; CelEsterC12 and CelEsterC18) were added to PCL producing composites. Alkaline treatments did not improve the compatibility with the matrix but it slightly increased the cellulose aspect ratio (*l/d*) (better matrix/fiber load transference efficiency). The esterification treatment produced the opposite result where the best compatibility with the matrix but strong reduction on the fibers *l/d* was achieved. Best composites properties were found with the 2 hours acetylated fibers with good matrix/fiber compatibility and slight decrease on the cellulose *l/d*. Mathematical models were used to correlate experimental mechanical behavior. Best agreement was obtained by the Hull´s model which takes into account the matrix-fiber adhesion and the *l/d.*

Nanocomposites: 5 wt.% of bentonites (1; 2; 3; 9 and 11) were added to PCL producing nanoomposites. DRX pattern indicates probably intercalation or some degree of exfoliation of the clay platelets between polymeric chains. All clays act as nucleation agent because X_{cr} increased when bentonites were incorporated. Whereas the stiffness increased in all cases, the tensile strength decreased for PCL/clay 3. The elongation at break decreased in all cases because the intercalation of the clay reduces the plasticity of the polymer. The water vapor rate, whose are very important for packaging, decreased in all cases.

CONCLUSIONS

The results obtained in the present study indicates that increasing the matrix/filler compatibility is one way to improve the mechanical properties of PCL/filler composites but other variables should always be taken into account. Future works will be conducted on changing the processing parameters as another strategy to improve the final behavior of such materials.

ACKNONWLEDGEMENTS

Authors acknowledge to (PICT1560) and CONICET (PIP 6254) for the financial support.

REFERENCES

BALA P, SAMANTARAY BK, SRIVASTAVA SK (2000) Synthesis and characterization of Na-montmorillonite-alkylammonium intercalation compounds *Mat Resear Bull* 35, 1717-1724

DUBOIS P, JACOBS C, JEROME R, TEYSSIE P (1991). Macromolecular engineering of polylactones and polylactides. 4. Mechanism and kinetics of lactide homopolymerization by aluminum isopropoxide. *Macromolecules*, 24(9), 2266–2270.

HEDLEY CB, YUAN G, THENG BKG (2007) Thermal analysis of montmorillonites modified with quaternary phosphonium and ammonium surfactants *Applied Clay Science* 35, 180-188

LEPOITTEVIN B, DEVALCKENAERE M, PANTOUSTIER N, ALEXANDRE M, KUBIES D, CALBERG C, JÉROME R, DUBOIS P. (2002).Poly (ε-caprolactone)/clay nanocomposites prepared by melt intercalation:. *Polymer,* 43(14):4017–4023.

MOHANTY AK, MISRA M, HINRICHSEN G. BIOFIBERS (2000). Biodegradable Polymers and Biocomposites: An Overview. *Macromol Mater Eng,* 277(1), 1–24.

MORÁN J, ALVAREZ V, CYRAS VP, VÁZQUEZ A (2008) Extraction of Cellulose and Preparation of Nano-Cellulose from Sisal Fibers. . *Cellulose,* 15, 149-159.

PLACKETT D, VÁZQUEZ A. (2004) Polymer composites and the environmental. In: Caroline Baillie, Editor, Cambridge: Woodhead Publishers, p. 123-153.

ROOHANI M, HABIBI Y, BELGACEM NM, EBRAHIM G, KARIMI AN, DUFRESNE A. (2008) Cellulose whiskers reinforced polyvinyl alcohol copolymers nanocomposites. *European Polymer Journal,* 44(8), 2489-2498.

Functional regulation of photo-responsive nano-arrays composed of ordered metal-coordinated peptide-redox protein conjugates

X. Wang, K. Nagata, M. Higuchi
Department of Materials Science and Technology, Graduate School of Engineering,
Nagoya Institute of Technology, Japan

SUMMARY

With the aim of a unidirectional electron transfer, we prepared vertically oriented metal coordinated $Leu_2Ala(4\text{-}Pyri)(Co(II))Leu_6Ala(4\text{-}Pyri)(Co(II))Leu_6$ peptide nano-arrays by the stepwise polymerization on a self-assembled monolayer (SAM) surface having ferrocene moieties. The Ala(4-Pyri) moieties were formed complexes with Co(II), and the peptide assemblies obtained oriented vertically and unidirectionally. We investigated the electron transfer through the peptide nano-arrays. As a result, the complexation between Ala(4-Pyri) and Co(II) accelerated the electron transfer coupled with the macro-dipole moments of the peptide assemblies. Furthermore, the redox proteins were fixed on the surface of the peptide nano-array. Upon photoexcitation of ferrocenyl group on the SAM surface, electron transfer occurred from the excited ferrocenyl group to the redox protein. The system may be useful for the novel nano-devices.

1. INTRODUCTION

Vectorial signal transfer such as a directional electron transfer is a basic feature of many biological processes. For example, in a photosynthesis system, the special location of particular functional groups bound a vertically oriented α-helix peptide bundle in the lipid membrane yields a photo-induced vectorial electron transfer through the membrane (Babcock at to. 1993, Deisenhofer at to. 1985). Vertical and unidirectional α-helical peptide assemblies are focussed as novel nano-devices capable of transferring information because of its optical characteristic and large macro-dipole moment along its molecular axis. Studies on the vertically and unidirectionally oriented peptide assembly may be not only important for mimicry of biological signal transduction, but also may provide the basis for fabrication of novel molecular devices.

We report fabrication of vertically and unidirectionally oriented metal coordinated peptide assemblies by stepwise polymerization on Au electrodes. The amino acid sequence of peptide is chosen as $Leu_2Ala(4\text{-}Pyri)Leu_6Ala(4\text{-}Pyri)Leu_6$, because its two 4-Pyri groups of Ala motieties are located in the same direction of one side surface of the α-helical rod to form a stable peptide bundle by the metal-coordination. We investigated the structures of metal coordinated peptide assemblies on the electrodes. We prepared self-assembled monolayers composed of the same sequencial metal coordinated peptide having thioctic acid at the *N*-terminal on the Au electrodes. The metal coordinated peptide monolayers obtained by stepwise polymerization aligned nearly perpendicularly to the electrode surface in comparison with the self-assembled peptide monolayers. Activity of redox protein fixed on the metal coordinated peptide nano-array could be regulated by the photo-induced unidirectional electron transfer through the nano-array. We believed the system would be useful for the novel nano-devices.

2. RESULTS AND DISCUSSION

2.1 Preparation of Peptide Nano-arrays

We fabricated the $Leu_2Ala(4\text{-}Pyri)(Co(II))Leu_6Ala(4\text{-}Pyri)(Co(II))Leu_6$ nano-array by a stepwise polymerization of amino acids using the modified conventional solid-phase peptide synthesis (SP method) on a mixed self-assembled monolayer (SAM) surface consisting of amino-alkanethiol, dialkyl disulfide and ferrocenyl alkanethiol, which was prepared on the Au electrode (Fe-$L_{14}A_2$Co SP) (Higuchi at to. 2008). The metal coordinated peptide nano-array on a ferrocenyl group free mixed SAM ($L_{14}A_2$Co SP) was also obtained by the same protocol. For comparison, we prepared the metal coordinated peptide nano-array on the Au electrode by the self-assembled monolayer method (SAM method) using $Leu_2Ala(4\text{-}Pyri)Leu_6Ala(4\text{-}Pyri)Leu_6$, which has thioctic acid at *N*-terminal ($L_{14}A_2$Co SAM). Furthermore, we prepared metal free peptide nano-arryas $Leu_2Ala(4\text{-}Pyri)Leu_6Ala(4\text{-}Pyri)Leu_6$ on the Au eletrode by both SP method and SAM method (Fe-$L_{14}A_2$ SP, $L_{14}A_2$ SP, $L_{14}A_2$ SAM). The Nitrate Redutase (NR) as a electron acceptor was fixed on the peptide nano-array surface. Structures of the peptide assemblies on the Au electrode were investigated by the FTIR-RAS measurement. Electrochemical properties of the peptide nano-arrays were examined. We demonstrated the activity control of the redox protein on the peptide nano-arrays by the photo-induced vectrorial electron transfer through the metal coordinated peptide nano-arrays.

2.2 Structural Study

We investigated the secondary structure of the peptide on the Au electrode by FTIR-RAS, and the tilt angle of α-helical rod from the surface normal was determined on the basis of the radio of the amino I and II absorbance (Enriquez at to.1992). The results were shown at Table 1.

Table 1. The percentage of secondary structure and tilt angle of the α-helix rod from the surface normal for peptide nano-arraye on the Au electrodes.

	α-helix (%)	*β*-sheet (%)	random coil (%)	tilt angle (deg)
$L_{14}A_2$ SAM	88.0	0.1	11.9	60
$L_{14}A_2$Co SAM	87.2	6.7	6.1	43
$L_{14}A_2$ SP	45.9	6.8	47.3	68
$L_{14}A_2$Co SP	65.1	9.1	25.8	36
Fe-$L_{14}A_2$ SP	45.9	4.5	49.6	67
Fe-$L_{14}A_2$Co SP	65.7	5.4	28.9	37

The Co coordinated peptide nano-arrays which were fabricated by SAM ($L_{14}A_2$Co SAM) and SP method ($L_{14}A_2$Co SP and Fe-$L_{14}A_2$Co SP) took a mainly α-helical conformation. However, in the case of metal free peptide assemblies prepared by SP method ($L_{14}A_2$ SP and Fe-$L_{14}A_2$ SP), the helicities were lower than that of $L_{14}A_2$Co SP and Fe-$L_{14}A_2$Co SP. This result could be explained that the complexation between 4-Pyri and Co(II) stabilized the α-helical conformation owing to the peptide bundle formation. The molecular orientation of the Co coordinated α-helical rods of $L_{14}A_2$Co

SAM, $L_{14}A_2Co$ SP and Fe-$L_{14}A_2Co$ SP aligned nearly perpendicularly to the electrode surface in comparison with Co free peptide rods of $L_{14}A_2$ SAM, $L_{14}A_2$ SP and Fe-$L_{14}A_2$ SP. These imply that the Co(II) coordination to the 4-Pyri groups of the peptides result in the formation of the vertically oriented α-helical peptide bundle on the electrode surface.

2.3 Electrochemical Measurements

The electrochemical properties of the peptide nano-arrays which were prapared by SAM method and SP method on a mixed SAM composed of amino-alkanethiol and dialkyl disulfide were examined. A conventional three-electrode setup was used. The supporting electrolyte was KCl aqueous solution (0.1 M). Fig. 1a shows the I-V plot for Co coordinated peptide nano-array (circle), which was prepared by SAM method. A current increase was observed in any event at positive and negative potentials. It is noted that we did not observed the current response for the Co free nano-array (square). On the other hand, the case of the Co coordinated peptide nano-array fabricated by SP method on the mixed SAM, the significant current was observed at the only negative potentials (Fig. 1b). This result suggests that the macro-dipole moment of the α-helical rod in the nano-array fabricated by SP method is aligned unidirectionally. Presumably, the non-linear effect of electron flow through the nano-array fabricated by SP method occurs along the peptide macro-dipole moment coupled to Co(II)-(4-Pyri) complexes.

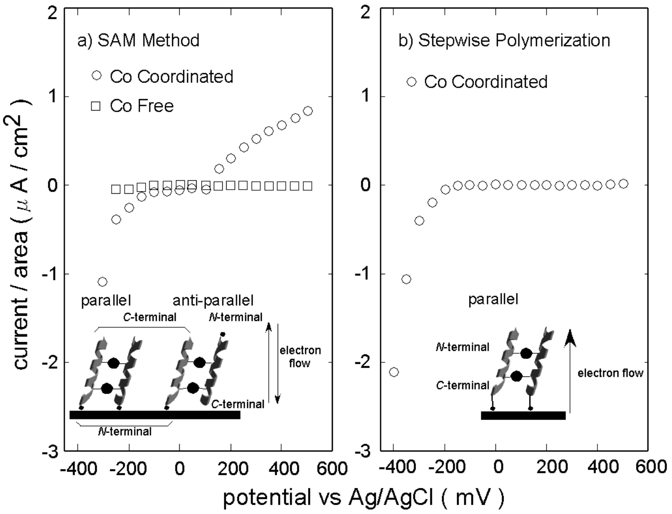

Fig.1. Current-voltage plots for peptide nano-arrays on the Au eletrodes. a) prepared by SAM method. b) fabricated by SP method.

2.4 Photo-induced vectorial electron transfer through the peptide nano-arrays

Photo-induced vectorial electron transfer through Co coordinated peptide nano-arrays prepared by SP method, which had electron donor, ferrocenyl group, on the electrode, and the electron acceptor, NR, at the *N*-terminal of the peptide, was investigated by using the three-electrode setup described above. The supporting electrolyte was KNO_3 aqueous solution (0.1 M) as a substrate for NR. The measured photocurrent generated by photo-irradiation of the Co coordinated nano-arrays having the ferrocenyl group on the electrode was shown in Fig. 2 with the repeating on-off switching of the photo-irradiation. A remarkable photocurrent was observed. The photocurrent caused by the electron transfer from the ferrocenyl group on the Au electrode to the NR, which located on the peptide nano-array surface. The photocurrent of the NR free Fe-$L_{14}A_2Co$ SP was lower than that of the Fe-$L_{12}A_2Co$ SP having NR on the surface. This result suggested that the vertical electron flow through the nano-array activated the surface NR by the photo-irradiation. The activated NR reduced the NO_3^- in the aqueous phase.

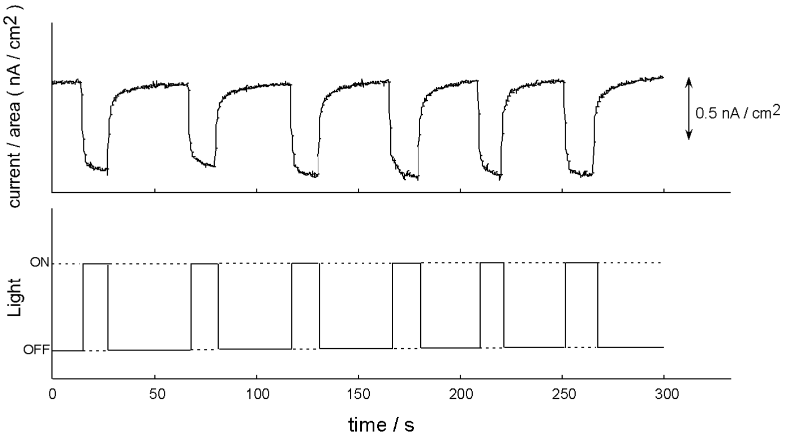

Fig.2. Time course of the photocurrents of Leu_2Ala(4-Pyri)(Co(II))Leu_6Ala (4-Pyri)(Co(II))Leu_6 nano-arrays prepared by SP method on a mixed ferrocenyl SAM upon photo-irradiation.

3. CONCLUSIONS

In summary, the vertically and unidirectionally oriented metal coordinated peptide nano-arrays were easily fabricated by the stepwise polymerization on a photo-responsive mixed SAM surface having ferrocenyl group. We demonstrated that vectorial and unidirectional electron transfer across the peptide nano-arrays on the mixed SAM. The electron transfer was accelerated by Ala(4-Pyri)-Co(II) complexes coupled with the macro-dipole moment of the peptide through the nano-arrays. The unidirectional electron transfer regulated the activity of the surface redox protein as the electron acceptor. This system may be useful for the novel molecular nano-devices.

REFERENCES

BABCOCK, G. (1993) *Proc. Natl. Acad. Sci. U.S.A.* **90** 10893

DEISENHOFER, J., EPP, O., MIKI, K., HUBER, R., MICHEL, H. (1985) *Nature* **318**, 618

ENRIQUEZ, E.P., SAMULSKI, E.T. (1992) *Mater. Res. Soc. Symp. Proc.* **255** 423

HIGUCHI, M. (2008) *Thin Solid Films* **516** 4312

Effect of interface modification with styrene-co-maleic anhydride oligomers on the mechanical properties of recycled polystyrene-lignocellulosic fiber composites

M. Poletto, J. Dettenborn, M. Zeni, A.J. Zattera
Laboratory of Polymers (LPOL), Center of Exact Sciences and Technology (CCET),Caxias do Sul University (UCS), Caxias do Sul/RS, Brazil

SUMMARY

The effect of the addition of three poly (styrene-co-maleic anhydride), SMA, oligomers with different content of maleic anhydride (MA), as interfacial modification agent on sawdust/PS composites properties was studied. The composites were manufactured in a twin-screw extruder using 20 wt% of sawdust. Were incorporated 1, 2 and 4 wt % of SMA in the composites. Mechanical properties were analyzed. This interface modification improves the compatibility of hydrophilic sawdust with hydrophobic PS. The addition of oligomers improves the mechanical properties of the composites with the incorporation of 2 wt% of SMA. Scanning electron microscopy (SEM) was used to investigate the fiber-matrix interface.

1. INTRODUCTION

The utilization of biomass for processing of novel composites has attracted growing interest because of this eco-friendly and renewable nature (Hillig et al., 2008). Industrial region of Caxias do Sul, situated in Rio Grande do Sul/Brazil, generates a big amount of industrial and urban wastes. The furniture industry generates approximately 6000 m^3/month of sawdust (Hillig et al., 2004). The estimate generation of expanded polystyrene waste in Caxias do Sul is about 1240 m^3/month (Poletto et al., 2008), deposited in the city landfill reducing drastically the area of the landfill.

The objective of this work was to investigate the interfacial adhesion of different SMA in composites whit sawdust and PS. The influence of the MA concentration in the copolymers on the mechanical properties of sawdust/PS composite was evaluated.

2. EXPERIMENTAL

2.1 Materials and composites preparation

EPS wastes were supplied by Associação de Recicladores Serrano, Caxias do Sul/Brazil. It has a MFI of 20 g/10min (200ºC/5 kg). Sawdust of *Pinus elliottii* was obtained from Madarco Co., Caxias do Sul/Brazil, with particle size 53-105 μm. Three types of SMA were obtained from Sartomer Co., Exton/USA, used with coupling agents. SMA2000 contains 30 wt% of MA groups and weight average molecular weight, M_w of 7500 g/mol; SMA3000 whit 25 wt% of MA and M_w of 9500 g/mol; SMAEF40 contains 20 wt% of MA and M_w of 10500 g/mol, these properties were obtained from Sartomer Co. Were incorporated 1, 2 and 4 wt% of coupling agents.

For reduction of apparent density the EPS was molded by compression in a hot press (5 min/130 ºC). The EPS were then grinded in a rotary knife mill getting flakes of PS. The sawdust was dried in an oven at 105°C for 24h. Composites whit 20 wt% of sawdust were processed with 1, 2 and 4 wt% of three types of SMA in a co-rotante twin-screw extruder, at 200rpm. The nine barrel temperature zones were controlled between 170ºC and 190ºC. Specimens for mechanical tests were injection-molded at a barrel temperature of 180ºC and mold temperature of 40 ± 2ºC.

2.2 Mechanical properties measurements and scanning electron microscopy

The tensile test was conducted according to ASTM D638 at 5 mm/min, with extensometer of 50 mm. Un-notched Izod impact strength was measured according ASTM D256. The flexural tests were conducted according to ASTM D790. The composites were tested at 1,5 mm/min. The fiber/matrix interface was investigated using a SHIMADZU Superscan SS-550, operated at an accelerating voltage of 15 kV. The cryo-fractured surfaces were sputter-coated with gold.

3. RESULTS AND DISCUSSIONS

3.1 Mechanical properties

The tensile strength and Young’s modulus increased with increasing SMA content, as showed in Figure 2.

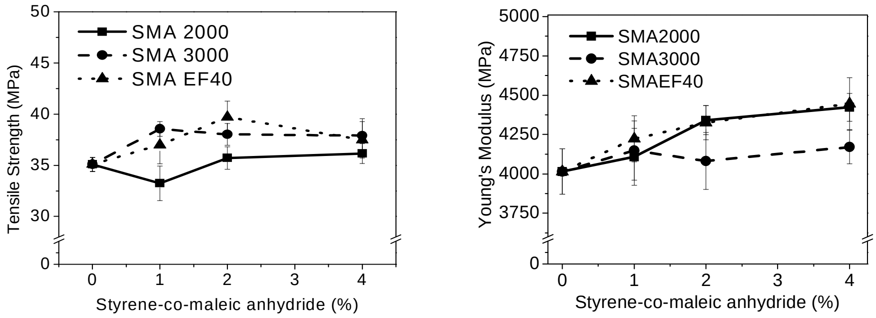

Fig. 2. Tensile strength and Young’s modulus of sawdust reinforced PS as a function of styrene-co-maleic anhydride content.

Figure 3 showed the flexural strength and flexural modulus of composites. The maximum value was obtained with 2 wt% of the SMA 2000. This coupling agent contains 30% by weight of MA groups, more content than others, and M_w of 7500 g/mol, the lowest M_w. The low M_w gives them sufficient fluidity in the molten state and thus supports their migration towards the fibre surface (Devaux, et al., 2002). This phenomenon causes a preferential localization os SMA to the fibre-matrix interface, and thus increases the possibilities of interaction with sawdust (Devaux, et al., 2002).

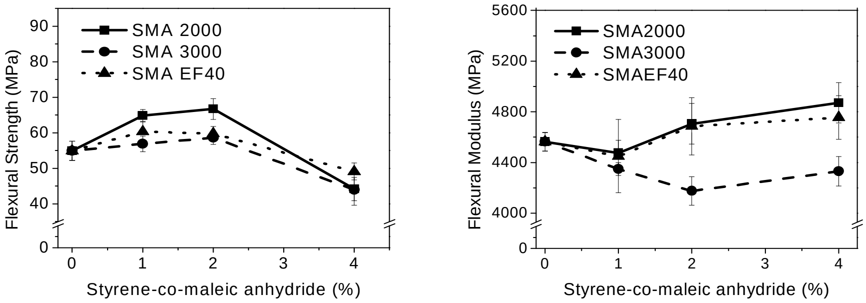

Fig. 3. Flexural strength and flexural modulus of sawdust reinforced PSr as a function of styrene-co-maleic anhydride content.

Impact strength decrease with SMA content probably because occurs increase in formation of entanglement between the fiber and PS, Figure 4 exhibits this behavior. Furthermore, the sufficient number of MA groups in SMA 2000 attached into the PS chains causes strong interfacial interaction, probably due the formation of chemical bonds between MA groups and hydroxyl groups of sawdust (Kim et al., 2007). Thus, composites whit 2 wt% of SMA 2000 showed more brittle behavior.

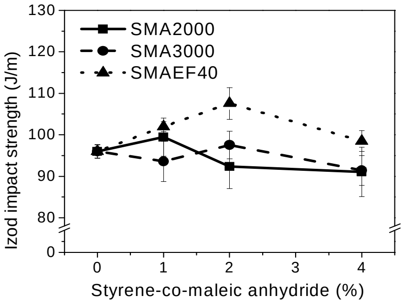

Fig. 4. Impact strength of sawdust reinforced PSr as a function of styrene-co-maleic anhydride content.

3.2 SEM observations

Figure 5 shows SEM micrographs of the composites prepared without (a) and with (b) SMA. The micrographs of composites prepared without SMA indicated presence of pulled-out traces and gaps between the sawdust and PS, which is evidence of weak interfacial adhesion. However, the adhesion between the fiber and the PS improved with addition of SMA. The appearance of the fiber surface is rough because it contains traces of matrix adhering to the surface. This indicates strong interfacial adhesion and good wetting (Kim et al., 2007) between the sawdust and PS.

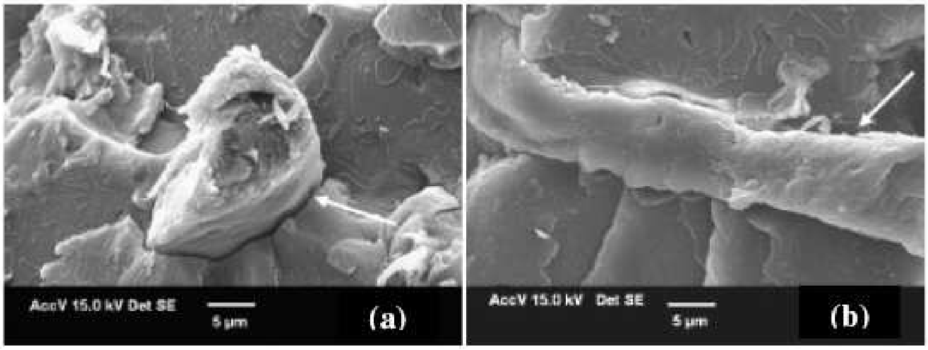

Fig. 5. SEM images (2000x): without SMA (a) and whit SMA (b).

3. CONCLUSIONS

The improvement in mechanical properties of the composites using SMA as a compatibilizing agent was strongly dependent on the amount of MA and the M_w of SMA. Low M_w gives sufficient fluidity for SMA in the molten state and thus supports the migration towards the fibre surface improving the adhesion of the sawdust and PS. The mechanical properties of SMA-treated composites were significantly increased compared to those of SMA non-treated composites. The satisfactory results were obtained with 2 wt% of SMA 2000. The SEM micrographs confirm better adhesion between the sawdust and the PS matrix.

ACKNOWLEDGMENT

The authors want to be grateful to Associação de Recicladores Serrano, Madarco Company and Sartomer Company for supplying materials and CNPQ for the financial support.

REFERENCES

DEVAUX, E., PAK, S.H., CAZÉ, C. (2002). Effects of the structure os styrene-co-maleic anhydride oligomers on the interfacial properties in a glass fibre reinforced polystyrene composite material. *Polymer Testing*,21, 773-779.

HILLIG, É., FREIRE, E., ZATTERA, A.J., ZANOTO, G., GRISON, K., ZENI, M. (2008). Use of sawdust in polyethylene composites. *Progress in Rubber, Plastics and Recycling Technolog*,, 24, 73-79.

HILLIG, É., SCHNEIDER, V. E., PAVONI, E.T. (2004). Pólo moveleiro da serra gaúcha: geração de resíduos e perspectivas para sistemas de gerenciamento ambiental. Educs, Caxias do Sul (Brazil).

KIM, H-S., LEE, B-H., CHOI, S-W., KIM, S., KIM, H-J. (2007). The effect of types of maleic anhydride-grafted polypropylene (MAPP) on the interfacial adhesion properties of bio-flour-filled polypropylene composites. *Composites Part A*, 38, 1473-1482.

POLETTO, M., ZATTERA, A. J., SCHNEIDER, V. E. (2008). Management of recyclable waste: associated problems with post consumption expanded polystyrene *in VI Simpósio Internacional de Qualidade Ambiental*, Porto Alegre, Brazil.

Crystallinity characterization of HDPEr/PVA blend biodegraded under composting conditions - biofilm

R.N. Brandalise
Centro de Ciências Exatas e Tecnologia
Grupo de Tecnologia de Polímeros
Universidade de Caxias do Sul / Caxias do Sul / Brazil
M. Zeni
Centro de Ciências Exatas e Tecnologia
Grupo de Membranas
Universidade de Caxias do Sul / Caxias do Sul / Brazil
M.M.C. Forte
Pós-Graduação em Engenharia de Minas, Metalúrgica e de Materiais.
Universidade Federal do Rio Grande do Sul / Porto Alegre / Brazil

ABSTRACT

Post-consumer high-density polyethylene (HDPEr) is one of the mass-produced non-degradable polymers and various types of polyethylene are used extensively in many fields, including agricultural and food-packing films. There has been a growing interest in enhancing the biodegradability of HDPE by blending it with a biodegradable water-soluble polymer, poly (vinyl alcohol) (PVA). A material like maleic anhydride (AM) grafted in HDPEr (HDPEr-AM) compatibilizer was used in this work. PVA might influence the blend properties, reducing the cristallinity blend HDPEr/HDPEr-AM/PVA, 35/5/60 to 33%, evaluated by differential scanning calorimetry, improving the biological degradation in composting conditions The HDPEr films submitted to composting showed a beginning of biofilm formation, with an increased mass in the 30, 40 and 50-day collection attributed to the presence of microorganisms within the polymer matrix, evaluated by optical microscopy. Until the fiftieth day of exposure to composting, the HDPEr/HDPE-AM/PVA films showed weight loss after that period, extending up to 120 days. The accumulation of water, penetrating the polymer matrix causes the swelling of the same. The HDPEr/HDPE-AM/PVA blend composition of 35/5/60 deteriorated most in 50 days of composting, with a mass loss of more than 15% from all blends, possibly due to the lower crystallinity presented associated with PVA solubility. The crystallinity index results obtained for the HDPEr/HDPE-AM/PVA blend composition of 35/5/60 were significantly lower than the polyethylene index (56%), improving the biological degradation, since biodegradation occurs preferentially in the amorphous regions.

1. INTRODUCTION

High density polyethylene is a ubiquitous material with versatile properties and it is widely used due to its mechanical strength, low cost, easy processability and resistance to chemical and biological attack (KIM, 2001). It is used extensively in many fields, including agricultural and food-packing films (HUANG, 2005). However, there has been some concern about pollution, since plastic waste accumulates in the environment, leading to long-term environmental and waste management problems. There has been an increased interest in enhancing the polyethylene biodegradability and blending it with polar biodegradable polymers such as amide, poly (vinyl alcohol)(PVA), polyhydroxylbutyrate (PHB), and poly(lactic acid)(PLA)(LEE,2002; WESTPHAL,2001). However, biodegradable polymers have unsatisfactory mechanical properties, which restrict their use or increase their cost for use in certain applications.

In this study, biofilm formation and the crystallinity index of blends prepared with post-consumer high density polyethylene (HDPEr) and PVA were evaluated. The characterization techniques used were differential scanning calorimetry(DSC) and optical microscopy(MO). Maleic anhydride grafted post-consumer polyethylene (HDPEr-AM) was used as a compatibilizer in order to obtain an HDPEr/PVA, a more suitable material with biodegradable potential after being used in agricultural lands.

EXPERIMENTAL

Recycled HDPE (HDPEr) showed Mn and Mw of 4.5 $x10^4$ and 1.5 x 10^5 Dalton, respectively. PVA with Mn and Mw of 4,060 and 85,298 Dalton, was provided by Vetec Química Fina. The compatibilizer (HDPEr-AM) (0.5wt%) was obtained by grafting reaction of maleic anhydride on HDPEr using dicumyl peroxide under N_2 atmosphere in a SEIBT single-screw extruder (L/D = 32, D = 35 mm, Fc = 2.5) with a temperature profile of 150, 160, 170 and 190ºC, 1050 rpm during 9 min.

The blending process of the polymers was carried out in molten state in the same SEIBT single-screw extruder, with a temperature profile of 180, 210, 220 and 210ºC. The PVA content in the blend varied from 20 to 80 wt% and the compatibilizer content (HDPEr-AM) was 5 or 10 wt%.

The differential scanning calorimetry(DSC) measurements were carried out in a Shimadzu DSC-50 Instruments. The samples were heated from -30 to 270˚C at a constant heating rate of 10˚C/min, two runs. The crystallinity index of the polymers was calculated using the expression (Equation 1), where X_c is the crystallinity index (%), $\Delta H_{f\ polymer}$ is the fusion enthalpy of the polymer normalized to its content in the blend, and $\Delta H_{f\ 100\%}$ is the fusion enthalpy of the hypothetical 100% crystalline polymer, 293 $J.g^{-1}$ (FU,2005) for the HDPEr and 156 $J.g^{-1}$ for the PVA (GOH,2005).

$$X_c = (\Delta H_{f\ polymer} / \Delta H_{f\ 100\%}) \times 100 \qquad (1)$$

The crystallinity index of the blend was calculated using the expression (Equation 2), where n and m are the HDPEr and PVA quantities in the blend, $X_{c\ HDPEr}$ and $X_{c\ PVA}$ are the crystallinity index of HDPEr and PVA.

$$X_{c\ mixture} = n\ .(X_{c\ HDPEr}) + m\ .(X_{c\ PVA}) \qquad (2)$$

The optical microscopy (MO) measurements were carried out using a NIKON optical microscope, model EPIPHOT 200.

The compostage where the films were placed to degrade was prepared using waste from organic matter and tree-pruning waste (80/20%), in the form of heaps (1x1x1m) and the degradation process of HDPEr and of the blends was monitored for a 120-day period.

RESULTS AND DISCUSSION

Figure 1 shows the micrographs of HDPEr and HDPEr/HDPE-AM/PVA - 35/5/60, after 10, 50 and 120 days of exposure in the compostage.

HDPEr - 10 days

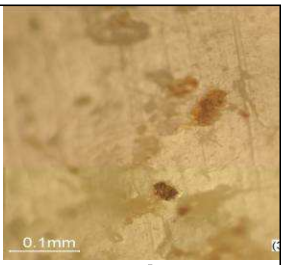

35/5/60 - 10 days

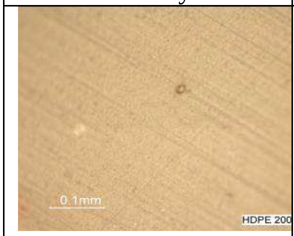

HDPEr - 50 days

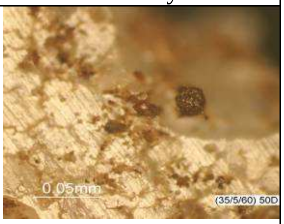

35/5/60 - 50 days

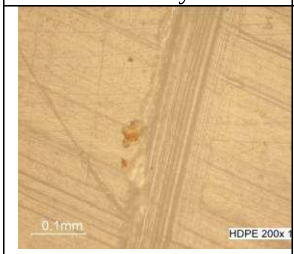

HDPEr - 120 days

35/5/60 - 120 days

Figure 1. Optical microscopy of HDPEr and of the HDPEr/HDPE-AM/PVA blend with a 35/5/60 composition after 10, 50 and 120 days of composting.

Figure 1 shows the HDPEr film with the beginning of biofilm formation, in with colonies of bacteria are established (GU, 2000). After 120 days of exposure this process is found to increas. For the HDPEr/HDPE-AM/PVA-35/5/60 blend characteristics of the polymeric surface can be visualized with biofilm formation. Removal of part of the polymeric material is seen; possibly desorption of additives and monomers out of the matrix by microbial degradation, fragility and loss of mechanical stability, which is characteristic of the attack by the enzyme from a biological source; finally, pigmentation of the surface and inside of the material, which can also be attributed to the excretion of microbial pigments (FLEMMING,1989). The removal of PVA through the action of enzymes promoted the degradation of the interface regions between the polymers, weakening the whole surface that was exposed to biodegradation.

The HDPEr/HDPE-AM/PVA - 35/5/60 blend was the most deteriorated in 50 days of composting, with the greatest mass loss of 15% of all blends, possibly due to the lower crystallinity presented associated with the solubility of PVA.

Table 1 shows the crystallinity index of the net polymers and their crystallinity index in the blends determined by DSC runs.

HDPEr/HDPEr-AM/PVA (wt %)	Xc (1°) HDPEr (%)	Xc (2°) HDPEr (%)	Xc (1°) PVA (%)	Xc (2°) PVA (%)	Xc (1°) blend (%)	Xc (2°) blend (%)
HDPEr	56.20	56.50	--	--	--	--
PVA	--	--	27.1	11.62	--	--
75/5/20	70.7	65.6	6.4	2.5	58	53
55/5/40	66.3	62.4	4.7	3.1	42	38.6
35/5/60	73.1	65.0	7.1	4.1	33.5	28.5
15/5/80	81.8	80.0	1.6	1.6	18	18

(1°) -1° Heating, (2°) - 2° Heating

Table 1. Crystallinity index of the polymers and HDPEr/HDPE-AM/PVA blends.

The crystallinity of the mixture ($X_{c\ \mathrm{mixture}}$) decreased since the PVA has very low crystallinity. This can be associated with a high intermolecular interaction between the carbonyls of the compatibilizer HDPEr-AM and the hydroxyl groups of the PVA that could nucleate and immobilize the polyethylene chains in a more favored conformation in the crystallite environmental.

CONCLUSIONS

The HDPEr films submitted to composting showed a beginning of biofilm formation, with an increased mass in the 30, 40 and 50 days, attributed to the presence of microorganisms within the polymer matrix **which was evaluated** by optical microscopy. The HDPEr/HDPE-AM/PVA-35/5/60 deteriorated most in 50 days of composting, with the greatest mass loss of 15% of all blends, possibly due to the lower crystallinity presented associated with the solubility of PVA. The crystallinity index results obtained for the HDPEr/HDPE-AM/PVA-35/5/60 was significantly lower than the polyethylene index (56%), improving the biological degradation, since the biodegradation occurs preferentially in the amorphous regions.

REFERENCES

FU,Q.; BING,N.;WANG,K.; ZHANG, Q.;RONHNI,D.(2005)- Polymer,v.46, p.3190-3198.

GOH,S.; YI,H.; (2005) - Polymer, 46, p.9170-9175.

GU. J.D.(2000) – Microbial deterioration and degradation of polymeric materials in: Renie, W. (Ed). The uhlig corrosion handbook, 2nd, Edition, Wiley, New York, p. 439-460.

FLEMMING H.C.(1989) – Relevance of biofilms for biodeterioration of surfaces of polymeric materials – Polymer Degradation and Stability, 59, p. 309-315.

HUANG, C.Y.;ROAN, M.L.;KUO, M.C .;LU,W.L. (2005) - Polymer Degradation and Stability v.90, p.95-105.

KIM,J.H.;SHIN,T,K.;CHOI, H.J..JHON. M.S .(2001) - *European Polymer Journal* v.37, p.2131-2139.

LEE, J.A.;KIM, M.N. (2002) – J. of Polymers and the environment, v.9, p.91-95.

WESTPHAL,C.;PERROT,C.;KARLSSON.S.(2001)- Polymer Degradation and Stability, v.73, p. 281-287.

Improvement of the interfacial adhesion of plasticized PVC filled with natural fillers

J. Balart, L. Sánchez-Nacher, O. Fenollar, D. García-Sanoguera
Materials Technology Institute (ITM) Polytechnic University of Valencia (UPV), Plaza Ferrándiz y Carbonell, sn, 03801, Alcoy, Alicante, Spain - dagarsa@dimm.upv.es

ABSTRACT

The aim of this work is improve the interfacial adhesion between the plasticized PVC matrix and fibres coming from agave Americana by using plasma technology. Different plasma processing variables were used in order to establish the optimum treatment conditions. The plasma treatment promotes the surface activation of natural fibres and by this way, an increase in the interfacial adhesion polymer-filler has been achieved and consequently an improvement of mechanical properties.

1. INTRODUCTION

In the last years, the use of natural fibres as reinforcement in both thermoplastic and thermosetting matrix composites is increasingly replacing the conventional inorganic fibres. Especially, natural fibre reinforced thermoplastics have a good potential in the future as a substitute for wood-based material in many applications (Van de Velde, et al. 2002). The development of bio-based composites is because of natural fibres biodegradability, light weight, low cost, high specific strength compared to glass and carbon, recycling and renewing natural sources of plants such as coir, sisal, jute, Agave Americana, kenaf, flax, ramie, abaca, kapok, hemp.... (Doan, et al. 2006; Rana, et al. 1998).

Agave Americana is a monocotyledon plant, which belongs to the amaryllidaceae family. The basic fibre of Agave American is hard and is derived from the leaf structure of the plant (Jaouadi, et al. 2009). The organic matrix is composed by hemicelluloses, pectin matter, lignin and gums and the reinforcing fibres are mainly composed of cellulose. Cellulose fibres extracted from Agave Americana is characterized by a lower lignin content value and a high humidity absorption.

On the other hand interfacial behaviour between the fibres and polymer matrices has long been recognised as a key factor influencing the overall properties of composite materials (Crespo, et al. 2008; El Oudiani, et al. 2009). Fibre-matrix interfacial phenomena is an important factor that determine the main mechanisms of damage accumulation and propagation (Gassan, et al. 1999). The use of coupling or compatibility agents, which are reacted or deposited onto the fibre or in some cases into the polymer is a commonly technique to improve the fibre-matrix adhesion. On the other hand the physical surface activation by electric discharge (corona, cold plasma) is other popular technique for surface oxidation and activation by changing the surface energy of the cellulose fibres increasing its wettability (Rana, et al. 2003). However due to the high instability of the species generated during and after the plasma treatment, hydrophilic properties achieved by the plasma treatment are rapidly lost (Bhat, et al. 2002). This process is well known as “hydrophobic recovery” and represents a significant restriction for storage of fillers.

2. EXPERIMENTAL

Mechanical properties have been determined by tensile test. The tensile tests were carried out using a universal tensile test machine ELIB 30 (S.A.E. Ibertest, Madrid, Spain) following ISO 527. A 20 mm min^{-1} crosshead speed was used to obtain the tensile graph with a load cell of 5 kN. All specimens were tested at room temperature and a minimum of five samples were analyzed and average values of tensile strength and elongation at break were calculated. SEM photographs of different samples were carried out by a scanning electron microscopy JEOL 6300 (JEOL USA Inc., Peabody, USA). Samples were previously coated with gold, the coating process was performed in vacuum conditions. The fracture surfaces observed were obtained in the different tensile tests at room temperature.

3. RESULTS AND DISCUSSION

In this work we have use a new type of plasma treatment to activate the fibre surface and by this way improve the interfacial adhesion between plasticized PVC and the cellulosic fibre. The results obtained demonstrate that the plasma treatment conditions determine the behaviour of the composite. In any case the plasma treatment increases the mechanical performance of composite by improving the interaction between filler and polymer matrix.

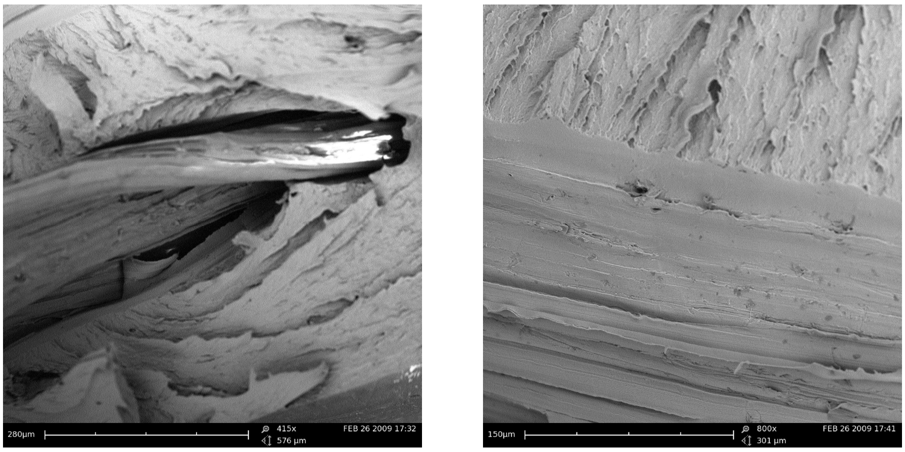

a) b)

Fig. 1. **SEM microphotographs of fracture surfaces vinyl plastisols with a 10% of Agave Americana fillers. a) No plasma-treated fibre, b) Plasma-treated fibre.**

Fig. 1a shows a SEM micrograph of composite without plasma treatment, while Fig. 1b shows a SEM micrograph of composite using the cellulosic fibre treated with atmospheric plasma. As can be observed the interfacial adhesion is higher with the sample plasma treated.

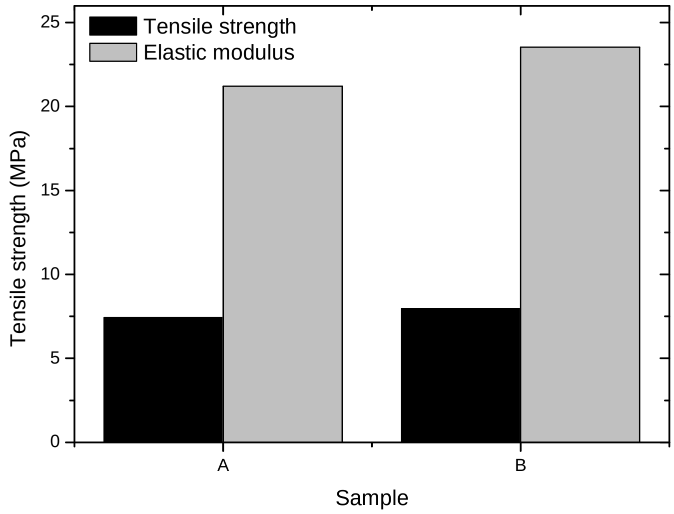

Fig. 2. Variation of tensile strength and elastic modulus for samples of plasticized PVC with 2 wt% of Agave Americana fibre: a) treated with plasma; b) without treatment.

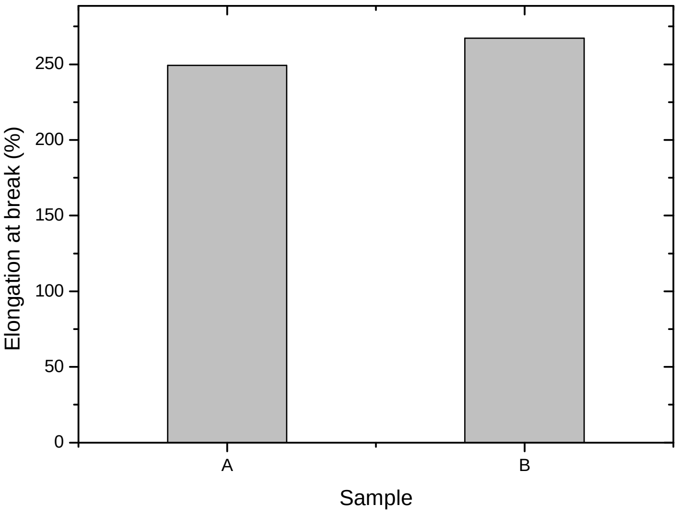

Fig. 3. Variation of elongation at break for samples of plasticized PVC with 2 wt% of Agave Americana fibre: a) treated with plasma; b) without treatment.

Regarding to mechanical properties in Fig 2 can be observed the variation of tensile strength and elastic modulus for samples of plasticized PVC with 2 wt% of Agave Americana fibre with and without atmospheric plasma treatment. Both tensile strength and elastic modulus increase with the plasma treatment.

Fig 3 shows the variation of elongation at break for samples of plasticized PVC with 2 wt% of Agave Americana fibre with and without atmospheric plasma treatment. As previous properties, elongation at break increases with the plasma treatment. These results confirm that the mechanical properties are strongly associated with the interfacial adhesion between fibre and polymer matrix.

4. CONCLUSIONS

The results obtained in this study demonstrate that the atmospheric plasma treatment increase the interfacial adhesion between Agave Americana fibre and polymer matrix. This interfacial adhesion improvement promotes an increase in the mechanical properties both resistant and ductile.

ACKNOWLEDGEMENTS

Authors thank “Ministerio de Ciencia y Tecnología”, Ref: DPI2007-66849-C02-02 and “Ministerio de Ciencia e Innovación”, Ref: CIT-020000-2008-14 for financial support.

REFERENCES

BHAT, N.V.; UPADHYAY, D.J. (2002). Plasma-induced surface modification and adhesion enhancement of polypropylene surface. *J. Appl. Polym. Sci.*, 86, 925-936.

CRESPO, J.E.; SANCHEZ, L.; GARCIA, D.; LOPEZ, J. (2008). Study of the mechanical and morphological properties of plasticized PVC composites containing rice husk fillers. *J. Reinf. Plast. Compos.*, 27, 229-243.

DOAN, T.T.L.; GAO, S.L.; MADER, E. (2006). Jute/polypropylene composites I. Effect of matrix modification. *Compos. Sci. Technol.*, 66, 952-963.

EL OUDIANI, A.; SGHAIER, B.; MSAHLI, S.; CHAABOUNI, Y.; SAKLI, F. (2009). Elastic Recovery and Viscoelastic Behavior of Agave americana L. Fibers. *Text. Res. J.*, 79, 166-178.

GASSAN, J.; BLEDZKI, A.K. (1999). Possibilities for improving the mechanical properties of jute epoxy composites by alkali treatment of fibres. *Compos. Sci. Technol.*, 59, 1303-1309.

JAOUADI, M.; M'SAHLI, S.; SAKLI, F. (2009). Optimization and Characterization of Pulp Extracted from the Agave Americana L. Fibers. *Text. Res. J.*, 79, 110-120.

RANA, A.K.; MANDAL, A.; BANDYOPADHYAY, S. (2003). Short jute fiber reinforced polypropylene composites: effect of compatibiliser, impact modifier and fiber loading. *Compos. Sci. Technol.*, 63, 801-806.

RANA, A.K.; MANDAL, A.; MITRA, B.C.; JACOBSON, R.; ROWELL, R.; BANERJEE, A.N. (1998). Short jute fiber-reinforced polypropylene composites: Effect of compatibilizer. *J. Appl. Polym. Sci.*, 69, 329-338.

VAN DE VELDE, K.; KIEKENS, P. (2002). Biopolymers: overview of several properties and consequences on their applications. *Polym. Test*, 21, 433-442.

T6. NANOCOMPOSITES

Compatibility of block copolymer/nanoparticle blends depending on block copolymer architecture

M. R. Bockstaller[1], A. Avgeropoulos[2], J. Listak, I. F. Hakem, H. Ju Ryu, S. Rangou[2], N. Politakos[2], K. Misichronis[2]
[1]Department of Materials Science and Engineering, Carnegie Mellon University, 5000 Forbes Ave., Pittsburgh, PA 15213, USA
[2]Department of Materials Science and Engineering, University Campus-Dourouti, University of Ioannina, Ioannina 45110, Greece

ABSTRACT

The effect of block copolymer chain connectivity on the structure formation in binary blends comprising block copolymer hosts and enthalpically neutralized particle fillers is investigated for linear di- (AB) and triblock (ABA and BAB) as well as four-arm star copolymer architectures (AB_3 and A_3B). For particles with approximately constant effective size (defined here as the ratio of filler particle diameter to host polymer radius of gyration), miscibility was observed only within diblock copolymers and within the domains formed by the endblocks of triblock copolymers. The limitation of particle miscibility within the triblock mid-domain is interpreted as a consequence of the entropy loss associated with particle deposition due to the stretched configuration of bridged midblock chains (direct constraint). Particle aggregation was observed in both star-copolymer samples irrespective of the architecture of the particle-loaded polymer domain. In the case of particle-loading of the branched copolymer domain, this is rationalized as a consequence of the increased effective particle size (direct constraint), whereas the incompatibility of particle fillers in the linear block domain of miktoarm copolymer hosts is interpreted as a result of the reduced compressibility of the particle-free star-domain along with the coupling of conformational changes within the microstructure (indirect constraint). The sensitive dependence of the particle compatibility on the chain architecture of the polymer host illustrates a yet unexplored parameter space that will need to be taken into account if particle blends are to be designed with branched or multiblock host copolymer architectures.

1. INTRODUCTION

In this contribution we present a systematic study of the implications of block copolymer chain architecture on the compatibility of nanoparticle fillers that are enthalpically neutralized to one of the copolymer domains. Three types of copolymer architecture have been explored in order to understand the effect of chain connectivity and branching on the segregation of particle fillers: linear diblock (AB), triblock (ABA, BAB) and four-arm star (A_3B, AB_3) copolymers. The materials in the present study are based on polyisoprene (PI) and polystyrene (PS) block composition and oligostyrene-functionalized gold nanoparticles (AuPS, core diameter $d_{\mathrm{core}} \cong 2.8$ nm, cumulative particle core and shell diameter $d_{\mathrm{P}} \cong 3.8$ nm) as enthalpically neutralized additives to the PS domain. Block copolymer compositions and molecular weights were chosen such as to facilitate lamellar (*L*) and cylindrical (*C*) microdomain structures and similar values of the effective particle size parameter $s \cong 0.5$ for all BCP/NP blends. This rather large value of s (previous studies were focused on $s \sim 0.1$-0.3) was chosen based on the expectation that the implications of constraining effects related to chain connectivity increase with particle size. For all samples the particle concentration was chosen to be $c_P = 1$ wt. % (corresponding to a net particle volume filling fraction $\phi_P \cong 0.005$, including the volumes of both particle core and shell) in order to neglect effects related to changes of the overall polymer composition. The different polymer architectures used in the present study are illustrated in Figure 1.

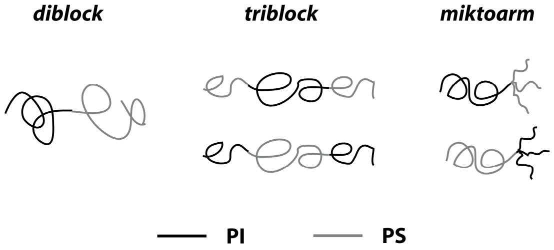

Figure 1. Polymer architectures used for incorporation of Au nanoparticles.

2. EXPERIMENTAL SECTION

A series of lamellar and cylindrical diblock (SI) and triblock (SIS and ISI) copolymers with approximately constant block molecular weight were mixed with polystyrene or polyisoprene coated gold nanoparticles (AuPS or AuPI). Block copolymer characteristics are described in Table 1. Various molecular characterization methods were adopted for verification of successful synthesis such as: size exclusion chromatography (SEC), membrane osmometry (MO), vapor pressure osmometry (VPO) and proton nuclear magnetic resonance spectroscopy (^{1}H-NMR). The synthesis of thiol-terminated oligostyrene ligands (degree of polymerization $N_{PS} \sim 10$) using anionic polymerization as well as the synthesis of oligostyrene-capped gold particles was performed using a modification of the phase-transfer technique developed by Schiffrin et al. [Bockstaller et al. 2001 and Schiffrin et al. 1994]. The average particle diameter (*i.e.* the cumulative diameter of particle core and shell) was determined to be $d_P \cong 3.8$ nm. Particle solutions were filtered through membrane filters (0.25 μm pore diameter) prior to use. Particle size analysis for each BCP/NP composition was performed by analyzing about 1000 particles for at least five different electron micrographs per sample using the NIH ImageJ software that is available for free at http://rsbweb.nih.gov/ij/download.html.

Transmission electron microscopy (TEM) was performed in thin sections from specifically prepared annealed films using a JEOL 2000 EX electron microscope operated at 200 kV. Imaging was done by amplitude and phase contrast, and images were acquired using a Gatan Orius SC600 high resolution camera.

3. RESULTS AND DISCUSSION

Our experiments reveal that particle compatibilization depends on the architecture of both the particle-loaded and the particle-free domain. The mutual relevance of the architecture of both domains is interpreted in terms of *direct* and *indirect* constraints that relate to constraining effects due to the connectivity of the particle-loaded domain and to the coupling of dimensional changes that is implied by the covalent linkage between the two blocks. The results thus point to a more complicated parameter space for controlling structure formation in BCP/NP blends that will need to be taken into account if the particle-blending approach is to be applied to copolymer hosts with branched or multiblock architectures.

Linear di- and triblock copolymer architectures. Figure 2a depicts the cross-sectional electron micrographs for the lamellar SI-*L*/AuPS system revealing that particles are single dispersed within the PS domain, as can be deduced from the average particle diameter that is approximately equal to the neat particle size. A trend is observed for larger particles to segregate within the domain center regions in agreement with previous reports on BCP/NP systems.

Table 1. Molecular characteristics of the copolymers synthesized and the characteristic size (s).

Sample	$(\bar{M}_n)^a_{1^{\text{st}}\text{ arm}}$ (kg/mol)	$I^b_{1^{\text{st}}\text{ arm}}$	$(\bar{M}_n)^a_{\text{total}}$ (kg/mol)	I^b_{total}	$(\phi_{PS})^d_{copolymer}$	s^e
SI-*L*	45.8	1.03	71.5	1.10	0.61	0.57
SIS-*L*	26.0	1.02	93.0	1.05	0.48	0.77
ISI-*L*	24.5	1.05	98.5	1.05	0.46	0.56
I$_3$S-*L*	41.8	1.02	87.6	1.06	0.48	0.58
IS$_3$-*L*	43.2	1.02	85.3	1.06	0.45	1.04
SI-*C*	75.8	1.06	94.1	1.09	0.77	0.44
SIS-*C*	42.6	1.02	94.4	1.06	0.76	0.60
ISI-*C*	14.2	1.03	102.5	1.08	0.72	0.45

[a] Membrane osmometry (MO) in toluene at 35°C. [b] Size Exclusion Chromatography (SEC) in THF at 35°C. [c] Using the equation: $f(PS)_{\text{copolymer}} = \frac{M_n(\text{PS})}{\bar{M}_{n\,\text{copolymer}}}$. [d] Volume fraction based on ^{1}H-NMR values using the equation: $\phi_{PS,\text{ copolymer}} = \frac{f_{PS}\,\rho_{PI}}{f_{PS}\,\rho_{PI} + [1-f_{PS}]\rho_{PS}}$ ($\rho_{\text{PS}} =$ 1.06 g/ml, $\rho_{\text{PI}} =$ 0.93 g/ml). [e] $s = d_{\text{AuPS}}/R_{\text{G,PS-block}}$

ABA-type triblock copolymers differ from the diblock homologues in that the midblock is tethered at both ends, and thus – due to the covalent linkage – must assume either looped or bridged conformations in the microphase separated state. The effect of chain architecture in linear multiblock copolymers is shown in Figure 2b, which depicts electron micrographs of the SIS-*L* and ISI-*L*/AuPS systems. Analysis of the particle size distributions reveals that particles are single dispersed within SIS-*L*, and – analogous to SI-*L* – larger particle sizes are found to preferentially segregate within the center region of PS domains. In contrast, particle aggregation is observed for the ISI-*L*/AuPS system where an average aggregate size of $d_{\text{ISI}} \cong 12.1$ nm suggests clustering of about 32 individual nanocrystals (assuming spherical aggregate shape).

Miktoarm star copolymer architectures. Star-copolymer architectures differ from their linear homologues in both constitutional and conformational asymmetry that results in a shift of the morphological stability regions as compared to linear block copolymers. Figure 2c depicts electron micrographs of the SI$_3$-*L*/AuPS and S$_3$I-*L*/AuPS systems, revealing particle aggregation in both miktoarm samples irrespective of the architecture of the particle-bearing polymer domain. The average diameter of particle aggregates is found to be similar (and about equal to the PS-layer thickness), *i.e.* $d_{\text{SI3-}L} \cong d_{\text{S3I-}L} \cong 18$ nm, suggesting the clustering of about 106 nanocrystals per aggregate. We rationalize the reduced compatibility of particle fillers within the S_3I-*L*/AuPS system to be a consequence of the large effective particle size $s \cong 1$ that implies a significant penalty in conformational entropy if particles are to be accommodated by the polymer chains. This effect is expected to be more pronounced in star polymer systems where segmental crowding in the vicinity of the interface results in stretching of the polymer chains.

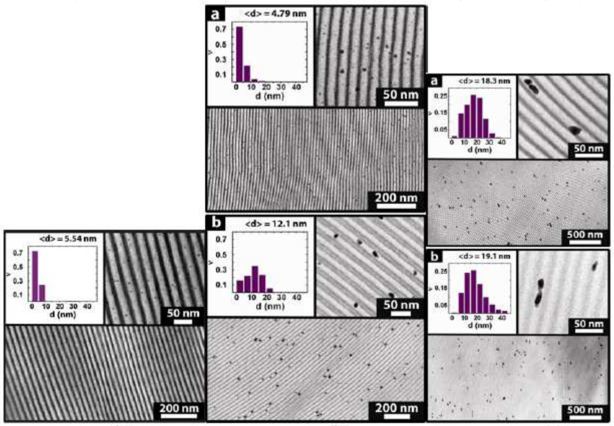

(a) (b) (c)

Figure 2. (a). Electron micrograph of the SI-*L*/AuPS, (b). Electron micrographs of triblock copolymer/particle [a: SIS-L/AuPS and b: ISI-L/AuPS] and (c). Electron micrographs of the SI_3-*L*/AuPS (panel a) and S_3I-*L*/AuPS (panel b). In each case the inset depicts the particle size distribution (y denotes the frequency) and the right inset shows a magnified area element.

4. CONCLUSIONS

The compatibility of enthalpically neutralized particle fillers with effective size $s \cong 0.5$ has been found to sensibly depend on the architecture of block copolymer host materials. For linear triblock copolymers, the connectivity of the midblock domain extends a *direct* constraint impeding particle sequestration that has been interpreted as a consequence of the entropy loss associated with the accommodation of particle fillers due to the stretched configuration of bridged midblock chains. For four-arm star-copolymers, both *direct* and *indirect* constraints associated with the characteristic dimension, *s*, and the mutual dependence of conformational changes due to the covalent linkage are proposed as rationale for the observed particle aggregation. In summary, our results point to a more complicated parameter space for controlling structure formation in BCP/NP blend systems that will need to be taken into account if the particle-blending approach is to be applied to branched or multiblock copolymer architectures.

ACKNOWLEDGEMENTS

Financial support by the National Science Foundation via grant DMR0706265, the MRSEC program of the National Science Foundation under Award Number DMR-0520425 (MB) as well as by the Greek Secretariat for Research & Development through the bilateral project 05-NONEU-229 handled by the Research Committee from the University of Ioannina (AA) is gratefully acknowledged.

REFERENCES

Bockstaller, M. R.; Kolb, R.; Thomas, E. L. *Adv. Mater.* **2001**, 13, 1783.

Brust, M.; Walker, M.; Bethell, D.; Schiffrin, D. J.; Whyman, R. *J. Chem. Soc. Chem. Commun.* **1994**, 801.

Preparation and conductive properties of graphite/polymer nanocomposites

R. Quintero Restrepo, K. Nagata, M. Higuchi
Department of Materials Science and Engineering, Graduate School of Engineering,
Nagoya Institute of Technology, Japan
T. Kinoshita
Department of Frontier Materials, Graduate School of Engineering,
Nagoya Institute of Technology, Japan

SUMMARY

Two different kinds of isocyanate functionalized graphite oxide are prepared and used in the processing of polymer nanocomposites by solution blending method. XRD and FT-IR techniques are used to characterize the modified graphite oxide and the results show the incorporation of new functional groups into the structure. Thermal and electrical properties at different filler loads are studied with TGA and electrical volume resistivity measurements respectively. The results suggest a good dispersion of graphite sheets into the polymer matrix that leads to the improvement of thermal stability and a formation of an electrical conductive network with low filler content.

1. INTRODUCTION

Within the field of functional materials, electrical conductive composites with low percolation threshold are the aim of many recent semiconductor researches (Chen et to. 2002). Graphene, defined as individual 2-D graphite sheets made of sp^2-bonded carbon atoms have special electronic, thermal and mechanical properties, giving it many possibilities as a filler in composites. However, graphene is only available after overcoming the strong van der Waals attractive forces present in natural graphite. Graphite oxide and its affinity to water has proved to be an effective way to separate the sheets in the form of stable aqueous solutions, however, it's poor compatibility with organic solvents doesn't allow to use it in conjunction with general organic materials.
In this study, graphite oxide was treated with isocyanate (iGO) in order to improve its compatibility with organic solvents and achieve a good dispersion of the individual graphene nanosheets within a polymer matrix in solution (Stankovich et to. 2006). After blending and reducing the oxidized sheets, the resulting composite's electrical and thermal properties were studied in order to determine the influence of the isocyanate types.

2. MATERIALS AND METHODS

Graphite oxide (GO) was prepared from Expanded graphite (ITO Co., JP, average particle size=5μm) following the Hummers method (Hummers et to, 1958). Expanded graphite was stirred in concentrated H_2SO_4 for 24 hrs, then $KMnO_4$ was added slowly keeping the temperature below 20°C. The mixture was heated till 35°C for 1 hr and H_2O_2 was added to terminate the reaction. The product was washed with 10% aqueous solution and distilled water, centrifugated and freeze-dried (EYELA, FD-5N).

The isocyanate treating step was carried out by mixing, under N_2 atmosphere, graphite oxide 50 mg with isocyanate 2mmol (Tokyo Kasei Kogyo Co., Ltd.) in *N,N*-dimethylformamide (DMF), and stirring for 24 hrs. The solution was poured into dichloromethane (DCM), filtrated, washed with DCM and dried in vacuo for 12 hrs.

n-Propyl Isocyanate

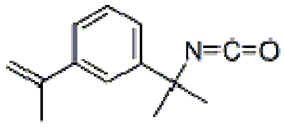

3-Isopropenyl-*α*,*α*-dimethyl benzyl Isocyanate

The characterization was made through FT-IR (Jasco FT/IR-460 plus) and XRD (Rigaku, RINT X-Ray Difractometer) techniques.

The composite blending was performed by adding iGO to DMF in a 1 mg/ml ratio. Polystyrene (PS Japan Corp.) was then added and dissolved by magnetic stirring. In order to reduce the iGO, the solution was heated to 80 °C and Hydrazine (Sigma-Aldrich, 30%) was added in a 1 ml/gram of iGO ratio. The mixture was poured into methanol, filtrated, washed with additional methanol and dried in vacuo. The composite was milled into powder and hot-pressed at 255 °C and 2.2 MPa for 15 min. Silver conductive paint was applied on the surface of the samples to improve the contact with the electrodes. Thermogravimetric analysis (TGA) was carried out by using a Seiko Instruments TG/DTA220. The temperature was ramped from 27 °C - 600 °C at a rate of 10 °C/min. Electrical volume resistivity measurement was performed on Advantest R8340A Ultra High Resistance Meter.

3. RESULTS AND DISCUSSION

The XRD pattern (Fig.1) shows that the sharp peak for graphite appeared at 24.6°, corresponding to a *d*-spacing of 3.34 Å. It can be seen in the pattern for the treated graphite oxide that a new peak appeared at 9.1°, corresponding to an increased *d*-spacing of 9.71 Å and the previous peak at 24.6° is absent.

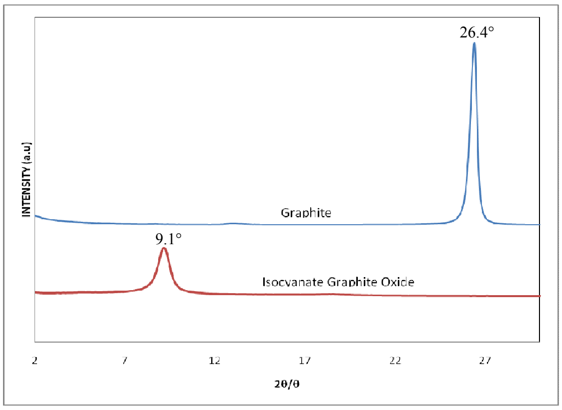

Fig. 1. XRD patterns of Graphite and Isocyanate Graphite Oxide.

The FT-IR spectra (Fig. 2) show the peaks corresponding to the functional groups present in the original GO and in the modified iGOpropyl and iGObenzyl. The 1719 cm^{-1} stretching and the 1614 cm^{-1} bending on the GO pattern correspond to –C=O and -O-H groups. The vibrations in the 1630 cm^{-1} – 1480 cm^{-1} interval on the iGO paterns can be assigned to amides (I, II) groups and carbamates. Additional aromatic stretching is present for iGObenzyl in the 1530 cm^{-1}-1450 cm^{-1} interval due to C-C stretching and in 794 cm^{-1} due to C-H bending.

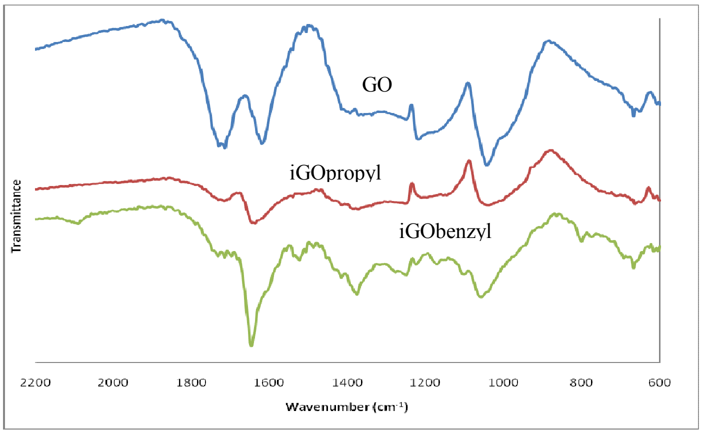

Fig. 2. FT-IR spectra of GO, iGOpropyl and iGObenzyl.

Figure 3 shows the TGA curves for PS and PS/iGO composites. Compared with the one of PS, it can be seen a significant improvement in thermal stability of composites as the degradation temperature becomes higher, even for the smallest load of 0.5 wt.%. This effect is attributable to a good dispersion of graphite layers inside the polymer matrix, which provides chemical and physical stability at high temperature due to the refractory properties of graphite.

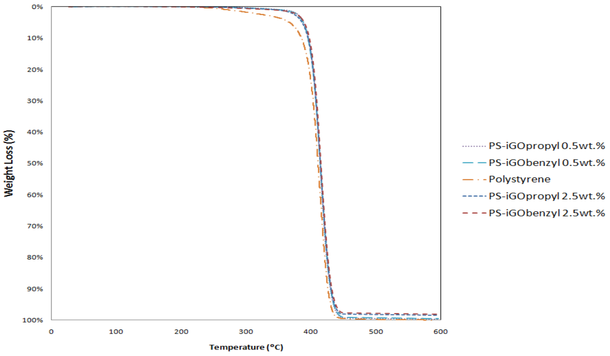

Fig. 3. TGA curves of PS, PS/iGOpropyl and PS/iGObenzyl nanocomposites.

Electrical resistivity measurements of PS/iGO composites are shown in Figure 4. The volume resistivities of iGOpropyl filled composites were overall lower than those of iGObenzyl. With a 0.5 wt.% load, the material exhibited a value of $2x10^7$ Ω cm.

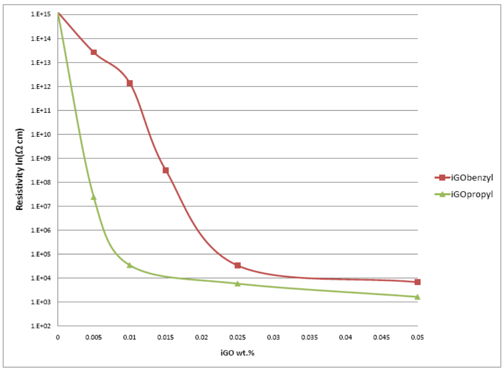

Fig. 4. Electrical resistivity measurements of PS/iGO composites.

4. CONCLUSIONS

The thermal and electrical behavior of the PS/iGO composites showed a combined interaction effect: first, between the iGO and the organic solvent and second, between iGO and the polymer matrix. The aliphatic isocyanate treated GO could form a conductive network within the polymer with a smaller load. At larger filler ratios, the difference between volume resistivity of PS/iGOpropyl and PS/iGObenzyl became smaller.

REFERENCES

CHEN, X., SHEN, J., HUANG, W. (2002) Novel electrically conductive polypropylene/graphite nanocomposites, *J. Mater. Sci. Let.*, 21, 213-214.

HUMMERS, W., OFFEMAN R. (1958) Preparation of Graphitic Oxide, *J. Am. Chem. Soc.,* 80, 1339.

STANKOVICH, S. (2006) Graphene-based composite materials, *Nature*, 442, 282-286.

Mezclas sinérgicas de nanocargas y aditivos ignífugos convencionales para la mejora al fuego de materiales termoplásticos

S. Fita, I. Buezas, V. Martínez
Instituto Tecnológico del Plástico - AIMPLAS, Valencia, España
A. González-García, P.P. Martín
Boeing Research & Technology Europe, S.L., Madrid, España

RESUMEN

El objetivo principal de este trabajo es la ignifugación de un polipropileno copolímero mediante la combinación de aditivos intumescentes y nanoarcillas, para la obtención de materiales con alta resistencia al fuego que puedan ser utilizados en aeronáutica.

En lo que respecta al procesado de los distintos *compounds*, la adición de nanoarcillas mejoró el flujo de los compuestos y la calidad superficial de las láminas obtenidas a partir de ellos, frente a los que contenían solamente aditivos intumescentes convencionales.

En relación a las propiedades ignífugas de las láminas extruidas, la resistencia al fuego dependió del tipo y porcentaje de nanoarcilla añadida. Además, el uso de nanoarcillas permitió reducir la cantidad de aditivos necesaria para poder alcanzar la clasificación V0.

1. INTRODUCCIÓN

El uso de materiales termoplásticos en aplicaciones aeronáuticas está sujeto a una estricta normativa en lo que respecta a su comportamiento frente al fuego. Debido a la naturaleza orgánica de la matriz, es necesario utilizar retardantes de llama. Por razones de toxicidad, el uso de compuestos halogenados se está limitando en la mayor parte de sectores industriales (Directive 2002/95/EC) siendo reemplazados por sistemas libres de halógenos, si bien, con menor efectividad que los basados en bromo y/o cloro. Entre ellos, unos de los más efectivos son los sistemas intumescentes. Ejemplos son el polifosfato de amonio (APP), que durante la combustión forma una capa carbonosa que protege al material, o el grafito expandible, que combinado con el APP puede mejorar las propiedades ignifugantes de las poliolefinas (Xie et al., 2001).

El tamaño de la partícula es un parámetro estructural importante de los aditivos ignífugos, que no sólo afecta a las propiedades ignífugas del material sino también a las propiedades mecánicas y de fluidez de los composites (Giannelis et al, 1998). A menor tamaño de la partícula mejor dispersión de la carga y por lo tanto, mejores propiedades ignífugas. Las nanoarcillas son una nueva clase de materiales que, utilizadas en pequeñas cantidades (0.5 - 5%), adecuadamente dispersadas en la matriz y combinadas junto con los agentes compatibilizantes apropiados, permiten aumentar las propiedades ignífugas del material (Suárez et al. 2006). De las posibles nanoestructuras (Morgan 2006), es la exfoliada la más interesante porque presenta la mayor área superficial expuesta al polímero, mejorando la interacción polímero-carga y, en consecuencia, las propiedades ignífugas del material. Durante la combustión, las nanoarcillas crean una estructura carbonosa tridimensional que evita el goteo del material.

Los copolímeros de bloque o heterofásicos del polipropileno presentan una elevada fluidez (Moore, 1996) lo que los hace muy adecuados para aceptar grandes cantidades de carga y, por lo tanto, convertirlos en compuestos ignífugos.

2. EXPERIMENTAL

2.1 Materiales

Los composites fueron elaborados a partir de un copolímero de bloque, PP ISPLEN PB 180 G2M (REPSOL YPF). Para mejorar la compatibilidad con los retardantes a la llama se utilizó un anhídrido maleico, INTEGRATE NP 570-030 (Equistar Chemicals). Los sistemas intumescentes han sido un polifosfato amónico, BUDIT 3167 (Budenheim Ibérica Comercial) y un grafito expandible, Ex JF300-50N BIC (NGS Naturgraphit GMBH). Las nanopartículas seleccionadas fueron tres nanoarcillas de estructura exfoliada presentadas en forma de masterbatch de PP (FERRO SPAIN): Masterbatch B1 con un 40 % de nanoarcillas, Masterbatch B2, con un 20 % de nanoarcillas de distinta naturaleza al B1 y Masterbatch B3, que contiene el mismo tipo de nanoarcillas que E2 pero una concentración del 30%.

Todos los porcentajes reseñados son porcentajes en peso.

2.2. Preparación de los compounds

Se añadieron distintas cantidades de agentes intumescentes a la matriz de polipropileno. Se tuvieron en cuenta aspectos como la dispersión de las cargas y las propiedades ignífugas para evaluar la adecuación de las distintas composiciones. Los respectivos *compounds* fueron procesados mediante una extrusora Coperion de doble husillo de 25 mm. En la tabla 1 se muestran las composiciones preparadas.

Muestra	**Composición (%)**						
	PP	**anhídrido maleíco**	**polifosfato amónico**	**Grafito**	**Master B1**	**Master B2**	**Master B3**
1	36	4	50	10	----	----	----
2	51	4	40	5	----	----	----
3	46	4	40	10	----	----	----
4	40	----	50	10	----	----	----
5	36.8	----	46	9.2	8	----	----
6	36	----	45	9	10	----	----
7	33.6	----	42	8.4	----	16	----
8	32	----	40	8	----	20	----
9	20	----	50	10	----	20	----
10	24	----	50	10	----	----	16
11	20	----	50	10	----	----	20

Tabla 1. Composición intumescente para el PP heterofásico.

2.3 Obtención de las láminas

Los *compounds* fueron obtenidos mediante el proceso de extrusión de lámina plana. Para ello se utilizó una extrusora Collin monohusillo, de diámetro 25 mm y una relación L/D = 25.

2.4 Determinación del comportamiento frente al fuego.

Para evaluar la inflamabilidad de las distintas láminas se aplicó el Test de Inflamabilidad Vertical según la norma UL 94. Este test es el más restrictivo dentro de esta norma. Los materiales se pueden clasificar como V-0, V-1 o V-2, siendo la clasificación V-0 la que representa un mayor grado de ignifugación de las muestras. Las probetas fueron obtenidas mediante el troquelado de las láminas procesadas.

3. RESULTADOS Y DISCUSIÓN

3.1 Procesado de los *compounds*

En la figura 1 se muestran los valores de la presión y el torque implicados en la preparación de las distintas mezclas a partir del PP y los aditivos ignífugos.

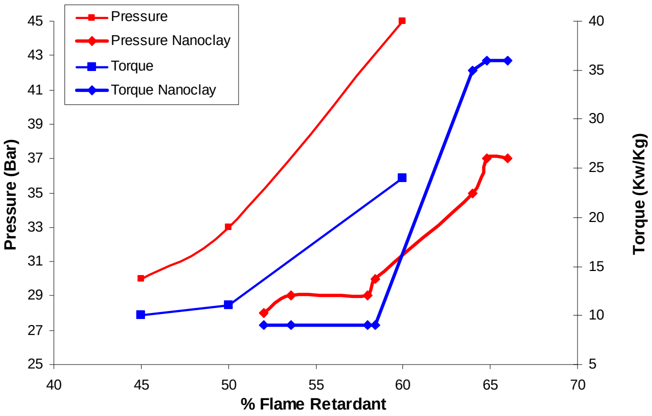

Figura 1. Presión y torque para el procesado de los distintos compounds.

Como puede observarse, al aumentar la cantidad de aditivos intumescentes y grafito, se produce un aumento de la presión en la boquilla de extrusión, asociado a una disminución progresiva de las propiedades de flujo. La adición de nanocargas permite reducir la viscosidad de las mezclas aunque necesitan de un mayor torque que las muestras que no las contienen. De esta manera se concluye que las nanocargas mejoran el flujo de los aditivos intumescentes convencionales. Sin embargo, para niveles de nanocargas superiores, la adición de un masterbatch más concentrado da lugar a una reducción en el índice de fluidez (MFI). En la tabla 2 se muestran los MFI de los distintos compounds, medidos a 190ºC y con una carga aplicada de 5 kg.

Muestra	1	2	3	4	5	6	7	8	9	10	11
MFI (g / 10 min)	5.13	9.93	9.05	6.78	14.29	14.04	13.55	15.68	6.58	3.85	3.41

Tabla 2. Índices de fluidez de las muestras ignifugadas

3.2 Obtención de las láminas

Las muestras obtenidas con aditivos ignífugos convencionales muestran una superficie rugosa en ambos lados de las láminas, debido probablemente a una mala distribución del flujo polimérico en el cabezal de la extrusora. Al añadir las nanocargas, aumenta el MFI del *compound*, mejorando la procesabilidad y el aspecto superficial de las láminas.

3.3 Comportamiento al fuego

En la tabla 3 se clasifican los *compounds* según el test de inflamabilidad vertical (UL94).

Muestra	1	2	3	4	5	6	7	8	9	10	11
Clasificación	V0	V2	V2	V0	V2	V0	V0	V2	V0	V0	V0

Tabla 3. Clasificación al fuego según el test de inflamabilidad vertical (UL94).

Como puede observarse, en el caso de los compounds ignifugados de forma convencional, la mejor clasificación frente al fuego se obtiene para las muestras con un 50 % de BUDIT 3167 y un 10 % de grafito expandible. En general, la adición de nanoarcillas da lugar a buenos grados de ignifugación a excepción de las muestras en las que el contenido en Master B1 fue del 8 % o en aquella en la que el contenido en Master B2 es del 20 % pero con menor porcentaje de cargas ignífugas convencionales.

4. CONCLUSIONES

La adición de bajas concentraciones de nanoarcillas exfoliadas sobre los compounds de PP ignifugados con aditivos convencionales, reduce la viscosidad de las mezclas. Esto facilita el procesado de las mismas mediante extrusión, mejorando de esta manera el aspecto superficial de las láminas obtenidas. El efecto de las nanoarcillas sobre las propiedades ignífugas de las muestras tratadas con aditivos ignífugos convencionales depende tanto del tipo como de la cantidad añadida. Todo apunta a que la adición de un mayor porcentaje de nanocargas mejora las propiedades ignífugas de los materiales, a excepción del Masterbatch B2 que al ser menos concentrado parece que diluya la muestra de tal forma que se reduzca su resistencia al fuego.

AGRADECIMIENTOS

Proyecto financiado por el CDTI dentro de las ayudas del subprograma aeroespacial, del programa nacional de proyectos de investigación aplicada 2008.

REFERENCIAS

Xie R., Qu B. (2001). Synergistic effects of expandable graphite with some halogen-free flame retardants in polyolefin blends *en Polym Degred Stab.*, 71, 375-384.

Morgan A. B. (2006) Flame retarded polymer layered silicate nanocomposites: a review of commercial and open literature systems *en Polym. Adv. Technol.*, 17, 206-217.

Moore E. P. (1996) *Polypropylene handbook*, Ed. Hanser Publisher, Munich, Vienna, New York.

Suárez M. J., Matellanes L., Ballesteros J. (2006). Nanocomposites: efecto sinérgico en la ignifugación de poliolefinas *en Plásticos Universales*, 110, 108-113.

Giannelis E.P., Manias E. (1998). Flame retardant Nanocomposite Materials en Annual Conference on Fire Research. *Book of Abstracts*. November 2-5.

Structural variations and transcrystallinity in polymer nanocomposites

A. Dasari[1,2], **Y.W. Mai**[2]
1Madrid Institute for Advanced Studies of Materials (IMDEA-Materials), E. T. S. de Ingenieros de Caminos, 28040 Madrid, Spain
[2] Center for Advanced Materials Technology (CAMT), School of Aerospace, Mechanical & Mechatronic Engineering, The University of Sydney, Sydney, NSW 2006, Australia
e-mail: aravind.dasari@imdea.org

ABSTRACT

There are many questions surrounding the occurrence of preferential orientation of lamellae (transcrystalline regions) in the vicinity of fillers and their influence on interface and ultimate mechanical properties in polymer composites [1]. More significantly, preferential oriented growth due to epitaxy *versus* geometric confinement effect (offered in particular by nano-fillers) during crystallization, size range and dimension of fillers, differences in thermal conductivities of fillers (and polymers), and the toughness of the resultant nanocomposites. In this talk, polymer lamellae orientations in the vicinity of different nano-fillers (carbon nanofiber, organoclay, calcium carbonate and carbon black) will be discussed and more importantly, their role during the deformation processes. Further, correlations and comparisons will be made with the recently introduced 'mobility' concept [2, 3] concerning the enhanced ductility in polymer nanocomposites. Briefly, it was revealed that the ductility of polymer nanocomposites is system dependent and that the presence (due to lattice matching) or absence of transcrystalline regions does not have a significant bearing. Besides, mobility of nanoparticles is also only one of the mechanisms and not exclusively responsible for ductility.

REFERENCES

[1] A. Dasari, Z.-Z. Yu, Y.-W. Mai. Transcrystalline regions in the vicinity of nano-fillers in polyamide 6. Macromolecules, 2007, 40(1): 123-130.
[2] D. Gersappe. Molecular mechanisms of failure in polymer nanocomposites. Physical Review Letters, 2002, 89(5): 058301-058304.
[3] T.H. Zhou, W.H. Ruan, M.Z. Rong, M.Q. Zhang, Y.L. Mai. Keys to toughening of non-layered nanoparticles/polymer composites. Advanced Materials, 2007, 19(18): 2667-2671.

Dielectric and magnetic properties of magnetic liquids and composites on the basis of iron oxide nanoparticles

R. Moučka, N. Kazantseva, J. Vilčáková, A. Lopatin, P. Sáha
Polymer Centre, Faculty of Technology, Tomas Bata University in Zlín, Czech Republic
N. Chekina
Department of Applied Research, University Institute, Tomas Bata University in Zlín, Czech Republic

SUMMARY

Electromagnetic properties of ferrofluids comprising magnetite particles are discussed. Magnetite particles were synthesized by co-precipitation method from mixture of Fe^{III} and Fe^{II} chlorides whose ratio varied from 0.33 to 2.30. Particles were stabilised by dextran or gelatine. Prepared particles were characterized by electron microscopy, X-ray diffraction, magnetostatic measurement as well as dielectric and magnetic spectroscopy. Considerable differences in electromagnetic properties recorded in liquid form are explained on the basis of various structures, into which particles tend to organise. Such materials are discussed in relation to their possible utilisation in radiactive hyperthermia through the combine effect of magnetic and dielectric losses.

1. INTRODUCTION

Ferrofluids (FFLs) based on polymer-coated magnetic nanoparticles have attracted much attention for medical diagnostics and cancer therapy such as magnetic hyperthermia [1-3] Magnetic hyperthermia is non-invasive method of malignant tumour treatment based on heating up the cancerous tissue because of temperature enhancement which occurs in MNPs (embedded into the tumour) under the influence of an external magnetic field. The heating effect of FFLs in magnetic field is caused by magnetic losses which often do not provide sufficient specific loss power (SLP), considered to be 10 kW/g. However, in radiative hyperthermia to SLP contributes not only magnetic but also dielectric losses. Although different mechanisms can be responsible for dielectric losses of magnetic materials, in FFLs based on iron oxides the most important one is connected with electric conductivity. In this regard, good prospects are exhibited by magnetite, which is characterized with high enough magnetic properties ($M_S = 90$ emu/g) and high electrical conductivity ($\sigma_{DC} = 10^{-2}$ S/cm). Thus the goal of present study was to evaluate a variety of magnetite based FFLs in relation to their total losses.

2. EXPERIMENTAL

2.1. Materials and Methods

Ferrofluids were prepared by co-precipitation method in alkaline media from a mixed $FeCl_3{\times}6H_2O$ and $FeCl_2{\times}4H_2O$. Aqueous ammonia was used as a precipitating agent and dextran or gelatine was chosen as stabilisers. Substantially, several types of ferrofluids with different structural and electromagnetic properties were prepared under the different Fe^{III}/Fe^{II} molar ratio, which we refer to as samples N1-7 (dextran) and N8 (gelatine) (see Table 1). Additionally, iron oxide powders were prepared from ferrofluids by lyophilizing with a view to comparing electromagnetic properties of liquid and solid states. Electric and magnetic properties of these materials were determined by various methods both static and dynamic in the broad frequency range. Structure and particle size was determined from X-ray diffraction (XRD), light scattering analysis measurement and transmission electron microscopy (TEM), the last mentioned also proved organisation of particles into structures.

3. RESULTS AND DISCUSSION

TEM images show that the particle size as well as particle size distribution depend on used stabiliser (coating). In case of dextran, individual spherical particles with diameter of approximately 10 nm coated by thin dextran overlayer (core-shell structure) are obtained (Fig. 1a, b). On the other hand, if gelatine is used size distribution of particles is much broader and no traces of core-shell are apparent (Fig. 1c). It was found that the particles tend to organise themselves into different type of aggregates (chain-like, globular, ring-like, etc.). Moreover, we determined that the shape and size of these are given by a synthesis condition, namely a pair of stabiliser concentration and corresponding molar ratio of iron salts. For example, for 15 wt. % of dextran only molar ratio of Fe^{III}/Fe^{II} 1:1 yields particles organised into chain-like aggregates, typically 100 nm long, which are interconnected to form an infinite cluster (Fig. 1b).

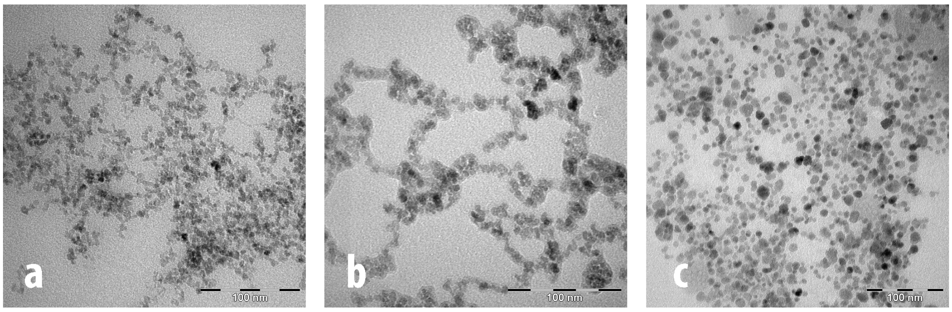

Fig. 1. TEM of samples: N1(a), N4(b) and N8(c).

Powder XRD pattern of particles showed a spinel phase. The line position and relative intensities were consistent with the spectrum of either magnetite (Fe_3O_4) or maghemite (γ-Fe_2O_3). The lattice constant a_0 varied from 8.32 Å to 8.35 Å depending on Fe^{III}/Fe^{II} molar ratio (Table 1).

sample N	1	2	3	4	5	6	7	8
lattice const. a_0 (Å)	8.325	8.315	8.333	8.320	8.350	8.319	8.355	8.342
Fe^{III}/Fe^{II}	1.70	1.43	0.73	1.10	0.33	2.00	2.30	1.10

Table 1. Lattice parameters of samples 1-8 obtained by XRD.

Although measured lattice parameters (Table 1) indicate either magnetite (8.396) or maghemite (8.345), which both have lattice parameters close to observed ones, complex magnetic permeability spectrum (Fig. 2) clearly marks magnetite showing typical character of ferromagnetic material. Particularly it displays two dispersion regions. The latter is connected with magnetization rotation with critical resonance frequency around 1 GHz.

As can be seen from the magnetization curve (Fig. 3), the magnetite particles in liquid state exhibit superparamagnetic behaviour. Though the recorded values of saturation magnetization (M_s), varying from 0.003 to 0.015 emu/g, are rather negligible compared to crystalline magnetite M_s = 90 emu/g, this stems from low concentration of magnetic phase in liquid.

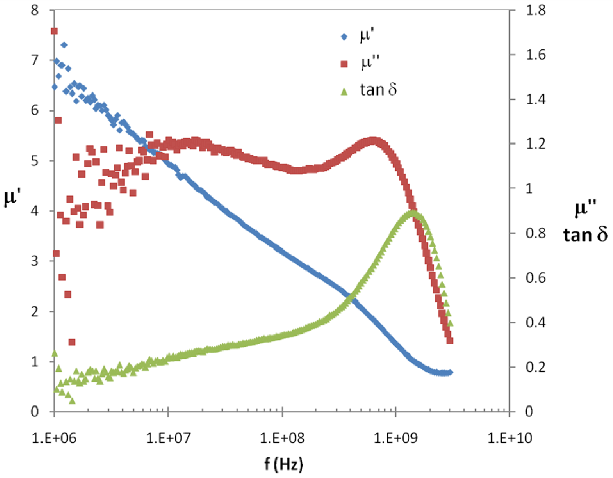

Fig. 2. Magnetic permeability spectrum of compressed (powder) sample N4.

Significant topological differences in ferrofluid clusters accordingly influence their dielectric properties. When the particles arranged themselves into chains forming an infinite cluster spanning throughout the volume of the sample the dielectric losses are significantly higher than values recorded for other morphologies. The enhancement of imaginary part of complex permittivity was observed in frequency range below 1 GHz (Fig. 4).

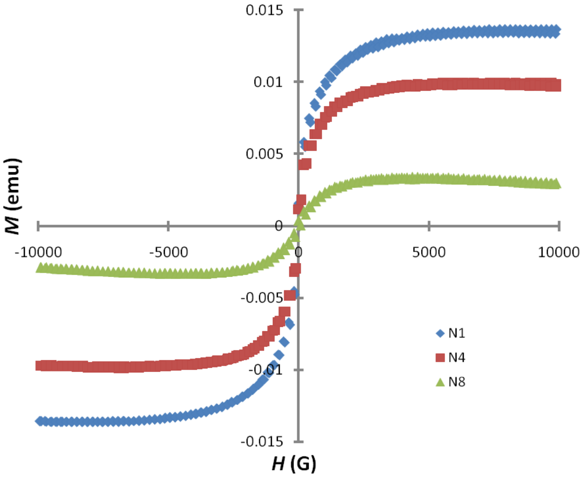

Fig. 3. Magnetization curves for colloidal samples N1, N4 and N8.

The observed difference is, most probably, due to the formation of special microstructure of ferrofluid with organization of magnetic nanoparticles into path-like chains interconnected into an infinite cluster. The average length of chain-like aggregates is around 100 nm and thus, it is possible to consider these as nanowires with high aspect ratio. It is well known that the dielectric losses for such type of structure are significantly higher than for individual particles due to different boundary condition of electrical field [4].

Therefore, we suppose that such type of magnetic liquids could be employed in radiative hyperthermia as the necessary heat would come from both magnetic and dielectric losses, where the latter may be as significant as the former, if not more so.

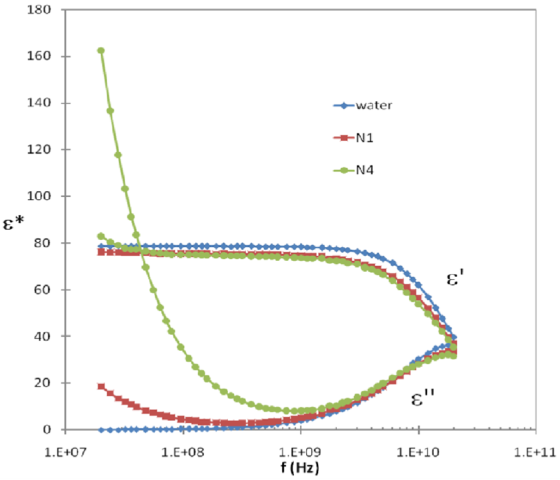

Fig. 4. Dielectric relaxation spectroscopy of liquid samples N1 and N4.

4. CONCLUSION

A significant difference in the electromagnetic properties of ferrofluids based on polymer-coated magnetite is attributed to the microstructure of ferrofluid.

The formation of assemblies is closely associated with magnetic dipolar interaction and thus can be controlled by changes of the ratio between average particle diameter and the thickness of dextran coating.

The structured ferrofluids exhibit high value of dielectric losses in frequency range below 1 GHz which should make them applicable as a medium in radiative hyperthermia.

ACKNOWLEDGMENT

The authors want to thank Ministry of Education, Youth, and Sports of the Czech Republic, particularly projects ME 883 and MSM 7088352101, by which the research was financed.

REFERENCES

[1] Behrens, S., et al., *Synthesis and characterization.* Lecture Notes in Physics, 2009. **763**: p. 1-82.

[2] Szasz, A., et al., *An energy analysis of extracellular hyperthermia.* Electromagnetic Biology and Medicine, 2003. **22**(2-3): p. 103-115.

[3] Trahms, L., *Biomedical applications of magnetic nanoparticles.* Lecture Notes in Physics, 2009. **763**: p. 327-358.

[4] Landau, L.D., Lifshitz, E.M. *Electrodynamics of Continuous Media*. Pergamon press, 1984 (Chap. 2, §8, pp. 39-42).

Development and characterization of PEEK/carbon nanotube composites

A. Diez-Pascual, M. Naffakh, M. Gómez, G. Ellis, C. Marco
Departamento de Física e Ingeniería de Polímeros. Instituto de Ciencia y Tecnología de Polímeros, CSIC. C/ Juan de la Cierva 3, 28006, Madrid, Spain
T. Martínez, A. Anson, J. González-Domínguez
Grupo de Nanoestructuras de Carbono y Nanotecnología. Instituto de Carboquímica, CSIC. C/ Miguel Luesma Castan 4, 50018 Zaragoza, Spain
Y. Martínez-Rubi, B. Simard
Steacie Institute for Molecular Sciences, National Research Council of Canada. 100 Sussex Drive, Ottawa, ON, K1A 0R6, Canada

SUMMARY

New poly(ether ether ketone) (PEEK) based nanocomposites have been fabricated by incorporation of arc and laser grown single-walled carbon nanotubes (SWCNT) using melt processing. The structure, morphology, thermal and mechanical properties of composites containing different SWCNT contents have been investigated. SEM observations demonstrated a more uniform distribution of the CNTs for samples prepared following a processing method based on ball milling and dispersion in ethanol. Increasing the SWCNT loading resulted in a decrease in the crystallization temperature of the matrix, and a substantial increase in its degradation temperatures. Further, a non-linear growth in the storage modulus by addition of increasing SWCNT contents was observed, attributed to weaker interfacial interactions nanotube-PEEK at higher loadings. CNTs restrict molecular motions, and thus increase the glass transition temperatures; the largest increment is found among composites including laser grown SWCNTs.

1. INTRODUCTION

PEEK is a semi-crystalline thermoplastic polymer with excellent thermal and chemical stability, currently used in a wide range of applications, especially for the automobile and aerospace industries. Since its commercialization in 1981, many studies have been reported on the structural, thermal and mechanical characterization of this high-performance thermoplastic material. In the literature there are many reports related to the integration of SWCNTs into polymer matrices, but only a few papers deal with such composites with a PEEK matrix; the most relevant being those published by Shaffer et to. (2002), working with carbon nanofibres/PEEK composites and by Baaba et to. (2007), dealing with multi-walled nanotubes functionalized with sulfonated PEEK.

This study approaches two main objectives: firstly, the development of strategies to efficiently incorporate SWCNTs into the PEEK matrix; secondly, the characterization of the PEEK composites. The influence of the preparation and processing conditions, as well as SWCNT concentration on the morphology, thermal and dynamic mechanical properties of the resulting composite materials is analyzed in detail in this work.

2. EXPERIMENTAL

2.1 Materials

The matrix used was a commercially available poly(ether ether ketone), PEEK 150P, supplied by Victrex plc, UK (M_w ~ 40000 g/mol, T_g = 147 ºC, T_m = 345 ºC). The polymer was vacuum dried at 120 ºC for 4 h, and stored in a dry environment before blending. Arc-grown SWCNTs were synthesized by the Institute of Carbon Chemistry (ICB-CSIC), Zaragoza, Spain, using Ni/Y ~2/0.5 atomic ratio as catalyst. In order to decrease the metal catalyst content (~13 wt% Ni, Y), these arc-grown SWCNTs were treated in a reflux of HNO_3 1.5 M, at 150 ºC for 2 h, and then centrifuged at 10000 rpm for 4 h. Laser grown SWCNTs were prepared by the Steacie Institute for Molecular Sciences (SIMS-NRC), Canada. The residual catalyst (Ni, Co) was lower than 4 wt%, and they were used without further purification.

2.2 Preparation of PEEK/SWCNT composites

Raw arc-grown and laser grown SWCNTs (see Table 1) were mixed with dried PEEK powder as received. Purified arc-grown and laser grown SWCNTs were dispersed in 30 mL of ethanol, sonicated in an ultrasonic bath for 30 min and dried under vacuum (70 mbar) at 50 ºC until the ethanol was completely eliminated. All types of PEEK/SWCNT composites studied in this work, containing concentrations of 0.1, 0.5 and 1 wt% SWCNTs, were prepared by melt-blending in a Thermo-Haake MiniLab micro-extruder at 380 ºC, using 5 g of material, with a rotor speed of 150 rpm and mixing times of 20 min.

Preparation Method	Metal (%) (TGA)	G/D ratio (Raman)	Purity (%) (NIR)	D (nm) SEM	Sample Code
Arc (as-grown)	12.7	5.6	35.7	21.8	ZC1
Arc-purified	3.2	14.3	50.4	20.4	ZC1p*
Laser (as-grown)	3.9	7.2	38.8	39.8	LC1&LC1m*

Table 1. Characteristics of the SWCNTs used for the preparation of the composites. Those SWCNTs indicated with (*) were integrated by pre-dispersion in ethanol.

3. RESULTS AND DISCUSSION

In order to determine the state of dispersion of the fabricated composites, the surfaces of cryo-fractured films were examined by SEM. The SWCNTs were quite agglomerated in samples prepared by direct mixing. However, those prepared with previous mechanical treatments showed a good dispersion of the SWCNTs. The size of the domains in the dispersed phase was smaller and CNTs were evenly distributed through the whole matrix.

To study the thermal stability of the composites, TGA characterization was carried out under dry air and nitrogen atmospheres. The degradation curves of pure PEEK and composites containing 1 wt% SWCNTs are displayed in Figure 1.

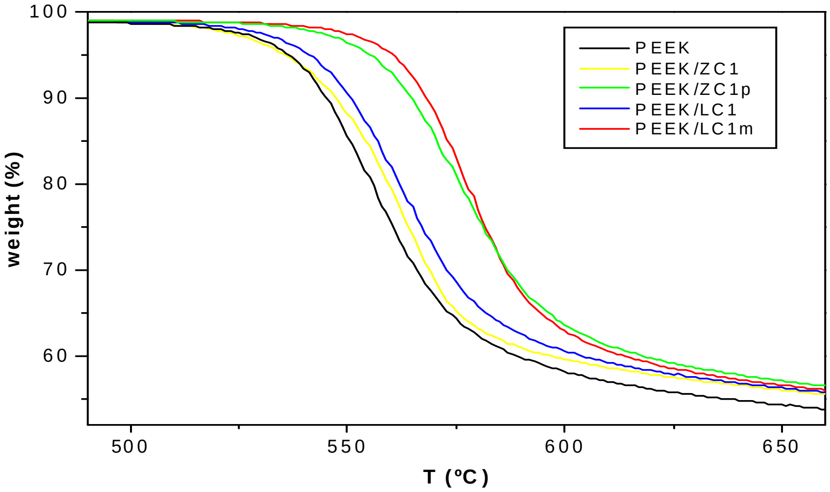

Fig. 1. TGA curves for different types of 1 wt% PEEK/SWCNT composites in nitrogen atmosphere, at a heating rate of 10 ºC/min.

The incorporation of SWCNTs induces a remarkable thermal stabilization of the matrix; the addition of 1 wt% LC1m or ZC1p increases the initial degradation temperature (T_i) by 25 ºC, and delays the temperature of maximum degradation rate T_{mr} by about 20 ºC. DSC was employed to evaluate the effect of SWCNTs on the crystallization and melting behaviour of PEEK/SWCNT composites. The crystallization temperature T_c is 309 ºC for pure PEEK, and decreases by incorporation of SWCNTs ($T_{c\text{-}0.1wt\%}$ = 307.5 ºC, $T_{c\text{-}0.5wt\%}$ = 305.1 ºC, $T_{c\text{-}1wt\%}$ = 303.3 ºC). However, the cystallization enthalpy ΔH_c and therefore the crystallinity, remain almost unchanged. This unusual behaviour can be explained by a confinement effect: CNT network imposes a confinement on polymer chain diffusion and crystal growth which slows down the crystallization process, leading to lower T_c values for the composites. Their crystalline structure was characterized using wide angle x-ray diffraction. Four peaks were observed at 2θ of 18.8º, 20.7º, 22.9º and 28.9º, which correspond to (110), (111), (200) and (211) crystalline planes of the orthorhombic unit cell. All composites exhibit similar diffractogram to the PEEK matrix.

The mechanical properties of the composites were explored by DMA. Figure 2 shows the temperature dependence of the storage moduli and loss moduli of PEEK/LC1m composites. At room temperature, composites containing 0.1, 0.5 and 1 wt% SWCNTs increased E′ of the matrix by approximately 16, 23 and 27%, respectively. The observed enhancement in the mechanical response is attributed to the effective load transfer from the matrix to the fillers likely resulting from an improvement in the SWCNT dispersion.

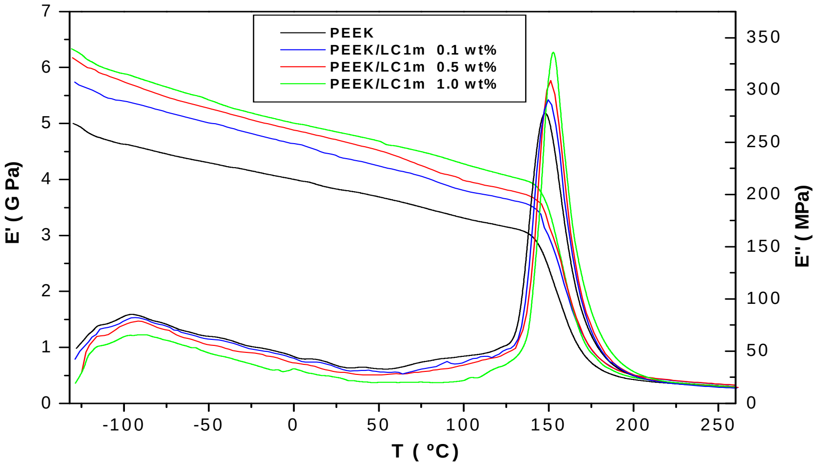

Fig. 2. Temperature dependence of the storage modulus and loss modulus of PEEK/LC1m composites, at different CNT loadings and frequency 1 Hz.

The addition of SWCNTs causes small increases in T_g, and thus, in the stiffness of the systems, because CNTs restrict rotational motion within the chains.

4. CONCLUSIONS

PEEK/SWCNT nanocomposites with different SWCNT content have been prepared by melt blending. An efficient dispersion of the CNTs in the matrix was achieved by the combination of ball milling and mechanical treatments in ethanol media. The nanocomposites are thermally more stable than the pure matrix, and present lower crystallization temperatures, attributed to nanoconfinement and multiple nucleation effects. They present higher storage modulus and glass transition temperature than the matrix, in particular those incorporating laser grown SWCNTs, probably due to the improved quality and properties of this type of filler.

ACKNOWLEDGMENT

Financial support from a coordinated project between the National Research Council of Canada (NRC) and the Spanish National Research Council (CSIC) is gratefully acknowledged. A.D. thanks the CSIC for Postdoctoral contract.

REFERENCES

BAABA, M-R., BANTIGNIES, J-L., ALVAREZ, L, PARENT, P, LE NORMAND, F., GULAS, M. (2007) NEXAFS study of Multi-Walled Carbon Nanotubes functionalization with Sulfonated poly(ether ether ketone) Chains. *J. Nanosci. Nanotechnol.*, 7, 3463-3467.

SANDLER, J., WERNER, P., SHAFFER, M. S. P., DEMCHUCK, V., ALTSTADT, V., WINDLE, A.H. (2002) Carbon-nanofibre-reinforced poly(ether ether ketone) composites. *Composites A,* 33, 1033-1039.

Core-shell magnetic nanoparticles based on polylactones

A. Nan, R. Turcu, I. Craciunescu, C. Leostean, I. Bratu
National Institute of Research and Development for Isotopic and Molecular
Technologies, Donath 65-103, 400293 Cluj-Napoca, Romania, sanda@itim-cj.ro
J. Liebscher
Institute of Chemistry, Humboldt-University Berlin, Brook-Taylor 2, 12489 Berlin,
Germany

SUMMARY

In this study we describe the polymerization of ε-caprolactone and lactic acid and also the copolymerization between ε-caprolactone and lactic acid. The surface initiated ring opening polymerization (ROP) of ε-caprolactone and lactic acid was initiated by the common catalysts, tin (II) 2-ethylhexanoate to produce *core-shell* magnetic nanoparticles based on poly(ε-caprolactone), polylactic acid, poly(ε-caprolactone)-polylactic acid copolymers respectively, containing one hydroxyl chain. Moreover we performed the surface initiated ROP of ε-caprolactone and lactic acid microwave assisted in the presence of tin (II) 2-ethylhexanoate. The chemical structure of the obtained poly (ε-caprolactone) was characterized by FT-IR and XPS spectroscopy. The properties of the magnetic-polymer hybrid nanostructures were investigated by differential scanning calorimetry (DSC), XRD spectroscopy and magnetization measurements. The morphology of magnetic core-shell nanostructure was determined by TEM.

1. INTRODUCTION

Homopolymers and copolymers of, lactides (LA), and ε-caprolactone (CL) are increasingly investigated worldwide for pharmacological, biomedical, agricultural, and environmental purposes (Langer, 2000; Langer, 1998; Mecerreyes et al., 1999; Lofgren et al., 1995). In contrast to the traditional step-polycondensation method, the ring-opening polymerization of cyclic esters is an effective method for the preparation of the related aliphatic polyesters. The rapidly growing interest in biodegradable materials has also increased interest in catalysts and mechanisms concerning the ring-opening polymerization of lactones and lactides (Kricheldorf et al., 2000).

Biodegradable polymers are widely studied because of their non-toxic property and biodegradability. Among these polymers, poly(lactic acid), poly(glycolic acid), especially their copolymer—poly(lactic-co-glycolic acid) (PLGA) have been investigated extensively as drug delivery system (Chandy et al., 2002; Shi et al., 2003; Fu et al., 2005), But their acidic degradation products and possibility of initiating inflammatory limit their developments.

Poly(_-caprolactone) (PCL), as one of the most popular synthetic polymers, has been researched as biodegradable carrier for controlled drug release (Dhanaraju et al., 2006; Lim et al., 1998; Barbato et al., 2001). PCL is suitable for controlled drug release because of its high permeability to many drugs and biocompatibility in physiological environments (Murthy, 1997). Preparation methods of microspheres were primarily determined by the solubility of the drug and the polymer in various solvent systems, such as: single emulsion solvent evaporation (Perez et al., 2000), double emulsion solvent evaporation (Dhanaraju et al., 2006; Cleek et al., 1997) or spray drying technique (Chu et al., 2006) and so on.

2. EXPERIMENTAL DETAILS

2.1. Synthesis and Stabilization of Magnetite Surface

The synthesized magnetite nanoparticles were surface-stabilized *in situ* by the addition of *L*-serine or glycolic acid strongly stirred for 2 h at 80 ^{0}C, under argon atmosphere (Scheme 1).

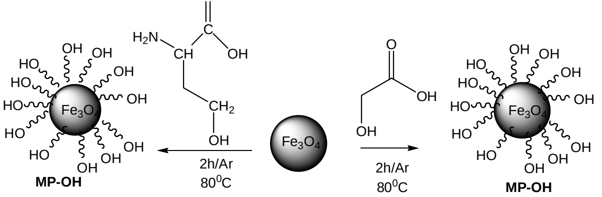

Scheme 1

2.2. Polymerization of CL and LA in the precense of magnetic nanoparticles

The surface-initiated ROP of ε-CL and LA onto magnetite was carried out was carried out according to the procedure shown in Scheme 2. The stabilized magnetic nanoparticles (**MP-OH**) were mixed, in the presence of SnOct$_2$, with freshly distilled CL, lactic acid, respectively and strongly shacked at 100^{0}C for 5 h at 1200 rot./min..

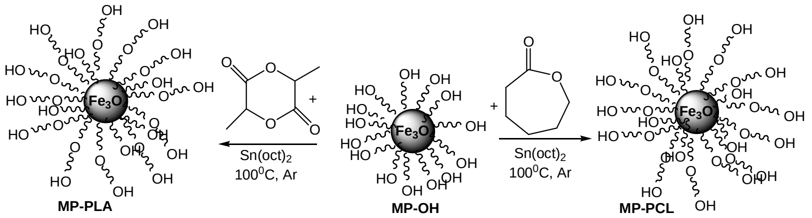

Scheme 2

The polymerization of CL onto magnetite nanoparticles was performed also by microwave irradiation (**MP-OH-MW-CL**). The reaction was performed at the (200 ^{0}C) at a microwave power of 200 W for 7 minutes while the pressure reached 8 bar. The energy uptake finished after 100 seconds.

2.3. Formation of block copolymer on the iron oxide nanoparticles

The surface-initiated ring-opening copolymerization of CL and LA in the presence of magnetic nanoparticles is a two step reaction and will direct us to obtain hybrid material containing a block copolymer and iron oxide (**MP-PCL-b-PLA**): (a) first step is the ring opening polymerization of CL, the reaction condition was mention before; (b) second step is polymerization of lactic acid in the same reaction condition as was mention before.

3. CHARACTERIZATION OF THE HYBRID MATERIAL

3.1. Morphologic characterization

The TEM images (Figure 1) of magnetic nanoparticles modified with serine **MP-OH** (Figure 1a) and the hybrid material **MP-PCL** presented in Figure 1b, prove the core-shell structure.

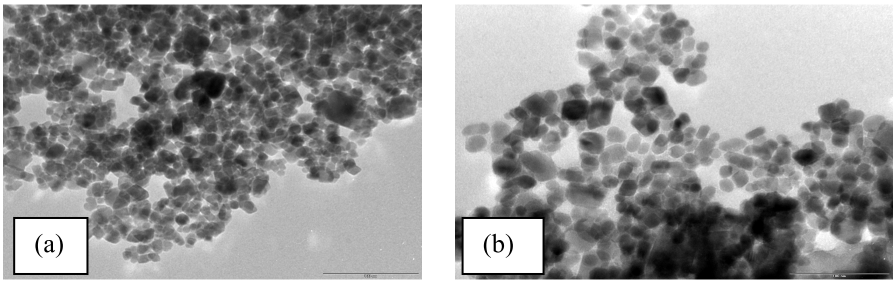

Figure 1: (a) the TEM image of MP-OH, (b) the TEM image of MP-PCL (bar size 100 nm)

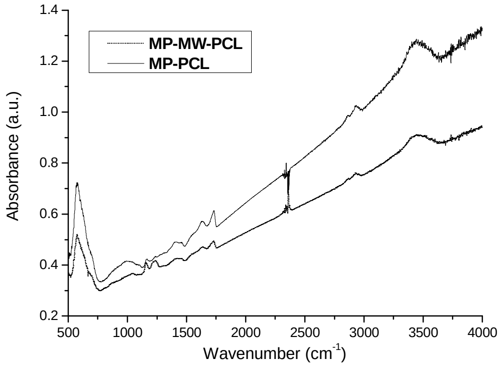

Figure 2. FTIR spectra of **MP-PCL** and **MP-MW-PCL**

3.2. FTIR spectroscopy

FTIR spectra, shown in figure 2, exhibited characteristic adsorption bands of both component materials, namely the MP-OH and hybrid materials. The intense band located at 572 cm^{-1} is characteristic of magnetite. The characteristic bands of PCL appear between 1157 cm^{-1} and 2949 cm^{-1}.

4. CONCLUSIONS

We obtained for the first time block copolymers based on PCL and PLA on the iron oxide nanoparticles surface. The Sn(oct)$_2$ catalyzed surface-initiated ROP of ε-CL in the presence of surface modified magnetite was successfully conducted by microwave irradiation for the first time. The effect of microwave irradiation on the polymerization involves the enhancement of chain propagation of PCL and the restraint of growing centre formation and allowed to finish the polymerisation in 10 min. In addition, solvents are not necessary in this process. The FTIR spectra contain the characteristic absorption bands of both constituents, namely, hybrid materials and magnetite. TEM revealed the the size of the magnetite nanoparticles increased by the ROP from 13 – 16 nm to 22 – 27 nm.

ACKNOWLEDGMENT

The authors want to be grateful to Dr. Holger Scharf from Federal Institute for Materials Research and Testing, Berlin, Germany for determining the iron concentration of our samples. This work was supported by the Romanian Ministry of Education and Research under the research programs, 4-th PNCDI Programe, Project No 71-068/14.09.2007.

REFERENCES

BARBATO, F., ROTONDA, M. I. L., MAGLIO, G., PALUMBO, R., QUAGLIA, F. (2001) Biodegradable microspheres of novel segmented poly (ether-ester-amide)s based on poly(ε-caprolactone) for the delivery of bioactive compounds. *Biomaterials*, 22, 1371–1378.

CHANDY, T., DAS, G. S., WILSON, R. F., RAO, G. H. R. (2002) Development of polylactide microspheres for protein encapsulation and delivery. *J. Appl. Poly.*, 86, 1285–1295.

CLEEK, R. L., KING, K. C., ESKIN, S. G., MIKOS, A. G. (1997) Microparticles of poly (DL-lactic-co-glyconic acid) / poly (ethylene glycol) blends for controlled drug delivery. J. Control. *Release*, 48, 259–268.

DHANARAJU, M. D., GOPINATH, D., AHMED, M. R., JAYAKUMAR, R., VAMSADHARA, C. (2006) Characterization of polymeric poly(ε-caprolactone) injectable implant delivery system for the controlled delivery of contraceptive steroids. *J. Biomed. Mater. Res.*, 76A, 63–72.

FU, X., PING, Q., GAO, Y. (2005) Effects of formulation factors on encapsulation efficiency and release behaviour in vitro of huperzine A-PLGA microspheres. *J. Microenc.*, 22, 705–714.

KRICHELDORF, H. R.; KREISER-SAUNDERS, I.; STRICKER, A. (2000) Polylactones 48. $SnOct_2$-initiated polymerizations of lactide: A mechanistic study. *Macromolecules*, 33, 702.

LANGER, R. (2000) Biomaterials in drug delivery and tissue engineering: one laboratory's experience. *Acc. Chem. Res.*, 33, 94.

LANGER, R. (1998) Drug delivery and targeting, *Nature*, 392, 5-10,

LIM, L. Y., GOULD, P., DICKINSON, N. A., COLLETT, J. H. (1998) The influence of environmental conditions on damage in L-poly-lactic acid during gamma irradiation. *Control. Release. Bioact. Mater.*, 15, 111–112.

LOFGREN, A.; ALBERTSSON, A. -C.; DUBOIS, P.; JEROME R. (1995) Recent advances in ring-opening polymerization of lactones and related compounds, *J. Macromol. Sci., Rev. Macromol. Chem. Phys.*, C35, 379.

MECERREYES, D.; JEROME, R.; DUBOIS, P. (1999) Novel Macromolecular Architectures Based on Aliphatic Polyesters: Relevance of the Coordination-Insertion Ring-Opening Polymerization, *in Advances in Polymer Science* (Ed. Hilborn, J. G.), 1, Springer-Verlag: Berlin.

MURTHY, R. S. R. (1997) Biodegradable polymers. *Controlled and novel drug delivery*. (Ed. Jain, N.K.), 27–51, CBS Publisher, New Delhi.

PEREZ, M. H., ZINUTTI, C., LAMPRECHT, A., UBRICH, N., ASTIER, A., HOFFMAN, M., BODMEIER, R., MAINCENT, P. (2000) The preparation and evaluation of poly(ε-caprolactone) microsparticles containing both lipophillic and hydrophilic drug. *J. Control. Release*, 65, 429–438.

Nanocomposite organically modified silica coatings with embedded inorganic fullerene-like tungsten disulfide

H. Hattermann, T. Hübert, M. Griepentrog
BAM Federal Institute for Materials Research and Testing, Division VI.4 Surface Technologies, D-12200 Berlin, Germany

SUMMARY

A promising method to improve the tribological properties of thin coatings is by the incorporation of dry lubricant nanoparticles. We have used a sol-gel process to prepare such nanocomposite coatings with a matrix of organically modified silica filled with up to 30 wt.-% inorganic fullerene-like tungsten disulfide. Gracing incidence X-ray diffraction proved that the hexagonal crystal structure of the tungsten disulfide remains intact during the sample preparation. Scanning and transmission electron microscopy showed a homogeneous distribution of small aggregates and single WS_2 particles in the silica-based matrix. Through nanoindentation testing the hardness and modulus of the composite coatings were measured. The tribological behavior of the composite coatings was investigated for dry sliding with ball-on-disc tests. The incorporation of tungsten disulfide particles into the organically modified silica coatings leads to a strong reduction of the coefficient of friction from 0.6 to 0.15.

1. INTRODUCTION

Inorganic fullerene-like materials like tungsten disulfide are a new and interesting class of materials (Tenne et al. 1992). Due to their layered structure they exhibit good lubricating properties (Rapoport et al. 2003) and are well suited for the incorporation into thin protective coatings because of their small particle sizes of about 50 to 300 nm. Such composite coatings with embedded inorganic fullerene-like WS_2 and an improved tribological behavior have already been prepared successfully based on a galvanic Ni-P matrix (Chen et al. 2002) or on a PEEK matrix (Hou et al. 2008).

In this work we have used a sol-gel process to prepare organically modified silica coatings with embedded WS_2 particles. The structure of these composite coatings was determined and their hardness, modulus and coefficient of friction was measured and compared with values of pure organically modified silica coatings.

2. EXPERIMENTAL

The investigated nanocomposite coatings were prepared through a sol-gel process described in detail by Hübert et al. (2009). The precursor was prepared from a mixture of 3-glycidoxypropyltrimethoxysilane (SIGMA-ALDRICH), aqueous colloidal silica (LUDOX 34 wt.-%, SIGMA-ALDRICH), ethylenediamine (J. T. BAKER), water and ethanol (J.T. BAKER) in the molar ratio of 0.3 : 1 : 0.5 : 6.5 : 1 adjusted at pH 4 with HNO_3.

Tungsten disulfide powder (single particle size 80 to 220 nm, NanoMaterials Ltd.) was added to the precursor. Through ultrasound treatment (BANDELIN SONOPLUS HD 2200) and the addition of the surfactant cetyltrimethyl ammoniumbromide (CTAB, SIGMA) the homogenization and dispersion of the WS_2 in the sol was obtained.

Lapped stainless steel substrates (AISi 316Ti) were then dip-coated, dried in air and finally heat-treated at temperatures in the range from 150 to 300 °C for 1 h in air. For reference, organically modified silica coatings without incorporated inorganic fullerene-like WS_2 were prepared, too.

The tungsten disulfide content in the sol-gel coatings was estimated by an X-ray fluorescence method (XRF) using a Fisherscope XDAL, calibrated with screen printed reference samples on stainless steel of 10 and 50 wt.-% WS_2 (mixture of WS_2 and ACROS silica gel ultra pure 5-15 µm). The morphology of the coatings with the embedded inorganic fullerenes was investigated using scanning electron microscopy (SEM) (HITACHI 2460N) and transmission electron microscopy (TEM). X-ray diffraction in gracing incidence arrangement (GI-XRD) (XRD 3000 PTS, SEIFERT FPM, CuK_α radiation, incidence angle of 2.5 °) was used for phase identification.

The indentation hardness and modulus of the silica films were measured by an instrumented indentation test using the continuous stiffness measurement option (Nano Indenter XP, MTS NanoInstruments). On each sample 30 measurements were performed with a Berkovich indenter tip and an assumed Poisson’s ratio of 0.2. The coefficient of friction of organically modified silica coatings with and without embedded tungsten disulfide particles was determined for dry sliding with a ball-on-disc test (counterpart: steel ball with 10 mm diameter, frequency 2 Hz, sliding distance 4 mm, rel. humidity: 50 %). The applied load was varied from 1 to 10 N.

3. RESULTS AND DISCUSSION

The nanocomposite coatings have a WS_2 content between 20 and 30 wt.-% and different coating thicknesses between 1 and 5 µm. GI-XRD measurements of inorganic fullerene-like WS_2 powder and of nanocomposite coatings show that the hexagonal crystal structure of the inorganic fullerene-like tungsten disulfide remains unchanged during the sample preparation and that the organically modified silica matrix has an amorphous structure.

Scanning electron microscopy reveals that the tungsten disulfide particles are embedded as single particles and small agglomerates evenly distributed inside the silica matrix (see figure 1).

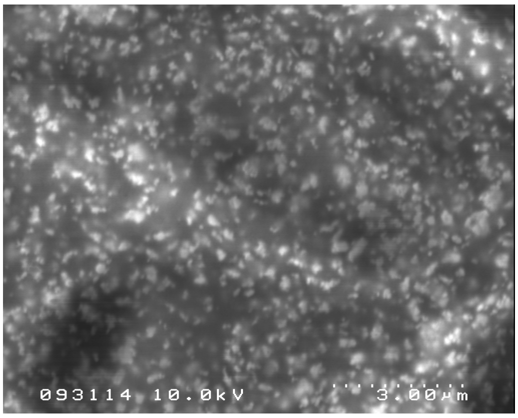

Figure 1. SEM image of an organically modified silica coating containing WS_2 particles.

TEM images show that the embedded tungsten disulfide particles are well connected to the matrix i.e. that there are no visible pores at the particle-matrix interface.

The indentation modulus and hardness of the composite coatings containing tungsten disulfide and of pure organically modified silica coatings are listed in table 1.

Table 2. Indentation modulus E_{IT} and indentation hardness H_{IT} of organically modified silica coatings and of composite coatings containing WS_2 particles.

Coating	Curing temperature [°C]	E_{IT} [GPa]	Std. dev. E_{IT} [GPa]	H_{IT} [GPa]	Std. dev. H_{IT} [GPa]
Silica	150	2.7	0.1	0.23	0.01
Silica + WS_2	150	1.8	0.1	0.12	0.01
Silica	200	4.6	0.3	0.41	0.02
Silica + WS_2	200	2.2	0.2	0.25	0.01
Silica	250	6.5	0.4	0.60	0.05
Silica + WS_2	250	7.0	0.3	0.54	0.02
Silica	300	8.2	0.6	0.56	0.06
Silica + WS_2	300	11.7	1.4	0.80	0.06

The results are similar compared to values from the literature (Ferchichi et al. 2002). Both indentation hardness and modulus rise strongly when the temperature of the final heat treatment is increased. This can be explained by a higher degree of polymerization of the matrix. The incorporation of 20 to 30 wt.-% of inorganic fullerene-like WS_2, however, leads only to small changes of the mechanical properties.

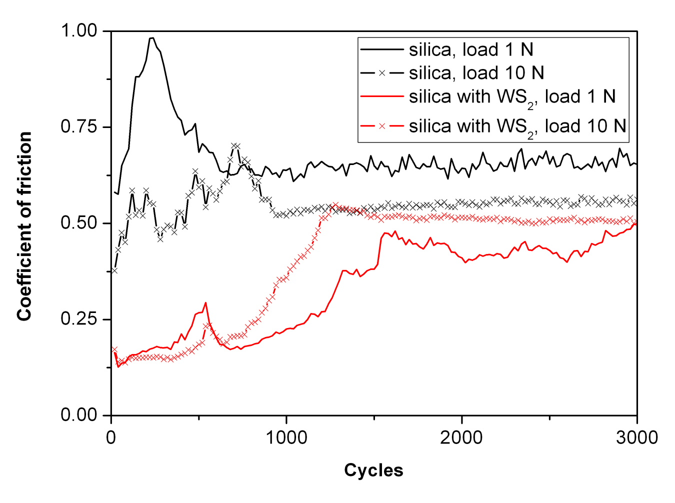

Figure 2. Coefficient of friction of organically modified silica coatings with and without embedded WS_2 particles measured for two different applied loads.

Figure 2 shows the effect of the embedded inorganic fullerene-like WS_2 onto the tribological behavior of the composite coatings. The coefficient of friction of the composite coatings is reduced from about 0.6 to 0.15 for both applied loads.

4. CONCLUSIONS

We have prepared organically modified silica coatings with embedded inorganic fullerene-like WS_2 on stainless steel substrates through a sol-gel process. GI-XRD measurements show that the hexagonal crystal structure of the tungsten disulfide remains unchanged during the sample preparation. The inorganic fullerene-like WS_2 particles are embedded as homogeneously distributed single particles and small agglomerates as can be observed from SEM and TEM images. The indentation modulus and hardness of the organically modified silica coatings depend strongly on the temperature of the final heat treatment, whereas the incorporation of tungsten disulfide particles into the coatings leads only to a small modification of hardness and modulus. However, a strong reduction of the coefficient of friction from 0.6 to about 0.15 can be observed for the nanocomposite coatings due to the embedded WS_2 particles.

ACKNOWLEDGMENT

We are grateful to H. Lorenz and N. Hoffmann for support with the sample preparation, M. Sahre and S. Reetz for the XRD and XRF measurements, B. Strauß for SEM and I. Dörfel for TEM analysis and M. Hartelt for the tribological testing. The presented study has been conducted in the framework of the European project FOREMOST (FP6-515840).

REFERENCES

CHEN, W., TU, J., Xu, Z., TENNE, R., ROSENTSVEIG, R., CHEN, W., GAN, H. (2002) Wear and friction of Ni-P electroless composite coating including inorganic fullerene-like WS_2 nanoparticles, *Adv. Eng. Mat.*, 4, 686-690.

FERCHICHI, A., CALAS-ETIENNE, S., SMAIHI, M., ETIENNE, P. (2002) Study of the mechanical properties of hybrid coating as a function of their structures using nanoindentation, *J. Non-Crystalline Sol.*, 354, 712-716.

HOU, X., SHAN, C.X., CHOY, K.-L. (2008) Microstructures and tribological properties of PEEK-based nanocomposite coatings incorporating inorganic fullerene-like nanoparticles, *Surf. & Coat. Technol.*, 202, 2287-2291.

HÜBERT, T., HATTERMANN, H, GRIEPENTROG, M. (2009) Sol-gel-derived nanocomposite coatings filled with inorganic fullerene-like WS_2, *J. Sol-Gel Sci. Technol.*, DOI 10.1007/s10971-009-1896-3.

RAPOPORT, L., LESHCHINSKY, V., LAPSKER, I., VOLOVIK, Y., NEPOMNYASHCHY, O., LVOVSKY, M., POPOVITZ-BIRO, R., FELDMAN, Y., TENNE, R. (2003) Tribological properties of WS_2 nanoparticles under mixed lubrication, *Wear*, 255, 785-793.

TENNE, R., MARGULIS, L., GENUT, M., HODES, G. (1992) Polyhedral and cylindrical structures of tungsten disulphide, *Nature*, 360, 444-446.

Fracture toughness of carbon fiber laminate joints with nanoreinforced adhesives

M.R. Gude, S.G. Prolongo, A. Ureña
Materials Science and Engineering Department. Universidad Rey Juan Carlos. Móstoles, Madrid, Spain

SUMMARY

The effect of the nanoreinforcement of an epoxy adhesive in the mode I fracture toughness of carbon fiber/epoxy laminate joints has been studied. Three different methods were used to analyze the results of the double cantilever beam (DCB) test, providing very similar results. The addition of carbon nanofibers and, specially, carbon nanotubes to an epoxy adhesive increases the mode I adhesive fracture energy, G_{IC}, of carbon fiber laminate joints.

1. INTRODUCTION

Carbon fiber/epoxy laminates are a very used type of composite materials in several industrial applications, like automobile, aerospace and energy. In many of these applications, the large size and complexity of the structures require the use of joining techniques to assemble different parts. In the case of carbon fiber reinforced polymers (CFRP), adhesive bonding presents many advantages compared with the use of mechanical joints (Chin et al. 1996).

Epoxy resins are one of most important structural adhesives, because of their good adhesive properties and high thermal and chemical resistance. For the joint of carbon fiber/epoxy laminates, they also present high chemical compatibility with the composite matrix. One of their main limitations is their low fracture toughness and very high electrical resistivity. In order to increase the toughness of epoxy resins, one of the most used solutions is the addition of elastomeric particles. This has enhanced the fracture toughness of epoxy adhesives at the expense of deteriorating other properties. More recently, the use of nanometric particles has been researched. Gilbert et al. (2003) achieved an important enhancement of the mode I fracture toughness of cocured CFRP joints by adding alumina nanoparticles to the adhesive. However, when laminates were previously cured, fracture toughness values obtained were even lower than the ones of unreinforced adhesive. Moreover, this kind of nanoparticles does not solve the problem of electrical conductivity.

This work explores a new alternative, which consists of the reinforcement of an epoxy adhesive with carbon nanofibers and nanotubes, in order to increase the mode I fracture toughness of CFRP joints without damaging other adhesive properties. In previous works, it has been demonstrated that the addition of these nanoreinforcements does not affect the lap shear strength. In addition, nanoreinforced adhesives maintain an adequate viscosity for their application and they drastically decrease the electrical resistivity with regard to the neat adhesive, from $10^{17}\ \Omega\cdot$cm down to $10^{4}\ \Omega\cdot$cm (Prolongo et al. 2009).

2. EXPERIMENTAL

2.1 Materials and processing

The adhesive used in this work is a basic epoxy formulation based on diglycidyl ether of bisphenol A (DGEBA). The curing agent was an aromatic amine, 4,4'-diaminodiphenylmethane (DDM). Both were supplied by Sigma-Aldrich. Two types of carbon nanoreinforcements were used: nanofibers and nanotubes. Carbon nanofibers (CNF), manufactured by Grupo Antolín (Spain), have a diameter between 10-90 nm. Multiwall carbon nanotubes (CNT) have an average diameter smaller than 10 nm and they have been amino-functionalized by the manufacturer, Nanocyl (Belgium).

The processing of nanoreinforced adhesives was carried out in several steps, in order to achieve a good dispersion of CNFs and CNTs in the adhesive. This process includes the use of chloroform and several dispersion techniques, and has been optimized in a previous work (Prolongo et al. 2008). The content of CNFs was 0.5 wt% with regard to the DGEBA mass. In the case of CNTs, only 0.25 wt% was added due to their high specific area. The curing process of neat and reinforced adhesives was carried out in two steps: 3 h at 150 °C and then 1 h at 180 °C.

Unidirectional carbon fiber/epoxy laminates were used as adherends. They were manufactured by Instituto Nacional de Técnica Aeroespacial (INTA, Spain) using prepregs HEXCEL HEXPLY 8552/34%/UD134/AS4 12K. Before curing, a polyester peel ply was placed over the last prepreg. This ply was removed just before the adhesive bonding, to generate a clean, rough surface.

2.2 Characterization

Double cantilever beam (DCB) tests were used to determine the mode I fracture toughness of adhesive joints. Adherend dimensions were 150 x 25 x 3.3 mm^3 and the adhesive thickness was 0.4 mm. A non-adhesive insert was placed in one of the ends of the joint, between both adherends, in order to act as crack initiator. DCB tests were carried out loading the specimens at a constant cross-head rate of 1.0 mm/min. Five samples of each adhesive composition were tested.

For the calculation of mode I critical strain energy release rate, G_{IC}, three different methods were employed: corrected beam theory (CBT), experimental compliance method (ECM) (Blackman et al. 2003) and area method (Whitney et al. 1982). The last method provides a mean value, while the first ones allow the determination of the resistance curve (R-curve), which is a graph of the propagation values of the adhesive fracture energy G_{IC} versus crack length.

3. RESULTS AND DISCUSSION

For each tested joint, the three calculation methods were applied. Using CBT and ECM, the mean values and standard deviation were calculated for each measured crack length (between 5-60 mm of crack propagation, every 5 mm). Figure 1 shows the mean R-curves of each adhesive composition, using the G_{IC} values calculated by CBT.

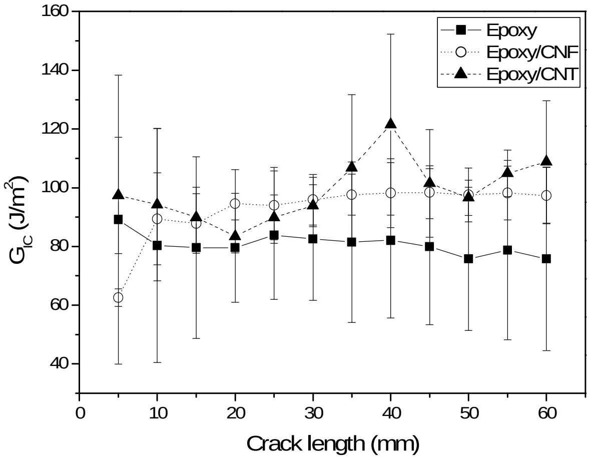

Fig.1. Resistance curves calculated using CBT for DCB joints with different adhesives.

Although the standard deviation is quite high, mean values clearly indicate that the addition of carbon nanoreinforcements to the adhesive increases the fracture toughness of the DCB joints. This agrees with the results of the two other calculation methods (figure 2). In general, the mean values of each adhesive are very similar, independently of the method used for the calculation.

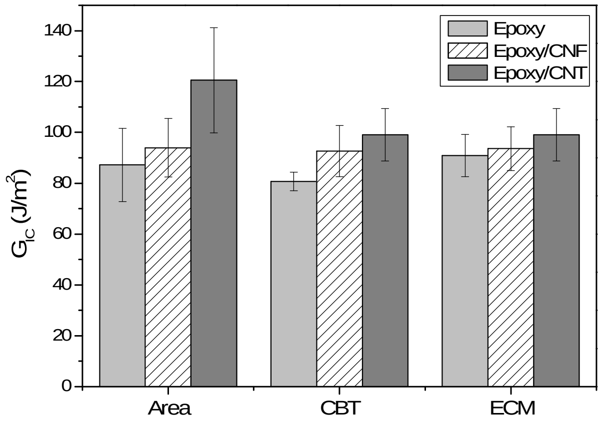

Fig.2. Comparison of the mean propagation values of G_{IC} as a function of the adhesive composition and the calculation method.

The reinforcement of epoxy adhesives with carbon nanofibers increases the mode I fracture toughness of DCB joints of carbon fiber/epoxy laminates in an 8.5 % with regard to the neat adhesive, while the increase with carbon nanotubes is 23.3 %. In all the tested joints the failure was found macroscopically adhesive. However, in the samples bonded with epoxy/CNT adhesive, crack moves from one side of the joint to other, meaning that carbon nanotubes are preventing the crack to propagate along the adherend/adhesive interface. Fracture surfaces have to be studied in depth using a scanning electron microscope (SEM) to determine how the nanoreinforcements are working to increase the adhesive fracture energy.

To conclude, it is important to stand out that the mean G_{IC} values are not very high, compared with others found in bibliography (Blackman et al. 2003, Gilbert et al. 2003), but two facts must be taken into account: the adhesive used is a basic epoxy formulation instead of a commercial adhesive, and the surface preparation is not the best for this kind of materials. In a previous work (Prolongo et al. 2009) it has been found that grit blasting or plasma provide higher lap shear strength for the same adherends and adhesives. However, peel ply has been chosen because it is very used in the aerospace industry. In a future work, plasma treatment and grit blasting will be used to prepare the laminate surfaces for the calculation of mode I fracture toughness.

4. CONCLUSIONS

Carbon nanoreinforcements are found to be a very good option in order to enhance the adhesive properties of epoxy resins. It has been determined that both CNTs and CNFs increase the mode I fracture toughness of DCB joints using carbon fiber/epoxy laminates as adherends. Also, it was confirmed that the three calculation methods employed for determining G_{IC} provide very similar results.

ACKNOWLEDGMENT

The authors wish to thank to *Ministerio de Educación y Ciencia* (project MAT2007-61178). María R. Gude also thanks *Consejería de Educación de la Comunidad de Madrid* and *Fondo Social Europeo* for her research contract.

REFERENCES

BLACKMAN, B.R.K., KINLOCH, A.J., PARASCHI, M., TEO, W.S. (2003). Measuring the mode I adhesive fracture energy, G_{IC}, of structural adhesive joints: the results of an international round-robin. *Int J Adh Adh*, 23, 293-305.

CHIN, J.W., WIGHTMAN, J.P. (1996). Surface characterization and adhesive bonding of toughened bismaleimide composites. *Compos A*, 27A, 419-428.

GILBERT, E.N., HAYES, B.S., SEFERIS, J.C. (2003). Nano-alumina modified epoxy based film adhesives. *Polym Eng Sci*, 43, 1096-1104.

PROLONGO, S.G., BURÓN, M., GUDE, M.R., CHAOS-MORÁN, R., CAMPO, M., UREÑA, A. (2008). Effects of dispersion techniques of carbon nanofibers on the thermo-physical properties of epoxy nanocomposites. *Compos Sci Technol*, 68, 2722-2730.

PROLONGO, S.G., GUDE, M.R., SANCHEZ, J., UREÑA, A. (2009). Nanoreinforced epoxy adhesives for aerospace industry. *J Adh*, 85, 180-199.

PROLONGO, S.G., GUDE, M.R., UREÑA, A. (2009). Synthesis and characterisation of epoxy resins reinforced with carbon nanotubes and nanofibers. *J Nanosci Nanotech*, doi:10.1166/jnn.2009.1554.

WHITNEY, J.M., BROWNING, C.E., HOOGSTEDEN, W. (1982). A double cantilever beam test for characterizing mode I delamination of composite materials. *J Reinf Plast Compos*, 1, 297-313.

Orientation of acicular nanoreinforcement in composite materials

G. Marom
The Institute of Chemistry, The Hebrew University of Jerusalem,
91904 Jerusalem, Israel

SUMMARY

Flow processes such as shear and extensional are known to affect orientation. Various studies usually consider orientation of long chain molecules, such as of high molecular weight polymers, and of fibers and whiskers embedded with the liquid. In this paper previous results on orientation of discontinuous fiber reinforced polymer melts are used in a new study of the effect of flow on orientation of acicular nanoparticles. This is also considered as a new technique for obtaining oriented nanocmposites.

1. INTRODUCTION

The effect of flow on orientation was initially studied in short fiber reinforced composites. In one of the studies, the shear induced crystallization behavior of isotactic polypropylene (iPP) composite melt containing chopped aramid fibers was investigated by means of WAXD (wide-angle X-ray diffraction) and SAXS (small-angle X-ray scattering) techniques using synchrotron radiation. The study was carried out on composites subjected to post shear isothermal crystallization at different temperatures in the range of 140-160 °C. A number of parameters pertaining to the crystallization morphology and kinetics were analyzed, such as the total crystallinity and the orientated fraction thereof, the fraction of the orientated amorphous phase, the dimensions of the formed shish-kebab structure and the induction time and rate of crystallization. The separate contributions of shear and fibers were determined and compared with their combined effect, which for most of the studied parameters exhibited a synergistic rather than an additive effect.

The results and observations of such preliminary studies on discontinuous micron fibers were then applied to acicular nanoreinforcement. A number of examples will be presented in this paper, including of processing and characterization of extruded drawn MWNT-PAN (multiwalled carbon nanotube-polyacrylonitrile) composite filaments, of characterization and correlation to nematic order of drawn monofilaments of liquid crystalline polymer/carbon nanoparticle composites and of orientated crystallization in drawn thermoplastic polyimide modified by carbon nanofibers.

2. RESULTS AND DISCUSSION

Our current work on orientation techniques for acicular nanofillers by flow was precedent by a number of studies on orientated crystallization in discontinuous aramid fiber(AF)/polypropylene(iPP) composites under shear flow conditions or under extensional drawing. Under shear conditions, the fibers became aligned in the flow direction [Larin et al (2005)] and then, combined with the effect of shear on the polymer matrix, a highly aligned shish-kebab/transcrystalline morphology was produced, as demonstrated in Fig. 1 [Larin et al (2008)].

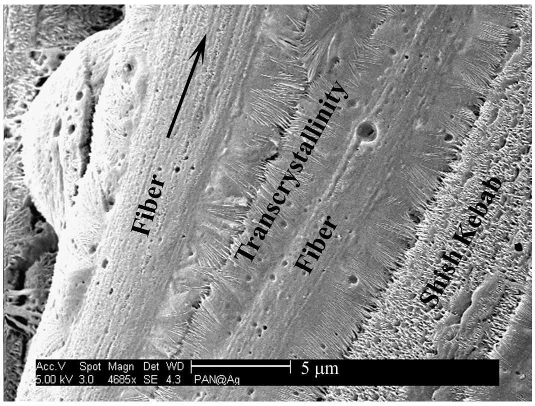

Fig. 1. High resolution SEM image of an etched tapered cross-section of shear crystallized AF-iPP composite (the arrow marks the shear direction), showing a highly oriented morphology structured around the flow-aligned fibers.

Based on this observation a number of nanocomposites were studied for the effect of flow on orientation. The study of processing and characterization of extruded drawn MWNT-PAN composite filaments [Vaisman et al (2007)] showed that Herman's factor (f_H), used to express the level of molecular orientation, increased with the draw ratio (Fig. 2) and that the strength and modulus increased correspondingly (Fig. 3).

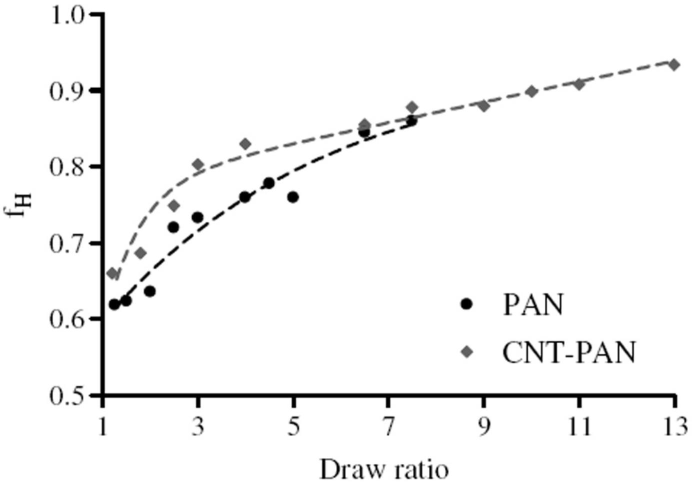

Fig. 2. Herman's factor (f_H) of PAN and CNT-PAN (1 wt.% MWNT) extruded filaments as a function of draw ratio.

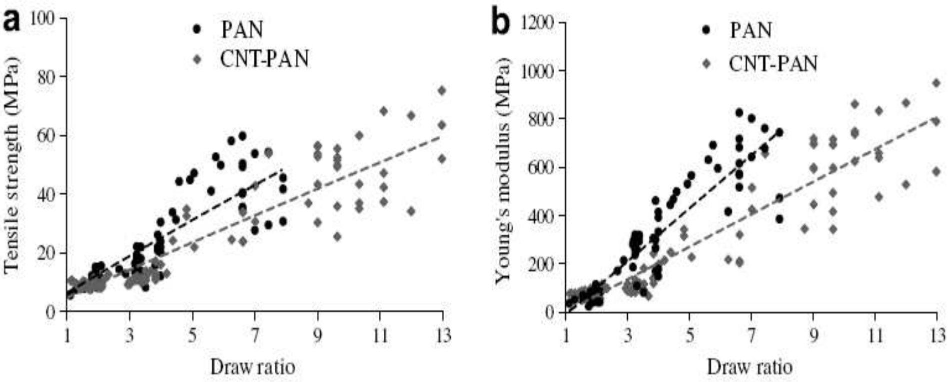

Fig. 3. The mechanical properties of PAN and CNT-PAN (1 wt.% MWNT) extruded filaments as a function of draw ratio: (a) the ultimate tensile strength , (b) the apparent Young's modulus.

The study of orientated crystallization in drawn thermoplastic polyimide (PI) modified by carbon nanofibers (VGCF) showed that the degree of orientation of nanofibers and crystallization increased with their content and with the draw ratio. And that drawing generated a unique orientated layered lamellar structure, characteristic of smectic-like mesophase, as demonstrated in Fig. 4 [Smirnova et al (2009)].

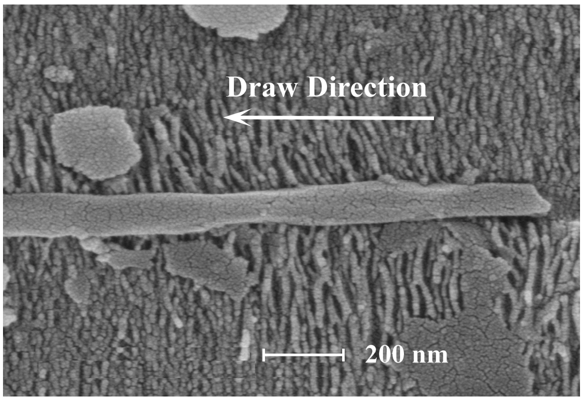

Fig. 4. Scanning electron micrograph of typical PI lamellar morphology around a single VGCF in a drawn (DR = 6, annealed, 1 wt.%) PI film. The lamellae are by and large perpendicular to the fiber.

The characterization of drawn monofilaments of liquid crystalline polymer (vectra)/carbon nanoparticle composites correlated to nematic order also showed that the

VGCF were individually dispersed and highly aligned along the filament axis (as shown in Fig. 5), generating significantly higher mechanical properties [Kalfon-Cohen et al (2009)].

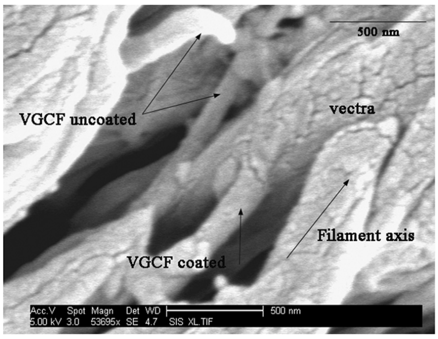

Fig. 5. Scanning electron micrograph of VGCF inclusions in a vectra/VGCF monofilament at a draw ratio 5.

3. CONCLUSIONS

Flow processes such as melt extrusion and extensional drawing can generate high alignment of acicular nanofillers. They can be utilized to produce aligned nanocomposites.

ACKNOWLEDGMENT

The author acknowledges his colleagues whose combined studies (cited bellow) contributed to this paper.

REFERENCES

KALFON-COHEN E., MAROM G., WACHTEL E., PEGORETTI A. (2009). Characterization of drawn monofilaments of liquid crystalline polymer/carbon anoparticle composites correlated to nematic order. *Polymer*, 50, 1797-1804.

LARIN B., MAROM G., AVILA-ORTA C.A., SOMANI R.H., HSIAO B.S. (2005). Orientated crystallization in discontinuous aramid fiber/isotactic polypropylene composites under shear flow conditions. *J. Appl. Polym. Sci.*, 98, 1113-1118.

LARIN B., AVILA-ORTA C.A., SOMANI R.H., HSIAO B.S., MAROM G. (2008). Combined effect of shear and fibrous fillers on orientation-induced crystallization in discontinuous aramid fiber/isotactic polypropylene composites. *Polymer*, 49, 295-302.

SMIRNOVA V.E., GOFMAN I.V., YUDIN V.E., DOBROVOLSKAYA I.P., SHUMAKOV A.N., DIDENKO A.L., SVETLICHNYI V.M., WACHTEL E., SHECHTER R., HAREL H., MAROM G. (2009). Orientated crystallization in drawn thermoplastic polyimide modified by carbon nanofiber. *Polym. Eng. Sci.*, 49, 217-222.

VAISMAN L., LARIN B., DAVIDI I., WACHTEL E., MAROM G., WAGNER H.D. (2007). Processing and characterization of extruded drawn MWNT-PAN composite filaments. *Compos. Pt. A-Appl. Sci. Manuf.*, 38, 1354-1362.

Microstructure, thermal, viscoelastic and mechanical properties of metallopolymers polyesterurethane-Co(II)

G. Moroi
Polyaddition Department. Institute of Macromolecular Chemistry “Petru Poni” of Iaşi, Romania

SUMMARY

A series of metallopolymers polyurethane/cobalt(II) (PUCo) having different cobalt contents were synthesized from a MDI-based polyesterurethane (PU) and cobalt chloride. PUCo were characterized in comparison with PU by AAS, UV–vis absorption spectroscopy, FTIR spectroscopy, DSC, DMA, TGA and tensile testing. Cobalt(II) ions form intermolecular tetrahedral complexes with the urethane nitrogen atoms in the hard segments, which results in the disturbance of hydrogen-bond system and crystallinity of the hard-segment domains. For PUCo compared with PU the values of soft-segment glass transition and storage modulus increase, due to the reduction in chain mobility induced by the coordination crosslinking, and the thermal stability is diminished. PUCo present lower values of tensile breaking strength and elongation at break than PU.

1. INTRODUCTION

In the last decades, the study of the systems formed of synthetic functional polymers and metal ions have attracted considerable attention as valuable information concerning the influence of the latter on the synthesis, processing and properties of the former can be thus obtained. Metallopolymers suitable for a variety of potential applications may be tailored by selecting the appropriate preparation conditions. Since polyurethanes constitute an important class of industrial polymeric materials, it is of great interest to establish the manner in which they are affected by the presence of metal ions. Polyurethane-based metallopolymers may be used as polymeric electrolytes, actuators, transducers etc. In our previous papers, the interactions between different types of polymers and various metal ion species have been studied. The objective of the present work was to investigate the effect of cobalt(II) ions on the microstructure and properties of a polyurethane material (cobalt is used in humidity indicators, fertilizers, as well as in electroplating and catalysis etc.). To this purpose, a series of PUCo were prepared in the form of films and characterized in comparison with PU.

2. EXPERIMENTAL

PUCo were synthesized from a polyesterurethane (PU) and cobalt chloride hexahydrate, $CoCl_2 \cdot 6H_2O$. PU was obtained from poly(ethylene-co-diethylene adipate)diol (PEDA), 4,4’-diphenylmethane diisocyanate (MDI) and ethylene glycol (EG); it contains PEDA soft segments and MDI/EG hard segments and its concentration of urethane groups is 3.26×10^{-3} mol g^{-1}. Four PUCo having distinct cobalt contents in the range 0.04–0.95% were prepared by the method presented elsewhere (Moroi et al. 2002 Thermochim. Acta). PUCo are partially crosslinked materials (as indicated by their improved solvent resistance), which is consistent with the occurrence of intermolecular complexation. Compared with PU, PUCo exhibit enhanced adherence to various substrates.

The cobalt content was determined by AAS using a Perkin Elmer AA800 spectrometer. The UV–vis absorption spectra were recorded using a SPECORD M42-Carl Zeiss Jena spectrophotometer in the wavelength range 280–770 nm. The FTIR-ATR spectra were acquired using a Brucker VERTEX 7-Specac Golden Gate spectrophotometer at a resolution of 2 cm^{-1}. The DSC analyses were conducted on a Mettler DSC 12E instrument from ambient temperature to 360 °C at a heating rate of 20 °C min^{-1}, the sample mass being about 2 mg. The DMA measurements were performed using a TA Instruments DMA 983 apparatus from –120 to 200 °C at a heating rate of 3 °C min^{-1} on multilayer samples of 50 × 30 × about 0.8 mm. The TGA measurements were carried out on a TGA V5.1A DuPont 2000 thermoanalyzer under dynamic nitrogen atmosphere from ambient temperature to 950 °C at a heating rate of 9 °C min^{-1}, the sample mass being 10 mg. The tensile tests were conducted on a computer-controlled tensile tester at a crosshead speed of 5 mm min^{-1}; the dimensions of the dumbbell-shaped specimens were 45 × 7 mm with gauge dimensions 14 × 4 mm.

3. RESULTS AND DISCUSSION

PUCo contain lower quantities of cobalt than those used in their synthesis (Moroi 2009). The cobalt content of PUCo increases roughly linearly with increasing initial cobalt concentration; the curve slope suggests that the former could be further increased by additionally increasing the latter.

By contrast to PU, which is colorless, PUCo exhibit a characteristic greenish-blue color, evidencing that cobalt(II) ions form coordination complexes with polyurethane functional groups. The UV-vis spectra reveal that the absorbance (A) of PUCo is higher than that corresponding to PU over the entire wavelength range. Whereas the spectrum of PU displays no absorption maximum, the spectra of PUCo exhibit two absorption maxima in the visible region around 440 and 670 nm, which probably arise from transitions taking place within the d-shell of Co(II) ion. The predominant tetrahedral geometry of the complexes, indicated by PUCo color, is confirmed by the absorption in the region 600–700 nm (Chen 1996). The intense band exhibited, as a shoulder around 315 nm, by the metallopolymers synthesized from PU and other transition metal ion species and assigned to a charge transfer electronic transition could be shifted in PUCo towards lower wavelengths overlapping PU absorption (Moroi 2009).

The FTIR spectra indicate that the polyurethane functional groups provide active sites (mainly the nitrogen atoms) capable to form coordination complexes with cobalt ions. The complexation involving the urethane groups in the hard segments is likely to result in the disturbance of the hydrogen-bond system existing in the hard-segment domains.

Based on spectroscopic results and literature data, the predominant complex structure may be assumed. This has a tetrahedral symmetry with the four-coordinated central Co(II) ion bonded with two urethane nitrogens and two chlorides (Shibata 2003, Zumdahl 1986). Since the two urethane groups belong to different polymer chains, coordination crosslinking appears within the polymer matrix.

The DSC thermograms of PU and PUCo show endotherms caused by the melting of the crystalline hard-segment domains. For PUCo compared with PU, changes of the melting endotherm take place as cobalt content increases (for the PUCo with the highest cobalt content, this endotherm is partially overlapped towards higher temperatures by a broad endotherm assigned to the thermal decomposition onset): its magnitude gradually diminishes, revealing a reduction of the crystallinity degree, and its position shifts towards lower temperatures, suggesting a decrease in order.

The DMA curves represent the dependence on temperature of loss tangent (tan δ) and elastic modulus (E'). On tan δ vs. temperature curve of PU, peaks α and β are ascribed to the glass transition of the soft segments (T_{gs}) and to a secondary relaxation occurring in the soft-segment phase, respectively (Hale et al. 1997, Bajsic 1996). For PUCo as compared with PU, the increase in T_{gs} suggests that limitations in soft-segment mobility are produced by the coordination crosslinking occurring within the hard-segment domains, whereas the modification of β peak could indicate changes in the hydrogen bonding occurring between the hard and soft segments. PUCo present higher values of E' than that corresponding to PU throughout the temperature range of DMA measurements, which shows the increase in chain stiffness.

The TGA results reveal that cobalt ions favor to different extents the processes involved in the thermal degradation of PU, i.e. the scission of the urethane linkage, as well as the decomposition of polyesterurethane chain sequences (MDI, PEDA and EG) and products formed via MDI secondary reactions (Moroi et al. 2002 Polym. Degrad. Stab., Moroi 2004).

The PU stress-strain curve is typical for elastomers. The stress-strain curves of PUCo are largely similar in shape with that of PU. For the two PUCo having lower cobalt contents, the curves are located close to that of PU. For the other PUCo, the tensile strength values are lower than that corresponding to PU (the difference becomes more and more significant as the strain increases), revealing that the higher amounts of cobalt ions render the polyurethane matrix less resistant than the lower cobalt amounts. Tensile testing results show that PUCo with maximum cobalt content has a lower resistance as compared with PUCo with minimum cobalt content, which seems to be consistent with DMA data. The values of the tensile breaking strength for PUCo are lower than for PU. It appears that the structural changes induced in the polymer matrix by the presence of cobalt ions do not compensate, as far as the tensile strength is concerned, for the loss of the initial structure (hydrogen bonding and crystallinity) of the hard-segment domains. Although, with increasing cobalt content, the stress necessary to produce a certain strain tends to decrease, the reverse situation would be expected from the standpoint of crosslinking level. It may be assumed that the mechanical behavior of PUCo is the resultant of several interrelated phenomena (e.g. coordination crosslinking, hydrogen bonding and crystallinity of the hard-segment domains and stress-induced crystallinity of the soft-segment phase). For PUCo compared with PU, the values of the elongation at break are generally lower, confirming the role of cobalt ions in enhancing the rigidity of the polyurethane matrix.

4. CONCLUSIONS

PUCo synthesized from a segmented polyesterurethane and cobalt(II) ions as chloride exhibit a characteristic color and, compared with PU, are more adherent to different substrates and less soluble in DMF. Cobalt(II) ions form coordination complexes of tetrahedral geometry with the urethane nitrogen atoms in the hard segments, the intermolecular complexation resulting in the crosslinking of the polymer chains; as a consequence, the hard-segment domains undergo the disturbance of the original hydrogen bonding. The complex formation interferes with the packing of the hard segments, causing modifications in the crystallinity of the hard-segment domains. In comparison with PU, PUCo present changes in both viscoelastic and mechanical behaviors due to the decrease in chain mobility caused by the coordination crosslinking (higher values of soft-segment glass transition and storage modulus, and lower values of tensile breaking strength and elongation at break). For PUCo compared with PU, the main steps of the thermal decomposition process are favored. Generally, the higher the cobalt content of PUCo, the more pronounced the differences in their properties as compared with PU.

ACKNOWLEDGMENT

The author is grateful to Dr. C. Ciobanu (Institute of Macromolecular Chemistry “Petru Poni” Iaşi, Romania) for providing the polyurethane and Prof. X. Han (Changchun Institute of Applied Chemistry, People’s Republic of China) for AAS analyses.

REFERENCES

BAJSIC, E.G., REK, V., SENDIJAREVIC, A., SENDIJAREVIC, V., FRISH, K.C. (1996) The effect of different molecular weight of soft segments in polyurethanes on photooxidative stability. *Polym. Degrad. Stab.*, 52, 223-233.
CHEN, L., XU, H., ZHU, Y., YANG, C., SHEN, G. (1996) Synthesis of novel coordination polyurethanes. *Polymer J.*, 28, 481-488.
HALE, A, BAIR, E.H. (1997) Polymer blends and block copolymers, *in Thermal Characterization of Polymeric Materials*, Second Edition (Ed. Turi, E.A.), 752, Academic Press, San Diego (USA).
MOROI, G., CIOBANU, C. (2002) Aspects of polyesterurethane interaction with metallic ions. II. Synthesis and thermal behavior of polyurethane interaction products with manganese and copper ions. *Thermochim. Acta*, 385, 153-162.
MOROI, G., CIOBANU, C. (2002) Thermal behaviour of polyurethane interaction products with cobalt ions. *Polym. Degrad. Stab.*, 78, 287−293.
MOROI, G. (2004) Influence of ion species on the thermal degradation of polyurethane interaction products with transition metal ions. *J. Anal. Appl. Pyrolysis*, 71, 485−500.
MOROI, G. (2009) Preparation and characterization of polyesterurethane metallopolymers containing transition metal ions. *Macromol. Symp.*, 279, 29-40.
SHIBATA, M., ITO, T. (2003) Metallization of cross-linked polyurethane resins by reduction of polymer-incorporated metal ion. *Polymer*, 44, 5617-5623.
ZUMDAHL, S.S. (1986) *Chemistry*, 838, D.C. Heath and Comp., Lexington, Massachusetts, Toronto.

Effect of nanoclay on long-term water absorption behavior of wood polymer nanocomposite

B. Kord
Scientific Member, Department of Wood and Paper Science and Technology,
Islamic Azad University, Chalous Branch, P.O. Box 46615/397, Chalous, Iran
Email: behzad_k8498@yahoo.com

SUMMARY

Polypropylene/wood flour composites with different nanoclay and maleated polypropylene (MAPP) contents were fabricated by melt compounding and then injection molding. The long-term water absorption of the composites was evaluated by immersing them in water at room temperature for several weeks (up to 3000 hours). Water diffusion coefficients were also calculated by evaluating the water absorption isotherms. Results indicated that water absorption decreased with increase of clay loading, and also the effect of compatibilzer was positive in terms of enhancing the dimensional stability of the composites. The maximum water absorption and diffusion coefficients decreased by increasing the proportion of clay and MAPP contents. Water absorption of the studied composites was proved to follow the kinetics of a Fickian diffusion process.

1. INTRODUCTION

New applications and end uses of wood plastic composites (WPCs) for decking, flooring and outdoor facilities, window frames, various construction materials and bathroom parts for example, and their exposure to atmosphere or contact with aqueous media has made it necessary to evaluate the water uptake characteristics of these materials. Water absorption is one of the most important characteristics of WPCs exposed to environmental conditions that determine their end use applications. Therefore, as a limiting parameter, water absorption has to be taken into account in the design of WPCs for final applications. Generally, water absorption in WPCs is governed by two significant mechanisms: the hygroscopic nature of natural fillers/fibers and the penetration of water into the composites (diffusivity) via gaps and flaws at the interfaces between fibers and plastics. Poor resistance of the fibers to water absorption can have undesirable effects on mechanical properties and dimensional stability and in long–term, embrittlement linked to the degradation of the macromolecular skeleton by hydrolysis. Therefore, it is important to study in detail the water absorption behavior in order to estimate not only the consequences that the water absorbed may have, but also how this water uptake can be minimized in some way. A number of attempts have been madetoreduce waterabsorption of WPCs.

The impressive enhancement of material properties achieved with the inclusion of submicron-size fillers in plastics and has stimulated active research in polymer composites. The aim of this study was to investigate the effect of nano-scale filler on the long-term water absorption behavior of polypropylene/wood flour composite.

2. EXPERIMENTAL

Polypropylene, V30S (MFI=18 g/10min, density=0.92 g/cm^3) was supplied by Arak Petrochemical Co, Iran. Beech wood-flour (100 mesh size) was from Cellulose Aria Co, Iran. Maleic anhydride grafted polypropylene (PP-g-MA) provided by Solvay with trade name of Priex 20070 (MFI=64 g/min, grafted maleic anhydride 0.1 wt%) was used as coupling agent. Cloisite 30B (CEC=90 meq/100 g clay, d_{001}=18.5 A) was obtained from Southern clay Products Co, USA as Nanoclay. Before preparation of samples, wood flour were dried in an oven at (65 ± 2) °C for 24 hours. Then polypropylene, wood flour and nanoclay were weighed and bagged according to formulations given in Table 1. The mixing was carried out by a HAAKE internal mixer, the total mixing time was 13 min. The compounded materials were then ground using a pilot scale grinder. Then, the resulted granules were dried at 105°C for 4 hours. Test specimens were prepared by injection molding. The specimens were stored under controlled conditions for at least 40 hours prior to testing. Water absorption tests were carried out according to ASTM D-7031-04.

Table 1. Composition of the Studied Formulations.

Code	Polypropylene content (Wt. %)	Wood flour content (Wt. %)	Nanoclay content (phc)*	PP-g-MA (phc)
50W50P	50	50	0	0
50W50P2M	50	50	0	2
50W50P4M	50	50	0	4
50W50P3N	50	50	3	0
50W50P2M3N	50	50	3	2
50W50P4M3N	50	50	3	4
50W50P6N	50	50	6	0
50W50P2M6N	50	50	6	2
50W50P4M6N	50	50	6	4

*Per hundred compound

3. RESULTS AND DISCUSSION

Water absorption curve is illustrated in figure 1 where the percentage of water absorption is plotted against time for all samples. As it is clearly seen, generally water absorption increases with immersion time, reaching a certain value at saturation point where no more water was absorbed and the composites water content remained constant. Time to reach the saturation point was not the same for all formulations. The 50W50P4M6N and 50W50P samples showed minimum (13.26%) and maximum (14.29%) water absorptions, respectively. The hydrophilic nature of wood flour causes the water absorption in manufactured WPCs (the plastics have negligible water absorption). Because of constant wood flour content (50 Wt. %) in all formulations, the different water absorption among all manufactured compositescan be attributed to the roleof coupling agent and nanoclay. Figure 1 also shows that water absorption decreases by adding the MAPP. This means that it is the interface region which influences the water absorption of the composite. Because uncompatibilized wood flour composite has weak fiber/matrix adhesion in nature, at the presence of the compatibilizer the interface is enhanced. Generally it is necessary to use compatibilizers or coupling agents in order to improve the polymer/fiber bonding and in turn to enhance water resistance. The MAPP chemically bonds with the OH groups in the lignocellulosic filler and limits the water absorption of the composites. As a result, it is important to use coupling agents to improve the quality of adhesion between plastics and fibers, to reduce the gaps in interfacial region and to block the hydrophilic groups. The another reason for less water absorption could be the change in crystallinity of WPCs coupled by coupling agent (MAPP) and existence of nanoclay as a nucleating agent. It was reported that crystallinity of the WPCs is much greater than that of the corresponding WPCs without the MAPP modification. On the other hand the nucleation efficiency and the crystallinity of the hybrid composite can be improved at the presence of the nanofiller as a nucleating agent. As the crystalline regions are impermeable to penetrate, the water absorption is less in the composites.

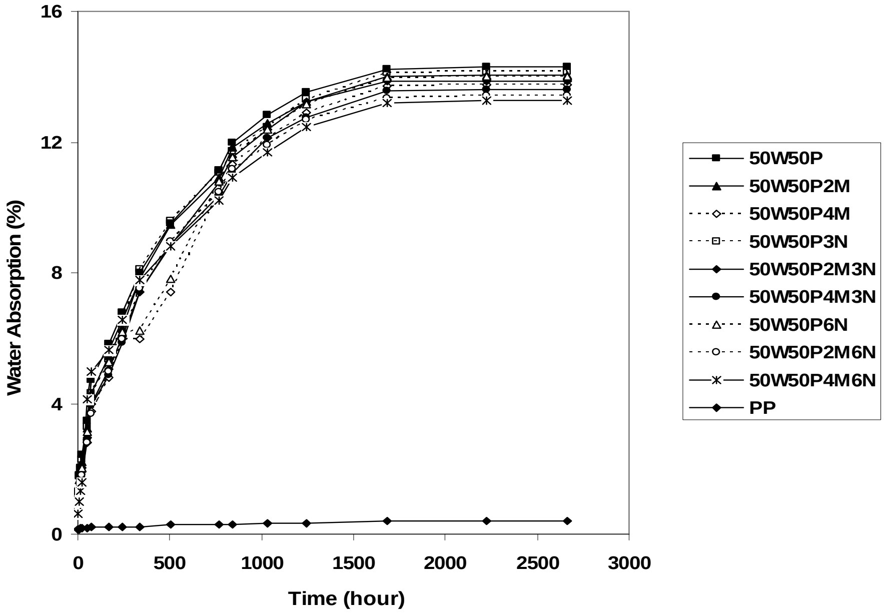

Figure 1. Water absorption of the samples.

Another result in figure 1 is that the composites containing clay exhibited lower water absorption as compared with those made without clay. By increasing the clay content to 6%, the water absorption of composites was reduced. It seems the barrier properties of nano scale filler inhibit the water permeation in the polymer matrix. Two mechanisms have been reported for this phenomenon. First is based on the hydrophilic nature of the clay surface that tends to immobilize some of the moisture, second, surfactant-covered clay platelets form a tortuous path for water transport. This barrier property hinders water from going into the inner part of the nanocomposite. It seems both of afore said mechanisms could be more efficient when the morphology is exfoliated. In other words in exfoliated morphology, there is more available surface of organoclay (with hydrophilic nature) and surfactant (tortuous path), so the water transport goes down under the severe conditions. In general, three mechanisms for water transport in polymer composites are known which are: Fickian diffusion, Relaxation controlled and non-Fickian or Anomalous. The dominant mechanism depends on factors such as chemical structure of the polymer, dimensions and morphology of the wood filler and polymer-filler interfacial adhesion. Table 2 shows the water diffusion coefficients for all formulations. The results show the water diffusion coefficients decrease with incorporation of MAPP into hybrid composite. The 50W50P4M composite exhibited the lowest diffusion coefficients.

Table 2. Water diffusion, maximum water Absorption, n and k coefficients for all formulations.

Formulation	Maximum Water Absorption	n	K(h^2)	Water Diffusion Coefficient ($\times 10^{-12}$ m2s-^{1})
50W50P	14.2861	0.3845	0.0594	3.9295E-12
50W50P2M	14.0547	0.4132	0.0466	3.7667E-12
50W50P4M	13.7526	0.4352	0.0397	3.2589E-12
50W50P3N	14.1606	0.3912	0.0561	4.016E-12
50W50P2M3N	13.8785	0.4249	0.0445	4.1368E-12
50W50P4M3N	13.6163	0.4632	0.0357	4.1589E-12
50W50P6N	14.0224	0.3818	0.0546	4.0374E-12
50W50P2M6N	13.4081	0.4688	0.0342	3.9933E-12
50W50P4M6N	13.2577	0.4774	0.0348	3.8925E-12

4. CONCLUSIONS

The following conclusions could be drawn from the results of the present study:
1. Water absorption of the hybrid composite increased with immersion time, reaching a certain value at saturation point and the composites water content remained constant
2. With increase of the MAPP and organoclay content in composite, water absorption decreased.
3. The mechanism of water transport in hybrid composite was Fickian diffusion and it seems, the water transport could be more restricted in exfoliated morphology through this mechanism.

REFERENCES

Han, G., Lei, Y., Wu, Q., Kojima, Y. and Suzuki, S. 2008. Bamboo–fiber filled high density polyethylene composites; effect of coupling treatmentand nanoclay. Journal of Polymer Environment, Vol 21, 1567-1582.
Lei, Y., Wu, Q., Clemons, C.M., Yao, F. and Xu, Y. 2007. Influence of nanoclayon properties of HDPE/wood composites. Journal of Applied Polymer Science, Vol 18, 1425-1433.
Rana HT, GuptaRK, GangaRao HVS, Sridhar LN. 2005. Measurement of Moisture Diffusivity through Layered-Silicate Nanocomposites, AIChE Journal, 51, 3249-3256.
Utracki, L.A., Sepehr, M. and E.Boccaleri, E. 2007. Synthetic, layered nanoparticles for polymeric nanocomposites (PNCs); A review. Journal of Polymers for Advanced Technologies, Vol 18, 1-37.

Improved biodegradable materials for packaging

J. Alonso, M. Gallur, M. Jorda, S. Aucejo
“Advanced 'Materials for Packaging”. Packaging, Transport and Logistics Research Centre (ITENE).C/Albert Einstein, 1. Parque Tecnológico de Paterna, Valencia, Spain.
E-mail: jalonso@itene.com Phone contact:+34 963905400 Fax:+34 963905401

ABSTRACT

The use of polymers in packaging is widespread nowadays. However, most of the conventional polymers used in packaging are not degradable is a reasonable period of time, and hence high quantity of wastes are accumulated during long periods of time, taking up a lot space in landfills. Moreover oil is running out, and prices are rising more and more each day.

One solution to this problem is the use of renewable materials. These materials are obtain from the feedstocks, like corn or sugar, and after making use of them, are degradable or compostable.

Among other materials, starch, polylactic Acid (PLA), and polyhydroxybutyrates (PHB) are the materials most commonly used in packaging. However, these raw materials suffer from poor properties for some packaging applications. In order to get better features, different nanoreinforcements can be added to the polymer matrix to obtain enhanced materials.

In this paper, nanocomposites of starch and PLA have been prepared in order to evaluate the improvement in properties (related to the neat matrix), studying important parameters for packaging like barrier, mechanical, or thermal properties obtaining improved properties comparing to the neat matrix.

1. INTRODUCTION

The industrial use of plastics produced from non-renewable raw materials, especially in the case of packaging, and consumables, is continuous increasingly in worldwide. In 2007 the amount of waste plastic generates in Spain was 2.7 millions tons, a 58 % of total plastic waste, and a 1.65 millions tons was only generates in packaging applications (Infopack nº 142, 2007). These numbers make necessary the search of alternatives materials more sustainable and eco-efficient that can compete in packaging market.

The development and use of biodegradable polymers from renewable resources has been strongly encouraged in last years in response to concerns about disposal of plastics. Biopolymers have attracted more and more interest due to increasing environmental concern and decreasing fossil resources. This evolution motivates the research to develop novel materials labelled as “environmentally-friendly”, i.e., materials produced from alternative resources, with lower energy consumption, biodegradable and non-toxic to the environment Since biopolymers are biodegradable and the main productions are obtained from renewable resources, they represent an interesting alternative of conventional plastic substitution for short-life range applications as packaging .

Nevertheless, until now, most biopolymers are sometimes too weak for practical use. Therefore, it appears necessary to improve these biopolymers to make them fully competitive with common thermoplastics. Nanocomposites are novel materials with drastically improved properties due to the incorporation of small amounts (less than 10 wt %) of nano-sized fillers into a polymer matrix. Nanofillers can be classified according to their morphology (P. Bordes et al, 2009). Nano-biocomposites are obtained by adding nanofillers to biopolymers, resulting in very promising materials since they show improved properties with preservation of the material biodegradability, without eco-toxicity.

Starch is a semicrystalline polymer stored in granules as a reserve in most plants. Barrier properties of starch films have been characterized before (Forssell P. et al., 2002). Starch films are good oxygen barriers, due to their tightly packed, and ordered network structure, bonded by hydrogen bonds, however, its hydrophilic nature and poor mechanical properties has restricted its application as packaging material.

A possible alternative to enhance the material properties is the use of different reinforcements such as fibres. A lot of progress and research has been devoted to study and develop new nanosized reinforcements derived from cellulose materials (Zimmermann, T et al. 2004). Acid hydrolysis of cellulose is a well-known process used to remove amorphous regions and obtain cellulose crystallites/whiskers from various cellulose sources (Devis A., 2008).

An interesting aspect of poly(lactic acid) (PLA) is its availability from a monomer/cyclic dimer (lactide) produced by fermentation of agricultural crops such as corn, potato, and waste products. Because of this “green” feature combined with its benign degradation behavior, PLA is considered as a potential packaging material in many fields. Biomedical uses of PLA have been widespread, which include bioabsorbable surgical sutures and implants, controlled drug delivery, and tissue culture. However, the strength and some other properties such as thermal stability, gas barrier, solvent resistance, and flame retardance of the pure polymer are often not enough for end use. Confinement of polymer in a two-dimensional silicate gallery, so-called polymer nanocomposite, is one of the effective ways to improve material performance (Maiti et al. 2007).

2. EXPERIMENTAL

2.1 Materials

Purified sodium montmorillonite (MMT) (Closite®Na+) was purchased from Southern Clay Products. Modified clay were prepared in our laboratory as is described at (Jordá-Beneyto M. 2008). Cellulose Nanowhiskers were obtain following a process explain at (Devís A. 2008). Microcrystalline Cellulose Avicel, (FMC Biopolymer), was used as substrate for obtaining the cellulose nanowhiskers.

Polylactide pellets were purchased from Cargill Dow (NatureWorks® PLA polymer 7032D) for the preparation of filled biopolymers. Pea starch was obtained by Roquette Laisa S.A.

2.2 Nanocomposites preparation

Different nanocomposites samples have been obtained filled with the different reinforcements. For this purpose a DSM Explore Microcompounder (15.5 cc) was used. Pellets (dried overnight at 60ºC) are blended with different weight percentages of nanoreinforcements and plasticizers, in this counter-rotating micro-extruder. After extrusion the melted materials were transferred through a preheated cylinder to the mini injection moulder (DSM Explore) to obtain bone-like specimen samples (ISO 527 standard; probe type 5A-B).

2.3. Characterization

Nanocomposites were characterized using different techniques. TGA (Thermogravimetric Analysis) analyses were performed on samples using a Thermal

Analyzer Q5000 IR (TA Instruments). DSC (Differential Scanning Calorimetry) was carried out on nanocomposite samples trough a Q2000 MDSC equipment (TA Instruments). Finally, Mechanical Properties of nanocomposites samples were determined from tensile tests, performed on a universal testing machine at a constant elongation rate of 20 mm/min (ISO 527 standard). Water Vapour Transmission Rate (WVTR) was evaluated following standard ASTM E96-93 using the desiccant method.

3. RESULTS AND DISCUSSION

3.1. Starch composites

Pea starch-cellulose nanowhiskers composites with 2%wt, 4%wt and 6%wt were developed. Mechanical properties (Young's modulus and elongation at break) of the nanocomposites of pea starch obtained with the addition of CNW showed an increase on the Young's Modulus as a function of reinforcements content compared with the neat starch matrix value, as shows 1. This phenomenon is combined with a decrease on elongation at break when increase filler content (Gallur M. et al, 2008). Thermal results showed a slightly displacement of melting point towards higher temperature. Both results proved that cellulose nanowhiskers and starch matrix have a good interfacial adhesion. (Averous L. et al, 2001).

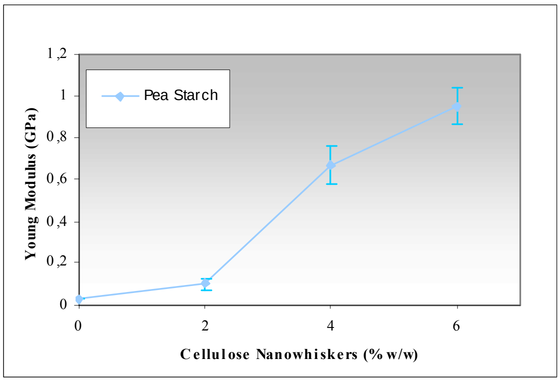

Fig. 1. Mechanical properties of pea starch bionanocomposites.

3.2. PLA composites

Water vapour transmission rate of different PLA composites prepared with organo – modified clay was evaluated. Results are shown in Fig. 2. It can be observed the improvement in WVTR of sample when modified clays are used. The best result is achieved with a 55 % in WVTR reduction.

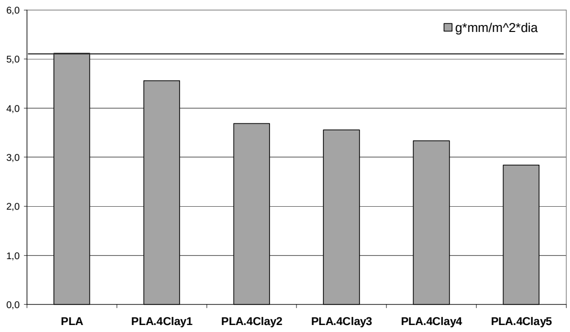

Fig. 2. WVTR of different PLA bionanocomposites.

4. CONCLUSIONS

Pea starch bionanocomposites were developed and characterized. Results obtained shown an improvement in thermal and mechanical properties. PLA nanocomposites have been obtained with improved barrier properties. 55 % of reduction in WVTR is achieved.

ACKNOWLEDGMENTS

Authors would like to thank to the IMPIVA for the financial support, and Roquette Laisa S.A for providing Starch materials.

REFERENCES

AVEROUS L, FRINGANT C AND MORO L (2001) Plasticizers starch-cellulose interactions in polysaccharide composites. Polymer 42:6565-6572.

BORDES. P, POLLET. E, AVEROUS. L, (2009) Nano-biocomposites: Biodegradable polyester/nanoclay systems. Progress in Polymer Science 34 125–155

DEVÍS A., S. J., ALONSO J.M., GALLUR M., JORDÁ M. AND AUCEJO S. (2008). Bionanocomposites based on cellulose nanowhiskers and renewable polymeric matrices. *Bangkok (Thailand)*,

FORSSELL, P., et al.,(2002) Carbohydrate Polymers, 47(2): p. 125.

GALLUR M., DEVIS.A, SALAS.J, ALONSO.J, JORDÀ-BENEYTO. M AND AUCEJO. S. (2008) “Starch Blends reinforced with cellulose nanowiskers and nanoclays for biopackaging” Proceedings of the Polymer Processing Society 24th Annual Meeting ~ PPS-24 ~ June 15-19, 2008 Salerno (Italy).

JORDÁ-BENEYTO M., A. J., SALAS J., GALLUR M., AUCEJO S., CLEGG F., BREEN C. (2008). Processed Biopolymer Films Filled With Modified Montmorillonite For Food Packaging Applications. *Salerno (Italy)*,

MAITI, P., BATT, C. A. and GIANNELIS, E. P. (2007). New biodegradable polyhydroxybutyrate/layered silicate nanocomposites. *Biomacromolecules.* 8, 11, 3393-3400.

ZIMMERMANN, T., E. POHLER, AND T. GEIGER,(2004) Advanced Engineering Materials. 6(9): p. 754.

HEBM, a new route for preparing LDPE-silica nanocomposites. Influence of the process and the silica content

D. Olmos, J.González-Benito
Dpto. Ciencia e Ing. de Materiales e Ing. Química, universidad Carlos III de Madrid.
Avda. Universidad 30, 28911-Leganés, Madrid, Spain. e-mail: javid@ing.uc3m.es
G. González-Gaitano
Departamento de Química y Edafología. Universidad de Navarra,
31080 Pamplona, Spain

RESUMEN

The aim of this work is to evaluate a new route, high energy ball milling (HEBM), for preparing nanocomposites based on low density polyethylene (LDPE) filled with silica nanoparticles. The influence of HEBM process and the presence of silica nanoparticles on the thermal properties and the morphology of the materials were studied. Different composites were prepared as a function of: i) the milling time and ii) the amount of silica added to the polymer. Thermal (TGA, DSC), spectroscopic (FTIR) and morphological (AFM) characterizations of the nanocomposites were carried out. The HEBM led to the incorporation of pure alumina particles coming from the milling balls and jar into the LDPE. The amount of alumina incorporated varied with the milling time and the amount of the silica added. The decomposition temperatures of the samples occurred ca. 450 ºC, regardless the grinding time (amount of alumina) or the silica content. Although the final properties of the samples did not differ much of those of the neat LDPE, the presence of the nanoparticles play an important role in certain properties such as the coefficient of thermal expansion (CTE) of the composites.

1. INTRODUCTION

Polymers filled with nanoparticles usually show unique or enhanced properties (mechanical, electrical, thermal, optical…) at rather low loadings compared to conventional composites. Although the enhancement of a certain property depends on several factors, an efficient dispersion of the nanoparticles in the polymer matrix is a critical issue. Several experimental approaches can be found in literature describing different protocols to obtain uniformly dispersed nanofillers in a polymer matrix. Typically these processes are based either on solution or on molten state methods which have as major disadvantages the use of solvents or high processing temperatures. Recently, the solid-state methods such as *high-energy ball milling* (HEBM) have been proven to be a good alternative to efficiently disperse different nanoparticles in polymeric matrixes (González-Benito et al. 2007, González-Benito et al. 2009, Vittoria et al. 2007). In this work we examine the effect of HEBM as an alternative method of dispersion and preparation of nanocomposite materials based on a LDPE and commercial silica nanoparticles (diameter of 14 nm). Firstly, the effect of milling time at constant loading of silica (2% by weight) in LDPE was studied. As reference system neat LDPE was used considering the same milling times. Secondly, the influence of the amount of silica nanoparticles in the LDPE was investigated preparing samples with different content of nanoparticles (1, 2, 4, 8, 10 and 20% w/w). Thermal (TGA, DSC), spectroscopic (FTIR) and morphological (AFM) characterizations were used to monitor the effects of milling conditions and silica content on the samples under study.

2. EXPERIMENTAL PART

2.1 Materials and sample preparation

Commercial low density polyethylene, LDPE, as well as 14-nm diameter fumed silica nanoparticles were supplied by Sigma-Aldrich. Samples were prepared as follows: 20 g of LDPE and silica nanoparticles mixtures (1, 2, 4, 8, 10 and 20% by weight of silica) were introduced in an alumina grinding jar together with 190 g of alumina balls. The whole system was placed in a Pulverisette 5 Fritsch apparatus where the powder was milled (400 rpm) at room temperature. To study the effect of the milling time on the blending process, samples of LDPE-silica (2% wt) were extracted at different milling times (1, 2, 4, 8, 10 h) letting the equipment to rest for 15 min every hour of active milling. To avoid overheating in the system a milling sub-cycle was considered. Neat LDPE was also subjected to the same milling cycles to have samples as references.

2.2 Techniques

TGA experiments were performed with a Mettler TGA/SDTA851 from 25 to 900ºC in N_2 atmosphere. Sample of 10-20 mg were flattened in open Pt crucibles and the thermograms recorded at different heating rates (15, 20, 25 and 30 ºC/min). The non-isothermal crystallization and melting processes of all the samples were studied in a Mettler Toledo 822^e *DSC* under N_2 atmosphere using the following scan sequence: i) 35-170 ºC (10 ºC/min); ii) 170 ºC (5 min); iii) 170-35 ºC; iv) 35 º C (3 min); v) 35-170 ºC (10 ºC/min). *FTIR-ATR* spectra were recorded with a Nicolet Avatar spectrometer with a Golden Gate diamond, single bound, ATR. Each spectrum is the average of 32 scans, at 4 cm^{-1} resolution in the wave number range 4000-600 cm^{-1}. A pellet of blend was kept during 1h at 140ºC and then annealed to 40ºC by cooling at a 50ºC/h rate. *AFM* studies were done with a scanning probe microscope MultiMode Nanoscope IVA (Veeco) at ambient conditions in tapping mode with etched silicon probes (40 N/m).

3. RESULTS AND DISCUSSION

At each heating rate, the decomposition onset of the LDPE occurs at the same temperature regardless the milling time or the silica content. However, the residue after thermal degradation increases with milling time (Fig. 1a). X-ray microanalysis, XRD and FTIR analyses of the residues proved that cross-contamination is solely due to Al_2O_3 arising from the corundum sintered balls used for milling. Although not strictly parallel, in the presence of a 2% of silica nanoparticles the trend is similar and a crossover at 6h of milling is observed (Fig. 1a). Beyond this point the difference between both curves corresponds to the initial content in silica (2%). The presence of nanoparticles in higher amounts seems to have a buffering effect on the wearing of the balls. In fact, the extra mass registered upon thermal degradation at a constant milling time (6h) is lower the higher the silica content is (Fig. 1b).

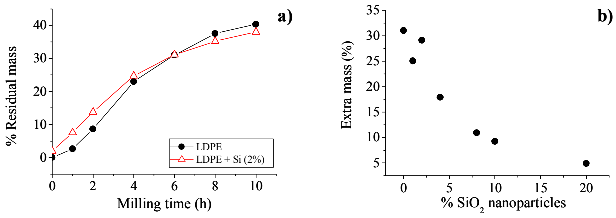

Fig. 1. a) Residual mass (%) of LDPE samples with milling time; b) Variation of the extra mass (%) registered as a function of the content in silica particles.

Fig. 2 shows the FTIR-ATR spectra of the samples milled for 6h with different SiO_2 content. The narrow doublet at 1472-1462 cm^{-1} is the bending mode of CH_2 and the broad band at 1098 cm^{-1} corresponds to SiO_2. In the mid IR region, Al_2O_3 absorbs below 900 cm^{-1} in a broad band, in which the rocking vibration mode of CH_2 at 728-718 cm^{-1} is overlapped. Although the presence of nanoparticles does not modify the bands of the polymer there is a marked drop in the absorbance of the corundum band at higher silica contents which is in accordance with TGA results (Fig. 1b). One possible explanation might be related with the brittleness of the milled polymer because this contamination was not observed in the case of polymers whose glass transition temperature was higher than the milling temperature. To overcome this difficulty, further experiments will be carried out under cryogenic conditions.

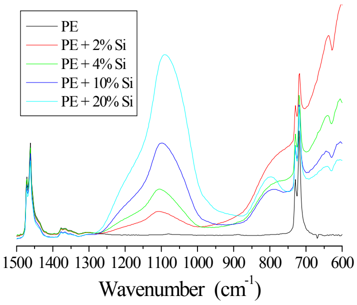

Fig. 2. FTIR–ATR spectra as a function of the content in silica nanoparticles.

DSC experiments revealed slight variations in the crystallization process within the first 4h of milling. A slight increase in the crystallization temperature, T_c, of LDPE was observed. Furthermore, as milling time proceeds, the bandwidth of the crystallization exothermal trace decreases. This result may indicate that the type of crystallites is more uniform. A similar trend with milling time was also observed for the LDPE-2% SiO_2 samples. However, a slight decrease in T_c is observed when the amount of silica increases. These variations were attributed to the amount of alumina microparticles.

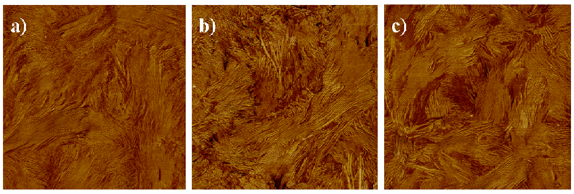

Fig. 3. AFM Phase images of: a) LDPE; b) LDPE-6h and c) LDPE-20% SiO_2 samples. (Phase scale 50°, 10x10 μm).

On the other hand, lamellar thicknesses of 17-27 nm were estimated from AFM images (Fig. 3), being in good agreement with results published in literature. Moreover, being concordant with the DSC results, the tendency observed seems to indicate that the thickness of lamellas slightly changes when the amount of alumina increases while they do not seem to change as a function of the silica content.

Figure 4 shows the thermal expansion of LDPE and nanosilica filled LDPE (2% and 20% wt) in a small range of temperatures. Coefficients of thermal expansion, CTE, calculated for these samples were: $3.0\cdot10^{-4}$; $3.1\cdot10^{-4}$ and $1.9\cdot10^{-4}$ $^{o}C^{-1}$ respectively. This result suggests that presence of high enough amounts of silica nanoparticles (20% w/w) rather than the presence of alumina allows reducing considerably the coefficient of thermal expansion (40% of reduction).

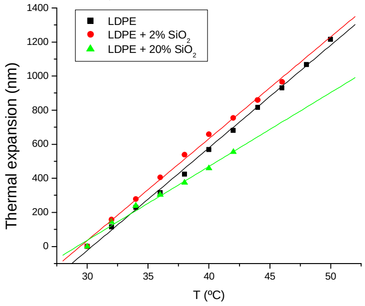

Fig. 4. Thermal expansion of LDPE, LDPE-2% and LDPE-20% samples.

3. CONCLUSIONS

LDPE-silica nanocomposites were prepared using high energy ball milling (HEBM). Thermogravimetric analyses as well as FTIR and XRD experiments revealed a cross-contamination due to the balls and jar used for milling. Although, the presence of corundum microparticles within the nanocomposites may slightly affect the morphology of the polymer they did not seem to affect the CTE of the materials. However, the CTE seems to be dependent on the amount of silica nanoparticles.

ACKNOWLEDGEMENTS

Authors gratefully acknowledge financial support from projects MAT2007-61607 and HH2006-0007.

REFERENCES

CASTRILLO, P.D., OLMOS, D., AMADOR, D.R., GONZÁLEZ-BENITO, J. (2007). Real dispersion of isolated fumed silica nanoparticles in highly filled PMMA prepared by high energy ball milling. *J. Coll. Interf. Sci.*, 308, 318-324.

GORRASI G, SARNO M, DI BARTOLOMEO A, SANNINO D, CIAMBELLI P, VITTORIA, V. (2007) Incorporation of carbon nanotubes into polyethylene by high energy ball milling: Morphology and physical properties. J. Polymer Science: Part B.,45, 597-606.

OLMOS D., DOMINGUEZ, C., CASTRILLO, P.D., GONZÁLEZ-BENITO, J. (2009). Crystallization and final morphology of HDPE: Effect of the high energy ball milling and the presence of TiO_2 nanoparticles. *Polymer*, 50, 1732-1742.

Novel polylactide-microfibrillated cellulose laminated films

I. Siró, D. Plackett
Risø National Laboratory for Sustainable Energy, Technical University of Denmark,
P.O. 49, DK-4000 Roskilde, Denmark
e-mail: istvan.siro@risoe.dtu.dk

SUMMARY

Due to its easy processibility and outstanding features, polylactide (PLA) could be a substitute for conventional polymers in several application domains. However, PLA also has some shortcomings which restrict its wider application, such as its inherent brittleness, low thermal stability, limited oxygen barrier and relatively high price. Preparation of nanocomposites of PLA and natural nanofibers has been considered as a promising method. The use of microfibrillated cellulose (MFC) in combination with PLA could lead to fully degradable and renewable nanocomposites with a range of practical applications. MFC (also referred as nanocellulose) offers unique possibilities as a reinforcing material due to its fine scale, high stiffness and strength[1,2]. However, deriving from the highly hydrophilic nature of MFC its application as reinforcement for nanocomposites has so far been limited to water-based polymers[3,4,5].

A practical way to combine beneficial properties of MFC and polylactide might be lamination of the two materials, which to our knowledge has not previously been reported. To explore this possibility, two types of plasticized MFC film, differing in terms of the starting raw materials, were cast from dispersion in deionized water and L-PLA films were extruded from commercial granulate in a single screw extruder. Sandwich structures of PLA/MFC/PLA films were fabricated using an office laminator. The key properties of these laminated films, such as transparency, oxygen and water vapor permeability and adhesion were tested and are reviewed in this presentation.

REFERENCES

1. Sakurada, I.; Ito, T.; Nakamae, K. *Makromol. Chem.* **1964**, 1-10.
2. Yano, H.; Nakahara, S. *J. Mater. Sci.* **2004***, 5,* 1635-1638.
3. Cheng Q, Wang SQ, Rials TG, Lee SH. *Cellulose.* **2007**, 14 (6): 593-602
4. Henriksson M, Berglund LA. *J Appl Poly Sci.* **2007**, 106(4): 2817-2824.
5. Zimmermann T, Pohler E, Geiger T. *Adv Eng Mater.* **2004**, 6(9):754–761.

Development and characterization of HDPE/EVA/POSS nanocomposites

P. Scapini, C.A. Figueroa, C.L.G. Amorim, J.S. Crespo
Centro de Ciências Exatas e Tecnologia, Universidade de Caxias do Sul, Brazil
R.S. Mauler, R.V.B. Oliveira
Instituto de Química, Universidade Federal do Rio Grande do Sul, Brazil

SUMMARY

In this study, composites with a polymeric matrix comprising a blend of high density polyethylene (HDPE) and the copolymer ethylene vinyl acetate (EVA), and with polyhedral oligomeric silsesquioxane (POSS) as the nanoclay, were processed and characterized. The composites were processed in a closed mixing chamber and characterized in terms of their thermal and morphological properties. For the preparation of the composites, the concentrations of the blend components (0, 25, 75 and 100%wt) and of the POSS (0, 2 and 10%wt) were varied. The results of the processing showed that an increase in the POSS concentration in the polymeric matrix caused the aggregation of the system. The X-ray results indicated that the presence of EVA in the composites led to the appearance of crystalline domains at lower POSS concentrations. Scanning electron microscopy of the blends without POSS reveals that the two polymers are immiscible and incompatible. The differential scanning calorimetry and thermogravimetry analyses indicated that the POSS did not affect the melt and degradation temperatures of the polymer matrix.

1. INTRODUCTION

The demand of polymers requirements for new applications, has increased, including higher temperatures of use and greater resistance to oxidation. The polymer industry has been able to keep abreast of these market demands through the use of additives, fillers, and polymer blends. More recently, the diverse and entirely new chemical technology of polyhedral oligomeric silsesquioxane (POSS) nanostructured polymers has been developed. This technology affords the possibility of preparing plastics that contain nanoscale reinforcements directly bound to the polymer chains. Unlike previous systems, the POSS technology materials have the additional advantage of being employed in the same manner as organic monomers or in the form of blendable resins (SCHWAB et to. 1998). The silsesquioxanes include random, ladder, cage and partial cage structures. However, much more attention has been directed to the silsesquioxanes with specific cage structures designated by the abbreviation POSS (LI et to. 2002). The chemical nanostructure of POSS, with a diameter of 1 to 3 *nm*, can be seen as the smallest possible particles of silica (MARK 2004). The incorporation of POSS cages into polymer materials may result in improvements in polymer properties, including increased temperature of usage, oxidative resistance and surface hardening, resulting in better mechanical properties as well as a reduction in flammability and heat evolution (WADDON et to. 2002).

This article reports a new approach for the modification of HDPE/EVA by the incorporation of POSS nanostructures by melt mixing. Thus, the processability, thermal properties and morphology of the produced systems were investigated.

2. EXPERIMENTAL

2.1 Preparation of nanocomposites

For the preparation of the composites, the concentrations of the blend components (0, 25, 75 and 100%wt) and of the POSS (0, 2 and 10%wt) were varied. In this study, a torque rheometer equipped with a mixing chamber with a volume of 65 *cm*^{3} was used to estimate the processability of the composites. The experiments were carried out at 180 *ºC*, 90 *rpm*, for 10 *min*, with a torque precision of ± 1.0 *N*.

2.2 Characterization of composites

The thin films (≈ 1 *mm*) used in the composite characterization were prepared by compression molding at 190 *ºC* for 10 *min* under a pressure of 7.5 *MPa*.

The X-ray diffraction (XRD) measurements were taken at room temperature on a Shimadzu XRD 6000 diffractometer in normal reflection mode with CuKα radiation. The samples were scanned at 0.5 ^{o} *min*$^{-1}$.

Scanning electron microscopy (SEM) and Si mapping of the composites samples were carried out using a Shimadzu SSX-550 scanning electron microscope equipped with an energy dispersive X-ray detector at an operating voltage of 15 *kV*. Before analysis, cryogenic fracture surfaces were covered with a thin gold layer in a P-S2 diode sputtering system metalizer for 2 *min*.

The calorimetric measurements were taken on a Shimadzu DSC-50 differential scanning calorimeter in a dry nitrogen atmosphere (50 *mL min*$^{-1}$). All the samples (around 10 *mg*) were heated from ambient temperature to 200 *ºC*. For the normalization of the thermal history (first run, 10 *ºC min*$^{-1}$), the data reported here were collected for the second melt event with a heating and cooling scan of 10 *ºC min*$^{-1}$.

A Shimadzu thermal gravimetric analyzer (TGA-50) was used to investigate the thermal stability of the composites. The samples (about 10 *mg*) were heated under nitrogen atmosphere from ambient temperature up to 900 *ºC* at a heating rate of 10 *ºC min*$^{-1}$.

3. RESULTS AND DISCUSSION

Table 1 gives the stabilized torque, which can be related to the viscosity of the sample, the totalized torque, which is related to the work required to mix the components, and the specific energy, which is the ratio between the energy required to carry out the mixing and the sample mass.

In the HDPE and HDPE/EVA systems, the presence of 2 *wt%* of POSS slightly increases the values for the stabilized and totalized torque and specific energy. This result suggests that the viscosity of these two samples is higher. The decrease of these values for a POSS content of 10 *wt%* was also observed, suggesting that in high concentrations POSS form aggregates, which are not incorporated into the polymer, leading to a decrease in viscosity. However, for the EVA system there was an increase in the stabilized and totalized torque and the specific energy with an increase in the POSS content. This increase was proportional to the POSS content and is probably due to auto-reticulation of the EVA caused by the temperature and shearing (MARCILLA et to. 2001).

Table 1. Processability results of composites.

System	POSS content (wt%)	Stabilized torque (N m)	Totalized torque (N m min)	Specific energy (J g^{-1})
HDPE100	0	5.1 ± 1.0	57.5 ± 10.0	636.6 ± 95.1
	2	5.5 ± 1.0	60.0 ± 10.0	660.0 ± 94.7
	10	4.8 ± 1.0	55.7 ± 10.0	618.3 ± 93.5
HDPE75/EVA25	0	4.7 ± 1.0	52.0 ± 10.0	585 ± 95.0
	2	5.1 ± 1.0	59.3 ± 9.1	645.0 ± 95.2
	10	4.6 ± 1.0	50.4 ± 10.0	568.3 ± 93.3
HDPE25/EVA75	0	7.7 ± 1.0	68.5 ± 10.0	740.0 ± 94.3
	2	7.5 ± 1.0	66.5 ± 9.1	721.7 ± 95.0
	10	6.4 ± 1.0	61.7 ± 10.0	675.2 ± 93.30
EVA100	0	7.0 ± 1.0	69.7 ± 10.0	751.7 ± 94.9
	2	19.5 ± 1.0	144.9 ± 10.0	1460.0 ± 94.2
	10	14.7 ± 1.0	117.1 ± 10.0	1198.3 ± 95.0

The pure POSS XRD diffractogram shows peaks at 2θ = 8, 8.8, 10.9, 11.7, 18.3 and 19.7 ^{o}, which are characteristic of its crystalline structure. The neat HDPE showed peaks at 2θ = 21.6 and 24.1 ^{o}, which correspond to the 110 and 200 reflections of the crystalline structure of PE, respectively. The EVA copolymer shows broad peaks (2θ ranging for 21 to 25 ^{o}) related to the PE structure in the EVA copolymer. For the systems the XRD results indicating that the presence of EVA in the composite led to the appearance of POSS aggregates at lower concentrations, probably due to the increase in the polarity of the polymer matrix.

In the SEM micrographs in Figure 1, it can be observed that the addition of EVA (dark phase) to the HDPE (light phase) produces a biphasic system with a co-continuous morphology, that is, it is not possible to distinguish which polymer is the matrix and which the dispersed phase.

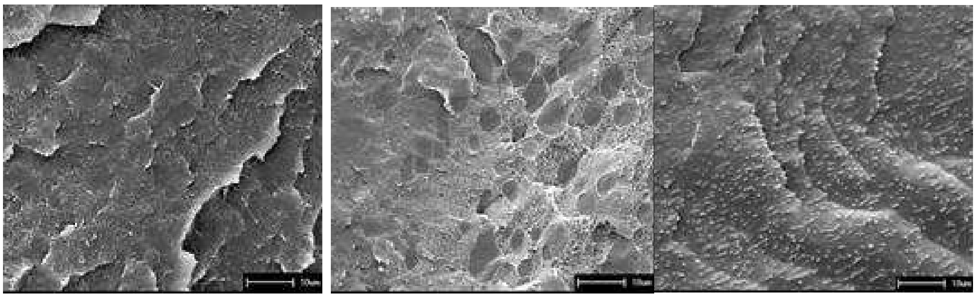

(a) **(b)** **(c)**

Fig. 1. SEM micrographs of the composites without POSS: (a) HDPE100, (b) HDPE75/EVA25 and (c) HDPE25/EVA75.

The DSC curves of POSS, HDPE and EVA had T_m values of 56, 128 and 84 ºC, respectively. It can be observed that in the composites HDPE/EVA, regardless of the POSS content, has T_m values of about 84 and 128 ºC, which is characteristic of HDPE and EVA, respectively, suggesting that the polymers have a certain immiscibility, as observed previously on the SEM micrograph. The HDPE/EVA and EVA systems with 10 wt% of POSS also had a third melt peak, at approximately 56 ºC, also characteristic of POSS.

The TGA curves of POSS showed two mass losses: one at 285 ºC (65 %) and another at 360 ºC (28 %). For the HDPE system can be observed that the samples had only one mass loss stage, in the temperature range of 488 to 492 ºC, corresponding to the thermal degradation of HDPE. For the other systems the first mass loss was observed in the temperature range of 356 to 374 ºC, which is related to the elimination of the acetic acid of EVA and the degradation of POSS. At higher temperatures, 488 to 497 ºC, the thermal degradation of HDPE occurs, as well as the formation of cross-linking in the EVA. Apparently, the presence of POSS did not affect the degradation mechanism of the polymer matrix.

4. CONCLUSIONS

In this study, the morphology and thermal properties of HDPE, EVA, and HDPE/EVA composites with POSS nanostructure were analyzed and compared with those of the pure polymers. POSS underwent aggregation in higher concentration during composites processing indicating a solubility limit above 2 wt%. The presence of EVA in the composite favors the POSS aggregation due to the increase in the polarity of the polymer matrix. These aggregates are characterized by the presence of a melt peak of POSS, and they indicate that the polarity of polymeric matrix plays a major rule in composite morphology even in immiscible systems.

ACKNOWLEDGMENT

The authors are grateful to CAPES and CNPq (481748/2007-5) for financial support.

REFERENCES

LI G., WANG L., NI H. PITTMAN JR C.U. (2002). Polyhedral Oligomeric Silsesquioxane (POSS) Polymers and Copolymers: a Review. *J Inorg Organomet P.,* 11, 123-153.

MARCILLA A., REYES-LABARTA J.A., SEMPERE F.J. (2001). DSC and TGA study of the transitions involved in the thermal treatment of binary mixtures of PE and EVA copolymer with a crosslinking agent. *Polymer,* 42, 5343-5350.

MARK J.E. (2004). Some novel polymer nanocomposites. *Accounts Chem Res.,* 37, 946-953.

SCHWAB J.J., LICHTENHAN J.D. (1998). Polyhedral oligomeric silsesquioxane (POSS)-based polymers. *Appl Organomet Chem.,* 12, 707-713.

WADDON A.J., ZHENG L., FARRIS R.J., COUGHLIN E.B. (2002). Nanostructured Polyethylene-POSS Copolymers: Control of Crystallization and Aggregation. *Nano Lett.,* 2, 1149-1155.

Ultrahydrophobic coatings based on polydimethylsiloxane nanocomposites

N. García, E. Benito, J. Guzmán, P. Tiemblo
Instituto de Ciencia y Tecnología de Polímeros (CSIC), Juan de la Cierva 3, 28006-Madrid, Spain

ABSTRACT

Polydimethylsiloxane (PDMS) coatings are usually applied to prepare hydrophobic and antiadhesive surfaces useful in a wide variety range of applications including autocleaning and antifouling surfaces. Furthermore, the biocompatibility of this polymer makes it suitable for biomedical uses in which low energy surfaces are also demanded such as microfluidic devices. The surface properties of these PDMS coatings will be determined by their static and dynamic hydrophobicity, which, in its turn, depends on the surface chemical nature and roughness. The control over both, chemistry and topology, allows us to develop tailored coatings with special features. With this aim in mind, we report in this work the preparation, characterization and properties of nanostructured coatings based on PDMS and nanosilica particles.
At a first stage, low molecular PDMS chains were grafted onto the nanoparticles surface by using a newly reported high-efficient method. These as-modified particles were finely dispersed in ethanol and PDMS resins and these mixtures were used to prepare the final coatings.

The surface structure and properties of these coatings were evaluated by water contact angle measurements and AFM imaging. The results show that hydrophobicity of the coatings can be modulated (water contact angles covering the range from 100º to 170º) by varying the nature and content of the nanosilica organic coverage. That is, the addition of these nanosilica particles enables the modulation of the surface energy and surface roughness of the coating.

1. INTRODUCCIÓN

La combinación de propiedades que caracteriza al polidimetilsiloxano (PDMS), biocompatibilidad, tenacidad, transparencia, permeabilidad a los gases, hidrofobia, adherencia y la poca energía necesaria para su preparación, entre otras, hacen que los materiales y recubrimientos basados en este polímero estén adquiriendo un creciente interés tanto en estudios básicos como en áreas de gran importancia tecnológica. Es de destacar su uso en medicina o en sistemas de microfluidos, aplicaciones en las que se precisa un riguroso control sobre las características superficiales del material, de ahí que hayan proliferado las técnicas de tratamiento superficial para conseguir materiales con distintas propiedades, sobre todo en lo que se refiere a hidrofobia/hidrofilia y adhesión (Makamba et al. 2003).
A la hora de diseñar superficies con una mojabilidad característica se requiere un control sobre la composición química y la estructura superficial en la micro y nanoescala (Feng et al. 2006). Las estrategias experimentales más usadas se basan en (i) crear micro/nanoestructuras en sustratos hidrofóbicos o (ii) modificar químicamente superficies micro/nanoestructuradas con materiales de baja energía superficial. De esta

forma, se han podido obtener recubrimientos superhidrofóbicos basados en PDMS con estructuras texturizadas de morfología multiescalar (Sun et al. 2005; Ming et al. 2005), aunque los métodos preparativos siguen siendo complejos y difícilmente escalables, lo que impide un uso más generalizado.

En este trabajo presentamos un modo simple para preparar recubrimientos ultra y superhidrofóbicos basados en híbridos organo/inorgánicos de PDMS y nanopartículas de sílice. La ventaja de esta aproximación experimental reside en el hecho de poder modular de forma sencilla el comportamiento frente al agua de una superficie.

2. PARTE EXPERIMENTAL

Se ha llevado a cabo la modificación superficial de nanopartículas de sílice de 12 nm de diámetro nominal (Aerosil 200, Degussa) usando un método experimental (García et al. 2007) que proporciona excelentes resultados en la incorporación de materia orgánica en un tiempo muy inferior a los procedimientos convencionales. Como agentes modificantes se ha usado una serie de PDMS (ABCR) con un intervalo de peso molecular entre 550 y 4200 Da (DMS1=550, DMS2=1750 y DMS3=4200) y terminados en grupos hidroxilo. Se prepararon dispersiones (3% en peso) de las nanopartículas modificadas en etanol y en PDMS (DMS1) mediante agitación mecánica, obteniéndose en todos los casos dispersiones estables en el tiempo. A las dispersiones en DMS1 se les añadió una cantidad estequiométrica de 3-aminopropiltrimetoxisilano (APTS, Aldrich) como endurecedor. Se prepararon recubrimientos en soporte de vidrio a partir de estas dispersiones.

Como técnicas de caracterización se usaron RMN de sólidos (^{29}Si y ^{13}C) y microanálisis en el caso de las nanopartículas modificadas y la determinación de los ángulos de contacto con el agua y AFM para los recubrimientos.

3. RESULTADOS Y DISCUSIÓN

En la figura 1 se muestran los espectros de RMN de ^{29}Si y ^{13}C de las partículas de sílice con el injerto de cadenas de PDMS en superficie. La estructura de la región Q del espectro de ^{29}Si (entre -90 y -120 ppm) asignada a la parte inorgánica indica un buen rendimiento de incorporación en la reacción de modificación. Este rendimiento es independiente de la longitud de las cadenas de PDMS injertadas al ser muy similar esta región del espectro en las tres muestras sintetizadas. El porcentaje de incorporación de PDMS se calcula mediante los datos de microanálisis siendo de 9,6% para las partículas modificadas con DMS1, 19,1% cuando se usa DMS2 y 24,9% en el caso del DMS3. La región del espectro de ^{29}Si entre -5 y -30 ppm muestra la estructura de las cadenas de PDMS injertadas. La aparición de una señal aguda situada en -22 ppm indica la presencia de cadenas largas de PDMS alejadas de la superficie inorgánica. Este mismo efecto se observa en el espectro de ^{13}C con la banda localizada a 1,4 ppm.

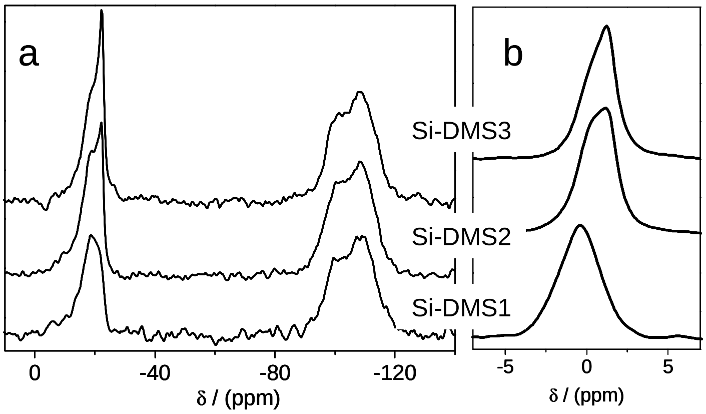

Fig. 1. Espectros de RMN de ^{29}Si (a) y ^{13}C (b) de las nanopartículas modificadas.

En la figura 2 se muestra la topografía de los recubrimientos preparados a partir de las dispersiones en etanol de las partículas modificadas. Se observa que la rugosidad media de la superficie aumenta al incrementarse la longitud de las cadenas injertadas. Sin embargo, estos cambios en la topografía no provocan significativas diferencias en el comportamiento frente al agua, siendo las tres superficies superhidrofóbicas con ángulos de contacto que varían entre 165º para el recubrimiento de las partículas Si-DMS1, y 169º para las partículas Si-DMS3. Por lo tanto, la hidrofobia, en este caso, está influenciada más por la naturaleza química de la superficie que por su topografía.

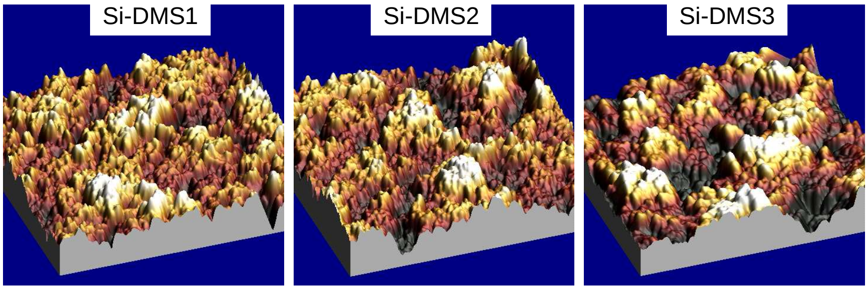

Fig. 2. Topografía (AFM) de los recubrimientos preparados a partir de las dispersiones en etanol de las nanopartículas modificadas.

Con el fin de dotar de mayor estabilidad mecánica a los recubrimientos, se usaron dispersiones de las partículas en un PDMS de bajo peso molecular (DMS1). En estos recubrimientos se observó una disminución clara de la rugosidad media de la superficie, en comparación con los recubrimientos de las partículas en solitario, lo que también provoca la pérdida del carácter superhidrofóbico. Los ángulos de contacto para estos recubrimientos varían entre 125º para las partículas Si-DMS1 en DMS1 y 138º para las Si-DMS3 en el mismo dispersante. La mayor diferencia en los ángulos de contacto respecto a los recubrimientos anteriores de las partículas en solitario, se debe a los cambios en la rugosidad de la superficie, que esta vez sí son determinantes en el comportamiento frente al agua del recubrimiento.

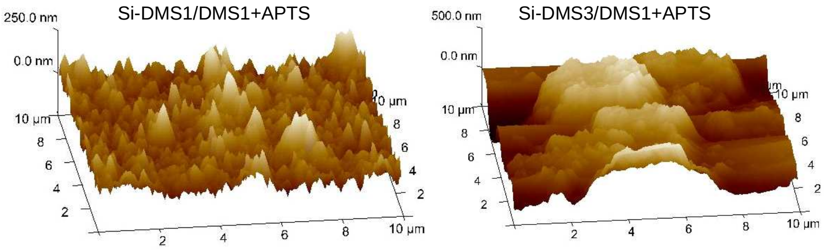

Fig. 3. Topografía (AFM) de los recubrimientos preparados a partir de las dispersiones en DMS1 + APTS de las nanopartículas modificadas.

En la figura 3 se muestra la topografía de los recubrimientos preparados a partir de dispersiones de las nanopartículas sintetizadas en mezclas de DMS1 y APTS. Se observa que para las nanopartículas con injerto de DMS1 se obtiene un recubrimiento con una rugosidad uniforme y sin embargo las partículas modificadas con el PDMS de más alto peso molecular dan lugar a una rugosidad en la micro y nanoescala. A pesar de identificar este tipo de estructuras en superficie que, *a priori*, serían las más adecuadas para dotar al recubrimiento de un carácter superhidrofóbico, todos los recubrimientos preparados con las mezclas de DMS1+APTS presentan ángulos de contacto muy similares y no superiores a 110º. Parece evidente que el grupo amino del APTS es el responsable de esta disminución de los ángulos de contacto.

4. CONCLUSIONES

El injerto controlado de cadenas de PDMS en la superficie de nanopartículas de sílice permite la preparación de recubrimientos de carácter super y ultrahidrofóbicos. La longitud de las cadenas injertadas y el agente dispersante determinan la estructura superficial del recubrimiento y permiten modular la hidrofobia del material.

AGRADECIMIENTOS

Los autores agradecen al Ministerio de Ciencia y Tecnología la financiación recibida (MAT2008-06725-C03-01 y Programa Ramón y Cajal).

REFERENCIAS

FENG, X., JIANG, L. (2006) Design and creation of superwetting/antiwetting surfaces. *Adv. Mater.,* 18, 3063-3078.

GARCÍA, N., BENITO, E., GUZMÁN, J., TIEMBLO, P. (2007) Use of p-toluenesulfonic acid for the controlled grafting of alkoxysilanes onto silanol containing surfaces: Preparation of tunable hydrophilic, hydrophobic, and super-hydrophobic silica. *J. Am. Chem. Soc.,* 159, 5052-5060.

MAKAMBA, H., KIM, J.H, LIM, K., PARK, N., HAHN, J.H. (2003) Surface modification of poly(dimethylsiloxane) microchannels. *Electrophoresis*, 24, 3607-3619.

MING, W., WU, D., van BENTHEM, R., de WITH, G. (2005) Superhydrophobic films from raspberry-like particles. *Nano Lett.,* 5, 22298-2301.

SUM, M., LUO, C., XU, L., JI, H., OUYANG, Q., YU, D., CHEN, Y. (2005) Artificial lotus leaf by nanocasting. *Langmuir,* 21, 8978-8981.

Simultaneous reinforcement and compatibilization of toughened polymer systems by organoclay

I. Kelnar, J. Rotrekl

SUMMARY

In polymer blends, organophilized montmorillonite acts as reinforcement and compatibilizer, both effects are significantly influenced by localization of clay and degree of its dispersion. This work demonstrates that simultaneous influencing of structure and also of numerous parameters of polymer constituents may lead to synergistic or antagonistic effects on mechanical performance. Presented are thermoplastic and thermosetting matrix nanocomposites containing dispersed polymeric phase combined with clay having favourable core shell structure with a shell formed by stacks of clay platelets leading to more fair balance of mechanical properties. Possibilities to regulate morphology of dispersed phases by varying clay polymer affinity, e.g., by application of clays with different modifications and/or by mixing procedures are discussed.

Phenolic resin/montmorillonite nanocomposites prepared by one step in situ intercalative polymerization

M. Huskić, M. Žigon

SUMMARY

Phenolic resin/montmorillonite (MMT) nanocomposites have been the subject of research for only 10 years. As most of other polymer/MMT nanocomposites, the resol and novolac types of phenolic resin have been mixed with various modified and non-modified MMT. The use of modified MMT ensures good intercalation of resin between the alumosilicate layers but it is relatively expensive. Therefore, alternative methods, such as one step *in situ* intercalative solution polymerization have been proposed. This method involves simultaneous modification of MMT with quaternary ammonium salts (QAS), polymerization and polymer intercalation. It has been successfully used to produce intercalated PMMA/MMT nanocomposites.

The same method has now been applied to produce phenolic resin/MMT nanocomposites. We prepared both, resol and novolac type of nanocomposites. Phenol, formalin, catalyst, QAS and Na-MMT were mixed and heated to reflux for 4 hours. Nanocomposites were precipitated by cooling, dried and analysed by XRD, DSC and TGA. Alternatively, some nanocomposites were prepared without QAS, and some by pre-swelling MMT in a water/QAS mixture for 24 hours. Two types of QAS were used: with one long alkyl chain (cetyl-trimethylammonium bromide - CTMAB) and one with three medium sized alkyl chains (tricaprylyl methylamonium chloride – TCMAC). The intercalation of phenolic resin between the layers in the nanocomposite is better when CTMAB is used. Pre-swelling did not show any improvement in intercalation. Subsequent curing of nanocomposite resins only slightly influenced the intercalation. The influence was not straightforward and it will be discussed in details in present contribution.

Nuevos avances en el desarrollo de nanocompuestos elastoméricos

J. Carretero-González, R. Verdejo, M. Hernández, M. Arroyo,
M.A. López-Manchado
Instituto de Ciencia y tecnología de Polímeros, CSIC, Juan de la Cierva, 3 28006-
Madrid (España)

RESUMEN

En este trabajo se presentan nuevos desarrollos llevados a cabo en el campo de los nanocompuestos poliméricos basados en matrices elastoméricas reforzados con nanopartículas de arcilla. Se pretende relacionar la microestructura del material con sus propiedades macroscópicas y dar una explicación a la significativa mejora de propiedades que se alcanzan con estas nanopartículas en relación con las cargas convencionales, tales como el negro de carbono o sílice. Para ello, se ha analizado el efecto de las nanopartículas sobre la cristalización del caucho natural bajo deformación uniaxial así como, su efecto sobre la dinámica molecular del caucho natural.

1. INTRODUCCIÓN

Durante los últimos años, los nanocompuestos poliméricos han adquirido un enorme interés científico e industrial debido a las excelentes propiedades que exhiben incluso con la adición de pequeñas cantidades de carga (Pinnavaia, 2000). De hecho, prácticamente todos los polímeros se han usado para la preparación de nanocompuestos poliméricos. Sin embargo, la gran mayoría de estos trabajos se han centrado en estudiar la síntesis, morfología y propiedades de los nanocompuestos, pero sin profundizar en el conocimiento del mecanismo de interacción polímero/nanopartícula. En particular, en el caso de las matrices elastoméricas, es necesario ahondar en el efecto de las nanopartículas sobre la red elastomérica, que permitirá explicar la significativa mejora de propiedades alcanzada con estas nanopartículas en relación a las cargas convencionales como el negro de carbono o la sílice. En este trabajo, se analizará la estructura molecular de la red polimérica por espectroscopia dieléctrica y el efecto de las nanopartículas sobre la cristalización inducida del caucho natural bajo deformación uniaxial mediante medidas de sincrotrón in-situ.

2. PARTE EXPERIMENTAL

Se ha utilizado caucho natural, NR suministrado por Malasyam Rubber bajo el sobrenombre de CV 60 (Viscosidad Mooney, ML (1+4) 100 ºC 60) y una montmorillonita: sódica y orgánicamente modificada provista por Southern Clays Products.

Los materiales compuestos se prepararon en un mezclador de rodillos abiertos con 10 ppc (partes por cien de caucho) de carga, usando azufre como sistema de vulcanización. La dispersión y morfología del sistema se analizó mediante difracción de rayos X y microscopia electrónica de transmisión. Las medidas de espectroscopia dieléctrica se realizaron en un Novocontrol Turnkey Concept N40 broadband, y las medidas de cristalización in-situ se llevaron a cabo mediante experimentos de esfuerzo-deformación acoplados a difracción de rayos X con radiación sincrotrón en X27C beamline del National Synchrotron Light Source (NSLS), Brookhaven National Laboratory (BNL).

3. RESULTADOS Y DISCUSIÓN

En estudios previos, Arroyo et al. (2003) y Lopez-Manchado et al. (2003), observaron que la incorporación de 10 pcc de organoarcilla daba lugar a una mejora significativa de las propiedades mecánicas del material comparables a las que se obtenían con 40 pcc de negro de carbono, sin además, provocar un deterioro de las propiedades elásticas del material. La mayoría de los trabajos atribuyen esta mejora de propiedades a la obtención de una estructura exfoliada en la que las nanopartículas se encuentran homogéneamente dispersas en la matriz polimérica. En la Figura 1, se aprecian las imágenes de TEM tomadas para los compuestos reforzados con la arcilla sódica (C6A) donde se aprecian grandes aglomerados y con la organoarcilla (C15A) donde se aprecian láminas individuales de arcillas homogéneamente dispersas en la matriz elastomérica.

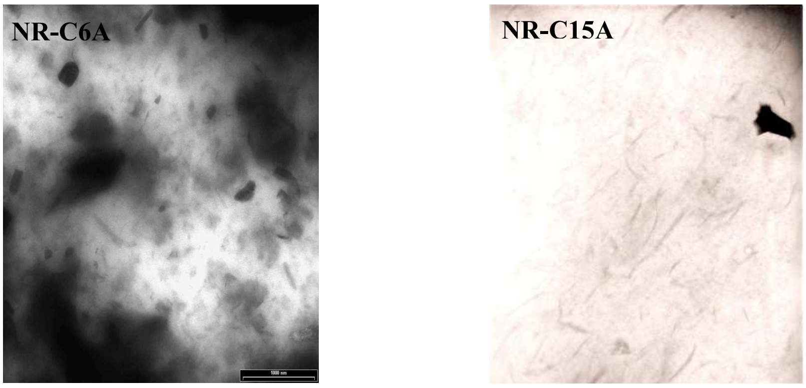

Figura 1. Imágenes TEM nanocomposites NR-arcilla sódica (NR-C6A) y orgánicamente modificada (NR-C15A).

Es evidente, que esta estructura es necesaria para alcanzar una mejora de las propiedades pero esta explicación no es suficiente para comprender el mecanismo de refuerzo que tiene lugar en muchos sistemas. Es necesario profundizar en el mecanismo de interacción carga-polímero para poder entender el diferente efecto reforzante de estas nanopartículas respecto a las cargas convencionales. Una de las peculiaridades del NR es su capacidad de cristalizar bajo deformación uniaxial. Esto hace que el NR exhiba excelentes propiedades incluso sin cargar a diferencia de otros cauchos sintéticos. Por ello, analizamos el efecto de las nanopartículas sobre la cristalización del caucho natural bajo deformación mediante medidas de sincrotrón in-situ. Mediante este método, podemos controlar los cambios estructurales a nivel local que se producen en el material durante su deformación.

En la Figura 2, se aprecian las curvas de esfuerzo-deformación y los correspondientes difractogramas de WAXD seleccionados durante la deformación y relajación del material. La cristalización del caucho natural queda reflejada en la alineación de las reflexiones de (120) y (200). Es importante destacar que las reflexiones del cristal aparecen a menores deformaciones en presencia de las nanopartículas. Así, el onset de la deformación se desplaza desde 3.3 para el caucho sin cargar a 1.2 para la muestra cargada con la nanoarcilla. Por otro lado, la cristalinidad total del caucho natural aumenta drásticamente en presencia de las nanopartículas. El caucho natural presenta un 25% de cristalinidad a una deformación del 500% mientras que en las muestras reforzadas con las nanopartículas, la cristalización aumentaba hasta un 48%. Este aumento se puede atribuir a la formación de fuertes interacciones interfaciales entre la carga y el polímero, que facilitan la transferencia de esfuerzo a través de la matriz. Esta gran región interfacial puede favorecer la orientación de las cadenas poliméricas, promoviendo la nucleación bajo deformación.

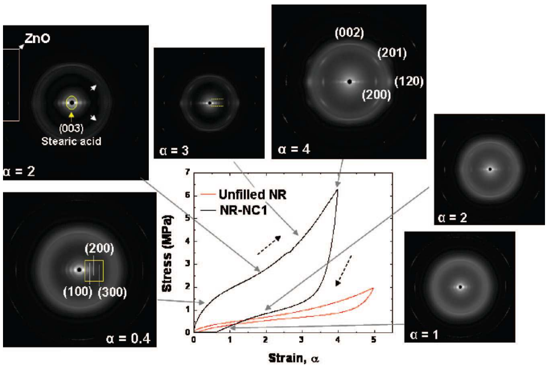

Figura 2. Curvas esfuerzo-deformación y difractogramas de rayos X con sincrotrón durante la deformación y retracción.

Por su parte, se analizó el efecto de las nanopartículas sobre la dinámica molecular del caucho natural mediante medidas de espectroscopia dieléctrica de banda ancha. La Figura 3 muestra las curvas tridimensionales de la pérdida dieléctrica en función de frecuencia y temperatura para el caucho natural y sus nanocomposites. El caucho natural vulcanizado únicamente presenta una única relajación dieléctrica correspondiente al modo segmental. La incorporación de las nanopartículas no afecta a la relajación segmental, es decir, que ambas muestras presentan una temperatura de transición vítrea similar. Sin embargo, en presencia de las nanopartículas, se aprecia una nueva relajación más lenta que la segmental. Esta nueva relajación se asocia a las cadenas de caucho interaccionando con la superficie de las nanoarcillas que inducen un nuevo modo segmental más lento con una T_g aproximadamente 90 º mayor que la del polímero puro.

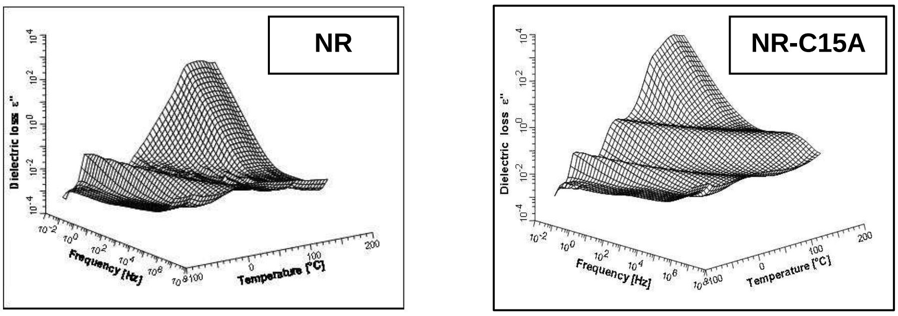

Figura 3. Pérdida dieléctrica en función de frecuencia y temperatura en NR y NR-C15A.

4. CONCLUSIONES

Se puede concluir que la presencia de fuertes interacciones interfaciales entre las nanopartículas y el polímero favorece la orientación de las cadenas de caucho natural e inducen a una prematura cristalización y a un aumento de la cristalinidad total del sistema. Esta mayor cristalinidad no observada con otras cargas convencionales, como el negro de carbono o la sílice precipitada, permite explicar la sorprendente mejora de las propiedades mecánicas de estos sistemas en relación con las cargas convencionales. Por otro lado, las medidas dieléctricas muestran un cambio en la dinámica molecular del caucho natural en presencia de las nanopartículas. Así, las nanopartículas originan una nueva relajación más lenta que la segmental del caucho natural puro, debido a las cadenas de caucho interaccionando con la superficie de la organoarcilla.

AGRADECIMIENTOS

Los autores desean agradecer al Ministerio de Ciencia e Innovación por la financiación del proyecto MAT-2007-61116.

REFERENCIAS

ARROYO, M. (2003). Organo-montmorillonite as substitute of carbon Black in natural rubber compounds, *Polymer* 2003; **44**: 2447-2453

LOPEZ MANCHADO, M.A. (2003). Preparation and characterization of organoclay nanocomposites based on natural rubber. *Polymer International* 2003; **52**: 1070-1077

PINNAVAIA, TJ (2000). *Polymer Clay Nanocomposites.* Weinheim: Wiley-VCH

Dispersión mecánica en la fabricación de nanocomposites para su uso como matrices en materiales multiescalares

A. Jiménez-Suárez, M. Campo, M. Sánchez, C. Romón, A. Ureña
Departamento Ciencia E Ingeniería de Materiales, ESCET. Universidad Rey Juan Carlos, Móstoles, Madrid, España

RESUMEN

La adición de nanorrefuerzos presenta dificultades durante el procesado debidas a la tendencia a formar aglomerados. El uso de una calandradora consigue mejorar la dispersión sin necesidad de emplear disolventes facilitando la escalabilidad del proceso. Variando los parámetros del proceso, se consiguen diferentes resultados en cuanto a dispersión y daño del nanorrefuerzo. En este estudio se ha optimizado el proceso de dispersión mecánica por calandrado, obteniéndose dispersiones homogéneas hasta porcentajes añadidos del 5% en masa de nanofibras de carbono (CNFs). Se ha analizado la efectividad de la dispersión por diferentes técnicas de microscopía y análisis termomecánico de los nanocomposites.

1. INTRODUCCIÓN

El empleo de materiales compuestos con refuerzos tradicionales de fibra continua de carbono embebidas en resinas epoxi está ampliamente extendido en diferentes industrias, destacando por su volumen, la industria aeronáutica. Sus excelentes propiedades mecánicas en la dirección de las fibras y un amplio conocimiento del diseño con este tipo de materiales, les han llevado a ser usados como componentes estructurales. La adición de nanorrefuerzos a la matriz polimérica se plantea como una alternativa para mejorar las propiedades mecánicas dominadas por la matriz, causando también modificaciones en otros campos como el comportamiento eléctrico por la aparición de fenómenos cuánticos de conducción por efecto túnel entre los nanorrefuerzos, disminuyendo notablemente el umbral de percolación para la conducción eléctrica.

La excepcionalidad de su tamaño también supone nuevas dificultades en el procesado de estos materiales. La elevada superficie específica disponible hace que tiendan a formar aglomerados, quedando ésta por tanto reducida y aumentando el tamaño final del refuerzo. Esto provoca un descenso de las propiedades predichas mediante simulación. La dispersión del nanorrefuerzo en el polímero para el posterior impregnado de la fibra continua, se puede conseguir mediante métodos químicos empleando disolventes y aplicando sonicación simultáneamente (Prolongo et al., 2008). Sin embargo, se requiere la eliminación del disolvente en una etapa previa al curado, puesto que a las temperaturas de curado éste podría evaporarse dejando poros en el material. La vía mecánica se presenta como una alternativa, en la cual la mezcla pasa a través de un sistema de rodillos, que ejerciendo fuerzas de cizalladura sobre la mezcla, separará progresivamente los aglomerados (Thostenson et al., 2006; Gojny et al., 2004).

2. MÉTODO EXPERIMENTAL

2.1 Materiales

La matriz polimérica del nanocomposite utilizada ha sido una resina epoxi de nombre comercial *Araldite* LY556 basada en bisfenol A mezclada con un endurecedor basado en amina aromática de nombre comercial *Araldite* XB3473 en una proporción 100:23 en masa. El nanorrefuerzo utilizado son nanofibras de carbono (CNFs) suministradas por el *Grupo Antolin*, encontrándose varios tipos como son las denominadas *platelets*, y *cup-stacked*. Las propiedades y características varían según el tipo de CNF, con una longitud media de 35 µm, y diámetros entre 20 y 47 µm (Chaos et al, 2008)

2.1 Procesado de los nanocomposites

El procesado de los nanocomposites está constituido fundamentalmente por dos estapas: 1) dispersión de las CNFs en la matriz y 2) curado de las mezclas. La dispersión de las CNFs en la matriz se realiza mediante el uso de una calandra de tres rodillos. Controlando los sentidos y velocidades de giro de los rodillos se consigue que las fuerzas ejercidas sobre la mezcla sean de cizalladura pura, evitandoo fuerzas de compresión que podrían dañar las CNFs. Controlando la separación entre rodillos (GAP 1 y 2), así como el número de veces que se introduce la mezcla en el sistema, se variará la fuerza ejercida sobre la misma, y por tanto la dispersión y el daño sobre las CNFs. La tabla 2.1 resume las condiciones utilizadas en cada uno de los métodos estudiados.

MÉTODO I	**GAP 1 (µm)**	**GAP 2 (µm)**	**Rep**	**ω (rpm)**	**MÉTODO II**	**GAP 1 (µm)**	**GAP 2 (µm)**	**Rep**	**ω (rpm)**
	120	40	1	250		15	5	8	250
	75	25	1						
	45	15	1						
	15	5	4						

Tabla 2.1. Condiciones de calandrado seleccionadas para los métodos estudiados.

Tras el proceso de calandrado, se eleva la temperatura de la mezcla hasta 90ºC para disminuir su viscosidad y facilitar su procesado posterior manteniendo una agitación magnética sobre la mezcla. Tras alcanzar la temperatura fijada, se añade el agente endurecedor líquido manteniendo la agitación durante unos minutos para que se mezcle homogéneamente. Finalmente se inyecta la mezcla resultante en un molde abierto que se introduce en una estufa para realizar el curado.El ciclo de curado realizado es isotermo a 140ºC durante 8 horas.

3. RESULTADOS

La comparación de los nanocomposites fabricados siguiendo los dos métodos de calandrado se ha realizado mediante caracterización por microscopía óptica de luz transmitida (TOM) de las mezclas sin curar, y por microscopía eléctronica de transmisión TEM para las muestras curadas. Además los ensayos dinámicos termomecánicos (DTMA) permiten determinar la temperatura de transición vítrea de las muestras.

Las imágenes tomadas mediante TOM a 100 aumentos para ambos métodos muestran diferencias principalmente en el número de aglomerados presentes en las mezclas tras el calandrado. Estas diferencias son más significativas en las dispersiones de contenido 1,5% en masa de CNFs (Fig. 3.1 a,b) dónde se puede apreciar mayor número de aglomerados en el método II, con un tamaño medio ligeramente superior. Las diferencias observadas por TOM para mayores contenidos de CNFs son menores. En este tipo de imágenes no se puede observar si el daño causado sobre las nanofibras es diferente según el método de calandrado. El análisis de las imágenes obtenidas por TEM para contenidos del 3% en masa de CNFs (Fig. 3.1 c,d) revelan como en ambos métodos el daño de la nanofibra es similar, pero se observan diferencias en la homogeneidad de la dispersión, que es mejor para el método I de calandrado.

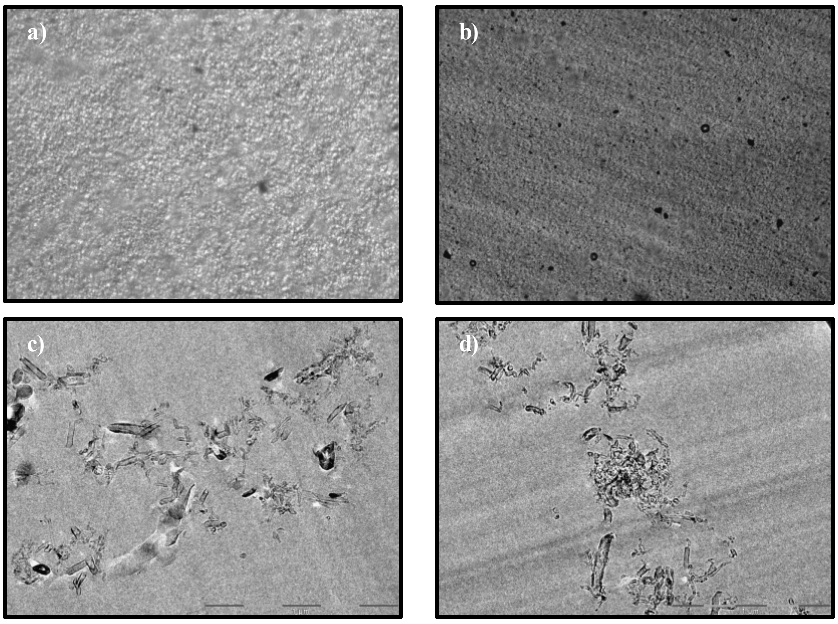

Fig. 3.1. Imágenes de TOM, 1,5% en masa CNFs, según a) Método I, b) Método II, y de TEM 3% en masa CNFs, según c) Método I, d) Método II.

Como resultado del análisis de las imágenes obtenidas mediante las dos técnicas de microscopía, parece que la disminución gradual del espaciado entre rodillos de la calandra es aconsejable para conseguir una mejor dispersión de las CNFs en la matriz polimérica. No obstante, el estudio de la temperatura de transición vítrea de los nanocomposites debe ser también tenido en cuenta, puesto que dificultades durante el proceso de curado debido a la presencia de grandes o numerosos aglomerados podrían comprobarse de esta manera.

La temperatura de transición vítrea muestra un claro descenso cuándo la dispersión se realiza mediante el método II de calandrado, este descenso es más acusado para menores contenidos de CNFs, probablemente debido a que con contenidos del 3% en masa, el método I también posee cierta cantidad de aglomerados, y por lo tanto las diferencias entre las dispersiones conseguidas con ambos métodos, son menores, como se ha observado con el estudio por microscopía. El descenso mostrado se puede asociar con una mayor dificultad del movimiento y reacción de las cadenas de polímero, debido a la presencia de grandes aglomerados, o de un mayor número de estos, por lo tanto, el método I tras este análisis es el más adecuado para obtener una dispersión homogénea.

CNFs	Tg – Método I (ºC)	Tg – Método II (ºC)
0%	172,50 ± 0,02	172,50 ± 0,02
1,5%	169,55 ± 0,57	117,78 ± 4,44
3%	167,56 ± 3,05	147,35 ± 1,81

Tabla 3.1. Variación de la temperatura de transición vítrea

3. CONCLUSIONES

- Se ha optimizado el proceso de dispersión mecánica de CNFs en matriz epoxi mediante el control de los parámetros que más influencia tienen sobre la dispersión final como son la distancia entre rodillos y el número de pasadas sobre la mezcla.
- El método I de dispersión mediante calandra permite la obtención de mezclas epoxi/CNFs homogéneas hasta porcentajes del 3% en masa para su posterior utilización como matrices en materiales compuestos multiescalares.

AGRADECIMIENTOS

Los autores agradecen la financiación para la realización de la investigación al Ministerio de Educación y Ciencia (Proyecto MAT 2007-61178) y a la Comunidad de Madrid-Uniersidad Rey Juan Carlos (Proyecto CCG08-URJC/MAT-3524)

REFERENCIAS

CHAOS-MORÁN R, CAMPO M, PROLONGO S.G, ESCALERA M.D, UREÑA A. (2009).The functionalization of carbon nanofibers with 4,4'-diaminodiphenylmethane, a curing agent for epoxy resins. Journal of Materials Research, 24 (4),1435- 1445.
GOJNY F.H., WICHMANN M.H.G., KÖPKE U., FIEDLER B., SCHULTE K. (2004), Carbon nanotube-reinforced epoxy-composites: enhanced sittness and fracture toughness at low nanotube content. Composites Science and Technology, 64,2363-2371.
PROLONGO S.G, BURÓN M,GUDE M.R, CHAOS-MORÁN R, CAMPO M, UREÑA A. (2008). Effects of dispersión techniques of carbon nanofibers on the thermo-physical properties of epoxi nanocomposites. Composites Science and Technology. 68, 2722-2730.
THOSTENSON E., CHOU T. (2006). Processing-structure-multi-functional property relationship in carbon nanotube/epoxy composites, Carbon, 44, 3022-3029.

Compatibilization and property control of polyolefin and polyester composites containing natural fibres

M. Pracella, G.D. Guerra
Institute of Composite and Biomedical Materials, IMCB- CNR,
Via Diotisalvi 2, Pisa 56122, Italy
pracella@ing.unipi.it
M. Minhaz-Ul Haque, N. Barbani
Department of Chemical Engineering & Materials Science, University of Pisa, Via Diotisalvi 2, Pisa 56122, Italy
E. Piorkowska
Centre of Molecular & Macromolecular Studies, Polish Academy of Sciences,
Sienkiewcza 112, Lodz 90363, Poland

SUMMARY

Composites of isotactic polypropylene (PP) and polylactide (PLA) with hemp fibres (*cannabis sativa*), and composites of polystyrene (PS) with cellulose fibres, oat (*avena sativa*) and $CaCO_3$ particles respectively, obtained by melt mixing, were examined by FT-IR analysis, optical and SEM microscopy, EDS, WAXS, DSC, TGA and mechanical tests. For PP/hemp composites, grafting of glycidyl methacrylate (GMA) either onto fibres (Hemp-GMA) and polymer chains (PP-*g*-GMA) was carried out to improve the fibre–matrix interfacial interactions. For composites with PS matrix the effect of addition of maleic anhidride functionalized copolymers (SEBS-*g*-MA, PS-*co*-MA, PP-*g*-MA) and oligomers (PEG, PPG) was investigated. The properties of binary and ternary systems were analysed as function of fibre characteristics, compatibilizer concentration and mixing parameters.

1. INTRODUCTION

Polymer composites based on natural fillers are currently attracting great attention as alternative materials to glass or synthetic fibre reinforced plastics in several applications, mostly for automotive, appliance and packaging products. The main advantage of employing natural fibres is that these are biodegradable and renewable, and exhibit low cost, low density and high toughness. However the low compatibility between fibres and polymer matrix generally leads to weak mechanical performances, limiting the use of these materials. In order to improve the interfacial interactions between the components, surface modification of the fibres and/or polymer functionalization, as well as addition of compatibilizers is required [George *et al* 2001]. In the present communication we analyse the effect of reactive compatibilization processes on the morphological, thermal and mechanical properties of composites of PP, PLA and PS with hemp, cellulose or oat.

2. EXPERIMENTAL

Composites of PP (Targor, MFR= 12 g/10min), PP-g-GMA (5 wt.% grafted GMA) [Pracella 2003] and PLA (Cargill-Dow, M_w= 126,000) with hemp fibres (PP/Hemp, PP-*g*-GMA/Hemp) and GMA modified hemp (PP/Hemp-GMA) at various composition ratios were prepared in a Brabender internal mixer at 170°C using different compounding procedures. Composites of PS (mixture of crystal type and high impact PS) with cellulose fibres (Technocel 75, Neuchem) (PS/Cell), oat (Chemical Net, Poland) (PS/Oat) and with $CaCO_3$ (PS/$CaCO_3$) were obtained by melt mixing in Brabender at 180/200°C.

The morphology of blends was examined on the freeze-fractured surfaces of bulk samples with a Jeol T300 scanning electron microscope. FT-IR spectra of compression moulding films were recorded by means of a Perkin-Elmer 2000 spectrophotometer. X-ray analysis (WAXS) was performed with DRON-20 diffractometer, using the CuKa radiation. The thermal behaviour was examined with a Pyris Diamond DSC (Perkin-Elmer) at a heating/cooling rate of 10 °C/min, under nitrogen flow. Thermal degradation of composites and pure components was analysed with a TGA MK2 (Rheometric Scientific) in the range 50-800°C at a heating rate of 10°C/min, in N_2 atmosphere. Tensile tests were carried out at room temperature by means of an Instron testing machine using cross-head speeds of 0.5 mm/min for PP composites and 5 mm/min for PS composites.

3. RESULTS

3.1 Composites with PP and PLA matrix

Modification of NaOH treated hemp fibres was performed by exploiting the reaction of the hydroxyl groups of fibres with GMA monomer (in TEA solution), that gives rise to the formation of ether bonds at the fibre surface (Hemp-GMA) (Fig. 1). Hemp-GMA can react with PP during melt mixing, in the presence of a radical initiator (BTP), through the attack of PP macroradicals to the double bond of GMA, as monitored by FT-IR spectroscopy. SEM analysis of PP/Hemp-GMA and PP/Hemp/PP-g-GMA composites indicated an improved adhesion of the fibres to the polymer matrix.

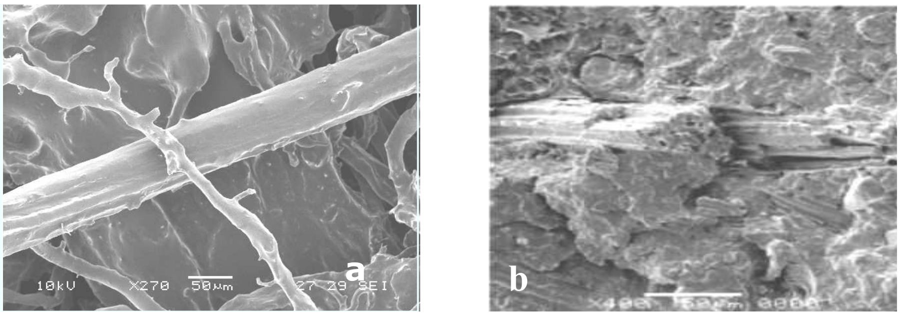

Fig.1. SEM micrographs of (a) Hemp-GMA, (b) PLA/Hemp (80/20)

The isothermal crystallisation behaviour of PP/Hemp and PLA/Hemp was examined in the range 120–138°C using the Avrami model [Pracella *et al* 2006, Masirek *et al* 2007]. An increase of about one order of magnitude in the crystallization rate of composites was found with respect to neat PP and PLA, which was related to an increased nucleation density of polymer crystals on the fibres surface. The results of TGA analysis of PP composites evidenced a higher thermal stability of the GMA modified fibres with a maximum degradation rate at 321°C. The tensile tests pointed out large changes of the Young modulus for all samples when compared to plain polymers, while the impact strength and elongation at break decreased [Lezak *et al* 2008]. Values of modulus above 3000 MPa were found for PP/Hemp samples added with 10 phr PP-*g*-GMA [Pracella *et al* 2006].

3.2 Composites with PS matrix

The SEM analysis of fracture surfaces of PS composites with cellulose, oat and $CaCO_3$ displayed in all cases a good filler dispersion with a poor adhesion between matrix and particles. Significant changes of composite morphology and thermal properties were recorded on the addition of compatibilizer, depending on the copolymer structure and content of functional groups. For PS/Cell compatibilized with SEBS-*g*-MA, the glass transition temperature of PS increased with increasing the fibre content. The effect of the compatibilizer at the polymer-fibre interface was analysed by FT-IR on samples with different content of SEBS-*g*-MA and PS-*co*-MA copolymers. FT-IR spectra showed changes of the MA carbonyl stretching and ester band (1750-1850 cm^{-1}), as well as shifts of the alcohol and ether bands of cellulose (1000-1200 cm^{-1}), supporting the occurrence of chemical reactions between maleic anhydride and hydroxyl groups of cellulose [Pracella *et al* 2008].

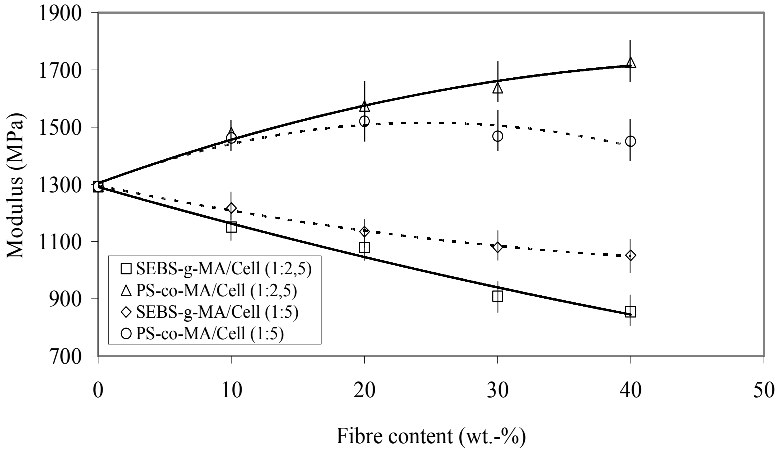

Fig. 2. Elastic modulus of PS/Cell composites compatibilized with PS-*co*-MA and SEBS-*g*-MA (at different copolymer/fibre ratio) as a function of cellulose content.

A marked increase of the modulus up to about 1750 MPa was found for PS/Cell (60/40) upon addition of PS-*co*-MA (16 phr), while the strength at max and elongation at break decreased, as compared to plain PS and uncompatibilized samples (Fig. 2). Otherwise, the addition of SEBS-*g*-MA copolymer caused a ductile behaviour with lower modulus and increased elongation at break [Oksam *et al* 1998]. SEM analysis of SEBS-g-MA/Cell samples pointed out a stronger surface adhesion accompanied by extended fibre fraying with respect to PS-*co*-MA/Cell samples (Figure 1b). For PS/Oat composites the addition of PEG (5-10 phr), as plasticizer, resulted in a decrease of modulus and a neat improvement of elongation at break.

4. CONCLUSIONS

The morphology, thermal behaviour and mechanical properties of the examined composites resulted to be significantly affected by the chemical modification of the fibres, as by the addition of compatibilizers containing reactive groups (PP-*g*-GMA, SEBS-*g*-MA, PS-*co*-MA). The modified systems showed enhanced fibre dispersion and interfacial adhesion as a consequence of chemical interactions between the functional groups on the polymer chains and the hydroxyl groups of the fibres, as confirmed by FT-IR analysis. Marked changes in the spherulitic morphology and melt crystallisation rate of polymer matrix were also observed both for PP/Hemp and PLA/Hemp composites due to the nucleating effect of the fibres. The mechanical analysis showed that modulus, tensile strength and elongation at break are largely affected by the type and amount of fibre, as well as by the structure and concentration of compatibilizer. In particular, the addition of PP-*g*-GMA to PP/Hemp samples resulted in an increased stiffness owing to a higher fibre–matrix adhesion.

In the case of PS/Cell composites a higher interfacial adhesion was noticed in samples compatibilized with the graft copolymer, SEBS-g-MA, as compared to those containing the random copolymer, PS-*co*-MA. This can be ascribed to the fact that the block copolymer is mostly located at the interface between filler particle and matrix, giving rise to more effective interactions with the polar groups of the fibres.

REFERENCES

GEORGE J., SREEKALA M.S., THOMAS S. (2001) A Review on Interfacial Modification and Characterization of Natural Fiber Reinforced Plastic Composites. *Polymer Engineering Science*, *41*,1471-1485.

PRACELLA M., CHIONNA D. (2003) Reactive Compatibilization of Blends of PET and PP Modified by GMA Grafting. *Macromolecular Symposia*, ***198***, 161-171

PRACELLA M., CHIONNA D., ANGUILLESI I., KULINSKI Z., PIORKOWSKA E., (2006) Functionalization, Compatibilization and Properties of Polypropylene Composites with Hemp Fibres. *Composites Science and Technology*, *66*, 2218–2230

MASIREK R., KULINSKI Z., CHIONNA D., PIORKOWSKA E., PRACELLA M. (2007) Composites of Poly(L-lactide) with Hemp Fibres. Morphology, Thermal and Mechanical Properties. *J. Applied Polymer Science*, *105*, 255-268

LEZAK E., KULINSKI Z., MASIREK R., PIORKOWSKA E., PRACELLA M., GADZINOWSKA K. (2008) Mechanical and thermal properties of green polylactide composites with natural fillers. *Macromolecular Bioscience*, *8*, 1190-1200

PRACELLA M., PANCRAZI C., D'ALESSIO A., CORTI A., CHIELLINI E. (2008) *Property Improvement and Degradability Control of Polyolefin Based Composites Containing Natural Fibres and Mineral Fillers.* 13th European Conference on Composite Materials, ECCM13, June 2-5, Stochkolm, Sweden, ID-2640

OKSAM K, LINDBERG H, HOLMGREN A. (1998) The Nature and Location of SEBS-MA Compatibilizer in Polyethylene-Wood Flour Composites. *J. Applied Polymer Science,* 1998;69:201-209.

One-dimensional polymer based nanocomposites. From tailored fabrication to applications

J. Martín, J. Maiz, C. Mijangos
Instituto de Ciencia y Tecnología de Polímeros (CSIC), Juan de la Cierva,3 (28006)
Madrid, cmijangos@ictp.csic.es

SUMMARY

Template synthesis is one of the most effective methods for the preparation of one-dimensional polymer-based nanostructures. Hexagonal alumina pores provides an exceptional route for the generation of 1D nanostructured polymers and polymer nanocomposites. Several infiltration methods were employed to obtain polymer nanofibers and nanotubes of any diameter and length of a wide chemical nature: PS, PVC, PVDF, PMMA and hybrid polymers. Morphological and chemical characterization was carried out by SEM, Raman Confocal spectroscopy and X-Ray. The crystallisation, local dynamics and dielectric properties of some semicrystalline polymers were studied by means of DSC, dielectric spectroscopy and neutron scattering.

1. INTRODUCTION

Over the last few years, one-dimensional polymeric nanostructures (1D) have attracted increasing interest from, both, fundamental and applied point of view. Alumina template synthesis (AAO) and subsequent polymer infiltration, is one of the most effective methods for the preparation of such nanostructured polymer materials (1). The main lines of investigation in this field are dealing with: i) Development of new infiltration methods and bigger nanostructured surfaces; low cost and rapid technological process and the possibility of reusing the AAO template (reclying); ii) Determination of the polymer properties at nanoscale and the study of correlation of new properties with the polymer confinement. In this way, the behaviour of polymer composites under nanoscale confinement seems to hold out a new perspective to deal with some classical problems in polymer composites physics, i.e. the early stages of the crystallization [2], magnetic properties (3), the glass transition, etc. and iii) Development of nanostructured composites for applications in photonics, electronics, sensors, catalysis or biomedicine in tissue engineering.

For the last few years, we have carried out a systematic study on the preparation of nanotubes and nanofibers of almost any kind of polymer (of very different chemical nature) with taylor size, their chemical and morphological characterization; the study of polymer properties under confinement and investigation of potential applications.

The aim of the present work is to report i) the infiltration methods of PEO, PVDF, SWCNT/PVDF and PVA into porous aluminum oxide (AAO) templates of different porous diameter and length; ii) the determination of the chemical composition distribution gradient of SWCNT/PVDH by Raman Confocal Spectroscopy and iii) the study of polymer properties under confinement with two examples: the effect that confinement produces, first, in the crystallization and morphology of PEO nanotubes and, second, in the segmental dynamics of a semicrystalline PVDF.

2. EXPERIMENTAL PART

Sample preparation and morphological characterization. AAO templates have been prepared by a two-step electrochemical anodization process of aluminium at different anodization conditions, following the procedure described in the literature (4). Wetting based methods, either by precursor film or melt capillarity, were employed to obtain: PVDF nanofibers and nanotubes, SWCNT/PVDF nanofibres, PEO nanofibres and nanotubes and PVA nanofibres of various diameter and length.

AAO templates and PVDF, SWCNT/PVDF, PEO and PVA nanotubes and nanofibres were morphologically and chemically characterized by scanning electron microscopy (SEM) (Philips XL-30 ESEM); X-Ray diffactometer (Bruker D8 Advance) equipped with nickel-filtered CuKα radiation operated at 40kV and 40mA and by Raman Confocal spectroscopy to characterize the chemical composition profile along the length of SWCNT/PVDF nanofibres.

Effect of the confinement on polymer properties. The calorimetric measurements of PEO bulk and PEO nanotubes were carried out on a TA Q100 differential scanning calorimeter under nonisothermal conditions. Dielectric measurements were carried out over a broad frequency windows and temperature interval

3. RESULTS

Depending on the anodization conditions, AAO templates of different pores size have been obtained. The average porous diameter was 70, 160, 170, and 360 nm and the porous length varied from hundreds of nanometers to hundreds of microns.

A birds-eye view (a) and cross section view (b) of one of these templates is shown in Figure 1.

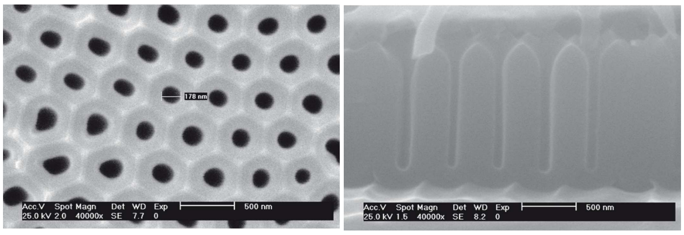

Fig 1. SEM picture of AAO. (a) Surface and (b) cross section.

Depending on the infiltration conditions, chemical nature of the polymer and template dimensions two wetting regimes are possible. High molecular mobility conditions (high temperature, low molecular weight, etc.) leads to the complete wetting regime, whereas low mobility conditions (low temperature, high molecular weight, etc.) leads to the partial wetting regime. In Fig 2, a birds-eye view of PS nanotubes is shown. The inset micrographs show broken nanotubes in which the tubular shape of the nanostructure can be observed.

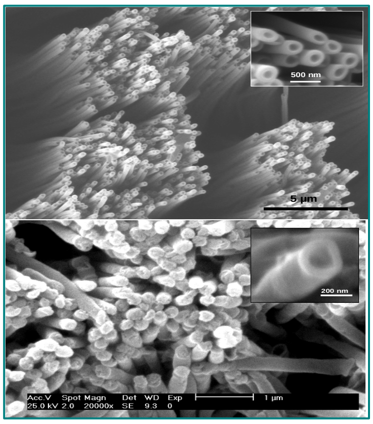

Fig 2. Birds-eye view of PS nanotubes. The inset micrographs show broken nanotubes.

The crystallization of PEO appears to be strongly influenced with the confinement. From the thermograms of bulk PEO and PEO nanotubes is observed i) no change in melting temperature of both samples, being 62ºC, and ii) bulk PEO crystallizes at higher temperature than PEO nanotubes, 40C and -10C, respectively. These results have been confirmed by WAXS. WAXS profiles of PEO nanotubes acquired during non isothermal crystallization at different temperatures are compiled in Figure 3. On this figure can be observed that the principal Bragg reflection peak only appear below -15 ºC. BulK PEO has the same Bragg peaks at room temperature (5)

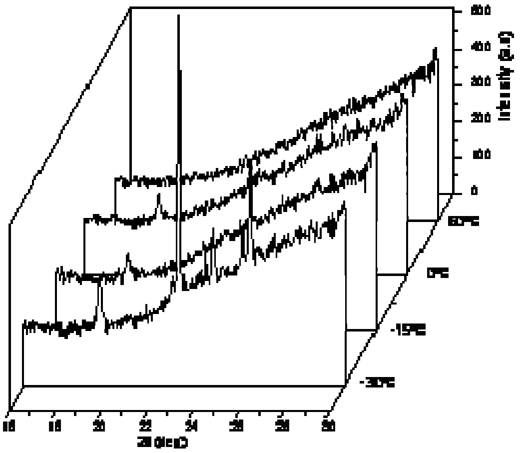

Fig 3. Crystallization of PEO nanotubes followed by temperature resolved WAXS.

A slight acceleration of the segmental dynamics was found comparing to the bulk when the PVDF is confined into nanopores due to the partial hindering of crystallization. On the other hand, the existence of a highly constrained relaxation was found and associated with the polymer-alumina interface (6). Similar results have been obtained for the crystallization of PVDF nanofibres. Although no shown here, the counterbalance between the consequences of spatial confinement and interfacial interactions controls the dynamics and semicrystalline structure of PVDF.

4. CONCLUSIONS

Anodic Aluminum Oxide (AAO) is a suitable template for the preparation of 1DPN by “template synthesis” due to its relatively low cost, good quality architecture with long-range order and adjustable and uniform nanopores with hexagonal symmetry. It enables the preparation of all types of 1D nanostructured polymer (nanofibres, nanotubes and ordered arrays of them) of any kind of chemical structure. Confinement of polymers in one-dimensional structure has a strong effect on polymer properties. Particularly, the confinement of PEO and PVDF nanotubes has a great influence on both crystallization mechanism and crystal morphology.

ACKNOWLEDGEMENTS

This work was financed by MICINN (MAT 2008-1073). Authors thank D. Gómez for SEM experiments and JM thanks MICINN for the grant FPU AP2005-1063.

REFERENCES

1. Masuda, H.; Fukuda, K. *Science* 1995, 268, 5216, 1466-1468
2.-Richter, S.; Steinhart, M.; Hofmeister, H.; Zacharias, M.; Gösele, U.; Gaponik, N.; Eychmüller, ; Rogachy, A. L.;. Wendorff, J. H ; Scweizer, S. L.; Rhein, A.; Wehrspohn, (2005) Appl. Phys. Lett. 2005, 87, 142107.
3. Martin J, Vazquez M, Hernandez M, Mijangos C (2008) *One-dimensional magnetopolymeric nanostructures with tailored sizes*, Nanotechnology 19(17)
4. Martin J, Mijangos C (2009) *Tailored polymer-based nanofibers and nanotubes by means of different infiltration methods into alumina nanopores* Langmuir 25(2) 1181-1187
5. Martín J, Maiz J, Mijangos C (2009) *Crystallization of PEO nanotubes. Some evidences of induced crystallization,* to be sent
6. Martin J, Mijangos C, Sanz A, Nogales A, Ezquerra T (2009) “Segmental dynamics of semicrystalline polymer nanorods” Macromolecules DOI: 0.1021/ma900754v

Estudio y caracterización de envases de nanocompuestos de PET con sepiolitas elaborados por termoformado

T. Fernández, A. Fernández
Departamento de I+D+i, LINPAC PACKAGING S.A. La Calzada - Vegafriosa, 33128 Pravia – Asturias, España
D. García-López
CIDAUT, Fundación para la Investigación y Desarrollo en Transporte y Energía. Parque Tecnológico de Boecillo, Parcela 209, 47151 Boecillo – Valladolid, España
J. Viña
Departamento de Ciencia de los Materiales e Ingeniería Metalúrgica, Universidad de Oviedo, Campus Universitario, s/n, 33203 Gijón - Asturias, España
A. Argüelles
Departamento de Construcción e Ingeniería de Fabricación, Universidad de Oviedo, Campus Universitario s/n, 33203 Gijón - Asturias, España

RESUMEN

En el presente trabajo se han obtenido láminas de nanocompuestos de PET reforzadas con una nanoarcilla fibrilar como la sepiolita, mediante un proceso de extrusión a escala industrial. Las láminas de PET reforzadas con nanosepiolita han sido caracterizadas microscópica y macroscópicamente. Mediante estos análisis se han observado las diferencias en cuanto a morfología y dispersión de las nanosepiolitas en la matriz de PET en función de la concentración de nanosepiolita en el máster de partida y el porcentaje final de ésta en la lámina. Además se han analizado sus propiedades físicas, así como sus propiedades mecánicas y de barrera al oxígeno, al dióxido de carbono y al vapor de agua. Una vez caracterizadas las láminas de nanocompuestos de PET, se han termoformado para obtener los envases deseados. Estos envases han sido también caracterizados mecánicamente para evaluar la influencia del nanocompuesto.

1. INTRODUCCIÓN

El PET es uno de los materiales más ampliamente utilizados en el sector del envase y embalaje debido, principalmente, a sus propiedades mecánicas, barrera y de transparencia. Sin embargo, desde el punto de vista del sector de envases para la alimentación, sus propiedades no son suficientes para cubrir las exigencias del mercado. Así pues, hoy en día, para satisfacer estas exigencias, se utilizan una gran variedad de materiales con distintas propiedades, lo que complica ampliamente el proceso industrial. En el presente trabajo se pretende mejorar las propiedades del PET con la adición de partículas de sepiolita con dimensiones nanométricas. Se ha realizado un estudio sobre las condiciones de extrusión y termoformado necesarias para la obtención de envases a partir de un material nanocompuesto, así como la influencia de éstas en las propiedades del nanocompuesto final.

2. PARTE EXPERIMENTAL

2.1. Materiales utilizados

Este trabajo se ha desarrollado utilizando PET como matriz polimérica para el nanocompuesto. El material de refuerzo escogido es la sepiolita (Pangel HV/Tolsa S.A), que es un silicato de magnesio hidratado cuya fórmula teórica de la celda unidad es $Si_{12}O_{30}Mg_8(OH,F)_4(OH)_4{\cdot}8H_2O$ (Darder et al., Kavas et al.). Tiene estructura fibrilar formada por dos capas tetraédricas de sílice unidas a una capa central octaédrica discontinua de óxido e hidróxido de magnesio. Esta estructura forma túneles de tamaño nanométrico que crecen en la dirección de la fibra y proporcionan un gran área superficial. Además a lo largo de las fibras de sepiolita se forman grupos silanol (Si-OH) que facilitan su modificación y de esta manera mejoran la interacción interfacial entre la sepiolita y los polímeros. Por otra parte, la sepiolita tiene buena resistencia mecánica y estabilidad térmica (Bokobza, Rong et al., Ruiz-Hidalgo). Como agente modificante se ha empleado el silano metacriloxipropil trimetoxisilano (MEMO). Los nanocompuestos de PET/sepiolita (máster) han sido obtenidos por Repol mediante extrusión y los porcentajes de sepiolita han variado entre el 10 y el 18%. A partir de estos máster se realizaron pruebas de extrusión con porcentajes de sepiolita en lámina entre el 1 y 3 %.

2.2. Obtención de los envases nanocompuestos

A partir del concentrado de PET/nanosepiolita se han obtenido láminas de nanocompuesto mediante un proceso de extrusión a escala industrial. Esta extrusión se ha llevado a cabo en una extrusora de doble husillo corrotante (Luigi Bandera SpA.). La velocidad de producción se ha ido variando desde 500 Kg/h hasta 1200 Kg/h. Controlando de esta forma los parámetros de extrusión y la calidad de la lámina obtenida en función de los porcentajes de nanoarcilla y la velocidad de la máquina.

Una vez obtenida la lámina de PET/nanosepiolita ésta se ha termoformado en una termoformadora Kiefel controlando los parámetros utilizados tanto en moldeo como en corte. Se han termoformado envases con distintas aplicaciones en el mercado para poder finalmente comparar las prestaciones de los envases realizados en sus materiales originales y con el nanocompuesto de PET.

2.3. Caracterización de los materiales y envases

En primer lugar se ha llevado a cabo una caracterización microestructural mediante Microscopía Electrónica de Barrido (SEM) y Microscopía Electrónica de Transmisión (TEM). Estas caracterizaciones se han complementado con Análisis Termogravimétricos (TGA) para poder controlar el porcentaje de nanosepiolita en cada muestra.

Los análisis de SEM se realizaron sobre la superficie obtenida al fracturar los materiales después de sumergirlos en nitrógeno líquido, empleando un microscopio Hitachi 3400N. Mientras que para los análisis de TEM se realizaron en un microscopio JEOL 2000FX operado a 200 kV. La preparación de las muestras para estos análisis se realizó por corte con ultramicrotomo en nitrógeno líquido, depositando la película obtenida en una rejilla de cobre que soporta una película de grafito. Por último, los Análisis Termogravimétricos se ha empleado un equipo METTLER TOLEDO 851E donde se realizaron dos etapas, una primera etapa de 50 a 600ºC en atmósfera de nitrógeno y una segunda etapa desde 600 hasta 900ºC en atmósfera de aire a una velocidad de 20ºC/min.

Una vez realizada la caracterización microscópica se han analizado las propiedades de barrera al oxígeno, al dióxido de carbono y al vapor de agua de los nanocompuestos.

Tanto las láminas como los envases se han analizado mecánicamente. Los ensayos realizados sobre las láminas han sido: Resistencia a Tracción e Impacto Puncture. El ensayo de tracción a Rotura se ha realizado en base a la norma ISO 527-3 con probetas halterio (tipo 5). Mediante el Impacto Puncture se ha analizado el comportamiento a la perforación a distintas temperaturas en un equipo MTS-831 bajo la norma UNE-EN ISO 6603-2.

La caracterización mecánica de los envases se ha hecho bajo ensayos no normalizados de impacto y de aplastamiento axial y lateral. Los ensayos de aplastamiento axial se han realizado en una máquina de compresión digital, serie CDF. Los ensayos de aplastamiento lateral se han realizado en una máquina de compresión Hounsfield y los e de impacto en un equipo TMI (Monitor/Impact Testing Machines Inc.).

3. RESULTADOS Y DISCUSIÓN

La caracterización microscópica realizada por SEM ha revelado la presencia de agregados micrométricos en las láminas con más de un 2% de nanosepiolita. Con el fin de analizar la dispersión nanométrica de las nanosepiolitas en la matriz de PET, en función del porcentaje de nanosepiolita se han realizado análisis de microscopía de transmisión (TEM) cuyos resultados se muestran en la Figura 3. Se observa una morfología heterogénea y sin orientación preferente, con nanofibras individuales de nanosepiolita (rectángulos) acompañadas de agrupaciones de nanofibras (resaltadas con flechas). También se observa que algunas nanofibras tienen más de 500 nm de longitud, aunque la mayoría son más cortas, e incluso algunas se ve que están rotas (círculos).

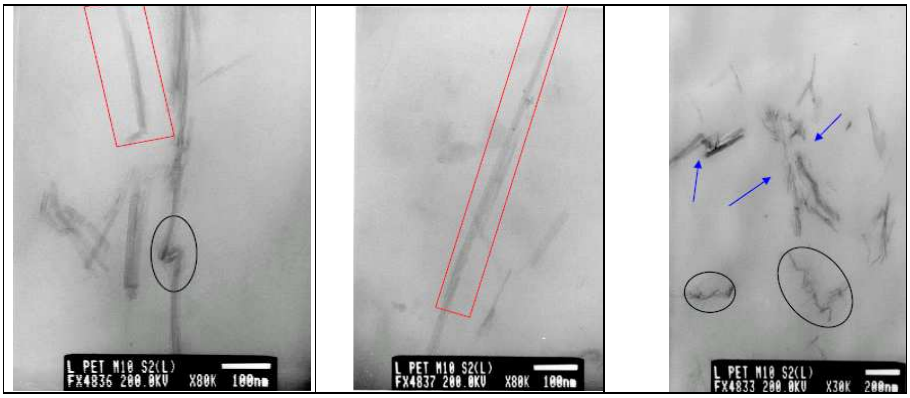

Figura 3. Micrografías de TEM de muestras tomadas en sentido longitudinal a la dirección de extrusión con 1.2 % de nanosepiolita.

Para analizar la barrera a los gases de los nanocompuestos se utilizará el coeficiente de permeabilidad, que se obtiene a partir de la velocidad de transmisión de un gas a través de la muestra y el espesor de la misma. Los resultados de permeabilidad se muestran en la Tabla 1. Las láminas de nanocompuesto de PET presentan, frente a las de PET puro, una menor permeabilidad al O_2, aproximadamente igual al vapor de agua y mayor al CO_2. Y, aunque no se observan diferencias significativas entre los distintos valores, parece que la concentración del 2% en nanosepiolita es la que presenta mejores propiedades barrera.

% nS máster	**PET puro**	**10 % nS**	**18 % nS**	
% nS lámina	**-**	**2 %**	**2 %**	**3 %**
C.P al O_2	3,38	3,00	2,79	3,02
C.P al $H_2O_{(v)}$	0,89	0,86	0,86	0,91
C.P al CO_2	7,6	14,3	13,5	15

Tabla 1. Coeficiente de permeabilidad (cc/m^2/mm/día).

Los nanocompuestos de PET/sepiolita presentan mayor resistencia a la tracción que las láminas de PET puro. Esta resistencia aumenta con el contenido en nanosepiolita. El comportamiento de las láminas de nanocompuesto al impacto puncture depende mucho de la composición del material, y se comprobó que otros parámetros como la temperatura de ensayo y el espesor de la lámina influyen en su comportamiento final y modo de rotura.

Los ensayos realizados sobre los envases finales termoformados con lámina de nanocompuesto de PET han demostrado que la rigidez por gramo aumenta en todos los casos respecto a los envases de referencia, fabricados con PET y otros polímeros sin aditivar. Por el contrario, la resistencia al impacto de los envases fabricados con lámina de nanocompuesto disminuye.

4. CONCLUSIONES

En el presente trabajo se ha optimizado el proceso de extrusión y termoformado industrial para la obtención de envases a partir de lámina de nanocompuestos de PET/sepiolita.

AGRADECIMIENTOS

El presente trabajo no se habría podido realizar sin la concesión por el CDTI de un proyecto CENIT a la empresa LINPAC PACKAGING Pravia. El desarrollo y caracterización de los nanocompuestos se ha llevado a cabo gracias a la colaboración de empresas como Tolsa y Repol y de los centros tecnológicos Cidaut y Ainia.

REFERENCIAS

DARDER. M., LOPEZ-BLANCO, M., ARANDA, P., AZNAR, J. J., BRAVO, J., RUIZ-HITZKY, E., (2006) Microfibrous chitosan-sepiolite nanocomposites. Chem. Mater. 18(6), 1602-1610.

KAVAS, T., SABAH, E., ÇELIK, M. S., (2004) Structural properties of sepiolite-reinforced cement composite, Cem. Concr. Res. 34(11), 2135-2139.

BOKOBZA, L., (2004) Elastomeric composites, I. Silicone. J. Appl. Polym. Sci. 93(5), 2095-2104.

RONG, J., PING, Z., HONG, X., ZHANG, W., U. S. Patent 6444742 (2002).

RUIZ-HITZKY, E., (2001) Molecular access to intracrystalline tunnels of sepiolite, J. Mater. Chem. 11(1), 86-91.

Synthesis and characterization of nanocomposites based on furan resins

G. Rivero, V. Pettarin, L. B. Manfredi
Instituto de Investigaciones en Ciencia y Tecnología de Materiales (INTEMA). Facultad de Ingeniería, Universidad Nacional de Mar del Plata, Argentina.
A. Vázquez
Laboratorio de Polímeros y Materiales Compuestos. Instituto de Tecnologías y Ciencias de la Ingeniería (INTECIN). Facultad de Ingeniería. Universidad de Buenos Aires, Argentina

ABSTRACT

Furan resins obtained from furfural and phenol were synthesized to obtain a resin to be used as metal coating or matrix of composite materials. These resins should have similar properties to the phenolic resins because they are obtained by replacing formaldehyde by furfural. So, it should be possible to obtain a material with an excellent thermical and oxidative resistance but reducing the formaldehyde emissions. Moreover, the addition of nanoparticles to the furan resin should enhance their performance. The synthesis and characterization of a furan resin was made in this work. Nanocomposites were obtained by the in-situ addition of different type of clays to the resin. The prepolymer formation reactions were studied by infrared spectroscopy (FTIR) and the variation of viscosity with the time was measured. It was observed that the addition of clay to the resin accelerates the prepolymer formation. It was then cured using hexamethylenetetramine as catalyst and their chemical structure was also studied by FTIR. It was concluded that the type of clay has an important influence on the final structure of the resin. It could be due to the compatibility among the surfactants of the clay with the resin. The curing kinetics of the furan resin and their composites was characterized by differential scanning calorimetry applying free kinetic models.

1. INTRODUCTION

During the last years, the use of biomass wastes as row materials for the development of new polymeric materials has been increasingly promoted. Furan resins are similar to phenolic resins as formaldehyde is replaced by furfural, which is easily produced from a wide range of agricultural or forestry wastes containing pentoses. As formaldehyde is a dangerous atmospheric pollutant, its replacement in paints and metal coatings would decrease its potential emissions. Furthermore, it was reported (Hussain et al. 2006) sizeable properties improvement after the addition of low quantities of nanoparticles to a polymeric matrix. The purpose of this work is to study the chemical reactions involved in the synthesis and curing of a furan resin and their nanocomposites. Then, it is significant to understand the changes in the chemical structure and the properties of the nanocomposites that determine potential specific applications.

2. EXPERIMENTAL

Furan resin (F) was synthesized using phenol and furfural, 1:1 molar ratio in K_2CO_3 solution media. Nanocomposites were obtained similarly by the in-situ addition of

Cloisite®clays: Na^+ (FNa) and organically modified 30B (F30B) and 10A (F10A) (Southern Clay Products). Then, resins were cured by a temperature treatment after the addition of 12% of hexamethylentetramine as catalyst.

Prepolymer samples were collected from the reactor every 30 minutes and direct measurements of the viscosity at 25 ºC (Brookfield Cone/Plate Viscometer) were performed. Fourier Transform Infrared (FTIR) spectra of the prepolymer samples were obtained in a Mattson Genesis II. FTIR technique was also used to follow the resin curing up to 180°C, running scans every 10°C. Spectra were normalized with the band at 1595 cm^{-1}, assigned to the C=C str, that was expected to remain constant.

Ozawa, Ortega and Vyazovkyn isoconversional methods (Ortega, 2008) were applied to the systems to calculate the activation energy as function of the curing conversion using dynamic DSC data at different heating rates: 2, 5, 10, 20 and 25°C/min.

3. RESULTS AND DISCUSSION

As a result of the measures of viscosity at 25°C to the different fractions obtained during the progress of reaction (**Figure 1**), it was observed that the addition of clays actually accelerates the reaction. It was also observed that the materials that showed a faster increment in the viscosity are the ones with higher solid content and refractive indexes. Then, FTIR analysis was performed in the materials to study the influence of the clay addition in the chemical structure of the furan resin.

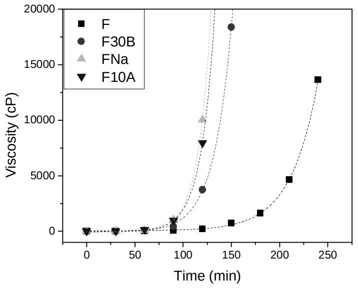

Fig. 1. Viscosity vs time.

Chemical reactions shown in **Figure 2** lead to interpret the proposed possible chemical changes that take out during the synthesis (Zeitsch, 2000).

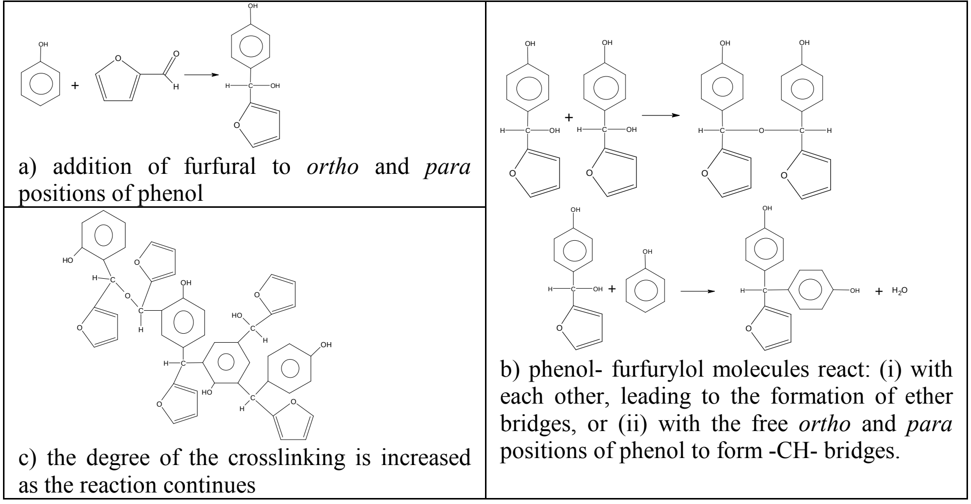

a) addition of furfural to *ortho* and *para* positions of phenol

b) phenol- furfurylol molecules react: (i) with each other, leading to the formation of ether bridges, or (ii) with the free *ortho* and *para* positions of phenol to form -CH- bridges.

c) the degree of the crosslinking is increased as the reaction continues

Fig. 2. Diagram of the phenol-furfural reactions (Idem in the *ortho* position).

FTIR spectrum was scanned for each resin and the variation of the bands corresponding to the characteristic functional groups along the reaction time was analyzed in the neat furan prepolymer. Thereafter, the influence of the clay addition in the chemical structure of the furan resin was also studied.

The consumption of furfural was evidenced by the decrease of the bands at 1692 cm^{-1} (C=O str) and at 1512 cm^{-1} (C=C in ph-str if double bond is conjugated to a saturated group) with time (**Figure 3**). The growing substitution extent on the phenol ring with the reaction advancement was evidenced as a reduction of mono-substituted rings at 690 cm^{-1} as well as the intensity enhancement of the bands associated to substituted rings in positions 1,2- and 1,2,4- (736 cm^{-1}) and, 1,4- and 1,4,6- (840 cm^{-1}) (**Figure 4)**. The *ortho* positions of the phenol were more easily substituted than *para* position. The bands at 1440 cm^{-1} and 1456 cm^{-1}, assigned to the *para-para′* and *ortho–ortho′* -CH- bridges between phenols, increase their intensity with time (**Figure 5**). O*rtho-ortho′* bridges formation is favoured over *para-para′* bridges. This result is in accord to the higher quantity of *ortho* substituted benzene rings.

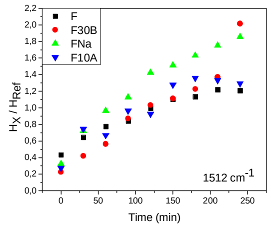

Fig.3. Furfural decrease.

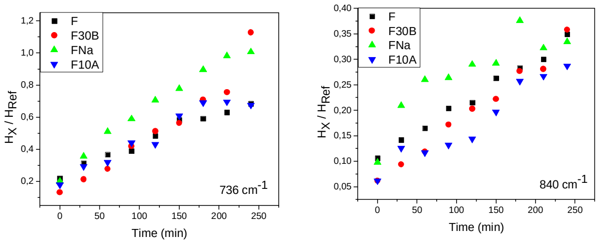

Fig. 4. Substitution of phenol rings.

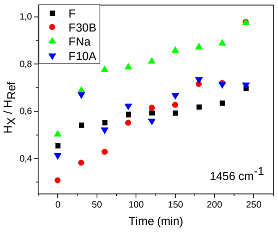

Fig. 5. –CH- bridges.

Curing kinetic analysis of thermosetting resins is usually complex because simultaneous chemical reactions take place and their activation energy changes depending on the conversion. A continuous tendency of activation energy *E* as a function of conversion was calculated for each material applying the mentioned methods (**Fig.6**). As the curves obtained by Ozawa method are not constant with conversion, the suppositions assumed on its expressions become invalid.

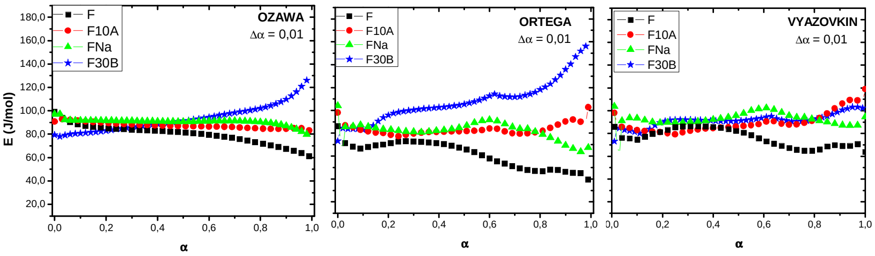

Fig. 6. Activation energy as function of conversion.

Curves of the systems studied obtained by Vyazovkin method show that initial *E* values are quiet similar until a conversion of approximately 0,5 is reached. FTIR analysis of the cured materials evidenced that at this point, drastic changes of chemical functional groups take place because of the simultaneous occurrence of addition and crosslinking reactions. At this range of conversion, nanocomposite curves of E exhibit a peak that does not appear in the curve of the neat resin. Additionally, E values were higher for the composites than for the neat resin, independently of the clay used. This may be due to the polymer chains mobility impediment introduced by the clay sheets, which may act as a barrier. Finally, the accuracy and sensibility of Ortega and Vyazovkin methods were optimized by the evaluation of the minimization of errors affected during the numerical calculus. It was observed that the curve tendency and the absolute values are notably affected by the $\Delta\alpha$ selected.

4. CONCLUSIONS

Furan resin and nanocomposites were obtained by the in-situ addition of three different clays. FTIR analysis performed indicated that the proposed reactions are consistent with the structural chemical changes in the functional groups during the synthesis and curing reactions. It can be concluded that the clay addition to the furan resin accelerates the formation reaction of the materials. Anyway, differences between each nanocomposite were detected in relation to their final chemical structure. FNa showed the most advanced reaction rate evidenced by the most rapid disappearance of free reagents as well as the earliest increase of functional groups characteristic of the reaction products and a major rate of benzene substitution. It could be explained due to the formation of chelates in the presence of Na^+ (Gardziella et al. 2000) that also favours the *ortho* position substitution. The differences on the rate and extent of reaction and final chemical structure among the materials may be due to the chemical nature of the clay organic modifiers that are compatible with the furan resin.

Activation energy of the curing process as a function of conversion was calculated applying isoconversional methods. Ozawa´s method is not suitable to this system because as E changes during the reaction, the suppositions assumed became invalid. Nevertheless, Vyazovkin numerical analysis provides the most accurate method to analyze the E variation with the conversion. Even if Ortega method results simpler, its precision is more affected by the selected $\Delta\alpha$. Nanocomposites E profile showed a peak at conversion 0,5 approximately, independently of the kind of clay added to the polymer. The furan resin E curve did not exhibit it. It seems that this increment in the activation energy may be due to the clays that act as physical barriers to the polimerization when a certain conversion has been reached.

ACKNOWLEDGMENTS

The authors gratefully acknowledge the support from the National Research Council of Argentina (CONICET), PIP6254 and ANPCYT (PICT 1560).

REFERENCES

ORTEGA A. (2008) A simple and precise linear integral method for isoconversional data. *Thermochim Acta*, 474, 81-86

HUSSAIN F., HOJJATI M., OKAMOTO M., GORGA R.E. (2006) Polymer-matrix nanocomposites, processing, manufacturing and appl. *J Compos Mater,* 40, 1511-75.

GARDZIELLA A., PILATO L.A., KNOP A. (2000) *in: Phenolic Resins*, Springer-Verlag, Berlín, Heidelberg.

ZEITSCH K.J. (2000) *in: The chemistry and technology of furfural and its many by-products*, Ed. Elsevier, Amsterdam, the Netherlands. 214-16.

Nanocompuestos epoxi/CNT: estudios sobre su preparación y curado de la matriz

M.T. Lacorte
Departamento de Ciencia de Materiales e Ingeniería Metalúrgica, ETSEIAT (UPC)
P.Pagès
Departamento de Ciencia de Materiales e Ingeniería Metalúrgica, ETSEIAT (UPC)
F. Carrasco
Departamento de Ingeniería Química, EPS (UdG)
C. Comes
Composites ate, S.L., 08330 Sant Boi de Llobregat

RESUMEN

Se ha procedido a la preparación de muestras de nanocompuestos a partir de una matriz epoxi trifuncional reforzada con nanotubos de carbono (CNT) : Una proporción de CNT de 0.0.5% en masa, pudo dispersarse satisfactoriamente en la resina sin necesidad de oxidación ni funcionalización previa. Posteriormente se procedió a añadir el endurecedor en la proporción adecuada, procediéndose seguidamente al curado no isotérmico de la matriz siguiendo el ciclo térmico indicado por el suministrador. Un primer control de la dispersión se ha realizado mediante microscopía óptica de transmisión con objeto de establecer el tiempo de inmersión en el baño ultrasónico, en función del estado de los aglomerados de nanotubos que se apreciaba mediante esta técnica.

Las microfotografias tomadas de distintas zonas de fractura en muestras curadas de nanocompuesto realizadas mediante SEM, mostraron una aceptable dispersión de los CNT en la resina con la práctica desaparición de los aglomerados presentes en el producto comercial de CNT utilizado.

El avance del curado térmico de la resina, se ha seguido mediante espectroscopía FTIR calculando el parámetro α a partir de la evolución de una banda característica epoxi de la resina observándose una significativa aceleración de dicho avance en determinadas fases del ciclo de curado debido a la presencia de los nanotubos dispersados.

1. INTRODUCCIÓN

Los nanotubos de carbono (CNT) son objeto de una amplia investigación y caracterización por parte de muchos autores (LI et al. 2003), (THOSTENSON et al. 2003), actualmente se fabrican a escala industrial y desde su descubrimiento se han perfeccionado sus técnicas de obtención, consiguiéndose diversos tipos: nanotubos de pared simple (SWCNT), doble (DWCNT) y múltiple (MWCNT). En todos los casos se ha ido mejorando asimismo la pureza de los nanotubos y su calidad. Son materiales nanométricos, que por ello poseen una extraordinaria área efectiva (del orden de 1300 m^2/g) así como una relación de aspecto del orden de varios miles, que actuando como aditivos pueden cambiar las propiedades de otro material. De acuerdo con su estructura grafítica los CNT poseen una alta conductividad térmica y eléctrica, pudiendo comportarse como semiconductores o parecidos a los metales.

Para aprovechar al máximo las propiedades excepcionales de los CNT, deben conseguirse dos objetivos : obtener una buena dispersión de los nanotubos en la matriz, y lograr una buena adhesión interfacial con ella . Se han ensayado diversos métodos para conseguir buenas dispersiones, entre ellos la agitación mecánica, la agitación por ultrasonidos y en algunas ocasiones los CNT han sido previamente funcionalizados con objeto de lograr una afinidad con la matriz polimérica (el tratamiento básico consiste en una oxidación destinada a abrir la estructura de los CNT, complementada la mayoría de las veces por una reacción química con objeto de incorporar grupos amina primaria a dicha estructura).

En el presente trabajo, se ha obtenido una aceptable dispersión de una proporción de MWCNT del 0.05% en masa, en un sistema constituído por una resina epoxi trifuncional y un endurecedor de diamina con una combinación de agitación mecánica, ultrasonidos y temperatura sin funcionalización previa de los nanotubos. La técnica de control utilizada ha sido la microscopía electrónica SEM.

Se ha comparado el curado no isotérmico del sistema en ausencia y con la presencia de una dispersión de MWCNT mediante utilización de la espectroscopía FTIR, siguiendo la evolución de una de las bandas características de los grupos epoxi de la resina, observándose una apreciable diferencia entre ambos avances de curado, lo que demuestra que los nanotubos influyen en el curado de la resina ejerciendo el papel de catalizadores en determinadas etapas del curado, efecto que es importante conocer de cara al procesado industrial de piezas de este tipo de nanocompuestos.

2. MATERIALES Y EQUIPOS

El sistema utilizado como matriz, consiste en una resina epoxi trifuncional TGAP, Araldite MY0510 y un endurecedor 4-4´diamino difenilsulfona, HT-976-1, ambos suministrados por HUNTSMAN. La proporción resina/endurecedor es de 100/52 en masa.

El nanorefuerzo está constiuído por nanotubos de pared múltiple (MWCNT), Baytubes C150P suministrados por BAYER MATERIALS SCIENCE. La proporción nanorefuerzo/resina utilizada ha sido del 0.05% en masa.

El baño ultrasónico utilizado ha sido un Bransonic DTH-3510 de 42 KHZ.

El espectrómetro FTIR utilizado ha sido el modelo 6700 de NICOLET y el intervalo de registro seleccionado está comprendido entre 4000 y 600 cm^{-1}.

El microscopio electrónico SEM utilizado ha sido el modelo JEOL 610.

3. EXPERIMENTAL Y RESULTADOS

Para la preparación de las muestras de nanocompuestos, se ha procedido a la dispersión de los MWCNT (0,05% en masa) en 20ml de etanol, colocando esta mezcla en el baño de ultrasonidos durante 4h. A continuación se añade la resina a 80ºC y se coloca nuevamente la mezcla en el baño de ultrasonidos durante 2h manteniendo la temperatura del baño a 69ºC. Este método se fundamenta en el propuesto por determinados autores (LAU et al. 2003) .

Una vez evaporado el etanol (12 h en estufa a 80ºC) se realiza un control previo de la calidad de la dispersión y distribución de los MWCNT mediante microscopía óptica, observándose la práctica desaparición de agregados. A continuación se añade el endurecedor en una proporción de 100/52 a la mezcla previamente calentada a 80ºC con agitación mecánica durante 30min. Se sonifica 1h manteniendo el baño de ultrasonidos a 69ºC, se procede al curado no isotérmico en estufa de la muestra de nanocompuesto siguiendo el siguiente proceso de calentamiento que es el recomendado por el suministrador : 4 h a 100ºC, 2h a 150ºC y 2 h a 200ºC.

El avance de curado de la matriz durante el proceso utilizado, se ha seguido mediante espectroscopía FTIR calculando el parámetro α, a partir de los valores del cociente de la absorbancia de la banda característica de los grupos epoxi de la resina tomados cada hora (906 cm-^{1}), que disminuye gradualmente con el avance del curado, y de la absorbancia de la banda de los grupos bencénicos de la resina (1513 cm-^{1}), que permanece invariable durante dicho proceso (PAGÈS et al. 2008).

En la tabla 1 se indica la comparación de los valores del parámetro α del sistema matriz sólo y en presencia de una concentración de MWCNTS del 0.05%,obtenidos durante sucesivas etapas el proceso de curado no isotérmico.

T curado (h acumul.)	T curado (ºC)	Curado matriz (α %)	Curado nanocompuesto (α %)
0.5	100	0.0	0.0
4.0	100	22.2	17.0
5.0	150	81.5	88.0
6.0	150	82.3	92.7
7.0	200	100.0	100.0
8.0	200	100.0	100.0

Tabla 1. Evolución del parámetro α durante el proceso de curado de la matriz y del nanocompuesto.

Con objeto de controlar la calidad de la distribución y dispersión de las nanotubos en la matriz, además de un primer examen realizado con microscopía óptica en la fase inicial de preparación de la muestra para observar el estado de los agregados de los nanotubos dispersados, se realizan una serie de microfotografías SEM a las muestras totalmente curadas. Con objeto de visionar mejor los nanotubos dispersados en la resina, la muestra se ataca superficialmente con unas gotas de ácido oxidante (H2SO4) (LI et al. 2008). En la Figura 1 se muestran varias microfotografías SEM captadas mediante esta técnica que constatan una buena dispersión y distribución de los nanotubos en la matriz.

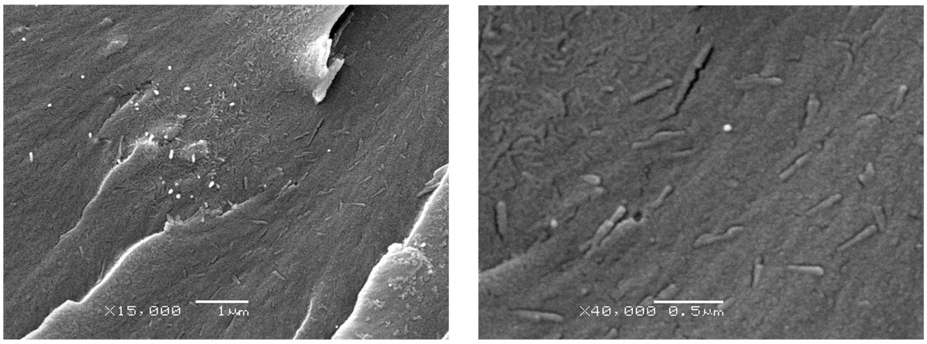

Fig. 1. Microfotografías SEM de muestras de nanocompuestos con un 0.05 % de MWCNT.

4. CONCLUSIONES

1. Se ha desarrollado un método de preparación de nanocompuestos epoxi trifuncional/MWCNT, sin necesidad de efectuar una funcionalización previa de los nanotubos.
2. Se ha demostrado que existe una fuerte interacción entre la matriz y los nanotubos dispersados en ella, puesto que el avance del curado se ha llevado a cabo más rápidamente en presencia de nanotubos, los cuales ejercen un efecto catalítico en el curado (excepto en las fases iniciales del mismo ya que a temperaturas inferiores a 100ºC, los nanotubos no consiguen activarse).
3. La microscopía SEM, con ataque superficial de la muestra, indica una aceptable dispersión y distribución de los nanotubos en la matriz con el método de preparación propuesto.
4. El conocimiento del efecto de la dispersión de nanotubos en el curado de la matriz se considera importante en la tecnología industrial de procesado de este tipo de nanocompuestos.

AGRADECIMIENTOS

Agradecemos a la empresa BAYER MATERIALS SCIENCE el suministro desinteresado de los MWCNT utilizados en el presente estudio.

REFERENCIAS

LAU K-T, SHI SQ, CHENG H-M, Micro-mechanical properties and morphological observation on fracture syrfaces of carbon nanotube composites pre-trated at different temperatures, Composites Sci. Technol. 2003, 63, 1161-1164.
LI C, CHOU TW. Elastic moduli of multi-walled carbon nanotubes and the effect of van der Waals forces. Compos Sci Technol 2003;63:1517–24.
LI X-F, LAU K-T, YIN Y-S, Mechanical properties of epoxy-based composites using coiled carbon nanotubes, Composites Sci. Technol. 2008, 68, 2876-2881.
P.PAGÈS, T.LACORTE, M.LIPINSKA, F.CARRASCO. Study of Curing of Layered Silicate/Trifunctional Epoxy Nanocomposites by Means of FTIR Spectroscopy: Journal of Applied Polymer Science, vol. 108, 2107-2115 (2008).
THOSTENSON ET, CHOU TW. On the elastic properties of carbon nanotube-based composites: modeling and characterization. J Phys D: Appl Phys 2003;36:573–82.

Thermally conductive nanocomposites: development and characterization

M. Chapartegui, B. Pérez, **S. Florez**
Inasmet-TECNALIA, Mikeletegi 2, 20009 San Sebastian, Spain
A. Santamaría, **M.E. Muñoz**
Polymers Science and Technology Department and Polymat, Faculty of Chemistry, University of the Basque Country, E-20080 San Sebastian, Spain

SUMMARY

The aim of this study is to develop a thermally conductive, electrically insulating nanoreinforced epoxy system with well balanced mechanical properties as an alternative to the already used non-reinforced epoxy systems for electroforming coils coating.
For this purpose, a low viscosity epoxy system based in DGEBA and an amine hardener was selected. Aluminium Nitride (AlN) and Boron Nitride (BN) were selected as the thermally conductive and electrically insulating nanomaterials. Nanocomposites were manufactured with nanoceramic percentages between 2 and 20% wt. The dispersion of the nanomaterials within the organic matrix was analyzed by SEM and the influence of the addition of nanomaterials on rheological properties was evaluated. Standard nanocomposite samples were subjected to flexural test, as well as to thermal conductivity measurements. Best results are obtained for epoxy/10%wt.AlN nanocomposites where thermal conductivity is enhanced by 90% and flexural modulus and flexural strength are increased by 70% and 30%, respectively.

1. INTRODUCTION

Coils used in electroforming are usually covered with an epoxy resin to ensure thermal and mechanical performance during the process. However, their life time is reduced due to the fragility of the resins so production possibilities for electroforming are limited. Nanoreinforced resins can help to enhance its impact and wear resistance (Wetzel et al. 2004) and thus coil durability. Together with mechanical properties improvement, nanomaterials offer the possibility of increasing the capability for the resin to dissipate the heat generated during the electroforming process (Iwata et al. 2006), (Xu et al. 2000). Electrically insulating resins are required for these applications.
The aim of this study is to develop a thermally conductive, electrically insulating nanoreinforced epoxy system with well balanced mechanical properties as an alternative to the already used non-reinforced epoxy systems for electroforming coils coating.

2. EXPERIMENTAL

2.1 Materials

A low viscosity epoxy system based on a Bisphenol A epoxy resin and an amine curing agent was selected. The characteristics of the studied system are shown in Table 1.

	Araldite DBF / Aradur HY 956 EN
Chemical origin of epoxy/hardener	DGEBA/aliphatic tetramine
Mix ratio (pbw)	100:20
Initial mix viscosity at RT (mPa.s)	1800
Cure schedule	4h @ 25ºC + 6h @ 60ºC
Supplier	Huntsman

Table 1. Characteristics of the investigated epoxy system.

Aluminium Nitride (AlN) and Boron Nitride (BN) nanoparticles from PlasmaChem GmbH were selected as the thermally conductive and electrically insulating nanomaterials.

2.2 Nanocomposite manufacturing

AlN and BN nanoparticles were dispersed in the resin by a three roll mill. The three roll mill device allows to monitor the gap between the rolls, the force between the rolls and the speed of the rolls, so that nanofillers are well dispersed in the matrix due to the shear forces generated between the rolls.

Hardener was added and mixed with the dispersion by mechanical stirring during 10 minutes, keeping the mixture under vacuum. The mixture was poured in an opened mould and cured in an oven following the cure schedule indicated in Table 1.

Nanocomposite coupons with 2 wt %, 10 wt % and 20 wt % of nanoparticle content were manufactured.

2.3 Nanocomposite characterization

2.3.1 Microstructural characterization

Scanning Electron Microscopy (SEM) technique was used to evaluate the dispersion of the nanoparticles in the epoxy matrix. Figure 1 presents the SEM micrographs for the nanocomposites with 10 wt % of nanofiller content.

Fig. 1. SEM micrographs for Araldite DBF nanocomposites with: a) 10 % wt BN, b) 10 % wt AlN .

For the same content of nanofiller, AlN nanocomposites exhibit better dispersion than BN nanocomposites.

2.3.2 Rheological properties of the dispersions

A rheometer in parallel-plate geometry mode was used to study the rheological behavior of the epoxy/AlN dispersions before curing, that is, before adding the hardener. In Figure 2 viscosity as a function of shear rate is presented:

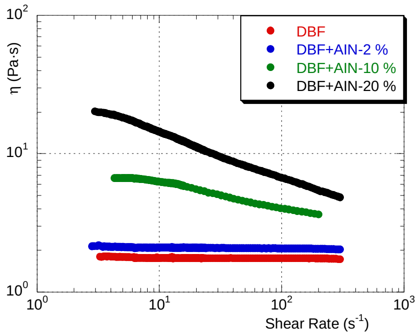

Fig. 2. Viscosity curves for Araldite DBF/ AlN nanocomposites.

The shear rate dependence of the viscosity changes for high AlN contents.The neat resin and the nanocomposite with 2 wt % AlN exhibit Newtonian behavior, whereas the nanocomposite with 10% wt. nanoparticle content shows a pseudoplastic behavior. A viscoplastic response is hinted from viscosity data of 20 wt % AlN. This is indicative of the existence of a physical network which is destroyed as shear rate is increased, leading to a significant viscosity decrease that facilitates the processing of this highly charged system. Preliminary results (not shown here) indicate that the existence of such a physical network modifies the curing process of the dispersion.

2.3.3 Mechanical properties

Flexural test was carried out according to the norm UNE – EN ISO 178. Results are shown in Table 2:

Araldite DBF		Flexural strength		Flexural modulus	
Nanoparticle	wt %	Strength (Mpa)	Increase vs. neat resin (%)	Modulus (MPa)	Increase vs. neat resin (%)
-	-	93±3.5	-	2967±3.8	-
BN	2	118±1.1	27	3545±2.6	19
BN	10	109±1.4	17	3531±2.1	19
AlN	10	124±1.9	33	5131±3.7	73

Table 2. Flexural test results for Araldite DBF nanocomposites.

When 10 % wt. of AlN is added to the epoxy matrix, the flexural modulus is increased by 73 % and the flexural strength is increased by 33 %.

2.3.4 Thermal conductivity

Thermal conductivity of the manufactured nanocomposite coupons was measured using the Guarded Hot Plate method. In Figure 3 the obtained results can be seen:

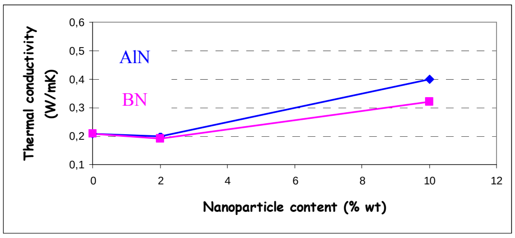

Fig. 3. Thermal conductivity results for Araldite DBF nanocomposites.

When 10 % wt. of AlN is added to the epoxy matrix, the thermal conductivity is increased by 90 %.

3. CONCLUSIONS

In this work a polymer matrix nanocomposite was developed for electroforming coils coating application. A low viscosity commercial epoxy system was used as a matrix and aluminium nitride and boron nitride nanoparticles were selected as nanofillers. Nanoparticles were dispersed in the matrix by calendaring. SEM micrographs revealed that with AlN nanoparticles a better dispersion was achieved. For the highest nanofiller content dispersion the rheological analysis indicated the formation of a physical network before curing. With the addition of 10% wt. AlN both mechanical properties and thermal conductivity of cured samples improved significantly.

ACKNOWLEDGEMENTS

This research group kindly thanks ARKEMA for lending the ceramic three roll mill used in this work.
This investigation has been supported by European project PROFORM, “An innovative manufacture process concept for a flexible and cost effective production of the vehicle body in white: Profile Forming”, Contract nº026706.

REFERENCES

IWATA, M. et al. (2006) CRIEPI Report HOS008.
WETZEL, B. et al. (2004). Impact and wear resistance of polymer nanocomposites at low filler content, *Polymer Engineering & Science,* 42, 1919-1927.
XU, Y., CHUNG, D. D. L (2000) Increasing the thermal conductivity of boron nitride and aluminum nitride particle epoxy-matrix composites by particle surface treatments, *Composite Interfaces,* 7, 243-256.

Bacterial cellulose production from Colombian agroindustrial waste

C. Castro[1], R. Zuluaga[1], I. Mondragon[2], P. Gañán[1]
[1]School of Engineering, New Materials Research Group, Pontificia Bolivariana University
[2]'Materials + Technologies' Group, Chemical and Environmental Engineering Department, Polytechnic School, Universidad del País Vasco/Euskal Herriko Unibertsitatea

ABSTRACT

The production of bacterial cellulose from agroindustrial waste was examined. Carbon resources, like sugar cane juice and pineapple peel were used. The yields were increased by addition of carbon resources from pineapple peel and sugar cane juice. In addition, it was confirmed that these residues are a potential resource to the production of cellulose with morphological, chemical and physical properties as those reported in others work.

1. INTRODUCTION

Cellulose is the most abundant biopolymer on the earth and it can be synthesized by plants, animals and a large number of microorganisms, one of them *Acetobacter xylinum*. From the point of view of the chemical structure, the bacterial cellulose is identical as the produced by plants, besides it has higher crystallinity and purity (free of lignin, hemicellulose and other natural components). These features make it an interesting raw material for applications such as nutritional component, artificial skin, composite reinforcement, electronic paper and in traditional applications where vegetal cellulose is used (Bielecki S. et al 2005).

In recent years there has been increasing concern for studying the production of bacterial cellulose using other carbon sources, as regards the production cost reduction (Kurosumi et al 2009). There are in Colombia a lot of organic waste from different stages in the agroindustrial productions that in many cases they can not be marketed due to their poor quality. The aim of this work has been the production of bacterial cellulose using Colombian agroindustrial wastes like pineapple peel and sugar cane juice (no refining sugar source) as a carbon source. The cellulose microfibrils obtained were characterized by infrared spectroscopy (FTIR), liquid chromatography (HPLC), atomic force microscopy (AFM), mechanical test, intrinsic viscometry and X-ray diffraction.

2. EXPERIMENTAL

2.1 Methods

The Acetobacter xylinum sp used in this study was previously isolated from a commercially available homemade vinegar culture. The culture medium was prepared at different ratios of sugar cane juice to pineapple peel 100:0, 70:30, 50:50, 30: 70, 0:100, as shown in Table 1. The acidity was adjusted to pH=3.3 by adding acetic acid. Then, the inoculum was added and the mediums were incubated without agitation at 25 °C for 13 days.

After incubation, the pellicles were successively washed with water and 5 wt% potassium hydroxide solution to remove microbial contaminants. Thereafter, the pellicles were dried in an oven at 60 °C all night.

The cellulose produced was characterizated by atomic force microscopy to observe its morphology, in a NanoScope IIIa, Multimode TM from Digital Instruments with a frequency of 200 kHz, and a spring constant of 12-103 N/m. The chemical structure was determined using Attenuated total reflection Fourier transform infrared spectroscopy using a FTIR spectrometer (Nicolet 6700 Series) equipped with a single-reflection ATR. The degree of polymerization was calculated from intrinsic viscosity data according to UNE 57-039-92 (which agrees with ISO 5351-1:1981, option B). The mechanical properties were evaluated in a Minimat 2000 according to ASTMD 1708 and ASTMD 882-02.

2.2 Results and discussion

Figure 1 shows the amount of bacterial cellulose produced from different concentration of culture medium adjusted to pH 3.3 after 13 days incubation. More cellulose was produced from the medium 100/0, followed of 70/30 and 50/50 what is due to the increase the carbon resources amount.

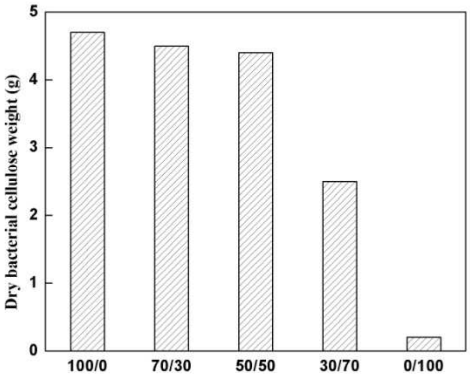

Fig. 1. Bacterial cellulose product from different concentrations of sugar cane juice / pineapple peel.

Figure 2(a) shows the atomic force microscopy of the cellulose samples, a fibril structure is observed with diameters between 20-30 nm and several millimeter in long. These results are within the range expected for this type of cellulose (Bielecki et al 2005).

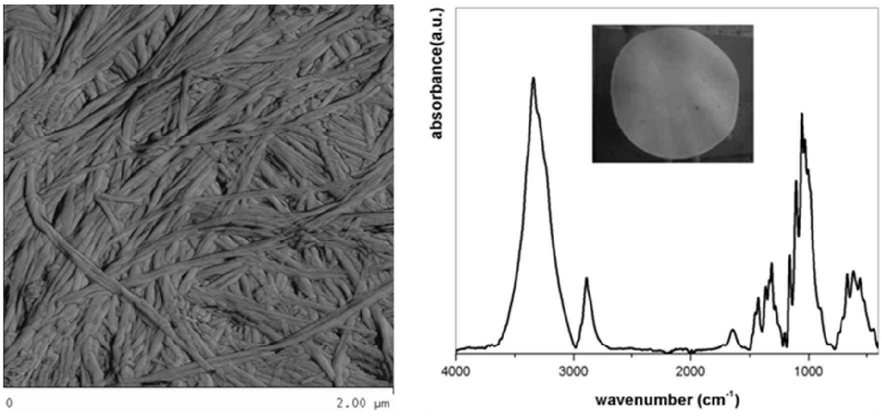

(a) (b)

Fig. 2. Atomic force microscopy (a) and ATR-FTIR spectrum (b) of bacterial cellulose produced at a ratio of sugar cane juice to pineapple peel 100:0.

The infrared spectrum for cellulose obtained from the 100:0 medium is show in figure 2(b). This spectrum is similar to cellulose obtained from the others mediums and typical bands of bacterial cellulose were presented (Shirk et al. 1952). Infrared spectroscopy can also be used for the determination of the Iα/Iβ ratio (Pecoro et al. 2008) and infrared crystallinity indice (O´Connor et al. 1964). To all mediums, the Iα/Iβ ratio was around 0.54 indicating that cellulose is richer in polymorphism Iβ unlike what was reported to cellulose of this origin (Pecoro et al. 2008). These results could be associated with other sugars such as glucomannan and xyloglucan present in agroindustrial waste, that can change the crystalline structure of cellulose (Hackney et al. 1994).

Table 1 shows the comparison of tensile properties, moisture content and polymerization grade to bacterial cellulose produced at a ratio of sugar cane juice to pineapple peel 100:0 with other results reported in literature. All values obtained experimentally fit within the ranges presented in the literature with the exception of Young's modulus, which is closer to values reported for cellulose of plant origin of 5.5-12.6 GPa (Pecoro et al.), this could be explained by the presence of most polymorphism Iβ than Iα like the case of the cellulose of plant origin (Sturcová et al. 2004).

Properties	Experimental	Reported	References
Strength at break	130 MPa	100-260 MPa	Iguchi et al.
Young´s modulus	7000 MPa	15000-30000 MPa	Pecoro et al.
Polymerization grade	5900	2000-10000	Pecoro et al.
Water content	95 %	92-99 %	Pecoro et al.

Table 1. Comparison of some properties of bacterial cellulose produced from different concentrations of sugar cane juice / pineapple peel with those reported in the literature.

3. CONCLUSIONS

The culture mediums to the production bacterial cellulose from Colombian agroindustrial wastes like pineapple peel and sugar caña juice were examined. The yields were increased to the addition of sugar amounts but their properties remained constants. The presence in all mediums of other sugars like glucomannan and xyloglucan could affect the Iα/Iβ ratio, producing more Iβ polymorphism.

The cellulose produced presented morphological, chemical and physical properties as those reported in another works, so it is possible produce bacterial cellulose with interesting properties from agroindustrial wastes.

ACKNOWLEDGEMENTS

The authors would like to thank COLCIENCIAS and SENA in the concerning to the financial support that has made this research work possible. We also thank to students Semillero New Material Research for their collaboration.

REFERENCES

BIELECKI S., KRYSTYNOWICZ A., TURKIEWICZ M., KALINOWSKA H. (2005) Bacterial Cellulose *in Biotechnology of polymer*. (Ed. Wyley), 381-434.

HACKNEY J., ATALLA R., VANDERHART D. (1994) Modification of crystallinity and crystalline structure of Acetobacter xylinum cellulose in the presence of water-soluble ß-1,4-linked polysaccharides 13C-NMR evidence *in International Journal of Biological Macromolecules*, 16, 215-128.

KUROSUMI A., SASAKI C., YAMASHITA Y., NAKAMURA Y. (2009) Utilization of various fruit juices as carbon source for production of bacterial cellulose by *Acetobacter xylinum* NBRC 13693 *in Carbohydrate Polymers,* 76, 333-335.

NELSON M.L., O´CONNOR R.T. (1964) Relation of certain infrared bands to cellulose crystallinity and crystal lattice type. Part II. A new infrared ratio for estimation of crystallinity in cellulose I and II *in Journal of Applied Polymer Science*, 8, 1325-1341.

PECORO E., MANZANI D., MESSADDEQ Y., RIBEIRO S. (2008) Bacterial cellulose from *Glucanacetobacter xylinus*: Preparation, properties and applications *in Monomers, Polymers and composites from renewable resources*.(Ed. Elsevier), 369-383.

SHIRK H.D., GREATHOUSE G.A. (1952) Infrared Spectra of Bacterial Cellulose *in Analytical Chemistry*, 24, 1774-1775.

STURCOVÁ A., HIS I., APPERLEY D.C., SUGIYAMA J., JARVIS M.C. (2004) Structural Details of Crystalline Cellulose from Higher Plants *in Biomacromolecules*, 5, 1333-9.

Fiber reinforced nanocomposites based on carbon nanofibers for stress monitoring

M. Monti[1], L. Torre[1], M. Natali[1], R. Petrucci[1], J.M. Kenny[1*], N. Markaide[2]
[1]University of Perugia - INSTM Research Unit, Terni (Italy)
[2]INASMET - Tecnalia, San Sebastian (Spain)
*Current address: ICTP-CSIC, Madrid (Spain)

1. INTRODUCTION

In recent years, the possibility of tailoring the properties of a material depending on its final goal has experienced a enormous breakthrough due to the development of nanotechnology. In fact, the ability on modifying and modelling materials at nanoscale level is leading modern society to advancements which were unthinkable just a decade ago [1]. Among the nano-scaled particles that are commonly included in plastics for enhancing their properties, carbon nanotubes and nanofibers have a particular role, because of their capability of significantly modifying even the electrical properties of a plastic materials [2,3]: for this reason they can be considered as intrinsically multifunctional nanoparticles.

Nowadays, polymer-based composite materials are widely used in applications in which they have a structural role, in many different sectors such as aerospace, automotive and machinery in general, as well as in civil engineering. In the applications in which they have a structural role, it is very important to have the possibility of detecting the presence of strain accumulation and even the presence of any damages.

The use of techniques that exploit electrical properties of the composite to monitor damages has been recognized as a non-invasive way in carbon fiber reinforced plastic, since the good electrical conductivity of carbon fibers themselves [4]. In fact, in this case, fracture of fiber results in a strong increase of electrical resistance. Nonetheless, this approach does not consider the fractures involving the matrix and the fiber-matrix interface, so it can give just a partial view of what could happen inside the composite during a mechanical solicitation. Moreover, it can not be employed with non-conducting fibers, e.g. glass or aramid. For this reason, some researchers has begun to investigate the possibility of the employment of electrical modified polymeric matrices [5].

In this study, we doped an unsaturated polyester resin with carbon nanofibers, in order to get a matrix with enhanced electrical conductivity for the production of a glass fiber reinforced composite. In the present work the calendering technique was employed for the dispersion of the nanoparticles in the matrix. The benefits of the calendering process are strictly related to the fact that it is already an industrial process, although in different applications, and so it can be considered an easily up-scalable technique.

In the present study, composites produced by mean of resin transfer molding process, were studied by mechanical and electrical tests. In fact, at the same time as mechanical tests were performed, electrical resistance was measured, in order to verify whether any change in resistance is related to a mechanical change, such us strain accumulation, cracks formation and delamination. When nanocomposites with 0.5 and 1 wt% of nanofibers were used as matrices for the composite laminate very interesting results were obtained in this sense.

2. EXPERIMENTAL

Vapour-grown carbon nanofibers (Grupo Antolin - Spain) were employed as a reinforcement and sensing material for the final composite. The resin utilized as a matrix in this study is a low-viscosity ortophtalic unsaturated polyester (UP) resin supplied by Cray Valley (Enydyne I 68835). Finally, E-Glass fibers were used as a 0/90 plain woven fabric and chopped strand mat.

The equipment used in this work for performing the dispersion was a three roll mill, consisting of three chrome-plated hardened steel rolls (80 mm in diameter), supplied from EXAKT Technologies Inc., model EXAKT 80E.

Vacuum assisted resin transfer molding (VARTM) was used to manufacture the composite laminates. An in-depth study on the injection temperature was carried out, comparing rheological and thermal results of the reactive system, in order to check the possibility of raising up the initial temperature.

In this study, the mechanical behaviour of the materials was observed simultaneously with the electrical resistance, in order to check if it is possible to correlate the presence of a tensional state or a damage, with an increase of electrical resistance. In all cases, a Keithley electrometer, model 6517B, was employed to measure electrical resistance.

3. RESULTS AND DISCUSSION

The opportunity of exploiting electrical properties of a material as a non-invasive tool for damage sensing, is obviously related to the real ability in conducting electricity of the material itself. Since plastic materials are typically electrical insulators, the possibility of raising up the electrical properties was investigated, using in this study carbon nanofibers. Different concentrations of this nanofiller were employed and the result obtained is in figure 1.

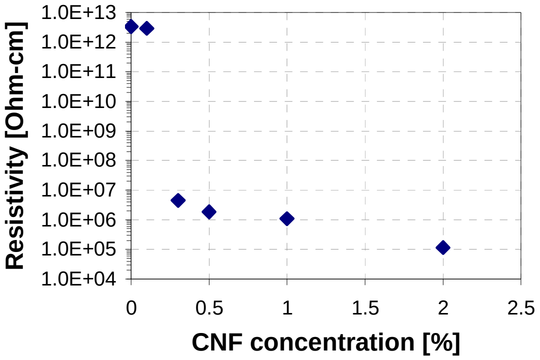

Fig. 1. Electrical resistivity of the nanocomposites as a function of CNF content.

As a consequence of this analysis, and taking into account that the rheology of the system does not change significantly till 1%, it was decided to produce glass-fiber reinforced composites with 0.5-and-1%-CNF nanocomposites as matrices.

The opportunity of obtaining the maximum performances by the laminate produced for this study has led, to investigate the possibility of raise up, at least a little, the injection temperature of the resin. For this reason, the reactive system (neat resin, without nanofibers) was studied at two different temperature, that is 25°C and 40°C. In figure 2 both rheological and thermal results are shown: as it is possible to observe the increase of the injection temperature to 40°C makes the cure reaction too fast for carrying out the whole process before the gelation of the system has occurred. For this reason, 25°C turned out to be the best temperature for the composite process.

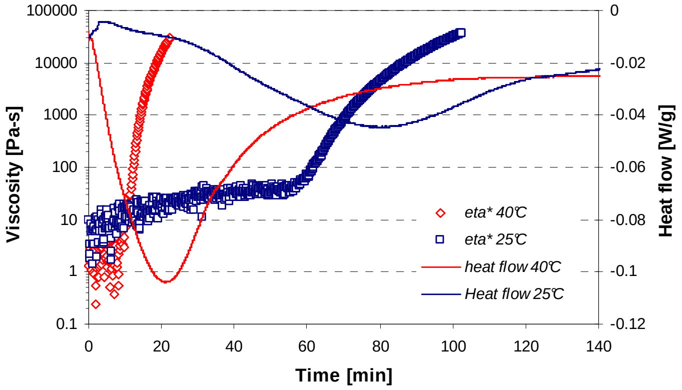

Fig. 2. Results of rheological and thermal analysis on the reactive system, formed by neat resin without nanofibers, during isothermal tests at 25°C and 40°C.

As a result of the electro-mechanical characterization it is possible to verify whether the presence of a mechanical strain, as well as the final failure of the material, due to the mechanical solicitation, involves a variation in the electrical resistivity of the material itself. The measurement of the electrical resistance of the samples before the mechanical test has revealed that, in the case of the glass fiber composite, there is a significant change in this gap: in fact, resistance of flexural samples (i.e. 80×10×2.5 mm) passes from around 2.4×10^9 Ω to 1.3×10^6 Ω. This result involves the fact that, in the 1%-CNF nanocomposite the current signal is stronger and so easier to control, corresponding in the tests performed in a clearer signal. In figure 3 a typical result of these tests is shown, in particular, in this case, the matrix is the one with 1% of CNFs.

Observing this graph, it is possible to see how the mechanical failure of the sample obviously corresponds to a strong increase of electrical resistance, due to the breakage of the continuity of the material, involving the delamination of the single plies, the fiber fracture, and the matrix failure. Moreover it is very interesting to point out that at the failure point, resistance variation is around 5% in the all cases studied, enabling to expect the failure point of this materials for this value of resistance change. Eventually, it is possible to observe that resistance variation starts to increase when the load is just at the middle of the maximum, giving the possibility to foresee the failure to be with large advance.

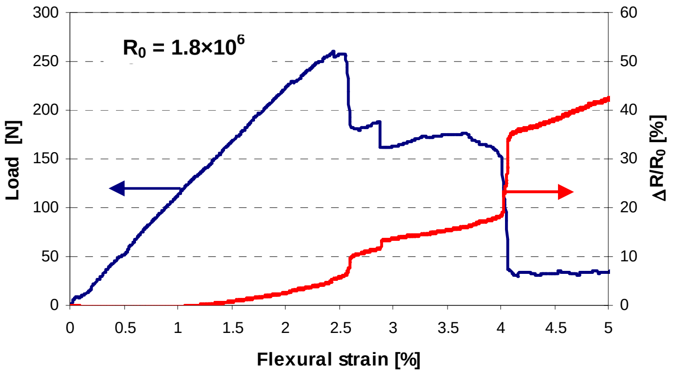

Fig. 3. Electro-mechanical results on composite based on the nanocomposite with 1% of CNFs.

3. CONCLUSIONS

Carbon nanofibers have turned out to be a very interesting tool to modify electrical properties of a thermosetting matrix, even at low concentrations. When employed in glass fiber composites, they can be exploited as a tool for strain and damage sensing, especially in applications in which the constant knowledge of the health status of the material is a key factor for its use, for example in structural applications. The results obtained in this direction are very encouraging, in fact a very low content of nanofiber lead to a completely different electrical behaviour of the matrix and to the final glass fiber composite, offering great possibilities, that are not exploitable with the neat resin as a matrix.

REFERENCES

[1] E. T. Thostenson, C. Y. Li, T. W. Chou; Nanocomposites in context – Composites Science and Technology, 65 (3-4) (2005) 491-516.

[2] E. Hammel, X. Tang, M. Trampert, T. Schmitt, K. Mauthner, A. Eder, P. Peotschke; Carbon nanofibers for composite applications - Carbon 42 (2004) 1153-1158.

[3] J. Sandler, M.S.P. Shaffler, T. Prasse, W. Bauhofer, K. Schulte, A.H. Windle; Depvelopment of a dispersion process for carbon nanotubes in an epoxy matrix and the resulting electrical properties – Polymer 40 (21) (1999) 5967-5971.

[4] X. Wang, D. Chung - Sensing damage in carbon fiber and its polymer-matrix and carbon-matrix composites by electrical resistance measurement – Journal of Material Science 34 (1999) 2703-2713

[5] E. Thostenson, T. Chou – Carbon nanotube networks: sensing of distributed strain and damage for life prediction and self healing – Advanced Materials 18 (2006) 2837-2841.

Wood fibres and wood microfibrillated cellulose as reinforcement of natural rubber

I. González, F. Vilaseca, P. Mutjé
Grup LEPAMAP, Escola Politècnica Superior, Universitat de Girona, Avda. Lluís Santaló, 17071 GIRONA (Spain). Telf: 972 41 84 63, fabiola.vilaseca@udg.edu
J. Bras, A. Dufresne
Grenoble Institute of Technology (INP) – The International School of Paper, Print Media and Biomaterials (PAGORA) - 461 rue de la Papeterie, DU, BP 65 - F-38402 Saint Martin d'Hères Cedex (France)
D. da Silva Perez, A. Lavalette
FCBA Institut Technologique, Domaine de Saint-Clément, 34980 Saint-Clément-de-Rivière (France)

ABSTRACT

In the present work, fibres and microfibrillated cellulose (MFC) extracted from softwood were used to reinforce natural rubber. It is reported the influence of the reinforcement nature on the mechanical and thermal properties of the ensuing composite. The surface of both fibers and MFC was chemically modified in order to improve their compatibilization. The thermal behavior (Tg) and the mechanical properties of the composites in both the linear and non linear range were determined using differential scanning calorimetry (DSC) and tensile tests, respectively. Significant differences were reported according to the nature and the amount of the fillers used as reinforcement. It was also proved that the chemical treatment dearly improve the ultimate properties of the composites.

1. INTRODUCTION

Nowadays there is a simultaneous and growing interest in developing bio-based products and innovative process technologies that can reduce the dependence on fossil fuel and move to a sustainable materials basis [Pandey et al., 2005; Espert et al., 2004]. In parallel, researchers have focused their works on the processing of nanocomposites (materials with nanosized reinforcement) to enhance mechanical properties [Dufresne, 2006; Bondeson et al.. 2006]. There are several possibilities to obtain nanoelements from renewable resources depending on their biological origin (e.g. cellulose, starch, and chitin). In the present work cellulose was used as a nanostructured high-performance constituent, in the form of microfibrilated cellulose-(MFC). Besides the low cost of the raw material, the use of MFC as a reinforcing phase in biocomposites has numerous advantages, e.g. low density; renewable nature; wide variety of filler available through the world; low energy consumption; high specific properties; modest abrasivity during processing; biodegradability; relatively reactive surface, which can be used for grafting specific groups and availability almost unlimited [Tserki et al., 2005; Pasquini et al., 2006]. However, when the application as reinforcement of polymeric matrix is considered, natural fibers can present some disadvantages, as for instance high moisture absorption; poor wetability; incompatibility with most of the polymeric matrices and limitation of the processing temperature of the nanocomposites. Indeed lignocellulosic materials start to degrade near 230 °C restricting the type of matrix that can be used in association with natural fillers. In this work, some chemical modification on the fibre surface was carried out. The goal was oxidizing the –OH groups located in the carbon 6, replacing the hydroxyl groups by –COOH groups. This oxidation will allow the following amidation without degradation of cellulose.

On the other side, natural rubber is an elastomeric material which is obtained from the rubber tree *Hevea brasiliensis* (*Euphorbiaceae*). It is a polymer of isoprene (mainly *cis*-1,4-isoprene) with molecular weights ranging from 100,000 to 1,000,000. Nowadays rubber can be synthetically produced. The aim of the present study is to evaluate the thermomechanical behavior of biocomposite films obtained from natural Rubber and cellulose fibers (MFC) focusing on the differences induced by the nature of the filler, fibers versus microfibril, and its surface chemical modification.

2. EXPERIMENTAL

2.1 Materials

Wood fibers were obtained from softwood pulp. MFC were produced using a microfluidizer; previously, cellulose fibres were degraded with enzymes (cellulase).

2.2 Surface modification

The method used was the cellulose oxidation by means of TEMPO (2,2,6,6-tetramethylpiperidine-1-oxyl) which has been recognized as the quickest, most selective and best controlled method. TEMPO is a very stable chemical product when put in contact with air, humidity and light, so it can be preserved and used easily. Afterwards, the oxidized cellulose surface was amidated with aniline.

2.3 Biocomposite films preparation

The natural rubber was used as latex. Different amounts of fibers or MFC were used to prepare the composite films, viz. 0, 3 and 12 wt%. The corresponding amounts of particles in suspension in water were mixed and magnetically stirred for 6 h with the NR latex. The suspensions were casted in Teflon molds, where the films were obtained by solvent evaporation at 40ºC.

2.4 Biocomposite characterizations

Differential scanning calorimetry (DSC) experiments were carried out with a DSC Q100 differential calorimeter (TA Instruments) fitted with a manual liquid nitrogen cooling system. The heating and cooling rates were 10 °C.min-1 from -100 °C to 100 °C and from 100 °C to -100 °C, respectively, in N_2 atmosphere. Sample weights were between 6 mg and 8.5 mg.

Tensile tests were carried out with a RSA3 (TA Instruments, USA) equipment with a 100 N load cell. Measurements were performed with a cross head speed of 10 mm·min-1 at 25 °C. The samples were prepared by cutting strips of the films 20 mm long and the distance between jaws was 10 mm, whereas the width and the thickness of the samples were measured before each measurement. 2-4 samples were used to characterize each composite.

3. RESULTS & DISCUSSION

The results show that mechanical properties of natural rubber were substantially enhanced by the addition of cellulose fibres from softwood. Young's Modulus increased from 0.77 MPa for non reinforced rubber until 9.46 MPa for 12% wt reinforced composites without any chemical modification. As expected, elongation decreased after the addition of the reinforcement, dropping from 409% for non-reinforced matrix to 66% for 12% reinforced composites. Chemical modification on fibres improved the interface between fibres and matrix. Composites based upon oxidized fibres showed and increasing in Young's Modulus until 34.55 MPa, far higher than the results obtained for non-modified fibres. However, an increasing in oxidation rates of fibres did not show an improvement in the mechanical properties of composites; instead, those properties decreased when compared with composites based upon lower-rate oxidized fibres, obtaining Young's Modulus results of 12.06 MPa for 12% reinforced composites. A resume of those results can be observed in the next table. Thermal properties did not show significant modifications after the addition of the reinforcement. Glass transition temperature remained around – 65 ºC with little variation. After oxidized, fibres were amidated with aniline in order to improve interfaced even more. However, amidated-fibres based composites showed lower mechanical properties when compared to no-amidated ones, but still an improvement in such properties is observed when compared to not-reinforced natural rubber.

Name	Tg (ºC)	E (MPa)	Ɛ (%)	σ (MPa)
STG0 3%	- 64.02	2.26±0.6	213±9.19	1.1±0.31
STG0 12%	- 65.92	9.46±0.58	66±3.53	0.99±0.02
STG02 3%	- 65.68	2.95±0.3	302±82.02	1.17±0.31
STG02 12%	- 66.86	34.55±9.24	275±44.54	1.88±0.25
STG03 3%	- 63.78	2.7±0.27	253±36.76	0.95±0.16
STG03 12%	- 66.86	12.06±4.38	161±101.82	0.94±0.16
AMa-STG02 3%	- 65.68	0.86±0.26	366±9.19	0.79±0
AMa-STG02 12%	- 65.68	9.66±1.40	227±2.12	1.16±0.07
Natural Rubber	- 65.68	0.77	409	0.65

Table I. Thermal and mechanical properties of natural rubber composites reinforced with softwood fibres at different oxidation and amidation degrees. Tg, glass-transition temperature. E, Young's Modulus. Ɛ, deformation and σ, tensile strength.

Microfibrilated cellulose (MFC)-based composites showed similar behaviour. Young's Modulus increased after adding MFC in the matrix. Ɛ dropped while Tg remained constant. Oxidation on MFC also improved the interface between matrix and reinforcement; after oxidation, MFC was amidated in order to improve interface. Results showed no improvement in mechanical properties when compared to non amidated fibres. Tg remained around – 65º C.

Name	**Tg (ºC)**	**E Mpa**	**ε (%)**	**σ (MPa)**
MF000 3%	- 65.68	4.47±2.05	230±88.05	1.18±0.2
MF004 3%	- 65.68	2.86±0.96	408±73.53	1.68±0.23
MF004 8%	- 65.44	33.94±14.54	219±104.65	2.13±0.16
MF005 3%	- 64.26	5.32±0.49	307±50.91	1.75±0.25
MF005 12%	- 66.15	75.75±19.61	191±62.93	7.82±0.53
AMa-MF004 3%	- 64.73	1.2±0.04	455±184.55	1.01±0.3
AMa-MF005 3%	- 64.34	8.51±2.85	377±96.43	1.77±0.04
AMa-MF005 12%	- 64.97	17.82±3.31	51±9.19	7.07±0.91
Natural Rubber	- 65.68	0.77	409	0.65

Table II. Thermal and mechanical properties of natural rubber composites reinforced with microfibrillated cellulose at different oxidation degrees and after amidation.

4. CONCLUSIONS

Addition of cellulose fibres and microfibers increased the mechanical properties of natural rubber to a significant degree. Chemical modification (oxidation) of those fibres increased the interface between cellulose and natural rubber, showing a significant increasing in Young's Modulus. With the increment in rigidity, percentage deformation diminished, as expected. However chemical oxidation is effective until a certain rate, after which mechanical properties decreased when compared to composites based on fibres with a lower rate of oxidation. Amidation showed also an enhancement in mechanical properties, but not better than those fibres only oxidized.
Besides, addition of cellulose as reinforcement provoked no modification in thermal properties of the matrix, Tg remained with little variation.

REFERENCES

- Bondeson, D.; Mathew, A.; Oksman, K., *Cellulose* **2006,** *13*, 171-180.
- Dufresne, A., *Journal of Nanoscience and Nanotechnology* **2006,** *6*, 322-330.
- Espert, A.; Vilaplana, F.; Karlsson, S., *Composites Part A-Applied Science and Manufacturing* **2004,** *35*, 1267-1276.
- Pandey, J. K.; Kumar, A. P.; Misra, M.; Mohanty, A. K.; Drzal, L. T.; Singh, R. P., *Journal of Nanoscience and Nanotechnology* **2005,** *5*, 497-526.
- Pasquini, D.; Belgacem, M. N.; Gandini, A.; Curvelo, A. A. D., *Journal of Colloid and Interface Science* **2006,** *295*, 79-83.
- Tserki, V.; Zafeiropoulos, N. E.; Simon, F.; Panayiotou, C., *Composites Part A-Applied Science and Manufacturing* **2005,** *36*, 1110-1118.

Preparation and electrical resistivities of Ag/PP nanocomposites

K. Nagata*, M. Shinkai, K. Ichihara, R. Quintero Restrepo, M. Higuchi
Department of Materials Science and Engineering, Graduate School of Engineering,
Nagoya Institute of Technology, Japan
T. Kinoshita
Department of Frontier Materials, Graduate School of Engineering,
Nagoya Institute of Technology, Japan

SUMMARY

Silver nanofillers are used as metallic conductive fillers, chemically synthesized based on the polyol process and applied in PP to produce silver-filled PP nanocomposites by the *ex-situ* technique. X-ray photoelectron spectroscopy (XPS), TEM and SEM are used to characterize their structure and morphology. Their thermal stability and electrical resistivity are measured by thermogravimetric analyses and digital electrometer. The results of XPS, TEM and SEM indicate the synthesized nanofillers are silver metal *ca.* 400 nm in diameter and *ca.* 10 μm in length. Ag/PP nanocomposites exhibit higher thermal stability than neat PP and lower electrical resistivity above 40 wt% of Ag content.

1. INTRODUCTION

Recently, interest has been growing in the fabrication of metallic-organic nano-composites consisting of polymers and metal nanofillers for advanced materials applications. In particular, the fabrication of one-dimensional (1D) nanostructures for nanocomposites, including particles, wires, rods, and tubes, is crucial because the unique properties of nanoparticles and nanowires, such as electronic, optoelectronic, and magnetic functions, can provide real-world applications. Among all metals, silver nanofillers are particularly interesting to fabricate and study because bulk silver exhibits the highest electrical and thermal conductivity among all metals. Silver is also an important material that has been used in a rich variety of commercial applications, and its performance in these applications could be potentially enhanced by processing it into 1D nanostructures with controllable dimensions and aspect ratios.

In the present study, silver nanofillers were used as metallic conductive fillers and applied in PP to produce silver-filled PP nanocomposites. Silver nanofillers were chemically synthesized based on the polyol process [1-3] for large-scale synthesis. The electrical resistivity (electrical conductivity) of PP nanocomposites filled with silver nanofillers as functions of filler loading was investigated. Furthermore, morphological studies were carried out to evaluate the dispersivity of silver nanofillers in nanocomposites.

2. Materials and Methods

Ag nanofillers were synthesized by reducing silver nitrate ($AgNO_3$) in ethylene glycol in the presence of poly(vinylpyrrolidone) (PVP). The following is the preparation procedure for the Ag nanofillers. First, anhydrous ethylene glycol (10 ml, 99.8%, Aldrich) was heated at 160ºC for 1 hr under argon gas as the shielding atmosphere; then 3 ml of acetyl acetone iron(III)/EG solution (0.2 mM) was added to a three-necked round-bottom flask and stirred at 160ºC for 10 min. Second, separate solutions of $AgNO_3$ (99+%, Aldrich) and PVP (Mw~55,000, Aldrich) in ethylene glycol (250 mM and 375 mM respectively, each 50 ml) were simultaneously injected into the reaction flask using a two-channel syringe pump at a rate of 1.0 ml/min. Then, the mixture was refluxed in a flask at 160ºC for 2 hrs. The liquid was centrifuged and repeatedly washed with acetone and ethyl alcohol. The products were characterized by X-ray photoelectron spectroscopy (XPS, Surface Science Instrument SSX-100) and transmission electron microscopy (TEM, Hitachi H-7000).

To prepare the Ag/PP nanocomposites, Ag nanofillers were combined in an appropriate ratio with PP (Japan Polypro Co., Novatec-PP, MA3, density: 0.90g/cm^3) dissolved in xylene. Ag nanofillers were mixed with MALIALIM (NOF Co.) as a solid dispersant, in a 1:2 ratio in xylene. The preparation procedure of the Ag/PP nanocomposites is as follows. PP was dissolved at 120ºC for 20 min. Ag nanofiller solution was added and vigorously mixed at 120ºC for 2 min. After removing the xylene, the products were compression-molded at 200ºC to make sheets about 0.5 mm thick. The films of the Ag/PP nanocomposites were measured by thermogravimetric analyses (SII, TG/DTA 200) and digital electrometer (R8340A, Advantest Co.). Electrical resistivity (room temperature volume resistivity) was measured with a two-probe system. The film sample (50 mm in diameter, 0.5 mm thick) was placed between Ni probes. Silver paste (Three Bond Co., Ltd., 3350C) was painted on each surface of the sample to ensure electrical contact with the electrodes. All values of resistivity reported in this study are values of dc resistivity.

3. Results and Discussion

Figure 1 shows the TEM images taken from the silver nanofillers synthesized by the polyol method. The product after purification was mainly composed of nanofibers. Figure 1(a) indicates that this method could produce uniform silver nanofibers that are smooth and have a diameter of *ca.* 400 nm and a length of *ca.* 10 μm, respectively. Therefore, the aspect ratio was *ca.* 25. However, a few silver nanoparticles were obtained as by-products.

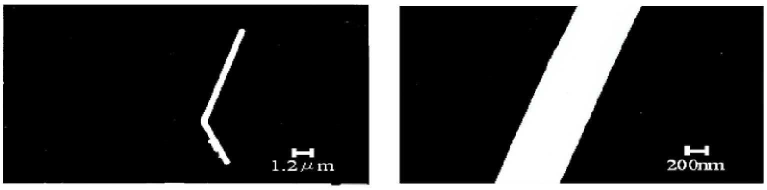

a) × 5000 b) × 50,000

Fig. 1. TEM images of Ag nanofiber: (a) x 5,000 and (b) x 50,000.

Figure 2 shows the XPS spectra for the silver nanofibers. The observed peaks can be assigned to silver. The peaks of Ag $3d_{5/2}$ and Ag $3d_{3/2}$ were found at 367.9 and 373.9 eV, significantly lower than 368.2 and 374.2 eV, respectively, the value for silver metal [4].

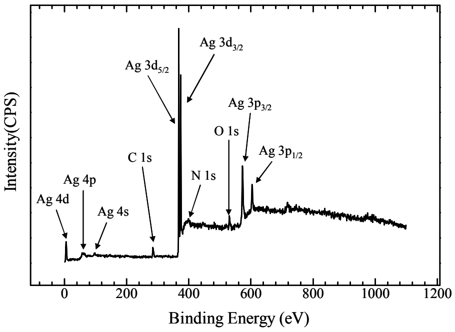

Fig. 2. X-ray photoelectron spectra of silver nanofiber.

Figure 3 shows the TGA curves for the neat PP and Ag/PP nanocomposites with different Ag contents. An improvement in the thermal stability of the nanocomposite can be seen with an increase in the nanofiller content. The onset of thermal degradation is shifted to higher temperature by about 47ºC for the composite with 10 wt% of Ag nanofibers. This suggests that the nanofibers in the polymer matrix play a role in retarding heat penetration and preventing diffusion from the decomposed polymeric material.

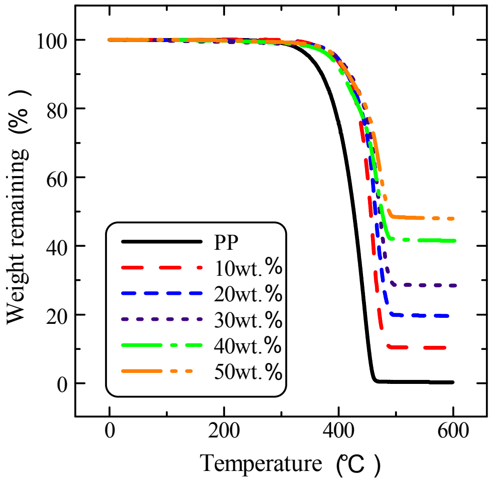

Fig. 3. TGA curves of neat PP and Ag/PP nanocomposites obtained under nitrogen atmosphere and heating rate of 10ºC /min.

Figure 4 shows the effect of Ag content on the resistivity of Ag/PP nanocomposites. The electrical resistivity and the percolation threshold of nanocomposites were dependent on the Ag content. When the Ag content increased from 30 to 40 wt%, the resistivity, ρ decreased from 10^{13} to $10^{9}\Omega$cm. This suggests that the conductive network of Ag at 40 wt% is more efficiently formed than at 30 wt% in the PP matrix.

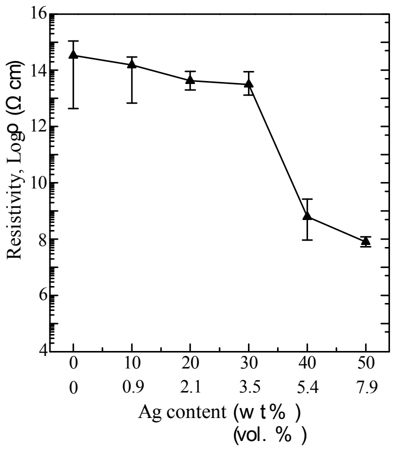

Fig. 4. Dependence of electrical resistivity, ρ, of nanocomposites on Ag content.

3. CONCLUSIONS

In summary, uniform silver nanofibers with a diameter of about 400 nm and length of about 10 μm were chemically synthesized based on the polyol process for large-scale synthesis. Ag/PP nanocomposites were prepared by the *ex-situ* technique: first, nanofillers were produced by chemical methods and then distributed into a polymer solution. Ag/PP nanocomposites remarkably improved the thermal stability in the presence of Ag-nanofibers and the lower electrical resistivity above 40 wt% of Ag content.

ACKNOWLEDGMENT

This research was supported in part by the Nagoya Industrial Science Research Institute Foundation. We thank Dr. Hanaichi and Mr. Takase (Hanaichi Ultrastructure Research Institute Co., Ltd., Japan) for their help with the TEM and SEM observation.

REFERENCES

[1] WILEY, B., SUN, Y., MAYERS, B., XIA, Y. (2005) Shape-controlled Synthesis of Metal Nano-structures: The Case of Silver, *Chem. Eur. J.*, **11**, 454-463.

[2] SUN, Y., XIA, Y. (2002) Large-scale synthesis of uniform silver nanowires through a soft, self-seeding, polyol process, *Adv. Mater.*, **14**, 833-837.

[3] CHEN, C., WANG, L., JIANG, G., YANG, Q., WANG, J., YU, H., CHEN, T., WANG, C., CHEN, X. (2006) The influence of seeding conditions and shielding gas atmosphere on the synthesis of silver nanowires through the polyol process, *Nanotechnology*, **17**, 466-474.

[4] MOULDER, J.F., CHASTAIN, J., KING, R.C. (1995) *Handbook of X-ray Photoelectron Spectroscopy: A Reference Book of Standard Spectra for Identification and Interpretation of XPS Data*, Physical Electronics, Eden Prairie, MN.

Efecto de las nanoparticulas de Fe_2O_3 sobre las transiciones de fase y la conductividad ionica del $CsHSeO_4$

O. Checa[a,b], E. Olaya, J.E. Diosa[b], R.A. Vargas[b]
[a]Departamento de Ciencias Básicas, Universidad Nacional de Colombia, Palmira, Colombia
[b]Departamento de Física, Universidad del Valle, A.A. 25360, Cali, Colombia

RESUMEN

El CsHSeO4, pertenece a la familia de cristales que presentan enlaces de hidrógeno con formula general $AHXO_4$, donde A = Cs, K, NH, Rb, and X = S, Se. Estos compuestos experimentan varias transiciones de fase con el incremento de la temperatura y exhiben fases conductoras superionicas, en las que la conductividad esta relacionada con la movilidad de los protones. Este tipo de conductores protónicos son investigados con el afán de avanzar en el almacenamiento de energía y celdas combustibles. El $CsHSeO_4$, presenta dos transiciones de fase conocidas por encima de la temperatura ambiente. La transición a la fase supersónica esta bien establecida a $T_s = 128°C$ y aparece en muchos experimentos. Pero este no es el caso para la otra transición cercana a 80ºC cuyo origen aun no esta establecido.

Por otro lado el dopaje heterogéneo con materiales cerámicos tales como Al_2O_3, SiO_2, TiO_2, ZrO_2, ha sido ampliamente utilizado para mejorar propiedades eléctricas, mecánicas, así como su estabilidad térmica y química de diferentes materiales. En este trabajo se utilizan las técnicas de calorimetría diferencial de barrido, el análisis termogravimétrico y la espectroscopia de impedancia eléctrica, para estudiar el efecto de las nanoparticulas de Fe_2O_3 sobre las propiedades térmicas y eléctricas del electrolito sólido $(1-x)CsHSeO_4$-xFe_2O_3, en un rango de concentraciones $x = 0.0 - 0.6$. Los compuestos son preparados por aleación mecánica seguida de un tratamiento térmico a una temperatura de 50ºC durante 6 horas. El compuesto puro CsHSeO4 muestra dos anomalías alrededor de 80ºC y 128ºC respectivamente. La conductividad muestra un comportamiento tipo Arrhenius del orden de 10^{-4} $(\text{ohm cm})^{-1}$, para las diferentes concentraciones de Fe_2O_3, los resultados muestran que la conductividad incrementa y que térmicamente son mas estables a medida que aumenta la concentración de Fe_2O_3. Este efecto puede atribuirse a una fuerte interacción entre el $CsHSeO_4$ and Fe_2O_3.

Conductive hybrid fillers in nanocomposites

J. Sarlin, K. Immonen
VTT, P.O.Box 1300, (Sinitaival 6), FI33101
Tampere, Finland

SUMMARY

Carbon nanotubes (CNT) are a key component in present technologies to produce high conductive plastic composites. In our work we have studied a method to synthesize hybrid conductive fillers using CNT and an inherently conductive polymer, polyaniline (PANi), witch hybrid material is used in polypropylene (PP) compounds. In hybrid fillers CNT are more or less coated by thin PANi layer but the components, CNT and PANi, are not connected by covalent bonds, only secondary interactions bonds these components. Composites show good conductivities, values over 20 S/cm were measured.

In this work we have studied PP composites with pure CNT or CNT/PANi hybrid fillers and PPCNT/ PANi hybrid composites with gallate dispersing agents. Used dispersing agent was ethyl gallate (EG). In semicrystalline systems fillers induce crystallization. During annealing changes in crystallinity can control more or less forming structure. In our work we have characterised crystallinity in the mentioned composites by nonisothermal DSC analysis and by WAXS. CNT as a conductive filler causes a remarkable effect on crystallinity, instead effects induced by hybrid fillers were less notable. Crystalline forms of PP are sensitive in fillers.

An interesting issue of these composites is (stable) change of conductivity as a result of high temperature annealing. This phenomenon has been observed also in thermoplastic composites with CNT. In our work after heat treatment PP composites including hybrid and CNT conductive fillers showed remarkable decrease of surface resistance, over 4 decades were recorded. This change is a result of reorganisation of conductive fillers caused by thermal activation; fluctuation of polymer segments drives conductive fillers in new morphology which is characterised by essentially higher conductivity compared to the values measured before annealing. The rate of the change depends on the interactions between conductive filler and polymeric host. Addition of dispersing agent causes remarkable effects in conductivity.

Comparative study on compressive strength of high performance binder incorporating nano-silica and silica fume

F. Albino de Souza
Master Science Degree Student, Departament of Structure – DE - School of Civil Engeneering, Architecture and Urban Design- FEC - State University of Campinas – UNICAMP - BRAZIL
A. de Almeida
Master Science Degree Student, Departament of Structure – DE - School of Civil Engeneering, Architecture and Urban Design- FEC - State University of Campinas – UNICAMP - BRAZIL
N. de Oliveira Pinto Júnior
Prof. Phd Departament of Structure – DE - School of Civil Engeneering, Architecture and Urban Design- FEC - State University of Campinas – UNICAMP - BRAZIL

SUMMARY

Recently many researchers are using the nanotechnology concept to create Portland concrete composites, where they look for the comprehension of the hidration of cement particles and addition of nanometrics (nm) particles, as nano-silica.

The main focus of this article is to show a comparative study on compressive strength of high performance binder incorporating nano-silica and silica fume. To this, were studied several mixture varying the rate of addition of nano-silica in the weight of cement (3%, 5% and 10%), also changing the method of cure: cure in pressure atmospheric air and submerged in water with calcium hydroxide. To complement the results measured is the consistency of mortars in the fresh state.

For a parameter of the microstructure of the mortars were using scanning electron microscopy images showing the interface between the matrix and the aggregates.

Efecto de las condiciones de procesado en la estructura de nanocomposites de polipropileno/nanoarcilla modificados con poliolefinas elastoméricas

M.J. Abad, M. Ladra, A. Ares, J. Cano, A. Torres
Grupo de Polímeros, E.U.P., Universidad de A Coruña, Ferrol, España
S.G. Pardo
Centro Galego do Plástico (CGaP), Ferrol, España
Grupo de Polímeros, E.U.P., Universidad de A Coruña, Ferrol, España

RESUMEN

La variación en la composición y las condiciones de procesado de nuevos nanocompuestos de polipropileno y nanoarcilla, modifican las propiedades reológicas de los mismos, debido, entre otras variables, a que el grado de exfoliación obtenido por la nanoarcilla no es igual. En este trabajo se han medido las propiedades reológicas mediante ensayos dinámicos y la distancia interlaminar de la nanoarcilla mediante difracción de rayos X. Los resultados demuestran que la adición de un copolímero elástomérico (POE) y un compatibilizante, provoca el aumento de la viscosidad de los materiales y el valor de su módulo de almacenamiento. Por la contra, aunque existe cierto grado de exfoliación de la nanoarcilla en los composites comparado con la nanoarcilla original, la incorporación de los modificadores disminuye la distancia interlaminar. Sin embargo, el descenso de la temperatura de procesado y el aumento de la velocidad de los husillos durante la extrusión mejora el grado de exfoliación obtenido.

1. INTRODUCCIÓN

Los materiales nanocompuestos basados en nanoarcillas tipo montmorilonita (MMT) modificadas con un grupo orgánico, pueden mejorar notablemente las propiedades como la estabilidad térmica, la resistencia al fuego, las propiedades mecánicas o las propiedades barrera de los materiales compuestos tradicionales. Por sus potenciales aplicaciones, han producido gran interés en los ámbitos académicos e industriales. La combinación de estas nanocargas con polímeros comerciales de bajo coste, como por ejemplo el polipropileno, permite obtener un material de altas prestaciones a un precio reducido. Sin embargo, las propiedades del material compuesto final van a depender de la morfología obtenida en el material, en particular, del grado de intercalación alcanzado por las cadenas poliméricas entre las laminillas de la nanoarcilla y este, dependerá en gran medida del tipo de procesado y de los parámetros utilizados, de la adición de compatibilizantes, etc (LERTWIMOLNUN et al. 2006) (NGUYEN et al. 2008)

Por otro lado, una de las debilidades del PP es su fragilidad en impacto a bajas temperaturas, lo que lo invalida para su utilización en algunas aplicaciones en el sector del automóvil. En este trabajo, se ha estudiado el comportamiento reológico de materiales compuestos de matriz de PP modificada con distintos contenidos de nanoarcilla, a los que se le ha añadido una poliolefina elastomérica (POE) con el fin de mejorar su comportamiento a impacto a bajas temperaturas. Además de analizar la influencia de la composición en el comportamiento reológico de los materiales compuestos, mediante ensayos dinámicos, también se ha intentado relacionar los parámetros de extrusión utilizados,con el grado de intercalación alcanzado entre el polímero y la nanoarcilla, ya que es sabido que las mejores propiedades se logran cuando existe exfoliación de la nanocarga e intercalación de las moléculas del termoplástico. Así, mediante análisis de difracción de rayos X se midió la distancia entre las distintas laminillas de la nanoarcilla para medir el grado de intercalación obtenido.

2. MATERIALES Y METODOS

2.1 Materiales

En este trabajo se ha utilizado un polipropileno (ISPLEN PP 070 G2M de REPSOL-YPF) con un índice de fluidez (MFI) de 12 g/10 min (230ºC/2.16 kg); un copolímero de etileno-octeno (POE) comercialmente denominado ENGAGE 8402 (DOW Chemical company) con un MFI de 30 g/10 min (190º C/2.16 kg); como compatibilizante, un polipropileno injertado con anhídrido maleico (PP-g-MA), Fusabond MZ203D, (Dupont) con un MFI de 41 g/10min (190ºC/1 kg) y finalmente, una nanoarcilla modificada orgánicamente (MMT) cuyo nombre comercial es 1.31 PS (Nanocor).

2.2 Preparacion de los nanocompuestos

Los distintos nanocompuestos fueron preparados mediante una extrusora corrotante bihusillo de laboratorio, DSE20 (Brabender). Con el objetivo de ver la influencia de los parámetros de procesado en las propiedades de los materiales obtenidos, se varió la velocidad de los husillos (N) y la velocidad de alimentación (Q) de la extrusora, obteniéndose muestras con diferentes cocientes N/Q. Además, se estudiaron dos temperaturas distintas de procesado. La Tabla 1 resume la composición de los nanocompuestos estudiados y sus parámetros de procesado.

Nomenclatura PP/POE/PP-g-MA/nanoarcilla	PP (%)	POE (%)	PP-g-MA (%)	Nanoarcilla (%)	N/Q	T (ºC)	d (nm)
95/0/0/5	95	-	-	5	2	200	2.20
90/10/0/0	90	10	-	-	2		-
90/5/0/5	90	5	-	5	2		2.18
85/10/0/5	85	10	-	5	2		
75/20/0/5	75	20	-	5	2		2.17
80/10/5/5	80	10	5	5	2		2.01
70/10/15/5	70	10	15	5	2	180	
80/10/5/5i	80	10	5	5	2		2.11
80/10/5/5ii	80	10	5	5	6		

Tabla 1. Formulaciones de los nanocompuestos y distancia interlaminar.

2.3 Métodos

Las medidas reológicas fueron realizadas usando un reómetro de deformación controlada (ARES, TA Instruments) con geometría de platos paralelos (25 mm de diámetro, espesor de 1mm) a 200ºC. Los ensayos reológicos fueron realizados en la región viscoelástica lineal (LVE). Esta región viscoelástica fue determinada mediante un ensayo de deformación antes del estudio de la viscoelasticidad de los compuestos bajo un ensayo de frecuencia. Las medidas de barrido de frecuencias fueron realizadas en el rango de $1x10^{-2}$ a $6x10^{1}$ rad/s

Los experimentos de difracción de rayos X (WAXD) fueron realizados con una radiación CuKα con una longitud de onda (λ) de 1,54 Å y un voltaje de aceleración de 40 kV. El espectro de difracción fue obtenido en un rango de 2θ de entre 2 y 60º. El espacio entre laminillas (d) ha sido calculado usando la ecuación de Bragg ($\lambda = 2d$ sen θ), donde θ indica el ángulo de la reflexión característica del plano {001} de la nanoarcilla (Ver difractograma de la Fig.1)

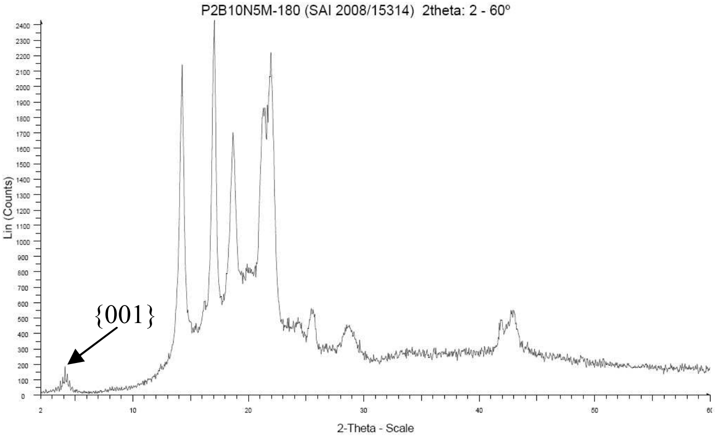

Fig. 1. Difractograma de rayos X. Muestra 80/10/5/5i.

3. RESULTADOS Y DISCUSION

Para caracterizar el estado de dispersión de la nanoarcilla en la matriz termoplástica, se realizaron ensayos dinámicos de los distintos nanocompuestos. La Figura 2 muestra los datos del modulo de almacenamiento (G`) en función de la frecuenta del ensayo para los distintos materiales. Los datos muestran que los valores de los módulos y de la viscosidad aumentan en función de la cantidad de copolímero añadido, debido a la mayor viscosidad del POE con respecto al PP. Se estudió también, el efecto del compatibilizante (PP-g-MA) en las propiedades reológicas de los nanocompuestos. Los datos muestran un claro aumento en los valores del módulo de almacenamiento y de la viscosidad compleja, lo que es indicativo de un buen grado de compatibilización. En cuanto a la influencia de las distintas condiciones de procesado, el aumento de la temperatura de extrusión provoca una disminución en los valores de viscosidad de los compuestos obtenidos. Si tenemos en cuenta el efecto de los distintos ratios N/Q apreciamos una disminución del módulo de almacenamiento (G’) cuando la velocidad de extrusión aumenta.

Los resultados proporcionados por la técnica de difracción de rayos X (WAXD) permitieron calcular la distancia interlaminar (d) de la nanoarcilla, una vez procesados los nanocompuestos. Comparando los datos de los nanocompuestos (Tabla 1) con el valor de d de la nanoarcilla original (2.12 nm), puede observarse que d aumenta después del procesado en todas las muestras sin compatibilizante, aunque disminuye al aumentar el contenido de POE. En cuanto a la influencia de los parámetros de procesado, la disminución de la temperatura aumenta la distancia interlaminar, seguramente debido a que aumenta la viscosidad del material dentro de la extrusora y por tanto, el esfuerzo de cizalla que sufre durante la extrusión, de acuerdo con los datos reológicos obtenidos previamente.

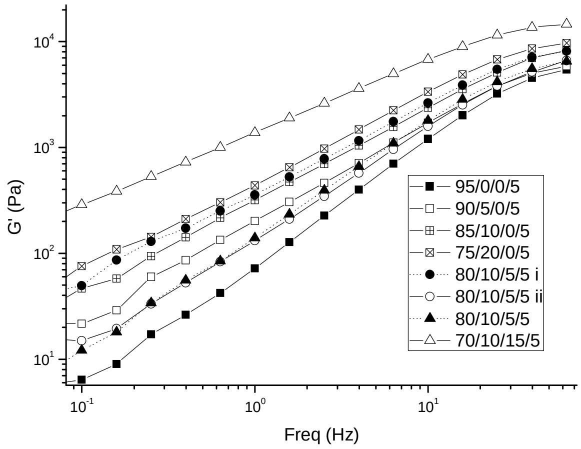

Fig. 12. Módulo de almacenamiento como función de la frecuencia de los composites PP/POE/PP-g-MA/nanoarcilla.

4. CONCLUSIONES

El comportamiento reológico de los nanocompuestos PP/nanoarcilla depende del contenido de copolímero incorporado (POE) y el compatibilizante utilizado. Tanto uno como otro aumentan el modulo de almacenamiento y la viscosidad compleja de los materiales en todo el rango de frecuencias. La variación de los parámetros de procesado también modifica las propiedades reológicas de los nanocompuestos, la disminución de la temperatura de procesado produjo materiales mas viscosos, mientras que el aumento de la velocidad de los husillos diminuyó el modulo de los materiales.

Por último los datos de distancia interlaminar d, que depende del grado de exfoliación obtenido por la nanoarcilla durante el procesado de los materiales, indica que este aumenta respecto a la nanoarcilla original, si bien, el mayor grado de exfoliación se obtiene en las muestras que no están modificadas con el copolímero y que no poseen compatibilizante.

AGRADECIMIENTOS

Este trabajo ha sido financiado por la Secretaría Xeral de Investigación e Desenvolvemento, Xunta de Galicia (XUGA-PGIDT06DPA172PR9)

REFERENCES

BAGHAEI, B., JAFARI, S.H., KHONAKDAR, H.A., REZAEIAN, I., AS'HABI, L., AHMADIAN, S. (2009). Interfacially compatibilized LDPE/POE blends reinforced with nanoclay: investigation of morphology, rheology and dynamic mechanical properties. *Polym. Bull.*, 62, 255-270.

LERTWIMOLNUN, W., VERGNES, B. (2006). Effect of processing conditions on the formation of Polypropylene/organoclay nanocomposites in a twin screw extruder. *Polym. Eng. Sci.*, 46, 314-323.

NGUYEN, Q.T., BAIRD, D.G. (2008). Dispersion of nanoclay into polypropylene with carbon dioxide in the presence of maleated poplypropylene. *J.Appl.Polym.Sci.*, 109, 1048-1056

Increment in oxygen permeability of polyethylene by inclusion of acicular nanofillers

R. Martini, S. Barbosa
PLAPIQUI (UNS-CONICET), Cno. La Carrindanga Km. 7, 8000 Bahía Banca, Argentina
S. La Tegola, A. Iannoni, A. Terenzi, J.M. Kenny
Materials Engineering Center, University of Perugia, Località Pentima Bassa, 21, 05100 Terni, Italy

ABSTRACT

Polyethylene (PE) - sepiolite nanocomposites are very interesting materials because they combine their properties in a synergetic manner. Chemically, sepiolite is a hydrated magnesium silicate with a needle-like structure, instead of clays typical plate-like. For this reason sepiolite has the greatest surface area of all the clay minerals with a high density of silanol groups (-SiOH) which explain the high hydrophilicity of this filler. The high surface area and porosity account for the remarkable adsorptive properties of this clay.

In this work, a systematic study of oxygen permeability and mechanical properties on films was performed in order to investigate the influence of the sepiolite content and modification on the basic properties of PE. The nanocomposites were prepared in a laboratory twin screw extruder. Samples with 1, 3, 5 and 10 wt % and using sepiolite with and without surface modification were prepared and tested. Results show important increment oxygen permeability as the nanoclay content increases, without loose the good film processability.

1. INTRODUCTION

Polyethylene (PE) - sepiolite nanocomposites are very interesting materials because they combine their properties in a synergetic manner. Chemically, sepiolite is a hydrated magnesium silicate with the ideal formula $Si_{12}Mg_8O_{30}(OH)_4(OH_2)_4.8H_2O$. It is not a layered phyllosilicate, it's structure can be considered a quincunx of talc type sheets: planes formed by an octahedral layer (Mg) between two external tetrahedral layers (Si), these sheets are separated by so called zeolitic channels, characterized by the presence of atoms of zeolitic water. The particular arrangement of atoms produces a needle-like structure, instead of typical plate-like one. For this reason sepiolite has the greatest surface area of all the clay minerals with a high density of silanol groups (-SiOH) which explain the high hydrophilicity of this filler. The silicate lattice has not a significant negative charge and so the cation exchange capacity of this clay is very low.

These particles are arranged forming loosely packed and porous aggregates with an extensive capillary network which explains the high porosity and light weight because of the high amount void space. The high surface area and porosity account for the remarkable adsorptive and absorptive properties of this clay: it adsorbs vapour and odours and can absorb approximately its own weight of water and other liquids (Ma et al, 2007)

The use of sepiolite fillers also can improve processing, dimensional stability, mechanical strength and thermal resistance of polyethylene as well as, they allow controlling the rheological behavior of the polymer enhancing their stability under a wide temperature range (García et al., 2009; Hotta and Paul, 2004; Araújo et al. 2007). In this work, a systematic study of oxygen permeability and mechanical properties on films was performed in order to investigate the influence of the sepiolite content and modification on the basic properties of PE.

2. EXPERIMENTAL

Materials: Linear Low Density Polyethylene Dowlex 2045, with Mw: 119000 g/mol, Mn: 29900 g/mol and PD = 4, kindly supplied by DOW Chemicals, has been used as matrix. Two different grades of commercial sepiolite were purchased to TOLSA Group (from Spain). Samples were PRG4, a non modified sepiolite and a PRG5, compatibilized with vinyl-trimethoxysilane.

Nanocomposites Compounding: It was performed in a laboratory twin screw extruder with recirculation at 150 rpm for 1 min, with a temp. profile of 135, 160 and 185 °C, from feed to die. Films for permeability measurements were prepared by compression molding.

Tensile Properties Measurement: The tests were carried out in an LLOYD Instruments LR 30K tester over films of 10 x 100mm and with 25 μm of thickness approximately. The measurements were performed at 25 ºC, 50 mm/min using a cell of 50 N.

Tear-Propagation Resistance Test: the measurements were carried out in an LLOYD Instruments LR 30K tester, according to the ASTM D 1938 norm, at 25 ºC, 250 mm/min using a cell of 20 N.

Oxygen permeability measurements: The equipment used was a MOCON OX-TRAN 2/21. The oxygen barrier properties were determined at 23 ºC with 0% of relative humidity over films.

3. RESULTS

The film mechanical properties are shown in Fig. 1. It can be observed an important increment in the elastic modulus respect to the pure PE. This value is almost constant for the nanocomposites analyzed, but a decrement was observed for the blend with 10 wt% of sepiolite. The tensile strength suffer a decrement when the sepiolite content is low but increases with the nanofiller content to decrease again when the sepiolite content is 10 wt %. Also, the elongation at break slightly decreases, but for all of the nanocomposites remains over than 300 %, a very good value for film processing.

On the other hand, the oxygen permeability as a function of sepiolite content and compatibilization is shown in Fig. 2. The permeability increases as the filler content increases. The permeability increment lightly increases with sepiolite content and seems to be dependent of the sepilolite type. The values for non compatibilized ones are higher than for those compatibilized. This behavior, in opposite at the normal response of laminar nanocomposite, can be due to the acicular form of the filler. The increment in barrier properties of laminar fillers proceeds from the increment in tortuosity, because clays have two dimension so grether than the third. However, sepiolites have one dimension higher than the other two, then the tortuosity is not incremented by the inclusion of this kind of filler. The increment in oxygen permeability proceeds from the nature of sepiolites. They have a porous structure with channels and OH in the surface, as shown in figure 3. In this sense, taking into account that the dispersion is good in both cases, the less permeability in compatibilized sepiolites could be due that compatibilization reduce the amount of OH and then reduce the oxygen permeability as shown in Fig. 2.

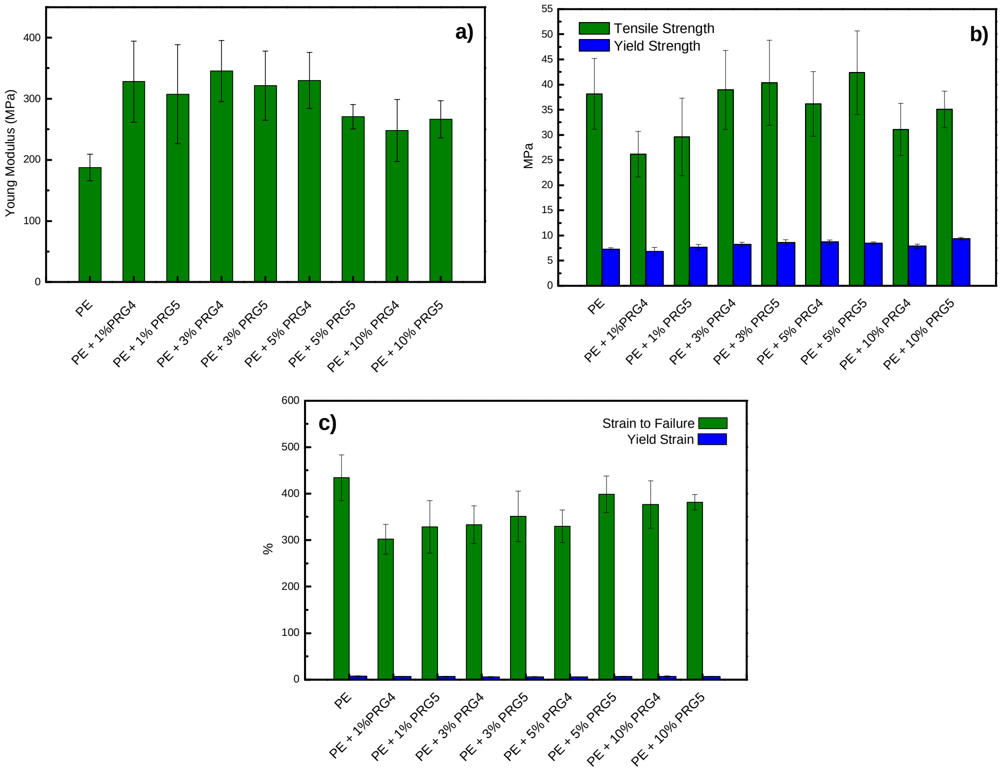

Fig. 1. Tensile properties of nanocomposite films. a) Young modulus; b) Tensile and Yield strength; c) Yield strain and elongation at break.

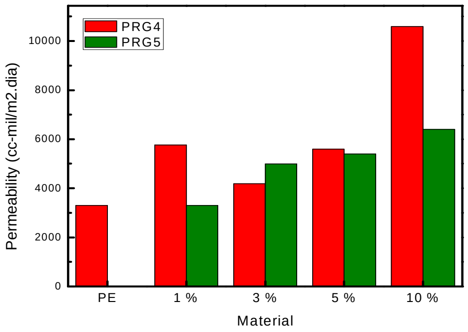

Fig. 2. Oxygen permeability of nanocomposite films.

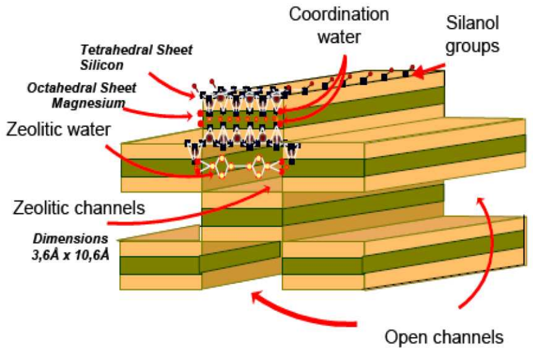

Fig. 3. Sepiolite structure.

3. CONCLUSIONS

In this work was demonstrated that it is possible to obtain polyethyelene/ sepiolite films with increased permeability properties without deterioration of the mechanical properties.

REFERENCES

ARAÚJO, E.M., BARBOSA, R., MORAIS, C.R.S., SOLEDADE, L.E.B., SOUZA, A.G., VIEIRA, M.Q.J. (2007) Effects of organoclays on the thermal processing of PE/clay nanocomposites. *Therm. Analy. Calor.*, 90, 841- 848.

GARCIA, N., HOYOS, M., GUZMAN, J., TIEMBLO, P. (2009) Comparing the effect of nanofillers as thermal stabilizers in low density polyethylene. *Pol. Deg. Stab*, 94, 39-48.

HOTTA, S., PAUL, D.R. (2004) Nanocomposites formed from linear low density polyethylene and organoclays, *Polym*er, 45, 7639-7654.

MA, J., BILOTTI, E., PEIJS, T., DARR, J.A. (2007) Preparation of polypropylene/sepiolite nanocomposites using supercritical CO_2 assisted mixing. *European Polymer Journal,* 43, 4931–4939.

Nano-talc reinforced PP composites. Final properties improvement through interfacial modification

L. Castillo, S. Barbosa, N. Capiati
Planta Piloto de Ingeniería Química (Universidad Nacional del Sur-CONICET)
Bahía Blanca, Argentina

SUMMARY

The gas barrier and mechanical properties in two series of polypropylene (PP)/talc composites were studied. These composites were prepared in a laboratory batch mixer: PP/untreated talc and PP/treated talc. Different mineral concentrations of untreated talc and treated talc were used, from 0 up to 5%. The barrier properties were analyzed in terms of water vapor permeability while mechanical ones, through the elastic modulus, elongation at break and strength. The influence of talc concentration and superficial treatment on these film properties was studied. The increase of talc content gives a reduction in water vapor permeability without losing ductility. The talc treatment changes either the particle size or the particle surface energy and has a marked influence on the behavior of the composites properties. The barrier properties obtained with the incorporation of 1wt% of treated talc are similar to those obtained with 5 wt% of untreated one. Thus, the elongation at break of pure PP is reduced in 30 % in the first case while it decreased in a 46% in the case of composites with 5% of untreated talc.

1. INTRODUCTION

The increment in barrier properties of polymeric materials is very important in their use for food packaging, particularly in controlled atmosphere packaging. Packaging must control the oxygen, carbon dioxide and humidity content in order to increase the time in which the food is kept under the optimal conditions for its consumption (Bertuzzi et al., 2002). The laminar nanofiller inclusion is a manner to increase the barrier properties. In this sense, polymer clay nanocomposites have very good barrier properties against gases (oxygen, nitrogen and carbon dioxide), water and hydrocarbons. Previous works demonstrated that the reduction of permeability is strongly depended on the aspect ratio of mineral particles, with high ratios dramatically enhancing gaseous barrier properties. The best gas barrier properties would be obtained when mineral is fully delaminated, with uniform distribution on the polymeric matrix (Choudalakis et al., 2009). The barrier properties enhancement in polymer nanocomposites can be explained by the concept of tortuosity. In a polymer nanocomposite film, the sheet-like layers are oriented in parallel with the film surface. As a result for traversing equivalent film thickness, in polymer nanocomposite gas molecules have to take more way than in pristine polymer matrix. In nanocomposites, molecules must move around the impermeable clay layers. Besides, it seems that the enhancement of barrier properties does not arise from the chemical interactions since it does not depend on the kind of gas or liquid molecule (Massey, 2004).

Polypropylene is one of the most used resins in packaging because it is a versatile thermoplastic material, compatible with many processing techniques and a favorable price/performance ratio. Then, the increment of their barrier properties maintaining good mechanical properties are the challenge of this work. In this way, talc was chosen as laminar filler because it is so economic and induces special crystallization in PP (Ferrage, et al., 2002). However, commercial talc has not nanometric particles, then, in this work, a formulation of isotactic PP with nanoparticles talc obtained by us is proposed, in order to increment barrier properties maintaining the mechanical properties to obtain good films.

1. EXPERIMENTAL

Polypropylene (PP) homopolymer Cuyolén 1102 H (Mn=72200 g/mol, Mw=309300 g/mol), gently provided by Petroquímica Cuyo SA, was used as matrix. High purity talc from Australia, named A10, was kindly supplied by Dolomita SAIC. Talc chemical composition is: SiO_2=61%, MgO=31%, Fe_2O_3=1.1%, CaO=0.3%, MnO=0.1%, Al_2O_3=0.9%; its average diameter is 5.6 μm and the average thickness is 32 nm.The modified talc, named A10T, is the result of an esterification reaction between talc and an organic acid. Details of this modification could be obtained in Barbosa et al., 2006. As a result of this reaction, the average diameter of particles is 2.2 μm and the thickness is 9 nm.

Two sets of composites were prepared, with natural and treated talc. They were prepared in a laboratory batch mixer Brabender Plastograph, under nitrogen atmosphere, at 185 ºC during 20 min, with rotor speed of 30 rpm. The composites obtained were called *PP(Talc percent)(Talc type).* The filler concentrations were 1 and 5 wt% for composites with talc A10 and 1 and 2 wt% for composites with A10T. The composite films to measure barrier and mechanical properties were made by compression molding. The talc dispersion in PP films was characterized by Scanning Electronic Microscopy (SEM), using a Jeol 35CF Microscope. Film samples were fracture under cryogenic conditions and the surfaces to be analyzed were coated with gold for make it conductive. The water vapor permeability measurements were performed following ASTM E96-80 method, using T=38 ºC and HR=90% during 160 hours. Film mechanical properties were measured in an Instron Universal testing machine (model 3369). Tensile strength, elastic modulus and percent elongation were determined using a load cell of 1 kN and crosshead speed of 2 mm/min.

2. RESULTS AND DISCUSSION

Figure 1 shows the water vapor permeability coefficient as a function of talc concentration for the two sets of composite films prepared. It can observe that in both cases, as talc concentration increases, the permeability decreases, as expected. This tendency can be explained through the concept of tortuous path. When the talc concentration increases, there are more layers that difficult the gas molecules. Also, talc particles are PP crystal nucleators, then as the talc concentration increases, more nucleators are present and the PP crystallization degree increases. Tortuosity and nucleation character of talc particles increases as the particle dimensions decreases. Diameter particle average from A10T diminishes 61 % from those of original A10, and the thickness is reduced in 80%, then the contact talc/PP surface increases around of 500 %, assuming talc particles as rod like ones. These changes are reflected in the water vapor barrier of each kind of composites. The incorporation of 1 wt% of treated talc in the film produces the same grade of barrier than the composite with 5 wt % of natural talc. The barrier increased in 34% when 1% of natural talc was added, but the increase was much higher (45%), when the concentration of treated talc was 1%. Figure 2 shows the particle dispersions in the films from both kinds of composites. The above observations are corroborated in the micrographs. Modified talc (Fig. 2b) has less particle dimensions and is better distributed in PP matrix than unmodified one (Fig. 2a).

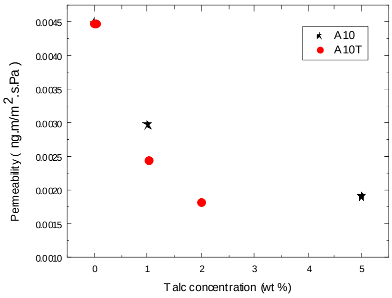

Fig. 1. Water vapor permeability measurements of PP/Talc films.

Figure 3 shows the influence of the filler content on the elastic modulus of the composites. The values were normalized with matrix ones to emphasize the increment produced by the incorporation of talc. As expected, the elastic modulus increases as the talc content increases. This is due to the fact that first, PP is substituted by the largely more rigid filler particles; second, the talc presence increases the PP crystallinity and lastly, the filler presence restricts the mobility and deformability of the matrix by introducing a mechanical restraint. PP/A10T composites have higher values of modulus than PP/A10 composites for the same concentration and the increment of the modulus with talc concentration seems to be higher, too. Although, theories indicate that the elastic modulus of a composite material should be independent of the size of filler particles, our results shows that for a similar concentration, as the particle size decreases, composite modulus increases. This fact agrees with results of other authors (Nielsen et al. 1994). They propose several reasons for this discrepancy. As the particle size decreases, surface area increases, then, if the polymer is changed in some manner at the interface, the properties should change with particle size because the values of the matrix modulus change. This fact agrees with the present case because talc particles change the matrix crystallization behavior (Ferrage et al., 2002).

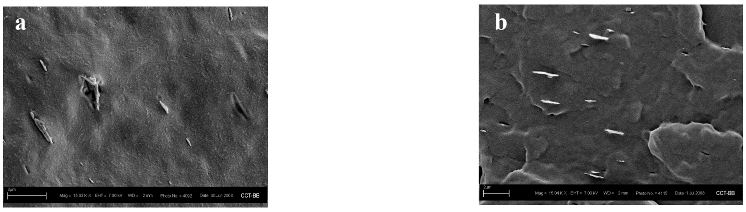

Fig. 2. SEM micrographs at 15000x of a) PP/ 1% A10 and b) PP/ 1% A10T films.

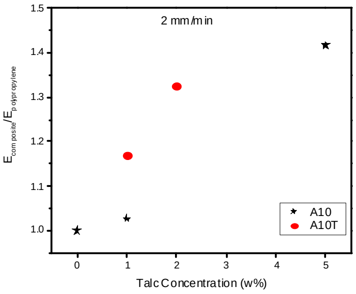

Fig. 3. Relative elastic modulus of PP/Talc films.

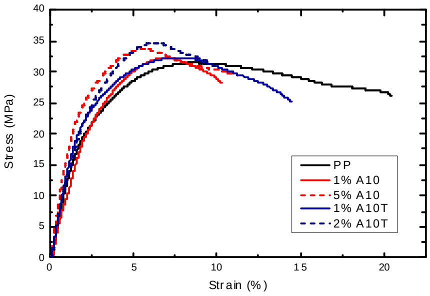

Fig. 4. Tensile Stress-Strain curves of PP/talc.

Figure 4 shows representative stress-strain curves of the composites films. It is clear that strength increases as talc content increases. However, the strength of composites with 2 wt% of A10T is higher than PP1%A10, corroborating the good influence of the diminution of particle dimension. Also, the results are good for elongation at break, for the same talc content: composites with 1% of A10T have large elongation at break than those without modification. Its shows that the filler is better adhered to the matrix. This behavior proceeds from the fact that as the particle size decreases and the surface area increases, the surface energy of the particles increases, increment the modulus and the adherence particle-matrix. This effect was found in other nanocomposites like PP/fumed silica or PP/carbon black.

3. CONCLUSIONS

The nanotalc reinforced PP composites prepared with talc modified by us shows a so good relation between barrier properties and mechanical ones. It is possible to obtain a nanocomposite with an increment in barrier to water vapor of 45%, with 1% of nanotalc, respect to pure PP and with high possibilities of blow molding because its elongation at break remain around 70% of those of pure PP.

REFERENCES

BARBOSA, S., CASTILLO, L., CAPIATI, N. (2006) Purificación de talcos por extracción selectiva de carbonatos. Desagregación de la estructura laminar. *XXII Congreso Interamericano de Ingeniería Química y V Congreso Argentino de Ingeniería Química (XXII CIIQ / V CAIQ)*, Buenos Aires, Argentina.

BERTUZZI, M. A., ARMADA, M., GOTTIFREDI, J. C., APARICIO, A. R., JIMENEZ, P. (2002) Estudio de la permeabilidad al vapor de agua de films comestibles para recubrir alimentos. *Congreso Regional de Ciencia y Tecnología NOA 2002, Catamarca, Argentina*, 1-10.

CHOUDALAKIS, G., GOTSIS, A. D. (2009) Permeability of polymer/clay nanocomposites. A Review. *European Polymer Journal*, 45, 967-984.

FERRAGE, E., MARTIN, F., BOUDET, A., PETIT, S., FOURTY, G., JOUFFRET, F.(2002) Talc as nucleating agent of polypropylene: morphology induced by lamellar particles addition and interface mineral-matrix modelization. *Journal of Materials Science*, 37, 1561-1573.

MASSEY, L. K., (2004) *Film Properties of Plastics and Elastomers* (Ed. Plastics Design Library Handbook).

NIELSEN, L., LANDEL, R. (1994) *Mechanical Properties of polymers and composites* (Ed. Marcel Dekker, Inc).

$ZnFe_2O_4$ / SiO_2 nanocomposites: iinfluecnce of the matrix in the magnetic properties of the embedded nanoparticles

V. Blanco Gutiérrez, M.J. Torralvo Fernández, R. Sáez Puche
Departamento de Química Inorgánica, Facultad de Químicas, Universidad Complutense
Madrid, 28040 Madrid. Spain

Magnetic nanocomposites comprised of nano-sized magnetic crystals embedded in an amorphous matrix have promising applications in many areas such as optics, electronics, mechanics or medicine (1). These nanocrystalline particles have a high surface/volume ratio, leading to magnetic properties different from those of bulk materials. Thus, it is well known that nanosized spinel $ZnFe_2O_4$ behaves as superparamagnetic at room temperature while their bulk counterparts are antiferromagnetic.

It has been observed that not only the size and shape of the ferrite nanoparticles but also the presence of a matrix in which the nanoparticles are embedded influence in the magnetic behaviour of the material (2).

Well dispersed zinc ferrite nanoparticles were prepared embedded in a silica matrix that was obtained by sol-gel reactions (3) (see figure 1). In the silicon alkoxide polimerization, the zinc ferrite precursors remain motionless in the polymeric gel and after thermal treatment the $ZnFe_2O_4$ nanoparticles are obtained.

It is shown in figures 2 and 3 how these zinc ferrite nanoparticles, present different magnetic properties to those free nanocrystals with similar size. Although in both cases they behave as superparamagnetic, however, they show different blocking temperature and magnetic susceptibility. A remarkable fact is how the coercive field of embedded zinc ferrite nanoparticles is one order of magnitude higher as a consequence of the encapsulation process in the matrix. This suggests that the nanocrystals are firmly embedded and consequently the movement of the magnetic domains is avoided.

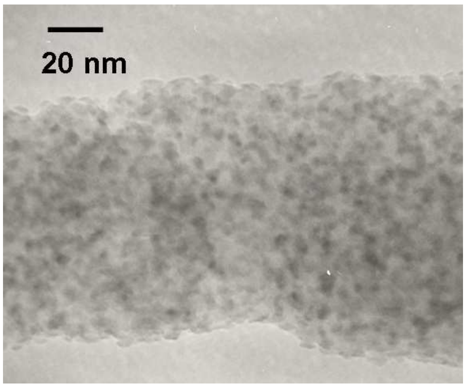

Fig. 1. TEM image of 3 nm $ZnFe_2O_4$ nanoparticles embedded in silica matrix.

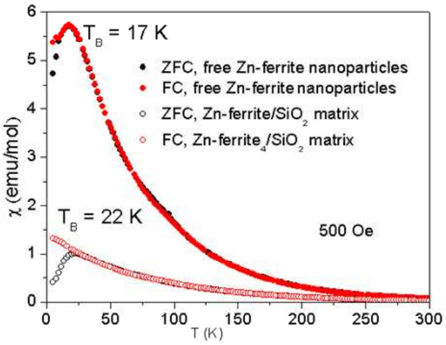

Fig. 2. ZFC y FC curves for free and embedded $ZnFe_2O_4$ nanoparticles of 3 nm, measured at 500 Oe.

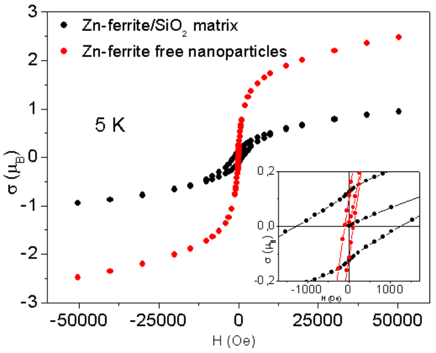

Fig. 3. Hysteresis loops measured at 5 K for both free and embedded $ZnFe_2O_4$ nanoparticles of 3 nm.

REFERENCES

1. Ya-Juan Hao et al., 2006, Materials Letters 60, 1334–1337
1. Sophie Laurent, Delphine Forge, Marc Port, Alain Roch, Caroline Robic, Luce Vander Elst, and Robert N. Muller, Chem. Rev. 2008**,** 108*,* 2064–2110
2. Qing Song and Z. John Zhang J. Phys. Chem. B 2006**,** 110*,* 11205-11209
3. L.A. Garcıa-Cerda, V.A. Torres-Garcıa, J.A. Matutes-Aquino, O.E. Ayala-Valenzuela, Journal of Alloys and Compounds 2004, 369, 148–151

Efecto de la montmorillonita en la morfología y propiedades termomecánicas de los nanocomposites poliéster/poli (ε-caprolactona)/montmorillonita

S. Calvo del Valle, R.Mª. Masegosa Fanego
Dpto. Física y Química Aplicadas a la Técnica Aeronáutica. E.U.I.T. Aeronáutica
Univ. Politécnica de Madrid, España
M.G. Prolongo, C. Salom
Dpto. Materiales y Producción Aeroespacial. E.T.S.I.Aeronáuticos
Univ. Politécnica de Madrid, España

RESUMEN

En este trabajo se ha elegido un sistema ternario de matriz resina de poliéster insaturado, (UP), modificada con el termoplástico, poli (ε-caprolactona), (PCL) y como nanorrefuerzo una arcilla, la montmorillonita orgánicamente modificada (OMMT). Se ha fijado el contenido de PCL y OMMT en el 4% en peso, utilizando dos muestras de PCL de distinto peso molecular. Se han estudiado las propiedades termo-mecánicas de los sistemas poliéster/PCL/OMMT y se han correlacionado con la estructura/morfología de los nanocompuestos obtenidos.

1. INTRODUCCIÓN

Los aditivos juegan un papel importante en la modificación de las propiedades de los polímeros y de los materiales compuestos derivados de los mismos. Entre los materiales inorgánicos utilizados como aditivos refuerzo para la mejora de las propiedades de los polímeros, los silicatos laminares (arcillas) modificados orgánicamente, han centrado últimamente la atención dado que dependiendo del método de preparación y de la interacción entre el arcilla y el polímero se pueden generar tres tipos de morfologías según el estado de dispersión de la organoarcilla en el polímero: estructuras que corresponden a separación de fases de los dos componentes, estructuras intercaladas y nanocompuestos en los que se consigue la exfoliación. En nanocompuestos con silicatos laminares en los que se consigue la exfoliación, se ha comprobado que cuanto mas exfoliada esté la arcilla en la matriz más se impide la coalescencia de los dominios dispersos en la matriz (Hong et al. 2006). El estudio de nanocompuestos ternarios persigue conseguir un balance óptimo de propiedades (Wang et al. 2008). El objetivo de este trabajo es estudiar la propiedades termomecánicas de los sistemas ternarios UP/PCL/OMMT con el fin de conseguir una mejora de propiedades respecto a los sistemas binarios, UP/OMMT; se han elegido dos muestras de poli (ε-caprolactona) de distinto peso molecular y se ha analizado si el peso molecular del termoplástico influye de manera significativa en el estado de dispersión de la OMMT cuando coexisten PCL y UP y por tanto en la estructura del nanocompuesto UP /PCL/OMMT.

2. EXPERIMENTAL

2.1 Materiales

La resina de poliéster insaturado utilizada en este estudio es del tipo isoftálica y fue suministrada por Cray Valley bajo el nombre comercial de Norsodyne 44233. Dicha resina contiene un 38wt% de estireno. La C30B, suministrada por Shouther Clay Products, Inc. es una montmorillonita orgánicamente modificada con una sal de amonio cuaternaria cuyos sustituyentes son metil, bis-2-hidroxietil y una cadena carbonada de composición ~ 65% C18, ~ 30% C16, y ~ 5% C14. La concentración del modificador es de 90 meq/100g arcilla. Las dos muestras de PCL corresponden a pesos moleculares: Mn=2000g/mol (PCL2) suministrada por Aldrich Chemical Company, Inc., y Mn=50000g/mol (PCL50) suministrada por Polyscience, Inc.

2.2 Preparación de los nanocompuestos y reacción de curado

Los nanocompuestos UP/C30B/PCL se prepararon por dispersión de la C30B en la resina (4% de Cloisita respecto a la masa total de UP + PCL) a 50ºC con agitación a 300rpm durante 2h. La PCL (4% respecto a la masa de UP) se añadió a la mezcla a 50ºC con agitación a 200rpm durante 3h.

La reacción de curado de la resina UP tuvo lugar utilizando como iniciador peróxido de benzoílo (1.5% respecto a la masa de UP). El protocolo consistió en: curado isotermo a 80ºC durante 1 hora y posteriormente un post-curado a 110 ºC durante 3 h.

2.3 Técnicas experimentales

Para las medidas de análisis térmico mecánico dinámico se ha utilizado un equipo Rheometric Scientific DMTA V trabajando en el modo de flexión en doble voladizo. Las medidas se realizaron a frecuencia 1, 2, 5, 10 y 50 Hz, con un barrido de temperaturas desde 25ºC hasta 220°C a 3ºC/min. Los máximos en la curvas tanδ-temperatura se identificaron con las relajaciones α asociadas a la transición vítrea.

La propiedades mecánicas a tracción de las muestras se midieron en una máquina de ensayos MTS modelo QTest 2L con un extensómetro modelo 63411F-54. Las muestras se cargaron a velocidad constante de 1mm/min hasta fractura. Se midieron cinco probetas de cada muestra. Los valores de las propiedades mecánicas de las muestras corresponden al valor promedio de las cinco probetas medidas.

La dispersión de las láminas de Cloisite 30B en las resinas se ha estudiado a través de los espectros de difracción Rayos X de ángulo rasante. Se ha utilizado un equipo XPERT-PRO.

3. RESULTADOS

3.1 Caracterización de los nanocompuestos

La Figura 1 muestra los espectros de difracción de la C30B y de los nanocompuestos que se especifican. En los sistemas ternarios hay un desplazamiento del pico de difracción hasta valores del ángulo $2\theta = 2{,}2^{\circ}$ lo que supone un aumento del espaciado de las galerías de la arcilla, entre 2,1 y 2,2 nm, respecto a la C30B. En la Tabla 1 se muestran los valores del espaciado para los sistemas binarios UP+C30B y PCL+C30B. Estos valores suponen aumentos entre 1,9 y 1,6 nm respecto a los valores de la C30B pura. Los resultados de difracción de Rayos X son compatibles con la obtención de nanocompuestos con estructuras mixtas intercaladas/exfoliadas en las que las cadenas de polímero se insertan en las galerías de la arcilla.

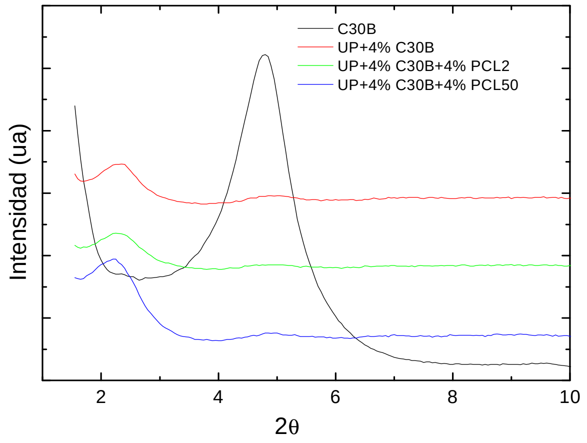

Fig.1. RX de las muestras estudiadas.

Muestra	**d** nm
C30B	1.8
UP+4%C30B	3.7
UP+4%C30B+4%PCL2	4.0
UP+4%C30B+4%PCL50	3.9
PCL2+4%C30B	3.7
PCL50+4%C30B	3.4

Tabla 1. Valores del espaciado interlaminar, d

3.2 Propiedades térmicas y mecánicas de los nanocompuestos

Los resultados de DSC se muestran en la Tabla 2. La T_g calorimétrica de la resina UP curada es 108ºC. Con la adición de C30B la T_g de la resina se incrementa, hasta alcanzar el valor de 118ºC para el 4% de Cloisita. Ello es debido a las interacciones entre el polímero y las láminas de arcilla nano-dispersadas que restringen los movimientos segmentales de la resina UP. En trabajos previos se estudiaron los sistemas binarios UP+Cloisita 30B variando el contenido de arcilla, observando que el contenido óptimo del nanocompuesto se conseguían para porcentajes bajos de arcilla (~4%). Con la adición de PCL al sistema UP+C30B se observa una ligera disminución de la T_g respecto al sistema sin PCL, pero en cualquier caso superior al valor de la T_g de la resina pura. Los resultados de calorimetría muestran además que no hay cambios significativos en los valores de la energía de activación de la reacción de curado del nanocompuesto UP+C30B+PCL lo que indica que la presencia de Cloisita y PCL no afecta al mecanismo de la reacción de curado de la resina.

Muestra	**E_a(kJ/molUP)**	**ΔH(Jg^{-1})**	**T_g(ºC)**
UP	86±1	-352±10	108
UP+4%C30B	83±2	-364±8	118
UP+4%C30B+4%PCL2	81±2	-356±10	111
UP+4%C30B+4%PCL50	84±2	-346±10	115

Tabla. 2 Resultados obtenidos por DSC a partir de curados dinámicos.

En la medidas de DMTA se llevaron a cabo determinaciones de tan δ, módulo de almacenamiento, E´ vs temperatura, a distintas frecuencias. En la tabla 3 están resumidos los resultados obtenidos a 1 Hz.

Muestra	T_g (ºC)	E´(25ºC) (Pa)	E´(180ºC) (Pa)
UP+4%C30B	142	$2.1*10^9$	$3.2*10^7$
UP+4%C30B+4%PCL2	136	$2.1*10^9$	$1.9*10^7$
UP+4%C30B+4%PCL50	142	$1.9*10^9$	$2.6*10^7$
UP	137	$1.9*10^9$	$2.5*10^7$

Tabla 3. Resultados obtenidos por DMTA.

Las T_g de la Tabla 3 corresponden a los valores del máximo del pico de tanδ correspondiente a la relajación α. Estos valores son coherentes con los determinados por DSC. Los valores de E´ a temperatura ambiente apenas varían en relación a la UP mientras que si hay una variación apreciable en E´ "rubber" en los sistemas ternarios, dependiendo del peso molecular de la PCL. En cuanto a las propiedades mecánicas a tracción (ver Tabla 4) cabe destacar una disminución (20%) del módulo de Young (E) en los sistemas ternarios respecto al binario UP+C30B, pero un aumento importante de la ductilidad (entorno al 25%) manteniéndose la resistencia mecánica.

Muestra	σ(MPa)	ε (%) (a fractura)	E (GPa)
UP+4%C30B	40±5	1.1±0.1	4.5±0.1
UP+4%C30B+4%PCL2	43±3	1.4±0.2	3.6±0.1
UP+4%C30B+4%PCL50	42±4	1.4±0.2	3.6±0.1
UP	43±3	1.3±0.1	3.8±0.1

Tabla 4. Resultados obtenidos de los ensayos de tracción.

4. CONCLUSIONES

Se han caracterizado y determinado las propiedades termomecánicas de los sistemas ternarios UP/PCL/C30B. El espaciado interlaminar de la C30B en estos sistemas indica que se trata de nanocompuestos con estructuras mixtas intercaladas/exfoliadas. La presencia de PCL en el sistema provoca un buen balance de las propiedades termomecánicas entre las que cabría destacar el aumento de la ductilidad de estos sistemas respecto a los binarios UP+C30B.

REFERENCIAS

HONG J.S., NAMKUNG H., AHN K..H., LEE S.J., KIM C. (2006). The role of organically modified layered silicate in the breakup and coalescence of droplets in PBT/PE blends Polymer, 47, 3967

WANG K., CHEN Y., ZHANG Y. (2008). Effects of organoclay platelets on morphology and mechanical properties in PTT/EPDM-g-MA/organoclay ternary nanocomposites. Polymer, 49, 3301-3309.

AGRADECIMIENTOS

Este trabajo ha sido financiado por los proyectos MEC (MAT 2006-0213) y CAM (S-.0505/MAT2007).

Morphological and mechanical properties of TPU/clay nanocomposites

L. Pizzatto
Autotravi Borrachas e Plásticos Ltda, Caxias do Sul, Brazil
R. Fiorio, G. Machado*, M. Giovanela, A.J. Zattera, J.S. Crespo
Centro de Ciências Exatas e Tecnologia, Universidade de Caxias do Sul, Brazil
*Centro de Tecnologias Estratégicas do Nordeste, Brazil

SUMMARY

In this study thermoplastic polyurethane (TPU) composites were obtained with different nanoclay contents. The nanoclay Cloisite®30B (C30B) was dispersed in the TPU matrix by melt processing (twin-screw extruder; TPU-E composites) and during bulk polymerization (TPU-S composites). The characterization of TPU/nanoclay composites was carried out by means of scanning electron microscopy (SEM) and X-ray diffraction (XRD). The mechanical characterization was performed through determination of the tensile and tear strengths. The TPU-E 3 wt% composite showed the best improvement with increases in stress and strain at break and energy (28%, 35% and 88%, respectively), compared to the TPU-E (sample without nanoclay).

1. INTRODUCTION

In recent years, polymer/clay nanocomposites have attracted great attention in the industrial sector, since the use of nanoclay as reinforcement for polymers results in materials with excellent mechanical properties. These nanocomposites exhibit remarkable improvement compared to the conventional microcomposites in various properties such as mechanical strength, heat resistance, gas permeability, and inflammability. Some researchers have reported the preparation of TPU/nanoclay composites and nanocomposites through bulk (PATTANAYAK et to. 2005a, 2005b and 2005c) and solution (CHENG et to. 2006) polymerization, melt processing (DAN et to. 2006, CHAVARRIA et to. 2006) and reactive extrusion (CAI et to. 2007) using montmorrilonite and organically modified nanoclay and observed an improvement in the mechanical properties.

The aim of this work is to compare two methods of incorporation of nanoclay into TPU matrix (bulk polymerization and meting process). In this study, TPU composites were prepared with different C30B contents. We investigated the dispersion state of the nanoclay particles and its effects on the mechanical properties of the composites, before and after accelerated ageing.

2. EXPERIMENTAL

2.1. Preparation of the TPU and TPU composites

The base TPU (TPU-S) was synthesized with a 1.75:0.5:1 molar ratio of MDI: polyol:1,4-butanediol and contained 34.5 wt% of hard segments. The prepolymer was prepared under nitrogen atmosphere by reacting the MDI with the polyol at 80^{o}C in an industrial mixer, at 600 rpm for 5 min. TPU-S was synthesized in a industrial mixer from the chain extension of the prepolymer with the 1,4-butanediol at 80^{o}C for 15 min. TPU-S composites (TPU-S 1 wt% and TPU-S 3 wt%) were prepared by adding C30B after 1 min of chain extension reactions and further mixing at 600 rpm the system for approximately 5 min. TPU-S was dried for 4 h at 80ºC prior to melt processing. TPU-S with different amounts of C30B (0, 1, 3 and 10 wt%) were dry-mixed before melt processed once in a co-rotating, intermeshing twin screw extruder at 210ºC and 200 rpm. The melt processed TPU composites samples were named TPU-E, TPU-E 1 wt%, TPU-E 3 wt% and TPU-E 10 wt%.

The sample specimens used in the TPU-S and TPU-E composites characterization were prepared by compression molding at 200ºC for 5 min under a pressure of 7.5 MPa. The specimens were post-cured at 80ºC for a period of 24 h.

2.2. Characterization of the TPU and TPU composites

The change in gallery distance of silicate layers in the nanoclay was determined on an X-ray diffractometer (Shimadzu XRD 6000) using Cu Kα radiation. The samples were scanned at 0.5º min^{-1}. Scanning electron microscopy (SEM) images of TPU and TPU composites samples were obtained using a Shimadzu SSX-550 scanning electron microscopy with an operating voltage of 15 kV. Before analysis, all samples were covered with a thin gold layer in a P-S2 diode sputtering system metalizer for 10 min. Tensile and tear properties were determined using a universal testing machine (EMIC DL 300), according to ASTM D638-04 type V method and ASTM D 624-00 type C method, respectively. Mechanical properties were determined before and after accelerated ageing (170 h, 70ºC) according to ASTM D 573-03 in an Erzinger oven model 90/65/70.

3. RESULTS AND DISCUSSION

The dispersion state of the nanoclay particles can be inferred from Figs. 1a and 1b. The diffraction peaks in Fig. 1 at 2θ = 4.9º (d-spacing ca. 1.7 nm) are related to C30B. A broad peak at 2θ = 20º relates to the TPU.

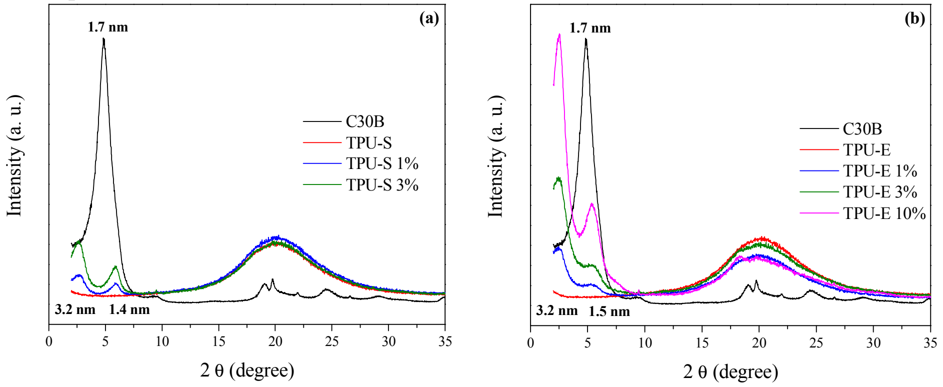

Fig. 1. X-ray diffraction patterns of C30B, (a) TPU-S and (b) TPU-E.

In Fig. 1a (TPU-S composites) the X-ray diffraction pattern shows d-spacings of ca. 3.2 and 1.4 nm. A peak observed with a d-spacing of 3.2 nm indicated partial intercalation of nanoclay layers by the polymer chains. The peak with a d-spacing of 1.4 nm, similar to that observed for C30B, indicated the presence of nanoclay tactoids in the composites. This is also evidenced by the presence of agglomerated C30B nanoclay particles in the SEM images shown in Figs. 2b and 2c. The presence of nanoclay tactoids induced a nucleation process in TPU-S composites (Figs. 2b and 2c), resulting in a reduction in the size of the spherulite, comparing to the TPU-S, sample without nanoclay (Fig. 2a).

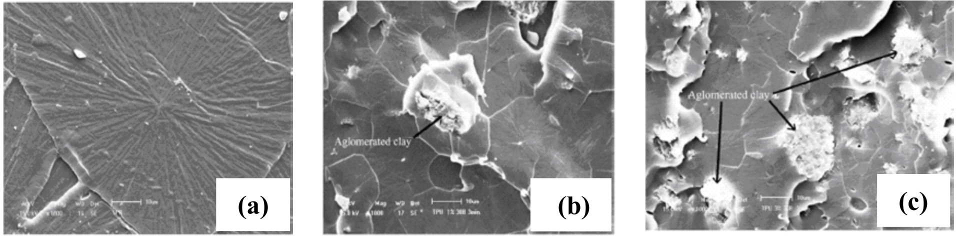

Fig. 2. SEM images: (a) TPU-S, (b) TPU-S 1 wt%, and (c) TPU-S 3 wt% (1000 x).

Figure 1b shows the results for TPU-E composites. Compared with the TPU-S composites, a stronger peak at d-spacing 3.2 nm was observed, indicating that the majority of the silicate layers of C30B were intercalated by the TPU chains. At d-spacing 1.5 nm, a peak was observed only for the TPU-E 10%, probably due to an excess of nanoclay in this composite, and consequently poor dispersion.

For the extruded sample without nanoclay (TPU-E) the cooling, after the extrusion process, led to the formation of small spherulites and a more elongated morphology, in comparison with TPU-S sample. The reduction in the size of these spherulites is due to quenching, immediately after the extrusion process. The SEM analysis for the TPU-E 1 wt%, TPU-E 3 wt% and TPU-E 10 wt% composites showed the absence of spherulites probably due to the high degree of intercalation of C30B in the polymeric chain.

The values for the tensile modulus, stress and strain at break, energy and tear strength of TPU and its composites are presented in Table 1. For the TPU-S samples, as a general trend, the values for the mechanical properties (stress and strain at break, energy and tear strength) decreased with an increase in the nanoclay content. However, the tensile modulus value was not found to be dependent on the nanoclay content. The C30B could not reinforce TPU because of poor system dispersion observed through XRD and the presence of agglomerated nanoclay tactoids shown by the SEM analysis.

Sample	Tensile modulus (MPa)	Stress at break (MPa)	Strain at break (%)	Energy (J)	Tear strength (kN m^{-1})
TPU-S	11.8 ± 0.3	28.1 ± 3.3	350.5 ± 18.3	27.3 ± 2.8	102.3 ± 6.9
TPU-S 1 %	12.1 ± 0.4	22.6 ± 3.0	315.4 ± 20.1	21.4 ± 2.8	95.4 ± 2.8
TPU-S 3 %	12.7 ± 0.3	9.2 ± 0.8	119.4 ± 15.3	4.7 ± 0.8	87.4 ± 8.9
TPU-E	13.6 ± 0.4	20.5 ± 2.2	293.0 ± 17.9	19.6 ± 2.8	101.2 ± 7.8
TPU-E 1 %	14.4 ± 0.6	16.6 ± 2.4	235.9 ± 32.7	14.8 ± 3.2	112.4 ± 4.3
TPU-E 3 %	19.4 ± 1.1	26.2 ± 2.2	396.6 ± 35.1	37.0 ± 4.2	124.1 ± 8.8
TPU-E 10 %	44.0 ± 2.1	12.6 ± 0.8	192.8 ± 41.2	13.4 ± 3.3	121.2 ± 2.7

Table 1. Tensile and tear properties of TPU composites.

For TPU-E composites, TPU-E 3 wt% showed the greatest improvement in terms of stress and strain at break (increase of 28% and 35%, respectively) and energy (increase of 88%), compared to the TPU-E. Hence, for TPU-E 3 wt%, the increase in the values for the mechanical properties can be attributed to the good dispersion and intercalation of the nanoparticles observed by XRD. TPU-E 10 wt% had the highest tensile modulus (increase of 224%, compared to the TPU-E); however, the other properties had lower values compared with those of TPU-E. TPU-E 1 wt% had lower values for stress and strain at break, as well energy, than TPU-E and TPU-E 3 wt%. This behavior can be related to poor particle dispersion during the melt processing, compared to TPU-E 3 wt%. On the other hand, the results concerning tear strength for TPU-E composites were similar (considering the standard deviation) and independent of the nanoclay content and dispersion.

As a general trend, the accelerated ageing process for TPU composites promoted an increase in the values for the mechanical properties. Samples with C30B showed significant improvement in the mechanical retention properties compared to TPU-S and TPU-E. One hypothesis for this is that ageing at 70ºC may have completed the extension of the chains (post-cure process). Strain at break and energy were the properties that showed highest increases with ageing. A better conformation of the soft segments of TPU, induced by ageing, facilitated stretching of these chains during stress-strain analysis, increasing both strain at break and energy.

4. CONCLUSIONS

For TPU-S composites the X-ray diffraction patterns show the presence of C30B tactoids in the TPU matrix. The SEM images corroborated this result and evidenced the presence of agglomerated nanoclay particles. The method used in the synthesis did not provide sufficient shear stress for exfoliation and good dispersion of the nanoclay. Intercalation and better dispersion occurred in the TPU-E samples due to the high shear viscosity during the melt processing. TPU-E samples show better mechanical properties than TPU-S samples, since the low degree of particle dispersion observed in TPU-S samples may have induced a lowering of the polymer-nanoclay interactions and promoted stress concentration. The accelerated ageing process applied to the TPU composites led to an increase in the values for the mechanical properties, compared to samples without nanoclay.

REFERENCES

CHAVARRIA, F., PAUL, D.R. (2006). Morphology and properties of thermoplastic polyurethane nanocomposites: Effect of organoclay structure. *Polymer*, 47, 7760-7773.

CHENG, A., WU, S., JIANG, D., WU, F., SHEN, J. (2006). Study of elastomeric polyurethane nanocomposites prepared from grafted organic-montmorillonite. *Colloid Polym. Sci.*, 284, 1057-1061.

DAN, C.H., LEE, M.H., KIM, Y.D., MIN, B.H., KIM, J.H. (2006). Effect of clay modifiers on the morphology and physical properties of thermoplastic polyurethane/clay nanocomposites. *Polymer*, 47, 6718-6730.

PATTANAYAK, A, JANA, S.C. (2005a). Synthesis of thermoplastic polyurethane nanocomposites of reactive nanoclay by bulk polymerization methods. *Polymer*, 46, 3275-3288.

PATTANAYAK, A., JANA, S.C (2005b). Properties of bulk-polymerized thermoplastic polyurethane nanocomposites. *Polymer*, 46, 3394-3406.

PATTANAYAK, A. JANA, S.C. (2005c). Thermoplastic polyurethane nanocomposites of reactive silicate clays: effects of soft segments on properties. *Polymer*, 46, 5183-5193.

CAI, Y., HU, Y., SONG, L., LIU, L., WANG, Z., CHENG, Z., FAN, W. (2007). Synthesis and characterization of thermoplastic polyurethane/montmorillonite nanocomposites produced by reactive extrusion. *J. Mat. Sci.*, 42, 5785-5790.

Morphologycal study of a PP/EPDM/organoclay nanocomposite deformed by uni-axial compression

A. Thompson, C.L.G. Amorim , J.S. Crespo, C. Giacomelli, G. Machado*
Centro de Ciências Exatas e Tecnologia, Universidade de Caxias do Sul, Brazil
*Centro de Tecnologias Estratégicas do Nordeste, Brazil
O. Bianchi, D. Samios, S.R. Teixeira
Universidade Federal do Rio Grande do Sul, Brazil

SUMMARY

Morphological and structural properties of a polypropylene (PP)/ethylene propylene diene terpolymer rubber (EPDM)/organoclay nanocomposite, submitted to uni-axial plain strain deformation, at room temperature and under compression rates of 50, 100 and 1000 MPa, have been investigated using wide angle X-ray diffraction (WAXD), small angle X-ray scattering (SAXS) and scanning electron microscopy (SEM) analysis. The composition of PP in the blend was 75%. During the melt process of mixing 1, 2 and 4 phr of organoclay C15A was added in the blend. The WAXD results indicate that the silicate layers of organoclay were intercalated by the polymer chains. These results were supported by SEM/Si mapping analysis.

1. INTRODUCTION

The use of blends of polypropylene (PP) and ethylene-propylene-diene terpolymer rubber (EPDM) has become ubiquitous in the industry, basically due to their excellent chemical and thermal properties. However, in certain cases these materials show low mechanical resistance, which leads the manufacturers to introduce fillers, aiming this property improvement. The introduction of small quantities of fillers with particles of nanometric dimensions inside the macromolecules of a plastic resin (WANG et to. 1998) became usual. The works carried out with addition of modified clays in these materials have been showing improvement in their mechanical properties, since intercalation of the clay is observed in the polymer chains (Lee et to. 2005). One of the clays most used in these researches is the montmorillonites (MISHRA et to. 2005), such as the Cloisite®15A (C15A). The C15A is a montmorillonite modified with salts of quaternary ammonia. Still attempting to improve the properties of the polymeric materials, studies of structural modifications with the use of uni-axial deformation have been carried out in semi-crystalline polymers (ASAMI et to. 2004). The main purpose of this work is to characterize the morphology of PP/EPDM blend, with and without the presence of clay, as well as to understand the mechanism of functioning of the clay in the lamellar structure of the polymer, before and after the uni-axial deformation.

2. EXPERIMENTAL

2.1. Sample Preparations

The samples were prepared by melt mixed method in a Haake Rheocorder at 190° C and 100 rpm rotor speed with a mixing time of 15 min. Four types of blends were prepared, the pure one and the others with the following concentrations of C15A: 1, 2 and 4 phr. All the blends have 50 g of polymer and the ratio of 75/25 wt% of PP/EPDM. After the extrusion, the moisture material was grounded in a Primotécnica 75BA’s mill and then hot pressed, under a temperature of 190° C and 7.5 MPa, for 5 minutes, in a press Schulz PHS, in order to get samples of 2 mm of thickness, used for the nanocomposites’ characterization. The uni-axial compressions in these samples were made at room temperature, in a hydraulic press Carver Monarch G30-H, under deformation pressures of 50, 100 and 1000 MPa.

2.2. Measurements

The morphology of the material was examined by a Shimadzu SSX-550 Scanning Electron Microscope (SEM). Images of the surface were obtained and also the mapping of Si was made in the samples. The accelerating voltage used was 10 kV.

In order to identify the crystalline peaks and to evaluate the clay intercalation in the chains of the polymer, Wide Angle X-Ray Diffraction (WAXD) studies of the samples were carried out in a Shimadzu XRD-6000 operating at 40 kV and 30 mA (CuKα radiation). The scanning rate was 0,5°/min and the measure range was 1,5 to 35°.

The Small Angle X-Ray Scattering (SAXS) were used to identify the lamellar long period (L) of the nanocomposites, as well as to check the lamellar rotation angle (φ). The analysis were made in the Laboratório Nacional de Luz Síncroton (LNLS, Campinas, SP), the time of exposure to SAXS radiation was 60 s, the distance between the plane of detection and the sample was 1244 mm and the value of λ wavelength was 1,488 Å.

3. RESULTS AND DISCUSSION

The WAXD diffraction patterns of the blends of PP and EPDM with and without different concentrations of C15A are shown in Fig. 1. The pattern of Fig. 1e. shows two peaks that are characteristic of the clay (2,70° and 7,20°) and correspond to its crystalline reflections. A shift of these clay related peaks was observed (these dislocations take place of 2,70° to 2,30° and of 7,20° to 4,40°) in the case of blends, what suggests intercalation of the clay by the polymer chains.

The WAXD diffraction patterns shown in the Fig. 2 allows to observe a change in the crystalline structure of the material. The difference of intensity in the peaks, checked between the pattern of the undeformed material and the deformed ones, indicates a reduction in the crystalline fraction (partial amorphization) of the deformed materials. This amorphization grows with the increase of the deformation pressure also.

In the Fig. 3 (SEM images of the blends) can be seen a variation in the microstructure of the blends with the addition of clay, this is due to the intercalation observed previously by WAXD analysis. There are not observed agglomeration points of clay in the polymer, which is an indicative of good dispersal of the clay into the polymer matrix. Furthermore, in Fig. 4, the uniformity of the silica particles can be observed, indicating that the C15A is homogeneously dispersed in the polymer matrix and at the micrometric scale.

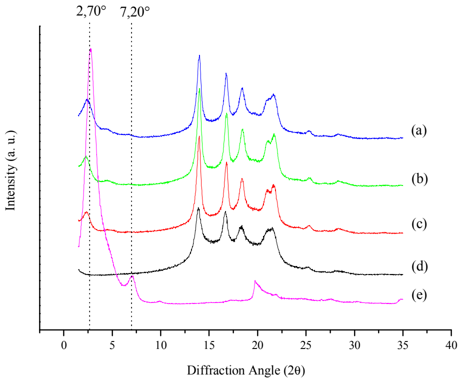

Fig. 1. WAXD diffraction patterns of (e) C15A and the blends with: (a) 4 phr C15A, (b) 2 phr C15A, (c) 1 phr C15A, (d) 0 phr C15A.

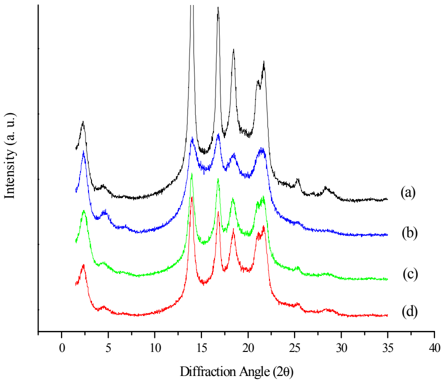

Fig. 2. WAXD diffraction patterns of the blend with 2 phr of C15A (a) undeformed and deformed samples: (b) 50 MPa, (c) 100 MPa, (d) 1000 MPa.

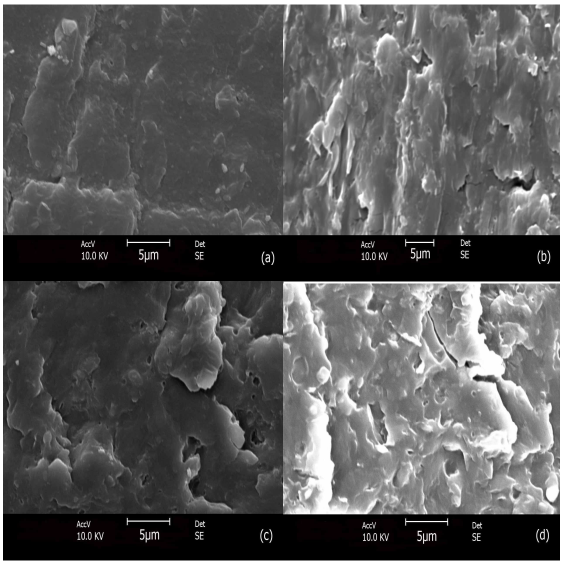

Fig. 3. SEM images of blends with: (a) 0 phr C15A, (b) 1 phr C15A, (c) 2 phr C15A, (d) 4 phr C15A.

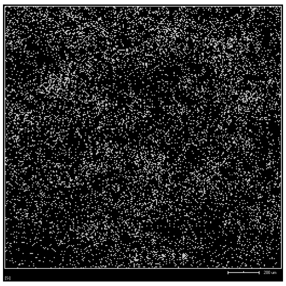

Fig. 4. Si mapping for the blend with 2 phr C15A.

In the Table 1 is noticed that the L, in relation with polymer undeformed, obtained via SAXS profile analysis, increases with the introduction of clay into the blends. The uni-axial deformation of the blends induces the slight reduction of this spacing that leads to the disappearance of the reflection peak of the clay, which owes in part of cristallinity reduction in the blends, already shown in the WAXD diffraction patterns, but also to the lamellar rotation of the material. The values of the φ increase with the deformation, principally regarding the peak of qmáx referent to the clay in the blends, which explains the disappearing of qmáx clay peaks after the deformation in the blends. It is still noticed that the addition of clay increases the lamellar movement in the blend, that is shown up by the increase of the φ. But it is important to stand out that with the addition of more clay this rotation has a tendency to stabilize. The lamellar movement of the clay follows the polymer and the φ for the lamellae's of clay also increases with the addition of clay. L also decreases with the deformation, which makes the lamellar spacing shorter and explains the fact of the φ practically not to be altered for deformed samples, even with the addition of clay. Already for the lamellae's of the clay, the angle φ of deformed samples follows the tendency of the undeformed ones and increases with the introduction of clay.

Table 1. Values of lamellar long period (L) and rotation angle (φ) for the blends.

Parameters	**Sample**							
	Undeformed				**Deformed 1000 MPa**			
	0*	**1***	**2***	**4***	**0***	**1***	**2***	**4***
L polymer (nm)	11.85	12.08	12.31	12.08	11.85	11.42	11.63	11.21
L clay (nm)	0	3.31	3.39	3.32	0	0	0	0
φ (polymer)	240°	180°	225°	220°	255°	255°	260°	270°
φ (clay)		145°	160°	190°		260°	280°	205°

* C15A content in phr

4. CONCLUSIONS

A composite was obtained by addition of clay C15A to a blend of PP and EPDM. It was demonstrated in this work that the clay was intercalated by the polymers chains. The analysis of SAXS demonstrated that there was variation in the angle of rotation φ of the polymer and clay's lamellae with the addition of the C15A and this variation has a tendency to stabilize when it took place the introduction of the biggest amount of clay and the consequent restriction of molecular movement. Besides, we're been able to demonstrate that the uni-axial deformation of the composites produced a partial amorphization in the material.

ACKNOWLEDGMENT

The authors are grateful to Ciaflex Indústria de Borrachas Ltda and Braskem for supplying the EPDM and PP polymers, respectively, CAPES and CNPq are acknowledged for financial support, the LNLS for SAXS analysis.

REFERENCES

ASAMI, T., NITTA, K. (2004). Morphology and mechanical properties of polyolefinic thermoplastic elastomer I. Characterization of deformation process. *Polymer,* 45, 5301-5306.

LEE, H., FASULO, P.D., RODGERS, W.R., PAUL, D.R. (2005). TPO based nanocomposites. Part 1. Morphology and mechanical properties. *Polymer,* 46, 11673-11689.

MISHRA, J.K., HWANG, K.J., HA, C.S. (2005). Preparation, mechanical and rheological properties of a thermoplastic polyolefin (TPO)/organoclay nanocomposite with reference to the effect of maleic anhydride modified polypropylene as a compatibilizer. *Polymer,* 46, 1995-2002.

WANG, Z., PINNAVAIA, T.J. (1998). Nanolayer Reinforcement of Elastomeric Polyurethane. *Chemistry of Mats.,* 10, 3769-3771.

Nanocomposites based on polyhydroxybutyrate and different organically modified montmorillonites

D.A. D'Amico, L.B. Manfredi, V.P. Cyras
Instituto de Investigaciones en Ciencia y Tecnología de Materiales (INTEMA). Facultad de Ingeniería. Universidad Nacional de Mar del Plata, Argentina
A. Vázquez
Laboratorio de Polímeros y Materiales Compuestos. Instituto de Tecnologías y Ciencias de la Ingeniería (INTECIN). Facultad de Ingeniería. Universidad de Buenos Aires, Argentina

ABSTRACT

Development of polymer/clay nanocomposites is one of the latest revolutionary steps of the polymer technology. Preparation of blends or nanocomposites using low percentages of inorganic fillers is among the routes to improve some of the properties of biodegradable polymers such as barrier, thermal and oxidative, when compared with traditional composites. Montmorillonite (MMT) is among the most commonly used layered silicates because it is environmentally friendly and readily available in large quantities with relatively low cost. Therefore, the aim of this work is to improve the properties of biodegradable polymers by the addition of small amounts of clay. Films were prepared from a polyhydroxybutirate (PHB) solution by casting. Nanocomposites were similarly obtained by the addition of different percentages and type of MMT to the polymer. Crystallinity, thermal degradation and hidrophobicity of films containing 2, 4, 6 and 10 wt% of two MMTs were investigated. From X-Ray diffraction analysis a different behaviour was observed. The Cloisite® Na^+ showed an increment in their interlayer distance, but the galleries of the Cloisite® 15A contract during the formation of the film. On the other hand, the thermal resistance of the composites containing the modified MMT was higher than the ones with Cloisite® Na^+ and PHB film. These results could be related with the different crystallinity and morphology of the final materials.

1. INTRODUCTION

Packaging waste have increase industrial and scientific interests in the field of biopolymeric materials. Poly(hydroxybutyrate) (PHB) is a well-known biodegradable, hydrophobic and semicrystalline polyester, that can be use in packaging applications in replacement of non degradable commodity polymers. Polyhydroxyalkanoates (PHA´s), of which poly(hydroxybutyrate) (PHB) is the most common, are carbon energy storage materials produced by numerous bacterial species. PHA´s are now under intensive investigation because of its inherent property as a biodegradable thermoplastic. A very interesting property of PHB with respect to food packaging applications is its low water vapour permeability, which is close to that low-density polyethylene. However, they are still expensive and quite brittle and have low velocity of crystallization (Gerardus et al. 1999; Sudesh et al. 2000, Zhang, 1999). It is well known that nanocomposites obtained by the addition of low percentages of clay to polymers exhibited an improvement in the properties such as barrier, thermal and oxidative when compared with traditional composites (Huang et al., 2005; Pukánszky et al, 2006; Cyras et al, 2008).

The aim of this work is to obtain nanocomposites based on PHB and nanoreinforcements with improved properties related to the neat polymer.

2. MATERIALS AND METHODS

A biodegradable polymer, Polyhydroxybutyrate (PHB) (Mn=42500) was kindly supplied by PHB Industrial S. A., Brazil. Montmorillonite Cloisite®Na$^+$ and Cloisite®C15A was supplied by Southern Clay Products (Texas, USA).

X-ray diffractograms (XRD) were obtained with KCuα (λ=1.54Å) radiation in a Philips PW 1710 X-ray diffractometer system. The X-ray tube was operated at 45 kV and 30 mA, at 2°/min.

Different amounts of two kind of montmorillonite (2, 4, 6, 10 %w/w) and PHB were homogeneously dispersed using $CHCl_3$ as common solvent. Films were obtained by casting on glass Petri dishes at room temperature.

Thermal gravimetric analysis was performed on the samples with a Mettler TA 4000 at a heating rate of 10ºC/min under a nitrogen atmosphere. The sample weight was between 3-7 mg.

Differential Scanning Calorimetric (DSC) analysis of composites was made using a Perkin Elmer Pyris 1. The dry and conditioned (at 75% RH) samples were subject to heating scans between -40°C and 230°C to obtain the fusion temperature. The scanning rate was 10^0C/min.

Transmission optical microscopy (TOM) was performed on the PHB and nanocomposite films employing a Leica DMLB microscope, with crossed polarizers, provided with a video camera Leica DC 100.

3. RESULTS AND DISCUSSION

In order to investigate the dispersion of the montmorillonite layers, XRD analyses were performed on the composites (Fig 1). MMT exhibits a single 001 diffraction peak around 7.5 2θ. In the composite with Cloisite®Na$^+$ the 001 diffraction peak of the MMT (12.2Å) was shifted to lower angles regardless the clay content. These results should indicate that the polymer chains entered into the silicate layers forming intercalated PHB/MMT nanocomposites, without reaching complete exfoliation. Inversely, the Cloisite®C15A (33.9Å) showed a contraction when was incorporated to the PHB, except for 4% of clay. This could be due to the (Park et al, 2002).

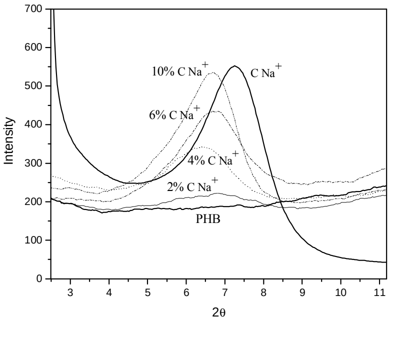

Fig 1 a. DRX of nanocomposites with Cloisite®Na$^+$

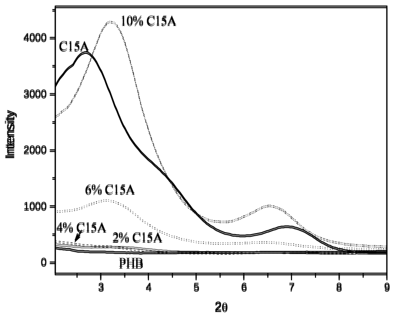

Fig 1 b. DRX of nanocomposites with Cloisite®C15A.

Thermal behavior of the PHB in the nanocomposites was studied by DSC. The enthalpy of fusion (ΔH) and the percerntage of crystallinity (X_c) was calculated. It was observed a disminution in the crystallinity with the increment in the amount of clay.

Table 1. Enthalpy of fusion and % of crystallinity of the materials

C Na+	ΔH (J/g)	X_c	**C15A**	ΔH (J/g)	X_c	**ΔH_{PHB} (J/g)**	$X_{c\ PHB}$
2%	95.1	65.1%	**2%**	91.4	62.6%	97,2	66.6
4%	94.3	64.6%	**4%**	96.2	65.9%		
6%	92.8	63.6%	**6%**	90.6	62.1%		
10%	92.0	63.0%	**10%**	93.8	64.3%		

From the micrograph obtained by TOM, Fig 2, it was observed that the crystallization morphology was similar among the materials. In order to study the isothermal kinetic of PHB crystallization, the films were observed by means of transmission optical microscopy. The velocity of crystallization of PHB was enhanced by the presence of the clay, especially for the C15A.

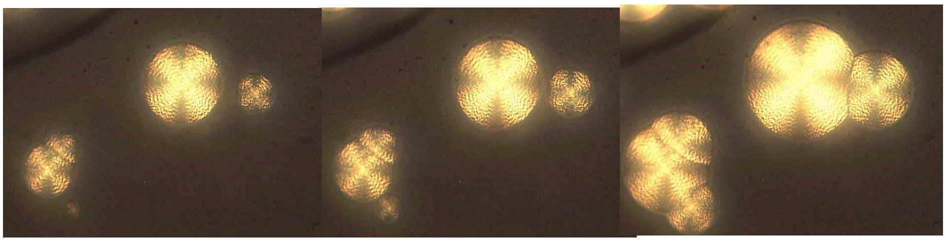

Figure 2. TOM images.

Thermal analysis was performed in order to determine if the addition of clay produces any change on the thermal decomposition behavior of PHB (Fig 3). The DTG curves show one peak at 260°C that represents the decomposition of PHB. This peak shifted to higher temperatures in the nanocomposites with C15A, indicating that the introduction of clay improve the thermal stability of PHB. However, the composites containing CNa^+ showed lesser thermal stability.

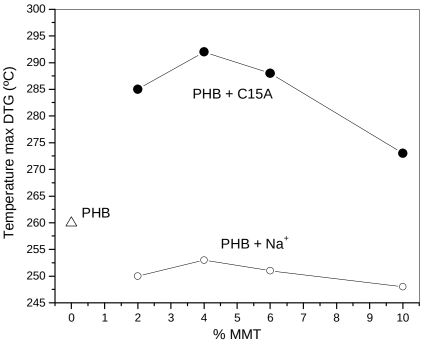

Fig. 3. Temperature max DTG vs. % of clay.

4. CONCLUSIONS

It was possible to prepared PHB/clay composites films from PHB and two different MMT by casting. The CNa^+ is more hydrophilic than C15A, which has the highest interlayer distance.

The C15A was the better dispersed in the PHB in spite of the expantion of the CNa^+ layers.It could be due to the higher initial interlayer gallery of the C15A.

The crystallinity diminished as clay was incorporated, but the global morphology was not changed. However, it was observed that the addition of clay enhanced the velocity of crystallization of PHB, acting as nucleating agent.

The nanocomposites studied showed a different thermal degradation behavior. The inorganic material has better thermal stability than the organic material due to its chemistry. It was reported that the well dispersed clay acts as a heat barrier, enhancing the overall thermal stability of the nanocomposites (Cyras el al, 2008). This was the behavior of the nanocomposites with C15A clay, due to its better dispersion in PHB compared with CNa^+. The variation of the thermal behaviour with the percentage of clay is in accordance to the cristallinity of the samples. The higher cristallinity lead to a higher thermal resistance.

ACKNOWLEDGMENTS

The authors thank the financial support of CONICET (PIP nº6254) and SECYT (PICT 12-1560).

REFERENCES

CYRAS, V.P.; MANFREDI,L.B.;TON-THAT, MINH-TAN AND VÁZQUEZ, A.. (2008) "Physical and Mechanical Properties of Thermoplastic starch/montmorillonite films" *Carbohydrate Polymers*, 73, 1, p 55-63

GERARDUS A., VAN der WALLE, GODFRIED J., BUISMAN, RUUD A., WEUSTHUIS and GERRIT E. (1999) Development of environmentally friendly coatings and paints using medium-chain-length poly(3-hydroxyalkanoates) as the polymer binder. *International Journal of Biological Macromolecules*, 25, 123-128

HUANG, M., YU, J., MA X. & PENG JIN. (2005). High performance biodegradable thermoplastic starch—EMMT nanoplastics. *Polymer*, 46, 9, 3157

PUKÁNSZKY, B., MÜLLER, P. & BAGDI, K. (2006) Thermoplastic starch/layered silicate composites: structure, interaction, properties. *Composite Interfaces.* Vol13, nº1, pp1-17.

SUDESH, K., ABE, H. AND DOI, Y. (2000) Synthesis, structure and properties of polyhydroxyalkanoates: biological polyesters; *Progress in Polymer Science*; 25; 1503-1555.

Biocomposites obtaining with natural fillers and potato starch polymer

J. Morán, L.B. Manfredi, V.P. Cyras
Instituto de Investigaciones en Ciencia y Tecnología de Materiales (INTEMA). Facultad de Ingeniería. Universidad Nacional de Mar del Plata, Argentina
A. Vazquez
Laboratorio de Polímeros y Materiales Compuestos. Instituto de Tecnologías y Ciencias de la Ingeniería (INTECIN). Facultad de Ingeniería. Universidad de Buenos Aires, Argentina

RESUMEN

Starch is a biodegradable polymer produced in abundance from many renewable resources. As a consequence it is easily available and very cheap. However, it is necessary to reduce their water absorption, as well as improve their mechanical properties. Gelatinized potato starch in the presence of water and glycerol was used as references material. In order to decrease their hydrophibicity starch was acetylated (with acetic acid and anhydride), maleated (with maleic anhydride) and esterified with octanoyl chloride. Films were prepared from potato starch and montmorillonite. The clay dispersion in the films was analyzed by X-ray diffraction (XRD). It was observed that the 001 diffraction peak of clay was shift to lower angles in the nanocomposites patterns providing strong evidence that the clay nanolayers formed an intercalated structure but not complete exfoliation. The water absorbed by the nanocomposites measured in an environment with a 75% of constant relative humidity was reduced by the addition of montmorillonite to the starch. The micro-tensile test was performed on the nanocomposite films showing significant improvement in the Young modulus up to 500% for the nanocomposite containing 5 wt% of clay.

1. INTRODUCTION

Starch is cheap, produced in abundance, biodegradable and available from many renewable sources. The processing and manipulation of starch is vital for many industry usages (Frignant, et al, 1996). Starch is a semicrystalline polymer stored in granular form as a reserve in certain plants. It is composed of repeating 1,4-α-D-glucopyranosyl unit: amylose and amylopectin. The amylose is linear, the repeating units are linked by α (1-4) linkages, the amylopectin has a α (1-4) linked backbone and about 5% α (1-6) linked branches. Potato starch granules normally contain 16-23% amylase (Myllärinen et al, 2004; Plackett and Vazquez, 2004). In native form, the starch granules are insoluble in cold water and most uses involve a heating treatment in the presence of excess of water. Below a critical temperature (gelatinization temperature) starch granules absorb water and undergo swelling to many times their original size. Beyond this temperature, the swollen starch granules can undergo a disruption into smaller aggregates or particles, and result in a gelatinized starch. Starch can be chemically modified in order to enhance the properties demanded by the industry, such as mechanical properties, crystallinity and water absorption (Bastioli, 1995).

Preparations of blends or nanocomposites using inorganic or natural fibers are among the routes to improve some of the properties of biodegradable polymers. Nanoomposites obtained by the addition of low contents of clay to polymers exhibit an improvement in the properties such as barrier, thermal and oxidative when compared with traditional composites. Clay minerals are aluminum silicates of a layered type classified as phyllosilicates (Huang et al., 2005; Pukánszky et al, 2006; Cyras et al, 2008).

The aim of the work is to study the modification of the chemical structure of native potato starch and the influence of the addition of low percentages of clay on the barrier, thermal and mechanical properties of plasticized starch.

2. MATERIALS AND METHODS

Materials: Native Potato Starch was kindly provided by AVEBE, Argentina S. A. (Buenos Aires, Argentina).Glycerol was purchased from Aldrich, USA. Sodium montmorillonite (Cloisite® Na+) with a cation exchange capacity (CEC) of 92.6 meq/100g clay was supplied by Southern Clay Products (Texas, USA).

Preparation of starch-plasticized films. Native starch was dispersed in distilled water and 30% w/w of glycerol. The suspension was heated to 90ºC for 15 min. The dispersion was poured into rectangular moulds and dehydrated at 50ºC, to constant weight. On the other hand, the montmorillonite (MMT) was dispersed in distilled water by sonication during 10 min at room temperature. The clay dispersion was added to the aqueous dispersion of starch and the mixture was continued to sonicate for another 30 min. **Acetylating treatment.** The starch (15 g) was immersed in a solution of glacial acetic acid (80 ml) and toluene (100ml) at 25ºC, for 4 h. Then was washed and dried at 50ºC. The acetylated starch was stored at room temperature in vacuum desiccators. The films were prepared with 30 wt% of glycerol. **Maleic anhydride treatment.** The starch (20g) was immersed in a solution of maleic anhydride (1.6g) (8%w/starch) with acetone (200ml) at 25ºC, for 24 h, then washed and dried at 50ºC. The films were prepared with 30wt % of glycerol. **Octanoyl starch.** The starch (20g) was immersed in a solution of octanoyl chloride (1.6g) (8%w/starch) with acetone (200ml) at 25ºC, for 24 h, then washed and dried at 50ºC. The films were prepared with 30wt % of glycerol.

Testing performed on starch and films. The specimens were investigated by *X-ray* using a Philips Model PW 1830 X-Ray, from 5 to 60 2θ, with CuKα radiation, at room temperature and a scanning rate of 1º/min (RX). *Infrared Spectroscopy* (FTIR) of specimen were obtained using a Mattson mod Genesis 2, in ATR and DRIFT, using 32 scans at 2cm^{-1} resolution. *The constant relative humidity* environment (rh) was generated with aqueous saturated NaCl solutions (75%rh) (ASTM E 104-85). The starches were dried at 45ºC until a constant weight (m_0). The mass was determinate at different times (m_t). The samples were subjected to *micro-tensile test* on an Instron Universal Testing Machine, Model 1123, at 23ºC and 90% HR. Test specimens were cut using the punch to obtain a dog-bone sample following ASTM D882-97. The crosshead speed was 1mm/min and an extensometer video F.O.V.: 50 mm was used.

3. RESULTS AND DISCUSSION

The effectiveness of chemical treatments was studied by FTIR (Fig 1). The 2933 cm^{-1} peak corresponding to the absorption of the CH_2 group present in the starch does not change with the treatment. Hence, it was used as internal standard. The peak at 1740 cm^{-1} and at 1240 cm^{-1} in esterified starch, indicates the presence of an ester group (C=O and C-O stretching bands). These results confirm the esterification of starch.

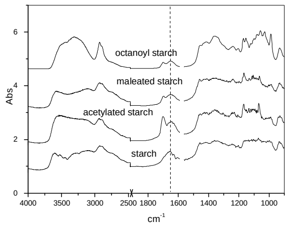

In order to investigate the dispersion of the montmorillonite, X-ray diffraction was performed on the composites (Fig 2). In the composite films the 001 diffraction peak of the MMT (12.1 Å) was shifted to lower angles regardless the clay content. These results should indicate that the glycerol and/or the polymer chains entered into the silicate layers forming intercalated nanocomposites. This could be due to the strong polar interactions between the hydroxyl groups present in the polymer chain, in the glycerol and in the silicate layers (Park et al, 2002).

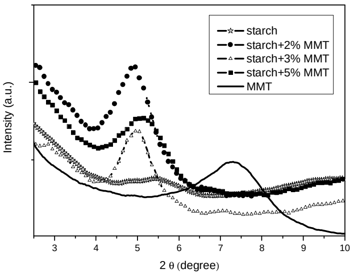

Fig 2. DRX of nanocomposites starch

The moisture content as a function of time was determined in order to measure the equilibrium moisture content (Fig 3a and b) . The percentage increase in weight value (m%) was calculate as follows:

$$m\% = \frac{m_t - m_0}{m_0} \times 100 \qquad (1)$$

where, m_t is a wet weight of starch at each time; m_0 is the initial weight of dry starch. The esterifications produce a decrease in the maximum moisture sorption when the potato starch is in powder. Because this treatments reduces the OH^- concentration and this reduces the maximum water sorption (Fringant, 1997) producing an starch more hydrophobic. The addition of glycerol and gelatinization produce higher water absorption due to a greater interchain distances in the presence of glycerol. The addition of clay improve the water resistance of starch. The reason could be that the starch is able to form hydrogen bonds with the hydroxyls of the MMT layers and this strong structure could reduce the diffusion of water molecules in the material. The clay produces a tortuous path-way and also a diminution of the length of free way for water-uptake.

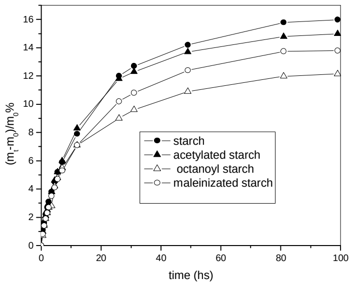

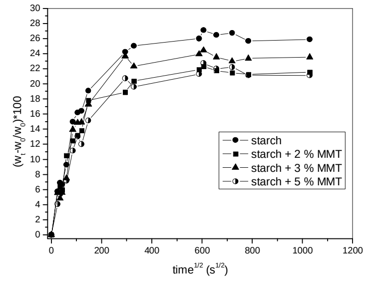

Moisture absorption: Fig. 3a. Esterified starches. Fig. 3b. Nanocomposites.

Mechanical properties resulted from the tensile test are shown in Table 4. It was observed an important increase of 5 and 6-fold in the modulus when 3wt% and 5wt% of MMT was added to the starch, respectively. This behavior was expected and was attributed to the resistance exerted by the clay itself and to the orientation and aspect ratio of the intercalated silicate layers. In addition, the stretching resistance of the oriented backbone of the polymer chain in the gallery bonded by hydrogen interaction also contributed to enhancing the modulus and the stress. The layered silicate acts as a mechanical reinforcement of starch reducing the flexibility of the polymer.

Table 1. Mechanical Properties of nanocomposites.

Sample	Max Stress (MPa)	Young's modulus (MPa)	Deformation at break (%)
starch	3.3 ± 0.4	29.8 ± 4.4	62.6 ± 10.1
+ 2% of MMT	3.1 ± 0.3	29.6 ± 12.1	55.1 ± 17.2
+ 3% of MMT	3.2 ± 0.7	150.5± 25.6	37.6 ± 14.5
+ 5% of MMT	5.2 ± 0.8	195.6±38.6	46.8 ± 19.2

3. CONCLUSIONS

The esterification of starch reduce the water sorption respect to that of the untreated starch, due to hydrophilic character of acetylated and maleated starch is lower than the native starch.

The nanocomposites exhibited a remarkable improvement in the mechanical properties such as Young modulus and tensile stress. However a diminution in the deformation was observed due to the reinforcing action of MMT. The main reason for this improvement in the properties in polymer clay nanocomposites is the strong interfacial interaction between matrix and clay which has a high modulus (170 GPa) and change the morphology of the matrix of starch.

4. ACKNOWLEDGMENTS

The authors thank the financial support of CONICET (PIP nº6254) and SECYT (PICT 12-1560).

5. REFERENCES

BASTIOLI, C. (1995). Starch Polymer Composites. *In Degradable Polymer*. Chapman and Hall: . p 112

CYRAS, VIVIANA P., TOLOSA ZENKLUSEN, M.CAROLINA & VAZQUEZ, ANALÍA. (2006). Relathionship between Structure and Properties of Modified Potato Starch Biodegradables Films". *Journal of Applied Polymer Science.* 101 (6) 15:4313

FRIGNANT, C.; DESBRIERES, J.; RINAUDO, M. (1996). Physical properties of acetylated starch-based materials: relation with their molecular characteristics. *Polymer*, 37, 2663.

FRINGANT, C.; RINAUDO, M.; GRENOBLE, N.; GONTARD, S.; MONTPELLIER; DERRADJI, H. (1998)Biodegradable Starch Based Coating to Waterproof Hydrophilic Materials. *Starch.* 7, 292

HUANG, M., YU, J., MA X. & PENG JIN. (2005). High performance biodegradable thermoplastic starch—EMMT nanoplastics. *Polymer*, 46, 9, 3157

MYLLÄRINEN, P.; PARTANEN, R.; SEPÄALLÄ, J; FORSSELL, P. (2002) Effect of glycerol on behaviour of amylase and amylopectin films. *Carbohydr. Polym.*, 50, 355.

PARK, H.M., LI, X., JIN, C.Z., PARK, C.Y., CHO, W.J. & HA, C.K. (2002) Preparation and properties of biodegradable thermoplastic starch/clay hybrids. *Macromolecular Materials and Engineering,* 287, 553.

PLACKETT D. and VAZQUEZ, A. (2004), In Green Composites. Polymer Composites and the Environmental. Chaper 7: Natural Polymer Source. Ed by Caroline Baillie. CRC Press, Washington, DC. Cambridge. England.. 123-153.

PUKÁNSZKY, B., MÜLLER, P. & BAGDI, K. (2006) Thermoplastic starch/layered silicate composites: structure, interaction, properties. *Composite Interfaces.* 13, 1, 1-17.

CYRAS, V.P.; MANFREDI,L.B.;TON-THAT, MINH-TAN AND VÁZQUEZ, A.. (2008) "Physical and Mechanical Properties of Thermoplastic starch/montmorillonite films" *Carbohydrate Polymers*, 73, 1, 55-63.

Towards self-assembled nanocomposites based on block copolymers containing magnetic nanoparticles

H. Etxeberria, G. Kortaberria, I. Mondragon
'Materials + Technologies' Group, Departamento Ingeniería Química y M. Ambiente,
Escuela Politécnica. Universidad del País Vasco/Euskal Herriko Unibertsitatea

ABSTRACT

Following previous attempts to functionalize magnetic nanoparticles (MN) with acrylic polymers, the functionalization of iron oxide nanoparticles (Fe_3O_4) with polystyrene (PS) brushes via atom transfer radical polymerization (ATRP) 'grafting from' technique has been carried out in order to prepare block copolymer-based nanocomposites. Several poly(styrene)-b-poly(methylmethacrylate) (PS-b-PMMA) block copolymers, with different contents of PMMA are being studied to prepare the nanocomposites. The effect of the nanoparticles and their content in the obtained nanostructures and the influence of the molecular weight of PMMA block is being investigated.

1. INTRODUCTION

During the last years nanocomposites containing nanoparticles have received increasing interest as potential candidates to replace traditional materials. Magnetic nanoparticles in particular have been a subject of extensive research due to their potential applications in many diverse fields like ferrofluids, magnetic resonance imaging contrast enhancement and biological and mineral separation. One significant problem is that magnetic nanoparticles tend to aggregate into large clusters. To overcome this problem nanoparticles surface is functionalised with surfactants or polymer chains which ensures effective control of dispersion.

Self-assembly of block copolymers is an interesting property that is used because of the rich variety of nanostructures that can be generated depending on the nature of the blocks. Nanostructures are generated by the repulsion between the different blocks of the copolymer.

In this work, different attempt to functionalise magnetic iron oxide nanoparticles (Fe_3O_4) have been carried out with polystyrene (PS) brushes via atom transfer radical polymerization (ATRP) "grafting from" technique. PS-PMMA block copolymers with different PMMA contents are being studied to get nanostructured block copolymers for the dispersion of the modified nanoparticles.

2. MAIN RESULTS

Magnetic nanoparticle surface was modified with a silane (2-(4-chlorosulfonylphenyl) ethyl trichlorosilane) (CTCS) that contains an initiator group that allows the polymerisation from the surface of the nanoparticles (Marutani et al. 2004, Garcia et al. 2007). The introduction of CTCS onto MNs is of a great importance for anchoring PS brushes onto the MN surface because the sulfonyl chloride groups of CTCS control the growth of PS chains on the surface. The reaction between hydroxyl groups sited in the surface of the nanoparticle and CTCS was confirmed by Fourier transform infrared spectroscopy (FTIR) (fig. 1). Two new peaks were observed compared to the neat

CTCS FTIR spectrum. The first peak (at 1039 cm^{-1}) is attributed to the formation of new Si-O-Si bonds that indicates a self-condensation reaction to form a polysiloxane film on the iron oxide surface. The second one (situated at 1129 cm^{-1}) is attributed to the MN-O-Si bond that was formed after the reaction. Other peaks that appear in both spectra are assigned to the symmetric stretching of the S=O bond (1337 cm^{-1}) and to the asymmetric stretching of the S=O bond (1178 cm^{-1}). The presence of the silane was also confirmed by thermogravimetric analysis (TGA) (not shown here).

CTCS-MNs were subjected to ATRP. The polymerization of the polystyrene on the surface of the magnetic nanoparticles was followed by FTIR (Ejaz et al. 1998, Sun et al. 2006) and TGA (not shown here). There are three new peaks that were assigned to polystyrene (1600, 1500 and 1450 cm^{-1}) and there is a large increase in the characteristic stretching bands of alkyl and aryl groups (between 3250 cm^{-1} and 2750 cm^{-1}) compared to the CTCS-MNs. The position of the band (Ar-SO_2-Cl) at 1377 cm $^{-1}$ is shifted to 1318 cm $^{-1}$ (Ar-SO_2-R). This displacement was attributed to the influence of the neighbouring groups.

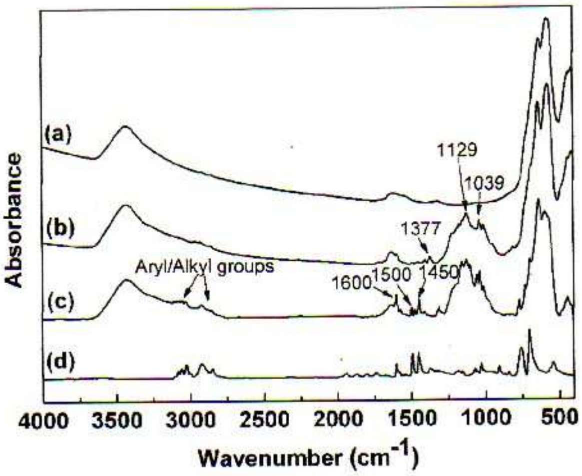

Fig. 1. FTIR spectra of (a) MN, (b) CTCS-MN, (c) PS-MN, and (d) PS.

The formation of nanostructures of the copolymers of PS-b-PMMA was studied by atomic force microscopy (AFM). The copolymers were solved in toluene and deposited onto a silicon wafer by spin-coating using toluene solutions of 3 wt % PS-b-PMMA. The samples were annealed in a vacuum oven at several temperatures and periods of time. As seen in fig. 2. nanostructures are achieved after annealing treatment. Ongoing work is being carried out to achieve different nanostructures using several PS-PMMA block copolymers.

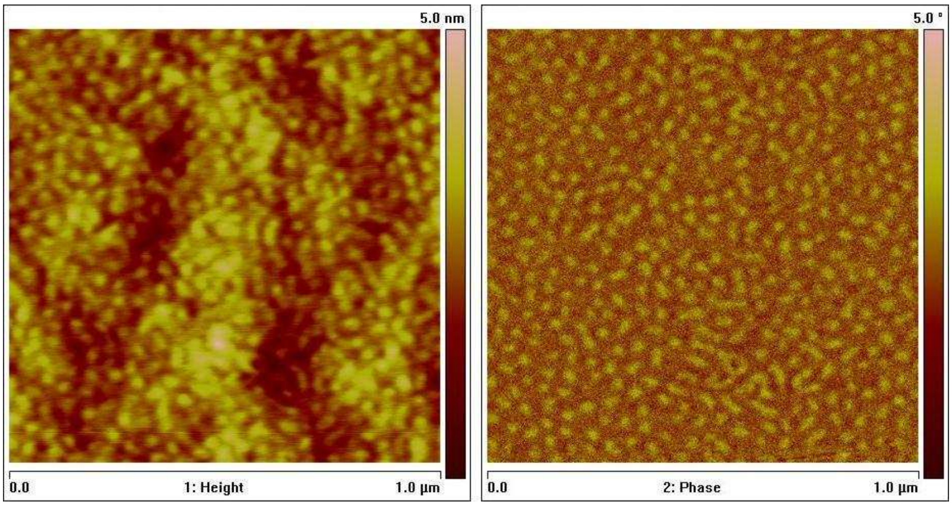

Fig. 2. PS-PMMA block copolymer AFM image [height (left) and phase (right)] after annealing.

Once the nanostructured block copolymers are achieved the next step is to get nanocomposites of MNs with PS brushes and PS-b-PMMA block copolymers compounding both and sonicating before spin coating the samples. The modified MNs will place in the PS block domains because of their affinity (Xu et al. 2008)

3. CONCLUSIONS

Commercial magnetite MNs surface were functionalised using "grafting from" technique by ATRP achieving a corona of PS brushes. Those functionalised MNs were characterized by FTIR and TGA to confirm the presence of PS chains on their surfaces. PS-b-PMMA block copolymers were nanostructurated by annealing and a good dispersion of the modified MNs in the block copolymers was achieved by adding the modified MNs to the block copolymers.

ACKNOWLEDGEMENTS

The authors want to be grateful for the support of Basque Country Government in the frame of Grupos Consolidados (IT-365-07), inanoGUNE (IE08-225) projects and also the Spanish Ministry of Science and Innovation for MAT2006-06331.

REFERENCES

Ejaz, M.; Yamamoto, S.; Ohno, K.; Tsuji Y.; Fukuda, T. (1998) Controlled graft polymerization of methyl methacrylate on silicon substrate by the combined use of the Langmuir-Blodgett and atom transfer radical polymerization techniques, *Macromolecules*, 31, 5934-5936.

Garcia, I.; Tercjak, A.; Zafeiropoulos N. E.; Stamm, M.; Mondragon, I. (2007) Generation of core/shell iron oxide magnetic nanoparticles with polystyrene brushes by atom transfer radical polymerization, *Journal of Polymer Science. Part A: Polymer Chemistry*, 45, 4744-4750.

Marutani, E.; Yamamoto, S.; Ninjbadgar, T.; Tsujii, Y.; Fukuda, T.; Takano, M. (2004) Surface initiated atom transfer radical polymerization of methyl methacrylate on magnetite nanoparticles, *Polymer*, 45, 2231-2235.

Sun, Y.; Ding, X.; Zheng, Z.; Cheng, X.; Hu, X.; Peng, Y. (2006) Surface initiated ATRP in the synthesis of iron oxide/polystyrene core/shell nanoparticles, *European Polymer Journal*, 43, 762-772.

Xu, C.; Ohno, K.; Ladmiral, V.; Russell, J. C. (2008) Dispersion of polymer-grafted magnetic nanoparticles in homopolymers and block copolymers, *Polymer*, 49, 3568-3577.

Composites based on biodegradable thermoplastic starch and carbon nanotubes

L. Famá
LPyMC, Departamento de Física, Facultad de Ciencias Exactas y Naturales.
Grupo de Materiales Avanzados. INTECIN. Departamento de Ingeniería Mecánica.
Facultad de Ingeniería. Universidad de Buenos Aires, Argentina
C. Bernal
Grupo de Materiales Avanzados. INTECIN. Departamento de Ingeniería Mecánica.
Facultad de Ingeniería. Universidad de Buenos Aires, Argentina
S. Goyanes
LPyMC, Departamento de Física, Facultad de Ciencias Exactas y Naturales.
Universidad de Buenos Aires, Argentina

ABSTRACT

Novel nanocomposites were developed adding multi-walled carbon nanotubes (MWCNTs) to a very low cost biodegradable matrix, in order to improve the material viscoelastic and water vapor permeability behaviour. Composite materials were obtained dissolving MWCNTs (wrapped in an aqueous solution of a starch-iodine complex) in a starch matrix. The morphology of the samples was studied by SEM. A vein pattern that became thinner and denser with increasing volume fraction of filler was observed. Moisture content and water vapour permeability were found to increase with carbon nanotubes content. In dynamic mechanical experiments, two different relaxations were observed. These relaxations were found to be sensitive to the introduction of the higher fraction of MWCNTs. An important increment in the storage modulus at room temperature was also found for the composites.

1. INTRODUCTION

Over the last years, there has been increasing interest in the use of biodegradable and low cost packagings based in polymeric materials like starch. However, starch based materials have poor mechanical properties and high permeation in comparison to other polymers. It is well known that the addition of fillers to polymers can lead to an improvement in these properties. Fillers with high modulus are usually employed to increase composites stiffness. Besides, according to tortuous pathway, the presence of the fillers also changes the diffusivity way improving permeation properties. A particular type of fillers, well studied recently due to their high aspect ratio and modulus, is carbon nanotubes; therefore they make ideal materials to employ as reinforcement in starch.

In this research, starch-MWCNTs composites were developed and different properties associated with their use as packaging materials were studied.

2. MATERIALS AND METHODS

Biodegradable starch matrix composites have been prepared using different weight fractions (ϕ_f, 0 wt.%, 0.027 wt.% and 0.055 wt.%) of multi-walled carbon nanotubes (MWCNTs) as filler. As carbon nanotubes are not soluble in an aqueous solution of stach, an aqueous solution of a starch-iodine complex was used to wrap the nanotubes (Star et al., 2003). The appropiate amount of filler was incorporated into the starch-iodine complex (93 wt.%) and the mixture was sonicated in an ultrasonic bath for 1 h. Tapioca starch (4.5 wt.%) and glycerol as plasticizer (2.5 wt.%) were added to the system, wich was heated at ~ 3°C/min, till the mixture achieved a temperature 5 % higher than the temperature of gelatinization. The gel was degassed for 10 min., distributed in plastic dishes and dried at 52°C for 24 h. Samples with thickness of 0.26 ± 0.01 μm were obtained.

Cryogenic fracture surfaces of the different materials were studied by means of field emission scanning electron microscopy (FE-SEM). Moisture content was determined by the oven drying method at 100 ºC for 24 h (AOAC, 1995). The crystalline fraction was also determined from X-Ray diffraction patterns and water vapor permeability (WVP) at 25ºC was obtained using a modified ASTM E96-00 (1996) procedure.

The rheological behaviour of the different materials was characterized using a Dynamic Mechanical Thermal Analyser (DMTA IV) equipment in the Regular Tension mode at 1 Hz, in the temperature range between -100°C and 25ºC, at a heating rate of 2 °C/min.

3. RESULTS

Fig. 1 shows FE-SEM micrographs of the samples studied. For the composites (Fig. 1 b and c) a well-developed vein pattern can be observed, suggesting that the residual amorphous matrix controlled the fracture behaviour. The space between veins was found to decrease with filler content. This result is similar to that observed in materials containing nanocrystals (Bian et al., 2002), where the vein pattern becomes thinner and denser with increasing volume fraction of nanocrystals.

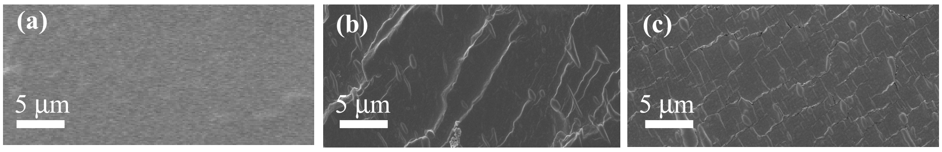

Fig. 1. SEM micrographs of the cryogenic fracture surface of the matrix (a) and the composites with 0.027 wt.% (b) and 0.055 wt.% (c) of MWCNTs.

The X-ray diffraction patterns of the composites only differed from those of the matrix in the peak placed around 2θ =24. This peak is more evident in the composite with the highest filler content investigated (ϕ_f = 0.055 wt.%). The presence of this peak leads to an increase in the crystalline fraction of the composites. However, it should be notes that are not differences in the matrix crystalline fraction.

Moisture content and WVP were found to decrease as the fraction of carbon nanotubes increased as it can be seen in Table 1. The same trend was observed for the moisture content when it was normalized by the matrix weight. This suggests that the addition of MWCNTs modified the quantity of available OH.

ϕ_f (wt.%)	Moisture content (%)	WVP x10^{-10} (g/smPa)
0	37.5 ± 0.4	2.8 ± 0.1
0.027	36.5 ± 0.2	2.3 ± 0.1
0.055	34.6 ± 0.8	1.6 ± 0.1

Table 1. Moisture content and WVP.

The decrease in WVP values with filler concentration is expected taking into account the theory of tortuous pathway of composite materials (Matayabas, 2000).

Fig. 2a and b, shows the dependence of loss tangent (*tan δ*) and storage modulus (*E'*) with temperature for the different materials investigated. It can be observed in *tan δ* curves, that the relaxation peak around -60 °C associated with the glycerol-rich phase (T_g) did not shift horizontally with the addition of a small amount of MWCNTs, but its width was found to decrease. This result suggests that the presence of carbon nanotubes did not change the distribution of glycerol in the matrix, but they also restricted the movements responsible for friction (relaxation movements). However, the filler strongly modified the transition observed in the matrix around 0 ºC, broadening and diminishing its intensity. This effect was well-developed in the composite with 0.055 wt.% of MWCNTs, and might be associated with the decreased water content of this material (Table 1). Following García et al. (2009), this relaxation may be associated with a rearrangement of amorphous starch chains in the presence of moisture. The peak was more evident as the water content increased. Therefore, the lower intensity of this peak in the composite with 0.055 wt.% of filler is expected taking into account the lower moisture content of this material.

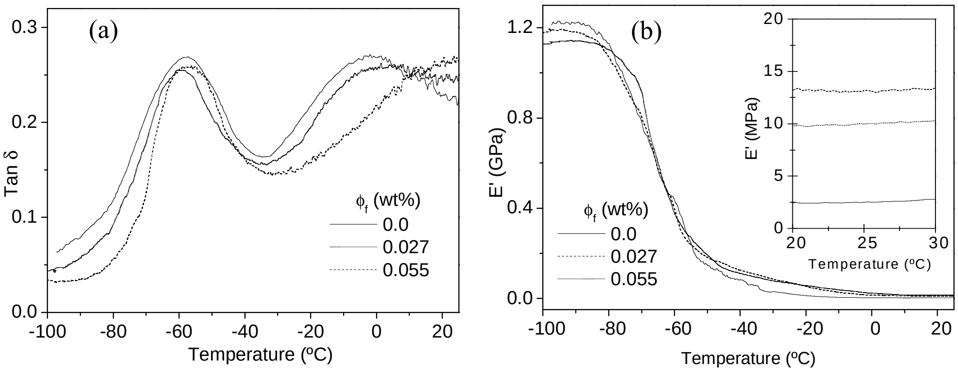

Fig. 2. (a) Tan δ and (b) E' as a function of temperature.

As it can be observed in Fig 2 (b), the addition of carbon nanotubes to starch also changed the dependence of storage modulus with temperature. *E'* showed a slight decrease in the glassy zone, while a strong increment in its value was observed in the rubbery zone. The filler had a greater effect in raising the modulus above the T_g than below it. This difference could be explained considering that filled systems are never perfectly dispersed, because always exist some agglomerated particles. Below T_g the polymer can exert large forces on the agglomerates due to its high modulus, so a great deal of nanotubes–nanotubes motion is expected to occur. However, above T_g, the forces may be not strong enough to overcome the friction at contact points breaking up the agglomerates. When there is no slippage ($T > T_g$), the agglomerate plus some immobilized polymer act as a single unit, while when slippage can occur ($T<T_g$), the flow units becomes smaller and less polymer is immobilized between nanotubes (Goyanes et al., 2000).

3. CONCLUSIONS

The incorporation of multi-walled carbon nanotubes into the starch matrix changed the composite morphology showing a well-developed vein pattern that became thinner and denser with increasing filler content. The addition of only 0.055 wt.% of MWCNTs led to a decrease in the moisture content of 7.7 % and in the WVP of around of 43 %. Furthermore, the composites exhibited at room temperature *E'* values approximately 63 % higher than that of the starch matrix. The relaxations observed in $\tan\delta$ curves were sensitive to the introduction of carbon nanotubes, suggesting that they are not a relocation of the main plasticizer with the addition of the filler. These results would show that the starch-MWCNTs nanocomposites developed in this work have an important advantage for their use as intelligent packaging.

ACKNOWLEDGEMENTS

The authors acknowledge the financial support of UBA, CONICET and ANPCyT.

REFERENCES

ASTM Standar test methods for water vapor trasmission of material, E96-00 (1996) Anual book of ASTM, American Society for Testing and Materials, Philadelphia, USA.

BIAN Z., HE G., CHEN G.L. (2002) Investigation of shear bands under compressive testing for Zr-base bulk metallic glasses containing nanocrystals. *Scripta Material* 46, 407-412.

GARCÍA, N.L., RIBBA, L., DUFRESNE, A., ARANGUREN, M., GOYANES, S. (2009). Physico-mechanical properties of biodegradable starch nanocomposites. *Macromol. Mat. Eng*. In press

GOYANES, S.N., MARCONI, J.D., KONIG, P.G., MARTIN, M.D., MONDRAGÓN, I. (2000) Dynamic properties of epoxy composites filled with quartz powder. *J. Alloy Comp* 310, 374-377

MATAYABAS, J.C., TURNER, S.R. (2000). Nanocomposite technology for enhancing the gas barrier of polyethylene terephthalate, *in Polymer-Clay Nanocomposites* (Ed Pinnavaia, T.J., Beall, G.W), 207-226, Wiley, J. & Sons, Ltd., England.

Official Methods of Analysis of AOAC International. 950.46 (1995) 16th Ed., AOAC International, Gaithersburg, MD, USA.

STAR, A., LIU, Y., GRANT, K., RIDVAN, L., STODDART, J.F., STEUERMAN, D.W., DIEHL, M.R., BOUKAI, A., HEATH, J.R. (2003) Noncovalent side-wall functionalization of single-walled carbon nanotubes. *Macromolecules* 36, 553-560.

Mechanical behaviour of starch-based nanocomposites

L. Famá
LPyMC, Departamento de Física, Facultad de Ciencias Exactas y Naturales.
Grupo de Materiales Avanzados, INTECIN (UBA-CONICET). Departamento de Ingeniería Mecánica. Facultad de Ingeniería. Universidad de Buenos Aires, Argentina
V. Pettarín
División Polímeros, INTEMA (UNMdP-CONICET), Departamento de Ing. en Materiales, Universidad Nacional de Mar del Plata, Mar del Plata, Argentina
S. Goyanes
LPyMC, Departamento de Física, Facultad de Ciencias Exactas y Naturales.
Universidad de Buenos Aires, Argentina
C. Bernal
Grupo de Materiales Avanzados, INTECIN (UBA-CONICET). Departamento de Ingeniería Mecánica. Facultad de Ingeniería. Universidad de Buenos Aires, Argentina

ABSTRACT

In this work, novel nanocomposites based in tapioca starch polymer reinforced with multi-walled carbon nanotubes (MWCNTs) were developed. The effect of the addition of small fractions of MWCNTs (0.027 wt.% and 0.055 wt.%) in the quasistatic tensile and in the biaxial impact response of the nanocomposites was investigated. An aqueous solution of starch-iodine complex was used to wrap the filler before adding it to the polymer. Under both loading conditions investigated, the nanocomposites exhibited improved mechanical behaviour in comparison to the starch matrix. In addition, it was observed that carbon nanotubes were properly wrapped by the starch-iodine complex used. From the above findings, good dispersion of individual nanotubes or bundle of them in the starch matrix and adequate adhesion between phases could be expected.

1. INTRODUCTION

Over the last few years, a number of researchers investigated the use of different fillers in composite materials with the object of improving mechanical properties of packaging. Due to shortage or relatively high price of traditional materials, starch is viewed as an alternative source by companies for its use in biodegradable formulations for packaging. In addition, offering attractive mechanical properties, carbon nanotubes have been the object of interest due to their wide scope of possible applications such as composite reinforced materials (Smith et al., 2003) constituting a potential system to achieve a significant improvement in bulk properties.

The objective of this research was to study the influence of the addition of small fractions of MWCNTs in the bulk mechanical behaviour of nanocomposites through the evaluation of the quasistatic uniaxial tensile and the biaxial impact response of the materials.

2. MATERIALS AND METHODS

Carbon nanotubes are not soluble in an aqueous solution of starch hence, an aqueous solution of a starch-iodine complex was used to wrap them before they were incorporated into the polymer. Iodine is expected to preorganise the backbone of the amylose in starch into a helical conformation and to make its hydrophobic cavity accessible to a single carbon nanotube or bundles thereof (Star et al., 2003). Starch-iodine complex was prepared by stirring 0.5 % starch in distilled water with saturated iodine for 5 min at room temperature and then stabilised during one night. The proper amount of MWCNTs was inmersed in 93 wt.% of the starch-iodine complex and the mixture was sonicated in an ultrasonic bath for 1 h.

Biodegradable starch matrix composites were prepared using different weight fractions of MWCNTs as filler (ϕ_f, 0 wt.%, 0.027 wt.% and 0.055 wt.%). Tapioca starch (4.5 wt.%) and glycerol as plasticizer (2.5 wt.%) were added to the system with the proper amount of nanotubes dispersed in the aqueous solution of the starch-iodine complex. The mixture was heated at ≅ 3 °C/min, till a temperature 5 % higher than the temperature of gelatinization was reached. After gelatinization, the gel was degassed (10 min.), distributed in petris and dried 24 h at 52 °C. Samples were conditioned over NaBr ($a_W \cong 0.575$ at 25 °C) before characterisation. Sample thickness (e) was 0.26 ± 0.01 µm.

MWCNTs wrapped with the aqueous solution of the starch-iodine complex were observed using scanning electron microscopy (FE-SEM) at 130 KX.

Mechanical properties of the different materials were characterized by uniaxial tensile and biaxial impact tests. Uniaxial tensil tests were carried out in an Instron dynamometer at 2.10^{-5} m/s following ASTM 638-02 standard recommendations. Biaxial impact tests were performed using a falling weight Fractovis of Ceast at 3 m/s. The thickness related perforation energy (U/e) was obtained by numerical integration of the load-displacement curves. Disc maximum strength (σ_d) was evaluated as $\sigma_d = 2.5\frac{P_{\max}}{e^2}$, where P_{max} is the maximum load attained in the test.

3. RESULTS

3.1 Morphology of carbon nanotubes

Fig. 1a and b shows SEM micrographs of the MWCNTs dispersed in alcohol and in the aqueous solution of starch-iodine complex, respectively. It can be seen in this figure, that MWCNTs dispersed in the starch-iodine complex (Fig 1 (b)) are coarser than the original ones, confirming that they were properly wrapped as expected. The irregularity observed in their walls can be attributed to the form of the amylopectin of the starch used to wrap them.

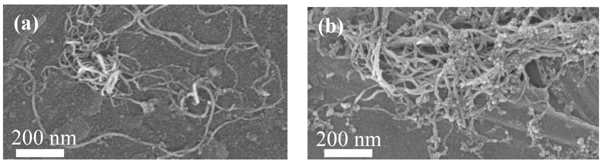

Fig. 1. SEM micrographs of MWCNTs dispersed in alcohol (a) and in the aqueous solution of the starch-iodine complex (b). (At 130 KX)

3.2 Mechanical response of nanocomposites

Figure 2 shows typical nominal stress-strain curves obtained under quasistatic tensile loading conditions. All materials exhibited non-linear behaviour until failure with a precipitous drop of load at the maximum stress with no necking before fracture.

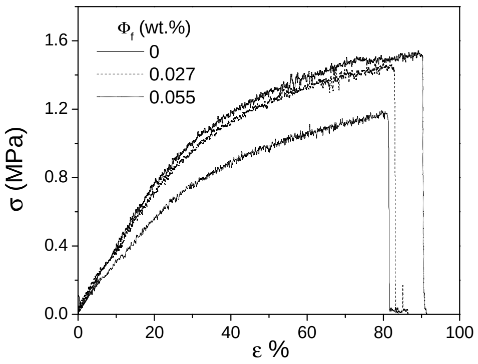

Fig. 2. Typical nominal stress-strain curves for the matrix and the composites.

Table 1 lists tensile parameter values for the matrix and the different nanocomposites investigated. A significant improvement in stiffness (E) and tensile strength (σ_u) values was found with the incorporation of the carbon nanotubes to the starch matrix without any loss in ductility (moreover, strain at break values also increased). In addition, this improvement was higher as the nanotubes content increased. Consequently, tensile toughness also increased for the nanocomposites and with filler loading.

ϕ_f (wt.%)	E (MPa)	σ_u (MPa) [± 0.02]	Tensile toughness x 10^{-5} (J/m^3)
0	2.56 ± 0.02	1.15	6.4 ± 0.1
0.027	3.55 ± 0.08	1.44	8.4 ± 0.1
0.055	3.91 ± 0.04	1.52	9.9 ± 0.1

Table 1. Tensile parameter values for the materials investigated.

Force-displacement traces obtained under biaxial impact conditions are shown in Fig. 3. Typical macrophotographs of the impacted area of a matrix sample and a composite are also included in Figure 3, as an example. All the samples exhibited semi-brittle fracture behaviour as judged from the non-linear load-deflection records which dropped to zero immediately upon reaching the maximum load (Fig. 3 (A)). Some radial cracks responsible for the final failure of specimens (Fig. 3 (B)) were observed around the hole area in impacted samples.

Thickness related perforation energy (U/e), disc maximum strength (σ_d) and maximum displacement (d_{max}) values are reported in Table 2. All these parameters significantly increased with filler content, showing that the addition of even a very small fraction of carbon nanotubes to the biodegradable matrix is an efficient way to improve the impact fracture behaviour.

Fig. 3. (A) Impact load-displacement curves for the different materials. (B) Macrophotograph of impacted discs.

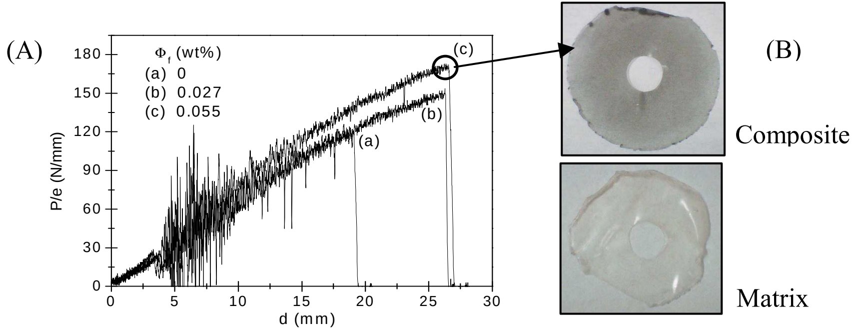

ϕ_f (wt.%)	*U/e* (N/mm^2)	σ_d (N/mm^3) [± 2]	d_d (mm) [± 0.2]
0	1212.3	3225	19.0
0.027	2174.2	6040	26.2
0.055	2577.8	6324	26.8

Table 2. Parameters obtained under biaxial impact conditions.

3. CONCLUSIONS

The mechanical properties of starch-MWCNTs nanocomposites showed an increasing trend with filler content under both quasistatic uniaxial tensile and biaxial impact conditions. In addition, carbon nanotubes were found to be properly wrapped by the starch-iodine complex used to preparate the composites. Hence, a homogeneous distribution of carbon nanotubes or bundle of them in the matrix and a suitable interaction between carbon nanotubes and starch could be expected in our nanocomposites. Thus, a successful method to develop novel nanocomposites based on a biodegradable polymer and carbon nanotubes was found and the incorporation of MWCNTs seems to be an efficient mean of improving bulk mechanical properties.

ACKNOWLEDGEMENTS

The authors acknowledge the financial support of UBA, CONICET and ANPCyT.

REFERENCES

SMITH, B.W., LUZZI, D.E. (2003) Carbon nanotubes *in Introduction to Nanoscale Science and Technology* (Ed Ventra, M.D., Evoy, S., Heflin, J.R.Jr.), 172-182, USA.

STAR, A., LIU, Y., GRANT, K., RIDVAN, L., STODDART, J.F., STEUERMAN, D.W., DIEHL, M.R., BOUKAI, A., HEATH, J.R. (2003) Noncovalent side-wall functionalization of single-walled carbon nanotubes. *Macromolecules* 36, 553-560.

Preparación de nanocomposites PP-nanotubos/nanofibras de carbono para la fabricación de fibras textiles con propiedades de apantallamiento electromagnético

J. Pascual[1], E. Fages[1], O. Fenollar[2], L. Sánchez-Nacher[2], R. Balart[2]
[1]Instituto Tecnológico Textil (AITEX), Pl. Emilio Sala 1, 03801, Alcoy, Spain
[2] Instituto de Tecnología de Materiales (ITM), Universidad Politécnica de Valencia (UPV), Plaza Ferrandiz y Carbonell 1, 03801, Alcoy, Spain

RESUMEN

En los últimos años se ha trabajado intensamente en el campo de la adición de partículas de tamaño nanométrico en matrices poliméricas con el fin de incrementar sus prestaciones. El potencial incremento de estas prestaciones está en relación con la elevada superficie específica que presentan las nanopartículas, lo cual permite un alto grado de interacción con la matriz en la que se encuentran inmersas. Una de las posibilidades que brindan algunas partículas nanométricas, tales como los nantubos y las nanofibras de carbono, son las de conseguir aumentos significativos en la conductividad eléctrica del polímero.

Los resultados obtenidos muestran cómo la dispersión de las nanopartículas en la matriz polimérica se ha llevado a cabo de forma satisfactoria, quedando las partículas bien dispersas y de forma homogénea en toda la superficie del material. Es importante resaltar la mejora en las propiedades mecánicas resistentes que se obtienen y en cuanto a su comportamiento térmico, tenemos que la adición, tanto de nanotubos como de nanofibras, aumenta de forma importante la estabilidad térmica a altas temperaturas y retrasa la temperatura de inicio de procesos de degradación termo-oxidativa.

1. INTRODUCCIÓN

Los nanotubos y nanofibras de carbono son una nueva generación de materiales que presentan unas propiedades superiores a los materiales convencionales. Los nanotubos de carbono (CNTs) son unos materiales formados por carbono, donde la unidad básica es un plano grafítico enrollado que forma un cilindro, formando unos tubos cuyo diámetro es del orden de algunos nanómetros. Las nanofibras de carbono (CNFs) por su parte, se consideran como materiales intermedios entre las fibras de carbono convencionales y los nanotubos, desarrolladas con objeto de producir unas fibras de carbono de tamaño nanométrico alternativas a los nanotubos, más económicas y con la posibilidad de ser producidas en grandes volúmenes, puesto que el interés que suscitan debido a sus múltiples posibles aplicaciones, ha provocado que se haya trabajado en optimizar y trasladar su proceso de producción a nivel industrial. (COLEMAN 2006, COLEMAN 2006, GRADY 2002, MA 2003)

El interés en estos productos radica en sus excelentes propiedades mecánicas, alta conductividad térmica y eléctrica y su buena estabilidad a altas temperaturas, lo que hace de este tipo de fibras un material muy interesante para ser empleado como refuerzo de polímeros. Sin embargo, los materiales compuestos que se ha conseguido obtener hasta la fecha presentan unas propiedades muy inferiores a las inicialmente esperadas, debido a la naturaleza de los materiales y la elevada incompatibilidad existente entre la

matriz polimérica y el nano-refuerzo. Ésta provoca la aglomeración de la nanofibra y la formación de una interfase polímero-nanofibra de malas propiedades mecánicas, donde la transferencia de tensión entre la matriz y el refuerzo no es efectiva.
El objetivo de este trabajo es evaluar la influencia en las propiedades mecánicas y térmicas de la incorporación de distintas cantidades tanto de nanofibras de carbono (CNFs) GANF como de nanotubos de carbono (CNTs) a una matriz de polipropileno (PP), ampliamente utilizado en la fabricación de fibras textiles, mediante un proceso de extrusión de doble husillo co-rotante. Esta fase se plantea como etapa previa en la obtención de fibras textiles de alto rendimiento mecánico y térmico a partir de la modificación mediante la incorporación de estos aditivos base carbono.

2. EXPERIMENTAL

Se ha efectuado un análisis mediante termogravimetría analítica para estudiar los procesos de degradación y estabilidad térmica a altas temperaturas. Además, se han llevado a cabo de ensayos de tracción, que permiten determinar parámetros resistentes fundamentales como el módulo de elasticidad, el alargamiento a rotura y la tensión de rotura. La caracterización mecánica se ha llevado a cabo según la norma UNE-EN ISO 527-1 y 4. Esta caracterización se realiza siguiendo la norma citada en una máquina universal de ensayos IBERTEST ELIB 30 (S.A.E. Ibertest, Madrid, España) a una velocidad de 20 mm min-1 a temperatura ambiente. Los ensayos de caracterización de la estabilidad térmica y procesos de degradación de las mezclas de PP con nanofibras y con nanotubos de carbono se han llevado a cabo con una balanza termogravimetrica con una célula de medida Mettler-Toledo 1100 TG (Mettler-Toledo Inc., Schwerzenbach, Switzerland), perteneciente al conjunto de técnicas de análisis térmico integrables de la serie STAR e-2000.

3. RESULTADOS Y DISCUSIÓN

Los resultados para las mezclas de PP con nanofibras de carbono revelan un incremento sustancial en el inicio de degradación y pérdida de peso a altas temperaturas. El PP virgen presenta un inicio de degradación sobre los 290 ºC, medido como temperatura en la que se produce la caída del 1% del peso sobre la caída de peso total. Este valor aumenta de forma lineal con el incremento de la cantidad de nanofibras GANF, hasta alcanzar un valor máximo de 443ºC para el contenido de nanofibras del 5%wt. Para cantidades mayores, 10 y 20%wt, esta temperatura desciende ligeramente, produciéndose un efecto contrario al deseado. Destacar el residuo de material que queda después de llevar el material hasta los 800 ºC. A esta temperatura, el PP se ha volatizado totalmente, con lo que el único residuo posible es la carga de nanofibras.

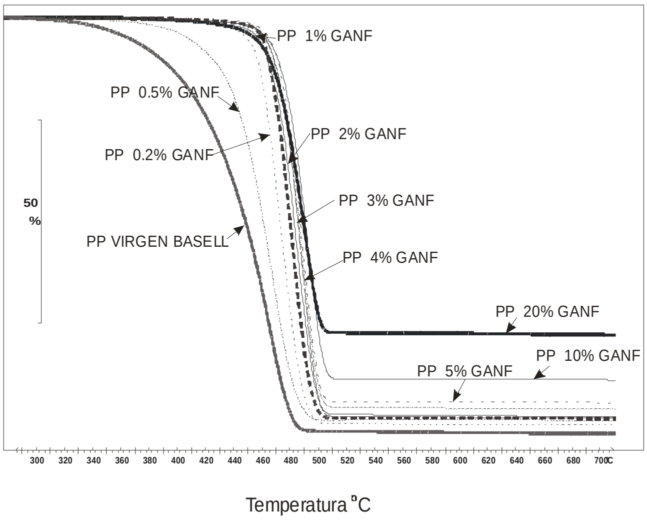

Fig 1. Influencia de la cantidad de GANF en el comportamiento térmico a altas temperaturas de los composites PP-GANF.

La tensión de rotura inicial del polipropileno, en torno a 27,9 MPa, se incrementa de forma apreciable hasta valores en torno a 32-33 MPa con el empleo de diferentes contenidos en nanofibras de carbono (CNFs) comprendidos entre 0,2% y 5%. A partir de este contenido, se aprecia una disminución de la tensión de rotura. Con un 10% de CNFs la tensión de rotura ya no mejora sino que disminuye ligeramente y sobre todo es con un 20% donde se aprecia la mayor reducción de la tensión de rotura que alcanza incluso valores inferiores a los iniciales de la matriz de polipropileno.

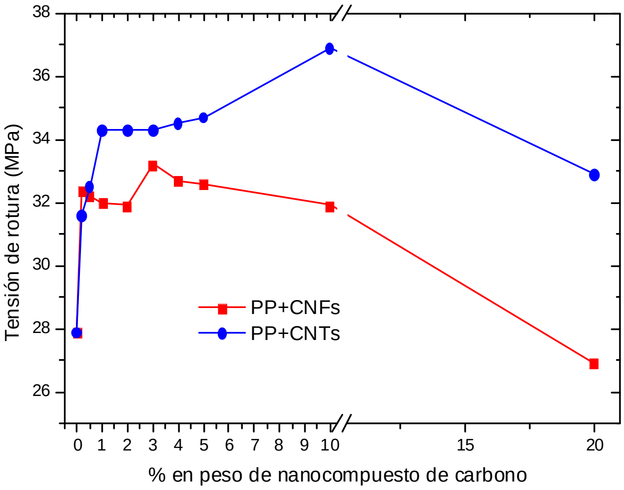

Fig 2. Gráfico de la evolución de la tensión de rotura de los composites PP con diferentes nanocompuestos de carbono.

En relación al comportamiento de los compuestos con nanotubos de carbono (CNTs), la evolución es similar. La incorporación de pequeñas cantidades mejora ligeramente la tensión de rotura (con un 0,2% se consigue incrementar la tensión de rotura hasta valores cercanos a 32 MPa) y relamente para valores comprendidos entre 1% y 5% se consigue una tensión de rotura en torno a 34 MPa. En este caso, la tendencia creciente se mantiene hasta el 10% de CNTs que permite alcanzar una tensión de rotura en torno a 37 MPa. En este sentido, existe una buena cohesión – interacción entre la matriz y los nanotubos de carbono hasta un 10% en peso. A partir de esta composición, se produce un deterioro de la tensión de rotura debido a la dificultad de procesado de estos materiales en tanto en cuanto el volumen específico de los nanotubos es muy elevado y aunque en peso represente solo un 20%, en volumen representa unos niveles muy elevados y ello da lugar a la formación de agregados no coherentes con la matriz polimérica.

4. CONCLUSIONES

La utilización tanto de nanotubos como de nanofibras de carbono confieren al polipropileno una mejora significativa en su comportamiento térmico. En cuanto a los procesos termo-oxidativos, los mejores resultados se dan en el caso de máxima carga de nanofibras y nanotubos (20% en peso). Por lo que respecta a la degradación a altas temperaturas, la incorporación de un 5% de GANF y un 10% de CNT ofrecen los mejores resultados en cuanto a retraso en el inicio de la degradación.

En lo que respecta al comportamiento mecánico, en este caso, la incorporación de cargas hace que aumente ligeramente el comportamiento a rotura del material. Los máximos valores se dan en el caso de cantidad de carga del 10%, tanto en el caso de los nanotubos como en las nanofibras. Para cantidades del 20%, además presentar importantes problemas de procesabilidad, las propiedades mecánicas presentan un descenso importante. El incremento más significativo se da en el caso del módulo de elasticidad, llegando a doblar los valores del módulo de elasticidad con un 5-10% de cargas nanometricos.

AGRADECIMIENTOS

Los autores agradecen al “Ministerio de Ciencia y Tecnología” Ref: DPI2007-66849-C02-02 por la financiación recibida para el desarrollo de este trabajo de investigación.

REFERENCIAS

J.N COLEMAN, ET AL., Carbon. 44(9): p. 1624-1652(2006).
J.N COLEMAN, AND Y.K. GUN'KO, Advanced Materials. 18(6): p. 689-706(2006).
P GRADY. ET AL., Journal Of Physical Chemistry B. 106(23): p. 5852-5858(2002).
H.M MA ET AL., Composites Science And Technology. 63(11): p. 1617-1628(2003).

Antibacterial effect of nanosilver particles as fillers for polypropylene matrices

E. Fagés[1], J. Pascual[1], D. García-Sanoguera[2], R. Balart[2], L Sánchez-Nácher[2]
[1]Textile Research Institute (AITEX), Plaza Emilio Sala 1,
03801, Alcoy, Alicante (Spain)-efages@aitex.es; *jpascual@aitex.es*
[2]Materials Technology Institute (ITM), Polytechnic University of Valencia
Plaza Ferrándiz y Carbonell s/n, 03801, Alcoy, Alicante (Spain)
- dagarsa@dimm.upv.es; rbalart@mcm.upv; lsanchez@mcm.upv.es

SUMMARY

The overall effect of nanosilver particles as fillers for polypropylene matrices is studied in this work. Optimum dispersion of nanoparticles is needed in order to obtain the maximum specific surface to achieve antimicrobial behavior. In this work, dispersion of nanosilver particles is evaluated by transmission electron microscopy (TEM). The overall results show good antibacterial efficiency against staphylococcus aureus and escherichia coli.

1. INTRODUCTION

In the recent years it has been detected a growing interest on the knowledge regarding the risks associated to continuous exposure to bacterial contamination. So that, many industrial and technological sectors have introduced new multifunctional additives to optimize formulations in order to minimize health damage; so we can find these additives in different products such as clothes, liquid soaps, paper, polymeric materials and medical devices. Silver has been widely used as antibacterial additive in last decades. Nevertheless, the use of this antibacterial agent has been carried out at a micro-scale range. Recently, some processes have been developed to obtain nanosilver particles which offer new interesting possibilities. (JEONG 2005, BOITEUX 2006, DAMM 2008, HAN 2007, LIANG 2007, MORONES 2005, SHRIVASTAVA 2007).

In this research work we have evaluated the multifunctional properties of composites based on the use of a polypropylene matrix and different nanosilver particles as additives for antibacterial purposes. Dispersion of nanosilver particles is one of the main parameters to be controlled in order to obtain the optimum specific surface and subsequently, enhance optimum antibacterial behavior. So that, TEM techniques have been used to study the dispersion level. Also, antibacterial behavior against staphylococcus aureus and escherichia coli is evaluated.

2. EXPERIMENTAL

As polymer matrix, a polypropylene commercial grade Moplen HP561S (Basell Polyolefins) has been used. Nanosilver fillers used in this study were S2-30 (particle size between 25-45nm) and S2-80 (particle size in 30-80 nm range) supplied by Nanodynamics, Inc.

Composites were prepared by a co-rotating extruder system ZSK 18 MEGAlab, by Coperion.

TEM analysis was performed on a JEOL mol. JEM-2010.

Antibacterial properties against sthapylococcus aureus ATCC 6538 and esherichia coli ATCC 8379 were evaluated following the guidelines of the JIS Z 2801:2006 y JIS L 1902:2002.

3. RESULTS ANS DISCUSSION

Dispersion of nanoparticles is one of the main parameters in order to obtain maximum specific surface and subsequently, antibacterial activity. TEM analysis shows intermediate dispersion of nanosilver particles (Figure 1), for both particle sizes (30 and 80).

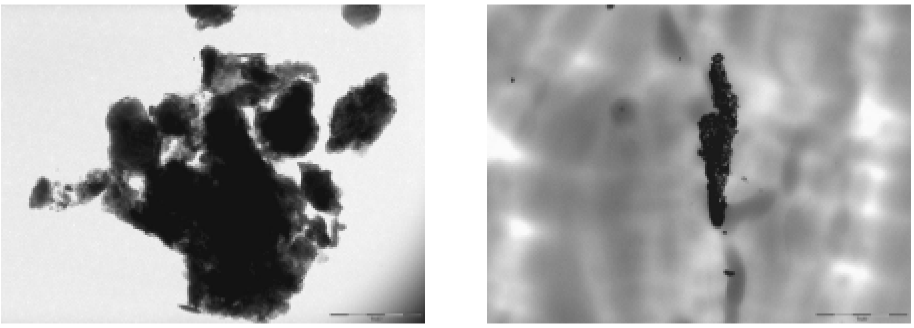

Fig 1. TEM microphotographs of PP-nanosilver (2% w/w) composites extruded at 500 rpm (5200x). a) nanosilver particles S2-30, b) nanosilver particles S2-80.

As it can be observed in Figure 1, presence of aggregates is evident. One of the parameters to be controlled is the extrusion rate. Optimum dispersion results are obtained for low extrusion rates in the 200-300 rpm range

Regarding antibacterial performance of composites, it is important to remark that there are many variables influencing this behavior; among this wide variety, nanosilver content and dispersion are the main parameters. As the nanosilver content increases, the antibacterial efficiency increases; furthermore, optimum dispersion of nanoparticles will provide maximum specific surface thus leading to optimum antibacterial properties.

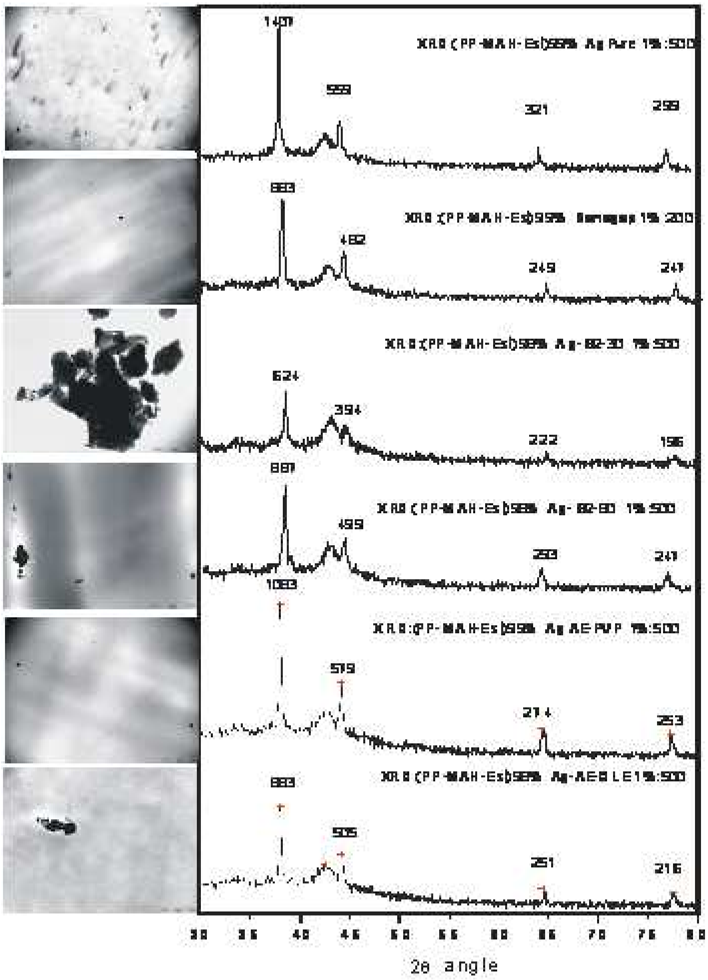

Fig 2. TEM microphotographs with XRD analysis of PP-nanosilver (2% w/w) composites extruded at 500 rpm (5200x) with different nanosilver particles.

The antibacterial effects can be observed in Figure 3 which shows the antimicrobial activity of PP-nanosilver composites with different amount of nanosilver particles and different particle size. Antimicrobial activity is defined as strong for values higher than 3, significative for values ranging from 1 to 3, slight for values comprised between 0.5 and 1 and non significative for values lower than 0.5. As it can be observed, antibacterial activity is higher for small particle size (1 PP-Ag ND and5 PP Ag ND) with values close to 3, and even higher, for both sthapylococcus aureus and esherichia coli. Regarding the amount of nanosilver particles, as expected, better results are obtained for 2% w/w (1 PP-Ag ND and 6 PP Ag ND). The overall results also show better antimicrobial activity against sthapylococcus aureus than to esherichia coli.

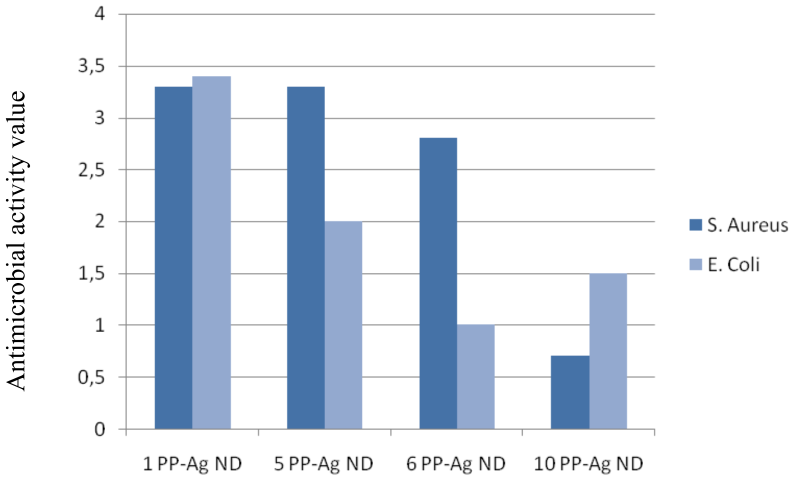

Fig 3. Antimicrobial activity of PP-nanosilver composites. 1PP-Ag ND (2% w/w, S2-30 particles), 5PP-Ag ND (2% w/w, S2-30 particles), 6PP-Ag ND (2% w/w, S2-80 particles), 10PP-Ag ND (2% w/w, S2-80 particles).

4. CONCLUSIONS

The effect of nanosilver particles on the overall antimicrobial behavior of PP-nanosilver composites is interesting. The amount of nanosilver needed to obtain significative activity is about 1% w/w and excellent behavior is detected for higher amounts (2% w/w). Regarding particle size, optimum results are obtained for particle diameters ranging from 30 to 45 nm. Furthermore, TEM analysis revealed presence of individual and small nanosilver clusters and some big aggregates. Despite this, good antimicrobial properties are obtained thus showing that nanosilver addition is an efficient method to increase antibacterial behavior of polymer matrices.

ACKNOWLEDGEMENTS

Authors thank “Ministerio de Ciencia y Tecnología”, Ref: DPI2007-66849-C02-02 for financial support.

REFERENCES

JEONG, S. H.; HWANG, Y. H.; YI, S. C., J. Mater. Sci. 40, 5413 2005.
BOITEUX, G.; BOULLANGER, C.; CASSAGNAU, Macromol. Symp. 233, 246 2006.
DAMM, C.; MUNSTEDT, H.; ROSCH, A., Mater. Chem. Phys. 108, 61 2008.
HAN, J. K.; SAITO, F.; LEE, B. T., Mater. Lett. 61, 4177 2007.
LIANG, G. D.; C., Mater. Sci. Eng. B-Solid State Mater. Adv. Technol. 142,55 2007.
MORONES, J..; ELECHIGUERRA, J..; KOURI, J. B.; Nanotechnology 16, 2346 2005.
SHRIVASTAVA, S.; BERA, T.; ROY, A.; SINGH, P.; Nanotechnology 18, 9 2007.

Policondensación interfacial de melamina-formaldehido para microencapsulado de PCM's para obtener materiales termorreguladores

M.L. González, S. Pavón, B.González, A. Valea
Departamento de Ingeniería Química y del Medio Ambiente, Escuela Universitaria de Ingeniería Técnica Industrial, UPV/EHU
Plaza de la Casilla, 3, 48012 Bilbao
marialuz.gonzaleza@ehu.es

RESUMEN

El objetivo del presente trabajo es sintetizar microcápsulas conteniendo PCM's mediante el procedimiento de polimerización "in situ" de un prepolímero de melamina-formaldehído en una preemulsión acuosa del PCM's. Se analiza el efecto de la disminución de la energía superficial de las gotas de PCM's emulsionadas, aportando energía de agitación y agregando un sistema tensioactivo y estabilizante coloidal, sobre el proceso de microencapsulación del material PCM's y sobre su morfología y propiedades. Se han utilizado dos tipos de parafinas, el hexadecano y el tetradecano, de diferente peso molecular para analizar la permeabilidad y estabilidad de las paredes poliméricas durante los ciclos de cambio de fase y frente a solicitaciones mecánicas.

1. INTRODUCCIÓN

Los PCM's (Phase Change Materials) son un subgrupo de HSM's (Heat Storage Materials) con un proceso de intercambio dinámico de calor que tiene lugar a la temperatura de fusión. Cuando un PCM's sufre la transición de fases sólido-líquido, la energía se almacena en forma de calor latente a temperatura constante. La energía térmica latente acumulada se libera cuando la PCM's solidifica de nuevo. Los PCM's orgánicos son hidrocarburos de alto peso molecular como las parafinas, alcoholes pesados y ácidos grasos. Las parafinas de 13-28 átomos de carbono tienen temperaturas de fusión entre -5,5ºC a +61ºC y, comparadas con otros PCM's, tienen alta densidad de almacenamiento de energía, elevadas temperaturas de ebullición y estabilidad hasta 250ºC. Son químicamente inertes, no corrosivas, baratas, ecológicamente aceptables y no tóxicas. Estas características las hacen adecuadas para múltiples aplicaciones. Para resolver los problemas prácticos de estabilidad del PCM's y mantenerlo funcional durante de un número de ciclos durante su aplicación, pueden ser encapsulados en micro ó nanocápsulas de un material polimérico. Es necesario que las paredes de las cápsulas sean impermeables para evitar la liberación del PCM's y posean alta resistencia a esfuerzos mecánicos y térmicos. La mayor parte de las investigaciones sobre microencapsulado se han orientado a su preparación y caracterización, ó a su aplicación funcional. Sin embargo, existen pocos estudios sobre los mecanismos de formación de las estructuras core-shell de las microcápsulas de PCM's durante los diferentes procedimientos de microencapsulado.

El objetivo del presente trabajo es sintetizar microcápsulas conteniendo PCM's mediante el procedimiento de polimerización "in situ" de un prepolímero de melamina-formaldehído en una preemulsión acuosa del PCM's. Se analiza el efecto de la disminución de la energía superficial de las gotas de PCM's emulsionadas, aumentando la energía de agitación y agregando un sistema tensioactivo y estabilizante coloidal, sobre el proceso de microencapsulación del material PCM's y sobre su morfología y propiedades. Se han utilizado dos tipos de parafinas, el hexadecano y el tetradecano, de diferente peso molecular para analizar la permeabilidad y estabilidad de las paredes poliméricas durante los ciclos de cambio de fase y frente a solicitaciones mecánicas.

2. METODOLOGÍA EXPERIMENTAL

En primer lugar se ha sintetizado el prepolímero a partir de una disolución acuosa de melamina/formaldehído en relación molar 1/3 en medio regulado (pH = 8,5-9,0) a 60ºC. La preemulsión acuosa del material PCM's (hexadecano ó tetradecano) al 10% wt se ha llevado a cabo utilizando agitación mecánica y sonicación y diferentes sistemas tensioactivos basados en dodecilbencensulfonato de sodio (SDBS) y heptanol (C7OH) para las diferentes formulaciones que se reflejan en la tabla 1. En una tercera fase se han mezclado 100ml de la disolución acuosa del prepolímero y 100 ml de la preemulsión de la parafina, se ha llevado el pH del medio hasta 4,0 utilizando ácido acético y se ha llevado a cabo la polimerización a 65 ºC adicionando gota a gota, durante 1 h, la disolución de polivinilalcohol (PVA) con la concentraciones indicadas en la tabla 1.

Muestra	PCMs	SDBS /C7OH	[PVA] (mol/L)
S0	-	1,0 g/ 0g	
S1	Hexadecano	1.0g / 0g	0,001 M
S6*	Hexadecano	0,5g / 0,5g	0,001 M
S7*	Hexadecano	0,5 g/ 0 g	0,001 M
S8*	Hexadecano	0,5 g / 0 g	0,005 M
S5	Tetradecano	1,0 g / 0 g	0,001 M

* La preemulsión de parafina se ha sometido a sonicación

Tabla 1. Relación de las variables de formulación.

Después de la polimerización, las microcápsulas se han separado por coagulación, filtración, lavado y secado en estufa. Las propiedades térmicas de las microcápsulas secas se han observado mediante análisis térmico DSC y TGA (de Mettler) en barridos de 10ºC/min. El análisis de la composición superficial se he realizado con un FTIR de Perkin Elmer Spectrum con dispositivo para ATR - Golden Gate Specac. Los ensayos de resistencia mecánica de realizaron midiendo la pérdida de masa que sufren las microcápsulas sumergidas en agua caliente tras someterlas a esfuerzos de cizalla durante 2 h.

3. RESULTADOS Y DISCUSIÓN

La formación de las paredes poliméricas se debe a reacciones de policondensación entre las moléculas del prepolímero, inicialmente disueltas en la fase acuosa. Durante la policondensación el polímero que se origina debe depositarse sobre la superficie de las gotas de parafina (core) para continuar la polimerización y originar el polímero entrecruzado (shell) que debe encapsular el PCM's. En este sentido, se ha utilizado un tensioactivo aniónico (SDBS) cuyos grupos –SO_3^- quedarían en la superficie de las gotas de PCM's, de forma que los prepolímeros protonados, que se producen durante la policondensación en medio ácido, tendrían cierta afinidad por dichos grupos superficiales favoreciendo la aproximación y formación del shell polimérico. Por el contrario, si el prepolímero crece en medio acuoso hasta que supera su solubilidad, la fase polimérica segregada tenderá a depositarse sobre las superficies de las gotas de PCM's y, en este caso, el grupo -SO_3^- superficial podría dificultar la deposición del polímero segregado sobre la superficie de las gotas de PCM's. En la tabla 2 se reflejan los resultados de los rendimientos calculados a partir del sólido obtenido para los sistemas estudiados. En la misma tabla 2 se refleja la pérdida de peso sufrida por el sólido obtenido al someterlo al ensayo de resistencia a cizalla cuando el sólido esta suspendido en agua a 50ºC (2h)

Sistema	S0	S1	S6*	S7*	S8*	S5
Rend(%)	78,52	56	**	96%	80,72%	60,87
% perd.	21,02	38,04	70,34	44,83	58,39	55,59

** superiores al 100% posiblemente debido a la presencia de otros ingredientes ó agua

Tabla 2. Rendimientos calculados y de las pérdidas de masa por agitación en agua.

Las formulaciones en las que se ha homogenizado la preemulsión de PCMs por sonicación (*), en principio, parecen conducir a mayores rendimientos aunque, tras el ensayo de resistencia, se observa también una mayor pérdida de masa. En los espectros FTIR del hexadecano puro aparece una fuerte banda de adsorción entre 1570 - 1236 cm^{-1} asociada a la vibración de los C-H alifáticos. Cuando la parafina está encapsulada este pico debería desaparecer si en la superficie solo hubiera polímero. Pero si el material core no ha sido completamente encapsulado aún aparecerían bandas entre 2935-2852 cm^{-1} y la presencia de las moléculas de los tensioactivos utilizados adsorbidos en la superficie también poseen grupos –C-H alifáticos. En las formulaciones S6, S7 y S8, a pesar de contener menor cantidad de tensioactivo, se observan la mayor absorción en las bandas indicadas debido a la existencia de parafina sin encapsular.

Las características térmicas de las microcápsulas que contienen hexadecano se muestran en las curvas TGA y DSC de las figuras 1 y 2. En la curva TGA del hexadecano puro se observa una rápida pérdida de peso del material con la temperatura desde 137ºC hasta 207ºC. En contraste, en las curvas TGA de la microcápsulas, aparece un primer tramo de pérdida de peso que se desplaza ligeramente a mayores temperaturas para las formulaciones S1 y S7 y puede asociarse a la mayor resistencia de las paredes poliméricas. A partir de 270ºC debido al "cracking" del shell polimérico aparecen otro/s tramo/s de pérdida de peso que llega hasta 440ºC. Los resultados se reflejan en la tabla 3. También cabe resaltar la baja relación parafina/polímero obtenido para la formulación con tetradecano, lo cual evidencia la mayor penetración de éste a través de las paredes poliméricas, debido a su menor peso molecular.

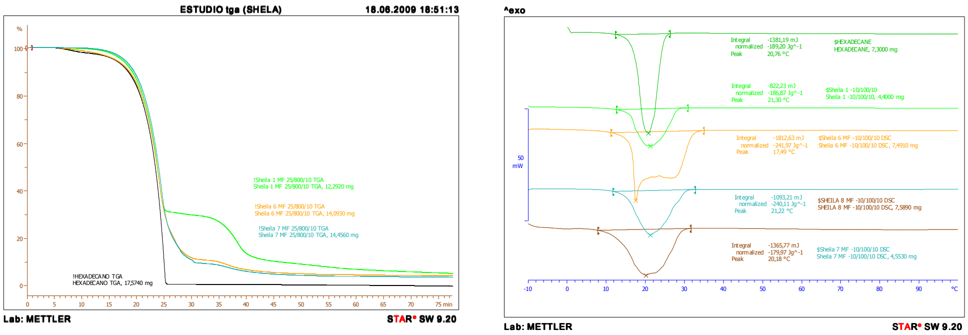

Figuras 1 y 2. Curvas TGA y DSC obtenidas en los análisis térmicos a 10ºC/min.

Sistema	S0	S1	S6	S7	S8	S9	S5
% parafina y otros	5,22 130-250	67,75 167-288	90,40* 169-341	85,88* 146-339	69,19 131-282		33 100-238
%polimero	69,10	18,75	4,56 *	3,42*	22,9		45,27

* Un único tramo que se extiende fuera del rango del punto de ebullición de la parafina.

Tabla 3. Resultados de las pérdidas de peso registradas en las TGA.

Similares resultados se obtienen del análisis de las curvas DSC. Los picos exotérmicos alrededor de la temperatura a la que aparece el pico de fusión de la parafina (21ºC y ΔH_m = 200 $J.g^{-1}$) a 10ºC/min se observa que poseen unas entalpías superiores a la de la parafina, lo cual se debe a la presencia de otros ingredientes de bajo peso molecular, sobre todo en las formulaciones llevadas a cabo con baja concentración de tensioactivo aniónico y sonicación. Estos resultados podrían interpretarse en base a la presencia de polímero de menor peso molecular las paredes sean muy delgadas y poco resistentes, lo que justifica también mayores pérdidas de peso tras el ensayo de resistencia a cizalla en agua caliente. Puede deducirse que mayores grados de división obtenidas por sonicación (S7) conducen, con esta formulación, a paredes más delgadas, polímero de menor grado de polimerización que queda entre las microcápsulas, y son menos estables que las obtenidas con agitación mecánica y mayor concentración de SDBS. Este efecto parece compensarse aumentando la concentración del estabilizante coloidal (PVA) (S8) adicionado durante la policondensación, debido posiblemente a que impide la floculación de las microcápsulas durante la policondensación, impidiendo que oligómeros queden retenidos entre microcápsulas, obteniéndose resultados similares a la S1.

REFERENCIAS

ZANG, HUANZHI, XIAODONG. “Fabrication and performance of microencapsulated phase change materials based on n-octadecane core and resorcinol-modified melamine-formaldehide shells”. Colloids and Surfaces A. Physicochemical and Engineering Aspects (2009), 332(2,3), 129-138.

Kinetic study on the thermal performance of a block copolymer-SWNT-trifunctional epoxy nanocomposite

J.M. González-Domínguez, A. Ansón-Casaos, P. Castell, M.T. Martínez
Group of 'Carbon Nanostructures and Nanotechnology', Department of Nanotechnology.
Instituto de Carboquímica (CSIC), C/ Miguel Luesma Castán 4, 50018 Zaragoza, Spain

SUMMARY

The thermal behaviour and degradation profile of triglycidyl p-aminophenol (TGAP), a trifunctional epoxy, crosslinked with 4,4'-diaminodiphenylsulfone (DDS), was studied using different techniques. Nanocomposites based on this epoxy system with Single Walled Carbon Nanotubes (SWNTs) as the reinforcer were also studied. SWNTs were previously debundled and wrapped by a block copolymer (Pluronic F68) to enhance their integration. This study deepens on the influence of both Pluronic and SWNTs in the thermal cleavage of the epoxy system. From thermogravimetric analysis (TGA) data, isoconversional kinetic calculations were carried out to obtain the Activation Energy (AE) variations along the degradation process, in both inert and oxidative environments. Other experimental techniques such as Thermal Programmed Heating coupled to Mass Spectrometry (TPH-MS) complemented this study, showing the possible degradation mechanisms as well as the effects of the Pluronic and SWNTs presence.

1. INTRODUCTION

Epoxy polymers are the most widely used thermoset materials, commonly employed as the matrix in composites fabrication. The excellent performance of an epoxy resin is observed in mechanical, electrical and thermal resistance. For this reason, some epoxy materials represent key elements in science and engineering, for the automotive or aerospace industries. Multifunctional composite materials based on epoxy systems can be prepared by adding other components such as fibres or thermoplastic polymers. In the nanocomposites field, there is a large research activity on these matrices with nanoscale fillers, such as SWNTs. They lay in the forefront of nanoscience research because of their unique physical properties and outstanding performance. Nowadays, there is a high interest in epoxy nanocomposites for a wide diversity of applications, but some aspects relating their proper integration and physical properties must be more deeply analyzed. The thermal behaviour and degradation profile is of specific interest in the present work. In our previous research, we have worked on unbundling and dispersing SWNTs with a block copolymer (González-Domínguez et al, 2009). Their integration into a trifunctional epoxy resin was successfully achieved by a solvent-free optimized method. Differential scanning calorimetry (DSC) was applied to study the curing mechanism. An important effect on the curing reaction was specially observed with the presence of Pluronic, which exhibited lower curing AE values in the extreme stages of the reaction compared to the neat resin. This improvement in the curing AEs revealed a positive effect of this block copolymer in the integration of SWNTs. Scanning electron microscopy showed a highly homogeneous distribution of SWNT in the matrix when Pluronic wrapped SWNTs were used instead of unwrapped SWNTs. The corresponding nanocomposites were briefly characterized, among others, by the TGA technique. It was then noticed the complex degradation mechanism when shifting from inert to oxidative atmosphere. A deeper study of the thermal behaviour, emphasizing the influence of SWNTs and Pluronic, is aimed in the present work.

2. EXPERIMENTAL

2.1 Materials

The epoxy system used in this work is a trifunctional epoxy monomer, triglycidyl p-aminophenol (TGAP) with 4,4'-diaminodiphenylsulfone (DDS) as the curing agent. SWNTs were produced by the arc discharge method, purified by nitric acid treatment and then wrapped with commercial Pluronic F68 in aqueous medium (González-Domínguez et al, 2009).

2.2 Composites manufacturing

The epoxy nanocomposites were made from the integration of Pluronic wrapped SWNTs into the TGAP by a premixing stage which included hot stirring and sonication (González-Domínguez et al, 2009). The curing agent was afterwards added in stoichiometrical functionality ratio. The blend was cast in an aluminium mould and then cured in a Carbolyte HT4/30 oven at 200ºC for 4.5h.

A nanocomposite sample, called "TGAP+DDS+2%SWNTs-Pluronic", was prepared with a fixed loading of Pluronic wrapped SWNTs (2 wt%). In order to compare Pluronic and SWNTs isolated effects, three blank samples were also prepared, all of them subjected to the same premixing stage. One of them, "Blank-Pluronic (2%)", contained an identical amount of Pluronic as the "TGAP+DDS+2%SWNTs-Pluronic" sample (10mg/g of TGAP). Another one, "TGAP+DDS+2%SWNTs", contained an identical ratio (2 wt%) of acid treated SWNTs. The last one, "Blank w/o Pluronic", did not contain any component different from TGAP and DDS.

Sample Name	**Kind of SWNTs**	**SWNTs ratio (wt%)**	**Amount of Pluronic (mg/gTGAP)**
Blank w/o Pluronic	---	0	0
Blank + Pluronic (2%)	---	0	10
TGAP+DDS+2%SWNTs w/o Pluronic	Acid treated	2	0
TGAP+DDS+2%SWNTs-Pluronic	Pluronic wrapped	2	10

Table 1: Sample names and specifications.

2.3 Thermal analysis

TGA analyses, performed under either nitrogen or air atmosphere (both at 50 mL/min), were registered with a SETARAM Setsys Evolution 16/18 equipment at different heating rates: 1, 2, 5 and 10ºC/min, in the range from room temperature to 800ºC. TPH-MS experiments were carried out in a home-made oven with an Eurotherm 2408 temperature controller, coupled to a Balzers Instruments GSD 300-O mass spectrometer, in two different atmospheres: inert (Ar) and oxidative (synthetic air, O_2+Ar) respectively at 10ºC/min heating rate. From dynamic heating experiments obtained with the TGA at different heating rates, the kinetics of the degradation process was studied. Using the "advanced isoconversional kinetics" methodology (Viazovkyn, 1997 and 2000), AE variations were calculated along the degradation process in both atmospheres.

3. RESULTS AND DISCUSSION

TGA thermograms show a totally different behaviour in N_2 atmosphere with respect to air atmosphere (González-Domínguez et al, 2009). In inert environment, only a single weight loss is observed (centered in the range of 350-400 ºC, depending on the sample and the heating ramp), attributable to a purely thermal process. In air atmosphere (Fig. 1), the same thermal peak is observed. It is a very complex process, composed by several stages. Another weight loss is observed only in air environment at high temperatures. It is slightly overlapped with the thermal process, and may be attributed to the oxidative degradation of the thermal process residue. The maximum peaks positions (in both thermal and oxidative processes) are affected by the Pluronic and SWNTs presence.

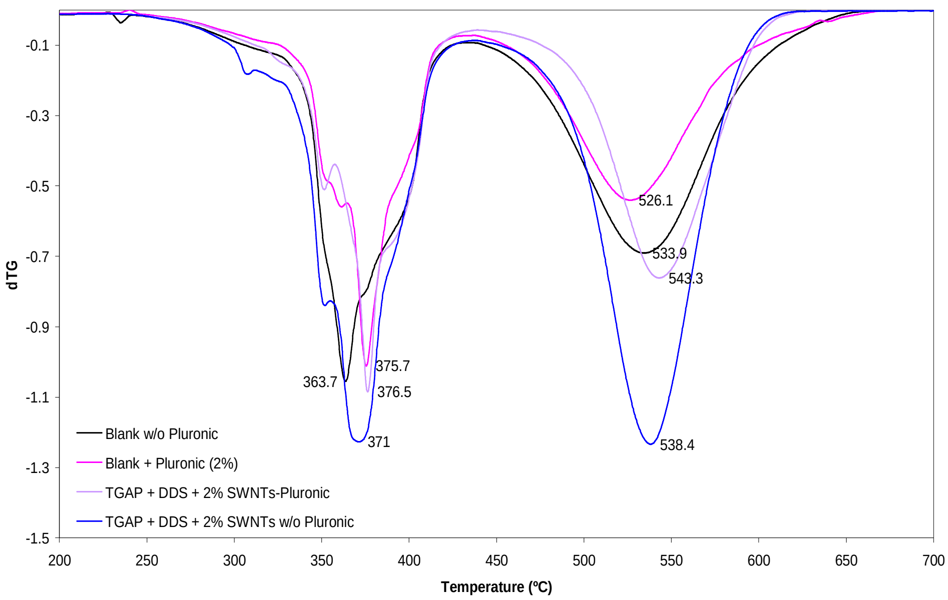

Figure 1. Differential thermograms (dTG) for the different samples at 10ºC/min in air.

To each of the aforementioned TGA peaks (thermal and oxidative), the "advanced isoconversional method" was applied. The complexity of the thermal degradation is evident, and there is a remarkable improvement of the thermal stability (higher AEs) at low conversions when Pluronic wrapped and unwrapped SWNTs are compared. Both Pluronic and SWNTs isolated presence seem to delay the latter stages of the thermal process. In the oxidative process (Fig. 2) very neat and steady values of AE are observed, indicating a single step process. The presence of Pluronic provides a higher oxidative stability (higher overall AE) while the SWNTs presence seems to change the oxidation mechanism, as a drastic change on the AE curve trend is observed. Again, the Pluronic wrapped SWNTs offer higher AE values than unwrapped SWNTs.

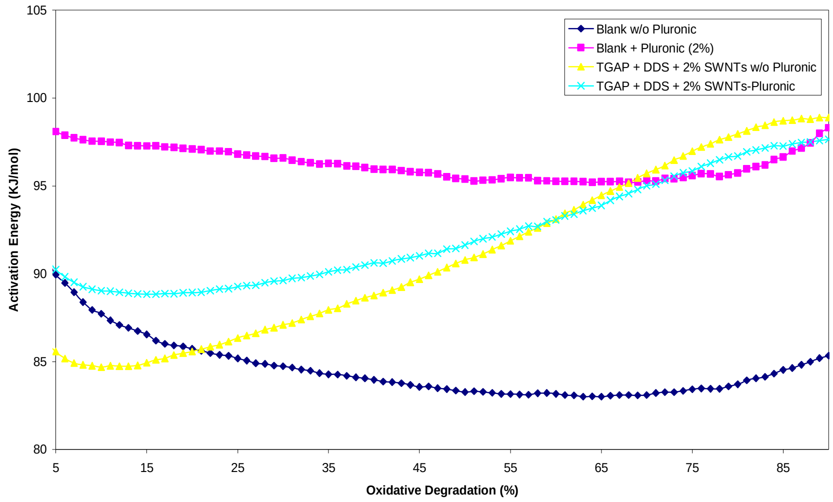

Figure 2. AE plots vs oxidative progress.

From the TPH-MS registers, several clear conclusions were drawn. The oxidative weight loss is governed by CO/CO_2 release (probably corresponding to the oxidation of the thermal residue). In the thermal peak, the cleavage process seems to undergo by the three steps represented as peaks or knees in the dTG, as they fit with registered m/z maximum peaks. Around 350ºC carbon oxides coming from the aliphatic part are observed; at about 375ºC nitrogen and more carbon oxides are released; and at around 400ºC sulphur and phenyl species are observed (indicating the aromatization of the residue). In oxidative atmosphere sulphur peaks are advanced ≈20ºC.

CONCLUSIONS

Integrating Pluronic-wrapped SWNTs into a trifunctional epoxy system (TGAP + DDS) leads to the development of novel nanocomposite materials with enhanced properties. In this study, an improvement in the thermal and oxidative stability has been shown by means of isoconversional kinetic studies applied to TGA peaks. TPH-MS technique helped to unravel the possible cleavage mechanisms.

REFERENCES

GONZÁLEZ-DOMÍNGUEZ J.M., CASTELL P., ANSON A., BENITO A.M., MASER W.K., M.T. MARTINEZ (2009). Block copolymer assisted dispersion of SWNTs and integration into a trifunctional epoxy. *J. Nanosci. Nanotechnol.,* DOI: 10.1166/jnn2009.1575

VYAZOVKIN S. (1997), Evaluation of activated energy of thermally stimulated solid-state reactions under arbitrary variation of temperature. *J. Comput. Chem.*18, 393-402.

VYAZOVKIN S. (2000), Modification of the integral method to account for variation in the activation energy.. *J. Comput. Chem.*22, 178-183.

Interactions between multi-walled carbon nanotubes and an azo-dye, Disperse Orange 3

G. Díaz Costanzo
LPyMC, Departamento de Física, Facultad de Ciencias Exactas y Naturales.
LPI, Departamento de Física, Facultad de Ciencias Exactas y Naturales. Universidad de Buenos Aires, Argentina
I. Mondragon
'Materials + Technologies' Group, Dep. Ingeniería Química y M. Ambiente,
Escuela Politécnica. Universidad País Vasco/Euskal Herriko Unibertsitatea
S. Goyanes
LPyMC, Departamento de Física, Facultad de Ciencias Exactas y Naturales.
Universidad de Buenos Aires, Argentina and CONICET, Argentina
S. Ledesma
LPI, Departamento de Física, Facultad de Ciencias Exactas y Naturales. Universidad de Buenos Aires, Argentina and CONICET, Argentina

ABSTRACT

The interactions between multi-walled carbon nanotubes (MWCNT) and an azo-dye molecule were studied. The MWCNT were dispersed in different solutions of the dye Disperse Orange 3 (DO3) in tetrahydrofuran. An absorption band at 321 nm in the ultraviolet visible absorption spectra of the mixture, which does not belong to the dye neither the nanotubes, reveals the interactions. These interactions reach its maximum for a specific weight ratio DO3/MWCNTs equal to 2/3.

1. INTRODUCTION

In the last years special attention has been paid to carbon nanotubes and particularly they have been studied for the development of novel optoelectronic nanocomposites. In this sense, it is relevant to explore the interaction of the tubes with azobenzene derivatives. Azobenzene derivatives have the possibility of stack the nanotubes by their benzene ring structure. The interactions of nanotubes with azo-dye molecules become an important task since they could enhance their dispersion in organic solvents, or induce in carbon nanotubes a specific optical response. Moreover, by making carbon nanotubes and Disperse Orange 3 molecules interact in an organic solvent like tetrahydrofuran (THF), it could allow the immersion of the nanotubes in different polymer matrices such as epoxy resins.

In this work, we explore the interactions between MWCNT and DO3 molecules by studying changes in the ultraviolet visible absorption spectra.

2. MATERIALS AND METHODS

Commercial MWCNT (Nanocyl 3100) were used as received. Six different concentrations of Disperse Orange 3 (Sigma) in tetrahydrofuran were prepared, 1, 2, 4, 6, 8 and 20 µg/mL. Equal concentration solutions, 1, 2, 4, 6, 8 and 20 µg/ml, were prepared with DO3 in THF with the addition, in all samples, of a fixed amount of

MWCNT, 6 μg/mL. The MWCNT were first sonicated in THF during 20 min and then pipetted to the DO3 solutions. The molecular structure of the DO3 is shown in Fig.1.

The UV-Vis absorption behavior of the two different kinds of samples, with and without MWCNT, was studied at room temperature immediately after being sonicated for 20 min with an UV-Vis spectrometer HP8453 of 1 nm resolution.

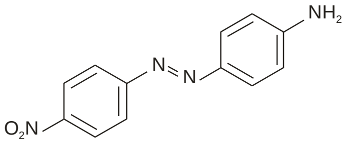

Fig. 1. Molecular structure of Disperse Orange 3.

3. RESULTS

Fig. 2a-b shows the UV-Vis absorption spectra obtained. In Fig. 2a the spectra of solutions of DO3 in THF at different concentrations have been superimposed. As it can be seen, there are two absorption bands specially marked. The one at lower wavelengths, around 280 nm, is attributed to the π-π* electronic transition while the one around 443 nm corresponds to the n- π* transition of DO3. The π-π* and n-π* electronic transitions are associated to the trans-cis and cis-trans isomerization of the DO3 molecule respectively. Although not shown here, the absorption maxima of both bands grow linearly upon DO3 concentration indicating that they follow Beer's law. In Fig. 2b we superimposed the spectra of the same six different concentrations of DO3 in THF, all of them with the same fixed concentration, 6 μg/mL, of MWCNT. It should be noted that the two characteristic bands of the dye have not changed, with exception of the background of the nanotubes. In fact, the linear growth of the absorption maxima upon DO3 concentration was maintained. The main interesting result here is that in addition to the two absorption bands of the dye two other peaks appeared. As it is shown in Fig. 2b, there is a first shoulder in the spectra around 257 nm, while there is a stronger peak around 321 nm.

The new absorption at 257 nm is attributed to the π -plasmon transition of MWCNT (Pichler et al., 1998) while the band around 321 nm reveals a different interaction between MWCNTs and DO3 molecules.

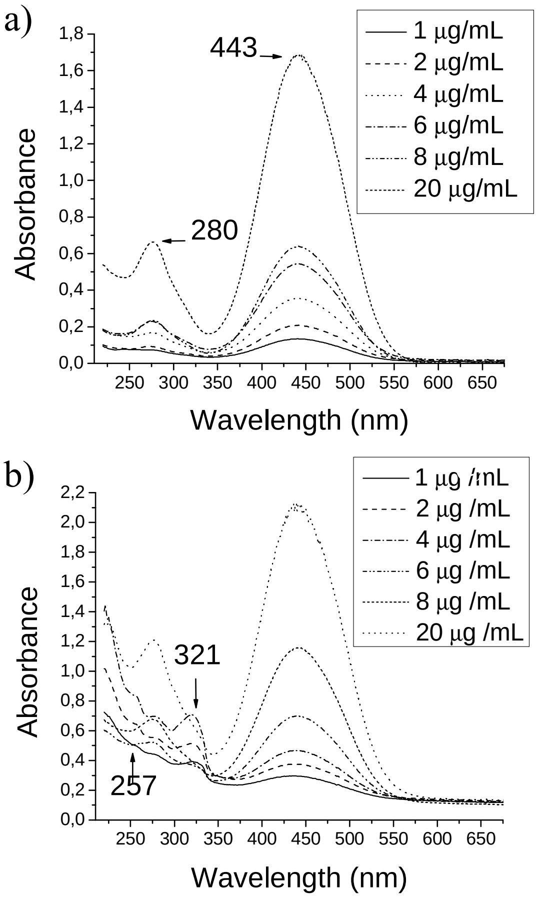

Fig. 2. UV-Vis absorption spectra: (a) DO3 in THF at six different concentrations (b) DO3 in THF with a fixed amount of MWCNT, 6 µg/mL.

It is known (Lu et al., 2006) that MWCNT and aromatic molecules, such as those of DO3, can interact via π-π* stacking by charge transfer. Interesting enough is to mention that both new absorptions obtained in the samples of DO3 and MWCNT change their height upon DO3 concentration. Specifically, the band around 321 nm can be attributed to π-π* stacking interaction. This band reaches a maximum for the particular weight relation DO3/MWCNTs equal to 2/3. On the other hand, for the highest concentrations (8 and 20 µg/mL) spectra do not show significant changes when MWCNT were added, with exception of the background. This can be clearly seen in Fig. 3 where these spectra are plotted in the range of 290 and 350 nm to show the peak associated to π-π* stacking interactions in detail and where the highest concentrations where not plotted to make the figure clearer. No absorption band around 321 nm is found for samples with MWCNTs, 6 µg/mL, and higher DO3 concentration, 8 µg/mL and 20 µg/mL. In all cases, the MWCNT background was subtracted for better comparison. In this figure, we plotted together the MWCNT – DO3 spectra for DO3 concentrations of 1, 2, 4 and 6 µg/mL. As mentioned, for higher concentrations, the absorption band attributed to the π-π* stacking interaction is not present. In this sense, finding the optimum stacking of DO3 molecules to MWCNT could be considered when trying to induce a certain optical response to the tubes or when trying to disperse them.

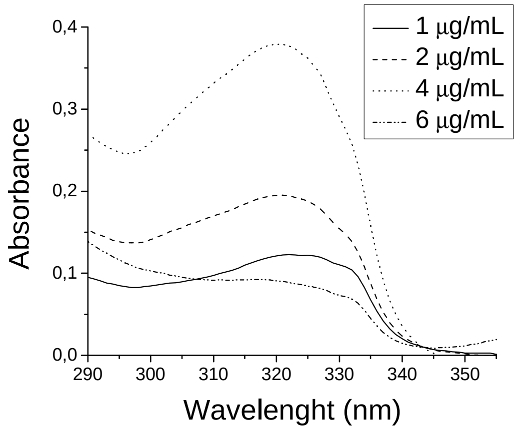

Fig. 3. Detail of the UV-Vis absorption spectra obtained for samples of different DO3 concentration and fixed concentration of MWCNT (6 µg/mL).

3. CONCLUSIONS

Accurate evidence about the interactions between MWCNT and Disperse Orange 3 azoderivative molecules has been obtained using UV-Vis absorption spectroscopy. The interactions were revealed by means of the presence of an absorption band at 321 nm, which can be associated to π-π* stacking interactions. The capability for interaction reaches its maximum for a specific weight ratio DO3/MWCNTs equal to 2/3.

On the basis of this research, the new optical response of the nanotubes induced by the stacking of the Disperse Orange 3 molecules could be explored for the development of novel optoelectronic nanocomposites.

ACKNOWLEDGEMENTS

The authors acknowledge the financial support of UBA (X094 and X118), CONICET (PIP 5959 and PIP 112-200801-03047), ANPCyT (25834 and 2284), Basque Country Government (IT-365-07 and inanoGUNE) and MEC (MAT2006-06331).

REFERENCES

LU, J.; NAGSE, S.; ZHANG, X.; WANG, D.; Ni, M.; MAEDA, Y.; WAKAHARA, T.; NAKAHODO, T.; TSUCHIYA, T.; AKASADA, T.; GAO, Z.; YU. D.; YE, H.; MEI, W. N.; ZHOU, Y. Selective Interaction of Large or Charge-Transfer Aromatic Molecules with Metallic Single-Wall Carbon Nanotubes: Critical Role of the Molecular Size and Orientation *J. Am. Chem. Soc.*2006, 128, 5114.

PICHLER, T.; KNUPFER, M.; GOLDEN, M. S.; FINK, Localized and Delocalized Electronic States in Single-Wall Carbon Nanotubes *J. Phys. Rev. Lett.* 1998, 80, 21, 4729.

Nanocomposites of polyethylene and montmorillonite: rheological and tribological characterization

M. Fernanda Horst
Planta Piloto de Ingeniería Química, PLAPIQUI (UNS/CONICET). Bahía Blanca, Argentina
W. Tuckart
Departamento de Ingeniería (UNS). Bahía Blanca, Argentina
L.M. Quinzani
Planta Piloto de Ingeniería Química, PLAPIQUI (UNS/CONICET). Bahía Blanca, Argentina
M.D. Failla
Planta Piloto de Ingeniería Química, PLAPIQUI (UNS/CONICET), Departamento de Ingeniería (UNS). Bahía Blanca, Argentina

ABSTRACT

Polyethylene nanocomposites based in a commercial organophylic montmorillonite were prepared by melt mixing the components in a laboratory mixer. The relationship between the morphology and the rheological and tribological properties of the mixtures subjected to different thermal and mechanical treatments is analyzed. The phase structure of the materials is analyzed using X-ray diffraction and electron microscopy. The pin-on-disk tests were performed on cylindrical probes of the composites to determine the friction coefficient and wear rate. The composites show rheological properties that are affected by the annealing time in the molten state. Furthermore, the low-frequency dynamic moduli of the annealed materials are larger than the corresponding data of fresh mixtures signaling a more solid-like rheological behavior.

1. INTRODUCTION

Polymer–clay nanocomposites (PNC) continue to generate much interest due to their potential for exceptional improvements in mechanical and barrier properties when compared to conventional polymer-composites. These improvements are achieved when the clay exfoliates into the polymer matrix generating high aspect ratio particles. One of the most common nanoscopic fillers used for the preparation of PNCs is the montmorillonite (MMT). Dispersal of nanolayers of MMT in a polymeric matrix produces an 'exfoliated PNC' while the mere infiltration of polymer molecules between the clay layers produces an 'intercalated PNC'. In practice, complete exfoliation of the clay is rarely reached and both intercalated and exfoliated structures coexist in the polymeric matrix.

The use of MMT in PNCs requires an initial step of purification of the clay followed by the interchange of the interlayer inorganic cations (Na^+, Ca^{2+}, etc) with short chain organic ones such alkylammonium ions. This step not only increases the interlayer spacing but also improves the compatibility with the polymer, most of all if the polymer is a polyolefin. In addition, in the case of polymers of low polarity, like polyethylene (PE), the dispersion of the clay platelets is improved with the addition of a compatibilizer, such as maleic anhydride grafted polyethylene (PEg).

In the present study, a commercial organophylic montmorillonite (MMT) and a commercial polyethylene (PE) were used to prepare PNCs by melt mixing this components with a functionalized PE. The relationship between the morphology and the rheological and tribological properties of the mixtures subjected to different thermal and mechanical treatments is analyzed.

2. EXPERIMENTAL

The PE is a high density polyethylene from *PBB-Polisur* (M_w= 65.000 g/mol). The PEg was prepared by reactive mixing the PE with maleic anhydride in a counter-rotating twin screw extruder (*Goetffert*, D=35 mm, L/D=15) using an organic peroxide as initiator. The PEg presents a grafting degree of 0.2 wt%. The clay used as reinforcement is the *Nanomer I.44P* from *Nanocor*. Irganox 1010 from *Aldrich* was added as an antioxidant.

The composites were prepared by melt mixing the polymers with the clay during 25 min in a *Brabender Plastograph* at 160°C under nitrogen atmosphere. The PNCs have 5 wt% of clay and PEg/clay weight ratio of 3:1, 2:1, and 1:1. The PE/PEg/MMT composites are termed PEN5-*xy* where *xy* represent the PEg:clay ratio.

X-ray diffraction was used to analyze the structure of the materials. The average size of the *d*-spacing or basal spacing d_{001} (sum of a layer and an interlayer distance) in clay powders and nanocomposites was determined from the 2θ position of the (001) diffraction peak of each material using Bragg´s law. The study was done using a *Philips PW 1710* X-ray diffractometer equipped with a Cu Kα radiation source of wavelength 1.54 Å operated at 45 kV and 30 mA. The dynamic moduli of the polymers were measured in a rotational rheometer (*Rheomoetrics RDAII*) using small amplitude oscillatory shear flow between parallel plates under nitrogen atmosphere. The dynamic moduli were obtained using ~2mm thick samples in a frequency range between 0.04 and $400s^{-1}$. Dynamic strain sweeps were also performed on samples of all the materials to determine the strain range of linear response. To analyze the effect of annealing, sequences of tests were applied to each sample. An initial dynamic frequency sweep (DFS) was applied at 150°C, followed by a period of 1 h at rest at 200°C. The temperature was then lowered back to 150°C and DFSs were performed every 10°C up to 200°C. Finally, a DFS at 150°C was applied.

The friction and wear behavior of the composites were investigated using a pin-on-disc wear test-machine. Pins of 6 mm diameter and 20 mm length were used. Tests were performed without lubrication loading the pins against stainless steel (*SAE 4140*) discs of 40 mm diameter. The friction coefficient and the wear resistance were determined according the ASTM G99 norm measuring the weight loss of the pins after 1728 m of sliding at a constant speed of 375 rpm using different loads.

3. RESULTS and CONCLUSIONS

Figure 1 displays the elastic modulus and the dynamic viscosity ($\eta' = G''/\omega$) at 150 °C of PE, PEg and the blends PE/PEg that constitute the polymeric matrices of the composites. The PE was previously processed in the blender under the same conditions than the blends. The blends have elastic moduli larger than those of the polymers, mainly at low frequencies. The possibility of immiscibility of the polymers suggested by these results is being further analyzed using calorimetric and microscopy techniques.

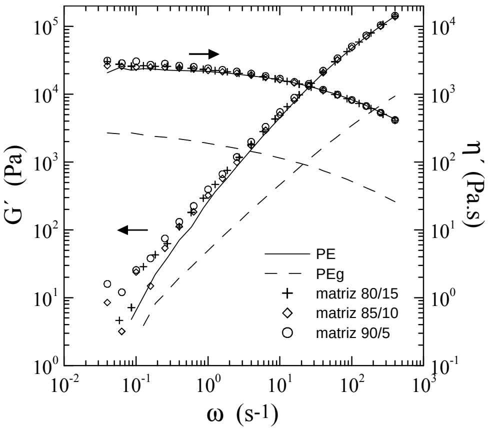

Fig. 1. Elastic modulus and dynamic viscosity at 150°C of PE, PEg and the blends.

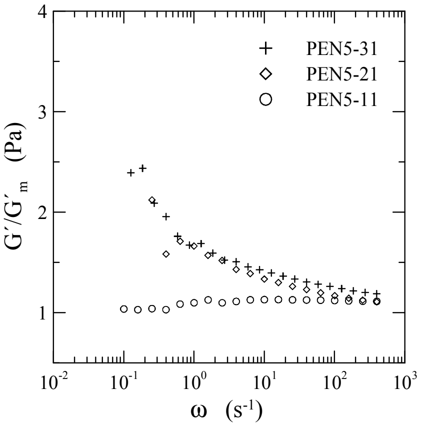

Fig. 2. Elastic modulus of composites at 150°C relative to the elastic modulus of the matrices.

Figure 2 shows the G′(ω) data of the composites at 150°C obtained in the initial DFS. The data are presented relative to those of the corresponding polymeric matrices (G'_m) already displayed in Fig. 1. According to these results, PEN5-11 has elastic moduli very similar to those of the matrix (G'/G'_m~1) while the other two composites have moduli larger than those of the matrices, mainly at low frequencies. This result indicates that there is a more "solid-like" behavior in this two materials that may be due to higher interaction among particles.

Figure 3 displays the elastic moduli of the composites measured during the second DFS. This data were obtained at 150°C after 1 h of annealing at 200°C, and are reported relative to the elastic moduli of the fresh samples ($G'_{initial}$). The composites show rheological properties that are affected by the annealing time in the molten state. Furthermore, the low-frequency dynamic moduli of the annealed materials are larger than the corresponding data of fresh mixtures signaling a more solid-like rheological behavior, even in the case of PEN5-11.

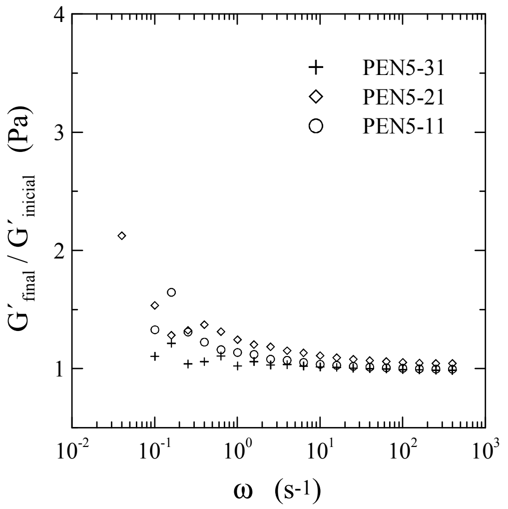

Fig. 3. Elastic modulus of annealed composites at 150°C, relative to the data measured during the initial DFS.

The results in Figs. 2 y 3 suggest that, as it happens with other nanocomposites, the blending and annealing in molten state help to break apart and delaminate the clay particles producing a more solid-like rheological behavior of the composites. However, these results need further analysis since they may be affected by the possible immiscibility of the polymers. Calorimetric and scanning electron microscopy (SEM) studies are presently been performed.

With respect to the DRX results, the position and shape of the d_{001} diffraction peak in the composite diffractograms suggest that the interlayer spacing of the original MMT (approximately 2.6 nm) slightly increases during the mixing with no significant delamination. The phase structure of the composites will be further analyzed using SEM. According to the preliminary results of the wear behavior, PE displays melting of the pin surface with adhesive wear mechanism. Its friction coefficient continuously increases during the test due to the temperature rise of the pin surface. PEN5-31 does not show this behavior. On the contrary, at the speed and load testing conditions used, this material presents very low wearing.

ACKNOWLEDGEMENTS

The authors wish to thank CONICET, ANPCyT and UNS for their financial support.

REFERENCES

HOTTA, S., PAUL, D.R. (2004). Nanocomposites formed from linear low density polyethylene and organoclays. *Polymer,* 45, 7639-7654.

DEVENDRA, R., HATZIKIRIAKOS, S.G., VOGEL, R. (2006) Rheology of metallocene polyethylene-based nanocomposites: Influence of graft modification. *J. Rheol.*, 50, 415-434.

Development of novel nanocomposites based on PLA and clays for food packaging applications

M. Jordá, M. Gallur, J. Alonso, S. Aucejo
Packaging, Transport & Logistics Research Centre (ITENE)
C/ Albert Einstein, 1. Parque Tecnológico de Paterna, Valencia, Spain.
mjorda@itene.com

SUMMARY

Montmorillonite is one of the most interesting layered silicates since it is easy to functionalize its surface due to the high Cation Exchange Capacity (CEC), and surface area. When these clays are use for food packaging applications special concern should be taken into account with the selection of modifiers.

In this work, one sodium montmorillonite, and other calcium montmorillonite (K10) are used in order to functionalize them with food compliant modifiers. Both clays are characterized, and differences are evaluated.

After that, different biodegradable nanocomposites based on PLA have been developed with both types of clays. Nanocomposites have been characterized comparing the results with the nanocomposites prepared with unmodified clays.

1. INTRODUCCIÓN

Inorganic fillers are commonly used to improve a variety of physical properties, such as stiffness, strength, or thermal stability, and in some cases to reduce plastic costs having sizes ranging from several microns to few millimeters (Cho*, et al.* 2001, Davis*, et al.* 2002, Hasegawa*, et al.* 1998). During the last decade, a new nanofiller technology for polymer reinforcement has attracted a lot of attention. Compared with conventional composites, nanocomposites present at low percentages addition an enhancement in properties when compared to bulk properties.

Polymer layered nanocomposites are based mainly on sodium montmorillonite, which is a 2:1 layered smectite. To improve the miscibility and interactions between clays and polymers it is necessary to substitute sodium and calcium cations in the interlayer space, replacing them by organophilic cations such as alkylammoniums or alkylphosphoniums, leading to organomodified layered silicates (OMLS) (Okamoto 2006).

There are three techniques to produce polymer nanocomposites: in situ polymerization, solvent blending, and melt processing. This last process involves mixing a mixture of polymer and OMLS under shear and above melting temperature. This technique does not involve the use of solvents, and can be processed in existing melt processing equipments.

In packaging, huge amounts of plastics materials are used. Conventional plastic are not degradable in a reasonable period of time and therefore efforts are focused towards reduction or use of biodegradable/biocompatible polymers. Some biopolymers have already an application in food packaging industry but these applications would be increased if materials were reinforced. One approach to such improvement is the use of nanofillers in bioplastics leading to biopolymer nanocomposites. Addition of modified clays to obtain nanocomposites has provided the means to improve materials performance; these improvements can include high moduli (Cho, *et al.* 2001, Hasegawa, *et al.* 1998), increased strength (Cho, *et al.* 2001, Hasegawa, *et al.* 1998) and heat resistance (Davis, *et al.* 2002), decreased gas permeability (Messersmith, *et al.* 1995) and flammability (Zhao, *et al.* 2005).

2. EXPERIMENTAL

2.1. Materials

Purified sodium montmorillonite (MMT) (Closiste®Na+) was purchased from Southern Clay Products. Activated Calcium Montmorillonite (K10) was purchased from Fluka. Organic modifiers were supplied by Acros Organics. Three quaternary ammonium salts were selected from the list of additives approved for food contact applications. Each modifier has an alkyl chain with different polarity. Modifier 1 present more polarity than Modifier 2 and Modifier 3. Modifier 3 is the least polar modifier. Polylactide pellets were purchased from Cargill Dow (NatureWorks® PLA polymer 7032D) for the preparation of filled biopolymers.

2.2. Organo-modified clays preparation

Three different methods (Mittal 2007, Salas-Vicent, *et al.* 2007, Tiwari, *et al.* 2008) have been tested in order to obtain the best experimental procedure for the preparation of organo-modified nano-clays. A cation exchange reaction between the hydrated cations (inside the MMT layers) and the alkyl ammonium ions is carried out in an aqueous solution. After the process the modified clay is dried at 80ºC during one day, milled in a ball mill and sieved to obtain particle size below 25 microns.

2.3. Nanocomposite preparation

Different PLA nanocomposites samples have been obtained with the modified clays prepared. For this purpose a DSM Explore Microcompounder (15.5 cc) was used. PLA pellets (dried overnight at 60ºC) are blended with 4% in weight of clay in this counter-rotating micro-extruder. The temperatures of processing are 195 ºC. The rotation speed of the screw is maintained at 100 r.p.m. After extrusion the melted materials were transferred through a preheated cylinder (195ºC) to the mini injection moulder (DSM Explore) to obtain bone-like specimen samples (ISO 527 standard; probe type 5A-B).

2.4. Characterization

Both, clays and filled composites were characterized using different techniques. FTIR (Fourier Transform InfraRed) Spectra were obtained on an Equinox 55 spectrometer (Bruker), coupled to a microscope modulus with ATR objetive (Hiperion, Bruker). WAXD (wide-angle X-ray diffraction) analyses were performed on samples using a Bruker AXS D5005 difractometer. TGA (Thermogravimetric Analysis) analyses were performed on samples using a Thermal Analyzer Q5000 IR (TA Instruments). Water Vapour Transmission Rate (WVTR) was evaluated following standard ASTM E96-93 using the desiccant method. Finally, Mechanical Properties of nanocomposites samples were determined from tensile tests, performed on a universal testing machine at a constant elongation rate of 20 mm/min (ISO 527 standard).

3. RESULTS AND DISCUSSION

3.1. Organo-modified Clays

Different modified clays have been obtained from MMT following the method explained previously. The summary of the organo-modified clays obtained are presented in Table 1. Using the same procedure different exchange capacities relative to CEC are obtain. MOD3 results in an optimum % Exchange for MMT; however, MOD2 is the best option for K10 clay.

Table 1. Modified clay obtained from MMT, and yield of the cation exchange reaction. * % Exchanged relative to CEC as determined by TGA.

Clay	**Modifier**	**Exchange (%)***	**Clay**	**Modifier**	**Exchange (%)***
MMT	-	-	K10	-	-
MMTMOD1	MOD1	56.1	K10MOD1	MOD1	35.2
MMTMOD2	MOD2	77.2	K10MOD2	MOD2	84.1
MMTMOD3	MOD3	78.3	K10MOD3	MOD3	43.4

The presence of modifiers in the clay was determined by FTIR. It is observed in the results the presence of a peak under 1200 cm^{-1} which corresponds to Si-O absorptions and OH bands that are typical of clay minerals (Madejova 2003). Inner hydroxyl groups, lying between the tetrahedral and octahedral sheets, give the absorption near 3620 cm^{-1}, as it is seen in all the spectra. The C-H stretching bands of alkylammnium cations occur in the 3020-2800 cm^{-1}. Two strong bands near 2930 cm^{-1} and 2850 cm-1 are present in spectra. A characteristic C-H bending vibration of the (CH3)4N^{+} cation at 1487 cm^{-1} (Xie*, et al.* 2001) is seen in the spectrum of all the modified clays.

The X-ray diffraction (XRD) patterns of MMT, K10 and the modified clays were carried out over all the samples. From the diffractograms it is observed the change in clay interlayer spacing (corresponding to the d(001) diffraction peak). By the preparation of modified clay, interlayer space is increase with respect to original clay.

3.1. Filled nanocomposites

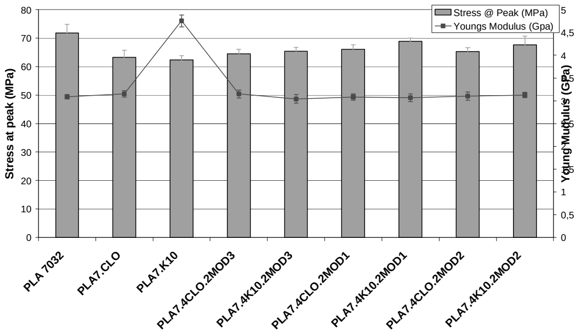

Fig. 1. Mechanical properties of prepared nanocomposites, tensile tests.

Filled PLA nanocomposites samples have been prepared with the organo-modified clays produced. Neat PLA has been also studied for comparison purposes. In Figure 1 it is shown the mechanical properties of the different nanocomposites prepared with MMT, and K10. It is observed that not appreciable differences are observed in the results. Both stress at peak and Young Modulus, are at the same values that neat PLA. However permeability results show an improvement of 55 % when using modified clays (with MOD3). This reduction has been observed through the evaluation of the water vapour transmission.

4. CONCLUSIONS

MMT and K10 clays have been modified using three different alkylammonium salts approved for food contact applications. XRD patterns and FTIR spectra evidence the presence of the modifiers between the silicate layers. PLA nanocomposites have been prepared using the organo-modified clays as fillers. Clays seem to be well dispersed in the polymer matrix, and barrier properties are significantly improved.

ACKNOWLEDGMENTS

Authors would like to thank to the IMPIVA for the financial support.

REFERENCES

CHO, J. W. and PAUL, D. R. (2001). Nylon 6 nanocomposites by melt compounding. *Polymer.* 42, 11.

DAVIS, C. H., *et al.* (2002). Effects of melt-processing conditions on the quality of poly(ethylene terephthalate) montmorillonite clay nanocomposites. *Journal of Polymer Science Part B-Polymer Physics.* 40, 23, 2661-2666.

HASEGAWA, N., *et al.* (1998). Preparation and mechanical properties of polypropylene-clay hybrids using a maleic anhydride-modified polypropylene oligomer. *Journal of Applied Polymer Science.* 67, 1, 87-92.

MADEJOVA, J. (2003). FTIR techniques in clay mineral studies. *Vibrational Spectroscopy.* 31, 1, 1-10.

MESSERSMITH, P. B. and GIANNELIS, E. P. (1995). SYNTHESIS AND BARRIER PROPERTIES OF POLY(EPSILON-CAPROLACTONE)-LAYERED SILICATE NANOCOMPOSITES. *Journal of Polymer Science Part a-Polymer Chemistry.* 33, 7, 1047-1057.

MITTAL, V. (2007). Esterification reactions on the surface of layered silicate clay platelets. *J Colloid Interface Sci.* 315, 1, 6.

OKAMOTO, M. (2006). Polymer/layered silicate nano-composites - Structure development and processing operations. *International Polymer Processing.* 21, 5, 487-496.

SALAS-VICENT, J., *et al.* (2007). Amino Acid Modified Montmorillonite As Reinforcement In Polyhydroxybutyrate Matrices. *Alicante*,

TIWARI, R. R., *et al.* (2008). Synthesis and characterization of novel organo-montmorillonites. *Applied Clay Science.* 38, 3-4, 203-208.

XIE, W., *et al.* (2001). Thermal characterization of organically modified montmorillonite. *Thermochimica Acta.* 367, 339-350.

ZHAO, C. G., *et al.* (2005). Mechanical, thermal and flammability properties of polyethylene/clay nanocomposites. *Polymer Degradation and Stability.* 87, 1, 183-189.

Investigation on the mechanical and microstructural properties of polypropylene/wood flour/clay hybrid nanocomposite

Behzad Kord
Scientific Member, Department of Wood and Paper Science and Technology,
Islamic Azad University, Chalous Branch, P.O. Box 46615/397, Chalous, Iran
Email: behzad_k8498@yahoo.com

SUMMARY

Polypropylene/wood flour composites with different nanoclay and maleic anhydride grafted polypropylene (PP-g-MA) contents were fabricated by melt compounding and then injection molding. The mechanical properties such as flexural modulus, tensile modulus and impact strength were evaluated. Results indicated that the flexural and tensile modulus increases with increase of nanoclay up to 3phc at the same concentration of PP-g-MA and then decreases. However the impact strength of the composites decreases with increasing the nanoclay loading. Also the effect of compatibilzer was positive in terms of enhancing the mechanical properties of the composites. The morphology of the nanocomposites has been examined by using X-ray diffraction (XRD) and transmission electron microscopy (TEM). Morphological findings revealed that intercalation form the sample with 3phc concentration of clay, wich implies to formation of the intercalation morphology and better dispersion than 6phc, and the d-spacing of clay layers were improved in the composite in presence of compatibilizer.

1. INTRODUCTION

Wood plastic composites (WPCs), which are defined as composite materials containing wood (in various forms such as wood flour and fiber, kenaf fiber, hemp, sisal etc) and thermoplastic materials (e.g. polyethylene, polypropylene, PVC etc.), are a relatively new family of composite materials. Compared to the traditional synthetic fillers, the natural fibers present lower density, less abrasiveness, lower cost and they are renewable and biodegradable. WPCs are becoming more and more commonplace and are also gaining considerable popularity in the world. Recently, to improve of the physical and mechanical properties of WPCs, some approaches such as: foaming, chemical treatments of wood fiber, hybridization with other fillers, etc have been considered by the researchers. Hybrid composites are materials made by combining two or more different types of fibers in a common matrix. By hybridization, it is possible to to achieve a balance between performance properties and cost of the composites, which would not be obtained with a single kind of reinforcement.

The impressive enhancement of material properties achieved with the inclusion of submicron-size fillers in plastics and elastomers has stimulated active research in polymer composites. Clay nanocomposites, especially nanoclay/polymer composites, exhibit dramatic increases in modulus, strength, barrier properties, flammability resistance, and heat resistance compared with conventional or microcomposites. The aim of this study was to investigate the effect of nanoclay and coupling agent on the clay dispersion and mechanical properties of the WPC composites.

2. EXPERIMENTAL

Polypropylene, V30S (MFI=18 g/10min, density=0.92g/cm^3) was supplied by Arak Petrochemical Co, Iran. Beech wood-flour (100 mesh size) was from Cellulose Aria Co, Iran. Maleic anhydride grafted polypropylene (PP-g-MA) provided by Solvay with trade name of Priex 20070 (MFI=64 gr/min, grafted maleic anhydride 0.1 Wt.%) was used as coupling agent. Cloisite 30B (CEC=90meq/100gclay, d_{001}=18.5A^0) was obtained from Southern clay Products Co, USA as Nanoclay. Before preparation of samples, wood flour were dried in an oven at (65 ± 2) °C for 24 hours. Then polypropylene, wood flour and nanoclay were weighed and bagged according to formulations given in Table1. The mixing was carried out by a HAAKE internal mixer, the total mixing time was 13 min. The compounded materials were then ground using a pilot scale grinder. Then, the resulted granules were dried at 105°C for 4 hours. Test specimens were prepared by injection molding. The specimens were stored under controlled conditions for at least 40 hours prior to testing.

Table 1: Composition of the Studied Formulations.

Code	Polypropylene content (Wt. %)	Wood flour content (Wt. %)	Nanoclay content (phc)*	PP-g-MA (phc)
50W50P	50	50	0	0
50W50P2M	50	50	0	2
50W50P4M	50	50	0	4
50W50P3N	50	50	3	0
50W50P2M3N	50	50	3	2
50W50P4M3N	50	50	3	4
50W50P6N	50	50	6	0
50W50P2M6N	50	50	6	2
50W50P4M6N	50	50	6	4

*Per hundred compound

The flexural, tensile and impact tests were measured according to the ASTM D790-03, D638-03 and D256 respectively. Wide angle X-ray diffraction (XRD) analysis was carried out with a Seifert-3003 PTS with CuKα radiation (λ =1.54 nm, 50kV, 50mA) at room temperature, scanning rate was 1^0 /min. The morphology structure of the nanocomposites was investigated by a Philips transmission electron microscope (TEM) with an acceleration voltage of 100kV. The ultrathin slides were obtained by a Leica Ultracut UCT.

3. RESULTS AND DISCUSSION

Figure 1 shows that the flexural modulus of nanocomposites increases with increase of PP-g-MA at different levels of nanoclay. It is well established that presence of the PP-g-MA as coupling agent enhances the interface adhesion between wood flour and pp matrix and brings better encapsulation of wood particles by the plastic which consequently results in higher flexural modulus. Another interesting result in figure (1) is that, the flexural modulus increases with increase of nanoclay up to 3phc at the same concentration of PP-g-MA and then decreases. It is well known that the nano-scale filler with very high aspect ratio can improve the flexural modulus of the polypropylene.

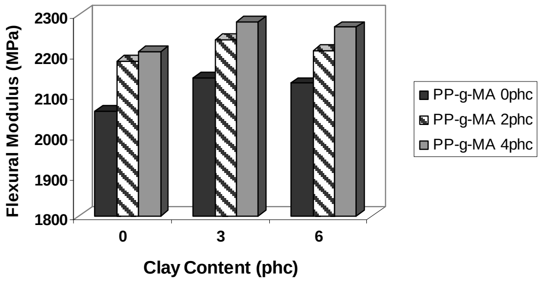

Figure 1. Flexural modulus of samples versus clay content at different PP-g-MA levels.

The x-ray diffraction of the samples with different levels of nanoclay at the 2phc PP-g-MA concentration demonstrates that, the $2\theta=4.76^0$ is related to neat clay with d_{001}=18.5nm. In the sample with 3phc concentration of clay, the peak was shifted to a lower angle ($2\theta=4.480^0$, d_{001}=19.70nm) wich implies to formation of the intercalation morphology. The peak related to 6phc of nanoclay was appeared at $2\theta=4.54^0$, d_{001}=19.44nm. These data shows that the order of intercalation is higher for 3phc of nanocaly than the 6phc of nanoclay concentration. It seems, this is because of the limitted value of PP-g-MA in the nanocomposites. The same trend was observed in the x-ray diffraction of samples with the different levels of PP-g-MA to the same concentration of nanoclay. With increase of PP-g-MA in the composite, the d_{001} is increased. Because of the strong interaction between clay layers and coupling agent, PP-g-MA molecules could enter and penetrate the gallery between clay layers when the clay was mixed with 4phc PP-g-MA. Also TEM micrographs confirmed the x-ray results.

Fig 2 shows that the tensile modulus of the composite is similar to flextural modulus, a maximum tensile modulus was observed at 3phc of nanoclay content. Reinforcing efficiency of the nanofiller is balanced by two opposite phenomenon. The negative affect is attributed to migration of nanoparticles in to the interface of wood-plastic which caused to decrease on its performance. At 6phc of nanoclay, agglomeration of nanoparticles could decreases the reinforment of clay. Dispersion of nanoclay as positive effect could be enhanced the modulus, therefore it can be concluded in 3phc of nanoclay content in hybrid composite, the former phenomenon has dominated and the tensile modulus increases.

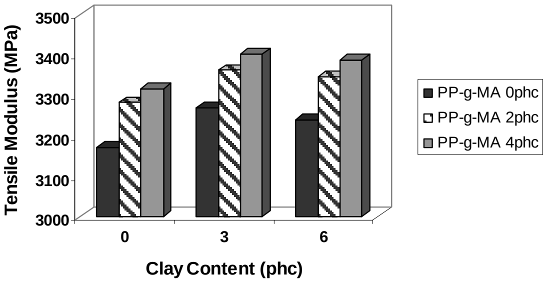

Figure 2. Tensile modulus of samples versus clay content at different PP-g-MA levels.

Figure 3 shows that the the impact strength of the composites decreases with increasing the nanoclay loading at the same concentration of PP-g-MA. The decrease in impact strength at higher clay content levels is probably due to the formation of clay agglomeration, and the presence of un-exfoliated aggregates and voids. Also figure 3 illustrates, the impact strength increases with increase of PP-g-MA at different levels of nanoclay. The enhancement in the impact strength could be attributed to the more homogeneous dispersion of the fiber resulting from the increasing wettability of the fiber with increasing concentration of the coupling agent.

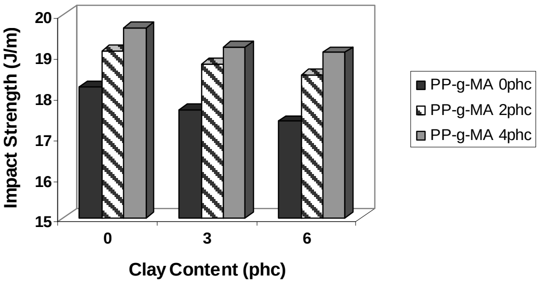

Figure 3. Impact strength of samples versus clay content at different PP-g-MA levels

4. CONCLUSIONS

The following conclusions could be drawn from the results of the present study:

1. The flextural and tensile modulus of composites increases with increase of nanoclay up to 3phc at the same concentration of PP-g-MA and then decreases. However, the impact strength was decreased with increased of nanoclay loading.
2. The mechanical properties of polypropylene/wood flour/nanoclay hybrid composites was improved by increase of PP-g-MA content.
3. The X-ray diffraction (XRD) patterns and TEM images showed that the order of intercalation is higher for 3phc of nanocaly than 6phc of nanoclay concentration. Also, the clay dispersion can improved in the PP matrix in presence of compatibilizer.
4. It seems, with increase of compatabilizer the fully exfoliation morphology could be obtained.

REFERENCES

Alexandre M, Dubois P. (2000). Polymer-Layered silicate nanocomposites: Preperation, properties and use of a new class of materials; A review, Journal of Material Sciencd and Engineering, 28, 1-63.

Mohanty S, Nayak SK. (2007). Effect of clay exfoliation and organic modification on morphological, dynamic mechanical, and thermal behavior of melt compounded polyamide-6 nanocomposites, Journal of Polymer Composite, 28, 153-162.

Tjong SC. (2006). Structural and mechanical properties of polymer nanocomposites; A review, Journal of Material Science and Engineering, 53, 73–197.

Wu Q, Lei Y, Clemons CM, Yao F, Xu Y, Lian K. (2007). Properties of HDPE/clay/wood nanocomposites, Journal of Plastic Technology, 27, 108-115.

Hetzer M., Kee D. (2008). Wood/polymer/nanoclay composites, environmentally friendly sustainable technology; A review, Journal of Chemical Engineering, 16, 1016-1027.

Preparation and mechanical properties of PS/clay nanocomposites based on recycled expanded polystyrene

K. Nagata, D. Wu, S. Matsumoto, R. Quintero Restrepo, M. Higuchi

Department of Materials Science and Engineering, Graduate School of Engineering,
Nagoya Institute of Technology, Japan

SUMMARY

Polystyrene/clay nanocomposites are investigated by melt-compounding polystyrene (PS) with an imidazolium-treated montmorillonite (organoclay). The structural, thermal and mechanical properties are characterized using FT-IR, X-ray diffraction, TGA, TEM and an instron universal testing machine. The results from these experiments show that organoclay is successfully prepared and intercalated. The thermal degradation temperatures were no less changed regardless of organoclay content, compared to the PS matrix. TEM observation indicates that organoclay is dispersed in the PS matrix and either partially exfoliated or intercalated to improve the flexural properties of PS/clay nanocomposites.

1. INTRODUCTION

Plastics are widely used in everyday life, and thus their consumption in Japan has reached *ca.* 10 million tons per year according to the 2007 data of the Plastic Waste Management Institute. However, the constant generation of plastic wastes and their disposal generates environmental problems along with economic loss. Among plastic wastes, expanded polystyrene foam (EPS) is used as packing "peanuts" and molded packing material for cushioning fragile items inside boxes in the automotive, electronic, and IT fields, and has many unique properties such as light weight and energy efficiency. To ameliorate the related environmental problems, current technologies recycle EPS into low-value products such as clothes hangers, flower pots, and toys in what is known as mechanical recycling. The conversion of EPS to high-value products (up-cycling) should lead to higher levels of EPS recycling.

We have previously reported the preparation and mechanical properties of poly-lactide/organoclay nanocomposites prepared using a melt-compounding method [1]. Also, many other researchers have reported that clays, as a filler in nanocomposite with general purpose plastics, have exhibited significantly improved mechanical and thermal properties [2]. Their layers possess a large amount of surface area, which adds to the possibility of intercalation inside the interlayer space with a strong interaction, and yields a dramatic improvement in physical and chemical properties with small loading.

In the present study, PS/clay nanocomposites were made using imidazolium salt with a long alkyl chain to modify the clay. The mechanical and thermal properties of PS nanocomposites filled with organoclay as functions of filler loading were investigated. Furthermore, morphological studies were carried out to evaluate the dispersivity of organoclay in PS nanocomposites.

2. Materials and Methods

General-purpose polystyrene (GPPS) was provided by PS Japan Ltd. and used as received. Na-type montmorillonite (MMT) as clay mineral (clay) was Kunipia-F, obtained from Kunimine Co. The cation exchange capacity (CEC) cited by the manufacturer was 115 mmol/100 g and the clay was used as received. Reagent grade 1-octadecyl-3-methylimidazolium chloride (C18mim) was purchased from Acros Organics. Standard ion-exchange procedures were employed for the preparation of the organic-treated clay [3]. The C18mim-terated MMT (C18-MMT) was characterized using an FT-IR spectrophotometer (Impact400, Nicolet), an X-ray diffractometer (XRD, RINT2000, Rigaku Co.) and a thermogravimetry/differential thermal analyzer (TGA, TG/DTA 220, SII NanoTechnology Inc.).

The preparation procedure of the PS/clay nanocomposites is described as follows. C18-MMT was mixed with the PS matrix in different ratios and blended in a twin-screw extruder (Technovel Co.) at *ca.* 100 rpm for 3-5 min at 210ºC. The products were compression-molded at 200ºC to make sheets. The PS/clay nanocomposites were characterized using XRD, TGA and transmission electron microscopy (TEM, H-7000, Hitachi Ltd.), and examined through three-point bending tests using a Tensilon (UTM-4).

3. Results and Discussion

To confirm cation exchange of montmorillonite (MMT) by C18mim, FT-IR spectroscopy was used. The strong aliphatic absorption bands observed in the C18-MMT hybrids are the methylene modes between 3,000 and 2,800 cm^{-1} and between 1,520 and 1,400 cm^{-1} (figure not shown). These results can be assigned to the C18mim intercalation into the interlayer space of MMT.

C18-MMT was analyzed by XRD to determine whether the spacing between the layers (*d* spacing) had changed. Figure 1 shows the XRD profiles of MMT and C18-MMT. These profiles show a peak at 9.1º for MMT and two peaks at 4.0º and 8.2º for C18-MMT, respectively. The peak moved to lower 2θ for C18-MMT, which indicates higher spacing for MMT galleries. The C18-MMT pattern has a visible increased intensity peak due to the C18mim intercalation, corresponding to a 12.36 ångström increase in the interlayer distance. The same behavior can be observed in Figure 2 for the composites made with C18-MMT (modified clay) and MMT, but with a variable layer interspacing assignable to the shear force of the twin-screw extruder.

Figure 3 shows the flexural modulus and strength for PS/C18-MMT nanocomposites. The exfoliated polymer/clay systems generally exhibit higher mechanical properties than the neat polymer. The flexural moduli of PS/clay nanocomposites were higher than that of the PS matrix (3.4 GPa). On the other hand, the flexural strength of PS/clay nanocomposites was lower than that of the PS matrix (50.0 MPa). When the PS matrix was filled with 5wt% C18-MMT, the flexural strength exhibited 40.3 MPa.

Figure 4 shows the TGA curves for the neat PS and PS/C18-MMT nanocomposites with different C18-MMT contents. Although C18-MMT content was different, no fewer changes in the onset temperature of thermal degradation (T_D) were observed for their nanocomposites (T_D: 392.0 ºC to 395.8 ºC) compared to the PS matrix (T_D: 395.5 ºC).

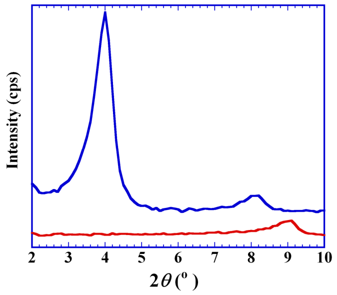

Fig. 1. XRD patterns of C18-MMT and MMT.

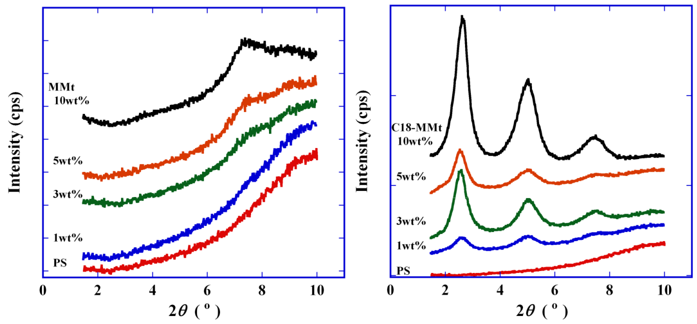

Fig. 2. XRD patterns of (a) PS/MMT and (b) PS/C18-MMT nanocomposites.

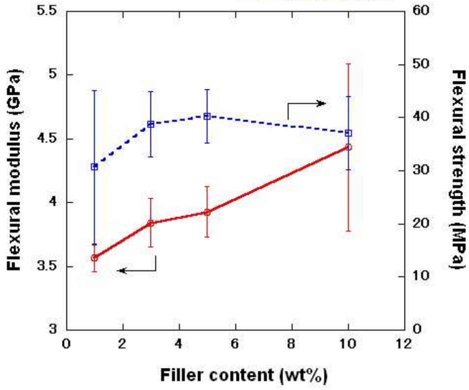

Fig. 3. Flexural properties of PS/C18-MMT nanocomposites.

This suggests that the addition of C18-MMT, whether it was intercalated, exfoliated, or not, had little or no effect on the T_D of their nanocomposites, except for the glass transition temperature (Tg).

Figure 5 shows the TEM images taken from the PS/C18-MMT nanocomposite filled with 5wt% C18-MMT. Figure 5(b) indicates that some individual layers appear in the PS matrix, as well as some smaller (*ca.* 8-layers) tactoids with expanded layer spacing. However, the degree of exfoliation of C18-MMT was smaller than what we expected in the PS matrix; therefore, the mechanical and thermal properties of their nanocomposites might be improved remarkably.

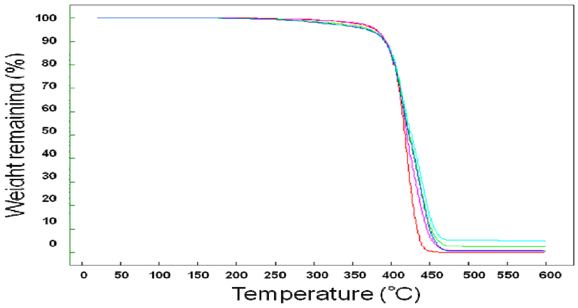

Fig. 4. TGA curves of neat PS and PS/caly nanocomposites obtained under nitrogen atmosphere and heating rate of 10ºC /min.

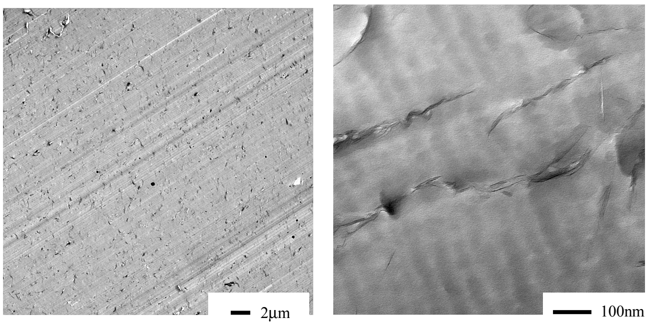

Fig. 5. TEM images of PS/C18-MMT nanocomposite filled with 5wt% C18-MMT: magnification (a) x 700 and (b) x 25,000.

3. CONCLUSIONS

In summary, PS/clay nanocomposites were made by melt-compounding using imidazolium salt to modify the clay. The organoclay was successfully intercalated. The thermal degradation temperatures were no less changed regardless of organoclay content, compared to the PS matrix. TEM observation indicates that organoclay was dispersed in the PS matrix and either partially exfoliated or intercalated to improve the flexural properties of PS/clay nanocomposites.

ACKNOWLEDGMENT

This research was supported in part by the Japan Expanded Polystyrene Recycling Association (JEPSRA).

REFERENCES

[1] MATSUMOTO, S., QUINTERO RESTREPO, R., MATSUYAMA, A., WU, D., NAGATA, K., HIGUCHI, M. (2009) Polylactide/organoclay nanocomposites: Preparation and mechanical properties, *in Proceeding of the 3rd Asian Conference on Adhesion (ACA2009)*, *Hamamatsu, Japan*, PA31. [2] KATO, M., USUKI, A. (2000) Polymer-Clay Nanocomposites, i*n Polymer-Clay Nanocomposites* (Ed. Pinnavaia, T.J., Beall, G.W.), 97-110, John Wiley & Sons Ltd., Chichester, West Sussex (England). [3] Vaia, R.A., Teukolsky, R.K., Giannelis, E.P. (1994) Interlayer structure and molecular environment of alkylammonium layered silicates, *Chem. Mater.*, 6, 1017-1022.

Nanostructured systems based on block copolymer and well-dispersed alumina/epoxy matrix nanocomposites. Optical and thermomechanical properties

C. Ocando, L. Martin, A. Tercjak, I. Mondragon
'Materials + Technologies' Group, Departamento Ingeniería Química y M. Ambiente,
Escuela Politécnica. Universidad del País Vasco/Euskal Herriko Unibertsitatea

SUMMARY

Optical, thermal and mechanical properties of composites based on Al_2O_3 nanoparticles dispersed into a neat epoxy matrix and the modified one with 30 wt% epoxidized poly(styrene-*b*-butadiene-*b*-styrene) (SBS) block copolymer (BC) are presented. The T_g of polystyrene- and epoxy-rich phases in BC-modified epoxy matrix were enhanced with the introduction of Al_2O_3. Mechanical and fracture characterization showed that it is possible to improve the stiffness of the BC-modified epoxy matrix with the incorporation of Al_2O_3, while the fracture toughness was maintained in these systems. It was found that Al_2O_3 nanoparticles were uniformly dispersed in the resulting BC-modified epoxy nanocomposite, preserving their optical properties.

1. INTRODUCTION

The poor fracture toughness of epoxy resins has represented an important drawback for many potential applications. In order to overlap this problem, the preparation of nanostructured materials via self-assembly or reaction induced microphase separation of block copolymers modified epoxy matrices has been widely used. This strategy can further optimize the fracture toughness of brittle epoxy maintaining their transparency because the phase separation in these mixtures generally occurs at nanometer scale. Epoxidized SBS triblock copolymers have been used for this purpose (Ocando et al. 2008). Nevertheless, one disadvantage of block copolymers is the risk of sacrificing the stiffness and the glass transition temperature (T_g) of the epoxy matrix. A new approach can be the inclusion of inorganic nanoparticles into epoxy matrix to enhance final mechanical properties suppressing the plasticization effect obtained with organic additives and preserving the optical transparency (Zhao et al. 2008, Zhen et al. 2009). With this goal, the aim of this work was to obtain nanostructured hybrid materials based on epoxidized SBS triblock copolymer and well-dispersed alumina/epoxy matrix nanocomposites with superior optical, thermal and mechanical properties.

2. EXPERIMENTAL PART

Block copolymer was SBS, Dynasol C500, with 30 wt% PS, kindly supplied by Repsol-YPF. The weight-average molecular mass was 136 000 g/mol, being the T_g of PS and PB blocks 70 ºC and -80 ºC, respectively. Epoxidized C500 block copolymer, C500epI, being I the epoxidation mol% with respect to PB double bonds, was obtained by epoxidation of polybutadiene block. The epoxidation reaction was described elsewhere (Ocando et al. 2008). Alumina nanoparticles with an average diameter size of 39 nm and specific surface area 44 m^2/g were purchased from Nanophase Technologies Corp.

Dodecanethiol and toluene, from Sigma Aldrich, were used as surfactant and solvent, respectively. The epoxy monomer, diglycidyl ether of bisphenol-A (DGEBA), DER 332, was purchased from Dow Chemical. It has an epoxy equivalent around 175 and an average number of hydroxyl groups per two epoxy groups $n = 0.03$. The hardener used was an aromatic diamine, 4,4′-methylenebis(3-chloro 2,6-diethylaniline) (MCDEA), supplied by Lonza. An amino-hydrogen-to-epoxy stoichiometric ratio equal to 1 was maintained for all prepared systems.

Alumina nanoparticles were added into both neat epoxy matrix and epoxy modified with 30 wt% C500ep46. Nanocomposites containing 1 wt% Al_2O_3 and a weight ratio 4:1 (dodecanethiol:Al_2O_3) were prepared. Firstly Al_2O_3 nanoparticles were dried in vacuum at 125 ºC for several hours. Nanocomposites were prepared in solution by sonication technique. Al_2O_3, surfactant, epoxidized SBS and DGEBA were dispersed in toluene for 4 h. The resultant solution was heated at 70 ºC in an oil bath, and then under vacuum up to complete solvent removal. MCDEA was added to the mixture at 140 ºC and mixed for 5 min. The samples were degassed under vacuum and cured in parallelepipedic moulds at 140 ºC during 24 h and post-cured at 165 ºC for 2 h.

3. RESULTS AND DISCUSSION

In figure 1 an AFM image of an epoxy mixture containing 30 wt% C500ep46 is presented. The mixture shows microphase-separated morphology, where spherical and wormlike PS micelles do appear confined in the epoxy matrix with long-range order.

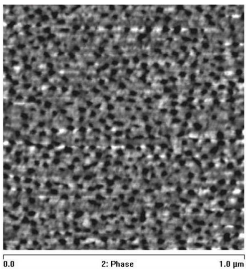

Fig. 1. TM-AFM phase image for epoxy mixture containing 30 wt% C500ep46.

Table 1 summarizes the final properties of an epoxy matrix containing 1 wt% Al_2O_3 and those of the nanostructured BC-modified epoxy matrix containing 30 wt% C500ep46 and 1 wt% Al_2O_3, with and without surfactant. It is possible to point out that better optical and thermal properties were obtained for the nanocomposites based on BC-modified epoxy than for the one with neat epoxy. Treatment of nanoparticles with surfactant clearly improved thermal properties of both epoxy- and PS-block phases. On the other hand, the incorporation of Al_2O_3 into BC-modified epoxy improved its modulus considerably. The modulus improvement is expected because of the high Al_2O_3 modulus. Figure 2 shows DMA spectra for BC-modified epoxy matrices containing Al_2O_3. As can be seen, in accordance with results of tensile tests, storage modulus (E') for the nanocomposite with surfactant was higher. At temperatures higher than T_g, the improvement of E' was dramatic for the mixture containing surfactant, which could be related to enhanced nanoparticle dispersion.

Systems	**T (%) 700 nm**^{a}	**T_g (ºC) matrix**^{b}	**T_g (ºC) PS**^{b}	**E' (MPa)**^{c} **at T_g+50ºC**	**E (MPa)**^{d}	K_{Ic}^{e}
Epoxy	80	160	-	270	2800±45	0.80±0.02
1 wt% Al_2O_3	40	166	-	320	2500±110	0.70±0.10
30 wt%C500ep46	80	110	63	120	2600±160	1.30±0.20
1 wt% Al_2O_3	60	105	60	140	2700±110	1.10±0.05
4 wt% S	70	92	51	160	2500±80	1.15±0.10
1 wt% Al_2O_3-4 wt% S	65	120	87	270	2800±50	1.05±0.05

[a]Transmittance in the UV-visible range of 700 nm, the thickness of the samples was 1.5 mm. [b]T_g of epoxy-rich and PS-rich phases, determined by DSC. [c]Storage modulus in rubber plateau zone, determined by DMA. [d]Young's modulus determined by three point flexural tests. [e]Critical stress intensity factor, K_{Ic}, values were obtained from three-point bending tests performed on single edge notched specimens (SENB).

Table 1. Properties of neat epoxy and its nanocomposites containing 1 wt% Al_2O_3 and 30 wt% C500ep46, with and without surfactant.

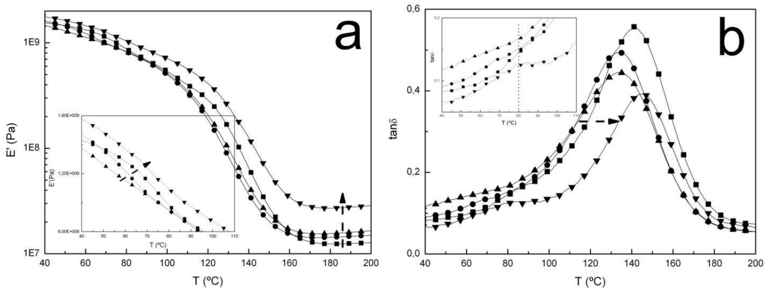

Fig. 2. DMA spectra: (a) storage modulus and (b) loss factor obtained at 1 Hz for the mixtures containing 30 wt% C500ep46 (■), and its nanocomposites containing 1 wt% Al_2O_3 (●), 4 wt% S (▲) and 1 wt% Al_2O_3-4 wt% S (▼).

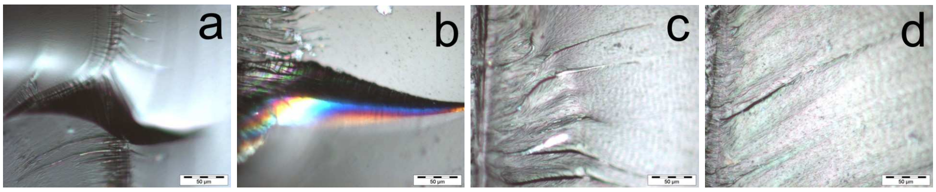

Fig. 3. OM image of fracture surface of: (a) neat epoxy, (b) 1 wt% Al_2O_3 epoxy nanocomposite, (c) mixture containing 30 wt% C500ep46 and (d) its nanocomposite containing 1 wt% Al_2O_3 with surfactant.

As can be seen from table 1, although the addition of Al_2O_3 nanoparticles produced a slight decrease on fracture toughness properties, the K_{Ic} values of both BC-modified epoxy matrix and their alumina nanocomposites were higher than that of neat epoxy matrix. In addition, optical and atomic force microscopy (AFM) analyses of fracture surfaces were also performed. As can be seen in figures 3 and 4, the fracture surface of neat epoxy and its alumina nanocomposite was very smooth, revealing that the resistance to crack was very low. On the contrary, the fracture surfaces of the BC-modified epoxy and its alumina nanocomposite were rougher showing significant toughening effect of BC. In BC-modified epoxy system, the worm-like micelles can act as nanocavities within the epoxy, allowing more facile deformation of the matrix, therefore contributing to energy absorption. Furthermore, the dispersion of Al_2O_3 in the neat epoxy was worse than the obtained in the BC-modified epoxy matrix (figure 4).

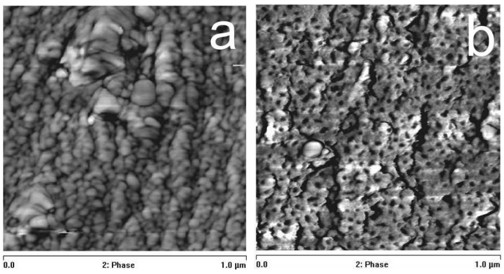

Fig. 4. TM-AFM phase image of fracture surface of 1 wt% Al_2O_3 nanocomposites of: (a) epoxy matrix and (b) 30 wt% C500ep46 with surfactant.

3. CONCLUSIONS

The optical, thermal and mechanical properties of neat epoxy were successfully improved by the preparation of nanostructured hybrid material based on SBS epoxidized triblock copolymer and well-dispersed alumina/epoxy matrix nanocomposites. The addition of Al_2O_3 nanoparticles on BC-modified epoxy matrix increased the T_g and tensile properties maintaining the fracture toughness and optical properties.

ACKNOWLEDGEMENTS

The authors want to be grateful for the support of Basque Country Government in the frame of Grupos Consolidados (IT-365-07), inanoGUNE (IE08-225) projects and also the Spanish Ministry of Science and Innovation for MAT2006-06331.

REFERENCES

OCANDO, C., TERCJAK, A., SERRANO, E., RAMOS, J.A., CORONA-GALVÁN, S., PARELLADA, M.D., FERNÁNDEZ-BERRIDI, M.J., MONDRAGON, I. (2008) Micro-and macrophase separation of thermosetting systems modified with epoxidized styrene-*block*-butadiene-*block*-styrene linear triblock copolymers and their influence on final mechanical properties. *Polym. Int.,* 57, 1333-1342.

ZHAO, S., SCHADLER, L.S., HILLBORG, H., AULETTA, T. (2008) Improvements and mechanism of fracture and fatigue properties of well-dispersed alumina/epoxy nanocomposites. *Compos. Sci. Technol.,* 68, 2976-2982.

ZHENG, Y., CHONUNG, K., WANG, G., WEI, P., JIANG, P. (2009) Epoxy/nano-silica composites: curing kinetics, glass transition temperatures, dielectric, and thermal-mechanical performances. *J. Appl. Polym. Sci.,* 111, 917-927.

EFM imaging of carbon nanotube confinement into poly(styrene-b-isoprene-b-styrene) block copolymer matrix

L. Peponi, M. Cardinali, L. Valentini, J.M. Kenny
Dipartimento di Ingegneria Civile e Ambientale, Università di Perugia, INSTM,
UdR Perugia, 05100 Terni -Italy
A. Tercjak, J. Gutierrez, I. Mondragon
'Materials + Technologies' Group, Departamento Ingeniería Química y del Medio
Ambiente, Escuela Politécnica. Universidad del País Vasco/Euskal Herriko
Unibertsitatea

ABSTRACT

In this work, atomic and electrostatic force microscopes (AFM and EFM) have been used to demonstrate the sequestering of octadecylamine functionalized single-walled carbon nanotubes (ODA-SWCNTs) in the polystyrene phase of the polystyrene-b-polyisoprene-b-polystyrene (SIS) block copolymer matrix. To disperse the ODA-SWCNTs in the SIS block copolymer matrix, dodecanethiol (DT) has been used as surfactant. From a morphological point of view a change from cylindrical self-assembled nanostructures of neat SIS to ordered lamellar domains, when 1 wt % of DT-ODA-SWCNTs has been added to the SIS matrix, has been observed. Due to the excellent electrical properties of carbon nanotubes, their confinement into the lamellar domains of the PS block has been detected by EFM.

1. INTRODUCTION

Phase-segregated block copolymers have received significant attention in the last decade as enabling materials for future technologies and represented a subject of broad current research emphasis across the full spectrum of macromolecular chemistry and physics due to their versatility of this unique class of polymers offers tremendous potential for their use as templates and scaffolds for applications in microelectronics, separation devices, optics, and optoelectronics as reported by Lodge et al., by Mauritz et al. and by Krishnamoorthy et al. In general, block copolymers consist of two or more chemically distinct polymer chains. Chemical incompatibility between the constituent blocks leads to microphase separation. Due to the covalent linkage between blocks their phase separation has been restricted to the length scale of the polymer molecules (typically 10–100 nm) as reported in literature by Mauritz et al. and by Krishnamoorthy et al. The self-assembly processes, leading to the formation of well-ordered nanostructures, are dictated by the Flory–Huggins interaction parameter, the volume fraction of the blocks, the molecular weight of the blocks and the time–temperature experimental conditions as reported by Serrano et al. and by Liu et al. So, depending also on the relative length of the constituents, block copolymers can segregate into microphase lamellae, cylinders and spheres, with several novel microstructures intervening between these broad boundaries. Most recently it has been reported by Sung how the dispersion of single-walled carbon nanotubes in a non-polar solvent is controlled with a series of polystyrene-block-polybutadiene-block-polystyrene block copolymers that contain cholesteryl chloroformate in side-chains. The fabrication of a solution of single-walled carbon nanotubes (SWCNTs) with good dispersion and stability has been of great interest because most of the potential applications of SWCNTs are based on solution processes such as spin coating and dip coating.

2. RESULTS AND DISCUSSION

In this study instead of using the block copolymer as dispersant for the carbon nanotubes, we investigated the role of an organic surfactant for the confinement of the nanotubes inside the self-assembled block copolymer matrix. More in general a surfactant consists of two parts one hydrophilic and the other one hydrophobic and due to this architecture it is used as a bridge between nanofillers and polymeric matrices as reported by Niu et al.. In particular when a block copolymer matrix is used an adequate surfactant can be used to selectively disperse nanofillers in one of the blocks of the block copolymer matrix as reported in our previous works. This selectivity is important in designing the properties of block copolymer based composites. The effect of surfactant on final neat SIS and ODASWCNTs/SIS composite morphologies has been investigated by FE-SEM technique. Fig. 1a shows the FE-SEM image of neat SIS. Even if the FE-SEM analysis does not provide any information on the topography of the samples, the self-assembled morphology of the different blocks of the block copolymer matrix is observable. In fact, Fig. 1a shows the cylindrical self-assembled nanostructure of the PS phase with the most of the cylinders placed parallel to the free surface (diameter - 15 nm). When DT modified ODA-SWCNTs have been used for the realization of nanocomposite films, the self-assembled cylindrical morphology observed for the neat SIS switched to well-ordered lamellar nanostructure (interlamellar periodicity of about 20 nm).

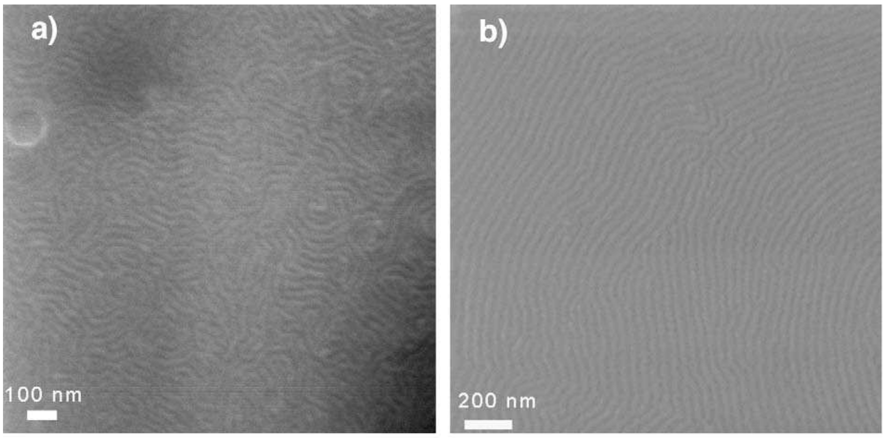

Fig. 1. FE-SEM images for (a) neat SIS block copolymer, (b) ODA-SWCNTs/SIS.

This fact is also confermed by AFM. The electrical conductivity of the nanocomposites and the formation of a conductive network of the carbon nanotubes is confirmed taking into account the electrical properties of the film, measured using a semiconductor characterization system.

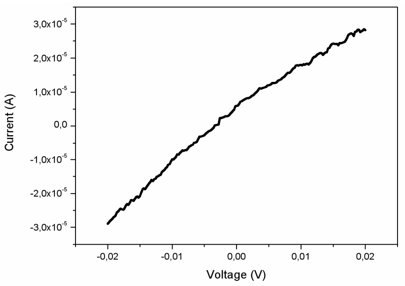

Fig. 2. Current-Voltage curve of DT-ODASWCNTs/SIS.

Due to the electrical conductive behaviour of the DT modified ODA-SWCNT/SIS nanocomposite films, in order to investigate the positioning of the nanotubes into the SIS matrix, the electrical behaviour of the nanocomposite films has been investigated by electrostatic force microscopy. This non-invasive technique has been used to qualitatively map the nanocomposite surfaces evidencing the contrast between the conductive ODA-SWCNTs and the insulating SIS block copolymer matrix.

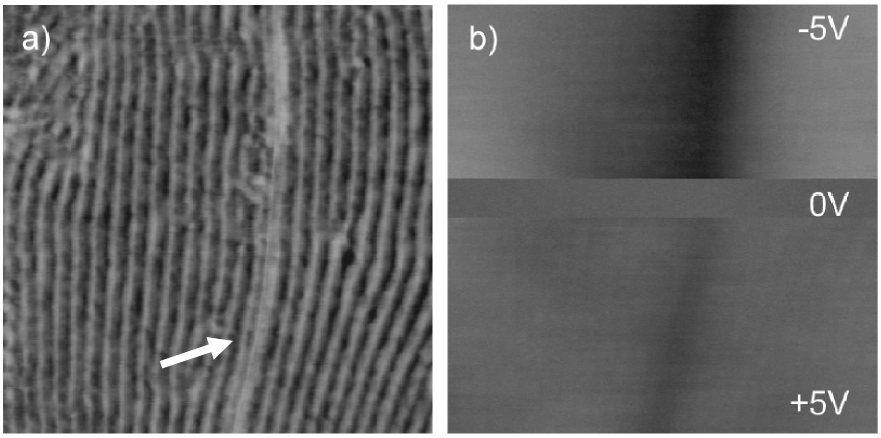

Fig. 3. (a) TM-AFM and (b) EFM phase images (1x1μm) obtained on the DT-modified ODA-SWCNTs/SIS sample varying the bias from negative to positive values passing thorough 0V. The arrow in Figure 5a serves to the eyes to indicate the nanotube inside the PS lamella.

3. CONCLUSIONS

The use of EFM to investigate thin nanocomposite films, brings important new insights on the self-assembling behavior of block copolymer matrices as host for the nanotube positioning, and more specificallym for the imaging of the nanotubes inside the block copolymer domains. Extension to other types of hybrid nanocomposites can be expected to provide valuable information on the conformational properties on the local scale in functional self-assembled architectures.

REFERENCES

KRISHNAMOORTHY S, HINDERLING C, HEINZELMANN H. (23006) Nanoscale patterning with block copolymers. *Mater. Today, 9, 40-4.*
LIU T, BURGER C, CHU B. (2003) Nanofabrication in polymer matrices. *Progr. Polym. Sci., 28, 5-26.*
LODGE TP. (2003) Block copolymers: past successes and future challenges. *Macromol. Chem. Phys. 204, 265-73.*
MAURITZ, K.A., STOREY, R.F., MOUNTZ, D.A., REUSCHLE, D.A. (2002) Poly(styrene-b-isobutylene-b- styrene) block copolymer ionomers (BCPI), and BCPI/silicate nanocomposite. 1. Organic counterion: BCPI sol–gel reaction template. *Polymer, 43, 4315-23.*
NIU, S., SARAF. R.F. (2007) Selective assembly of nanoparticles on block copolymer by surface modification. *Nanotechnology,18, 125607-10.*
SUNG J, et al. (2007) Control of SWNT dispersion by block copolymers with a side-chain polarity modifier. *Macromol. Rapid Commun., 28, 176-82.*

Confinement of graphene nanosheet into poly(styrene-b-isoprene-b-styrene) block copolymer matrix

L. Peponi, J.M. Kenny
Dipartimento di Ingegneria Civile e Ambientale, Università di Perugia, INSTM, UdR Perugia, 05100 Terni - Italy
A. Tercjak, I. Mondragon
'Materials + Technologies' Group, Departamento Ingeniería Química y del Medio Ambiente, Escuela Politécnica. Universidad del País Vasco/Euskal Herriko Unibertsitatea
R. Verdejo, M.A. Lopez Manchado
Institute of Polymer Science and Technology (CSIC), Juan de la Cierva, 3 28003-Madrid - Spain

ABSTRACT

The successful confinement of exfoliated graphene nanosheets into a nanostructured poly(styrene-b-isoprene-b-styrene), SIS, block copolymer matrix has been reported in this work. The incorporation of carbon nano-objects in these self-organized matrices provides new opportunities for scientific insights into the physics of self-organization, as well as a vast range of multifunctional properties for potential technological applications.

1. INTRODUCTION

Nanocomposites based on the block copolymers ability to self-assemble into well order nanostructured morphology constitute a multidisciplinary area of great interest since they self-assemble to form well-defined, ordered, periodic nanoscale morphologies as reported by Bockstaller et al., by Hamley et al., by Warren et al., by Park et al., by Lazzari et al., by Caseri et al. and by Segalman et al.

Graphene is a giant aromatic macromolecule with an enormous specific surface area and excellent mechanical, electrical and thermal conductivity properties as reported in literature by Kotov and Novoselov. So, the incorporation of individual graphene sheets into polymer matrices could lead to a new class of polymer composite materials with enhanced properties and new functionalities as reported by Stankovich. Self-assembling of block copolymers (BC) has been reported as a powerful method to generate well-ordered structures at the nanometer scale. BC can spontaneously self-organize into well-defined spherical, cylindrical and lamellar morphologies with domain dimensions of 5-100 nm as reported by Lazzari et al.. This self-assembling is controlled by a reduction of the enthalpy as the blocks demix, but also by the loss of entropy as the blocks arrange in ordered structures. The resulting equilibrium morphologies depend on the copolymer composition, the volume ratio of each block and the experimental conditions, among other factors. In this work, the dispersion of graphene sheets in the block copolymer matrix was confirmed by atomic and electrostatic force microscopies.

2. RESULTS AND DISCUSSION

A stable suspension of individual graphene sheets in toluene is obtained by sonication. In Figure 1 are reported FE-SEM images of the grapheme nanosheets, after sonication. It is worth to note the exfoliation of the graphene into single transparent sheets. In fact, the morphology of the substrate, FTO, can be detected.

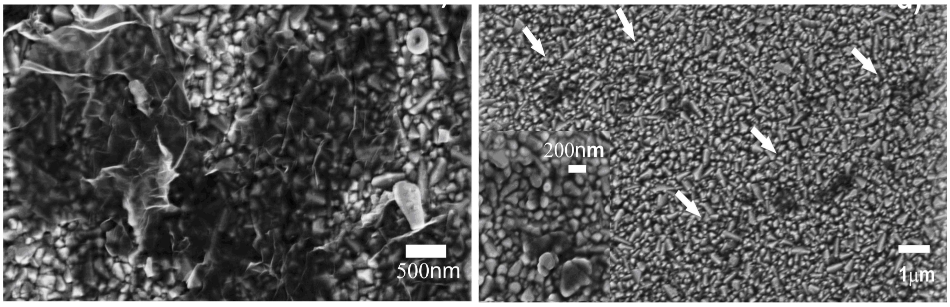

Fig. 1. FE-SEM images exfoliated graphene nanosheets.

The block copolymer was then dissolved in the well-dispersed suspension of FG sheets in toluene and the nanocomposite system was processed by spin-coating obtaining transparent thin nanocomposite films with 0.5wt% of graphene.

AFM analysis revealed a drastic change of the self-assembled morphology of the nanocomposite. The poly(styrene-b-isoprene-b-styrene) (SIS) neat matrix presented well-ordered cylindrical domains of PS block parallel to the free surface with an average diameter of about 20 nm (Fig. 2).

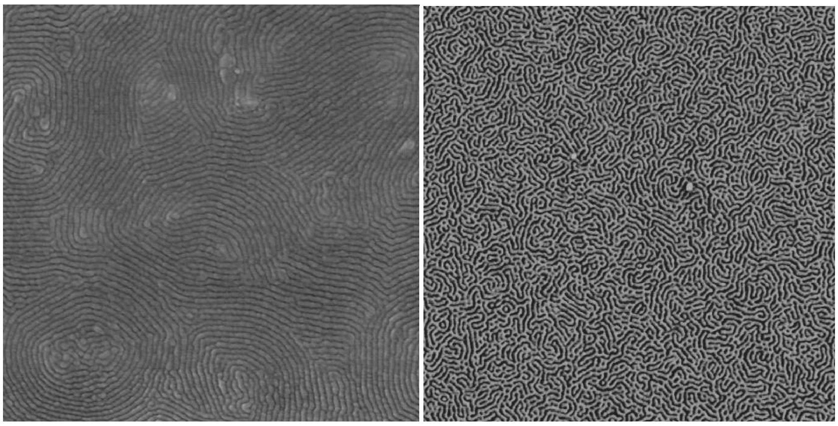

Fig. 2. FE-SEM images for (a) neat SIS block copolymer, (b) FGS/SIS.

The confinement of the graphene by the PS block was also confirmed by DSC analysis. The glass transition (Tg) of the PI block remains invariant at about -58 ºC for both SIS and NG, while the Tg of PS block shifts from 78 ºC for neat SIS to 84 ºC for NG. The glass transition (Tg) of PI block remains invariant at about -58 ºC for both SIS and NG, while the Tg of PS block shifts from 78 ºC for neat SIS to 84 ºC for NG. This increment in the PS Tg indicated the stiffening of the PS segments which is coherent with the reduced mobility of the PS domains as a consequence of the sequestering of graphene nano-sheets in the PS phase. Moreover, this mobility reduction can be also responsible of the morphological changes in the nanocomposite.

The topography height profile reported in Figure 3, corresponding to the FG sheets evidenced by arrows, showed a minimal number of "superficial" graphene sheets, height profile of 1-10 nm, on well-ordered block copolymer-based nanocomposites. (Fig. 3)

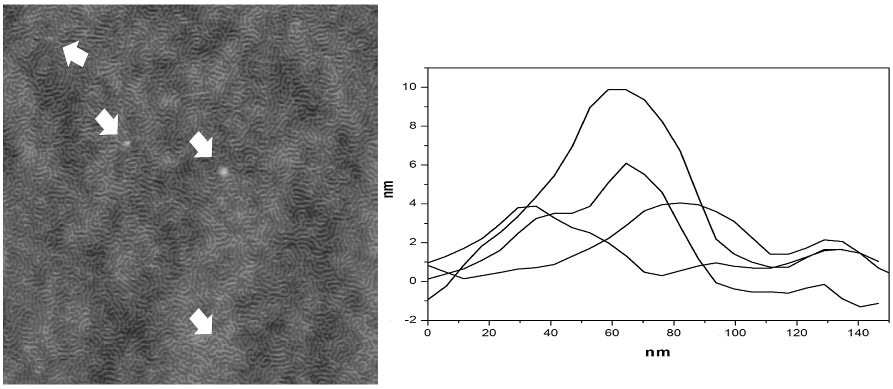

Fig. 3. (3 x 3 μm) tapping-mode AFM topography (left) and the corresponding topography height profile (right). The arrows indicate some graphene nano-sheets corresponding to the height profile.

3. CONCLUSIONS

The results indicated that the graphene sheets were confined in the PS domains of SIS block copolymer and that this confinement induced a change in the nanostructured morphology of the matrix. We expect that this facile approach for preparation of graphene-based block copolymer nanocomposites will lead to the development of a new class of materials with enhanced properties.

REFERENCES

BOCKSTALLER M.R., MICKIEWICZ R.A., THOMAS E.L. (2005). Block Copolymer Nanocomposites: Perspective for tailored functional materials. *Adv. Mater., 17, 1331-1349.*

CASERI W. (2000) Nanocomposites of polymers and metals or semiconductors: historical background and optical properties. *Macromol. Rapid. Commun., 21, 705–22.*

GEIM A.K., NOVOSELOV K.S., (2007) The rise of graphene, *Nat. Mater. 6,* 183-191.

HAMLEY IW. (2003) Nanostructure fabrication using block copolymers. *Nanotechnology, 14, R39–54.*

LAZZARI M, LOPEZ-QUINTELA MA. (2003) Block copolymers as a tool for nanomaterial fabrication. *Adv. Mater. 15, 1583–94.*

LODGE TP. (2003) Block copolymers: past successes and future challenges. Macromol. Chem. Phys. *204, 265–73.*

KOTOV A.N. (2006) Materials science: Carbon sheet solutions. *Nature*, *442, 254-255.*

PARK C, YOON J, THOMAS EL. (2003) Enabling nanotechnology with self assembled block copolymer patterns. *Polymer 44, 6725–60.*

WARREN SC, MESSINA LC, SLAUGHTER LS, KAMPERMAN M, ZHOU Q, GRUNER SM, et al. (2008) Ordered mesoporous materials from metal nanoparticle-block copolymer self-assembly. *Science 320,1748–52.*

STANKOVICH, S. DIKIN D.A., DOMMETT G.H.B., KOHLHAAS, K.M., ZIMNEY, E. J., STACH, E. A., PINER, R. D., NGUYEN, S.-B. T., RUOFF, R. S. (2006) *Nature 442,* 282-286.

Nanocomposites de poliuretano preparados mediante polimerización in situ con nanocargas de silicato reactivas

L. Rueda, M. A. Corcuera, I. Mondragón, A. Eceiza
'Materials + Technologies' Group, Departamento Ingeniería Química y del Medio Ambiente, Escuela Politécnica. Universidad del País Vasco/Euskal Herriko Unibertsitatea

RESUMEN

En este trabajo se presentan la síntesis y caracterización de nanocomposites en base poliuretano incorporando montmorillonita modificada (Cloisite 30B®), que consiste en láminas de silicato orgánicamente modificadas con una sal de amonio cuaternaria.

1. INTRODUCCIÓN

Una de las áreas de investigación que ha evidenciado un desarrollo importante en la última década corresponde al estudio de los nanomateriales en general y de los nanocomposites poliméricos en particular aplicables en muy diversos campos (Ramakrishna et al. 2001). En los últimos años, los nanocompuestos poliméricos incorporando cargas naturales tipo motmorillonita han sido objeto de numerosos estudios debido a la mejora en propiedades mecánicas, térmicas y barrera (Xiong et al. 2007). Entre las matrices poliméricas utilizadas en la síntesis de dichos nanocompuestos, los poliuretanos termoplásticos segmentados (STPU) poseen unas propiedades únicas que los hacen atractivos en diversos sectores (Wang el al. 2008, Liu et al. 2009).

Sin embargo, la mejora observada en las propiedades finales del nanocomposite está condicionada por la efectiva dispersión del nanorrefuerzo en la matriz polimérica. Una forma de aumentar la compatibilidad entre los nanorrefuerzos inorgánicos y la matriz polimérica de naturaleza orgánica es mediante la incorporación de montmorillonita modificada con cationes orgánicos de hidrofobicidad similar a la matriz y/o con grupos capaces de intervenir en los procesos de polimerización de la matriz (Wang et al. 2007). En este sentido se ha incorporado una montmorillonita modificada con agentes compatibilizantes $N^+(CH_2CH_2OH)_2(CH_3)T$, Cloisite® 30B (C30B), que aumentan la hidrofobicidad de la carga y poseen grupos hidroxilo (-OH) que podrán intervenir directamente en la reacción para alcanzar una óptima dispersión en la matriz polimérica.

En este trabajo se presentan los resultados obtenidos en la funcionalización del nanorrefuerzo y preparación de nanocomposites basados en matrices de poliuretano biocompatibles con diferente contenido de C30B y el estudio de su caracterización enfocado hacia la mejora de sus propiedades influenciadas por la efectiva dispersabilidad del nanorrefuerzo en la matriz.

2. PARTE EXPERIMENTAL

2.1 Síntesis de matriz poliuretano biocompatible

La síntesis de la matriz de tipo poliuretano STPU con 18 wt% de segmento rígido se ha llevado a cabo mediante polimerización en 2 etapas. El segmento flexible (SS) está formado por poli(caprolactona-b-politetrahidrofurano-b-caprolactona) diol (PCL-b-PTHF-b-PCL) y el segmento rígido (HS) por 1,6 hexametilendiisocianato (HDI) y 1,4 butanodiol como extendedor de cadena. La primera etapa de la síntesis se ha llevado a cabo incorporando el poliol y el diisocianato a un reactor a 100 ºC durante 6 h en atmósfera de N_2. En la segunda etapa se añade el extendedor de cadena y la mezcla se transfiere a un molde completándose la reacción en estufa de vacío a 100 ºC durante 24 horas.

2.2 Funcionalización de C30B y preparación de los nanocomposites

La funcionalización de C30B mediante los grupos isocianato del HDI y su capacidad de anclaje químico a la matriz se ha analizado siguiendo la reacción entre los grupos hidroxilo de C30B y el grupo isocianato de HDI. La reacción se ha llevado a cabo en un reactor a 100ºC durante 300 minutos incorporando el nanorrefuerzo dispersado mediante sonicación (Vibracell 75043, Bioblock Scientific) en tetrahidrofurano (THF) previamente secado y el HDI en relación estequiométrica.

Los nanocomposites en base a una matriz de poliuretano con 18% de segmento rígido (STPU-18) han sido sintetizados incorporando en la primera etapa de la reacción diferentes porcentajes de C30B dispersados mediante sonicación en THF seco. La síntesis de los nanocomposites se ha completado siguiendo el mismo procedimiento que para la matriz. La tabla 1 recoge la nomenclatura de los nanocomposites sintetizados y el contenido de C30B.

Nanocomposites de poliuretano	Contenido de C30B (wt%)
STPU-18-1	1
STPU-18-2	2
STPU-18-4	4

Tabla 1. Nomenclatura y composición de los nanocomposites de poliuretano sintetizados indicando el correspondiente porcentaje de C30B.

3. RESULTADOS Y DISCUSION

La funcionalización del nanorrefuerzo C30B con grupos isocianato del HDI se ha estudiado mediante Espectroscopia Infrarroja de Transformada de Fourier (FT-IR). En la figura 1 se observa la aparición de diversas bandas, banda a 1730 cm^{-1} correspondiente al grupo carbonilo de uretano, banda a 1540 cm^{-1} correspondiente a la vibración de tensión del grupo amida I, así como la aparición de la banda a 3425 cm^{-1} de los grupos –NH, que confirman el anclaje químico del HDI en la superficie del nanorrefuerzo a través de la reacción del grupo isocianato del HDI y los grupos hidroxilo de C30B.

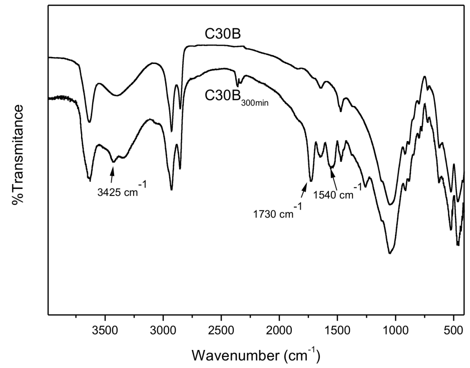

Fig. 1. Espectros FT-IR de C30B y C30B tras 300 min de reacción (C30B$_{300min}$).

La caracterización de los nanocomposites sintetizados se ha llevado a cabo mediante diversas técnicas de análisis térmico y morfológico. La respuesta viscoelástica de la matriz y los nanocomposites sintetizados se ha evaluado mediante Análisis Mecánico-Dinámico (DMA). La figura 2 muestra el módulo de almacenamiento (E’) y el factor de pérdidas (tan δ) de la matriz y de los nanocomposites sintetizados. Se observa que la temperatura de transición vitrea (T_g) se desplaza hacia valores de temperatura mayores al incrementar el contenido de nanorrefuerzo, atribuyéndose a restricciones de movilidad en el SS debido a interacciones entre la matriz y las láminas de silicato funcionalizadas. Además se observa que los nanocomposites con mayor contenido de C30B muestran un incremento en el E’ pudiéndose atribuir al mecanismo de refuerzo que ejerce el material inorgánico (Pattanajak et al. 2005).

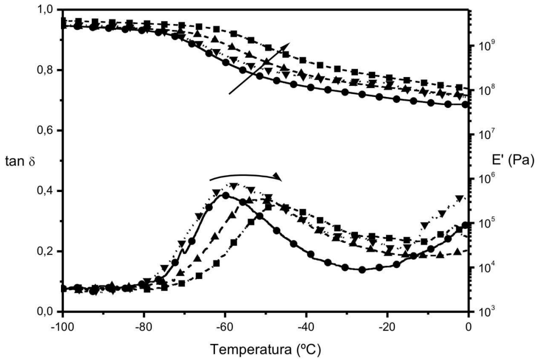

Fig 2. Tan δ y E’ vs. Temperatura de STPU-18 (■), STPU-18-1 (▲), STPU-18-2 (●) y STPU-18-4 (◆).

El estado de la dispersión de la carga en los nanocomposites se ha examinado mediante Microscopía de Fuerza Atómica (AFM). La figura 3 muestra el estado de exfoliación del refuerzo a escala nanométrica para materiales conteniendo 1 wt% de C30B mientras que para STPU-18-4 se puede observar evidencia de estructuras intercaladas, que puede ser debido a la alta viscosidad que se alcanza como resultado del incremento del porcentaje de C30B.

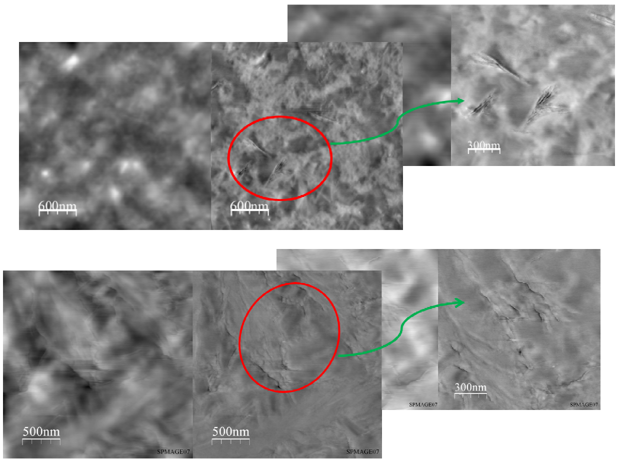

Fig 3. Imágenes de AFM de STPU-18-1 (abajo) y STPU-18-4 (arriba).

4. CONCLUSIONES

Se han sintetizado nanocomposites con diferentes porcentajes de nanorefuerzos orgánicamente modificados capaces de intervenir en la reacción de polimerización de la matriz de tipo poliuretano termoplástico segmentado observándose una efectiva dispersión a escala nanométrica mediante el anclaje químico.

AGRADECIMIENTOS

Se agradece a la Universidad del País Vasco/Euskal Herriko Unibertsitatea (PIFA01/2006/045) y al Gobierno Vasco (Saiotek S-PE08UN11, CIC inanoGUNE-ETORTEK 0911 y Grupos de Investigación Consolidados IT-365-07) por la ayuda económica prestada para este trabajo.

REFERENCIAS

RAMAKRISHNA, S., MAYER, J., WINTERMANTEL, E., LEONG, K.W. (2001). Biomedical applications of polymer-composite materials: a review. *Compos Sci Technol.*, 61, 1189-1224.

XIONG, J., ZHENG, Z., JIANG, H., YE, S., WANG, X. (2007). Reinforcement of polyurethane composites with an organically modified montmorillonite. *Compos. A: Appl. Sci. Manuf.,* 38, 132-137.

WANG, W., GUO, Y., OTAIGBE, J.U. (2008). Synthesis and characterization of novel biodegradable and biocompatible Poly (ester-urethane)s thin films prepared by homogeneous solution polymerization. *Polymer,* 49, 4393-4398.

LIU X.-Y., ZHANG Ch.-C., XU W.-L., OUYANG Ch.-X. (2009). Controlled release of heparin from blended polyurethane and silk fibroin film. *Mate. Let.*, 63, 263-265.

WANG, H.H., CHEN, K.V. (2007). A Novel Synthesis of Reactive Nano-Clay Polyurethane and Its Physical and Dyeing Properties. *J. Appl. Polym. Sci.,* 105, 1581-1590

PATTANAYAK, A., JANA, S.C. (2005) Synthesis of thermoplastic polyurethane nanocomposites of reactive clay by bulk polymerization methods. *Polymer,* 46, 3275-3288.

Compuestos nanoestructurados de polipropileno con nanotubos de carbono. Mezclado por ultrasonido

Y. Sánchez , A. Karam
Laboratorio de Polímeros, Centro de Química, Instituto Venezolano de Investigaciones Científicas (IVIC), Caracas, Venezuela
C. Albano, C. Candele
Laboratorio de Polímeros, Centro de Química, IVIC, Caracas, Venezuela.
Escuela de Ingeniería Química, Universidad Central de Venezuela, Caracas, Venezuela
G. González
Centro Tecnológico, IVIC, Caracas, Venezuela

RESUMEN

En este trabajo se realizó el estudio del mezclado en solución mediante ultrasonido (US) y el empleo de agentes surfactantes como posible solución a la tendencia que poseen los nanotubos de carbono (NTCs) a aglomerarse, al emplearse como carga en matrices poliméricas, como el caso del polipropileno (PP). Se elaboraron nanocompuestos de PP/NTC´s variando el contenido de carga entre 0,02- 0,5 % y el tiempo de mezclado entre 13 y 35 min., en presencia de un surfactante como agente dispersante. Se evaluaron dos clases de surfactante: uno el dodecil sulfato de sodio (DSS) del tipo aniónico: y el nonil fenol etoxilado (NFE-10) del tipo no iónico. Los compuestos obtenidos fueron caracterizados mediante ensayos mecánicos,calorimetría diferencial de barrido (DSC) y análisis termogravimétrico (TGA). Se observó que la adición de NTCs produce un incrementó la rigidez del PP. Las mejores propiedades mecánicas (incremento de la rigidez en un 67%) se obtuvieron a 0,05% p/p de NTC´s, 35 min y DSS. Respecto a las propiedades térmicas se encontró que los NTC´s actúan como agentes nucleantes durante la cristalización del PP, evidenciado por el incremento de la temperatura de cristalización, a medida que incrementa el contenido de carga. Adicionalmente se observó un aumento tanto de la temperatura de inicio de descomposición como de la Energía de activación a la descomposición, que sugiere que la incorporación de NTC´s permite mejorar la estabilidad térmica del PP. Se encontró que las propiedades térmicas dependen más del contenido de carga que del agente surfactante empleado.

1. INTRODUCCIÓN

El empleo de NTC´s como cargas reforzantes ha permitido obtener un mejoramiento significativo de las propiedades mecánicas y térmicas de diversas matrices poliméricas, superando los resultados obtenidos con otras cargas.(López Manchado y col. (2005)). Sin embargo, su uso se ha visto limitado por su la alta tendencia a aglomerarse debido a las fuerzas de Van der Waals que mantienen una fuerte atracción entre ellos, (Zhu y col. (2003)). Adicionalmente, su superficie poco reactiva evita la adecuada interacción interfacial con matrices apolares.

La obtención de nanocompuestos homogéneos con una adecuada dispersión y distribución uniforme, se ha convertido en un verdadero reto científico y tecnológico. Entre las soluciones se han propuesto: el mezclado por ultrasonido, el mezclado en fundido, la funcionalización superficial, la adición de surfactantes y agentes compatibilizantes, etc. (Dondero y col. (2006)).

Respecto al ultrasonido, las condiciones extremas de temperatura y presión generadas por el fenómeno de cavitación acústica, permiten que este método pueda ser empleado para generar una dispersión y mezclado efectivo (Chang y col. (2005)). Mientras que la doble afinidad de los agentes surfactantes (hidrofílica e hidrófoba) podría mejorar la dispersión de NTC´s en polímeros apolares (Gong y col. (2000))

En este sentido, este trabajo plantea la elaboración de nanocompuestos de PP y NTC´s mediante la técnica del mezclado en solución con ultrasonido (US), empleando dos tipos de surfactantes, con el propósito de mejorar la dispersión.

2. PARTE EXPERIMENTAL

2.1 Materiales

PP comercial grado J600, suministrado por PROPILVEN, S.A. Nanotubos de carbono de paredes múltiples, 88% de pureza, suministrados por Nanocyl S.A. Decalina, cis y trans, 99% de pureza, Riedel-de Haën. Dodecil sulfato de sodio (DSS), surfactante aniónico, 95% de pureza, Sharlau Chemie S.A. Nonilfenol etoxilado con 10 moles de óxido de etileno (NFE-10), surfactante no iónico, suministrado por Couttenye & Co. S.

2.2. Preparación de los compuestos

Se realizó una dispersión en decalina de los NTPMs en una proporción entre 0,02- 0,5 %. Se añadió surfactante en una relación 1:5 p/p y se aplico ultrasonido por 3 min. Se diluyó el PP en decalina bajo agitación y calentamiento controlado. Esta solución fue agregada a la dispersión de NTPMs. Se sometió la mezcla a ultrasonido variando el tiempo de mezclado entre 15 y 35 min. El compuesto fue recuperado añadiendo hexano en lavados sucesivos, para luego ser filtrado y secado al vacío.

2.3 Caracterización de los compuestos

Las propiedades mecánicas fueron realizadas en una maquina de ensayos Universales Instron 4204 según la norma ASTM D638. La calorimetría diferencial de barrido fue realizada en un Metter Toledo DSC822. La temperatura de inicio de degradación (Tid) fue determinada a partir de la primera derivada los termogramas obtenidos en un equipo de análisis termogravimetrico Mettler Toledo TGA851. La energía de activación fue calculada a partir del método de la función E2, propuesto por Hsi-Jen y col. (2004).

3. DISCUSIÓN DE RESULTADOS

Al analizar las propiedades mecánicas de los compuestos se encontró que cuando el PP es sometido a US (PPJ600 US) el módulo elástico presenta un descenso. Este resultado permite inferir que el PP se degrada cuando se expone a la radiación ultrasónica durante el tiempo de mezclado con los NTPM´s (Figura 1)

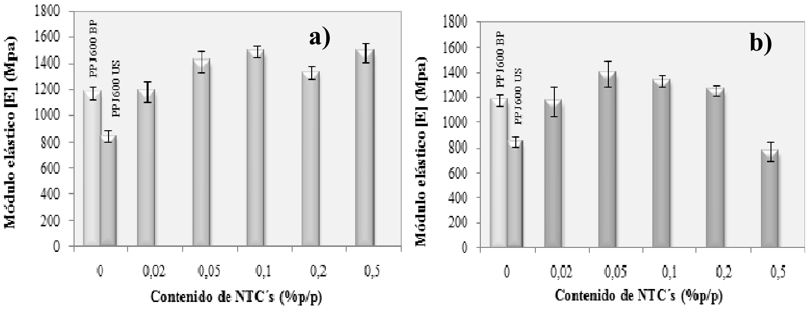

Fig 1. Módulo elástico de compuestos PP- NTCs dispersos con DSS a diferentes tiempos de mezclado a) 13 min b) 35 min.

Al comparar el tiempo de mezclado en US en las mezclas con DSS, se encontró que al emplear 13 min, el módulo elástico incrementa con el contenido de carga hasta 0,05 % luego de lo cual comienza a disminuir. Esto fue atribuido a una mayor formación de aglomerados a mayores contenidos de carga, lo que aumenta la concentración de esfuerzos, afectando negativamente la rigidez del compuesto. Al aumentar a 35 min, el módulo mostró un incremento con la carga que se mantiene invariable a contenidos superiores al 0,05 %. Lo que demuestra que a un mayor tiempo de mezclado se puede lograr una mejor disgregación de los aglomerados, además de permitir una mayor adsorción de las moléculas de surfactante sobre la superficie de la carga. Resultados similares fueron obtenidos al emplear NFE10. Sin embargo se encontró que el mayor aumento en esta propiedad fue del 76 % a 0,05 de NTCs. % empleando DSS respecto al PP sometido a US, mientras que con el NF10 fue del 42 % a la misma concentración.

Se encontró que la adición de NTCs produjo un ligero aumento en la resistencia a la ruptura y una ligera disminución en deformación a la ruptura. Sin embargo los nanocompuestos no mostraron variaciones significativas con el incremento de carga presentando valores entre (30-32 ±2,01 MPa) y (9- 11 %) respectivamente.

Independientemente del surfactante utilizado, se observó un incremento de la temperatura de cristalización con la adición de NTCs, con respecto al valor del PP puro (desde 120 º C hasta aproximadamente 124 ºC) Lo que sugiere que los NTC´s ejercen un efecto nucleante sobre el PP, lo que induce una disminución del tiempo de inducción para la cristalización de este polímero. Sin embargo la temperatura no mostró cambios significativos, mientras que el porcentaje de cristalización, disminuyo ligeramente a mayor contenido de carga (0,5%) desde 66% hasta 64 % para el caso del DSS y 62 % para el NF10. Lo cual podría ser consecuencia de los aglomerados, puesto que se conoce que estos son capaces de interferir con el crecimiento de los cristales.

La temperatura inicial de degradación (Tid) de los nanocompuestos presentó una tendencia a incrementar con la cantidad de NTPM´s, alcanzando el mayor valor para el caso de 0,5 % p/p (Figura 2) Este comportamiento sugiere que la incorporación de NTC´s como cargas reforzantes puede mejorar la estabilidad térmica del PP.

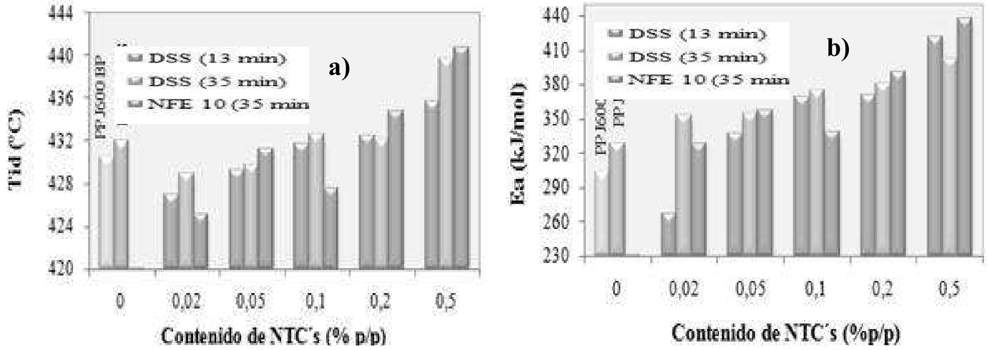

Fig. 2. Temperatura de inicio de descomposición (a) y Energía de Activación (b) de compuestos PP- NTCs dispersos con DSS a diferentes tiempos de mezclado.

4. CONCLUSIONES

Un mayor tiempo de mezclado permite una mejor dispersión de la carga y mejor absorción del agente surfactante. A bajos contenidos de NTC´s (0,05% p/p) se alcanzó un incremento en la rigidez del 67%, empleando como surfactante DSS y un tiempo de mezclado de 35 min. Independientemente del tipo de surfactante la adición de NTCs tiene un efecto nucleante sobre la cristalización de PP por lo que se produce un incremento en la Tc y confiere a los compuestos una mayor estabilidad térmica. La presencia de aglomerados a altos contenidos de carga desmejora las propiedades térmicas y las mecánicas.

5. REFERENCIAS

CHANG, T.E., JENSEN, L.R., KISLIUK, A., PIPES, R.B., PYRZ, R. & SOKOLOV, A.P. (2005). Microscopic mechanism of reinforcement in single-wall carbón nanotube/ polypropylene nanocomposite. *Polymer*, 46: 439-444.

DONDERO, W.E., & GORGA, R.E. (2006). Morphological and mechanical properties of carbón nanotube/polymer composites via melt compounding. *Journal of Polymer Science Part B: Polymer Physics*, 44: 864-878.

GONG, X., LIU, J., BASKARAN, S., VOISE, R.D. & YUNG, J.S. (2000). Surfactant-assisted processing of carbon nanotube/polymer composites. *Chemistry of Materials*, 12:1049-1052.

HSI-JEN C., KUAN-MIN L.,YEH-CHIN L.(2004). Methods for determining the kinetic parameters from nonisothermal thermogravimetry*J. Chem. Eng. Japan*, 37, 1172-1178

LÓPEZ MANCHADO, M.A., VALENTINI, L., BIAGIOTTI, J. & KENNY, J.M. (2005). Thermal and mechanical properties of single walled carbón nanotubes polypropylene composites prepared by melt proccesing. *Carbon*, 43:1499-1505.

ZHU, J., KIM, J., PENG, H., MARGRAVE, J.L., KHABASHESCU, V.N & BARRERA, E.V. (2003). Improving the dispersión and integration of single-walled carbón nanotubes in epoxy composites through functionalization. *Nano Letters*, 3(8): 1107-1113.

Innovative natural fiber honeycomb cores for sandwich structures based on vinylester resin reinforced with jute fabrics

A. Stocchi, E. Rodríguez
Institute of Material Science and Technology (INTEMA)
University of Mar del Plata - National Research Council (CONICET),
Av. Juan B. Justo 4302 - B7608FDQ - Mar del Plata, Argentina
C. Bernal
Advanced Materials Group (GMA)
INTECIN (UBA-CONICET)
Department of Mechanical Engineering-Engineering Faculty University of
Av. Paseo Colón 850 – 1063 – Buenos Aires, Argentina
A. Vázquez
Laboratorio de Polímeros y Materiales Compuestos. Instituto de Tecnologías y Ciencias de la Ingeniería (INTECIN). Facultad de Ingeniería. Universidad de Buenos Aires, Argentina

ABSTRACT

In this work the fabrication of new honeycomb cores were investigated, focusing in a novel process methodology. Renewable materials and industrial waste as jute fiber and flyash particles respectively were used as reinforcement. The obtained cores were characterized in compression tests and compared with available commercial honeycomb cores. The tests results and the density measurement indicated good specific properties.

1. INTRODUCTION

Structural sandwich panels are widely used in many structures, especially in the aeronautic and transportation industry due to several properties like high specific strength and stiffness, acoustic isolating capacity and low thermal conductivity.

The sandwich composites are a special type of composite laminate where 2 thin but stiff and strong faces are separated by a core material. By separating the skins in this way, the strength and stiffness of the structure is increased with little increase in weight (Shahdin et. al, 2009)

Such sandwich structures are wide used as a way to obtain lightweight components with high bending strength and stiffness (Ole Thybo Thomsen, 2009). The core provides flexural stiffness and out-of-plane shear and compressive strength. There are several groups of core materials and they can be classified by the type of support that the cores provide to the skins. Typical core materials are foams or balsa cores. Those cores with open cells, closed cells or without cells provides a homogeneous support of the skins. Other type of cores can act as unidirectional supports such as corrugated cores, and are widely used. On the other hand the honeycomb core provides bidirectional support of the facesheets. (Ole Thybo Thomsen, 2009) Aluminium, Nomex, polymer and composites are the most used materials in honeycomb fabrication.

The sandwich construction is not only used in terms of lightweight potential. This construction with low-cost cores is also an effective way to reduce costs (Jochen Pflug et al, 2006), however this cost-reduction capacity generally is ignored.

Over the recent years there is an increasing interest in natural fibers as a substitute for glass fibers mainly because of their low specific gravity, low cost, as well as their renewable and biodegradable nature (Aziz et. al, 2004). However, there are no references in the literature about the use of natural fiber composites for producing core materials for sandwich constructions. In this preliminary work a novel honeycomb materials made from natural resources are investigated, focusing on the use of natural fibers as jute and industrial waste as flyash particles.

2. EXPERIMENTAL

2.1 Material

Commercially available woven jute fabrics (Casthanal, Textil CIA, Brazil), and Fly ashes kindly supplied by Industrias del Tablero S.A. (INTASA, Spain) were used as reinforcement. They were obtained from the biomass combustion and subsequently separated using a 20 μm mesh sieve.

The matrix material was prepared from general purpose vinylester resin (Derakane Momentum 411-350 from Dow, provided by Poliresinas San Luis, Buenos Aires, Argentina) and accelerator in a weight ratio of 1:0.05.

2.2 Honeycomb fabrication

Two experimental laboratory-scale compression moulding process to obtain honeycomb cores was used. They were fabricated with different size of hexagonal aluminum cells.

The resulting material is a honeycomb core of 10 x 30 x 120 mm^3 which had to be machined to remove the edges. The final aspect of the different honeycomb cores obtained is seen in Figure 1.

Honeycomb cores were fabricated with different materials: Vinylester resin (VE), Vinylester reinforced with 40 wt % of flyash and vinylester reinforced with jute fabrics.

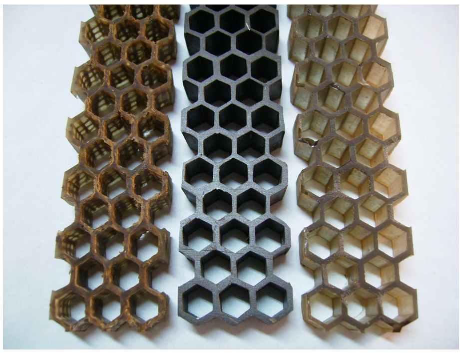

Figure 1. Honeycomb cores obtained: a) jute/VE, b) VE/flyash, c)VE.

2.1 Compression tests

Flatwise compression test were performed following ASTM C365 standard recommendations. Samples of 22 x 55 x 10 mm were used. The test speed was 0.5 mm/min. Stress-strain curves were obtained from these tests and yield strength values were determined from the obtained curves.

3. RESULTS AND DISCUSSION

3.1 Honeycomb density measurement

In order to compare the mechanical properties to a unique parameter, a sample with known volume of each core prepared was weighted. The density values are shown in Table 1. The table also list values of commercial cores for comparison.

Core type	Kg/m^3	cell size
VE/flyash honeycomb core	370	6
VE honeycomb core	326	6
Jute/VE honeycomb core	290	6
Aluminium Plascore*	126	6,35
Stainless Plascore*	92	9,52
Euro composite (special fibre)*	42	6,4
PN2 aerospace grade Aramid fibre honeycomb core*	30	6,4

* Data obtained from product data sheet

Table 1. Honeycomb cores densities.

3.2 Flatwise compression tests

Figure 2 shows the compressive true stress-strain curves for the different cores obtained.

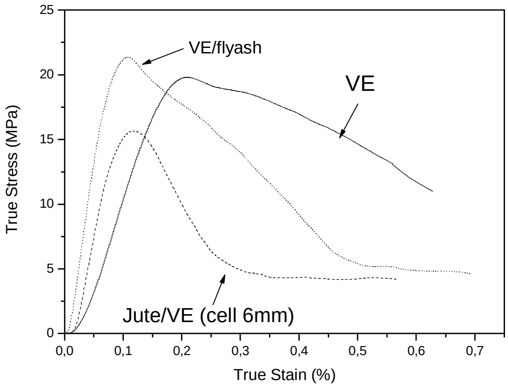

Figure 2. Stress-strain curves for the obtained honeycomb cores.

All materials exhibited ductile behavior under uniaxial compression, characterized by the initial linear elastic response followed by yielding and strain softening. Only the Jute-vinylester honeycomb core showed a marked drop in the load after the peak load whereas the other materials exhibited a more gradual strain softening.

3.3 Specific properties

In lightweight structures design, the specific properties of the cores are often more important than the absolute properties. Figure 3 shows the specific compression strength of the cores in comparison with commercial available cores.

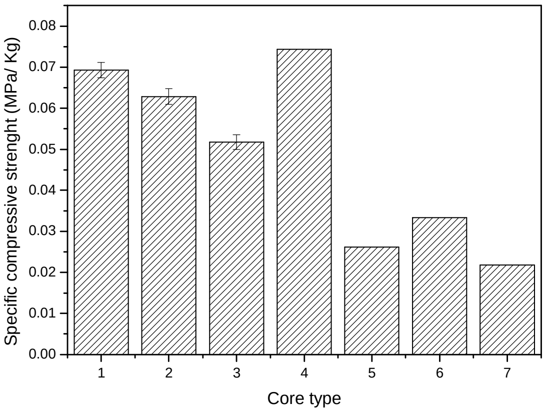

Figure 3. Specific compression strength of the cores in comparison with commercial available cores 1) VE/flyash, 2) VE, 3) Jute/VE 4) Aluminium Plascore* 5) Stainless Plascore* 6) Euro composite (special fibre)* 7) PN2 aerospace grade Aramid fibre honeycomb core*
*** Data obtained from product data sheet.**

In the figure is clearly observed that all the obtained honeycomb cores have superior specific properties than non-metallic commercial ones. On the other hand, all the obtained cores have inferior specific values than the aluminum commercial core.

CONCLUSIONS

In this work the fabrication of new honeycomb cores were investigated. A novel laboratory-scale process was designed and implemented. The obtained cores show higher densities than the commercial honeycomb cores. Nevertheless good specific compression strength in comparison with commercial available ones was found for the processed materials.

REFERENCES

AZIZ SH, ANSEL MP. (2004) The effect of alkalization and fibre alignment on the mechanical and thermal properties of kenaf and hemp bast fibre, *Comp Sci Techol*;64:1219-1230].

PFLUG JOCHEN and VERPOEST IGNAAS (2006) Sandwich Materials Selection Charts, *Journal of Sandwich Structures and Materials* 8..

SHAHDIN AMIR , MEZEIX LAURENT , BOUVET CHRISTOPHE, MORLIER JOSEPH , GOURINAT YVES (2009) Fabrication and mechanical testing of glass fiber entangled sandwich beams: A comparison with honeycomb and foam sandwich beams *Composite Structures,* 90, 404–412.

THOMSEN OLE THYBO, (2009) Sandwich Materials for Wind Turbine Blades Present and Future, *Journal of Sandwich Structures and Materials* 11.

Nanocomposites based on multiwalled carbon nanotubes and nanoclays for VOC detection

C. Vera, I. Bustero, I. Obieta
Departamento de Biomateriales y Nanotecnología
Inasmet-Tecnalia, San Sebastian (Spain)

ABSTRACT

Nowadays, gas sensors are receiving considerable attention in industrial processes and environmental controls for measurement and detection of organic emissions. Different gas sensing devices have been developed over the past years based on metal oxides and/or conductive polymers. However, these sensors operate at high temperature and their response time and sensibility are not fully satisfactory. Composites based on carbon nanotubes (CNT) exhibit new electrical properties that make them potential candidates to be used as chemiresistor sensors at room temperature. In this study, nanocomposites have been fabricated by solvent casting, incorporating multi wall carbon nanotubes, MWNTs, into two different polymeric matrix; PMMA, Polymethil methacrylate and PS, Polystyrene. The change in electrical resistance of these nanocomposites in the presence of different saturated atmospheres of volatile organic compounds (VOC) has been studied. Carboxilic functionalizated MWNTs and different percentages of MWNTs in the polymeric matrix have been used to study their effect in the chemiresistor behavior.

1. INTRODUCTION

Composites based on multiwalled carbon nanotubes (MWNT) exhibit new electrical properties (Zhang et al. 2005) that make them potential candidates to be used as chemiresistor sensors (Abraham et al. 2004) for in-situ measurements. Their simplicity, robustness and response at room temperature (Sinhan et al. 2006) are some of their advantages versus the existing sensors based on metal oxide and conductive polymer which operate at high temperatures.

2. EXPERIMENTAL

In this study, we investigated PMMA, Polymethil methacrilate and PS, Polystyrene based nanocomposites to be used as sensing materials in chemiresistors for the detection of volatile organic compounds (VOC). Multiwalled carbon nanotubes MWNT, and Sepiolite type nanoclays were used as active fillers. Solution blending method was used for the fabrication of the nanocomposite film. MWNT were previously dispersed by ultrasound techniques in chloroform and toluene before being blended with PMMA and PS respectively. Sepiolites were dispersed in PMMA nanocomposites by high-shear stirring with Cowles disk.

2.1. Electrical characterization

Nanocomposites with different percentages of conductive fillers (MWNT) were fabricated to study the variations of the electrical properties. The percolation threshold was established at 2% of MWNT. The nanocomposites were observed by Scanning electron microscopy (SEM). Besides, 2%w of sepiolites was added to the PMMA/MWNTs nanocomposites to study the sensing effect of these nanofillers.

Fig 1 shows the 3D network of multiwalled carbon nanotubes dispersed in PMMA matrix. This phenomenon increases the conductivity of the final material and is explained by the percolation theory.

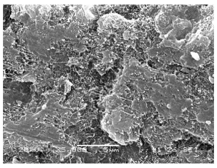

Fig. 1. SEM image of PMMA/MWNT nanocomposite.

2.2. Structural characterization

We characterized the dispersion of the nanoparticles using Raman spectroscopy. As it can be observed on Fig. 7 the spectra obtained at different points of the PS based nanocomposite are more overlapped than in the case of PMMA. This suggests a better dispersion of the nanofillers in the PS matrix.

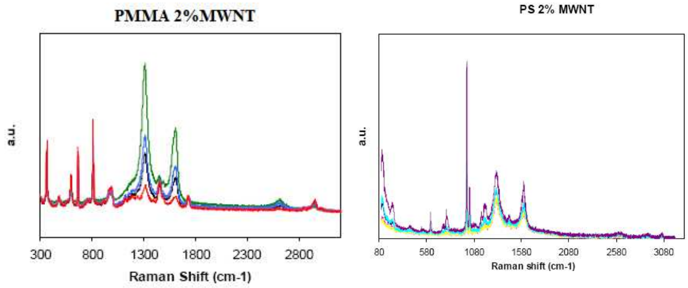

Fig. 2. Raman spectra of nanocomposites with 2% of MWNT.

The mechanical properties of the PMMA nanocomposite at different concentrations of MWNT (2 and 5%) were characterized by flexural bend text according to Standard ISO I78.

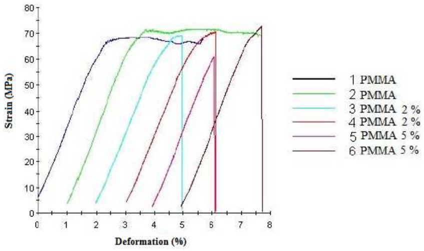

Fig. 3. PMMA/MWNT nanocomposite behaviour in flexion probe.

The Fig 3. shows an increase of the dimensional stability of the material with the addition of MWNT. Significant variations were not observed in flexural strain and strength modulus between the polymer without MWNT and the nanocomposite.

3. Sensing measurements

Nanocomposite films were cut into 20x10 mm pieces and two gold electrodes were placed by evaporation using a mask directly on the nanocomposite surface as shown in Fig. 4 The distance between electrodes was fixed at 1 mm.

Fig. 4. Device for electrical measurements.

The sensing measurements were carried out by standard resistance equipment with four wires. The change in the electrical resistance of these nanocomposites in the presence of different saturated atmospheres of volatile organic compounds (VOC) was studied. Two different mechanisms of interaction were observed:

In one case, sorption of organic vapours in the polymeric matrix phase leads to swelling of the nanocomposite and the conductivity decreases. This phenomenon can be explained by the percolation theory. The distance between the conductive particles in the matrix is enlarged provoking a decrease in the conductivity of the nanocomposite.

In the other case, an electrical effect of charge transfer from the carbon nanotube to the vapour molecules will occur enhancing the conductivity. This mechanism is governed by physisorption and dipole type forces (Abraham et al. 2004). The Fig 5 presents the two different behaviours for the of PMMA/2%MWNT nanocomposite when exposed to acetone vapours.

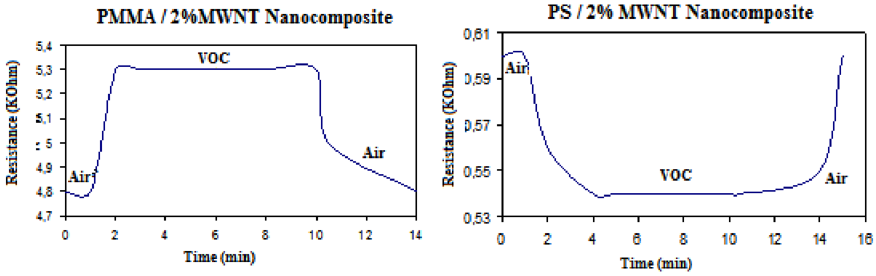

Fig. 5. Variation of the nanocomposite´s resistance upon acetone vapour exposure.

The electrical responses of the nanocomposites based on PS are higher than those of PMMA when exposed to all the vapours.

The mechanisms observed are the following:

1. **PMMA**: The predominant mechanism for the response of vapour such as acetone, methanol, dichloromethane, triclhoromethane and toluene is **matrix swelling**.

2. **PS:** The mechanism involved depends on the type of vapour: Solvents with affinity to PS like tetrahydrofuran, dichloromethane and tricloromethane the chemiresistor behaviour of PS nanocomposites is governed by matrix swelling

For polar molecules like acetone, methanol and ethanol the main mechanism is the **polar interaction** between the CNTs surface and the vapour molecules.

Finally, the effect of nanoclays (sepiolite) in the electrical response of the PMMA/2%MWNT nanocomposites at different atmospheres was also studied and it can be observed on Fig. 6.

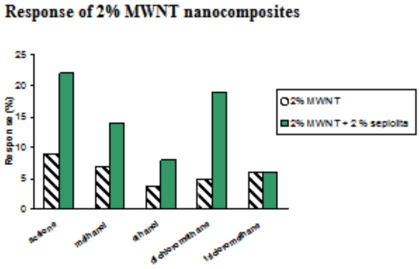

Fig.6. Comparison between PMMA nanocomposite with and without sepiolite nanoclays.

Fig 6 shows the increase of the response when adding the sepiolite nanoclays, the swelling of the matrix vastly increases with the addition of high absorbent particles increasing the sensing properties of the device.

The reversibility of these mechanisms needs further study, but the results seem to be very promising.

4. CONCLUSIONS

The electrical responses of the nanocomposites based on PS are higher than those of PMMA. Both mechanisms can be observed in the case of PS matrixes: matrix swelling and dipolar type interaction. In the case of PMMA nanocomposites only the swelling effect is observed.

Thus, nanocomposites obtained in this work open new possibilities in development of new sensors for environmental applications.

REFERENCES

ABRAHAM J.K., Philip B., Witchurch A., Varadan V.K., (2004) *Reddy Smart Mater Struct* 13, 1045-1049.

SINHA.N, Ma J., Yeow J.T. , (2006), *Journal of Nanoscience and Nanotechnology,* 6, 573-590.

ZHANG B., Fu R.W., Zhang M.Q., Dong X.M., (2005), *Sensors and actuator B*, 323-328.

Effects of surfactants on the dispersive ability and electromagnetic properties of carbon nanotube/silicone composites

J. Vilčáková, R. Moučka, P.Vilčák, K. Maloňová, M. Ilčíková, M. Hřibová, P.Sáha
Polymer Centre/Faculty of technology Tomas Bata University in Zlin/Czech Republic
M. Omastová, M. Mičuštík
Polymer Institute/Slovak Academy of Science/Bratislava/Slovak Republic

SUMMARY

The effects of ionic surfactants and organic solvents on the separation and dispersion uniformity of multi-wall carbon nanotubes (MWCNTs) in silicone matrix were investigated. Different procedures were used for dispersion of MWCNTs in matrix. Homogeneity and morphology was analyzed by electron microscopy (SEM, TEM). These properties were also reflected in concentration dependence of electrical and thermal conductivity. Hence for investigated concentration span (up to 6 vol. %) the less homogeneous system yielded lower percolation threshold and lower thermal conductivity. These effects stem from partial individualisation of nanotubes due to surfactant modification.

INTRODUCTION

Owing to their great potential, particularly unprecedented mechanical but also electrical and thermal properties, carbon nanotubes (CNTs) have rightfully attracted much scientific attention and been subject of innumerable studies since their development in early 1990s [1-3]. However, full exploitation of their physical possibilities poses whole number of challenges starting with their preparation and ending with incorporation of these into other materials reinforcing them so. During their synthesis, carbon nanotubes tangle together, forming bundles. These subsequently substantially hinder their ability to reinforce composite material. To solve this problem, several methods of carbon nanotubes disentanglement have been developed. Basically, they can be divided into mechanical and chemical methods. Regarding chemical methods, most common ones comprise utilisation of surfactants, which are non-covalently bonded onto the surface of nanotubes [4].

This work deals with two different approaches to CNTs separation, the first one being exclusively mechanical (ultrasonic treatment) while the second combines mechanical way with chemical modification by surfactant.

EXPERIMENTAL

a. Materials

Commercially available multiwall carbon nanotubes (MWNT–2040, Conyuan Biochemical Technology, Thaiwan) were used as filler for silicone elastomer (Sylgard 184, Down Corning, USA). For modification of CNTs anionic surfactant, dodecylbenzenesulfonic acid (DBSA), was chosen.

b. Preparation of composites

Two sets of composites, varying in CNTs volume content (0-6 vol. %), were prepared. One of which was based on neat nanotubes while other comprised CNTs modified by DBSA. In both cases CNTs were pre-treated by ultrasound in order to partially separate them from each other. CNT/DBSA modification was carried out by stirring DBSA aqueous solution with CNTs at ambient temperature. Finally the product was filtrated and dried at 60°C. Polymer composites in both cases were prepared by ultrasonic mixing of pre-treated CNTs with corresponding mass of polymer matrix. The mixture was casted into mould compressed and cured for 2 hrs at 100 °C.

c. Methods

The composite structure and the rate of CNTs' entanglement were assessed by scanning electron microscopy (SEM). Electrical conductivity of prepared composite samples was determined from current-voltage measurements in two-point setup using programmable electrometer (Keithley 6517A, USA). Thermal conductivity was measured using experimental setup by Fitch [5].

RESULTS AND DISCUSSION

The effect of ultrasonic pre-treatment of raw CNTs is depicted in **Fig. 5***a*. However, even better separation of nanotubes before their incorporation into polymer matrix can be achieved by their modification by surfactant (**Fig. 5***b*).

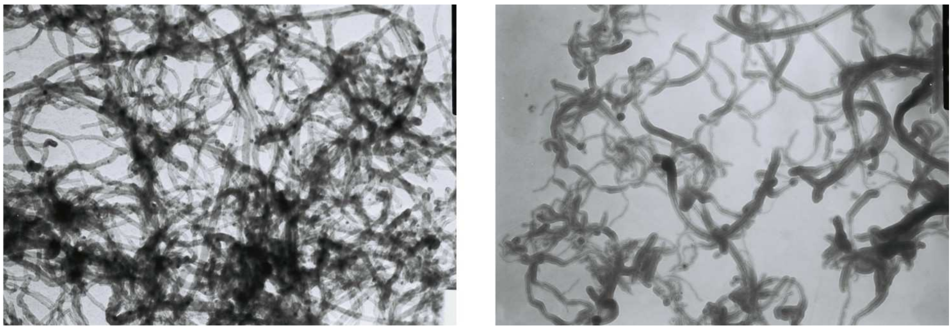

Fig. 5. TEM of pretreated raw CNTs: a) ultrasonic treatment; b) ultrasonic tretment and DBSA modification.

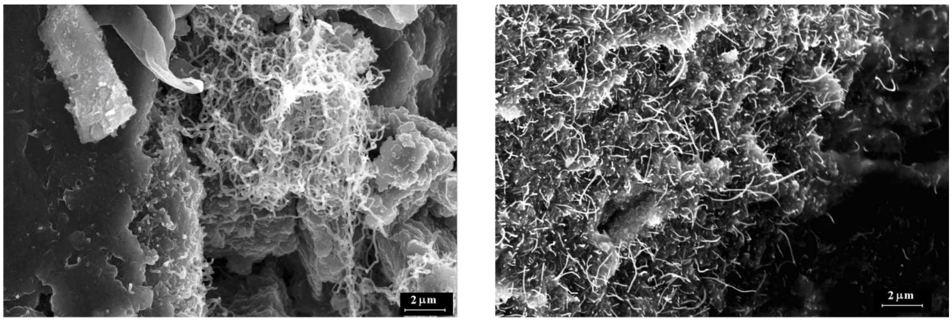

Fig. 6. SEM of composites on the basis of CNTs. a) CNT/silicone composite with 3.5 vol. %; b) CNT-DBSA/silicone composite with 6 vol. %.

Both composites exhibit sudden change of electrical conductivity on filler content (**Fig. 7**). In accordance with percolation theory it is connected with creation of infinite conductive cluster throughout the volume of composite material (**Fig. 6**). However the position of this change, referred to as percolation threshold (φ_c), significantly differed. Thus, lower φ_c ($\varphi_c = 2$ vol. %) is recorded for unmodified CNTs whereas CNT-DBSA yielded $\varphi_c = 4.7$ vol. % (**Fig. 7**). Latter effect is connected with individualization of CNTs in polymer (**Fig. 6***b*) decreasing the probability of creation of infinite clusters.

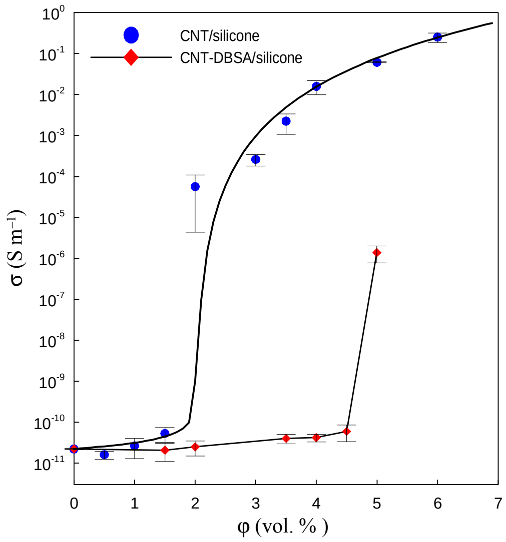

Fig. 7.Percolation dependence of electrical conductivity of silicone composites.

The considerable morphological difference of investigated systems was as well reflected in thermal conductivity (λ) of studied composites, with higher values determined for composite filled with unmodified CNTs. However due to different character of thermal conductivity compared to electrical conductivity the concentration dependence has linear character with not so pronounced dissimilarities as in case of electrical conductivity (**Fig. 8**).

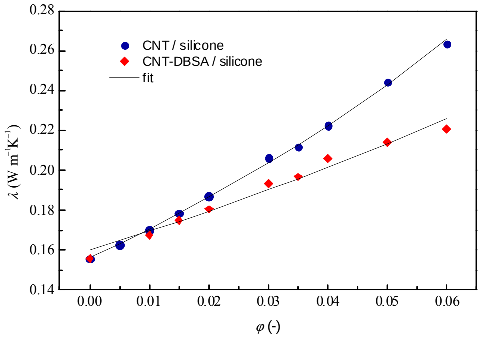

Fig. 8. Dependence of thermal conductivity of silicone composites on filler concentration.

CONCLUSIONS

The structural, electrical and thermal properties of composites containing neat CNTs and ones modified by DBSA were investigated. CNTs were modified in order to improve their dispersion in silicone matrix. The property package of CNT-based composites was discussed in regard to filler concentration and its arrangement in matrix. The difference of percolation threshold for neat and modified CNTs indirectly proves alternations in composite structure depending on used CNTs. Thus, better dispersion in case of modified CNTs leads to higher value of percolation threshold and lower thermal conductivity of composites on their basis.

ACKNOWLEDGMENT

The research was supported by the Ministry of Education, Youth, and Sports of the Czech Republic (ME 883 and MSM 7088352101). Science and Technology Assistance Agency APVV-51-050505 (Slovakia).

REFERENCES

[1] Breuer, O. and U. Sundararaj, *Big returns from small fibers: A review of polymer/carbon nanotube composites.* Polymer Composites, 2004. **25**(6): p. 630-645.
[2] Coleman, J.N., et al., *High-performance nanotube-reinforced plastics: Understanding the mechanism of strength increase.* Advanced Functional Materials, 2004. **14**(8): p. 791-798.
[3] Coleman, J.N., et al., *Small but strong: A review of the mechanical properties of carbon nanotube-polymer composites.* Carbon, 2006. **44**(9): p. 1624-1652.
[4] Cui, S., et al., *Characterization of multiwall carbon nanotubes and influence of surfactant in the nanocomposite processing.* Carbon, 2003. **41**(4): p. 797-809.
[5] Tye, R.P., *Thermal Conductivity*. 1969, London: Academic Press INC.

Aumento de la tenacidad de fractura y resistencia al desgaste de recubrimientos sol-gel de sílice reforzados con nanotubos de carbono

A.J. López, A. Ureña, J. Rams
Dept. Ciencia e Ingeniería de Materiales, ESCET, Universidad Rey Juan Carlos

RESUMEN

En el presente trabajo se estudia la viabilidad de la fabricación de recubrimientos cerámicos de sílice reforzados con nanotubos de carbono de pared múltiple (MWCNTs) sobre sustratos de aleación de magnesio empleando la ruta orgánica del proceso sol-gel y la técnica de generación de recubrimientos por inmersión (*dip-coating*). Se han estudiado dos procedimientos, agitación magnética y agitación por sonda de ultrasonidos, para la generación de la disolución precursora. Como resultados más relevantes se puede destacar la presencia del mecanismo de puenteo de grietas en los recubrimientos reforzados.

1. INTRODUCCIÓN

Desde el descubrimiento de los nanotubos de carbono (CNTs) por Ijima (1991), y debido a sus interesantes propiedades mecánicas se han realizado un considerable número de estudios empleando este material como nanorefuerzo en materiales compuestos. Se espera que la incorporación de los CNTs en matrices cerámicas conlleve aumentos en la tenacidad de fractura, y aumentos en su resistencia mecánica y en su resistencia al desgaste (Xia et al. 2004). La técnica sol-gel es una vía novedosa de fabricación de materiales cerámicos reforzados con CNTs (de Andrade et al. 2008).

En el presente trabajo de investigación se describen los resultados preliminares obtenidos en cuanto a la viabilidad de generación de recubrimientos de matriz cerámica de sílice reforzados con CNTs empleando dos métodos de preparación basados en la técnica sol-gel. Dicha viabilidad se estudia en términos de la incorporación y efectiva dispersión del nanorefuerzo, la morfología superficial de los recubrimientos, la tolerancia del recubrimiento a la deformación, y el comportamiento frente a desgaste.

2. PROCEDIMIENTO EXPERIMENTAL

2.1. Material empleado

El sustrato utilizado, con dimensiones 22 x 22 x2 mm^3, es la aleación de magnesio-itrio WE54 (Magnesium Elektron Company). Los sustratos fueron desbastados con papel de SiC hasta P800, y posteriormente desengrasados con propanol y secados con aire caliente.

Como refuerzo se emplearon nanotubos de carbono de pared múltiple funcionalizados con grupos hidroxilo (OH-MWCNTs) (Nanocyl Company), con un diámetro medio de 9.5 nm y longitud media inferior a 1 μm.

2.2. Generación de los recubrimientos

Los recubrimientos sol-gel de sílice se fabricaron partiendo de una disolución alcohólica de tetraetil-ortosilicato (TEOS) con proporciones molares 4:4:1 de TEOS:etanol: agua acidulada, y empleada anteriormente por los autores (Rams et. Al 2006). Se generaron dos tipos de recubrimientos en función del proceso de fabricación de la disolución sol-gel:

A) Tipo T: suspensión de etanol/OH-MWCNTs sonicada (45 minutos) y adición al resto de reactivos del sol-gel con posterior agitación magnética durante 2 horas.

B) Tipo U: adición directa de los OH-MWCNTs a los precursores del sol-gel y agitación mediante sonda de ultrasonidos durante 45 minutos.

El refuerzo fue incorporado en ambos casos en una proporción del 0.005 % en peso respecto al total de la disolución, con el fin de obtener recubrimientos finales de sílice tras secado y sinterización con una proporción final de refuerzo del 0.1 % en peso.

Para la deposición de los recubrimientos por inmersión se empleó una velocidad controlada de extracción de 10 cm/min. Posteriormente, todos los recubrimientos fueron secados a temperatura ambiente durante 30 minutos para generar la evaporación lenta de los disolventes, y densificados a 400 ºC durante 2 horas con posterior temple en aire.

2.3. Caracterización de los recubrimientos

La caracterización morfológica de los distintos recubrimientos y su comportamiento a fractura se realizó mediante microscopia electrónica de barrido (SEM, Hitachi SN 3400; FEG-SEM, Nova NanoSEM 230). Mediante ensayos de dureza Vickers empleando cargas de 2 kg se analizó la integración del refuerzo en la matriz cerámica así como la respuesta a la fractura de los distintos recubrimientos. Los ensayos de desgaste (pin on-disc) sin lubricación fueron realizados empleando una carga nominal de 1 N, bola de acero de 5 mm de diámetro, velocidad de 0.1 m/s, y una distancia total de 60 m. Los ensayos permitieron determinar la tasa de desgaste (k) de las muestras ensayadas.

3. RESULTADOS

En la figura 1 se muestran las morfologías superficiales de los distintos recubrimientos generados. Los recubrimientos tipo T (figuras 1a y 1b respectivamente) son homogéneos, libres de agrietamiento y porosidad, y replican la rugosidad superficial del sustrato desbastado. Sin embargo, los recubrimientos U (figuras 1c y 1d) presentan porosidad superficial, siendo ésta extremadamente elevada en los recubrimientos reforzados, lo que implica que el nanorefuerzo está influyendo en las etapas de hidrólisis y condensación del sol-gel formador de la matriz de sílice. En cualquier caso, todos los recubrimientos obtenidos presentan espesores cercanos a las 3 μm independientemente del método de obtención, tal como se desprendió del análisis de los cortes transversales y posterior observación en SEM.

Tras los ensayos de dureza se pudo comprobar la distinta capacidad de absorción de la deformación de los recubrimientos (figura 2). Resulta evidente que el recubrimiento de sílice sin reforzar (figura 2a) presenta una elevada densidad de grietas alrededor de las huellas residuales (marcada en la figura), mientras que el recubrimiento nanoreforzado (figura 2b) posee una muy baja densidad de grietas. Al analizar las grietas originadas en el recubrimiento reforzado a mayores aumentos mediante FEG-SEM (figura 2d) se comprobó la presencia de los nanotubos de carbono puenteando las grietas, siendo éste uno de los mecanismos de aumento de tenacidad en materiales cerámicos reforzados; mientras que en el recubrimiento sin reforzar las grietas eran las típicas de una cerámica no reforzada (figura 2c).

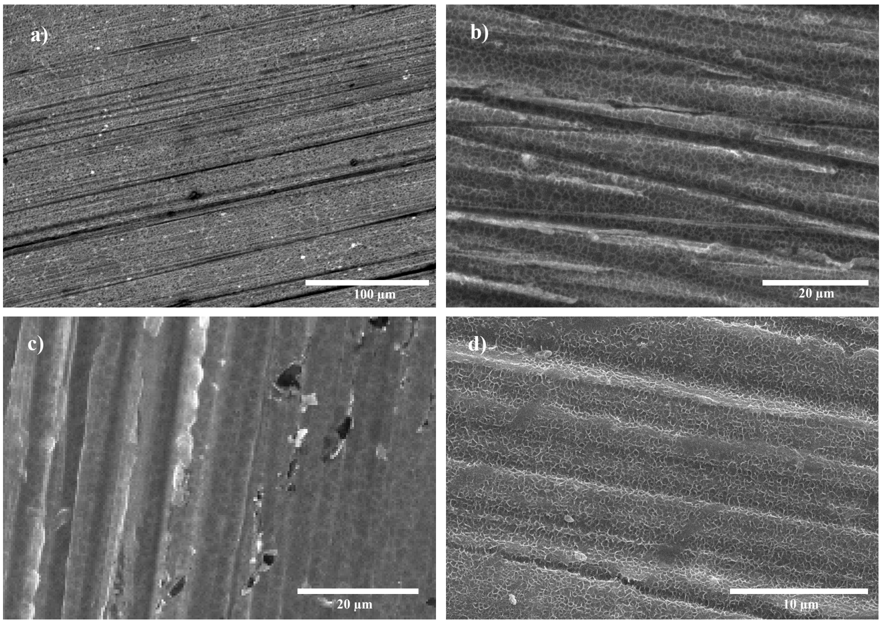

Figura 1. Micrografías SEM de los distintos recubrimientos: a) tipo T; b) tipo T+CNTs; c) tipo U; d) tipo U+CNTs.

Los mismos resultados se obtienen en los recubrimientos generados mediante ultrasonidos (tipo U): presencia de puenteo de grietas en el recubrimiento reforzado y sin puentear en el no reforzado.

Los resultados de los ensayos de desgaste se recogen en la tabla 1 en términos de la variación de la tasa de desgaste (k) respecto al sustrato sin recubrir. Los recubrimientos tipo T disminuyen la tasa de desgaste de la aleación de magnesio en torno a un 6%, pero la incorporación de tan solo un 0.1 % en peso de nano-refuerzo no mejora de forma apreciable (6.5 %) dicho comportamiento, aunque al menos no actúa como defecto, por lo que la distribución del refuerzo puede considerarse como óptima. En cuanto a los recubrimientos tipo U, su comportamiento es inferior que el del sustrato de partida, aunque la presencia del refuerzo mejora apreciablemente el comportamiento del recubrimiento. Ya se comprobó anteriormente cómo los recubrimientos tipo U presentaban elevada porosidad superficial, factor que limita en gran medida su comportamiento a desgaste.

Material	**% □k (mm^3/N m)**
Sílice tipo T	-6.0
Sílice tipo T + OH-MWCNTs	-6.5
Sílice tipo U	8.7
Sílice tipo U + OH-MWCNTs	1.8

Tabla 1. Variación de la tasa de desgaste respecto al sustrato sin recubrir.

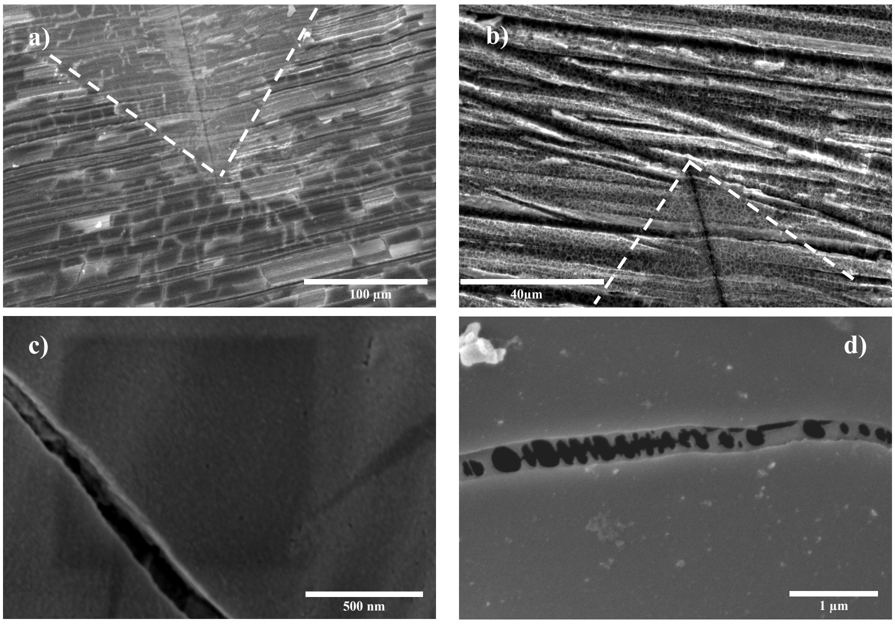

Figura 2. Micrografías SEM (a y b) y FEG-SEM (c y d) de los distintos recubrimientos fabricados: a y c) tipo T sin refuerzo; b y c) tipo T+CNTs.

3. CONCLUSIONES

- Se ha comprobado la eficacia de los métodos empleados en cuanto a la incorporación efectiva y dispersión de los nanorefuerzos en la matriz cerámica de los recubrimientos.
- La morfología superficial de los recubrimientos de sílice está influida por la técnica de generación del sol-gel, siendo la agitación magnética de los precursores empleados la que genera los mejores recubrimientos (tipo T).
- En los recubrimientos tipo T reforzados el daño generado tras los ensayos de dureza es muy inferior al observado en los no reforzados, debido al mecanismo de puenteo de grietas que los MWCNTs generan con tan sólo un 0.1 % en peso de refuerzo añadido, con lo que se puede inferir un aumento en la tenacidad de fractura del recubrimiento.
- Los recubrimientos tipo T mejoran el comportamiento a desgaste respecto al sustrato sin recubrir, sin embargo, la incorporación de tan sólo un 0.1 en peso de refuerzo conlleva un ligerísimo aumento del comportamiento a desgaste del recubrimiento.

4. REFERENCIAS

DE ANDRADE, M.J., LIMA, M.D., BERGMANN, C.P., DE O RAMMINGER, G., BALZARETTI, N.M., COSTA, T.M.H.,GALLAS, M.R., (2008), Nanotechnology, 19, 265607.

IJIMA, S. (1991), Nature, 354-356.

RAMS, J., UREÑA, A., LÓPEZ, M.D., LÓPEZ, A.J., (2006),Surf. Coat. Technol., 201, 3715-22.

XIA, Z., RIESTER, L., CURTIN, W.A., LI, H., SHELDON, B.W., LIANG, J., CHANG, B., XU, J.M., (2004) , Acta Mater., 52, 931-944.

Vacuum infusion technique using natural fibers as reinforcement

G. Francucci, E.S. Rodríguez
Instituto de Investigación en Ciencia y Tecnología de Materiales (INTEMA), Facultad de Ingeniería, Universidad Nacional de Mar del Plata, Argentina
A. Vazquez
Laboratorio de Polímeros y Materiales Compuestos. Instituto de Tecnologías y Ciencias de la Ingeniería (INTECIN). Facultad de Ingeniería. Universidad de Buenos Aires, Argentina

ABSTRACT

The main goal of this work is to understand how the main processing variables are affected when glass fibers are replaced by natural fibers in reinforced plastics. A jute fabric was characterized in terms of its saturated and unsaturated permeability. It was found that fluid absorption and swelling are mechanisms present in natural fibers that reduce both permeabilities. Fluid absorption removes fluid from the main stream as it travels through the reinforcement, acting as a sink component and thus decreasing flow velocity during the unsaturated flow. Also, the saturation of the natural fibers cause swelling, reducing the porosity and increasing flow resistance during saturated flow.

1. INTRODUCTION

Over the recent years there is an increasing interest in natural fibers as a substitute for glass fibers mainly because of their low specific gravity, low cost, as well as their renewable and biodegradable nature. But one of the keys of its success is the possibility of using the well-studied glass fiber composites processing techniques, like RTM, VARTM or SCRIMP. Therefore, it is crucial to understand how the main processing variables are affected when glass fibers are replaced by natural fibers, which have different structure, different fabric architecture and different chemical interactions with the resins. One of those variables is the fabric permeability, which is the key parameter that governs the flow in the fiber bed, together with the fluid viscosity. One key aspect that has been studied by several authors in glass fibers is the difference between saturated and unsaturated permeability. Saturated permeability takes into account the flow resistance when the fluid goes through the reinforcement already impregnated, while the unsaturated permeability refers to the liquid flow through a dry reinforcement.

The aim of this work is to achieve knowledge on mechanisms related to natural fibers impregnation in order to understand the resin flow behavior through natural fiber preforms, and improve the quality and performance of their composites. The relation between permeability (saturated and unsaturated) and porosity of jute bidirectional fabrics is obtained. The Carman – kozeny model is used in order to get an analytical relation between permeability and porosity. Furthermore, a brief analysis on jute fibers water absorption and its effect on permeability values is performed. Jute fabrics are coated with Polyhydroxybutyrate (PHB) in order to reduce the fiber fluid absorption. PHB is a biodegradable thermoplastic polymer with a high hydrophobic character. Permeability tests results obtained with jute and PHB treated jute fabrics are compared in order to study the fluid absorption effect on the permeability values. Also, the swelling degree of the treated and untreated fibers is determined.

2. EXPERIMENTAL

Commercial bidirectional jute fabrics (Castanhal Textil, Brasil; surface density = 0.0300 g/cm2) have been used in this study. In order to study the fluid absorption effect on permeability measurements, jute fibers were coated with Polyhydroxybutyrate (PHB). Surface density of the treated fabrics reached 0.046 g/cm2.The test fluid used for the flow experiments was a 22 % V/V water/glycerin solution, leading to viscosity values near 0.150 Pa.s. For the swelling tests, besides glycerin, two thermosetting resins were used: a commercial vinylester (Derakane 411-350, from Ashland) and a phenolic resin synthesized in our laboratory (molar ratio:1.3 ; solid content: 53,67%).

Unidirectional injection experiments were performed in a rectangular metallic mold with an acrylic lid. The depth of the mold cavity used for each injection was set in order to obtain the desired values of porosity. The viscosity of the fluid used was measured before every infusion in a Brookfield DV–II+ cone and plate viscometer. A vacuum pump was used to force the fluid flow through the mold cavity. The pressure gradient achieved was measured with a vacuometer, located at the outlet line of the mold. In this study, Darcy's Law for unidirectional flow was used to estimate the permeability. Unsaturated permeability can be obtained using Equation 1.

$$K_{unsat} = \frac{(\Phi.m.\mu)}{2\Delta P} \qquad (1)$$

Where K_{unsat} is the unsaturated permeability (m^2), m is the slope of the curve x^2 (square of the flow front position) vs. Time, μ is the fluid viscosity (Pa.s) and ΔP (Pa) is the pressure drop along the fiber bed. The relation between the flow front position and the injection time was obtained by recording the infusion process with a camera mounted on top of the transparent flow cell. Saturated permeability was calculated by measuring the fluid volumetric flow rate, once the reinforcement was fully saturated (Equation 2). A standard flow meter connected at the output line of the mold was used for this purpose and a plot of volume vs. time could be obtained.

$$K_{sat} = \frac{(Q.\mu.\Delta L)}{(A.\Delta P)} \qquad (2)$$

Where K_{sat} is saturated permeability (m^2), Q is the volumetric flow rate (m^3/s), ΔL the preform length (m) and A, the mold cavity transverse area (m^2). The modified Carman – Kozeny model was used to establish a relationship between permeability and porosity. The model has the following expression, where n and C are empirical parameters:

$$K = \frac{\phi^{n+1}}{C(1-\phi)^n} \qquad (3)$$

Swelling degree was evaluated for treated and untreated jute fibers by optical microscopy. Single fibers were put with the test fluid (glycerin + water) between glass slides, and the change in fibers diameter was measured by taking pictures at different times. The pictures were analyzed using image processing software.

3. RESULTS AND DISCUSSION

Saturated and unsaturated permeability values as a function of the porosity are shown in Figure 5. The Carman-Kozeny model (Equation 3) was used to fit the experimental data. The fitting parameters resulted: n =0.9146, C = 8.464 E9, for saturated permeability, and n=1.289, C=1.338 E10, for unsaturated permeability. As expected, both saturated and unsaturated permeabilities increase as porosity does. Also, it was observed accordingly with other authors (Shojaei A et al. 2004, Lundström et al. 2000, Foley et al. 1991) that the permeability is higher when the reinforcement is fully saturated than during the filling process. This observation can be attributed to the delayed impregnation of the dense fiber tows, with respect to the macroscopic flow front, due to the difference in the local permeability of the inter-tow and intra-tow regions (Chan A. et al. 1993). Fiber tows acts as a sink, removing fluid from the main stream as it travels along the mold cavity, leading to lower permeability values. In natural fibers, unsaturated permeability is affected by fluid absorption and saturated permeability is affected by fiber swelling (a consequence of fluid absorption), both effects leading to a decrease in the value of the permeability. Absorption acts as another sink component, removing more liquid from the main fluid stream and retarding the fluid flow, thus the flow resistance increase and permeability values drop. Furthermore, saturation of natural fibers can cause swelling (Siddiqur rahman et al. 1997), and it could reduce the porosity and increase flow resistance during saturated flow. This statement is confirmed by the results obtained from permeability tests performed on PHB treated jute samples shown in Table 1. Between brackets are the permeability values of untreated jute that were extrapolated using the Carman-Kozeny model. It was found that the permeability of PHB coated jute fabrics were higher than for untreated ones. As seen before, the PHB coated the fibers reducing fluid absorption and therefore increasing unsaturated permeability. This procedure also reduces fibers swelling, increasing saturated permeability.

Figure 1. Permeability as a function of porosity.

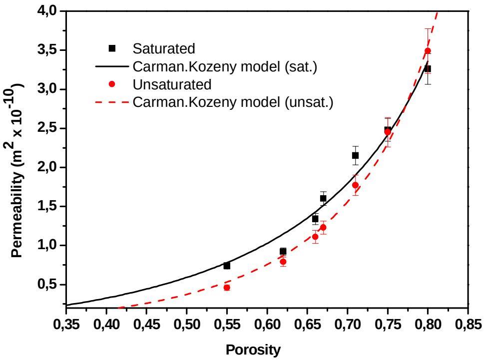

Table 1. Permeability values for treated jute fabrics.

Sample	Porosity (%)	K $_{unsat}$ (m^2 x 10^{-10})	K $_{sat}$ (m^2 x 10^{-10})
J - TA	45	1.25 (0,263)	1.74 (0,446)
J - TB	40	1.54 (0,177)	1.86 (0,326)

Regarding the swelling tests, after 30 minutes of immersion in different fluids, untreated jute fabrics showed an increase in diameter of 22 % when immersed in a glycerin +water solution, while the PHB coated fibers showed almost no swelling. In addition, jute fibers showed an increase in diameter of about 6% when immersed in vinyl ester and phenolic resins. Therefore, swelling of the fibers during the infusion process is not only a mechanism that arises in permeability determination with water-based model fluids, but also occurs in the infiltration of composite parts with true resins. The highly hygroscopic components of the fibers like cellulose and specially hemicellulose are responsible for this phenomenon. These results show the importance of taking into account the chemical and physical interaction of the test fluid with the fibers when measuring permeability of natural reinforcements.

3. CONCLUSIONS

As expected, both saturated and unsaturated permeabilities increase as porosity does. Also, it was observed that saturated permeability values are higher than unsaturated permeability values, but this difference tends to vanish for porosities above 75%.

Also, it was found that Jute reinforcements absorb great amount of fluid during the infusion process, when compared to glass fiber reinforcements. The fluid absorption affects the permeability value of the preform, because it removes fluid from the main stream as it travels through the reinforcement, acting as a sink component and thus decreasing flow velocity during the unsaturated flow. Furthermore, saturation of natural fibers can cause swelling, thus reducing the porosity and increasing flow resistance during saturated flow. So both saturated and unsaturated permeability values of the Jute preform are reduced because of the fluid absorption. Also, in the infusion of composite parts with true resins the swelling of the fibers is still present, as could be demonstrated with swelling test with vinylester and phenolic resins.

REFERENCES

SIDDIQUR RAHMAN M, NILUPAR M, MAJID MA, SOBHAN SHEIKH MA (1997). Swelling characteristics of jute fibre with water and different organic and inorganic vapours and liquids. Cellulose Chemistry and Technology; 31: 87-92.

SHOJAEI A, TROCHU F, GHAFFARIAN SR, KARIMIAN SMH, LESSARD L (2004). An Experimental Study of Saturated and Unsaturated Permeabilities in Resin Transfer Molding Based on Unidirectional Flow Measurements. Journal of reinforced plastics and composites; 23(14): 1515-1536.

LUNDSTRÖM TS, STENBERG R, BERGSTROM R, PARTANEN H, BIRCKELAND PA (2000). In-plane permeability measurements: a nordic round-robin study. *Composites: Part A*; 31(1):29-43.

FOLEY FM, GUTOWSKI T (1991). The effect of process variables on permeability in the flexible resin transfer molding (FRTM) process. *In: Proceedings of 23rd International SAMPE Technical Conference. Kiamesha Lake (US*A); p. 326-339.

CHAN A, MORGAN RJ (1993). Tow impregnation during resin Transfer molding of Bi-directional nonwoven fabrics. Polymer Composites; 14(4):335-340.

Performance of multi-walled carbon nanotubes/epoxy nanocomposites obtained by sonication and mechanical dispersion

S.B. Susin, M. Zeni, A.J. Zattera
Polymers Laboratory (LPOL), Center of Exact Sciences and Technology (CCET)
Caxias do Sul University(UCS), Caxias do Sul/RS, Brazil
S.C. Amico
Polymers Laboratory, Department of Materials Engineering,
Federal University of Rio Grande do Sul(UFRGS), Porto Alegre/RS, Brazil.
L.A.F. Coelho, S.H. Pezzin
http://www.udesc.br/http://www.sc.gov.br Polymers Laboratory, Center for Science
Tecnology (CCT) Santa Catarina State University(UDESC), Joinville/SC, Brazil.

ABSTRACT

Since the discovery of carbon nanotubes (CNT), notable properties were predicted for this new class of carbon, such as extremely high elastic modulus (about 1 TPa), thermal conductivity higher than that of diamond and aspect ratio of about a thousand. However, these properties are not being successfully transferred to thermoset polymer composites produced with CNT, which is usually attributed to poor nanotubes dispersion within the matrix due to their entanglement. In order to promote the disentanglement and dispersion of nanotubes, many techniques have been reported, including mechanical dispersion and sonication. In this work, the performance of carbon nanotubes/epoxy nanocomposites obtained through sonication and mechanical dispersion were compared. After processing, the samples were analyzed by transmission and scanning electron microscopy, differential scanning calorimetry and tensile tests. The results indicated only a small increase in the mechanical properties of epoxy, which may indicate a poor interaction between resin and nanotubes.

1. INTRODUCTION

Today, nanocomposites represent a new boundary in material science since the reinforcements migrated from micro to nano scale. Due to that, the efficiency of standard mixing processes was no longer adequate, thus such processes have been adapted for processing nanofillers and many other mixing techniques have been proposed [1]. Within the area of nanomaterials, CNTs are one of the most researched [1-3] and dispersion was identified as one of the major challenges holding back the mass production of CNTs based products. In fact, commercial nanotubes comes in bundles due to intense van der Walls forces acting between the nanostructures, once it is built up of pure sp^2 carbon. Besides, it is very difficult to achieve a homogeneous dispersion of CNTs within polymer matrices. With that in mind, many attempts were carried out to solve the mixing problems and to achieve the properties stipulated for CNT reinforced composites. Nowadays, the most employed techniques to promote bundle disentanglement and nanotubes dispersion are mechanical mixing and sonication. Basically mechanical mixing processes use shear forces to break the bundles whereas sonication uses ultrasound energy [4, 5, 7-10]. Although results from both methods have demonstrated interesting dispersion states, it is not clear yet which technique is the best [3, 10]. In this context, CNT/epoxy composites were produced by sonication and by mechanical mixing and their mechanical properties were compared.

2. METHODOLOGY

2.1. Materials

The chosen matrix was a DGEBA epoxy resin Araldite GY 251. This resin was cured with a Diethylenetriamine (DETA) based hardener type Ren HY 956 BR at a volume ratio of 1 part of hardener to 5 parts of resin. Baytubes® C150P multi-walled carbon nanotubes (MWCNT) were used.

2.2. Composite preparation

In order to only compare the processes, a single base mixture was used consisting of 0.25 wt% of MWCNT and 80 g of epoxy. For the mechanical mixing, a DRAIS mixer (Fig. 1), operating at 1000, 3000 and 5000 rpm for 10 and 20 min, was used. For the sonication process, a sonicator SONICS model VCX 750 was employed working at 20 and 30% of amplitude and also for 10 and 20 min.

Fig. 1. Drais mixing chamber.

2.3. Specimen preparation and curing cycle

After processing, the hardener was mixed to the resin and the system was poured into silicone moulds to produce ASTM D638 Type I tensile specimens. The system was cured for 48 h at room temperature followed by 24 h at 60ºC.

3. RESULTS AND DISCUSSION

Tensile tests have demonstrated little increase in stress at break (σ*) and young modulus (*E*) (Fig. 2). This may indicate that the interactions between MWCNTs and epoxy were not strong enough to promote any significant increase in the nanocomposites properties.

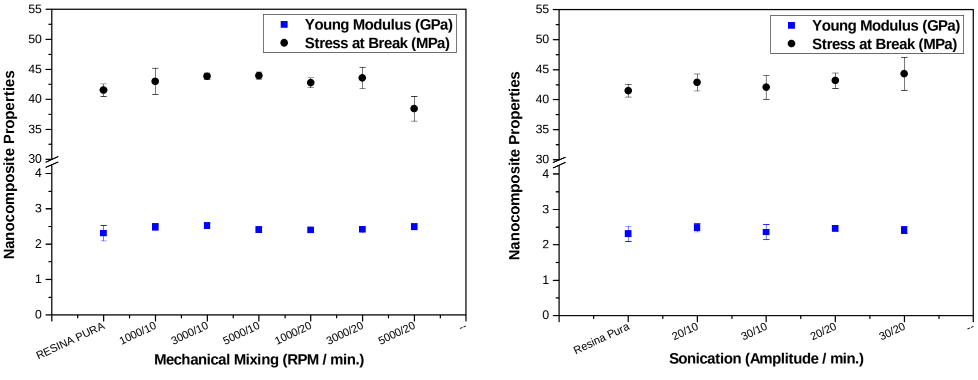

(a) (b)

Fig. 2. *E* and σ* for the composites, mechanical mixing (a) and sonication (b).

	Neat epoxy	**Mechanical Mixing**		**Sonication**	
	-	**Composite**	**Variation (%)**	**Composite**	**Variation (%)**
Modulus (Gpa)	2,31	2,46	+6,49	2,42	+4,88
Stress at break (MPa)	42,50	42,42	+2,22	43,12	+3,90
Strain at break (%)	4,94	3,77	-23,62	2,97	-39,89

Table 1. Tensile tests - mean values (n = 6).

The large decrease in strain at break (Table 1) may have been caused by two factors. The first one is that the nanotubes are stiffening the resin, as seen by the increase in modulus. The second one is that the MWCNT may be acting as impurities within the matrix, since the fractures initiated and propagated from a bundle (Fig. 3). Analyzing SEM images (Fig. 3), it was possible to define an intermediary phase between the matrix and the filler.

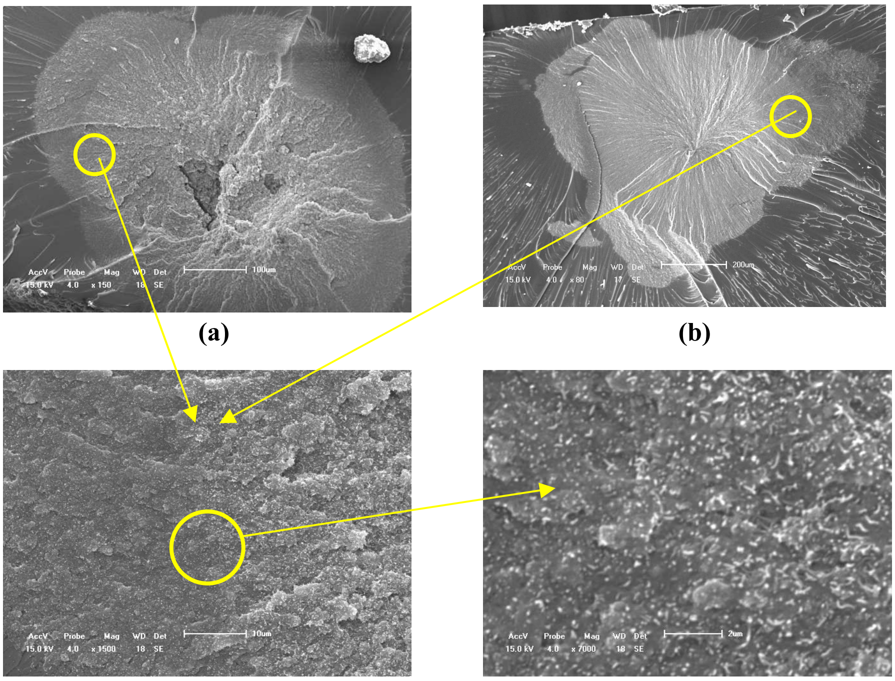

(a) **(b)**

Fig. 3. SEM images of composites produced by mechanical mixing (a) and sonication (b).

It is possible to see that there are more nanotubes in the intermediate phase then in any other region of the fracture surface and that the distance between the nanostructures is larger then in the inner regions of the bundle. Thus, these images suggest the preliminary stage of a disentanglement and dispersion process. Therefore, the nanocomposite may be stiffer then the matrix due to the small amount of disentangled CNTs dispersed within the matrix. However, this increase is small due to the presence of bundles that indeed would be acting as impurities across the matrix.

4. CONCLUSIONS

The results indicate that both techniques allow some degree of bundle disentanglement and dispersion of nanotubes. However, the SEM images of the preliminary stage of bundle disentanglement reveals that the ultrasound seems to act at specific regions of the bundles since the disentanglement took place in their extremities whilst the shear forces from the mechanical mixing seem to act in the overall structure of the bundles because the disentanglement process took place in the whole area around the bundle. Considering that, the intense shear forces from mechanical mixing may, in some way, stands out over sonication.

ACKNOWLEDGMENTS

The authors would like to thank CNPQ and CAPES for the financial support, to BAYER for the CNTs samples and especially to Prof. MSc. Rudinei Fiorio for all the support and collaboration.

REFERENCES

1. THOSTENSON, E.T., CHOU, T.W. (2006) Processing-structure-multi-functional property relationship in CNT/epoxy composites. *Carbon*, *44*, 3022-3029.

2. DE VILLORIA, R.G., MIRAVETE, A., CUARTERO, J., CHIMINELLI, A., TOLOSANA, N. (2006) Mechanical properties of SWNT/epoxy composites using two different curing cycles. *Composites: Part B*, *37*, 273-277.

3. GOJNY, F.H., WICHMANN, M.H.G., KÖPKE, U., FIEDLER, B., SCHULTE, K. (2004) Carbon nanotube-reinforced epoxy-composites: enhanced stiffness and fracture toughness at low nanotube content. *Comp. Sci. and Tech.*, *64*, 2363-2371.

4. IBEH, C.C., HUI, D., SHIVAKUMAR, K. (2007) Literature Survey of Current State of Research on Nanocomposites & Multifunctional Materials. Pittsburg State University, Pittsburg KS, New Orleans University, New Orleans LO, A&T University of North Carolina, NC. Disponível em: www.pittstate.edu/cncmm/documents/NanocompositesSURVEY-Ibeh%20et%20al01.pdf acessed in 02/13/2008.

5. THOSTENSON, E.T., REN, Z., CHOU, T.W. (2001) Advances in the science and technology of carbon nanotubes and their composites: a review. *Comp. Sci. and Tech.*, *61*, 1899-1912.

6. SONG, Y.S., YOUN, J. R. (2005) Influence of dispersion states of carbon nanotubes on physical properties of epoxy nanocomposites *Carbon*, *43*, 1378-1385.

7. LOOS, M.R., COELHO, L.A.F., PEZZIN, S. H., AMICO, S. C. (2008) Effect of Carbon Nanotubes Addition on the Mechanical Properties of Epoxy Matrices. *Mat. Res.*, v. *11*, n. *3*, 347-352.

8. KIM, J. A., SEONG, D. G., KANG, T. J., YOUN, J. R. (2006) Effects of surface modification on rheological and mechanical properties of CNT/epoxy composites *Carbon*, *44*, 1898-1905.

9. XIE, X.L., MAIA, Y.W., ZHOU, X.P. (2005) Dispersion and alignment of carbon nanotubes in polymer matrix: A review. Mat. Sci. and Eng. R 49, p. 89-112.

10. 10. BAL, S., SAMAL, S.S. (2007) Carbon nanotube reinforced polymer composites - A state of the art. Material Science Bulletin, v. 30, n. 4, p. 379-386, 20

Powders of DNA-wrapped carbon nanotubes

F. Güller, C. Sendra, S. Goyanes
LP&MC. Dep. de Física, FCEyN-UBA. * Consejo Nacional de Investigaciones
Científicas y Tecnológicas (CONICET), Argentina
J.A. Ramos, I. Mondragon
'Materials + Technologies' Group, Dep. Ingeniería Química y del Medio Ambiente,
Escuela Politécnica. Universidad del País Vasco/Euskal Herriko Unibertsitatea
G.H. Rubiolo
LP&MC. Dep. de Fisica, FCEyN-UBA,. Departamento de Materiales (GIDAT-CAC),
Comisión Nacional de Energía Atómica, Bs. As. Consejo Nacional de Investigaciones
Científicas y Tecnológicas (CONICET), Argentina

ABSTRACT

Artificial deoxyribonucleic acid (DNA) has been used to wrap multiwalled carbon nanotubes (MWCNTs). A procedure is given to obtain and to purify powders of DNA-wrapped MWCNTs. The powders can be conserved at low temperature during several months and they can be again water dispersed.

1. INTRODUCTION

Many applications of carbon nanotubes require good dispersion in different solvents. The functionalization with different molecules was proposed to reach this goal. Zheng et al (2003) showed that bundled single-walled carbon nanotubes can be effectively dispersed in water by their sonication in the presence of single-stranded DNA (ssDNA). However, to the author's knowledge nobody has yet reported powders of carbon nanotubes wrapped in DNA (wDNA-MWCNTs). Here we report a procedure to do those powders and the results of its characterization by means of microscopic techniques and Fourier transform infrared spectroscopy (FTIR).

2. EXPERIMENTAL PROCEDURES

DNA-MWCNTs aqueous solutions were prepared following the procedure given by Zheng et al. (2003). An aqueous solution 0.1M NaCl with 1 mg/mL DNA (Polycytidylic Acid Potassium Salt, Poly(C) Sigma) and 1 mg/mL CNT (Nanocyl 3100) was prepared. The aqueous solution was prepared with purified water (MilliQ standard) and its pH was fixed at 7.4 using a buffer HEPES (4-2-hydroxyethyl-1-iperazineethanesulfonic acid) 0.05 M. The solution was then sonicated for 90 min in ice water and centrifuged at 5580g for 90 min to separate the wDNA-MWCNTs from the non-functionalized nanotubes which stayed as a non-soluble material, which we name the pellet in what follows. The supernatant, containing the wDNA-MWCNTs, was sucked with a pipe and deposited in other different recipient that the pellet. Both recipients were kept at 8 ºC to preserve the biological material.

Dry wDNA-MWCNTs were obtained from the supernatant solution through vacuum evaporation of the water. However, this dry wDNA-MWCNTs mat contained some NaCl and residual DNA. For wDNA-MWCNTs purification the powders were put in 10 mL ethylic alcohol, the mixture kept in ice water and sonicated for 15 min. Two types of aggregates appeared in the bottom of the container, a white one associated with residual DNA (Piskur et al. 1995) and other black one we associated with wDNA-MWCNTs.

Using a small clamp, the black aggregate was removed from alcohol and dried in vacuum oven. These wDNA-MWCNTs free of DNA excess and NaCl is named *f*-DNA-MWCNTs in what follows.

The powders of wDNA-MWCNTs and *f*-DNA-MWCNTs were characterized by FE-SEM, AFM microscopy and FTIR.

3. RESULTS AND DISCUSSION

Naked eye observations suggest that wDNA-MWCNTs powders can be effectively dispersed in water at pH 7.4, as opposed to pristine MWCNTs where agglomerations of nanotubes can be easily seen in the solution. On the other hand, the solution of wDNA-MWCNTs in water was homogeneous gray, suggesting the functionalized nanotubes were well dispersed, in agreement with results published by Zheng et al. (2003) and Malik et al. (2007). Keeping the solution at 8 ºC, no sedimentation was observed after six months, meaning that wDNA-MWCNTs were well-dispersed for at least that time.

Carbon nanotubes in the pellet could also be dispersed in water at pH 7.4 but they precipitated to the bottom of the container after one day. This fact indicates that carbon nanotubes in the pellet were not functionalized, and that the centrifugation process effectively separates them from wDNA-MWCNTs.

The percentage of MWCNTs wrapped with Poly(C) was between 15 wt% and 35 wt%. These values are in agreement with those reported by Zheng et al. (2003).

FE-SEM micrographs of pristine nanotubes and wDNA-MWCNTs aqueous solution drops are shown in Figure 1.

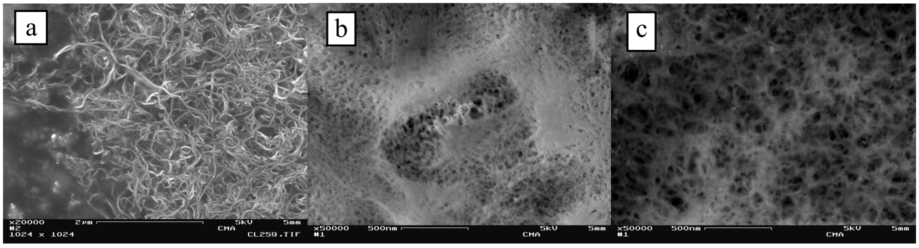

Fig. 1. FE-SEM micrographs: (a) MWCNTs; (b) and (c) wDNA-MWCNTs.

As can be seen in Fig. 1a, the pristine nanotubes are clearly not dispersed and heavily entangled. Figure 1b is the image of wDNA-MWCNT immediately they are focused with FE-SEM and Fig 1c the same image a few seconds later. This result shows that organic material is burned by the electronic beam and suggests that there is a great amount of DNA in the wDNA-MWCNTs sample.

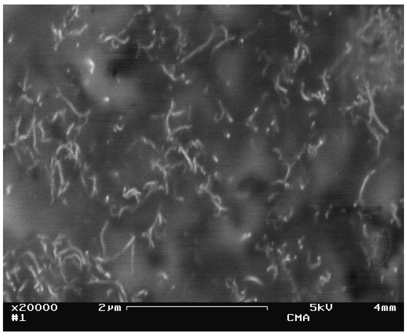

Fig. 2. *f*-DNA-MWCNT aqueous solution, FE-SEM.

As mentioned above, wDNA-MWCNTs samples were purified to eliminate residual DNA leading to *f*-DNA-MWCNT samples. To ensure that these CNT were still wrapped by DNA, dry *f*-DNA-MWCNTs were put in water at pH 7.4 and good dispersion was observed with the naked eye. This solution remained stable for at least six months like that of wDNA-MWCNTs samples.

Figure 2 shows a FE-SEM micrograph of a *f*-DNA-MWCNTs aqueous solution drop.

Comparing this micrograph with Fig. 1a, two clear differences can be seen. First, *f*-DNA-MWCNTs were well dispersed. Second, the lengths of all *f*-DNA-MWCNTs observed were much less than the ones of the pristine nanotubes. This reduction in length has also been reported by Zheng et al. (2003), who attributed it to the sonication process of the solution containing DNA and MWCNTs. However, the sample of pristine MWCNTs in water (Fig. 1a) was also sonicated with similar powder and time as *f*-DNA-MWCNTs solution. Besides, FE-SEM micrograph in Fig. 2 does not show DNA excess seen in Fig. 1b and 1c. It should be noted that the reduction in length and effective dispersion in water are not a consequence of the alcohol treatment.

Figures 3a and 3b show AFM images of a drop of wDNA-MWCNTs solution (topography and phase, respectively). The wrapped DNA on the MWCNTs can be observed with more detail at high resolution (Fig. 3c and d) as evidenced by the irregular surface (Takahashi et al. (2006)).

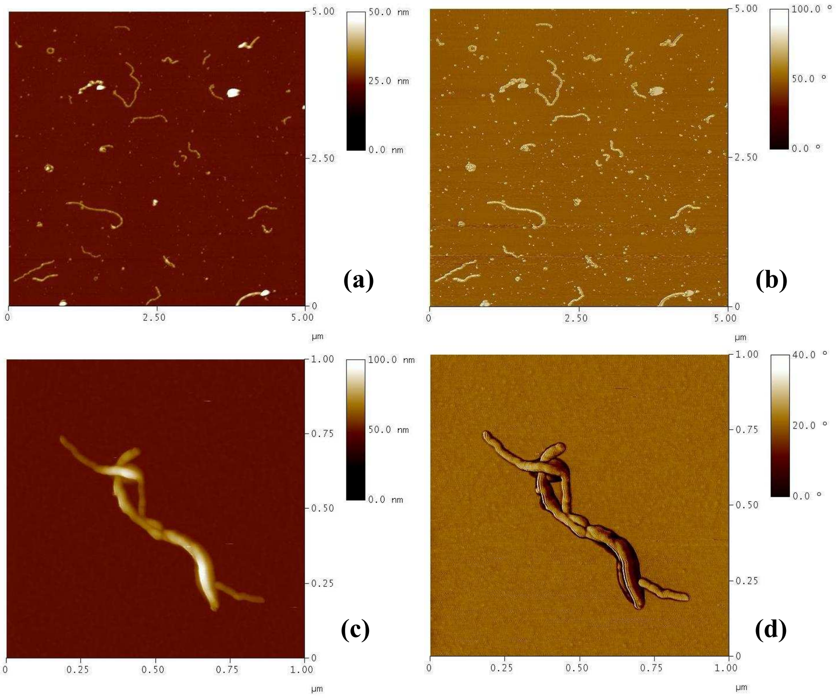

Fig. 3. AFM images of wDNA-MWCNTs.
Topography: (a) and (b). Phase: (c) and (d).

Finally, a FTIR study was performed on *f*-DNA-MWCNTs sample to confirm the presence of DNA. Figure 4 shows the pristine CNT and *f*-DNA-MWCNTs spectra.

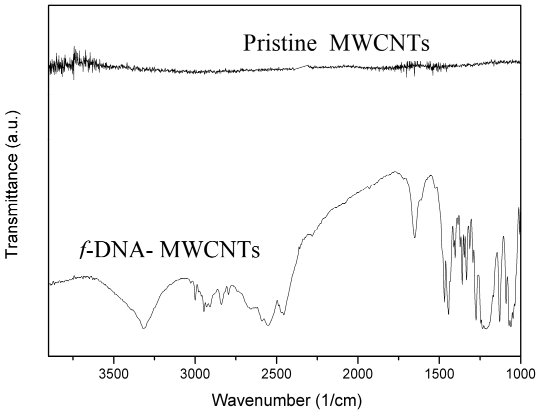

Figure 4. FTIR spectra

The *f*-DNA-MWCNTs spectrum shows several of the characteristic bands of Poly(C). Bands between 1411 cm^{-1} and 1500 cm^{-1} are attributed to C-C and C-N stretching. The bands at 1230 cm^{-1} and 1058cm $^{-1}$ are assigned to antisymmetric and symmetric stretching vibration modes of PO_2. The peak at 1656 cm^{-1} can be attributed to a vibration of the CO group. Bands around 2500 cm^{-1} correspond to NH_2 stretching, and bands around 2900 cm^{-1} to CH_x stretching. Finally, the band at 3300 cm^{-1} is assigned to OH stretching of the polymeric structure. These features indicate the presence of DNA attached to the nanotubes.

CONCLUSIONS

DNA wrapped MWCNTs powders can be obtained in a purified form by vacuum drying of an aqueous solution containing them and posterior precipitation in ethylic alcohol. The system DNA-MWCNTs in the powder form is able to retain the capacity of dispersion in water for a long time.

ACKNOWLEDGEMENTS

The authors acknowledge the financial support of UBA (X094), CONICET (PIP 5959) and ANPCyT (PICT 25834), Basque Country Government (IT-365-07 and inanoGUNE) and MEC (MAT2006-06331).

REFERENCES

ZHENG, M. et al. (2003). DNA-assisted dispersion and separation of carbon nanotubes. *Nature Materials*, 2, 338-342.
PISKUR, J., RUPPERECHT, A. (1995). Aggregated DNA in ethanol solution. *FEBS Letters*, 375, 174-178.
MALIK, S. et al. (2007). Physical chemical characterization of DNA-SWNT suspensions and associated composites. *Compos. Sci. Technol.*, 67, 916-921.
Takahashi, H. et al. (2006). AFM imaging of wrapped multiwall carbon nanotubes in DNA. *Chem. Phys. Lett.*, 418, 535-539.

Síntesis y caracterización de nanopartículas compuestas de oro con copolímeros en bloque biodegradables

C. Saldías, A. Leiva, L. Gargallo and D. Radic
Departamento de Química Física, Facultad de Química, Pontificia Universidad Católica de Chile e-mail: casaldia@uc.cl

Las nanopartículas metálicas, principalmente de elementos nobles, han sido de gran interés en este último tiempo debido a sus usos en medicina, informática, electrónica, catálisis, fotografía, espectroscopía de superficie, entre otras variadas aplicaciones. Además, como se ha confirmado en distintos estudios, las propiedades de una nanopartícula metálica son fuertemente dependientes de parámetros, tales como: tamaño, morfología, cristalinidad y estructura.

Por otra parte, los copolímeros en bloque sintéticos se han utilizado ampliamente en la obtención de micelas y nanoestructuras en agua u otros solventes y también como agentes estabilizadores estéricos para evitar la aglomeración excesiva de las nanopartículas.

Existe en literatura reportes de la utilización de agentes reductores, tales como, $NaBH_4$, $LiBH_4$, hidrógeno e hidrazina en el proceso de reducción de sales metálicas. Una clase de agente reductor muy interesante, son los alcoholes que permiten controlar la velocidad en la etapa de reducción, ya que su poder reductor depende de la longitud de su cadena alquílica.

En este trabajo se reporta un método para la síntesis de nanopartículas compuestas oro-copolímero mediante la reducción de tetracloroaurato de potasio ($KAuCl_4$) por copolímeros en bloque de Poli (N-vinil-2-pirrolidona) (PVP) y Poli (ε-caprolactona) (PCL) en disolución acuosa. Los copolímeros utilizados (Figura 1) poseen un doble rol, es decir, actúan como agentes reductores y estabilizantes en la síntesis de nanopartículas metálicas. Este poder reductor de los copolímeros podría estar dado por los grupos hidroxilo terminales que poseen.

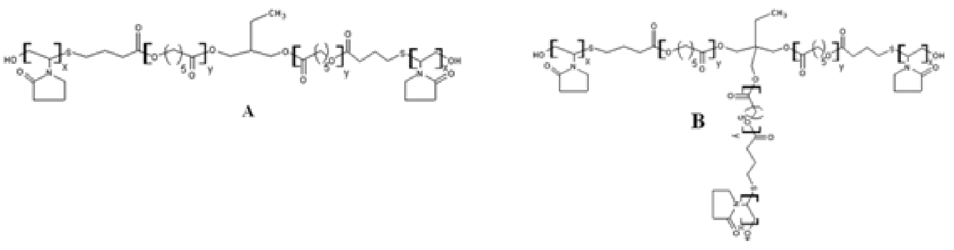

Figura 1. Estructura química de los copolímeros en bloques, PVP-b-PCL-b-PVP (A) y PCL-b-$(PVP)_3$ (B).

En la Figura 2 se muestran los espectros de absorbancia UV-visible de las nanopartículas de oro obtenidas con ambos copolímeros. Se observa en las imágenes de Microscopía de Transmisión Electrónica (TEM), Figura 3, nanoplatos con geometría triangular, hexagonal y ramificada, con un tamaño aproximado de 50 nm.

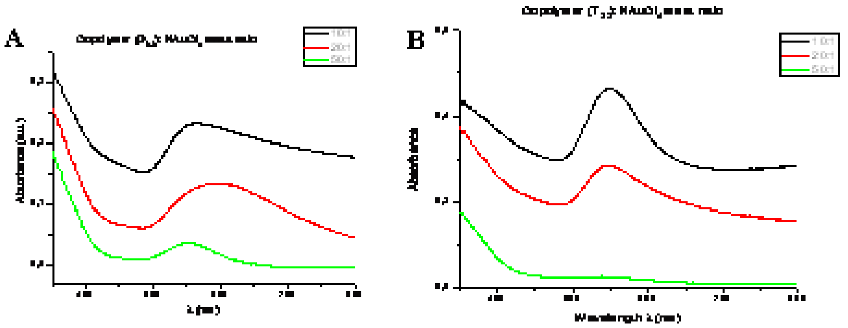

Figura 2. Espectro de absorbancia UV-visible de nanopartículas de oro obtenidas con PVP-b-PCL-b-PVP (A) y PCL-b-$(PVP)_3$ (B).

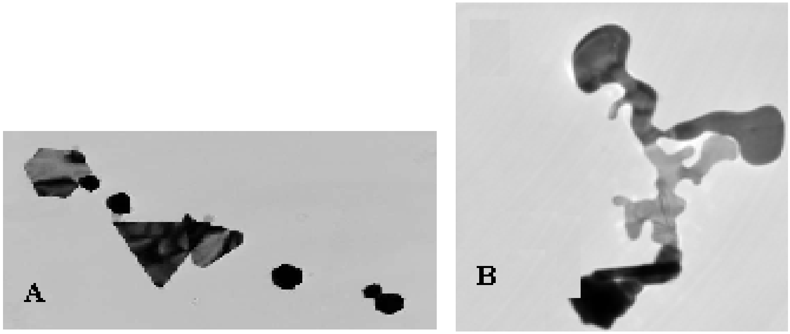

Figura 3. Imágenes TEM de nanopartículas de oro obtenidas con PVP-b-PCL-b-PVP (A) y PCL-b-$(PVP)_3$ (B).

REFERENCIAS

I. Washio, Y. Xiong, Y. Yin, Y. Xia, *Adv. Mater*. 2006, 18, 1745-1749.
Y. Xiong, I. Washio, J. Chen, H. Cai, Z. Li, Y. Xia, *Langmuir* 2006, 22, 8563-8570.
T. Sakai and P. Alexandridis *Langmuir* 2005, 21, 8019-8025.
T. Azzam and A. Eisenberg *Langmuir* 2007, 23, 2126-2132.

AGRADECIMIENTOS

Los autores agradecen al proyecto Fondecyt 1080238 por el financiamiento parcial de esta investigación. C.S agradece a Conicyt por Beca Doctoral.

T7. MANUFACTURING
PROCESADO

Effect of chemical modification on mechanical properties of textile fibers/HDPE composites

C.A.A. Lima
Universidade Federal de Alfenas, Campus Poços de Caldas, Brazil
D.R. Mulinari, H.J.C. Voorwald, M.O.H. Cioffi, P.H. Ozaki
Grupo de Fadiga e Materiais Aeronáuticos (DMT/FEG). Universidade Estadual Paulista, Brazil

ABSTRACT

In the work, mechanical properties of textile fibers/HDPE composites were studied. Residues textile fibers were treated with 10% sulfuric acid solution, followed by centrifugation, to remove impurities such as waxes, pectins and hemicellulosics fibers and analyzed by FTIR. These fibers were mixed with the polymeric matrix (HDPE) in a thermokinetic mixer, model MH-50H, with speed rate maintained at 5250 rpm, in which fibers were responsible for 5 to 15 wt% in the composition. After the mixture, composites were dried, ground in mill and placed in an injector camera according to ASTM D-638 specification. Results showed the addition of fibers in matrix increased the tensile strength and modulus compared to the matrix polymeric.

1. INTRODUCTION

The utilization of lignocellulosic materials in the production of polymeric composites is attractive particularly because of low cost and high volume applications, as well as advantages other, low density, availability of renewable natural resources, biodegradability and the concern with environment (Satyanarayana *et al.*, 2008; Farag, 2008).

Many studies have been developed on composites containing natural lignocellulosic fibers from agroindustrial or agricultural residues (Zah *et al.*, 2008; Lei *et al.*, 2007). Depending on their origin, natural fibers can be grouped into bast (jute, flax, hemp, kenaf), leaf (pineapple, sisal, henequen), and seed or fruit fibers (coir, cotton, oil palm). Cellulose is the main component of natural fibers, and the elementary unit of a cellulose macromolecule is anhydro-Dglucose, which contains three hydroxyl (OH) groups. However, the hydrophilic nature of these natural fibers is a major disadvantage for their application as reinforcement for polymeric composites.

There are several strategies of surface modifications to improve the compatibility between cellulose fibers and polymer matrices. The methods for surface modification can be physical or chemical according to the way they modify the fibre surface. Other frequently used treatments are bleaching, esterification, silane treatment, use of compatibilizer, plasma treatment, acetylation, alkali treatment and treatment with other chemicals (Mulinari *et al.*, 2009; GU, 2009).

Many researches have been conducted to study the mechanical properties, especially interfacial performances of the composites based on natural fibers due to the poor interfacial bonding between the hydrophilic natural fibers and the hydrophobic polymer matrices (Li *et al.*, 2008; Luz *et al.*, 2008).

The objective of this work was to study the effect of chemical modification on mechanical properties of residue textile fibers/HDPE composites.

2. EXPERIMENTAL

2.1 Chemical modification residue textile fibers

To remove the soluble extractives and to facilitate adhesion between fibers and matrix, the residue textile fibers were modified by pre-treatment with 10% sulfuric acid solution, followed by centrifugation.

2.2 FTIR characterization

The chemical structure of textile fibers modified and non-modified was evaluated by FTIR. FTIR spectra were obtained on a FTIR spectrophotometer (Perkin Elmer). Samples were prepared by mixing the materials and KBr in a proportion 1.5:300 (w/w). For all spectra, 16 scans were accumulated with a 4 cm^{-1} resolution.

2.3 Composites preparation

Residue textile fibers modified were mixed with the HDPE in a thermokinetic mixer, model MH-50H, with speed rate maintained at 5250 rpm, in which fibers were responsible for 5 to 15 wt% in the composition. After the mixture, composites were dried and ground in mill, model RONE. Composites and pure HDPE were placed in an injector camera at 165 ^{o}C and 2 ºC min^{-1} heating rate in a required dimensions pre-warm mold to obtain tensile specimen.

2.4 Mechanical properties

The mechanical strength of residue textile fibers reinforced HDPE composites was determined using an INSTRON universal-testing machine (model 8801). Tests were carried out according to ASTM standards D638 with 10 mm.min^{-1} crosshead speed. Tensile strength and modulus values are average results of five tested specimens.

3. RESULTS AND DISCUSSION

3.1 FTIR characterization

Infrared spectra of residue textile non-modified and modified are displayed in Fig. 1.

The most visible differences between the spectra of residue textile fibers modified and modified are the modifications of the signal at 2885 cm^{-1} and 1732 cm^{-1}, characteristics of the stretching of symmetrical CH groups and stretching of unconjugated CO groups present in polysaccharides and xylans. Considering the first region, the ratio between intensity of the C-H stretching band (~2900 cm^{-1}) is lower in the spectrum of the residue textile fibers modified material than that observed for the residue textile fibers non-modified. On the other hand, at the second region it may be observed modifications, especially in the ratio between the intensities of the C=O stretching band (~1730 cm^{-1}).

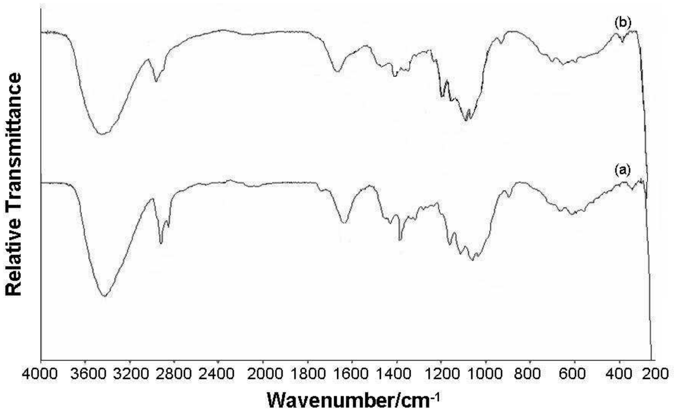

Figure 1. FTIR spectra: (A) residue textile non-modified (B) residue textile modified.

3.2 Mechanical Properties

Table 1 indicates the mechanical properties of residue textile fibers/HDPE composites and pure HDPE, in special the effect of chemical modification on residue textile fibers. Residue textile fibers/ HDPE composites show decrease in elongation at break in comparison to high-density polyethylene. With respect to tensile strength, it was obtained higher average value compared to the pure HDPE, but composites presented results similar. Therefore an amount reinforcement influenced in the tensile modulus.

Table 1. Mechanical properties of the composite.

Samples	*Properties*		
	Elongation at break (%)	*Tensile strength (MPa)*	*Tensile modulus (MPa)*
HDPE	8.9 ± 0.8	15.7 ± 1.1	732.45 ± 90.6
Residue textile fibers modified/HDPE 5%	7.2 ± 0.05	24.1 ± 0.3	1364.1 ± 42.3
Residue textile fibers modified/HDPE 15%	6.2 ± 0.01	23.9 ± 0.15	1557.3 ± 14.25

Reinforcement in wt%.

These results may be explained by the good interaction observed between fibers and matrix during the mixture process, confirming that fibers modification improves the fiber and matrix adhesion. This can be observed by the fracture surface. SEM micrograph of the fractured surface for the composite is shown in Fig. 2. It corresponds to surface of fractured residue textile fibers/HDPE composite 15 wt%.

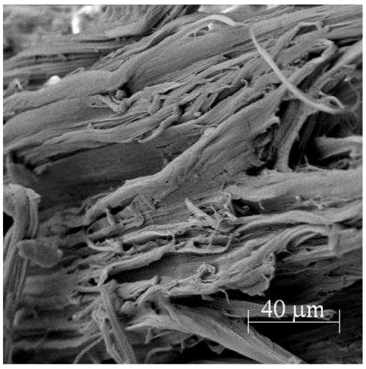

Figure 2. SEM of residue textile fibers modified (15 wt%)/HDPE composite 1000X.

4. CONCLUSIONS

The use of residue textile fibers as an alternative reinforcement in thermoplastics was verified. Modified fibers were studied to demonstrate the effect on mechanical properties and the practicability of processing these fibers with thermoplastics. Results were successfully accomplished and it was verified an improvement in the tensile strength and modulus compared to the high-density polyethylene.

ACKNOWLEDGEMENTS

The authors are grateful for the research support by CAPES.

REFERENCES

FARAG, M.M. (2008). Quantitative methods of materials substitution: Application to automotive components. *Materials & Design,* 29, 374-380.

GU, H. (2009). Tensile behaviours of the coir fibre and related composites after NaOH treatment. *Materials & Design*, 30, 3931-3934.

LEI Y, WU Q, YAO F, XU Y. (2007). Preparation and properties of recycled HDPE/natural fiber composites. Compos Part A, 38, 1664–1674.

LI, Y., HU, C., YU, Y. (2008). Interfacial studies of sisal fiber reinforced high density polyethylene (HDPE) composites. *Compos. Part A*, 39, p.570-579.

LUZ, S. M., DEL TIO, J., ROCHA, G. J. R., GONÇALVES, A. R., DEL'ARCO, A. P. (2008). Cellulose and cellulignin from sugarcane bagasse reinforced polypropylene composites: Effect of acetylation on mechanical and thermal properties. *Compos. Part A*, 39, p1362–1369.

MULINARI, D.R., VOORWALD, H.J.C., CIOFFI, M.O.H., DA SILVA, M.L.C.P., DA CRUZ, T.G., SARON, C. (2009). Sugarcane bagasse cellulose/HDPE composites obtained by extrusion. *Compos. Sci. Technol.*, 69, 214-219.

SATYANARAYANA, K.G., GUIMARÃES, J.L., WYPYCH, F. (2008). Studies on lignocellulosic fibers of Brazil. Part I: Source, production, morphology, properties and applications. *Compos Part A,,* 38, 1694–1709.

ZAH R, HISCHIER R, LEÃO AL, BRAUN I. (2007). Curauá fibers in the automobile industry - a sustainability assessment. J Cleaner Prod, 15, 1032-40.

Flexural and nondestructive tests on NC2/RTM6 composites manufactured by RTM for aerospace applications

M.Y. Shiino, M.O.H. Cioffi, H J.C. Voorwald
Grupo de Fadiga e Materiais Aeronáuticos DMT/FEG/UNESP.
Universidade Estadual Paulista, São Paulo – Brasil
M.C. Resende
Instituto Tecnológico da Aeronáutica, São Paulo – Brasil

SUMMARY

This work focused on the components manufactured by RTM for landing gear applications. This process produces excellent superficial finishing, reduces emission of monomers and produces complex geometry parts without reworkings.

A research project in partnership with the EMBRAER and CTA was conducted. NC2/RTM6 laminates provided by Hexcel composites were mechanically tested to verify the structural application possibility in future projects. Flexure mode was conducted to evaluate the material behavior during the operation. Ultrasonic inspections using C-scan methodology, with transdutor of 10 Mhz, to check the presence of descontinuties and possible defects in the material structure and the scanning electron microscopy in fractured samples were also conducted. The methodology used was the comparison between fractures from the tests, using SEM, and the quantitative results.

A good homogenity in the C-scan maps was observed, but poor regions of resin in the stitch area were verified. In flexure mode specimens presented excellent behavior, showing an excellent reproducibility in the RTM process. By using scanning electron micrograph analisys, it was possible to check the good interface and the fracture pattern produced during the tests.

1. INTRODUCTION

Carbon epoxy composite can be considered as a high performance material due to the high strength/weigth specific relation. Another attractive factor is the possibility of repairing little damages in field, without the need to disassemble the aircraft components (SURESH, S. to. 2003).

However the development of technology to produce carbon epoxy composite in relation to the material, shaping and manufacturing methods has improved and produced components with superior properties and consequently replaced metalic parts of the aircraft (BRYAN, H. to. 2003).For unidirecional composites the flexural mudulus is usually calculated by Classical Beam Theory(CBT), equation 1, and has an intermediate value between tensile and compressive modulus (MUJIKA, F. et al. to. 2006).

$$M = \frac{E_f \times I}{\rho} \qquad (1)$$

In the three-point bending test the flexural modulus can be calculated according to equation 2 by taking into account equation 1, where L, b and h are the dimensions of the beam and m is the slope of the load-displacement curve.

$$E_f = \frac{m \times L^3}{4 \times b \times h^3} \quad (2)$$

Gere and Timoshenko considered the difference between the tensile and compression modulus as a particular case of the assimetric behaviour(MUJIKA, F. et al. to. 2006).

In great span-to-depth ratio the shear effects, caused by loading noses, are negliged. As the loading nose increases the cross section of the beam starts the deformation processes at the cylindrical supports (MUJIKA, F. to. 2006).

In quasi-isotropic and cross laminates the number of interface interfers on the results of bending test, as the number of interface increases the maximum load and maximum displacement tend to increase as well (LEE, S. C. et al. to. 2009).

In laminated composites the mode of failure and its prediction is influenced by the properties of resin, fiber, the stacking sequence of the laminae, residual stress and environmental degradation. The failure might begin at the local level in an individual ply or in the interface of the plies and for multi-directional laminates the ultimate failure takes place when it has propagated in several plies (WILLIANS, J. C. et to. 2003).

In flexural it is common the ocurrance of buckling or kinking failure process which is associated with compression load in the upper part of the beam, whereas the part subjest to tensile stress the failure occurs by fiber rupture, and in the case of non-symetric laminates usually delamination takes places by coupling fenomena in which shear stress is predominant between the plies (GAY, D. et al. to. 2000).

2. MATERIALS AND METHODS

Composites tested is a combination of Hexcel intermediate modulus IM7-12k carbon fiber non-crimp quadri-axial orientated $[+45/0/-45/90]_{2S}$ with epoxy resin RTM6

The speed of the nose during the test was about 1.30 mm/min, calculated according to equation 3 (ASTM D790).

$$R = \frac{Z \times L^3}{6 \times d} \quad (3)$$

Where, R is the speed, L is support span and d is the deaph of beam.

The ultrasonic inspection was performed by using the C-scan method and imersing specimen to verify possible descontinuties in the composites, excess of resin and voids. The inspection was carried out with the equipment model MUIS32 manufactured by MATEC.

3. RESULTS AND DISCUSSION

Table 1 indicates the variation of the flexural modulus for the 27 specimens analised. These results are very expressive when compared with other materials used in the airspace industry, as, for example, 7050 aluminium alloy.

Results (GPa)							
Heats/ Specimens	IR384	IR385	IR386	IR387	IR388	IR389	IR390
1	31,88	32,95	21,40	26,36	32,35	24,41	27,54
2	24,25	30,15	29,89	27,19	31,73	30,03	29,84
3	30,71	27,95	30,96	28,18	27,97	26,44	26,97
4	29,76	28,82	28,55	31,68	31,41		29,33
Average	**29,15**	**29,97**	**27,70**	**28,35**	**30,87**	**26,96**	**28,42**
STD	**3,38**	**2,18**	**4,31**	**2,34**	**1,97**	**2,85**	**1,38**

Table 1. Results of the flexure test.

As observed in Figure 1, the load-displacement curve obtained for composite specimens tested in flexure presented elastic behavior from the begining to the end of the curve and the rupture ocurred in the specimen close to the maximun load, in Figure 1 shows each curve from IR384 to IR390.

To identify the causes of the composite failure, it was carried out analysis via SEM and via optical microscopic.

It was possible to verify stress concentration effects by fractograph analysis, according to Figure 2, in which the nucleation of the failure on the polyester fiber that keep the fabric together is indicated.

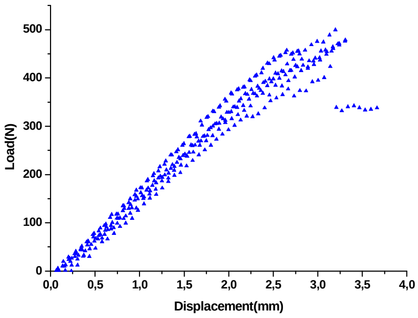

Fig. 1. Load-displacement curve of each heat tested.

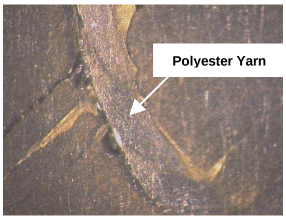

Fig. 2. Macrograph showing nucleation at the stitch.

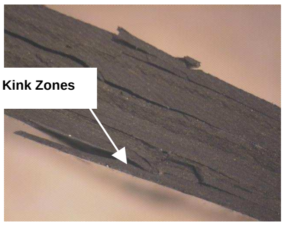

Fig. 3. Macrograph showing delamination at several places.

In Figures 4 and 5, failure process in the composite can be observed. In Figure 5 good adhesion of the resin on the fiber is verified which implicates on better results for the interlaminar strength.

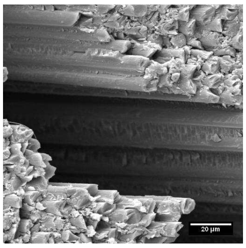

Fig. 4. Delamination 1000X magnification.

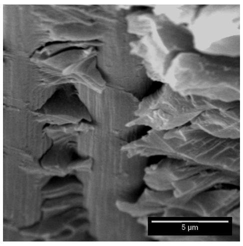

Fig. 5. Fracture with 7500X magnification.

Using ultrasonic analysis it has observed regular soaking of the fibers and good distribution of the resin along the plate, according to Figure 6.

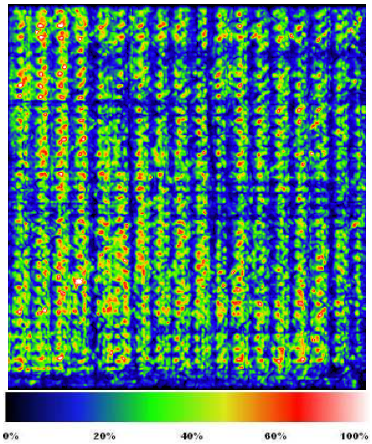

Fig. 6. Visualization of the impregnation map.

3. CONCLUSIONS

The stitch points were identified as one of the weakness of the composite, which act as a stress concentration, this was observed in many specimens tested.

From the fractograph analysis it was possible to verify the high compatibility of the NC2/RTM6 system with RTM process, by considering the good inteface and therefore good adhesion between fiber and matrix. Moreover it was possible verify the coesive fail of the resin associated to low tenacity of the matrix.

ACKNOWLEDGEMENT

The authors aknowledge the financial assintance of FAPESP by process number 2007/03182-1 and 2006/02121-6.

REFERENCES

ASTM D790 (2003). *Standard Test Methods for Flexural Properties of Unreinforced and Reinforced Plastics and Electrical Insulating Materials.*

BRYAN, H (2003). *Fatigue in Composites***.** First Edition, CRC, Cornwall – England, pág. 4.

GAY, D.,HOA, S. V (2007). *Composite Materials: Design and Applications***.** Second Edition, CRC.

LEE, S. C., JEONG, S. T., PARK, J. N., KIM, S. J., CHO, G. J.(2008) *A study on mechanical properties of carbon reinforce plastics by three-point bending testing and transverse static response.* Jornal of Materials Processing Technology 20I.

MUJIKA, F. (2006). *On the difference between flexural moduli obtained by three-point and four-point bending test*. Polymer Testing (25).

MUJIKA, F.; CARBAJAL, M.; ARRESE, A.; MONDRAGON, I. (2006) *Determination of tensile and compressive moduli by flexural tests*. Department of Mechanical Engineering, Polytechnical University College, University of Basque Country, Plaza Europa, 1, 20018, San Sebastián, Spain.

SURESH, S (2003). *Fatigue of Material***.** Second Edition, Cambridge University Press, United Kingdom, p.200.

WILLIAN, J. C., STARKE Jr., E.A. (2003). *Progress in structural materials for aerospace systems*. Acta Materialia, Vol. 51, pp. 5775-5799.

Mechanical properties of curaua fibers-cement based composites

A.L.F.S. d`Almeida, J.A. Melo Filho, R.D. Toledo Filho
Civil Engineering Department, COPPE, Universidade Federal do Rio de Janeiro, Brazil

SUMMARY

The development of eco-friendly materials that can reduce CO_2 emissions and aggregate value to a natural fiber, setting man at the countryside and increasing the income of poor populations is a challenge. Lignocellulosic fibers such as curaua are cheap and readily available reinforcement, requiring only a low degree of industrialization for their processing. The main drawback of using such fibers as reinforcement in cement composites is that they can be mineralized inside the alkaline environment. In this work, Portland cement was partially replaced by metakaolinite in order to produce a matrix free of calcium hydroxide, avoiding fiber mineralization. Cement composites reinforced with 6 and 10% of long aligned curaua fibers were manufactured and submitted to four pointing bending and to direct tensile tests in order to determine their mechanical behavior. The preliminary results obtained were compared with those found for cement composites reinforced by sisal fibers.

1. INTRODUCTION

Nowadays, environmental challenges due to the necessity of reducing worldwide levels of CO_2 emissions and energy consumption for the production of eco-friendly building materials is increasing the interest in natural products. Therefore, researches using lignocellulosic fibers such as sisal, curaua and jute as reinforcement of cementitious composites are increasing (d`Almeida et al. 2009, Toledo Filho et al. 2008, Silva et al. 2008, Silva 2009, Silva et al. 2009). Special attention should be given to natural fibers, in respect to energy conservation and environment protection. In fact, these materials possess many advantages, like low density, high specific strength, no healthy hazards, and also availability as renewable resources.

The main drawback to use lignocellulosic fibers as reinforcement in cement based composites is the fibers mineralization due to the migration of calcium hydroxide to the fiber lumen, middle lamella and cell walls. In this work, 50% of Portland cement (PC) was replaced by metakaolinite (MK) in order to produce a matrix completely free of calcium hydroxide, thus avoiding the problem of fiber mineralization. Moreover, the replacement of Portland cement by metakaolinite reduces CO_2 emissions and increases strength and durability of the material (Toledo Filho et al. 2009). Cement composites reinforced with 6 and 10% of long aligned curaua fibers were produced and tested under bending and direct tension.

2. MATERIAL AND METHODS

Curaua fibers are extracted from the leaves of *Ananas erectifolius* plants, which are a natural occurring *bromeliaceous* from Amazon region, Brazil. This fiber can reach 1.5 m long. For this work, the cuarua fibers were washed in hot water, brushed to separate the individual fibers and cut to the size of the molds (400 mm). The fibers were weighted and separated into five different layers resulting in a total volume fraction of 6% and 10%. The curaua fibers were stitched by three cotton fibers to make a homogeneous spacing between the fibers so as to facilitate the molding process.

The matrix was composed by Portland cement (PC) CPII F-32, metakaolinite (MK), river sand with maximum diameter of 1.18 mm and density of 2.67 g/cm^3 and naphthalene superplasticizer (Fosroc Reax Complast SP 430) with a solid content of 44%. The superplasticizer was used in order to increase the fluidity of the matrix. The mortar matrix had a mix proportion of 1:1:0.4 (cementitious material:sand:water, by weight). More details about the composites manufacture can be found in previous work (Toledo Filho et al., 2008, d`Almeida et al., 2009,).

The mechanical behavior of the composites was evaluated after 28 days of aging in a Shimadzu AGX – 100kN test equipment. Specimens 400 mm long, 80 mm large and 12 mm thick were tested in four point bending, at a crosshead rate of 0.5 mm/min. Three specimens were tested with a 300mm span, for each manufactured composite. Also, direct tensile tests were carried out in five specimens 400 mm long, 40 mm large and 12 mm for the composite reinforced with 6% of curaua fiber.

From the load deflection curves, the first-cracking strength (FCS), the post crack strength (PCS) and the toughness of the composites were calculated. The toughness was calculated as the area under the load versus displacement curve up to a displacement of 45 mm. Besides, the first-cracking strength for direct tension (FCSDT) and the post crack strength for direct tension (PCSDT) were also obtained.

3. RESULTS AND DISCUSSIONS

Figures 1a and 1b show typical equivalent flexural stress-displacement curves obtained for composites reinforced with 6 and 10% curaua fibers and a direct tensile stress displacement curves for composite with 6% curaua fibers, respectively.

Table 1 presents the average values and standard deviation for first-cracking bending strength (FCS), post crack bending strength (PCS), flexural toughness and first-cracking strength (FCSDT) and the post crack strength (PCSDT) under direct tension of the composites were calculated. Figures 2a and 2b present the typical cracking patterns for the specimens with 6% of fibers tested under bending and direct tension loads, respectively.

Observing the curves presented in Figure 1 it can be noted that the composites present a deflection hardening behavior under bending and a strain hardening behaviour under direct tension. The results presented in Table 1, indicate that PCS values as high as 27.5 MPa can be reached with the use of 6% of curaua fiber as reinforcement. For the same volume fraction a PCSDT value of about 10 MPa was observed. Regarding to the effect of fiber volume fraction, one can see a 21% decrease in FCS values and a 44% decrease in PCS when the volume fraction of curaua fiber was increased from 6% to 10%. The bending toughness calculated until a displacement of 45mm was also reduced (by about 13%) when the fiber volume fraction was increased. It is important to note that the 10% curaua reinforced composite presents a quite gradual softening behaviour (see Figure 1a) indicating that the composite can still present a post-cracking strength superior to 10MPa even at a deflection as high as 80 mm.

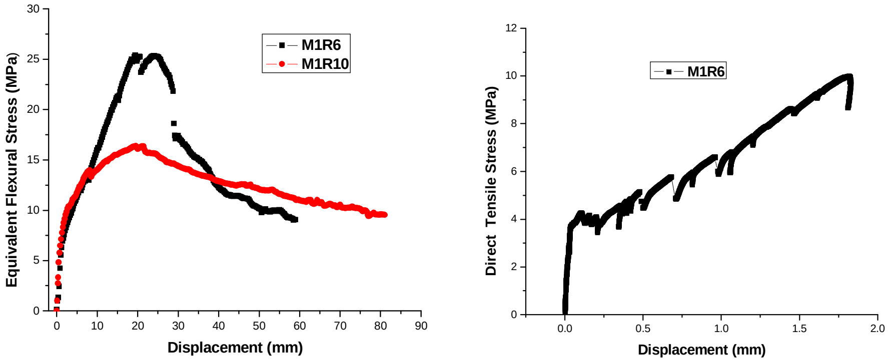

Fig. 1. (a) Typical four point bending curves for composites reinforced by 6 and 10% curaua fibers (b) Typical direct tension curve for composite reinforced by 6% curaua fibers.

Composites	FCS (MPa)	PCS (MPa)	Toughness (kJ/m^2)	FCSDT (MPa)	PCSDT (MPa)
M1R6	5.60 ± 1.17	27.52 ± 2.65	28.87 ± 2.12	3.65 ± 0.53	9.65 ±0.73
M1R10	4.39 ± 0.27	15.56 ± 1.10	25.13 ± 2.71	-	-

Table 1. Four Point Bending and Direct Tensile Results.

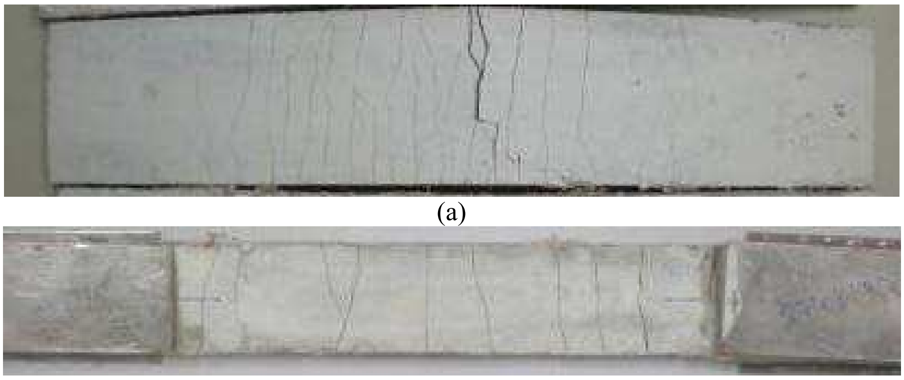
(a)

(b)

Fig. 2. Cracking pattern for the specimens reinforced with 6% of fibers submitted to (a) Four point bending test and (b) Direct tension loads.

The multiple-cracking patterns exhibited by the composites (see Figure 2) both in bending and direct tension shows elevated performance of the developed composites. A similar behaviour was also observed for cement composites reinforced with continuous and aligned sisal fiber (Toledo Filho, 2008, Silva, 2009). This behaviour was expected because sisal and curaua are high performance natural fibers (Silva, 2009) with similar modulus, tensile strength and strain at failure (Silva, 2009, Zah et al., 2007).

3. CONCLUSIONS

This work demonstrates the potential of long aligned curaua fibers as reinforcement in thin cement based laminates. The material presented a multiple cracking process with a strain hardening behavior under direct tension which demonstrates that it can be used in structural applications. The elevated ductility of the material can even make them ideal for use under blast, impact or dynamical loads. In addition, the use of a natural reinforcement in a matrix with a low content of Portland cement results in a sustainable material to be used in the construction industry.

ACKNOWLEDGMENT

The authors want to be grateful the CNPQ for financial support.

REFERENCES

D`ALMEDA, A.L.F.S., MELO FILHO, J.A., TOLEDO FILHO, R.D., (2009), Use of curaua fibers as reinforcement in cement composites, *Chemical Engineering Transactions*, V. 17, 1717-1722.

SILVA, F.A. (2009), Durabilidade e propriedades mecânicas de compósitos cimentíios reforçados por fibras de sisal, Ph.D. *Thesis, COPPE-UFRJ, Brazil.*

SILVA, F.A., Chawla, N., TOLEDO FILHO, R. D. (2009). An experimental investigation of the fatigue behavior of sisal fibers. *Materials Science & Engineering. A, Structural Materials: properties, microstructure and processing,* v. 516, p. 90-95.

SILVA, F.A., CHAWLA, N ; TOLEDO FILHO, R. D.(2008), Tensile behavior of high performance natural (sisal) fibers. Composites Science and Technology, v. 68, p. 3438-3443, 2008.

TOLÊDO FILHO, R.D, FAIRBAIN, E.M.R., MELO FILHO, J.A. AND SILVA, F.A.(2009), Durability of compression molded sisal fiber reinforced mortar laminates. Construction & Building Materials, v. 23, p. 2409-2420, 2009.

ZAH, R., HISCHIER, R, LEAO, A. L., BRAUN, I .(2007) Curauá fibers in the automobile industry - a sustainability assessment.. *Journal of Cleaner Production*, v. 15, p. 1032-1040, 2007.

Prediction of cure cycle in manufacturing process of thick-sectioned fiber reinforced composite materials using artificial neural networks

P. Eghbal Jahromi
Pertropars Ltd.,Tehran, Iran
S.M.R. Pishvaie
Chemical and Petroleum Engineering Department.
Sharif University of Technology, Tehran, Iran
A. Shojaei
Chemical and Petroleum Engineering Department.
Sharif University of Technology, Tehran, Iran

SUMMARY

Curing of thermoset based composites especially of thick ones has always been a matter of importance and consideration by many of researches due to its relevant serious problems such as non-uniformity, residual stress and consequently composite cracks. These mentioned faults are originated from the thermal gradients throughout the part caused by large amount of heat released along with the low thermal conductivity of the composites. Compared to experimental investigation, the approach of numerical simulation not only saves time and cost, but also provides a flexible, exact and vivid knowledge of the process behavior. The scope of this work is first to prepare a finite volume-based 3 dimensional simulation of the curing process and a parametric study using a CFD commercial package. However speeding up the simulation process is a substantial concern especially as a pre-requisition of practical aspects such as optimization or on-line control. As an alternative the numerical simulation is therefore substituted with a trained dynamic artificial neural network. The developed numerical simulation has been used as a data bank of the network training.

The numerical simulation is validated with the experimental data and a good consistency is achieved. More ever the neural network is also well trained with a defined performance of .006. While the numerical simulation lasted about 25-30 minutes, the neural network approach lasted only as much as 5-7 seconds and adjusted well for purposes of time-saving requirements.

1. INTRODUCTION

Fiber reinforced thermoset matrix composites are being used in a wide variety of applications such as aerospace and automobile industries because of their higher specific strength and stiffness than those of conventional materials. These composites can be fabricated successfully by many continues and batch processes. Regardless of the manufacturing method, they are all common in the critical and important step of curing process (Oh et. to. 2002 and Rai et. to. 1997).

The curing process has always been a challenge, since a combination of low thermal conductivity, acting like a thermal barrier, and high rate of released heat through the composite part causes thermal gradients and temperature overshoot and consequently leads to non-uniformity of the final cured products with the probability of composite cracks.

Although curing process has been widely simulated through a variety of special case models (Shojaei to. 2006), non of these efforts has applied a general package with reliable and precise results and attractive post-processing capabilities. However numerical simulations are always slow and time-consuming. This flaw specifically gets dominant in exact investigation of the behavior of rapid exothermic reactions while small time steps are required and this leads to much more slower processes. On the other hand simulations are usually purposed for subsequent practical applications such as optimization or on-line control where speed computation is a vital factor.

Artificial neural networks have been used as alternatives for these applications (Rai et. to. 1997 and Su et. to. 1998). Rai and Pitchumani designed a static (conventional) neural network as a rapid cure simulator in optimization application. However among the numerous possible configurations of ANNs, the recurrent neural networks (RNNs) are known to be practically effective in learning transient problems and superior in performing long-term predictions (Su et. to. 1998). Among all, only Su et al. have used RNNs. They have applied them as the soft sensor to predict on-line changes only in degree of cure in a bag-molding process. In this work, therefore, according to the transient nature of the problem, RNNs have been designed to simulate the profiles of temperature and degree of cure of a composite part purposed for rapid repetitious use during optimization process. However prior to this step, a finite volume-based numerical simulation of curing process has been performed using the CFD package of FLUENT in order to provide training datasets.

2. THEORETICAL BASIS AND METHODOLOGY

Temperature and degree of cure (conversion) distributions inside the mold can be predicted by the appropriate form of energy and mass balance equations. These equations can be written as below:

$$\rho c\frac{\partial T}{\partial t}=\frac{\partial}{\partial x}(K_x\frac{\partial T}{\partial x})+\frac{\partial}{\partial y}(K_y\frac{\partial T}{\partial y})+\frac{\partial}{\partial z}(K_z\frac{\partial T}{\partial z})+\dot{q} \tag{1}$$

$$\dot{q}=\rho H_u\frac{d\alpha}{dt} \tag{2}$$

$$\frac{d\alpha}{dt}=(k_1+k_2\alpha^m)(1-\alpha)^n \tag{3}$$

Solving the coupled Equations (1) and (3), needs using appropriate numerical methods where as in this paper the finite volume-based CFD package of FLUENT 6.3.26 has been used. Each CFD Packages primitively needs a pre-processor to prepare the geometry, meshes and definition of the zones. Gambit 2.3.16 is the CAD pre-processor applied in this work.

The massively parallel distributed processors called Artificial Neural Networks (ANNs) with the neurons as their structuring units are used as the accelerators of simulation process. In order to be able to learn the dominant pattern of the system, every network needs to see a set of data. In this work the dataset is a series of 1422 cure cycle data provided by running the numerical simulation, with manipulating the boundary conditions in a relatively good diversity. This set of data is randomly divided into three subsets of training (60%), validation (20%) and testing (20%). Among different available transfer functions, hyperbolic tangent sigmoid function is selected for all neurons due to its better prediction performance. According to the bounded range of the transfer function, the input and target data are normalized in the range of [-1, 1]. The performance function of the network is defined as $msereg = \gamma mse + (1-\gamma)msw$ where mse is the mean square error of the outputs; msw is the mean square of weighting factors and γ is the optimized performance ratio. (Rai et. to. 1997, Su et. to. 1998 and Mackey to. 1992)

3. RESULTS AND DISCUSSIONS

The mold used in this study has a cubic geometry with dimensions of $50\ mm \times 50\ mm \times 30\ mm$. The composite material is an epoxy/glass fiber system in which the volume fraction of fiber is assumed to be 0.3. The materials properties and the kinetics parameters used in this investigation are taken from the literature (Oh et. to. 2002). Initial temperature of the system is assumed to be 298 K and the convective heat transfer coefficient of 70 (w/m^{2}K) is used between the surrounding environment and the mold wall. As a sample the results for temperature trend through the thickness are reported in Fig.1 under an applied B.C.

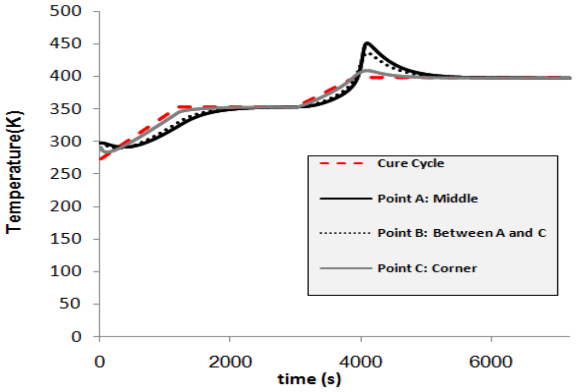

Fig. 1. Temperature profile through the thickness.

As we expected the temperature profile experiences an overshoot especially at the middle of the geometry and a significant non-uniformity will be appeared as a result.
Among the numerous possible configurations of ANNs, NARX (Nonlinear Auto-Regressive Network with Exogenous Inputs) models are suitable for training the problems in which the next value of the dependent output is regressed on previous values of outputs and inputs. This model with an arrangement of [6-7-7-2] of neurons is then used as the design basis of our network for prediction of temperature trends in the middle and corner of the mold. A schematic of this design is shown in Fig.2; where T is temperature, m and c abbreviate middle and corner and k denotes the time steps. The same can bee used for conversion. The performance of training of this net is about 0.006 for all training sets. Moreover the best linear fit of output data obtained from the network versus the targets can be expressed with the equations of $y = 0.9989\ t + 0.5814$

& *$y = 0.9996\ t + 2.0153$* compared to *$y = t$* respectively at the middle and corner. It worth to consider that while the numerical simulation lasted about 25-30 minutes, the neural network simulation lasted only about 5-7 seconds.

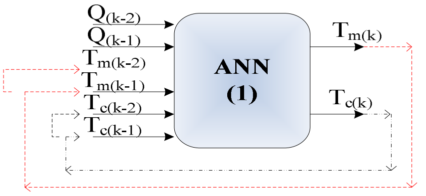

Fig. 2. An illustrative figure of the designed neural network.

3. CONCLUSIONS

A dynamic artificial neural network was developed to predict the cure cycle of a thick composite part. Training of the network was performed using the numerical results obtained using the three-dimensional finite volume method. The numerical study revealed that the neural network method reduces the computation time substantially compared to the conventional numerical methods.
Include always at the end a paragraph with the most relevant conclusions of the work.

ACKNOWLEDGMENT

The authors want to be grateful of Petropars Ltd. for the financial supports.

REFERENCES

1. MACKAY, D.J.C. (1992). Bayesian interpolation, neural computation, 4, 415-447.
2. OH, J.H. and LEE, D.G. (2002). Cure cycle for thick glass/epoxy composite laminates*, Journal of Composite Materi*als, 36, 19-45.
3. RAI, N. and PITCHUMANI, R. (1997). Rapid cure simulation using artificial neural networks, *Composites Part A*, 28, 847-859.
4. RAI, N. and PITCHUMANI, R. (1997). Optimal cure cycles for the fabrication of thermosetting matrix composites*, Polymer Composites*, 18, 566–81.
5. SHOJAEI, A. (2006). A numerical investigation on the cure cycle of railroad composite brake blocks**,** *International Polymer Processing*, 4, 421-431.
6. SU, H.B., FAN, L.T. and SCHLUP, J.R. (1998). Monitoring the process of curing of epoxy/graphite fiber composites with a recurrent neural network as a soft sensor, *Engineering Applications of Artificial Intelligence*, 11, 293–306.

Tool geometry evaluation for carbon reinforced composites laminates

L.M.P. Durão, D.J.S. Gonçalves
Instituto Superior de Engenharia do Porto
CIDEM – Centro de Investigação e Desenvolvimento em Engenharia Mecânica
R. Dr. António Bernardino de Almeida, 431 – 4200-072 PORTO, PORTUGAL
J.M.R.S. Tavares, V.H.C. de Albuquerque, A. Torres Marques
Faculdade de Engenharia da Universidade do Porto
Instituto de Engenharia Mecânica e Gestão Industrial
Rua Dr. Roberto Frias, s/n – 4200-465 PORTO, PORTUGAL

SUMMARY

The use of composite laminates in complex structures has increased significantly. However, there are still some issues when considering their use, mainly related with machining, leading to some difficulties and lack of acceptance. In this work, a methodology to evaluate drill geometry and feed rate based on thrust force and delamination extension is presented.

INTRODUCTION

For the past decades composite materials are increasing their importance as one of the most interesting group of materials, due to their unique properties of low weight, high strength and stiffness.

One of the main machining operations needed in composite structures is drilling, as it is required when bolts, rivets or screw are used to join different parts. Usually, it is accepted that drilling can be carried out using conventional machinery, with proper adaptations. However, as composites are non-homogeneous, drilling causes some difficulties. In fact, some damage in the region around the hole boundary is evident after the completion of the operation, being delamination the most serious damage as it can reduce the load carrying capacity of the joint. The main mechanism responsible for delamination is the indentation effect caused by the quasi-stationary drill chisel edge (Hocheng et al. 2005). This effect can be diminished by a correct choice of tool geometry and/or cutting parameters (Hocheng et al 2006). In general, it is accepted that a drilling process that reduces the thrust force exerted by the drill chisel edge can prevent delamination occurrence (Dharan et al 2000, Davim et al 2003, Durão et al. 2008). Another possibility for delamination reduction is an adequate design of the cutting tool – drill – which, combined with proper machining parameters, can help in delamination prevention (Persson et al 1997, Piquet et al 2000, Hocheng et al 2006, Tsao et al 2007).

In this work, a comparison on the thrust force during drilling and delamination extension after drilling has been accomplished considering five different drill geometries – twist with two point angles, Brad type, Dagger type and bidiametral, figure 1. The thrust force was monitored during hole machining and the delamination extension was computational analyzed by enhanced radiography and techniques of image processing and analysis. An experimental procedure was planned and results evaluated.

MATERIALS AND METHODS

In order to perform the experimental work planned, plates using prepreg CC160 ET 443 with a cross-ply stacking sequence and 24 layers were produced. The plates were cured under 300 kPa pressure and 130 ºC for one hour, followed by cooling. In the end, plate thickness was 4 mm. The plates were then cut in coupons of 165x96 mm^2.
The experimental work was divided in drilling of the laminate plates for thrust force monitoring with a *Kistler 9257B* dynamometer associated to an amplifier and a personal computer for data acquisition and processing. Drilling operation was carried out in a 3.7 kW *DENFORD Triac Centre* CNC machine. The second step was delamination evaluation by enhanced radiography and techniques of image processing and analysis. With this goal, plates were immersed in di-iodomethane for contrast for one and a half hour and radiographed. Acquired radiographies were scanned for delamination around the hole measurement. Details of this process can be found in Durão et al (2008).

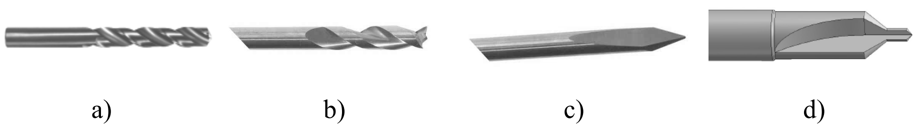

Figure 1. Drills: a) twist (120º / 85º); b) Brad; c) Dagger; d) bidiametral.

A total of five tungsten carbide drills with 6 mm diameter and different geometries were used: a twist drill with a point angle of 120º, a twist drill with a point angle of 85º, a Brad drill, a Dagger drill and a customized step drill, Figure 1. Cutting parameters, whose selection was based on previous work, were the following: cutting speed of 53 m/min, corresponding to a spindle speed of 2800 rpm; three feed rates, respectively 0.02, 0.04 and 0.06 mm/rev.

RESULTS AND DISCUSSION

Results considered for thrust force are the maximum values observed during drilling. The force values were always averaged over one spindle revolution, due to signal variation along drill rotation and are the average of six experiments performed under identical conditions.
Variation of thrust force with feed rate and drill geometry can be observed in Figure 2. From that figure, is clear that larger feed rates cause an increase in the value of the maximum thrust force during drilling, whatever drill is used. For this reason, the likelihood of delamination damage, closely linked to the existence of a trigger value for delamination onset (Hocheng /Dharan 1990), becomes greater with larger feeds.
Regarding tool geometry, Brad drill has always the highest values of thrust force while the lower ones were obtained with Dagger drills. When comparing the two twist drills, a 120º point angle allows for larger thrust force reduction than an 85º point angle drill. The bidiametral drill has not confirmed the predicted reduction of thrust force.
Regarding delamination, considering Delamination factor – F_d – (Chen, 1997) and results of delaminated diameter accomplished by enhanced radiographies and techniques of image processing and analysis, a comparison graphic is presented in figure 3. From the results of damaged region is possible to identify a relationship between feed rate and

delamination. So, an increase in feed will cause extended delamination. This result confirms that an appropriate feed rate selection can help on delamination prevention.

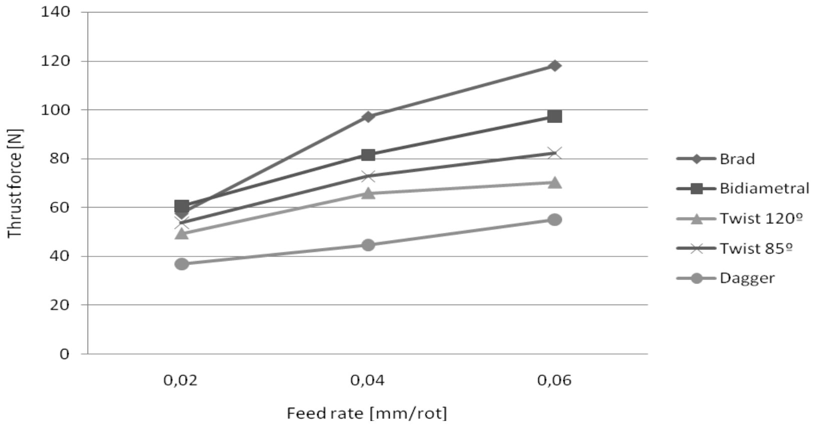

Fig. 2. Evolution of thrust force with feed rate for the drills used in this work.

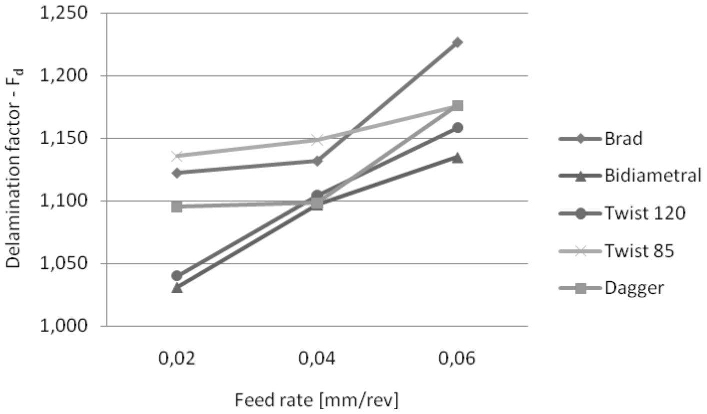

Fig. 3. Evolution of delamination factor – F_d – with feed rate for the drills used.

For the feed rates selected, the behavior of the five drill geometries becomes different with each feed rate. For the medium one, the values of delamination are very similar, while for the smaller and larger feeds, there is an advantage on the use of bidiametral or 120º point angle twist drill. Corresponding to higher thrust forces during drilling, Brad drills had the higher damaged zone. The lower thrust force values of Dagger drill did not correspond to less delamination, evidencing the importance of tool tip geometry on delamination onset and propagation.

CONCLUSIONS

Carbon/epoxy laminates were drilled with the objective of comparing five different tool geometries. Results used for drill geometry comparison were the maximum axial thrust force during drilling and delamination around the hole. Experimental work has involved three feed rates combined with a pre-selected cutting speed. Results show that an adequate combination of drill geometry and parameters can help to reduce delamination. Low feed rates seem appropriate for laminate drilling, reducing the axial thrust force and, therefore, the risk of delamination onset and propagation.

Additionally, an adequate tool selection can help on damage minimization. For the experimental conditions considered the most adequate commercial tool is the 120º point angle twist drill. Bidiametral drill represents an adequate option for a tool as well.

Tool geometry had influenced the results both for force and delamination. It is interesting to remark the diverse effect of feed rate on delamination according to the tool used, as the slope of the delamination values lines for each tool is dissimilar.

Based on the work accomplished and parameters used, a 120º twist drill should be used for minimal delamination while the bidiametral drill still needs further improvements.

ACKNOWLEDGEMENTS

This work is supported by the Portuguese FCT – Fundação para a Ciência e Tecnologia, under project PTDC/EME-TME/66207/2006, “Drilling of polymeric matrix composites structures”.

REFERENCES

CHEN W.C. (1997). Some experimental investigations in the drilling of carbon fibre-reinforced plastic composite laminates”, *Int J Machine Tools & Manuf,* 1097-1108.

DAVIM J.P., REIS P. (2003). Drilling carbon fibre reinforced plastics manufactured by autoclave – experimental and statistical study. *Materials & Design*, 24, 315-324.

DHARAN C.H.K., WON M.S. (2000). Machining parameters for an intelligent machining system for composite laminates. *Int J Machine Tools & Manuf*, 40, 415-426.

DURÃO, L.M.P., TAVARES, J.M.R.S., MARQUES, A.T., BAPTISTA, A.M., MAGALHÃES, A.G. (2008). Damage analysis of carbon/epoxy plates after drilling, *Int. J. Materials & Product Technology*, 32, 226-242.

HOCHENG H., DHARAN C.K.H. (1990). Delamination during drilling in composite laminates, *J. Engineering for Industry*, 1990, 112, 236-239

HOCHENG, H., TSAO, C.C. (2005). The path towards delamination-free drilling of composite materials, *J. Materials Processing Technology*, 167, 251-264.

HOCHENG, H., TSAO, C.C. (2006) Effects of special drill bits on drilling-induced delamination of composite materials, *Int. J. Machine Tools & Manuf.*, 46, 1403-1416.

PERSSON E, ERIKSSON I, ZACKRISSON L. (1997). Effects of hole machining defects on strength and fatigue life of composite laminates. *Composites A*, 28, 141-151.

PIQUET R, FERRET B, LACHAUD F, SWIDER P. (2000) Experimental analysis of drilling damage in thin carbon/epoxy plate using special drills. *Composites A*, 31, 1107-1115.

TSAO C.C., HOCHENG H. (2007). Parametric study on thrust force of core drill. *J. Materials Processing Technology*, 192/193, 37-40.

Thermal regulation in NCF/RTM6 composites

M.O.H. Cioffi; H.J.C. Voorwald
Fatigue and Aeronautics Materials Research Group, DMT/FEG/UNESP,
Av. Dr. Ariberto Pereira da Cunha no. 333, Cep 12516-420, Guaratinguetá/SP, Brazil
M.C. Rezende
Divisão de Materiais /IAE/CTA. Praça Marechal Eduardo Gomes, 50 Campus do CTA -
Vila das Acácias 12228-904 São José dos Campos/SP – Brazil
V. Ambrogi, C. Carfagna, V. Antonucci
University of Naples Federico II, Department of Materials and Production
Engineering, P.le Tecchio 80, 80125 Naples, Italy

ABSTRACT

The RTM process is one of most efficient techniques to produce advanced fibers reinforcing polymeric matrix composites. During the process the resin in liquid state is passed into the closed mold until the saturation of preform is allowed when the cure is started. The quality of impregnation depends on the permeability of reinforce by the resin, which represent the resistance of the fiber to the resin flow expressed by Darcy's law. Anomalies in the preform may affect the mechanical properties of composites, consequently significant changes in stiffness, strength and fatigue life may occur. Thermal regulation is an important action to improve polymer composites properties and in this work a NCF/RTM6 composites with and without microencapsulated in polymer shell phase was investigated by dynamical-mechanics analysis in order to obtain mechanical properties influence. Panel Composite was also investigated by Acoustic microscopy analysis in C-Scan method to verify edge effect as incomplete wetting of the fiber reinforcement, dry spot formation and voids.

1. INTRODUCTION

Fiber reinforced polymer to form composites introduces specific better properties, typically, mechanical behavior considered as adequate alternative to substitute the conventional one (Larsen T. O. et al., 2008). Depending on the application, these materials could offer a set of properties as low-density, high-strength, high-stiffness, high damping, chemical resistance, thermal-shock resistance (Melo J. D. D., Radford D. W., 2005).

However, composite processing, which uses unlocked molds, should be avoided in view of tight requirements and also due to possible environmental contamination.

The RTM process is one of most efficient techniques to produce advanced fibers reinforcing polymeric matrix composites (Antonucci V. et al., 2004). Is associated to an effective low cost technology to produce great scale composites components. It was developed as an economic method of high quality composites to produce more complexes components to than those obtained from the traditional methods (Hillermeier R. W., Seferis J.C. 2001), present excellent control of mechanical properties and shorter cycle of process (Luo J., Liang Z., Wang B. 2001) , other advantage is the elimination of autoclave and the reinforcements need not be limited by shelf life as pre-preg (Pandita S. D. et al., 2001) .

Parameters as temperature and frequency affect the composites performance. A range of temperatures is considered for design of some advanced structures as aircraft components, including operating low and high temperatures. Also the frequency is so important to be considered due to the vibration influence on the performance of polymers (Melo J. D. D., Radford D. W., 2005).

The influence of these parameters can be successfully known using a dynamic mechanical analysis (DMA). The DMA analysis provides an accurate temperature control and allows the characterization regarding temperature and frequency (Melo J. D. D., Radford D. W., 2005).

For thermal regulation the latent heat is an important phenomenon considering the possibility of high storage density and homogeneous temperature characteristics (Li J. et al, 2009). Micro phase change materials microencapsulated is an alternative for fibers thermal regulation (Zhang H., Wang X., 2009).

2. EXPERIMENTAL

2.1 Materials description

The reinforcement is a combination of Hexcel intermediate modulus IM7-12k carbon fiber non-crimp quadri-axial orientated +45/0/-45/90, a real weight 772g/m², and its mirror 90/-45/0/+45, stitched by a polyester yarn. The RTM6 is a mono-component liquid epoxy resin system developed by Hexcel Composites, which can be used in service temperature range from –60°C to 180°C. With and without microencapsula in polymer shell phase change material was used. Both material was processed by RTM.

2.2 Scanning microscopy inspection

Ultrasonic non-destructive testing measurement was used for panels composites, method through which the C-Scan images were obtained, which presents a relative attenuation of ultrasonic waves across the surface of a component. An ultrasonic transducer is used to scan the surface of a material mechanically in an x–y raster scan mode while generating and receiving waves.

2.3 Dynamics -Mechanical analysis

Dynamic measurements were carried out using 2980 TA Instruments dynamic mechanical analysis equipment at different frequency range (1, 5, 10, 100 Hz) and temperature range from 25ºC to 250ºC, with a heating rate of 3.0 °C/min, 3°C/min. A 3-point bending testing mode, with a 40.0 mm span between the supports was selected as the preferred testing geometry since clamped boundaries are reported to affect the damping measurements. All dynamic tests were carried out under a sinusoidal strain-controlled mode. Strain amplitude of 10 µm was used during measurements for viscoelastic parameters acquisition. Composites specimens were pre-stressed with an applied force 10 N and a force track of a 150%.

3. RESULTS AND DISCUSSION

3.1 Scanning inspection microscopy

It was conduct scanning in the three distinct layer of panel indicated in the Figure 1. Figure 2, 3 and 4 show the C-Scan map resulted of ultrasonic analysis using a scanning inspection microscopy. The figure 2 the impregnation map was obtained in respect to the more superficial layer of panel and it is possible verify low impregnated sites, indicated for green colour referred to the polyester yarn. In a deeper layer, indicated for the figure 3, a homogeneous distribution is represented by the blue color with low impregnation fails, by the green color. As seen in the Figure 2, the deepest layer indicated in the Figure 3, it was observed a good impregnation in consequence of optimized process.

Fig 1. NC2/RTM6 composite.

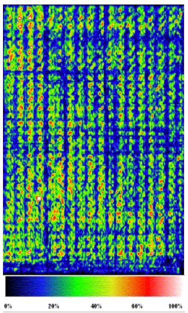

Fig 2. Scan layer 1

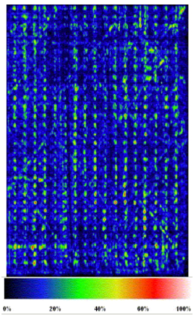

Fig 3. Scan layer 2

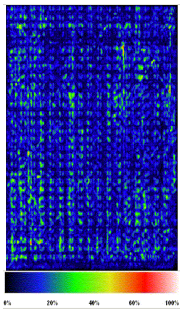

Fig 4. Scan layer 3.

To verify the influence of phase change material the resin was mixture with polymer shell microencapsule after that the composite was processed, indicated in Figure 5. No influence of microcapsule in the impregnation process was observed according to the C-Scan analysis, Figure 6.

Fig 5. NC2/RTM6 composite.

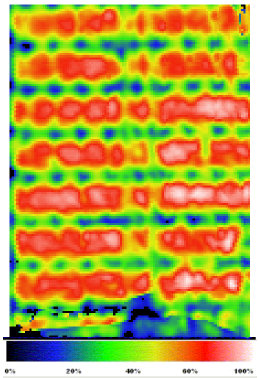

Fig 6. Scan layer 1.

3.2 Dynamic Mechanical Analysis

DMA Curves were indicated in Figure 7 for frequencies 1, 5, 10, 100 Hz. In all cases it was observed a correlation between viscoelastic parameters and the frequency variation. Among them it can be cited a better performance of the laminate with the frequency increase. In this case, the glass transition temperature (Tg) increases with the increase in the frequency, which is observed in the DMA curves, where it is possible to see for 1Hz, 5 Hz, 10 Hz and 100 Hz a variation in the Tg value equivalent to 195°C, 203°C, 208°C and 230°C. It was also observed that the storage modulus is relatively constant over the frequency range, which is associated to the better dimensional stability of the samples due to the lower time of test. The loss moduli present an increase according the frequency variation.

In the same way, for microencapsulated NC2/RTM6 composite was tested in frequencies 1, 5, 10, 100 Hz. The correlation between viscoelastic parameters and the frequency variation was also observed.

In this case, the glass transition temperature (Tg) increases according to the frequency, indicated in Figure 8 where it is possible to see for 1Hz, 5 Hz, 10 Hz and 100 Hz a variation in the Tg value.

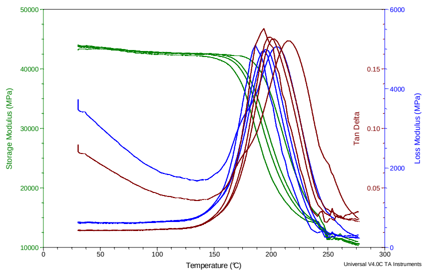

Fig 7. NC2/RTM6 composite DMA.

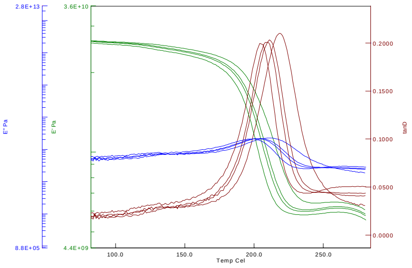

Fig 8. Microencapsulated NC2/RTM6 composite DMA.

equivalent to 205°C, 210°C, 212°C and 225°C, which in comparison to the composite without microcapsule represent a higher thermal stability due to the better distribution of temperature in the bulk of composite. For storage modulus was observed also a correlation with frequency, as example for the composite without microcapsule

4. CONCLUSIONS

It was observing a suitable impregnation for NC2/RTM6 composite with and without microencapsulated in polymer shell phase change material, whit show that the presence o microcapsule do not influence in the permeability. Both composite presented a correlation between frequency e viscoelastic parameters. The phase change material conferred higher thermal stability for the composite moving to write the DMA curves.

ACKNOWLEDGEMENTS

The authors are grateful for the research support by FAPESP through the process 2006/02121-6.

REFERENCES

Larsen T. O., Andersen T. L., Thorning B., Vigild M. E. (2008) Changes in the tribological behavior of an epoxy resin by incorporating CuO nano particles and PTFE microparticles. *Wear* 264, 9-10, 857.

Melo J. D. D., Radford D. W. (2005) Time and temperature dependence of the viscoelastic properties. *Comp. Struct*., 70, 240.

Antonucci V., Giordano M., Nicolais L., Di Vita G., (2004) A simulation of the non-isothermal resin transfer molding process *Pol Eng and Sci.* 40, 12, 2471.

Hillermeier R. W., Seferis J.C. (2001). Interlayer toughening of resin transfer molding composites *Comp:. part A*., 32, 721.

Luo J., Liang Z., Wang B. (2001) Optimum tooling design for resin transfer molding with virtual manufacturing and artificial intelligence *Comp.: part A*., 32, 877.

Pandita S. D., Huysmans G., Wevers M., Verpoest I. (2001) Tensile behavior of glass-plain weave fabric composites in on-and off axis directions *Comp.: Part A*. 32, 1533.

Jianli Li , PingXue, Wenying Ding, Jinmin Han, Guolin Sun. Micro-encapsulated paraffin/high-density polyethylene/wood flour composite as form-stable phase change material for thermal energy storage. *Solar Energy Materials & Solar Cells* Available online 24 June 2009.

Zhang H., Wang X. (2009). Synthesis and properties of microencapsulated n-octadecane with polyurea shells containing different soft segments for heat energy storage and thermal regulation. *Solar Energy Materials & Solar Cells* 93 (2009) 1366-1376.

Paclitaxel-eluting stents based on electropolymerized prodrugs

Jeong-Sun Sohn
Department of Polymer Science & Engineering, Chosun University, 375 Seosuk-dong,
Dong-gu, 501-759, Gwangju, Republic of Korea
Eun-Sun Choi, Byung-Wook Jo
Department of Chemical & Biochemical Engineering, Chosun University,
375 Seosuk-dong, Dong-gu, 501-759, Gwangju, Republic of Korea

SUMMARY

A series of electrically initiated in-situ polymerization was conducted for surface treatment of a stent with a hydrophilic microtubulin stabilizing-drug. For the electropolymerization, a series of water-soluble paclitaxel prodrug (PP7) analogues were synthesized by using several vinyl containing monomers. Finally we have tried the electropolymerization of polymer-modified paclitaxel prodrugs for practical application. The surface properties of electropolymerized steels were investigated by scanning electron microscopy (SEM). Also, the electropolymerized steels were characterized by test of blood platelet adhesion and whole blood clots in vitro.

1. INTRODUCTION

Paclitaxel is a unique tubulin-interacting agent unlike other conventional antimitotic agents, which inhibit the microtuble assembly process (Wani et al. 1971). In spite of paclitaxel's promising clinical drug activities, the drug has presented problems during it's administration to patients because of it's severe insolubility in water. Therefore, we have developed a water-soluble paclitaxel prodrug (PP7) based on PEG conjugates with a newly developed self-immolating group which gave a rapid hydrolysis rate to convert a prodrug into a parent drug without any reduction in drug efficacy (Jo et al. 2004, 2008). And we have investigated its properties, such as self-diffusion behavior, phase behavior (Hess et al. 2006), hydrodynamic property, molecular conformation (Sohn et al. 2005) and interaction with protein (Jo et al. 2009) etc, until now.

Paclitaxel has a special mechanism of action that inhibits SMC (smooth muscle cell) proliferation and migration. So, introduction of coated stents, which have become the most universal means of treating coronary artery disease, was a significant progress in suppression of cellular proliferation. But, most of the conventional paclitaxel-eluting stents are of layer by layer coatings by physical adsorption in which the drug coated is released rapidly into blood with decreasing drug efficacy.

Herein we present incorporation of several monomers containing a vinyl group onto the carbon 2’ of water soluble paclitaxel prodrug (PP7). The incorporation of the monomeric units has been successfully carried out and the analogues synthesized were characterized. And then, we have developed an electrochemically initiated in-situ polymerization of a drug directly on-to the surface of the stent.

2. EXPERIMENTAL

For purification of the water-soluble paclitaxel prodrug (PP7) analogues synthesized, preparative HPLC measurements (Waters Delta Prep 4000, Waters 2478 Dual λ absorbance detector) were performed, using an Xterra® RP C8 column (7 μm, 19×300 mm, Waters Co.), under gradient conditions with a mixture of solution A (95% acetonitrile-5% water) and solution B(5% acetonitrile-95% water) as the mobile phase. Peak elutions were monitored at 230 nm with the UV detector. To evaluate the finished surfaces, electropolymerized stainless steels were observed under a scanning electron microscope (SEM, Hitechi S-4800). The whole blood from a domestic rabbit was collected in a syringe containing 3.8 % sodium citrate buffer solution. Platelet-rich plasma (PRP) containing 4 x 10^8 cells/mL was prepared by mixing PRP and platelet-poor plasma (PPP) that were obtained by centrifuging the whole blood at 4℃ for 15 min at 1200 and 2000 rpm, respectively. Test samples and the control were incubated in obtained PRP(1 mL) in a shaking water bath (at 37 ℃, 2 h). Each sample was observed with SEM to check platelet adsorption.

3. DISCUSSION

2.1 Synthesis of the water-soluble paclitaxel prodrug analogue

For the electropolymerization, a series of water-souble paclitaxel prodrug (PP7) analogues were synthesized by using several vinyl containing monomers such as acrylic acid (AA), 5-hexenoic acid (HA) and pyrrole propanoic acid (PPA). The incorporation of the monomeric units has been successfully carried out. These compounds synthesized were characterized by FT-NMR and crosschecked by analytical-HPLC. The PP7 analogue, HA-PP7, showed only one peak in the analytical HPLC chromatogram at a retention time of 32 min after purification by prep-HPLC. This confirmed its purity to over 99% (Fig. 1).

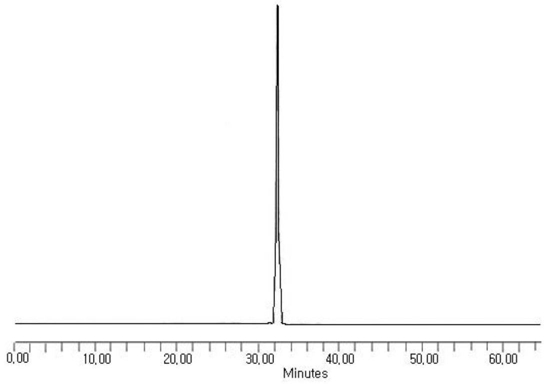

Fig. 1. Analytical-HPLC chromatogram of 2'-hexenoic carbonyl-PP7 (HA-PP7) after prep-HPLC.

2.2 SEM analysis

Finally we have tried the electropolymerization of polymer-modified paclitaxel prodrugs for practical application. The electropolymerization for the prodrug was conducted and optimized in order to determine the polymerization parameters such as concentrations of monomers and electrolytes, electrical current density, reaction time and shape of stainless-steel or other implant-materials. The Fig. 2 shows scanning electron microscopy (SEM) images of electro-polymerized paclitaxel prodrugs on the surface of stainless steel.

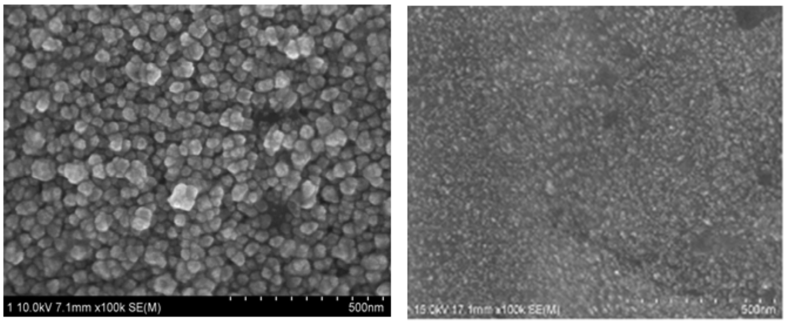

Fig. 2. Electropolymerized paclitaxel prodrug on the surface of stainless steel.

Also, the electropolymerized steels were characterized by test of blood platelet adhesion in vitro. Fig. 3 shows SEM images after blood platelet adhesion tests in vitro. The surface of the bare stainless steel was covered with many platelets, however, a electropolymerized stainless steel with PP7 analogue showed less platelet adhesion. In Fig. 3 (B), only a few platelets were found on the surface of the treated steel. The electropolymerized steels showed effectively reduced blood platelet adhesion .

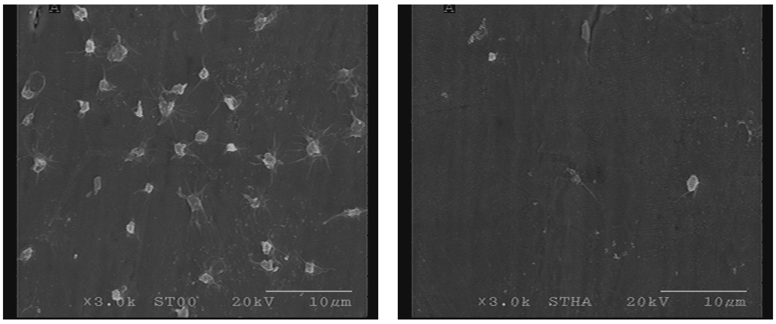

(A) (B)

Fig. 3. Platelet adhesion of (A) a bare stainless steel and (B) a electropolymerized stainless steel with PP7 analogue (x3.0K).

3. CONCLUSIONS

A series of water-soluble paclitaxel prodrug (PP7) analogues with several monomers containing a vinyl group were designed, successfully synthesized, and characterized. These PP7 analogues synthesized were polymerized directly on-to the surface of a stainless-steel by an electrochemical polymerization. And it was conducted and optimized in order to determine the polymerization parameters. The present study reports on the investigation of the surface properties of electropolymerized steels.

ACKNOWLEDGMENT

This work was supported by the Korea Research Foundation Grant funded by the Korean Government (MOEHRD, Basic Research Promotion Fund) (KRF-2008-314-D00117).

REFERENCES

HESS, M., WERMECKES, B., DEHNE, S., JO, B.-W., SOHN, J.-S., (2006) Characterization of PEG-modified paclitaxel. *Mat. Res. Innovat.,* 10, 364-375

JO, B.-W., KOLON, (2004) USPAT 6,703,417

JO, B.-W., SOHN, J.-S., HESS, M., CHOI, S.-K., CHOI, J.-K., (2008) Synthesis and anti-cancer efficacy of rapid hydrolysed water-soluble paclitaxel pro-drugs. *J. Biomater. Sci. Polymer Edn.,,* 19, 311-324.

JO, B.-W., HESS, M., WUNDERLICH, S., (2009) Paclitaxel-albumin interaction in view of molecular engineering of polymer-drug conjugates. *Pure Appl. Chem.,* 81, 439-450.

SOHN, J.-S., JO, B.-W., HESS, M., SCHWARK, K., DEHNE, S., ZAHRES, M., (2005) Effects of polymer modification of an anti-cancer drug with poly(ethylene oxide). *Macromol. Symp.,* 225, 31-42.

WANI, M., TAYLORE, H.L., WALL, M.E., COGGON, P., McPhail, A.T., (1971) The isolation and structure of taxol, a novel antileukemic and antitumor agent from *Taxus Brevifolia. J. Am. Chem. Soc.,* 93, 2325-2337.

Fabricación en fibra de carbono de un sistema de fijación externo para la consolidación de fracturas de huesos largos

J. Justo, J.C. Marín, J. Cañas
Grupo de Elasticidad y Resistencia de Materiales
Escuela Técnica Superior de Ingenieros de la Universidad de Sevilla
J.M. García Aznar
Dpto. Ingeniería Mecánica. I3A. Universidad de Zaragoza

RESUMEN

Los materiales compuestos, debido a sus excelentes propiedades mecánicas específicas (entendiendo por específico el valor de la propiedad dividido por su densidad), han permitido el desarrollo de piezas mucho más ligeras para la sustitución de elementos que tradicionalmente se fabricaban con materiales metálicos.

Muchos son los campos que se han visto beneficiados del uso de estos materiales, entre los que cabe contar el de la medicina. En operaciones de consolidación de fracturas óseas, es requerido un sistema de fijación que estabilice la zona afectada adecuadamente, y que actúe de puente mecánico entre los fragmentos óseos. Este sistema es deseable que presente el menor peso posible, ya que el paciente debe soportarlo durante bastante tiempo. Debido a este hecho, los diseños en metal requieren grandes aligeramientos de los espesores, con el consiguiente peligro de poder romperse la pieza (y sin conseguir reducciones de peso que resulten cómodas para el paciente). Con el diseño en material compuesto, pueden obtenerse piezas bastante robustas y que resultan fáciles de llevar y manipular.

En el presente trabajo se describe la metodología y el proceso llevado a cabo para la definición y fabricación del sistema de fijación en fibra de carbono, como una evolución a partir de diseños previos en metal. El proceso comporta la elección de materiales (tipos de preimpregnados), el diseño de útiles de moldeo y conformación de la bolsa de vacío, el curado en autoclave, y el mecanizado final de las piezas. Se detallan en particular las dificultades encontradas en la elaboración del elemento, y las soluciones adoptadas para solventarlas.

1. INTRODUCCIÓN

En la fig. 1 (a) se muestra el montaje del sistema completo, con el tubo de unión de fibra de carbono y los tornillos de apriete.

Para la fabricación de las piezas de sujeción se optó por fabricar una pieza en forma de T de la que se sacarían los distintos trozos (fig. 2 (b)). Debido a la necesidad de realizar orificios en las piezas (tanto para el paso de tornillería como para el paso del tubo de unión) y basándose en las piezas metálicas originales, se optó por asumir un espesor de 14 mm necesitándose para ello apilar 64 capas siguiendo el esquema de la fig. 2 (a). Como se observa, se han realizado dos apilados en L confrontados y se les ha superpuesto un apilado plano, introduciendo un macillo de fibra unidireccional en la unión de las tres partes.

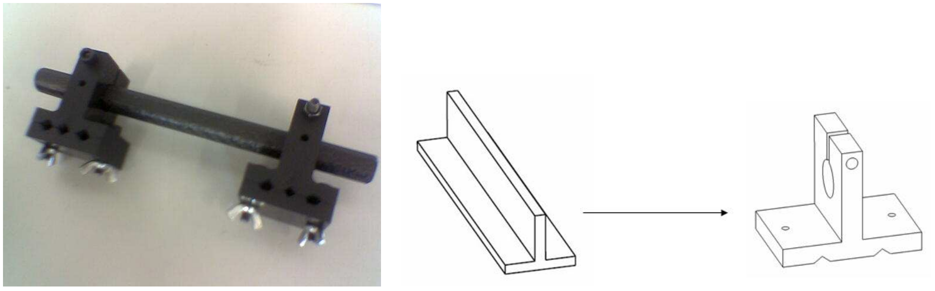

Fig. 1. (a) Montaje del sistema completo. (b) Esquema de producción de las piezas.

El material seleccionado para las láminas es un tejido Hexply M26T/50%/AGCP193T2 (Hexcel Composites 2007) y el proceso de fabricación elegido ha sido compactación con bolsa de vacío y curado en autoclave.

2. APILADO, CONFORMADO Y COMPACTACIÓN DE LAS LÁMINAS

Para el conformado de las láminas en L se utilizaron dos prismas de aluminio (fig. 2 (b)). Antes del apilado se colocó una lámina de teflón a modo de desmoldeante. Una vez se apilaron dichas láminas, se unieron los prismas, usándose a tal efecto presillas metálicas. Para que la unión permanezca así durante el curado, se utilizaron tornillos en los extremos de los prismas antes de retirar las presillas. En principio puede parecer que la contracción debida al curado puede ocasionar que el apriete de los cilindros deje de ser efectivo durante el proceso de polimerización, pero el sobreapriete de los tornillos y la presión externa aplicada consiguen paliar este efecto y la pieza obtenida no tendrá problemas de compactación.

Una vez apretados los prismas se procede a colocar el macillo de fibra unidireccional en la unión de las piezas en forma de L para que las láminas superiores no se vean afectadas de la falta de material en ese lugar. La elección del tamaño del macillo se ha realizado en base a la experiencia en piezas de estructura similar. Una vez colocado el macillo se procede a apilar las láminas superiores. El apilado se realiza según Justo (2007).

Para el apilado de todas las láminas se utilizó un sistema de calefacción y una espátula de teflón para conseguir las formas deseadas y una correcta eliminación del aire ocluido entre las láminas y, por ende, una buena compactación.

Tras el apilado de las láminas se colocan tiras de corcho de modo alrededor del laminado para mantener la forma de la pieza evitando que la resina escape una vez se vuelva fluida (fig. 3 (a)).

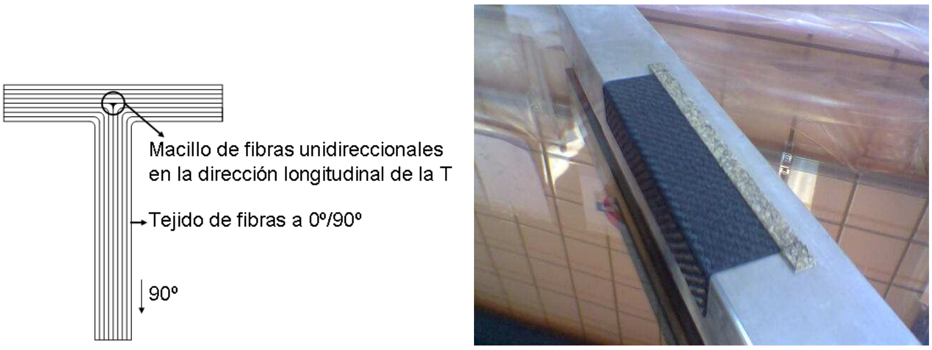

Fig. 2. (a) Esquema del apilado (b) Apilado de las láminas sobre el útil prismático.

Fig. 3. (a) Cierre con corcho del perímetro de la pieza (b) Bolsa de vacío.

3. CIERRE DE LA BOLSA DE VACÍO, CURADO EN AUTOCLAVE Y MECANIZADO FINAL DE LA PIEZA

Antes de proceder al cierre de la bolsa de vacío hay que tener en cuenta las zonas del montaje más susceptibles de rotura de la bolsa. Éstas son las zonas de separación entre los útiles prismáticos. La presión y el vacío podrían ocasionar un intento de penetración de la bolsa por estos orificios y la consiguiente rotura de la misma. Para solucionar esta fuente de fallo se procedió a sellar la zona de unión con cinta resistente a las altas temperaturas, de forma que se protegiera durante todo el proceso de curado.

Una vez protegido el montaje se procede al cierre de la bolsa según Justo (2007). En primer lugar, se coloca teflón sobre la pieza de forma que la proteja. A continuación se sitúan dos termopares, uno sobre la pieza y otro sobre el útil, de modo que se puedan seguir las temperaturas a lo largo del proceso de polimerización. Se cubren la pieza y los termopares con tejido "Airweave®" y se rebordean con cinta de vidrio, de modo que el vacío se pueda extender uniformemente dentro de la bolsa. Se sitúan dos almohadillas de tela de vidrio en uno de los extremos y, sobre estas, la parte inferior de las tomas de vacío. En la periferia del conjunto se hace un rectángulo de cromato y sobre el mismo se cierra la bolsa con plástico de cierre. Debido a la altura del útil, es necesario hacer dobleces en la bolsa (sellándolas con pinzas de cromato) para evitar que quede muy tensionada y se rompa al hacer el vacío. Una vez cerrada la bolsa se ajusta la parte superior de las tomas de vacío y se succiona (fig. 3 (b)). Debe comprobarse que se experimentan pérdidas de vacío inferiores a 0.17 bares/minuto.

Tras hacer el vacío se introduce la bolsa en el autoclave. Aquí se polimerizará la resina a través de un ciclo de curado, en el que se aplica temperatura, presión y vacío. Las condiciones para este material son: temperatura de 120ºC durante dos horas con una rampas de calentamiento y enfriamiento de 2 ºC/min, presión de 3.5 bares y vacío de -0.75 bares.

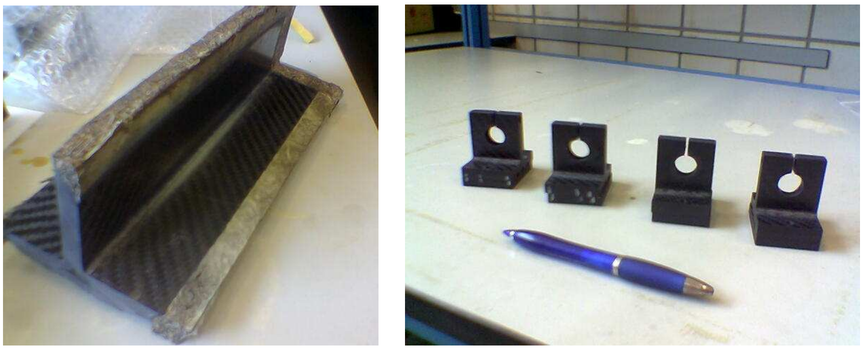

Fig. 4. (a) Vista de la T una vez curada. (b) Vista de las piezas mecanizadas.

Al finalizar el ciclo se extrae la pieza (fig. 4 (a)), que habrá que mecanizar para obtener las piezas de fijación. El corte de las distintas piezas se hace con sierra de disco de diamante, mientras que los taladros se realizan con escariador (fig. 4 (b)).

4. CONCLUSIONES

Se han fabricado piezas de un sistema de fijación de huesos en fibra de carbono. En el trabajo se han descrito tanto el material y el apilado considerados más apropiados para estas piezas como el proceso de fabricación utilizado. A su vez se han comentado los problemas que han aparecido durante la fabricación y la manera de solventarlos.

AGRADECIMIENTOS

Este proyecto se ha realizado con la financiación del Proyecto DPI2006-09692.

REFERENCIAS

JUSTO, J. (2007) Puesta en marcha, calibración y certificación de un sistema de fabricación, y aplicación a la fabricación de piezas de material compuesto. *Proyecto Fin de Carrera*. Universidad de Sevilla.

Hexcel Composites (2007) HexPly M26/M26T Product Data. www.hexcel.com. FTA 125a.

Simulación no-isotérmica de la infusión de resina polimérica termoestable en procesos productivos con bolsa de vacío

M. Gascons, N. Blanco
Advanced Materials and Analysis for Structural Design, Escola Politècnica Superior,
University of Girona, Campus Montilivi s/n, E-17071 Girona, Spain
K. Matthys
School of Engineering and Design, Brunel University, Kingston Lane, Uxbridge,
Middlesex, UB83PH, UK

RESUMEN

La proliferación de los materiales compuestos de matriz polimérica en nuevos mercados y aplicaciones ha permitido el desarrollo de elementos con mayores grosores. Dadas las dimensiones de estas piezas, es habitual su fabricación mediante procesos de infusión de resina con bolsa de vacío fuera de autoclave, habiendo en este proceso ciertas peculiaridades en la disipación de la temperatura. El uso de una fuente de calor para reducir la viscosidad de la resina y el tiempo de infusión es una práctica frecuente de estos procesos y, junto al curado, son la causa de una distribución no homogénea de temperaturas en la pieza. El presente trabajo muestra el desarrollo de una estrategia de simulación basada en el software LIMS^{TM}, del Center for Composite Materials de la University of Delaware, para poder obtener el perfil de temperaturas que generan estos procesos. La estrategia consiste en la definición de un perfil tridimensional y su posterior implementación en subrutinas de usuario para obtener la evolución de la temperatura a lo largo del tiempo de infusión, que será usada posteriormente para determinar sus efectos en las cualidades mecánicas de la pieza.

1. INTRODUCCIÓN

La producción de piezas de material compuesto de matriz polimérica termoestable es una técnica en auge debido a la excelente relación entre peso y propiedades mecánicas, motivo por lo que cada vez son más presentes en aplicaciones aeroespaciales, aeronáuticas y marinas, así como en otros muy diversos sectores industriales.

Debido a la mejora en la predicción y simulación de su comportamiento, dichas piezas están adquiriendo cada vez más responsabilidad dentro de las estructuras, por lo que cada vez se producen piezas más gruesas y de mayor tamaño, creando nuevos retos para su diseño y cálculo, tanto por su proceso productivo, su comportamiento en servicio y las posibles interacciones entre ambos.

La tendencia industrial en la producción de grandes estructuras de material compuesto apunta a las técnicas de bolsa de vacío como la principal metodología de fabricación, ya que reducen de forma significativa el coste en moldes de las tecnologías tipo RTM y a la vez puede evitar el proceso de curado en autoclave. Para la fabricación mediante esta técnica, la introducción de una fuente de calor mediante el molde o la resina es una práctica frecuente para conseguir disminuir la viscosidad de la resina, mejorando su difusión, pero generando una distribución de temperaturas que pueden afectar a las propiedades finales del material. Existen programas comerciales para la simulación del proceso de inyección de resina en este tipo de aplicaciones, los cuales presentan ciertas limitaciones para la consideración del gradiente de temperatura en el grosor de la pieza, sobretodo para elementos de grosor elevado.

2. DESCRIPCIÓN DE LA ESTRATEGIA DE SIMULACIÓN

Con la finalidad de obtener la distribución de temperaturas a lo largo del proceso de infusión, se han desarrollado subrutinas de usuario sobre el módulo térmico del software LIMS^{TM}, descrito por Simacek et Advani, (2004, 2005).

Dicho módulo es capaz de obtener la temperatura en geometrías 2D durante el proceso de infusión. El código resuelve la distribución de calor en el plano mediante una combinación de las técnicas de elementos y volúmenes finitos y de balances de energía. Para que el proceso evolucione, es necesaria la especificación de condiciones iniciales como son la temperatura de la resina y la preforma (tejido seco), así como la conductividad y difusividad de ambas. La dependencia de la viscosidad con la temperatura se introduce mediante la ecuación de Arrhenius, y la cinética de curado mediante un modelo representativo de la ecuación de Kamal-Sourur, ambos descritos en Halley et Mackay, (1996). El resultado que se puede obtener son las temperaturas en el plano medio y ambos lados del molde para un mallado bidimensional.

A diferencia de los sistemas de producción en molde cerrado, el uso de sistemas con bolsa de vacío implica una asimetría en las condiciones de contorno térmicas del sistema, ya que la transmisión de calor por el lado del molde rígido será de tipo conductivo mientras que la bolsa disipará por convección. Dicha asimetría tiene un efecto notable en la generación de tensiones residuales provocadas por efectos térmicos, por lo que la simulación 2D que ofrece el código LIMS^{TM} es insuficiente y justifica la necesidad de evolucionar a un sistema de predicción de temperaturas tridimensional, sobretodo para piezas de espesores elevados.

Dicha información es usada para crear una extrusión de la pieza y generar la distribución de temperaturas suponiendo una distribución parabólica a lo largo del grosor de la pieza como se sugiere en Simacek et Advani (2003) y Deleglisè et al. (2007).

En las subrutinas desarrolladas, las ecuaciones (1) a (3) se usan para obtener la temperatura en cada punto de cálculo de la geometría tridimensional generada a partir de la malla bidimensional, describiendo la evolución de la temperatura de cada punto (T(z,x,y,t)) en función de su posición y el instante de tiempo considerado. Para obtenerla, se usa la interacción de dos perfiles complementarios $T_1(z)$ i $T_2(z)$ que describen la temperatura según la influencia de uno de los moldes a lo largo del grosor del laminado, siendo *h* el grosor total, *z* la posición dentro de éste grosor i T_M la temperatura en el plano medio del laminado.

$$T(z;x,y,t) = T_1(z)\cdot T_M(x,y,t) + T_2(z) \tag{1}$$

$$T_1(z) = 4\frac{z\cdot(h-z)}{h^2} \tag{2}$$

$$T_2(z) = 2\cdot T_{(h=0)}\frac{(h-z)(h/2-z)}{h^2} + 2\cdot T_{(h=h)}\frac{(h-z)(h/2-z)}{h^2} \tag{3}$$

3. RESULTADOS

La figura 1 muestra los resultados obtenidos para un caso tipo de aplicación de las subrutinas creadas, donde resina epóxica es introducida a temperatura ambiente en una preforma de fibra de vidrio situada sobre un molde calefactado, con bolsa de vacío.

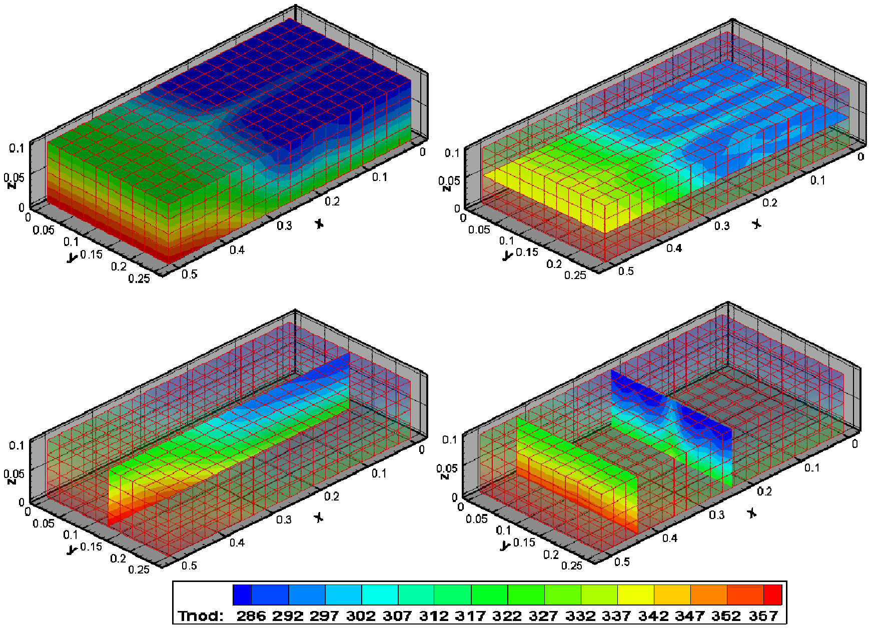

Fig. 1. Distribución de temperatura durante la infusión no-isoterma de resina. Infusión de izquierda a derecha, escala en Kelvin.

La difusión de la temperatura provocada por la entrada de resina puede ser observada, al igual que la influencia de la temperatura que introduce al sistema el molde calefactado a través de la parte inferior. La subrutina tiene la capacidad de determinar la influencia de la no homogeneidad de la difusión de temperatura en el plano medio del laminado hacia los bordes del mismo, pudiendo determinar como evoluciona el perfil en los distintos puntos del laminado. Los resultados permiten detectar el peligro de sobrecalentamiento de puntos centrales debido al inicio de la reacción de curado, así como el gradiente de temperaturas en el momento de iniciar el proceso de curado.

4. CONCLUSIONES

Se ha obtenido una herramienta de simulación capaz de reproducir el perfil de temperaturas generado a lo largo de la infusión en un proceso de producción mediante bolsa de vacío. Los resultados muestran razonable parecido con el trabajo experimental realizado, que será objeto de una comunicación futura. De esta forma, se confirma la necesidad de la obtención de un perfil 3D de temperaturas durante el proceso de inyección y curado de elementos de material compuesto con grosor elevado para la correcta predicción de la geometría final y sus respectivas tolerancias dimensionales.

AGRADECIMIENTOS

Los autores desean agradecer la colaboración del Center for Composite Materials de la University of Delaware y al proyecto CICYT MAT2006-14159-C02-01.

5. REFERENCIAS

Simacek, P and Advani, S. G. (2004) Desiderable features in mould filling simulations for liquid moulding processes. *Polymer Composites*, 24(-):355–367.
Simacek, P and Advani, S. G. (2005) Simulation three-dimensional flow in compression resin transfer moulding process. *Rev Eur Elements Finis*, 14(6-7):777–802,.
Halley, P. J. and Mackay, M. E. (1996) Chemorheology of Thermosets-An overview. Polymer Engineering and science, mid-march, Vol.36, No. 5
Simacek, P and Advani, S. G. and BINETRUY C. (2004) Liquid injection moulding simulation (lims) a comprehensive tool to design, optimize and control the filling process in liquid composite moulding. *JEC Composite*, 8(-):58–61,
Simacek, P and Advani, S. G. (2003) "Approximate Numerical method for Prediction of Temperature Distribution in Flow through Narrow Gaps containing Porous Media,", *Computational Mechanics*, Volume 32, pp, 1-9.
Deléglise M., Binétruy, C., Castaing, P. Krawczak P.,(2007) Use of non local equilibrium theory to predict transient temperature during non-isothermal resin flow in a fibrous medium *International Journal of Heat and Mass Transfer*, Volume 50, Issues 11-12, June, Pages 2317-2324.

Caracterización geométrica y mecánica del proceso de impresión tridimensional

O. Olvera, S. Gasca, C. Signoret, J.L. Ortíz
Centro de Investigación en Diseño, Manufactura y Automatización, Instituto
Tecnológico y de Estudios Superiores de Monterrey, Campus Querétaro, México

RESUMEN

El proceso de impresión tridimensional (3DP) es uno de los más populares en el mundo del prototipado rápido (RP), con gran potencial para diversas aplicaciones. Aún cuando se han realizado algunos estudios sobre este proceso, todavía existe una gran carencia de información acerca del comportamiento geométrico y mecánico de las partes fabricadas por el mismo, lo cual limita su aplicación en áreas tales como herramentales rápidos (rapid tooling, RT) y/o manufactura rápida (rapid manufacturing, RM). El objetivo de este estudio es obtener información sobre el comportamiento geométrico y mecánico del proceso de impresión tridimensional. La evaluación se realizó a través de la medición de tolerancias geométricas y la resistencia a la compresión. Para evaluación geométrica se diseñaron probetas especiales, mientras que para la evaluación de propiedades macánicas se emplearon probetas estandarizadas. Se puede concluir que la orientación de construcción afecta tanto las propiedades geométricas como mecánicas. Asimismo, se observa que el método de infiltrado tiene un efecto significativo en la resistencia a la compresión. Como resultado de este estudio se recomienda un método de fabricación que elimine el efecto de las condiciones ambientales y garantice la obtención de probetas repetitivas. También se sugieren varias recomendaciones para el mejor aprovechamiento del proceso de impresión tridimensional.

1. INTRODUCCIÓN

Los sistemas de RP juegan un papel importante en el desarrollo de nuevos productos. Su participación no sólo se limita a la modelación y transmisión de conceptos, sino también al desarrollo de los herramentales necesarios para la fabricación en serie (herramentales rápidos), o a la fabricación de partes reales y funcionales (manufactura rápida). Las principales ventajas de estas dos áreas, con respecto a sus contrapartes tradicionales, son el bajo costo para el desarrollo de los herramentales o prototipos funcionales, así como el corto tiempo de fabricación. Sin embargo para que las tecnologías de prototipado rápido puedan ser empleadas efectivamente en estas aplicaciones, deben cumplir con requerimientos específicos. Es de aquí donde surge la necesidad de conocer el comportamiento de los sistemas de prototipado rápido tanto en lo que respecta a variación dimensional y geométrica, como a propiedades mecánicas.

2. REVISIÓN BIBLIOGRÁFICA

Se han realizado diversos estudios sobre la caracterización de los sistemas de RP, donde el enfoque principal ha sido la comparación dimensional (Grimm, 2004) y geométrica (Mahesh et al. 2004) de diversos procesos: sinterizado selectivo por láser (selective laser sintering, SLS), estéreolitografía (stereolithography, SL), modelado por deposición fundida (fused deposition modeling, FDM) y manufactura laminada de objetos (laminated object manufacturing, LOM). De estos estudios se concluye que es necesaria la caracterización y comparación de los diversos procesos de RP, mediante el empleo de estándares y geometrías comparativas, generando una base de datos que permita la selección apropiada de los procesos de RP.

Dimitrov et al. (2006) evaluó el comportamiento dimensional del proceso de 3DP, al realizar mediciones sobre diferentes longitudes y la influencia de la dirección en construcción en la precisión dimensional. Se encontró que el proceso de 3DP oscila entre los grados IT 9 al 15. También evaluó, aunque de manera limitada el comportamiento geométrico del proceso.

Se han realizado diversos estudios para la caracterización mecánica de los procesos de RP, donde la prueba principal que se realiza es la prueba de tensión (Ahn et al. 2002, Gibson et al. 1997, Chockalingam et al. 2006); dejando en segundo plano a la de compresión (Ahn et al. 2002, Ang et al. 2006). También se evalúa el efecto de la orientación de construcción en las propiedades mecánicas (Ahn et al. 2002, Gibson et al. 1997). Los procesos caracterizados en dichos estudios son: FDM, SL y SLS.

De esta revisión, se puede observar que el proceso de 3DP no ha sido caracterizado en sus propiedades geométricas o mecánicas. Por lo tanto, es necesaria la realización de estudios que cubran estas áreas, cuyos resultados permitan nuevas aplicaciones de este proceso en la industria.

3. EXPERIMENTACIÓN

Para la construcción de todas las probetas, se empleó una impresora Z310 de ZCorporation, utilizando polvo zp102 y aglutinante zb56; en todos los casos se fabricaron con un espesor de capa de 0.125 mm y fueron infiltradas con resina Z-Max. La Figura 1 muestra las direcciones de construcción, donde el eje Y indica la dirección de movimiento de la boquilla que deposita el aglutinante. El eje X, representa la dirección de movimiento del mecanismo que soporta la boquilla de aglutinante.

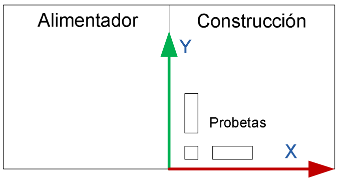

Fig. 1. Direcciones de construcción de las probetas de compresión.

Para la evaluación de las tolerancias geométricas, se fabricaron probetas empleando las recomendaciones dadas por la norma ASME Y14.5M-1994 para la evaluación de las tolerancias de forma y de orientación, Figura 2. El número de mediciones varía entre 1 y 4, dependiendo de la tolerancia geométrica. Todas las mediciones se realizaron en una máquina de medición por coordenadas.

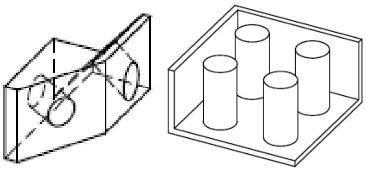

Fig. 2. **Probetas empleadas en la caracterización geométrica.**

Respecto a las propiedades mecánicas, se decidió evaluar la resistencia a la compresión, ya que como lo menciona Dimitrov et al. (2006), las diversas aplicaciones que se pueden tener para partes construidas por el proceso 3DP, están sujetas a esfuerzos de compresión (patrones para moldes, diseño y fabricación de herramentales, directa o indirectamente). Para ello se construyeron probetas prismáticas de base cuadrada, de dimensiones 12.7x12.7x25.4 mm, de acuerdo a la norma ASTM D695-02^{a}. Para evaluar el efecto del método de infiltrado se consideraron dos métodos: infiltrado por inmersión e infiltrado al vacío (10 probetas). Una segunda prueba, evalúa el efecto que tiene la orientación de construcción en las probetas en la resistencia a la compresión (15 probetas). La resistencia a la compresión fue medida en una máquina universal.

Durante la experimentación, se observó que las condiciones ambientales, particularmente la humedad relativa, tenían un efecto significativo en la preparación de las probetas, por lo que se estableció un proceso de fabricación que permita la obtención de probetas repetibles. El proceso establece que todas las probetas "en verde", fabricadas de acuerdo con el procedimiento establecido por Z-Corp, deben ser secadas en horno durante 2 horas y a una temperatura de 100 °C. Al finalizar el secado, las probetas deberán ser infiltradas por el método seleccionado: con brocha, por inmersión o al vacío.

4. RESULTADOS

En las Tablas 1 y 2 se muestran los resultados obtenidos de los estudios realizados sobre las tolerancias geométricas y la resistencia a la compresión, respectivamente.

Efecto de la orientación en las propiedades geométricas										
Tolerancia	Variante	Orientación / Promedio[mm]								
		Plano XY	Plano YZ	Plano XZ	Eje X	Eje Y	Eje Z	Planos XY-YZ	Planos XY-XZ	Planos YZ-XZ
Linealidad					0.140	0.062	0.127			
Planicidad		0.246	0.240	0.264						
Redondez		0.168	0.417	0.323						
Cilindricidad					0.290	0.202	0.237			
Paralelismo	Superficial	0.192	0.254	0.200						
	Axial				0.764	0.244	0.290			
Perpendicularidad	Superficial							0.212	0.213	0.186
	Superficie-Eje	0.259	0.491	0.625						
Angularidad	Superficial	0.107	0.192	0.299						
	Superficie-Eje	0.037	0.004	0.057						

Tabla 1. Efecto de la orientación de construcción en las propiedades geométricas.

Resistencia a la compresión [MPa]			
Dirección Infiltrado	Eje X	Eje Y	Eje Z
Inmersión	7.5	---	---
Vacío	20.1	16.7	14.6

Tabla 2. Resistencia a la compresión.

5. CONCLUSIONES Y RECOMENDACIONES

Los resultados obtenidos muestran que la dirección de construcción afecta al comportamiento geométrico y la resistencia a la compresión. Es posible que las desviaciones obtenidas en las tolerancias geométricas puedan ser compensadas mediante modificaciones a las dimensiones del diseño; así como con la generación de geometrías de soporte. También se observó que la resistencia a la compresión disminuye en un 28% aproximadamente, dependiendo de la orientación. Se puede concluir que el método de infiltrado ejerce una gran influencia en la resistencia a la compresión. Con el infiltrado al vacío, se obtiene una resistencia 2.7 veces mayor a la obtenida con el infiltrado por inmersión. Como resultado de este estudio, se recomienda un método de fabricación que elimine el efecto de las condiciones ambientales y garantice la obtención de probetas repetitivas. También se proponen varias recomendaciones para el mejor aprovechamiento del proceso de impresión tridimensional.

REFERENCIAS

AHN, SUNG-HOON, et al. (2002) Anisotropic material properties of fused deposition modeling ABS, *Rapid Prototyping Journal*, 248-257.

ANG, KER CHIN, et al. (2006) Investigation of the mechanical properties and porosity relationships in fused deposition modelling-fabricated porous structures, *Rapid Prototyping Journal*, 100-105.

CHOCKALINGAM, K., et al. (2006) Influence of layer thickness on mechanical properties in stereolithography, *Rapid Prototyping Journal,* 106-113.

DIMITROV, D., et al. (2006) Investigating the achievable accuracy of three dimensional printing, *Rapid Prototyping Journal*, 42-52

GIBSON, IAN, et al. (1997) Material properties and fabrication parameters in selective laser sintering process, *Rapid Prototyping Journal*, 129-136

GRIMM, TODD (2004) Comparing Technologies: Stereolithography, Selective Laser Sintering, Fused Deposition Modeling and Powder-Binder Printing *en Rapid Prototyping & Manufacturing Conference, Dearborn, Michigan,* TP04PUB194.

MAHESH, M., et al. (2004) Benchmarking for comparative evaluation of RP systems and processes, *Rapid Prototyping Journal*, 123-135.

Influencia de la geometría del molde en la permeabilidad flexible de refuerzos y núcleos en los procesos de infusión de resina

E. Díaz[1], J.A. García[2], C. Sanz[1]
[1]AIMPLAS, Avda. Gustave Eiffel, 4, 46980, Paterna, Valencia
[2]Universidad Politécnica de Valencia, Camino Vera s/n, 46022, Valencia
ediaz@aimplas.es, jugarcia@mcm.upv.es, csanz@aimplas.es

RESUMEN

Los procesos de transferencia de resina cobran cada día mayor importancia en la industria de transformación de los materiales compuestos. En concreto, los procesos de infusión, en los que la resina impregna el refuerzo gracias a un gradiente de presiones provocado por la realización del vacío parcial en la cavidad del molde, han encontrado una gran aplicación en la fabricación de piezas de composite de gran tamaño, tales como palas de aerogeneradores y cascos de barco. En este tipo de procesos, la obtención de un prototipo virtual previo a la fabricación del molde permite optimizar el diseño del mismo sin incurrir en gravosos costes de modificaciones posteriores. En el presente trabajo se detalla el diseño y la puesta a punto de un método de caracterización de permeabilidad para refuerzos y núcleos empleados generalmente en el proceso de infusión de resinas que presenta ciertas ventajas sobre los métodos existentes. Por un lado, la permeabilidad se determina en condiciones similares a las del propio proceso de infusión, obteniendo de esta manera una pseudo-permeabilidad o *permeabilidad flexible* que permite el empleo de los modelos tradicionales de simulación mediante elementos finitos sin tener que incorporar como variable el cambio de sección de la cavidad con el tiempo. Por otro lado, el dispositivo experimental permite la determinación de la permeabilidad flexible para diferentes radios de curvatura del molde, lo que permite incluir el efecto de dicha deformación en el propio valor de la permeabilidad flexible. Por último, en el presente trabajo se llevan a cabo diversas simulaciones que permiten comparar los resultados obtenidos mediante una caracterización de permeabilidad convencional y la realizada con el método experimental propuesto.

Implementación numérica de un modelo de curado de resinas

J. Justo[1], E. Graciani[1], F. París[1], R. Avila[2]
[1]Grupo de Elasticidad y Resistencia de Materiales
Escuela Técnica Superior de Ingenieros de la Universidad de Sevilla
c/ Camino de los Descubrimientos, s/n. 41092 Sevilla, España
[2]Composite Technology (EDSWCM) Materials and Processes Airbus Spain.
Pº. John Lennon s/n 28906 Getafe, España

RESUMEN

Se ha implementado un modelo de curado de una resina HEXCEL 8552 en un programa comercial de Elementos Finitos. Para ello se ha empleado un modelo cinético previamente ajustado experimentalmente por Airbus y se ha acoplado con un modelo térmico.

A partir de las medidas experimentales del grado de curado, α, medido como el consumo de grupos epoxi durante la reacción de polimerización frente al número inicial de grupos epoxi presentes en la resina, se ha obtenido el comportamiento de la derivada del grado de curado respecto del tiempo en función del grado de curado y de la temperatura.

Por tanto, el acoplamiento entre el modelo térmico y el modelo cinético permite determinar la evolución del grado de curado, en conjunción con la variación de la temperatura en el componente a lo largo del proceso de curado, mediante un análisis no-lineal con el Método de los Elementos Finitos.

In-situ process monitoring and reliable cure control applied in RTM production of epoxy/carbon fibre parts

A.G. Mamalis, N. Pantelelis, K. Spentzas
National Technical University of Athens
N. Efentakis
Technika Plastika

SUMMARY

An innovative PC-based monitoring system (Synthesites, Greece) has been used for the real-time sensing of composite manufacturing processes. The system comprises an optimised durable non-intrusive electrical and temperature sensor, an electronic sensing system and the appropriate software for data acquisition and control running in a PC. The sensors have been designed for the sensing of the complete process i.e. resin arrival detection, viscosity changes as well as material transformation up to the end-of-cure. The sensors' feedback is recorded and processed by the sensing system providing real-time material state information (viscosity, degree of cure etc.). Furthermore based on the monitoring feedback a control algorithm decides when to terminate the curing of each part leading to shorter and more reliable production.

This monitoring system and sensors have been installed at Technica Plastika and successfully used for the first time in the production of epoxy/ carbon fibre parts using closed mould injection (RTM). The resin injection takes place at 50°C with injection pressure that reaches 12 bars. After the end of filling the mould is heated to 100°C and remains there for a specific time to ensure fully cured part.

To ensure part quality and optimal cure time sensors have been installed near the injection and venting gates so real-time information of the resin state in the mould cavity during injection and curing is monitored and used for the quality and process control of the production. After the initial trials of the system a 30% reduction of the curing time has been attained while the monitoring system helped in better overall fine tuning of the production.

Fabricación, caracterización y modelización de paneles sandwich compuestos por cores de espumas de polietileno y pieles de aluminio

P. Alvarez, A. Echeverría, M.M. Petite
Asociación Centro de Investigación en Tecnologías de Unión LORTEK, Bº La Granja s/n, 20240 Ordizia, Spain
M.A. Rodríguez-Pérez, J. Pinto, S. Estravis
Laboratorio de Materiales Celulares (CellMat), Departamento de Física de la Materia Condensada, Facultad de Ciencias, Universidad de Valladolid, 47011 Valladolid, Spain
M.A. Martínez, J. Abenojar
Grupo de Comportamiento en servicio de Materiales. Dpto. C. e Ing. de Materiales e Ing. Química. Universidad Carlos III de Madrid, Spain

RESUMEN

Los paneles sándwich compuestos por núcleos (cores) de espumas poliméricas y pieles metálicas son materiales estructurales de amplio uso en diversas industrias (aeronáutica, ferroviaria, eólica, construcción) en las que es necesario el aligeramiento de estructuras resistentes. Estos materiales compuestos presentan además unas buenas propiedades de aislamiento térmico y acústico y una alta capacidad de absorción de energía a impacto. El desarrollo de estos materiales requiere de estudios que combinen diversos aspectos de la ciencia de materiales como son la fabricación de los cores espumados, la adhesión a las láminas metálicas externas y la caracterización y modelización de su comportamiento mecánico, térmico y acústico. En este trabajo se ha trabajado en paralelo en la mejora integral de los procesos de fabricación (espumado y adhesivado) y en el desarrollo de herramientas de modelización multiescala que predigan el comportamiento mecánico de estos materiales y puedan ser utilizadas en la optimización de las prestaciones y en la mejora del diseño conceptual de estos componentes. A partir de este estudio combinado se ha concluido que la mejora de la adhesión espuma-piel y la consideración del efecto de la presión hidrostática en la descripción de la espuma resultan vitales para mejorar el comportamiento y compresión de estos materiales.

1. FABRICACIÓN DE LOS NÚCLEOS CELULARES DE LDPE

Se han fabricado bloques circulares de espuma polimérica de polietileno de baja densidad (LDPE) de celda cerrada para ser utilizados como núcleos de la estructura sándwich. El espumado se llevó a cabo en un molde con forma de disco de dimensiones 150 mm de diámetro y 8 mm de espesor. La formulación empleada ha consistido en granza de LDPE, azodicarbonamida como agente espumante, peróxido de dicumilo como agente reticulante, óxido de zinc como catalizador y ácido esteárico como ayudante del proceso (Rodríguez-Pérez et al. 2005, Eaves 2004). El espumado se produjo en horno a una temperatura de 180ºC.

La densidad final de las espumas se controló ajustando la cantidad de material introducido inicialmente en el molde. La densidad final de las espumas fabricadas ascendió a 200 Kg/m^3 aproximadamente, esto es, una densidad relativa de 0.22. Las espumas fabricadas se cortaron en tiras de 80 x 20 mm y se procedió a su unión a las láminas de aluminio A2024 de 1.26 mm de espesor.

Fig. 1. Preparación de los cores de LDPE para la fabricación de paneles sándwich.

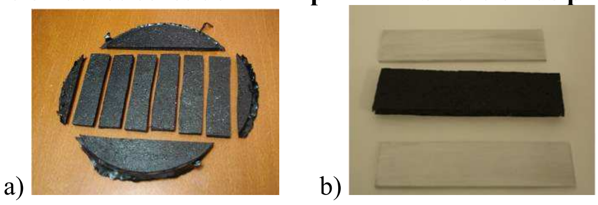

a) b)

2. ADHESIÓN DE LOS NÚCLEOS CELULARES A LAS PIELES METÁLICAS

Para la adhesión de los núcleos de espuma polimérica a las pieles de aluminio se seleccionó un adhesivo elástico de base poliuretano monocomponente (Sikaflex® 252.). Para mejorar la adhesión núcleo-piel se prepararon adecuadamente la superficie de las láminas de aluminio mediante lijado y limpieza con MEK y de las espumas mediante tratamiento con plasma atmosférico.

El tratamiento con plasma atmosférico activa la superficie del polímero sin llegar a degradarla o quemarla dado que la temperatura de la boquilla no supera los 40ºC. El efecto del tratamiento de plasma atmosférico sobre el polímero puede valorarse determinando la energía superficial mediante la medición de los ángulos de contacto con varios líquidos de tensiones superficiales conocidas y aplicando el modelo de OWKR (Zhang et al. 2009). Este modelo permite determinar las componentes dispersiva y polar de la energía superficial y está especialmente recomendado para superficies poliméricas. En la fig. 2b se observa que tras el tratamiento con plasma atmosférico se produce un aumento muy importante de la energía superficial de las piezas al pasar de 23 mN/m a 63 mN/m. Este aumento es debido al aumento de la componente de energía polar (generación de grupos funcionales polares) y su efecto se mantiene hasta al menos 750 h después de aplicar el tratamiento.

Fig. 2. a) Equipo para determinar ángulos de contacto y b) variación de la energía superficial en la espuma de LDPE tras el tratamiento de plasma atmosférico.

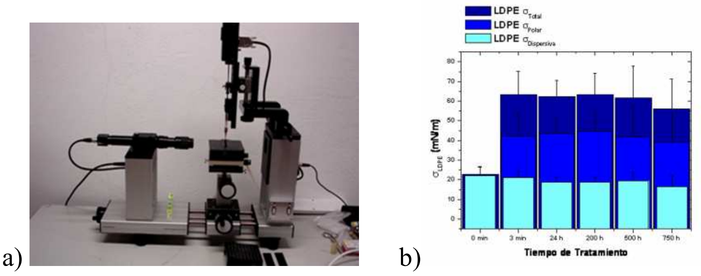

a) b)

3. CARACTERIZACIÓN DE LOS PANELES SÁNDWICH FABRICADOS

Los paneles sándwich fabricados se caracterizaron realizando ensayos de flexión en tres puntos (64 mm de distancia entre apoyos). La fig. 3b muestra la curva carga-desplazamiento obtenida en los paneles fabricados a partir de las espumas de LDPE. El fallo se debió a la falta de adhesión core-aluminio para un valor de flecha de 11 mm.

Fig. 3. a) Ensayo de flexión en tres puntos y b) curva carga-desplazamiento de los paneles sándwich fabricados.

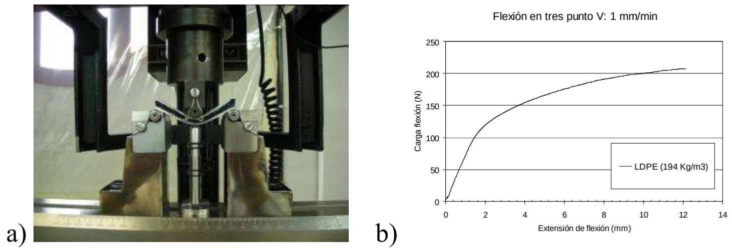

4. MODELIZACIÓN MULTIESCALA DE LOS PANELES SÁNDWICH

Para predecir el comportamiento a flexión y el modo de fallo de los paneles fabricados, se han realizado ensayos de modelización por elementos finitos (FEM). A las espumas poliméricas se les ha aplicado un modelo de comportamiento macroscópico equivalente del tipo CRUSHABLE FOAM que describe una superficie de colapso elíptica en el plano tensión de Mises – presión hidrostática. Dicho comportamiento se verificó y calibró por medio de un proceso de homogenización FEM consistente en la realización de ensayos multiaxiales virtuales con unidades microscópicas representativas (RVE) (fig. 4a) (Alvarez et al. 2009). El desarrollo de esta metodología de modelización multiescala ha permitido calibrar el comportamiento de una espuma con una densidad dada sin necesidad de realizar físicamente los ensayos mecánicos mínimos necesarios (compresión uniaxial y compresión multiaxial) (fig 4b).

Fig. 4. a) Unidad virtual RVE utilizada para el proceso de homogenización FEM y b) superficie de colapso determinada para dos espumas de LDPE (densidades relativas 0.22 y 0.69).

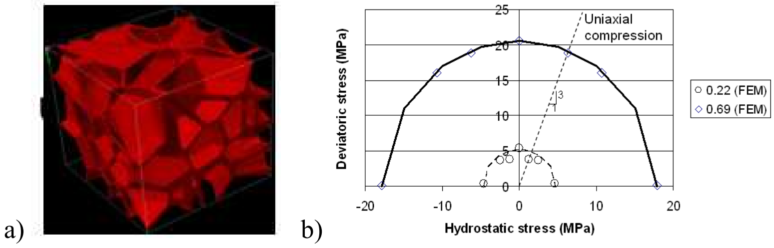

La asignación del comportamiento CRUSHABLE FOAM es esencial para predecir el comportamiento de espumas ante solicitaciones multiaxiales. Debido a la naturaleza celular de estos materiales, la presión hidrostática del interior de las celdas genera un colapso (plastificación) prematuro en comparación con el criterio de Mises independiente de esta presión y que se emplea con materiales totalmente densos. Este efecto es mucho más acusado en las solicitaciones a tracción y para su estudio debe considerarse el efecto de la presión del gas en el interior de las celdas. (Alvarez et al. 2009).

A partir de la simulación macroscópica del ensayo de flexión en tres puntos, se puede visualizar y predecir correctamente el modelo de fallo del panel, la distribución de tensiones y deformaciones y la geometría final del panel (fig. 5). Tal y como se muestra en la fig. 5b, le deformación plástica a cortadura se concentra en la intercara inferior espuma-aluminio (sometida a tracción) y constituye la causa de fallo de este panel, tal y como se corroboró en los ensayos de flexión reales realizados.

Fig. 5. a) Campos de tensiones y b) deformaciones a cortadura (PE12) determinados en la simulación del ensayo de flexión en tres puntos de los paneles.

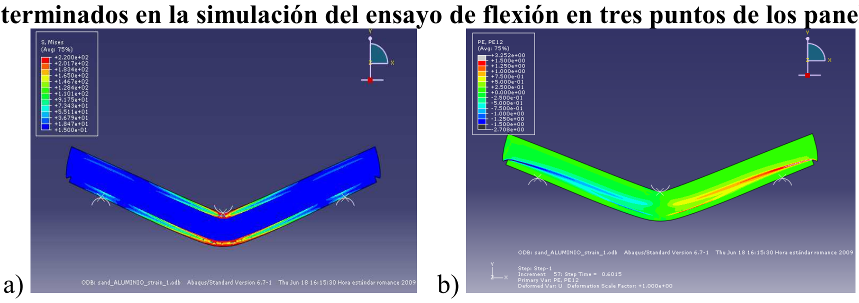

5. CONCLUSIONES

La mejora de las prestaciones de los paneles sándwich compuestos por núcleo de espuma de LDPE y pieles de aluminio pasa por la mejora de la adhesión entre los dos componentes. El objetivo es evitar el fallo del adhesivo que evite la transmisión efectiva de carga sobre todo ante solicitaciones tractivas.

La aplicación del tratamiento de plasma atmosférico al núcleo antes de su adhesivado permite mejorar de forma duradera las condiciones de adhesión al incrementar la energía superficial.

Se ha desarrollado una metodología de modelización multiescala de materiales celulares a través de la cual es posible determinar el comportamiento equivalente de estos materiales sin necesidad de realizar ensayos experimentales reales y obtener una respuesta detallada de su comportamiento ante solicitaciones multiaxiales. Esta metodología se ha aplicado con éxito al caso de los paneles estudiados.

REFERENCIAS

ALVAREZ P. et al. (2009) *ACEX-09*, Junio 2009, Roma

EAVES D. (2004). *Handbook of Polymeric Foams*, Rapra Technology, UK.

RODRIGUEZ-PEREZ M.A. (2005) *Adv Polym Sci* 2005, 184, 97.

ZHANG S., LI L., KUMAR A. (2009). *Materials Characterization Techniques*, Taylor & Francis Group. USA, 15-16.

Cure and permeability characterization of RTM and infusion processes by dielectric spectroscopy

I. Harismendy, I. Arrizabalaga, J. Gayoso, A. Irazusta, R. Mezzacasa
Plastics and Composites Department
Inasmet-Tecnalia
San Sebastián /Spain
isabel.harismendy@inasmet.es
G. Maistros
INASCO Hellas
Argyroupolis
Athens / Greece
g.maistros@inasco.com

SUMMARY

In this study, dielectric spectroscopy for liquid composite moulding processes (LCM) monitoring is investigated. Dielectric sensors are used to monitor both the resin flow and cure. An experimental setup is built in order to characterize the in-plane permeability and degree cure for both RTM (hard tooling) and infusion (flexible tooling). Results are compared to those obtained by visual determination (flow) and DSC kinetic models predictions (cure).

1. INTRODUCTION

Liquid composite moulding processes (LCM) such as RTM and infusion are gaining increasing interest in the industry due to their cost effectiveness and their ability to produce complex shapes. Process simulation and real-time process control are key issues to reduce development costs as well as to improve the quality and reliability of LCM processes.

For high performance composites, curing is one of the most relevant and time consuming production steps. The magnitude and the duration of the applied temperature (time-temperature profile) will determine the final properties of the part. On the other hand, for LCM processes, the selection of a good injection strategy is crucial to assure a complete saturation of the preform and thus the desired quality.

Numerical modelling of LCM (cure, viscosity and flow through the preform) can aid to better understand and improve the process by choosing the correct parameters. However, differences between raw material batches, the variability associated to manual operations as well as uncertainties in permeability characterization can lead to different curing behaviour or flow that progresses in a different manner than predicted. For this reason, it is recommended to monitor cure and flow in order to better control the process.

There are several approaches to process monitoring: externally inside (pressure, heat sensors) or outside the mould (thermography, optical) or internally (intrusive methods) within the part like embedded optical fibres. In this study, dielectric sensors located in the mould together with the proper software are used to monitor both the cure and flow in LCM process. Also, an experimental setup is built in order to characterize the permeability of the preform.

2. CURE MONITORING

In a first step, a kinetic study of the resins kinetics was performed. For this purpose, both isothermal and dynamic calorimetric tests were carried out in a TA Q100 DSC. Results were fitted to an autocatalytic model with diffusion (1):

$$\frac{d\alpha}{dt} = k(T)\alpha^{m(T)}\left[\frac{\alpha\max(T) - \alpha}{\alpha\max(T)}\right]^{n(T)} \tag{1}$$

Where α is the degree of cure or conversion and α_{max} is the maximum conversion at each temperature. The rate constant (k) and orders or reactions (m, n) are functions of temperature.

Figure 1 and 2 show the cure monitoring setup used in this study. The setup consists of a mould with electrical resistances and tool-mounted dielectric sensors (designed and assembled by INASCO) with integrated thermocouples.

Figure 1. Cure monitoring setup.

Figure 2. Sensor.

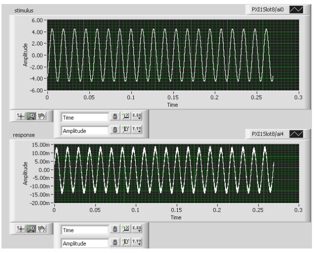

Figure 3. Sensor signal.

The signal from the dielectric sensors and the thermocouples was recorded and treated with the DiAMon Plus™ software from INASCO. An AC current was applied at a frequency range ranging from 0.2 to 10 kHz. The gain (Z) and phase (θ) were obtained by comparing input signal to stimulus voltage (Figure 3). Z and θ yield the real (Z') and imaginary (Z") impedance. Degree of cure evolution was followed by the changes in Z" maximum value, as the peak was shifted to lower frequencies. Figure 4 shows the results for a laminate of EA9396 resin with carbon fibre.

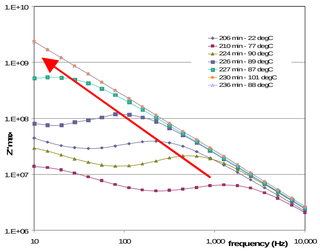

Figure 4. Z”max variation with frequency.

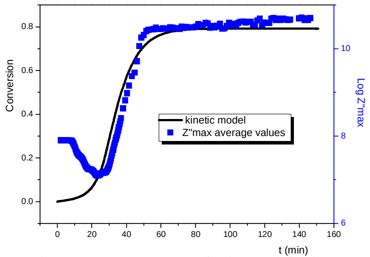

Figure 5. Z”max evolution with time

Figure 5 shows the comparison of the dielectric signal to the kinetically estimated conversion for a cure cycle at 66ºC (heating rate 2ºC/min). As it can be seen, from α=0.1 a good correlation was observed. From α=0 to α=0.1 the signal was dominated by the decrease of viscosity.

3. FLOW MONITORING

Figures 6, 7 and 8 show the setup for flow monitoring and in-plane permeability calculation. The setup consists of a lower steel plate with electrical resistances and integrated temperature and dielectric sensors distributed along the length of the plate. A pressure sensor is located at the feeding point in order to record the pressure gradient. For RTM tests an upper glass plate is used. Infusion tests are performed with a vacuum bag.

Figure 6. RTM permeability setup.

Figure 7. Infusion permeability setup

Figure 8. Flow sensor

In-plane permeability tensors, k1 and k2, are calculated following the method of the ellipse by measuring the evolution of flow front position with time at different fabric orientations (0º, 45º and 90º). Permeability values at each orientation are calculated by rearranging Darcy’s law equation.

$$\underline{\underline{k}} = (1 - Vf)\mu\left(\frac{x^2}{2t\Delta P}\right) \qquad (2)$$

Where $\underline{\underline{k}}$ is the preform permeability tensor, V_f is the fibre volume content, μ the fluid viscosity, t is the time and ΔP is the pressure gradient.

In order to check the validity of the sensors for flow detection, several trials were performed with fluids of different conductivity. Figure 9 shows the results of the tests performed with epoxy resin (EA9396, low conductivity) and acetone (high conductivity).

In this case, a DC current of 20 volts was used and the intensity of the signal was measured. As shown in the figure, sensors where able to detect both the resin and acetone.

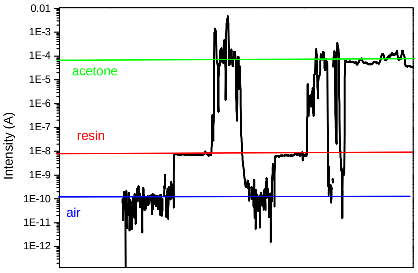

Figure 9. Flow detection trials.

4. CONCLUSIONS

In this study dielectric sensors were used to monitor both the resin flow and cure. Experimental setups were built in order to characterize the in-plane permeability and cure degree. In the cure tests, a good agreement between sensor signal and DSC kinetic model predictions was found. An accurate detection of resin arrival was also observed in the flow tests. Results show that dielectric spectroscopy can be a reliable method for LCM process monitoring.

ACKNOWLEDGMENTS

This work was partly supported by the EU in the frame of SENARIO project (Advanced Sensors and Novel Concepts for Intelligent and Reliable Processing in Bonded Repairs) under contract nº AST5-CT-2006-030982.
Financial support from the *Ministerio de Ciencia e Innovación* under contract n ºPTQ-08-03-07711 is also acknowledged.

REFERENCES

DEVILLARD, M., HSIAO, K.T., ADVANI, S.G. (2005), Flow sensing and control strategies to address race tracking disturbances in resin transfer moulding**,** *Composites Part A*, 36, 1581-1589.
FERNALD, P., GUITARD, D., TROCHU, F. (1996), Cocurrent methods for permeability measurement in resin transfer moulding, *Polymer Composites*, 17, 149-158.
PANTELELIS, N., MAISTROS, G. (2006), Process monitoring for liquid composite moulding using durable sensors, *27th Riso International Symposium on Materials Science*, Roskilde, Dennmark, 279-285.
PANTELELIS, N (2005), Towards the dynamic optimization for the cure control of thermoset-matrix materials, *Composite Science and Technology*, 65, 1254-1263.

Mecanizado de materiales compuestos de fibra de carbono y matriz termoplástica

A. López-Arraiza, J. Santos
Laboratorio de Composites. Centro Tecnológico IDEKO-IK4, Spain.
A. Agirregomezkorta, M. Sarrionandia, J. Aurrekoetxea
Departamento de Mecánica y Producción Industrial. Mondragon Goi-Eskola Politeknikoa, Universidad de Mondragón, Spain.

RESUMEN

En el presente trabajo se ha estudiado el proceso de taladrado de placas de fibra de carbono con matriz termoplástica (pCBT). El objetivo del presente proyecto se centra en conseguir las herramientas y condiciones de mecanizado óptimas que eviten la presencia de imperfecciones o malos acabados en la pieza final. Se han utilizado cuatro brocas diferentes de uso típico en aeronáutica y se han realizado ensayos de taladrado a bajas y altas revoluciones. Los agujeros resultantes se inspeccionaron dimensionalmente, se evaluó su rugosidad y se observaron igualmente al microscopio óptico y electrónico. Los mejores resultados en cuanto a acabado y tolerancias dimensionales se obtuvieron a bajas revoluciones (3000 rpm) con geometrías de herramienta que facilitan la salida de viruta. Esta viruta obtenida puede utilizarse posteriormente como carga de refuerzo en procesos de transformación en fundido de termoplásticos.

1. INTRODUCCIÓN

El mecanizado de los polímeros reforzados con fibras de carbono (CFRP), materiales de creciente utilización en el sector aeronáutico, automovilístico, eólico o naval, difiere en gran medida del mecanizado convencional de metales debido a su anisotropía y heterogeneidad (Guidossi et al. 2004, Tsao et al. 2004). Los compuestos de matriz termoplástica fabricados mediante vía líquida como RTM ("resin transfer moulding"), son materiales de reciente aparición que presentan numerosas ventajas frente a los termoestables como son: mayor tenacidad, mayor resistencia al impacto y reciclabilidad (Mohd Ishak et al. 2007).

Este trabajo presenta un estudio del proceso de taladrado de pCBT reforzado con fibra de carbono utilizando distintas herramientas y condiciones de mecanizado. Si bien el mecanizado de compuestos de matriz termoestable ha sido objeto de diversos estudios, el mecanizado de los compuestos termoplásticos obtenidos por vía líquida es inédito, de ahí el interés del presente trabajo de investigación.

2. PARTE EXPERIMENTAL

2.1 Materiales y procesado

La matriz objeto de estudio es CBT160 (Cyclics®Corporation), que tras polimerizar y cristalizar da como resultado el termoplástico de ingeniería Poli(tereftalato de butileno) (pCBT). El refuerzo utilizado es un tejido plano equilibrado [0º/90º] de fibra de carbono de alta resistencia con un gramaje de 200 g/m^2 (suministrado por Hexcel). En cada laminado se han utilizado 14 capas de dicho tejido obteniéndose placas rectangulares

(250 mm x 300 mm x 3 mm) mediante moldeo TP-RTM asistido por vacío (Agirregomezkorta et al. 2008).

2.2 Parámetros de mecanizado

El proceso de mecanizado se ha desarrollado en seco para evitar la posible absorción de fluido de corte por la matriz termoplástica. Se ha trabajado a dos velocidades distintas de corte: 3.000 rpm y 15.000 rpm; con un avance de herramienta de 0,05 mm/rev. Las características y geometrías de las herramientas se pueden observar en la tabla 1.

Tipo de broca	
Helicoidal HSSCo Ø6,35 (LATZ) 	Helicoidal MD Ø6,10 (K10 ARDATZ) 
Fresa dentado diamante con punta broca de MD Ø6,00 (SGS®FGR-6M) 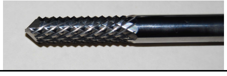	Espada de MD Ø6,35 (LATZ) 

MD: Metal Duro, HSSCo: Acero rápido al cobalto

Tabla 1. Herramientas de taladrado utilizadas.

Los ensayos de taladrado se han realizado en un centro de mecanizado MML-500 (Módulo Motores Lineales), diseñado y fabricado en IDEKO, con velocidad máxima del cabezal de 24.000 rpm y potencia del cabezal de 23 KW. La placa se colocó sobre una base de madera para evitar la flexión de la placa al mecanizar y para minimizar los efectos de delaminación a la salida de la herramienta. Se realizaron diez agujeros por cada herramienta y condición de taladrado.

2.3 Métodos de inspección y control

Se han realizado medidas dimensionales con un micrómetro de agujeros para verificar el diámetro de taladrado. La rugosidad a lo largo del espesor del taladro se ha inspeccionado a 0,5 mm/s con un rugosímetro marca Mitutoyo (Surftest SJ-301). Las imágenes de microscopía óptica se han obtenido con un dispositivo USB Digital Microscope de la marca BigCatch^{TM} que permite trabajar de 20 a 200 aumentos y observar tanto la entrada como la salida de herramienta. El microscopio electrónico de barrido (SEM) es un modelo EVO$^{®}$40 de la marca Zeiss que permite trabajar a bajo vacío y observar directamente las muestras sin metalizar. Se inspeccionó la parte interior de los taladros para ver el efecto de la herramienta sobre el termoplástico y las fibras de carbono.

3. DISCUSIÓN DE RESULTADOS

Se ha observado una variación importante entre el diámetro de las herramientas y los agujeros según las condiciones de taladrado utilizadas. La fresa con punta de broca es la que mayor precisión dimensional aporta tanto a bajas como a altas revoluciones, por el contrario, la espada de MD y las brocas helicoidales a altas revoluciones presentan incrementos medios de diámetro entre un 5,6 y 10,5 %, siendo despreciable la variación a bajas revoluciones.

Las imágenes en la zona de entrada de los taladros realizados a 3.000 rpm (fig. 1) revelan mejores acabados utilizando la fresa con punta de broca (c). Las brocas helicoidales de HSSCo (a) y MD (b) presentan acabados con rebabas y fibras rotas, y con la espada (d) se observa la presencia de "pieles" de termoplástico en todo el perímetro superficial del agujero. La salida de la herramienta presenta peores acabados que la entrada pero sin llegar a apreciarse delaminación o separación de la capa final por la presencia del bloque de madera de sacrificio. Al aumentar las revoluciones de mecanizado a 15.000 rpm no se obtienen mejoras en el acabado, incluso la presencia de rebabas y fibras rotas es mayor que a bajas revoluciones de taladrado.

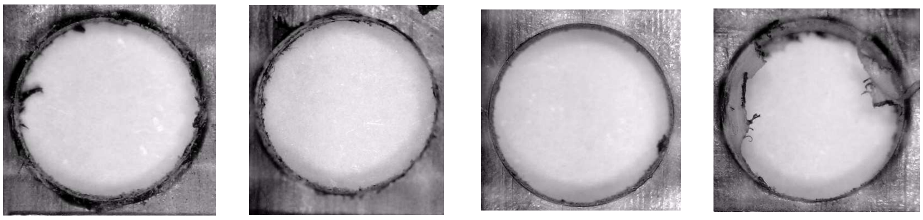

(a) HSSCo (b) MD (c) Fresa Ø (d) Espada

Fig. 1. Entrada de los taladros realizados a 3.000 rpm. Fotos con 30X.

En la tabla 2 se puede observar el valor típico de rugosidad R_a (área entre la curva de rugosidad y la línea de referencia) para las distintas herramientas y las dos condiciones de taladrado. Se observa que a bajas revoluciones la rugosidad obtenida es mejor que a altas revoluciones para todas las herramientas. La espada de metal duro presenta los mejores valores, típicos del proceso tradicional de taladrado (1-3 μm). La influencia de la velocidad de taladrado no es la misma para todas las herramientas, ya que mientras con la espada hay un factor próximo a dos, con la broca MD la rugosidad se multiplica por un factor próximo a seis.

	HSSCo		MD		Fresa		Espada	
	3.000 rpm	15.000 rpm	3.000 rpm	15.000 rpm	3.000 rpm	15.000 rpm	3.000 rpm	15.000 rpm
Ra (μm)	2,25	8,04	1,94	11,78	3,42	7,24	1,71	3,60

Tabla 2. Rugosidades según tipo de herramienta y condición de mecanizado.

Para explicar estas diferencias de rugosidad frente a velocidad de taladrado se han estudiado las superficies mecanizadas mediante SEM. En la figura 2 se muestran los resultados de la broca helicoidal de MD por ser los más significativos. Como se puede apreciar a 3.000 rpm (figura 2a), la superficie es relativamente lisa, hecho que puede deberse al comportamiento dúctil del material que se confirma con la generación de viruta continua. Sin embargo, al aumentar las revoluciones, y como consecuencia de la marcada naturaleza viscoelástica de la matriz, el comportamiento pasa a ser más frágil, generando una superficie más rugosa (figura 2b). La viruta generada en estas condiciones no es alargada como a bajas revoluciones sino que son partículas de polvo.

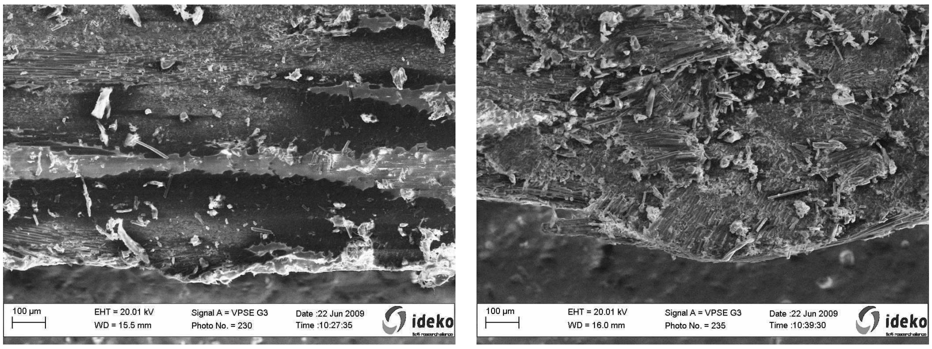

(a) MD 3.000 rpm (b) MD 15.000 rpm

Fig. 2. Imágenes 200X de la entrada de la broca en el material

4. CONCLUSIONES

El estudio del taladrado de compuestos de matriz termoplástica reforzada con fibra de carbono obtenidos por RTM ha demostrado que:

1. Taladrar a bajas revoluciones proporciona mayor precisión dimensional, mejor rugosidad y menores rebabas a la entrada y a la salida de la herramienta.
2. La mejor precisión dimensional se obtiene mediante la fresa con dentado de diamante, mientras que con la espada se obtiene la mejor rugosidad.
3. La naturaleza viscoelástica de la matriz hace que a bajas revoluciones de taladrado presente un comportamiento dúctil, generando viruta larga, mientras que a altas revoluciones el comportamiento es frágil con viruta en polvo, lo que genera una menor precisión dimensional y peor acabado superficial.

AGRADECIMIENTOS

Los autores desean agradecer la colaboración de Iker Altuna y Guillermo Arriola por su ayuda en los ensayos de mecanizado y rugosidad respectivamente.

REFERENCIAS

AGIRREGOMEZKORTA, A., HOYOS, G., ARETXAGA, G., SARRIONANDIA, M., AURREKOETXEA, J. (2008). Propiedades mecánicas de composites pCBT/fibra de carbono fabricados mediante RTM. *Actas del X Congreso Nacional de Materiales, pp. 711-714.*

GHIDOSSI, P., EL MANSORI, M., PIERRON F. (2004). Edge machining effects on the failure of polymer matrix composite coupons. *Composites: Part A 35, 989-999.*

MOHD ISHAK, Z.A., LEONG, Y.W., STEEG, M., KARGER-KOCSIS, J. (2007). Mechanical properties of woven glass fabric reinforced in situ polymerized poly(butylene terephthalate) composites. *Composite Science and Technology 67, 390-398.*

TSAO, C.C., HOCHENG, H. (2004). Taguchi analysis of delamination associated with various drill bits in drilling of composite material. *International Journal of Machine Tools & Manufacture 44, 1085-1090.*

Tecnología pre-preg fuera de autoclave

A. Pipó
Departamento de investigación y Desarrollo. PROSIX COMPOSITES ENGINEERING,
San Sebastián, España.
Alvaro.pipo@prosix.es

RESUMEN

La producción de grandes estructuras de altas prestaciones en el sector náutico ha experimentado una gran evolución desde las técnicas de laminado manual a las actuales con materiales pre-impregnados. Una de estas grandes estructuras para la que es necesario la optimización de las técnicas de fabricación con pre-pregs en bolsa de vacío, es la fabricación de los barcos de Copa América. Las normas de esta antigua regata, que se inició hace 150 años, prohíbe el uso de autoclave para la fabricación del casco. Sin embargo, la evolución y optimización en diseño de estas estructuras de 25 m de largo, sometidas a elevadas solicitaciones mecánicas, ha derivado en la necesidad de conseguir niveles de porosidad y calidad de sus laminados equivalentes a los obtenidos con el curado en autoclave. El presente estudio, agrupa los principales desarrollos que realizó Prosix Composites Engineering en el campo de la minimización de la porosidad de laminados con materiales compuestos pre-impregnados para la fabricación de los dos barcos del Desafío Español para la Copa América de vela de Valencia 2007. Diferentes factores de la fabricación como las compactaciones intermedias, la composición del stack y su posicionamiento relativo al laminado y las variables del ciclo de curado, fueron estudiadas y analizadas para la obtención de su combinación óptima en función de las propiedades reológicas del sistema pre-preg utilizado. En este estudio, se presentan técnicas para la optimización de los procesos de fabricación de grandes estructuras con pre-pregs fuera de autoclave que pueden aplicarse tanto en la náutica como en otros sectores.

1. INTRODUCCIÓN

Actualmente, las grandes estructuras de composites como los cascos de los barcos de Copa América son fabricadas con estructuras sándwich compuestas por núcleos de nido de abeja y pieles de carbono-epoxy en los que se requiere: (1) la adhesión entre las pieles y el núcleo debe ser perfecta para evitar deslaminaciones que pueden producir un fallo crítico en la estructura, (2) las pieles deben contener la fracción volumétrica de fibra más elevada posible y el mínimo nivel de porosidad para obtener las mejores propiedades mecánicas (principalmente rigidez y resistencia) de la estructura sándwich.
En aplicaciones espaciales o aeronáuticas, estos requerimientos ya son actualmente alcanzados procesando las piezas de composite dentro de autoclaves. Con esta técnica, aplicando presiones de hasta 10 bar. se consigue una elevada compactación entre las capas de material y un bajo nivel de porosidad, (Eom et al. 2001). Es muy escasa la documentación existente para las técnicas de procesamiento por bolsa de vacío al contrario de lo que sucede para el procesado en autoclave. Stringer (1989), señala en su estudio la crítica influencia de la viscosidad del sistema de resina empleado en el nivel

de porosidad del laminado final. Mas recientemente, Pepecka et al (2002) desarrollaron sistemas pre-pregs con niveles de permeabilidad a los gases optimizados.
En este estudio, se controlarán por tanto, factores como la temperatura, de la que depende directamente el comportamiento de la viscosidad del sistema de resina, y la distribución de presiones en el laminado. También se controlarán otros parámetros del proceso como las compactaciones intermedias durante la laminación de las diferentes capas y la composición del stack para el curado de las piezas

2. MATERIALES UTILIZADOS Y METODO DE ENSAYO

El sistema pre-preg utilizado fue el SE84LV unidireccional carbono-epoxy, contenido nominal de resina 32% en peso y gramajes 150, 200 y 300 gr/m^2 de la empresa SP-GURIT (UK) Ltd. Las pieles se laminaron siguiendo un esquema de laminación de 6 capas (2x150, 2x200, 2x 300) y orientación variable en función del área de la estructura objetivo de cada estudio. Las dimensiones de las probetas utilizadas fueron 600 x 600 mm. Una vez realizado el proceso de laminación siguiendo en cada caso los procedimientos de compactaciones intermedias que se expondrán en el siguiente apartado, se prepararon los materiales del stack con las diferentes configuraciones, también presentadas en el siguiente apartado. Los materiales de stack utilizados fueron: peel ply seco de Nylon , 82 gr/m^2 (Ply A); film perforado P3 y P90; tejido de vidrio plain 202 gr/m^2 (RE210D) y manta de poliéster 150 gr/m^2 (Econoweave 44W) como aireadores-sangradores; red aireadora de polipropileno (breatherflow 20) y bolsa de vacío. Una vez preparado cada panel de ensayo se realizo el proceso de curado siguiendo ciclos de curado reproducibles en hornos de grandes dimensiones, controlando y monitorizando las temperaturas por medio de termopares (min. 2 por panel) y el nivel de vacío por sensores de presión. Los diferentes parámetros del ciclo de curado estudiados se presentan en el siguiente apartado. Una vez curados los paneles se procedió al corte de 3 muestras de la zona central de cada panel. Tras su preparación metalográfica, se controló la distribución de porosidad respecto al espesor del laminado por microscopía óptica con equipo Nikon Microphot-FX. Posteriormente se obtuvo de porcentaje de porosidad global del laminado siguiendo ensayos de digestión de resina según norma ASTM D 3171-76.

3. RESULTADOS

3.1. Compactaciones intermedias durante la laminación

Los factores que se estudiaron para la definición de las compactaciones intermedias fueron: la frecuencia, la temperatura y el tiempo de compactación. Los resultados obtenidos se muestran en la tabla 1. El esquema de laminación, el ciclo de curado y el stack utilizado para todas las muestras fue el mismo.

	TIEMPO COMPACTACION	TEMPERATURA COMPACTACION	FRECUENCIA	POROSIDAD MEDI
1	1 hr	20ºC	1 capa	0,90%
2	1 hr	45ºC	1 capa	1,50%
3	4 hr	20ºC	1 capa	0,88%
4	1 hr	20ºC	3 capas	1,81%
5	1 hr	45ºC	3 capas	2,01%
6	4 hr	20ºC	3 capas	1,80%
7	0	0	sin compactacion	5,40%

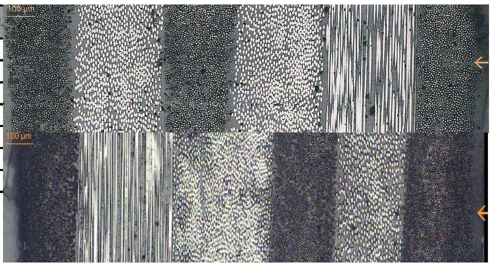

(Izq.) Tabla 1. Efecto de la frecuencia, tiempo y temperatura de las compactaciones intermedias en la calidad final del laminado.
(Dcha.) Figura 1. Arriba distribución de porosidad para caso 1 (tabla 1). Abajo distribución de porosidad para caso 4 (tabla 1).

Como puede observarse en la tabla 1, el porcentaje de porosidad media del laminado disminuye principalmente cuando aumenta la frecuencia de las compactaciones, aumenta el tiempo de compactación y ésta se realiza a temperatura ambiente. Por otra parte, respecto a la distribución de la porosidad en la sección del laminado se pudo observar en todos los casos cómo ésta se concentra en las intercalas de las capas laminadas entre compactaciones sucesivas. La figura 1 muestra a modo de ejemplo la microscopía óptica del caso 1 y 4 de la tabla 1.

3.2. Ciclos de curado

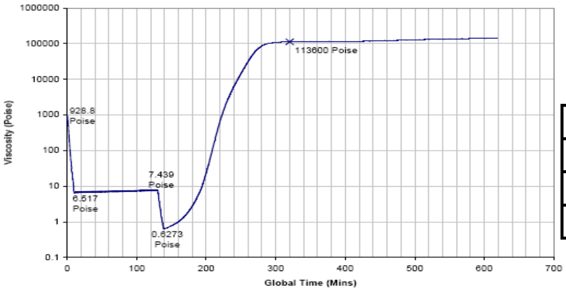

	MESETA INICIAL	POROSIDAD MEDIA
1	2 HR@ 50ºC	1,10%
2	2 HR@ 65ºC	0,88%
3	3 HR@ 65ºC	0,89%
4	1,5 HR@ 70ºC	0,95%

(Izq.) Figura 2. Variación de la viscosidad de la resina SE84LV para ciclo de curado 2hr@65ºC, 8hr@85ºC, rampas 3ºC/min.(SP Technical Service).
(Dcha.) Tabla 2. Efecto de la meseta inicial del ciclo de curado en la porosidad final del laminado.

La figura 2 muestra la variación de la viscosidad de la resina SE84LV respecto a la variación de tiempo y temperatura. Como se observa, en las primeras etapas del ciclo de curado, se puede conseguir mantener un estado de baja viscosidad de la resina realizando mesetas a temperatura constante durante cierto tiempo previo a la llegada del punto de gel de la resina. Por tanto, variando el tiempo y temperatura de las mesetas en las primeras etapas del ciclo de curado se puede optimizar el flujo de resina y favorecer la salida de aire del laminado. La tabla 2 muestra el efecto de estas mesetas en el porcentaje de porosidad del laminado. Resultados para mismos esquemas de laminación y configuración de stack.

3.3. Configuración del stack

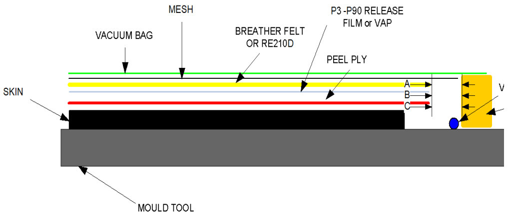

	A	B	C	POROSIDAD MEDIA
1	0 mm	0 mm	50 mm	1,12%
2	0 mm	0 mm	0 mm	0,90%
3	0 mm	50 mm	0 mm	0,85%

(Izq.)Figura 3. Configuración típica de stack utilizada. (Dcha.) Tabla 3. Efecto de la configuración del stack en la porosidad media del laminado final.

Los parámetros de configuración del stack fueron estudiados con el objetivo de potenciar la circulación del aire del laminado durante ciclo de curado. La figura 3 muestra una configuración típica del stack utilizado durante este estudio siendo las dimensiones, A,B y C , la distancia al tubo de vacío del breather, el release film y el peel ply respectivamente. La tabla 3 muestra las diferentes configuraciones ensayadas y su efecto en la porosidad del laminado. Resultados para laminados con mismos esquemas de laminado y ciclos de curado.

3. CONCLUSIONES

El control del nivel de porosidad de los laminados fabricados con técnicas de bolsa de vacío resulta un sistema complejo gobernado principalmente por la variación de la viscosidad de la resina, la permeabilidad a los gases y los parámetros de procesamiento. En este estudio se ha mostrado que, para un sistema de resina particular dado, es posible fijar los parámetros de procesamiento para las compactaciones intermedias de laminación, los ciclos de curado y la configuración del stack, que permiten minimizar el nivel de porosidad del laminado a niveles comparables a los obtenidos por técnicas en autoclave. Las técnicas mostradas en este estudio, junto con las desarrolladas por Prosix en otros campos de la fabricación, fueron implementadas en la construcción de los dos barcos del Desafío Español de la 32º Copa América de vela de Valencia, resultando unas estructuras de alta calidad (porosidad <1,02%) que superaron sin problemas la prueba de esfuerzos y no registraron ningún defecto durante la competición.

AGRADECIMIENTOS

Se agradece especialmente el trabajo realizado por Agustín Zulueta para la consecución del equipo español de la 32º Copa América de vela y a Ezequiel Sirito, Pablo Santarsiero y Gabriel Mariani por su ayuda durante la construcción de los barcos.

REFERENCIAS

Eom, Y., Boogh, L., Michaud, V., Sunderland, P., Månson, J.-A.E., Polymer Composites, 22 (1) (2001) : 22. y ., Polymer Eng. Sci., 41 (3), (2001) : 492.
Stringer, L.G., Composites 20, nº5, september (1989):441.
Repecka, L., Boyd, J., in Proc. SAMPLE 2002, May 12-16 2002, Long Beach, CA, CD version, (2202).

T8. MODELLING
MODELIZACIÓN

Numerical simulation of composite materials and structures using the unit cell homogenization approach

H. Badillo[1], **S. Oller** [1,2]
[1]Centro Internacional de Métodos Numéricos en la Ingeniería. Universidad Politécnica de Cataluña. Edificio C1, Campus Norte UPC C/ Gran Capitán S/N 08034 Barcelona, Spain. hbadillo@cimne.upc.edu
[2]Departamento de Resistencia de Materiales y Estructuras en la Ingeniería, Universidad Politécnica de Cataluña. Jordi Girona 1-3, Módulo C1, Campus Norte UPC, 08034 Barcelona, Spain. sergio.oller@upc.edu

ABSTRACT

This methodology proposes to find reliable estimates of the overall response of the structure, independently of the geometrical arrangement and of the material properties of the constituents using a homogenization technique based on a periodic microfield approach by studying a unit cell which represents the composite to be analyzed. The methodology is implemented based on a finite element code in two scales. A macro scale treats the composite as a homogeneous material and deals with the boundary conditions and loads. A micro scale deals with the geometry and the material properties of the constituents to obtain the homogenized response of the composite.

The homogenized constitutive tensor is obtained for any unit cell corresponding to each Gauss point of the macroscale that enters in the nonlinear range thru perturbations. Periodic boundary conditions, by means of the Lagrange multipliers are applied to ensure compatibility of deformations. The homogenization technique is developed to obtain the response of 2D models for composite materials and structures with constituents that have classic constitutive equations, such as damage or plasticity.

1. INTRODUCTION

Several alternative methods have been developed to compute the mechanical behavior of composite structures since full microscopic modeling is difficult to apply due to the computational difficulties that such task implies. Among those methods there is the theory of multiscale homogenization. This method proposed initially by Sanchez-Palencia (1980), is based on the assumption that the internal structure of the composite material is periodic, which makes possible to divide the whole structure into unit cells that can adopt any form.

The local periodicity hypothesis suggests that the symmetries of the fields arise as a consequence of the energy minimization principle, which ensures that the periodic field of the state variables, such as displacements and forces, and strains and stresses, tend to be periodic as its geometry in the space of small deformations. Therefore the magnitudes of the macroscopic stress and strains are calculated, based on the microscopic fields that represent the behavior of the composite as if it were a homogeneous material.

2. APPROACH TO THE PROBLEM USING HOMOGENIZED VARIABLES

The problem of homogenization is based on the relationship between the deformations at the macroscopic scale (x) with the transformation experienced by the periodicity vectors that are contained on a structural scale much smaller called microscale (y).

The homogenized strain tensor calculates the global field of the space of the cell in a displacement periodic field and it corresponds to the average value of strain that matches the classic definition given by the average method as shown in equation (1). Following the same considerations for the homogenized stress tensor and considering that the cell volume is very small it can be expressed as noted in equation (2).

$$\tilde{\varepsilon}_{ij} = \left\langle \varepsilon_{ij}(y) \right\rangle_{\Omega_C} = \frac{1}{V_C} \int_{\Omega_C} \varepsilon_{ij}(y) dV_C \tag{1}$$

$$\tilde{\sigma}_{ij} = \frac{1}{V_C} \int_{V_C} \sigma_{ij} dV \tag{2}$$

where ε is the strain tensor in the micro scale and V_C is the volume contained in Ω_C.

For macroscopic purposes the homogenized stress tensor $\tilde{\sigma}$ satisfies the same requirements as the stress tensors in homogeneous materials, therefore it is feasible to obtain the macroscopic level response based on an analysis performed in the microstructure of the composite. The homogenized equilibrium equation expressed it in terms of homogenized variables is given by:

$$\int_V \tilde{\sigma}_{ij,j} \, dS + \int_V \tilde{b}_i dV = 0 \tag{3}$$

This equation is valid for any region of the composite Ω, therefore it is valid if there is any small domain, whose boundary is the domain of the cell, i.e. $\Omega \to \Omega_C, \Omega_C \to 0$.

3. LINEAR-ELASTIC HOMOGENIZED FORMULATION

This study obtains the composite elastic constitutive tensor based a formulation by in two-scales (microscopic and macroscopic). At microscopic level, the problem is reduced to solve a boundary value problem in the domain Ω_C of the cell that represent the static equilibrium at the microstructural level, ignoring the volume forces. The constitutive behavior of the components of the composite is given by the local constitutive tensor $C(y)$ and can represent any type of mechanical behavior.

Meanwhile, in the macroscopic scale if we consider that all the constituents of the composite are elastic and without admitting the possibility of debonding among the component materials, the problem becomes a boundary value problem of a homogeneous solid in which there is a field of displacements and strains. For more detail on this formulation refer to Zalamea (2001) and Oller et al. (2005). The homogenized elastic constitutive tensor $\tilde{C}(x)$ can be determined from applying small perturbations to the cell, in order to activate the elastic properties of the composite, expressed mathematically as follows:

$$\tilde{C}_{ijkl}(x) = \tilde{\sigma}_{ij}(x) : (\tilde{\varepsilon}_{kl}(x))^{-1} \tag{5}$$

If the condition orthotropy it is considered and applying a perturbation in each of the principal directions by separately, the homogeneous constitutive tensor can be obtained component by component, thus making the problem to have a unique solution.

The problem that represents equation (5) can be addressed using the finite element method. However, in this case the mathematical formulation needs to ensure the periodicity of displacements and forces.

3.1 Implementation of Periodicity Conditions

Periodic boundary conditions, by means of the Lagrange multipliers are applied to ensure compatibility of deformations. Although this method has some drawbacks, such as increasing the number of equations and bandwidth, they can be solved by applying the boundary conditions as suggested by Anthoine (1995) by dividing the Lagrange multipliers into two groups, λ_1 and λ_2. The steady state of increased functional with the Lagrange multipliers is given by the well-conditioned system of linear equations,

$$\begin{bmatrix} K & {k_p}^T & {k_p}^T \\ {k_p}^T & I & -I \\ {k_p}^T & -I & I \end{bmatrix} \begin{bmatrix} \tilde{u} \\ \lambda_1 \\ \lambda_2 \end{bmatrix} = \begin{bmatrix} F \\ \Delta D \\ \Delta D \end{bmatrix} \tag{6}$$

where I is the identity matrix, ΔD is the nodal displacement vector between the nodes on the contour and k_p is the matrix that relates the degrees of freedom of the nodes in the contour of the cell.

The solution of the system of equations allows determining the microscopic stress field in the domain of the cell, which gets the homogenized stress tensor $\tilde{\sigma}$ for each of the strains applied, on each of the directions. Once the homogenized elastic tensor is obtained the problem in the macrostructure is solved by applying the standard finite element method using the classic procedure of equilibrium for a homogeneous solid.

4. NON-LINEAR HOMOGENIZED FORMULATION

The procedure to calculate the nonlinear homogenized tensor consists in identifying if any Gauss point of any element of the unit cell has entered in the nonlinear range. If this is the case the homogenized tangent constitutive tensor needs to be calculated for that unit cell. To obtain the local tangent constitutive tensor a perturbation method is used following the method proposed by Martinez (2008) and it is defined as follows:

$$\dot{\sigma} = C^t : \dot{\varepsilon} \tag{7}$$

The tangent constitutive tensor can be obtained as the sum of n stress vectors, which are the product of the j component of the strain vector rate and the j column of the tangent stiffness tensor of the matrix description of equation (7). This is:

$$\dot{\sigma} \equiv \sum_{j=1}^{n} \delta^{j}\sigma = \sum_{i,j=1}^{n} c^{t}{}_{j} \cdot \dot{\varepsilon}_{j} \tag{8}$$

Equation (8) can be used to obtain the j column stiffness tensor, which is unknown:

$$c^{t}{}_{j} = \frac{\overset{j}{\dot{\sigma}}}{\dot{\varepsilon}_{j}} \equiv \frac{\delta^{j}\sigma}{\delta\varepsilon_{j}} \tag{9}$$

The perturbation method consists in defining n small variations, or perturbations, of the strain vector $\delta\varepsilon_j$, to obtain n stress vectors $\delta^{j}\sigma$ that will be used in Equation (9) to obtain the numerical expression of the tangent constitutive tensor.

The homogenized tangent nonlinear constitutive tensor $\tilde{C}^{t}(x)$ is obtained by computing the average value of all the tangent constitutive tensors for each Gauss point of the unit cell. It must be noted that if the Gauss point still lies within the linear range, the tangent tensor will be equal to the linear constitutive tensor of the material, i.e. $c^{t}=C(y)$. This computation also matches the classic definition given by the average method and it is defined in equation (10).

$$\tilde{C}_{ij}{}^{t}(x) = \frac{1}{V_C} \int_{V_C} c^{t}{}_{ij}\, dV \tag{10}$$

5. CONCLUSIONS

A homogenization method that deals with the problem of analyzing the structural behavior of composite material and structures is presented in this paper. One of the most relevant aspects of this study is the method to compute the homogenized nonlinear tangent constitutive tensor. The tensor is obtained by computing the average value of all the tangent constitutive tensors for each Gauss point of the unit cell. The method proposes an alternative to previous homogenization methods that are not completely effective in calculating the response of composite material and structures.

ACKNOWLEDGEMENTS

The first author would like to thank to the International Center for Numerical Methods in Engineering (CIMNE) for the fellowship grant awarded to perform this research.

REFERENCES

ANTHOINE, A. (1995). “Derivation of the in-plane characteristics of masonry through homogenization theory.” *Int. J. Solids Struct.*, 32(2), 137–163.

MARTINEZ, X.; OLLER, S.; RASTELLINI, F.; BARBAT, A.H. (2008). “A numerical procedure simulating RC structures reinforced with FRP using the serial/parallel mixing theory”. *Computers & Structures*, 86 (15-16): 1604-1618. ISSN: 0045-7949

OLLER S, MIQUEL J, ZALAMEA F. “Composite material behaviour using a homogenization double scale method”. *J Eng Mech 2005*;131(1): 65–79.

SANCHEZ-PALENCIA, E. (1980). Vol. 127, “Nonhomogeneous media and vibration theory”. *Lecture notes in physics*, Springer, Berlin.

ZALAMEA, F. (2001). “Composite modelling by means of the homogenization theory”. *PhD thesis*, Technical Univ. of Catalonia, Spain (in Spanish).

Plasticity in bimaterial joints

A. Barroso, D. Vicentini, V. Mantič, F. París
Grupo de Elasticidad y Resistencia de Materiales, Universidad de Sevilla, España

ABSTRACT

The aim of this work was to analyze the influence of different yielding criteria in adhesive joints with metallic and composite materials. Isotropic hardening behaviour with the von Mises, Drucker-Prager and Raghava criterion were considered for the adhesive, while for Carbon Fiber Reinforced Polymer (CFRP) and aluminium, linear elastic behaviour was used. At failure load a local yielding was found at the CFRP-adhesive bimaterial corner in all the criteria. The pressure dependent criteria have shown a tendency to lead the plastic zone to follow a certain angle. Comparisons with experimental evidences indicate that a pressure dependent criterion (i.e. dependency of hydrostatic stress) is more suitable for this kind of polymeric adhesive. The numerical analyses were made by standard Finite Element simulations.

1. INTRODUCTION

Failure mechanisms in adhesive joints are not completely understood yet due to the complex stress state induced at the corner (Barroso *et al.*, 2009 and Barroso, 2007), including several materials with very different characteristics and anisotropy in some of them. The particular corner considered in the present study is shown in Fig. 1.

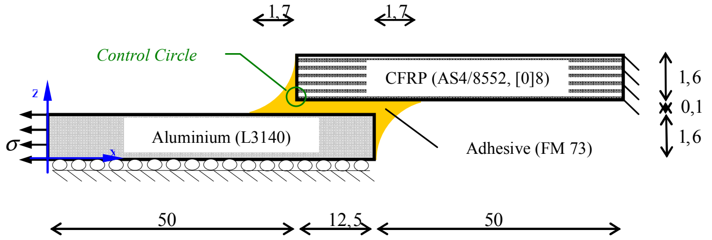

Fig. 1. Geometry (units in mm).

A Linear Elastic Fracture Mechanic (LEFM) approach could be inadequate in the case of relevant plasticity in the corner. Bowden et al. (1972) found experimentally that plasticity in polymers is very dependent on the hydrostatic component of the stress tensor. Considering plasticity in polymers, Broughton et al. (2001) simulated it with von Mises and Drucker-Prager criteria, Chiang et al. (1994) and Chowdhury et al. (2000) with Drucker-Prager, Crocombe et al. (1995) and Aydin (2008) with the criterion proposed by Raghava et al. (1973), between others. Also the cohesive model is being used to simulate the failure process in polymers (Chowdhury et al., 2000; Liljedahl et al., 2006) and damage (Crocombe et al., 1995). In this paper, a double lap joint between CFRP and aluminium plates bonded by a structural adhesive is presented (Fig. 1). In the 2D plane strain FE analysis the adhesive-fillet was considered and the results were compared with the linear elastic plane strain solution (Barroso, 2007).

The mesh was sufficiently refined at the corner tip (inside a control circle of radius r=0.33 μm placed at the corner, Fig. 1). The three following plasticity models were considered for the adhesive: von Mises, Drucker-Prager and Raghava, all assuming bilinear isotropic hardening. Aluminium and CFRP were modeled as linear elastic, isotropic and orthotropic materials respectively. The smallest finite elements utilized in the meshes were around 0.9 μm. The FE simulation was performed by FE code ANSYS and some details of each plasticity model will be discussed in the next session.

2. PLASTICITY MODELS

Von Mises criterion for metallic materials and Drucker-Prager for soils propose a cylindrical and a conical surface in the principal stress space, being widely detailed in the literature (Chen et al., 1988; Drucker et al., 1952; Vicentini, 2008; Wilson, 2002) and thus they will not discussed here. The Raghava model (Raghava et al., 1973) for polymers needs more explanation to correctly introduce it into a FE code (ANSYS in this work). This criterion proposes the following yield function:

$$(\sigma_1-\sigma_2)^2+(\sigma_2-\sigma_3)^2+(\sigma_3-\sigma_1)^2+2(\sigma_e^C-\sigma_e^T)(\sigma_1+\sigma_2+\sigma_3)=2\sigma_e^C\sigma_e^T \quad (1)$$

where σ_e^C and σ_e^T are the material yield stresses in compression and tension respectively. Equation (1) can be rewritten as:

$$q^2+(\sigma_e^C-\sigma_e^T)I_1=\sigma_e^C\sigma_e^T \quad\Rightarrow\quad q^2+(\sigma_e^C-\sigma_e^T)3\sigma_m=\sigma_{adm}^2 \quad (2)$$

Were the σ_{adm} is the geometric average (or an equivalent admissible stress) between the yield stress in tension and compression, i.e. $\sigma_{adm}=\sqrt{\sigma_e^C\sigma_e^T}$. We can define another parameter relating the yield stress in tension and compression ($\lambda=\sigma_e^C/\sigma_e^T$) to obtain:

$$q^2+\alpha\,\sigma_m=\sigma_{adm}^2 \quad (3)$$

where $\alpha=3\sigma_e^T(\lambda-1)$ and $\sigma_{adm}=\sigma_e^T\sqrt{\lambda}$ have dimensions of stresses.

This criterion is a conic surface in the principal stress space with its cone tip rounded. The transformation shown above is necessary to understand and introduce properly the parameters in some FE codes (e.g. ANSYS or ABAQUS) through the Extended Drucker-Prager (EDP) option.

3. RESULTS

The material properties used in the analyses presented were: $E=68670\ MPa$, $\nu=0,33$ and $E=3000\ MPa$, $\nu=0,35$ for aluminium and adhesive respectively. The CFRP was modeled as an equivalent homogeneous orthotropic material: $E_x=141300\ MPa$, $E_y=9580\ MPa$, $E_z=9580\ MPa$, $G_{xy}=5000\ MPa$, $G_{yz}=3500\ MPa$, $G_{xz}=5000\ MPa$, $\nu_{xy}=0,3$, $\nu_{yz}=0,32$, $\nu_{xz}=0,3$. For all cases the applied stress was the one at failure (determined experimentally, i.e. $\sigma=172\ MPa$, see Fig.1). The finite element PLANE42 (four nodes with two degrees of freedom, DOF in what follows) was used in the von Mises model, with 37733 nodes and 37306 elements in total. Hardening behaviour was activated with the TB,BISO command, considering a tangent modulus of $K_T=12\ MPa$ and yield stress in tension as $\sigma_e=50\ MPa$ for the adhesive. The Drucker-Prager and Raghava model were simulated using the EDP option (activated via TB,EDP command), with Linear and Power law yield functions respectively. The finite element PLANE182 (four nodes with two DOF) was used, with 115343 nodes and

114507 elements in total. Associated flow rule was considered for both cases. The hardening was activated with TB,MISO command for these EDP models. The Linear EDP was activated by using $\alpha = 0,98$ (dimensionless) and $\sigma_y = \sigma_e^T = 50\ MPa$ parameters, and the Power EDP by using $\alpha = 69\ MPa$, $b = 2$ (a quadratic function), and $\sigma_y = \sigma_{adm} = \sigma_e^T \sqrt{\lambda} = 60,4\ MPa$ parameters defined in (3), where $\lambda = 1,46$. Figure 2 shows the circumferential stress evolution at *r=0.33 μm* (for angle θ varying from 90º to 360º) in the bimaterial corner. The results for the Raghava model mostly coincide with those by von Mises, except for the interval between 90º and 190º, where the stress level decays up to an 18% with respect to the linear-elastic response. The Drucker-Prager model presents the biggest yielding extent.

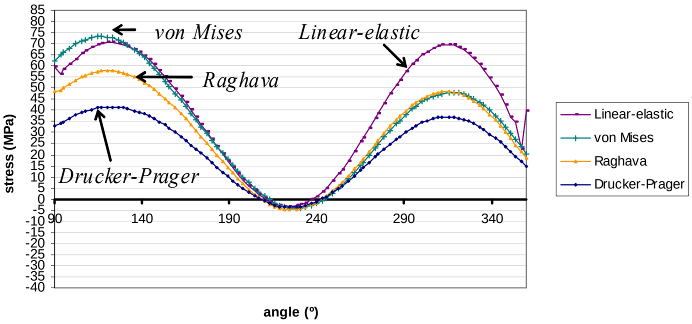

Fig. 2. Circumferential stresses (σ_θ) evolution.

Figure 3 presents the hydrostatic stress for the adhesive inside the control circle radius *r=0.33 μm* obtained by the three yielding criteria considered and for the simple linear elastic case. For Drucker-Prager and Raghava criteria (both include the pressure effect) the strong tendency to lead the stress state at a certain angle is observed. This fact suggests that a yielding criterion that includes the hydrostatic pressure leads the plasticity path in that direction (around 30º from the CFRP-adhesive vertical interface in the corner). This angle was experimentally observed in the failure path by Barroso et al. (2009).

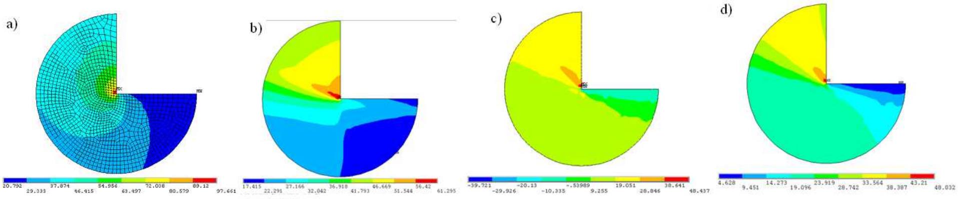

Fig. 3. Hydrostatic stress in the case a) Linear Elastic (the mesh used included), b) von Mises, c) Drucker-Prager and d) Raghava.

4. CONCLUSIONS

Some plasticity effects were analyzed in a bimaterial corner, by using a FE commercial code. The presence of plasticity in the corner can change significantly the specimen response, i.e. the stress state when comparing to the linear-elastic behaviour in the adhesive. In this work the von Mises, Drucker-Prager and Raghava models were applied to consider plasticity in the adhesive, the last two models being dependent on the hydrostatic stress component. For the particular configuration considered here, the hydrostatic stress contribution affects the yielding path at the corner at a certain angle around 30º counter-clock wise from the CFRP-Adhesive vertical interface.

ACKNOWLEDGEMENTS

This work was supported by CAPES Brazilian Ministry of Education and also by the Junta de Andalucía through the Projects of Excellence P08-TEP-04071 and P08-TEP-04051.

REFERENCES

AYDIN, M. D. (2008). 3D nonlinear stress analysis on adhesively bonded single lap composite joints with different ply stacking sequences, The Journal of Adhesion, 843, 15 - 36.

BARROSO, A.; MANTIČ, V.; PARIS, F. (2003) Singularity analysis of anisotropic multimaterial corners, Int Journal of Fracture 119: 1-23.

BARROSO, A. (2007). Characterization of Singular stress states at multimaterial corners. Application to adhesively bonded joints with composite materials, University of Seville, PhD Thesis (in Spanish).

BARROSO, A.; PARIS, F; MANTIČ, V. (2009) Representativity of the singular stress state in the failure of adhesively bonded joints between metals and composites, Compos. Sci. Technol., doi:10.1016/j.compscitech.2008.11.029.

BOWDEN, P. B.; JUKES, J. A. (1972). The plastic flow of isotropic polymers, J. Mat. Science, 7, 52-63.

BROUGHTON, W. R.; CROCKER, L. E.; URQUHART, J. M. (2001). Strength of adhesive joints: a parametric study, NPL Report MATC(A)27.

CHEN, W. F.; HAN, D. J. (1988). Plasticity for Structural Engineers, Springer-Verlag.

CHIANG, M. Y. M.; CHAI, H. (1994). Plastic deformation analysis of cracked adhesive bonds loaded in shear. Int. J. Solids Struct., 31, 2477-2490.

CHOWDHURY, S. R.; NARASIMHAN, R. (2000). A finite element analysis of quasistatic crack growth in a pressure sensitive constrained ductile layer, Eng. Fract. Mech., 66, 551-571.

CROCOMBE, A. D.; RICHARDSON, G.; SMITH, P. A. (1995). A unified approach for predicting the strength of cracked and non-cracked adhesive joints, J. Adhesion, 49, 211-244.

DRUCKER, D. C.; PRAGER, W. (1952). Soil mechanics and plastic analysis or limit design, Q. Appl. Math., 10, 157-165.

LILJEDAHL, C. D. M.; CROCOMBE, A. D.; WAHAB, M. A.; ASHCROFT, I. A. (2006). Modelling the Environmental degradation of the interface in adhesively bonded joints using a cohesive zone approach, The Journal of Adhesion, 82, 1061-1089.

RAGHAVA, R.; CADDELL, R. M.; YEH, G. S. Y. (1973). The macroscopic yield behaviour of polymers, J. Mat. Science, 8, 225-232.

VICENTINI, D. F. (2008). Análisis 3D elástico y 2D elastoplástico de una esquina bimaterial en uniones adhesivas, Universidad de Sevilla, MSc Thesis (in Spanish).

WILSON, C. D. (2002). A critical re-examination of classical metal plasticity. J. Appl. Mech., 69, 63 – 68.

Método de elementos discretos: compuestos laminados sometidos a impacto de baja velocidad

R.C. Hidalgo, E. V. González, P. Maimí, P. Badalló, J. Costa
(AMADE) Análisis y Materiales Avanzados para el Diseño Estructural
Escola Politècnica Superior. Universitat de Girona. España

RESUMEN

En el presente trabajo, se describe un modelo de elementos discretos en dos dimensiones para caracterizar la aparición y evolución del daño intralaminar en materiales compuestos laminados, sometidos a impactos de baja velocidad. El modelo considera capas de láminas multidireccionales que se discretizan usando una teselación de Voronoi. La respuesta elástica de las capas se ha idealizado utilizando un arreglo de vigas elásticas y una regla de interacción no lineal. Además, la disipación energética se describe a través de fuerzas disipativas normales y tangenciales. La simplicidad del modelo permite estudiar varios tipos de laminado, secuencias de apilamiento y efectos de tamaño finito, esclareciendo su interrelación con la aparición y la propagación del daño.

1. INTRODUCCIÓN

El estudio de la respuesta a impacto en estructuras laminadas de material compuesto es de especial interés para el diseño y evaluación de la resistencia al daño (Abrate 1998). Los eventos de impacto se pueden dar en cualquier momento de la vida de la estructura (fabricación, servicio y mantenimiento). En estructuras de compuesto, los impactos pueden crean daño interno que a menudo no se detecta por simple inspección visual. Este daño interno causa reducciones severas en la resistencia de la estructura y puede crecer bajo estados de carga.

En los últimos años, simulaciones numéricas de la respuesta a impacto se han realizado a diversas escalas. Actualmente se desarrollan modelos muy sofisticados de elementos finitos para el estudio de la evolución del daño intralaminar e interlamiar (Lopes et al 2009; González et al 2009; Miamí et al 2007). Sin embargo, estos algoritmos son numéricamente muy costosos y comúnmente no permiten describir la aparición y la evolución del daño a escala microscópica, así como su interrelación con la existencia de defectos locales, aleatoriamente distribuidos (Chakrabarti et. al. 1997).

2. MODELO

En este proyecto presentamos un modelo multicapas en 2D, el cual es una generalización de un modelo discreto del sólido deformable que fue desarrollado años atrás (Kun et. al. 1999 y D'addetta et. al. 2001). Siguiendo dicha aproximación el cuerpo sólido es discretizado en partículas independientes que interactúan entre si localmente. De esta manera, la estructura del sólido es descrita a través de polígonos convexos cuya configuración inicial se construye a través de una teselación aleatoria de Voronoi (Kun et. al 1999 y D'addetta et. al. 2001). Así, cada elemento se considera como una gran colección de átomos, que interactúan elásticamente entre ellas a escala mesoscópica.

El modelo describe el comportamiento elástico no lineal de los sólidos de la siguiente manera. Los polígonos son considerados como cuerpos rígidos no deformables. Sin embargo, cuando se presionan uno contra el otro pueden superponerse sin variar su forma, lo cual representa en cierta medida deformaciones locales. Por lo general, la superposición de polígonos está caracterizada por dos puntos de intersección que definen la línea de contacto. Con el fin de simular la fuerza elástica de contacto entre los granos se introduce una fuerza repulsiva proporcional al área superpuesta. Por otro lado la disipación es modelada a través de un término disipativo proporcional a la velocidad relativa v_{rel}, de las partículas en contacto. Finalmente, la dirección de la fuerza normal es elegida perpendicular a la línea de contacto de los polígonos, resultado

$$f_{ij}^{(n)} = E_n A - \gamma^{(n)} m_{eff} v_{rel}^{(n)}$$

donde E_n representa el modulo de elasticidad normal, A área de solapamiento, m_{eff} la masa efectiva y $\gamma^{(n)}$ es el coeficiente de disipación normal. Las partículas también experimentan una fuerza tangencial del tipo

$$f_{ij}^{(t)} = E_t\, \xi(t) - \gamma^{(t)} m_{eff} v_{rel}^{(t)}$$

donde E_t representa el modulo de elasticidad tangencial $\xi(t)$ es el desplazamiento tangencial relativo y $\gamma^{(t)}$ es el coeficiente de disipación tangencial. Aquí es importante remarcar que el cálculo de la fuerza tangencial es efectuado teniendo en cuenta el límite de Coulomb.

$$f_{ij}^{(t)} = \min\left(\left|f_{ij}^{(t)}\right|,\ \mu\left|f_{ij}^{(n)}\right|\right) \times sign\,[f_{ij}^{(t)}]$$

donde μ es el coeficiente de fricción estático.

Finalmente, para mantener el sólido en conjunto, es necesario introducir una fuerza de cohesión entre los polígonos vecinos. Con este fin introducimos un arreglo de vigas, ampliamente utilizadas en modelos de crecimiento defectos en sólidos (Herrmann et al 1990, Kun et. al 1999 y D'addetta et. al. 2001). De esta manera, los centros de masa de los polígonos vecinos están conectados por vigas elásticas, que ejercen una fuerza atractiva. Las vigas independientes pueden fracturarse y presentan límites de fractura aleatorios, lo cual describe la evolución del daño local.

En dos dimensiones, cada polígono presenta tres grados de libertad: las dos coordenadas posicionales de su centro de masa y el ángulo de rotación. El algoritmo calcula numéricamente la solución de ecuaciones de movimiento de cada una de las “partículas” que constituyen el sólido, para unas condiciones de contorno establecidas se resumen en:

$$\sum_{j=1}^{c} \vec{f}_{ij}^{(n)} + \vec{f}_{ij}^{(t)} = m_i\, \vec{a}_i$$

$$\sum_{j=1}^{c} \vec{R}_{ij} \times (\vec{f}_{ij}^{(n)} + \vec{f}_{ij}^{(t)}) = I_i\, \vec{\alpha}_i$$

Estas ecuaciones de movimiento son integradas usado un algoritmo predictor-corrector de quinto orden. Una descripción más detallada de este modelo puede encontrarse en (D'addetta et. al. 2001).

La simplicidad del modelo permite estudiar varios tipos de laminado, secuencias de apilamiento así como efectos de tamaño finito. Por simplicidad, en el presente trabajo presentamos resultados correspondientes a un sistema (0/X/0/0/X/0). La disposición angular de las capas X se estima con el factor $\alpha=E_x/E_f$, $(\alpha\leq 1)$ donde E_f representa el modulo de elasticidad de las capas en la dirección longitudinal a fibra (capa orientada en la dirección 0) y E_x el modulo de elasticidad de la capa orientada en la dirección X. De ese modo $a=1$ representa un composite laminado de capas unidireccionales (0/0/0/0/0/0) y $\alpha_m=E_f/E_m$ representa el caso límite (0/90/0/0/90/0) donde E_m cuantifica el modulo de elasticidad en la dirección transversal a la fibra. En lo adelante hemos asumido que $\alpha_m=E_m/E_f=0.1$

2. RESULTADOS PRELIMINARES

Hemos simulado el impacto a baja velocidad de un impactador sobre el laminado descrito anteriormente. Por simplicidad, hemos fijado la velocidad del impactador y sus dimensiones (v=10 m/s; d= 6 mm). El impactador interactúa con el laminado durante un tiempo τ, el cual caracteriza la energía adsorbida. El impacto se produce en la parte inferior, exactamente en el centro geométrico del laminado (Fig. 1).

Fig 1. La figura muestra el estado final de un laminado con dimensiones (350 × 30 mm) después de finalizado un impacto de τ=0.2 s. a) Ilustra resultados para un laminado con α=0.1 por su parte b) Ilustra el caso α=0.5, el modelo captura de forma cualitativa la evolución preferencial del daño debido a la discontinuidad de las propiedades elásticas.

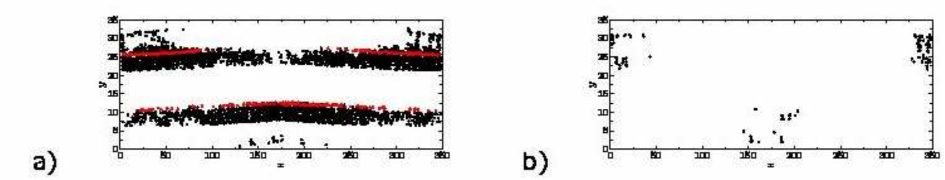

Fig 2. La figura muestra el estado final de un laminado con dimensiones (350 × 30 mm) después de finalizado un impacto de τ=0.2 s. a) Ilustra resultados para un laminado con α=0.1. Los símbolos negros caracterizan el daño, si se considera que el laminado posee una distribución homogénea de límites de rotura local (breaking thresholds). Por su parte, los símbolos rojos representan la localización del daño, cuando el límite de ruptura de la interfase es cuatro veces menor que la de las capas. b) Ilustra los restados obtenidos para α=0.5. La disminución daño es evidente.

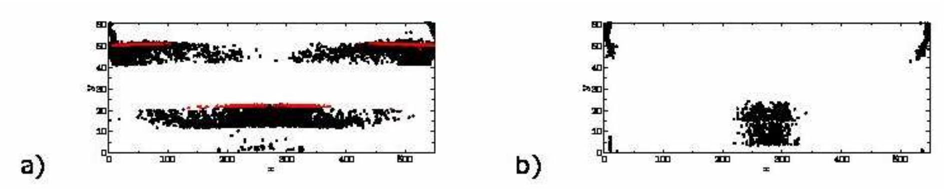

Fig 3. La figura muestra el estado final de un laminado con dimensiones (650 × 60 mm). En condiciones similares al presentado en la figura 2. Los resultados para el laminado asimétrico son muy similares, sin embargo efectos de tamaño son evidentes en el caso simétrico. La localización del daño sugiere que la influencia de factores inerciales es determinarte.

AGRADECIMIENTOS

Este trabajo ha sido financiado parcialmente por Ministerio de Ciencia e Innovación, proyectos (FIS2008-06034-C02-02, MAT2006-14159C02-01, TRA2006-15718-C02-01/-TAIR). E.V González agradece a la Generalitat de Catalunya y a los Fondos Sociales Europeos. R.C. Hidalgo agradece la financiación del Ministerio de Ciencia e Innovación a través del programa Ramón y Cajal.

REFERENCIAS

ABRATE, S. (1998). Impact on composite structures. *Cambridge University Press*, UK.
CHAKRABARTI, B. K. and BENGUIGUI, L. G., (1997) *Statistical Physics of Fracture and Breakdown in Disordered Systems*, Clarendon Press, Oxford
D'ADDETTA, G, KUN, F., RAMM, E., HERRMANN, H.J. (2001), From solids to granulates - discrete element simulations of fracture and fragmentation processes in geomaterials, in *Continuous and Discontinuous Modelling of Cohesive-Frictional Materials*, eds. P.A. Vermeer, et al., Springer Lecture Series in Physics 568, p.231-258
GONZÁLEZ, E.V., MAIMÍ, P., TURON, A., CAMANHO, P.P., RENART, J. (2009). Simulation of delamination by means of cohesive elements using an explicit finite element code. *Computers, Materials, & Continua (Tech Science Press)*, 9, 51-92.
LOPES, C.S., CAMANHO, P.P., GORDAL, Z., MIAMI, P., GONZÁLEZ, E.V. (2009). Low-velocity impact damage on dispersed stacking sequence laminates: Part II: Numerical simulations. *Composites Science and Technology*, 69, 937-947.
KUN, K., D'ADDETTA G., HERRMANN H.J., RAMM E. (1999), Two-dimensional dynamic simulation of fracture and fragmentation of solids, *Comp. Ass. Mech. and Eng. Sci*. **6**, 385-402
MAIMÍ P., CAMANHO P.P., MAYUGO J.A., DÁVILA C.G. (2007), A continuum damage model for composite laminates. Part I: Constitutive model. *Mechanics of Materials*, 39 (10), 897-908.

Dynamical models for the low energy impact

A.B. Martínez, D. Arencón, O.O. Santana, J.I. Velasco
Centre Català del Plàstic. Universitat Politècnica de Catalunya
C/Colom 114, 08222 Terrassa, Spain
G. Xiang
Beijing Institute of Technology
5 South Zhongquanain Street , Haidian District, 100081 Beijing

ABSTRACT

In this work, a epoxy-fiber composite material has been impacted with a hemispheric dart in the flexion plate configuration. The geometry of the model is analyzed through a dynamic model non-conservative that considers both flexion and the local contact with the dart. The application of the model allows obtaining the force and energy where the failure takes place, as well as the value of the elastic modulus and rupture strain.

INTRODUCTION

The methods applied to predict the force–time evolution in a low-energy impact are, in general, derived from a simple spring–mass model [1]. This approach considers the material perfectly elastic and to behave in a conservative way. When working in high-energy conditions the energy losses are negligible with respect to the falling one; however, in low-energy arrangements these losses cannot be ignored. On the other hand, all materials are nonconservative to some degree, so an approach to its experimental behavior needs to include the deformation on plastic and viscoelastic phenomenon.
The specimen behavior during impact could be separated in two parts: the contact with the falling dart and the plate deflection. As shown in previous work [1], the contribution of the contact can be studied separately using a specific experimental set up and its corresponding mechanical model based on the Hertz law. The specimen deflection can be modeled with the theory of small deflection of plates. Although many published models for predicting the behavior of materials during low energy impacts in flexed plate configuration are conservative, i.e. they assume no energy loss, the dynamic response of materials in such conditions can never be considered fully elastic. Consequently, a better approach is founded by the non-conservative methods that are based on lumped mass-spring models, aim of the present work.

MATERIALS

The specific laminate material used in the experiments was M21E/IMA, supplied by Hexcel Company. It is a modified form of Hexcel's M21 epoxy thermoset resin that is currently used with a TorayT8oo carbon fibre on the A38o. M21E/IMA with resin and fibre both from Hecel exhibits improvements in damage tolerance over the basic M21 through the addition of thermoplastic resin. The stacking sequence is as follow:
[0/90]5S=[0/90/0/90/0/90/0/90/0/90/90/0/90/0/90/0/90/0/90/0]

EXPERIMENTAL PROCEDURE

Plate bending tests were performed using a striker mounted in a Ceast Dartvis apparatus with a 12.7 mm diameter hemispherical dart head. The different drop masses of 0.503 kg, 1.503 kg, 2.003 kg, 2.503 kg were used. The sample plates were simply supported on two different metallic rings of 30 mm and 39.75 mm internal radius R. Force vs time data was acquired for 5 ms at a scanning frequency of 1 MHz (1 million values per second). The impact energy of the device was modified either by a change in the drop height or in the total mass of the dart. In that situation the tested specimens could not be damaged. So further low energy impacting tests were performed in a different tower using a striker with a 20 mm diameter hemispherical dart head. The drop mass of striker was 3.607 kg. In this situation, the tested specimens will be sure to be damaged.

THEORETICAL MODEL

The transversal collision between a rigid striker and a specimen made of a uniform material with linear elastic behavior can be modeled by a mass-spring system. The bending-indentation model with the mass effective of specimen is shown in figure 1. If the plate mass is very small in front of the drop mass, then the spring can be considered mass less and the system is reduced to a single degree of freedom shown in figure 2.

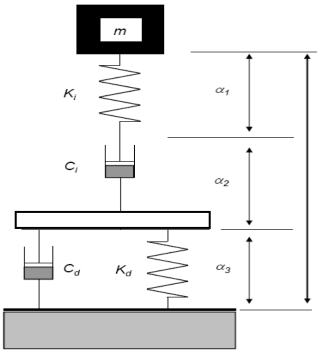

Fig. 1. Scheme of the lumped mass spring model with the mass effective specimen.

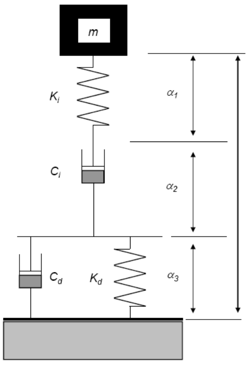

Fig. 2. Scheme of a single degree of freedom of lumped mass spring model.

Since almost all real systems are not conservative to a greater or lesser degree, a better approach can be expected by means of non-conservative systems. With this aim, two dashpots can be introduced into the conservative system, one in a serial disposition for the energy dissipation in the contact and another one in a parallel disposition for the energy dissipation during the plate deflection.
The system motion of flection-indentation model with the mass effective of specimen shown in figure 2 has been described [2,3].

RESULTS AND DISCUSSION

From the experimental tests, (Figure 3) we have observed the consistency of the model, as using 2 different masses, two indenters diameters and two support ring diameters the result of the elastic modulus was the same, 55 GPa.

From the plot of the maximum force vs initial velocity (Figure 4), a rupture load of 6662.38 N at an initial velocity of 2 m/s was obtained for the M21E/IMA material. The rupture stress of 850 MPa was obtained. The absorbed kinetic energy of 17.12 J was calculated for M21E/IMA material.

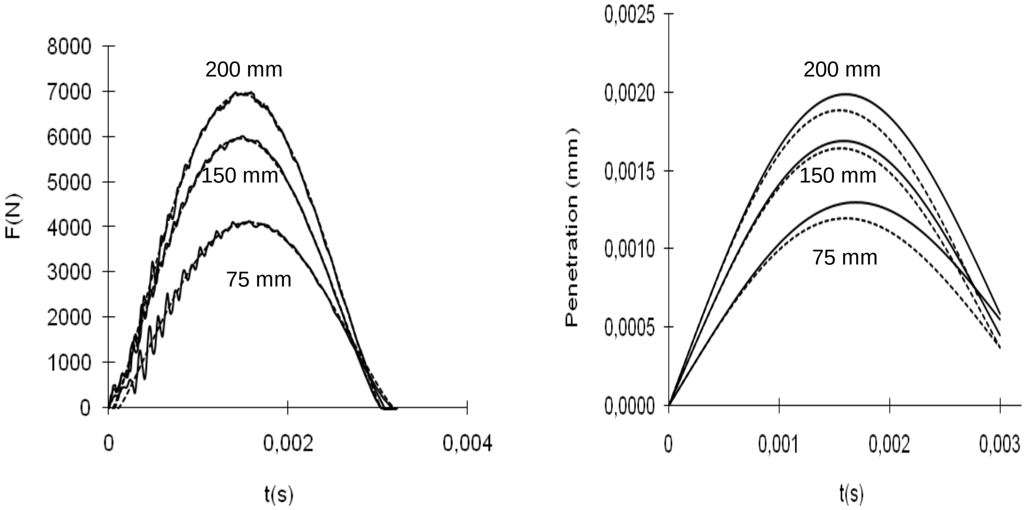

Fig. 3. Plots of (a) force vs time and (b) penetration vs time performed on the material at different impact heights. Continuous lines represents experimental record and dashed lines to the model prediction.

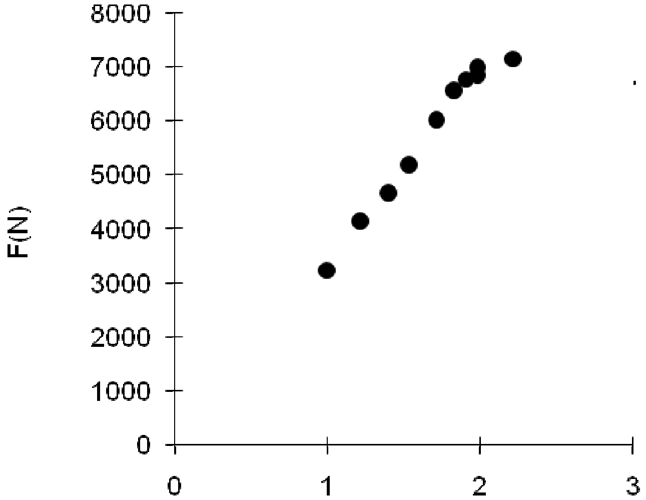

Fig. 4. Maximum load (F_m) versus striker v_0 for high energy impacts.

CONCLUSIONS

Low energy impact methods are very powerful tool to characterize materials material. Different models for predicting the contact duration, force, indentation and displacement under impact has been developed for impact a plate with a hemispherical indenter.
Comparisons between the different models predictions and the experimental results are in very good agreement. Comparison of the impact force history also shows good accord. Both tested materials showed nonconservative impact response and could be successfully modeled by the different models used in this work. Calculated numerical curves were in great agreement with registered experimental curves and values. The model is consistent as the change of the geometrical parameters gives identical results.
Using this method, rupture stress and elastic modulus could be readily obtained for M21E/IMA material. The impact behavior of M21E/IMA material was well characterized

REFERENCES

1. Jiménez O, Sullcahuaman JA, Sanchez-Soto M, Martinez AB. Low energy impact evaluation using non conservative models. Int J Solids Struct 2005;42:5758–64.
2. Martínez AB, Arnau J, Santana OO, Gordillo A. Impacto de plásticos: impacto de baja energía. Información Tecnolo´gica 1994;5: 19–24.

Modelling matrix cracking in composite materials

S. Sadaba[1], C. Gonzalez[1,2], J. Llorca[1,2]
[1]Madrid Institute for Advanced Studies of Materials (IMDEA-Materials), Spain
[2]Department of Material Science, Civil Engineering, Polytechnic University of Madrid

SUMMARY

Simulation of failure of polymer matrix composites PMC's materials is particularly complex as different failure modes are observed depending on the loading direction and the stress state, including (intralaminar) ply damage and (interlaminar) ply delamination. Traditionally, most of the composite damage models have been developed following the continuum damage mechanics approach (CDM). Within this framework, the constitutive behavior of the cracked composite material, by the different failure modes considered, is homogenized using internal damage variables representing the actual crack density in the composite material. This framework is especially well suited when diffuse and homogeneous micro-cracking driven by external loads occurring at the ply level and the behavior of the composite material can be represented by a damaged homogeneous material. However, not fully understood limitations of CDM models arise when dealing with discrete matrix cracking at the ply level such as shear stress locking effects or the impossibility to represent adequately matrix cracking patterns following fiber directions. X-FEM formulations deal with discontinuities of the continuum media by using a local enrichment of displacement fields in a FEM discretization. This allows to capture solutions with pronounced non smooth characteristics such as for example physical cracks, interface cracks, etc. The work here presents an X-FEM implementation to deal with matrix cracking at the ply level in composite materials. The X-FEM formulation has been implemented within the commercial finite element code ABAQUS Explicit as a user element subroutine VUEL.

1. X-FEM FORMULATION

The Extended Finite Element Method is an extension of the standard Finite Element Method in which the conventional shape functions $N_i(x)$ are enriched by additional degrees of freedom representing a displacement discontinuity (Remmers 2006):

$$\bar{u}(\bar{x},t)=\sum_{i=1}^{Nnod} N_i(\bar{x})\cdot\left(\bar{u}_i(t)+H(\bar{x})\cdot\bar{q}_i(t)\right) \qquad (1)$$

where $\bar{u}(\bar{x},t)$ is the displacement field, $\bar{u}_i(t)$ the nodal displacement degrees of freedom, $H(\bar{x})$ a function representing a displacement jump at the discontinuity and $\bar{q}_i(t)$ the additional DOF's.

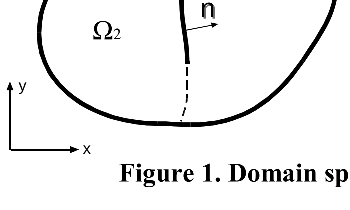

$$H(\bar{x})=\begin{cases}-1\,if\ \bar{x}\in\Omega_1\\+1\,if\ \bar{x}\in\Omega_2\end{cases} \qquad (2)$$

Figure 1. Domain split by a discontinuity.

Choosing the discontinuity function as a unit symmetric function (equation (2)), a linear combination of the standard and enriched functions can be used to simplify the implementation in a conventional FE code (Song et to. 2006), also known as the "phantom node" method:

$$\overline{u}_i^{e1} = \begin{cases} \overline{u}_i \; if \; node\, i \in \Omega_1 \\ \overline{u}_i - \overline{q}_i \; if \; node\, i \in \Omega_2 \end{cases} \qquad \overline{u}_i^{e2} = \begin{cases} \overline{u}_i - \overline{q}_i \; if \; node\, i \in \Omega_1 \\ \overline{u}_i \; if \; node\, i \in \Omega_2 \end{cases} \tag{3}$$

The resulting formulation consists of two superimposed standard finite elements e1 and e2 (with conventional formulation) with a coupling given by the discontinuity law. Special degrees of freedom including displacement and discontinuity DOF's are defined as "phantom nodes" and are not attached to the conventional mesh.

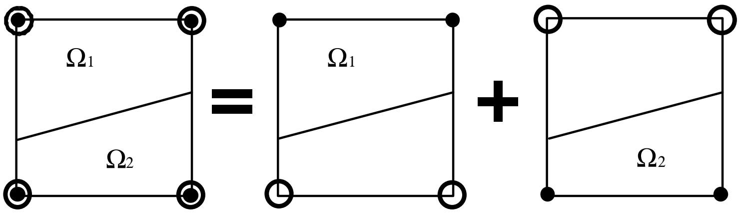

Figure 2. The extended element is split into two standard elements with reduced integration domain. Filled circles represent the standard nodes whereas hollow circles are "phantom nodes" representing the discontinuity.

The kinetic, internal and cohesive forces for both elements e=1,2 can be calculated as:

$$\begin{aligned} f_e^{kin} &= \int_{\Omega^e} N^T N \rho \, d\Omega_e \ddot{u} \\ f_e^{\text{int}} &= \int_{\Omega^e} (\nabla^S N)^T \sigma \, d\Omega_e \\ f_e^{coh} &= (-1)^e \cdot \int_{\Omega^e} N^T \overline{\tau}_C \cdot \overline{\mathbf{n}} \, d\Omega_e \\ f_e^{kin} + f_e^{\text{int}} + f_e^{coh} &= f_e^{ext} \end{aligned} \tag{4}$$

which should be consistent with the external forces acting on the element as in (4). Using this formulation instead of the original XFEM, the standard DOF inside the elements (filled circles) can be directly attached to a conventional FE mesh.

2. CASE STUDY

The material is considered as laminas of linear elastic orthotropic solids and a cohesive law is used for the discontinuity behaviour. A mixed-mode cohesive law using Turon's (2006) with the Benzeggagh-Kenane mixed-mode implementation is used for the interface. The relevant parameters are shown in Table 1.

E1 (GPa)	E_2 (GPa)	G_{12} (GPa)	ν_{12}
137	8.76	3.63	0.25

N (MPa)	G_I (J/m^2)
80	580

Table 1. Lamina elastic material properties (left) and interface properties (right).

A Double Cantilever Beam (DCB) test according to ASTM D5528 (1994) has been modelled as a plane-strain 2D specimen with stacking sequence $[0]_{18}$. An initial regular mesh with size 0.3 mm has been created in ABAQUS/Explicit and then a discontinuity along the interface between plies is placed with a preprocessing script. The elements split by the potential discontinuity are converted to user elements defined by a VUEL. The initial crack is modelled as a traction-free discontinuity inside the user elements.

The results were compared with the analytical solution given by the LEFM in the DCB specimen.

3. RESULTS & DISCUSSION

The specimen is loaded elastically until the point of maximum load is reached. After that point, the load decreases following the condition of LEFM in opening mode I for stable crack growth. Due to the fact that the cohesive stiffness changes dramatically at the onset of damage, high frequency oscillations among the mean value are observed. These oscillations increase with the penalty parameter, as observed in similar references using traditional cohesive elements (Elmarakbi et to. 2009).

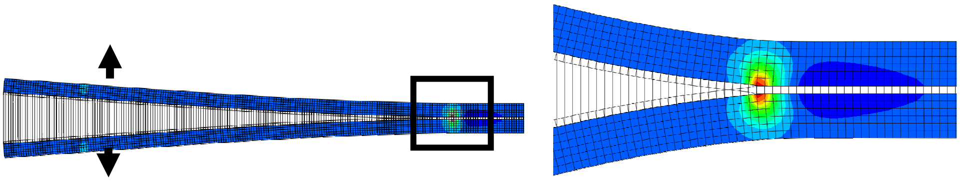

Figure 3. Double Cantilever Beam deformed shape (left) and detail of crack tip (right). Shape of superimposed user elements can be observed at the interface and open crack.

The crack mouth opening distance (CMOD) is plotted against the opening force in figure 4:

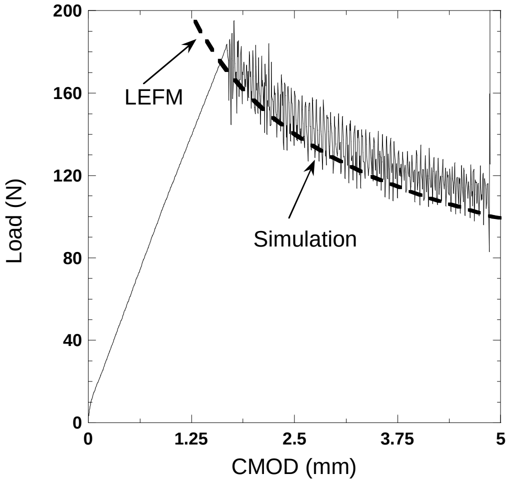

Figure 4. Comparison simulation results vs analytical predictions.

4. CONCLUSIONS

The developed X-FEM technique is able to model a discontinuity for a regular mesh regardless of the discontinuity position. The results agree with the theoretical predictions of the LEFM for the DCB test. Additionally, oscillations arise due to the formulation of the discontinuity behaviour, also appearing in traditional cohesive elements.

The main advantages of this technique with respect to traditional cohesive elements are the use of simplified mesh, the good scalability due to the architecture of the ABAQUS/Explicit scheme and the compatibility with the code.

ACKNOWLEDGMENT

This investigation was supported by the Ministerio de Eduación y Ciencia de España through the Grant MAT 2006-2602 and by the Comunidad de Madrid through the program ESTRUMAT-CM (reference MAT/0077).

REFERENCES

ASTM D5528 (1994) Standard Test Method for Mode I Interlaminar Fracture Toughness of Unidirectional Fiber-Reinforced Polymer Matrix Composites.

ELMARAKBI A.M., HU, N., FUKUNAGA H. (2009) Finite element simulation of delamination growth in composite materials using LS-DYNA. *Composites Science and Technology.* In press.

PINHO S.T., IANNUCCI L., ROBINSON P. (2006). Formulation and implementation of decohesion elements in an explicit finite element code. *Composites: Part A* 37: 778-789.

REMMERS J. (2006) Discontinuities in materials and structures. A unifying computational approach. *Ph D dissertation, Delft University of Technology*.

SONG, J-H, AREIAS, P.M.A, BELYTSCHKO, T (2006). A method for dynamic crack and shear band propagation with phantom nodes. *Int. J. Numer. Meth. Engng*, 67:868-893.

TURON A. (2006) Simulation of delamination in composites under quasi-static and fatigue loading using cohesive zone models, *Ph D dissertation, University of Girona*.

Análisis numérico de postpandeo de paneles rigidizados de material compuesto

J. Reinoso, A. Blázquez, F. París
Grupo de Elasticidad y Resistencia de Materiales. Escuela Técnica Superior de Ingenieros, Universidad de Sevilla, España

RESUMEN

Los paneles rigidizados están formados por una lámina o piel delgada a la que se unen rigidizadores para aportarle la rigidez necesaria. La presencia de elementos delgados hace que estos componentes sean muy sensibles a fenómenos de inestabilidad local de la piel. Aún así, estos elementos disponen de una capacidad portante (en ocasiones muy elevada) en régimen de postpandeo. Es por ello, que los criterios de diseño permiten sobrepasar la primera carga de pandeo en un cierto margen. El fallo global suele venir caracterizado por la aparición de despegues entre la piel y los rigidizadores, delaminaciones o fallos intralaminares (Starnes et al, 1985). Es claro que para aprovechar adecuadamente la capacidad resistente de estos elementos en régimen de postpandeo, se requiere un conocimiento adecuado del comportamiento de los mismos, lo que conlleva incluir en el análisis no linealidades geométricas (grandes desplazamientos y deformaciones). Existen numerosas publicaciones en las que se analiza el comportamiento en postpandeo de paneles rigidizados ante cargas de compresión o cizalladura, pero son escasos los análisis sobre paneles sometidos a presión (Romeo y Frulla, 1995). En este trabajo se llevan a cabo simulaciones computacionales sobre el comportamiento en régimen de post-pandeo de un panel cilíndrico con dos rigidizadores con sección transversal en forma de Ω, sometido a una presión uniforme sobre una de las caras del espécimen, considerando los efectos de la introducción imperfecciones geométricas adicionales en la geometría de la estructura que suelen ser comunes en este tipo de paneles. El análisis se realiza con el programa de Elementos Finitos ABAQUS/Standard, empleando elementos lineales tipo lámina de integración reducida para la discretización de la estructura.

1. INTRODUCCIÓN

En el estudio del comportamiento de paneles rigidizados en régimen de postpandeo habitualmente se tienen en consideración numeroso factores que afectan a la respuesta estructural como son el número de rigidizadores, sus posiciones, sección transversal, etc. Sin embargo, en ese tipo de elementos tan esbeltos existen ciertas desviaciones de la geometría del panel que influirán de forma relevante en la evolución del componente [2]. Es por ello que en este trabajo se muestra la importancia de la cuantía y orientación de estas imperfecciones en la evolución en postpandeo para un panel genérico.

2. CARACTERIZACIÓN DEl PANEL RIGIDIZADO

La geometría general del panel considerado es la mostrada en la Figura 1. Se trata de un panel curvo, con radio de curvatura 1950 mm, longitud de arco 2500 mm y ancho 1020 mm, rigidizado con dos largueros dispuestos circunferencialmente y simétricos, siguiendo la curvatura. La distancia entre rigidizadores considerada será de 600 mm.

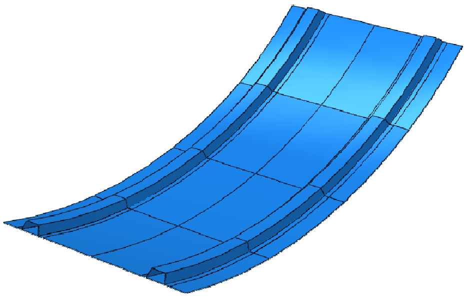

Fig. 1. Tipología de panel rigidizado analizado.

Las propiedades de los materiales empleados para la fabricación de los materiales son recogidos en la Tabla.1, mientras que las secuencias de apilado para cada una de las zonas del panel se muestra en la Tabla.2.

Propiedad	**Cinta**	**Tejido**
Módulo elástico en dirección de la fibra E_1 (Pa)	122 10^9	61 10^9
Módulo elástico en dirección transversal a la fibra E_2 (Pa)	8.5 10^9	61 10^9
Módulo elástico tangencial en el plano G_{12} (Pa)	3.4 10^9	2.2 10^9
Módulo elástico tangencial en el plano G_{13} (Pa)	3.4 10^9	2.2 10^9
Módulo elástico tangencial fuera del plano G_{23} (Pa)	2.2 10^9	1.5 10^9
Coeficiente de Poisson en el plano de la lámina ν_{12}	0.3	0.05

Tabla 1. Propiedades mecánicas de los materiales.

Zona	**Material**	**Nº Telas**	**Laminado**	**e (mm)**
Cabeza de Ω	Cinta (capas a 90º) Tejido (capas a 0º&45º)	7	(45/90/90/0/90/90/45)	1.576
Alma de Ω	Tejido	3	(45/0/45)	0.84
Piel	Cinta	7	(90/45/-45/0/-45/45/90)	1.288

Tabla 2. Composición del material utilizado (0º la circunferencial del panel).

Por otro lado, la forma de solicitación de los componentes se realiza mediante una carga de presión uniformemente distribuida sobre la superficie de la piel, siendo las condiciones de contorno en los bordes de los paneles de empotramiento, es decir, impidiendo desplazamientos y giros. Se considerarán la existencia de imperfecciones geométricas en la estructura. Estas imperfecciones son tenidas en cuenta computacionalmente mediante una combinación lineal de los primeros modos de pandeo del panel. La cuantía y signo de las imperfecciones consideradas quedan recogidos en la Tabla 3.

Panel	Modos	Cuantía	Signo
P0	Ninguno		
P2+	2 primeros	0.0001	+
P2-	2 primeros	0.0001	-
P5+	5 primeros	0.00001	+
P5-	5 primeros	0.00001	-
P10+	10 primeros	0.00001	+
P10-	10 primeros	0.00001	-

Tabla 3. Cuantía y signo de las imperfecciones consideradas en el panel.

3. RESULTADOS

Los resultados numéricos de las simulaciones del panel se recogen en la Figura 2. En ésta se representa la envolvente de desplazamientos radiales máximos, u_r, en valor absoluto de los nodos centrales del panel (que son los más desfavorables) frente a la carga de presión. En esta figura, además se tiene en cuenta la variabilidad de las magnitudes de las imperfecciones geométricas introducidas.

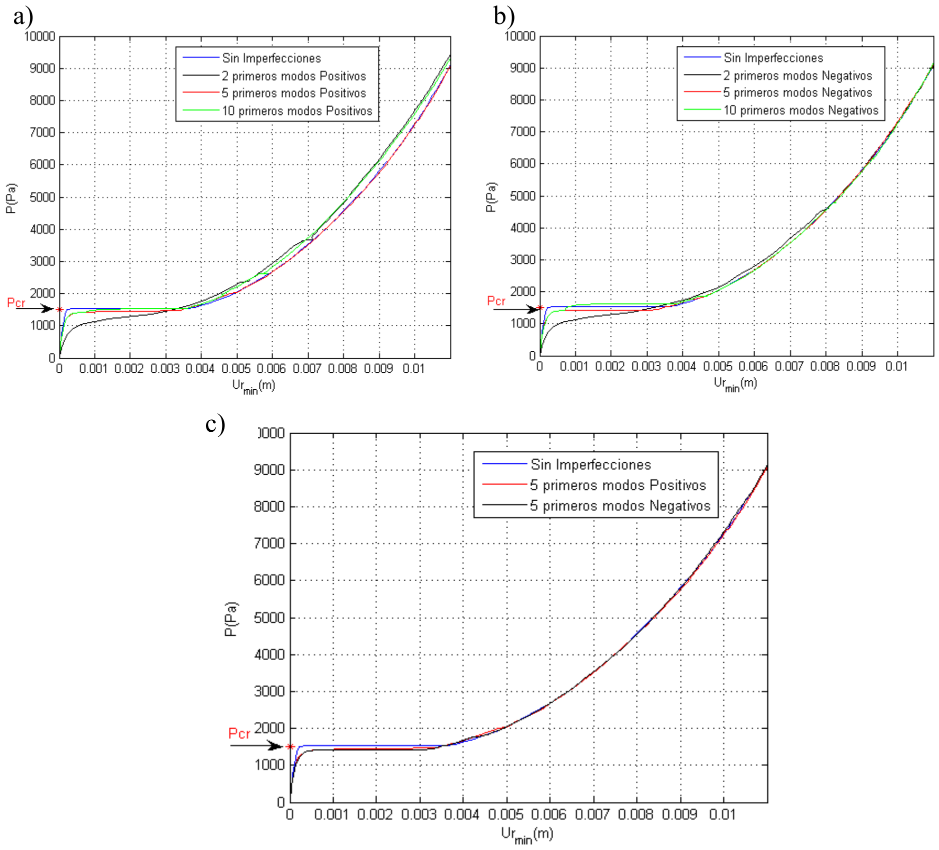

Fig. 2. Comparación de las evoluciones de la envolvente de u_r para los casos (a) P0, P2+, P5+ y P10+, (b) P0, P2–, P5– y P10–, y (c) P0, P5+ y P5–.

Las deformadas asociadas a la evolución del panel en postpandeo con las imperfecciones consideradas se recogen en la Figura 3, para una carga de 20000 Pa.

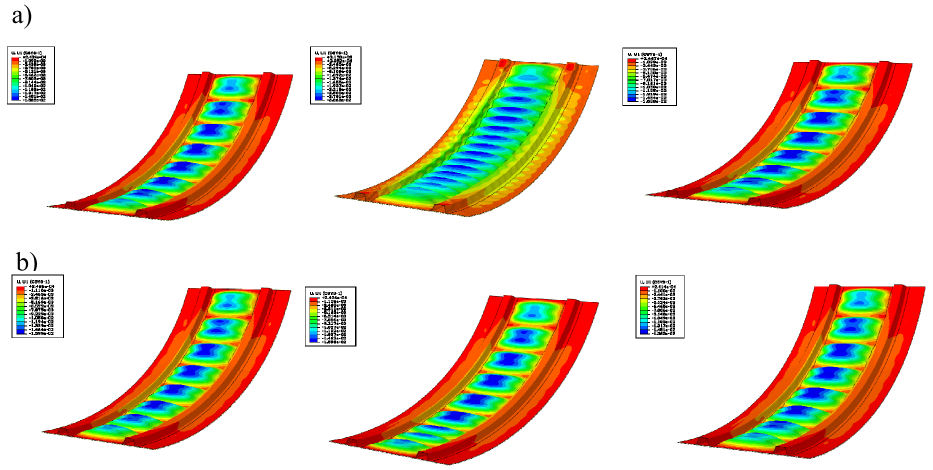

Fig. 3. Deformada para los casos (a) P2+, P5+ y P10+ respectivamente, y (b) P2–, P5– y P10– respectivamente.

4. CONCLUSIONES

Analizando los resultados expuestos, puede concluirse que las imperfecciones geométricas presentes en el panel juegan un papel determinante en la evolución en postpandeo de éste. Ello es debido a que éstas hacen que preponderen la activación unos modos de pandeo frente a otros con lo que la deformada del componente sufrirá variaciones. Debido a ésto, es recomendable efectuar una revisión pormenorizada de las posibles desviaciones existentes en la geometría del panel con el fin de poder realizar simulaciones numéricas más ajustadas a la realidad. Por todo ello se pone de manifiesto la existencia de una amplia variabilidad en los resultados derivados de los cálculos si fueran tenidas en cuenta combinaciones adicionales de entre modos de pandeo.

AGRADECIMIENTOS

Los autores desean agradecer la financiación de este trabajo por los proyectos P06-TEP-02045 de la Junta de Andalucía

REFERENCIAS

FALZON, B.G., STEVEN, G.P. (1997) “Buckling mode transition in hat-stiffened composite panels loaded in uniaxial compression”. *Composite Structures*, **37** (2), pp. 253-267.

ROMEO, G., FRULLA, G. (1995) “Nonlinear analysis of graphite/epoxy wing boxes under pure bending including lateral pressure”. *Journal of Aircraft*, **32** (6), pp. 1375-1381.

STARNES JR., J.H., KNIGHT JR., N.F., ROUSE, M. (1985) “Postbuckling behavior of selected flat stiffened graphite-epoxy panels loaded in compression”. *AIAA Journal*, **23** (8), pp. 1236-1246.

STEVENS, K.A., RICCI, R., DAVIES, G.A.O. (1995) “Buckling and postbuckling of composite structures”. *Composites*, **26** (3), pp. 189-199.

In-plane impact behaviour of CFRP laminates. Experimental and FEM results using inter and intra-lamina progressive damage models

E. Pajares
Airborne Composites SL', Parque Científico i Tecnológico de la Universitat de Girona,
E.V. Gonzalez, J.A. Mayugo, J. Costa
Analisis de Materiales Avanzados y Diseño Estructural (AMADE). Universitat de Girona, España.

SUMMARY

To improve the damage tolerance of composite structures, the out-of-plane impact loads such as those resulting from lateral impact by foreign objects are extensively studied. However, the in-plane impact is not deeply investigated because it is not a typical loading case. The aim of the work is to predict the global behaviour of the structure, in order to save manufacturing costs and experimental testing efforts in advanced structures required for future projects. This paper presents a study of the in-plane low velocity impact damage of composite plates. Both impact experimental tests and numerical simulations using intralaminar and interlaminar progressive damage models have been used. Finally, a correlation between experimental and FEM tests is presented.

1. INTRODUCTION

The in-plane impact is not deeply investigated because it is not a typical loading case. Experimental test using the drop tower to impact thick CFRP plates and FEM simulations using advanced constitutive models to understand the behaviour of the material are used. The goal of this work is to compare and correlate the obtained results.

2. EXPERIMENTAL TESTS

In-plane impact tests have been conducted using two different lay-ups. The same material is used for both transversally isotropic lay-ups, whose configurations are [0/90/45/-45]3s (samples A) and [0/60/-60]4s (samples B). CFRP unidirectional material (K63712/MTM49) is used.

Impact tests have been performed using the drop-weight tower from the Faculty of Aeronautics at TU Delft. The impact average speed is 10m/s and the impactor mass is 1.055Kg. To assure the in-plane impact, a cylindrical nose with 30mm of diameter and 40mm length has been used. The dimensions of the CFRP specimen are 87x87mm, and the thickness is 9.6mm. The impact velocity is determined using infrared sensors and measuring the time it takes for the impactor to travel a predetermined distance. The time required for the impactor to travel this distance is measured by a counter which is triggered when the impactor passes through the infrared sensors. The average velocity is derived from this data. Using a data reduction method, the displacement and the impact energy are also calculated. Newton’s law of motion is applied to calculate the acceleration. The velocity and the displacement are obtained by means of integration.

Figure 1 shows a typical force-displacement chart obtained from several performed test.

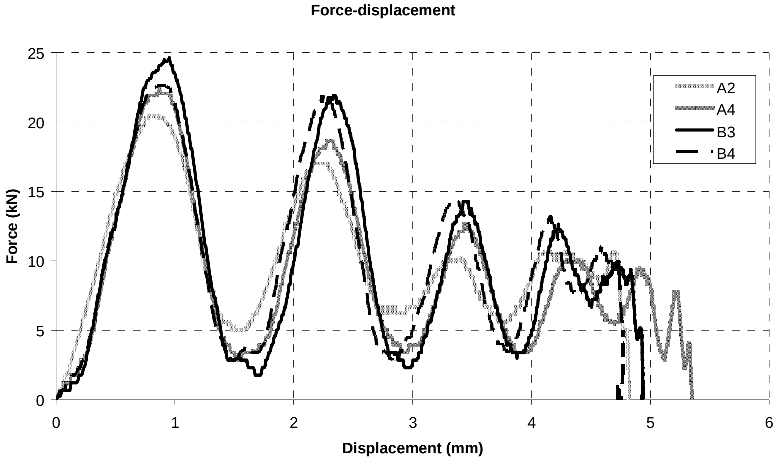

Fig. 1. Force- displacement chart obtained from several test data

3. FE MODELS

FE models have been implemented in explicit finite elements code in order to simulate the impact conditions during the tests. Two different specific formulations have been used for the behaviour of the material: intraply and interply continuum damage models. The intraply damage behaviour model has been developed by Maimí et al (2007) and it is capable to simulate the onset of intraply damage using the LaRC04 failure criteria for the prediction of the fibre breakage and matrix cracking. The model is also capable to simulate the material degradation (reduction of the elastic properties) due to damage growth. On the other hand, an interply damage model developed by Turon et al (2006) that can predict the onset and evolution of the interface material behaviour between the different layers has been used. The physical progressive failure behaviour of fibres, matrix and interfaces is taken into account with the use of these advanced formulations. These special formulations are implemented in ABAQUS software via user subroutines and input file. Because the analysis is expected to be a high non-linear problem, ABAQUS/EXLICIT time integration method is used.

The interface between the different layers is simulated by means of a resin rich thin layer with specific material properties. This cohesive region is controlled by the bilinear cohesive constitutive relation that controls the opening of the cohesive elements.

The FE analysis model contains two different bodies: the impactor and the composite plate. The steel impactor (30mm diameter and 40mm length) is modelled as a rigid body with C3D8R elements. The entire impactor spear mass (1’055 kg) is reduced to a cylinder volume, so the fictitious density for the analysis is modified to 37’136·10^6 kg/m^3. The plate is composed by two different materials: the composite itself and the interface material, both with different properties and material formulation as described. The selected element type is C3D8R again. The thickness for the layers of composite material is 0.388mm and 0.012mm for the interface layers. The length of the elements close to the impact area is approximately 0.9mm. This length is increased in the areas where the delaminations or damage are not expected to be critical.

Several modelling techniques have been taken into account to simulate the test and to get improved results: contact, damping, element deletion and mass scaling. The aim of using the deleting elements technique, damping and mass scaling is to increase the stable time increment and reduce the computational time. It depends directly on the density of the material and is determined by the most distorted element. The contact algorithm is necessary to simulate the contact between the impactor and the plate but also from the new created surfaces that appear when deleting fully damaged elements (both composite and cohesive material elements) from the plate. The mass scaling option is used for the severe damaged elements with a maximum total change of 3% of the mass.

4. RESULTS

The comparison between experimental and numerical results is shown in Figure 2 in a force-displacement chart.

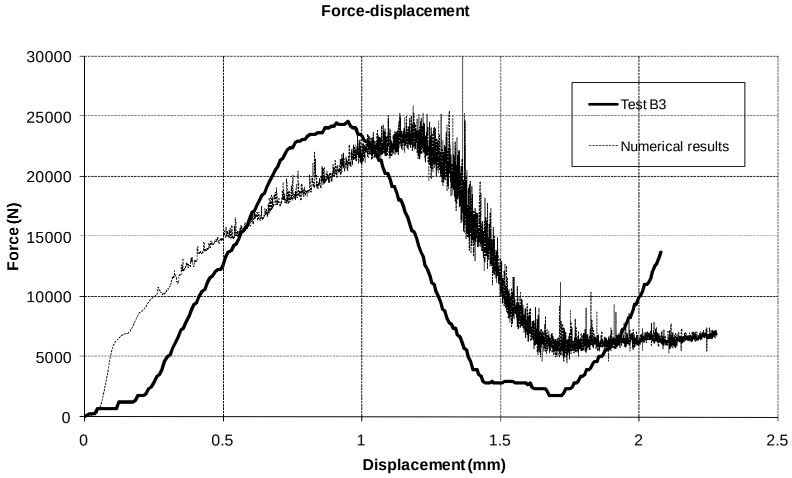

Fig. 2. Force-displacement chat. Experimental vs numerical results.

Force-displacement relation does not fully agree at the first load ramp, but the maximum expected force obtained with the numerical simulations agrees with test results. Moreover, many oscilations occur when the delaminations starts and the elements are distorted, this phenomenon takes place at high loads. The model is not yet capable to simulate the rebounds observed in the tests and the maximum impactor displacement is not calculated accurately.

Graphical results for an impacted plate are shown in Figure 3. The tested sample shows a big amount of delaminations, fibre breakage and matrix cracking at the impacted zone and surrounding areas. The FEM contour plot represents the matrix damaged area and the delaminations that occur at the impact and surrounding areas, which are in agreement with the experimental result. Specially, the delaminations in the external 0° layers can be observed.

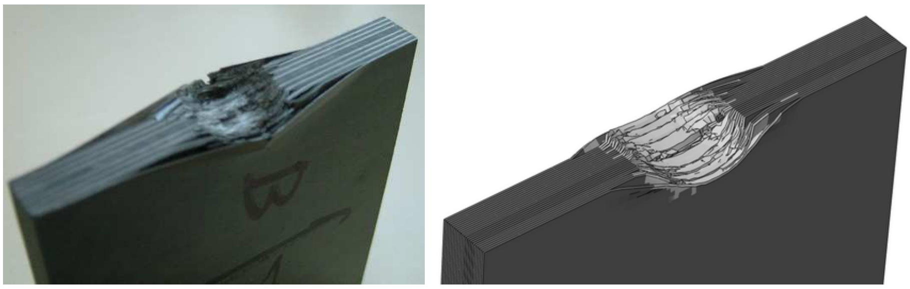

Fig. 3. Tested sample and numerical output of the matrix damage variable.

5. CONCLUSIONS AND FUTURE WORK

The results obtained from the test are well correlated; it indicates that acceptable results have been achieved at the impact tower. On the other hand, the use of the advanced continuum damage model for the composite material and the use of advanced cohesive formulation for the interface elements offers good correlations for the maximum force, delaminations and impact footprint when the first rebound of the force takes place. Following rebounds can not be simulated with the current model.

Future work will improve the current model by means of: include penalty stiffness and friction for the contact bodies and eroding surfaces, improve the element deletion control, add the geometry for the fixture and verify the energy balanced and correlation in order to capture the impact behaviour and correlated the rebounds, force and displacements obtained in the tests.

6. REFERENCES

E. González, P. Maimí, A. Turon, P. Camanho, J. Renart. (2009) Simulation of delamination by means of cohesive elements using a finite explicit element code. *Computers, Materials and Continua, vol. 9, no.1, pp. 51-92.*

P. Maimí, P. Camanho, J. Mayugo, C. Dávila. (2007) A continuum damage model for composite laminates – part i: Constitutive model, *Mechanics of Materials*, 39, 897-908.

P. Maimí, P. Camanho, J. Mayugo, C. Dávila. (2007) A continuum damage model for composite laminates – part i: Constitutive model, *Mechanics of Materials*, 39, 897-908.

A. Turon, P. Camanho, J. Costa, C. Dávila. (2006) A damage model for the simulation of delamination in advanced composites under variable-mode loading, Mechanics of Materials, 38, 1072-1089.

Tension dominated inter-fibre failure under bi-directional loads. Micromechanical approach

E. Correa, F. París, V. Mantič
Grupo de Elasticidad y Resistencia de Materiales. Mecánica de Medios Continuos,
Teoría de Estructuras e Ingeniería del Terreno. Escuela Superior de Ingenieros,
Universidad de Sevilla, España

ABSTRACT

The growth of interface cracks corresponding to tension dominated inter-fibre failure under bi-directional loads is studied. The Boundary Element Method is employed for the analysis of the fracture process and the results evaluated by means of Interfacial Fracture Mechanics. The conclusions of the numerical analysis contribute to clarify the failure onset.

1. INTRODUCTION

The inter-fibre failure under uniaxial tension has already been the objective of several studies by the authors, París et al. (2007). These studies allowed the first stages of the mechanism of damage at micromechanical level to be identified, showing that it starts with the appearance of small debonds at the fibre-matrix interfaces. The initial defects grow unstably and symmetrically along the interfaces (interface cracks). This period ends when these cracks have reached a certain length at the interface coinciding with the appearance of a physically relevant contact zone at the tip. From that moment on the growth of the interface cracks becomes stable, which favours the occurrence of the kinking towards the matrix. The coalescence between different cracks in the matrix leads to the final macro-failure.

Many of the existing proposals for the prediction of the inter-fibre failure at lamina level are based on the hypothesis that the failure taking place at a plane is governed by the components of the stress vector associated to that plane. In the present work this assumption is revised for the tension dominated inter-fibre failure by means of a single-fibre Boundary Element model, Fig. 1, using the same bi-material system employed in París et al. (2007). An analysis of the influence of an out of failure plane stress component (tension or compression) on the generation of the damage dominated by a transverse tension is carried out. Several aspects of this problem have already been analysed by the authors in París et al. (2003). Interfacial Fracture Mechanics has been used to analyse the numerical results.

2. ORIGIN OF FAILURE

The presence of an external secondary load, σ_{33}, acting at the same time as σ_{22} could alter the origin of the failure and, thus, the development of the interface crack. The initiation of the failure at the interface has been considered in this work to be controlled by the σ_{rr} distribution, Goodier (1933), at the undamaged interface, as was already done in París et al. (2007). Then it is fundamental to analyse the influence that the different levels of σ_{33} have on σ_{rr} of the undamaged interface. Three different values of n coefficient have been considered: 0, 0.5 and 1. Based on this the notation employed to distinguish between the different bi-directional cases follows the scheme: T-*n*C and T-*n*T (T=tension, C=compression).

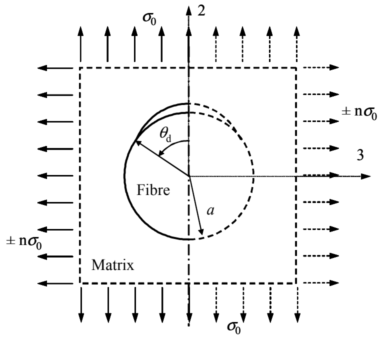

Fig. 1. Single fibre BEM model.

Curves presented in Fig. 2a (T-*n*C case) show that the presence of σ_{33} does not qualitatively alter the distribution of σ_{rr} at the interface. Quantitatively, and with reference to the T-0 case, compressive σ_{rr} significantly increases as σ_{33} does, whereas maximum tensile σ_{rr} increases only slightly. Referring to the T-*n*T case, Fig. 2b, the σ_{rr} level at the interface is maintained with reference to the T-0 case though presenting some qualitative alterations, consisting in an increase of the σ_{rr} level in those interfacial points that were less stressed in the unidirectional case. Thus the tendency generated is to level the σ_{rr} state between all interfacial points, as is shown in the limit case T-T.

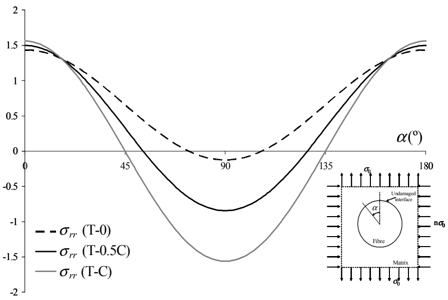

Fig. 2a. σ_{rr} distribution. (T-*n*C case).

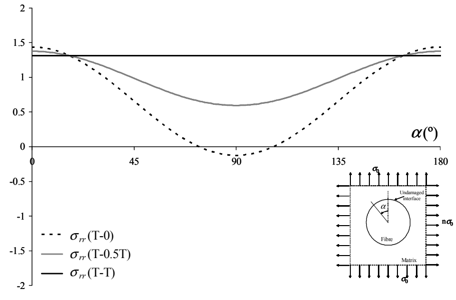

Fig. 2b. σ_{rr} distribution. (T-*n*T case).

Based on the former evidence, an initial debond at the interface of 10º length centred in axis 2 (position at which σ_{rr} is maximum) will be assumed for the study of the growth of the interface crack, both for the T-*n*C case and the T-*n*T case.

3. INTERFACIAL GROWTH

The evolution of the first debond at the interface is studied by means of the BEM model (París and Cañas (1997), Graciani (2006)), shown in Fig. 1a and its growth evaluated in terms of the Energy Release Rate, G (Irwin (1957)).

3.1 Tension-compression biaxial case

The results obtained show that the presence of $\sigma_{33} < 0$ does not qualitatively alter the evolution of G versus θ_d, though it is found that its level increases as $\sigma_{33} < 0$ does, which means that the load level required for crack propagation is lower.

The prediction of growth of the interface crack is made by comparing G with its corresponding critical value, G_c, Hutchinson and Suo (1992). G - G_c comparisons for the cases T-0 and T-C (taken as representative of all T-*n*C cases) are plotted in Fig. 3. A value of 0.2 has been chosen for λ and G_{1c} has been taken as the value that makes G and G_c coincide for the first debonding angle, $\theta_d = 10^\circ$ in this case. This criterion for the election of G_{1c} can be implemented once a scaled representation of the G curves, that makes all curves to coincide at $\theta_d = 10^\circ$, has been considered.

The results shown in Fig. 3 predict an unstable growth of the interface crack that reaches lower debonding angles as the presence of $\sigma_{33} < 0$ increases, though the value of σ_0 needed for the initiation of the crack growth is lower as the presence of σ_{33} increases, which means that the presence of a compression superimposed on the tension nominally responsible for the failure accelerates the failure.

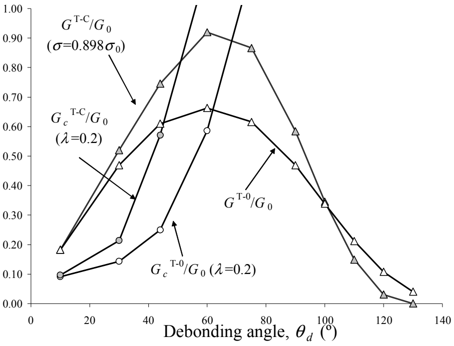

Fig. 3. *G*-*G_c* comparison. (T-*n*C case).

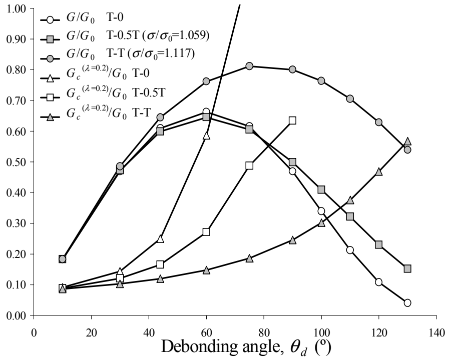

Fig. 4. *G*-*G_c* comparison. (T-*n*T case).

3.2 Tension-tension biaxial case

The results obtained for this case show that the presence of $\sigma_{33} > 0$ does not significantly alters the G level obtained in the T-0 case, though a translation of the position of the maxima has been detected. It can also be deduced that the propagation of the initial debond requires a slightly higher level of the external load as *n* increases. G and G_c curves associated to T-*n*T cases corresponding to *n*=0,0.5 and 1 are represented together in Fig. 4, having used the same scaled representation as in the T-*n*C case (Fig. 3). The results obtained predict an unstable growth of the interface crack that extends towards larger debonding angles as the presence of $\sigma_{33} > 0$ increases, though the amount of load required for the initiation of growth is also greater as this presence increases. For the T-T limit case this tendency could lead to a particularly large extension of the crack at the interface that, in conjunction with the special morphology of the crack detected in this case (consisting in the opening of the previously developed contact zone near the tip), would impede the kinking of the crack towards the matrix.

3. CONCLUSIONS

The first stages of the development of the tension dominated inter-fibre failure under bidirectional loads have been studied by means of a single fibre BEM model. A secondary external load has been considered to act simultaneously with the tension nominally responsible for the failure, and both cases (tension and compression) have been analysed. The results obtained show that the presence of a secondary load could alter several aspects of the stages already detected for the tension uniaxial case leading then to the conclusion that the presence of an out plane stress component could affect the development of the failure.

ACKNOWLEDGEMENTS

This work was supported by the Spanish Ministry of Education and Science (Project TRA2006 08077) and Junta de Andalucía (Projects of Excellence TEP-02045 and TEP-04051).

REFERENCES

GOODIER, J.N. (1933). Concentration of stress around spherical and cylindrical inclusions and flaws. *Applied Mechanics,*55(7), 39-44.

GRACIANI, E. (2006). Formulación e implementación del método de los elementos de contorno para problemas axisimétricos con contacto. Aplicación a la caracterización de la interfase fibra matriz en materiales compuestos, *PhD Thesis*. University of Seville.

HUTCHINSON, J.W., SUO, Z. (1992). Mixed mode cracking in layered materials, *Advanced Applied Mechanics*, 29, 63-191.

IRWIN, G.R. (1957). Analysis of stresses and strain near the end of a crack transversing a plate. *Journal of Applied Mechanics*, 24, 361-364.

PARÍS, F., CAÑAS, J. (1997). Boundary Element Method. Fundamentals and Applications. Oxford, OUP.

PARÍS, F., CORREA, CAÑAS, J. (2003). Micromechanical view of failure of the matrix in fibrous composite materials. *Composites Science and Technology*, 63, 1041-1052.

PARÍS, F., CORREA, E. MANTIČ, V (2007). Kinking of transverse interface cracks between fibre and matrix. *Journal of Applied Mechanics*, 74(4), 703-716.

Una nueva aproximación para el análisis de laminados multidireccionales con geometría de tira

F. Mujika
Grupo 'Materiales + Tecnologías', Departamento Ingeniería Mecánica, Escuela
Politécnica. Universidad del País Vasco/Euskal Herriko Unibertsitatea

RESUMEN

Se propone una nueva aproximación para el análisis de laminados compuestos multidireccionales con geometría de tira, denominada Teoría de Tiras Laminadas (TTL). La configuración geométrica de tira es la que se utiliza en los ensayos mecánicos. Habitualmente se utiliza la Teoría Clásica de Placas Laminadas (TCPL) imponiendo las condiciones de que los momentos y fuerzas por unidad de longitud son nulos en los bordes longitudinales de la probeta. En el caso general de un laminado multidireccional, de acuerdo con tal hipótesis, existen estados de tensiones no nulos que proporcionan resultante y momento resultante nulos. Se considera más adecuado realizar la hipótesis de que sean nulas las tensiones en los bordes longitudinales y a lo largo del ancho de la tira. La consecuencia inmediata es la obtención de nuevos coeficientes de rigidez reducidos de cada lámina y la subsiguiente modificación de los coeficientes de rigidez del laminado.

1. INTRODUCCIÓN

En los ensayos de tracción y flexión, si los ejes de la probeta no son ejes principales de otrotropía aparecen fuerzas y momentos debido a los efectos de acoplamiento en los extremos (Pagano et al. 1968, Mujika et al. 2003). La Fig. 1(a) muestra las fuerzas y momentos en un ensayo de tracción cuando se aplica una fuerza *P*. La Fig. 1(b) muestra las reacciones de los apoyos y la fuerza aplicada *P* en un ensayo de flexión de tres puntos. En este caso, se supone que el contacto entre la probeta y los apoyos está localizado en cuatro puntos. En ambos casos se considera un laminado multidireccional general, cuyo comportamiento puede incluir todos los efectos de acoplamiento.
Habitualmente, en los ensayos mecánicos se utilizan configuraciones de laminado que carecen de efectos de acoplamiento o éstos se consideran directamente despreciables a pesar de no estar cuantificados. Dado que las probetas utilizadas en los ensayos mecánicos tienen geometría de tira, el objetivo del presente trabajo es mostrar los aspectos principales de una nueva aproximación denominada Teoría de Tiras Laminadas (TTL) que permite obtener las incógnitas hiperestáticas que aparecen en la Fig. 1. Como consecuencia, las tensiones y desplazamientos causados por los efectos de acoplamiento pueden ser incluidos en la interpretación de resultados. Ello permite profundizar en la interpretación de resultados de los ensayos mecánicos de laminados multidireccionales incluyendo también los efectos higrotérmicos.

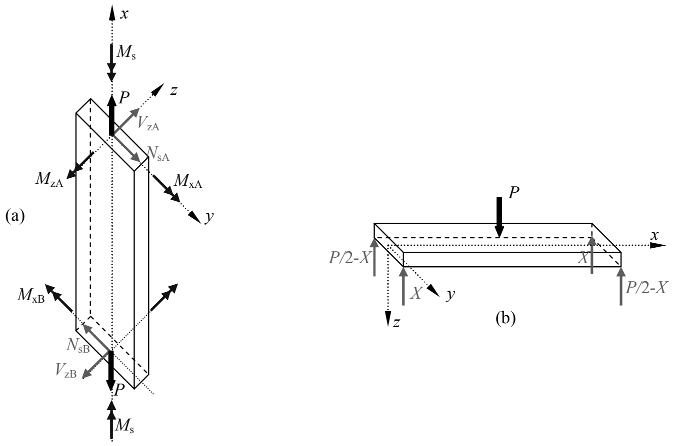

Fig. 1. Fuerzas y momentos en ensayos de tracción y flexión.

2. CAMPO DE DESPLAZMIENTOS

Se supone que el campo de desplazamientos viene dado por la superposición de otros dos, correspondientes a configuraciones plana y de canto, como sigue:

$$\begin{aligned} u(x,y,z) &= u_0(x) + z\varphi(x,y) + y\psi(x) \\ v(x,y,z) &= v_1(x) + y\eta(x) + (z - z_C)\theta(x) \\ w(x,y,z) &= w_0(x) - y\theta(x) \end{aligned} \tag{1}$$

φ y ψ son ángulos rotados respecto a los ejes y y z, respectivamente. θ es el ángulo de torsión y η es la deformación media en la dirección y. z_C es la posición del centro de torsión, localizado en el eje z.

3. CAMPO DE DEFORMACIONES

Utilizando primas para las derivadas con respecto a x de funciones que sólo dependen de x, la deformación normal ε_x en la dirección longitudinal de la tira y la deformación tangencial $\gamma_{xy} = \gamma_s$ en el plano xy son:

$$\begin{Bmatrix} \varepsilon_x \\ \gamma_s \end{Bmatrix} = \begin{Bmatrix} \varepsilon_x^0 \\ \gamma_s^0 \end{Bmatrix} + y \begin{Bmatrix} \kappa_z \\ \eta' \end{Bmatrix} + z \begin{Bmatrix} \kappa_x \\ \kappa_s \end{Bmatrix} = \begin{Bmatrix} \varepsilon_x^1 \\ \gamma_s^1 \end{Bmatrix} + z \begin{Bmatrix} \kappa_x \\ \kappa_s \end{Bmatrix} \tag{2}$$

$$\varepsilon_x^0 = u_0' \quad \gamma_s^0 = v_1' + \psi - z_C\theta' \quad \varepsilon_x^1 = \varepsilon_x^0 + y\kappa_z \quad \gamma_s^1 = \gamma_s^0 + y\eta'$$

donde

$$\kappa_x = \frac{\partial\varphi}{\partial x} \quad \kappa_s = \frac{\partial\varphi}{\partial y} + \theta' \quad \kappa_z = \psi'$$

El valor medio de la deformación tangencial fuera del plano $\bar{\gamma}_z$ es:

$$\bar{\gamma}_z(x,y) = \varphi(x,y) + w'_0 - y\theta' \qquad (3)$$

$\bar{\gamma}_z$ y φ se descomponen en partes simétrica y antisimétrica. Se supone que la parte simétrica está relacionada con la flexión (*b*) y que la parte antisimétrica está relacionada con la torsión (*t*). Además, se supone que los términos $\bar{\gamma}_z^b$ y φ^b son uniformes en el ancho de la tira y que φ^t no depende de *x*. Así, las curvaturas de flexión y torsión de (2) vienen dadas por:

$$\kappa_x = \frac{\partial \varphi^b}{\partial x} = \frac{\partial \bar{\gamma}_z^b}{\partial x} - w_0'' \qquad \kappa_s = \frac{\partial \varphi^t}{\partial y} + \theta' = \frac{\partial \bar{\gamma}_z^t}{\partial y} + 2\theta' \qquad (4)$$

Por otra parte, el valor medio de γ_s en el espesor es γ_s^0. El valor medio en la sección completa es:

$$\bar{\gamma}_s(x) = \psi + v_1' - z_C\theta' \qquad (5)$$

4. RELACIÓN TENSIÓN-DEFORMACIÓN

Se supone que $\sigma_y = 0$ y $\tau_{yz} = 0$. Teniendo en cuenta los efectos higrotérmicos dados por $e_i = \alpha_i \Delta T + \beta_i \Delta c$ la relación tensión-deformación en el plano del laminado viene dada por:

$$\begin{Bmatrix} \sigma_x \\ \tau_s \end{Bmatrix}_k = \begin{bmatrix} q_{xx} & q_{xs} \\ q_{xs} & q_{ss} \end{bmatrix}_k \left(\begin{Bmatrix} \varepsilon_x^1 \\ \gamma_s^1 \end{Bmatrix} + z \begin{Bmatrix} \kappa_x \\ \kappa_s \end{Bmatrix} - \begin{Bmatrix} e_x \\ e_s \end{Bmatrix}_k \right) \text{donde} \begin{bmatrix} q_{xx} & q_{xs} \\ q_{xs} & q_{ss} \end{bmatrix}_k = \begin{bmatrix} S_{xx} & S_{xs} \\ S_{xs} & S_{ss} \end{bmatrix}_k^{-1} \qquad (6)$$

La relación entre los coeficientes de rigidez reducidos q_{ij} and Q_{ij} es:

$$q_{xx} = Q_{xx} - \frac{Q_{xy}^2}{Q_{yy}} \qquad q_{xs} = Q_{xs} - \frac{Q_{xy}Q_{ys}}{Q_{yy}} \qquad q_{ss} = Q_{ss} - \frac{Q_{ys}^2}{Q_{yy}} \qquad (7)$$

Se puede apreciar que la diferencia entre los coeficientes es máxima para 45º. La relación fuera del plano viene dada por $\gamma_{zx} = S'_{55}\,\tau_{zx}$. Dado que se utilizarán valores medios a lo largo del espesor, las flexibilidades equivalentes correspondientes a la flexión y a la torsión se obtienen mediante principios energéticos.

5. FUERZAS Y MOMENTOS DE SECCIÓN

Tras integrar las tensiones en el espesor, se pueden obtener las fuerzas y momentos por unidad de longitud, incluyendo los efectos higrotérmicos. Integrando estas fuerzas y momentos a lo largo del ancho, se obtienen las fuerzas y momentos de sección. La relación que tienen éstas con las deformaciones y curvaturas son:

$$\begin{Bmatrix} \varepsilon_x^0 \\ \bar{\gamma}_s \\ \hdashline \kappa_x \\ \kappa_s^1 \end{Bmatrix} = \left[\begin{array}{cc:cc} f_{xx} & f_{xs} & g_{xx} & g_{xs} \\ f_{xs} & f_{ss}^1 & g_{sx} & g_{ss} \\ \hdashline g_{xx} & g_{sx} & h_{xx} & h_{xs} \\ g_{xs} & g_{ss} & h_{xs} & h_{ss} \end{array}\right] \frac{1}{b} \begin{Bmatrix} N_x^* \\ N_s^* \\ M_x^* \\ M_s^* \end{Bmatrix} \text{donde } \kappa_s^1 = 2\theta' + \frac{\bar{\gamma}_z^t(b_1)}{b_1} \qquad (8)$$

Las fuerzas y momentos con asterisco de (8) indican la suma de los correspondientes términos mecánicos e higrotérmicos. El coeficiente f_{ss} se modifica por f_{ss}^1 dado que se usan tensiones medias. Se obtienen las siguientes relaciones para el momento flector M_z:

$$M_z = \frac{b^3}{12}\left(a_{xx}\kappa_z + a_{xs}\eta'\right) \qquad \begin{Bmatrix} \kappa_z \\ \eta' \end{Bmatrix} = \frac{12}{b^3} \begin{bmatrix} f_{xx} & f_{xs} \\ f_{xs} & f_{ss} \end{bmatrix} \begin{Bmatrix} M_z \\ 0 \end{Bmatrix} \qquad (1)$$

6. OBTENCIÓN DE DESPLAZAMIENTOS Y TENSIONES

Suponiendo conocidas las fuerzas y momentos en la sección recta de la probeta, se pueden determinar las incógnitas hiperestáticas que aparecen en la Fig. 1 aplicando las condiciones de contorno correspondientes. Con ello, se obtienen los campos de tensiones y desplazamientos. Los resultados obtenidos con esta aproximación coinciden con los resultados obtenidos para los ensayos de tracción y flexión oblicua referidos en la introducción.

7. CONCLUSIONES

De acuerdo a TTL, los coeficientes de rigidez reducida varían con respecto a la TCPL. En consecuencia, existen diferencias en los resultados de tensión obtenidos según ambas aproximaciones. Las fuerzas y momentos hiperestáticos que aparecen en los ensayos de tracción y flexión de laminados multidireccionales pueden ser calculados de acuerdo al campo de desplazamientos de la TTL. Se pretende con ello profundizar en la interpretación de los ensayos mecánicos de configuraciones de laminados multidireccionales.

REFERENCIAS

PAGANO, N.J., HALPIN, J.C. (1968). Influence of End Constraint in the Testing of Anisotropic Bodies, *Journal of Composite Materials*, 2: 19-31.

MUJIKA F., MONDRAGON I., (2003). On the displacement field for unidirectional off-axis composites in 3-point flexure - Part 1: Analytical approach, *Journal of composite materials*, 37 (12): 1041-1066.

MUJIKA F., DE BENITO A., MONDRAGON I., (2003). On the displacement field for unidirectional off-axis composites in 3-point flexure - Part 2: Numerical and experimental results, *Journal of composite materials*, 37 (13): 1191-1217.

3D edge effects in adhesive CFRP-AL double-lap joints

A. Barroso, D. Vicentini, V. Mantič, F. París

Grupo de Elasticidad y Resistencia de Materiales, Universidad de Sevilla, España

ABSTRACT

2D numerical models of Carbon Fiber Reinforced Plastic and Aluminium (CFRP-AL) adhesively bonded double-lap joints are typically used instead of more computationally expensive 3D models. Although in most cases, a 2D stress state (generalized plane strain) can be assumed, it is well known that edge effects appear at the free lateral faces of the joint. In this work, the extent of these edge effects has been quantified by performing a 3D numerical model of a CFRP-Al double-lap joint and comparing the results with the 2D plane strain solution. For the particular case under study, the edge effects were shown to be significant at a distance of around one adherent thickness with lower stresses than those found in the 2D model. Stress comparisons between numerical 2D and 3D solutions where carried out at a distance of few fiber diameters from the corner edge were failure is expected to initiate. The results showed that edge effect is significant only near the free-edge of the sample for this configuration.

1. INTRODUCTION

Some difficulties of reliable failure prediction of adhesively bonded components make the use of adhesive joints limited. The aim of this work is the study of an adhesive CFRP-Al double-lap joint commonly employed in the aeronautic industry. The geometry includes the adhesive spew-fillet, which can reduce the stresses at the corner (Belingardi et al. 2002, Tsai et al. 1994, Bodganovich et al. 1999).

There are many 3D Finite Elements (FE) analyses including multimaterial adhesive joints. We can highlight the work of Bodganovich et al. (1999) again using submodelling in the analysis. Andruet et al. (2000) and Gonçalves et al. (2002) used special FE, considering geometric nonlinearity. Their results are limited to single-lap joints, and do not consider any spew-fillet. Ishikawa et al. (2008) evaluated the strength of the stepped-lap joints in 3D and carried out an experimental analysis. Aydin (2008) presents a 3D analysis limited to single-lap joints without fillet.

3D effects in corners are analyzed in Tsai et al. (1994); Aydin (2008); Bogdanovich et al. (1999); Ortiz et al. (2006), da Silva et al. (2008). Another important point is that experimental tests can measure (using strain gauges, for example) the stress state on the free lateral surfaces of the specimen, while these surfaces do not exist in the mathematical problem formulation for plain strain.

In this paper, a double lap joint between carbon-epoxy composite (AS4/8552 unidirectional fiber $[0]_8$) and aluminium (L3140) plates bonded by a structural adhesive (FM73) is considered. The 3D FE analysis considers the spew-fillet and the results are compared with the strain plane solution obtained by Barroso (2007). The present work is focused on the singular stress field in a particular bimaterial corner (CFRP-adhesive), inside a control area of 33 μm radius, where the failure initiation is expected to appear in real specimens.

2. THREE-DIMENSIONAL MODEL

The geometry of the problem represented in Fig. 1 was chosen according the ASTM D 3528-96 (2002).

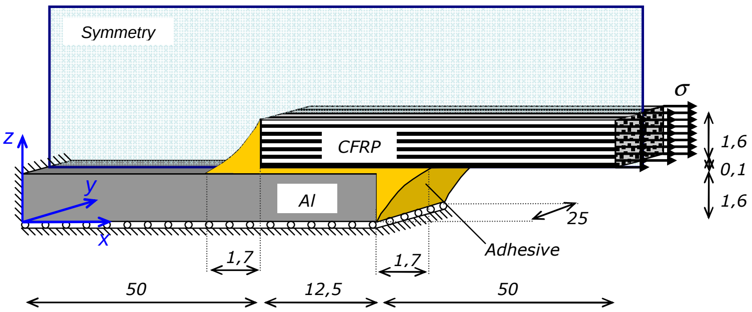

Fig. 1. Geometry (dimensions in millimeters).

The symmetries indicated were considered to simplify the problem (parallel to the *xy* and *xz* planes) and to reduce computational costs.

A set of two cylindrical volumes were used to control the mesh in the critical area around the corner edge, where singularity is known to occur (Barroso 2007). In this control cylinder the mesh was refined (the edge of the smallest element being $\cong 0.74\ \mu m$), the cylinder radius is 1/3 of the adhesive thickness. Each finite element on the circumference of the cylinder was established to have a $10.4\ \mu m$ width, thereby giving 1200 uniform elements along the *y* axis. The Fig. 2 shows the mesh used in the analysis.

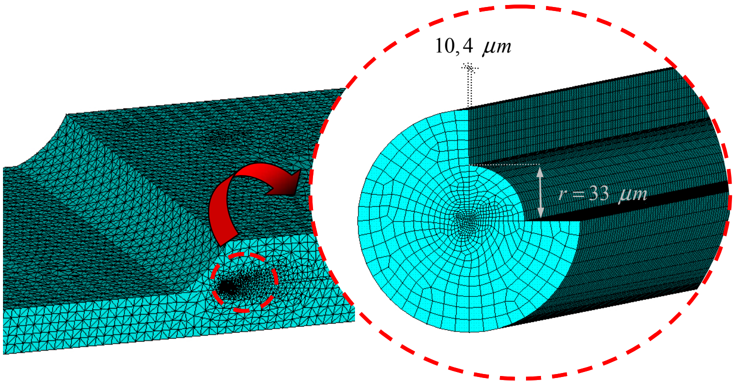

Fig. 2. Mesh and detail of control cylinder in the corner (adhesive-CFRP).

The 3D linear elastic analysis was carried out using the following material properties are: $E = 68670\ MPa$, $\nu = 0.33$ and $E = 3000\ MPa$, $\nu = 0.35$ for aluminium and adhesive respectively. The CFRP was modeled as an equivalent homogeneous orthotropic material: $E_x = 141300\ MPa$, $E_y = 9580\ MPa$, $E_z = 9580\ MPa$,

$G_{xy} = 5000\ MPa$, $G_{yz} = 3500\ MPa$, $G_{xz} = 5000\ MPa$, $\nu_{xy} = 0.3$, $\nu_{yz} = 0.32$, $\nu_{xz} = 0.3$. The applied stress is $\sigma = 100\ MPa$ (see Fig.1).

ANSYS FE code was used, with SOLID45 (8 nodes, 3 Degrees Of Freedom – DOF in what follows – per node) finite element for both the aluminium and adhesive, and SOLID64 (8 nodes, 3 DOF per node) finite element for the CFRP. The model has 1.010.060 nodes and 2.131.998 elements. Due to the very refined mesh in the control cylinder, it was necessary to control well all the geometry to allow a smooth transition between all the elements and to warrant a good aspect ratio for the adherent panels and adhesive layer due the need to capture the stress singularities in the corner.

3. RESULTS

The stresses along the surface of the control cylinder were taken to evaluate the stress state at the corner. In Fig. 3 the 3D FE solution (i.e. the distribution of circumferential stresses) is presented, comparing with the plane strain Boundary Elements (BE) solution (Barroso 2007). In Fig. 3 a) one can appreciate a representative surface distribution that gives a qualitative idea of the edge effect. In Fig. 3 b) the angular distribution of circumferential (σ_θ) stresses for different positions of y axis (according coordinate system in Fig. 1) is presented and the edge effect is clearly observed, where *y = 0* represents the free edge and where *y = 12.5 mm* the symmetry plane. The stresses at the free edge were reduced by $\cong 11\ MPa$ in the most critical case.

It can be appreciated that the stresses are quite constant along the *y* axis and present a little dispersion about the 2D BE solution excepting the free edge where the solution decreases for *y* approaching to zero.

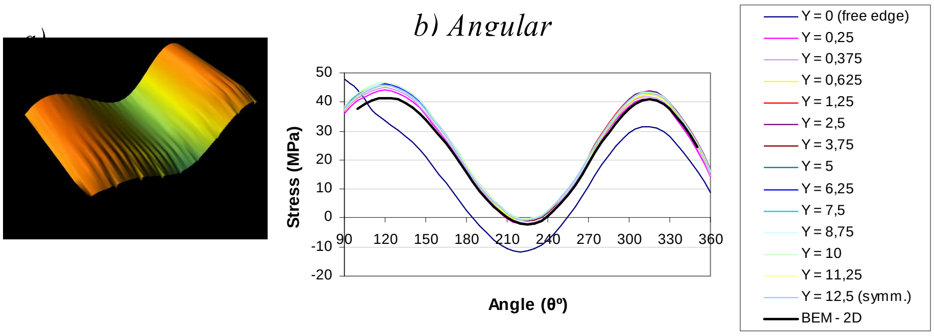

Fig. 3. Distribution of circumferential σ_θ stresses.

4. CONCLUSIONS

3D edge effect was analyzed in a particular adhesive CFRP-AL double-lap joint. The size of the adhesive thickness (0.1 mm) makes the 3D model computationally expensive (a large area with a very low thickness and stresses varying in the thickness direction need a very fine mesh). In the free edge, the circumferential and tangential stresses presented a reduction with respect to the plain strain solution, for this kind of configuration, the plain strain solution being approximately valid in about 97% the width of specimen (i.e. along Y direction). The validity of the commonly used 2D plane strain analysis has been shown to be sufficiently accurate for predicting the stress state in the region away from free edge, for the configuration analyzed. Not all material combinations lead to the same result (stresses less severe at the free edge) so in each case this fact should verified before using representative 2D models. The use of submodeling (Bogdanovich et al. 1999) would be a known alternative to the present expensive 3D numerical simulations.

ACKNOWLEDGEMENTS

This work was supported by CAPES Brazilian Ministry of Education and also by the Junta de Andalucía through the Projects of Excellence P08-TEP-04071 and P08-TEP-04051.

REFERENCES

AYDIN, M. D. (2008). 3D Nonlinear stress analysis on adhesively bonded single lap composite joints with different ply stacking sequences, The Journal of Adh., 843, 15-36.

ANDRUET, R. H.; DILLARD, D. A.; HOLZER, S. M. (2000). Two and three-dimensional geometrical nonlinear finite elements for analysis of adhesive joints, Int. J. Adh. Adhesives, 21, 17-34.

BARROSO, A. (2007). Caracterización de estados singulares de tensión en esquinas multimateriales. Aplicación a uniones adhesivas con materiales compuestos, Universidad de Sevilla, PhD Thesis (in Spanish).

BELINGARDI, G., GOGLIO, L., TARDITI, A. (2002). Investigating the effect of spew and chamfer size on the stresses in metal/plastics adhesive joints. Int. J. Adh. Adhesives, 22, 273 - 282.

BOGDANOVICH, A. E.; KIZHAKKETHARA, I. (1999). Three-dimensional finite element analysis of double-lap composite adhesive bonded joint using submodeling approach, Composites: Part B 30, 537 – 551.

DA SILVA, L. F. M., NEVES, P. J. C., ADAMS, R. D., SPELT, J. K. (2008). Analytical models of adhesively bonded joints – Part I: Literature survey. Int. J. Adh. Adhesives 29, 319-330

GONÇALVES, J. P. M.; MOURA, M. F. S. F.; CASTRO, P. M. S. T. (2002). A three-dimensional finite element model for stress analysis of adhesive joints, Int. J. Adh. Adhesives, 22, 357-365.

ICHIKAWA, K.; SHIN, Y.; SAWA, T. (2008). A three-dimensional finite element stress analysis and strength evaluation of stepped-lap adhesive joints subjected to static tensile loadings, Int. J. Adh. Adhesives, 28, 464-470.

ORTIZ, J., MANTIČ, V., PARÍS, F. (2006). A domain-independent integral for computation of stress intensity factors along three-dimensional crack fronts and edges by BEM, Int. J. Solids & Struct., 43, 5593-5612.

TSAI, M. Y.; MORTON, J. (1994). Three-dimensional deformations in a single-lap joint, J. Strain Analysis, 29, 1, 137 – 145.

Análisis micromecánico del crecimiento de grieta interlaminar en modo I en un compuesto de fibra de carbono

D. Trias, J. Costa, E. Oliveras, N. Hereu
Análisis y Materiales Avanzados para el Diseño Estructural (AMADE)
Universitat de Girona. Escola Politècnica Superior II.
Av Lluís Santaló s/n. 17071 Girona
dani.trias@udg.edu

RESUMEN

El modelado micromecánico de un compuesto permite el análisis y cuantificación de los mecanismos de fallo que producen el daño en el material con elevada precisión y mediante pocas hipótesis de partida. Si bien este tipo de análisis es ya frecuente hoy en día en la literatura científica, generalmente se limita al análisis de tensión y deformación.

Este trabajo utiliza un modelo micromecánico para analizar el frente de grieta y la zona cohesiva en un compuesto de fibra de carbono bajo crecimiento de grieta en modo I. Se utiliza una distribución de fibra obtenida mediante una micrografía y una ley de degradación para la matriz. La simulación permite tanto la simulación del estado tensional durante el crecimiento de grieta como la obtención de los parámetros propios de la mecánica de la fractura, como la estimación del valor crítico de la energía necesaria para abrir la grieta. También permite estimar la longitud de la zona cohesiva, la cual es de interés para la aplicación de elementos cohesivos.

1. INTRODUCCIÓN

La micromecánica computacional, eso es, el modelado y simulación de los materiales en su escala microestructural está recibiendo recientemente el interés y atención de investigadores tanto del campo de la ingeniería estructural como de la ciencia de materiales. Gracias a la capacidad de computación disponible hoy en día se pueden emplear modelos que contengan un menor número de hipótesis y permitan analizar el comportamiento de los materiales compuestos de un modo más realista.

Bien es sabido que la deslaminación es uno de los modos de fallo más comunes en materiales compuestos laminados. Las técnicas más extendidas para su simulación son aquellas basadas en la mecánica de la fractura como la Técnica del Cierre Virtual de Grieta (VCCT) (Ribicki y Kanninnen 1977) y como los elementos cohesivos (Dávila et al 2008).

Ambas técnicas incluyen suposiciones que limitan su uso a determinadas condiciones y necesitan ser alimentadas con algunos parámetros del material. El uso de un modelo micromecánico para la simulación de la deslaminación permite por un lado, un enfoque más realista desde el punto de vista del material y por otro, la obtención de los parámetros que necesitan estas técnicas numéricas. Las únicas referencias que se encuentran en la literatura que empleen simulación micromecánica para el fenómeno de la delaminación provienen de finales de los años 80 (Crews et al 1986, Crews et al 1988). Los equipos de computación actuales permiten sin duda nuevos enfoques.

El presente trabajo muestra la modelización del mecanismo de fallo de la deslaminación usando un modelo de elementos finitos micromecánico.

2. MODELIZACIÓN

2.1 Construcción del modelo de elementos finitos

Para la modelización se emplea una distribución de fibras de un compuesto laminado de fibra de carbono obtenida mediante microscopio óptico. Mediante software propio se obtiene la posición de las fibras y se convierte en un modelo de elementos finitos para MSC.Marc o bien para Abaqus.

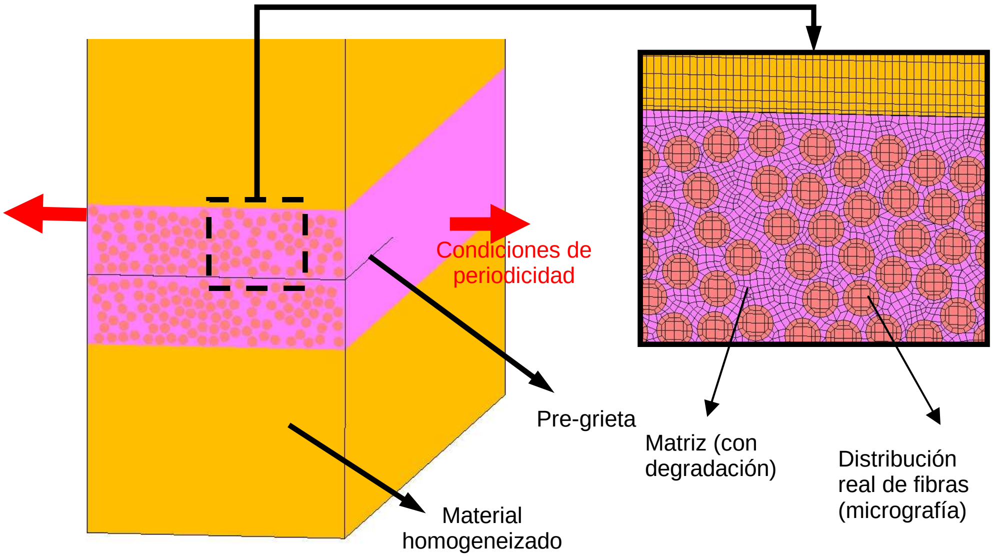

Fig. 1. Esquema del modelo creado.

2.2 Condiciones de contorno

En la Figura 1 se esquematiza el modelo realizado, usando condiciones de periodicidad para simular el ancho de una lámina y un material homogeneizado para ocupar el espesor competo de una lámina.

2.3 Propiedades de los materiales

La fibra se considera un material lineal elástico y, teniendo en cuenta el modo de fallo modelizado, se prescinde de simular su fallo. La matriz se considera Para las propiedades elásticas de los materiales se emplean valores usados en trabajos anteriores (Trias et al 2006) y para la degradación de la matriz se emplean distintos modelos: (1) Brittle cracking de Abaqus (2) Mohr Coulomb de Abaqus (3) Modelo de daño propio.

3. RESULTADOS Y CONCLUSIONES

Los modelos empleados constan de unos 300.000 a 500.000 elementos y llevan del orden de días a una semana en completar la simulación en un clúster con 33 procesadores Intel Opteron 2.6 GHz, de los cuales se usaban 8 simultáneamente.
Los resultados obtenidos permiten obtener la distribución de tensiones, analizar la longitud cohesiva y observar la aparición de grietas diferentes a la principal (provocada por pre-grieta). Asimismo, permiten analizar la trayectoria que sigue la grieta durante su propagación.

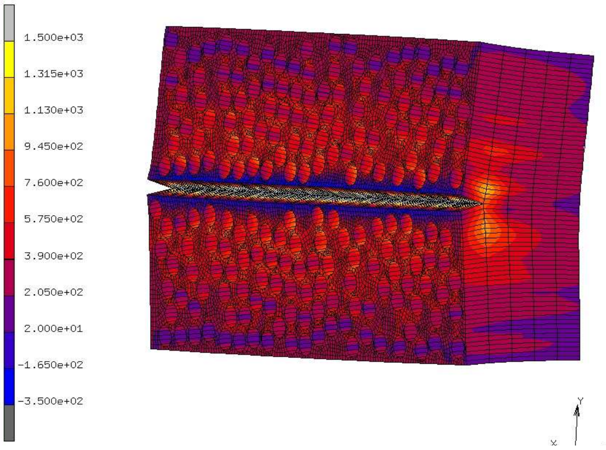

Fig. 3. Ejemplo de resultado del modelo: tensiones principales máximas

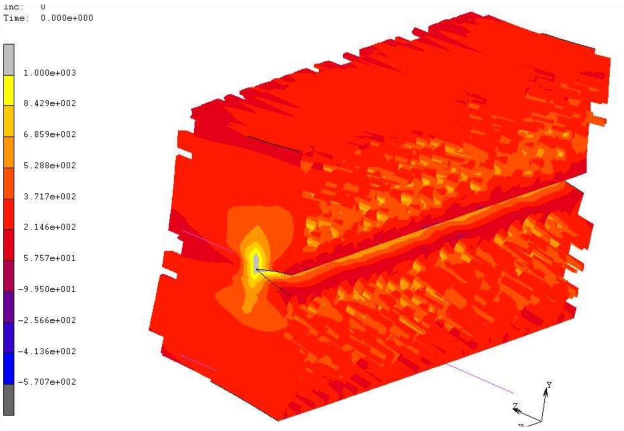

Fig. 4. Ejemplo de resultado del modelo: tensión de Von Mises.

AGRADECIMIENTOS

Los autores desean agradecer al Ministerio de Ciencia y Tecnología por la concesión del proyecto MAT2006-14159-C02-01.

REFERENCIAS

CREWS J.H., SHIVAKUMAR K.N., RAJU I.S. (1986) Factors influencing elastic stresses in Double Cantilever Beam specimens. *NASA Technical Memorandum 89033*.
CREWS J.H., SHIVAKUMAR K.N., RAJU I.S. (1988) A fiber-resin micromechanics analysis of the delamination frint in a DCB specimen. *NASA Technical Memorandum 100540*
DÁVILA, C.G.; CAMANHO, P.P.; TURON, A. (2008) Effective simulation of delamination in aeronautical structures using shells and cohesive elements. *Journal of Aircraft* 45 (2008): 663-672.
RYBICKI E.F, KANNINEN M.F. (1977) A finite element calculation of stress intensity factors by a modified crack closure integral. *Engineering Fracture Mechanics*, 9(4):931-938, 1977.
TRIAS D., COSTA J., FIEDLER B., HOBBIENBRUNKEN T., HURTADO J.E. (2006) A two-scale method for matrix cracking probability in fibre-reinforced composites based on a statistical representative volume element *Composites Science and Technology* 2006, 66(11-12):1766-1777

Herramienta para el análisis parametrizado de paneles reforzados con larguerillos bajo cargas de compresión

J. Bofill, J. Torres, J.A. Mayugo
AMADE, Escuela Politécnica Superior. Universitat de Girona, España
F. Cabrerizo
INTA, Área de Materiales Compuestos, 28850, Torrejón de Ardoz-Madrid

RESUMEN

Se presenta una metodología para el estudio de un ensayo a compresión de un panel de material compuesto reforzado con tres larguerillos. Se ha creado un modelo parametrizado que permite realizar una gran cantidad de análisis con cierta agilidad mediante el método de elementos finitos. Con ello, se ha creado una herramienta que admite cambiar tanto la configuración geométrica como la configuración del laminado que definen el revestimiento y los refuerzos. La metodología se completa con la implementación de métodos de análisis de los resultados, con lo que es posible realizar el post-procesado con un alto grado de automatización.

El modelo proporciona datos sobre la capacidad de resistencia de la estructura, con lo que se puede valorar la capacidad de carga del panel. Por otro lado, la esbeltez que poseen este tipo de estructuras propicia que se produzca pandeo local combinado con una flexión global del conjunto panel-rigidizador cuando están sometidas a cargas a compresión. Por lo tanto, la herramienta también valora la rigidez del panel en forma de su modo de pandeo local y su flexión global.

1. INTRODUCCIÓN

El objetivo de este trabajo es desarrollar una metodología para el análisis paramétrico de un ensayo de compresión de un panel de material compuesto rigidizado con tres larguerillos. Los revestimientos de materiales compuestos reforzados con larguerillos son una solución estructural ampliamente usada en medios de transporte aéreo y espacial. Esto conlleva que el estudio de éste tipo de estructuras sea un elemento idóneo para validar el desarrollo de herramientas de cálculo para la ayuda al diseño de componentes fabricados con materiales compuestos laminados.

Se han realizado análisis modal, para obtención de los modos de pandeo, análisis elástico y análisis no-lineal. Cada tipo de análisis se divide en tres fases. En el primer paso se desarrolla un sistema automatizado para generar el conjunto de parametrizaciones. A continuación, se genera el modelo en elementos finitos con una serie de parámetros variables para analizar el efecto que producen estos sobre el comportamiento del panel. El último paso es el post-procesado o análisis de resultados.

2. DESCRIPCIÓN DEL PANEL Y ENSAYO

El panel utilizado para el desarrollo de la herramienta paramétrica se fabrica con *cinta prepreg* de matriz de epoxi reforzada con fibras de carbono unidireccionales, cuya referencia es T800/M21. El panel es rectangular y está reforzado con tres larguerillos en forma de T, como se puede observar en la Figura 1.

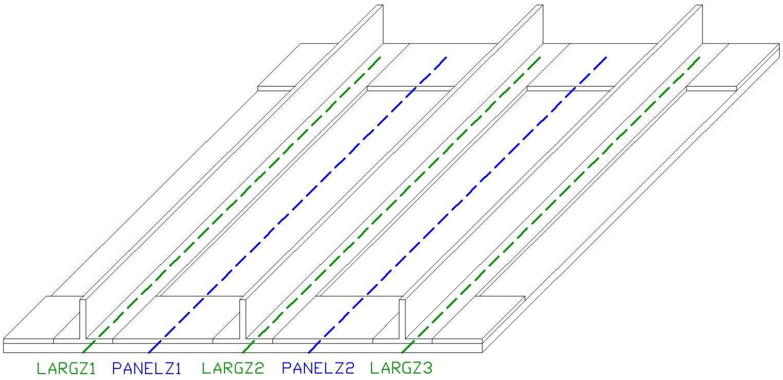

Fig. 1. Esquema del panel reforzado con tres larguerillos.

Las propiedades del laminado de todas las partes del panel se muestran en la Tabla 1.

Referencia	**Secuencia apilamiento**	**Nº capas**	**Espesor [mm]**
Refuerzo	$(\pm45,0_2,90,0)_S$	12	2.208
Base del refuerzo	$(\pm45,0_2,90,0)$	6	1.104
Panel	$(\pm45,90,0)_S$	8	1.472

Tabla 1. Propiedades del laminado.

El ensayo se realiza en una máquina convencional de tracción-compresión de dos columnas, con uno de los platos de compresión móvil y que comprime el panel 1mm. Al no ser una sujeción encastada, se colocan unas láminas adicionales en la base del panel para aumentar la superficie de contacto y así la robustez de los extremos (ver Figura 1).

3. MODELIZACIÓN Y ANÁLISIS PARAMÉTRICO

El análisis paramétrico se realiza en función de tres variables geométricas de diseño. Estos parámetros variables son la base del panel, la base del refuerzo y la cota vertical del larguerillo. En total, el análisis se realiza sobre 80 combinaciones de parámetros.

El modelo en elementos finitos se genera mediante el programa ABAQUS/Standard. Las variables de estado usadas en el análisis paramétrico para estudiar la respuesta del panel son las siguientes:

1. **Carga crítica de desestabilización:** Carga máxima que puede soportar el panel antes de desestabilizarse por pandeo. Se calcula multiplicando el valor propio (λ) del análisis modal con la carga teórica que soporta el panel.
2. **Índice de flexión global:** Avaluación de la deformación que sufre el panel en todo su conjunto. Su valor es el desplazamiento en la dirección perpendicular al plano del panel en la línea central LARGZ2 (Figura 1).
3. **Índice de pandeo local:** El pandeo local aparece a causa del comportamiento no lineal del panel al someterlo a cargas de compresión. Se calcula como la diferencia entre el desplazamiento máximo en la dirección

perpendicular al plano en las líneas PANELZ1 y PANELZ2 (Figura 1) y el índice de flexión global.

4. Índice de fallo intralaminar: En la modelización en elementos finitos con ABAQUS/Standard se ha implementado la subrutina LARC-03 para obtener el índice de fallo para todos los elementos de las capas más críticas del panel.

Estas variables de estado se calculan con la combinación de los resultados del análisis modal, análisis lineal y el análisis no lineal. En la Figura 2 se puede observar a partir de que análisis se obtiene cada una de ellas.

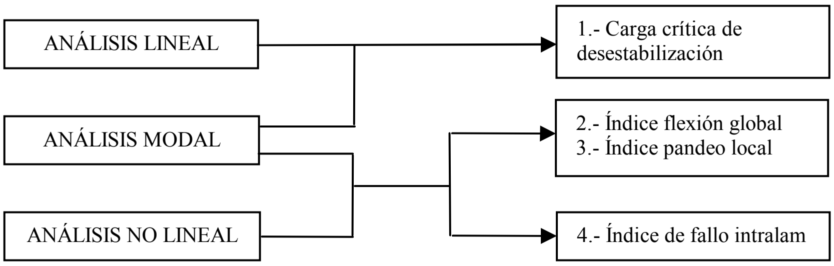

Fig. 2. Combinación de análisis para la obtención de los distintos resultados.

4. ANÁLISIS DE LOS RESULTADOS

4.1 Análisis modal

El análisis modal es usado para obtener los diferentes modos de pandeo que puede sufrir el panel sometido a cargas de compresión. Se acepta que el modo con menor carga crítica es el modo con más probabilidades de aparecer.

El análisis modal demuestra la existencia de dos modos de pandeo principales, cuyas cargas críticas de desestabilización son muy similares y que pueden aparecer indistintamente. Para conseguir resultados uniformes y equiparables para todas las parametrizaciones, se han introducido imperfecciones en la geometría inicial para obligar al panel a deformarse en el mismo modo.

Variable de diseño	**Consecuencia**	**Grado de influencia**
Incremento de la altura del refuerzo	Incremento	Significativa
Incremento de la base del refuerzo	Incremento	Significativa
Incremento de la base del panel	Disminución	Determinante

Tabla 2. Resumen de la influencia de las variables de diseño en la carga crítica de desestabilización (P_{CR}).

El análisis modal incluye el análisis paramétrico de la carga crítica de desestabilización (P_{CR}) para el modo de pandeo impuesto. En la Tabla 2 se muestra un resumen de las tendencias observadas en los resultados de este análisis.

4.2 Análisis del pandeo local y flexión global

La Tabla 3 contiene el resumen de los resultados obtenidos del análisis no lineal.

Variable de estado	Variable de diseño	Consecuencia	Grado de influencia
Pandeo local	Incremento altura refuerzo	Disminución	Determinante
	Incremento base refuerzo	Disminución	Poco significativa
	Incremento base panel	Incremento	Poco significativa
Flexión global	Incremento altura refuerzo	Incremento	Significativa
	Incremento base refuerzo	Disminución	Poco significativa
	Incremento base panel	Incremento	Determinante

Tabla 3. Resumen de la influencia de las variables de diseño en el pandeo.

4.3 Análisis del fallo intralaminar

La compresión a 1mm produce unas tensiones intralaminares en las diferentes partes del panel. Estas tensiones se evalúan mediante el criterio de fallo LaRC03 (Dávila et al. 2005, Pinho et al. 2005) para predecir el fallo.

5. CONCLUSIONES

Se ha presentado una metodología para el análisis paramétrico de un ensayo de un panel de material compuesto reforzado con tres larguerillos. Este análisis permite realizar cambios en distintas variables geométricas para estudiar la influencia de estas en diferentes variables de estado que determinan capacidad de carga por pandeo, modos de pandeo y de flexión global, y aparición de daño intralaminar.
Esta herramienta de análisis podrá ser usada en un futuro para la optimización de este tipo de ensayos.

AGRADECIMIENTOS

Se agradece la financiación del presente trabajo por el Ministerio de Educación y Ciencia mediante los proyectos TRA2006-15718-C02-01 y TRA2006-15718-C02-02.

REFERENCIAS

Dávila, C. G., Camanho, P. P., Rose, C. A., (2005) Failure criteria for FRP laminates. Journal of Composite Materials 39 (4), 323-345.
Pinho, S. T., Dávila, C. G., Camanho, P. P., Iannucci, L., Robinson, P., (2005) Failure Models and Criteria for FRP Under In-Plane or Three-Dimensional Stress States Including Shear Non-linearity. NASA/TM-2005-213530. National Aeronautics and Space Administration.

Modelling ultrasonic debulking of tape lamination

J. Justo, E. Graciani, F. París
Grupo de Elasticidad y Resistencia de Materiales
Escuela Técnica Superior de Ingenieros de la Universidad de Sevilla
R. Ávila
Composite Technology (EDSWCM) Materials and Processes, Airbus.

ABSTRACT

A numerical model is presented, which has been developed to study the quality of the ultrasonic debulking of a composite laminate. The quality of the debulking level will depend, primarily, of the temperature raised in the laminate. For that reason, the evolution in time of the temperature inside the composite laminate has been studied. To this end, a thermal model has been developed which leads to the determination of the temperature inside the laminate from the values of the temperature at the tip of the ultrasonic horn. To validate the model, the numerical results have been compared with experimental measurements in a particular case.

1. INTRODUCTION

The aim of the out-of-autoclave manufacturing technique in which the present study is focused is to obtain composite laminates of high performance. To this end, an automatic tape lamination head is employed that places the layers over a working table. The head is equipped with two compaction rollers with adjustable pressure and temperature and a ultrasonic compaction device (sonotrode) located between them, which has the function of continuously debulking the tape after it is placed. The main advantage of this system is that it eliminates the need for vacuum-bag debulking the laminate every certain number of plies. Instead, the layers are being compacted as they are placed. This means an enormous saving in time in the manufacturing process. It also permits the coupling with an out-of-autoclave curing system which may activate the polymerization of the resin in the tape, layer by layer, after it is placed and compacted.

The quality of the laminate is highly dependent on the debulking of the plies. The air entrapped between plies has to be properly removed and this will occur under sufficient applied pressure if the resin is fluid enough, that is, if the temperature in the laminate is raised to a certain level during a certain period of time.

The objective of the model presented in this paper is to analyze the heat flux and the temperatures reached in the composite laminate using as an input the temperature measured in the ultrasonic horn during the debulking process.

The use of this model will reduce the need of controlling the temperature in the laminate placing thermocouples in it. To validate the results obtained with the numerical model, a comparison is made with the experimental measurements of the temperature in the bottom of the laminate (obtained with a thermocouple) when the ultrasonic horn is maintained in the same position for 12 seconds. Note that it can not be a priori assured that the comparison yields good results, since the experiment is made on fresh material while the properties employed in the model have been measured on cured material.

The compaction equipment is shown in Fig. 1. This equipment consists of the ultrasound compactor with a titanium tip (sonotrode) that has the function of vibrating over the material to be compacted. The composite layers are placed with an automatic lay-up system (ATL). Below the laminate can be found, in the following order: a layer of peel-ply to fix the first ply to the tool surface, a polyamide film to demould the panels and an aluminium plate to give the panels their flat shape.

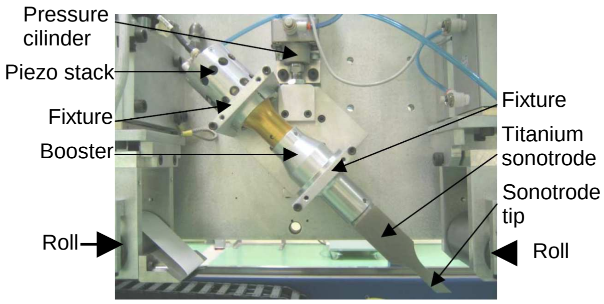

Fig. 1. Ultrasonic compactor.

2. FINITE ELEMENT MODEL

The components that have been considered in the model are the titanium tip of the sonotrode and the composite laminate to be compacted, see Fig. 2(a). The temperature measurements have been made at the node showed on Fig. 2(b), located at the bottom surface of the laminate under the sonotrode, since it is in this position where the thermocouple has been placed during the experiments. A conforming mesh has been employed in order to obtain smooth transitions in the heat transfer between the solids.

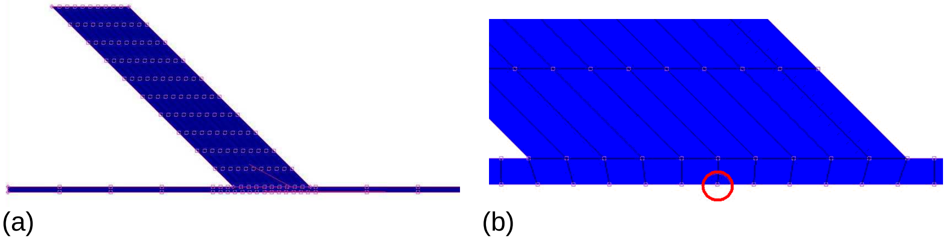

Fig. 2. (a) FEM model of the sonotrode and the laminate. (b) Measuring node.

It is assumed that the only heat exchanges that will affect the problem are: conduction between the sonotrode and the laminate, convection between the sonotrode and the environment and convection between the laminate and the environment. The properties of the materials are shown in the Table 1.

Material	ρ $[kg\,m^{-3}]$	c_P $[J\,kg^{-1}\,K^{-1}]$	k $[W\,m^{-1}\,K^{-1}]$
Titanium	4430	580	7,1
Composite laminate	1570	1180	0,6 (transverse) 1 (longitudinal)

Table 1. Material properties.

The problem is formulated in two steps. In the first step ($0 < t \leq 12\,s$) both bodies are in contact, initially at 25 ºC, and the temperature of the sonotrode increases, transferring heat to both bodies. The temperature rise in this stage is shown in Fig. 3(a); it has a high slope at the beginning and a lower slope afterwards, since it is supposed that the heating rate will decrease as the maximum temperature is being reached. It must be noted that in actual fact it is the sonotrode tip that heats up as a consequence of friction and heat generated within the composite when subjected to the ultrasonic vibration. In the second step ($t > 12\,s$) the sonotrode is removed instantaneously, allowing the laminate to cool freely, driving the stored heat away through the laminate itself (to the sides) and to the air by convection.

3. RESULTS

Temperature measured in the model at the node shown in Fig. 2(b), that coincides with the point where the temperature have been measured in the experiments, is shown in Fig. 3(b) as a function of time.

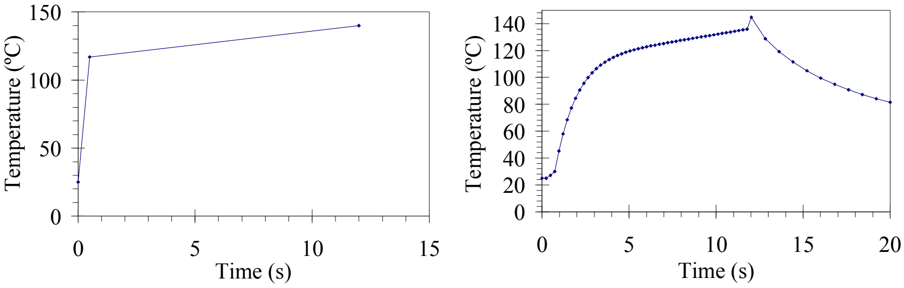

Fig. 3. (a) Imposed temperature on the sonotrode tip. (b) Numerical solution of the temperature at the monitored node.

As expected, a rapid initial increase of the temperature is obtained (in about 2 seconds). After that, once a 120 ºC temperature is reached, the temperature gradient becomes slower. Finally, the free cooling of the laminate is obtained. The 140 ºC peak appears immediately after the moment when the sonotrode is lifted.

The temperature distributions inside the laminate at the beginning of the heating and just after the cooling are respectively shown in Fig. 4(a) and (b). As can be observed, before lifting the sonotrode, the temperature raised in the laminate is uniform through the thickness (in a range of 133±5 ºC).

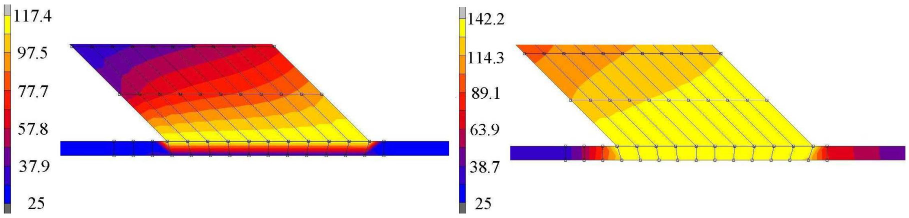

Fig. 4. Evolution of the temperature into the sonotrode and the lay-up (a) At the beginning of the process (b) Before cooling.

Taking the experimental results shown in Seebacher 2008 and superimposing this curve to the numerical results obtained in the thermal model described above, Fig.5 is obtained, where a reasonable agreement between the numerical and experimental data can be observed. As can be seen, the heating peak after the lifting of the sonotrode is not a distortion of the sensor, as was thought at the beginning. This peak appears as a consequence of the heat that was being evacuated through the titanium tip, which, in the absence of it, is concentrated in the laminate.

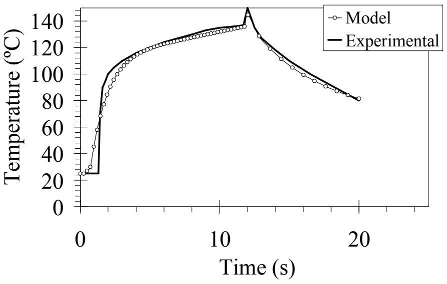

Fig. 5. Comparison with experiments.

4. CONCLUSIONS

A numerical model has been developed to determine, from the measured temperature of the ultrasonic sonotrode, the evolution of the temperature field inside the laminate. This model can be employed to determine the temperature reached in the laminate during the actual compaction process. It is expected that these measurements will be directly related to the quality of the compaction. Hence, the use of the present model avoids the need to install thermocouples in the panels (a more complex and expensive technique than monitoring the temperature of the sonotrode) to determine the temperature in-situ each time the manufacturing parameters are changed.

REFERENCES

SEEBACHER, S. (2008) Contributions to the investigation of in-situ ultrasonic tape lamination of composite thermoset prepregs. *Master Thesis.* Private Fachhochschule Göttingen, Germany.

Determinación de la resistencia a compresión longitudinal de composites de fibra larga mediante flexión de tres puntos

N. Carbajal, G. Vargas, A. Arrese, F. Mujika
Departamento Ingeniería Mecánica,
Escuela Politécnica de Donostia-San Sebastián
Universidad del País Vasco/Euskal Herriko Unibertsitatea

RESUMEN

En este trabajo se proponen dos métodos de ensayo para determinación de la resistencia a compresión longitudinal de composites de fibra larga mediante flexión de tres puntos. En el primer método se utilizan laminados unidireccionales, se analiza el efecto de la concentración de carga y se propone una expresión para calcular la longitud de la zona de contacto. En el segundo método se utilizan laminados cruzados de la forma $[0_m/90_n/0_p]$, y se realiza un análisis de tensiones en el cual se incluyen las tensiones témicas. En ambos métodos los resultados experimentales concuerdan con el valor de resistencia de compresión del material utilizado.

1. INTRODUCCIÓN

Existen numerosos métodos de ensayo de compresión así como numerosos modelos micromecánicos que estudian el fallo de compresión. El principal problema de los métodos existentes es la variabilidad de resultados que está asociada a factores difíciles de controlar.

En este trabajo se propone flexión de tres puntos de laminados unidireccionales y de laminados cruzados para determinación de la resistencia a compresión.

2. DETERMINACIÓN DE RESISTENCIA A COMPRESIÓN MEDIANTE FLEXIÓN DE LAMINADOS UNIDIRECCIONALES

2.1 Aproximación analítica

En la Figura 1 aparecen los parámetros geométricos del modelo así como la determinación del valor de la carga de indentación. La longitud de la zona de contacto d_c se ha obtenido según Turner (1966) a partir de las propiedades elásticas del material,

$$d_c = 0{,}19 \cdot \sqrt[3]{rP} \tag{1}$$

donde r es el radio de aplicador de carga y P es el valor de la carga donde la curva carga-desplazamiento cambia de no lineal a lineal (Mujika 2007)

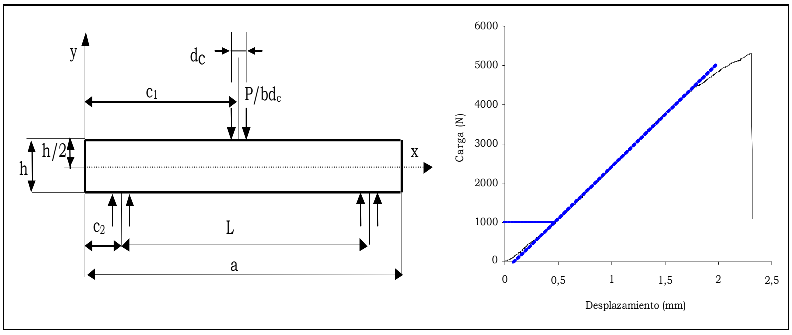

Fig. 1. Parámetros geométricos del modelo de efectos locales y carga de indentación.

La tensión del modelo de efectos locales σ_x se ha obtenido a partir del análisis de flexión de tres y cuatro puntos de materiales ortótropos (Whitney 1986) incluyendo la expresión de la longitud de la zona de contacto de la ecuación (1), resultando

$$\sigma_x = \frac{P_{\max} L}{bh^2}\sigma_\zeta \tag{2}$$

donde σ_ζ es la tensión en coordenada normalizada $\zeta = \frac{x}{a}$

2.2 Análisis de resultados

Se han ensayado dos tipos de muestras de T6T/F593: a) espesor menor que la anchura con espesores 6 y 7 mm y b) espesor mayor que la anchura con espesores 10 y 11 mm.

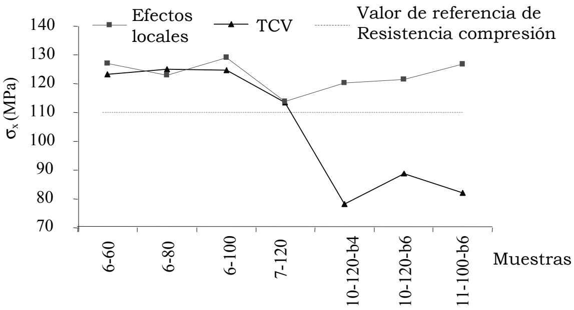

Fig. 2. Valores medios de resistencia obtenidos mediante TCV y mediante modelo de Whitney para las muestras de espesores nominales 6, 7, 10 y 11 mm.

En la Figura 2 se observa que los valores de tensión según el análisis de efectos locales y según la TCV son similares en el caso a) y muy diferentes en el caso b). Las diferencias en el caso b se deben a indentación. Además los valores de tension según la TCV en el caso a) son ligeramente mayores que el valor de referencia (Bombardier 2003), debido probablemente a los efectos del gradiente de tensiones presente en la flexión de tres puntos según Wisnom (1999). Según Fleck y Liu (2001) cuando la relación entre el espesor y el diámero de fibra es próximo a 1000, las tensiones de flexión tienden a la resistencia a compresión, condición que cumple la muestra 7-120.

3. DETERMINACIÓN DE RESISTENCIA A COMPRESIÓN MEDIANTE FLEXIÓN DE LAMINADOS CRUZADOS

3.1. Aproximación analítica

Según Pagano (1967) se han considerado las siguientes hipótesis de la TCV en flexión:

1. La deformación longitudinal en el eje *x* ε_x es una función lineal de z
2. Las únicas tensiones distintas de cero en cada lámina son σ_x y τ_s
3. Cada lámina tiene comportamiento linealmente elástico.

Imponiendo las condiciones de mayores tensiones de compresión que de tracción en las capas de 0º y que la capa a 90º esté sometida a esfuerzos de compresión se ha elegido la configuración $[0_r/90_r/0_{2r+2}]$. En este caso la tensión máxima de compresión σ_{xc}^M verifica

$$\frac{\sigma_{xc}^M}{\sigma_{3p}} = \frac{A + B\cdot\phi}{C + D\cdot\phi + F\cdot\phi^2} \tag{3}$$

donde $\sigma_{3p} = \dfrac{6m_x}{h^2}$, $\phi = \dfrac{E_T}{E_L}$ y *A*, *B*, *C*, *D*, *F* son funciones de $t_1 = \dfrac{h_1}{h}$ y $t_2 = \dfrac{h_2}{h}$, tal que A y C >1 con A > C y B, D y F < 1.

En caso de T6T/ F593 donde ϕ = 0,06, la ecuación (3) se puede simplificar obteniendo

$$\sigma_{xc}^M \approx \frac{A}{C}\sigma_{3p} \tag{4}$$

3.2. Análisis de resultados

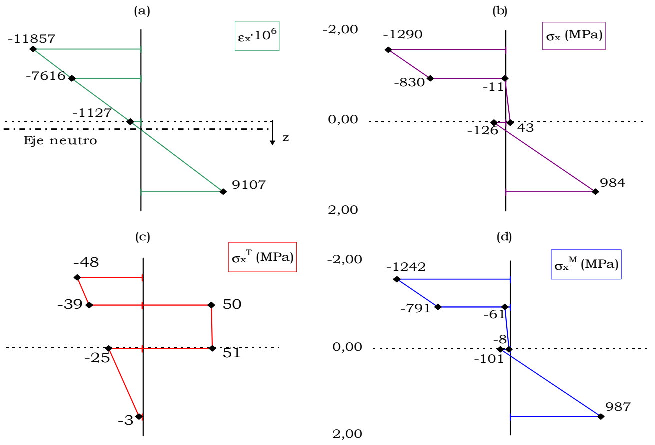

Fig. 3. Distribución de ε_x, σ_x, σ_x^T y σ_x^M en $[0_3/90_5/0_8]$-80.

En la Figura 3 se muestran los perfiles deformaciones longitudinales en el eje x ε_x, las tensiones mecánicas σ_x^M, las tensiones térmicas σ_x^T y las tensiones totales σ_x obtenidas mediante el modelo propuesto en la configuración $[0_3/90_5/0_8]$ con luz 80 mm. La tensión de compresión es mayor que la de tracción en las capas de 0º y las tensiones térmicas de tracción se contrarrestan con las mecánicas de compresión en la capa de 90º.

En la Figura 4 se muestra el fallo de compresión en $[0_4/90_6/0_{10}]$ con luz 100 mm

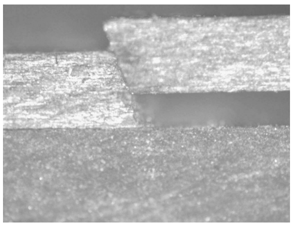

Fig. 4. Rotura a compresión en $[0_4/90_6/0_{10}]$-100.

3. CONCLUSIONES

En el primer método la resistencia a compresión puede ser obtenida de forma fiable mediante las ecuaciones correspondientes a la TCV una vez asegurado que no aparece indentación y que el fallo se produce por compresión.

En el segundo método se ha comprobado que la resistencia a compresión no depende de las propiedades elásticas del material, sino de la relación entre módulo transversal y módulo longitudinal.

AGRADECIMIENTOS

Se desea agradecer al Gobierno Vasco por la financiación de la tesis doctoral del autor mediante el programa IKERTU y a Hexcel Composites por el suministro del material.

REFERENCIAS

Fleck, N.A., Liu, D. Microbuckle initiation from a patch of large amplitude fibre waviness in a composite under compression and bending. European Journal of Mechanics A, 2001; 20: 23-37.

Mujika, F. On the effect of shear and local deformation in three point bending tests. Polymer Testing, 2007; 26:869-877.

Pagano, N.J. Analysis of the Flexural test of bidirectional composites. Journal of Composite Materials, 1967; 1: 336-342.

Turner, J.R. Contact on a transversely isotropic half-space, or between two transversely isotropic bodies. International Journal of Solids and Structures, 1966; 16: 409-419.

Whitney, J.M. Elasticity Analysis of Orthotropic Beams under concentrated Loads. Composites Science and Technology, 1985; 22: 167-184.

Wisnom, M.R. Size effects in the testing of fibre-composite materials. Composites Science and Technology, 1999; 59: 1937-1957.

Caracterización de inicio y crecimiento de grietas de interfaz entre fibra y matriz bajo cargas transversales usando el modelo de interfaz débil

L. Távara, V. Mantič, E. Graciani, F. París
Grupo de Elasticidad y Resistencia de Materiales. Escuela Técnica Superior de Ingenieros, Universidad de Sevilla, España

RESUMEN

Se estudia el inicio y crecimiento de un despegue en la interfaz entre fibra y matriz bajo cargas transversales biaxiales de tracción - tracción y compresión con tracción dominante. Se considera un problema simplificado en relación a una lámina unidireccional real, con una fibra embebida en una matriz cuyas dimensiones externas son mucho más grandes que el radio de la fibra. El objetivo es predecir las cargas de fallo (críticas) de la interfaz para distintas combinaciones de cargas biaxiales, y los ángulos de crecimiento inestable del despegue correspondientes a estas cargas críticas. En este modelo se considera una (posiblemente ficticia) interfase representada mediante una distribución continua de muelles, de rigidez adecuada. La rotura de estos muelles que trabajan con tensiones normales y tangenciales está controlada por una ley de comportamiento elástica lineal – frágil para modo mixto de fractura. Aunque estrictamente hablando no tiene que existir ninguna interfase (o adhesivo) entre la fibra y la matriz, se supone que el comportamiento de la interfaz fibra-matriz puede ser descrito razonablemente en el marco del modelo de interfaz débil. La obtención de la curva de fallo para cargas transversales biaxiales en el problema descrito se basa en el hecho que este modelo no sólo permite estudiar la propagación de grietas sino que también permite estudiar el inicio de grietas en una interfaz.

1. INTRODUCCIÓN

Las láminas unidireccionales de materiales compuestos sufren un mecanismo de rotura denominado fallo de la matriz o fallo entre fibras ante la aplicación de cargas en la dirección perpendicular a las fibras. Este mecanismo se caracteriza por la aparición de despegues en las interfaces entre las fibras y la matriz cuando está dominado por cargas de tracción. La conexión entre los despegues iniciales en las interfaces y la macro grieta final pasa por el crecimiento de estos despegues, convertidos en grietas de interfaz, a lo largo de las propias interfaces, su desvío posterior para internarse en la matriz, y la coalescencia final de las grietas provenientes de distintas interfaces.

2. INTERFAZ DÉBIL

El modelo de interfaz débil fue desarrollado, entre otros, por Lenci (2001). La interfaz débil es considerada como la conexión entre las dos superficies que se encuentran unidas por una capa fina de adhesivo elástico lineal - *interfase*, y la zona dañada consiste en la separación debido a la ruptura de dicha capa de adhesivo. La distribución continua de muelles que simulan la capa de adhesivo sigue una ley de comportamiento elástica lineal – frágil mostrada en la Figura 1, así:

$$\sigma = \begin{cases} k_1\delta_n & si \quad \delta < \delta_c, \\ 0 & si \quad \delta > \delta_c, \end{cases} \qquad y \qquad \tau = k_2\delta_t, \tag{1}$$

donde σ y τ son las tensiones normales y tangenciales respectivamente que actúan en un muelle, δ_n y δ_t son los desplazamientos normales y tangenciales relativos de los extremos del muelle, y k_1 y k_2 son las rigideces normal y tangencial de la *interfase*. σ_c y δ_c son la tensión normal crítica y desplazamiento normal relativo crítico que alcanza el muelle al romperse en Modo I puro.

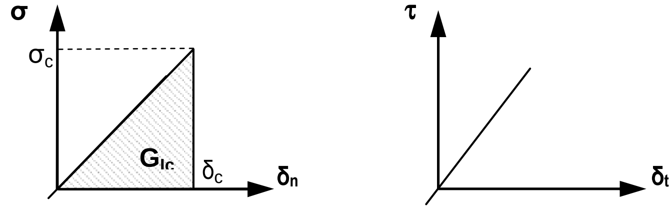

Fig. 1. Ley de comportamiento elástica lineal-frágil en las direcciones normal y tangencial.

Las leyes de la interfaz débil presentadas implican la inexistencia de singularidad en el campo de tensiones en el vértice de la grieta. El criterio de fallo de la interfaz, propuesto en Távara et al (2009b), está basado en el índice de liberación de energía G, definido como la energía almacenada en el muelle delante del vértice de la grieta (Lenci 2001):

$$G = G_I + G_{II} = \frac{\sigma\delta}{2} + \frac{\tau\delta_t}{2}, \tag{2}$$

el cual se rompe cuando la grieta se propaga. Se considera que la grieta se propaga cuando el índice de liberación de energía en el modo I, G_I, alcanza el valor de la tenacidad a la fractura en modo I, es decir cuando $G_I = G_{Ic}$ donde

$$G_{Ic} = \frac{\sigma_c\delta_c}{2} = \frac{\sigma_c^2}{2k_1}. \tag{3}$$

Luego, el índice de liberación de energía total de una grieta trabajando en modo mixto:

$$G = G_I + G_{II} = G_I(1 + \tan^2\psi_G), \tag{4}$$

donde $\tan^2\psi_G = G_{II}/G_I$, siendo ψ_G el ángulo (de fase) que define la mixticidad de los modos de fractura. Escribiendo el criterio de crecimiento de una grieta a lo largo de una interfaz débil en forma $G = G_c$; y combinándolo con (3) y (4) se obtiene:

$$G_c = G_{Ic}(1 + \tan^2\psi_G). \tag{5}$$

Los detalles de la implementación del modelo presentado aquí en el MEC así como su aplicación en el ensayo de fractura interlaminar en Modo I de materiales compuestos son mostrados en Távara et al (2009a).

3. INCLUSIÓN CILINDRICA BAJO CARGAS TRANSVERSALES BIAXIALES

Se considera una inclusión cilíndrica infinitamente larga, con sección transversal circular, dentro de una matriz infinita unida a la matriz a lo largo de su superficie lateral mediante una distribución continua de muelles que se comportan según el modelo de interfaz débil introducido en el Apartado 2. Se estudia no sólo el crecimiento de la grieta sino también el inicio del despegue. Tanto la inclusión como la matriz son consideradas como materiales isótropos lineales. Una carga biaxial uniforme con $-\sigma_x^\infty \le \sigma_y^\infty \le \sigma_x^\infty$ y $\sigma_x^\infty > 0$ es aplicada de manera perpendicular a la dirección de la inclusión. De esta manera un estado de deformación plana se genera en la inclusión y en la matriz.

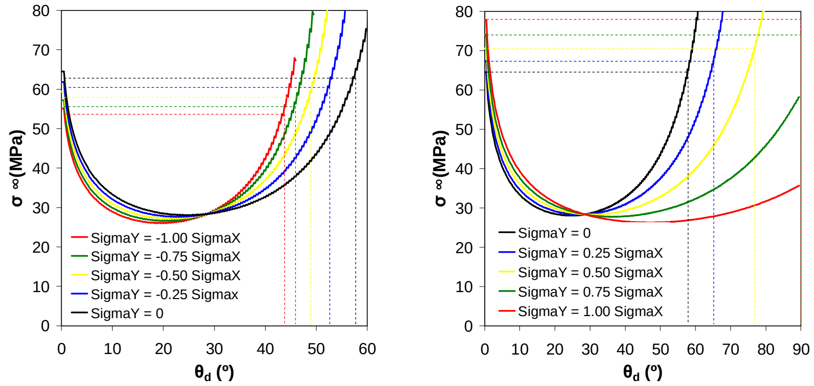

Fig. 2. Tensión aplicada frente al semiángulo de la grieta.

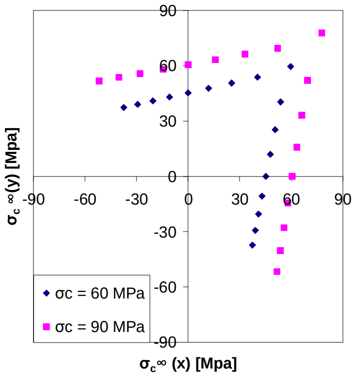

Fig. 3. Curva de fallo de una inclusión circular bajo cargas transversales biaxiales.

3.1 Solución Numérica usando MEC

Se ha elegido un sistema fibra de vidrio y matriz epoxi (Tabla 1). El modelo del MEC realizado consistió en una inclusión circular con radio de 7.5 μm dentro de un cuadrado de lado 1mm. El valor de k_2 es tomado como $k_1/2.66$ (Távara et al 2009b).

Material	Coeficiente de Poisson, ν	Modulo de Young, E
Matriz epoxi	$\nu_m = 0.33$	$E_m = 2.8$ GPa
Fibra de vidrio	$\nu_f = 0.22$	$E_f = 71$ GPa

Tabla 1. Las propiedades elásticas de la matriz y la fibra.

El valor de la tenacidad a fractura de la interfaz fibra matriz en modo I considerado fue $G_{Ic} = 2$ Jm^{-2} y valor de la tensión crítica de la interfaz fibra matriz en modo I, $\sigma_c = 90$ MPa. De la Figura 2, se puede obtener una estimación del semiángulo, θ_c, que alcanza la grieta creciendo de manera inestable, así como la carga que produciría dicho crecimiento, σ_c^∞, para diferentes combinaciones de cargas biaxiales de tracción – tracción y tracción – compresión. Se consideró una carga de tracción dominante en el eje "x" y se varió la carga en el eje "y" para obtener las combinaciones deseadas. Se observa que mientras mayor sea la carga de compresión en el eje "y", la carga necesaria para la iniciación de la grieta es menor; de igual manera el ángulo inicial de despegue disminuye mientras la carga de compresión aumenta. Por otro lado mientras mayor sea la carga de tracción en el eje "y", la carga necesaria para iniciar el despegue también es mayor, además el ángulo de despegue también crece produciendo prácticamente despegue total de la fibra en los casos con mayor tracción. Debido a que no se dispone de un valor exacto de σ_c, además del estudio hecho para σ_c = 90 MPa, se repitió el estudio para σ_c = 60 MPa. En la Figura 3 se presentan las curvas de fallo obtenidas para ambos casos.

4. CONCLUSIONES

Aunque estrictamente hablando no exista una interfase – una capa de adhesivo, entre la fibra y la matriz, el modelo de interfaz débil ha probado que puede ser aplicado para estudiar el comportamiento del sistema fibra-matriz sometido a cargas biaxiales. Se observó que con el criterio de fallo ($G = G_{Ic}$) utilizado se pueden obtener resultados bastante aproximados a los que se esperan en la realidad. Se obtuvo la curva de fallo de una inclusión circular bajo cargas transversales biaxiales.

AGRADECIMIENTOS

Los autores desean agradecer el financiamiento de este trabajo por los proyectos TRA2006 - 08077 del Ministerio de Educación y Ciencia y los Proyectos de Excelencia TEP – 1207, TEP – 02045 y P08-TEP 04051 de la Junta de Andalucía.

REFERENCIAS

CORREA E. (2008) Estudio micromecánico del "fallo de la matriz" en materiales compuestos fibrosos, Tesis Doctoral, 328 pags. ETSI – Universidad de Sevilla, España.

GRACIANI E., MANTIČ V., PARÍS F. Y BLÁZQUEZ A. (2005) Weak formulation of axi-symmetric frictionless contact problems with boundary elements. Application to interface cracks*, Comput Struct*, 83: 836-855.

LENCI S. (2001) Analysis of a crack at a weak interface, *International Journal of Fracture*, 108: 275-290.

MANTIČ V. (2009) Interface crack onset at a circular cylindrical inclusion under a remote transverse tension. Application of a coupled stress and energy criterion, *International Journal of Solids and Structures*, 46: 1287-1304.

PARÍS F., CORREA E., MANTIČ V. (2007) Kinking of transverse interface cracks between fibre and matrix*, Journal of Applied Mechanics*, 74: 703-716.

TÁVARA L., MANTIČ V., GRACIANI E., CAÑAS J., PARÍS F. (2009a) Analysis of a crack in a thin adhesive layer between orthotropic materials applied to composite interlaminar fracture toughness test, *2nd ECCOMAS Thematic Conference on the Mechanical Response of Composites, London, UK.*

TÁVARA L., MANTIČ V., GRACIANI E., PARÍS F. (2009b), Caracterización de grietas de interfaz entre fibra y matriz bajo cargas transversales uniaxiales usando la teoría de interfaz débil, *Congreso de métodos numéricos en Ingeniería 2009 SEMNI*, *Barcelona, España*.

Aplicación del método de fuerzas integrado dual en elementos membrana y placa para materiales compuestos

I. Adarraga, A. Cantera López de Silanes, J.M. Romera, F. Mujika
Departamento de Ingeniería Mecánica, Universidad del País Vasco, España

RESUMEN

En este estudio se muestra la utilización del método de las fuerzas integrado aplicado al Método de los Elementos Finitos (MEF) y su aplicación para materiales ortótropos y anisótropos. El Método de las Fuerzas Integrado y el Método Dual de Fuerzas Integrado, IFM y IFMD respectivamente, son dos métodos desarrollados por S. N. Patnaik, en los cuales se tienen en cuenta las ecuaciones de equilibrio y las de compatibilidad de las deformaciones, obtenidas éstas a partir del principio del trabajo virtual complementario.

Tras una descripción del método, se ha realizado el análisis de un elemento anisótropo sometido a tracción. El valor de la tensión a lo largo de la línea inferior del elemento mediante el IFMD varía en un 10% respecto del obtenido de la aplicación de la Resistencia de Materiales, y mediante el método de la rigidez, entre un 12% en el centro y un 300% en los extremos.

A continuación se aplica este método para obtener la matriz de rigidez de un elemento placa rectangular de cuatro nodos. Con este elemento se ha realizado el análisis de una placa en voladizo con dos cargas puntuales en el extremo. Los valores obtenidos mediante el IFMD con sólo dos elementos dan un 0,13% de error en el desplazamiento en la punta del voladizo y un 23% en la tensión máxima. Mediante el método de la rigidez, estos valores son del 6% y del 28% respectivamente.

La siguiente aplicación consiste en una placa rectangular con dos cargas puntuales iguales en dos extremos opuestos y dos apoyos en los otros dos. Los resultados obtenidos mediante el método de las fuerzas IFMD con un solo elemento muestran que el error en el momento M_{xy} es del 2%.

1. INTRODUCCIÓN

El método de la rigidez en elementos finitos puede interpretarse como una forma aproximada de resolver las condiciones de equilibrio, derivadas éstas del principio de los trabajos virtuales. En el método de la rigidez la ecuación de gobierno es

$$[K]\{x\}=\{P\} \tag{1}$$

En el método de las fuerzas integrado, en cambio, además de las condiciones de equilibrio, se tienen en cuenta también las condiciones de compatibilidad de las deformaciones, derivadas éstas del principio del trabajo virtual complementario. Estas condiciones de compatibilidad añadidas a las condiciones de equilibrio proporcionan la ecuación de gobierno del método de las fuerzas integrado o IFM (Patnaik, 2004) [i].

$$\left[\frac{\textit{Ecuaciones de equilibrio}}{\textit{Compatibilidad de las deformaciones}}\right]\{\textit{Fuerzas}\}=\left\{\frac{C\arg \textit{as externas}}{\textit{Deformación inicial}}\right\} \tag{2}$$

2. MÉTODO DE FUERZAS INTEGRADO DUAL (IFMD)

Las ecuaciones del IFMD para un elemento continuo discretizado en elementos finitos con n grados de libertad de fuerzas y m grados de libertad de desplazamientos, se obtienen por acoplamiento de las m ecuaciones de equilibrio (EE) y las $r = m - n$ condiciones de compatibilidad (CC). La ecuación de gobierno se transforma para que su aspecto sea idéntico a la ecuación de gobierno del método de la rigidez, es decir, que las incógnitas primarias sean los desplazamientos nodales.
La ecuación de gobierno y la matriz de rigidez son las que figuran en las ecuaciones (3) y (4) respectivamente, donde $[\mathrm{K}]_{ifmd}$ es la matriz de rigidez y $[\mathrm{P}]_{ifmd}$ es el vector de fuerzas.

$$[K]_{ifmd} = [E][G]^{-1}[E]^{-1} \tag{3}$$

$$[K]_{ifmd}\{x\} = \{P\}_{ifmd} \tag{4}$$

3. ELEMENTO CUADRILÁTERO DE 4 NODOS ANISÓTROPO

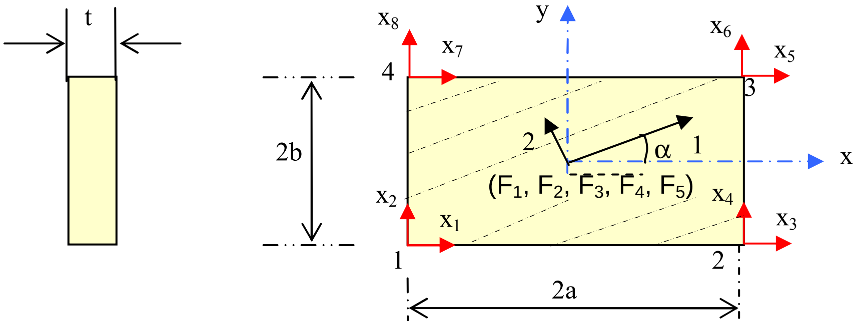

Fig. 1. Elemento rectángulo de 4 nodos.

3.1 Ensayo de tracción. Material anisótropo.

En la figura 2 se muestra una viga sometida a la que se ha sometido a un desplazamiento en un extremo de 0,015mm. Se ha realizado un análisis IFMD con 4 elementos cuadriláteros.

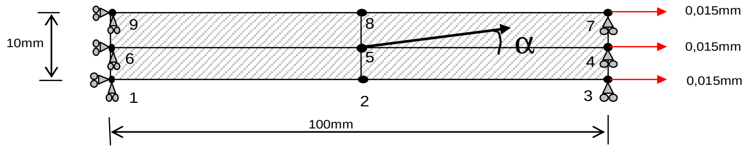

Fig. 2. Viga sometida a tracción.

Las tensiones obtenidas en la línea inferior de la viga se han comparado con los obtenidos mediante la aplicación del método de los desplazamientos y la resistencia de materiales [ii].

El error cometido mediante el análisis IFMD oscila entre el 11% en el centro y el 10-12% en los extremos. Mediante el método de los desplazamientos, sin embargo, el error en el centro de la viga es del 25,6% y el 83-300% en los extremos [iii].

4. ELEMENTO PLACA DE 4 NODOS ORTÓTROPO

Se muestran a continuación la aplicación del IFMD en un elemento placa de 4 nodos ortótropo [iv].

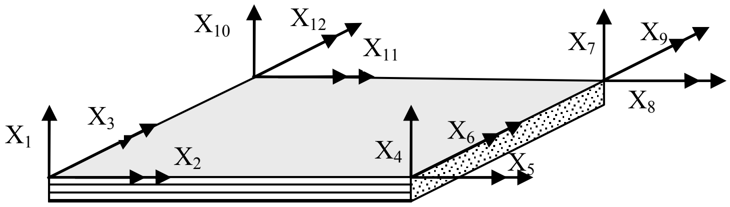

Fig. 3. Elemento placa de 4 nodos.

4.1 Placa en voladizo. Material ortótropo

A continuación se aplica el método IFMD para obtener la matriz de rigidez de un elemento placa rectangular de cuatro nodos. Con este elemento se ha realizado el análisis de una placa en voladizo con dos cargas puntuales de 5N en el extremo.

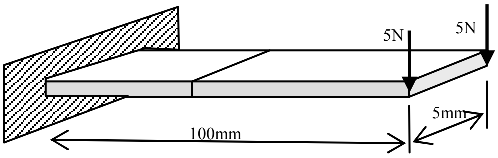

Fig. 4. Placa en voladizo con dos cargas puntuales.

En la figura 5 se pueden ver los diagramas de momentos obtenidos del análisis IFMD. Los valores obtenidos mediante este método con sólo dos elementos dan un 0,13% de error en el desplazamiento en la punta del voladizo y un 23% en el momento máximo. Mediante el método de la rigidez, estos valores son del 6% y del 28% respectivamente.

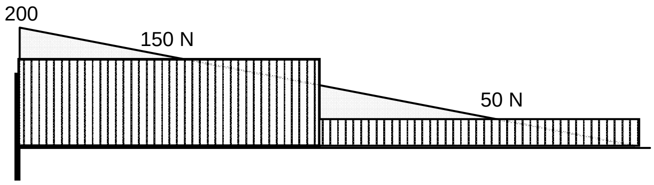

Fig. 5. Diagrama de momentos flectores IFMD y real.

En la tabla 1 se muestran los momentos y desplazamientos máximos obtenidos en los cuatro análisis.

	1 elem.	2 elem.	3 elem.	4 elem.	Real
Y_{max} (mm)	6,64	6,65	6,.66	6,66	6,666
M_{max}	100	150	175	180	200

Tabla 1. Momentos y desplazamientos máximos.

4.2 Placa rectangular con 2 cargas puntuales y 2 apoyos en extremos opuestos

La siguiente aplicación consiste en una placa rectangular con dos cargas puntuales iguales en dos extremos opuestos y dos apoyos en los otros dos.

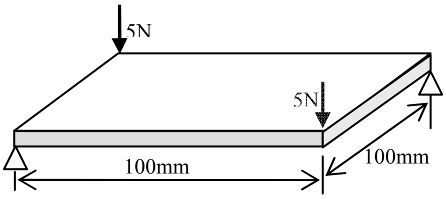

Fig. 6. Placa rectangular con dos cargas puntuales.

Los resultados obtenidos del análisis EF con hasta 4 elementos muestran que, mediante el método de las fuerzas IFMD, el error cometido en el momento M_{xy} es menos del 2%.

5. CONCLUSIONES

Los métodos IFMD aplicado a elementos finitos proporcionan resultados muy precisos en tensiones y desplazamientos, incluso en modelos de sólo dos elementos.

Simulación numérica y resultados experimentales del ensayo a tracción de un panel rigidizado de material compuesto

M.M. Real, A. Blázquez, E. Graciani, J. Cañas y F. París
Grupo de Elasticidad y Resistencia de Materiales, Escuela Técnica Superior de
Ingenieros, Universidad de Sevilla

RESUMEN

Se analiza numérica y experimentalmente un panel rigidizado plano solicitado por una tracción transversal a los rigidizadores. Se han realizado una serie de ensayos hasta rotura en el laboratorio y se cuenta con la lectura de varias bandas extensométricas en función de la carga aplicada. Se han realizado dos modelos de elementos finitos, resueltos con MSC PATRAN-NASTRAN, y se comparan los resultados con las mediciones experimentales. También se incluyen resultados numéricos incluyendo la evolución del daño.

1. INTRODUCCIÓN

El laboratorio de Elasticidad y Resistencia de Materiales de la E.T.S. de Ingenieros de Sevilla ha realizado numerosos ensayos experimentales para diversas empresas del sector aeronáutico. Uno de estos paquetes de ensayos consistió en analizar la influencia en el comportamiento de paneles rigidizados de la inclusión de una babette entre los rigidizadores. En la Fig. 1 se muestra un esquema de las probetas ensayadas.

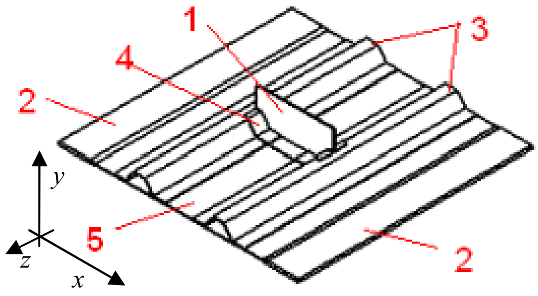

1 = babette
2 = zonas de mordazas
3 = rigidizadores (Ω)
4 = pie de la babette
5 = piel o recubrimiento

Fig. 1. Esquema de las probetas analizadas.

Se trata de un panel plano con dos rigidizadores en forma de Ω, perpendiculares a la dirección de aplicación de la carga, que están unidos transversalmente con una babette.

2. Modelos numéricos

Básicamente se han considerado dos modelos: un modelo monolítico y un modelo por componentes.

El modelo monolítico está constituido completamente por elementos tipo *shell*, para ello la probeta se ha dividido en zonas asignando a cada zona el laminado correspondiente. De esta forma, y a modo de ejemplo, en la zona en la que se superponen la piel y el ala del rigidizador los elementos tienen definido un laminado que está formado, conjuntamente, por las láminas de la piel y el pie del rigidizador dispuestas secuencialmente.

En el modelo por componentes, cada componente de la probeta (piel, rigidizador y babette) se modela por separado con elementos tipo *shell* y el laminado correspondiente. Un componente se enlaza con otro (por ejemplo piel con pie de rigidizador) mediante elementos sólidos. Hay que prestar especial cuidado a que las mallas entre las que se van a definir los elementos sólidos sean conformes, con lo que se evita la aparición de elementos muy distorsionados.

El panel estaba fabricado con dos tipos de material compuesto de fibra de carbono: uno tipo cinta (M21/T800) y otro tipo tejido (RTM: G0926). Las propiedades de ambos materiales se muestran en la Tabla 1.

	E_{11} [GPa]	E_{22} [GPa]	ν_{12}	G_{12} [GPa]	esp. [mm]
Cinta	170	8.0	0.30	4.5	0.184
Tejido	6.3	6.3	0.05	4.0	0.37
Adhesivo	2.6	2.6	0.44	0.9	0.2

Tabla 1. Composición del material utilizado.

Estos materiales se han dispuesto conformando los laminados que se muestran en la Tabla 2 para cada uno de los componentes del panel, siendo 0º la dirección de los rigidizadores (dirección z en la Fig. 1) y 90º la dirección de aplicación de la carga (dirección x en la Fig. 1).

	Material	Laminado
Alma de la babette	Tejido	$[45_6]$
Pie de la babette	Tejido	$[45_4]$
Refuerzo en los extremos	Cinta	$[+45/-45/90/0/90/-45/+45]_S$
Rigidizadores	Cinta	$[+45/-45/0_2/90]_S$
Revestimiento o piel	Cinta	$[+45/-45/0/-45/+45]_S$

Tabla 2. Composición del material utilizado.

En el modelo por componentes, los nodos de las zonas adheridas se han colocado en los planos medios de los laminados correspondientes, por lo que los elementos sólidos deben definirse con un material ortótropo ficticio, cuyas propiedades dependen de las del adhesivo y los laminados que unen y de la altura del elemento, para no rigidizar el modelo artificialmente. Las propiedades de estos materiales (hay varios, dado que hay varias uniones diferentes: piel-rigidizador, piel-babette y rigidizador-babette) se han calculado haciendo que un elemento de material ficticio se comporte de la misma forma que el elemento laminado real.

Las mordazas estaban fijas al panel en las zonas de refuerzo mediante dos filas de remaches de ∅6.4. Los extremos se han simulado como empotramientos en la primera línea de tornillos, una de las mordazas se ha mantenido fija y a la otra se le ha aplicado una carga uniformemente distribuida en la dirección x de la Fig. 1.

3. Resultados

En la Fig. 2 se comparan, a modo de ejemplo, los resultados numéricos obtenidos con las lecturas de algunas bandas.

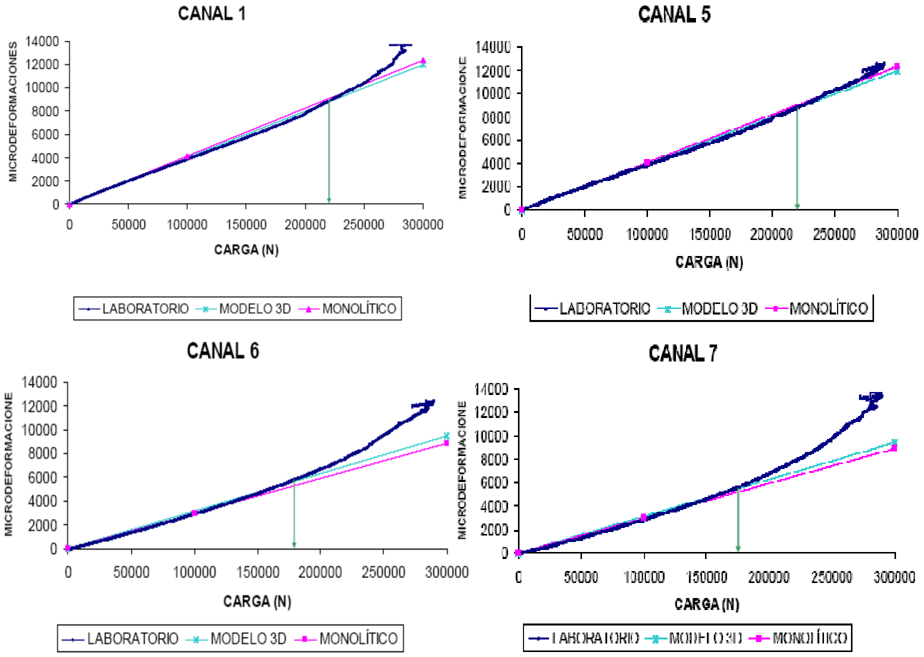

Fig. 2. Comparación de las predicciones numéricas y las lecturas de algunas bandas.

Ambos modelos se ajustan bastante bien a los resultados experimentales hasta que la aparición de daño en la probeta separa el comportamiento del lineal, lo que ocurre (dependiendo de cada banda), aproximadamente para una carga de 180 KN.

Aunque no se han incluido por motivos de espacio, el modelado de la capa de adhesivo con elementos sólidos permite una transmisión suave de las cargas entre los laminados de cada componente. No obstante, la principal ventaja del modelo por componentes es la capacidad para estimar las tensiones en la capa de adhesivo, posibilitando la aplicación de algún criterio de diseño apropiado. En la Fig. 3 se muestran las tensiones de pelado y cortadura en la capa de adhesivo.

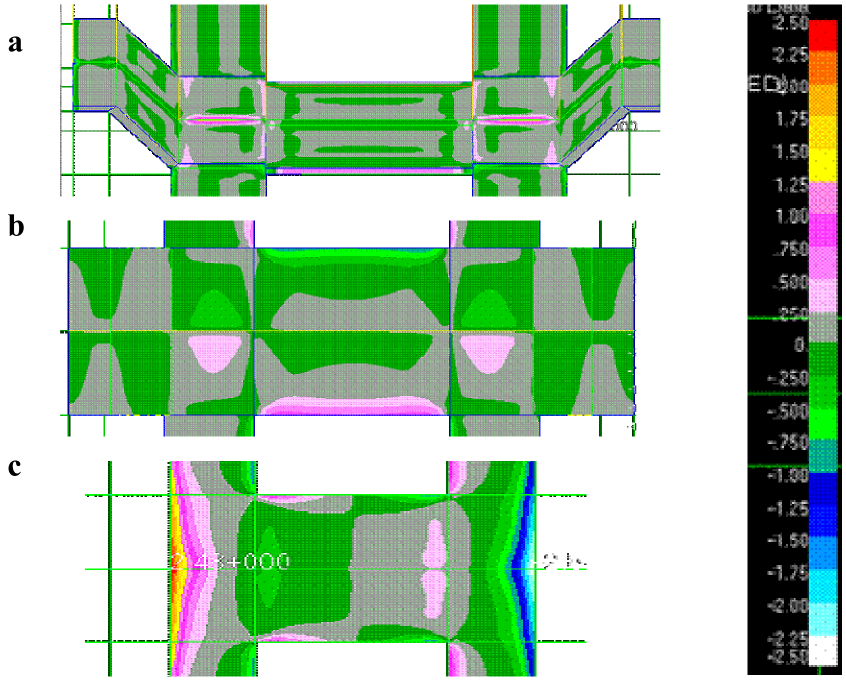

Fig. 3. Tensiones en la capa de adhesivo (a) pelado, (b) cortadura en dirección de los rigidizadores, y (c) cortadura en la dirección de la carga.

3. CONCLUSIONES

Los modelos desarrollados se ajustan muy bien con los resultados experimentales, lo que permite profundizar en el estudio de la influencia que la presencia de la babette tiene sobre el comportamiento del panel rigidizado.
La sustitución de los elementos sólidos que modelan el adhesivo por elementos cohesivos permitiría realizar un análisis sobre la propagación del daño por las intercaras entre los diferentes laminados.

REFERENCIAS

AIMS05-01-002. (2008). Airbus Material Specification. Carbon fibre reinforced epoxy prepeg. Unidireccional tape/180ºC – curing class. Intermediate modulus fibre. Structural material.
AIMS05-04-009. (2008). Airbus Material Specification. Standard modulus Carbon fibre fabric (with or without blinder). 5H satin, 370 g/m2. Liquid epoxy resin 180º curing.
JONES R.M. (1975) *Mechanics of Composite Materials* (Ed. B.J. Clark, McGraw-Hill) USA.
MSC.SOFTWARE (2007). *MSC Nastran Quick Reference Guide*

Modelling and characterization of carbon nanotubes oxidation to enhance dispersion

B. Coto, M. Blanco, L. Arzubiaga, I. Antia, J. Barriga
Deptartamento de Procesos de Fabricación. Fundación TEKNIKER-IK4. Eibar, España.
J.R. Sarasua, I. Martínez, E. Meaurio
Departamento de Ciencia de Materiales, Escuela de Ingeniería de Bilbao. Universidad del País Vasco/Euskal Herriko Unibertsitatea

ABSTRACT

Carbon nanotubes (CNT) poses remarkable mechanical and electrical properties but for many applications in which they have to be integrated in a given matrix, it is necessary to functionalize their surface to improve the CNT-matrix interaction. The effect of different oxidation treatments on CNTs has been analyzed in this work using modelling and experimental techniques.

1. INTRODUCTION

Carbon nanotubes have attracted considerable attention in some potential applications due to their remarkable properties. Therefore, they have been expected to be excellent fillers for polymer composites. In order to obtain nanocomposites with enhanced properties, it is necessary to oxidize or functionalize their surface in order to improve CNT-matrix interaction and CNT dispersion in the matrix.

Chemical treatments are being widely employed to oxidize CNT. The main disadvantage of these treatments is that CNT structure can be damaged during the process thus affecting CNT properties. In the present work, the effect of different oxidation treatments on CNTs has been studied using experimental and modelling techniques.

2. EXPERIMENTAL PART

Industrial grade multiwalled carbon nanotubes (MWCNT) (Graphistrenght C100, Arkema), were used as starting material. Purification and chemical oxidation of MWCNT were carried out with different treatments. Solvents employed and names of resultant MWCNT were collected in table 1.

Solvents	**Name**
NH_4OH:H_2O_2 mixture (ratio: 1:1)	MWCNT-NH
H_2SO_4:HNO_3 concentrated acid mixture (ratio: 3:1)	MWCNT-SN
HNO_3 diluted to 50 %	MWCNT-ND
HNO_3 concentrated	MWCNT-NC

Table 1. Solvents/solvent mixtures employed in the different treatments.

100 mg MWCNT were dispersed in 60 ml of solvent/solvent mixtures by ultrasonication and then refluxed under magnetic stirring for 2 h. All dispersions were then filtered, washed with deionised water until achieving pH=7 and dried at 110 ºC several days.

FTIR spectra were collected in KBr pellets at room temperature with a Perkin-Elmer Spectrum ONE spectrometer from 4000 to 400 cm^{-1} averaging 40 scans with 4 cm^{-1} resolution. TGA were carried out under nitrogen atmosphere from room temperature to 900 ºC at a heating rate of 10 ºC/min using a TA Q800 instrument. AFM images were carried out with a NT-MDT, Solver Pro atomic force microscope.

In oxidation processes several functional groups such as carboxylic (-COOH), carbonylic (C=O) and/or hydroxylic (-OH) are formed on CNT surface via oxidations of double bonds in the graphene wall, mainly CNT defects (Solhy et al. 2008). FTIR spectra of MWCNT before and after the different treatments are collected in figure 1a. All spectra show a band at 1575 cm^{-1} ascribed to the stretching vibrations of isolated C=C double bonds. This band appears superposed in some of the treated CNTs by a strong water band around 1630 cm^{-1} due to residual humidity. The band around 1730 cm^{-1} in oxidized CNTs, ascribed to C=O vibration of carboxylic groups, corroborates the efficiency of treatments. The band is more intense for CNT oxidized with acidic treatments. These treatments are more efficient in the generation of –COOH groups.

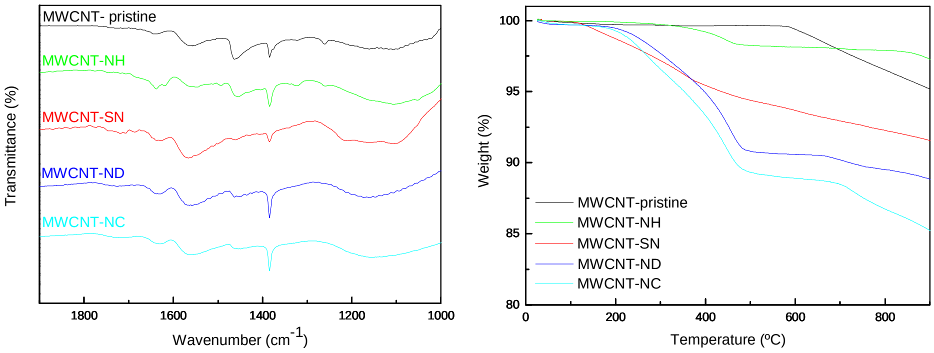

Fig. 1. a) FT-IR spectra and b) TG curves of pristine and oxidized MWCNT.

TGA curves were shown in figure 1b. The untreated MWCNT starts to degrade at about 550 ºC with a relatively slow degradation rate. Treated CNT degradation begins at lower temperatures. Up to 150 ºC a little weight loss corresponding to the adsorbed water is observed for some of the treated CNT. Then, degradation of oxidized carbon occurs. Datsyuk et al. (2008) attribute the loss from 150 to 350 ºC to the decarboxylation of carboxylic groups on walls and the degradation between 350-500 ºC to the elimination of hydroxyl functionalities attached to the walls. At higher temperatures, the weight loss corresponds to the thermal oxidation of remaining disordered carbon. MWCNT with the non-acidic treatment exhibited the highest thermal stability, whereas the treatment with concentrated HNO_3 acid is the most oxidative. According to FTIR spectra, the treatment with NH_4OH:H_2O_2 mixture seems to generate –OH groups (more than –COOH groups) resulting in a weight loss at temperatures around 350 ºC. Thermal oxidation of pristine CNTs at high temperature seems to be accelerated by the presence of catalyst particles.

Figure 2 shows AFM images of the MWCNT before and after treatments. A good structural integrity of MWCNT seems to be maintained after treatments.

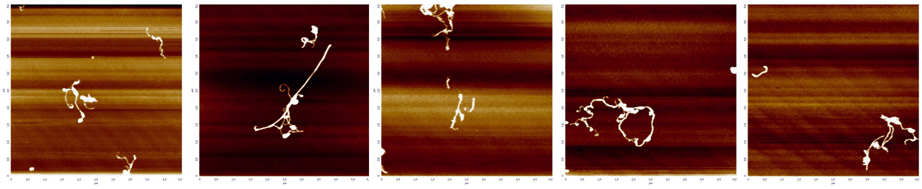

Fig. 2. AFM images of the MWCNT after treatments. From left to right: pristine MWCNT, MWCNT-NH, MWCNT-SN-, MWCNT-ND and MWCNT-NC.

3. MODELLING OF FUNCTIONALIZATION

A molecular modelling approach was used to analyze the influence of functionalization on the CNTs properties. Both classical molecular dynamics and DFT approaches were used to analyze different properties of SWCNTs. The initial model of the CNT had a length of 6.15 nm and a diameter of 0.814 nm. This model was used with the COMPASS forcefield (Accelrys) to study the optimal packing structure of the –COOH functional groups on the surface of the nanotubes using a self-assembled monolayer approach (Barriga et al. 2007). In this approach the energy of different patterns is examined for different percentages of functionalization. Molecular packing energies were determined by substracting CNT and -COOH energy contributions so we obtain the packing energy per -COOH functional group as is showed in equation (1):

$$E_{packing} = (E_{CNT\ functionalized} - E_{CNT} - N \cdot E_{COOH})/N \qquad (1)$$

Different patterns were analysed for degrees of functionalization from 0.167% to 15%.

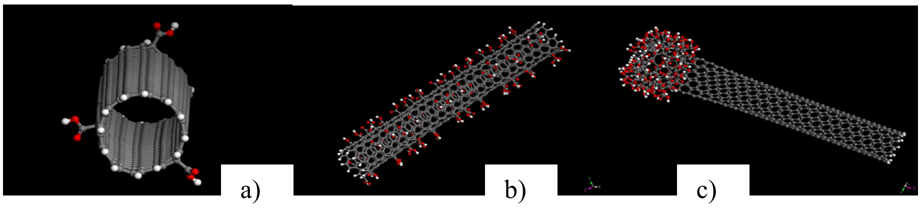
a) b) c)

Fig. 3. Different functionalization patterns. a) 0.5%; b) 12 % distributed pattern and c) 12% grouped pattern.

The minumum energy configurations were obtained for each degree of functionalization as showed in figure 4. A 12% degree of functionalization is the most favourable from an energetic point of view. Energies of different patterns for the same degree of functionalization showed that distributed (figure 3b) patterns are favored in front of grouped (figure 3c) patterns. Moreover for the patterns in which the functional groups are not well distributed on the CNT surface, the deformation of the CNT increases. Further molecular dynamics studies showed the influence of the functionalization patterns in the mechanical properties of the CNT.

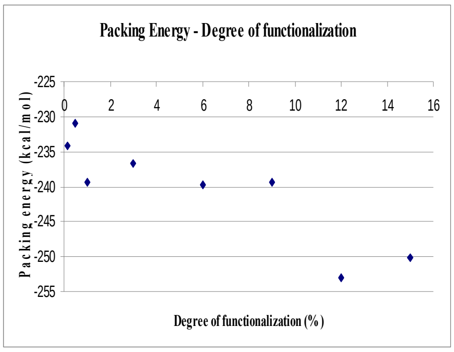

Fig. 4. Packing energy vs degree of functionalization

The solvation behaviour of the CNTs in water was analysed using a DFT COSMO model. Dmol3 software from Accelrys was used to perform the calculations. Firstly the influence of the length of the modelled CNT was analysed. A GGA-PW91 functional with a DNP basis set was used to perform the calculations. Results showed how for pristine CNTs the free energy of solvation raises with the length of the model of CNT as the effect of hydrogen atoms at the border of the CNT decreases while non-electrostatic term raises. Further studies analyse the influence of functionalization on solvation.

5. CONCLUSIONS

The selected oxidation treatments generated carboxyl and hydroxyl groups on MWCNT walls in different levels, depending on the type of acid/base and its concentration. However, for most treatments a good CNT structural integrity is maintained.

The modelling approach reveals that well distributed patterns of functionalization are energetically favored and the CNT is less deformed. A COSMO solvation model shows how the length and functionalization of the CNT influences its solvation behaviour.

ACKNOWLEDGEMENTS

Authors wish to thank EU (POCO project: CP-IP 213939-1) and Ministerio de Ciencia y Tecnología (NANOCIT: IAP-600100-2008-26) for the financial support.

REFERENCES

BARRIGA, J., COTO, B., FERNÁNDEZ B., (2007). Molecular dynamics study of optimal packing structure of OTS self-assembled monolayers on SiO_2 surfaces. Tribology International 40, issue 6, 960-966.

DATSYUK, V., KALYVA, M., PAPAGELIS, K., PARTHENIOS, J., TASIS, D., SIOKOU, A., KALLITSIS, I., GALIOTIS C. (2008). Chemical oxidation of multiwalled carbon nanotubes. *Carbon*, 46, 833-840.

SOLHY, A., MACHADO, B.F., BEAUSOLEIL, J., KIHN, Y., GONÇALVES, F., PEREIRA, M.F.R., ORFÃO, J.J.M., FIGUEIREDO, J.L., FARIA, J.L., SERP, P. (2008). MWCNT activation and its influence on the catalytic performance of Pt/MWCNT catalysts for selective hydrogenation. *Carbon*, 46, 1194-1207.

Análisis numérico del ensayo de fragmentación de fibra única, empleando elementos cohesivos

F. Curiel, E. Graciani, A. Blázquez, F. París
Grupo de Elasticidad y Resistencia de Materiales
Escuela Técnica Superior de Ingenieros de la Universidad de Sevilla

RESUMEN

Se ha llevado a cabo un análisis numérico, mediante el Método de los Elementos Finitos (MEF), del ensayo de fragmentación de fibra única empleando elementos cohesivos para modelar la aparición y crecimiento de las grietas de despegue. Dado que durante todo el proceso del ensayo la matriz tiende a contraerse más que la fibra en dirección radial, ha sido preciso tener en cuenta el contacto entre las caras de la grieta de despegue. Como resultado se ha observado que las caras de la grieta se encuentran cerradas a lo largo de toda su longitud. Por tanto, el crecimiento de la misma es en puro modo II de fractura. Los resultados obtenidos para diferentes valores del coeficiente de fricción se han comparado con resultados de análisis numéricos previos, obtenidos con el enfoque de la Mecánica de la Fractura Elástica Lineal (MFEL), empleando el Método de los Elementos de Contorno (MEC). En ausencia de fricción se ha observado un acuerdo excelente en los resultados de ambos enfoques. Sin embargo, si se tiene en cuenta el efecto de la fricción, los resultados obtenidos con elementos cohesivos y con la MFEL muestran comportamientos análogos pero con discrepancias cuantitativas.

1. INTRODUCCIÓN

El ensayo de fragmentación de fibra única (Kelly y Tyson ,1965) consiste en someter a tracción una probeta que contiene una única fibra alineada con la carga. El presente estudio considera una probeta con una fibra de vidrio embebida en resina epoxi, con las características mostradas en la Tabla 1.

	Fibra de vidrio	Resina epoxi
Módulo de elasticidad	70 000 MPa	3 500 MPa
Coeficiente de Poisson	0.2	0.3
Coeficiente de expansión térmica	$7\cdot10^{-6}$ K^{-1}	$50\cdot10^{-6}$ K^{-1}
Radio exterior(r_i)	5 μm	1 000 μm

Tabla 1. Características mecánicas y dimensiones de la probeta.

Dado que la fibra soporta menores alargamientos que la resina, una vez que la probeta alcanza una cierta deformación, la fibra comienza a fragmentarse. Cuanto más pequeño es un fragmento de fibra, más resistente se vuelve (puesto que es más difícil que haya un defecto en su interior). Por tanto, llega un momento en que deja de fragmentarse la fibra y comienza a fallar la interfase, apareciendo grietas de despegue entre la fibra y la matriz que nacen en los puntos de rotura de la fibra y crecen a lo largo de la interfase fibra/matriz, tal como se muestra en el esquema de la Figura 1.

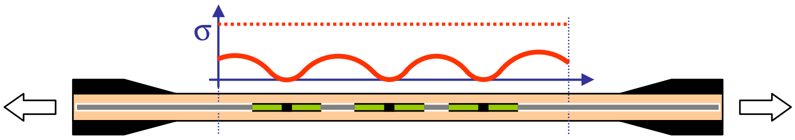

Fig. 1. Esquema de la probeta tras la fragmentación de la fibra y el crecimiento de las grietas de despegue.

El objetivo del presente trabajo es llevar a cabo una simulación numérica del ensayo que permita, mediante ajuste con los resultados experimentales, determinar la *tenacidad a fractura* de la interfase.

2. MODELO NUMÉRICO

Dado que los fragmentos en que se divide la fibra son muy largos, en comparación con su diámetro y con la longitud de las grietas de despegue, la solución es repetitiva en el extremo de los fragmentos y presenta, por un lado, simetría axial respecto al eje de la fibra y, por otro, simetría respecto al plano de rotura de la fibra. Por tanto el modelo numérico empleado es el mostrado en la Figura 2.(a), constituido por la sección radial del tramo de probeta correspondiente a la mitad de un fragmento de fibra.

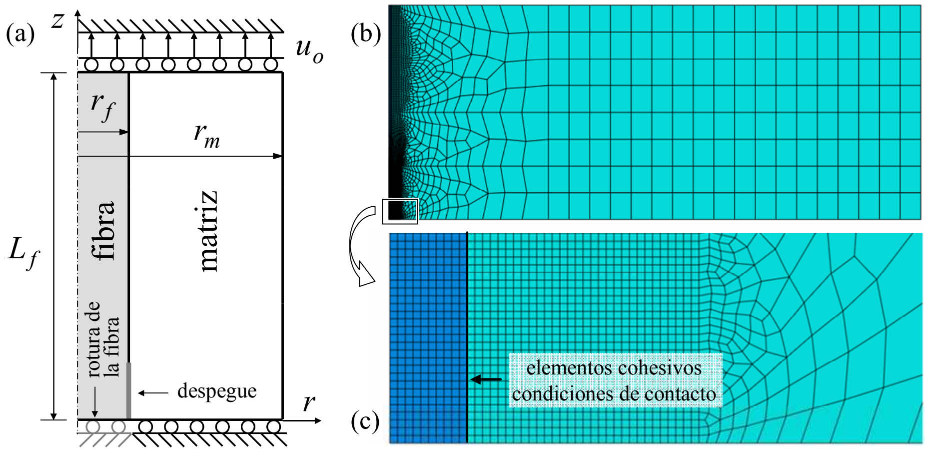

Fig. 2. (a) Esquema del modelo. (b) Malla de elementos finitos. (c) Detalle de la zona de rotura de la fibra y comienzo del despegue.

El proceso de carga se divide en cuatro pasos. En el primero, la probeta se somete a un decremento de temperatura $\Delta T_0 = -80\,\mathrm{K}$, para simular el enfriamiento tras la solidificación durante el proceso de fabricación de la misma. En el segundo paso se aplica tracción hasta un alargamiento medio $\varepsilon = 1\%$. En el tercer paso, se simula la rotura de la fibra, manteniendo constante la deformación aplicada, retirando la condición de contorno en desplazamientos en el plano de rotura. Por último, se aplica nuevamente tracción hasta un alargamiento medio $\varepsilon = 4\%$.

El análisis numérico se ha llevado a cabo mediante el MEF, empleando el programa ABAQUS. En la Figura 2.(b) se muestra la malla de elementos axisimétricos de cuatro nodos empleada. Como el diámetro de la fibra es varios órdenes de magnitud menor que el de la probeta, es preciso llevar a cabo una disminución progresiva del tamaño de la malla. En la Figura 2.(c) se muestra la malla uniforme empleada en la zona cercana a la rotura de la fibra.

Para simular el comienzo y la progresión del proceso de despegue se han empleado elementos cohesivos (de espesor nulo) COHAX4 en la interfase entre la fibra y la matriz. Dado que en dicha zona se esperan grandes desplazamientos relativos (en comparación con el tamaño de la malla), se ha realizado el análisis en grandes desplazamientos. Aunque los elementos cohesivos empleados permiten modelar los distintos modos planos de fractura, en el modelo actual la fractura se produce en modo II puro (Graciani et al. 2007). Por tanto, el comportamiento a cortadura de los elementos cohesivos empleados es el que se muestra en la Figura 3.

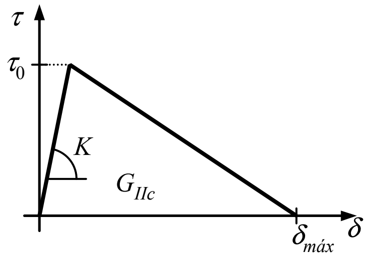

Características de la ley cohesiva:

$G_{IIc} = 50$ J/m^2

$\tau_0 = 210$ MPa

K = 70000 MPa/μm

Fig. 3. Ley cohesiva.

Por último, dado que la resina tiende a contraerse más que la fibra en dirección radial, una vez comienza a propagarse el despegue hay que tener en cuenta el contacto entre la fibra y la matriz. Los elementos cohesivos permiten modelar el fallo a cortadura de la interfase y la propagación del despegue, mientras que las restricciones de contacto previenen la interpenetración una vez que se ha comenzado el despegue.

3. RESULTADOS

En el enfoque cohesivo, mostrado en la Figura 3, se considera que la interfase comienza a dañarse en un punto una vez que se ha alcanzado la máxima tensión (τ_0), dado que, a partir de ese instante, la descarga se produciría por una recta de pendiente inferior a la original. A su vez, se considera que el vértice de la grieta ha alcanzado un punto cuando en dicho punto se supera la máxima apertura definida en la ley cohesiva ($\delta_{máx}$).

En la Figura 4.(a) se muestran los resultados obtenidos en la simulación de la propagación de la grieta de despegue con el modelo cohesivo (empleando el MEF) cuando se desprecia el efecto de la fricción. En la gráfica puede observarse como, tras la rotura de la fibra (ε = 1%), comienza a dañarse la interfase. La longitud de la zona dañada aumenta con la deformación media en la probeta hasta que se forma la grieta de despegue (en torno a ε = 2.2%). A partir de ese momento la longitud de la zona dañada permanece constante y la longitud despegada aumenta con la deformación media en la probeta. En el entorno de ε = 2.75% el crecimiento de grieta se vuelve inestable, con lo cual la pendiente de la curva a/ε se hace vertical. Se han incluido también en la Figura 4(a) los resultados obtenido con un modelo basado en el MEC con el enfoque de la MFEL (Graciani et al. 2007). Puede observarse que los resultados de ambos enfoques son bastante parecidos.

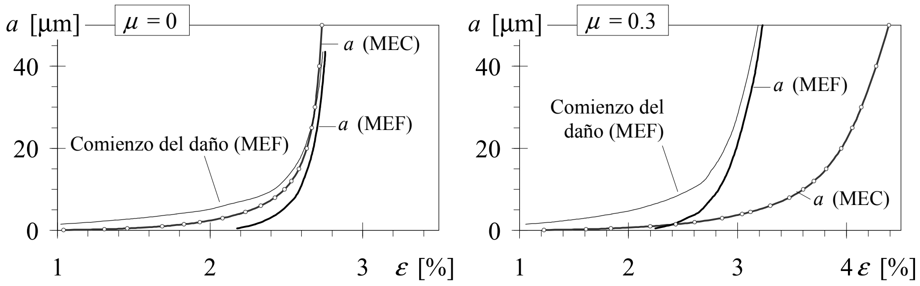

Fig. 4. Propagación de la grieta de despegue: (a) sin fricción, (b) con fricción.

Por último, en la Figura 4(b) se muestran los resultados obtenidos en la simulación de la propagación de la grieta de despegue, con los enfoques anteriormente mencionados, cuando se considera el efecto de la fricción (tomando $\mu = 0.3$). En este caso, ambos enfoques ofrecen resultados cualitativamente similares, el efecto de la fricción se traduce en un retraso en la propagación del despegue y un crecimiento más estable a altas deformaciones. Sin embargo las diferencias cuantitativas son manifiestas.

5. CONCLUSIONES

Se han presentado los resultados de un modelo del ensayo de fragmentación de fibra única empleando el MEF con elementos cohesivos. Dicho análisis ha confirmado que la fricción entre las caras de la grieta retrasa la propagación del despegue y hace que la propagación sea más estable. No obstante, para justificar el origen de las diferencias observadas con los resultados basados en la MFEL es preciso realizar un estudio más profundo de la solución de ambos enfoques.

REFERENCIAS

ABAQUS Inc. (2006). ABAQUS 6.6. Analysis User´s Manual.

GRACIANI, E., MANTIČ, V., PARÍS, F. (2007). Influencia de la fricción en el estado tensional en la fibra y la interfase en el ensayo de fragmentación de fibra única, *en Materiales Compuestos 07* (Ed: Güemes, A., Merino, J.C., Ureña, A.), 551-558, Gráficas 82, SL.

KELLY, A., TYSON, W.R. (1965). Tensile properties of fiber-reinforced metals: copper/tungsten and copper/molybdenum. *J Mech Phys Solids*, 13, 329-350.

Análisis numérico de pandeo de paneles rigidizados de material compuesto

J. Reinoso, A. Blázquez, F. París
Grupo de Elasticidad y Resistencia de Materiales. Escuela Técnica Superior de Ingenieros, Universidad de Sevilla, España

RESUMEN

Uno de los elementos estructurales que mayor interés ha despertado en las últimas décadas para su fabricación con materiales compuestos han sido los paneles rigidizados empleados en los recubrimientos de los fuselajes, estabilizadores y alas de las aeronaves. Estos componentes están formados por una lámina o piel delgada a la que se unen rigidizadores, siendo las secciones transversales más habituales las secciones tipo T, I y Ω, para aportarle la rigidez necesaria. La configuración de los paneles hace que sean estructuras muy sensibles a fenómenos de inestabilidad, fundamentalmente por abolladuras de la pie aunque ello no supongan el fallo del componente. Para aprovechar esta característica, los criterios de diseño permiten sobrepasar la primera carga de pandeo en un cierto margen. El objetivo de este trabajo es el análisis mediante simulaciones numéricas de las cargas y modos de pandeo de un panel rigidizado cilíndrico de material compuesto. El panel considerado tiene dispuestos dos rigidizadores en dirección circunferencial con sección transversal en Ω y se encuentra sometido a una presión uniforme sobre la piel. La resolución numérica de la estructura se ha realizado a través del programa de Elementos Finitos ABAQUS/Standard, usando elementos lineales tipo lámina de integración reducida para la discretización de la estructura. En esta investigación se han llevado a cabo diversas variaciones de ciertos parámetros del sistema, concretamente la secuencia de apilado de las láminas y la distancia entre rigidizadores, para proceder a realizar un análisis de la influencia de los mismos en las cargas y modos de pandeo del componente.

1. INTRODUCCIÓN

En la concepción del diseño de un componente estructural existen numerosos factores a ser tenidos en cuenta para la diseño final del mismo. En el caso de los paneles rigidizados de material se consideran las dimensiones y forma característica de la piel así como la sección transversal de los larguerillos que serán unidos a ésta para conferirle mayor rigidez. Este número de parámetros será incluso mayor en el caso de que el material de ejecución sea láminas apiladas de material compuesto unidireccional ya que la propia secuencia de apilado influirá en la respuesta estructural del componente. Así pues, es preciso realizar un estudio de la influencia de algunos parámetros

2. CARACTERIZACIÓN DE PANELES RIGIDIZADOS

La geometría general de los paneles considerados es la mostrada en la Figura 1. Se trata de un panel curvo, con radio de curvatura 1950 mm, longitud de arco 2500 mm y ancho 1020 mm, rigidizado con dos largueros dispuestos circunferencialmente y simétricos, siguiendo la curvatura. Uno de los parámetros de estudio en el presente trabajo es la influencia de la separación entre rigidizadores, denotada por D, que variará entre 500 y 700 mm en intervalos de 50 mm.

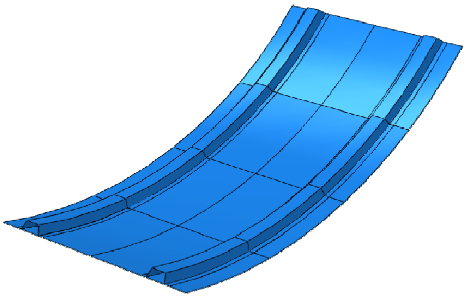

Fig. 1. Tipología de panel rigidizado analizado.

Las propiedades de los materiales empleados para la fabricación de los materiales son recogidos en la Tabla 1. Las secuencias de apilado para cada una de las zonas del panel se muestra en la Tabla.2, donde se ha considerado la variación de la secuencia de apilados en la piel como parámetro de estudio Piel A (láminas a 90º dispuestas exteriormente) y Piel B (láminas a 0º dispuestas exteriormente).

Propiedad	**Cinta**	**Tejido**
Módulo elástico en dirección de la fibra E_1 (Pa)	$122\ 10^9$	$61\ 10^9$
Módulo elástico en dirección transversal a la fibra E_2 (Pa)	$8.5\ 10^9$	$61\ 10^9$
Módulo elástico tangencial en el plano G_{12} (Pa)	$3.4\ 10^9$	$2.2\ 10^9$
Módulo elástico tangencial en el plano G_{13} (Pa)	$3.4\ 10^9$	$2.2\ 10^9$
Módulo elástico tangencial fuera del plano G_{23} (Pa)	$2.2\ 10^9$	$1.5\ 10^9$
Coeficiente de Poisson en el plano de la lámina ν_{12}	0.3	0.05

Tabla 1. Propiedades mecánicas de los materiales.

Zona	**Material**	**Nº Telas**	**Laminado**	**e (mm)**
Cabeza de Ω	Cinta (capas a 90º) Tejido (capas a 0º&45º)	7	(45/90/90/0/90/90/45)	1.576
Alma de Ω	Tejido	3	(45/0/45)	0.84
Piel A(90º)	Cinta	7	(90/45/-45/0/-45/45/90)	1.288
Piel B (0º)	Cinta	7	(0/45/-45/90/-45/45/0)	1.288

Tabla 2. Composición del material utilizado (0º la circunferencial del panel).

La forma de solicitación de los componentes se realiza mediante una carga de presión uniformemente distribuida sobre la superficie exterior de la piel. Por otro lado las condiciones de contorno en los bordes de los paneles son las de empotramiento, impidiendo desplazamientos y giros.

3. RESULTADOS

Los resultados numéricos de cargas y modos de pandeo son recogidos en Tablas 3-7, donde se recogen los valores cuantitativos y cualitativos referidos a los modos de pandeo ($m{\times}n$, siendo m el número ondas circunferenciales y n las ondas axiales) de las cinco primeras cargas de pandeo para cada uno de los paneles considerados.

Carga Crítica	**Carga Piel B (0º)**	**Modo 0º Piel B (0º)**	**Carga Piel A (90º)**	**Modo 90º Piel A (90º)**
1	4307.0	15x1	2055.1	19x1
2	4312.0	15x1	2056.1	19x1
3	4564.6	15x1	2110.8	20x1
4	4583.4	16x1	2114.7	21x1
5	4976.5	16x1	2194.6	21x1

Tabla 3. Cargas y modos de pandeo del panel D=500 mm

Carga crítica	**Carga Piel B (0º)**	**Modo 0º Piel B (0º)**	**Carga Piel A (90º)**	**Modo 90º Piel A(90º)**
1	3829.0	13x1	1740.2	18x1
2	3831.4	14x1	1741.0	19x1
3	4096.6	15x1	1795.3	19x1
4	4096.7	14x1	1798.5	20x1
5	4494.7	16x1	1879.4	20x1

Tabla 4. Cargas y modos de pandeo del panel D=550 mm

Carga crítica	**Carga Piel B (0º)**	**Modo 0º Piel B (0º)**	**Carga Piel A(90º)**	**Modo 90º Piel A(90º)**
1	3453.6	14x1	1512.2	17x1
2	3457.1	12x1	1512.7	18x1
3	3712.2	14x1	1567.2	18x1
4	3736.4	15x1	1569.8	19x1
5	4126.6	15x1	1653.2	19x1

Tabla 5. Cargas y modos de pandeo del panel D=600 mm

Carga crítica	**Carga Piel B (0º)**	**Modo 0º Piel B (0º)**	**Carga Piel A(90º)**	**Modo 90º Piel A(90º)**
1	3151.7	12x1	1339.0	16x1
2	3156.8	13x1	1339.8	17x1
3	3424.2	13x1	1394.7	17x1
4	3427.6	14x1	1396.1	18x1
5	3830.5	15x1	1480.0	19x1

Tabla 6. Cargas y modos de pandeo del panel D=650 mm

Carga crítica	**Carga Piel B (0º)**	**Modo 0º Piel B (0º)**	**Carga Piel A(90º)**	**Modo 90º Piel A(90º)**
1	2904.2	12x1	1203.4	14x1
2	2910.9	11x1	1203.7	15x1
3	3167.8	13x1	1257.9	17x1
4	3197.5	14x1	1261.6	16x1
5	3605.5	14x1	1342.4	18x1

Tabla 7. Cargas y modos de pandeo del panel D=700 mm

En la Figura 2 se aprecia una representación característica de los modos de pandeo de los diferentes componentes analizados y la evolución de las cargas de pandeo con la distancia entre rigidizadores.

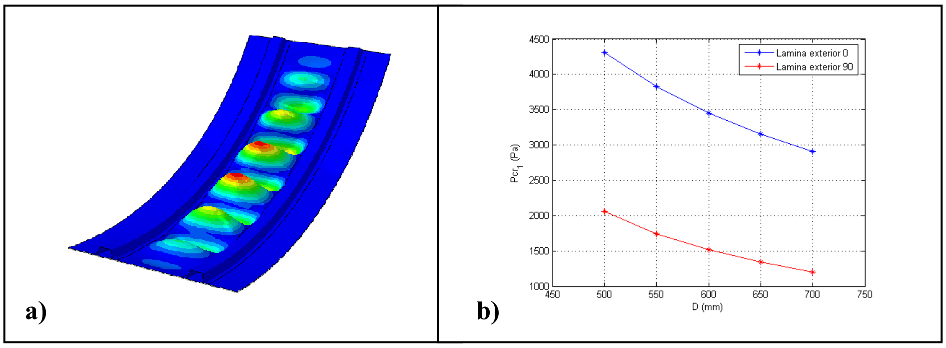

Fig. 2. (a) Forma cualitativa de los modos de pandeo de la estructura. (b) Evolución de las cargas criticas de pandeo con la distancia entre rigidizadores.

4. CONCLUSIONES

A tenor de los resultados expuestos, puede apreciarse como la distancia entre rigidizadores influye notablemente en las cargas y modos de pandeo. Concretamente el hecho de emplear larguerillos en Ω provoca que sólo aparezcan abolladuras en la zona central del componente, quedando aislados los extremos laterales, incluso quedando invariante ante diferentes condiciones de apoyo en los mismos. Con respecto a la secuencia de apilado, a tenor de los modos de pandeo de la estructura, la disposición de las láminas exteriores de la piel dispuestas a 90º resulta más propensas a la aparición de abolladuras que los paneles a 0º, al aportar las primeras menor rigidez que las segundas con lo que el valor de las cargas críticas de pandeo quedan reducidas significativamente.

AGRADECIMIENTOS

Los autores desean agradecer la financiación de este trabajo por los proyectos P06-TEP-02045 de la Junta de Andalucía

REFERENCIAS

ABRAMOVICH H., WELLER T., BISAGNI C. (2008) Buckling behavior of composite laminated stiffened panels under combined shear-axial compression. *J. Aircraft*, **45**, pp. 402-413.

FALZON, B.G., STEVEN, G.P. (1997) Buckling mode transition in hat-stiffened composite panels loaded in uniaxial compression. *Comp. Struct*, **37** (2), pp. 253-267.

ROMEO, G., FRULLA, G. (1995) Nonlinear analysis of graphite/epoxy wing boxes under pure bending including lateral pressure. *J. Aircraft*, **32** (6), pp. 1375-1381.

STARNES JR., J.H., KNIGHT JR., N.F., ROUSE, M. (1985) Postbuckling behavior of selected flat stiffened graphite-epoxy panels loaded in compression. *AIAA Journal*, **23** (8), pp. 1236-1246.

STEVENS, K.A., RICCI, R., DAVIES, G.A.O. (1995) Buckling and postbuckling of composite structures. *Composites*, **26** (3), pp. 189-199.

Three dimensional finite element model of a non-crimp fabric laminated using geometrically straight tows with crimped material properties

L.M. Ferreira
Departamento de Engenharia Mecânica. Escola Superior de Tecnologia de Abrantes do Instituto Politécnico de Tomar, Portugal
E. Graciani, F. París
Grupo de Elasticidad y Resistencia de Materiales. Escuela Técnica Superior de Ingenieros de la Universidad de Sevilla, España

ABSTRACT

The compressive failure of a $[0,90]_n$ non-crimp fabric laminate is studied using a 3D finite element model of the representative unit cell at mesoscopic scale. In previous analyses, tow elements coordinate systems were oriented in the actual direction of the fibres. Therefore, the same transversely isotropic mechanical behaviour was employed for every tow element (defined in the element coordinate system). A new approach is presented in this work, in which the geometrical crimp of the tows is neglected and straight tows are created. The actual crimp of the fibres is considered by introducing suitable anisotropic material properties in each zone of the tow. Anisotropic properties have been obtained by a rotation of the actual transversely isotropic mechanical behaviour, taking into account the actual orientation of the crimped fibres. This approach requires a larger amount of work to define the material properties but, on the contrary, the mesh can be easily created for any configuration. Results obtained with the new approach (i.e., the 'straight tows' model) have been successfully compared with those of the previous analyses (i.e., the 'crimped tows' model).

1. INTRODUCCIÓN

Non crimp fabric (NCF) composites have a complicated internal structure which affects the performance of the NCF composites, depending on the load scenario. It is then appropriate to develop a numerical model of a NCF composite prior to experimental characterization, in order to understand the influence of a significant number of parameters (for example, resin and fibre properties, internal geometry,…), in the elastic behaviour of the laminate and in the mechanisms of failure.

A full 3D finite element model, with a new approach in the definition of the crimp, has been developed to predict the failure mechanism under compressive loads.

2. MESOSCOPIC APPROACH OF THE NCF

The present study has been made at the mesoscopic level. Tows have been modelled as a homogenous material (without considering their microscopic constituents: resin and fibres). Different anisotropic properties (defined in the global coordinate system) have been employed in the different zones of the tows, obtained by a rotation of the transversely isotropic mechanical behaviour, taking into account the actual orientation of the crimped fibres. Resin pockets have been modelled as a homogeneous isotropic material occupying the spaces between the tows.

The analysis has been made under the hypothesis of large displacements (using ANSYS software) and the load has been applied in a linear and progressive manner, until instability is reached. Linear elastic material behaviour has been considered.

2.1 Description of the 3D FEM

To present the model analyzed in this study it is necessary to define the concept of the representative volume element (RVE). It is a minimum repeatable cell which allows us to build any part of the non-crimp fabric composite by stacking multiple RVE. Due to the symmetry of the RVE, only one quarter RVE has been considered. The process to obtain the RVE, as well as the model analysed, is represented in Figure 1.

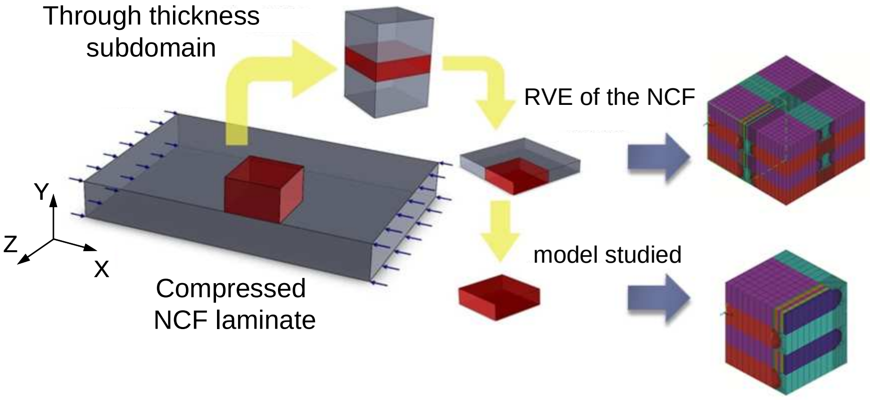

Fig. 1. Process to obtain the RVE and the analysed model.

2.2 Mechanical properties of the tows and resin

Structural solid element (SOLID185) with anisotropic behaviour in global coordinate system has been employed. The mechanical properties considered correspond to a T300/914 composite with a 55% volumetric fibre fraction, similar to the one used by Drapier and Wisnom (1999) and Graciani et al. (2005). The mechanical properties of resin and tows in a local coordinate system are presented in Tables 1 and 2. In the tows, direction 1 is the fibre direction, and directions 2 and 3 are the transverse directions.

Properties	Value
E_{11}	129 GPa
$E_{22} = E_{33}$	9.77 GPa
$\nu_{12} = \nu_{13}$	0.32
ν_{23}	0.45
G_{23}	1.5 GPa

Table 1. Tow's material constants.

Properties	Value
E_m	4.5 GPa
ν_m	0.4

Table 2. Resin's material constants.

A maximum crimp angle of 3° has been considered in the model. The properties of each tow element are defined taking into account the actual crimp in the fibres located at the position of the element. The crimped elements were identified and the corresponding angle of crimp was calculated for each element. The angle of rotation used to simulate the crimp in the elements transforms the mechanical properties from transversely isotropic to anisotropic. The stiffness properties calculated for every element/angle, are defined as distinct anisotropic materials in the finite element model.

2.3 Boundary conditions

The boundary conditions applied to the faces of the model serve to impose the compressive stress state and guarantee the displacements compatibility in the limits of the model with the rest of the structure. Symmetry conditions have been assumed in the faces parallel to the XY plane and one of the faces parallel to YZ plane. The opposite face parallel to the YZ plane has a pure compressive load applied and displacements of its nodes are coupled to ensure that all nodes displace the same in the load direction. The boundary conditions in the top and bottom faces (parallel to the XZ plane) must guarantee the compatibility of the RVE under consideration with the adjacent RVEs. Thus, displacements of the nodes in both faces are coupled to ensure that the extension in the thickness direction is constant through the whole model.

3. RESULTS

Considering the boundary conditions and the load imposed, it is expectable that the 0º tows suffer instability phenomenon, known as mesobuckling.

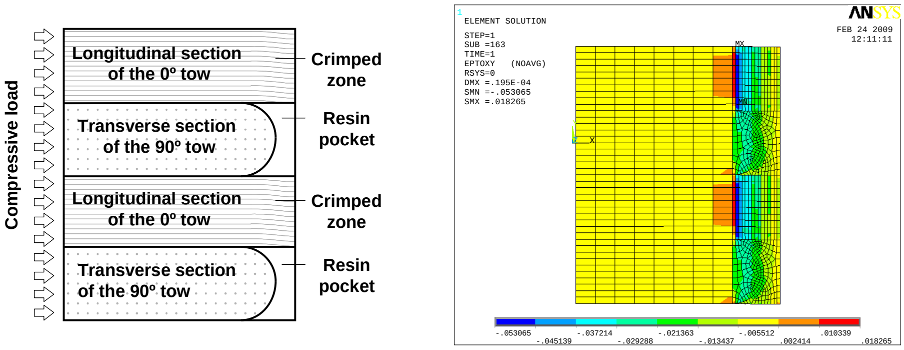

(a) (b)

Fig. 2. Results in $z = 0$ face. (a) Sketch of the model (b) γ_{xy} shear strains.

Figure 2(b) represents the γ_{xy} shear strain through the front face of the model (normal to Z axis). The model is sketched in Fig. 2(a) showing the different zones considered in the model. It is possible to appreciate the repetitive solution of strains within the tows having the same orientation. It can also be observed that the larger strain gradients arise in the zone where the 0º tows are affected by the crimp (i.e, where packages of resin appear between the 90º tows). Two consecutive vertical rows of elements appear in the 0º tows, one of them having the maximum positive value of γ_{xy}, and the other having the maximum negative value of γ_{xy}. The evolution of γ_{xy} strains along the ideal direction of the fibres in the 0º tows (called direction B) can be clearly appreciated in Figure 3.

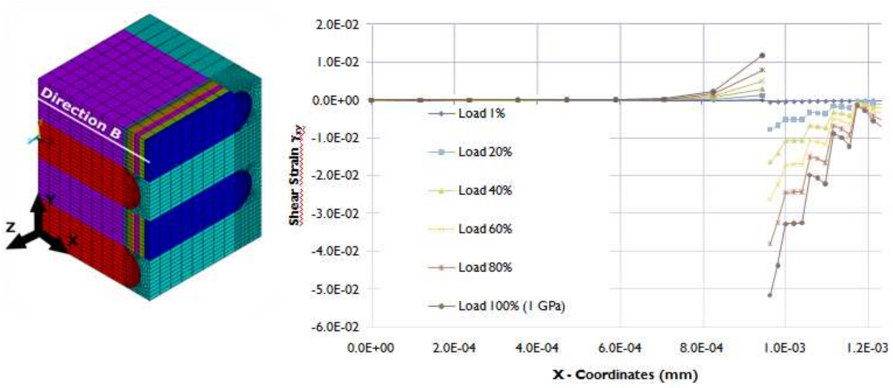

Fig. 3. Evolution of γ_{xy} shear strains along the represented direction.

The results lead to think that the failure of the NCF under this type of load is controlled by the shear strains that appear in the 0º tow. The abrupt jumps in the shear strain take place in the zone where the 0º tow stops to be in contact with the adjacent 90º tow, and start to be in contact with the resin. The difference between the stiffness of the 90º tow and the stiffness of the resin is responsible for this jump in the shear strain and consequently it is in the root of the failure of the composite. This failure mechanism is in agreement with the results shown by Graciani et al. (2005), using a more complicated FEM model in which the tow elements were oriented following the actual crimp of the fibres.

4. CONCLUSIONS

The behaviour of an antisymmetric $[0,90]_n$ NCF composite under in-plane compressive load has been studied using a new 3D finite element model. In this model the fibre crimp is modelled by means of an appropriate definition of the material properties in the elements. The results obtained are similar to those shown in Graciani et al. (2005).

The advantages of this model in comparison with previous models are the rapid modelling and meshing and the possibility of introducing complex crimps without changing the geometry of the model (to simulate, for example, the effect of stitching in the NCF composite). However the geometrical simplification implies the use of certain algebraic calculations to determine the mechanical properties in the crimped zones. As an additional advantage, the use of a simpler geometry in the new FEM results in a higher quality mesh, which leads to better convergence of the non-linear analysis.

REFERENCES

DRAPIER, S., WISNOM, M.R. (1999), Finite-element investigation of the compressive strength of non-crimp-fabric-based composites. *Compos Sci Technol,* 59, 1287-1297.
GRACIANI, E., GONZÁLEZ, A., PARÍS, F. (2005) Análisis del comportamiento a compresión de un laminado [0,90,0,90] de tejido no ondulado mediante un modelo 3D de elementos finitos. Materiales Compuestos 05 (Ed. Amigo, V., Payá, J.J., Salvador, M.D., Monzó, J.M., Segovia, F., Borrachero, V.), 877-884, Editorial de la UPV.

Desarrollo y validación de un modelo matematico para el cálculo de propiedades mecánicas de materiales compuestos

V. Barrera, C. Carvajal, J.S. Márquez, C. Quiroga
Universidad de San Buenaventura, Bogotá D.C.

RESUMEN

Para el desarrollo del proyecto en primera instancia se desarrolló un modelo matemático programado en el software matemático Matlab® utilizando diferentes teorías desarrolladas de mecánica de materiales compuestos y de criterios de falla como Máximo-Esfuerzo, Máxima-Deformación, Tsai-Hill, Tsai-Wu y Hashin-Rotem, capaz de estimar las propiedades mecánicas de un material compuesto en función de propiedades físicas y mecánicas de sus materiales constituyentes y de la orientación de las fibras de refuerzo, para de esta manera evaluar la interdependencia de dichas propiedades por medio de diferentes gráficas que las asocien; además se evalúa el comportamiento de laminados por medio de la teoría clásica de laminación, a partir de las propiedades del material compuesto, del número de láminas y la dirección de refuerzo.

Como segunda parte se validaron las teorías para el cálculo de algunas propiedades a partir de comparación y análisis entre las propiedades teóricas generadas por el modelo y las propiedades experimentales obtenidas de la caracterización bajo estándares ASTM de dos materiales compuestos de matriz polimérica de aplicación aeronáutica: fibra de vidrio/epóxico y fibra de carbono/epóxico; para finalmente establecer unos factores de corrección que ajustaron los resultados teóricos con respecto a los resultados empíricos que se obtuvieron al producir los materiales con las facilidades de fabricación con las que cuenta actualmente Colombia y específicamente la Universidad de San Buenaventura.

El modelo matemático validado permitirá tener una herramienta para el cálculo y diseño de materiales compuestos, útil para el desarrollo de los proyectos de la Universidad en la misma área que involucren el diseño de componentes, fabricados con materiales compuestos, ya que permitirá realizar una estimación de las propiedades mecánicas del material teniendo en cuenta diferentes factores que las afectan, y a su vez evaluar distintas configuraciones de material que cumplan con requerimientos de diseño establecidos; disminuyendo los costos y el tiempo necesario de realizar una evaluación experimental para hallar el material y la configuración adecuadas para el diseño de algún componente.

Energy absorbing bonded structures for increased aeronautic safety

P.N. Soeiro Ferreira
Altran Technologies, Madrid

RESUMEN

The security of an aircraft during impact can be defined as the ability to withstand damages without harming its occupants. Generally speaking, the sources of injuries in an aircraft impact crash are: High deceleration forces, trauma by direct impact against hard surfaces, exposure to after-impact environment (fire, smoke, etc). Thereby, the design of the aircraft structure should take into account every possible source of harm to the occupants and eliminate it. This implies redesigning the cabin structure, development of appropriate seats and fixing devices, reduction of the impact energy, elimination of injuring objects and choosing materials that do not produce harming smokes if ignited. Some of the most recent models of helicopters have special structures that were designed to absorb energy during impact. For reasons that are linked to structure certification and the use of approved calculus methodologies, the development of design concepts, namely structural joints, did not evolved in parallel with the more advanced materials that are used to build those structures. In the frame of this work we developed a line of investigation to characterize the performance of special designed structures that use structure debonding as a means of absorbing impact energy.

Análisis numérico del campo de desplazamientos del ensayo de flexión oblicua en composites unidireccionales

J.M. Romera, I. Adarraga, M.A. Cantera, F. Mujika
Departamento de Ingeniería Mecánica, Escuela Politécnica de Donostia - San Sebastián.
Universidad del País Vasco/Euskal Herriko Unibertsitatea

RESUMEN

El objetivo del presente trabajo es proponer una nueva alternativa a la modelización del ensayo de flexión oblicua de tres puntos desde una perspectiva numérica utilizando el Método de los Elementos Finitos para composites unidireccionales de resina epoxy reforzados con fibra de carbono. Además, se compararán los resultados obtenidos de estos modelos numéricos con los procedentes de unos modelos analíticos recientemente desarrollados. Para la modelización de los contactos entre los cilindros y la probeta se han utilizado elementos gap lineales.

1. INTRODUCCIÓN

Recientes estudios (Mujika et al. 2003) han tratado el ensayo de flexión de tres puntos desde un punto de vista analítico. En dichos trabajos se ha desarrollado un extenso número de ensayos experimentales con diferentes luces y ángulos de orientación de fibra, para contrastar el campo de desplazamientos real con el obtenido a partir de estos modelos analíticos. Concretamente se midió la deflexión en el punto central de la probeta, que resultó ser muy próxima a los valores estimados por los modelos.

El problema fundamental que surge es que existen dos tipos de comportamiento de las probetas al someterlas al ensayo. En unas ocasiones el contacto entre la probeta y los cilindros de apoyo es toda la generatriz de contacto (caso sin despegue), y, sin embargo, en otras, el contacto entre probeta y cilindros de apoyo se reduce a un punto en cada apoyo, colocados en extremos opuestos, levantándose la probeta por encima de ambos cilindros (caso despegue).

En este trabajo se va a llevar a cabo un análisis numérico de carácter estático y lineal basado en el Método de los Elementos Finitos, usando una formulación híbrida que combina el método de las fuerzas y el de los desplazamientos. El tipo de elemento usado son cáscaras basadas en la First Shear Deformation Theory (FSDT), concretamente cáscaras de la formulación de Belytschko (Belytschko et al. 1984). Para simular el contacto entre rodillos y probeta se han utilizado elementos de contacto del programa COSMOS/M denominados elementos gap lineales. En la Figura 1 se detalla el modelo numérico utilizado para el análisis con sus correspondientes condiciones de contorno.

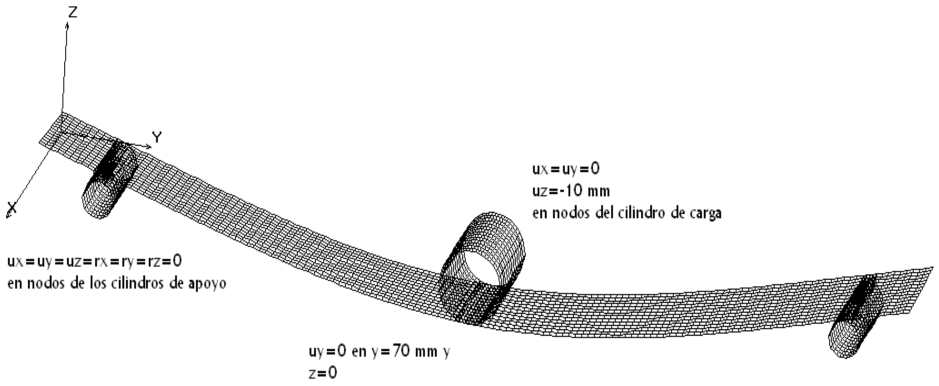

Fig. 1. Modelo, condiciones de contorno y deformada de la probeta.

2. RESULTADOS

Se analiza una probeta fabricada a partir de una secuencia de capas prepreg IM7-8552 de igual orientación de fibra. Las dimensiones de la probeta son: largo 140 mm, ancho 15 mm y espesor 2,118 mm. La luz entre apoyos y la orientación de la fibra con respecto a la dirección longitudinal de la probeta son respectivamente, 120 mm y 45º.

2.1 Selección del tipo de elemento y de la densidad de malla

Antes de preparar el modelo definitivo, se realizó un estudio comparativo, mostrado en la Figura 2, entre cuatro modelos diferentes para determinar el tipo de elemento y la densidad de malla apropiados.

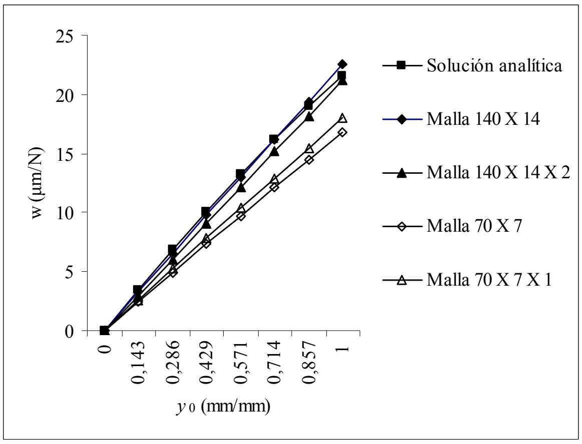

Fig. 2. Campo de desplazamientos en la línea de contacto con los apoyos.

2.2 Campo de desplazamientos del modelo numérico

La pendiente carga-desplazamiento obtenida en el punto medio de la probeta fue analíticamente 4,580 N/mm y numéricamente 4,591 N/mm, siendo el error 0,24 %.

Para esta combinación de luz con ángulo de orientación de fibra, el modelo analítico y el numérico preveían despegue. Los resultados de ambos son comparados en la Figura 3, donde se representa la distribución de desplazamientos verticales (w) frente a la coordenada normalizada de su anchura (y_0) en la línea de contacto entre la probeta y el cilindro de apoyo.

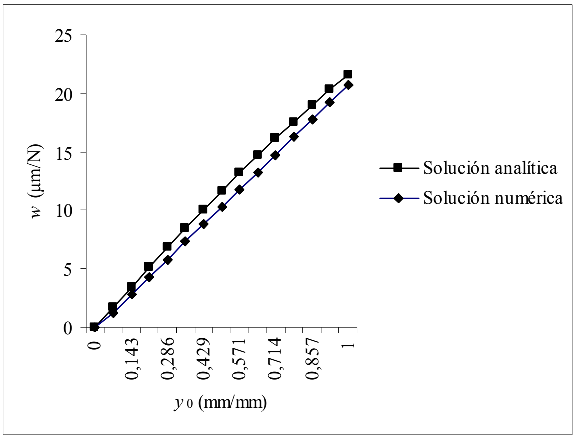

Fig. 3. Distribución de desplazamientos verticales a lo largo de la línea de contacto con el cilindro de apoyo.

Por otra parte, la Figura 4 presenta los resultados en los modelos analítico y numérico de la distribución de desplazamientos en la línea de contacto con el cilindro de carga.

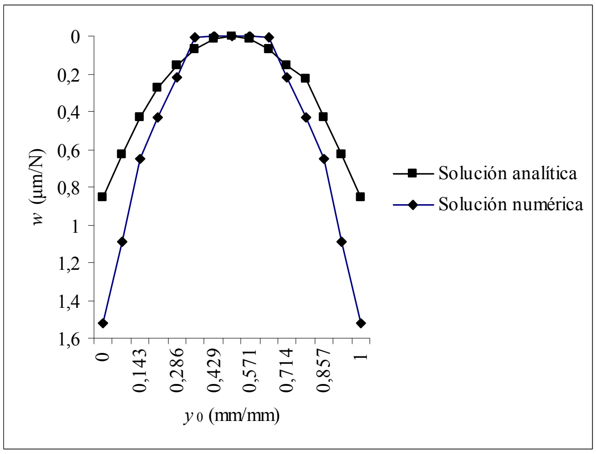

Fig. 4. Distribución de desplazamientos verticales a lo largo de la línea de contacto con el cilindro de carga.

3. CONCLUSIONES

Los resultados de los modelos numéricos se aproximan al del modelo analítico desarrollado en un estudio anterior. Si se observa, por ejemplo la deflexión en el punto medio se puede comprobar que entre ambos existe una discrepancia de un 0,24%.

Si se analizan los resultados de ambos modelos para la distribución de desplazamientos en la línea de contacto de la probeta con el cilindro de apoyo, se puede concluir que las estimaciones de ambos modelos concuerdan.

Sin embargo, en el caso de las distribuciones de desplazamiento a lo largo de la línea de contacto con el cilindro de carga, los resultados para ambos modelos presentan discrepancias. Por un lado, en el modelo analítico se supone un contacto puntual, mientras que el modelo numérico presenta una longitud de contacto de 3,2 mm. La razón de esta discrepancia es que en el modelo numérico se establece una línea de elementos gap de contacto para que sea el propio análisis el que establezca a través de qué gaps se transfiere la carga.

Se puede concluir que si bien el modelo analítico establece con precisión el campo de desplazamientos de la probeta a nivel global, la situación local correspondiente a las proximidades de la zona de aplicación de carga se complementa con los resultados del análisis numérico.

REFERENCIAS

BELYTSCHKO, T., STOLARSKY, H., CARPENTER, N. (1984). A Triangular Plate Element with one-point Quadrature. *International Journal for Numerical Methods in Engineering,* 20, 787-802.

MUJIKA, F., MONDRAGÓN, I. (2003). On the Displacement Field for Unidirectional Off-Axis Composites in 3 Point Flexure. Part I: Analytical Approach. *Journal of Composite Materials,* 37, 1041-1066.

T9. MECHANICAL AND PHYSICAL BEHAVIOUR
COMPORTAMIENTO FÍSICO Y MECÁNICO

Effect of poly(methyl metacrylate-co-acrylate amide) electrocoating on carbono fibre-epoxi composites: adhesion and mechanical properties

C. Tridech[1], P. Robinson[2], A. Bismarck[1]
[1]Polymer and Composite Engineering Group (PaCE),
Department of Chemical Engineering
[2]Composites Centre, Department of Aeronautics,
Imperial College London, South Kensington Campus, London SW7 2AZ UK.

SUMMARY

A continuous polymer electrocoating route has been applied to tailor adhesion between carbon fibres and an epoxy matrix. A copolymer coating consisting of methylmethacrylate (MMA) and acrylamide (AAm) was introduced as a flexible interface between fibres and matrix. Unidirectional unsized carbon fibres were successfully uniformly electrocoated with poly(methylmethacrylate-co-acrylamide) (p[MMA-co-AAm]). The electrocoating leads to an increase of fibre diameter from 7 to 8 μm as measured by the Wilhelmy technique. Interfacial shear strength between electrocoated fibre and epoxy matrix, which was studied by single fibre pull-out tests, has been improved from 91 MPa (PMMA electrocoated fibres) to 98 MPa (p[MMA-co-AAm] electrocoated fibres). Water contact angle shows that electrocoated fibres are more hydrophilic than unsized carbon fibres. The coating has altered the fibre surface properties and led to changes in carbon fibre-epoxy composite performance. Flexural modulus of fibre-epoxy composites, which was investigated by the three point flexural test, has been enhanced from 62 GPa of original fibre-epoxy composites to 87 GPa of p[MMA-co-AAm] electrocoated fibre-epoxy composites.

1. INTRODUCTION

Fibre reinforced composites provide advantages such as excellent thermal resistance and low density with high strength relative to ordinary bulk engineering materials, such as steel, wood, brass and aluminium (Jones 1999). However, the fibre-matrix adhesion needs to be optimised in order to effectively transfer stress between reinforcement and matrix to obtain optimal composite performance. The aim of this work is to introduce a flexible interface in between carbon fibres and epoxy matrix. Such interfaces could provide more roughness between reinforcement and matrix, as a result, more flexibility to the whole composite performance while using at high temperature. The more flexibility of the composite can result in a reduction of maintenance requirements.

Poly methyl methacrylate (PMMA) has been introduced as a coating for unidirectional unsized carbon fibres (Bismarck et al. 2005). They polymerised MMA onto carbon fibres by electro-deposition. However, PMMA has insufficient adhesion to an epoxy matrix. Therefore, PMMA was modified in order to improve the adhesion between PMMA coating and epoxy matrix. Acrylamide (AAm) was selected as a copolymer for the coating. It has been shown by Bismarck et al. (2002) that acrylamide provide an admirable adhesion to an epoxy matrix when it was electrocopolymerised with carbazole and used as a coating interface between carbon fibres and epoxy. Therefore, the coating, which will be deposited onto the carbon fibres surface, is poly(methyl methacrylate-co-acrylamide)

2. EXPERIMENTS AND CHARACTERISATION

Electrografting or electro-deposition, which offers uniform coatings all along the fibres length in a continuous process (Kumru et al. 2001), was selected as a method for applying poly(methyl methacrylate-co-acrylamide) coatings to carbon fibres. The electrocoated fibres were characterised by various methods in order to study surface properties and adhesion behaviour to an epoxy matrix.

As-received 12k unsized AS4 carbon fibres (Hexcel) was used for this study. The fibres was processed continuously at 0.35cm/s with 150g tension through a electrode tube which was immersed in the electrolyte mixture consisting of methyl methacrylate (Sigma-Aldrich) and acrylamide (Sigma-Aldrich) at 65°C. Electrical current at 0.4A was applied to the electro-deposition setup. The electrocoated fibre were washed with acetone (VWR) and dried overnight in an oven at 55°C. The electrocoated fibres were prepared in different electrolyte composition (MMA:AAm) to tailor the coating composition. Electrocoated fibre-epoxy composites were manufactured by vacuum bagging.

The electrocoated fibres were characterised by Scanning electron microscope (SEM) to study their surface morphology. Wilhelmy technique with dodecane testing liquid was used to measure the single fibre diameter. The technique also analysed contact angle between modified fibres and testing liquids such as deionised water and formamide. Then, surface free energy of electrocoated fibres were calculated from Wilhelmy characterisation data. Thermo gravimetric analysis (TGA) in air atmosphere was used to determine the mass of coating on the fibres. The adhesion behaviour between coated single fibre and epoxy matrix was studied by the single fibre pull-out test. Flexural modulus of electrocoated fibre-epoxy composites was investigated by the three point flexural test.

3. RESULTS AND DISCUSSION

Unidirectional unsized carbon fibres were successfully uniformly electrocoated with poly(methylmethacrylate-co-acrylamide). Typical scanning electron micrographs (SEM) of electrocoated carbon fibres (Fig. 1.) show that p[MMA-co-AAm] uniformly covered the carbon fibres. The coating is clearly distinguished by its surface roughness while an original surface of unsized carbon fibre is very smooth and clean.

The successful electrocoating leads to an increase of the single fibre diameter from 7 to 8 μm by the consistent deposition of p[MMA-co-AAm] as measured by the Wilhelmy technique using dodecane as the testing liquid. The results support the values measured from SEM images. The onset temperature of the degradation of the electrocoated carbon fibres in p[MMA-co-AAm] (494°C) was as expected, much lower as compared to original carbon fibres (555°C). From the original weight loss it can be inferred that 7 wt.% p[MMA-co-AAm] was coated onto the carbon fibres. The water contact angle of fibres decreased from 76° to 45° after the electrocoating with p[MMA-co-AAm]. The reduction of water contact angle of the fibres indicates that the surface of coated fibres is more hydrophilic due to presence of amine functional groups in the p[MMA-co-AAm] coating. Surface free energy of the electrocoated fibres were calculated by Fowkes theory (Fowkes 1964) using data from Wilhelmy characterisation with deionised water and formamide testing liquids. The surface free energy of the carbon fibres increased after applying an electrocoat. Modified fibres which were electrocoated in electrolyte containing higher AAm concentration had a higher surface free energy and polar component of surface free energy comparing to those of electrocoated fibres in low AAm concentration.

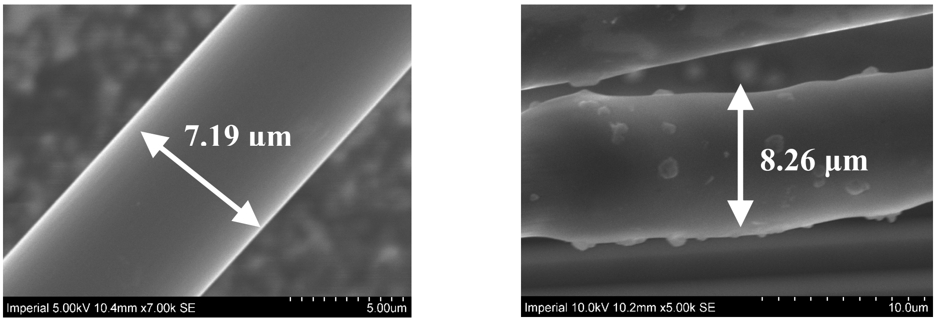

Fig. 1. Scanning electron micrographs of unsized carbon fibres (left) and poly(methylmethacrylate-co-acrylamide) electrocoated carbon fibres (right).

Single fibre pull-out tests indicate that the electrocoated fibres with high AAm content have a higher interfacial adhesion to an epoxy matrix (98 MPa) compared to those of modified fibres with low AAm content (91 MPa) whereas unsized carbon fibres show the highest interfacial adhesion to epoxy (103 MPa). The results support the hypothesis that AAm coating improves an adhesion between modified PMMA coating and epoxy matrix although the interfacial adhesion between electrocoated fibres and epoxy is slightly less than that of original fibres. Three point flexural tests of fibre-epoxy composites show that p[MMA-co-AAm] electrocoated fibre-epoxy composites have a highest flexural modulus (87 GPa) compared to those of PMMA electrocoated fibre-epoxy composites (80 GPa) and especially unsized carbon fibre-epoxy composites (62 GPa). It can be explained that the improvement is produced by the surface roughness of the electrocoated fibres which enhanced the adhesion between carbon fibres and epoxy matrix.

4. CONCLUSIONS

As shown in this study poly(methylmethacrylate-co-acrylamide) was successfully electrocoated onto unsized carbon fibres which can be clearly observed from SEM images. The fibre diameter increased from 7 to 8 µm after electrocoating with 7 wt.% p[MMA-co-AAm] coating deposited and water contact angle decreased from 76° to 45° indicating a more hydrophilic surface of modified fibres. The fibres surface free energy increased.

The electrocoating AAm improves an adhesion between modified PMMA coating and epoxy matrix as confirmed by the results from single fibre pull-out test. The interfacial shear strength of electrocoated fibre with AAm is higher than that of the electrocoated fibre without AAm although the unsized carbon fibres show the strongest interfacial adhesion to epoxy matrix. The enhancement in interfacial adhesion led to an improvement in composite performance studied by three point flexural tests. p[MMA-co-AAm] electrocoated fibre-epoxy composites show a higher flexural modulus comparing to those of original carbon fibre-epoxy composites

ACKNOWLEDGMENT

The authors are very grateful to the Royal Thai government for funding. The single fibre pull-out machine is kindly supported by BAM-Berlin. Technical assistance from PaCE group is gratefully acknowledged.

REFERENCES

BISMARCK, A., MENNER, A., KUMRU, M.E., SEZAI SARAC, A., BISTRITZ, M., SCHULZ, E. (2002). Poly(carbazole-co-acrylamide) electrocoated carbon fibers and their adhesion behavior to an epoxy resin matrix. *J. Mater. Sci.*, 37, 461-471.
BISMARCK, A., LEE, A.F., SEZAI SARAC, A., SCHULZ, E., WILSON, K. (2005). Electrocoating of carbon fibres: A route for interface control in carbon fibre reinforced poly methylmethacrylate?. *Compos Sci Technol.*, 65, 1564-1573.
FOWKES, F.M. (1964). *Ind. Eng. Chem.,* 5, 40.
JONES, R.M. (1999) *Mechanics of Composite Materials,* 519 p., Taylor & Francis, London (UK).
KUMRU, M.E., SPRINGER, J., SEZAI SARAC, A., BISMARCK, A. (2001). Electrografting of thiophene, carbazole, pyrrole and their copolymers onto carbon fibres: electrokinetics measurements, surface composition and morphology. *Synth. Met.*, 123, 391-402.

New advances for the topographic characterisation of sheet moulding compounds

A. Calvimontes, K. Grundke, A. Müller
Leibniz Institute of Polymer Research Dresden, Hohe Strasse 6, 01069 Dresden,Germany

ABSTRACT

For a comprehensive study of Sheet Moulding Compounds (SMC) surfaces, topographical data obtained by a contact-free optical method (white light chromatic aberration imaging) were submitted systematically to statistical, functional and volumetrical characterisation methods. Optimal sampling conditions (measure length and resolution) were obtained by a topographical-statistical procedure proposed on the present work.

The influence of moulding conditions (pressure, moulding time, metallic mold topography, metallic mold form, prepregs placement procedure, glass fibres content and glass fibres orientation) on resulting macro-, meso- and micro-morphology of the SMC surface were studied by using different measure lengths as well as mathematical filtering operations by the topographical data.

1. INTRODUCTION

SMC materials are based on glass fibres and unsaturated polyesters with styrene matrix as comonomer for crosslinking together with inorganic fillers (mainly calcium carbonate) and other chemicals for curing, aspect control, etc.

Due to the high heterogeneity of SMC materials it is difficult to fulfil optical requirements of the automotive industry. By controlling the processing conditions, surface properties of SMC can be optimized for subsequent coating. It was the aim of this study to perform a systematic topographical functional characterization of SMC materials in order to qualify and quantify the coatability and the optical parameters of these surfaces. Only a small number of studies using SMC materials for compression moulding have shown the effects of fibre type and length on resulting surface quality (Kim et al. 1997, Boylan et al. 2003).

2. MATERIALS

Samples of SMC were produced under defined temperature (147.5 ± 2.5°C), and different conditions of pressure (3.5 to 14 MPa) and moulding time (60 to 360 s). Plates having 0% and 10 % and 30% of glass fibres were studied.

3. EXPERIMENTAL

3.1 Measure of the topography

A 3D imaging measuring instrument was used for the optical analysis of the topography of SMC surfaces, MicroGlider® (FRT, Germany). This instrument uses an optical sensor based on the principle of chromatic aberration of light (Ruprecht et al. 2005). White-light is focused on the surface by a measuring head with a strongly wavelength-dependent focal length (chromatic aberration). The spectrum of the light scattered on the surface generates a peak in the spectrometer. The wavelength of this peak along with a calibration table reveals the distance from sensor to sample. The sensor works on transparent, highly reflective or even matt black surfaces (Ruprecht et al. 2004).

3.2 Topographic characterisation

Measure length (L_m) and resolution (Δ_x, assuming $\Delta_x = \Delta_y$) are the most important sampling parameters, that besides some particular instrumental dependent ones, must be optimal defined before characterising a topography.

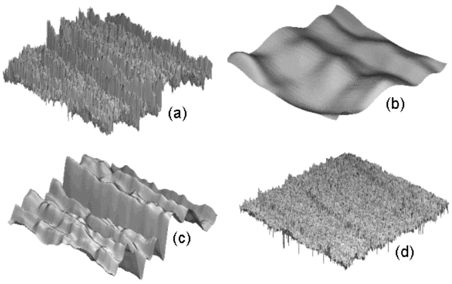

$L_m = 3$ mm; $\Delta_x = \Delta_y = 5$ µm; $\Delta_z = 1$ nm

Fig. 1. Total SMC topography (a), isolated short waviness (b), isolated mean roughness (c) and isolated arithmetic. mean

Before topographical characterisation, an adequate selection of optimal sampling conditions (cut-off length and resolution) were done by a systematic procedure proposed by Calvimontes (2009) for the characterisation of periodic and non periodic surfaces at different length scales (Figure 1). In order to probe the reliability of the optimized sampling conditions (L_m = 3 mm and Δ_x = 5 µm), seven independent topographic measurements were performed over different regions of the sample surface. Standard deviation of the resulting parameters show that R_a is statistically more reliable than W_z and R_z. However, this results also show how much dependent are the topographic parameters on measure position. The reasons will be analysed in the next paragraphs.

Using the obtained optimal parameters, about two hundred topographic measurements at the same and different coordinates of the SMC-plates (corresponding to identified positions of the metallic mold) were realized. The resulting surface data were processed by FRT-Mark III Software (FRT, Germany) using mathematical filtering by Fast Fourier Transformation Method, whose graphical 3D representation can be seen in Figure 1. Three meso-topographic parameters were calculated: short-waviness (W_z), mean-roughness (R_z) and number of long waves on L_m (N_z). Three micro-topographic parameters were obtained: arithmetic mean roughness (R_a), number of short waves on L_m (N_a), and porosity (V_o), which is defined as the filling quantity or void volume under the mean height of the surface per area unit.

Additional, long-waviness (L-W_z) using L_m=100 mm and Δ_x=100 µm was measured in order to study the macro-morphology of the surface.

4. RESULTS AND DISCUSSION

4.1 Moulding conditions and topographical transfer from metallic mold

Schubel et al. (2006) used microscopic and stylus profiling methods in order to correlate R_a values to study roughness effects on SMC surface quality. To our present work, three different SMC plates that correpond to defined moulding conditions (pressure and moulding time) were selected. On each one of them, the topography of sixty defined positions were characterised by chromatic confocal imaging using L_m = 3 mm and Δ_x = 5 µm. Figure 2 shows that, from a statistical point of view, mean values of W_z, R_z and N_z could characterise the topography as a function of moulding conditions. According to our results, moulding conditions control the meso-topography of the SMC surfaces studied and apparently not at all the micro-topography characterised using R_a values.

By comparing the measured topographic parameters between plates at the same position, it was clear that the topography of the metallic mold controls the resultant meso-topography of the SMC surface more specific than moulding conditions, by transference of its surface irregularities.

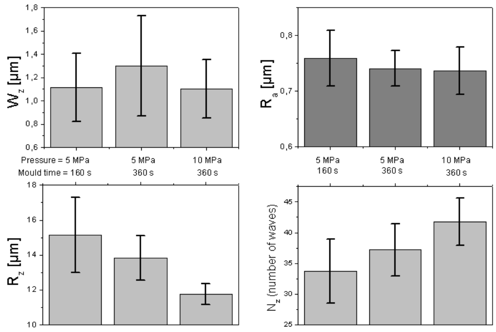

Fig. 2. Influence of moulding conditions (pressure, moulding time) on meso (W_z, R_z, N_z) and micro topography (R_a).

As a important conclusion, by SMC any topographic characterisation of surface modification processes (by cleaning by powerwash for example) must be realized by comparing topographical changes of identified mold-plate positions. For a systematic study of mold influence on resultant SMC surfaces, it is necessary to previously measure the topography of the metallic mold. However, a direct measure of the mold topography was not possible because the size and weight of the metall piece. For this reason, a print of the mould surface was obtained using polydimethilsiloxan (PDMS) (Fig.3), which is proved to reproduce nanoscale structures with great fidelity (Kim et al. 2003). Before applying this process to the metallic mold, an experimental probe and calibration of this procedure were realized by measuring the topography of a small metallic piece of the same material of the mold and comparing its topography with the topography of the obtained PDMS surface.

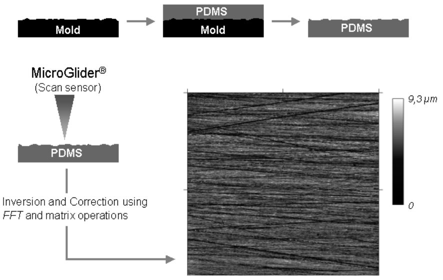

Fig. 3. Transference of mold grooves defines the meso-topography of third level (DIN 4760) of SMC surfaces. Moulding conditions: 5 MPa and 160s (a), 5 MPa and 360s (b), 10 MPa and 360s (c).

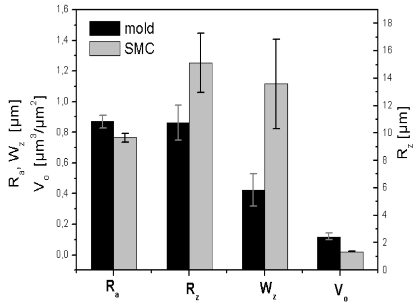

Fig. 4. Topographic transfer from metallic mold to SMC surface.

According to our results, the transference of micro-topographic irregularities from mold to SMC surface is relatively low (cf. Figure 4). The calculation of Wenzel roughness factor (the ratio between the real surface area and the geometric projected area) shows that the mold effective area is about only 1 % bigger than the effective area of SMC surface by using the optimal resolution of 5µm. However, the transference of meso-topography, characterised as R_z is strong, principally because a notable increase of the short waviness from mold to SMC surface, presumably due to adhesion during separation, that could be responsible for a "shrinkage effect" of 2D-profiles observed by Schubel et al. (2006) and atributed to mould surface and to a volumetric resine shrinkage.

Transfer of meso-waves (N_z) is only about 57%, but the transference of their height (characterized as R_z) is about is about 141% due to the notable transference of short waviness (cf. Figure 4).

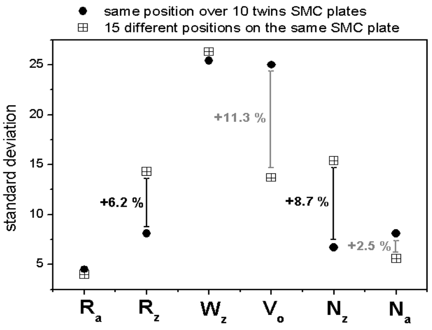

Fig. 5. Impact of sampling (positioning) criteria on statistical reliability.

After measuring of fifteen identified positions over ten different twin SMC plates (produced with the same moulding conditions: 5 MPa, 160s), it was possible to compare the influence of mold topography on the statistical reliability of the topographic parameters. Figure 5 shows that mold topography influence strongly the SMC meso-topography (R_z and N_z varies notably from position to position). By fixing a position over 10 twin plates, R_z and N_z are statistically more reliable, also only the effect of glass fibres orientation (prepreg orientation) reflected in porosity (V_o) seems to control the meso and probably micro-topography of each measured area.

5. CONCLUSIONS

After analysing the calculated topographic characterisation parameters by macro-, meso- and micro- length scales produced by constant temperature (147,5°C ± 2,5°C), the most important conclusions are:

- By a constant temperature, rheology during moulding, controlled by pressure and moulding time, defines the resulting long waviness (macro-morphology studied by L_m=100 mm), which is simultaneously controlled by the mold form and prepregs placement procedure.
- Mold morphology and prepregs placement also control short waviness (meso-morphology studied by L_m=3 mm) directly and due to adhesion between mold and SMC surface during detaching.
- Orientation and size of glass fibres can affect in some cases the short waviness through adhesion during detaching, but in general control the meso topography (characterized as R_z).
- Mold surface defines always the meso topography (R_z) but, depending on mold inhomogeneities can also influence on the micro topography (characterized as R_a).

Heat interchange (cooling) and conditions of residual volatiles evaporation already mentioned by Schubel et al. (2006, Part II) after moulding were not studied in the present work but can be assumed to be important in the definition of the resulting micro-topography.

REFERENCES

BOYLAN S., CASTRO J.M. (2003) Effect of reinforcement type and a length on physical properties, surface quality, and cycle time for sheet molding compound (SMC) compression molded parts. J. Appl. Polym. Sci., 90(9): 2557-71.

CALVIMONTES, A. (2009) Topographic characterization of polymer materials at different length scales and the mechanistic understanding of wetting phenomena, PhD. Thesis, Technische Universität Dresden, Germany.

KIM K., JEONG, J., IM, Y. (1997) Effect of molding parameters on compression molded sheet molding compounds parts. J. Mater. Process.Technol., 67: 105-11.

KIM, Y.S., LEE, H.H., HAMMOND, P.T. (2003) High density nanostructure transfer in soft molding using polyurethane acrylate molds and polyelectrolyte multilayers. Nanotechnology 2003; 14: 1140-1144.

RUPRECHT, A.K., KÖRNER, K., WIESENDANGER, T.F., TIZIANI, H.J., OSTEN, W., LÜCKE, P. (2005) Chromatic confocal sensors for micro-topography measurements. Presented in 50. Internationales Wissenschaftliches Kolloquium der TU Ilmenau, September 19-23.

RUPRECHT, A.K., KÖRNER, K., WiESENDANGER, T.F., TIZIANI, H.J., OSTEN, W. Chromatic confocal detection for high speed micro-topography measurements. Proceedings of SPIE 2004;5302:5360-61.

SCHUBEL, P.J., WARRIOR, N.A., KENDALL, K.N., RUDD, C.D., Characterisation of thermoset laminates for cosmetic automotive applications: Part I – Surface characterisation. Composites: Part A 2006 ; 37 : 1734-1746.

SCHUBEL, P.J., PARSONS, A.J., LESTER, E.H., WARRIOR, N.A., RUDD, C.D., Characterisation of thermoset laminates for cosmetic automotive applications: Part II – Cure of residual volatile assessment. Composites: Part A 2006 ; 37: 1747-1756.

ACKNOWLEDGMENTS

The work was supported by German Federal Ministry of Education and Research.

Caracterización de la morfología de resinas termoestables utilizadas en la industria aeronáutica mediante microscopía de fuerzas atómicas (AFM)

M. Burón, A. Sánchez-Blázquez, J. Sánchez-Gómez
Composite Technology (EDSWCM), Materials and Processes. Airbus
J. Rams
Departamento de Ciencia e Ingeniería de Materiales. Universidad Rey Juan Carlos,
Madrid, España

RESUMEN

El objetivo de este trabajo es determinar la morfología de matrices termoestables modificadas con termoplásticos de altas prestaciones, mediante microscopía de fuerzas atómicas (AFM). El estudio realizado comprende el análisis de las distintas morfologías resultantes de la incorporación de modificadores termoplásticos de distinta naturaleza, así como de la aplicación de distintas condiciones de procesado sobre diferentes matrices termoestables de potencial aplicación en la industria aeronáutica. La caracterización morfológica se ha realizado utilizando el modo de trabajo de contacto intermitente (modo "tapping") del AFM y ha permitido determinar la forma, distribución y tamaño de los modificadores termoplásticos en función de su naturaleza química y de las condiciones de procesado.

1. INTRODUCCIÓN

Las resinas termoestables son uno de los materiales más versátiles empleados como matriz de materiales compuestos en la industria aeronáutica. Debido a las altas prestaciones que requiere esta industria, las resinas de naturaleza epoxídica resultan las más adecuadas puesto que presentan una elevada estabilidad dimensional a altas temperaturas, excelente resistencia térmica y química, alta resistencia mecánica, elevada rigidez y facilidad para el procesado. Sin embargo, su alta densidad de entrecruzamiento (característica de este tipo de resinas termoestables y que confiere al material sus propiedades superiores) provoca una disminución de su capacidad de tolerancia al daño, lo que limita su aplicabilidad. Por lo tanto, a la hora de formular resinas termoestables para su utilización en materiales compuestos para aplicaciones estructurales, es interesante mejorar la tenacidad de la matriz polimérica, mediante la adición de modificadores que la mejoren sin disminuir el módulo elástico ni la temperatura de transición vítrea. Esto se consigue, en general, mediante la utilización de modificadores termoplásticos de altas prestaciones, ya que la opción de utilizar la adición de modificadores elastoméricos suele conllevar una disminución de la rigidez del material resultante. Las resinas modificadas suelen presentar una gran complejidad morfológica y su caracterización es un requisito necesario dado que la forma, el tamaño y la distribución de fases para las diferentes condiciones de procesado son críticos a la hora de lograr aumentar la tenacidad de la resina. [Goodman 1998 y Magonov 1997].

Por otra parte, la Microscopía de Fuerzas Atómicas (AFM) se ha convertido en una herramienta muy potente y útil para la caracterización morfológica de materiales complejos y, en particular, de materiales compuestos de matriz polimérica. El modo de trabajo más empleado es el de contacto intermitente (*tapping*) y en él se hace oscilar el fleje que soporta a la punta cerca de su frecuencia de resonancia natural con una amplitud que se mantiene constante. Bajo estas condiciones, los materiales presentan un módulo de rigidez más elevado que en condiciones cuasiestáticas, lo que permite analizar muestras con zonas blandas sin deteriorarlas [Howland et al.]. A partir de los movimientos de la punta y de la muestra se puede registrar la topografía del material compuesto a escala nanométrica, mientras que a partir de las variaciones en la oscilación de la punta (desfases) se puede apreciar la existencia de fases con diferente rigidez. En este trabajo se ha observado que el proceso de procesado de las resinas empleadas modifica tiene una clara influencia en la microestructura obtenida.

2. PARTE EXPERIMENTAL

Las tres resinas termoestables empleadas en este trabajo se encuentran modificadas con termoplásticos de altas prestaciones para mejorar su tenacidad. Las resinas se presentan en forma de "filme" en estado inicial de polimerización o estado β, en el que ya se encuentran mezclados el precursor termoestable, el endurecedor, modificadores termoplásticos y aditivos. La preparación de las muestras para el análisis morfológico mediante AFM, se realizó posicionando varias capas de "filme" (hasta alcanzar un espesor de aproximadamente de 2 mm) en un molde de aluminio sobre una película teflonada para facilitar su desmoldeo. Posteriormente se han procesado a través de un mismo ciclo de curado pero realizando diferentes ciclos previos al curado. En la tabla 1 se muestran las condiciones de procesado en estufa empleadas en este estudio.

Proceso	Ciclo previo al curado	Ciclo de curado
Proceso 1	-	2 horas a 180 ºC
Proceso 2	3 horas a 140ºC y posterior enfriamiento	2 horas a 180 ºC
Proceso 3	70 minutos a 110 ºC y posterior enfriamiento	2 horas a 180 ºC

Tabla 1. Condiciones de procesado en estufa.

Una vez procesadas, se realizó una preparación superficial de las muestras curadas para su caracterización morfológica realizando un corte con una cuchilla de diamante a 35º. Para ello se empleó con ultramicrotomo Leica® Ultracut UC6 a temperatura ambiente con una velocidad de corte de 1 mm/s y un espesor de 70 nm.

El análisis de AFM se realizó con el microscopio de aproximación (Nanoscope V Multimode de Digital Instruments) trabajando en modo de contacto intermitente (*tapping*). El escáner empleado es de tipo AS-12 ("E") con una capacidad de rastreo máxima de 10 μm × 10 μm, y un rango vertical máximo de 2,5 μm. Para el barrido en modo *tapping* se utilizaron puntas de silicio con una configuración de viga (TESP) de frecuencia de resonancia próxima a 320 kHz, longitud de 125 μm y radio nominal de 8 nm. Las áreas estudiadas variaron entre 10 × 10 μm y 500 × 500 nm empleando frecuencias de barrido de ~1 Hz En todos los casos, se realizaron imágenes en diferentes muestras y áreas para comprobar la reproducibilidad de los resultados.

3. RESULTADOS Y DISCUSIÓN

En la figura 1 se muestran las imágenes de topografía obtenidas por AFM de las tres resinas termoestables analizadas en este estudio, donde se aprecia la distinta naturaleza del modificador termoplástico utilizado en cada una de ellas. En la resina A se puede observar (figura 1a) que el termoplástico es soluble, ya que presenta una superficie completamente homogénea en todo el rango de escalas medido. La resina B presenta una morfología monopartícula donde el modificador termoplástico se encuentra embebido en la matriz termoestable continua (figura 1b) y tiene una distribución de tamaño no uniforme entre 10-50 µm (determinado mediante microscopía óptica). A diferencia de la matriz termoestable que aparece plana debido a su corte frágil, el modificador aparece rugoso a causa de los artefactos que se producen durante el corte puesto que se trata de un material de naturaleza más plástica. Finalmente, en la resina C (figura 1c) puede advertirse una morfología biparticulada más compleja; aparece el termoplástico escindido en partículas de dos tamaños diferenciados de 1-2 µm y 150-300 nm que no es posible observar mediante microscopía óptica a causa de su pequeño tamaño.

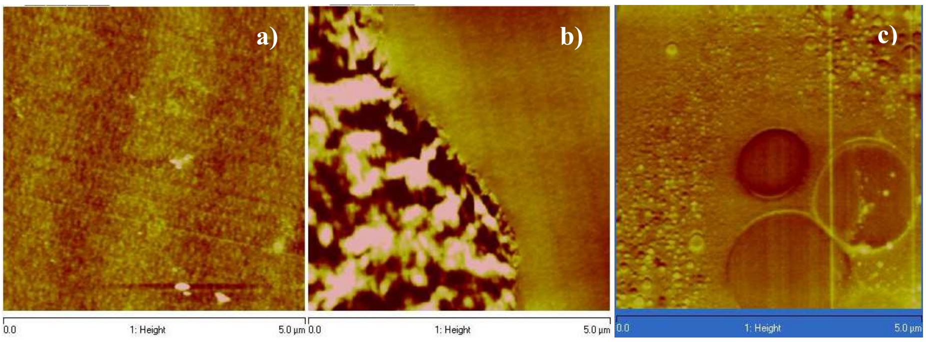

Fig. 1. Imágenes de AFM (imágenes de altura) de 3 resinas termoestables modificadas con termoplásticos: a) resina A con modificador soluble, b) resina B con morfología monopartícula y c) resina C con morfología bipartícula.

Adicionalmente, se ha analizado la influencia de las condiciones de procesado sobre la morfología resultante de las 3 resinas. El resultado de dicha caracterización ha puesto de manifiesto que no existe ningún cambio morfológico para las resinas A y B en función de las condiciones de procesado. Sin embargo, para la resina C, la existencia de un proceso de calentamiento previo al proceso de curado conduce a diferencias morfológicas. En la figura 2 se muestran las imágenes de fase de la resina C utilizando distintas condiciones de procesado. Como puede observarse, existe un cambio de morfología: se pasa de una morfología biparticulada con dos tamaños diferenciados de partícula como los indicados anteriormente (figura 2a) a una morfología monoparticulada con tamaños de partícula entre 25-150 nm (figuras 2b y 2c).

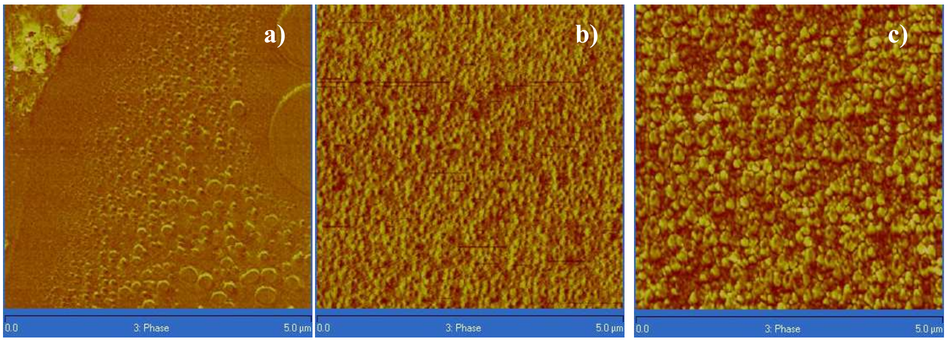

Fig. 2. Imágenes de AFM (imágenes de fase) de la resina C tratada con diferentes condiciones de procesado: a) proceso 1, b) proceso 2 y c) proceso 3.

La evidente evolución de la microestructura muestra que la realización de un ciclo previo al curado permite homogeneizar la distribución del modificador termoplástico evitando la aparición de grandes partículas. En particular, el uso de tratamientos de alta temperatura y menor tiempo (proceso 2) ha permitido obtener un tamaño de partícula más fino que podría dar lugar a un diferente comportamiento a fractura.

4. CONCLUSIONES

Se ha demostrado la capacidad del AFM para caracterizar en detalle la morfología de materiales poliméricos en los que se combinan matrices termoestables con modificadores termoplásticos. Se ha observado el efecto que las condiciones de procesado tienen en la morfología final de la resina y cómo un proceso previo al curado permite controlarla. Así pues, la microscopía de fuerzas atómicas se presenta como una técnica de gran utilidad para la caracterización de resinas utilizadas en la industria aeronáutica, así como para la optimización de los procesos aplicables a dichos materiales.

REFERENCIAS

GOODMAN, S. H. (1998). Handbook of Thermoset Plastics (Noyes Publications), Westwood.

HOWLAND, R., BENATAR, L. A practical Guide to scanning force microscopy Ed Park Scientific Instruments.

MAGONOV, S. N. (1997) Characterization of polymer surfaces with atomic force microscopy. *Annual Review of Materials Science,* 27, 175-222.

Fracture mechanisms of E-glass/epoxy composite laminates

Essam Totry*, G. Charalambous[†], J. Molina†, C. González*†
J. Llorca*†
* Departamento de Ciencia de Materiales, Universidad Politécnica de Madrid
E. T. S. de Ingenieros de Caminos. 28040 - Madrid, Spain
[†] Instituto Madrileño de Estudios Avanzados en Materiales (IMDEA-Materiales)
E. T. S. de Ingenieros de Caminos. 28040 - Madrid, Spain

SUMMARY

Fracture mechanisms of E-glass/epoxy laminates are studied in this work. Unidirectional $[0°]_{14}$, $[90°]_{14}$ and cross-ply composite laminates $[0°/90°]_{4s}$ were manufactured and fracture tested under three point bending conditions. Significant differences in the fracture behavior arise depending on the relative orientation of the initial notch respect to the fiber direction. Additional tests were interrupted and unloaded at different levels followed to CT scanning to assess the evolution of the deformation and failure mechanisms of the composite materials with respect to the initial notch introduced in the specimens.

1. INTRODUCTION

Fiber-reinforced polymers (FRP's) are nowadays used as structural materials in many different engineering lightweight applications. In contrast with standard metallic alloys, FRP's present very different physical fracture mechanisms depending on the loading conditions (static, fatigue, impact) and stress state: for instance, tensile deformation in the longitudinal direction in a single lamina (intralaminar failure) leads to fiber failure, compression in the same direction induces failure by localized fiber buckling and kinking while shear induce matrix cracking constrained along fiber directions. On the other hand, fracture in laminates can occur between adjacent plies originating the interlaminar failure mode by delamination.

As a result, even simple tests to characterize the basic mechanical properties to be used in the engineering design are not well understood due to the competition between the different failure modes mentioned which may lead to substantial identification errors. Despite the scientific interests to address physically deformation and failure mechanisms of composite materials, there is also a considerable interest from industry in developing accurate and reliable strategies to predict the critical conditions for failure in structural components made up of FRC (Cox and Yang, 2006).

2. MATERIALS AND EXPERIMENTAL TECHNIQUES

Pre-impregnated sheets of E-glass/MTM57 epoxy resin were purchased from Advanced Composite Group (UK). Rectangular panels of 350 x 300 mm^2 were heated at 3°C/min and consolidated at 120°C and 0.64 MPa in an autoclave for 30 minutes. They were cooled at the same rate of 3°C/min and the internal pressure was released at 80°C. Two different laminate configurations were manufactured: cross-ply ($[0°/90°]_{4s}$) and

unidirectional ([0°]$_{14}$ and ([90°]$_{14}$). The nominal fibre volume fraction was 54%. Panels were inspected to ensure that they were free of initial delaminations or other defects.
Three Point bending specimens (TPB) were cut from the panels laminates (both the cross-ply and the unidirectional) having the fibres parallel and perpendicular to the notch. The nominal depth, D, and span, S, of the TPB specimens was set to 8 and 32 mm respectively while the thickness corresponds to the plate thickness t, Figure 1 a). Straight notches were machined in the central section of the TPB specimens using a diamond wire of 0.3 mm in diameter with a notch depth of a_0=1.6 mm (20% relative notch depth). No fatigue precracking was used in this study. The specimens were tested under three point bending using a servo-electrical testing machine INSTRON 3305 under stroke control at constant cross-head speed of 0.2 mm/min. The load, P, was measured continuously with a 5 kN load cell, the displacement of loading point, δ, with the cross-head displacement and the crack mouth opening displacement CMOD on the side of each specimen using a digital image correlation system (VicSNAP, Correlated Solutions, Inc.). In the latter case, one of the specimen faces were painted in white and then black sprayed to create a random pattern for the digital image recognition. The DIC system acquired high resolution images of the face of the specimen at a rate of one image per second and thereafter post processed the images to obtain the displacement field within the specimen face.

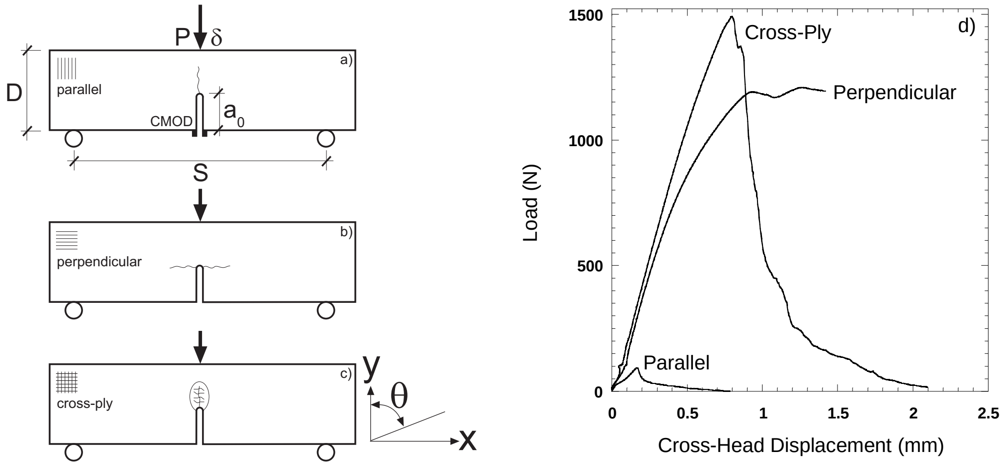

Figure 1. a) TPB specimen geometry definition. TPB specimen with fibers parallel to the notch [0°]$_{14}$. b) TPB specimen with fibers perpendicular to the notch [90°]$_{14}$.
c) TPB tests cross-ply laminates [0°/90°]$_{4s}$.
d) Representative Load-displacement curves of the TPB tests.

3. RESULTS

The typical P-δ curves of some of the TPB tests up to final failure were plot in Figure 1 d). The mechanical response is similar in all the cases; the load-displacement curves were initially linear elastic although some degree of nonlinearity is observed previous to the peak load. After this point, stable crack propagation was observed in all the cases but the physical fracture mechanisms differed substantially depending on the relative orientation of the notch with respect to the fibre direction.

The minimum peak load was observed in those specimens where the notch was introduced parallel to the fibre direction ($[0°]_{14}$). In these cases, the fracture was governed by the propagation of a mode I crack –the fracture energy corresponding to the epoxy matrix- constrained by the fibre direction along y axis, Figure 1 a). On the other hand, those tests with fibres perpendicular to the notch ($[90°]_{14}$), a T shaped matrix splitting emanating from the notch root was observed constrained again by the direction of the fibres along the x axis, Figure 1 b). No fibre failure was observed at all. After some unsymmetrical crack propagation, the compliance of the specimen increased substantially approaching to the one corresponding to an unnotched beam with the depth corresponding to the initial beam ligament ($D-a_0$). In this moment, the driving force for matrix crack propagation diminished and the tests was interrupted and finished. Finally, the tests performed in the cross-ply laminates ($[0°/90°]_{4s}$) exhibited totally different fracture behaviour with a fracture process zone where extensive damage was barely observed at the surface of the specimen and with overall stable crack propagation along the y axis, Figure 1 c). In this case, the coupling effects of the layered structure stabilized the T shaped splitting cracks observed in the $[90°]_{14}$ specimens and the fibres in this direction bridged matrix cracks appearing in the 0° layers. This mechanism is responsible of the increase of strength and toughness observed in the experiments.

4. CT SCANNING OF FRACTURE PROCESS ZONE

CT scanning images were used to assess the evolution of the deformation and failure mechanisms of the composite materials with respect to the initial notch introduced in the specimens (Wright *et al*., 2006). Some of the performed tests on cross-ply composites were interrupted at different levels of loadings (prior to peak loading, 80 % after peak loading, 50 % after peak loading and fully failed), Figure 2 (as shown in fig. 1b) to ascertain the fracture mechanisms (delamination, matrix splitting, fibre failure, etc.) using a X-ray tomography system (Phoenix Nanotom) with W radiation using 90 kV of voltage and voxel size of 5µm.

No major damage was found before the load peak using the X-Ray tomography system. Figure 2 presents the basic results of the CT scanning for a cross-ply interrupted test at 80% after peak loading confirming the main assumptions on the fracture mechanisms mentioned in the previous paragraphs. Despite of some minor fibre kinking observed in the region of the contact loads in the compression zone, Figure 2 a), matrix cracking in the 0° layers is observed (dark region in Figure 2 b)) and fibre bridging and pull-out in 90° layers (Figure 2 c).

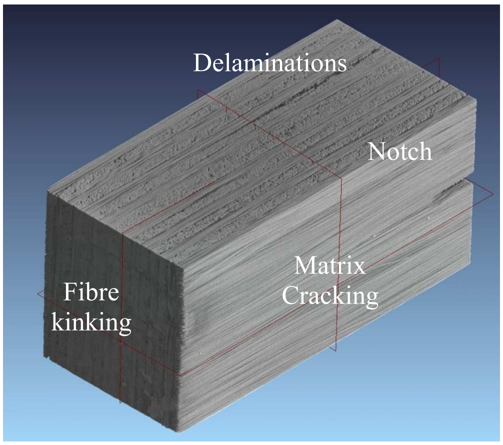

b) Fibre parallel to the notch (0° layers)

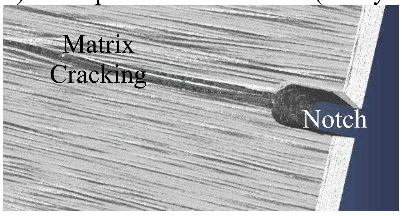

c) Fiber perpendicular to the notch (90° layers)

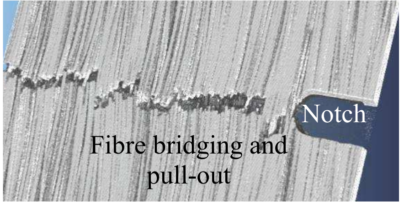

Figure 2. a) CT scanning images of the TPB cross-ply specimen (fiber/matrix topology is resolved) for interrupted tests at 80 % after peak loading. b) View of a ply with fibres parallel to the notch. c) View of a ply with fibres perpendicular to the notch.

5. CONCLUSIONS

Fracture mechanisms of E-glass/epoxy laminates were studied in this work. Significant differences in the behavior of unidirectional $[0°]_{14}$, $[90°]_{14}$ and cross-ply composite laminates $[0°/90°]_{4s}$ as a function of the relative orientation of the initial notch introduced in the specimens were observed. X-Ray Tomography was used to acquire 3D images of the micro/mesostructure and was used to address failure mechanisms within the composite laminates.

ACKNOWLEDGEMENTS

This investigation was supported by the Ministerio de Eduación y Ciencia de España through the Grant MAT 2006-2602 and by the Comunidad de Madrid through the program ESTRUMAT-CM (reference AT/0077). The composite materials used in this investigation were manufactured at INTA (Instituto Nacional de Técnica Aerospacial), and the authors want to express his gratitude to Dr. J. M. Pintado to Dr. M. A. de la Torre.

REFERENCIAS

COX, B., YANG, Q. (2006). In quest of virtual tests for structural composites. *Science* 314, 1102–1107.

WRIGHT P., FU, X., SINCLAIR, I., SPEARING, S.M. (2006), Ultra High Resolution Computed Tomography of Damage in Notched Carbon Fiber—Epoxy Composites *Journal of Composite Materials*, Vol. 42, No. 19, 1993-2002.

Test matrix definition and experimental results of low-velocity impact tests in laminated composites

E.V. González, P. Maimí
AMADE. Escola Politècnica. Universitat de Girona. Spain
P.P. Camanho
DEMEGI. Faculdade de Engenharia. Universidade do Porto. Portugal

ABSTRACT

This paper presents the procedure applied in order to define a suitable test matrix of laminated composite materials for low-velocity impact tests. This procedure is based on the analytical description of the impact elastic response. The analytical models allow to understand the effects of the impact governing parameters and thus to focus adequately the analysis on a selected parameter. Some experimental results are presented and compared with analytical predictions.

INTRODUCTION

The prediction of damage in laminated composite structures induced by the impact of a foreign object is a complex issue. Damage results from the interaction between different mechanisms (delamination, matrix cracking and crushing, fibre breaking, and fibre-matrix interface debonding), and it depends on the governing parameters of the impact event. These governing parameters are typically grouped in three sets: plate parameters (i.e. thickness, in-plane sizes, stacking sequence, elastic and fracture properties, density, boundary conditions, and lamina type), impactor parameters (i.e. velocity, mass, incidence angle, elastic properties, radius), and environmental conditions.

Experimental evidence shows that impact damage is directly related with the nature of the impact behaviour, which is also controlled by the governing parameters. Therefore, it is relevant to know the effects of each governing parameter on the impact behaviour, and thus to get a qualitative understanding of the possible damage mechanisms which can occur. In the literature there are approaches based on analytical models which predict the type of the impact response for a determined configuration, such as impact on monolithic and flat laminated composite plates (e.g. Christoforou and Yigit 1998; Olsson 2000). The initial knowledge of the impact behaviour not only assesses the possible types of damage induced, but it is also useful for the development of efficient numerical models, for planning test programs, and for selecting a proper simplified analytical model to describe the impact event.

The analytical models are a suitable and powerful tool to obtain fast predictive results for a given impact configuration. Generally, these analytical models are limited to simple geometries of the structure, and rely on stepwise solution of nonlinear differential equations or integral equations which describe the transitory response of the system until damage onset. The results given by these analytical models are suitable to compare different impact cases with different values of the governing parameters.

This paper presents a procedure to define coupons for low-velocity impact tests. The procedure relies on analytical models of the impact event for rectangular, flat, and monolithic laminated composite plates. Finally, some experimental results are presented and compared with analytical predictions.

PROCEDURE FOR IMPACT SPECIMEN DEFINITION

Before describing the procedure for the specimen's definition, it is useful to review the different types of plate impact behaviours. An impact initiates stress waves propagating from the impact point, where the influence of the waves gradually fades away due to material damping and wave scattering. For impact times in the order of the transition time for through-the-thickness waves the response is dominated by three-dimensional wave propagation which is associated with ballistic impact and causes localized and easily detectable damage. This behaviour is beyond the scope of the present paper. For longer impact times, flexural and shear waves govern the response. For times much longer than the time needed by these waves to reach the plate boundaries, the lowest vibration mode of the impactor-plate system predominates. Therefore, basically there are three behaviours (Olsson 1993): *response dominated by dilatational waves*, *flexural and shear wave-controlled or infinite plate behaviour*, and *quasi-static behaviour*. Additionally, if the impactor mass is very small and the global response of the plate can be neglected, this behaviour is called *half-space impact*. These behaviours can be described by means of analytical models, which give the response of the system until damage onset. The analytical models are often classified in function of how the plate is modelled (Davies and Olsson 2004): multi-degree-of-freedom models and one- or two-degree-of-freedom models. The first group yields to typically called *complete analytical models*, and are based on numerical mode summation which rarely allows explicit expressions for parameter influence. The second group includes *energy-balance models* and *spring-mass models*. These usually allow closed-form solutions which explicitly show the influence of the governing parameters, but have limited flexibility in handling complex geometries and different impact behaviours.

In Christoforou and Yigit (1998) a characterization diagram for behaviour type prediction as well as the maximum impact force for a wide range of impact cases is developed. This approach is based on simplified analytical models that use a linear contact law for local deflection description as shown in Fig. 1. The terms exposed are: the displacement of the impactor w_i and the transverse displacement of the plate w_o; velocity V_0 and mass M_i of the impactor; contact stiffness k_α and plate stiffness k_{bsm}; thickness h, density ρ, and flexural effective stiffness D^* of the plate (Olsson 1993). Using a dimensionless framework which defines the basic magnitudes as: $[M] = M_i$ (mass), $[T] = (M_i/k_\alpha)^{1/2}$ (time) and $[L] = V_0(M_i/k_\alpha)^{1/2}$ (length), the maximum dimensionless force for each extreme behaviour can be easily defined. In particular, the maximum force for half-space behaviour yields to the unity $\overline{F}_{hs,max} = 1$, for infinite plate behaviour it depends solely on the relative mobility parameter $\overline{F}_{w,max} = f\left(\zeta_w\right)$, and for quasi-static behaviour it is a constant function of the relative stiffness parameter $\overline{F}_{q,max} = f\left(\lambda\right)$. With those dependences, the characterization diagram can be built (see Fig. 1). The characterization parameters ζ_w and λ are defined as:

$$\zeta_w = \frac{1}{16}\sqrt{\frac{k_\alpha M_i}{\rho h D^*}} \qquad \lambda = \frac{k_{bsm}}{k_\alpha} \tag{1}$$

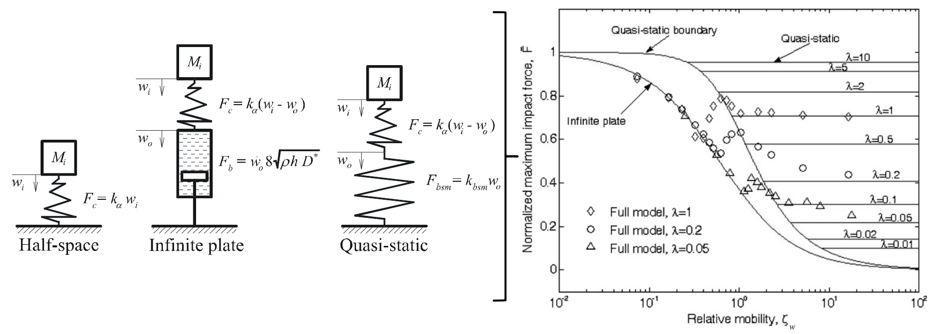

Fig. 1. Simplified analytical models and the impact characterization diagram based on the relative mobility ζ_w and the relative stiffness λ parameters.

The prediction of the maximum impact force is useful since it can be compared with a damage threshold. If the predicted maximum elastic impact force is greater than a threshold value, damage is triggered. For low velocity impact, the delamination is the main damage mechanism which reduces dramatically the stiffness of the structure and it can be predicted by means of (Davies et al. (1994)):

$$F_{cr}^2 = \frac{8\pi^2 E h^3 G_{IIc}}{9\left(1-\nu^2\right)} \qquad (2)$$

where E is the mean flexural module of the laminate, h is the laminate thickness, ν is the Poisson's ratio, and G_{IIc} is the fracture toughness in pure mode II.

EXAMPLE OF IMPACT ANALYSIS

As an example, the study of the ply thickness effect on the impact damage is presented. This study is carried out by selecting different laminates of AS4/8552 composite material with the same elastic impact behaviour which avoids the effect of other impact parameters. The selected laminates are: $[(45,0,-45,90)_4]_s$, $[(45_2,0_2,-45_2,90_2)_2]_s$ and $[45_4,0_4,-45_4,90_4]_s$. The impact energies considered are 20, 30 and 40J. For all cases, the impactor mass is of 5kg and the resulting impact behaviours are all quasi-static. Delamination is ensured for each impact energy case since the predicted maximum impact load is greater than the damage threshold load (see Eq. 2).

Fig. 2 shows the experimental results and the analytical prediction by using a complete analytical model for each laminate and impact energy. Despite the elastic behaviour for all laminate is the same, the resulting response and delamination threshold force are different.

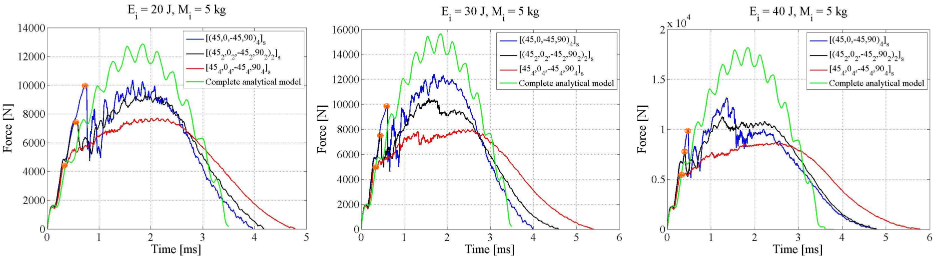

Fig. 2. Experimental and analytical force versus time charts for different impact energies. The orange points indicate the corresponding experimental critical loads.

CONCLUSIONS

A procedure to define coupons for low-velocity impact tests was presented. The procedure is based on an impact characterization diagram which gives the corresponding elastic impact behaviour as well as the maximum impact force those are determined by simply calculation of two key parameters. This procedure allows the understanding of the effects of any impact governing parameter and thus to focus adequately the analysis on a selected parameter. The resulting maximum impact force can be compared with a damage threshold criterion.

ACKNOWLEDGEMENTS

This work has been partially supported by the Spanish government under contracts: MAT2006-14159C02-01 and TRA2006-15718-C02-01/-TAIR. The first author would like to thank the Generalitat de Catalunya for the FI pre-doctorate grant partially supported by the European Social Funds. The third author acknowledges the financial support of the Portugal Foundation for Science and Technology under the project PDCT/EMEPME/64984/2006.

REFERENCES

CHRISTOFOROU, A. P., YIGIT, A. S. (1998). Characterization of impact in composite plates. *Composite Structures*, 43, 15-24.

DAVIES, G.A.O., OLSSON, R. (2004). Impact on composite structures. *The Aeronautical Journal*, paper num. 2909, 541-563.

DAVIES, G.A.O., ZHANG, X., ZHOU, G., WATSON, S. (1994). Numerical modelling of impact damage. *Composites*, 25, 342-350.

OLSSON, R. (1993). Impact response of composite laminates - a guide to closed form solutions. *Bromma: The Aeronautical Research Institute of Sweden*, FFA TN 1992-33.

OLSSON, R. (2000). Mass criterion for wave controlled impact response of composite plates. *Composites Part A- Applied Science and Manufacturing*, 31, 879-887.

Experimental research on open-hole tensile specimens made of carbon fibre reinforced plastics (CFRP) with an optimised curvilinear fibre pattern

A. Spickenheuer, K. Uhlig, K. Gliesche, G. Heinrich
Department of Composite Materials,
Leibniz Institute of Polymer Research Dresden (IPF), Dresden, Germany

SUMMARY

In this paper the experimental research on open-hole tensile specimens made of CFRP with a prior optimised curvilinear fibre pattern is considered. For generating the fibre layout a design tool for finite element analysis (FEA) based on local varying principal stress orientation was programmed. With help of the Tailored Fibre Placement (TFP) technology various CFRP open-hole specimens with curvilinear fibre pattern were manufactured. After testing the results were compared to specimens with standard multi-axial laminate stacking. For evaluation of the local strain conditions, especially next to the open-holes, an optical deformation measuring system was applied. The results showed both a significant reduction of strain peaks next to the hole as well as an improved tensile strength.

1. INTRODUCTION

The strength assessment and the perfection of composite structures containing open-holes is an outstanding task in lightweight engineering since a long time. Especially, since the usage of composite materials for aircrafts the study of stress concentration on notches and holes has become eminent. Mostly, multi-axial composites made of prepregs, non-crimp fabric (NCF) or woven materials have been focused on within those studies as described by Khot et al. (1973), de Morias (2000) and O'Higgins et al. (2008). On the other hand, new fibre placement technologies like, for example, the Tailored Fibre Placement (TFP) technology were developed within recent years with the capability to place fibres in arbitrary directions according to Gliesche et al. (1995) and Mattheij et al. (1998). This technology, in connection with appropriate optimisation methods, can generate fibre patterns that use the full potential of the fibre reinforcement for composite parts (Crothers et al. 1997, Weimer et al. 2000, Gliesche et al. 2003).

However, till now most studies of an optimal curvilinear fibre design have been carried out only theoretically, or only with simple fibre placement methods which are not suitable for industrial application (Hyer et al. 1988, Götz et al. 2000, Tosh et al. 2000). Thereby, mostly simple to test open-hole tensile specimens have been considered to demonstrate the potential of curvilinear fibre design. Nevertheless, the mechanical behaviour of composites with curvilinear fibre layout is not fully understood yet, and is much more complex than that of well-established multi-axial fibre material.

As an example, a material optimisation method using FEA, according to Spickenheuer et al. (2007), has been performed to numerically generate a curvilinear fibre pattern for a tensile loaded open-hole specimen. An optical strain measuring system has been used to assess the strain behaviour around the open-hole. A similar approach has been chosen on specimens with common laminate stacking according to Pandita et al. (2003) and Pierron et al. (2007).

2. Design of curvilinear fibre pattern

For generating the fibre pattern an optimisation method based on a principal stress optimisation criterion according to Hyer et al. 1988 and Götz et al. 2000 have been used. Therefore, an Ansys Parametric Design Language (APDL) program for the commercial FEA software ANSYS was programmed as described by Spickenheuer et al. (2007). For numerical simulation ’Shell99’ elements have been applied to a plane symmetrical quarter model of the considered open-hole specimen geometry. After an initial isotropic calculation an iterative realignment of the orthotropic finite element main directions according the calculated major principal stress directions has been performed. After 3 iterations the element wise in-plane shear stress has been nearly eliminated. From the thus achieved vector field element orientations a fibre pattern was deduced using a self developed line integration method for post processing. The obtained result can be seen on figure 1. In order to get planar load introduction zones for clamping of the specimens a constant fibre path distance of $w_R = 1.6\ mm$ at these areas was set. The specimen had a width of $w = 80\ mm$, a free length of $l_1 = 200\ mm$, a clamping length of $l_2 = 80\ mm$ and a hole diameter of $d = 20\ mm$.

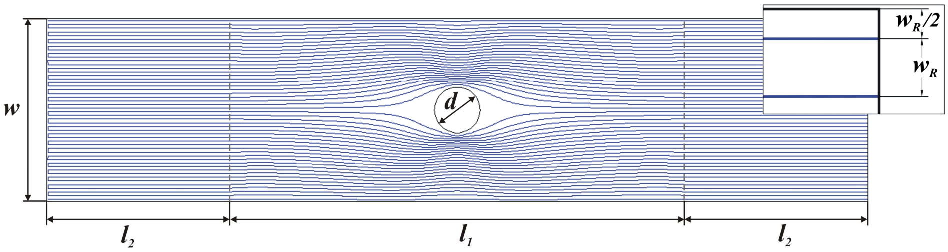

Fig.1. Deduced curvilniear fibre pattern of the open-hole specimen

3. Manufacturing

The obtained fibre pattern was applied via TFP onto bi-axial NCF material with [0/90] and [+45/-45] orientation and a weight per unit area of 514 g / m². For both NCF and the with TFP applied 6 k roving a HT carbon fibre material was chosen. As stitching threat a twisted polyester yarn with 10 tex and as base material filter paper was used. After textile manufacturing the preforms were infiltrated with epoxy resin (EPR L20 + EPH 161). For the applied vacuum assisted resin infusion (VARI) a half sided aluminium tool was used in order to ensure exact specimen geometry and a planar side for bonding. A Teflon® disc placed in the prior cut out centre of perform helped to minimize a machine finishing of the specimens. After infiltration two specimens halves were glued with the same epoxy as used for infiltration and finally provided with tabs for clamping made of glass fibre reinforced plastic (GFRP). To match the weight per unit area of the used reference NCF materials a final laminate stacking for type I_C $[C_1/0/90]_S$ respectively type II_C $[C_1/+45/-45]_S$ was set each with 1014 g / m². Thereby $[C_1]$ specifies the curvilinear layer according the major principal stress direction σ_1.

4. Experimental conditions and procedures

The tensile tests were conducted on a Zwick Z250 static testing machine equipped with wedge clamps. The test speed was set to 5 mm / min. In each case 4 specimens were tested until failure. On two of them the strain behaviour on the specimen surface was determined by using the commercial optical deformation measuring system ARAMIS. Next to the specimens with added curvilinear layers two additional specimen types made of NCF material were tested for reference. Type I according to type I_C possesses a stacking of $[0/90]_{2S}$ and a weight per unit area of 1028 g / m². Type II as reference to type II_C had a $[+45/0/-45]_S$ stacking and a weight per unit area of 962 g / m².

5. Results

The results of the tensile tests are summarised in Table 1. For an appropriate comparison with the reference specimens the failure load was normalised to the specific preform weight as well as to the fraction of fibres orientated mainly within the loading direction, represented by [0] and $[C_1]$.

Specimen	**Type I** $[0/90]_{2S}$	**Type I_C** $[C_1/0/90]_S$	**Type II** $[+45/0/-45]_S$	**Type II_C** $[C_1/+45/-45]_S$
Normalised failure load	2.4 ±0.1 kN / g	2.9 ±0.1 kN / g	3.3 ±0.04 kN / g	4.9 ±0.2 kN / g

Table 1. Results of the tensile tests

The results show a dramatic increased of normalised failure loads for the optimised composite specimens. For the comparable types I and I_C an improvement of about 21 % can be recognized. The increase of the type II_C compared to type II is 48 %.

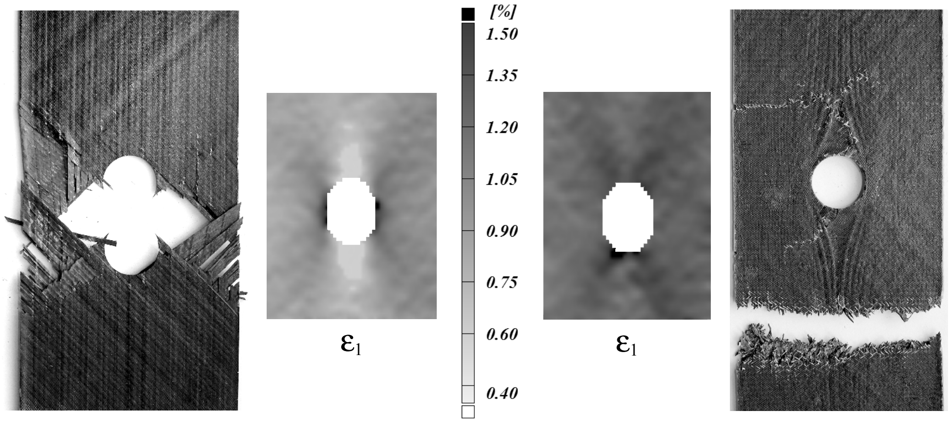

Specimen type II Specimen type II_C

Fig. 2. Comparison of fracture appearance and major principal strain distribution

In figure 2 a comparison of the fracture appearance of the specimen types II and II_C is presented as well as the measured major strain ε_1 distribution around the open-hole at a load level of 90 % of the failure load. On the shown specimen II the expected appearance of fracture of a tri-axial composite failure can be seen. Also the expected high major strain concentration horizontal next to the hole can be observed. However specimen II_C shows a totally different strain behaviour as there can no notch effect be found. The notch effect is even so much reduced that the failure did not began at the edge of the open-hole at all. This fracture pattern was found on all four tested specimens of type II_C.

6. Conclusion

The usage of numerically generated curvilinear fibre pattern applied on standard NCF material leads to a significant increase of failure load on laminates made of CFRP. With help of an optical deformation measuring system it was also found out that the strain distribution around the open-hole edge is nearly equalised. In case of a tri-axial fibre layout the stress concentration was even nullified and failure was not initialised on the open-hole edge.

ACKNOWLEDGMENT

The authors gratefully acknowledge the support of the Federal Ministry of Education and Research. Furthermore the authors want to be grateful to Mr. Mario Naumann and Mrs. Helga Kirsten for preparation of the specimens and Mr. Herbert Moldenhauer from the engineering office Moldenhauer GmbH for his fruitful discussions.

REFERENCES

Crothers, P. J., Drechsler, K., Feltin, D., Herszberg I., Kruckenberg T. (1997), Tailored fibre placement to minimise stress concentrations, *Composites Part A, 28A, 619-625*

Gliesche, K., Feltin, D. (1995), *Beanspruchungsgerechte Textilkonstruktionen für Composite-Bauteile*, Technische Textilien/Technical Textiles, 38

Gliesche, K., Hübner, T., Orawetz, H. (2003), Application of the tailored fibre placement (TFP) process for a local reinforcement on an "open-hole" tension plate from carbon/epoxy laminates, *Composites Science and Technology*, 63, 81-88

Götz, K. (2000), Die innere Optimierung der Bäume als Vorbild für technische Faserverbunde - eine lokale Approximation, Forschungszentrum Karlsruhe, Institut für Materialforschung, FZK 6552

Hyer, M.W., Charette, R.F. (1988), Innovative Design of Composite Structures: Further Studies in the Use of a Curvliniear Fiber Format to improve Structural Effiency, College of Enginieering, Virgina Polytechnic Institut and State University Blacksburg, Department of Engineering Science & Mechanics, Report No. VPI-E-88-8

Khot, N.S., Venkayya, V.B., Johnson, C.D., Tischler, V.A. (1973), Optimization of Fiber Reinforced Composite Structures, *Int. J. Solid Structures*, 9, 1225-1236

Mattheij, P., Gliesche, K., Feltin, D. (1998), Tailored Fiber Placement - Mechanical Properties and Applications, *Journal of Reinforced Plastics and Composites*, 17-9, 774-786

de Morais, A.B. (2000), Open-hole tensile strength of quasi-isotropic laminates, *Composites Science and Technology*, 60, 1997-2004

O'Higgins, R.M., McCarthy, M.A., McCarthy, C.T., (2008*),* Comparison of open hole tension characteristics of high strength glass and carbon fibre-reinforced composite materials, *Composites Science and Technology*, 68, 2770-2778

Pandita, S.D., Nishiyabu, K., Verpoest, I. (2003), Strain concentration in woven fabric composites with open holes, *Composite Structures*, 59, 361-368

Weimer, C., Preller, T., Mitschang, P., Drechsler, K. (2000), Approach to net-shape preforming using textile technologies. Part II: holes*, Composites Part A, 31, 1269-1277*

Pierron, F., Green, B., Wisnom, M.R., Hallett, S.R. (2007), Full-field assessment of the damage process of laminated composite open-hole tensile specimens. Part II: Experimental results, *Composites Part A*, 38, 2321-2332

Spickenheuer, A., Schulz, M., Gliesche, K., Heinrich, G. (2007), Using Tailored Fibre Placement Technology for Stress Adapted Design of Composite Structures, *Plastics, Rubber and Composites*, 37 (5/6), 227.

Tosh, M.W., Kelly, D.W. (2000), On the design, manufacture and testing of trajectorial fibre steering for carbon fibre composite laminates, *Composites Part A*, 31, 1047-1060

Influence of reactive electron beam processing on polypropylene-composite properties

S. Volke, U. Gohs, U. Wagenknecht, G. Heinrich
Leibniz Institute of Polymer Research Dresden

SUMMARY

Electron induced reactive processing is a novel technique where chemical reactions are induced by spatial and temporal precise energy input via high energy electrons under dynamic conditions of melt mixing. This method gives the possibility to increase surface energy of polypropylene (PP) effectively as well as to generate chemical couplings between filler and PP. The process was applied to a proved system consisting of PP (38 wt%), magnesium hydroxide (MH) (60 wt%), triallyl cyanurate (TAC) (2 wt%). Absorbed dose imparted per rotation of rotors is a new parameter controlling mechanical properties of polymer composites. Improved properties were found in tensile strength (140 %), elongation at break (500 %), and impact strength (170 %). Mechanical properties are increasing with lower absorbed dose per rotation. It can be shown that chemical couplings are generated during electron induced reactive processing in comparison to only compatibilized material.

1. INTRODUCTION

Because of incompatibility of non-polar PP and polar inorganic filler, resulting composites are brittle which has a detrimental effect on the desired properties. Improvements in mechanical properties can be reached by compatibilization [Jancar 1990, Hyche 1996], creating of chemical couplings between phases [Karger-Kocsis 1995] and by increasing of inhomogeneity [Grobler 1994]. Thus, maleic anhydride grafted PP is used as well as reactive processing of PP in presence of peroxide radical initiators. The temperature dependence of peroxide decay as well as the dependence of radical generation rate on time are two disadvantages of peroxide induced reactive processing.

Modification of polymers with high energy electron treatment is also well known and used to form parts (after) molding as well as raw materials (pellets, powders, fibers) in solid state and at room temperature [Gohs 2005]. The spatially and temporally precise input of energy is used to produce desired material properties on radical-induced chemical reactions.

Coupling of high energy electron modification of polymers and melt mixing offers a new possibility of reactive processing. In this case, radical generation is independent of temperature, can be easily controlled by beam current and kept constant over time. Absence of any crystallinity, high reaction rates as well as intensive macromolecular mobility and intensive mixing are reasons to expect novel structures and properties.

In present work, this novel method has been applied for a flame retardant PP composite consisting of 38 wt% PP, 60 wt% MH, and 2 wt% TAC. This composite system was successful tested in peroxide induced conventional reactive processing.

2. EXPERIMENTAL

2.1 Material

Polypropylene homopolymer HD120MO was supplied from Borealis, Germany. Triallyl cyanurate (TAC) was obtained from Cytec Surface Specialites, Netherlands. Magnesium hydroxide was got from Martinswerke Albemarle Corporation (grade Magnifin H7), Germany.

2.2 Sample preparation

Unique set-up which was used for electron induced reactive processing is shown in detail in [Gohs 2008]. An electron accelerator was directly coupled to internal mixer ($50\ cm^3$, Brabender, Germany) to induce chemical reactions by imparting high energy electrons under conditions of melt mixing [Gohs 2008, Wagenknecht 2009]. Mixing was done at an average temperature of 185 °C and 60 rpm for 11 minutes. Mixing time was controlled by safety regulations of electron accelerator. Electron induced reactive processing was done at an absorbed dose of 40 kGy with an electron energy of 1 MeV. The electron treatment time was 0,5 / 2 / 5 minutes. The penetration depth of electrons in electron induced reactive processing is limited to a part of mixing volume. The total mixing volume is modified due to the change of polymer mass in course of the mixing process. Composites without electron treatment were compounded in same way in internal mixer for 11 / 22 / 44 minutes. For mechanical and dynamic mechanical analyses dumb-bell shaped specimens were made by injection molding with BOY 22 A HV at constant set of parameters. IR Transmission foils ($d = 250\ \mu m$, 30 s) were made in a labor heating press at 185 °C.

2.3 Testing procedure

Tensile tests were carried out according to ISO 527-2/S2/50 (Zwick 8195.04, 40 %/min speed). Phase morphology was investigated by LEO 435 VP Ultra plus Scanning Electron Microscope (SEM) after breaking of dumb-bell shaped samples at -195 °C. IR studies were carried out using an FTIR spectrometer Vertex 80v (Bruker).

3. RESULTS AND DISCUSSION

In fig. 1, the intensity of carbonyl bonds in IR spectroscopy is shown for different PP samples. Electron induced reactive processing (3) gives highest yield in carbonyl bonds compared to conventional electron treatment at 185 °C (1) as well as plasticized polypropylene (2). Influence of electron induced reactive processing on tensile properties of composites is shown in fig. 2. In contrast to conventional electron treatment and untreated composites tensile strength and elongation at break are improved. Moreover, the tensile strength of about 32 MPa corresponds to that of original PP used in experiment. This is an indication for a good compatibility.

Further experiments have been done in order to get additional information on the reasons for theses improved tensile properties. Thus PP was plasticized for 22 and 44 min without any electron treatment in order to get a higher yield in carbonyl bonds (fig. 3). From fig. 3 it can be seen that further increase in carbonyl bonds (blue) only improves tensile strength up to about 30 MPa. This threshold is comparable to that value of electron induced reactive processing with an treatment time of 0,5 minutes. Longer treatment times during electron induced reactive processing result in higher tensile strength, higher elongation at break as well as impact strength (fig. 4).

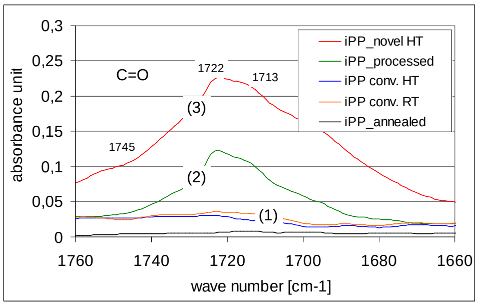

Fig. 1. FTIR-spectroscopy of different treated PP samples.

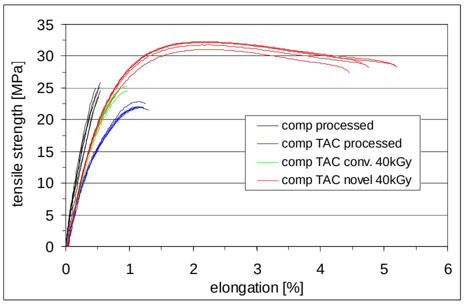

Fig. 2. Tensile test of different treated PP-MH composites.

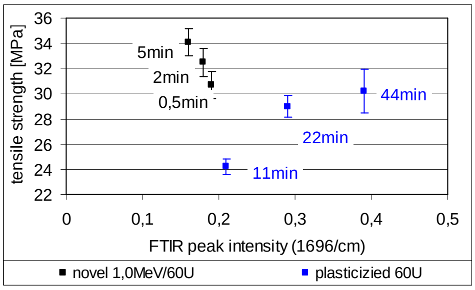

Fig. 3. Tensile strength of different treated PP-MH composites.

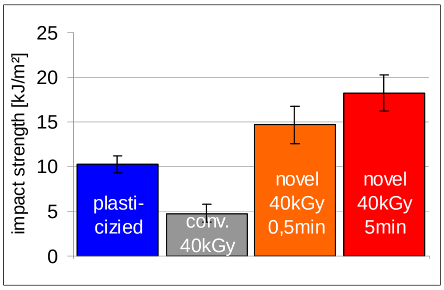

Fig. 4. Charpy impact test of different treated PP-MH composites.

3.1 Verification of compatibility

SEM pictures of the fracture surface are shown in fig. 6. There is no contact between MH and PP matrix in case of untreated sample. In contrast, electron induced reactive processing results in improved adhesion between filler and PP.

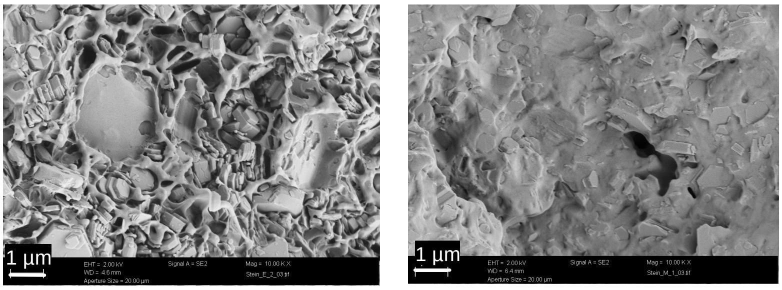

Fig. 5. SEM of untreated (left) and EB reactive processed composite (right)

3.2 Future investigations

Detailed investigations are running in order to get information about chemical coupling of MH and PP as function of composite treatment. In addition, further experiments are planned to investigate the role of electron energy in electron induced reactive processing PP-MH composite.

4. CONCLUSION

PP-MH composites were prepared by electron induced reactive processing as an alternative to conventional peroxide induced reactive processing. At fixed absorbed dose of 40 kGy this novel process results in improved tensile strength (140 %), elongation at break (500 %), and impact strength (170 %). Best properties have been achieved for an electron treatment time of 5 minutes.

The experimental results clearly indicate that two processes take place: (a) in-situ functionalization of PP and (b) in-situ improvement of adhesion between PP and MH. Functionalization of PP can be also achieved by a long mixing time (~ 44 min). But functionalization and improved adhesion is only achieved by electron induced reactive processing. This process depends on electron treatment time correlating with dose rate and radical generation rate. Thus we can conclude that radical generation rate of electron induced reactive processing controls adhesion of PP-MH composites at fixed mixing speed and same average mixing temperature. An influence of reaction rate in relation to mixing rate was already reported by Msakni et al. [Msakni 2006].

ACKNOWLEDGEMENT

The authors are thankful to diploma students H. Stein and B. Veselic and to IPF development association for financial assistance in case of conference.

REFERENCES

Gohs 2005	U. Gohs, R. Bartel, O. Röder, W. Schwarz, ASCEE-1, Cairo, Egypt, April 9 - 11, 2005
Gohs 2008	U. Gohs, G. Heinrich, M. Stephan, S. Volke, U. Wagenknecht, PPS-24, Salerno, Italy, June 15 -19, 2008
Grobler 1994	J.H.A. Grobler, W.J. McGill, J. Polym. Sci. Part B Polym. Physics, 32, 287, 1994
Hyche 1996	K.W. Hyche, Interntech Conference Proc., 1996
Jancar 1990	J. Jancar, J. Kucera, Polym. Eng. Sci., 30, 707, 1990
Karger-Kocsis 1995	J. Karger-Kocsis, Polypropylene Structure, blends and composites Vol 3, Chapman & Hall, London, 1995
Msakni 2006	A. Msakni, P. Chaumont, P. Cassagnau, Polym. Eng. Sci., 46, 1530, 2006
Wagenknecht 2009	U. Wagenknecht, U. Gohs, A. Leuteritz, M. Stephan, S. Volke, S. Wießner, G. Heinrich, PPS-25, Goa, India, March 1 - 5, 2009

Effect of triangular profile shape on the crushing behaviour of radial corrugated composite tubes subjected to axial quasi-static load

E.F. Abdewi
Mechanical Engineering Department,ering Academy Tajoura Libya
e-mail: abdewi301@yahoo.com

SUMMARY

This paper presents the effect of corrugation profile geometry on the crushing behavior, energy absorption, failure mechanism, and failure mode of woven roving glass fibre/epoxy laminated composite tube. Experimental investigations were carried out on composite tubes with two different profile shapes: sinusoidal and triangular. The tubes were subjected to axial compressive loading. On the addition to a radial corrugated composite tube, cylindrical composite tube, were fabricated and tested under the same condition in order to know the effect of corrugation geometry. The results showed that, corrugation geometry shows more stability under axial compression load than cylindrical tube. The results also show that, radial corrugated composite tube with a sinusoidal profile has more specific energy absorption than radial corrugated composite tube with a triangular profile.

1. INTRODUCTION

The use of composite materials in different kinds of applications is accelerating rapidly. As a part of engineering applications, composite tubes replacing metal products on many applications. High attention was given to produce composite tubes and testing it. They utilize these researches in composite crushing behavior and energy absorption. There is a considerable amount of published data on the response of composite tubes to axial crushing. Many of these studies utilize circular cross-section tubular specimens to determine the energy absorption capability of the material.

Hull (1991) stated that shape and dimensions of the component is one of the five important variables affecting specific energy absorption of composite materials. Farley (1986) studied the effect of specimen geometry on the energy absorption capability of composite materials. He found that, changes in section lay-up that lead to an increase in modulus lead to higher crush strengths and energy absorption. And many others such as Ross, and Shim.

Composite materials can be very effective energy absorbers. This was a fact achieved by researchers such as Thornton (1983), Provensal (1980), and Mahdi (2002).

Conventional shapes such as cylindrical, conical, rectangular, and many other regular cross sectional tubes have been tested. However, the literature shows no comprehensive study has been come across the study of radial corrugation shape of composite tube. This was one of the motivating factors behind this work. Therefore, this work adds more data to the prior contributions to the knowledge of the crashworthiness.

This paper presents the effect of corrugation profile geometry on the crushing behavior, energy absorption, failure mechanism, and failure mode of woven roving glass fibre/epoxy laminated composite tube. Experimental investigations were carried out on composite tubes with two different profile shapes: sinusoidal and triangular. The tubes were subjected to axial compressive loading. On the addition to a radial corrugated composite tube, cylindrical composite tube, were fabricated and tested under the same condition in order to know the effect of corrugation geometry.

2. EXPERIMENTAL WORK

As shown in Figure 1, different types of specimens have been investigated: Circular Composite Tube **(CCT)**, Radial Corrugated Composite Tube **(RCCT)**, and Triangular profile Corrugated Composite Tube **(TRCT).** All tubes are made of woven roving glass fibre/epoxy 600 G/sqm. According to Elfetori (2006), all specimens were fabricated under the same conditions with a fixed number of layers equal to six. The principle of wet winding process was used for the fabrication process. However, there is a difference in the details of fabrication for each type due to the difference of the final shape.

The specimens were tested in quasi-static axial as well compression between two flat platens (see Fig. 2). Instron 8500 digital testing machine with full scale load range of 250 kN was used. Five replicate tests were conducted for each type of composite tubes. Load platens were set parallel to each other before testing. All composite tubes were compressed at a rate of 10 mm/min until the end of the crush, which implies complete compaction of tested tube and load records increases sharply. Load and displacement were recorded by an automatic data acquisition system.

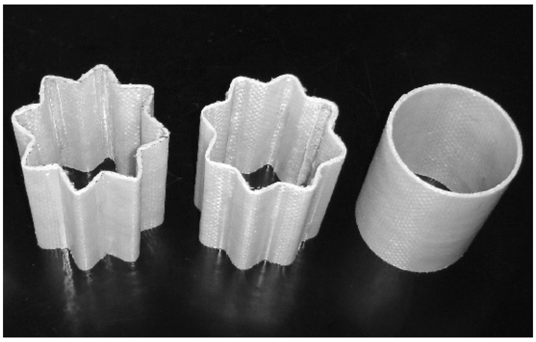

Fig. 1 Tested specimens (composite tubes).

Fig. 2 TRCT under compression load

3. RESULTS AND DISCUSSION

This work concerns of studying experimentally the effect of corrugation profile shape on energy absorption capability. In addition to corrugated tubes, cylindrical tube was tested as well for the purpose of comparison, since it has been set as a reference to examine the performance of radial corrugated composite tubes with respect to energy absorption capabilities. That means any improvement in the results obtained from testing any model over cylindrical tube defiantly will be a positive achievement, and a credit to radial corrugated composite tubes. Two different profiles have been tested; Sinusoidal profile and Triangular profile.

The specimen was loaded between two flat steel platens as shown in Figure 2. as the load increased slowly, crushing was started at the lower part of the specimen (see Figure 3a). The TRCT specimens collapsed following the failure mode of progressive crushing with micro-fragmentation of the composite material. Further collapse leads to formation of continuous fronds which spread radially outwards. As deformation proceeds, the externally formed fronds expand outwards with the simultaneous development of a number of axial splits, due to the developed tension in the circumferential direction of the tube followed by splaying of material strips. It was clearly observed that the formation of these strips was more distinct and the number of the splits was greater at the final stage of crushing (see Figure 3b).

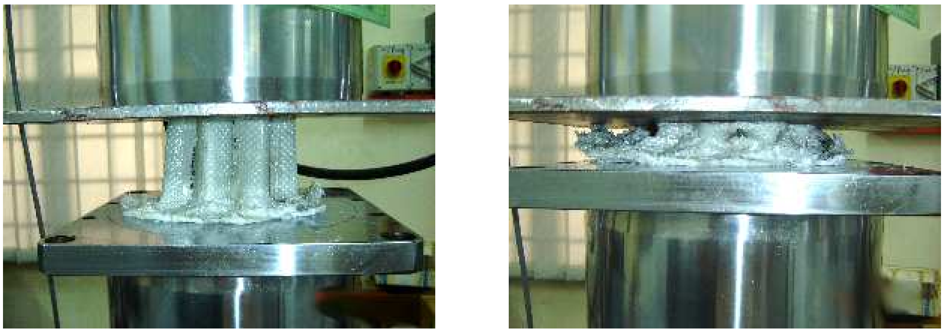

(a) (b)

Fig. 3 Deformation history of TRCT subjected to axial crushing load.

Table 1 presents the main parameters affecting the energy absorption characteristics of the three models. These parameters are: initial failure load P_i, total energy E_T, specific energy E_s, crushed length *u*, crushing force efficiency *CFE*, and stroke efficiency *SE*.

Model	P_i (kN)	E_T (kN.mm)	E_s (kj/kg)	*u* (mm)	*CFE* (%) (kN/kN)	*SE* (%) (mm/mm)
CCT	**41.788**	**3875.783**	**12.502**	**126.936**	**75.68**	**84.62**
RCCT	**62.047**	**6676.053**	**16.283**	**127.938**	**73.25**	**85.29**
TRCT	**49.228**	**4735.544**	**10.184**	**123.273**	**77.74**	**82.18**

Table 1. Crashworthiness parameters of CCT, RCCT, and TRCT subjected to axial compression load.

Typical load-displacement curves for different models (CCT3, RCCT,and TRCT) are shown in Figure 4. As it can be seen, the load increases linearly with the displacement until initial failure takes place. After that, the load falls and start fluctuates with sharp peaks and troughs increasing with displacement. This case of progress seems to continue until complete crushing of the specimens, consequently loads increases sharply.

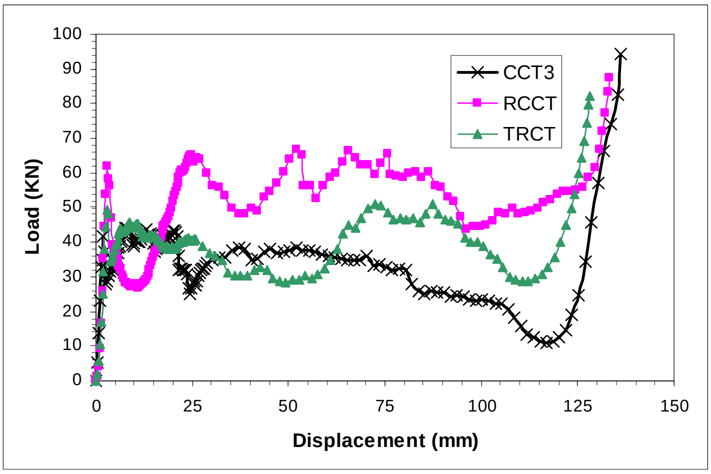

Fig. 4. Typical load-displacement curves for CCT, RCCT,and TRCT models subjected to axial crushing load.

4. CONCLUSION

The objectives of the paper have been achieved. The results obtained showed that, both models (RCCT, TRCT) crushed by the same failure mode. There is no significant effect of the corrugated profile on the energy absorption capabilities. RCCT model recorded the highest specific energy absorption amongst the tested models. The reason might be due to the sharp edges and corners that form the triangular profile. Hence this case was not exist considering comparison between corrugated tube with sinusoidal profile and cylindrical tube.

REFERENCES

ELFETORI F. Abdewi, S. Suliman, A.M.S. Hamouda, E. Mahdi. (2006), Effect of Geometry on the Crushing Behaviour of Laminated Corrugated Composite Tubes. Journal of Materials Processing Technology 172 394-399.

FARLEY, G. L. (1986), Effects of specimen geometry on the energy absorption capability of composite materials. J. Comp. Mat., 20, 390-400.

HULL, D. A. (1991) Unified Approach to progressive Crushing of Fibre-Reinforced Composite Tubes. Composites Science and Technology 40, 377-421.

MAHDI, E., Sahari, B.B., Hamouda, A.M.S., Khalid, Y.A. (2002), Crushing behaviour of cone-cylinder-cone composite system. Mech. Composite structure 2, 99-117.

PROVENSAL , J. and Cosatti, B. (1980), Energy Dissipation of composite structures. Proc., 18th International FISIIA Congress, May 5-8, , Hamburg, pp. 70-76.

ROSS, C. T. F, Bak Hock Huat, Tay Boon Chei, Chai Min Chong, and Mackney, M.D.A., (2003), The buckling of GRP hemi-ellipsoidal dome shells under external hydrostatic pressure. Ocean Engineering, V 30, 691-705.

SHIM, V.P., Quah, S.E. (2001), Effects of geometrical and loading parameters on wave propagation in a circular ring. International Journal of Impact Engineering 25,103-122.

THORNTON, P. H., Mahmood, H. F. & Magee, C. L. (1983), Energy absorption by structural collapse. Structural crashworthiness. pp. 96-117.

Caracterización a impacto de compuestos de origen renovable fabricados mediante la tecnología BMC

J.M. Cuevas, J.L. Ruiz, K. Gondra, S. Neira, S. Allue
GAIKER-IK4
M. Sarrionandia, A. Arostegui, J. Aurrekoexea
Departamento de Mecánica y Producción industrial, Mondragon Unibertsitatea

RESUMEN

El presente trabajo se centra en compuestos fabricados mediante la tecnología de BMC en base a resinas furánicas reforzadas con fibras cortas de lino (8 mm). Uno de los problemas que presentan este tipo de compuestos es su baja tenacidad y resistencia al impacto, por lo que se ha estudiado, mediante técnicas instrumentadas de impacto Charpy, el efecto de diferentes modificadores a impacto de naturaleza elastomérica (butil-acrilato, butadien-acrilonitrilo y carbamidas). En general, el BMC furánico presenta un comportamiento frágil, con niveles de tensión y alargamiento a rotura muy bajos. Los compuestos modificados siguen presentando un patrón de fractura frágil. Ningún aditivo elastomérico reduce la rigidez del compuesto de referencia, y todos mejoran la resiliencia, especialmente el de naturaleza carbamida.

1. INTRODUCCIÓN

El empleo de fuentes renovables como alternativa al petróleo es una estrategia prometedora para el desarrollo de polímeros con mayor ecoeficiencia (Yu et al. 2006). Por una parte, las matrices de procedencia natural son más fáciles de reciclar, se degradan con mayor facilidad y su balance neto de generación de dióxido de carbono es cero. Por otra parte, el uso de fibras naturales supone una serie de ventajas como son la disponibilidad de materias primas, bajo coste, y elevada rigidez y resistencia específica.
Hasta el momento actual, en el campo de las resinas furánicas se ha hecho poca investigación en la fisicoquímica de la preparación de los intermedios así como en los procesos de resinificación o curado (Hoydonck et al. 2008) ya que sus mas próximos competidores, las resinas fenólicas, parten de precursores derivados del petróleo, por tanto mas baratos, mas puros y se operaban con mayor rendimiento, lo que ha justificado el desarrollo de estas últimas en detrimento de las furánicas. Los problemas encontrados en la estabilidad, conservación y procesabilidad de los sistemas furánicos investigados por Gaiker en formatos de SMC, han planteado la alternativa del BMC como tecnología equivalente, al tratarse de un sistema en masa que no requiere de una evolución previa de la viscosidad con el tiempo (maduración), y es polimerizada y transformada por la misma técnica de compresión y temperatura que el SMC. Tradicionalmente, el proceso de fabricación de las resinas furánicas consiste en la polimerización discontinua por condensación de alcohol furfurílico con catalizadores, aditivos y modificadores en un reactor hasta obtener un grado adecuado de polimerización (controlando la temperatura del proceso). El alcohol furfurílico se obtiene del furfural, que a su vez se obtiene comercialmente por degradación de las hemicelulosas presentes en diferentes plantas (maíz, caña de azúcar,…) El alcohol furfurílico, considerado el precursor de las resinas furánicas, se obtiene por hidrogenación y es un compuesto muy reactivo, susceptible de resinificación en medio ácido y alta temperatura.

El objetivo ha consistido en validar la base de la composición de un BMC furánico y estudiar el efecto de diferentes modificadores de impacto.

2. DESARROLLO EXPERIMENTAL

2.1. Preparación del compuesto BMC furánico

La filosofía del BMC es formular una pasta resínica en base a matriz furánica, catalizador latente, desmoldeante interno, aditivos y refuerzo. La adicción final de la carga permite incrementar la viscosidad del sistema hasta alcanzar un grado de sequedad que equivale al estado de maduración de un sistema de SMC. En la etapa inicial del procesado del BMC, la resina furánica es mezclada mediante agitadores de alta velocidad con todos los aditivos, a excepción de la fibra y la mitad de la carga, componentes que se incorporan al final en un amasador de doble aspa. Esta etapa de amasado de las fibras con la pasta juega un papel determinante en la calidad de la pieza acabada, ya que existe el riesgo de romper la fibra. A fin de conseguir una completa humectación de la fibra, es necesaria la desfilamentación completa de las mismas, para lo que se ha optimizado el tiempo de amasado (175 s). Tras el procesado del BMC, el material es sometido a moldeo por compresión, obteniéndose probetas circulares de 250 mm de diámetro y 3,7 mm de espesor. Los principales parámetros a tener en cuenta son: la temperatura (130 ºC), la dosificación del material, la presión (60 bares) y el tiempo de ciclo (240 s), velocidad de cierre y apertura de la prensa.

Una vez optimizado el BMC furánico de partida, en cuanto a composición, procesabilidad y condiciones de moldeo, se han formulado tres nuevos compuestos, a los que se les han añadido modificadores de impacto elastoméricos de diferente naturaleza.

	BMC Ref.	BMC 1 MI butil acrilato	BMC 2 MI butadien-acrilonitrilo	BMC 3 MI carbamida
	PARTES			
Resina furánica	100,0	100,0	100,0	100,0
Cat. ácido (65% agua)	5,5	5,5	5,5	5,5
Modificador impacto (MI)	0,0	3,1	3,1	3,1
Desmoldeante interno	1,5	1,5	1,5	1,5
Carga inorgánica	116,7	116,7	116,7	116,7
% Fibra corta de lino	23,5			

Tabla 1. Formulaciones BMC furánicas preparadas.

2.2. Caracterización a impacto de los compuestos BMC

El estudio del comportamiento a impacto se ha efectuado mediante un péndulo Charpy instrumentado. Este sistema permite realizar la adquisición de datos en un intervalo de 2 μs, lo que asegura un gran número de puntos para el trazado de la curva fuerza-tiempo (*F-t*). Las dimensiones de las probetas prismáticas mecanizadas a partir de las placas obtenidas por BMC son 80 x 13 x 3,7 mm^3. La geometría de ensayo ha sido la de flexión tres puntos, con una luz entre apoyos de 50,8 mm, la masa del impacto es de 2,182 kg, temperatura ambiente y la velocidad de impacto ha sido de 0,33 m/s.

3. RESULTADOS Y DISCUSIÓN

Aunque el grueso del estudio, fue dirigido hacía el análisis del comportamiento a impacto del composite resultante, la caracterización mecánica se completó con ensayos de flexión, dureza y densidad. Como se puede observar la pérdida de rigidez es despreciable, mientras que la resistencia y la dureza disminuyen ligeramente.

	BMC Ref.	BMC 1 MI butil acrilato	BMC 2 MI butadien-acrilonitrilo	BMC 3 MI carbamida
Módulo flexión (GPa)	13,49 ± 0,51	13,27 ± 0,72	12,09 ± 0,68	12,45 ± 0,53
Resistencia flexión (MPa)	65,52 ± 4,79	67,33 ± 6,13	53,54 ± 2,48	57,05 ± 4,40
Densidad (g/cm^3)	1,75 ± 0,00	1,74 ± 0,00	1,76 ± 0,00	1,77 ± 0,02
Dureza Shore D	71,00 ± 4,12	65,00 ± 3,44	64,20 ± 2,76	65,20 ± 4,25

Tabla 2 .Caracterización mecánica.

En la figura 1 se muestran las curvas de impacto fuerza-tiempo más representativas de cada tipo de compuesto. Como se puede apreciar al inicio de las curvas hay efectos dinámicos que se atenúan antes de llegar al pico máximo, por lo que la medida de fuerza máxima no representa ninguna complicación ni se inducen errores de medida considerables. En lo que al patrón de deformación se refiere, en todos los casos la fuerza crece de forma lineal hasta llegar al máximo, tras el cual se produce una caída brusca de la fuerza, típica de las roturas frágiles.

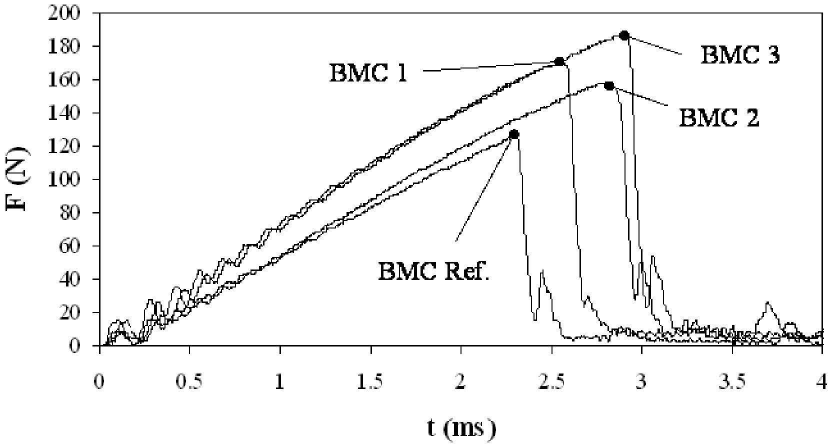

Fig. 1. Curvas representativas de impacto de los compuestos analizados.

El BMC de referencia es el que posee valores de fuerza y alargamiento más pequeños. Cabe desatacar que, al igual que en las medidas estáticas, la presencia de los modificadores de impacto no perjudican la rigidez del compuesto. La influencia sobre la tensión máxima o de fractura sin embargo es apreciable, ya que todos los modificadores mejoran la resistencia (figura 2). Este fenómeno es típico en los materiales de comportamiento frágil en los que se aumenta la deformación a la rotura. Como se ha comentado anteriormente, el compuesto de referencia es muy frágil y absorbe poca energía. Todos los modificadores de impacto mejoran dicha capacidad de disipar energía de impacto, aunque si bien se dobla el valor de referencia siguen siendo valores muy bajos. El compuesto BMC 3 modificado con carbamida es el más eficiente de los modificadores de impacto estudiados.

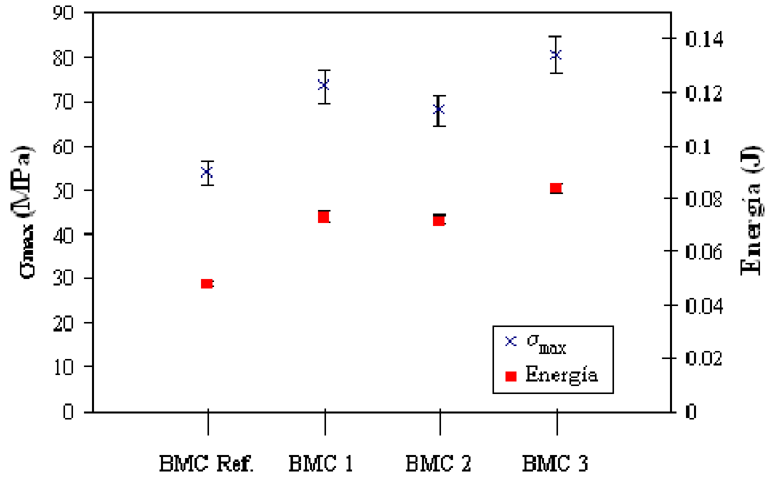

Fig. 2. Tensiones máximas y energías de impacto absorbidas para los compuestos BMC furánicos estudiados.

El estudio fractográfico ha demostrado que el mecanismo de pinzamiento de fisura, y no el aumento de volumen de matriz furánica deformada plásticamente, está en el origen tanto de la mayor resistencia como de la resiliencia.

4. CONCLUSIONES

El estudio a impacto de compuestos de BMC furánico reforzados con fibra de lino ha demostrado que su comportamiento a impacto es un punto débil y que si bien la adición de modificadores de impacto utilizados duplican la capacidad de disipar energía, los niveles alcanzados siguen siendo bajos comparado con otras matrices. La carbamida se ha mostrado como la mejor opción de las estudiadas en el presente trabajo.

5. AGRADECIMIENTOS

Los autores desean agradecer a la Comisión Europea (EC) (proyecto IP 515769-2 BIOCOMP, al Departamento de Innovación y Promoción Económica de la Diputación Foral de Bizkaia: Programa Ekinberri (2007-2008) (7/12/EK/2007/35) y al Ministerio de Ciencia e Innovación: Plan de Investigación Colaborativa (2008-2010) (CIT-420000-2008-18).

REFERENCIAS

HOYDONCK H.E., van RHIJN W.M. (2008). "Aplication of novel furan resins in composites", *Jec Composites 38, 34-35.*

YU, L., DEAN, K., LI, L. (2006). "Polymer blends and composites from renewable resources", *Progress in Polymer Science 31*, *576-602.*

On the flexural fatigue behaviour of glass fibre reinforced nanoclay modified epoxy matrix composites

G. Minak, D. Ghelli, R. Panciroli, A. Zucchelli
Alma Mater Studiorum - Università di Bologna, Mechanical Engineering Department
DIEM, viale del Risorgimento 2, 40136 Bologna, Italy

ABSTRACT

In the past few decades it has been demonstrated that the properties, specifically the mechanical ones, of thermo-set resins can be modified significantly by means of the addition of small quantities of nanoclay (such as montmorillonite).

In particular improvement of the elastic modulus, tensile strength and of the fracture toughness can be obtained, even if a reduction of the ductility is generally recorded.

Few works in literature deal with the fatigue behaviour of nano-modified resin systems, but the authors claim a tendency to better performances if compared with the original matrices. On the other hand, fatigue data are nearly not available at all for three phase composites, i.e. fibre reinforced nano-modified matrices.

To develop structural applications based on long fibre reinforced composite materials with nano-modified matrix essential aspects are the choice of the type and the percentage of nano-reinforcement in the matrix, together with the definition of techniques for the uniform dispersion of nano-reinforcement in the whole component.

Moreover new design criteria, especially as regards fatigue, which take account of the peculiarity of these triphasic materials, are needed.

In this work the three point bending fatigue behaviour of a glass woven fabric nanoclay modified epoxy matrix composite produced by infiltration in vacuum bag is experimentally investigated.

In order to enhance the differences in matrix properties short composite beams with different layups are tested at low frequency (to reduce the heat generation) on an Instron servo-hydraulic machine. The temperature of the specimen, its stiffness, the crack density in the thickness and the delamination onset and propagation are monitored.

1. INTRODUCTION

The damage in long fibre reinforced laminate composites is characterized by the competition of different failure mechanisms, among which the most important ones are: the matrix cracking, the delamination of the layers constituting the composite laminate, the transverse rupture of fibres (ductile or brittle depending on their nature) and the debonding between fibre and matrix.

Among the others, previous studies of the authors regarding the evaluation of the static and fatigue residual strength with initial damage (Cesari et al. 2007, Minak et al. 2009) highlighted the need to improve the properties of the matrix to limit the phenomenon of delamination.

One possibility to improve the mechanical properties of the matrix that was recently introduced (Becker et al., 2003, Subramaniyan and Sun, 2006, Meguid and Sun, 2004, Jen et al. 2005), is the addition of clay compounds having at least one dimension of the order of the nanometer, called nanoclays.

Considering the non-reinforced matrix alone, in Wang et al. (2006) an increase in elastic modulus and fracture toughness by adding exfoliated nanoclay is found while Ho et al. (2006) show an increase in tensile strength and a decrease in ductility of the matrix.

The relationship between the fractions of exfoliated and intercalated or even agglomerated nanoclay causes different effects on toughness and strength (Alexandre and Dubois, 2003, Zilg et al. 1999, Boo et al. 2006).

Few papers deal with the fatigue behaviour of nanoclay-reinforced matrix (e.g. Karaki et al. 2003, Juwono and Edward, 2005). They show a general tendency to an improvement, but without definitive conclusions.

As regards the properties of a three-phase composite, formed by a nano-reinforced matrix and long fibres, in (Chowdury et al. 2007) the addition of nanoclay leads to better impact behaviour of carbon-epoxy laminates in terms of higher peak force and lower damage at every energy level. In (Colavito et al. 2007) it is observed that the addition of a 5% nanoclay reduces the impact delaminated area by 46% while Avila et al. (2007) find that the addition of Montmorillonite, although intercalated and not exfoliated, in glass-epoxy composite laminates causes a significant increase in energy absorption and the fracture path changes from intra-laminar to inter-laminar.

The mechanisms that lead to the improvement (or sometimes worsening) of the properties are beginning to be understood (Quaresimin and Varley, 2008) but much experimental and modelling work is still needed to elaborate design criteria that might allow the use of the acquired knowledge in industrial components.

2. MATERIALS AND METHODS

Composite laminates were produces by vacuum bag resin infiltration. An epoxy resin system, with a Tg=80 °C was reinforced by means of glass long fibre in form of 2x2 balanced twill woven fabric with a mass per unit area of 0.35 Kg/m^2.

Different percentages of nano-metric Montmorillonite were added to the matrix system before the degassing phase of the infiltration process.

The laminate thickness was of 3.8 mm and it was obtained by a $[(0/90)_{10}]$ stacking sequence.

Rectangular specimens 25 mm wide and 100 mm long were cut from the laminas by means of a diamond-coated tool and their lateral edges were mirror polished by emery cloth.

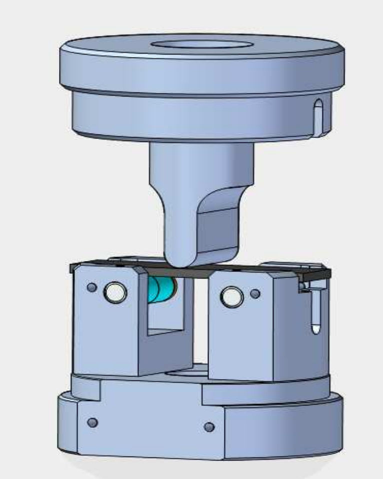

Fig. 1. Fatigue test set-up

Three-point bending fatigue test were performed in load control on an Instron servo-hydraulic machine equipped with a 100 kN Load cell and LVDT. The sinusoidal load (with load ratio R=0) frequency was chosen with the aim of reducing the time on test without increasing the specimen temperature, monitored by an infrared thermometer (type Optris LT CF2), more than 5 degrees. A 12.7 mm radius cylindrical indenter was used and the specimen was simply supported by two cylindrical roller bearings of a 12.5 mm radius in order to eliminate the friction on the supports. The initial span was of 70 mm (even in the case of large deflection the value of the shear stresses in the middle is not influenced by the actual span). Specimen failure criterion was a determined reduction of the stiffness, resulting in an increase of the displacement range.

At prescribed life stages optical micrographies of the samples' edges were acquired by means of a Zeiss Observer AX10 microscope (examples are shown in figures 2a and 2b) in order to monitor the crack density and the delamination onset and growth.

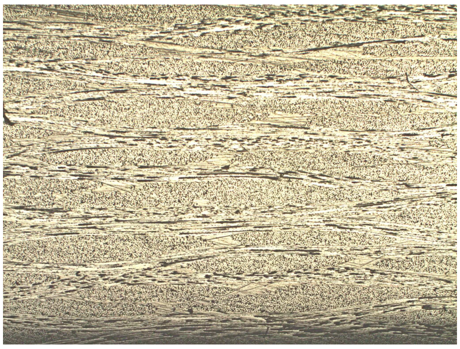

Fig 2a. Optical micrography.

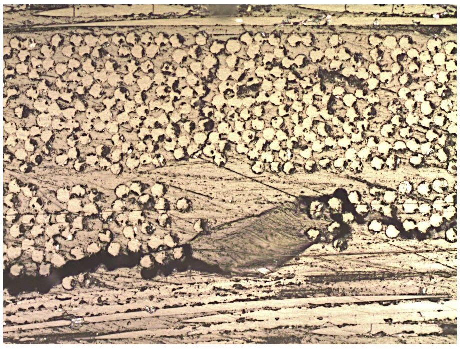

Fig 2b. Matrix damage.

3. EXPECTED RESULTS AND CONCLUSION

The study was focused on the possible improvement of the matrix system fatigue performances due to the addition of different percentages of Montomorillonite.

At the time in which this paper was written only preliminary results were available and they were not included.

By means of the experimental test campaign an evidence of positive (or negative) effects of the nano-modification was researched. The stresses on the matrix in three point bending are mainly tensile/compressive in the more external laminas and shearing in particular in the mid plane interface. The analysis of the crack density evolution and the measure of the growth of the delamination are expected to improve the understanding of the macroscopic effect of the matrix modification on its fatigue performances. A similar test campaign is under preparation by the authors with the aim of researching the effect of the matrix nano- modification on the compression-compression fatigue properties. Other Italian research units meanwhile are studying the impact behaviour, the inter-laminar properties and the high strain rate effects on the same material.

ACKNOWLEDGMENTS

The authors thank Dr. Fabrizio Lotti for the fatigue grips design. The present work was financed by the Italian Ministry for University and Scientific Research (MUR) with the grant n. 20075939JY_002.

REFERENCES

ALEXANDRE, M., DUBOIS, P., (2003) Polymer-layered silicate nanocomposites: a review from preparation to processing, *Prog Polym Sci*, 28 (11), 1539-1641

AVILA, A.F, SOARES, M.I, SILVA NETO, A., (2007) A study on nanostructured laminated plates behavior under low-velocity impact loadings, *Int J Imp Eng,* 34, 28–41

BECKER, O., VARLEY, R.J., SIMON, G., (2003) Use of layered silicates to supplementary toughen high performance epoxy-carbon fiber composites, *J Mater Sci Lett*, 22,1411-1414.

BOO, W.J., LIU, J., SUE, H.J., (2006) Fracture behaviour of nanoplatelet reinforced polymer nanocomposites, *Mater Sci Tech,* 22 (7), 829-834

CESARI, F., DAL RE, V., MINAK, G., ZUCCHELLI, A., (2007) Damage and residual strength of laminated carbon–epoxy composite circular plates loaded at the centre, *Compos A*, 38, (4), 1163-1173

CHOWDHURY, F.H., HOSUR, M., JEELANI, S., (2007) Processing, impact response and damage characterisation of plain-weave carbon/epoxy-nanoclay nanocomposites, *Polym Polym Compos*, 5 (6), 425-435

COLAVITO, K.W., KILIC, B., CELIK, E., MADENCI, E., ASKARI, E., SILLING, S., (2007) Effects of nanoparticles on stiffness and impact strength of composites, *Technical Papers AIAA* 4, 3950-3959

HO M., LAM, C., LAU K. , DICKON, H.L., Hui, D., (2006) Mechanical properties of epoxy-based composites using nanoclays, *Compos Struct*, 75, 415–421

JEN, M.H.R., TSENG, Y.C., WU, C.H. (2005) Manufacturing and mechanical response of nanocomposite laminates, *Compos Sci Tech*, 65, 775-779.

JUWONO, A., EDWARD, G., (2005) Fatigue performance of clay-epoxy nanocomposites, International Journal of Nanoscience, 4,4, 501-507

KARAKI, T., TIMMERMANN, J.F., SEFERIS, J.C., (2003) Tension-Tension Fatigue of Nanoparticle Modified Polymeric Matrix Composites, International SAMPE Symposium and Exhibition, 48, II, 1643-1650

MEGUID, S.A., SUN, Y., (2004) On the tensile and shear strength of nano-reinforced composite interfaces, *Mater Des* 25,4, 289-296

MINAK, G., MORELLI P., ZUCCHELLI, A.,(2009) Fatigue Residual Strength of Laminate Graphite-epoxy Composite Circular Plates Damaged by Transversal Load*, Compos Sci Tech,* 69, 1358–1363

QUARESIMIN, M, VARLEY, R.J, (2008) Understanding the effect of nanomodifier addition upon the properties of fibre reinforced laminates, *Compos Sci Tech*, 68 (3-4), 718-726

SUBRAMANIYAN, A.K., SUN, C.T., (2006) Enhancing compressive strength of unidirectional polymeric composites using nanoclay, Compos A, 37 (12), 2257-2268

WANG, L., WANG, K., CHEN L., ZHANG,Y.,HE, C, (2006) Preparation, morphology and thermal/mechanical properties of epoxy/nanoclay composite, *Compos A*, 37, 1890–1896

ZILG, C., MALHAUPT, R., FINTER, J., (1999) Morphology and toughness/stiffness balance of nanocomposites based upon anhydride-cured epoxy resins and layered silicates, *Macromol Chem Phys*, 200, 661-670

Mechanical and morphological properties of SBR/elastomeric vulcanized ground scraps composites

L.N. Carli
Programa de Pós-Graduação em Ciência dos Materiais, Universidade Federal do Rio Grande do Sul, Brazil
J.S. Crespo
Centro de Ciências Exatas e Tecnologia, Universidade de Caxias do Sul, Brazil

SUMMARY

Mechanical recycling of waste rubber has very important consequences since its natural degradation occurs over long time periods. It consists of the grinding of the rubber and reuse of the resulting powder as fillers in the production of new items. The aim of this study was to incorporate styrene-butadiene rubber (SBR) industrial scraps into a base formulation of identical composition. Eight composites with different proportions, varying from 10 to 80 phr of ground scrap (SBR-r), were prepared and evaluated by rheometric, physical-mechanical and morphological characteristics. The results obtained indicated that up to 50 phr of SBR-r can be added without adversely affecting these properties.

1. INTRODUCTION

Disposal of waste rubber is a serious environmental problem since its natural degradation occurs over long time periods due to the cross-linked structure. Mechanical recycling of waste rubber is a low cost alternative and has very important consequences including environmental, economic and social issues. It consists of the size reduction (grinding) of the rubber materials and reuse of the resulting powder as fillers in the production of new items (Fang et to. 2001). Several studies had reported significant losses in the mechanical properties even at low concentration of rubber scrap (Gujel et to. 2008, Ishiaku et to. 2000, Ismail et to. 2002). Therefore, when the main composition of the residue is known, the recycling process can be interesting in the achievement of better mechanical performance of the composites with higher scrap content (Zanchet et to. 2007). The aim of this study was to incorporate styrene-butadiene rubber (SBR) industrial scraps into a base formulation of identical composition used in the fabrication process of extruded profiles. Rheometric, physical-mechanical and morphological characteristics of the SBR-r composites were evaluated and the results were compared with the control sample (with 0 phr of SBR-r).

2. EXPERIMENTAL

2.1 Materials

The SBR base formulation and the extruded profile scraps were supplied by Ciaflex Indústria de Borrachas Ltda. (Caxias do Sul, RS, Brazil). The rubber scraps were collected according to ASTM E 300-03 and ground under ambient conditions. The obtained powder (SBR-r) showed a particle size distribution in the range of 28-35 mesh. The partial composition of the scraps, obtained by thermogravimetric analysis, was:

27.6% SBR, 34.1% $CaCO_3$, 24.1% oil, 12.1% carbon black and 2.1% other additives (Carli et to. 2009).

2.2 Preparation of SBR-r composites

Eight formulations with different contents (10 to 80 phr) of SBR-r were prepared in a laboratory two-roll mill (MH, model MH-600C), according to ASTM D 3182-06. The specimens for the physical-mechanical analysis were obtained by compression molding at 160°C under a pressure of 7.5 MPa in a Shultz electrically-heated hydraulic press.

2.3 Characterization of SBR-r composites

Cure characteristics were determined using an oscillating disk rheometer (ODR) Tech Pro-Rheotech OD+, at the vulcanization temperature (160 °C), according to ASTM D 2084-06. Tensile and tear strength tests were performed in an EMIC DL-3000 instrument, according to ASTM D 412-06a and ASTM D 624-00, respectively. A Shore A Teclock durometer, model GS709, was used to measure hardness (ASTM D 2240-05). The compression set test was carried out at 23 °C for 22 h in accordance with ASTM D 395B-03. Abrasion resistance was measured using a Maqtest equipment according to DIN 53516-87. The morphology of the cryogenically-fractured samples was analyzed using a Philips XL 30 scanning electron microscope (SEM).

3. RESULTS AND DISCUSSION

Fig. 1 shows the cure characteristics of SBR-r composites. The optimum cure time (t_{90}) and the scorch time (t_{s1}) values (Fig. 1a) were not affected by addition of SBR-r.

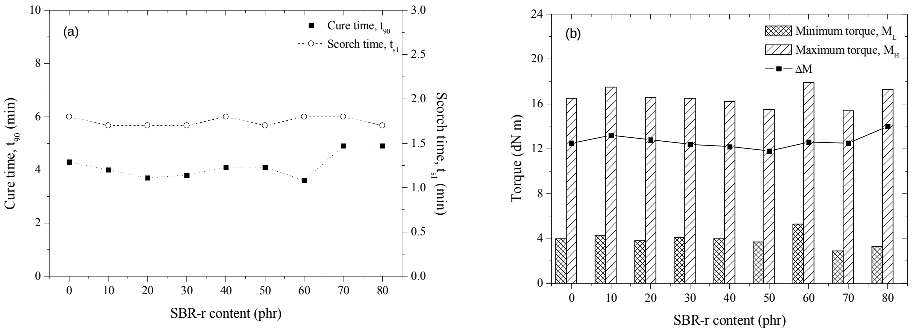

Fig. 1. Cure characteristics of SBR-r composites: (a) cure and scorch time and (b) torque values.

The minimum torque (M_L), a measure of stock viscosity, and maximum torque (M_H), related to the crosslink density, indicated that the addition of SBR-r to the composites did not significantly affect these properties up to 80 phr of SBR-r (Fig. 1b). The ΔM values, which are related to the influence of the residue on the composites, corroborated these findings.

Table 1 shows the variation in the mechanical properties of the SBR-r composites. The Shore A hardness and tear strength values showed a small variation with the addition of SBR-r up to 50 phr. For tensile strength, the results indicated that up to 40 phr of SBR-r can be added to the base formulation without adversely affecting the tensile behavior. Further increases in the SBR-r content led to a gradual decrease in these values. It is possible that with higher concentrations of SBR-r, agglomeration and particle-particle interaction of the rubber powder increase and the reinforcing effect of the filler is counteracted by the volume effect (Ishiaku et to. 2000, Ismail et to. 2002).

SBR-r content (phr)	Hardness (Shore A)	Tensile strength (MPa)	Elongation at break (%)	Tear strength (kN/m)	Compression set (%)	Abrasion loss (mm^3/40m)
0	44 ± 1	4,1 ± 0,2	472 ± 44	14,4 ± 0,3	1,7 ± 0,8	712 ± 30
10	42 ± 1	4,0 ± 0,3	448 ± 20	14,7 ± 0,3	2,5 ± 0,7	739 ± 26
20	42 ± 1	4,2 ± 0,2	469 ± 13	14,9 ± 0,7	1,9 ± 0,4	763 ± 40
30	41 ± 1	3,6 ± 0,3	494 ± 22	14,4 ± 0,9	2,5 ± 0,7	827 ± 16
40	42 ± 1	3,7 ± 0,2	475 ± 32	14,6 ± 0,7	2,4 ± 0,6	793 ± 28
50	43 ± 0	3,3 ± 0,2	438 ± 21	14,7 ± 0,5	1,6 ± 0,9	746 ± 15
60	41 ± 1	3,3 ± 0,6	398 ± 18	13,4 ± 0,7	2,5 ± 0,2	792 ± 54
70	40 ± 1	3,6 ± 0,1	402 ± 14	13,5 ± 1,0	3,0 ± 0,4	870 ± 18
80	41 ± 1	3,7 ± 0,1	395 ± 22	13,8 ± 0,9	3,0 ± 0,5	796 ± 31

Table 1. Mechanical properties of SBR-r composites.

The increase in the recycled rubber content in the SBR-r composites and hence the reduction in the virgin SBR content led to an increase in the compression set values. This can be attributed to the reduced elasticity of the elastomeric matrix, which facilitates irreversible flow under stress (Nelson et to. 2002). As a result, decreases in the elongation at break values were also observed for SBR-r contents above 50 phr.

SEM pictures of fractured surfaces of composites with 50 and 70 phr of SBR-r are shown in Fig. 2, with a magnification of 1000x.

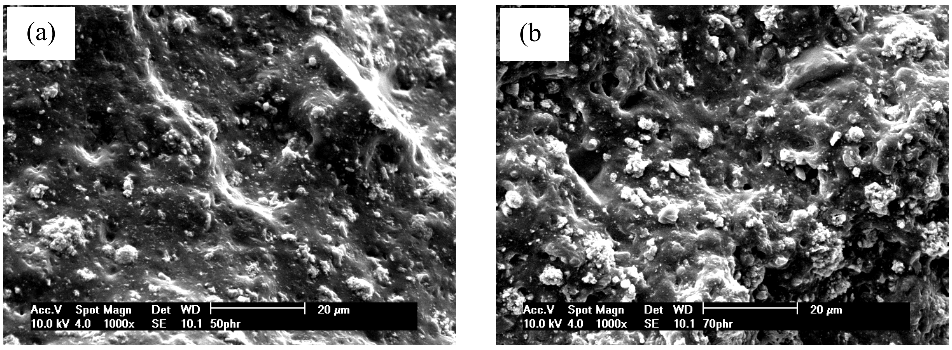

Fig. 2. SEM micrograph of composites with (a) 50 phr and (b) 70 phr of SBR-r.

In order to obtain rubber compounds with satisfactory mechanical properties, good dispersion of SBR-r in the matrix and strong interfacial adhesion are required (Bilgili et to. 2001). The micrograph of the failure surface of the SBR-r composite with 50 phr of SBR-r (Fig. 2a) evidenced the good distribution of the residue in the SBR matrix and the good adhesion between the matrix and the particles. However, as more SBR-r was incorporated, holes were formed as a result of the detachment of rubber particles from the matrix, as can be seen for the composite with 70 phr of SBR-r (Fig. 2b). It was possible to observe at least two phases in the SBR-r composites: rubber matrix and powdered rubber (lighter phase), evidencing the non-homogeneity of the composite.

This result corroborates the abrasion test, which the loss of materials increased with increasing SBR-r content, as a result of the poor powder-matrix interaction. Therefore, the abrasion resistance of control sample was slightly better than that of the composites with SBR-r as filler.

4. CONCLUSIONS

The results obtained for the SBR-r composites, related to the performance of the mechanical properties such as tensile and tear strength and abrasion resistance, indicated 50 phr as the limit of SBR-r content. Scanning electron microscopy corroborated this finding, evidencing the good distribution and the good adhesion between the matrix and the SBR-r particles.

ACKNOWLEDGMENT

The authors are grateful to Ciafex Indústria de Borrachas Ltda for supplying the SBR scraps and additives, and to CAPES and CNPq (481748/2007-5) for financial support.

REFERENCES

BILGILI, E., ARASTOOPOUR, H., BERNSTEIN, B. (2001). Pulverization of rubber granulates using the solid state shear extrusion process: Part II. Powder characterization. *Powder Technol.*, 115, 277-289.

CARLI, L.N., BONIATTI, R., TEIXEIRA, C.E., NUNES, R.C.R., CRESPO, J.S. (2009). Development and characterization of composites with ground elastomeric vulcanized scraps as filler. *Mater. Sci. Eng. C*, 29, 383-386.

FANG, Y., ZHAN, M., WANG, Y. (2001). The status of recycling of waste rubber. *Mater. Des.*, 22, 123-127.

GUJEL, Â.A., BRANDALISE, R.N., GIOVANELA, M., CRESPO, J.S., NUNES, R.C.R. (2008). Incorporação de pó de pneu em uma formulação para banda de rodagem de pneu de motocicleta. *Polímeros*, 18, 320-325.

ISHIAKU, U.S., CHONG, C.S., ISMAIL, H. (2000). Cure characteristics and vulcanizate properties of a natural rubber compound extended with convoluted rubber powder. *Polym. Testing*, 19, 507-521.

ISMAIL, H., NORDIN, R., NOOR, A.M. (2002). Cure characteristics, tensile properties and swelling behavior of recycled rubber powder-filled natural rubber compounds. *Polym. Testing*, 21, 565-569.

NELSON, P.A., KUTTY, S.K.N. (2002). Cure characteristics and mechanical properties of butadiene rubber/whole tyre reclaimed rubber blends. *Progr. Rubber Plast. Tech.*, 18, 85-97.

ZANCHET, A., DAL'ACQUA, N., WEBER, T., CRESPO, J.S., BRANDALISE, R.N., NUNES, R.C.R. (2007). Propriedades reométricas, e mecânicas e morfologia de compósitos desenvolvidos com resíduos elastoméricos vulcanizados. *Polímeros*, 17, 23-27.

Influencia de la temperatura en el comportamiento a fractura interlaminar de compuestos de matriz epoxi reforzada con fibra de carbono unidireccional bajo carga de impacto a baja velocidad

R. Zenasni
Department of Mechanics, Laboratory Sea2m, University of Mostaganem BP882, R.P., Algeria
B. Mustapha
Department of Quimical, Laboratory Sea2m, University of Mostaganem BP882, R.P., Algeria
A. Argüelles
Departamento de Construcción e Ingeniería de Fabricación, Universidad de Oviedo, Campus Universitario s/n, 33203 Gijón, España
J. Viña
Departamento de Ciencia de los Materiales e Ingeniería Metalúrgica, Universidad de Oviedo, Campus Universitario s/n, 33203 Gijón, España
I. Viña
Departamento de Construcción e Ingeniería de Fabricación, Universidad de Oviedo, Campus Universitario s/n, 33203 Gijón, España

RESUMEN

En este trabajo se estudia el comportamiento a fractura interlaminar en modo II de dos materiales compuestos reforzados con fibra de carbono unidireccional bajo carga de impacto de baja energía tras ser sometidos al efecto de la temperatura por encima y por debajo de la temperatura ambiente. El estudio se ha realizado sobre dos tipos de materiales compuestos de fibra de carbono y matriz epoxi, de denominaciones AS/8552 y AS4/3501-6. De cada material, se han fabricado laminados de 32 capas de fibra de carbono preimpregnado. Una película de PTFE ha sido introducida en el plano medio del laminado para generar una grieta artificial de longitud 60 mm. De cada material, se han realizado ensayos en modo II estático y dinámico a temperaturas de: -30, -15, 0. 20. 50 y 90ºC. De los resultados experimentales se deduce un comportamiento semejante entre ambos materiales, con escasa influencia de la temperatura.

1. INTRODUCCIÓN

El amplio campo de aplicación de los materiales compuestos en sectores tan dispares como la industria aeroespacial, del automóvil, construcción naval, equipos criogénicos, depósitos de líquidos y hasta componentes de turbobombas, aumenta día a día, debido a su facilidad de fabricación, su bajo coste relativo y a sus excelentes propiedades mecánicas. Este gran abanico de aplicaciones hace necesario conocer su comportamiento bajo la influencia de todo tipo de solicitaciones tanto mecánicas como térmicas o medioambientales. Así la temperatura puede originar cambios significativos en su respuesta termomecánica, al alterar sus mecanismos de fractura y de rotura. Por otra parte, en las diferentes aplicaciones industriales, pueden generarse diferentes tipos de daño que limitan, por lo general, su vida útil, uno de ellos, potencialmente muy peligroso, es el impacto de baja velocidad dado que puede producir una deslaminación de la sub-superficie, no visible en sus capas externas (Takayuki 2003), y que permite la entrada de humedad, lo cual afectará a la integridad y durabilidad del material. Cuando la temperatura disminuye hasta la temperatura criogénica (Usami et al. 1999), se generan tensiones internas en la matriz epoxi a causa de las contracciones térmicas. La rotura de la matriz se produce cuando las tensiones térmicas inducen un factor de intensidad de tensión que sobrepasa la tenacidad de fractura de la resina. La tenacidad a fractura de la matriz a temperatura criogénica puede mejorarse controlando la estructura química y la morfología (Uek et al. 2005). Estudios realizados han demostrado que la microestructura se vuelve más ordenada a bajas temperaturas (Zhang et al. 2001).

En este trabajo, se analiza el comportamiento de dos materiales compuestos carbono epoxi, sometidos a exposición térmica bajo solicitación a fractura dinámica en modo II, mediante impacto de baja energía.

2 PROCEDIMIENTO EXPERIMENTAL

2.1 Materiales

Se han utilizado dos materiales compuestos reforzados con fibra de carbono unidireccional y matriz epoxi. Uno de ellos del tipo (AS4/8552) de matriz epoxi modificada para mejorar su tenacidad y otro (AS4/3501-6), compuesto convencional de matriz epoxi 3501-06. Las probetas de espesor 6 mm, 25 mm de ancho y 160 mm de longitud, fueron cortadas a partir de laminados simétricos de 32 capas, introduciendo en su plano medio, en una longitud de 60mm, una película de material no adhesivo para así generar una grieta artificial. De cada tipo de material, se ensayaron cinco probetas las cuales fueron sometidas al efecto de la temperatura, altas y bajas. Las temperaturas seleccionadas fueron de: 90ºC, 50ºC, 20ºC(ambiente), 0ºC, -15ºC y -30 ºC.

2.2 Ensayos de impacto

Los ensayos de impacto se han realizado en una torre de caída de peso de 100J de capacidad máxima y a una velocidad de impacto es de 4.43 m/s. La geometría del ensayo (apoyos y distancias), figura 1, ha sido similar al ensayo ENF de acuerdo al protocolo ESIS (Davis et al. 2001) también se ha seguido este protocolo para la determinación de la energía requerida para la deslaminación G_{IIc} mediante los métodos propuestos y tomando el punto de carga máxima como referencia para los cálculos, según las diferentes teorías.

Calibración de la flexibilidad:

$$G_{IIC} = \frac{3ma^2P}{2B} \tag{1}$$

Teoría de la viga directa:

$$G_{IIC} = \frac{9a^2P\delta}{2B(2L^3+3a^2)} \tag{2}$$

Teoría de la viga corregida:

$$G_{IIC} = \frac{9a^2P^2}{16B^2Eh^3} \tag{3}$$

donde: B es la anchura, h el espesor medio, P la carga, δ el desplazamiento, *a* la longitud de grieta, L la distancia media entre los apoyos, C_0 la flexibilidad para *a*=0. La pendiente m se calcula de: $C=C_0+ma^3$

E es el modulo elástico determinado de la ecuación 4:

$$E=\frac{L^3}{4BC_0h^3} \tag{4}$$

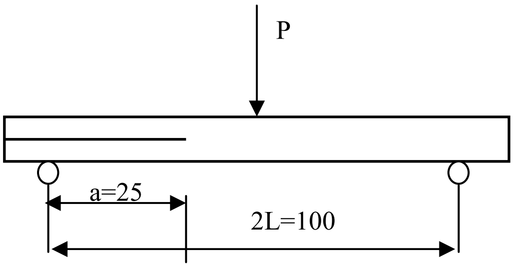

Fig. 1. Disposición del ensayo ENF

2.3 Resultados de los ensayos

En la figura 2 se muestran las variaciones de la energía de deslaminación de los dos materiales ensayados en función de la temperatura, para los diferentes métodos de cálculo empleados. Se observa un comportamiento ligeramente diferente según el método de cálculo empleado. Sí se considera el método de calibración de la flexibilidad, se puede apreciar, para el material 8552 un mantenimiento de la energía de fractura entre -30ºC y 0ºC, un ligero descenso a temperatura ambiente (20ºC) y a 90ºC y un mantenimiento a 50ºC.

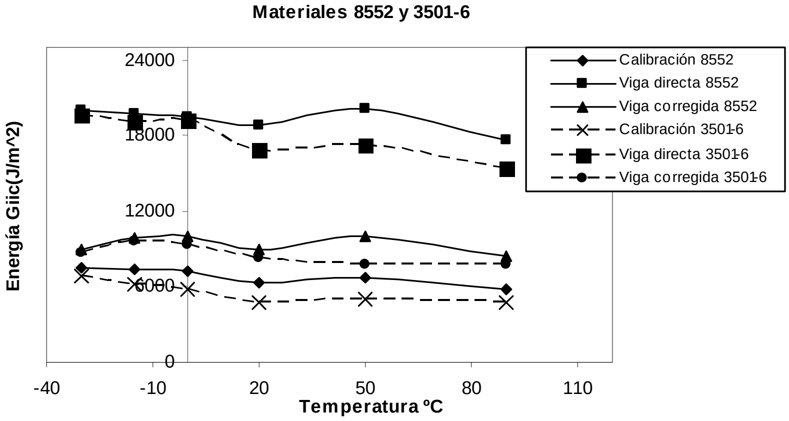

Fig. 2. Variación de energía de deslaminación en función de temperatura de exposición (8552 y 3501-6).

Para el material 3501-6 se aprecia, tomando como referencia la energía de deslaminación a -30ºC, una pérdida del orden del 15% a 0ºC, que alcanza el 20% a temperatura ambiente, valor que se mantiene a 50 y 90ºC. Considerando la teoría de la viga corregida, los dos materiales tienen un comportamiento similar entre -30ºC y 90ºC. Observando un ligero aumento de la energía de deslaminación a -15ºC y 0ºC del orden de un 10% del valor obtenido a -30ºC, manteniéndose la misma tendencia que la observada anteriormente para el resto de las temperaturas. El método de la viga directa da valores de energía de fractura sensiblemente superiores a los otros métodos, aunque la tendencia se mantiene, lo cual está condicionado por los valores de desplazamiento obtenidos directamente de los ensayos.

3. CONCLUSIONES

Dos compuestos han sido sometidos a daño por impacto en torre de caída de peso tras ser expuestos al efecto de temperaturas altas o bajas. A partir de los resultados obtenidos de la energía de deslaminación, bajo fractura en modo II, se deduce que los dos materiales muestran un comportamiento similar con ligeras variaciones en función de la temperatura de exposición, por lo que se puede concluir: que el tipo de resina no modifica de forma sustancial el comportamiento del material, además de que la formulación empleada en el cálculo de la energía de deslaminación proporciona resultados diferentes más elevados en el caso de la teoría de la viga directa.

AGRADECIMIENTOS

Los autores agradecen la financiación recibida de CICYT a través del proyecto de investigación MAT2007-60696

REFERENCIAS

TAKAYUKI Kusaka (2003). Experimental characterization of interlaminar fracture behaviour in polymer matrix composites under low velocity impact loading, JSME, Vol.46, Nº.3, 328-334.

USAMI S, SUZUKI, Ejima H, ASAN K.(1999). Thermomechanical properties of epoxy GFRPs used in superconducting magnet winding, cryogenics,39(11), 905-914.

UEK T, NISHIJIMA S, IZUMI Y (2005). Designing of epoxy resin systems for cryogenic use, Cryogenics,45(2),141-148.

ZHANG PQ, RUAN JH, Li WZ (2001). Influence of some factors on the damping property of fiber reinforced epoxy composites at low temperature, Cryogenics, 41(4),245-251.

DAVIES P., BLACKMAN B.R.K., BRUNNER A.J.(2001). Mode II delamination. Fracture Mechanics Testing Methods for Polymer Adhesives and Composites. Ed. Moore D.R., Pavan A. y Williams J.G., ESIS publication 28, Elsevier.

Medida del campo de deformaciones inducido por una delaminación mediante sensores de fibra óptica distribuida

A. Fernández-López, D. Llorente, A. Güemes
Departamento de Materiales y Producción Aeroespacial. Universidad Politécnica de Madrid, España

RESUMEN

Uno de los modos de fallo más comunes asociado a los materiales compuestos en aplicaciones aeronáuticas son las delaminaciones, debido a su influencia en las propiedades mecánicas, la aparición de modos de fallo no deseados y la vida a fatiga del material. Por todas estas razones, la detección de la existencia de delaminaciones es crucial en el mantenimiento aeronáutico, ya que la detección de una delaminación incipiente posibilita una reparación más sencilla y efectiva. Normalmente la detección de delaminaciones en el mantenimiento aeronáutico va asociada a técnicas de ensayos no destructivos basadas en ultrasonidos. En este artículo se estudian los cambios en el campo de deformaciones inducidos por una delaminación provocada por impactos de baja energía por medio de sensores de medida distribuida a lo largo de una fibra óptica. Las enormes posibilidades de monitorización estructural que permite esta técnica de medida, unida a la fácil integración de una red sensora de fibra óptica en el material compuesto hacen de ella una posible candidata para la mejora del mantenimiento.

1. INTRODUCCIÓN

La detección de delaminaciones es una de las prioridades del mantenimiento aeronáutico de estructuras de material compuesto. Debido a que en la etapa inicial de las delaminaciones provocadas por impactos de baja energía su influencia es únicamente local, las técnicas para la detección de daño mediante sensores integrados que permiten la detección de delaminaciones y la localización de las mismas están basadas en el estudio de la propagación de ondas elásticas, ya que hasta la fecha son las únicas que poseen una alta relación entre el área de medida y el peso que introduce la red sensora a la estructura. La dificultad para interpretar la señal obtenida, tanto para asignarla un nivel de daño como para localizar la posición del mismo han limitado su aplicación a ensayos en condiciones controladas, muy lejos de las condiciones de operación de una aeronave.

La medida distribuida a lo largo de una fibra óptica nos ofrece la posibilidad de medir deformaciones a lo largo de una fibra de varios kilómetros, posibilitando la medida en todos los puntos de la misma. Con la técnica utilizada en este artículo, basada en la dispersión de Rayleigh, es posible implementar una red ultra densa de sensores que nos permita la detección de daños con una influencia local, como pueden ser las delaminaciones, con la baja intrusividad y el bajo peso añadido que proporciona una fibra óptica. Así es posible detectar los cambios en el campo de deformaciones que inducen pequeños daños en el material compuesto, como pueden ser las delaminaciones, a pesar de que la influencia de estos sea únicamente local.

2. MEDIDA DEL CAMPO DE DEFORMACIONES INDUCIDO POR UNA DELAMINACION

2.1 Fundamento teórico

A pesar de que la fibra óptica es un sensor unidireccional, existen multitud de configuraciones que nos permiten medir el campo de deformaciones de una superficie completa. La configuración más común es la fibra en zig-zag, que nos permitirá cubrir extensas aéreas de una superficie (ver figura 1).

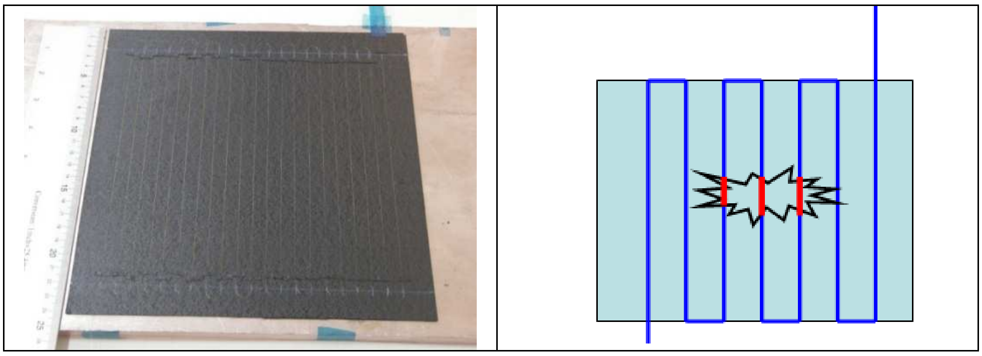

Fig. 1. Fibra óptica con configuración zig-zag.

Aunque una delaminación no tiene ninguna influencia significativa en el campo de deformaciones residuales producidas durante el curado, es posible encontrar en la bibliografía numerosos ejemplos en los que los impactos de baja energía provocan, junto con las delaminaciones, grietas intralaminares en la matriz. La rotura de la matriz provoca la liberación de las deformaciones residuales generadas durante el curado. Así, la liberación de las deformaciones residuales va a perturbar localmente el campo de deformaciones, permitiendo la detección de la existencia de delaminaciones por medio de sensores de deformación.

2.2 Fundamento teórico de la técnica de medida

La medida distribuida con sensores de fibra óptica no es una novedad. Equipos comerciales basados en el efecto Raman y el efecto Brillouin están disponibles en el mercado desde hace más de una década. Ambas técnicas han tenido escasa repercusión fuera de la ingeniería civil, donde su baja resolución espacial (superior a los 10 cm) no presentaba una limitación. La técnica de medida utilizada en este artículo está basada en la medida espectral de la dispersión de Rayleigh, que ofrece una alta resolución espacial (inferior a 1 mm) con altas prestaciones para la medida de deformaciones ($\pm\mu\varepsilon$). Durante la fabricación de la fibra se producen imperfecciones en el índice de refracción del núcleo. Dichas imperfecciones provocan pequeñas perdidas en la fibra, conocidas como dispersión de Rayleigh. El espectro de dicha dispersión en una sección de la fibra es estable en ausencia de perturbaciones exteriores, y se puede asemejar a una “huella dactilar” de la fibra, de forma que cualquier variación del las deformaciones en el sentido de la fibra o de la temperatura se ve reflejada en el espectro de la misma. La forma de cuantificar las variaciones en el espectro es mediante la correlación cruzada del espectro de la misma sección entre dos medidas. Así, las variaciones de temperatura y deformación van a ser proporcionales a la variación del paso espectral según la siguiente relación:

$$\frac{\Delta\lambda}{\lambda} = -\frac{\Delta\gamma}{\gamma} = K_T \Delta T + K_\varepsilon \varepsilon$$

2.3 Resultados experimentales

Se realizaron diferentes ensayos en placas de material compuesto con unas dimensiones de 150x100 mm., fabricadas con fibra unidireccional AS4/8552 con una configuración $[0_2,90_2,0_2]$. Se embebieron tres fibras ópticas con la configuración de la figura 2. Para provocar las delaminaciones, se realizaron impactos a 10 mm de la posición de la fibra para niveles de energía crecientes: 2.4, 4.4, 6.3 y 12 J.

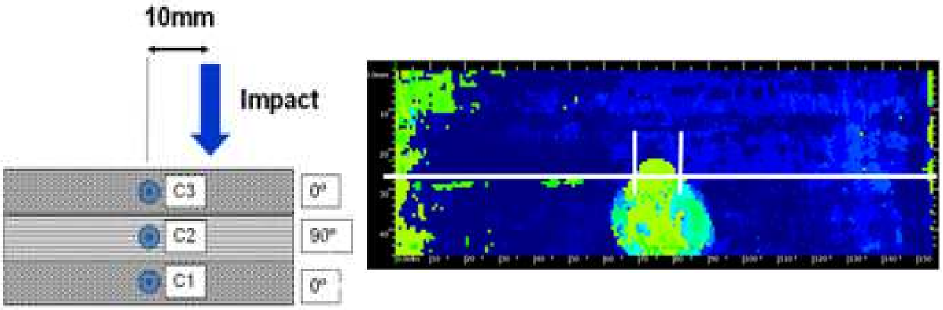

Fig. 2. Configuración del ensayo (izquierda). C-Scan de la delaminación (derecha).

En la figura 2 se puede apreciar el C-Scan después de un impacto de 4.4 J. Las fibras ópticas embebidas permitirán la medida del campo de deformaciones en el sentido de la fibra. Las deformaciones a lo largo de una de las fibras ópticas embebidas las podemos ver en la figura 3. Los valores del campo de deformaciones de la fibra muestran un salto correspondiente con el área delaminada, como consecuencia de la liberación de las deformaciones residuales en las tres fibras embebidas. Las medidas realizadas con C-Scan verifican la coincidencia del salto de deformaciones con la sección de fibra dentro de la delaminación. En este caso, la longitud de la fibra dentro del área delaminada permanece constante para los diferentes impactos, a pesar de que el área total de la delaminación va en aumento,

La influencia sobre el campo de deformaciones no se ciñe al área de la delaminación: el campo cercano a la misma también se ve afectado, disminuyendo su efecto a medida que nos alejamos del área delaminada.

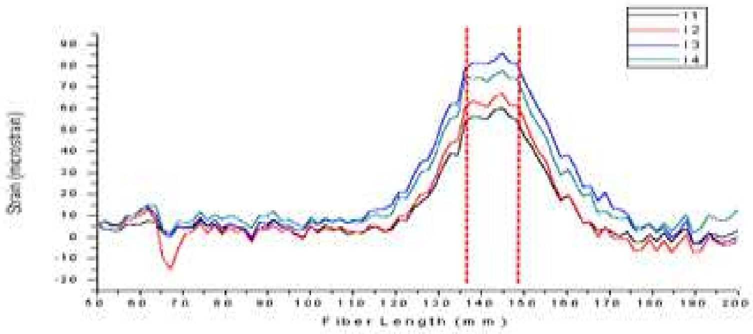

Fig. 3. Deformaciones a lo largo de la fibra óptica C3 para los diferentes impactos.

3. CONCLUSIONES

Los cambios del campo de deformaciones inducidos por un impacto pueden ser utilizados para la detección del área delaminada. En el caso de laminados cruzados, es posible establecer una relación directa entre el área delaminada y los valores obtenidos del campo de deformaciones. A pesar de que la influencia de las grietas interlaminares en la rigidez global del laminado es pequeña, la liberación de los esfuerzos residuales provocada por ellas es significativa y puede ser detectada por medio de sensores de deformación.

La medida distribuida abre la posibilidad de detectar pequeños cambios en el campo de deformaciones en piezas de material compuesto, como los inducidos por una delaminación, por medio de una red sensora integrada en la misma. A pesar de la alta densidad de la red sensora, la fibra óptica solo introduce un pequeño peso adicional, lo que la habilita para posibles aplicaciones aeroespaciales.

REFERENCIAS

KREGER, S., GIFFORD, D. K., SOLLER, B. J., WOLFE, M.S., FROGGAT, M. E. Fiber Calibration for Distributed Fiber-Optic Strain and Temperature Measurements using the Optical Backscatter Reflectometer.

KREGER, S., GIFFORD, D. K., SOLLER, B. J., WOLFE, M.S., FROGGAT, M. E. Fiber Calibration for Distributed Fiber-Optic Strain and Temperature Measurements using the Optical Backscatter Reflectometer.

KREGER, S., SOLLER, B. J., GIFFORD, D. K., DUNCAN, R. G., WOLFE, M.S., FROGGAT, M. E. Optical Backscatter Reflectometry as a Measurement Tool for Fiber-Optics in Avionics and Aerospace Applications.

MINAKUCHI, S., OKABE, Y., TAKEDA, N. (2007) Barely visible impact damage detection in sandwich structures using non-uniform strain along optical fiber sensors. *Proceedings of ICCM-16,* Kyoto, Japan

SANG, A. K., DUNCAN, R. G., KREGER, S., FROGGAT, M. E. High-Resolution ExtendedDistance Distributed Strain Measurements Using Swept-Wavelength Interferometry.

Influencia del tipo de matriz y de la temperatura, en materiales compuestos carbono-epoxi, sometidos a deslaminación bajo solicitación a fractura en Modo I

P. Coronado
Departamento de Construcción e Ingeniería de la Fabricación, Universidad de Oviedo, 33204 Gijón
A. Argüelles
Departamento de Construcción e Ingeniería de la Fabricación, Universidad de Oviedo, 33204 Gijón
J. Viña
Departamento de Ciencias de los Materiales e Ingeniería Metalúrgica, Universidad de Oviedo, 33204 Gijón
R. Zenasni
Departamento de Mecánica, Laboratorio Sa2m, Universidad Mostaganem, Argelia
M.A. Castrillo
Departamento de Construcción e Ingeniería de la Fabricación, Universidad de Oviedo, 33204 Gijón

RESUMEN

El presente trabajo analiza el comportamiento a fractura en Modo I y solicitación estática de dos materiales compuestos fabricados con el mismo refuerzo unidireccional de carbono tipo AS4 y dos tipos de matriz, uno con resina epoxi modificada para aumentar su tenacidad del tipo 8552 y el otro con resina epoxi tipo 3501-6, sin modificar, a distintas temperaturas. Para la realización del estudio se ensayaron probetas tipo DCB de ambos materiales, para cada una de las temperaturas objeto de análisis: 90, 50, 20 (temperatura ambiente), 0, -30 y -60ºC. Para analizar la resistencia a la deslaminación de ambos compuestos se determinó la tenacidad a la fractura (G_{IC}) según la norma ASTM D 5528-01.

1. INTRODUCCIÓN

Los materiales compuestos fabricados a partir de láminas manifiestan una preocupante susceptibilidad a la aparición y crecimiento de grietas entre capas. Este fenómeno conocido como deslaminación, es uno de los modos de fallo que más limita la vida útil de estos materiales y conduce a la reducción notable de la resistencia y rigidez de estos materiales pudiendo producir el fallo catastrófico de la estructura. Esta es una de las razones más importantes por las que en el pasado se ha limitado el uso de materiales compuestos a componentes de estructuras secundarias en las que las cargas se encuentran bien definidas y el fallo no supone una amenaza determinante para la estabilidad de la estructura total.

En los últimos años se han realizado un gran número de trabajos centrados en la determinación de las características a fractura interlaminar bajo solicitación estática, sin embargo, son escasas las investigaciones realizadas para este tipo de materiales en condiciones adversas de temperatura. S.G. Kalarikkal et al. (2006) realizaron un estudio sobre el efecto de las bajas temperaturas en la tenacidad a la fractura de compuestos formados por fibras de carbono y resina epoxi, para ello, emplearon distintos tipos de probetas DCB con nanopartículas y con tejidos de fibras planos. Otros autores como Y. Shindo et al. (2008) estudiaron el comportamiento de un compuesto reforzado con fibra de vidrio y matriz de resina epoxi también a temperaturas criogénicas pero en este caso se analizó el comportamiento a fractura interlaminar en Modo II.

2. PROCEDIMIENTO EXPERIMENTAL

En el presente estudio se analiza experimentalmente los fenómenos de iniciación y propagación de grietas interlaminares bajo solicitación estática en dos compuestos unidireccionales de fibra de carbono y dos tipos matrices epoxi.

2.1 Materiales y probetas

Se emplearon dos materiales compuestos, uno formado por resina epoxi tipo 8552 y refuerzo unidireccional de fibra de carbono AS4 y el otro por resina epoxi tipo 3501-6 y refuerzo unidireccional de fibra de carbono AS4. La orientación de ambos laminados es la misma: 16 láminas a 0º / inserto/ 16 láminas a 0º. Se utilizaron probetas tipo DCB para caracterizar la deslaminación en Modo I para los dos tipos de materiales y las distintas temperaturas, según la Norma ASTM 5528-01.

2.2 Procedimiento de ensayo

Las probetas se graduaron según la normativa, en uno de los bordes de las mismas cubiertos con pintura de spray blanca. El avance de la grieta se observó en todo momento mediante una videocámara instalada fuera de la cámara frente a un lateral de la probeta. El equipo empleado para realizar los ensayos está formado por una máquina servohidráulica marca MTS con una célula de carga acoplada de 1 KN. Para realizar los ensayos a temperaturas elevadas (50 y 90ºC) se utilizó una cámara térmica acoplada a la máquina de ensayos. Para los ensayos a bajas temperaturas (0, -30 y -60ºC) se utilizó la misma cámara con una botella de nitrógeno líquido acoplada.

2.3 Resultados experimentales

En las figura 1 se presentan los resultados de los valores de carga-desplazamiento durante la fase de iniciación de la grieta para las distintas temperaturas. En los gráficos se han representado los valores de las probetas consideradas más representativas para cada compuesto.

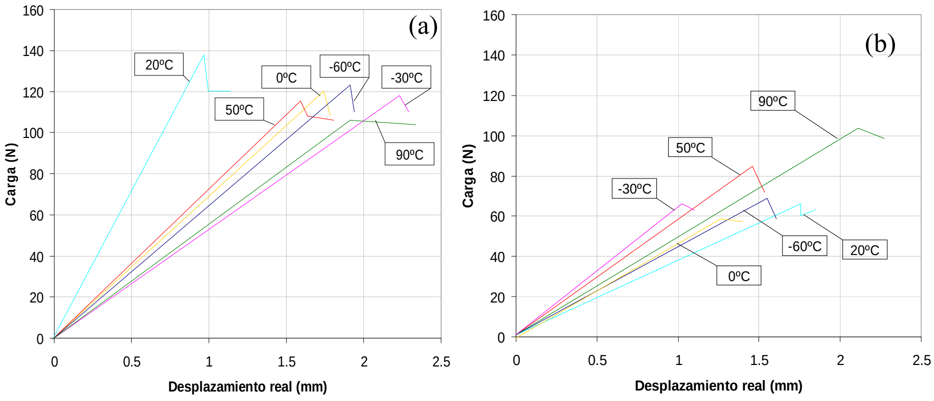

Fig. 1. Valores de carga y desplazamiento de las probetas más representativas para cada temperatura: (a) Material AS4/8552 y (b) Material AS4/3501-6.

Como se puede apreciar en las figuras anteriores la carga necesaria para iniciar el avance de grieta, es mayor para el material de resina modificada (AS4/8552) que para el material compuesto con matriz sin modificar para todas las temperaturas de ensayo, donde en la mayoría de los casos no se alcanzan los 100 N de carga.

Respecto a los valores tenacidad para la iniciación de la grieta obtenidos del análisis de los resultados de los ensayos realizados, se aprecian valores de G_{IC} más elevados para el material compuesto con matriz modificada para todo el rango de temperaturas estudiado, como podemos observar en la figura 2.

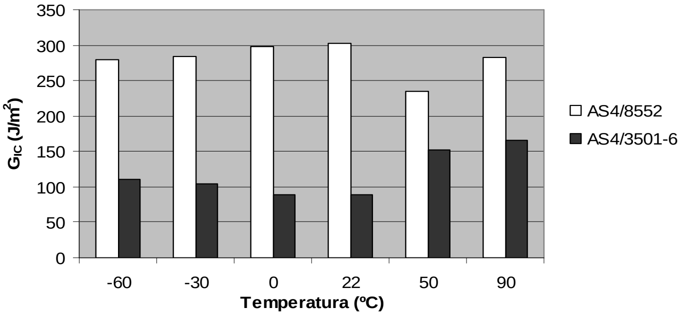

Fig. 2. Valores de G_{IC} durante la iniciación de la grieta para los dos tipos de compuestos a las distintas temperaturas de ensayo.

Por otra parte, para el material compuesto con matriz sin modificar la tasa de relajación de energía crítica para la iniciación de la grieta, aumenta ligeramente, respecto a los valores obtenidos a temperatura ambiente, a elevadas y bajas temperaturas, este fenómeno no se observa en el material compuesto de matriz modificada. Es decir, el material de matriz sin modificar presenta mejor comportamiento en condiciones adversas que a temperatura ambiente en base a los ensayos realizados, al contrario que ocurre con el material de matriz modificada (AS4/8552) que presenta mejor comportamiento (mayor G_{IC}) a temperatura ambiente.

En cuanto a los valores de tenacidad obtenidos durante la propagación de la grieta, se aprecian valores más bajos conforme avanza la grieta para el material de matriz modificada en todas las temperaturas de ensayo. Para el material de matriz sin modificar (AS4/3501-6) se aprecia un aumento de los valores de G_{IC} conforme avanza la grieta, debido probablemente a la formación de puentes de fibra que aumentan la resistencia del avance de grieta.

3. CONCLUSIONES

En base al estudio realizado podemos concluir que el material de matriz modificada (AS4/8552), presenta un mejor comportamiento en general, para todas las temperaturas objeto de estudio, presentando en todos los casos valores de G_{IC} más elevados tanto para la iniciación como para la propagación de la grieta. En cuanto al material de matriz no modificada (AS4/3501-6), observamos que durante la iniciación ofrece una mayor resistencia a la deslaminación a temperaturas adversas que a temperatura ambiente, al contrario que ocurre con el material AS4/8552.

Respecto a la propagación de la grieta en el material de matriz modificada observamos un incremento de G_{IC} durante la propagación de la grieta en la mayor parte de los casos. Esto puede ser debido a la influencia del elevado número de puentes de fibra formados en este material durante los ensayos. Este fenómeno se observa de manera menos significante en el material de matriz modificada, donde solo observamos un ligero aumento de tenacidad en los primeros mm de avance de grieta y luego comienza a disminuir progresivamente. En un compuesto unidireccional, después de la iniciación de la grieta, la mayor causa de resistencia a la deslaminación es la formación de puentes de fibra durante la propagación.

AGRADECIMIENTOS

Los autores agradecen la financiación recibida de CICYT a través del proyecto de investigación MAT 2007-60696.

REFERENCIAS

ASTM D 5528-01 Mode I Interlaminar fracture toughness of unidirectional fiber reinforced polymer matrix composites.
KALARIKKAL, S.G., SANKAR, B. V., IFJU, P.G. Effect of cryogenic temperature on the fracture toughness of graphite/epoxy composites (2006). *Journal of Engineering Materials and Technology, Vol. 18, 151-157.*
SHINDO, Y., SATO, T., NARITA, F. Mode II interlaminar fracture and damage evaluation of GFRP woven laminates at cryogenic temperatures using the 4ENF specimen (2008). *Journal of COMPOSITE MATERIALS, Vol. 42, No.11 (1089-1101).*

Nuevo método para determinar la curva de resistencia en modo II mediante el ensayo de flexión con entalla final en tres puntos

A. Arrese, N. Carbajal, G. Vargas, F. Mujika
Escuela Politécnica. Universidad del País Vasco-Euskal Herriko Unibertsitatea

RESUMEN

En el presente trabajo se propone un nuevo método para la determinación de la longitud de grieta y curva de resistencia en modo II basado en la complianza del punto de aplicación de carga. El desarrollo analítico se ha llevado a cabo teniendo en cuenta el efecto de las deformaciones locales, el cortante y las rotaciones de flexión.

1. INTRODUCCIÓN

La baja tolerancia a la fractura interlaminar de los materiales compuestos reforzados con fibra larga es una de la principales limitaciones de estos materiales para su uso en estructuras. Por ello, el conocimiento de los procesos de delaminación es necesario para poder diseñar estructuras de composite adecuadas y desarrollar materiales con mejores propiedades interlaminares (Corleto 1987).

El comportamiento a fractura de los materiales compuestos se caracteriza mediante la curva de resistencia o *R*-curva que se define como un registro continuo de la variación de la tenacidad a fractura en función del avance estable de grieta (Bueno 2007).

De acuerdo a Blackman et. al (2005, 2006), la dificultad para la determinación de la longitud de grieta durante el ensayo es la clave para acordar un protocolo para la fractura interlaminar en modo II de laminados composites.

En el presente trabajo se propone un nuevo método para la determinación de la longitud de grieta y la curva de resistencia en modo II basado en la complianza del punto de aplicación de carga. El desarrollo analítico se ha llevado a cabo teniendo en cuenta el efecto de las deformaciones locales (Mujika 2007), el cortante y las rotaciones de flexión. Esta nueva aproximación se ha denominado Teoría de Vigas con Rotaciones de Flexión *Beam Theory including Bending Rotation effects* (BTBR) y los resultados se ha comparado con los obtenidos para el método basado en CBTE propuesto por Blackman et al (2005, 2006) modificado incluyendo el efecto del cortante y la complianza del sistema denominado MCBTE *Modified Corrected Beam Theory with Effective Crack Length*.

2. ANÁLISIS

En el análisis que se realiza a continuación, se han tenido en cuenta el efecto del cortante, el efecto de las deformaciones locales y el efecto de las rotaciones de flexión.

La complianza del punto medio de aplicación de carga según BTBR es:

$$C^{II}=\frac{\delta}{P}=\frac{1}{8E_f wh^3}\left(3(a^{II})^3[1-3\alpha_a]+2L_0^3\right)[1-\alpha_f]+\frac{3L_0}{10G_{LT'}wh}[1-\alpha_s] \qquad (1)$$

siendo los α_i factores de corrección debidos al efecto de las rotaciones de flexión.

La complianza del punto de aplicación de carga según MCBTE, se calcula a partir de la ecuación (1), considerando nulos los factores de corrección.
siendo C la complianza experimental, despejando a^{II} de la ecuación (1) se obtiene la longitud de grieta según BTBR Cuando se desprecia el efecto del las rotaciones de flexión, la longitud de grieta a^I correspondiente a la aproximación MCBTE se obtiene de la ecuación (1) considerando nulos los factores de corrección.
La expresión de la tasa de liberación energía para el caso de la aproximación BTBR.

$$G_{II}^{II}=\frac{9P^2(a^{II})^2}{2E_f w^2(2h)^3}[1-\chi] \qquad \chi=\frac{2R}{(2h)}\frac{P(2L)}{E_f w(2h)^2}\left[4(a_0^{II})^3-5(a_0^{II})^2+6(a_0^{II})+\frac{2}{(a_0^{II})}\left(1+\frac{1}{5}\frac{E_f}{G_{LT'}}\left(\frac{h}{L_0}\right)^2\right)\right] \quad (2)$$

donde $a_0^{II}=a^{II}/L_0$ y χ es el factor de corrección de la tasa de liberación de energía.
La expresión de la tasa de liberación energía para el caso de la aproximación MCBTE.

$$G_{II}^{I}=\frac{9P^2(a^I)^2}{2E_f w^2(2h)^3} \quad (3)$$

3. RESULTADOS

Para comprobar experimentalmente la validez de la aproximación propuesta para la determinación de la longitud de grieta y R-curva, se han utilizado laminados unidirecccionales de material T300/F593.

3.1. Determinación de la longitud de grieta sin avance de grieta

La grieta inicial correspondiente a cada aproximación se determina realizando el promedio de los valores obtenidos punto a punto en el rango de deformaciones 0,05-0,2%.

Posición	***R*(mm)**	**$a^{\mathrm{II}}_{\mathrm{m}}$(mm)**	**$a^{\mathrm{I}}_{\mathrm{m}}$(mm)**	**a_{r}(mm)**
	R_1	30,2	29,9	
1	**R_2**	30,3	29,3	30,5
	R_3	30,5	29,4	
	R_1	40,3	40	
2	**R_2**	40,3	39,5	40,5
	R_3	40,1	39,1	
	R_1	50,4	50,1	
3	**R_2**	50,5	49,8	50,5
	R_3	50,6	49,6	

Tabla 1. $a^{\mathrm{II}}_{\mathrm{m}}$, $a^{\mathrm{I}}_{\mathrm{m}}$ y a_{r} para la probeta T300/F593 S1 con 120mm de luz.

siendo $a^{\mathrm{II}}_{\mathrm{m}}$ la grieta inicial correspondiente a al aproximación BTBR y $a^{\mathrm{I}}_{\mathrm{m}}$ la correspondiente a MCBTE. En la última columna se muestran las longitudes de grieta reales, las cuales se han determinado abriendo la probeta en modo I (Friedrich 1989).
Se comprueba que la precisión de la aproximación BTBR es excelente.

3.2. Determinación de la longitud de grieta durante avance de grieta

Para evaluar la precisión de las longitudes de grieta determinadas durante el avance, se provoca un avance estable en la grieta, descargando el ensayo tras el inicio del avance. La longitud de grieta se determina utilizando el valor de la complianza del último punto del ensayo. Para evaluar la precisión de las longitudes de grieta determinadas punto a punto, se realiza un segundo ensayo en el rango de deformaciones donde no se produce avance, determinando la longitud de grieta tal y como se ha explicado en el punto anterior.

R(mm)	Aproximación	a_{m1}(mm)	a_{lp}(mm)	a_{m2}(mm)
R_1	**BTBR (II)**	43,1	43,8	**43,8**
	MCBTE (I)	42,9	43	43,4
R_2	**BTBR (II)**	50,0	51,6	**51,4**
	MCBTE (I)	49,5	49,6	50,6
R_3	**BTBR (II)**	46,8	48,0	**47,9**
	MCBTE (I)	46,0	45,7	46,8

Tabla 2. Longitud de grieta durante el avance para la probeta T300/F593 S2.

En el caso de la aproximación BTBR la concordancia de las dos longitudes de grieta es excelente. Se comprueba por tanto la precisión de la aproximación BTBR para determinar la longitud de grieta durante el avance.

3.3. Determinación de las curvas de resistencia

Una vez comprobada la validez de la aproximación BTBR para la determinación de la longitud de grieta durante el avance, se evalúan la longitud de grieta y G_{II} en cada punto del ensayo estable a medida que avanza la grieta obteniendo la R-curva, utilizando para ello las aproximaciones BTBR y MCBTE.

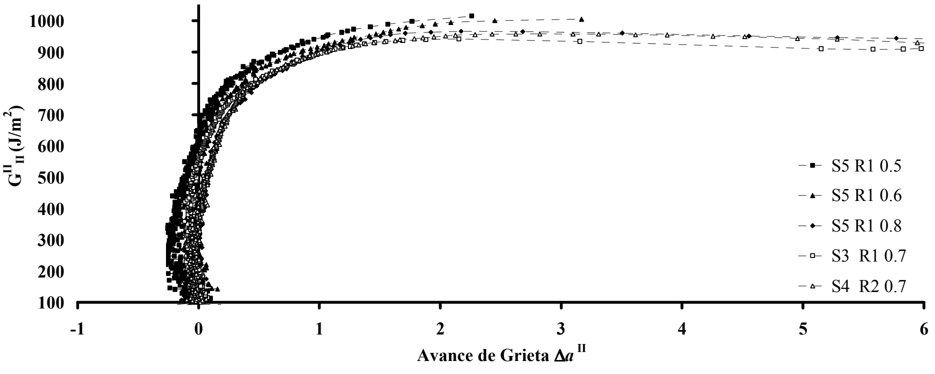

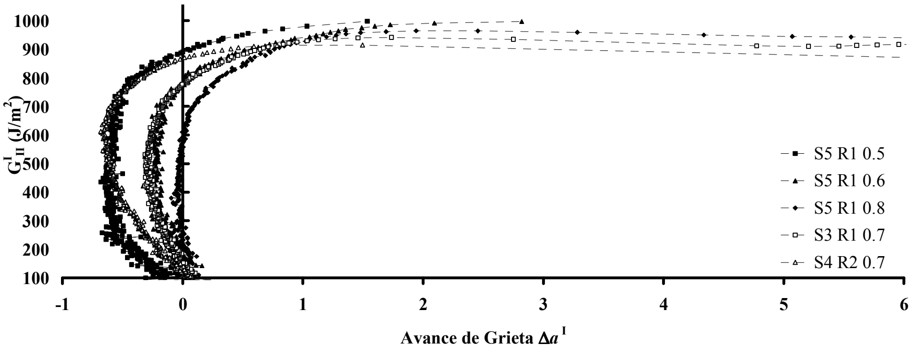

Fig. 1. R Curvas modificando las condiciones de ensayo. (a) BTBR (b) MCBTE.

Los resultados obtenidos muestran una clara repetitividad en las *R*-curvas obtenidas mediante BTBR en todos los casos ensayados. Sin embargo, los resultados obtenidos según MCBTE, presentan avances de grieta negativos, lo que induce a cuestionar la validez del este método para determinar las *R*-curvas.

3. CONCLUSIONES

El procedimiento BTBR propuesto resuelve los principales inconvenientes del ensayo ENF, ya que posibilita determinar tanto la longitud de grieta como la R-curva de una forma precisa, permitiendo la correcta caracterización de las propiedades interlaminares en modo II de una manera sencilla.

AGRADECIMIENTOS

Los autores desean agradecer a la Diputación Foral de Guipúzcoa.

REFERENCIAS

REFERENCIAS

CORLETO CR, BRADLEY WL. Mode II delamination fracture toughness of unidirectional graphite/epoxy composites. Composite materials: Fatigue and Fracture, Second 1987

BUENO S, BAUDIN C. Mechanical behaviour of structural ceramics. Boletin de la Sociedad Española de Ceramica. 2007; 46:103-118

BLACKMAN BRK, KINLOCH AJ, PARASCHI M. The determination of the mode II fracture resistance, GIIc, of structural adhesive joints: an effective crack length approach. Engineering Fracture Mechanics 2005; 72: 877-897.

BLACKMAN BRK, BRUNNER AJ, WILLIAMS JG. Mode II fracture testing of composites: a new look at an old problem. Engineering Fracture Mechanics 2006; 73: 2443-2455.

MUJIKA F. On the effect of shear and local deformation in three-point bending tests. Polymer Testing 2007; 26: 869–877

FRIEDRICH K. Fractographic Analysis of Polymer Composites. In: Pipes RB, editor. Application of Fracture Mechanics to Composite Materials. Elsevier. 1989. pp. 425-487.

Influencia del tipo de matriz, en compuestos carbono-epoxi sometidos a deslaminación bajo solicitación a fractura dinámica en modo I

A. Argüelles
Departamento de Construcción e Ingeniería de Fabricación, Universidad de Oviedo, 33204 Gijón
J. Viña
Departamento de Ciencia de los Materiales e Ingeniería Metalúrgica, Universidad de Oviedo, 33204 Gijón
A.F. Canteli
Departamento de Construcción e Ingeniería de Fabricación, Universidad de Oviedo, 33204 Gijón
J. Bonhomme
Departamento de Construcción e Ingeniería de Fabricación, Universidad de Oviedo, 33204 Gijón

RESUMEN

En este trabajo se estudia el comportamiento a fractura en modo I y solicitación dinámica, de dos materiales compuestos, fabricados con el mismo refuerzo unidireccional de carbono y dos tipos de matriz epoxi. Para ambos se ha obtenido bajo solicitación dinámica, el número de ciclos necesarios para comienzo de la deslaminación y la velocidad de crecimiento de grieta, Para diferentes fracciones de $G_{\text{crítica}}$.

De los resultados experimentales obtenidos se deduce, en lo referente a la iniciación de grieta, un comportamiento similar en la zona de fatiga de bajo número de ciclos, mientras que para alto número de ciclos la resina modificada, de comportamiento más tenaz, alcanza un límite de fatiga más alto. Respecto a la velocidad de crecimiento de grieta, bajo solicitación dinámica, se ha observado un comportamiento semejante en ambos materiales, así para pequeñas longitudes de grieta, zona inicial de crecimiento por debajo de 5mm, la velocidad es más elevada que en longitudes superiores.

1. INTRODUCCIÓN

El fallo por deslaminación en materiales compuestos laminados es un problema de gran interés, sobre todo en aquellas aplicaciones en las que el nivel de fiabilidad y seguridad exigida es importante.

La relación entre daño generado, deslaminación y estado de solicitación asociado es un dato relevante en el diseño de elementos fabricados con estos materiales y es la mecánica de fractura la herramienta utilizada para predecir su comportamiento, para lo cual se han desarrollado y se siguen desarrollando estudios que permiten obtener datos útiles para el diseño de piezas en condiciones de servicio real.

Uno de los parámetros relacionados con los procesos de deslaminación es la influencia que tiene la tenacidad de la matriz sobre la tenacidad del material compuesto (Gregory et al. 2003). Ensayos realizados en diferentes materiales ha demostrado que la relación entre la tenacidad de la matriz y la del laminado sigue una relación no lineal, (Hojo et al 2006).

En este trabajo se analiza experimentalmente el comportamiento frente a deslaminación de dos materiales compuestos, fabricados con el mismo refuerzo, fibras unidireccionales de carbono, y dos matrices epoxi diferentes una de ellas de comportamiento tenaz y la otra de comportamiento frágil. Para generar la deslaminación se han sometido a solicitación a fractura en modo I tanto en régimen estático como dinámico.

En solicitación dinámica, para ambos materiales se ha determinado por una parte el número de ciclos necesarios para el comienzo de la deslaminación para diferentes tasas de relajación de energía y por otra la velocidad de crecimiento de grieta para diferentes estados de solicitación.

2. PROCEDIMIENTO EXPERIMENTAL

2.1. Materiales y Probetas

El trabajo experimental se ha realizado sobre dos materiales compuestos fabricados a con el mismo refuerzo unidireccional de carbono tipo AS4, empleando una resina epoxi modificada del tipo 8552 y otra también epoxi 3501-6, sin modificar.

Para la caracterización de la deslaminación, en modos I, para ambos materiales se ha utilizado el mismo tipo de probeta DCB conforme a la norma ASTM D 5528-01 Las probetas, son rectangulares, de espesor y anchura uniforme, formadas por un número par de láminas unidireccionales (16/p.m./16), con un inserto no-adhesivo en su plano medio. Todos los ensayos, tanto estáticos como dinámicos se han realizado en una máquina servohidráulica, para la sujeción de la probeta a la máquina de ensayo se han empleado bisagras pegadas a la probeta.

2.2 Tenacidad a fractura estática

Para la determinación de la tenacidad a fractura de ambos materiales en régimen estático y modo I de fractura se ha empleado la norma ASTM D5528 Los datos obtenidos han sido utilizados para definir el nivel de solicitación en régimen dinámico.

2.3. Caracterización a fatiga

Los ensayos de fatiga realizados han tenido por objeto determinar, para ambos materiales:

1. El número de ciclos de carga necesarios para la iniciación de una grieta en el material, (determinación de curvas de fatiga $G_{máx}/G_{cri}$ - N, número de ciclos necesarios para comienzo de la deslaminación dada una determinada tasa de relajación de energía). Estos ensayos se han realizado aplicando la norma ASTM D 6115. Los ensayos se han realizado sometido a fatigada cíclica la probeta controlando, en la máquina de ensayos, el desplazamiento aplicado a los labios de la misma entre un mínimo y un máximo ($\delta_{mín.}$ y $\delta_{máx.}$). Estos valores se han ajustado para cada uno de los ensayos partiendo de los datos obtenidos de la caracterización estática del material, definiendo el desplazamiento máximo como un tanto por ciento del desplazamiento crítico obtenido de esta caracterización estática y calculando el desplazamiento mínimo como el $\delta_{máx.}$ x R [R=0.2]. Considerando que en régimen elástico lineal y para pequeñas desviaciones ($\delta/a<0.4$), la relación entre desplazamientos y cargas es proporcional. Se ha considerado iniciada la grieta cuando se ha observado visualmente mediante un microscopio móvil 100x, situado en una de las caras laterales de la probeta.
2. La velocidad de crecimiento de grieta para diferentes fracciones de $G_{crítica}$, como en el caso anterior para su realización se han empleado probetas sometidas a fatiga en una máquina dinámica de ensayos controlando la abertura de los labios de la probeta,

ajustando las cargas y desplazamientos a partir de los datos obtenidos de la caracterización estática del material, en su fase de crecimiento de grieta.
En ambos casos el método de cálculo empleado ha sido el de la teoría de vigas modificada [MBT].

3. RESULTADOS EXPERIMENTALES

Seguidamente se presentan los resultados experimentales obtenidos en el estudio del comportamiento a fatiga de ambos materiales.

3.1. Iniciación de la deslaminación

En la figura 1 se ha representado la energía de fractura normalizada frente al número de ciclos necesarios para la generación de una grieta por fatiga, que representan las curvas de caracterización a fatiga del material en su fase de iniciación de grieta, para los dos materiales ensayados. Los límites de fatiga obtenidos para cada uno de los materiales son, para el AS4/8552 y el AS4/3501-6 respectivamente del 50% y 30 % de la energía crítica de fractura obtenida en la caracterización estática, que corresponden con unas energías de deslaminación de 151.1J/m^2 y 26.58 J/m^2, para cada uno de ellos. Todos los cálculos se han realizado mediante la teoría de vigas modificada [MBT]. En ambos casos se ha considerado 3 millones de ciclos como límite de fatiga.

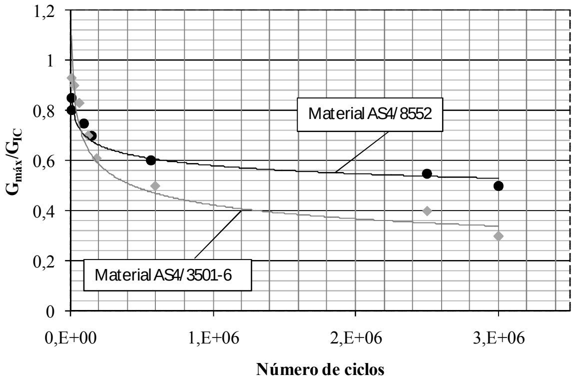

Fig. 1. Curvas de iniciación a fatiga.

3.2. Velocidad de crecimiento de la deslaminación

En la figura 2 se ha representado la velocidad de crecimiento de grieta en función de la longitud de grieta para los dos materiales ensayados, para un nivel de solicitación del 75% de la energía crítica de fractura obtenida en la caracterización estática.

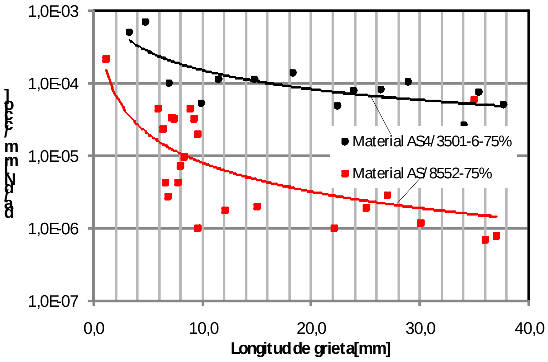

Fig. 2. Curvas de velocidad de propagación.

Para este nivel de solicitación y para ambos materiales la velocidad de crecimiento disminuye a medida que aumenta la longitud de grieta, pese a mantenerse durante todo el proceso del crecimiento de grieta la energía de fractura prácticamente constante, este fenómeno es más acusado en la resina modificada 8552, con velocidades de crecimiento medias del orden de: 2.681x10-5mm/ciclo. Para la resina sin modificar del tipo: 3501-6 la velocidad de crecimiento es más uniforme con velocidad de crecimiento medias de 1.526x10-4 mm/ciclo.

3. CONCLUSIONES

Las curvas de fatiga obtenidas en la fase de iniciación indican el mejor comportamiento global de la resina modificada 8552 más acusado en la fase de alto número de ciclos.

Respecto al crecimiento de grieta, la velocidad de crecimiento de grieta se ralentiza para grandes longitudes de grieta, llegando a detener su progresión, si no se aumenta la energía crítica de fractura por encima de los valores equivalentes obtenidos en la caracterización estática del material en su fase de crecimiento. Esto puede ser debido al aumento, en solicitación dinámica, de la flexibilidad de los labios de la probeta que absorbe parte de la solicitación aplicada al frente de entalla y la generación de puentes de fibra.

A medida que aumenta el rango de tensión la tendencia de la velocidad de crecimiento de grieta es a disminuir, para ambos materiales, aunque más acusado en el caso de la resina más tenaz 8552.

AGRADECIMIENTOS

Los autores agradecen la financiación recibida de CICYT a través del proyecto de investigación MAT2007-60696

REFERENCIAS

[1] GREGORY J. R., SPEARING S.M. (2003). Delamination initiation predictions from constituent behaviour. In: 14th International conference on composite materials, San Diego; CA, 14-18,

[13]. HOJO M., MATSUDA S., TANAKA M., OCHIAI S., MURAKAMI A. (2006). Mode I delamination fatigue properties of interlayer-toughened CF/epoxy laminates Composites Science and Technology 66, 665-675.

[10] ASTM D 5528-01 Modo I Interlaminar fracture toughness of unidirectional fiber-reinforced polymer matrix composites

[12] ASTM D 6115-97 Mode I fatigue delamination growth onset of unidirectional fiber-reinforced polymer matrix composites.

Failure analysis of impacted hybrid laminate composites using X ray tomography

A. Enfedaque[1], F. Gálvez[1], C. Gónzalez[1, 2], J. Molina[2], G. Charalambous[2], J. Llorca[1, 2]

[1] Departamento de Ciencia de Materiales, Universidad Politécnica de Madrid, E. T. S. de Ingenieros de Caminos, 28040 Madrid, Spain.

[2] Instituto Madrileño de Estudios Avanzados de Materiales (IMDEA-materiales), C/ Profesor Aranguren s/n, 28040 Madrid, Spain

ABSTRACT

Since 1980 the behavior of composite laminates subjected to low velocity and low energy impacts have been characterized. The dynamic response of carbon fiber laminates and glass fibers laminates have been tested many times before, but on the other hand hybrid laminates made up by carbon fiber layers and glass fiber layers have not been thoroughly studied.

Low velocity impact tests have been carried out in carbon fiber laminates and hybrid laminates of similar thickness using a drop weight testing machine. Impact energies close to the perforation limit were used in the tests, both in carbon and hybrid laminates. Behavior of carbon and hybrid laminates has been compared. A non destructive analysis of the tested samples have been carried out using X ray tomography that enables to relate the behavior differences with the failure mechanisms of the laminates. In this tests hybrid laminates have shown a greater capacity of absorbing energy than carbon laminates. These tendencies were confirmed for all thickness studied. However, failure mechanisms were different in hybrid and carbon laminates. In hybrid composites, damage was concentrated in carbon layers. In these areas a clear delamination can be seen while in glass fiber layers a greater strain can be observed.

1. INTRODUCTION

The response of composite materials subjected to impact loading has a growing interest in the last decades. The response of carbon fiber composites has been extensively studied by many authors (Abrate, S.1998, Abrate, S. 1991, Abrate, S. 1994, Cantwell et al. 1991). Also, great advances have been achieved in the understanding in deformation and failure mechanisms of glass fibers laminates during an impact event (Richardson et al. 1996).

However, there are only a few studies dealing with the impact response of hybrid laminates. Some work has been carried out (Hosur et al. 2005) and showed that hybrid laminates have a greater load carrying capacity than carbon /epoxi ones. While these investigations were performed in woven laminates, hardly any study has been carried out in non woven hybrid laminates.

Also there are few works dealing failure mechanisms of hybrid laminates. Non destructive testing (NDT) techniques such as X ray tomography are capable of studying failure mechanisms without damaging the samples.

2. TEST PROGRAMME

Tests were carried out using an 8250 Dynatup drop weight impact testing machine. This machine is equipped with a 15.8 mm diameter cylindrical impactor ended in a hemispherical tip. The impactor is rigidly attached to the drop weight that is used in the tests. A data acquisition system is connected to the impactor and all data is registered in a computer. Load, velocity and displacement of the loading point are recorded continuously during the test. The initial impact energy can be selected bye using different weights dropped from different heights. An image of the testing machine used and a detailed image of the drop weight and the impactor used can be seen in figure 1

Fig. 1. Drop weight impact test machine. Drop weight and impactor.

Samples were placed using a special device designed for these tests that left an open space of 127 mm between the samples sides. The corners of the samples were fixed using a system that can be seen in figure 2 and that avoided vibrations of the sample during the impact event.

Fig. 2. Fixation device. Sample fixed to the device.

To compare failure mechanisms between carbon composites and hybrid composites it was decided not to achieve a full penetration of the samples. Weights of 22.43 kg and 11.81 kg were chosen to perform the tests; with higher weights, samples were full penetrated and with lower weights hardly any damage was done.

Tested samples were performed in 145x145 mm^2 carbon and hybrid laminates. Samples were impacted in the geometric center of their area. Two different thicknesses were chosen. Although thicknesses of hybrid and carbon samples were not equal, they had variations of less than 3% in the thicker samples and around 5% in the thinner samples. Due to these slight variations, results obtained in the impact tests can be directly compared. In figure 3 results of the tests can be seen for both thin and thick samples.

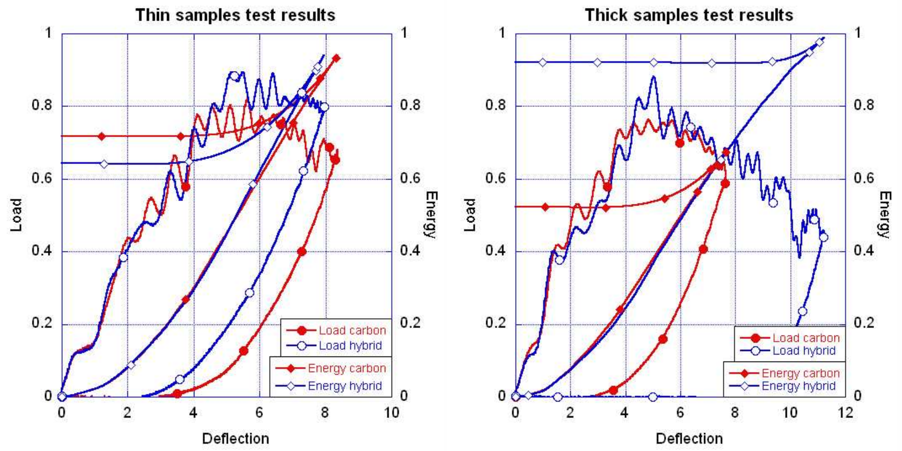

Fig. 3. Test results for thick and thin carbon and hybrid composites. Load, displacement and energy in adimensional units.

Test results showed that hybrid composites bear higher loads than carbon composites. However, the energy that the laminate absorbs depends mainly in the deformation capacity of the material. Due to this, composites capable of reaching higher deflection during the tests absorb more energy than stiffer laminates.

Thin carbon and hybrid laminates were both partially penetrated in the tests. Thick samples of hybrid laminates were almost completely penetrated while thick carbon fibre samples were only partially penetrated.

3. FAILURE MECHANISMS ANALYSIS

The different mechanical behavior of the composites registered in the tests was related to the failure mechanisms of laminates using X ray tomography (Phoenix Nanotom). The reconstruction performed using this system is a non destructive technique that is capable of making a full 3D image of the tested sample without damaging the sample during the inspection. The area reconstructed was limited to the central part of the laminates. The area studied was chosen according to the damaged areas that were noticeable during an ocular inspection. When a full reconstruction of the samples was carried out it was clear that no damaged area had been missed. In figure 4 some images of a hybrid sample can be seen.

In these images carbon layers appear as grey areas while glass fiber layers appear as white zones. The damaged area forms a cone that begins with the indentation damage in the upper layers and ends with the fiber breakage of the bottom layers. Glass fiber layers have higher strains due to its lower elasticity modulus and these higher strains distribute loads and introduce deformations in the carbon fiber layers beneath them. Damage in hybrid laminates is distributed in larger areas and due to this, hybrid laminates have a greater energy absorption capacity than carbon fiber laminates.

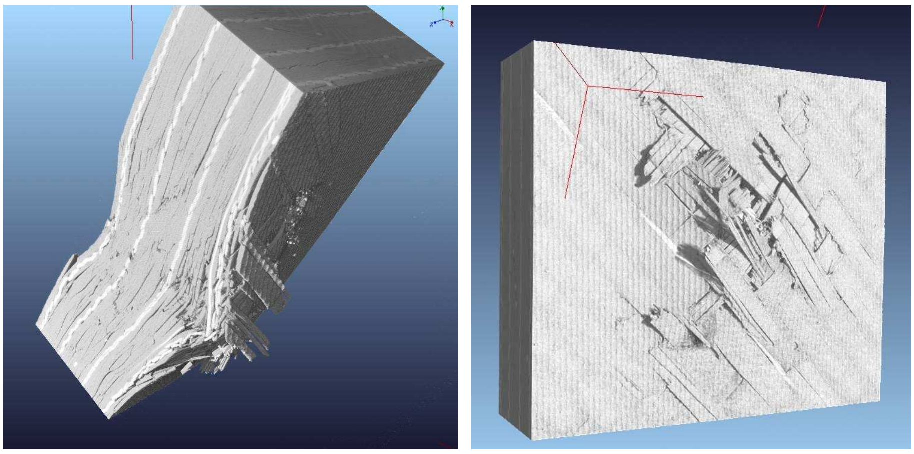

Fig. 4. Tomograph images of an hybrid sample.

4. CONCLUSIONS

Low velocity impact tests have shown that hybrid composites have a greater energy absorption capacity than carbon fiber laminates.

A complete reconstruction of tested samples has been performed using an X ray tomography system.

Reconstructed 3D images of tested samples showed that hybrid laminates have damaged areas larger than carbon fiber laminates. These differences in the damaged areas and in failure mechanisms are in good agreement with the results obtained in the impact tests .

REFERENCES

ABRATE, S. (1998) Impact on composite structures, Cambridge University Press, Cambridge.
ABRATE, S. (1991) Impact on laminated composite materials, *Appl Mech Rev* **44**, pp. 155–190.
ABRATE, S. (1994) Impact on laminated composites: recent advances, *Appl Mech Rev* **47**, pp. 517–544
CANTWELL, W.J. and MORTON, J. (1991). The impact resistance of composite materials – a review, *Composites* **22**, pp. 347–362
HOSUR, M.V., ADBULLAH, M, and JEELANI, S. (2005). Studies on the low velocity impact response of woven hybrid laminates
RICHARDSON, M.O.W. AND WISHEART, M.J.(1996) Review of low-velocity impact properties of composite materials, *Compos Part A* **27A** , pp. 1123–1131.

Caracterización de residuos del cepillado de piassava (*Attalea funifera Mart*) y evaluación del potencial para asociación con polietileno de alta densidad

S.P. Agrela
Universidad Federal de Bahia, Instituto de Química, Grupo de Energía e Ciencias dos Materiales, GECIM.
J.R. Cerchiaro
Universidad Federal de Bahia, Escuela Politécnica, Grupo de Investigación en Ingeniaría Ambiental Urbana.
N.M. José
Universidad Federal de Bahia, Instituto de Química, Grupo de Energía e Ciencias dos Materiales.
R.F. Carvalho
Universidad Federal de Bahia, Escuela Politécnica, Grupo de Investigación en Ingeniaría Ambiental Urbana. Rua Prof. Aristides Novis, 2. Federação , Salvador, Bahia, Brasil. ricardoc@ufba.br

RESUMEN

El empleo de recursos renovables en la preparación de nuevos materiales debe considerar los aspectos económicos, tales como la disponibilidad, posibles de usos y las consecuencias financieras. El estado de Bahía es el más grande productor de fibra piassava (*Attalea funifera Mart*) de Brasil. Podrían surgir nuevas aplicaciones con valor agregado agregado como un resultado del estudio de las propiedades físicas y mecánicas de fibras y residuo. En este trabajo, las fibras de piassava y el residuo fueron lavados y secos en vacuo durante 48 horas, luego, analizados por termogravimetría de barrido y microscopia electrónica de barrido. Los resultados mostraron que las fibras de piassava y el residuo tienen propiedades físicas similares, lo que sugiere que el residuo de piassava también pueden utilizarse como refuerzo de los materiales compuestos.

1. INTRODUCCIÓN

La Asamblea General de las Naciones Unidas declarar el año 2009 como el año internacional de las fibras naturales (Naciones Unidas, 2006). Además de ser un material sostenible fibras naturales alternativas son técnicamente factibles y ofrecen muchas connotaciones sociales positivas. En los últimos años ha habido un aumento en el uso de las hojas, frutas y fibras de la Palmera de Piassava.

En Brasil, existen tres especies de palmeras de piassava; la *Leopoldinia Piassaba* y *Natalia Aphandra* nativas de la Amazonía occidental y la *Funifera Attalea Mart* que proviene de la Mata Atlántica. Las fibras de la *Attalea funifera Mart* pueden llegar a 5 m de longitud, aproximadamente de 1 mm de diámetro, y son resistente al agua (Aquino, D´Almeida Monteiro, 2001, Voecks y Vinha, 1988). Las fibras de la palmera de piassava se han descripto como de más difícil procesamiento que otras fibras naturales.

Las palmeras de piassava son económicamente valiosas. El cultivo de piassava ocupa aproximadamente 2000 pequeños agricultores incuyendo beneficiadores y sus respectivas familias. Esto representa una parte importante de la economía regional tanto en la exportación como en la fabricación de escobas y cepillos. Desde os años 60, las exportaciones de fibra de piassava habían caído notablemente como resultado de la competencia con fibras y cuerdas sintéticas. Actualmente, se utilizan como rellenos de asiento y como refuerzo en matrices poliméricas. Residuos de cepillado de fibras, conocidos como la bucha, se utilizan como cubertura de pisos y aislamiento térmico industrial. En el presente 10.000 toneladas de esta materia prima se extraen anualmente la Mata Atlántica brasileña.

La investigación en *Attalea funifera Mart* como refuerzo de matrices de polímero es todavía poco común. Recientemente, cientistas brasileños han estado investigando las fibras de piassava como un posible refuerzo de compuestos poliméricos (Aquino, Monteiro, D´Almeida, 2003). Guimarães (1987) investigó el comportamiento mecánico de fibras piassava y de la bucha para reforzar compuestos de base de cemento. Este presente trabajo compara el comportamiento físico de fibras piassava y de la bucha.

2. FIBRAS DE RESÍDUOS DE PIASSAVA

Para una mejor comprensión es necesario definir y confirmar los términos utilizados para describir los materiales constantes en este trabajo. Las fibras individuales contienen células de esclerénquima que proporcionan apoyo mecánico a las plantas y a sus partes como hojas y tallo. Fibras técnicas, o fibras textiles, son paquetes de fibras individuales con propiedades mecánicas que dependen del origen de la planta, la naturaleza de la extracción, procedimientos extractivos, edad y componentes químicos (Vincent, 2000). Las fibras técnicas de piassava, que se muestra en la figura 1a y bucha, que se muestra en la figura 1b, se obtuvieron en una fábrica de escobas situada al sur del Estado da Bahia, Brasil.

a b

Figura 1. a) Fibras de piassava, b) Bucha de piassava.

En primer lugar, las fibras fueron lavadas y luego secadas al vacío durante 48 horas a fin de eliminar las impurezas y la humedad. Se calculó tanto la densidad de las fibras piassava como de la bucha, por medio de un picnómetro, en ambas se obtuvo 1,10 g/ml.

3. RESULTADOS Y DISCUSIÓN

El análisis por termogravimetria se usa comúnmente para estudiar el comportamiento térmico y las condiciones de procesamiento de piezas de polímeros. Los resultados de análisis TGA y DTG de la bucha se muestran en la figura 2a. La Descomposición de hemicelulosa puede observarse en la banda situada entre 320-260°C, y a 301°C se produjo un pico de degradación. La descomposición de la celulosa se situó entre 320-400 °C.

La masa residual de las fibras fue de un 31%, y de la bucha fue de un 26%. Se verificaron resultados similares de análisis termogravimetrica de fibras de piassava efectuados por Bonelli, et.alli (2005) y Aquino, Monteiro y D´Almeida (2006).

El resultado de Calorimetría diferencial de barrido también demostró degradación de la celulosa, como visto en la figura 2b, con un pico endotermico en 363ºC, que confirma resultados obtenidos por TGA.

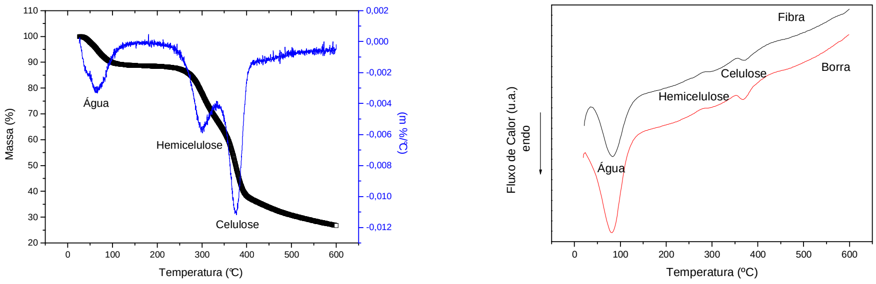

2ª 2b

Figura 2. a) TGA y b) DSC del bucha.

La morfología transversal de la bucha se muestra en figura 3. En la mayor ampliación de la imagen se comprueba que la composición celular del residuo es similar al de las fibras técnicas.

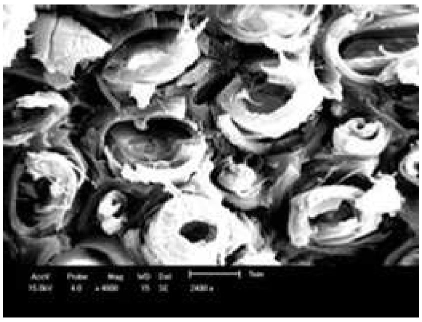

Figura 3. Microscopía electrónica de barrido en la bucha, 1200x.

4. Compuestos de PEAD y bucha de piassava

Los compuestos de residuo de piassava con polietileno de alta densidad (PEAD) fueran preparados con un 5% de la bucha en volumen y seccionados con 5mm de longitud. Las chapas de los compuestos fueran fabricadas en molde de acero con 150x150mm de longitud. Los ensayos de impacto fueran hecho en 6 probetas conforme la norma ASTM D256. Fue utilizado un equipo de entalle CEAST para obtener un entalle con 10,16mm de profundidad con un ángulo de 45º y la energía del impacto ha sido de 2.0 J. Los resultados son: PEAD puro 52,5 J/m y el incremento de un 5% de bucha en la matriz de PEAD amplió la tenacidad para 69,5 J/m.

5. CONCLUSIONES

La caracterización física por comportamiento térmico, densidad y arreglo morfológico, dos residuos de la industria de piasava demonstrar que estos tiene propiedades similares a las fibras técnicas y, como estas, son una alternativa importante en el refuerzo de termoplástico. Además, el residuo de piassava son de más fácil moldeo en procesos como inyección y extrusión.

Los resultados de los ensayos Izod con un 5% de bucha también indican una posibilidad concreta do uso de estos residuos como refuerzo estructural y no apenas como carga para henchimiento.

AGRADECIMIENTOS

Los autores desean agradecer la CAPES, CNPq y FAPESB por apoyo financiero en la investigación.

REFERENCIAS

AQUINO, R.C.M.P., D´ALMEIDA, J.R.M., MONTEIRO, S.N., (2001) "Flexural Mechanical Properties of Piassava Fibres (Attalea funifera)-Resin Matrix Composites. Journal of Materials Science Letters, v.20, p.1017-1019.

AQUINO, R.C.M.P., MONTEIRO, S.N., D´ALMEIDA, J.R.M., (2003). "Evaluation of the Critical Fibre Length of Piassava (Attalea funifera) Fibres using the Pullout Test". Journal of Materials Science Letters, v. 22, p. 1495-1497.

D´ALMEIDA, J.R.M.; AQUINO, R.C.M.P., MONTEIRO, S.N. (2006). Tensile mechanical properties, morphological aspects and chemical characterization of piassava (Attalea funifera) fibres. Composites: Part A, v.37, p.1473–1479.

GUIMARÃES, S.S. (1987). I Curso de Tecnologia do Concreto Estrutural. Escola Politécnica - UFBa. Salvador. In Portuguese.

UNITED NATIONS (2006). International Year of Natural Fibres, 2009. Resolution 189 session 61, on 20 December 2006. Available in http://www.unesco.at/pdf/res_natural_fibres.pdf

VINCENT, J.F.V. (2000). A unified Nomenclature for Plant Fibres for Industrial Use. Applied Composite Materials 7: 269–271.

VOECKS R.A.; VINHA S.G. (1988)Fire Management of the Piassava Fibre Palm (Attalea funifera) in Eastern Brazil. Conference of Latin Americanist Geographers, in Yearbook1988, pp. 7-13. Available in http://sites.maxwell.syr.edu/clag/yearbook1988/voecks.pdf

Determinación experimental de la resistencia a cortadura interlaminar por medio del ensayo de tracción *off-axis* y de flexión *off-axis*

G. Vargas, A. Arrese, N. Carbajal, F. Mujika
Grupo 'Materiales + Tecnologías', Departamento Ingeniería Mecánica, Escuela Politécnica. Universidad del País Vasco/Euskal Herriko Unibertsitatea

RESUMEN

El objetivo de este trabajo es comparar, desde el punto de vista teórico y experimental, dos métodos de ensayo para la determinación de la resistencia a cortadura en el plano de laminados unidireccionales: tracción *off-axis* y flexión *off-axis* a tres puntos. Se presentan algunos aspectos relacionados con los campos de tensiones y de desplazamientos, así como las condiciones para el uso de los métodos propuestos.

1. INTRODUCCIÓN

En una serie de artículos anteriores sobre la determinación de las propiedades a cortadura en el plano mediante ensayos *off-axis*, Mujika et al. (2005) estudiaron nuevas consideraciones relacionadas con los campos de tensiones y de desplazamientos para ambos ensayos. En dichos artículos, y en trabajos de otros autores, la determinación del módulo a cortadura interlaminar G_{LT} mediante ensayos *off-axis* ha sido demostrada y contrastada. En particular, Mujika et al. (2005) han presentado los métodos para medir G_{LT} mediante ensayos *off-axis* de flexión a tres puntos, y han demostrado experimentalmente su validez. Sin embargo, para el caso de la resistencia a cortadura interlaminar, X_{LT}, los trabajos de Mujika et al. (2005) aún no han sido demostrados de modo experimental. Así, los objetivos de este trabajo son comparar experimentalmente los ensayos *off-axis* de tracción y de flexión a tres puntos para la determinación de X_{LT}, y considerar varios criterios de fallo para el estudio de los modos de fallo.

2. MODELO ANALÍTICO

2.1 Ensayo de tracción *off-axis*

Para la determinación de la resistencia a cortadura interlaminar por medio del ensayo de tracción *off-axis,* se ha planteado un método analítico para el campo de tensiones basado en el 2º Teorema de Castigliano, considerando dos enfoques: un campo de tensiones simple que satisface las condiciones de equilibrio, y las constantes de integración del campo de tensiones en el modelo de Pagano y Halpin (1968). El procedimiento analítico para el cálculo de X_{LT} es el siguiente:

- Calcular los coeficientes de flexibilidad, S_{ij}, en los ejes del laminado ($i, j = x, y, s$).
- Calcular el coeficiente de acoplamiento, η, en función de los coeficientes de flexibilidad en los ejes del laminado, según la Eq. 1.
- Calcular la relación ente la fuerza de cortadura y la fuerza aplicada, k_1, en función de los coeficientes de flexibilidad en los ejes del laminado y de la relación longitud / ancho, $c = L/b$, según la Eq. 2.

- Determinar el punto de fallo *F'* después del ensayo, en el borde de la probeta, y cálculo de la coordinada normalizada de dicho punto $(x_{0F'}, y_{0F'}) = (x_{F'}/L, y_{F'}/b) = (x_{0F'}, -½)$, como se presenta en la Fig. 1a, donde $0 < x_{0F'} < ½$.
- Calcular la resistencia a cortadura en el plano, X_{LT}, a partir de la carga de fallo aplicada, P_f, y de la sección transversal de la probeta, *S*, y en función del ángulo de orientación de fibra, θ, según la Eq. 3.

$$\eta = \frac{S_{xs}}{S_{xx}} \tag{1}$$

$$k_1 = -\frac{S_{xs}}{S_{xx}c^2 + \frac{6}{5}S_{ss}} \tag{2}$$

$$X_{LT} = \frac{P_f}{2S} Sin\, 2\theta \left[1 + k_1(3c + 2\eta) - 6k_1 c\, x_{0F'}\right] \tag{3}$$

2.2 Ensayo de flexión *off-axis*

Para la determinación de la resistencia a cortadura interlaminar mediante el ensayo de flexión *off-axis* a tres puntos, se deben garantizar pequeños desplazamientos y se debe asegurar que ocurre un despegue (*lift-off*) entre la probeta y los soportes del útil de ensayo. Esta condición de despegue depende del valor crítico de la relación distancia entre apoyos / ancho de probeta, c_{LO}, que a su vez es función de los coeficientes de flexibilidad en los ejes del laminado, S_{ij}, y de la relación ancho / longitud total de la probeta, *b/L'*, y que se calcula según la Eq. 4.

$$c_{LO} = -\left(\frac{S_{ss}}{S_{xs}} + \frac{S_{ys}}{S_{xs}}\frac{b}{L'}\right) \tag{4}$$

Para calcular la resistencia a cortadura en el plano se deben seguir los siguientes pasos:

- Calcular la relación distancia entre apoyos / ancho, $c = L/b$, y de la relación distancia entre apoyos / longitud total de la probeta, $g = L/L'$.
- Determinar el punto de fallo *K'* después del ensayo, en la línea media transversal de la probeta (ver Fig. 1b), y cálculo de la coordinada normalizada de dicho punto $(x_{0F'}, y_{0F'}) = (x_{F'}/L, y_{F'}/b) = (½, y_{0F'})$, donde $y_{0F'} > 0$.
- Calcular X_{LT} en función de la carga de fallo aplicada, P_f, el espesor de la probeta, *h*, y el ángulo de orientación de fibra, θ, según la Eq. 5.

$$X_{LT} = \frac{3P_f}{4h^2}\left(-c\, Sin\, 2\theta + \frac{2g}{c} y_{0K'}\, Sin\, 2\theta + Cos\, 2\theta\right) \tag{5}$$

2.3 Criterios de fallo

Para estudiar los modos de fallo asociados a las probetas durante los ensayos *off-axis*, se han considerado los siguientes tres criterios de fallo para materiales compuestos: criterio de la deformación máxima, criterio de Hashin-Rotem, y criterio de Tsai-Wu.

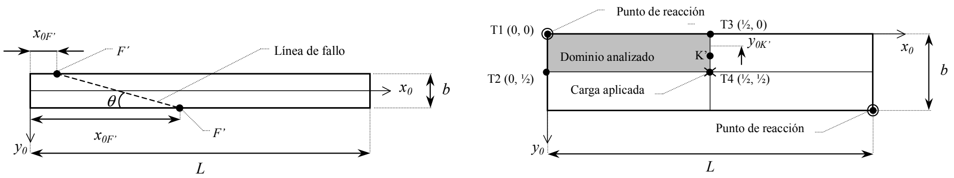

(a) (b)

Fig. 1. Parámetros geométricos de los ensayos *off-axis* y localización del punto de fallo. (a) Ensayo de tracción y punto *F'*, (b) Ensayo de flexión y punto *K'*.

3. EXPERIMENTAL

Se determinó experimentalmente la resistencia a cortadura en el plano de un laminado unidireccional de composite de resina epoxy reforzada con fibra de carbono, AS4/8552, proporcionado por la empresa Hexcel Composites. Los ensayos se han efectuado considerando varios ángulos de orientación de fibra: 10º, 20º, 30º y 45º, y variando los parámetros geométricos, como se presenta en la Tabla 1. Los ensayos de tracción *off-axis* se han llevado a cabo a una velocidad de aplicación de carga de 1 mm/ min y mordazas convencionales con papel de lija a lo largo de toda el área de sujeción. Para el ensayo de flexión *off-axis* a tres puntos las probetas se han sometido a una deformación del 1%/min y se ha empleado un sistema convencional de apoyos.

θ	Ensayo de tracción *off-axis*			Ensayo de flexión *off-axis*			
	L' (mm)	L (mm)	c	L' (mm)	L (mm)	c	c_{LO}
10º	275	175	14	90	80	6.5	6.34
20º	275	175	14	70	60	4.6	3.19
30º	250	150	12	60	50	3.8	2.25
45º	200	100	8	50	40	3.1	2.20

Tabla 1. Parámetros geométricos de los ensayos *off-axis*.

4. RESULTADOS

En la Fig. 2 se presenta la variación de las tensiones de cortadura en el plano en los puntos críticos, según el ángulo de orientación de fibra. Asimismo, se comparan dichas tensiones con el valor de resistencia a cortadura en el plano dado por el fabricante ($X_{LT\text{-}45^o}$ = 94 MPa), obtenido por el ensayo de tracción ±45º. La comparativa de las teorías de fallo para la determinación de X_{LT} se presenta en la Fig. 3. Los resultados revelan que para determinar la resistencia a cortadura en el plano es más adecuado el ensayo de flexión *off-axis* que el ensayo de tracción *off-axis*, ya que es más simple, considera la deformación de toda la probeta y supone que el fallo se inicia en un punto determinado.

Las condiciones para determinar X_{LT} mediante los métodos descritos son las siguientes:

- Bajos ángulos de orientación de fibra (e.g. θ = 10º - 20º) para obtener grandes tensiones de cortadura en el plano y bajas tensiones normales transversales

- Cálculo de la resistencia a cortadura interlaminar a partir de un criterio de fallo que considere la interacción entre las componentes de tensión (e.g. Tsai-Wu).
- Tracción *off-axis*: grandes relaciones longitud / ancho (e.g. $c > 8$) con el fin de reducir los efectos de restricción en los extremos; no es necesario el uso de sistemas de sujeción especiales, es suficiente con una superficie de sujeción con un alto coeficiente de fricción (e.g. con papel de lija).
- Flexión *off-axis*: relaciones longitud / ancho mayores que el valor crítico para asegurar el despegue ($c > c_{LO}$).

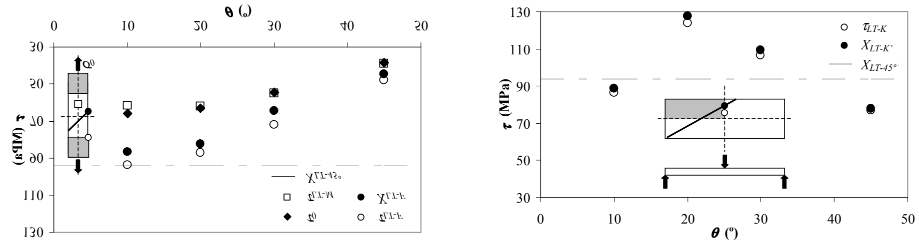

(a) (b)

Fig. 2. Variación de las tensones de cortadura en el plano con el ángulo de orientación de fibra. (a) Ensayo de tracción, (b) Ensayo de flexión.

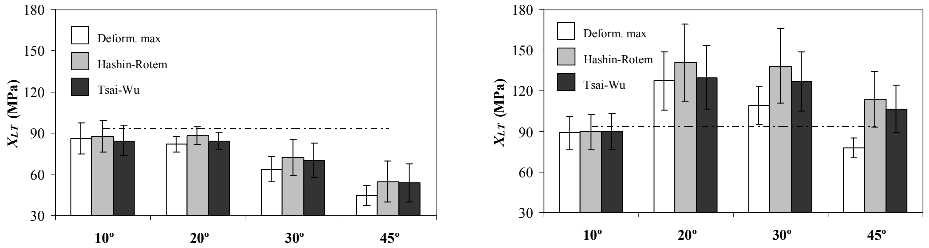

(a) (b)

Fig. 3. Comparativa de las teorías de fallo para la determinación de la resistencia a cortadura en el plano. (a) Ensayo de tracción, (b) Ensayo de flexión.

5. CONCLUSIONES

Se presenta una comparación experimental entre los ensayos de tracción *off-axis* y de flexión *off-axis* a tres puntos, para determinar la resistencia a cortadura en el plano de composites unidireccionales. Se resaltan sus ventajas e inconvenientes, y las condiciones de ensayo que garanticen la aplicabilidad de los dos métodos en cuestión.

REFERENCIAS

MUJIKA, F. (2005). New considerations on the stress field in an off-axis tensile test. *J. Comp. Mat.*, 39, 1909-1929.

MUJIKA, F., VALEA, A., GAÑÁN, P., MONDRAGON, I. (2005). Off-axis flexure test: a new method for obtaining in-plane shear properties. *J. Comp. Mat.*, 39, 953-980.

PAGANO, N.J., HALPIN, J.C. (1968). Influence of end constraint in the testing of anisotropic bodies. *J. Comp. Mat.*, 2, 18-31.

Propiedades mecánicas del ABS y sus nanocompuestos

F.C. Basurto [1], D. García-López [2], N. Villarreal-Bastardo [2], J.C. Merino [1,2], J.M. Pastor [1,2]
[1]Departamento de Física de la Materia Condensada, Cristalografía y Mineralogía, ETS de Ingenieros Industriales. Universidad de Valladolid. España
[2]Fundación CIDAUT – Centro de Investigación y Desarrollo en Transporte y Energía. Valladolid, España

RESUMEN

Mediante mezclado en fundido se han obtenido una serie de materiales nanocompuestos basados en acrilonitrilo-butadieno-estireno (ABS), un agente compatibilizante basado en ABS con injertos de anhídrido maleico (ABS-g-MAH) y una nanoarcilla fibrosa como la sepiolita. Se ha estudiado la influencia de los refuerzos nanofibrosos en las propiedades mecánicas del ABS. Para ello se han realizado ensayos termomecánicos sobre probetas estándar, midiéndose el módulo de Young, temperatura de deflexión bajo carga (HDT) e impacto Izod, y ensayos de termogravimetría (TGA) para conocer el porcentaje de carga añadida al nanocompuesto.

1. INTRODUCCIÓN

El uso de arcillas laminares para la obtención de nanocompuestos con propiedades mejoradas ha sido ampliamente estudiado en los últimos años. Los materiales minerales más utilizados han sido las montmorillonitas (MMT), que son silicatos pertenecientes a la familia de las esméctitas, con estructura laminar.

Sin embargo, existe otro tipo de minerales que no han sido tan ampliamente utilizados y que también aportan mejoras en las propiedades de las matrices. La sepiolita tiene una estructura similar a la MMT, pero presenta una diferencia fundamental respecto a la organización de las capas, ya que éstas se presentan en forma de estructuras fibrilares, con canales en su interior en la dirección de las fibras, donde se alojan moléculas de agua (Xie et al, 2007; Ruíz-Hitzky, 2001). Esta característica hace que la sepiolita tenga una alta área superficial y presente buenas propiedades de absorción, catalíticas y reológicas (Lemic et al. 2005).

Normalmente las nanoarcillas son tratadas con diferentes tipos de agentes modificantes para convertirlas en organofílicas y hacerlas más compatibles con las matrices poliméricas. Actualmente, existen dos métodos para ello: utilizando sales de amonio cuaternarias o silanos (Tartaglione et al. 2008). El primero de ellos consiste en una reacción de intercambio catiónico, a través de la cual tiene lugar la sustitución de los cationes inorgánicos hidratados situados entre las láminas de la nanoarcilla por cationes orgánicos. Por otra parte, el segundo método se basa en modificar la superficie de las nanoarcillas mediante un proceso de absorción de agentes tipo silanos con los grupos silanoles presente en la superficie de las nanoarcillas. En el presente trabajo se han seleccionado dos sales de amonio cuaternarias para modificar la sepiolita.

El ABS es un polímero de tipo ingenieril, ampliamente utilizado en la industria, debido a sus propiedades mecánicas, facilidad de procesado y resistencia química (Ma et al. 2006). Comercialmente, existen algunos productos modificados químicamente con MAH (Anhídrido Maleico) que, según varios autores, se injerta en las cadenas de butadieno (Qi et al. 2000). Esto hace que dichos materiales sean utilizados en diversas aplicaciones dentro del sector de automoción.

2. EXPERIMENTAL

2.1 Materiales

En este trabajo se han seleccionado dos grados de ABS distintos, que difieren en el contenido en butadieno (B), por un lado el ABS HI-100 (mayor contenido en B) suministrado por LG Chem. y por otro el ABS G-360 (menor contenido), suministrado por GE Plastic. Las nanoarcillas seleccionadas han sido basadas en una sepiolita estándar (Pangel HV) proporcionada por Tolsa S.A. que se han modificado con dos sales de amonio: el bencil metil 2 tallow hidrogenado (BM2TH) y trimetil tallow hidrogenado (3MTH). El material compatibilizante escogido ha sido un ABS injertado con MAH denominado B-6000 y suministrado por Polyram L. P, con un grado de funcionalización determinado por FTIR-ATR de aproximadamente 0.8 %.

2.2 Obtención de nanocompuestos

Los materiales nanocompuestos se han obtenido utilizando una extrusora doble husillo corrotante marca Leistritz 27 GL. La temperatura de extrusión ha sido de 230º C, con una velocidad de husillo de 200 rpm. Se han obtenido nanocompuestos con un 5 % y 10 % de sepiolita. El compatibilizante se ha añadido en un porcentaje del 10 %, y en una relación 1:1 y 2:1 respecto al porcentaje de sepiolita en el ABS. Una vez obtenidos los materiales en forma de granza, se han preparado las probetas tipo halterio 1A para la realización de los ensayos de caracterización, en una inyectora marca MARGARIT JSW, modelo JM 110.

2.3 Caracterización de materiales

Los ensayos que se realizaron sobre los materiales fueron: TGA, para analizar el porcentaje real de sepiolita; microscopía electrónica de transmisión (TEM); impacto Izod con entalla a temperatura ambiente; módulo de Young y temperatura de deflexión bajo carga (HDT).

Para el ensayo de TGA se empleó un equipo METTLER TOLEDO 851e, donde se utilizó atmósfera inerte en el rango de 50 a 550º C y atmósfera oxidante desde 550º C hasta 950º C, a una velocidad de 20º C/min.

En este tipo de materiales la sepiolita se dispersa a escala nanométrica, estructura que ha sido caracterizada mediante microscopía electrónica (TEM), utilizando un microscopio electrónico JEOL 2010 F operando a 120 kV, combinado con un tratamiento de teñido selectivo para diferenciar la fase elastomérica.

Los ensayos de caracterización termo-mecánica se realizaron bajo las condiciones especificadas en la normativa correspondiente, y son los siguientes:

- Módulo elástico, usando una máquina de ensayos universal MTS, modelo 831-59[1].
- Temperatura de reblandecimiento bajo carga (HDT), utilizando un analizador CEAST modelo HDT3VICAT P/N 6911.000[2].
- Impacto Izod con entalla a 23ºC: empleando un Péndulo “Resil Impactor” (CEAST)[3].

---

[1] Norma española UNE-EN ISO 527-1 y UNE-EN-ISO 527-2

[2] Norma española UNE-EN 75-1

[3] Norma española UNE-EN ISO 180/U.

3. RESULTADOS Y DISCUSIÓN

En la Tabla 1 se presentan los resultados de los nanocompuestos de ABS con las dos sepiolitas modificadas con diferentes sales de amonio y los dos porcentajes empleados.

Material	% Arcilla	HDT – 1.8 MPa (º C)	Módulo Young (MPa)	Izod (kJ/m^2)
HI-100	-	76.5	1810	26.8
G-360	-	79.2	2390	19.7
HI-100 + 5% BM2TH	3.7	80.0	2740	5.4
G-360 + 5% 3MTH	3.6	79.9	3310	5.2
HI-100 + 10% BM2TH	7.4	83.6	3530	2.5
G-360 + 10% 3MTH	7.4	89.1	4500	1.9

Tabla 1. Propiedades termomecánicas de nanocompuestos de ABS y sepiolita.

Los ensayos de TGA revelan que se han obtenido nanocompuestos con un porcentaje de carga ligeramente inferior al estimado teóricamente. Lo cual se debe a que las sepiolitas modificadas con sales de amonio poseen entre un 15-20 % de materia orgánica que se descompone durante el ensayo de TGA, no dejando residuo.

Respecto a las propiedades termo-mecánicas, tanto el HDT como el módulo han aumentado con el porcentaje de sepiolita, y el impacto Izod ha disminuido. Esto indica que la sepiolita ha rigidificado el polímero, disminuyendo la tenacidad del material. Se ha observado un aumento importante en los valores del módulo respecto a la matriz sin reforzar.

Material	% Arcilla	HDT – 1.8 MPa (º C)	Módulo Young (MPa)	Izod (kJ/m^2)
HI-100 + 10% B-6000	-	72.7	1860	21.9
G-360 + 10% B-6000	-	81.3	2420	15.6
HI-100 + 10% B-6000 + 5% BM2TH	3.7	77.6	2610	5.3
G-360 + 10% B-6000 + 5% 3MTH	3.9	80.1	3300	4.0
HI-100 + 10% B-6000 + 10% BM2TH	7.4	84.3	3550	2.1
G-360 + 10% B-6000 + 10% 3MTH	7.4	90.5	4410	2.0

Tabla 2. Propiedades termomecánicas de nanocompuestos de ABS y sepiolita compatibilizadas con ABS-MAH.

En la Tabla 2 se presentan los valores de las propiedades medidas ahora sobre nanocompuestos de ABS y sepiolitas, en los que se ha añadido un 10% de compatibilizante.

En primer lugar, los resultados de TGA indican que los porcentajes de sepiolita son ligeramente inferiores a los teóricos, aunque similares a los porcentajes obtenidos en el caso anterior (Tabla 1).

Por otra parte, podemos observar que el aumento en HDT ha sido pequeño en comparación con el aumento del módulo, incluso a porcentajes muy elevados. Teniendo en cuenta que el ABS es un material amorfo, la caída del módulo en torno a la zona de la transición vítrea es muy acusada, y se encuentra cercana a la temperatura de transición vítrea del material, por lo que son esperables pequeños aumentos de la temperatura de deflexión (Scobbo et al. 1994).

4. CONCLUSIONES

A la vista de las propiedades termomecánicas, la adición de sepiolita a la matriz de ABS ha aumentado la rigidez del material, disminuyendo la tenacidad. Cuanto mayor es el porcentaje de sepiolita, mayor es el incremento del módulo y HDT, y menor el valor del impacto. El compatibilizante no ha tenido un efecto significativo en los nanocompuestos, es decir, no ha mejorado la compatibilidad de la sepiolita con la matriz.

Por otra parte, los mínimos aumentos obtenidos en el HDT de estos materiales se deben a que el ABS es una matriz amorfa y estos valores se encuentran próximos a la zona de la transición vítrea, donde la caída del módulo en esa región es muy pronunciada.

AGRADECIMIENTOS

Este trabajo ha sido posible gracias a la subvención concedida por la Junta de Castilla y León (GR104) y el Ministerio de Educación y Ciencia (MAT2008-06379-C02).

REFERENCIAS

LEMIC, J., TOMASEVIC-CANOVIC M., DJURICIC M., STANIC T**.** (2005) Journal of Colloid and Interface Science, 292, 11-19.
MA H., XU Z., TONG L., GU A., FANG Z**.** (2006) Polymer Degradation and Stability, 91, 2951-2959.
QI R., QUIAN J., ZHOU C. (2000) Journal of Polymer Science, 90, 1249-1254.
RUÍZ-HITZKY E. (2001) Journal of Materials Chemistry, 11, 86-91.
SCOBBO J.J. Y COMETTI P.L. SPE-ANTEC, 40, 3326-3333.
TARTAGLIONE G., TABUANI D. Y CAMINO G. (2008) Microporous and Mesoporous Materials, 107, 161-168.
XIE S., ZHANG S., WANG F., YANG M., SÉGUÉLA R., LEFEBVRE J.M. (2007) Composites Science and Technology, 67, 2334-2341.

Impact response of injection-molded polypropylene/glass fiber parts

G. Viau, V. Pettarin, P. Frontini
Instituto de Investigaciones en Ciencia y Tecnología de Materiales INTEMA,
Universidad Nacional de Mar del Plata-CONICET, Mar del Plata, Argentina

SUMMARY

Parts of polypropylene (PP)/glass fiber composites were injection molded and processing conditions influencing multiaxial impact response were isolated. Developed skin-core microstructure was analyzed and its dependence on processing conditions and influence on impact response was also assessed. Results demonstrate that all factors that enlarge skin thickness benefit impact response of PP moldings.

1. INTRODUCTION

Injection molded PP composites have become very popular in various applications such as the consumer electronic products, the automotive components, and chemical industry, etc., due to their good combination properties-cost. Injection molding is an important manufacturing process to polymers; it provides products with high-dimensional steadiness, low manufacture cycles as well as low costs. Many studies found that the injection-molding processing parameters have crucial effects on the quality of products (Viana et al, 2002). A correct setting of injection-molding conditions is, therefore, a major concern in the plastics industry. Impact strength is often one of the fundamental material requirements used to measure the performance of plastics in many applications. Falling-dart impact tests on disc or plate specimens are widely used by the plastics industry to characterize the "practical" resistance of rigid thermoplastics, because they are intended to reproduce the real behavior of molded parts under impact loading. They are formalized product tests on representative components, rather than measurements of basic materials properties. One additional advantage of the falling-dart impact test is that it provides a convenient method for studying changes induced by surface modification in part performance (Bucknall, 2000). This works deals with the influence of injection-molding conditions on the impact response of PP/glass fiber composites.

2. EXPERIMENTAL

Three commercial materials gently provided by Petroken were used: propylene homopolymer (PP-H) SM 6100, 20% fiber reinforced polypropylene (PP-20GF) AJ 5007B and 30% fiber reinforced polypropylene (PP-30GF) AJ 5059B. 3mm thickness discs were injection molded in a one gate cold runner mold by using a Multiplas injection machine with 100kN clamping force. Influence of processing parameters on parts response was studied by injecting eight groups of samples following an experiment design according to L8 Taguchi orthogonal array (Rosse, 1996) (Table 1). ANOVA statistical analysis (Keppel et al, 1989) was applied to identify the most influencing processing parameters. Multiaxial dart impact experiments were conducted on a Fractovis Ceast falling weight type machine at room temperature at 3.5 m/s (ASTM D3763-93), using an instrumented high-speed dart with hemispherical end of 12,7mm and disk specimens clamped on a 40 mm diameter supporting rig. Impact perforation energy, *U*, was calculated from integration of load-displacement curves. Polarized light microscopy (PLM) was used to observe the morphology of the moldings. 10 μm thick specimens were microtomed from center of specimens with an Angila Scientific microtome and observed with an Olympus polarized light microscope.

Run	*Tm* (ºC)	*Tw* (ºC)	*Ct* (s)	*Ht* (s)	*Ph* (bar)	*Qj* (cm^3/s)
1	240	25	10	3	120	11
2	240	25	10	15	240	22
3	240	50	30	3	120	22
4	240	50	30	15	240	11
5	280	25	30	3	240	11
6	280	25	30	15	120	22
7	280	50	10	3	240	22
8	280	50	10	15	120	11

Table 1. Molding program defined according to a L8 Taguchi design matrix.

3. RESULTS AND DISCUSSION

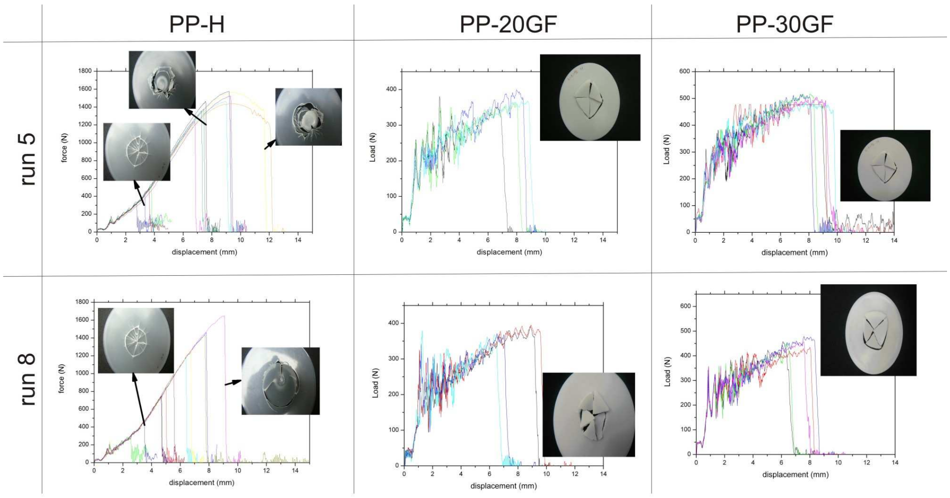

Fig. 1. Impact falling weight load-displacement curves for two PP moldings.

Fig. 1 shows load-displacement curves along with fracture patterns of materials under two processing conditions. PP-H moldings exhibited a great dispersion of behavior, i.e. different values of perforation energy and fracture patterns were observed. Some samples of run 1, 2, 5 and 6 underwent completely brittle fracture while others exhibited some or much plastic deformation before brittle fracture. Samples of runs 3, 4, 7 and 8 exhibited dispersion in absorbed energy but all fractured in a brittle manner. It seems that PP-H moldings are in the ductile-brittle transition zone under tested conditions: 1, 2, 5 and 6 moldings are in the upper transition (various samples exhibited ductile behavior), while 3, 4, 7 and 8 moldings are in the lower transition (all samples exhibited brittle behavior but with a great dispersion in absorbed energy). Fibers draw PP out of ductile-brittle zone: all samples exhibited a non-linearity of load-displacement curve followed by a brittle fracture. To compare *U* values, a threshold value was selected as media value minus standard deviation. These values and ANOVA analysis are shown in Fig. 2 and 3, respectively. It is clearly seen that composites exhibited better impact response than PP-H under almost all processing conditions. ANOVA analysis indicates that processing parameters that most influence *U* are different for PP-H and composites. PP-H is most influenced by wall temperature and mold temperature, while PP-20GF is most influenced by holding pressure.

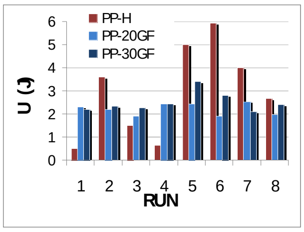

Fig. 2. Perforation energy

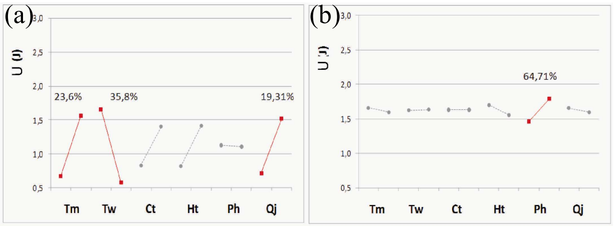

Fig. 3. ANOVA analysis of U (a) PP-H (b) PP-20GF.

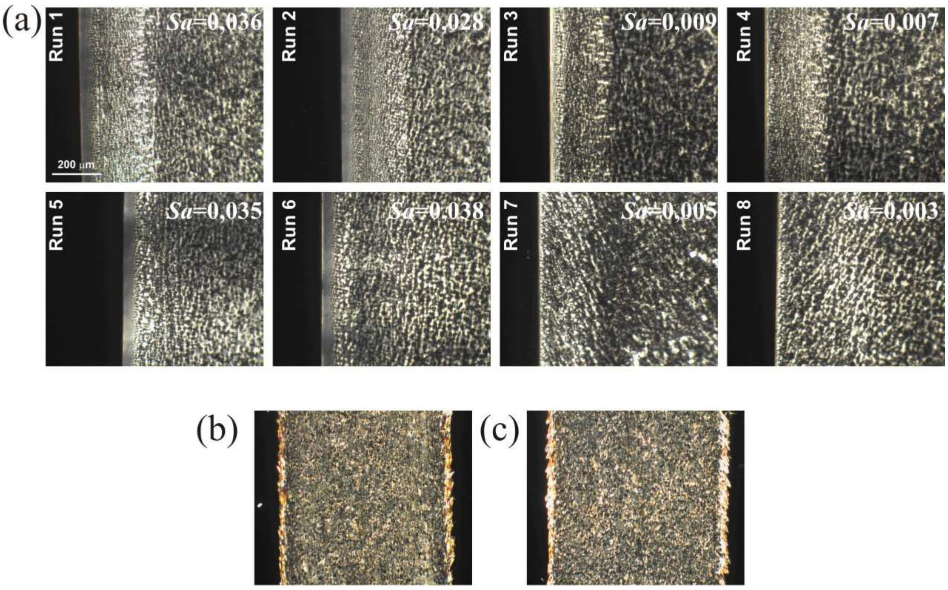

Fig. 3. PLM of (a) PP-H (b) PP-20GF (c) PP-30GF moldings.

As it is been reported that mechanical properties of injection-molded parts depend on microstructure (Viana et al, 2002), we analyzed molding's structure by PLM. PP-H samples showed a typical multilayered structure originated by the different thermo-mechanical history the melt undergoes through the thickness of injection molded parts (fig 4) (Kantz et al, 1972): a highly oriented nonspherulitic skin, a shear zone with molecular chains oriented essentially parallel to the injection direction, and a spherulitic core with essentially no preferred orientation. Skin-ratio (*Sa*) was calculated as skin thickness/sample thickness. It is evident that samples with higher *Sa* are in the upper transition and samples with lower *Sa* are in the lower transition. It is been stated that the D-B transition observed in polymers is in general due to an alteration in deformation mode, from distortional (shear banding) to dilational (crazing). On this basis, the experimental parameters and material variables which affect the relative importance of these deformation modes should in turn control the D-B behavior of the polymer (Jang et al, 1984). Molecular orientation tends to suppress the formation of crazes and promote the shear yielding mode, i.e. crazes usually do not develop in the highly oriented skin zone of injection molded PP. As a consequence, the bigger the *Sa* the lower the possibility of brittle fracture. Analysis of composites microstructure demonstrates that there is a very thin skin, if it actually exists (fig 5). This fact explains the out of ductile-brittle transition response exhibited by composites. It is also evident from previous analysis that factors influencing *Sa* are the most important processing parameters in PP-H, while in composites *U* is probably influenced by PP crystallinity.

4. CONCLUSIONS

Through this work the influence of injection-molding conditions on the multiaxial impact response of PP/glass fiber composites was assessed. It was found that processing parameters that most influence composites impact response are different from those of PP-H. This is due to diverse morphologies developed during molding: PP-H develops a typical skin-core structure while in composites this type of microstructure is not evident. Skin-core structure is also the explanation of different location of PP moldings in the ductile-brittle transition zone (upper or lower transition): the higher the skin thickness, the lower the occurrence of brittle fracture, i.e. samples are in the upper transition. Results demonstrate that special attention should be paid on processing conditions influencing moldings microstructure.

ACKNOWLEDGEMENTS

Authors would like to thank the financial support from CONICET, Universidad Nacional de Mar del Plata, and Agencia Nacional de Promoción Científica y Tecnológica from Argentina.

REFERENCES

BUCKNALL, CB (2000) Characterizing Toughness using Standard Empirical Tests, Chapter 21 in *Polymer Blends, Volume 2: Performance*, (Eds DR Paul and CB Bucknall), John Wiley & Sons Inc, 59-82

JANG, BZ; UHLMANN, DR; VANDER SANDE, JB (1984) Ductile-Brittle Transition in Polymers, *J. Appl. Polym. Sci.*, 29, 3409-3420

KANTZ, MR; NEWMAN, JHD; STIGALE, FH (1972) The skin-core morphology and structure-property relationships in injection-molded polypropylene, *J. Appl. Polym. Sci.*, 16, 1249-1260

KEPPEL, G. ZEDECK, S. (1989) Data Analysis for Research Designs: Analysis of Variance and Multiple Research/Correlation Approaches, W.H. Freeman, New York

ROSSE, P. (1996) Taguchi Techniques for Quality Engineering, Loss Function, Orthogonal Experiments, Parameter and Tolerance Design, McGraw-Hill, Toronto

VIANA, JC; CUNHA, AM; BILLON, N. (2002) The thermomechanical environment and the microstructure of an injection moulded polypropylene copolymer. *Polymer*, 43, 4185-4196

Thermal and oxidative degradation of epoxy based layered silicate nanocomposites

F. Román, Y. Calventus, J.M. Hutchinson, S. Montserrat
Departament de Màquines i Motors Tèrmics, ETSEIAT, Universitat Politècnica de Catalunya, 08222 Terrassa, Spain

SUMMARY

The thermal and oxidative degradation of several polymer/clay nanocomposites with a range of clay contents has been determined. It is found that the dispersion of the clay in the resin matrix plays a crucial role in the degradation process, and hence emphasises the importance of this aspect of nanocomposite preparation.

1. INTRODUCTION

There has been growing interest in recent years in the development of polymer layered silicate (PLS) nanocomposites (Alexandre and Dubois 2000), and in particular in those based upon epoxy resin (Becker and Simon 2005). Considerable attention has been directed towards the determination of the effects of the preparation method on their properties and nanostructure. There still remains, however, a lack of understanding of the interaction between the preparation procedure and the resulting nanostructure. To address this problem, we examine here the degradation, in nitrogen and in air, of PLS nanocomposites based upon epoxy resin as a function of their clay content and preparation procedure.

2. EXPERIMENTAL

A commercial octadecylamine modified montmorillonite (MMT), Nanomer I.30E from Nanocor Inc., was used. The epoxy resin was a commercial diglycidyl ether of bisphenol-A (DGEBA), Epon 828 (Shell Chemicals), and the curing agent was a polyoxypropylene diamine, Jeffamine D-230 (Huntsman Corporation).

Mixtures of resin and clay, with 2, 5 and 10 wt% clay, were prepared by simple mixing followed by an ultrasonic bath for 3h at 42ºC. The stoichiometric amount of curing agent was then added, and the mixture was finally degassed at room temperature (RT). The curing schedule for the samples, both with and without clay, was 2h at 70ºC and 8h at 120ºC. An additional mixture of resin with 10 wt% clay was pre-conditioned by storage at RT for about three years, and then cured with the stoichiometric quantity of Jeffamine D-230, the epoxy content having previously been determined by chemical analysis. The samples of neat resin are designated EPJ, the nanocomposites with 2, 5 and 10 wt% clay are designated NEPJ2, NEPJ5 and NEPJ10, respectively, and the pre-conditioned sample was designated NEPJ10pc.

A Mettler Toledo thermogravimetric analyser (TGA) was used to compare the thermal stability and weight loss of the different samples. The samples were heated from room temperature to 600ºC at different heating rates under dry nitrogen or dry air gas flow for thermal or oxidative degradation, respectively.

3. RESULTS AND DISCUSSION

3.1. Thermal degradation behaviour

The thermal degradation of the neat epoxy, the nanocomposites with 2, 5 and10 wt% clay, and the pre-conditioned samples is shown in the derivative TGA curves (DTGA) for one selected heating rate in Figure 1. For EPJ and the NEPJ nanocomposites, a single degradation process is observed, with a slight shoulder in the high temperature region, whereas the sample NEPJ10pc shows a marked shoulder, or even a peak, after the main degradation in the DTGA curves. For all the heating rates used in this study, the values of the temperature at the maximum degradation rate (T_{max}) were determined, which are shown in Figure 2. The addition of 2 and 5 wt% clay increases T_{max} by between 3 and 11ºC with respect to that of EPJ, with no systematic differences for these two clay contents. There is also no significant difference between the T_{max} of the main peak of NEPJ10pc and those of NEPJ2 and NEPJ5. On the other hand, NEPJ10 shows a significant reduction in T_{max} in comparison with NEPJ2 and NEPJ5, and even a slight reduction in comparison with EPJ.

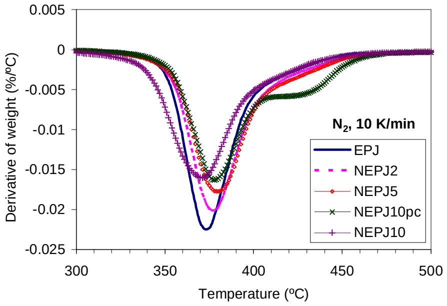

Fig. 1. DTGA at 10 K/min in nitrogen.

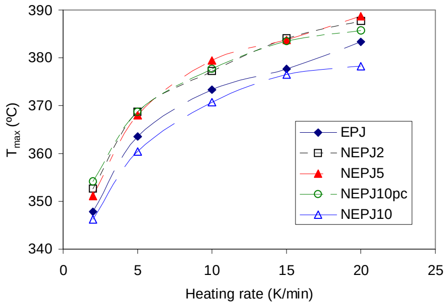

Fig. 2. T_{max} for degradation in nitrogen.

It is interesting to compare these results with some relevant reports in the literature. Brnardic et al. (2008) found almost identical or even slightly lower values of T_{max} in epoxy composites with 5 and 10 wt% MMT. Other authors (Gu and Liang 2003) have reported both higher and lower values of an initial degradation temperature, for 2 and 10 wt% clay, respectively, compared with the neat epoxy,. Thus, similar to our present results, they find that the 10 wt% nanocomposite has a reduced thermal stability in comparison with the neat resin. Guo et al. (2004) found increasing values of the degradation temperature for clay contents from 0 to 6 phr, followed by a slight decrease for clay contents up to 14phr, but with the nanocomposites always remaining more thermally stable than the neat resin. Despite the different systems studied by these several authors, there are some basic similarities in the degradation behaviours reported which suggest a common origin.

A possible explanation could lie in the quality of the dispersion of the clay in the resin. For clay contents of 2 and 5 wt%, the dispersion observed by optical microscopy is reasonably good. For 10 wt% clay, the dispersion is significantly worse, which means that the clay forms large agglomerates in the resin matrix, with no significant interaction between much of the clay and the resin, and hence no effective modification of the degradation behaviour, as observed in the present results. For NEPJ10pc, though, the interesting observation is that pre-conditioning results in a very significant improvement in the dispersion (Pustkova et al. 2009). Apparently the homopolymerisation that is taking place during pre-conditioning results in a de-aggregation of the clay, with important consequences not only for the dispersion but also for the subsequent cure kinetics and exfoliation (Montserrat et al. 2008). The present results therefore suggest that the quality of the dispersion of the clay in the resin is a very important determinant of degradation behaviour.

3.2. Oxidative degradation behaviour

The DTGA curves for weight loss in air at one selected heating rate are shown in Figure 3, and the dependence on heating rate of T_{max} for the main peak is shown in Figure 4. It can be seen that the main degradation step and the second peak (or shoulder) are advanced with respect to thermal degradation, but that in addition a third degradation peak appears at a higher temperature. The similarity of the first and second peaks for degradation in nitrogen and air suggests that they have a common origin, while the third peak at about 550ºC for degradation in air can be attributed to carbonisation.

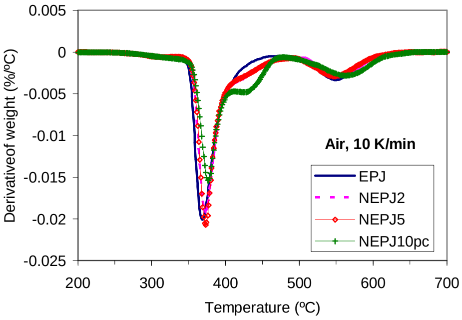

Fig. 3. DTGA curves at 10 K/min in air.

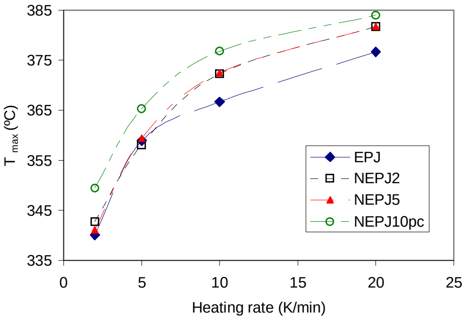

Fig. 4. T_{max} for degradation in air.

Similarly to the degradation in nitrogen, a pronounced shoulder or peak is observed in the DTGA curves for NEPJ10pc just after the first degradation step, and can be attributed to a change in the degradation mechanism induced by the homopolymerised epoxy formed during the pre-conditioning. Since the homopolymerisation which occurs at RT during pre-conditioning is catalysed by the onium ion of the organically modified clay, these homopolymerised chains that are formed are likely to be close to the clay surfaces, and in particular in the gallery regions of the intercalated clay. The protective environment of these interlamellar regions would delay the degradation process and lead to the observed behaviour.

In the oxidative degradation, a small increase of T_{max} for NEPJ2 and NEPJ5 with respect to EPJ is observed. In comparison, for NEPJ10pc, a somewhat larger increase of T_{max} with respect to EPJ, of about 8 to 9ºC, can be seen. Likewise, when we compare the oxidative and thermal degradation of NEPJ10pc, we see that the oxygen atmosphere advances the degradation by only 1 to 5ºC, whereas the equivalent advance for NEPJ2, NEPJ5 and NEPJ10, as well as for EPJ, was often as great as 10ºC or more. These results indicate that the stability of the pre-conditioned sample is not only better than that of the NEPJ nanocomposites, but also that it is very similar in both oxidative and thermal degradation. This behaviour results directly from the improvement in the clay dispersion and from the nanostructural changes that take place during the pre-conditioning, in which significant homopolymerisation of the epoxy resin takes place.

CONCLUSIONS

The effect of clay dispersion on the degradation behaviour of PLS nanocomposites has been studied, and it has been shown that it has an important influence on the thermal stability of these materials. An improvement in the thermal stability is observed for low clay contents (2 and 5 wt%), for which the dispersion is relatively good, whereas for higher clay contents (10 wt%) the dispersion is much poorer with a consequent reduction in the thermal stability. Pre-conditioning of the resin/clay mixture, which induces homopolymerisation, results in an improved dispersion and greater thermal stability.

ACKNOWLEDGEMENTS

We thank the Spanish Ministry for Project MAT 2008-06284-C03-03 and a Ramón y Cajal research contract for JMH, and the Huntsman Corporation for the Jeffamine.

REFERENCES

ALEXANDRE, M., DUBOIS, P. (2000). Polymer-layered silicate nanocomposites: preparation, properties and uses of a new class of materials. *Mater. Sci. Eng.*, 28, 1-63.

BECKER, O., SIMON, G.P. (2005). Epoxy layered silicate nanocomposites. *Adv. Polym. Sci.*, 179, 29-82.

BRNARDIC, I., MACAN, J., IVANKOVIC, H., IVANKOVIC, M. (2008). Thermal degradation of Epoxy/organically modified montmorillonite nanocomposites. *J. Appl. Polym. Sci.*, 107, 1932-1938.

GU, A., LIANG, G. (2003). Thermal degradation behaviour and kinetic analysis of epoxy/montmorillonite nanocomposites. *Polymer Degradation and Stability*, 80, 383-391.

GUO, B., JIA, D., CAI, C. (2004). Effects of organo-montmorillonite dispersion on thermal stability of epoxy resin nanocomposites. *Eur. Polym. J.*, 40, 1743-1748.

MONTSERRAT, S., ROMÁN, F., HUTCHINSON, J.M., CAMPOS, L. (2008). Analysis of the cure of epoxy based layered silicate nanocomposites: Reaction kinetics and nanostructure development. *J. Appl. Polym. Sci.*, 108, 923-938.

PUSTKOVA, P., HUTCHINSON, J.M., ROMÁN, F., MONTSERRAT, S. (2009). Homopolymerisation effects in polymer layered silicate nanocomposites based upon epoxy resin: implications for exfoliation. *J. Appl. Polym. Sci.*, in press.

Mecánica de la fractura de material compuesto de resina epoxi reforzada con nanofibras de carbono

R. Chaos-Morán, A. Salazar, M.D. Escalera, A. Ureña
Departamento de Ciencia e Ingeniería de Materiales. Escuela Superior de Ciencias Experimentales e Ingeniería. Universidad Rey Juan Carlos, España

RESUMEN

El uso de nanofibras de carbono se perfila como una alternativa económica al uso de nanotubos de carbono como refuerzo de matrices epoxídicas. Pese a sus modestas propiedades mecánicas en relación a los nanotubos de carbono, existe la posibilidad de que la incorporación de nanofibras de carbono mejore propiedades tales como la tenacidad de fractura. En este trabajo se estudia el efecto de la incorporación de pequeñas cantidades de nanofibras de carbono a una matriz epoxi sobre sus propiedades mecánicas y tenacidad de fractura. Si bien no se han logrado materiales con mejoras significativas, se aprecia que propiedades tales como el coeficiente de Poisson sí que se ven afectados por la presencia de un refuerzo nanométrico.

1. INTRODUCCIÓN

Los nanotubos (CNTs) y las nanofibras (CNFs) de carbono poseen excelentes propiedades eléctricas, térmicas y mecánicas. Tanto los estudios por dinámica molecular como las medidas experimentales han revelado módulos de Young < 1000 GPa y 200 GPa (Treacy et al. 1996), superficies especificas < 1300 m^2/g y 200 m^2/g (Peigney et al. 2001), relaciones de forma < 10^3 y 10^2 para los CNTs y CNFs, respectivamente. A pesar de las excelentes propiedades de los CNTs en comparación con CNFs, su utilización está condicionada por sus bajos volúmenes de producción y elevados costes. En este sentido es interesante considerar como posible alternativa la aplicación de las CNFs como nanorrefuerzo a escala nanométrica debido a sus menores costes y a sus comparativamente mayores volúmenes de fabricación (Chatterjee et al. 2002). A pesar de las predicciones teóricas, las propiedades mecánicas de los nanocompuestos de matriz polimérica están muy por debajo de las inicialmente previstas (Lozano et al. 2001). El motivo de este fracaso está en la dificultad de transferir las excelentes propiedades mecánicas de estos nanorrefuerzos a la matriz del compuesto. La única posibilidad de alcanzar esta transferencia es resolver dos problemas que surgen en el procesado: la dispersión del nanorrefuerzo y su baja adhesión con la matriz polimérica.La posible incorporación de CNFs a matrices poliméricas parece estar orientada a mejorar las propiedades a fractura de las matrices poliméricas de materiales compuestos convencionales arraigados en industrias como la aeronáutica o civil. Las propiedades a fractura del compuesto en la dirección perpendicular al plano del refuerzo están dominadas por la matriz. Una mejora en la tenacidad de fractura de estas matrices es equivalente a una mayor resistencia frente a la propagación de grietas.

El comportamiento en fractura de los materiales compuestos de matriz polimérica reforzada con CNFs aún no se ha estudiado utilizando los conceptos de la Mecánica de la Fractura aunque sí se puede encontrar una extensa bibliografía relacionada con el aumento de las propiedades mecánicas (tracción y flexión) de estos nanocompuestos. En general, un pequeño contenido de nanorrefuerzo mejora la resistencia a tracción y la rigidez de la matriz (Gojny et al 2003). Es por ello que el objetivo de este trabajo es analizar la influencia del contenido de nanofibras y del tratamiento de funcionalización de las mismas sobre las propiedades mecánicas y la fractura de nanocompuestos de matriz epoxídica.

2. PROCEDIMIENTO EXPERIMENTAL

2.1. Materiales

El monómero epoxi utilizado es el diglicidil éter de Bisfenol-A de 178 g/equivalente epoxi, suministrado por Sigma-Aldrich. Se ha usado como entrecruzante 4,4'-dimetilenanilina (DDM) suministrada también por Sigma-Aldrich. Se han usado como nanorefuerzo nanofibras de carbono (CNFs) GANF-1 suministradas por el Grupo Antolín, S.L. Éstas poseen un diámetro comprendido entre los 20 y los 100 nm y longitud media del orden a los 35 µm (dato del fabricante).

2.2. Preparación de los materiales

Se han utilizado dos tipo de nanofibras de carbono cono refuerzo: nanofibras en estado de recepción (CNF) y nanofibras (CNFo) de carbono oxidadas en ácido nítrico. Para fomentar la dispersión de las nanofibras de carbono en la matriz de resina epoxi se ha utilizado el método de puesta en suspensión en cloroformo optimizado previamente. La mezcla DGEBA-DDM-CNF en líquido se introduce en moldes con la forma deseada y es curada en estufa. Siguiendo este método se han fabricado materiales compuestos de matriz DGEBA-DDM reforzada con CNF y CNFo en contenidos de un 0,25 y 0,5 % m/m. Así mismo, se han fabricado muestras de material de resina de DGEBA-DDM sin reforzar como material de referencia.

2.3. Caracterización mecánica

Se han fabricado y ensayado materiales compuestos para la realización de ensayos de tracción bajo norma ASTM D 638 geometría Tipo IV y ensayos para el cálculo de K_{IC} por flexión a tres puntos según la norma ASTM D 5045. Los ensayos se han realizado a temperatura ambiente y en control de posición a una velocidad de 5 mm/min de desplazamiento de puente en una máquina universal electromecánica de ensayos mecánicos MTS, modelo Alliance RF/100. La carga se midió con una célula de carga de 5 kN de carga máxima y la deformación (en los ensayos de tracción) y el desplazamiento del punto de aplicación de carga (en los ensayos de flexión) se midió con un videoextensómetro Limess. Se ha realizado el estudio fratográfico correspondiente a las superficies de fractura obtenidas mediante microscopía electrónica de barrido (SEM) en un microscopio Hitachi S 3400 N.

3. RESULTADOS Y DISCUSIÓN

Las propiedades mecánicas generales de los materiales compuestos fabricados han sido determinadas mediante ensayos de tracción estandarizada. La figura 1 muestra los valores medidos de módulo elástico y de coeficiente de Poisson.

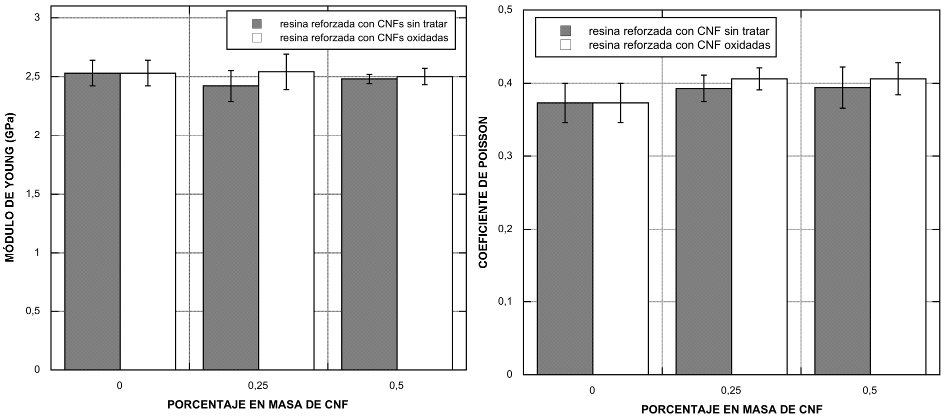

Fig. 1. Módulo elástico y coeficiente de Poisson de los materiales ensayados.

Tal y como se puede apreciar en la figura 1, tanto el módulo elástico como el coeficiente de Poisson de los materiales ensayados no presenta una variación significativa ni con el porcentaje de nanofibra utilizada como refuerzo ni con el tratamiento químico al que han sido sometidas las nanofibras.

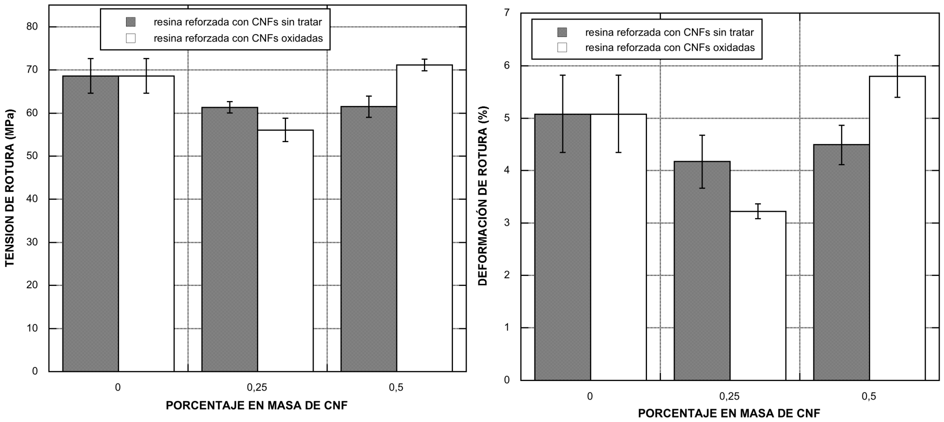

Fig 2. Tensión y deformación de rotura de los materiales ensayados.

Dicho comportamiento errático y poco concluyente se ve también especialmente reflejado en los valores de tensión y deformación de rotura (figura 2), en los cuales el efecto de los defectos tales como porosidad o falta de curado por presencia de cloroformo residual, identificados a través del estudio de las superficies de fractura, se hace especialmente patente.

El cálculo de la tenacidad a fractura de los materiales fabricados (figura 3) manifiesta dos efectos claros. En primer lugar, existe una clara dependencia del valor de K_{IC} con el radio de la entalla. Se puede apreciar un claro incremento del valor K_{IC} de la resina con un radio de entalla de 140 µm respecto de la resina con un radio de entalla de 60 µm. El efecto del redondeo de la entalla es un fenómeno anteriormente estudiado y que requiere en este caso un tratamiento específico. Además, se aprecia como los distintos materiales no presentan variaciones significativas de K_{IC} asociadas siempre a una elevada dispersión en los resultados.

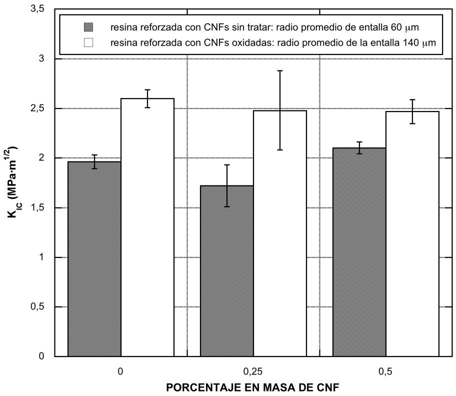

Figura 3. K_{IC} de los materiales fabricados.

4. CONCLUSIONES

- La incorporación de nanofibras de carbono, con y sin tratamiento químico o no, no supone mejoras significativas de propiedades elásticas de la resina epoxi. Se aprecian variaciones asociadas a la defectología presente en los materiales en las propiedades resistentes de las resinas reforzadas.
- La tenacidad de fractura de las resinas epoxi muestra una clara dependencia del radio de la entalla y no se ve afectada por la incorporación de CNFs.

5. REFERENCIAS

CHATTERJEE, A., DEOPURA, B.L. (2002) Carbon nanotubes and nanofibre: An overview. *Fibers and Polymers*.4 (134)

GOJNY, F.H., NASTALCZYH, J., ROSLANIEC, Z., SCHULTE, K. (2003) Surface modified multi-walled carbon nanotubes in CNT/epoxy-composites. *Chem. Phys. Lett.* 370 (820-824)

LOZANO, K., BARRERA, E.V. (2001) Nanofiber-reinforced thermoplastic composites. I. Thermoanalytical and nechanical analyses. *J. Appl. Polym. Sci.* 79 (125-133)

PEIGNEY, A., LAURENT, CH., FLAHAUT, E., BACSA, R.R., ROUSSET, A. (2001) Specific surface area of carbon nanotubes and bundles of carbon nanotubes. *Carbon.* 39 (507-514)

TREACY, M.M.J., EBBESEN, T.W., GIBSON, J.M. (1996) Exceptionally high Young's modulus observed for individual carbon nanotubes. *Carbon.* 381 (678-680)

AGRADECIMIENTOS

Los autores quieren agradecer a la Comunidad Autónoma de Madrid y a la Universidad Rey Juan Carlos la financiación para la realización de este trabajo (URJC-CM-2008-CET-3551)

Análisis experimental de los fenómenos de perforación en estructuras fabricadas con laminados vidrio/poliéster sometidas a cargas impulsivas

B.L. Buitrago Pérez
Departamento de Mecánica de Medios Continuos y Teoría de Estructuras. Universidad Carlos III de Madrid
Departamento de Tecnología Industrial. Universidad Simón Bolívar
S. K. García Castillo, E. Barbero Pozuelo
Departamento de Mecánica de Medios Continuos y Teoría de Estructuras. Universidad Carlos III de Madrid

RESUMEN

En este trabajo se estudió el comportamiento balístico de varias estructuras fabricadas a partir de laminados vidrio/poliéster, evaluando la velocidad residual del proyectil y la extensión del daño. Se analizaron tres laminados monolíticos de diferentes espesores y dos estructuras multicapa: una tipo sándwich con núcleo de espuma y otra formada únicamente por las pieles separadas una distancia igual al espesor del núcleo del sándwich. Se determinó que los laminados de mayor espesor presentan una mayor extensión del daño, y un mayor límite balístico. La influencia del núcleo en el límite balístico de las estructuras multicapas es despreciable, sin embargo, incrementa la extensión del área dañada en la piel posterior.

1. INTRODUCCIÓN

Las estructuras fabricadas a partir de laminados de vidrio/poliéster se emplean ampliamente en la industria naval y del transporte terrestre debido a sus buenas propiedades mecánicas. Aunque estas estructuras no estén diseñadas como blindajes, durante su vida en servicio pueden verse sometidas a cargas de tipo impulsivo, lo que hace necesario un mejor conocimiento de su respuesta frente a este tipo de cargas. Esta es una de las principales razones que limitan el uso de los materiales compuestos de tipo laminado (Hawyes et al. 2001), debido a que el daño generado por el impacto produce una importante disminución de su resistencia, aunque no sea detectable visualmente (Ibekwe et al. 2006).

Un parámetro que se emplea para estimar la resistencia frente a impactos de alta velocidad de una estructura es el límite balístico, que se define como la máxima velocidad de impacto, para un determinado proyectil, que no es capaz de perforar la estructura (Norma MIL-STD-662F). Otro parámetro importante es la extensión del área dañada, que está relacionada directamente con la resistencia residual del componente tras el impacto. Se ha observado que en impactos balísticos el daño generado es bastante extenso, por lo que se considera un parámetro crítico a la hora de diseñar estructuras (De Luca et al. 1998).

El comportamiento de una estructura multicapa no es el mismo que el de un laminado monolítico. En la literatura se pueden encontrar muchos estudios de estructuras multicapas o de estructuras monolíticas por separado. Sin embargo, para poder comparar su comportamiento balístico hay que someter las estructuras a las mismas condiciones de impacto, debiendo ser también iguales el resto de los parámetros (geometría, material, etc.)

En este trabajo se analiza, bajos las mismas condiciones de ensayo, el comportamiento frente a impacto balístico de tres laminados monolíticos de diferentes espesores y dos estructuras multicapa. En todos los casos se ha empleado el mismo tejido equilibrado de vidrio E/poliéster.

2. PROCEDIMIENTO EXPERIMENTAL

Se estudiaron cinco estructuras fabricadas a partir de laminados de tejido equilibrado de fibra de vidrio E/poliéster: tres laminados monolíticos de 3, 6 y 12 mm de espesor y dos estructuras multicapas; una tipo sándwich con pieles de 3 mm de espesor y núcleo de espuma de PVC de 30 mm de espesor y otra denominada placas espaciadas (PE) que consiste en dos laminados de 3 mm separados a una distancia de 30 mm.

Los ensayos de impacto se realizaron utilizando un cañón de gas Sabre Ballistics, modelo A1G+, con proyectiles esféricos de 7,5 mm de diámetro y 1,7 g de masa, en un rango de velocidades entre 80 m/s y 780 m/s. En los ensayos se utilizó una cámara de vídeo de alta velocidad, modelo PHOTRON FASTCAM-ultima APX. A partir de las imágenes registradas por la cámara se estimó la velocidad de impacto y residual del proyectil.

En todas las estructuras impactadas y aprovechando que las placas de material compuestos son traslúcidas, se determinó la extensión de área dañada con técnicas ópticas a partir de fotografías digitales (Nunes et al. 2004).

3. RESULTADOS

La Fig. 1 muestra la relación entre la velocidad de impacto y la residual en todas las estructuras ensayadas. Las curvas de ajuste representadas en la figura se calcularon empleando el modelo de Lambert-Jonas (Kasano 1999) que relaciona la velocidad residual con la de impacto mediante la siguiente ecuación:

$$v_R = A \cdot \left(v_o^p - v_{LB}^p \right)^{1/p} \tag{1}$$

donde v_o es la velocidad de impacto del proyectil, v_{LB} el límite balístico, v_R la velocidad residual del proyectil y A y p son parámetros de ajuste.

El límite balístico no se puede calcular de forma determinista, debido a que existe un intervalo de velocidades de impacto donde se puede producir o no la perforación completa de la estructura; y además la velocidad de salida del proyectil desde el cañón no puede ser controlada totalmente. Por ello en este trabajo, el límite balístico se estimó utilizando la ecuación 1. En la Tabla 1 recoge los resultados correspondientes.

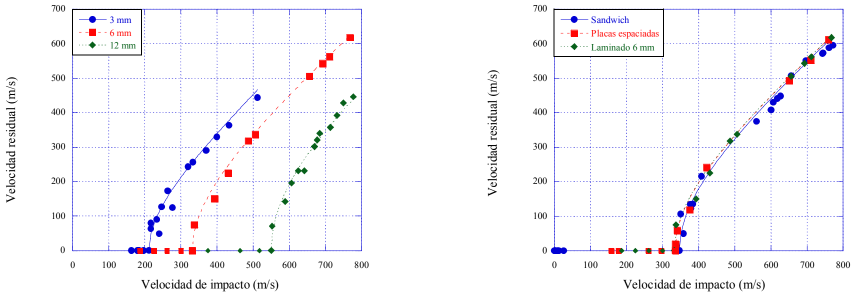

Fig. 1. Velocidad residual frente a velocidad de impacto.

La influencia del núcleo de espuma es depreciable, observándose en el límite balístico una diferencia del 3,5% entre las estructuras multicapas, mientras que entre el laminado monolítico de 6 mm y las PE la diferencia es mínima, debido a que en los tres casos la densidad areal es semejante. Por el contrario, en los laminados monolíticos el límite balístico aumenta con el espesor, producto del incremento de la densidad areal, así en el laminado de 12 mm aumenta hasta 2,6 veces con respecto al de 3 mm de espesor.

	Laminado de 3 mm	Laminado de 6 mm	Laminado de 12 mm	Placas espaciadas	Estructura sándwich
Limite balístico (m/s)	212	332	550	334	346

Tabla 1. Límite balístico.

En las Fig. 2 y 3 se muestran la influencia de la velocidad de impacto en la extensión del daño. En todas las estructuras se observa que las máximas extensiones de daño se alcanzan en el entorno del límite balístico. Para velocidades por debajo del límite balístico la extensión del daño se incrementa con la velocidad, mientras que para velocidades por encima se presenta una disminución con el incremento de la velocidad.

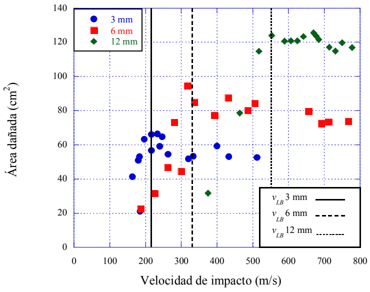

Fig. 2. Extensión del área dañada en los laminados monolíticos.

Para los laminados monolíticos, Fig. 2, se determinó que el área dañada se incrementa con el espesor de las placas. El laminado de 12 mm presentan una extensión del daño 2,4 veces la del laminado de 3 mm, que es un porcentaje semejante a la diferencia en el límite balístico.

La Fig. 3 muestra la extensión del daño en función de la velocidad de impacto para las estructuras multicapas y el laminado monolítico de 6 mm. En las estructuras multicapas la presencia del núcleo incrementa en un 25% el área dañada en la piel posterior en las proximidades del límite balístico, por el contrario, en la piel frontal el área dañada es tres veces mayor en las PE. El daño en la piel posterior de la estructura sándwich es similar al encontrado en el laminado monolítico de 6 mm de espesor.

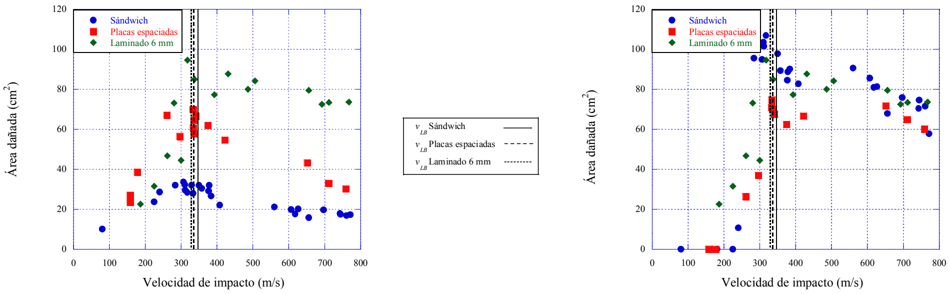

(a) (b)

Fig. 3. Área dañada en las estructuras multicapa y el laminado de 6 mm, (a) piel frontal y (b) piel posterior.

4. CONCLUSIONES

El límite balístico y la extensión de área dañada se incrementan con el espesor de los laminados monolíticos.

El límite balístico de las estructuras multicapas es similar al de un laminado monolítico de igual espesor. Sin embargo, la extensión del área dañada es diferente, siendo mayor en la piel posterior del sándwich respecto a las PE, y al contrario en la piel anterior.

REFERENCIAS

DE LUCA E. PRIFTI J. BETHENEY W. CHOU S.C. (1997). Ballistic impact damage of S2 glass-reinforced plastic structural armor. *Compos Sci Technol.,* 58,1453-1461.

HAWYES, V.J., CURTIS, P.T., SOUTIS, C. (2001). Effect of impact on the compressive response of composite laminates. *Compos Part A-Appl S.*, 32, 1263-1270.

IBEKWE, S.I., MENSAH, P.F., LI, G., PANG S.S., STUBBLEFIELD, M.A. (2007). Impact and post impact response of laminated beams at low temperatures. *Compos Struct.*, 79, 12-17.

KASANO, H. (1999). Recent advances in high-velocity impact perforation of fiber composite laminates. *JSME Int Journal,* 42(2), 147-157.

MIL-STD-662F Standard. V50 Ballistic test for armor. Department of Defense Test Method Standard.

NUNES, L.M., PACIORNIK S., D'ALMEIDA, J.R.M. (2004) Evaluation of the damage area of glass-fiber-reinforced epoxi-matrix composite materials submitted to ballistic impacts. *Compos Sci Technol.,* 64, 945-954.

Influencia del tipo de nanosilicato en las propiedades térmicas y mecánicas de nanocompuestos de matriz epoxi modificada con termoplástico

M. Sánchez-Cabezudo, R.M. Masegosa
Dpt. Física y Química Aplicadas a la Técnica Aeronáutica. E.U.I.T. Aeronáutica.
Univ. Politécnica de Madrid, España
M.G. Prolongo, A. García del Cid, C. Salom
Dpt. Materiales y Producción Aeroespacial. E.T.S.I. Aeronáuticos.Univ. Politécnica de Madrid, España

RESUMEN

Se han preparado materiales nanocompuestos formados por una matriz epoxídica, tipo diglicidileter de bisfenol A, modificada con poliacetato de vinilo (PVAc) en cantidad comprendida entre el 5 y 20% en peso y conteniendo un 4% en peso de silicatos laminares. Los silicatos laminares, denominados Cloisitas C30B y C93A, orgánicamente modificados, han sido comerciales. Se ha comprobado la influencia del grado de intercalación del nanosilicato sobre la cinética de curado, sobre las propiedades térmicas y sobre las propiedades mecánicas de los materiales epoxi/PVAc/C30B y epoxi/PVAc/C93A, comparándola con los correspondientes sistemas no reforzados.

1. INTRODUCCIÓN

Los materiales nanocompuestos formados por la unión de un material polimérico y un silicato laminar han sido objeto de numerosos trabajos de investigación (Ray el al, 2003). Este interés reside en que dichos materiales, potencialmente, poseen propiedades únicas derivadas de la gran superficie de contacto que resulta del tamaño nanométrico de los nanosilicatos que actúan como refuerzo. La utilización de nanorefuerzos en los termoestables epoxídicos modificados con termoplásticos adquiere un gran interés dado que contribuyen a contrarrestar el efecto de disminución de la resistencia mecánica del material termoestable provocado por la presencia del modificador. En la bibliografía existen pocos trabajos que aporten información sobre sistemas ternarios epoxi/termoplástico/nanosilicato y por tanto el objetivo principal de este estudio es obtener resultados sobre el comportamiento térmico y mecánico de un termoestable epoxídico tipo diglicidileter de bisfenol A (DGEBA), entrecruzado con 4,4´-diaminodifenilmetano (DDM), que ha sido modificado con un termoplástico, poliacetato de vinilo (PVAc) de moderada temperatura de transición vítrea ($T_g \sim 45$ºC), en cantidades comprendidas entre el 5 y el 20% en peso y que contiene un 4% en peso de silicatos laminares que actúan como nanorrefuerzo. La dispersión del nanorrefuerzo ha sido investigada mediante difracción de rayos X y la cinética de curado se ha estudiado por DSC, analizándose la influencia de la presencia de nanorefuerzo sobre la entalpía de curado (ΔH_R) y la posición del pico exotérmico, T_p, correspondiente a la reacción de curado. Por último, se ha determinado el comportamiento mecánico de los materiales mediante medidas del módulo elástico, la resistencia y la elongación en rotura.

2. EXPERIMENTAL

Las características de los materiales utilizados se resumen la Tabla 1.

Material	**Suministrador**	**Peso molecular (M_n)**	**Polidispersidad (r)**
DGEBA	Uneco S.A	380	-
PVAc	Polysciences	90000	2
DDM	Aldrich	198	-
NANORREFUERZOS			
Tipo	**Modificador**	**d interlaminar**	**Contenido**
Cloisita C30B Southern	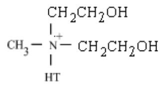 $CH_3-\overset{CH_2CH_2OH}{\underset{HT}{N^+}}-CH_2CH_2OH$	1.85 nm	90 (meq /100g silicato
Cloisita C93A Southern	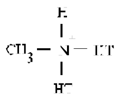 $CH_3-\overset{HT}{\underset{HT}{N^+}}-HT$	2.36 nm	95 (meq /100g silicato

Tabla 1. Características de los materiales utilizados.

Las muestras fueron preparadas siguiendo el siguiente protocolo: en primer lugar se mezclaron a 90ºC DGEBA y PVAc (5, 10, 15 y 20% en peso respecto a la mezcla DGEBA+DDM+PVAc) mediante agitación durante 4 horas, a continuación se añadió el 4% en peso de nanorrefuerzo, respecto a la masa total del sistema ternario, manteniendo las mismas condiciones de agitación y temperatura durante 18 horas más. Seguidamente las muestras fueron desgasificadas a vacío a 120ºC durante 2 horas. Se añadió el DDM, en cantidad estequiométrica, a 90ºC mediante agitación moderada. Las muestras fueron curadas en un horno a la temperatura de 120ºC durante 2 horas; realizando un poscurado adicional de 1 hora a 180 ºC. Los materiales obtenidos fueron caracterizados por difracción de rayos X utilizando un difractómetro XPERT_PRO_X-ray equipado con radiación CuKα, con objeto de determinar la distancia interlaminar.

Las medidas de DSC se realizaron en un equipo Mettler-Toledo mod.822e a 10ºC/minuto desde -60 a 300ºC. ΔH_R se obtuvo del área bajo la curva del pico exotérmico y la T_g de las muestras curadas se determinó como el punto medio del salto en la capacidad calorífica correspondiente al segundo barrido. Las medidas mecánicas fueron realizadas en una máquina universal de ensayos MTS mod. QTest 2L a la velocidad de elongación de 1mm/min. Los valores de módulo, resistencia y deformación en fractura son la media de al menos 5 probetas medidas de cada muestra.

3. RESULTADOS

El análisis por rayos X de todos los materiales muestra la presencia de un pico correspondiente a la distancia basal, situado a ángulos de difracción más bajos que los correspondientes a las Cloisitas puras. Mediante la ley de Bragg se ha calculado un valor de d_{100} ≈3.5 nm y d_{100} ≈3.3 nm para los materiales nanorreforzados con C30B y

C93A, respectivamente, independiente del contenido de PVAc y superior a los valores correspondientes a las Cloisitas puras d_{100}(C30B)=1.85 nm d_{100}(C93A)=2.36 nm. Aunque en ningún caso se ha conseguido la exfoliación del nanosilicato, las Cloisitas orgánicamente modificadas interaccionan con las moléculas orgánicas constitutivas del sistema ternario, provocando la separación de las láminas y aumentando el tamaño de las galerías interlaminares, alcanzándose en todos los casos una morfología intercalada. Aunque el espaciado interlaminar de los materiales obtenidos no depende significativamente del contenido de PVAc ni del tipo de nanosilicato empleado, si se toma como referencia la distancia d_{100} de los nanosilicatos puros se puede concluir que la mezcla DGEBA/PVAc/DDM penetra mejor en las galerías de C30B, lo que puede ser atribuido a la presencia de grupos hidroxilo en los modificadores orgánicos, que favorecería la interacción entre los componentes del sistema.

Los termogramas obtenidos para las mezclas DGEBA/PVAc/DDM conteniendo C30B y C93A muestran una transición vítrea a baja temperatura (T_g^o) que corresponde a la mezcla inicial no reaccionada, seguida de un pico exotérmico debido a la reacción de curado. Los valores del pico, T_p, y de ΔH_R referida a la masa de DGEBA se citan en la Tabla 2, comparados con los obtenidos para el sistema no reforzado.

	ΔH_R (J/g $_{DGEBA}$)			T_p(ºC)		
PVAc (%)	**sin**	**C30B**	**C93A**	**sin**	**C30B**	**C93A**
0	-583	-542	-535	164	162	162
5	-582	-561	-553	168	166	166
10	-555	-542	-549	172	170	171
15	-560	-534	-534	175	173	172
20	-539	-501	-505	182	180	172

Tabla 2. Datos correspondientes a los curados dinámicos de los materiales por DSC

En ausencia de modificador termoplástico, la presencia de Cloisitas provoca una disminución de ΔH_R respecto al sistema no reforzado, este comportamiento ya ha sido previamente observado para sistemas epoxi/DDM/C15A, C30B habiéndose comprobado que no puede ser atribuido a la existencia de reacción química entre el DGEBA y las Cloisitas (Prolongo et al, 2009). La presencia de termoplástico en el sistema atenúa la disminución del valor de ΔH_R. Se observan también diferencias en los valores de la temperatura del pico exotérmico. Para los sistema DGEBA/DDM/Cloisitas se aprecia un ligero desplazamiento de T_p hacia temperaturas más bajas, lo que indicaría la aceleración de la reacción. Este comportamiento puede atribuirse a la existencia de grupos hidroxilos (C30B) e hidrógenos ácidos (C93A) en los cationes alquilamonio modificadores, que actuarían como catalizadores de la reacción de curado. La presencia de termoplástico no afecta al descenso observado en T_p pudiéndose concluir que el sistema DGEBA/DDM/C30B se comporta de manera similar al sistema DGEBA/DDM/93A. Los barridos de DSC de los materiales totalmente curados indican la presencia de dos fases. Una fase rica en epoxi (T_g^{∞}) que coexiste con otra fase enriquecida en PVAc (T_{gPVAc}). En los sistemas no reforzados la presencia de PVAc provoca una ligera disminución del valor de T_g^{∞} (correspondiente a la fase epoxi), que no depende significativamente del contenido de PVAc en el sistema. De igual manera la presencia de epoxi rebaja el valor de la $T_{g\ PVAc}$ (correspondiente a la fase PVAc) cuando el contenido de PVAc en el sistema es inferior al 15% en peso. La presencia de nanopartículas minimiza el descenso observado en los valores de T_g correspondientes a la fase rica en epoxi mientras que no altera el comportamiento de la fase rica en PVAc. En la Tabla 3 se aportan los valores de las propiedades mecánicas determinadas para los sistemas epoxi/PVAc/Cloisitas.

PVAc	**Módulo (GPa)**			**Máxima Resistencia (MPa)**			**Deformación en fractura (%)**		
(%)	**sin**	**C30B**	**C93A**	**sin**	**C30B**	**C93A**	**sin**	**C30B**	**C93A**
0	2.5	3.0	2.8	63.0	64.5	53.9	3.8	3.4	2.9
5	2.4	3.0	2.7	62.0	65.7	51.7	4.4	3.1	3.0
10	2.2	3.0	2.9	59.2	59.6	56.4	5.9	4.1	3.8

Tabla 3. Propiedades mecánicas de los materiales estudiados.

La Tabla 3 indica que la presencia de la Cloisita C30B mejora los valores del módulo y la resistencia respecto a los sistemas sin nanorrefuerzo. Por su parte la Cloisita C93A sólo es capaz de mejorar ligeramente los valores del módulo. Este comportamiento puede ser justificado en función de la interacción más favorable entre la C30B y el material epoxídico modificado, así como por el mayor grado de intercalación conseguido para esta Cloisita que proporciona mayor superficie de contacto.

4. CONCLUSIONES

Se han preparado nanocompuestos formados por una matriz epoxi modificada con distintas cantidades de PVAc conteniendo un 4% de Cloisitas C30B y 93A. Mediante difracción de rayos X se ha comprobado que todos los nanocompuestos mostraban estructuras intercaladas con un espaciado interlaminar independiente del tipo de nanosilicato y del contenido de PVAc. El análisis por DSC ha permitido demostrar que la Cloisita C30B y C93A acelera la reacción de curado. La presencia de PVAc minimiza los cambios observados en la entalpía de reacción y en la posición del pico exotérmico. Los materiales obtenidos presentan una morfología heterogénea constituida por una fase enriquecida en epoxi que coexiste con una fase enriquecida en PVAc. Las propiedades mecánicas demuestran que la interacción favorable del refuerzo y un mayor grado de intercalación contribuyen a mejorar los valores del módulo y la máxima resistencia.

BIBLIOGRAFÍA

PROLONGO, M.G., MARTÍNEZ-CASADO, F.J., MASEGOSA, R.M., SALOM C (2009) Curing and dynamic mechanical thermal properties of epoxi/clay nanocomposites *Nanoscience and Nanotecnology. A*ceptado para publicación.

RAY, S.S., OKAMOTO, M. (2003) Polymer/layered silicate nanocomposites: a review from preparation to processing. *Progress in Polymer Science,* 28, 1539-1641.

AGRADECIMIENTOS

Este trabajo ha sido financiado por los proyectos MEC (MAT 2006-0213) y CAM (S-0505/MAT2007).

Análisis experimental del comportamiento a flexión dinámica de vigas sándwich

I. Ivañez, C. Santiuste, S. Sánchez-Sáez
Departamento de Mecánica de Medios Continuos y Teoría de Estructuras
Universidad Carlos III de Madrid, España

RESUMEN

En este trabajo, se ha analizado experimentalmente el comportamiento a flexión dinámica de vigas sándwich con pieles de fibra de vidrio/poliéster y núcleo de espuma de PVC. Se han llevado a cabo ensayos dinámicos de flexión en tres puntos, de los que se ha obtenido la fuerza de contacto, la energía absorbida y el desplazamiento máximo de ambas pieles. Se ha analizado la influencia de la energía de impacto sobre estas variables y en el modo de fallo de las vigas, observando que la compresión del núcleo bajo el área de contacto provoca una localización del daño que favorece la rotura de la piel superior.

1. INTRODUCCIÓN

Las vigas sándwich formadas por pieles de material compuesto y núcleo de espuma polimérica son utilizadas cada vez con más frecuencia como estructuras ligeras en las industrias automovilística, marina y aeroespacial, debido a la combinación de alta rigidez y resistencia a flexión, y bajo peso que presentan

Estas estructuras pueden estar sometidas a solicitaciones dinámicas que, por su naturaleza, pueden producir daños importantes que disminuyan la eficiencia de las vigas sándwich aunque, en general, los diseños de los que forman parte tienden utilizar su capacidad de deformación para absorber la energía del impacto y mitigar sus efectos. Por ejemplo, los vehículos sometidos a un impacto de baja velocidad, como pueda ser una colisión lateral en una zona urbana, deben poseer estructuras capaces de absorber la energía del impacto y soportar esfuerzos de flexión, reduciendo la transmisión de fuerzas a otras partes del vehículo y a sus ocupantes. Se resalta entonces la necesidad de realizar estudios detallados de cómo afecta la energía de impacto a los diferentes parámetros involucrados y de cómo se produce la absorción de energía en las estructuras.

Existen numerosos autores que describen el comportamiento a flexión estática de estas vigas (Stevees and Fleck 2004, Mines and Alias 2002, Shahdin et al. 2009), siendo menos conocido su comportamiento a flexión bajo condiciones dinámicas (Tagiarelli et al. 2007). En este trabajo se ha estudiado experimentalmente el comportamiento a flexión de vigas sándwich sometidas a impactos de baja velocidad, analizando la influencia de la energía de impacto sobre la fuerza máxima de contacto, la energía absorbida y los desplazamientos máximos de las pieles.

2. MATERIAL

Se ha utilizado un material sándwich formado por pieles de laminados de tejido de fibra de vidrio en matriz poliéster con 3 mm de espesor, y núcleo de espuma de PVC, de 100 kg/m^3 de densidad y 30 mm de espesor. El uso de estos materiales para conformar estructuras sándwich está bastante extendido debido a sus excelentes propiedades a flexión y se capacidad de absorción de energía.

3. ENSAYOS DINÁMICOS

Se han realizado ensayos de flexión en tres puntos en condiciones dinámicas utilizando una torre de caída de peso instrumentada, CEAST Fractovis 6785, que permitió registrar la fuerza ejercida por el percutor sobre la probeta. Se ha utilizado un percutor de cabeza Charpy de 20 mm de diámetro y 7,97 kg de masa total. Se han ensayado 20 vigas de sección rectangular (50 mm de anchura y 36 mm de espesor) y 480 mm de longitud, utilizando una distancia entre apoyos de 450 mm. Los ensayos, comprendidos en un rango de energías de impacto de entre 25 J a 75 J, se han grabado mediante una cámara de alta velocidad, lo cual ha permitido medir la velocidad de impacto del percutor sobre las probetas, la velocidad de rebote del percutor tras el impacto, así como el desplazamiento de ambas pieles. Tanto la energía de impacto como la absorbida, se calcularon a partir de las velocidades del percutor.

4. RESULTADOS

Las grabaciones de los ensayos han permitido realizar un examen visual del fenómeno del daño en las vigas sándwich. Se ha observado que para energías de impacto más bajas, la viga sándwich exhibe un comportamiento a flexión global, siendo similar el desplazamiento de ambas pieles durante todo el ensayo. Cuando aumenta la energía de impacto se produce bajo la zona del impacto una compresión localizada del núcleo, cuya densificación favorece la rotura de la piel superior. En la Fig. 1 se muestran dos imágenes en los momentos anterior y posterior a la rotura de la piel superior de la viga sándwich.

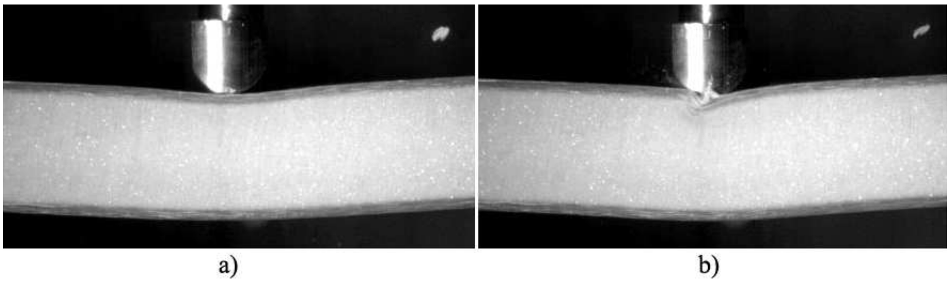
a) b)

Fig. 1. Imágenes correspondientes a un ensayo de energía de impacto de 52 J: a) antes de la rotura de la piel superior, b) después de la rotura de la piel superior.

Se ha obtenido la fuerza máxima de contacto en cada uno de los ensayos, Fig. 2.a. A pesar de que la rotura de la piel superior no se produjo para todas las energías de impacto utilizadas, la fuerza máxima exhibe valores prácticamente constantes para todos los ensayos, aumentando ligeramente con la energía de impacto.

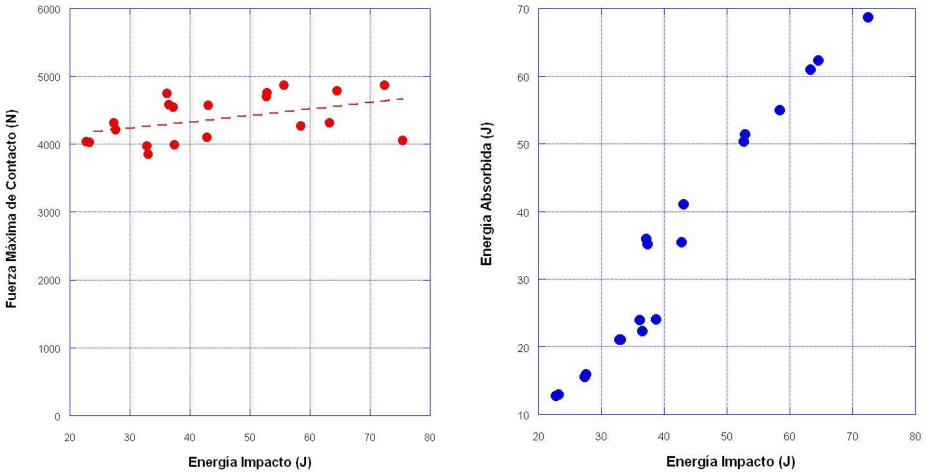

a) b)

Fig. 2. a) Fuerza máxima de contacto frente a energía de impacto, b) Energía absorbida frente a energía de impacto.

La energía absorbida en función de la energía de impacto se representa en la Fig. 2.b. Se puede distinguir en torno a los 37 J de energía de impacto un cambio brusco en los valores de energía absorbida, coincidiendo este cambio con la rotura de la piel superior. Para energías de impacto inferiores a ese valor, la energía absorbida por la viga corresponde a un 50-60% de la energía de impacto, mientras que para energías superiores, corresponde a un 94-97%. Para los niveles de energía de impacto en los que se produce la rotura de la piel superior, la energía absorbida se sigue incrementando con el aumento de la energía de impacto, lo que indica una contribución por parte de la deformación del núcleo de espuma al proceso de absorción de energía.

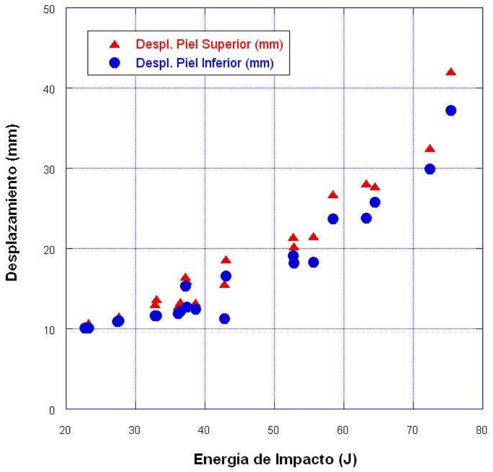

Fig. 3. Desplazamientos máximos de las pieles superior e inferior.

Los desplazamientos máximos de la piel superior e inferior se representan en la Fig. 3. Se observa un incremento de estos desplazamientos con el aumento de energía de impacto. La diferencia entre ambos desplazamientos máximos se hace más notable para energías de impacto superiores a 37 J, momento en el que se produce la rotura de la piel superior de las vigas sándwich. Para energías de impacto inferiores a 37 J, los desplazamientos máximos de ambas pieles son similares, debido a que la viga exhibe un comportamiento a flexión global.

5. CONCLUSIONES

El comportamiento a flexión dinámica de vigas sándwich con pieles de fibra de vidrio en matriz poliéster y núcleo de espuma de PVC, se ha analizado de forma experimental mediante ensayos de flexión en tres puntos en una torre de caída de peso. Se ha estudiado la influencia de la energía de impacto en la fuerza de contacto, la energía absorbida y el desplazamiento máximo de ambas pieles. La fuerza máxima de contacto presenta valores similares para todos los ensayos, a pesar de que la rotura de la piel superior no se produjo para todas las energías de impacto. Este hecho es significativo, pues aunque la energía de impacto aumente, los esfuerzos que se transmiten a los apoyos se mantienen prácticamente constantes. La energía absorbida presenta un salto en sus valores, que coincide con la energía de impacto a la que se produce la rotura de la piel superior de las vigas sándwich (aproximadamente 37 J). En los ensayos donde se produce la rotura de la piel superior, se ha observado una densificación del núcleo que favorece la absorción de energía. Esta densificación se confirma comparando los máximos desplazamientos de ambas pieles, cuyas diferencias aumentan notablemente a partir de ese valor de energía de impacto.

AGRADECIMIENTOS

Los autores desean agradecer a la Comunidad de Madrid y a la Universidad Carlos III de Madrid la financiación del Proyecto CCG08-UC3M/DPI-4348, que ha permitido la realización de este trabajo.

REFERENCIAS

MINES, R.A.W., ALIAS A. (2002). Numerical simulation of the progressive collapse of polymer composite sandwich beams under static loading. *Compos Part A-Appl S.,* 33, 11-26.

SHAHDIN A., MEZEIX L., BOUVET C., MORLIER J., GOURINAT Y. (2009). Fabrication and mechanical testing of glass fiber entangled sandwich beams: A comparison with honeycomb and foam sandwich beams. *Compos Struct.*, doi:10.1016/j.compstruct.2009.04.003.

STEEVES C.A., FLECK N. A. (2004). Collapse mechanism of sandwich beams with composite faces and a foam core, loaded in three-point bending. Part II: experimental investigation and numerical modelling. *Int J Mech Sci.*, 46, 585-608.

TAGARIELLI V.L., DESHPANDE V.S., FLECK N.A. (2007). The dynamic response of composite sandwich beams to transverse impact. *Int J Solids Struct.*, 44, 2442-2457.

Corrección de la flexibilidad en los ensayos de fractura intelaminar en modo I de materiales compuestos de fibra de carbono y matriz epoxi

J. Bonhomme[1], A. Argüelles[1], J. Viña[2], I. Viña[1], M.A. Castrillo[1]
[1]Departamento de Construcción e Ingeniería de Fabricación, Universidad de Oviedo, Campus Universitario s/n, 33203 Gijón, España
[2]Departamento de Ciencia de los Materiales e Ingeniería Metalúrgica, Universidad de Oviedo, Campus Universitario s/n, 33203 Gijón, España

RESUMEN

En este trabajo se evalúa la tasa de relajación crítica de energía (G_c) en modo I y la influencia que sobre dichos valores tiene la corrección por flexibilidad de los dispositivos de ensayo. El cálculo de G_{Ic} se llevó a cabo mediante métodos experimentales y numéricos en un material compuesto unidireccional de fibra de carbono y matriz epoxi AS4/8552

Los resultados preliminares, sin aplicación de correcciones, mostraron una diferencia del 20% entre los valores de G_{Ic} experimental y teórico utilizando la carga (P_c) como parámetro crítico para el cálculo y del 30% en caso de utilizar el desplazamiento crítico (δ_c). La introducción de correcciones por flexibilidad de los sistemas de ensayo permite disminuir la diferencia entre los valores numéricos y experimentales por debajo del 10%.

1. INTRODUCCIÓN

En este trabajo se ha caracterizado la tasa de relajación crítica de energía en modo I por procedimientos experimentales y numéricos aplicando el método de cálculo por elementos finitos (MEF).La convergencia de ambos métodos es muy importante con objeto de garantizar la seguridad en la predicción del fallo por deslaminación en las estructuras realizadas con materiales compuestos.

En trabajos previos se han encontrado diferencias del 20-30% entre los resultados numéricos y experimentales (Bonhomme et al. 2009). El objetivo de este trabajo es el de determinar las posibles causas de esta diferencia y mejorar la convergencia entre ambos métodos

2. MATERIALES Y MÉTODOS

Los ensayos experimentales se llevaron a cabo siguiendo la norma ASTM D 5528 utilizando probetas DCB (Double Cantilever Beam). Esta configuración de ensayo es la más común para la determinación del valor crítico de G en modo I. A diferencia del modo II en el que todavía existe una cierta controversia sobre el procedimiento de ensayo (Blackman et al. 2006), el modo I es un método ampliamente aceptado y establecido.

Con objeto de conectar las probetas con las mordazas de la máquina, se utilizó un sistema de bisagras. En la figura 1 se muestra un esquema del ensayo.

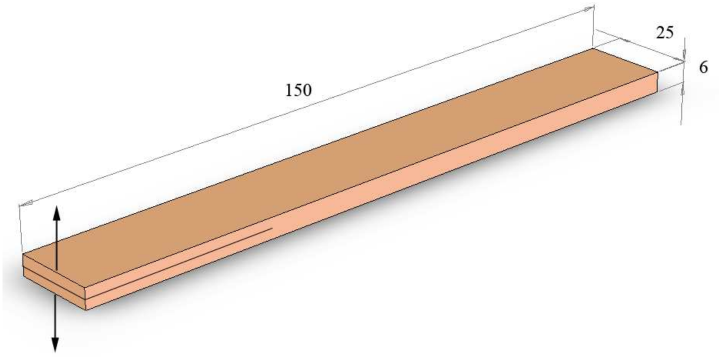

Figura 1. Probeta DCB.

El material usado en este estudio fue el Hexcel AS4/8552 de 6 mm de espesor y configuración unidireccional. La estructura del laminado era $[0°]_{16s}$. Se ensayaron cinco probetas. El ensayo se llevó a cabo en una máquina MTS con una velocidad de desplazamiento de 0,5 mm/min. Debido a la gran linealidad que presentaba la curva de ensayo, se tomó como valor crítico la carga máxima.

El valor de G_{Ic} se calculó por los tres métodos propuestos por la norma ASTM D 5528. Entre éstos métodos, la teoría de la viga modificada fue la que proporcionó un valor más bajo de la desviación estándar por lo que dicho método fue seleccionado como valor de referencia para comparaciones posteriores.

$$G_{Ic} = \frac{3P\delta}{2B\left(a+|\Delta|\right)} \qquad (1)$$

Por otra parte, los ensayos experimentales se modelizaron mediante el método de cálculo por elementos finitos (MEF). Existen varios métodos numéricos documentados en bibliografía para el cálculo de G_{Ic} (Wimmer et al.2006). Entre éstos, los métodos de cierre virtual de la grieta (VCCT) y extensión de la grieta en dos pasos son los más utilizados habitualmente (Krueger et al. 2004), (Rybicki y Kanninen 1997), (Singh et al. 1998), (Hellen 1975). En este estudio, G_{Ic} ha sido calculado por diferencia entre la energía elástica antes y después de la apertura de la grieta ya que este método fue validado en un estudio previo (Bonhomme et al. 2009). En ese mismo estudio se estudiaron diferentes tipos y tamaños de elementos. Se estudiaron elementos 2D y 3D con y sin nodos intermedios. También se estudiaron elementos colapsados y elementos estándar. En todos los casos se llegó a la conclusión de que estas variables no tenían un efecto significativo sobre el cálculo de G_{Ic}.

Respecto al tamaño de los elementos, se observó que los resultados convergían hacia un valor constante a medida que disminuía dicho tamaño. En el presente trabajo se utilizó una relación $a/a_0 = 1/150$ siendo:

- a: longitud de la deslaminación
- a_0: longitud inicial de grieta

3. RESULTADOS EXPERIMENTALES Y NUMÉRICOS

En la tabla 1 se comparan los resultados experimentales y numéricos obtenidos en este estudio.

	Experimental		MEF	
	Rigidez (N/mm)	G_{Ic} (J/m^2)	Rigidez (N/mm)	G_{Ic} (J/m^2)
	73,12 ± 10,20	298,12 ± 35,68	99,84 ± 11,31	250,06±55,27
Error	26%	20%	---	---

Tabla 1. Resultados numéricos y experimentales.

Como se puede ver en esta tabla, existe una diferencia notable entre la rigidez de los modelos numéricos y experimentales, y como resultado, una diferencia apreciable entre los valores de G_{Ic} obtenidos. Otra consecuencia de esta diferencia de rigidez es que los valores obtenidos en los cálculos numéricos dependen del valor crítico experimental utilizado como parámetro de entrada en el modelo de elementos finitos (P_c y δ_c).

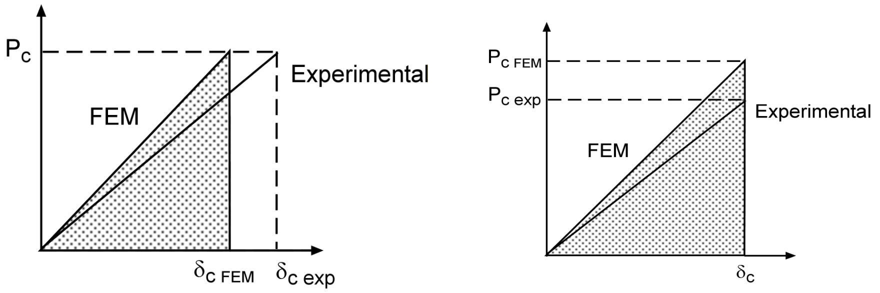

Figura 2. Diferencia de rigidez entre los modelos teóricos y experimentales.

A partir de estos resultados previos, se hizo necesario implementar un método para determinar la influencia de la flexibilidad propia de ensayo e introducir la correspondiente corrección en los cálculos numéricos y experimentales.

4. CORRECCIÓN POR FLEXIBILIDAD

Con objeto de determinar la flexibilidad propia de los útiles de ensayo se decidió ensayar probetas DCB sin grieta en su plano medio como se muestra en la figura 3.
Se realizaron cinco ensayos. El valor medio obtenido de la rigidez del sistema de ensayo fue 365.6 ± 29.0 N/mm. Esta corrección se aplicó en los modelos experimentales y numéricos y se recalcularon los valores de G_{Ic}. La diferencia obtenida entre los valores de rigidez de ambos modelos fue del 8% y la diferencia entre los valores de G_{Ic} disminuyó hasta el 9%.

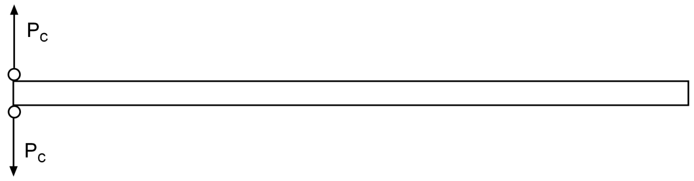

Figura 3. Ensayo para la determinación de la flexibilidad propia de ensayo en modo I.

5. CONCLUSIONES

La introducción de correcciones debidas a la flexibilidad propia del ensayo es una cuestión importante a tener en cuenta en la determinación de los valores de G_{Ic} ya que la norma de ensayo permite la utilización de diferentes procedimientos para conectar las probetas con la máquina de ensayo.

Para eliminar la influencia de estas flexibilidades es necesario utilizar un extensómetro adecuado para la medida correcta de los desplazamientos. Debido a que en ocasiones resulta difícil la aplicación de estos dispositivos, se ha demostrado que la realización de ensayos previos para la determinación de la flexibilidad de los útiles de ensayo y la posterior introducción de las correcciones en los cálculos, es un procedimiento adecuado para la obtención de los valores de G_{Ic} de una manera suficientemente precisa.

REFERENCIAS

BLACKMAN, B.R.K., BRUNNER, A.J., WILLIAMS, J.G. (2006) Mode II fracture testing of composites: a new look at an old problem *in Engineering Fracture Mechanics* (Ed. Elsevier), 73, 2443-2455

BONHOMME, J., ARGÜELLES, A., VIÑA, J., VIÑA, I. (2009) Numerical and experimental validation of computational models for mode I composite fracture failure *in Journal of Computational Material Science* (Ed. Elsevier), 45, 993-998

HELLEN, T.K., (1975), On the method of virtual crack extension, in International Journal for Numerical Methods in Engineering, (Ed. Wiley InterScience), 9(1), 187-207

KRUEGER, R., (2004), Virtual crack closure technique. History, approach and applications *in Applied Mechanics Reviews*, (Editor: J. N. Reddy Texas A&M University), 57, 109-143

RYBICKI, E.F., KANNINEN, M.F., (1977), A finite element calculation of stress intensity factors by a modified crack closure integral, *in Engineering Fracture Mechanics*, (Ed. Elsevier), 9, 931-938

SINGH, R., CARTER, B.J., WAWRZYNEK, P.A., INGRAFFEA, A.R., (1998), Universal crack closure integral for SIF estimation *in Engineering Fracture Mechanics*, C 60, 133-146

WIMMER, G., SCHUECKER, C., PETTERMANN, H.E., (2006) Numerical simulation of delamination, onset and growth in laminate composites, in Austrian Aeronautics Research, Network for Materials and Engineering, ILDSB, Vienna University of Technology.

Tensiones termomecánicas en materiales compuestos de fibra de carbono con matriz epoxi

M.A. Cantera, I. Adarraga, J.M. Romera, F. Mujika
Departamento Ingeniería Mecánica, Escuela Politécnica. Universidad del País Vasco/Euskal Herriko Unibertsitatea

RESUMEN

El enfriamiento en el proceso de fabricación en los laminados compuestos genera deformaciones a temperatura ambiente. En el caso de laminados asimétricos de configuración [θ/90-θ] con forma de tira estas deformaciones están asociadas a la existencia de tensiones residuales de flexión y torsión. El presente trabajo analiza las previsiones de la Teoría Clásica de Placas Laminadas (TCPL) y de una nueva aproximación teórica llamada Teoría de Tiras Laminadas (TTL) que asume una situación de tensión plana siendo en los bordes la tensión σ_y nula. Tras estudiar la sensibilidad de distintos factores en ambas aproximaciones, se aprecia que el coeficiente de dilatación térmico transversal α_2 es fundamental. Asimismo, para determinar desplazamientos de torsión se desarrolla una parte experimental de medición mediante máquina de medición tridimensional por coordenadas de deformaciones en laminados [θ/90-θ] de fibra de carbono T6T en matriz epoxi F593 obtenidos a partir de prepregs por compresión en caliente.

1. INTRODUCCIÓN

Las tensiones residuales de los materiales compuestos se generan durante el enfriamiento desde la temperatura de curado hasta la ambiente, principalmente debido a la desigualdad de coeficientes térmicos de expansión (CTE) entre la fibra y la matriz. Las propiedades de las capas unidireccionales en la dirección longitudinal están casi dominadas por el alto módulo de la fibra y el bajo coeficiente de expansión. Por el contrario, en la dirección transversal, las propiedades de la matriz predominan sobre la fibra, originado unos módulos menores y mayores coeficientes de dilatación térmica.

En el laminado, la secuencia de apilamiento de las capas y su disposición simétrica o asimétrica influyen tanto en la forma del material compuesto a temperatura ambiente como en las tensiones térmicas entre capas, que pueden original un fallo prematuro en la matriz. Estudios realizados por Hyer (1981) concluyen que en la práctica la forma del laminado depende de las relación del ancho/espesor. Los laminados delgados empleados por Hamamoto y Hyer (1987) tienen una relación lineal temperatura/curvatura en las que dos formas cilíndricas son posibles. Schlecht, Schulte e Hyer (1995) desarrollan para laminados cuadrados cruzados [$0_n/90_m$] una extensión de la TCPL basada en análisis por elementos finitos (FEA) para prever las formas deformadas de estos laminados.

Carbajal et al.(2008) proponen una aproximación analítica para predecir la curvatura cilíndrica de flexión en laminados cruzados asimétricos [$0_n/90_m$] con geometría de tira. En la literatura no se han encontrado análisis de tensiones fuera del plano para estos laminados asimétricos con geometría de tira. El presente trabajo profundiza en la torsión en laminados asimétricos de configuración [θ/90-θ].

2. MODELO TEÓRICO

El modelo teórico ampliamente empleado para el análisis de comportamiento elástico de materiales compuestos multidireccionales por numerosos autores es la TCPL. Mujika (2009) desarrolla un marco teórico para el estudio de laminados planos con geometría de tiras, llamado Teoría de Tiras Laminadas (TTL) que asume $\sigma_y = 0$ y $\tau_{yz} = 0$. Considerando los efectos higrotérmicos $e_i = \alpha_i \Delta T + \beta_i \Delta c$, las ecuaciones de tensión plana resultan:

$$\begin{Bmatrix} \sigma_x \\ \tau_s \end{Bmatrix}_k = \begin{bmatrix} q_{xx} & q_{xs} \\ q_{xs} & q_{ss} \end{bmatrix}_k \left(\begin{Bmatrix} \varepsilon_x \\ \gamma_s \end{Bmatrix} + z \begin{Bmatrix} \kappa_x \\ \kappa_s \end{Bmatrix} - \begin{Bmatrix} e_x \\ e_s \end{Bmatrix}_k \right) \text{donde} \begin{bmatrix} q_{xx} & q_{xs} \\ q_{xs} & q_{ss} \end{bmatrix}_k = \begin{bmatrix} S_{xx} & S_{xs} \\ S_{xs} & S_{ss} \end{bmatrix}_k^{-1} \tag{1}$$

Y la relación entre los coeficientes de la matriz de rigidez q_{ij} (TTL)con Q_{ij}(TCP) es:

$$q_{xx} = \left(Q_{xx} - \frac{Q_{xy}^2}{Q_{yy}} \right) \qquad q_{xs} = \left(Q_{xs} - \frac{Q_{ys} Q_{xy}}{Q_{yy}} \right) \qquad q_{ss} = \left(Q_{ss} - \frac{Q_{ys}^2}{Q_{yy}} \right) \tag{2}$$

Definiendo las fuerzas y momentos por unidad de longitud igual que en TCP, resulta:

$$\begin{aligned} \begin{Bmatrix} n_x \\ n_s \end{Bmatrix} &= \sum_{k=1}^{n} \int_{z_{k-1}}^{z_k} \begin{Bmatrix} \sigma_x \\ \sigma_s \end{Bmatrix}_k dz = [a] \begin{Bmatrix} \varepsilon_x^0 \\ \gamma_s^0 \end{Bmatrix} + [b] \begin{Bmatrix} \mathrm{k}_x \\ \mathrm{k}_s \end{Bmatrix} - \begin{Bmatrix} n_x^{TH} \\ n_s^{TH} \end{Bmatrix} \\ \begin{Bmatrix} m_x \\ m_s \end{Bmatrix} &= \sum_{k=1}^{n} \int_{z_{k-1}}^{z_k} \begin{Bmatrix} \sigma_x \\ \sigma_s \end{Bmatrix}_k z dz = [b] \begin{Bmatrix} \varepsilon_x^0 \\ \gamma_s^0 \end{Bmatrix} + [d] \begin{Bmatrix} \mathrm{k}_x \\ \mathrm{k}_s \end{Bmatrix} - \begin{Bmatrix} m_x^{TH} \\ m_s^{TH} \end{Bmatrix} \end{aligned} \tag{3}$$

siendo

$$a_{ij} = \sum_{k=1}^{n} q_{ij}^k (z_k - z_{k-1}) \quad b_{ij} = \frac{1}{2} \sum_{k=1}^{n} q_{ij}^k (z_k^2 - z_{k-1}^2) \quad d_{ij} = \frac{1}{3} \sum_{k=1}^{n} q_{ij}^k (z_k^3 - z_{k-1}^3) \tag{4}$$

Invirtiendo (3) y reagrupando queda

$$\begin{Bmatrix} \varepsilon_x^0 \\ \gamma_s^0 \\ \kappa_x \\ \kappa_s \end{Bmatrix} = \begin{bmatrix} f_{xx} & f_{xs} & g_{xx} & g_{xs} \\ f_{xs} & f_{ss} & g_{sx} & g_{ss} \\ g_{xx} & g_{sx} & h_{xx} & h_{xs} \\ g_{xs} & g_{ss} & h_{xs} & h_{ss} \end{bmatrix} \left(\begin{Bmatrix} n_x \\ n_s \\ m_x \\ m_s \end{Bmatrix} + \begin{Bmatrix} n_x^{TH} \\ n_s^{TH} \\ m_x^{TH} \\ m_s^{TH} \end{Bmatrix} \right) \tag{5}$$

El sistema de ecuaciones (5) permite estudiar los efectos acoplados de flexión y torsión mediante los valores de κ_x κ_s en laminados con capas de distinta orientación. Los valores asociados con la curvatura a flexión κ_x en TCP y TTL son similares.

3. ANÁLISIS DE SENSIBILIDAD DE FACTORES EN EL CÁLCULO DE κ_s

Se realiza un análisis de sensibilidad en el cálculo de κ_s de los siguientes factores:

- Los relacionados con características de material: E_1, E_2, G_{12},ν_{12}
- Los relacionados con la geometría de la probeta: espesor de cada capa y total *h*, anchura y longitud de la tira, pequeñas variaciones de ángulo de configuración.
- Los relacionados con comportamiento térmicos: Coeficiente de dilatación térmica longitudinal α_1 y transversal α_2 incremento de temperatura ΔT

Tomando como valores de referencia para el material T6T/F593, E_1 = 11.400 MPa, E_2,= 7.000 MPA, G_{12},= 4.500MPA y ν_{12} =0,3 se observa que variaciones de un 20% de los mismos tienen poco impacto en κ_s. (sensibilidad baja). El espesor total del laminado h tiene mayor influencia que los de cada capa y pequeñas variaciones de los ángulos de inclinación. Pero sin duda alguna, el factor más influyente es CTE α_2.

Bowles D.E. et al (1998) realiza una revisión de los distintos métodos de micromecánica existentes de distinto grado de complejidad para predecir CTE, sin embargo es difícil obtener valores fiables en la dirección radial a la fibra. Las mejores predicciones tienen una variación respecto al valor medido de hasta el 15% y otros análisis hasta el 50%.

4. DETERMINACIÓN DE DESPLAZAMIENTOS DE TORSIÓN

Se han fabricado 4 placas de T6T/F593 294x295mm por compresión en caliente en la prensa SANTEC de 30t de configuración $[0_n/90_m]$ de espesores nominales de 2,8 mm, 2,4mm, 1,60 mm. Se han obtenido probetas de configuración $[10_n/-80_n]$, $[30_n/-60_n]$, $[45_n/-45_n]$. n = 4,5, 6 En cada probeta se cuantificado la torsión en 5 líneas paralelas al extremo empotrado. Los espesores de las capas del laminado se han medido con microscopio óptico.

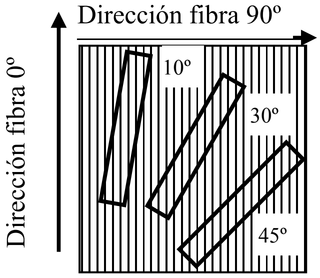

Fig 1. Orientaciones de probetas.

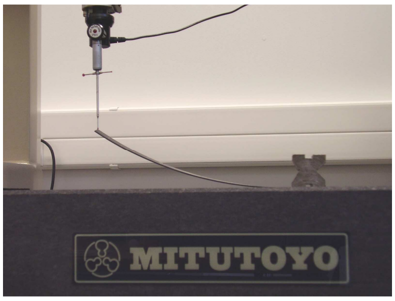

Fig 2. Maquina de medición empleada.

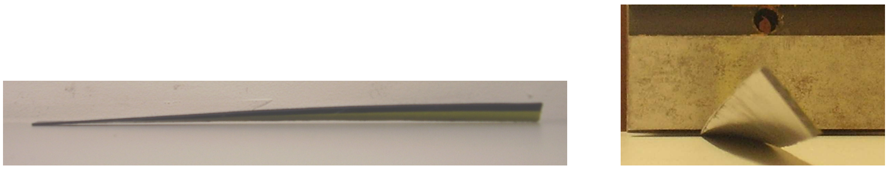

Fig 3. Probetas $[45_4/-45_4]$ donde se aprecian desplazamientos de torsión.

3. CONCLUSIONES

Las configuraciones asimétricas de laminados con forma de tira empleadas en el presente trabajo son adecuadas para el estudio de la flexión y torsión de origen térmico. Para la profundización de este análisis es conveniente utilizar aproximaciones micromecánicas adecuadas de α_2 con el fin de avanzar en la comparativa de los dos modelos teóricos expuestos.

AGRADECIMIENTOS

Los autores desean agradecer a HEXEL COMPOSITES el material suministrado T6T/F593 en forma de prepreg.

Mechanical and cure properties of devulcanizable SBR scraps composites

A. Zanchet, C. Ballico, M. Giovanela, J.S. Crespo
Centro de Ciências Exatas e Tecnologia, Universidade de Caxias do Sul, Brazil
L.N. Carli
Programa de Pós-Graduação em Ciência dos Materiais, Universidade Federal do Rio Grande do Sul, Brazil
R.C.R. Nunes
Instituto de Macromoléculas Professora Eloísa Mano, Universidade Federal do Rio de Janeiro, Brazil

SUMMARY

Environmental concern about waste management systems has stimulated the search of technological and economic alternatives, which waste can be introduced as raw material to the production cycles. The aim of this study was to develop and characterize styrene-butadiene rubber (SBR) composites containing industrial rubber scraps devulcanized by microwave. The scraps were ground under ambient conditions. From the obtained powder (SBR-r), 21 composites were prepared, varying the time exposure of the powder to the micro-waves (1, 2 and 3 min) and the SBR-r content. These composites were compared with a control sample (base formulation with 0 phr of SBR-r). The vulcanization parameters were determined by an oscillating disk rheometer. After curing, the composites were characterized by density and physical-mechanical properties (Shore A hardness, resilience, compression set, tensile and tear strength). The results showed that increasing the exposure time of the waste to the micro-waves had no significant influence in the composite properties.

1. INTRODUCTION

Among several techniques, the microwave devulcanization present some advantages that distinguish it as a most promising process of rubber recycling (Adhikari et to. 2000, Fang et to. 2001). The advantages include treatment of large amounts of material, the possibility of a continuous process with easy to adjust parameters, such as the power source and time of treatment. The latter is particularly important, as each type of rubber, with its own characteristics, will need a specific degree of devulcanization to produce a useful material (Scuracchio et to. 2006, 2007). In this context, the objective of this work is to develop and characterize formulations capable of vulcanizing and with technological applications, using industrial residues of butadiene-styrene copolymer (SBR-r). The development of the formulations was based on the devulcanization of residues with microwaves, followed by the incorporation of the processed residue into neat elastomer. The characterization determined the physical, rheological and mechanical properties of the residue and the obtained formulations.

2. EXPERIMENTAL

2.1Materials

The vulcanized elastomeric residues of SBR, composed of scraps from expanded extruded products, were collected according to ASTM E 300-03 at Ciaflex Indústria de Borrachas Ltda, RS-Brazil.

2.2 Grinding of scraps and characterization

The residue was ground mechanically, at ambient temperature. The obtained powder (SBR-r) presented an average particle size of 28 to 35 mesh (0.425 to 0.60 mm), and the following partial composition: 27.6% SBR, 34.1% $CaCO_3$, 24.1% oil, 12.1% carbon black, and 2.1% residual mass. The gel content was 95.8% (Carli et to. 2009).

2.3 SBR-r treatment with microwaves

The SBR-r was treated in adapted equipment, consisting of a Home Electrolux model 27E microwave oven with a stirring system. The equipment power was programmed to 700 W, and 100 g of SBR-r were added into a 600 mL beaker, and the sample was stirred at 40 rpm. The processing parameter used in this work is the time of exposure of the SBR-r to the microwaves, varying from 1 to 3 minutes.

2.4 Rheometry and specimens development

The curing characteristics were determined using an oscillatory disc rheometer Pro-Rheotech OD+, at 160 °C, according to ASTM D 2084-06. The vulcanization was carried out in a Luxor hydraulic press at 160 °C and under a 10 MPa pressure at the optimum vulcanization time values (t_{90}) determined by rheometric analysis.

2.5 Characterization of composites

The physical characterization of the specimens was carried out through the determination of mixtures and vulcanized composites densities (ASTM D 297-06). The Shore A hardness tests were carried out in a Shore A Teclock GS709 durometer (ASTM D 2240-05). The resilience test followed the ASTM D 1054-02, which was carried in a VEB TIW Rauenstein resiliometer. The compression set tests were carried following the ASTM D 395 B-03-Method A. The tensile strength, elongation at break and tear resistance properties were measured in an EMIC DL 3000, according to ASTM D 412-06a and ASTM D 624-00, respectively.

3. RESULTS AND DISCUSSION

Figure 1 presents the results concerning the vulcanization parameters of the developed composites. The minimum torque (M_L) is related with the viscosity of non-vulcanized compositions, while the maximum torque is (M_H) is related to the molecular stiffness, caused by the formation of crosslinks. The results showed that as the amount of SBR-r increased, the values of M_H decreased, indicating a lower molecular stiffness. This can be related to the decrease in the amount of unprocessed rubber, where the crosslinks are formed. The M_L values increased with the incorporation of the residue, indicating a higher viscosity of the material. The ΔM values, which are influenced by the amount of residue in the compositions, decreased with the addition of SBR-r for all studied compositions, particularly for the compositions without treatment (0 min of-exposure to the microwaves) and for higher amounts of SBR-r.

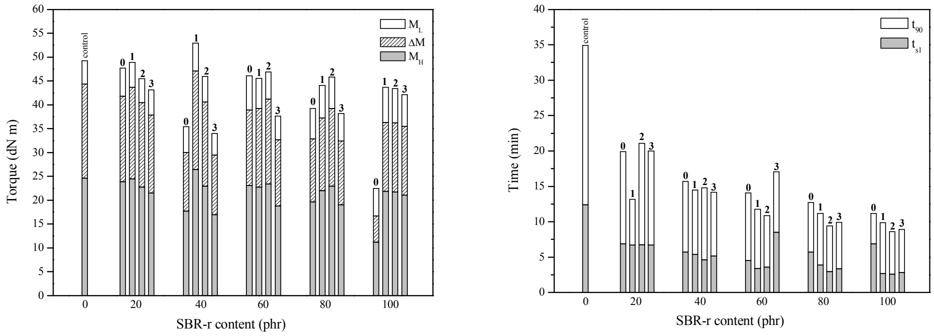

Fig. 1. Vulcanization parameters of the developed composites. The number 0, 1, 2 and 3 indicates the time (min) of exposition of the SBR-r to the microwaves.

The parameter t_{90} is of high importance, as it indicates the optimum vulcanization time of the specimens without degradation and aging of the mixtures. The addition of SBR-r caused a decrease of this parameter, indicating that the composites vulcanize at lower times. The t_{S1}, on the other way, indicates the safety time of the process before the formation of crosslinks. As it can be observed, this parameter decreased with the increasing amount of incorporated residue. The decrease of the t_{90} and t_{S1} values was caused by the presence of residual acceleration systems often present in this type of residue (Nelson et to. 2002). This reduction has not been influenced by the time of exposure of the SBR-r to the microwaves.

The values of density for the mixtures as well as for the vulcanized composites increased with the increasing amount of incorporated residues. It was also verified an increase in density of the vulcanized composites, compared to the mixtures, caused by the compression molding process. Figure 2a presents the values of hardness, resilience and compression set of the obtained composites, varying the amount of SBR-r and the exposure time to the microwaves. Observing the hardness results, considering the standard deviation, it was not observed a significant variation in the property with the incorporation of devulcanized residues. There was a slight decrease for the resilience values with the incorporation of the residue, indicating a decrease in the elasticity of the polymeric matrix, due to the incorporation of the SBR-r. Compression set values indicated that the higher amount of incorporated residue in the compositions caused a reduction on the values of this property. This result indicated an increase in the elastic recovery of the material to the imposed deformation. In a general way, these properties had not been influenced by the exposure time of the residue to the microwaves. Figure 2b shows the results of tensile strength and elongation at break for the developed composites. For tensile strength, it was observed that the higher amount of SBR-r and the exposure time to the microwaves caused a gradual decrease of this property. It is possible that, for higher concentrations of SBR-r, the reinforcing effect of the filler is counterbalanced by the filling effect, as a result of the weak interaction between the unprocessed matrix and the SBR-r (Ishiaku et to. 2002). As the concentration of SBR-r increases, the aggregation and particle-particle interaction of the powder also increase, which can cause a decrease on the mechanical properties. For elongation at break, it was verified an increase on the property values when compared with the control sample. This increase in elasticity of the composites was observed earlier in the compression set analysis. It was not observed a variation with the amount of incorporated residue and the time of devulcanization in the microwaves. It was also observed that the best result was obtained for the mixture with 80 phr of residue and 1 min of devulcanization. The data show that the increase in time of exposure to the microwaves and, mainly, the increase in the amount of SBR-r caused a significant loss of property, compared to the control sample.

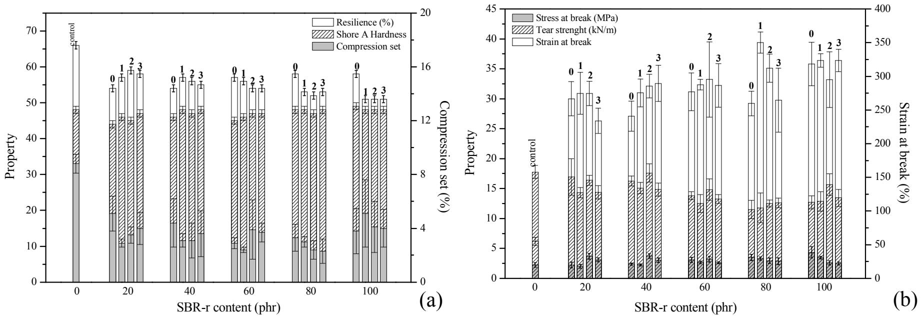

Figure 2: Physical-mechanical properties of the composites. The number 0, 1, 2 and 3 indicates the time (min) of exposition of the SBR-r to the microwaves.

4. CONCLUSIONS

The treatment of rubber with microwaves may cause breakage of crosslinks and the degradation of the main polymer chain. While the breaking of crosslinks allows the material to be reprocessed, the degradation of the main polymer chain, which is inevitable, causes a loss in the mechanical properties. As the main conclusion, this work showed that the treatment with microwaves is a viable technique for rubber recycling. However, it is necessary to study different ways to reduce the degradation of the main polymer chain and, consequently, obtain better mechanical properties.

REFERENCES

ADHIKARI, B., DE, D., MAITI, S. (2000). Reclamation and recycling of waste rubber. *Prog. Poly. Sci.*, 25, 909-948.

CARLI, L.N., BONIATTI, R., TEIXEIRA, C.E., NUNES, R.C.R., CRESPO, J.S. (2009). Development and characterization of composites with ground elastomeric vulcanized scraps as filler. *Mater. Sci. Eng. C*, 29, 383-386.

FANG, Y., ZHAN, M., WANG, Y. (2001). The status of recycling of waste rubber. *Mater. Des.*, 22, 123-127.

ISHIAKU, U.S., CHONG, C.S., ISMAIL, H. (2000). Cure characteristics and vulcanizate properties of a natural rubber compound extended with convoluted rubber powder. *Polym. Testing*, 19, 507-521.

NELSON, P.A., KUTTY, S.K.N. (2002). Cure characteristics and mechanical properties of butadiene rubber/whole tyre reclaimed rubber blends. *Progr. Rubber Plast. Tech.*, 18, 85-97.

SCURACCHIO C.H., WAKI, D.A., BRETAS, R.E.S. Caracterização térmica e reológica de borracha de pneu vulcanizada por microondas. (2006). *Polímeros*, 16, 46-52.

SCURACCHIO, C.H., WAKI, D.A., SILVA, M.L.C.P. (2007). Thermal analysis of ground tire rubber devulcanized by microwaves. *J. Therm. Anal. Calorim.*, 87, 893-897.

Propiedades de impacto, fractura y DMTA de una resina epoxi cargada con carbonato de calcio

F.J. Juanes, A. Valea, M.L. González, J.C. Míguez

Departamento Ingeniería Química y del Medio Ambiente. Escuela Universitaria de Ingeniería Técnica Industrial. Universidad del País Vasco/Euskal Herriko Unibertsitatea

RESUMEN

En el presente trabajo se estudian las propiedades mecánicas de un sistema compuesto basado en una resina epoxídica tetrafuncional (tetraglicidil difenil metano: TGDDM) curada en proporción estequiométrica con una diamina aromática (m-fenilen diamina: m-PDA). A dicho sistema se le ha adicionado carbonato cálcico de distintos tamaños micrométricos variando los porcentajes de la carga inorgánica incorporada. El estudio de los sistemas postcurados se ha realizado mediante ensayos de impacto, de fractura y de análisis termomecánicodinámico que informan sobre las propiedades del material básicas para su utilización en el diseño de piezas funcionales de alta rigidez. Esta rigidez se espera que se acentúe por la incorporación creciente de cargas inorgánicas. Por otra parte la disminución del tamaño de carga suele estar asociado a un incremento de la resistencia de estos materiales compuestos.

1. INTRODUCCIÓN

En los últimos años hay un interés muy considerable en la potenciación de sistemas multifase tales como los de resinas altamente entrecruzadas y partículas inorgánicas donde se puedan obtener mejoras en la tenacidad sin que disminuyan las resistencias del material. La mayor parte de los sistemas epoxídicos investigados han sido basados en resinas bifuncionales (Chin et al. 2001, Kornmann et al. 2001, Jiankun et al. 2001), aunque la mayoría de materiales para aplicaciones de alto rendimiento demandan epoxis de alta funcionalidad ya que se requieren mayores módulos y mayores temperaturas de transición vítrea. Estos sistemas más altamente entrecruzados son más difíciles de aumentar su tenacidad por lo que cualquier incremento será beneficioso.

2. IMPACTO

2.1 Resistencia al impacto

En la Figura 1 se recogen los valores de energía total a rotura por unidad de área (Rs, resistencia al impacto) obtenidos en los ensayos de impacto, mostrando sus variaciones según se incrementa la cantidad de carga incorporada y para los distintos tipos de carga utilizada. Estos valores son relativamente bajos pero acordes con los de otros trabajos con resinas TGDDM (Harismendy I. et al. 1998). Por otra parte, el comportamiento observado de la energía a impacto muestra un incremento general de la capacidad de absorción de energía con la incorporación de la carga. El incremento es, a porcentajes bajos, menor para la carga más pequeña, pero esta relación se invierte a altos porcentajes de carga, siendo la carga de menor tamaño la que ofrece los mejores resultados de energía de impacto y la carga mayor la que ofrece los peores resultados.

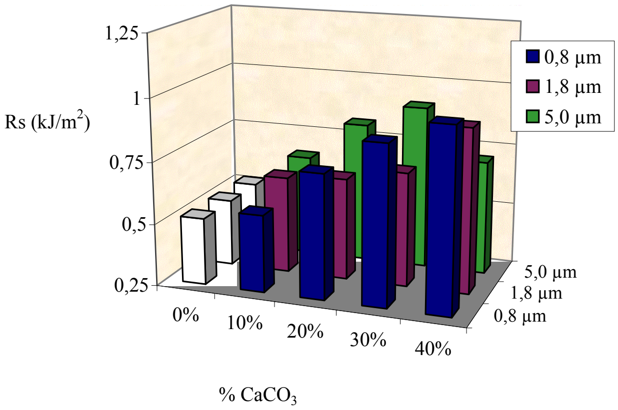

Figura 1. Variación de la resistencia al impacto (Rs) de los sistemas TGDDM/mPDA cargados con distintas proporciones y tamaños de $CaCO_3$.

3. FRACTURA

3.1. Factor crítico de intensidad de esfuerzos

La resistencia a la fractura se ha calculado a partir de la tensión crítica para la propagación de grieta y un factor de forma asociado a las probetas utilizadas. Las probetas estaban entalladas con borde o filo simple (SEN Single-Edge Notched) y fueron medidas y analizadas según la Mecánica de la Fractura Lineal Elástica (LEFM) (European Group on Fracture Task Group, 1990). Tal como puede observarse en la Figura 2, el factor crítico de intensidad de esfuerzos del material cargado con 0,8 µm es mayor que el del material no cargado, además el incremento en los valores de dicho factor es función de la carga añadida, obteniéndose los mejores resultados de tenacidad bajo condiciones de fractura para la composición de mayor cantidad de $CaCO_3$ de tamaño de 0,8 µm estudiada en este trabajo.

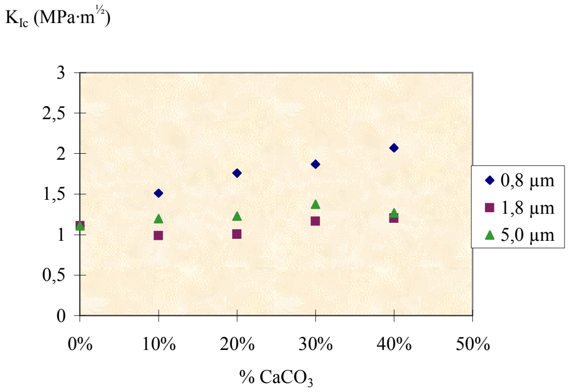

Figura 2. Variación de la resistencia a la fractura (K_{Ic}) para los sistemas de TGDDM/mPDA cargados con distintas proporciones y tamaños de $CaCO_3$.

4. PROPIEDADES DMTA

4.1 Relajación α (Temperatura de transición vítrea)

El análisis dinámico-mecánico-térmico se ha realizado sobre probetas mecanizadas procedentes de placas de los diferentes sistemas, curadas en un molde isotérmicamente a 90 ºC y postcuradas a 200 ºC para lograr la máxima Tg. La temperatura de transición vítrea, Tg, se ha tomado como la temperatura correspondiente al máximo de la relajación α, es decir, Tα.

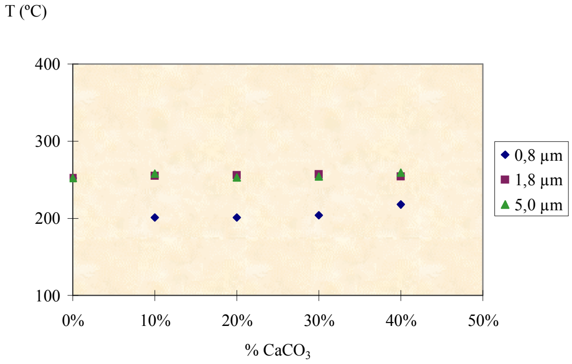

Figura 3. Variación de las temperaturas de transición vítrea correspondientes al máximo valor del factor de pérdida para el sistema puro y los modificados analizados con frecuencias de oscilación de 1 Hz.

Tal como se puede observar en la Figura 3, la adición de cargas de 1,8 y 5,0 µm apenas afectan al valor de la Tg. Los valores recogidos son muy próximos a los medidos para la matriz sin carga, aunque se puede resaltar que en todos los casos los valores de los materiales compuestos con estos tamaños de carga están ligeramente por encima del material no cargado. En el caso de la carga más pequeña se observa una disminución clara del valor de Tg que sólo se recupera ligeramente para altos porcentajes de carga.

4.2. Relajación ω y relajación β

Los valores de la temperatura de transición ω presentan un comportamiento similar para las cargas de 1,8 y 5,0 µm y son en todos los casos inferiores al del material no cargado. En cuanto a los valores de la temperatura de transición β de los materiales cargados con partículas de 1,8 y 5,0 µm no presentan grandes variaciones mientras que los correspondientes a partículas de 0,8 µm son significativamente menores que los del material no cargado.

4.3. Energía de activación de las relajaciones

Los valores obtenidos para las energías de activación de los distintos sistemas estudiados suponiendo una relación de tipo Arrhenius se encuentran representados en la gráfica de la Figura 4. Los valores se presentan agrupados según el tamaño de carga: cada grupo consta de cinco columnas que corresponden a porcentajes crecientes de carga: 0 %, 10 %, 20 %, 30 % y 40 %. Los valores obtenidos para la relajación α son del orden de 700 kJ/mol, similares a los observados para otros sistemas epoxídicos. Los obtenidos para la relajación ω varían entre 100 y 480 kJ/mol y para la relajación β entre

60 y 70 kJ/mol. Estos últimos valores son similares a lo referenciados en la bibliografía que sitúan la energía de activación de la relajación β entre 50 y 80 kJ/mol.

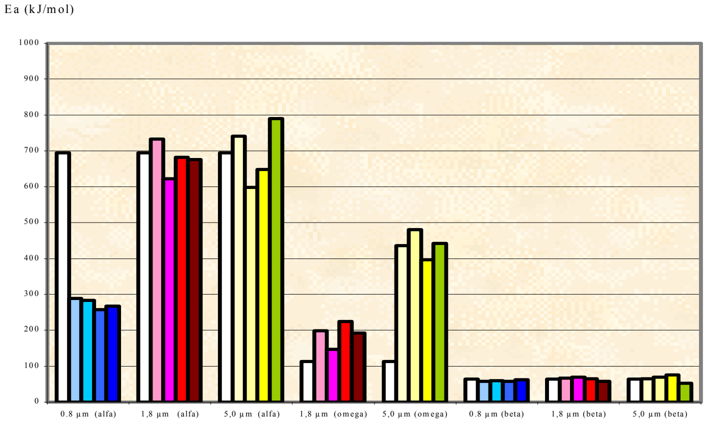

Figura 4. Valores de las energías de activación de las distintas relajaciones (α, ω y β) en función del tamaño y de la cantidad de carga incorporada.

3. CONCLUSIONES

Los valores de resistencia al impacto son relativamente bajos pero acordes con los recogidos en otros trabajos con resinas TGDDM. En cuanto al estudio de mecánica de la fractura de los materiales compuestos se ha observado un incremento del factor crítico de intensidad de esfuerzos, K_{Ic}, cuando se utiliza el tamaño más pequeño de partícula que puede asociarse con el aumento de zonas donde se desarrollan mecanismos que proporcionan una mayor resistencia a la propagación de grietas tales como la formación de bandas de cizalla.

En lo que respecta a la temperatura de transición vítrea de los distintos sistemas estudiados, la adición de cargas de 1,8 y 5,0 µm apenas afectan al valor de la Tg. En el caso de la utilización de partículas de 0,8 µm se observa una disminución clara del valor de Tg que sólo se recupera ligeramente para altos porcentajes de carga. En lo que respecta a la relajación α la inclusión de cargas de 0,8 µm causa una disminución muy significativa de la energía de activación necesaria para que los segmentos de cadena inicien el correspondiente proceso de relajación.

REFERENCIAS

KORNMANN X., LINDBERG H. AND BERGLUND L.A. (2001), *Polymer*, 42 (4), 1303

JIANKUN L., YUCAI K., ZONGNENG Q. AND XIAO-SU Y. (2001), *J. Polym. Sci.*, Part B: Polym. Phys., 39, 115

CHIN I. J., THURN-ALBRECHT T., KIM C.H., RUSSELL T.P. AND WANG J. (2001), *Polymer*, 42, 5947

HARISMENDY I., MINER R., VALEA A., LLANO-PONTE R., ANDRÉS M.A. AND MONDRAGON I. (1998), *J. Polym. Mater.*, 15, 205

EUROPEAN GROUP ON FRACTURE TASK GROUP, “Testing Protocol” (1990), Williams J.G. Ed., Imperial Collegue, London

Modified mortar with polymer admixture produced by recycling sugar cane bagasses

L.A.C. Motta
College of Civil Engineering, Federal University of Uberlândia, 38400-902, Uberlândia-MG, Brazil
R.M.N. Assunção
College of Pontal Integrated Science, Federal University of Uberlândia, 38302-000, Ituiutaba - MG, Brazil
G. Rodrigues Filho
Chemistry Institute, Federal University of Uberlândia, 38400-902, Uberlândia-MG, Brazil
N.G. Corrente
Chemistry Institute, Federal University of Uberlândia, 38400-902, Uberlândia-MG, Brazil
R.S. Cavalcanti
Chemistry Institute, Federal University of Uberlândia, 38400-902, Uberlândia-MG, Brazil

ABSTRACT

The work shows the using of the recycling materials as polymer admixture to produce polymer modified mortar. The products are obtained by the acetilation of the cellulose deriving sugar cane bagasses. The properties investigated were mortar consistence, compressive strength and air incorporation. The mortar factor water/cement was equal the 0.7 and the polymer content in relation to the cement mass was of 6%. The results had shown to rise of the consistence and air incorporated with reduction of the compressive strength of the modified mortar with cellulose admixture. The use of the recycling polymer is advantageous by the reduction of the modified system cost.

1. INTRODUCTION

The concept of polymer modification for cement based materials is not so new, considerable research and development of polymer modification for cement mortar and concrete have been conducted in various countries for the past 80 years or more (Ohama, 1998).

The polymeric admixture is effective at modifying or improving the properties such as workability, water retention, adhesion, waterproofness, strength and durability of cement mortar and concrete. Such a polymeric compound is a polymer latex, redispersible polymer powder, water-soluble polymer or liquid polymer. The cement mortar and concrete which are made by mixing with the polymer-based admixtures are called polymer-modified mortar (PMM) and concrete (PMC), respectively. In general, the properties of polymer-modified mortar and concrete depend on the polymer content or polymer-cement ratio, rather than the water-cement ratio compared with ordinary cement mortar and concrete. The polymer-cement ratio is defined as the mass ratio of the amount of polymer solids in a polymer-based admixture to the amount of cement in a polymer-modified mortar or concrete.

The polymer-based admixtures must present chemical stability towards the cement compounds, mechanical stability under actions, low air-entraining action, no adverse influence on cement hydration, formation of continuous polymer films in mortar or concrete, high adhesion of the polymer films to cement hydrates and aggregates, water resistance, alkali resistance, thermal stability for wide variations in temperature and weatherability of the polymer films formed in mortar or concrete.

2. EXPERIMENTAL

2.1 Production of the polymeric admixture

The sugar cane bagasse used for production of cellulose acetate was treated with a sodium hydroxide solution 1,0 mol.L-1 for one hour, for partial delignification. The acetylation of treated bagasse was carried out at room temperature. The acetic acid was used as solvent, the sulfuric acid as catalyser and acetic anhydride as acetylation agent at proportion of 1:10:0,2:10 (m:V:V:V – bagasse, acetic acid, sulfuric acid, acetic anhydride). The mixture was agitated for 45 minutes and then the produced polymer was precipitated with distilled water and washed until neutral pH.

The produced cellulose acetate was acetone-soluble that is a predominant characteristic of the cellulose diacetate. For use in the mortars polymer solutions were prepared containing 15 g polymer and 100 g acetone solvent.

2.2 Mortars preparations

Portland cement without mineral admixture (Brazilian Standard Type V- high early strength) and medium sand were used for mortar preparations. The physical and mechanical properties of cement and sand were determined second Brazilian standards (Table 1). Mortars were prepared with polymer/cement ratio (p/c) of 6.0%, a water/cement ratio (w/c) of 0.7 and sand/cement ratio (s/c) of 3.9. The polymeric solution was previously prepared and added to the cement/sand/water and mixe in a mechanic equipment. A reference mortar was prepared without polymer addition.

<table>
<tr><th colspan="4">Cement properties</th></tr>
<tr><th>Specific surface (Blaine)</th><th>Initial setting time</th><th>Bulk specific gravity</th><th>7-day compressive strength</th></tr>
<tr><th>(m^2/kg)</th><th>(h)</th><th>(g/cm^3)</th><th>(MPa)</th></tr>
<tr><td>434</td><td>3.0</td><td>3.08</td><td>36.38</td></tr>
<tr><th colspan="4">Sand properties</th></tr>
<tr><th>Bulk specific gravity</th><th colspan="2">Fineness modulus</th><th>Material minor than 75 µm</th></tr>
<tr><th>(g/cm^3)</th><th colspan="2"></th><th>(%)</th></tr>
<tr><td>2.51</td><td colspan="2">2.43</td><td>0.94</td></tr>
</table>

Table 1. Mechanical and physical properties of used materials.

2.3 Molding and cure of the specimens

Cylindrical specimens of diameter 50mm and height 100mm were prepared for determination of mortar compressive strength. The specimens were laboratory-cured until test age (28 days). Were tested four specimens for each mortar. The dry cure was adoted because polymer modified concrete and mortar present improved water retention. The water evaporation is inhibited due to the filling and sealing effects of impermeable polymer films formed. Accordingly, a sufficient amount of water required for cement hydration is held in the mortar and concrete. This good water retention of the modified composites contributes to an increase in the long-term strength in dry curing.

2.4 Consistency index and compressive strength

The consistency index of the fresh mortar was evaluated using a slump table according to the Brazilian standard NBR 13276: 2005. The fresh mortar is placed on a slump table, which is spun thirty times, then two orthogonal diameters are collected and, by the arithmetic average, the consistency index value is given. Compressive strength test was carried out by axial compression of cylindrical specimens at 28 days of age, according to the Brazilian standard 13279: 2005. The air content was determined according to the Brazilian standard NBR 9778: 2005, which specifies that the air content is the permeable voids volume/total volume ratio.

3. RESULTS AND DISCUSSION

Several factors such as polymer type, polymer-cement ratio, water-cement ratio, air content and curing conditions affect the properties of the fresh and hardened mortars. The cellulose acetate modified mortar (called CA) presented excellent resistance to bleeding and segregation, with a cohesive and homogeneous aspect, in spite of it improved flowability. Even with the same water-cement ratio 0.7 for both modified and reference mortar without polymer (called REF), it was observed an improved workability over the ordinary mortar and an increase of 26% on consistency index (CI) for the CA mortar in relation to the reference (Table 2). This modification was expected since the polymer improves the lubrication between the disperse cement particles, increase the entrained air, resulting in a fluid, homogeneous mortar.

Usually, in most modified mortars, a large quantity of air is entrained compared with in ordinary cement mortar because of the action of the surfactants contained as emulsifiers and stabilizers in the polymer. An excessive amount of entrained air causes a reduction in strength. The air content in the cellulose acetate modified mortar was not too larger then reference mortar, as can be seen in the Table 2, therefore the compressive strength was not strong affected.

Mortar	Compressive strength (MPa)	Consistency index (mm)	Air content (%)
REF	23.0	152.4	19.5
CA	20.1	192.0	20.2

Table 2. Mechanical and physical properties of mortars.

In general, polymer modified mortar and concrete show a considerable increase in tensile or flexural strength but no improvement in compressive strength compared with ordinary cement mortar. This can be explained in terms of the contribution of high tensile strength by the polymers themselves and an overall improvement in cement paste-aggregate bond.
The properties of the polymer modified mortar are influenced by various factors that tend to interact with each other. Factors such as the mix proportions, e.g., polymer-cement ratio, water-cement ratio, binder-void ratio, are being studied now and the results will be published son.

4. CONCLUSION

It was possible to produce cellulose acetate from sugar cane bagasse, aggregating value to this important residue. Based on the results of the essays of plastic consistency, air content and compressive strength, the produced polymer presented favorable properties for use in the mortar as improving fluidity without bleeding and segregation. Preliminary results indicated improving not only on the workability of the fresh mortar, but good properties also on the hardened mortar. Additional properties as water retention, permeability, absorption of water, bond strength, tensile strength, as well as other mixture are being studied now and the results will be published son.

REFERENCES

ASSOCIAÇÃO BRASILEIRA DE NORMAS TÉCNICAS-ABNT. (2005) NBR13276. *Argamassa para assentamento e revestimento de paredes e tetos* - Preparo da mistura e determinação do índice de consistência. Rio de Janeiro, 2005.
__________. (2005) NBR13279 *Argamassa para assentamento e revestimento de paredes e tetos* - Determinação da resistência à tração na flexão e à compressão. Rio de Janeiro.
_________. (2005) NBR9778 *Argamassa e concreto endurecidos* - Determinação da absorção de água, indice de vazios e massa específica. Rio de Janeiro.
OHAMA, Y. (1998) Polymer-based admixtures. *Cement and Concrete Composites*, v.20, p.189-212.

The swelling of a poly(*p*-phenylene benzobisoxazole) or PBO surface monitored in real time on the nanometer scale by atomic force microscopy (AFM)

K. Tamargo-Martínez[1], A. Martínez-Alonso[1], M. Gracia[2], J.I. Paredes[1], J.M.D. Tascón[1], M.A. Montes-Morán[1]
1. Instituto Nacional del Carbón, CSIC, Apartado 73, 33080 Oviedo
2. Instituto de Química Fisica "Rocasolano", CSIC, Serrano 119, 28006 Madrid

SUMMARY

The swelling of a poly(*p*-phenylene benzobisoxazole) (PBO) surface exposed to water has been monitored in real time on the nanometer scale using atomic force microscopy (AFM). The pristine PBO sample presents a morphology of long nanofibrils about 15-20 nm wide which are parallel to each other (and approximately parallel to the fiber axis). It also shows small patches or spots (15-40 nm large, which are interpreted to be contaminants). This morphology has been interpreted to reflect the orientation of the rigid-rod PBO macromolecules along the direction of the fiber axis. Following exposure to an oxygen plasma, the PBO surface displays a characteristic nanostructured morphology that is very different to that of the pristine polymer. It consists of different features (rounded, elongated), which coexist with others where a certain orientation along the fibre axis can be detected. Swelling of the plasma-treated sample following exposure to atmospheric water, or water from saturated atmospheres, was observed by tapping mode AFM operated in the attractive interaction regime. Monitoring the swelling of the plasma-treated polymer surface provided a means to reveal the nanometer-scale heterogeneity that this type of treatment produces on the polymer surface, something that would not be possible otherwise. The surface swelling induced in PBO was interpreted as arising from the incorporation of polar oxygen functionalities, as demonstrated by X-ray photoelectron spectroscopy (XPS). On the other hand, it is comparatively smaller than that observed for poly(*p*-phenylene terephthalamide) (PPTA). This difference can be attributed to both the molecular structure of the PBO polymeric chain and the intermolecular interactions among chains. In PBO, the presence of a heterocycle and the conjungation effect along the chain produce higher stability and rigidity than in the case of PPTA.

1. INTRODUCTION

Poly(*p*-phenylene benzobisoxazole) (PBO) provides great potential applications as reinforcing fibres for composites. This is due to their excellent thermal stability (Tamargo-Martínez et al. 2003a), chemical resistance and specific stiffness and strength (Toyobo 2001). However, PBO fibre-reinforced composites show a poor fibre-matrix interfacial adhesion (Luo et al. 2006, Park et al. 2003, Wu et al. 2004a, 2004b). This drawback can be overcome by changing the chemical and topographic surface properties of the fibres. Oxygen plasma treatments are able to improve the interfacial properties of PBO-based composites without altering the bulk properties of the PBO fibres (Wu et al. 2004b). On the other hand, it has been proved that O_2 plasma-treated poly(*p*-phenylene terephthalamide) (PPTA) fibres undergo a swelling effect (absorption of water molecules) during the post-treatment (2.5 h) (Paredes et al. 2006), which should diminish the adhesion force between the treated fibres and an epoxy resin. In this contribution, the swelling process of O_2 plasma-treated PBO fibres during the post-treatment (24 h) is investigated at the nanometer scale.

2. EXPERIMENTAL

PBO high-modulus fibres (labelled Z) were exposed to an oxygen plasma generated in a Technics Plasma 200-G apparatus by means of 2.45 GHz microwaves using 70 W, 1 mbar O_2 pressure and a treatment time of 4 min (ZO 4 samples). AFM investigations (tapping mode operation) were carried out under ambient conditions (relative humidity ~45 %, temperature ~22–23 ºC). The operating regime (attractive or repulsive) was established through proper setting of the free (A0) and setpoint (Asp) amplitudes (phase-distance curves) of cantilever vibration. We used rectangular silicon cantilevers (spring constant ~40 $N.m^{-1}$, resonance frequency around 250 kHz).

3. RESULTS AND DISCUSSION

The PBO sample presents a morphology of long nanofibrils about 15-20 nm wide, parallel to each other, and also approximately parallel to the fibre axis (figure 1-a1). Moreover, on the PBO sample the bright areas (15-40 nm large) in the phase image (small spots in figure 1a2) are interpreted as finish substances (Tamargo-Martínez et al. 2003b).

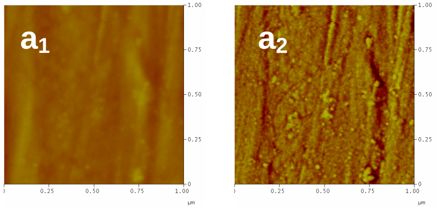

Fig. 1. Representative AFM images of untreated PBO fibre (Z) obtained in tapping mode operated in the attractive interaction regime: (a_1) topography and (a_2) phase images.

Figure 2 shows the height (subscript 1) and phase (subscript 2) images taken on the same area of a PBO fibre immediately after a 4 minute oxygen plasma treatment (Fig. 2a), as well as after exposure to the ambient atmosphere in the subsequent 24 h (Fig 2b and 2c). The sequence 2a and 2b was obtained in the attractive interaction regime, and the sequence 2c in the repulsive regime. Figure 2a shows a nanostructured morphology different to that of the untreated PBO fibre (Figure 1). The ZO 4 fibre is made up of irregular domains (rounded and globular nanostructures) which coexist with several areas arranged more or less parallel to the fibre axis (Figure 2a). Significant changes were observed 24 h after the plasma treatment (Figures 2b and 2c). The rounded and globular nanostructures of the treated fibre are not so distinctive after ambient exposure (compare sequence 2a and 2b). Similar observations for plasma treated PPTA fibres have been associated to a swelling effect induced by water molecules (Paredes et al. 2006). Moreover, the images of the post-treated PBO fibres recorded in the repulsive interaction regime are somewhat different from those obtained in the attractive regime. Comparison of Figures 2a and 2b reveals that the original morphology of the just treated fibre can be at least partially recovered when working under such regime. This is a consequence of the images recorded in the repulsive mode being obtained under hard tapping conditions (A_0 = 125 nm, r_{sp} = 0.5). The forces exerted by the tip under the repulsive regime are significantly larger than those produced in the attractive regime. As a consequence, the tip-sample interaction in the latter mode is extremely gentle and sample deformation is avoided (Paredes, 2002, Pignataro et al. 2002, San Paulo and Garcia, 2000), which is not necessarily the case of the repulsive regime. Thus, images obtained in the attractive regime provide a more accurate picture of the true sample surface topography.

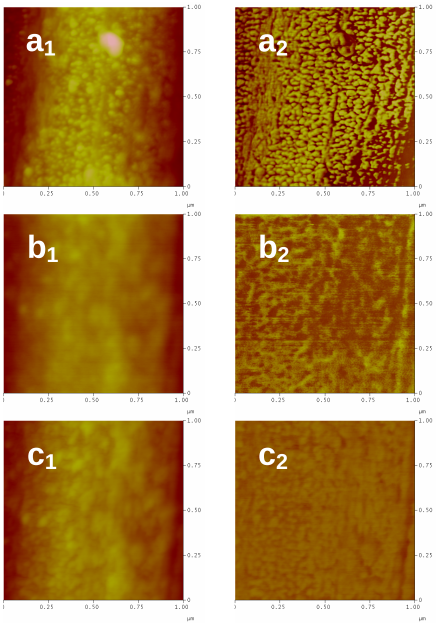

Fig. 2. In-situ evolution of a PBO surface treated in an oxygen plasma (ZO 4): images "a" and "b" were obtained by tapping mode AFM in the attractive regime (A_0 = 17 nm, r_{sp} = 0.8) immediately (a) and after 24 h plasma treatment (b and c). In each case, a height image (subscript 1) and a phase image (subscript 2) are shown. The sequence "b" and "c" was obtained on the same area, where the "c" was recorded in the repulsive mode (A_0 = 125 nm, r_{sp} = 0.5).

The ageing effect already described for PBO is comparatively smaller than that observed for plasma-treated PPTA under similar experimental conditions (Paredes et al. 2006). The PPTA surface swelling is noticeable just 2.5 h after the plasma treatment, mainly due to the enhancement of its hydrophilic character as a consequence of the introduction of oxygen functional groups (Paredes et al. 2006). However, XPS analysis performed on both Z and ZO 4 PBO samples have not detected any significant increase of the O/C atomic ratio after the treatment (Table 1).

SAMPLE	O/C	N/C
Z	0.34	0.05
Z cal	0.15	0.14
ZO 4	0.26	0.05
Ethanol-washed Z (Tamargo-Martínez et al. 2003a)	0.24	0.05

Table 1. Atomic ratios determined by XPS for PBO (Z), and plasma-treated PBO fibre (ZO 4). Z cal. corresponds to calculated atomic ratios.

Nevertheless, the high O/C atomic ratio detected on the PBO Z surface must be attributed to a standard finish treatment: the O/C ratio of the commercial PBO surface is much higher than that estimated from the molecular structure its monomer (Z cal., Table 1). This standard finish layer is removed with the oxygen plasma treatment, as shown in the AFM images (Figures 1 and 2a). The XPS atomic ratios (O/C and N/C) of ZO 4 are also very similar to those obtained for an ethanol-washed PBO surface (Tamargo-Martínez et al. 2003a) (Table 1), thus confirming that the oxygen plasma treatment is able to wipe the finish substances off the PBO fibre (cleaning effect of plasma).

Differences between both fibre structures, i.e., the molecular structure of their polymeric chains and the intermolecular interactions among chains, should also contribute to the smaller swelling observed for the treated PBO surface when compared to plasma-treated PPTA. Thus, the presence in the PBO fibres of a heterocycle (benzobisoxazole) and the conjugation effect along the chain results in a higher stability and rigidity than that of the PPTA fibres. In this latter type of polymeric fibres, important structural transformations in terms of cross-linking at the nanometer scale are prone to occur after the plasma treatment (Wu et al. 2004a).

4. CONCLUSION

The oxygen plasma-treated PBO polymer surface undergoes a slight swelling after 24 h under ambient conditions. XPS spectra have demonstrated that the capability to establish hydrogen bond interactions, through the formation of oxygen functional groups, increases only slightly after the oxygen plasma treatment.

ACKNOWLEDGMENT

Financial support from the Spanish MEC (project CTQ2005-01905-C04-02-PPQ) is gratefully acknowledged.

REFERENCES

LUO, K., LI, G., JIN, J., YANG, S., JIANG J. (2006). Surface analysis of PBO and modified SPBO fiber by contact angle measurements and XPS. *J. Macromol. Sci. B: Phys.*, 45, 631-637.

PAREDES, J.I. (2002). Las microscopías de efecto túnel y fuerza atómica aplicados al estudio de la modificación superficial de materiales de carbono mediante plasmas. *Doctoral Thesis, Oviedo University*, Oviedo, Spain.

PAREDES, J.I., VILLAR-RODIL, S., TAMARGO-MARTÍNEZ, K., MARTÍNEZ-ALONSO, A., TASCÓN, J.M.D. (2006). Real-time monitoring of polymer swelling on the nanometer scale by atomic force microscopy. *Langmuir*, 22, 4728-4733.

PARK, J.M., KIM, D.S., KIM, S.R. (2003). Improvement of interfacial adhesion and non-destructive damage evaluation for plasma-treated PBO and Kevlar fibers/epoxy composites using micromechanical techniques and surface wettability. *J. Colloid Interface Sci.*, 264, 431-445.

PIGNATARO, B., CHI, L., GAO, S., ANCYKOWSKI, B., NIEMEYER, C., ADLER, M., FUCHS, H. (2002). Dynamic scanning force microscopy study of self-assembled DNA protein nanostructures. *Appl. Phys. A*, 74, 447-452.

SAN PAULO, A., GARCÍA, R. (2000). High-resolution imaging of antibodies by tapping mode atomic force microscopy: attractive and repulsive tip sample interaction regimes. Biophys. J., 78, 1599-1605.

TAMARGO-MARTÍNEZ, K, VILLAR-RODIL, S., PAREDES, J.I., MARTÍNEZ-ALONSO, A., TASCÓN, J.M.D. (2003a). Studies on the thermal degradation of poly(p-phenylene benzobisoxazole)". *Chem. Mater.*, 15, 4052-4059.

TAMARGO-MARTÍNEZ, K., VILLAR-RODIL, S., PAREDES, J.I., MARTÍNEZ-ALONSO, A., TASCÓN, J.M.D., MONTES-MORÁN, M.A. (2003b). Surface characterization of PBO fibers. *Macromolecules*, 36, 8662-8672.

TOYOBO CO. LTD. TECHNICAL INFORMATION (2001). PBO Fiber ZYLON.

WU, G.M,, HUNG, C.H., YOU, J.H. (2004a). Surface modification of reinforcement fibers for composites by acid treatments. *J. Polym. Res.-Taiwan*, 11, 31-36.

WU, G.M., SHYNG, Y.T. (2004b). Surface modification and interfacial adhesion of rigid rod PBO fibre by methanesulfonic acid treatment. *Composites A*, 35, 1291-1300.

Low velocity impact in glass fibre/epoxy composites reinforced with cork interleaved layers

D. Dias, P.J.R.O. Nóvoa
Composite Materials and Structures Research Unit, Institute of Mechanical Engineering and Industrial Management (INEGI), FEUP Campus, Rua Dr. Roberto Frias 400, 4200-465 Porto, Portugal
A.T. Marques
Department of Mechanical Engineering, Faculty of Engineering, University of Porto, Rua Dr. Roberto Frias s/n, 4200-465 Porto, Portugal

ABSTRACT

The present work describes experimental studies where an interlayer toughening strategy was used with the objective of minimizing low velocity impact induced damage in composite materials. The interlayer material consisted of cork films, which were selected considering the high compressibility, high energy absorption and low density of cork. The composite plates were made by the hand lay-up moulding process. Mechanical characterization tests to study the mechanical behaviour of the composite materials included, flexural, interlaminar shear by "short beam" method, and Charpy impact tests. The results show a clear influence of the interlayer material on the composite structure behaviour. However, full advantage of the specific features introduced by the interlayer material is not achieved, mainly due to poor adhesion between the cork film and the polymer matrix, and/or the resistance of cork. With this case study, we were aiming to determine if cork was a viable option to be applied as an interlayer material, and if so, to optimize lay-up parameters so that performance could be maximized, but further research should be done, in order to achieve the ideal parameter combination that would allow achieving relevant improvements regarding low-velocity-impact damage in composite materials.

1. INTRODUCTION

Low-velocity impact damage is one of the most critical types of damage that can occur in composite materials. It is particularly harmful because in addition to the degree of damage it can produce, the fact that it is usually undetected by visual inspection may lead to unexpected failure during operation. The present work describes an experimental study set up to decrease the referred type of damage in composite materials, based on an interlayer toughening strategy (Duarte *et al.* 1999). In order to achieve the intended objective, cork was selected as the interlayer film material considering some of its specific performance features, namely, the excellent impact properties resulting from both high compressibility and high energy absorption. The additional fact that cork is a national, low density renewable natural product, adds up to the interest of its selection. Different interlayer film thicknesses and the surface treatments were considered. The mechanical characterization included the evaluation of tensile, flexural, interlaminar shear and Charpy impact properties, in order to obtain a thorough knowledge of the overall mechanical performance of the different laminate configurations included in the study.

2. EXPERIMENTAL

2.1 Materials

A laminating system from Sicomin® (France) composed of an epoxy prepolymer (SR 1500) and an amine hardener (SD 2505) was used as polymer matrix. The reinforcement consisted of both glass fibre *Twill* woven fabric and chopped strand glass fibre mat (450 g.m^{-2}) were used. Cork films supplied by Sá Rosas, S.A., obtained from virgin cork blocks with thicknesses of 0.5 mm and 0.2 mm. A 2% (v/v) aqueous solution of 3-aminopropylmethyldiethoxysilane (Aldrich) was used for surface treatment.

2.2 Composite laminate production

Composite plates were produced by the hand lay-up moulding process, from which all necessary specimens were cut for subsequent testing. Laminate compositions with different interlayer film thicknesses and the surface treatments were considered.

2.3 Composite laminate characterisation

The manufactured laminates had their flexural, interlaminar shear and Charpy impact properties evaluated, in order to obtain a thorough knowledge of their overall mechanical performance. In addition, scanning electron microscopy analysis was performed on cork film and laminate fracture surfaces.

3. RESULTS AND DISCUSSION

The results show a clear influence of the interlayer material on the composite structure. However full advantage of the specific features introduced by the interlayer material, is not achieved mainly due to poor adhesion between the cork film and the polymer matrix, and/or the resistance of cork. As an example of a result we present Fig. 1 where it can be observed that the use of thicker interleaves (B) leads to materials withstanding much higher deformations but with a high cost in loss of stiffness relative to the original laminate (A).

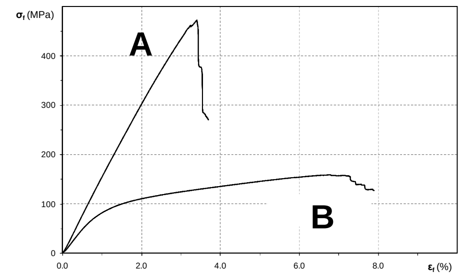

Fig. 1. Flexural stress vs. extension.

4. CONCLUSIONS

The work objective of determining if cork could be suitable option for an interlayer toughening material and, if so, under which conditions its performance could be maximized, failed to meet the initial expectations. The results suggest that either cork may not be an adequate material for the application, or that it was inefficiently used. This last possibility constitutes a motivation to further explore the use of cork with the sought objective, considering new parameter combinations that might result in relevant improvements regarding low-velocity-impact.

ACKNOWLEDGEMENT

The authors would like to thank the company Sá Rosas, S.A. and in particular to Mr. Eduardo Macedo, for supplying the cork films.

REFERENCES

DUARTE, A., Herszberg, I., Paton, R. (1999), Impact resistance and tolerance of interleaved tape laminates. *Compos. Struct.* 47, 753-758

Modificación de la resistencia a tracción de un composite de fibra de carbono al ser sometido durante un tiempo determinado a una corriente anódica constante en un medio electrolítico

J. Viña, I. Berdiales, J. Rojo
Departamento Ciencias de los Materiales e Ingeniería Metalúrgica, Escuela Politécnica, Campus Viesques, Universidad de Oviedo, España.
V. García
Departamento Química Física y Analítica, Escuela Universitaria de Ingeniería Técnica Industrial, Campus Viesques, Universidad de Oviedo, España.
A. Argüelles, R. García
Departamento Construcción e Ingeniería de Fabricación, Mecánica de los Medios Continuos, Escuela Politécnica, Campus Viesques, Universidad de Oviedo, España.

RESUMEN

En este trabajo se analiza la modificación de la resistencia a tracción de un composite de fibra de carbono, tras ser sumergido en un medio electrolítico (agua de mar) y sometido al paso de una corriente anódica constante (100 mA, 200 mA, 300 mA y con densidades respectivas 166.6 A/m^2, 333.3 A/m^2, 500 A/m^2) durante 2 horas.

El efecto de la corriente anódica (300 mA) sobre el refuerzo de fibra de carbono, origina una pérdida importante de la resistencia a tracción.

La conclusión es que cualquier estructura fabricada con fibra de carbono que se encuentre en un medio electrolítico, ha de ser protegida mediante pinturas que interrumpan la intercara de contacto fibra-electrolito, pues una corriente anódica de fuga de un circuito o vagabunda puede ocasionar el colapso de dicha estructura en poco tiempo.

1. INTRODUCCIÓN

Por todos es sabido que los metales son buenos conductores de la corriente eléctrica, pero existen otros materiales no metálicos que aun no siendo excelentes conductores, sí dejan pasar la corriente eléctrica. En este caso está la fibra de carbono.

Un plástico reforzado con fibra de carbono es conductor y al entrar en contacto con un metal en una estructura, forma un par galvánico que en el interior de un electrolito, provocará la corrosión del metal, pues el CFRP es más noble. Esta corrosión sería de tipo galvánica, siendo un proceso relativamente lento.

En el caso de una corriente impuesta el material que se degrada será siempre (Qin et al.) aquel por el que entra la corriente eléctrica.

1.1 Corrosión, degradación

Se entiende por corrosión la destrucción o deterioro de un material como consecuencia de su reacción química o electroquímica con el ambiente que le rodea.

En particular el término corrosión se aplica de forma general a los metales (M).

$$M \rightarrow M^{+n} + n \cdot e^{-}$$

Si el material que se deteriora es no metálico (CFRP), se prefiere hablar de degradación.

$$C \rightarrow C^{+n} + n \cdot e^{-}$$

Donde C^{+n} representa átomos de carbono o fragmentos carbonados, ver figura 1

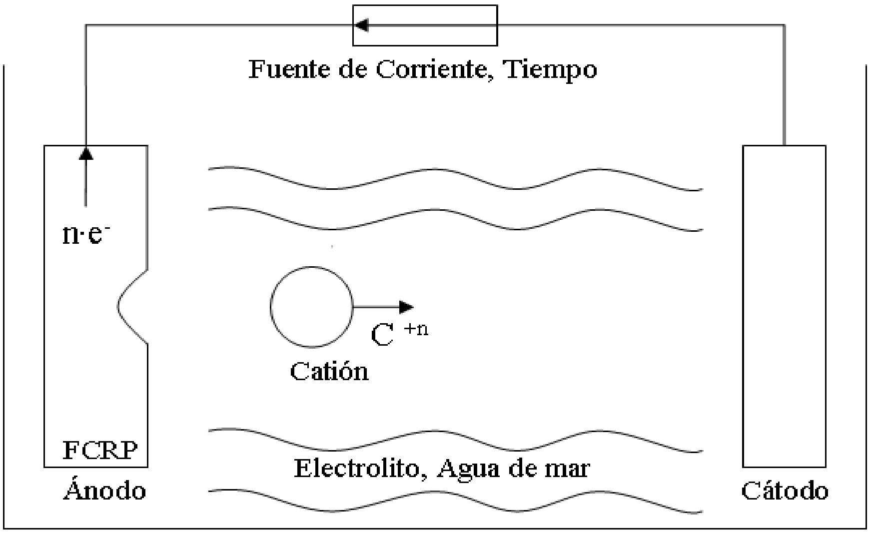

Fig. 1. Desprendimiento de átomos de carbono o fragmentos carbonados.

Los átomos de carbono o los fragmentos carbonados se desprenden de la estructura grafítica de la fibra, debilitándola y llegando incluso a romper la fibra (Ryu et al.), ocasionando una disminución de sus propiedades mecánicas.
En el proceso de degradación provocado por una corriente anódica, el deterioro puede producirse en cuestión de minutos o de horas. Sólo depende del producto de las magnitudes corriente-tiempo, pudiendo llegar a colapsar una estructura en cuestión de horas, sin que nadie se de cuenta del daño que estaba sufriendo dicha estructura.

1.2 Procedimiento

La preparación de la probeta para su degradación se hace de la siguiente manera:
Se aíslan todos los bordes y parte de la probeta dejando expuesta al electrolito la zona central de unos 300 mm^2 ((l=30 mm) · (a=10 mm)) por ambos lados.
Se sumerge la zona central de la probeta en agua de mar y se conecta a la fuente de corriente constante según figura 2.

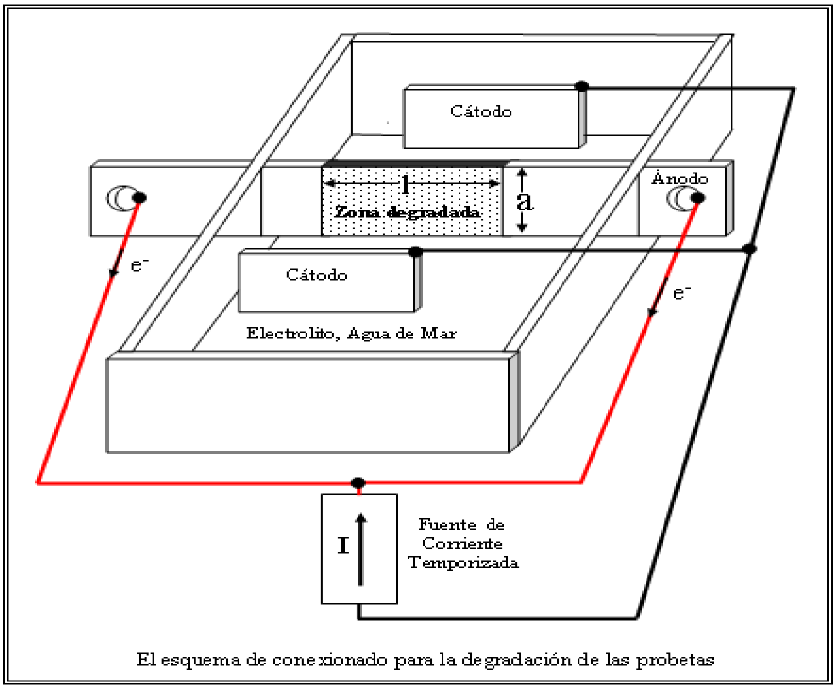

Fig. 2. Conexionado eléctrico de la probeta.

Una vez realizado el montaje, las variables a controlar durante el proceso de degradación son la corriente y el tiempo

2. RESULTADOS

Los ensayos de tracción se realizaron con una máquina de tracción Instron mod. 5580. Las deformaciones se midieron con un extensómetro de longitud inicial 50mm, expresando los resultados en mm/mm.

Los valores presentados para cada intensidad son la media de las cinco probetas ensayadas. En todos los casos el coeficiente de variación fue inferior al 5%. Los resultados obtenidos se reflejan en la tabla 1 y en la figura 3.

Probeta	I (mA)	t (s)	Tensión Rotura (MPa)	Disminución (%)
N-0H-000-1	0	0	587.75	0
N-2H-100-1	100	7200	548.59	6.66
N-2H-200-1	200	7200	458.13	22.05
N-2H-300-1	300	7200	416.61	29.11

Tabla 1. Resultados, ensayo de tracción.

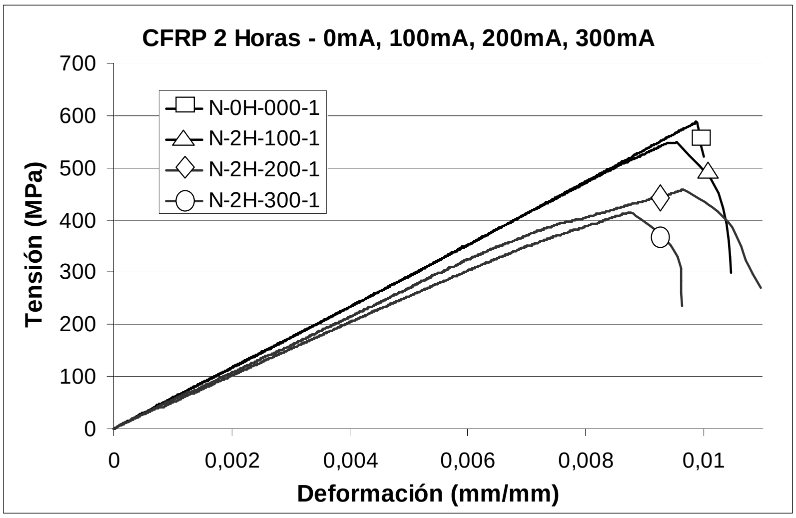

Fig. 3. Gráfica, ensayo de Tracción.

3. CONCLUSIONES

Las principales conclusiones que se derivan de este trabajo son:

- Un compuesto con refuerzo de fibra de carbono ha de encontrarse protegido de la degradación electroquímica si no se quiere que ésta provoque un fallo catastrófico en el elemento construido con ese material.
- La tensión de rotura a tracción de un compuesto con refuerzo de fibra de carbono sometido a degradación electroquímica se ve claramente disminuida conforme se incrementa la corriente anódica.

REFERENCIAS

QIN, J., BROWN, R., GHIORSE, S. and SHUFORD, R. (1994) The effect of carbon fiber type on the electrochemical degradation of carbon fiber polymer composites, Proceeding of the Tri-Service Conference on Corrosion.

RYU, S. -K., PARK, B.-J., (1999) XPS Analysis of carbon fiber surfaces-anodized and interfacial effects in fiber-epoxy composites. Journal of Colloid and Interface Science 215, 167-169.

Capacidad de absorción de sonido y comportamiento mecánico a compresión de esponjas de aluminio obtenidas por infiltración de preformas

P. Fernández M.
Escuela de Ingeniería, Grupo de Investigación sobre Nuevos Materiales,
Universidad Pontificia Bolivariana, Medellín, Colombia
R. Zuluaga
Escuela de Ingeniería, Grupo de Investigación sobre Nuevos Materiales,
Universidad Pontificia Bolivariana, Medellín, Colombia
H. González
Escuela de Mecánica, Universidad Tecnológica de Pereira, Grupo GIMI, Pereira,
Colombia
J. Cruz R.
Escuela de Ingeniería, Grupo de Investigación sobre Nuevos Materiales,
Universidad Pontificia Bolivariana, Medellín, Colombia

RESUMEN

En el presente trabajo se describe las propiedades mecánicas y funcionales de espumas de aluminio de porosidad abierta, denominadas esponjas. Específicamente fue evaluada la capacidad de absorción de sonido y el comportamiento mecánico a compresión de dichas espumas. La técnica de fabricación de las espumas fue la infiltración de preformas solubles, utilizando sal comercial (NaCl) como preforma y aleación de aluminio del tipo Al-Si-Mg. El método denominado “Absorción acústica mediante tubo de impedancia” fue utilizado para determinar la capacidad de absorción de sonido de las espumas a diferentes frecuencias y para cada tamaño de poro. De los resultados obtenidos, se observó que las esponjas con el menor tamaño de poros responde mucho mejor a diferentes niveles de frecuencia, presentando así mismo el mayor coeficiente de absorción de sonido. Similarmente, las pruebas de compresión evidenciaron que a menor tamaño de poro, mejor respuesta a la absorción de energía de deformación.

1. INTRODUCCIÓN

Las espumas metálicas son consideradas en esencia un material compuesto constituido por un metal como matriz y una red de poros asumida como el “relleno” de gas distribuido uniformemente a través de toda la matriz. Actualmente, se ha incrementado el interés en este tipo de materiales, particularmente en las espumas de aluminio, pues además de ser extremadamente livianas; ofrecen una combinación exclusiva de propiedades funcionales y mecánicas, tales como su excelente permeabilidad a fluidos, alta conductividad térmica, buenas propiedades acústicas junto a la gran capacidad de absorción de energía de deformación y amortiguación de vibraciones. Existen diversos métodos para la fabricación de espumas metálicas. Recientemente, Fernández et al. (2008) realizaron una revisión de los procesos reportados para la obtención de espumas metálicas, entre los cuales; el proceso de infiltración del metal fundido en preformas ofrece la posibilidad de obtener esponjas con poros de tamaño y forma controlados por la preforma, siendo común el uso de materiales removibles tales como espumas de poliuretano, carbamida o granos de sal para la elaboración de la preforma.

Aunque han sido pocos los trabajos abordados con referencia a la caracterización las propiedades acústicas de las esponjas metálicas, diferentes autores han reportado que estas poseen en general una buena capacidad de absorción de sonido. Lu et al. (1999), determinaron la capacidad de absorción de sonido de las espumas marca ALPORAS y, Hai-Jun et al. (2007) probaron sándwich de espumas fabricadas por espumado directo de una aleación de aluminio Al-Si, Kang et al. (2007) investigaron las propiedades acústicas de las esponjas fabricadas por fundición de precisión en preformas poliméricas, y Jiejun et al. (2003) estudiaron la capacidad de absorción de sonido de esponjas de aluminio reforzadas con SiC, obtenidas por infiltración positiva de preformas de sal. En cuanto a las propiedades mecánicas de las espumas metálicas, muchos estudios previos han sido enfocados hacia los mecanismos de deformación en compresión y en tensión; así como la influencia de la densidad relativa, la morfología y tamaño de los poros y, la fracción volumétrica de la porosidad. Gibson y Ashby (2001) establecieron relaciones entre la densidad relativa y; el módulo de Young y la resistencia a la fluencia.

En el presente artículo, las esponjas de aleación Al-Si-Mg fueron fabricadas mediante el proceso IPS con presión de vacío. Las muestras fueron sometidas a pruebas acústicas y a ensayos de compresión, a fin de determinar la influencia del tamaño y morfología de los poros en la capacidad de absorción de sonido y en el comportamiento a la deformación de las esponjas.

2. EXPERIMENTACIÓN Y RESULTADOS

2.1 Fabricación de las esponjas metálicas

El proceso de fabricación de las esponjas consistió en la infiltración del la aleación de aluminio fundida en la preforma mediante presión de vacío. Para la preforma, fueron utilizados tres tamaños de grano de la sal, 2.0 mm, 1.2 mm y 500 μm en promedio, que a su vez se reflejaron en los tamaños de poro de las esponjas producidas. Luego de infiltrar la preforma, el lingote de Al/NaCl fue sometido a disolución de la sal con agua corriente. Mediante el proceso descrito fue posible obtener esponjas con estructuras de porosidad completamente abierta e interconectada. En general, las esponjas metálicas así obtenidas presentaron densidades relativas promedio de 0.33; lo que significa un 67% de porosidad. Los tamaños de poro fueron una replica de los tamaños de grano de sal utilizados: 2.0 mm, 1.2 mm y 500 μm en promedio.

2.2 Absorción de sonido

Para determinar el coeficiente de absorción de sonido α, se realizaron pruebas en muestras cilíndricas de 30 mm de diámetro y 10 mm de espesor; mediante el método de tubo de impedancia basándose en la norma ASTM C384-04 "*Stantdard Test Method for Impedance and Absorption of Acoustical Materials by Impedance Tube* Method". El intervalo de frecuencia utilizado estuvo entre 250-4000 Hz. Los equipos necesarios para realizar esta prueba son básicamente, un tubo de impedancia, una fuente generadora de sonido, un micrófono y un osciloscopio.

Los resultados obtenidos permitieron determinar que las esponjas de aluminio bajo estudio poseen buenas propiedades de absorción de sonido, especialmente para valores bajos de frecuencia entre 250 y 450 Hz y para valores altos entre 1500 ~ 2000 Hz, para los cuales el coeficiente α presento valores entre 0.82 – 0.98; siendo mas eficientes aquellas esponjas con tamaño de poro mas pequeño. A frecuencias mayores a 2000 Hz no hubo una respuesta satisfactoria en prácticamente ninguna de las esponjas estudiadas. La fig. 1 ilustra una curva típica del coeficiente de absorción de sonido vs. la frecuencia de respuesta para esponjas con tamaño de poro promedio de 550 μm.

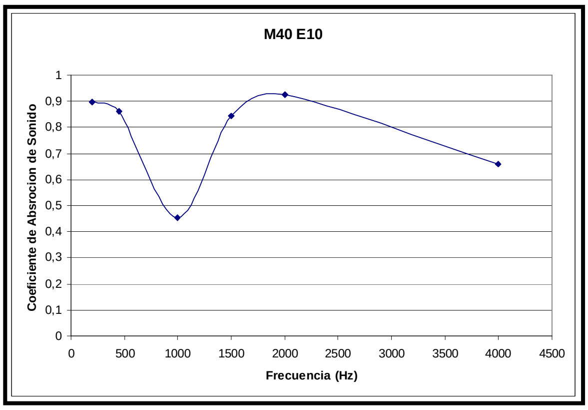

Fig. 1. Relación entre el coeficiente de absorción de sonido α y la frecuencia.

2.3 Comportamiento a compresión

El ensayo de compresión fue realizado en probetas cilíndricas de 20 de diámetro y 20 mm de altura, utilizando para ello una máquina universal Instron 5582 a una velocidad de cabezal de 0.5 mm/s. Del análisis de las curvas esfuerzo-deformación se estableció un patrón de deformación muy homogéneo, con tendencia a una alta capacidad de absorber energía de deformación debido al acomodamiento de la red porosa como se observa en la figura 2, estructura final.

En general, las curvas de esfuerzo-deformación exhibieron tres regiones de deformación típicas: i) una respuesta inicial lineal de tipo elástico, ii) un extensa región tendiente a formar una meseta (denominada *plateau region*) con un flujo de esfuerzos cuasi-constante en incremento y, iii) una región final de densificación debido al colapso de las celdas que se compactan, tal como se muestra en la fig. 2. Esta deformación característica es similar a la reportada por CAO et al. (2006) para espumas metálicas de aluminio obtenidas por proceso de infiltración en preformas de sal.

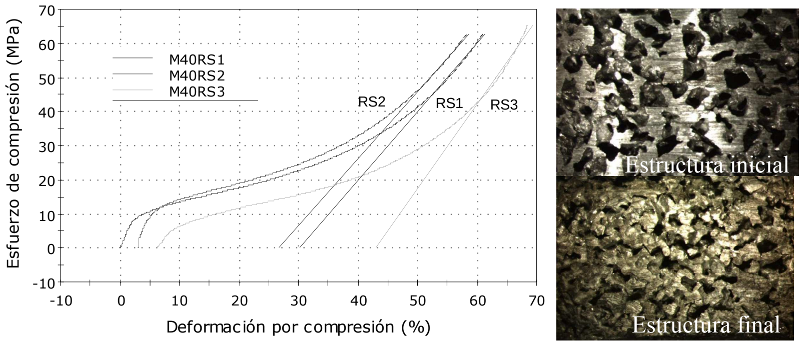

Fig. 2. Curva de esfuerzo vs deformación y estructuras inicial y final de la esponja.

3. CONCLUSIONES

Los valores obtenidos para el coeficiente de absorción de sonido α concuerdan con lo reportado por otros autores para los mismos niveles de frecuencia (Berg et al. 2008). Por otra parte, aunque la resistencia mecánica no es una de las propiedades de mayor relevancia en las esponjas, ya que su estructura de poros abiertos las hace ser más apreciadas para aplicaciones funcionales que para usos estructurales. No obstante, su comportamiento a la deformación demostró ser muy satisfactorio, observándose una mejor respuesta en las esponjas de menor tamaño de poro (550 µm).

AGRADECIMIENTOS

Los autores desean agradecer a Colciencias por la beca para estudios de doctorado otorgada a la Ing. Fernández mediante la cual fue posible realizar la investigación presentada en este artículo.

REFERENCIAS

BERG, A., MAYSENHÔLDER, W., HAESCHE, M. (2003). Noise reduction by open-pore aluminium foams. *en Proc. Cellular metals: Manufacture, Properties, Applications,* Berlin, Alemania MetFoam. MIT Press–Verlag, 487-492.
CAO X. et al. (2006). Effects of cell size on compressive properties of aluminum foam, *en Trans. Nonferrous Met. Soc. China* 16, 351-356.
FERNÁNDEZ, P., CRUZ, L. J., COLETO, J. (2008). Procesos de fabricación de metales celulares: Parte I, Procesos por vía líquida, *en Revista de Metalurgia*, 44, 6.
GIBSON, L.J., ASHBY, M.F. (2001). *Cellular solids: structure and properties,* Cambridge University Press, Cambridge, UK.
HAI-JUN, Yu et al. (2007). Sound insulation property of Al-Si closed-cell aluminium foam sandwich panels, *en Applied acoustics*, 68; 1502-1510.
KANG, B. et al. (2008). Heat Transfer and Acoustic Properties of Open Cell Aluminium Foams, *en: J. Mater. Sci. Technol*. Korea, 24, 1; 1-6.
JIEJUN, W et al. (2003) Damping and sound absorption properties of particle reinforced Al matrix composite foams, *en Composites Science Technology*, 63, 569-574.
LU, T.J., HESS, A., ASHBY, M.F. (1999) Sound absorption in metallic foams. *en: Journal of Applied Physics*, 85, 11; 7528-7539.

Comportamiento físico y mecánico de matrices cementantes con lodo de papel estucado activado

S. Ferreiro, M. Frías, M.I. Sánchez de Rojas, O. Rodríguez, B. Nebreda, J. Olmeda
Departamento de Síntesis, Caracterización y Reciclado de Materiales, Instituto de Ciencias de la Construcción “Eduardo Torroja” – CSIC. Madrid. España

RESUMEN

En el presente trabajo de investigación se aborda el estudio del comportamiento físico y mecánico de pastas y morteros normalizados elaborados con una substitución del 10% de cemento Portland CEM I-42.5 R por lodo de papel estucado activado (LPEA).
Los resultados obtenidos demuestran que los cementos elaborados con dicha substitución cumplen con todos los requisitos físicos y mecánicos exigidos dentro de la normativa vigente, siendo por tanto este residuo activado, un material susceptible a ser considerado como una adición puzolánica, con los consiguientes beneficios económicos, energéticos y medioambientales.

1. INTRODUCCIÓN

La incorporación de nuevos residuos industriales en la elaboración de cemento con adiciones, diferentes de los frecuentemente utilizados, tales como cenizas volantes, humo de sílice y/o metacaolín, es una de las líneas punteras del sector cementero. La posibilidad de obtener nuevos materiales a partir de recursos alternativos a los tradicionales está centrando la atención científica a nivel internacional. En esta línea de investigación, el lodo de papel estucado, residuo procedente del proceso de reciclaje de papel, se presenta como una fuente alternativa al metacaolín.

En esta línea, el grupo de investigación de Reciclado de Materiales del Instituto “Eduardo Torroja” ha demostrado en diversas investigaciones previas (Vegas et. al. 2006 y Frías et al. 2008) la viabilidad de la valorización de este residuo en una matriz de cemento, puesto que su comportamiento químico, si es apropiadamente activado, es compatible y admisible por ella.

2. MATERIALES

2.1 Lodos de Papel Estucado (LPE)

Los residuos industriales utilizados fueron lodos procedentes de la industria papelera de reciclaje, más concretamente, los generados en la unidad de destintado, utilizando como materia prima un lote de papel estucado. Dichos lodos presentan una morfología aglomerada de color grisáceo, compuesta por una fracción inorgánica, fibras de celulosa y tintas. Análisis realizados mediante DRX (no mostrados) ponen de manifiesto que los lodos de papel estucado están compuestos por minerales de calcita, caolinita, illita, talco y clorita, mientras que su composición química en base seca (Tabla 1) demuestra que sus óxidos principales son la sílice, la alúmina y el óxido de calcio.

En consonancia a la composición mineralógica de estos residuos, se escogieron 8 condiciones diferentes de activación (Tabla 2) con el objetivo de establecer un proceso óptimo, que logre la máxima activación de la caolinita como única fase susceptible de comportarse como una puzolana y la eliminación de la materia orgánica. Los métodos de activación empleados se basan en el tratamiento térmico del LPE en atmósfera oxidante, utilizando cuatro temperaturas diferentes y dos tiempos de residencia en la mufla (Tabla 2).

Materias primas	SiO_2 (%)	Al_2O_3 (%)	CaO (%)	MgO (%)	Fe_2O_3 (%)	SO_3 (%)	K_2O (%)	Na_2O (%)	L.O.I (%)
LPE	10.69	6.74	24.15	0.96	0.41	0.30	0.22	0.24	55.71
CP	19.48	5.95	62.96	1.63	2.13	2.28	1.18	0.32	3.02

Tabla 1. Composición química de las materias primas.

Denominación	LPEA1	LPEA2	LPEA3	LPEA4	LPEA5	LPEA6	LPEA7	LPEA8
Temperatura (ºC)	600		650		700		750	
Tiempo de residencia (h)	2	5	2	5	2	5	2	5
SiO_2 (%)	20.24	20.65	21.06	21.44	22.32	23.52	25.36	26.22
Al_2O_3 (%)	13.11	13.38	13.58	13.87	14.55	15.28	16.45	16.98
Cal libre (%)	0.31	0.31	0.35	0.82	7.15	22.49	25.11	26.46

Tabla 2. Denominación y contenido de SiO_2, Al_2O_3 y cal libre de los LPEA obtenidos al aplicar diferentes condiciones de activación.

A la vista de las determinaciones químicas realizadas, se observa que a medida que se aumenta tanto la temperatura como el tiempo de residencia en el tratamiento térmico de activación de los lodos, se favorece el proceso de descarbonatación de la calcita, incrementando la presencia de cal libre en la composición final del LPEA (Tabla 2).

2.2 Cemento Portland

El cemento utilizado para el estudio comparativo de las propiedades físicas y mecánicas de las mezclas, fue un cemento tipo CEM I 42.5R, según la designación impuesta por la norma UNE-EN 197-1:2000. Por norma, este tipo de cemento debe presentar un contenido en clínker igual o superior al 95%, por tanto puede incorporar hasta un 5 % de otros componentes minoritarios, siendo en este caso, un filler calizo. La composición de los principales óxidos del cemento (CP) también se recoge en la Tabla 1.

Como se ha citado anteriormente, la evaluación de la variación del comportamiento físico-mecánico del cemento Portland al incorporar el LPEA en función del tipo de activación aplicada, se realizó mediante una substitución del 10% de la masa del cemento por cada tipo de LPEA, obteniéndose un total de 9 muestras diferentes: el cemento patrón (CP) y 8 mezclas, denominadas: CP-LPEA1, CP-LPEA2,…y así sucesivamente hasta CP-LPEA8.

3. RESULTADOS Y DISCUSIÓN

Los requisitos físico-mecánicos exigidos para los cementos comunes están incluidos en la normativa vigente UNE-EN 197-1:2000, contemplando parámetros técnicos tales

como las resistencias mecánicas a compresión de morteros, los tiempos de principio de fraguado y la expansión admisible de pastas de cemento, que deben ser determinados según las respectivas normas de ensayo UNE-EN 196-1:2005 y UNE-EN 196-3:2005.
A la vista de los resultados obtenidos (Tabla 3) se observa que los cementos parcialmente substituidos con un 10 % de LPEA cumplen con todas las exigencias técnicas requeridas para un cemento con clase resistente 42.5, e incluso algunos de los cementos, más concretamente, CP-LPEA1, CP-LPEA2, CP-LPEA3 y CP-LPEA5 obtienen la clasificación tipo R a un solo día de curado.

Tipo de cemento	**Resistencia a compresión a 28 días de curado (MPa)**	**Tiempo de principio de fraguado (min)**	**Tiempo de final de fraguado (min)**	**Tiempo de fraguado (min)**	**Expansión (mm)**
CP	60.27 ± 1.32	129 ± 10	219 ± 10	90 ± 10	0
CP-LPEA1	62.13 ± 1.02	129 ± 10	219 ± 10	90 ± 10	0
CP-LPEA2	59.69 ± 0.50	119 ± 10	209 ± 10	90 ± 10	0
CP-LPEA3	61.70 ± 0.79	119 ± 10	199 ± 10	80 ± 10	0
CP-LPEA4	58.56 ± 1.17	109 ± 10	189 ± 10	80 ± 10	0
CP-LPEA5	58.41 ± 1.57	109 ± 10	189 ± 10	80 ± 10	0
CP-LPEA6	58.19 ± 0.67	109 ± 10	189 ± 10	80 ± 10	1
CP-LPEA7	54.04 ± 1.39	109 ± 10	179 ± 10	70 ± 10	1
CP-LPEA8	54.24 ± 0.79	99 ± 10	179 ± 10	80 ± 10	1
Requisitos	$42.5 \leq Rc \leq 62.5$	**≥ 60**	-	-	**≤ 10**

Tabla 3. Comportamiento físico-mecánico de matrices cementantes con y sin LPEA

La reducción de los tiempos de fraguado se atribuye a la sinergia de dos fenómenos:

1. La aceleración de la hidratación de la alita provocada por la saturación prematura de la fase líquida en portlandita, provocada por la hidratación de la cal libre contenida en el LPEA (Tabla 2), y por la mayor superficie aportada por la calcita para la nucleación de nuevas fases hidratadas.
2. La menor proporción de yeso disponible con respecto a la alúmina total del C_3A y del metacaolín del LPEA (Tabla 2), responsable de retrasar su hidratación (1), evitando un fraguado "flash" de la pasta de cemento.

$$Al_2O_3 + 4Ca(OH)_2 + 15H_2O \rightarrow Ca_4AH_{19}\downarrow \qquad (1)$$

Esta ligera aceleración del proceso de fraguado de las mezclas CP-LPEA 4 a 8 tendrá un efecto negativo en el subsiguiente desarrollo de las resistencias (Taylor, 1997), mientras que por el contrario, ciertas condiciones de activación (LPEA1 y 3) mejoran incluso las resistencias mecánicas del cemento a 28 días de curado, debido a la mayor cantidad de fases generadas en la reacción puzolánica, tales como, los geles C-S-H y los monocarboaluminatos cálcicos hidratados ($3CaO.\ Al_2O_3.CaCO_3{\cdot}11H_2O$).
Más allá de las exigencias de la normativa, existen otros parámetros recogidos por la misma que proporcionan información sobre el comportamiento de pastas y la manejabilidad de morteros en estado fresco, y que estarán íntimamente relacionados con la composición del cemento, en este caso modificada por el LPEA. Se comprueba que a medida que aumenta la temperatura como el tiempo del proceso de activación del LPE,

se reduce su manejabilidad, en términos de una mayor demanda de agua de consistencia normal (UNE-EN 196-3:2005) y una disminución del escurrimiento de los morteros (UNE 83811:1992 EX) (Fig. 1), ya que es necesario satisfacer inicialmente la hidratación de la cal libre. Al mismo tiempo, los análisis químicos y los ensayos de expansión confirman este fenómeno, puesto que los cementos con un contenido superior al 3 % en masa de cal libre, producen una expansión de 1 mm (Tabla 3), generando a su vez las mayores variaciones en el comportamiento en estado fresco (Fig. 1).

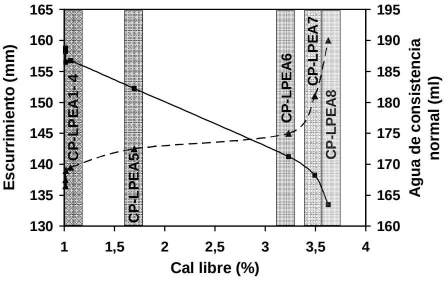

Fig. 1. Comportamiento de las pastas y morteros de cemento con LPEA.

4. CONCLUSIONES

De los resultados obtenidos, se deben resaltar las siguientes conclusiones:

1. Los residuos procedentes de la industria papelera son asimilables por una matriz cementante y son susceptibles de ser considerados como una adición puzolánica.
2. La substitución parcial de un 10 % de la masa de cemento por LPEA cumple con todos los requisitos físicos y mecánicos exigidos por la normativa para un cemento de clase resistente 42.5, independientemente de la condición de activación elegida.
3. Es más, utilizando las condiciones de activación más óptimas, 600 o 650ºC durante 2 horas, se consigue mejorar las resistencias mecánicas del cemento Portland a los 28 días de curado.

REFERENCIAS

FRÍAS M., RODRIGUEZ O., VEGAS I., VIGIL, R. (2008) "Properties of calcined clay waste and its influence on blended cement behaviour" J. Am. Ceram. Soc., 91 [4] 1226-1230.

TAYLOR, H. F. W. (1997) Cement chemistry (Ed. Thomas Telford) 2Ed., 218. USA.

VEGAS I., FRÍAS M., URRETA J., SAN JOSÉ J. T. (2006) Obtaining a pozzolanic addition from the controlled calcination of paper mill sludge. Performance in cement matrices. *Mater. Construcc.* 56 (283), 49-60.

AGRADECIMIENTOS

Se agradece al MEC la financiación del proyecto de investigación CTM2006-12551C03

Impacto de baja energía de compuesto de matriz pCBT reforzados con fibra de carbono fabricado mediante RTM asistido mediante vacío

A. Agirregomezkorta, G. Aretxaga, M. Sarrionandia, J. Aurrekoetxea
Departamento de Mecánica y Producción Industrial, Mondragón Unibertsitatea, España
A.B. Martínez
Departament de Ciència dels Materials i Enginyeria Metal.lúrgica, Centre Català del Plàstic, Universitat Politècnica de Catalunya, C/ Colom, 114, 08222 Terrassa, España.

RESUMEN

En el presente trabajo se ha caracterizado a impacto de baja energía del compuesto pCBT/CF obtenido mediante RTM asistido por vacío. El modelo no conservativo aplicado se ha mostrado válido para describir el comportamiento de este compuesto en el rango subcrítico. A su vez también, es efectivo para determinar el umbral de energía de generación de daño, incluso cuando el daño no es visible, lo que demuestra la sensibilidad del método. El módulo de elasticidad en indentación del pCBT/CF caracterizado es de 4,7 GPa y la tensión de inicio de daño es de 253,5 MPa.

1. INTRODUCCIÓN

Los compuestos de matriz polimérica reforzados con fibra de carbono en comparación con el acero o el aluminio, ofrecen ratios superiores de resistencia-peso y rigidez-peso, mejor comportamiento a impacto, reducen el ruido y las vibraciones y muestran una excelente resistencia a la fatiga (Cantwell et a1. 2007). Por otro lado presentan la desventaja de poder sufrir daños sin signos visibles tras un impacto de baja energía, lo que los excluye de ciertas aplicaciones estructurales (Salehi-Khojin et a1. 2006).

Las ventajas de los compuestos moldeados por transferencia de resina termoplástico (Resin Transfer Moulding, TP-RTM), sobre los de termoestables incluyen mejoras en la tenacidad, resistencia al impacto y posibilidad de reciclado (van Rijswijk et a1. 2007). El compuesto fabricado mediante TP-RTM a partir de butilén tereftalato cíclico (CBT), que tras polimerizar forma el polímero ingenieríl polibutilén tereftalato (pCBT). Las áreas principales de investigación se han centrado en los mecanismos de polimerización, microestructura y propiedades estáticas. Sin embargo, no se han llevado a cabo trabajos sobre las propiedades a impacto y comportamiento a la fractura de los compuestos reforzados con tejido de fibra de carbono.

En el presente trabajo se aplican técnicas de baja energía a los resultados experimentales obtenidos mediante ensayos instrumentados de caída de dardo e impacto-indentación sobre placa, cubriendo el rango de energías de impacto, que va desde el subcrítico, hasta la aparición de daño en el compuesto. Con el objetivo de identificar el módulo elástico y el umbral de daño a altas velocidades de solicitación con un pequeño número de ensayos.

2. MATERIALES Y MÉTODOS EXPERIMENTALES

2.1. Fabricación del compuesto mediante TP-RTM

El prepolímero utilizado en este estudio fue el oligómero CBT160® suministrado por Cyclics. Como refuerzo se utilizó un tejido plano equilibrado [0º/90º] de fibra de carbono de alta resistencia con un gramaje de 200 g/m^2 (Suministrado por Hexcel, ref. 43199). En cada laminado se han utilizado 10 capas. El oligómero fundido (230 ºC) se inyectó mediante vacío en un molde cerrado (calentado a 230 ºC), donde previamente se acomodó el refuerzo. Posteriormente, se enfrió a 190 ºC, manteniendo esta temperatura durante 30 minutos, y finalmente se enfrió fuera del horno durante 120 minutos hasta temperatura ambiente, antes de ser desmoldeado. Se moldearon placas de 250 x 250 x 3,5 mm^3 de CF-pCBT.

2.2. Ensayos de impacto-indentación e impacto flexión sobre placa

Los ensayos de impacto-indentación se llevaron a cabo en una máquina de caída de dardo instrumentado. La masa del impactor es de 1,803 kg, geometría hemisférica y 12,7 mm de diámetro. El espesor de probeta necesario para eliminar la influencia de la base de acero se estableció en 10,5 mm, para las alturas utilizadas durante el ensayo: 20, 30 y 40 mm. Los ensayos de indentación se modelizaron mediante un modelo viscoplástico compuesto de un sistema masa-muelle (no-lineal)-amortiguador en serie, donde el muelle sigue la ley de Hertz (Artús et a1. 2008).

Para los ensayos de flexión de placa las probetas (80 x 80 x 3,5 mm^3) fueron simplemente apoyadas sobre un anillo de 60 y 80 mm de diámetro interno y externo, respectivamente. Los ensayos de flexión se modelizaron utilizando un modelo no conservativo compuesto por dos partes. Una primera que considera la indentación en el contacto, y una segunda que considera la deflexión del plato y que está constituida por un muelle y un amortiguador en paralelo (Martínez et a1. 2006).

3. RESULTADOS Y DISCUSION

La resolución de las ecuaciones del modelo de impacto-indentación permite obtener la rigidez del muelle (K) y el coeficiente de amortiguamiento del amortiguador (C), mediante el ajuste con las curvas experimentales. El ajuste se realiza en base a dos parámetros: la fuerza máxima F_{max}, y el coeficiente de restitución. El valor del módulo de elasticidad a indentación obtenido para el compuesto fue de 4,7±0,1 GPa, valor que se utilizará para modelizar el impacto-flexión sobre placa.

En la figura 1.a se muestra un impacto subcrítico registrado experimentalmente, y superpuesta la curva calculada por el modelo, que es capaz de predecir de forma precisa el comportamiento del material, ajustándose en desplazamiento (tiempo de contacto), fuerza máxima y coeficiente de restitución (proporcional al área bajo la curva). La figura 1.b muestra un impacto supercrítico, con claros signos de rotura de fibras, que el modelo no es capaz de simular. Sin embargo la probeta ensayada no muestra signos de daño externo, ni huella indentación. Esto es debido a que el daño inducido por el impacto aumenta la flexibilidad de la probeta, por lo que el modelo se desvía del experimental.

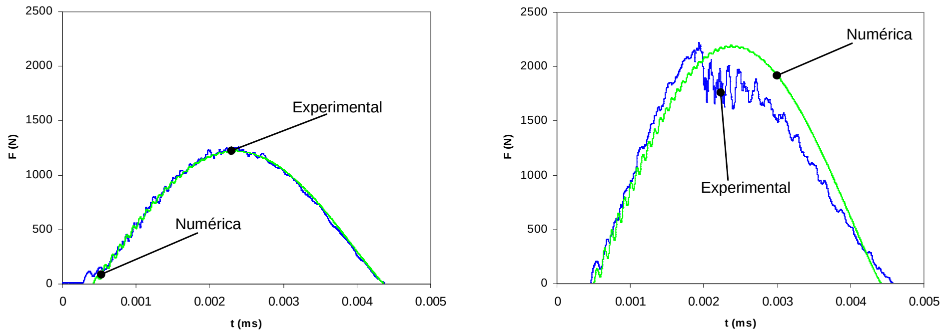

(a) (b)

Fig. 1. Evolución de la fuerza con el tiempo en un impacto subcrítico a 0,88 m/s(a), y en un impacto supercrítico a 1,62 m/s (b).

En la figura 2a se grafica el tiempo de contacto (t_c) en función de la velocidad de impacto. Dentro del rango subcrítico en los impactos de baja energía t_c tiende a disminuir levemente con el incremento de la velocidad de impacto. Una vez alcanzado el umbral de daño, el material gana en flexibilidad lo que se traduce en un aumento de t_c. Este punto de inflexión permite identificar el momento de inicio de daño, a partir del cual se pude calcular el umbral de energía, y consecuentemente la fuerza de generación de daño (figura 2.b). De la figura 2a se deduce que la velocidad de inicio de daño es 1,54 m/s y la fuerza correspondiente a la generación del daño es 2087 N (figura 2b), lo que equivale a una tensión 253,5 MPa.

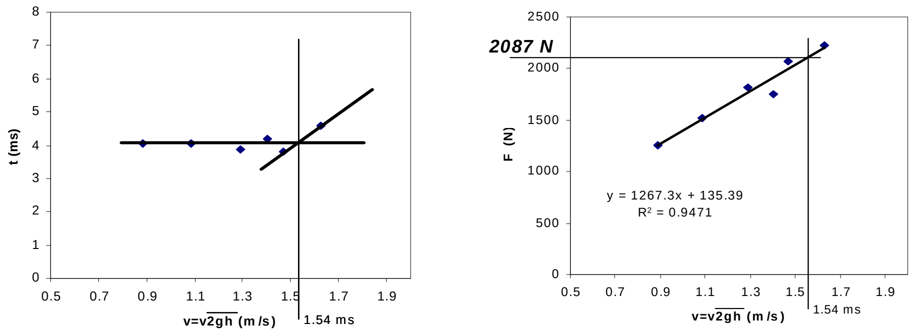

(a) (b)

Fig. 2. Evolución del tiempo de contacto con la velocidad de impacto (a) y evolución de la fuerza máxima con la velocidad de impacto (b).

4. CONCLUSIONES

En el presente trabajo se ha caracterizado a impacto de baja energía el compuesto pCBT/CF, para lo que se han realizado ensayos de caída de masa instrumentados sobre placa con punta hemisférica en configuraciones de impacto-indentación e impacto-flexión de placa. La aplicación de un modelo no conservativo que incorpora la respuesta local de la zona de contacto, y la global de flexión permite obtener curvas fuerza-tiempo que se ajustan con precisión a las experimentales siempre y cuando la naturaleza del impacto sea subcrítica. El modelo es válido para caracterizar el módulo de elasticidad en indentación a velocidades de impacto, que para el material objeto de estudio es de 4,7 GPa, y el umbral de daño estimado en 253,5 MPa.

AGRADECIMIENTOS

Se agradece al Ministerio de Ciencia e Innovación (PSE-370000-2008-4 proyecto LIGHTCARBONCARS) y al Departamento de Educación, Universidades e Investigación del Gobierno Vasco (PI2008-07) por la financiación del presente trabajo.

REFERENCIAS

ARTÚS, P., DÜRSTELER, J.C., MARTINEZ, A.B. (2008). Low-energy dynamic indentation method for analysis of ophthalmic materials. Optometry and Vision Science, 85, 49-53.
CANTWELL, W.J. (2007). Geometrical effects in the low velocity impact response of GFRP. Composite Science and Techology, 67, 1900-1908.
MARTINEZ, A..B., MASPOCH, M.Ll., SANTANA, O., NAVAS, J.A. (2006). Impacto de baja energía de poliésteres lineales. IX Congreso Nacional de Materiales –Vigo 06.
SALEHI-KHOJIN, A., BASHIRZADEH, R., MAHINFALAH, M., NAKHAEI-JAZAR, R. (2006). The role of temperature on impact properties of kevlar/fiberglass composite laminates. Composites Part : B, 37, 593-602.
van RIJSWIJK, K., BERSEE, H.E.N. (2007). Reactive processing of textile fiber-reinforced thermoplastic composites – An overview. Composites Part: A, 38, 666-681.

Dynamic mechanical and morphological characterization of starch/gluten/glycerol/coconut fibers composites

E. Corradini[1], L.H.C. Mattoso[2], J.A.M. Agnelli[3]
[1]DEMA, Univ. Federal de São Carlos, São Carlos, SP, Brazil
[2]Embrapa Instrumentação Agropecuária, São Carlos, SP, Brazil

ABSTRACT

Natural fibers like jute, sisal, coconut, jute, and cotton have been used as reinforcement in synthetic and natural polymer matrices [1,2]. Compared to inorganic fillers, the main advantages of vegetable fiber are: renewable nature, low cost, low density, high specific strength and modulus, comparatively easy processability due to their nonabrasive nature [3]. Starch and gluten are interesting natural polymers to be used as matrix in biocomposite due to their low cost, biodegradability and availability [4]. They can be processed in the presence of plasticizers, similarly to some conventional synthetic thermoplastic polymers. In addition, starch and gluten contain polar groups that can interact with the hydroxyl groups present in vegetable fibers. In this work the coconut fibers were used as reinforcement for biodegradable matrix of starch/gluten/glycerol. The effect of fiber content on dynamical mechanical properties and morphology was studied.

Fatigue and fractographic analysis in aeronautic composite NC2/RTM6, using Weibull distribution

G. Volpiano [1], M.O.H. Cioffi[1], H.J.C. Voorwald[1], M.C. Rezende[2]
[1]Grupo de Fadiga e Materiais Aeronáuticos DMT/FEG/UNESP, Av. Ariberto Pereira da Cunha, 333 Guaratinguetá, SP
[2]Instituto Tecnológico Da Aeronáutica, S.J.Campos, Sp, Brasil – Praça Marechal Eduardo Gomes – Vila Das Acácias Cep 12228-900 – São José Dos Campos/Sp - Brazil

ABSTRACT

Aeronautical industries study new possibilities to increase aircraft efficiency replacing conventional materials for composites with low density, considering the safe life criteria. The behaviour study in fatigue by the Weibull Distribution allowed the safe life forecast of the composite material, non-crimp fabric (NC2)/epoxy monocomponent system (RTM6) developed for the resin transfer moulding process (RTM). Laminates were produced using two different types of tooling, rigid and soft, had been submitted to uniaxials tensions between 58 and 72% of ultimate tensile strength, with load ratio R = 0,1 and a sinusoidal load of 8 Hz frequency. Fatigue tests were carried out in the Laboratory of Mechanical Properties at DMT/FEG-UNESP by an universal testing machine INSTRON 8801. Beyond making possible the safe life forecast of the material, Weibull parameters indicated that when increasing tension test, the material processed in soft tooling trends to increase the dispersion of results, instead of material processed in rigid tooling the inverse was observed. Scanning electron microscopy analyses were performed on the fracture surfaces of composite specimens, being identified standards fractures associated to materials submitted to cyclical loads.

Sinergia mecánica de la fibra de carbono con matriz epóxica y poliéster

J. Ramos
Universidad Autónoma de Occidente. Cali, Colombia

RESUMEN

En el presente trabajo se obtiene mediante vaciado y vibrado sobre un molde en caucho de silicona, probetas de resinas epóxica y poliéster, las cuales fueron catalizadas respectivamente al 20 y al 2%, (porcentaje en peso) a una temperatura de 25 °C y humedad relativa de aproximadamente el 65%. Las resinas se reforzaron con fibra de carbono unidireccional con un diseño [0/45/90]s. Con el fin de caracterizar las resinas y obtener los datos necesarios para realizar el respectivo diseño del compuesto reforzado con fibra de carbono unidireccional, primeramente se hace el ensayo de tensión a probetas con resina epóxica y con resina poliéster que no tuvieran sin ningún tipo de refuerzo. El material compuesto fibrorreforzado fue sometido a ensayos de flexión, tensión, torsión, impacto y permeabilidad. Los resultados muestran que la resina poliéster presenta un mejor modulo de elasticidad, esfuerzo de fluencia, limite elástico y mejor porcentaje de deformación que la resina epóxica. El compuesto con matriz epóxica muestra un mejor comportamiento a la flexión y absorbe mayor energía que el compuesto con matriz poliéster. Las propiedades mecánicas de las resinas epóxica y poliéster se ven notablemente mejoradas con la adición de fibra de carbono, debido que al tener un compuesto fibrorreforzado donde se genera una adherencia apropiada entre los diferentes elementos, estos presentan sinergismo en las propiedades mecánicas, evidencian una gran efectividad en el desvió de la fracturas y son una excelente alternativa para su utilización en diversos campos de la industria.

Optical drop contour analysis – Possibilities for the microscopic and macroscopic characterization of composite materials

W. Waibler
NEURTEK - DataPhysics Gmbh

ABSTRACT

The exact knowledge of the surface properties of composite materials is of particular importance for coating and painting of these materials. Polymer surfaces have relatively poor wetting and adhesion properties. To improve the wetting properties, the polymers are generally surface treated such as for instance with a plasma or a corona treatment. On base of optical contact angle measurement with test liquids of different polarity, the treatment effect as well as time dependant degradation effects could be determined reliably and easily.

In particular in field of nanotechnology optical drop contour analysis is also en vogue since several years. In many new technical applications the wetting behaviour of micron size liquid drops or even tinier droplets on solids affects the quality of recent products and the related production processes. Wetting and dewetting on a very small scale play a key role frequently. In particular the biotechnology and the genetic engineering profit already significantly from the latest progress and improvement in this exciting area of science.

Optical drop contour analyzing systems in combination with electrical heated high-temperature control units allow furthermore controlled measurement of the surface properties under inert gas atmosphere of polymer melts, liquid metals including solders, or hot melts at temperatures up to 700 °C. Furthermore, by the use of high temperature furnaces, temperatures up to 1800 °C could be reached.

Mechanical response of composite laminate containing fiber waviness

H.G. Rai, E.V. Honein, M.I. Najjar
University of Balamand
Koura, Lebanon

ABSTRACT

Fiber waviness is a defect associated with the manufacturing of unidirectional composite materials. It results from local buckling of prepreg, or from cure induced residual stresses. Generally, wavy fibers assumed a sinusoidal pattern. The sinusoid has two main parameters: its amplitude A and its wavelength L. Their ratio i.e. A/L determines the degree of waviness. This waviness defects have been observed to occur in, or through the thickness of, the plane of lamination. Composite parts containing fiber waviness were suspected to initiate failure in the part. It has been proven experimentally that composite containing wavy fibers have a reduced fatigue resistance, compressive strength, and stiffness.

The present research involves the development of mathematical model and numerical solution methods to investigate the effect of fiber waviness on the elastic behavior, stability, deflection, and free vibration of multilayered composite laminate. A theoretical model is developed for unidirectional lamina whose fiber is sinusoidal in the plane of the lamina. This model predict the elastic properties of the lamina and bending stiffness of laminate as function of A/L which are used in a numerical model to predict percent reduction of critical load, maximum deflection, and natural frequency of a multilayered laminate versus A/L. Several examples are illustrated to substantiate the model predictions. Results for critical buckling load, maximum deflection, and natural frequency versus fiber waviness for laminates containing fiber waviness are obtained.

Optimización del comportamiento mecánico de tableros aglomerados fabricados con compuesto PELD/AL contenido en los envases de Tetra Pak

M.A. Hidalgo*, E. Baena, J.C. Moya*****
*Grupo de investigación en tecnologías para la manufactura GITEM, Universidad Autónoma de Occidente, Campus Valle del Lili, km, 2 vía a Jamundí, Cali-Colombia
**RSI Ltda, Cali-Colombia, Calle 13 No 35A-60 Arroyohondo Yumbo, Cali Colombia
***Gestión Ambiental y Programas Sociales, Tetra Pak, Bogota-Colombia. World Trade Center, 100 No 8A-55

RESUMEN

Hoy en día es posible observar la sustitución del vidrio y del plástico empleados en la fabricación de algunos envases, por materiales laminados o multicapas cuyo diseño permite, una mas larga vida del producto en ellos envasado y una mayor eficiencia en el transporte del producto, estos materiales laminados tienen una alta resistencia mecánica y bajo peso. En sur America se viene incrementando el consumo de envases de cartón que contiene aluminio, este envase larga vida de Tetra Pak es un material compuesto de 5% aluminio, 20% polietileno, 75% cartón, materiales que tienen un período de degradación muy prolongado; la disposición final de este material una vez utilizado bien sea post-consumo o post-industrial representa un problema porque tarda muchos años en degradarse cuando se vierte en los basureros municipales. El proceso básico del reciclaje de envases larga vida de Tetra Pak obtenidos a partir de recolecciones voluntarias y selectivas a nivel industrial, ya fue desarrollado y actualmente se realiza en sur America; en este trabajo se presentan resultados sobre el estudio que facilita observar el comportamiento elástico y resistencia de tableros fabricados por moldeo por compresión en prensa de platos calientes (Hydraulic Laboratory Platen Presses modelo LabPro400 of FontijneGrotnes), con el material compuesto PELD/AL resultado del hidropulpeado de envases de Tetra Pak. Fue posible observar cinco variables de respuesta, tensión, compresión, flexión, impacto, y absorción de agua a variaciones en el proceso, es el caso de ciclos de presión alta y baja a temperatura constante, se vario dos tamaños de partícula, los cuales son posibles de reproducirse en la fabrica, obteniendo resultados favorables para potencializar la utilización que actualmente se le esta dando a este tipo de material, y como una investigación base para iniciar los estudios para reforzar el material con fibras naturales. A nivel mundial se vienen desarrollando proyectos similares, los cuales reflejan una utilización aceptable del material, en el caso de Colombia se espera desarrollar sobre esta investigación un estudio que favorezca, además de la utilización del PELD/AL, utilizar fibras naturales que se encuentran en la región, siendo posible fabricar nuevos compuestos a base de matriz polimérica recuperada.

Propiedades superficiales en materiales compuestos de matriz termoestable degradados en medios químicos

O. Sahuquillo[1], M.D. Salvador[1], E. Rayón[1], F. Segovia[1], J.M. Kenny[2]
[1]Instituto de Tecnología de Materiales (ITM). Universidad Politécnica de Valencia, España
[2]Dipartimento di Ingegneria Civile e Ambientale, Università di Perugia, INSTM-NIPLAB UdR Perugia, Terni, Italia

RESUMEN

El presente trabajo se centra en el estudio de las propiedades superficiales de materiales compuestos de matriz termoestable, que han permanecido inmersas en disoluciones de agua, NaCl (3.5% w/w) y NaOH (4% w/w), durante tiempos largos de inmersión. Se han empleado herramientas como la nanoindentación, AFM, y FESEM, con las que se pretende obtener valores de las propiedades superficiales y correlacionarlo con el efecto de la degradación producida en materiales compuestos y con la agresividad del medio. Se ha obtenido que la intensidad de la degradación está fuertemente relacionada con el pH de la disolución condicionando el mecanismo implicado. De esta forma es el NaOH es el que provoca un mayor efecto sobre las propiedades de los materiales estudiados.

1. OBJETIVO

El objetivo del presente trabajo se centra en el estudio de propiedades superficiales de materiales compuestos correlacionándolos con el efecto que la degradación produce sobre ellos, atendiendo a la naturaleza del medio de inmersión y al mecanismo implicado.

2. EXPERIMENTAL

Las matrices termoestables utilizadas son poliéster insaturado ortoftálico (UP) (P4 TV-29) y viniléster (VE) de bisfenol A (Atlac A-430.01), suministradas por BASF. Como refuerzo se ha empleado MAT de fibra de vidrio tipo E. Los compuestos se han obtenido por estratificación manual, y una vez curadas permanecen en inmersión, con tiempos máximos de degradación de 19000 horas, en disoluciones de agua, NaCl 3.5 % w/w y NaOH 4% w/w, con valores de pH de 7.71, 6.32 y 13.64.
La nanoindentación se realizó en un equipo Nanotest 600, con una punta tipo Berkovich, una profundidad de 1500 nm y una velocidad de 0.2 mN/s. La evaluación se realizó, con tres replicas por muestra, sobre áreas de resina de 150x125 μm. Los resultados se obtuvieron de acuerdo al método de Oliver and Pharr (1992). La Microscopía de Fuerza Atómica (AFM), se realizó con un equipo Nano Easy Scan AFM System en modo tapping, sobre una selección de muestras de las analizadas por nanoindentación. La observación superficial se realizó mediante un Field Emission Scanning Electron Microscopy (FESEM) Zeiss Supra 25.

3. RESULTADOS Y DISCUSIÓN

El módulo de elasticidad obtenido en nanoindentación en función del pH de la disolución se representa en la Fig. 1, se observa que, para las dos resinas termoestables empleadas, existe una correlación entre el carácter neutro o alcalino del medio y el efecto que produce sobre el compuesto. Por tanto, el NaOH (pH = 13.64) es el medio con un pH mayor y provoca unas pérdidas más significativas en los indicadores módulo de elasticidad y dureza obtenidos por nanoindentación. De otro lado, el agua (pH = 7.71) y NaCl (pH = 6.32), con carácter neutro, producen un efecto similar sobre el compuesto y de menor intensidad al producido por el NaOH. Además, las variaciones de las propiedades evaluadas en función del tiempo y por tanto el deterioro provocado son superiores en los compuestos de poliéster, Fig. 1 (a) y (b). En cuanto a los indicadores resistentes a partir de los valores de dureza, los resultados son similares a los mostrados para el módulo de elasticidad.

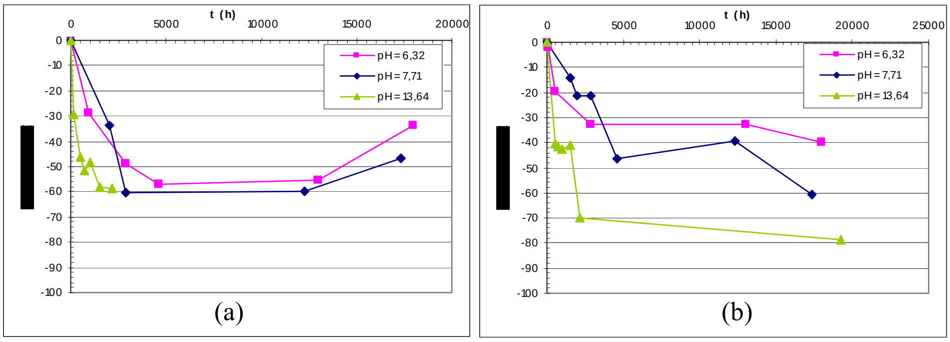

(a) (b)

Fig. 1. Resultados nanoindentación en compuestos: (a) Poliéster y (b) Viniléster.

Las pérdidas de masa producidas en los compuestos de poliéster en NaOH, Fig. 2 (a), junto con las pérdidas significativas de propiedades en nanoindentación, confirman que los mecanismos responsables de la degradación son la hidrólisis y la lixiviación de la matriz Chin et al. (2001), siendo este último el predominante. La pérdida de estas cadenas por lixiviación abre nuevos accesos para que la disolución pueda seguir penetrando y con ello producir una degradación más intensa si se compara con otras disoluciones Gu et al. (2001). En el caso de los compuestos de viniléster en NaOH, la hidrólisis cobra una mayor importancia, siendo coherente con la variación de masa obtenida, donde no se produce una pérdida significativa de misma Fig 2 (a).

En cambio, en el resto de materiales se produce un incremento de masa por la absorción del disolvente, Fig. 2 (b). En este caso predominan los mecanismos de hidrólisis de acuerdo con Mouritz et al. (2004), que aumentan el carácter hidrofílico de la matriz confirmado mediante la medida del ángulo de contacto y que provocan la caída de las propiedades evaluadas en nanoindentación, aunque de una forma menos intensa que la producida en NaOH. La pérdida del módulo de elasticidad en los medios con carácter neutro está relacionada con el aumento de la plasticidad de la matriz inducida por la hidrólisis, dando como resultado un material con menor dureza.

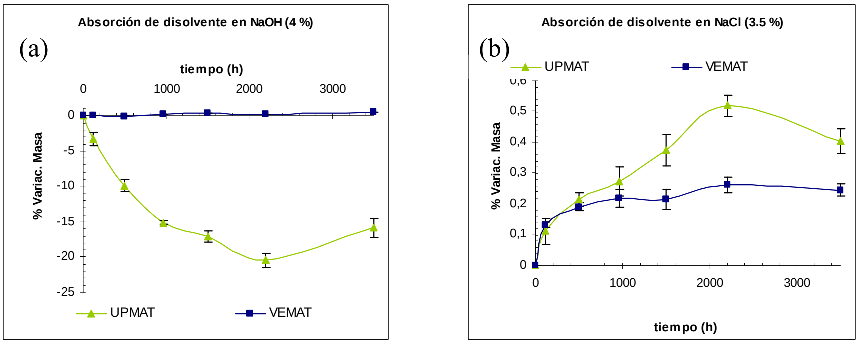

Fig. 2. Variación de masa: (a) NaOH y (b) NaCl.

En el estudio por AFM realizado, los resultados se han representado como la relación entre la variación de la rugosidad y tiempo en función del pH, Fig. 3 (a).

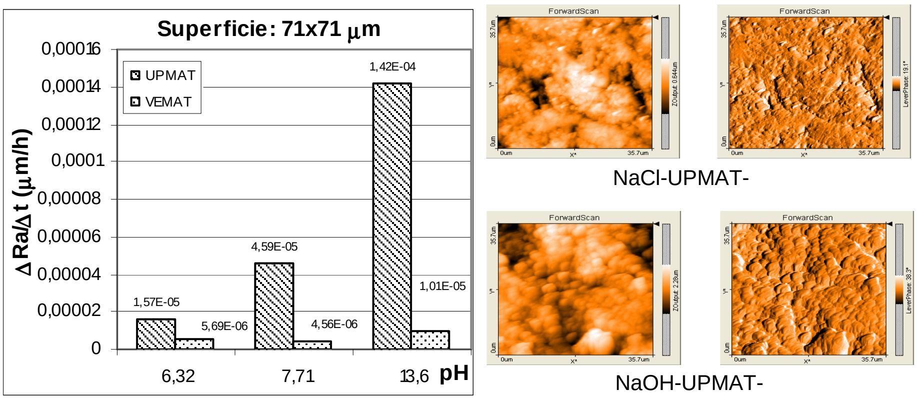

Fig. 3. Resultados AFM: (a) Rugosidad y (b) Imágenes superficiales.

Para las resinas utilizadas se observa un mayor cambio en rugosidad respecto a las otras disoluciones, en el medio con pH más elevado Fig. 3 (a), el NaOH, lo que implica un deterioro superficial cuantificado superior y por tanto una degradación más agresiva, Gu et al. (2001), lo que es concordante con el mecanismo de lixiviación propuesto, a partir de los resultados de nanoindentación y pérdida de masa, ya que provoca un cambio importante en el estado superficial del material tal y como se observa en la Fig. 3 (b). Se confirma la correlación entre el efecto de la degradación y el pH de la disolución, establecida a partir de los resultados de nanoindentación. Los cambios en rugosidad, son claramente inferiores en los compuestos de matriz viniléster comparado con los de poliéster. Estos resultados concuerdan con lo referenciado por Chin et al. (2001) and Mouritz et al. (2004), donde establecen que los compuestos de viniléster son menos susceptibles a la degradación que los de poliéster, debido a que los grupos funcionales éster son terminales y están protegidos por grupos metilos, mientras que en los compuestos de poliéster están distribuidos a lo largo de la cadena principal, siendo por tanto los primeros menos hidrolizables que los de poliéster en virtud de la estructura de las cadenas, como verifica el estudio mediante nanoindentación.

En las imágenes de FESEM Fig. 4, se puede observar que el NaOH es el medio que provoca un mayor efecto a nivel superficial Gu et. al. (2001) confirmando los resultados obtenidos de AFM, dejando una superficie irregular y con falta de material, producto de la lixiviación, Figura 4 (c), confirmado con las pérdidas de peso observadas. Medios menos agresivos presentan un estado superficial menos deteriorado, Fig. 4 (b). Un comportamiento similar se observa en los compuestos de viniléster.

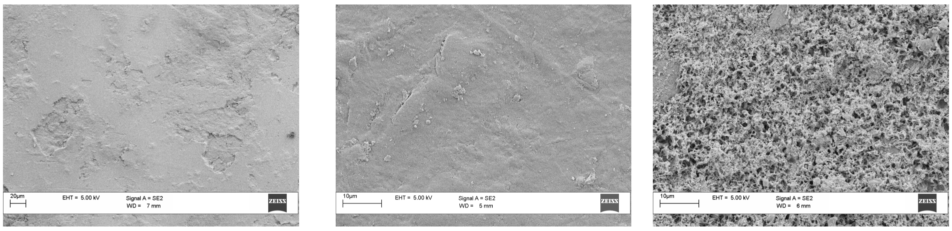

Fig. 4. FESEM de UPMAT: (a) Origen, (b) NaCl-12300h y (c) NaOH-2200h.

A partir de los resultados analizados en este trabajo, se diferencian dos niveles, desde el punto de vista de la agresividad del medio. De un lado tenemos el agua y el NaCl, con pH neutro alrededor de 7, que produce un efecto similar donde predominan los mecanismos de hidrólisis, y de otro lado, los de carácter fuertemente alcalino, con mecanismos preferenciales de lixiviación, que producen un mayor cambio en las propiedades del material dejando superficies muy deterioradas Gu et. al. (2001) comparado con el resto de medios analizados Fig. 3 (b) y 4 (b).

4. CONCLUSIONES

- Las herramientas empleadas para determinar las propiedades superficiales en los compuestos, nanoindentación y AFM, permiten cuantificar el nivel de degradación y aportar luz sobre los mecanismos responsables del deterioro.
- Existe una correlación entre el efecto de la degradación y el pH de la disolución, siendo el NaOH el medio más agresivo en virtud del efecto producido sobre las propiedades del material y sobre el estado superficial del compuesto.
- En los medios con carácter neutro predominan los mecanismos de degradación por hidrólisis y en los de carácter alcalino la lixiviación.

AGRADECIMIENTOS

Se agradece a la Universidad Politécnica de Valencia la financiación recibida para la realización de una estancia en la Università di Perugia (Italia), donde se llevaron a cabo parte de las caracterizaciones que se reflejan en este trabajo.

REFERENCIAS

CHIN, J.W., AOUADI, K., HAIGHT, M.R., HUGHES, W.L. Y NGUYEN, T. (2001), *Polymer Composite, vol. 22, No.2*, p. 282-297.

MOURITZ, A.P., KOOTSOOKOS, A., MATHYS, G. (2004), *Journal of Materials Science*, 39(19), p. 6073-6077.

OLIVER, W.C., PHARR, G.M. (1992), *Journal of Materials Research*, 7(6): p. 1564-1583.

GU, X., RAGHAVAN, D., et al., (2001), *Polymer Degradation and Stability*, 74 (1): p. 139-149.